HAI2024

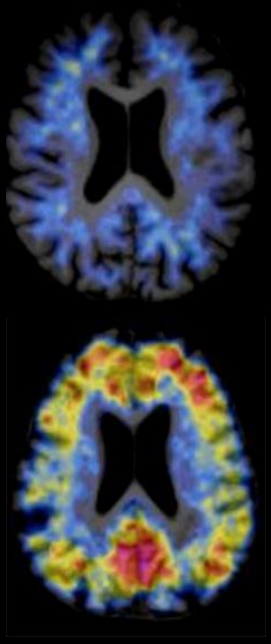

TABLE OF CONTENTS

WELCOME!

Dear Esteemed Attendees,

On behalf of the HAI2024 Executive Committee, it is my great pleasure to extend a warm welcome to each of you as we embark on this exciting journey into the realms of cutting-edge scientific exploration.

This year's response has been nothing short of spectacular, with an overwhelming 146 posters and 46 podium presentations selected from a pool of over 200 exceptional applications. This robust engagement demonstrates the dedication and enthusiasm of our scientific community, and we are thrilled to showcase the incredible work that lies ahead.

None of this would be possible without the unwavering support of our sponsors, to whom we extend our deepest gratitude:

Diamond Sponsors: Meilleur Technologies, Lantheus

Palladium Sponsors: Eli Lilly & Co., Alzheimer's Association

Gold Sponsors: Genentech, Eisai

Silver and Scholarship Sponsors: Rainwater Charitable Foundation. Bristol Myers Squibb

Silver Sponsors: Invicro. Life Molecular Imaging, Johnson & Johnson

Bronze Sponsors: AbbVie, C2N, Quanterix, Clario

We extend heartfelt appreciation to our Program Committee members, Theme Co-Chairs, and Executive Committee for their tireless efforts. Their invaluable contributions have paved the way for three days brimming with scientific exploration, networking opportunities, and mentorship possibilities.

This conference is not just an assembly of researchers; it's a dynamic community committed to advancing our field. So, as we gather in this space, let's celebrate the collaborative spirit that fuels scientific discovery.

Thank you for being an integral part of HAI2024, and here's to an inspiring conference filled with discovery, collaboration, and shared passion for advancing the frontiers of science.

Best wishes,

Dr. Keith Johnson
HAI2024 Conference Organizer

SUPPORTERS

NIH National Institute on Aging

DIAMOND

Meilleur Technologies

LANTHEUS CERVEAU

PALLADIUM

Lilly

ALZHEIMER'S ASSOCIATION

GOLD

Genentech
A Member of the Roche Group

Eisai

SILVER AND SCHOLARSHIP

RAINWATER Charitable Foundation

Bristol Myers Squibb

SILVER

Invicro

Life Molecular Imaging

Johnson&Johnson Innovative Medicine

BRONZE

abbvie

C2N DIAGNOSTICS

CLARIO.

Quanterix
The Science of Precision Health

HAI COMMITTEES

EXECUTIVE COMMITTEE

Keith Johnson, MD, *Massachusetts General Hospital*
Maria Carrillo, PhD, *Alzheimer's Association*
Teresa Gomez-Isla, MD, *Massachusetts General Hospital*
Thomas Karikari, PhD, *University of Gothenburg*
Beth Mormino, PhD, *Stanford University*
Julie Price, PhD, *Massachusetts General Hospital*

THEME CO-CHAIRS

Suzanne Baker, PhD, *Lawrence Berkeley Natl Laboratory*
Tobey Betthauser, PhD, *University of Wisconsin*
Anne Cohen, PhD, *University of Pittsburgh*
Brad Christian, PhD, *University of Wisconsin*
Teresa Gomez-Isla, MD, *Massachusetts General Hospital*
Ansel Hillmer, PhD, *Yale University School of Medicine*
Milos Ikonomovic, MD, *University of Pittsburgh*
Heidi Jacobs, PhD, *Massachusetts General Hospital*
Thomas Karikari, PhD, *University of Pittsburgh*
Susan Landau, PhD, *University of California, Berkeley*
Laetitia Lemoine, PhD, *Invicro*
Beth Mormino, PhD, *Stanford University*
Melissa Murray, PhD, *Mayo Clinic*
Julie Price, PhD, *Harvard Medical School*
Gil Rabinovici, MD, *University of California, San Francisco*
Pedro Rosa-Neto, PhD, *McGill University*
Suzanne Schindler, MD, PhD, *Washington University in St Louis*
Henrik Zetterberg, MD, *University of Gothenburg*

YOUNG INVESTIGATOR AWARD JUDGES

Hartmuth Kolb, PhD, *Janssen R&D*
Michael Pontecorvo, PhD, *Avid Radiopharmaceuticals*
Christopher Rowe, PhD, *Austin Health*
John Seibyl, PhD, *Invicro*

PROGRAM COMMITTEE

Suzanne Baker, PhD, *Lawrence Berkeley National Laboratory*
Tobey Betthauser, PhD, *University of Wisconsin*
Brad Christian, PhD, *University of Wisconsin*
Anne Cohen, PhD, *University of Pittsburgh*
Teresa Gomez-Isla, MD, *Massachusetts General Hospital*
Roger Gunn, PhD, *Imperial College*
Ansel Hillmer, PhD, *Yale University*
Kenji Ishii, MD, *Tokyo Metropolitan Inst. of Gerontology*
Milos Ikonomovic, MD, *University of Pittsburgh*
Clifford R. Jack, MD, *Mayo Clinic*
Heidi Jacobs, PhD, *Massachusetts General Hospital*
Renaud La Joie, PhD, *University of California, San Francisco*
Susan Landau, PhD, *University of California, Berkeley*
Laetitia Lemoine, PhD, *Invicro*
Beth Mormino, PhD, *Stanford University*
Melissa Murray, PhD, *Mayo Clinic*
Agneta Nordberg, MD, PhD, *Karolinska Institute*
Rik Ossenkoppele, PhD, *VU University Medical Center*
Julie Ottoy, PhD, *University of Toronto*
Julie Price, PhD, *Harvard Medical School*
Gil Rabinovici, MD, *University of California, San Francisco*
Susan Resnick, PhD, *National Institute on Aging*
Dorene Rentz, PsyD, *Brigham and Women's Hospital*
Pedro Rosa-Neto, MD, PhD, *McGill University*
Stephen Salloway, MD, *Brown University*
Sandra Sanabria, PhD, *Genentech*
Suzanne Schindler, MD, PhD, *Washington University in St Louis*
Christopher Schwarz, PhD, *Mayo Clinic*
Reisa Sperling, MD, *Brigham and Women's Hospital*
Rik Vandenberghe, MD, PhD, *KU Leuven*
Victor Villemagne, MD, *University of Pittsburgh*
Sylvia Villeneuve, PhD, *McGill University*
Christina Young, PhD, *Stanford University*
Henrik Zetterberg, MD, *University of Gothenburg*

POSTER INDEX (by presenter's last name)

Board #	Poster Title	Authors	Presenter
114	Comparison of FDG-PET in individuals with down syndrome and dominantly inherited Alzheimer's disease: genetic forms with elevated production of amyloid	Abdelmoity | Wisch | Gordon | Flores | Roman | Handen | Christian | Head | Mapstone | Hartley | Rafii | Lee | Krinsky-McHale | Lai | Rosas | Zaman | Schmitt | Ptomey | Bateman | Benzinger | Ances	**Abdelmoity, Omar**
104	Characterizing the relationship between the functional connectome and tau PET in preclinical Alzheimer's disease	Abuwarda | Trainer | Ju | Constable | Fredericks	**Abuwarda, Hamid**
77	Dynamic brain states are associated with Alzheimer's pathology and cognition	Adams | Kark | Chappel-Farley | Escalante | Stith | Rapp | Yassa	**Adams, Jenna**
55	Unraveling Alzheimer's disease heterogeneity: a comparative analysis using hydra and chimera	An | Sotiras | Gordon	**An, Zhaoqi**
41	Clinical phenotype and plasma biomarker associations of non-Alzheimer's hippocampal atrophy	Asken | Wang | McFarland | Barker | Adjouadi | Velez Uribe | Rosselli | Crocco | Armstrong | Curiel Cid | Vaillancourt | Loewenstein | Duara | Smith	**Asken, Breton**
123	Disentangling the relationships between tau-PET, amyloid-β-PET, hippocampal subfield volumes, and memory: a longitudinal study	Aumont | Bedard | Bussy | Fernandez Arias | Therriault | Rahmouni | Stevenson | Tissot | Servaes | C. Macedo | Gauthier | M. Chakravarty | Rosa-Neto	**Aumont, Etienne**
83	Early phase amyloid PET as a surrogate marker of brain metabolism in cases of cognitive impairment	Aye | Melzer | Keenan | Croucher | Tippett | Anderson | Le Heron	**Aye, William**
86	In vivo structural integrity of the hypothalamus and the spatiotemporal evolution of Alzheimer's disease	Baillet | Betthauser | Salmon | Jacobs	**Baillet, Marion**
139	Astrocyte reactivity influences cognitive decline in individuals across the Alzheimer's disease continuum	Bellaver | Povala | Ferreira | Bauer-Negrini | Lussier | Leffa | Ferrari-Souza | Zalzale | Soares | Rohden | Aguzzoli | Abbas | Benedet | Ashton | Tissot | Therriault | Servaes | Stevenson | Rahmouni | Hong | Rho | Karim | Zimmer | Zetterberg | Blennow | Villemagne | Klunk | Lopez | Tudorascu | Slachevsky | Rosa-Neto | Cohen | Karikari | Son | Pascoal	**Bellaver, Bruna**
95	Predictability of amyloid-PET status with plasma phospho-Tau217 in adults with Down syndrome	Bettcher | Janelidze | McLachlan | Zammit | McVea | DiFilippo | Betthauser | Laymon | Tudorascu | Cohen | Garimella | Price | Keator | Brickman | Lao | Klunk | Rosas | Zaman | Hartley | Head | Mapstone | Krinsky-McHale | Johnson | Lai | Ances | Handen | Hansson | Christian | Alzheimer Biomarkers Consortium – Down Syndrome	**Bettcher, Brecca**

52	Comparison of amyloid PET and plasma biomarkers in predicting future memory decline among cognitively normal individuals	Bilgel | An | Walker | Moghekar | Ashton | Kac | Karikari | Blennow | Zetterberg | Thambisetty | Resnick	**Bilgel, Murat**
18	Beyond quantity: fill states as a biomarker for the degree of pathology and neurodegeneration across the Alzheimer's disease continuum.	Doering | Hoenig | Giehl | Andrassy | Bader | Bauer | Dzialas | Elmenhorst | Emert | Frensch | Jäger | Jessen | Krapf | Kroll | Lerche | Lothmann | Matusch | Neumaier | Onur | Ramirez | Richter | Sand | Tellmann | Theis | Zeyen | van Eimeren | Drzezga | Bischof	**Bischof, Gerard**
65	Differential association between plasma biomarkers and established biomarkers of Alzheimer's disease	Bluma | Chiotis | Bucci | Savitcheva | Matton | Kivipelto | Jeromin | De Santis | Di Molfetta | Ashton | Blennow | Zetterberg | Nordberg	**Bluma, Marina**
92	The role of frontoparietal control network and default mode network functional connectivity in cognitive resilience in preclinical Alzheimer's disease	Boyle | Shirzadi | Coughlan | Seto | Properzi | Klinger | Yuan | Scanlon | Jutten | Papp | Amariglio | Rentz | Chhatwal | Buckley | Sperling | Schultz	**Boyle, Rory**
30	Predicting regional tau burden using structural connectivity from individualized epicenters	Brown | Das | Nasrallah | Detre | Yushkevich | McMillan | Wolk	**Brown, Christopher**
105	Estimating time-to-tau as a function of Aβ pathology in Alzheimer's disease using [18F]MK6240 and [18F]NAV4694 PET	Budd Haeberlein | Leuzy | Mathotaarachchi | Insel | Schöll | Moscoso | Villemagne | Doré | Rowe	**Budd Haeberlein, Samantha**
46	Establishing the interchangeability between CSF and PET for identifying patients with Alzheimer's disease pathology who are suitable for amyloid targeting therapies	Burnham | K Arora | Iaccarino | Kennedy | Kotari | Wijayawardana | Lu | Pontecorvo | Quevenco | Dell' Agnello | Neff | Petronzi | Viollet | Wang	**Burnham, Samantha**
133	Longitudinal white matter degeneration is associated with higher subsequent amyloid load across the Alzheimer's disease continuum	Burton | Blujus | Oh	**Burton, Courtney**
70	APOE, ABCA7, and KIF13B associations with earlier onset of amyloid positivity from over 4000 harmonized Positron Emission Tomography images	Castellano | Wang | Archer | Cody | Harrison | Wu | Durant | Janve | Engelman | Jagust | Albert | Johnson | Resnick | Sperling | Bigel | Saykin | Vardarajan | Mayeux | Betthauser | Dumitrescu | Mormino | Mormino | Hohman | Koran	**Castellano, Tonnar**
06	Amyloid pet positivity in Korean Dementia Syndromes: in relation to diagnosis, age, and Apoe genotypes	Chun | Jang | Yun | Kim | Woo | Seo	**Chun, Min Young**
130	Characterizing multi-site harmonized amyloid and tau PET across the Alzheimer's continuum	Cody | Johns | Carlson | Younes | Young | Mukherjee | Trittschuh | Gibbons | Dumitrescu | Archer | Durant | Nakano | Klinedinst | Choi | Lee | Scollard | Mez | Saykin | Crane | Cuccaro | Toga | Tosun | Hohman | Mormino	**Cody, Karly**
131	Characterization of tau PET accumulation relative to duration of entorhinal tau positivity	Cody | Langhough | Heston | Teague | Christian | Johnson | Betthauser	**Cody, Karly**

61	Clinical relevance of visually positive amyloid-PET burden in the occipital lobe	Collij | Smith | Palmqvist | Strandberg | Ossenkoppele | Hansson	**Collij, Lyduine**
62	Tau-PET subtypes show distinct profiles of cerebrospinal fluid biomarkers, neurodegeneration, and cognition in a large single-site cohort	Collij | Mastenbroek | Pichet Binette | Smith | Palmqvist | Mattsson-Carlgren | Strandberg | Ossenkoppele | Vogel | Hansson	**Collij, Lyduine**
125	Tau-PET spatial extent for predicting cognitive decline within tau-positive individuals	Coomans | van Tol | Groot | van der Flier | Pijnenburg | van de Giessen | Ossenkoppele	**Coomans, Emma**
91	Plasma ADRD biomarkers predict longitudinal declines in intra-network functional brain connectivity	Dark | Shafer | Cordon | An | Lewis | Moghekar | Landman | Resnick | Walker	**Dark, Heather**
08	Examination of synaptic density and neurofibrillary tau tangle burden in cognitively unimpaired and impaired older adults	DiFilippo | Jonaitis | Ennis | McLachlan | McVea | Bettcher | Pasquesi | Davenport-Sis | Schulz | Thor | Grover | Barnhart | Engle | Betthauser | Johnson | Bendlin | Christian	**DiFilippo, Alexandra**
17	Longitudinal hippocampal volume trajectories and their relationships with β-amyloid, tau, cerebrovascular, and cognition in a baseline cognitively unimpaired sample	Du | Betthauser | Jonaitis | Stephenson | Hermann | Rivera | Larget | Chappell | Cadman | Rowley | Eisenmenger | Johnson | Langhough	**Du, Lianlian**
85	Amyloid and tau burden relate to longitudinal changes in performance of everyday activities as measured using the performance-based Harvard Automated Phone Task	Dubbelman | Diez Palacio | Gonzalez | Amariglio | Becker | Chhatwal | Gatchel | Johnson | Locascio | Udeogu | Wang | Papp | Properzi | Rentz | Schultz | Sperling | Vannini | Marshall	**Dubbelman, Mark**
127	Will cerebral glucose metabolism measured using [18F]FDG PET substitute tau PET in clinical studies?	Edison	**Edison, Paul**
128	CSF sTREM2 is associated with neuroprotective microglial states early in Alzheimer's disease and deleterious effects later in the disease trajectory	Edison	**Edison, Paul**
112	Neighborhood disadvantage and the association between imaging biomarkers of Alzheimer's disease and cognition in a cohort of diverse older adults	Fan | Royse | Snitz | Reese | Karikari | Pascoal | Shaaban | Roush | Potopenko | Cisneros | Kotulsky | Kamboh | Lopresti | Villemagne | Lopez | Becker | Cohen	**Fan, Erica**
09	Association between plasma P-tau and cognition in the Alzheimer's disease spectrum	Fernandez | Therriault | Macedo | Servaes | Wang | Rahmouni | Aumont | Hosseini | Tissot | Mathotaarachchi | Stevenson | Stevenson | Pascoal | Ashton | Lessa | Karikari | Triana-Baltzer | Kolb | Zetterberg | Blennow | Rosa-Neto	**Fernandez, Jaime**
32	The TSPO circadian pattern: a [11C]ER176 test-retest study	Finn | Zanotti Fregonara | Appleton | Yu | Fujita | Masdeu | Pascual	**Finn, Quentin**
36	Early Aβ and tau-seeded functional networks derived in young adults reflect patterns of tau deposition and accumulation	Fonseca | Harrison | Chadwick | Ziontz | Baker | Jagust	**Fonseca, Corrina**

117	Increased CSF GAP-43 is associated with accelerated tau accumulation and spread in Alzheimer's disease	Franzmeier	Dehsarvi	Steward	Biel	Dewenter	Römer	Wagner	Brendel	Ewers	Moscoso	Blennow	Zetterberg	Schöll	**Franzmeier, Nicolai**
73	Elevated amyloid-ß and tau burden is associated with accelerated cognitive decline on a digital clock drawing test in preclinical AD	Fu	Robinson	Rodriguez Alonso	Francis Malave	Jutten	Del Carmen Montenegro	Thibault	Penney	Davis	Sperling	Johnson	Price	Rentz	**Fu, Jessie Fanglu**
13	Neurophysiological changes related to amyloid and tau pathology are associated with longitudinal cognition and Mild Cognitive Impairment progression	Gallego Rudolf	Wiesman	Baillet	Villeneuve	**Gallego Rudolf, Jonathan**
98	Visualization of endogenously generated Dutch-type Abeta oligomers that dysregulate presynaptic neurotransmission in the absence of detectable inflammation	Gandy	Castranio	Varghese	Argyrousi	Tripathi	Glabe	Levy	Wang	Zhang	Lubell	Guerin	Rahimipour	Dickstein	Arancio	Ehrlich	**Gandy, Sam**
53	Confocal microscopy assessment of flortaucipir binding by a fluorescence analog compound T726 shows 4RT overlap in frontotemporal lobar degeneration	Gatto	Youssef	Reichard	Whitwell	Josephs	**Gatto, Rodolfo**
54	Correlative histopathological evaluation of basal ganglia iron deposition and tau and PiB positron emission tomography in Alzheimer's disease and frontotemporal lobar degeneration	Gatto	Carlos	Reichard	Lowe	Whitwell	Josephs	**Gatto, Rodolfo**
29	An artificial neural network for PET brain amyloid imaging	Georgiou	Zhao	Deana	Sfakianaki	Curiel Cid	Loewenstein	**Georgiou, Mike**
22	Amyloid quantification is dependent on scanner: a head-to-head comparison of 18F-NAV4694 Centiloid measurements between three PET/CT scanners	Gillman	Bourgeat	Cox	Li	Villemagne	Fripp	O'Keefe	Huang	Krishnadas	Feizpour	Williams	Bozinovski	Rowe	Doré	**Gillman, Ashley**
78	Imaging synaptic density across the Alzheimer's disease continuum with [18]F-SynVestT-1	Giorgio	Soleimani-Meigooni	Chen	Toueg	Weimer	Zinnhardt	Baker	Janabi	Rabinovici	Jagust	**Giorgio, Joseph**
79	Data-driven analysis of 10,361 amyloid-PET scans from the IDEAS study reveals two primary axes of variation	Giorgio	Mundada	Blazhenets	Mejia Perez	Schonhaut	Carrillo	Hanna	Gatsonis	March	Apgar	Siegel	Hillner	Whitmer	Jagust	Rabinovici	La Joie	**Giorgio, Joseph**
120	Assessing the efficacy of BETTH-derived tau thresholds to predict cognitive decline	Gogola	Lopresti	Snitz	Tudorascu	Minhas	Dore	Ikonomovic	Shaaban	Kofler	Matan	Bourgeat	Mason	Rowe	Aizenstein	Mathis	Klunk	Lopez	Cohen	Villemagne	**Gogola, Alexandra**
121	Assessing the correlations between imaging and plasma biomarkers within the AT(N) framework	Gogola	Cohen	Zeng	Lopresti	Snitz	Tudorascu	Minhas	Ikonomovic	Pascoal	Kofler	Matan	Mason	Aizenstein	Mathis	Klunk	Zetterberg	Blennow	Lopez	Villemagne	Karikari	**Gogola, Alexandra**
115	Deep learning-based partial volume correction for tau PET imaging	Gong	Lois	Thibault	Tiss	Jang	Becker	Price	El Fakhri	Johnson	**Gong, Kuang**

138	Plasma NfL correlates to grey matter and white matter atrophy ambivalent to amyloid status in older adults	Hall | Rahmouni | Macedo | Servaes | Therriault | Fernandez-Arias | Trudel | Stevenson | Gauthier | Sanjeewa | Lussier | Pascoal | Benedet | Ashton | Zetterberg | Blennow | Rosa-Neto	**Hall, Brandon**
34	Reduced coupling between cerebrospinal fluid flow and global brain activity is linked to cortical tau and atrophy	Han | Lee | Chen | Ziontz | Ward | Landau | Baker | Harrison | Jagust	**Han, Feng**
59	PET staging of tauopathy using amygdala	Hanseeuw | Rubinstein | Schultz | Buckley | Properzi | Farrell | Gatchel | Amariglio | Beiser | Seshadri | Marshall | Sperling | Jacobs | Johnson	**Hanseeuw, Bernard**
11	Factors explaining tau onset age and time from tau onset to dementia	Heston | Teague | Ruiz de Chavez | Morse | Deming | Cody | Langhough | Zuelsdorff | Betthauser	**Heston, Margo**
144	Association between oxygen extraction fraction, tau, and amyloid pathology, and cognitive status in Alzheimer's disease: implications for advanced neuroimaging techniques	Hosseini | Servaes | Therriault | Tissot | Rahmouni | Macedo | Lussier | Stevenson | Wang | Fernandez-Arias | Socualaya | Aumont | Stevenson | Gauthier | Cho | Zhuang | Wang | Rudko | Pascoal | Rosa-Neto	**Hosseini, Seyyed Ali**
118	Investigating the impacts of tau status in Alzheimer's disease by using [18F]Flortaucipir tau cutoff	Huang | Lin | Huang | Hsu | Chang | Huang | Hsiao	**Huang, Shao-Yi**
02	Plasma Aβ42/40 ratio, GFAP, and NfL across the neurodegenerative diseases: cross-sectional and longitudinal study in a large multi-center cohort	Jang | Kim | Shin | Yoo | Lee | Yun | Na | Kim | Blennow | Zetterberg | Seo	**Jang, Hyemin**
137	Baseline plasma GFAP predicts longitudinal tau-PET uptake in Braak staging continuum	Jia | Rahmouni | Tissot | Servaes | Therriault | Cassa Macedo | Fernandez-Arias | Wang | Lussier | Kunach | Gauthier | Benedet | Ashton | Zetterberg | Pascoal | Blennow | Rosa-Neto	**Jia, Wan Lu**
75	Lower locus coeruleus function in associated with greater cognitive variability in preclinical Alzheimer's disease	Juneau | Baillet | Wiklund | Riphagen | Prokopiou | Papp | Jutten | Rentz | Sperling | Johnson | Jacobs	**Juneau, Truley**
129	The Mobile Toolbox for assessing cognition remotely: associations with amyloid and tau deposition in cognitively unimpaired older adults	Jutten | Burling | Fu | Properzi | Amariglio | Papp | Marshall | Price | Johnson | Sperling | Rentz	**Jutten, Roos**
71	Neuroinflammation in patients with mild cognitive impairment and Alzheimer's Disease	Kandimalla | Lee | Min | Botha | Graff-Radford | Jones | Vemuri | Kantarci | Knopman | Jack | Petersen | Lowe	**Kandimalla, Mahathi**
21	Distinct microbial species less abundant in Alzheimer's disease patients associate negatively with cerebrospinal fluid biomarkers of Alzheimer's disease	Kang | Khatib | Dilmore | Heston | Ulland | Johnson | Asthana | Carlsson | Chin | Blennow | Zetterberg | Knight | Kaddurah-Daouk | Rey | Bendlin	**Kang, Jea Woo**
141	Regional cell-type proportions are associated with AD pathological changes	Kang | Ottoy | Soucy | Massarweh | Black | Rosa-Neto | Goubran	**Kang, Min Su**

05	Distinct effects of cholesterol profile components on amyloid and vascular burdens	Kang | Yoo | Kim | Seo	**Kang, Sung Hoon**
84	Unlocking tau PET accessibility: a machine learning-based prediction of tau pathology from plasma, MRI and clinical variables	Karlsson | Vogel | Strandberg | Arvidsson | Åström | Seidlitz | Bethlehem | Stomrud | Ossenkoppele | Ashton | Blennow | Palmqvist | Smith | Janelidze | Pichet Binette | Mattson-Carlgren | Hansson	**Karlsson, Linda**
33	Tau PET signal within the default mode network predicts longitudinal clinical decline in atypical early Alzheimer's disease	Katsumi | Howe | Eckbo | Wong | Quimby | Hochberg | McGinnis | Putcha | Touroutoglou | Dickerson	**Katsumi, Yuta**
24	Relationship between enlarged perivascular space and beta-amyloid deposition among cognitively normal ADNI participants	Kim | Hudson | Yuan | Lipford | Lyu | Whitlow	**Kim, Jeongchul**
58	Chronic neuroinflammation in older adults with persistent Long COVID: the preliminary findings of [18F]FEPPA PET imaging	Kim | Taboada | Liu | Maciarz | Armstrong | Palekar | Weisenbach	**Kim, Min-Jeong**
96	Locus coeruleus metabolism relates to Alzheimer's disease pathology in amyloid-positive symptomatic individuals	Koops | Dutta | Becker | van Egroo | Hanseeuw | Sperling | Johnson | Jacobs	**Koops, Elouise**
142	Quantitative Gradient Recalled Echo (qGRE) MRI detects neuronal loss and iron accumulation in nucleus basalis of Meynert in preclinical and mild Alzheimer's disease	Kothapalli | Milchenko | Benzinger | Goyal | Eldeniz | Marcus | Morris | Yablonskiy | Raichle	**Kothapalli, Satya VVN**
108	"Treatment Related Amyloid Clearance" (TRAC): a framework to characterize a new biomarker state in the era of anti-amyloid therapies	La Joie | Sexton | Cummings | Galasko | Ikonomovic | Landau | Llibre-Guerra | Mummery | Ossenkoppele | Price | Risacher | Smith | Van Dyck | Carrillo	**La Joie, Renaud**
31	Microglia density across different clinical Alzheimer's disease variants	Lao | Johnson | Smith | Guzman | Okafor | Houlihan | Heuer | Rossano | Talmasov | Chikwem | Dass | Noble | Kreisl | De Jager | Small	**Lao, Patrick**
04	The impact of metabolic health on the relationship of obesity with and Alzheimer's and vascular markers	LEE | Yoo | Kim | Cheon | Kwak | Kim | Ryu | Chang | Jang | Kim | Kim | Na | Kang | Seo	**Lee, Eun Hye**
126	Association of sex and cerebral beta-amyloid with cortical gray matter brain age in cognitively impaired older adults	Li | Son | Chen | Wang | Aizenstein | Hong | Roh | Cho | Hong | Nam | Park | Kim | Lee | Choi | Moon | Seo | Choi | Kim | Wu	**Li, Jinghang**
119	Study of reference regions in the quantitation of [18F]Florzolotau tau PET imaging	Huang | Lin | Lin | Huang | Hsu | Chang | Huang | Hsiao	**Lin, Jyh-Ruei**
97	Correlating in vivo amyloid beta centiloid values with neuropathological burden: Insights from Down syndrome and Alzheimer's disease cohorts	Liou | Ikonomovic | Handen | Christian | Mapstone | Head | Tudorascu | Brickman | Price | Laymon | Rosas | Zaman | Hartley | Lai | Kofler | Ibrahim | Villemagne | Cohen	**Liou, Jr-Jiun**

132	Harmonization of multi-scanner PET data with ComBat: application to 18F-AV1451 data acquired on a Siemens ECAT HR+ PET and a GE Discovery MI PET/CT Scanner	Lois Gomez | Diez-Palacio | Price | Johnson	**Lois Gomez, Cristina**
47	Exploring A-T+ within the AT(N) framework	Lopresti | Cohen | Gogola | Ikonomovic | Snitz | Mason | Minhas | Matan | McGeown | Cieply | Chiang | Pascoal | Reese | Matela | Karikari | Sweet | Berman | Kofler | Lopez | Villemagne	**Lopresti, Brian**
124	Tau-PET Overlap Index; associations with Braak Stage and quantitative NFT measurements	Lee | Min | Moloney | Mester | Lund | Ghatamaneni | Senjem | Nguyen | Graff-Radford | Schwarz | Gunter | Kantarci | Boeve | Vemuri | Jones | Knopman | Jack | Petersen | Murray | Lowe	**Lowe, Val**
40	Longitudinal multicenter head-to-head harmonization of tau-PET tracers: an overview of the HEAD study	Lussier | Silva do Amaral | Povala | Negrini | Pascual | Gordon | Lowe | Oh | Soleimani-Meigooni | Klunk | Tudorascu | Rosa-Neto | Baker | Pascoal	**Lussier, Firoza**
81	Precuneus fMRI activity is associated with future Aβ burden in cognitively normal older APOE4 carriers	Maass | Molley | Binette | Vockert | Marquardt | Kreissl | Remz | Rajah | Villeneuve	**Maass, Anne**
82	PI-2620 binding in cognitively normal older adults including SuperAgers	Maass | Garcia-Garcia | Molley | Behrenbruch | Schuhmann-Werner | Vockert | Rullmann | Hochkeppler | Fischer | Svenja Schwarck | Baldauf | Schulze | Stephens | Patt | Barthel | Sabri | Duezel | Kreissl	**Maass, Anne**
23	Neuroinflammation follows and outstrips tau progression patterns in primary 4R tauopathies	Malpetti | Römer | Harris | Gross | Gnörich | Stephens | Mueller | Koglin | Levin | Höglinger | Brendel | Franzmeier	**Malpetti, Maura**
67	Data-driven disease progression modelling consistently reveals an occipital amyloid-β subtype in two independent cohorts	Mastenbroek | Collij | Young | Vogel | Salvadó | den Braber | Visser | Gispert | van der Flier | Strandberg | Smith | Palmqvist | Mattson-Carlgren | Oxtoby | Barkhof | Ossenkoppele | Hansson	**Mastenbroek, Sophie**
56	Prevalence of Alzheimer's disease pathology in studies of memory and aging	McKay | Millar | Barthelémy | Benzinger | Morris | Bateman | Schindler | Gordon	**McKay, Nicole**
66	PiB PET demonstrates early, elevated amyloid striatal binding compared to florbetapir in Down syndrome	McLachlan | Rouanet | Garimella | Price | Tudorascu | Laymon | Keator | Kreisl | Klunk | Handen | Fryer | Zaman | Head | Mapstone | Bettcher | LeMerise | McVea | DiFillipo | Zammit | Hartley | Christian | Investigators	**McLachlan, Max**
87	Cross-sectional comparison of extra-cerebral binding trends in [F-18]MK6240 PET images	McVea | DiFilippo | McLachlan | Betcher | Johnson | Betthauser | Christian	**McVea, Andrew**
88	Tau accumulation in Down Syndrome after onset of amyloid positivity	McVea | DiFilippo | Max McLachlan | Betcher | Zammit | Betthauser | Converse | Murali | Stone | Hartley | Johnson | Tudorascu | Laymon | Cohen | Minhas | Mathis | Ances | Zaman | Klunk | Handen | Christian | Investigators	**McVea, Andrew**
99	[18F]PI-2620 tau-PET binding patterns in American football players	Mejia Perez | Mosaheb | Schonhaut | Blazhenets | McKee | Stein | Farris | Mez |	**Mejia Perez, Jhony**

	with suspected Chronic Traumatic Encephalopathy	Stephens | Mueller | Keegan | La Joie | Rabinovici | Alosco	
26	Evaluating bidirectional effects of amyloid and tau on functional brain networks in preclinical Alzheimer's disease	Millar | Singhe | Macharia | Metcalf | Roman | Morris | Benzinger | Gordon | Ances	**Millar, Peter**
103	Evaluating CenTauRz harmonization of matched FTP and MK6240 tau PET images: the HEAD Study	Minhas | Delbene | Luo | Reese | Gogola | Villemagne | Dore | Lopresti | Laymon | Lussier | Bauer-Negrini | Povala | Cohen | Crainiceanu | Pascual | Gordon | Lowe | Oh | Soleimani-Meigooni | Klunk | Rosa-Neto | Baker | Pascoal | Tudorascu	**Minhas, Davneet**
146	Specific Tau networks are associated with different cognitive domains in the elderly	Nayak | Hojjati | Ozoria-Blake | Razlighi	**Nayak, Siddharth**
51	A head-to-head comparison between plasma p-tau217 and tau-PET for predicting future cognitive decline among cognitively unimpaired individuals	Ossenkoppele | Salvado | Pichet-Binette | Therriault | Jonaitis | Bourgeat | Doré | Masters | Johnson | Villeneuve | Rosa-Neto | Rowe | Hansson	**Ossenkoppele, Rik**
27	Tau propagates along principal axes of functional and structural brain organization in Alzheimer's disease	Ottoy | Tan | Kang | Bezgin | Lussier | Pascoal | Rahmouni | Stevenson | Soucy | Gauthier | Bernhardt | Black | Rosa-Neto | Goubran	**Ottoy, Julie**
64	Aβ and tau associations with sex and affected parent's sex in preclinical Alzheimer's disease	Ourry | St-Onge | Mohammediyan | Yakoub | Soucy | Poirier | Breitner | Villeneuve	**Ourry, Valentin**
16	NODDI-derived measures of microstructural integrity in medial temporal lobe white matter pathways are associated with Alzheimer's disease pathology	Parker | Adams | Kim | McMillan | Yassa	**Parker, Dana**
19	Successful aging reflects anterior cingulate preservation but not tau accumulation rate	Pezzoli | Giorgio | Chen | Harrison | Jagust	**Pezzoli, Stefania**
122	The effect of microglial activation on brain atrophy across the Alzheimer's disease continuum	Povala | Bellaver | Lukasewicz Ferreira | Ferrari-Souza | Schaffer Aguzzoli | Teixeira Leffa | Zalzale | Soares | Lussier | Negrini | Rohden | Benedet | Stevenson | Rahmouni | Tissot | Therriault | Servaes | Cohen | Klunk | Villemagne | Zatt | R Zimmer | Karikari | Rosa-Neto | A Pascoal	**Povala, Guilherme**
89	Greater locus coeruleus activity and locus coeruleus-amygdala hypoconnectivity during high arousal conditions are related to elevated concentrations of plasma p-tau231 in older individuals	Prokopiou | Van Egroo | Riphagen | Ashton | Janelidze | Sperling | Johnson | Blennow | Hansson | Zetterberg | Jacobs	**Prokopiou, Prokopis**
102	18F-MK-6240 Tau PET visual read algorithm for Alzheimer's disease: diagnostic accuracy and comparison with automated-quantitative Braak stage analysis	Provost | Soucy | Haeger | Macedo | Rahmouni | Stevenson | Servaes | Therriault | Arias | Rosa-Neto	**Provost, Karine**
110	Plasma p-tau217 outperforms [18F]FDG-PET in identifying	Quispialaya | Joseph Therriault | Aliaga | Benedet | Ashton | Karikari | Macedo |	**Quispialaya, Kely**

	biological Alzheimer's disease in atypical and early-onset dementia	Rahmouni | Stevenson | Tissot | Arias | Wang | Hosseini | Jean-Claude | Pascoal | Gauthier | Gilfix | Vitali | Soucy | Zetterberg | Blennow | Zimmer | Rosa-Neto	
106	Neuroinflammation potentiates the effect of amyloid-β on longitudinal tau accumulation	Rahmouni | Wang | Therriault | Servaes | Tissot | Macedo | Arias-Fernandez | Kunach | Stevenson | Hosseini | Hall | Trudel | Jia | Gauthier | Zimmer | Benedet | Pascoal | Rosa-Neto	**Rahmouni, Nesrine**
74	Significance of a positive tau PET scan with a negative amyloid PET scan	Robinson | Lee | Min | Przybelski | Josephs | Jones | Graff-Radford | Boeve | Knopman | Jack. Jr. | Petersen | Machulda | Fields | Lowe	**Robinson, Carling**
25	Examining inter- and intra-subject variability in digital clock drawing test performance in cognitively normal older adults	Rodríguez Alonso | Fu | Robinson | Francis Malave | Jutten | Del Carmen Montenegro | Thibault | Penney | Davis | Sperling | Price | Rentz | Johnson	**Rodríguez Alonso, Marina**
44	Amyloid-induced hyperconnectivity drives tau spreading across connected brain regions in Alzheimer's disease	Roemer | Wagner | Steward | Biel | Dewenter | Dennecke | Gross | Zhu | Zheng | Dehsarvi | Dichgans | Ewers | Brendel | Franzmeier	**Roemer, Sebastian Niclas**
14	Tau and amyloid associations with sustained attention and episodic memory performance in clinically unimpaired older adults	Romero | Winer | Tran | Rathmann-Bloch | Park | Schwartz | Miller | Anders | Morales | Wilson | Trelle | Andreasson | Davidzon | Mormino | Wagner	**Romero, America**
109	Alzheimer's disease biological PET staging using plasma p217+tau	Feizpour | Doré | Krishnadas | Bourgeat | Doecke | Saad | Triana-Baltzer | Laws | Shishegar | Huang | Fowler | Ward | Masters | Fripp | Kolb | Villemagne | Rowe	**Rowe, Christopher**
68	Mid-life perceived discrimination and late-life Alzheimer's disease pathology and cognition in African American and non-Hispanic White populations	Royse | Snitz | Saeed | Reese | Lopresti | Karikari | Kamboh | Villemagne | Reis | Lopez | Cohen	**Royse, Sarah**
113	Longitudinal association of mid-life ten year cardiovascular disease risk score with blood biomarkers of Alzheimer's disease and neurodegeneration: Heart SCORE Brain Study	Saeed | Chang | Swanson | Villemagne | Snitz | Royse | Lopresti | Kip | Reese | Gogola | Pascoal | Kamboh | Blennow | Zetterberg | Karikari | Lopez | Reis | Cohen	**Saeed, Anum**
63	ER176 neuroinflammatory PET profiles and relationships with flortaucipir tau PET in progressive apraxia of speech	Satoh | Utianski | Duffy | Clark | Botha | Lowe | Josephs | Whitwell	**Satoh, Ryota**
116	Plasma levels of an N-terminal tau fragment predict core AD and neurodegenerative biomarkers in autosomal dominant Alzheimer's disease	Schultz | Liu | Ostaszewski | Anderson | Karch | Cruchaga | Gordon | Benzinger | Hassenstab | Morris | Perrin | Goate | Allegri | Barthelemy | Berman | Chui | Farlow | Fox | Day | Jucker | Jack | Koeppe | Lee | Levey | Levin | Martins | Mori | Noble | Rosa-Neto | Salloway | Sanchez | Schofield | McDade | Sperling | Selkoe | Bateman | Chhatwal	**Schultz, Stephanie**
03	Publicly available software and FTP calibration data for CenTauR tau PET standardization	Schwarz | Przybelski | Prakaashana | Doré | Villemagne | Leuzy | Senjem | Lowe | Gunter |	**Schwarz, Christopher G.**

		Kantarci | Vemuri | Graff-Radford | Petersen | Knopman | Jack	
50	Parental history of memory impairment predicts β-amyloid burden and positivity in a preclinical population	Seto | Hohman | Mormino | Papp | Amariglio | Rentz | Johnson | Schultz | Sperling | Buckley | Yang	**Seto, Mabel**
07	Toward more representative estimates of the effect of tau on cognition	Shaaban | Wu | Kunicki | Chasioti | Tommet | Rich | Oh | Karikari | Cohen | Lopresti | Villemagne | Glymour | Jones	**Shaaban, C. Elizabeth**
136	[18F]RO-948 tau PET retention and correlation with fluid biomarkers in the early AD continuum	Shekari | González Escalante | Milà-Alomà | Falcon | López-Martos | Sánchez-Benavides | Brugulat-Serrat | Niñerola-Baizán | J. Ashton | K. Karikari | Lantero-Rodriguez | Snellman | Ortiz | Tonietto | Borroni | Klein | Minguillón | Fauria | Perissinotti | Molinuevo | Zetterberg | Blennow | Grau-Rivera | Suárez-Calvet | Gispert	**Shekari, Mahnaz**
76	Associations between regional tau pathology and cognitive decline across the AD continuum differ by sex	Singleton | Mattsson-Carlgren | Pichet Binette | Stomrud | Strandberg | Ossenkoppele | Hansson	**Singleton, Ellen**
45	A visual-read algorithm for tau pathology using [18F]RO948	Smith | Garibotto | Hägerström | Jögi | Ohlsson | Tonietto | Janelidze | Stomrud | Klein | Hansson	**Smith, Ruben**
135	A pretrained foundation model for learning representation of regional tau accumulation pattern and its downstream applications	Sohn | Song | Seong	**Sohn, JunYoung**
42	Synaptic loss in relapsing and progressive multiple sclerosis: an in vivo exploratory study using SV2A-PET	Soleimani-Meigooni | Giorgio | Abdelhak | Cordano | Chen | Toueg | Weimer | Zinnhardt | Baker | Janabi | Green | Jagust | Rabinovici	**Soleimani-Meigooni, David**
28	X-ray based amyloid index as a quantitative biomarker for neurodegenerative diseases	Suresh | Dahal | Badano	**Suresh, Karthika**
57	Depression in amyloid-positive individuals is associated with a faster rate of tau accumulation on longitudinal positron-emission tomography	Talmasov | Johnson | Lao | Marder | Miller	**Talmasov, Daniel**
140	Elevated Plasma Ptau-181 is associated with congestive heart failure	Tanner | Wiedner | Himali | Ramos-Cejudo | Beiser | Seshadri | Javier Aparicio | Himali	**Tanner, Jeremy**
90	Establishing tau-PET cut-points for cognitive diagnosis with [F-18]PI-2620	Tennant | Wheeler | Lee | Terner | Raman | Rissman | Christian | Petersen | Lee | Cohen | Ances | Zhou | Zhang | Nandy | Yaffe | O'Bryant | Braskie	**Tennant, Victoria**
134	Multimodal analysis of tau epicenters in heterogeneous Alzheimer's disease variants	Trainer | Vin | Xu | Chase | O'Dell | Toyonaga | Tun | Li | Ju | Mecca | van Dyck | Fredericks	**Trainer, Anne**
145	Association of plasma pTau epitopes with mesial temporal lobe cortical thinning	Trudel | Rahmouni | Macedo | Therriault | Servaes | Wang | Fernandez-Arias | Hall | Stevenson | Sanjeewa | Gauthier | Benedet |	**Trudel, Lydia**

		Ashton | Zetterberg | Blennow | Lussier | Tharick | Karikari | Rosa-Neto	
143	Head-to-head analysis of [18F]MK6240 and [18F]Flortaucipir standardized update values (SUVs): the HEAD Study	Tsai | Tissot | Tudorascu | Rosa-Neto | Gordon | Pascual | Lowe | Soleimani-Meigooni | Oh | Klunk | Jagust | Pascoal | Baker	**Tsai, Hsin-Yeh**
39	Validation of a novel visual read interpretation of flortaucipir PET for identification of participants with high tau burden: results from I7E-AV-A26 reader study	Tunali | Iaccarino | Wang | Arora | Lu | Shcherbinin | Pontecorvo	**Tunali, Ilke**
37	Gray matter GABA and Glutamate reflect amyloid beta burden in cognitively healthy individuals	Schreiner | Kirchner | Van Bergen | Gietl | Buck | Hock | Prüssmann | Henning | Unschuld	**Unschuld, Paul**
15	Sex differences in the relationships between 24-h rest-activity patterns and plasma markers of Alzheimer's disease pathology	Van Egroo | Beckers | Ashton | Blennow | Zetterberg | Jacobs	**Van Egroo, Maxime**
01	Longitudinal synaptic loss follows tau PET Braak staging in vivo and supports local neurodegeneration by tau accumulation in stages III-VI	Vanderlinden | Koole | Vandenbulcke | Van Laere	**Vanderlinden, Greet**
10	The role of biofluid markers in predicting near-term cognitive impairment	Yakoub | Ashton | Karikari | Strikwerda-Brown | St-Onge | Ourry | Schöll | Geddes | Ducharme | Rosa-Neto | Soucy | Breitner | Zetterberg | Blennow | Poirier | Villeneuve | Prevent-AD research group	**Villeneuve, Sylvia**
60	Discovery and optimization of [18F]ACI-15916, a promising PET tracer for the diagnosis of Parkinson's disease and other a-synucleinopathies	Vokali | Molette | Ravache | Delgado | Kocher | Pittet | Vallet | Luthi-Carter | Pfeifer | Kosco-Vilbois | Capotosti	**Vokali, Efthymia**
100	Regional amyloid-β burden in Lewy Body Disease	Vossler | Abdelnour | Young | Winer | Smith | Smith | Shahid | Wilson | Davidzon | Mormino | Poston	**Vossler, Hillary**
49	Comparison of visual interpretation and quantitation in detecting amyloid pathology using florbetapir F-18 PET imaging: results from nuclear medicine physicians or radiologists practicing at community healthcare settings	Wang | Lu | Iaccarino | Arora | Morris | Kim | Kennedy | Kotari | Burnham | collins | Pontecorvo	**Wang, Jian**
48	Sex-specific synergistic interaction between Aβ and p-tau predicts faster tangle accumulation in females	Wang | Therriault | Servaes | Tissot | Rahmouni | Macedo | Fernandez-Arias | Mathotaarachchi | Benedet | Stevenson | Ashton | Lussier | Pascoal | Zetterberg | Rajah | Blennow | Gauthier | Rosa-Neto	**Wang, Yi-Ting**
80	Lower locus coeruleus structural integrity is associated with greater intraindividual cognitive variability in older individuals	Wiklund | Van Egroo | Juneau | Riphagen | Papp | Jutten | Rentz | Sperling | Johnson | Jacobs	**Wiklund, Emma**
38	Amyloid PET scan reader agreement in IDEAS: expert readers vs local clinician readers	Windon | Siegel | Zeltzer | Hanna | Carrillo | Hillner, | Iaccarino | La Joie | March | Perez |	**Windon, Charles**

		Mundada | Arora | Buckley | Bullich | Sherwin | Gatsonis | Rabinovici	
93	Disrupted sleep and 24-hour rhythms are associated with 18F-PI-26260 tau PET in aging and neurodegenerative disease	Winer | Romero | Vossler | Young | Smith | Anders | Pacheco Morales | Davidzon | Henderson | Poston | Zeitzer | Mormino	**Winer, Joseph**
94	Cortical and substantia nigra 18F-PI-2620 tau PET are associated with cognitive and motor impairment in Lewy body disease	Winer | Vossler | Young | Romero | Smith | Shahid | Abdelnour | Wilson | Anders | Pacheco Morales | Davidzon | Mormino | Poston	**Winer, Joseph**
69	Comparison of amyloid positivity and global cortical SUVR between black and white non-Hispanic participants in the GAP Bio-Hermes study	Wolz | Hughes | Manber | Mohs | Dwyer | Beauregard	**Wolz, Robin**
111	A-T+ PET participants in preclinical AD: clinical progression and concordance with fluid biomarkers	Yakoub | St-Onge | Fajardo | Mohammediyan | Dery | Sylvain | Tremblay-Mercier | Remz | Gonneaud | Vogel | Soucy | Pichet-Binette | Villleneuve | Research Group	**Yakoub, Yara**
12	Evaluation of ComBat as a harmonization technique for reducing across-tracer variance in regional amyloid PET analyses	Yang | Earnest | Kumar | Gordon | Sotiras	**Yang, Braden**
107	Association between plasma pTau epitopes and synaptic density measured with [C-11]UCB-J PET	Yang | DiFilippo | Ma | Wilson | Thor | Pasquesi | Barnhart | Engle | Betthauser | Ashton | Johnson | Christian | Zetterberg | Bendlin	**Yang, Kao Lee**
43	[18F]-PI-2620 tau PET signal across the aging and Alzheimer's disease clinical spectrum	Young | Vossler | Romero | Smith | Park | Trelle | Winer | Wilson | Zeineh | Sha | Khalighi | Morales | Anders | Zaharchuk | Henderson | Andreasson | Wagner | Poston | Davidzon | Mormino	**Young, Christina**
35	Cognitive decline and Alzheimer's disease clinical status in Down syndrome are better distinguished by amyloid and neurofibrillary tau compared to age	Zammit | Schworer | Betthauser | Hartley | Laymon | Tudorascu | Cohen | Johnson | Converse | Minhas | Zaman | Ances | Mathis | Klunk | Handen | Christian | Alzheimer's Biomarker Consortium - Down Syndrome	**Zammit, Matt**
101	Pathology-weighted connectivity with medial parietal lobe drives neocortical tau accumulation	Ziontz | Fonseca | Giorgio | Harrison | Jagust	**Ziontz, Jacob**

POSTER INDEX (by board number)

Board #	Poster Title	Authors	Presenter
01	Longitudinal synaptic loss follows tau PET Braak staging in vivo and supports local neurodegeneration by tau accumulation in stages III-VI	Vanderlinden | Koole | Vandenbulcke | Van Laere	**Vanderlinden, Greet**
02	Plasma Aβ42/40 ratio, GFAP, and NfL across the neurodegenerative diseases: cross-sectional and longitudinal study in a large multi-center cohort	Jang | Kim | Shin | Yoo | Lee | Yun | Na | Kim | Blennow | Zetterberg | Seo	**Jang, Hyemin**
03	Publicly available software and FTP calibration data for CenTauR tau PET standardization	Schwarz | Przybelski | Prakaashana | Doré | Villemagne | Leuzy | Senjem | Lowe | Gunter | Kantarci | Vemuri | Graff-Radford | Petersen | Knopman | Jack	**Schwarz, Christopher G.**
04	The impact of metabolic health on the relationship of obesity with and Alzheimer's and vascular markers	LEE | Yoo | Kim | Cheon | Kwak | Kim | Ryu | Chang | Jang | Kim | Kim | Na | Kang | Seo	**Lee, Eun Hye**
05	Distinct effects of cholesterol profile components on amyloid and vascular burdens	Kang | Yoo | Kim | Seo	**Kang, Sung Hoon**
06	Amyloid pet positivity in Korean Dementia Syndromes: in relation to diagnosis, age, and Apoe genotypes	Chun | Jang | Yun | Kim | Woo | Seo	**Chun, Min Young**
07	Toward more representative estimates of the effect of tau on cognition	Shaaban | Wu | Kunicki | Chasioti | Tommet | Rich | Oh | Karikari | Cohen | Lopresti | Villemagne | Glymour | Jones	**Shaaban, C. Elizabeth**
08	Examination of synaptic density and neurofibrillary tau tangle burden in cognitively unimpaired and impaired older adults	DiFilippo | Jonaitis | Ennis | McLachlan | McVea | Bettcher | Pasquesi | Davenport-Sis | Schulz | Thor | Grover | Barnhart | Engle | Betthauser | Johnson | Bendlin | Christian	**DiFilippo, Alexandra**
09	Association between plasma P-tau and cognition in the Alzheimer's disease spectrum	Fernandez | Therriault | Macedo | Servaes | Wang | Rahmouni | Aumont | Hosseini | Tissot | Mathotaarachchi | Stevenson | Stevenson | Pascoal | Ashton | Lessa | Karikari | Triana-Baltzer | Kolb | Zetterberg | Blennow | Rosa-Neto	**Fernandez, Jaime**
10	The role of biofluid markers in predicting near-term cognitive impairment	Yakoub | Ashton | Karikari | Strikwerda-Brown | St-Onge | Ourry | Schöll | Geddes | Ducharme | Rosa-Neto | Soucy | Breitner | Zetterberg | Blennow | Poirier | Villeneuve | Prevent-AD research group	**Villeneuve, Sylvia**
11	Factors explaining tau onset age and time from tau onset to dementia	Heston | Teague | Ruiz de Chavez | Morse | Deming | Cody | Langhough | Zuelsdorff | Betthauser	**Heston, Margo**
12	Evaluation of ComBat as a harmonization technique for reducing across-tracer variance in regional amyloid PET analyses	Yang | Earnest | Kumar | Gordon | Sotiras	**Yang, Braden**

13	Neurophysiological changes related to amyloid and tau pathology are associated with longitudinal cognition and Mild Cognitive Impairment progression	Gallego Rudolf	Wiesman	Baillet	Villeneuve	**Gallego Rudolf, Jonathan**
14	Tau and amyloid associations with sustained attention and episodic memory performance in clinically unimpaired older adults	Romero	Winer	Tran	Rathmann-Bloch	Park	Schwartz	Miller	Anders	Morales	Wilson	Trelle	Andreasson	Davidzon	Mormino	Wagner	**Romero, America**
15	Sex differences in the relationships between 24-h rest-activity patterns and plasma markers of Alzheimer's disease pathology	Van Egroo	Beckers	Ashton	Blennow	Zetterberg	Jacobs	**Van Egroo, Maxime**
16	NODDI-derived measures of microstructural integrity in medial temporal lobe white matter pathways are associated with Alzheimer's disease pathology	Parker	Adams	Kim	McMillan	Yassa	**Parker, Dana**
17	Longitudinal hippocampal volume trajectories and their relationships with β-amyloid, tau, cerebrovascular, and cognition in a baseline cognitively unimpaired sample	Du	Betthauser	Jonaitis	Stephenson	Hermann	Rivera	Larget	Chappell	Cadman	Rowley	Eisenmenger	Johnson	Langhough	**Du, Lianlian**
18	Beyond quantity: fill states as a biomarker for the degree of pathology and neurodegeneration across the Alzheimer's disease continuum.	Doering	Hoenig	Giehl	Andrassy	Bader	Bauer	Dzialas	Elmenhorst	Emert	Frensch	Jäger	Jessen	Krapf	Kroll	Lerche	Lothmann	Matusch	Neumaier	Onur	Ramirez	Richter	Sand	Tellmann	Theis	Zeyen	van Eimeren	Drzezga	Bischof	**Bischof, Gerard**
19	Successful aging reflects anterior cingulate preservation but not tau accumulation rate	Pezzoli	Giorgio	Chen	Harrison	Jagust	**Pezzoli, Stefania**
21	Distinct microbial species less abundant in Alzheimer's disease patients associate negatively with cerebrospinal fluid biomarkers of Alzheimer's disease	Kang	Khatib	Dilmore	Heston	Ulland	Johnson	Asthana	Carlsson	Chin	Blennow	Zetterberg	Knight	Kaddurah-Daouk	Rey	Bendlin	**Kang, Jea Woo**
22	Amyloid quantification is dependent on scanner: a head-to-head comparison of 18F-NAV4694 Centiloid measurements between three PET/CT scanners	Gillman	Bourgeat	Cox	Li	Villemagne	Fripp	O'Keefe	Huang	Krishnadas	Feizpour	Williams	Bozinovski	Rowe	Doré	**Gillman, Ashley**
23	Neuroinflammation follows and outstrips tau progression patterns in primary 4R tauopathies	Malpetti	Römer	Harris	Gross	Gnörich	Stephens	Mueller	Koglin	Levin	Höglinger	Brendel	Franzmeier	**Malpetti, Maura**
24	Relationship between enlarged perivascular space and beta-amyloid deposition among cognitively normal ADNI participants	Kim	Hudson	Yuan	Lipford	Lyu	Whitlow	**Kim, Jeongchul**
25	Examining inter- and intra-subject variability in digital clock drawing test performance in cognitively normal older adults	Rodríguez Alonso	Fu	Robinson	Francis Malave	Jutten	Del Carmen Montenegro	Thibault	Penney	Davis	Sperling	Price	Rentz	Johnson	**Rodríguez Alonso, Marina**

26	Evaluating bidirectional effects of amyloid and tau on functional brain networks in preclinical Alzheimer's disease	Millar | Singhe | Macharia | Metcalf | Roman | Morris | Benzinger | Gordon | Ances	**Millar, Peter**
27	Tau propagates along principal axes of functional and structural brain organization in Alzheimer's disease	Ottoy | Tan | Kang | Bezgin | Lussier | Pascoal | Rahmouni | Stevenson | Soucy | Gauthier | Bernhardt | Black | Rosa-Neto | Goubran	**Ottoy, Julie**
28	X-ray based amyloid index as a quantitative biomarker for neurodegenerative diseases	Suresh | Dahal | Badano	**Suresh, Karthika**
29	An artificial neural network for PET brain amyloid imaging	Georgiou | Zhao | Deana | Sfakianaki | Curiel Cid | Loewenstein	**Georgiou, Mike**
30	Predicting regional tau burden using structural connectivity from individualized epicenters	Brown | Das | Nasrallah | Detre | Yushkevich | McMillan | Wolk	**Brown, Christopher**
31	Microglia density across different clinical Alzheimer's disease variants	Lao | Johnson | Smith | Guzman | Okafor | Houlihan | Heuer | Rossano | Talmasov | Chikwem | Dass | Noble | Kreisl | De Jager | Small	**Lao, Patrick**
32	The TSPO circadian pattern: a [11C]ER176 test-retest study	Finn | Zanotti Fregonara | Appleton | Yu | Fujita | Masdeu | Pascual	**Finn, Quentin**
33	Tau PET signal within the default mode network predicts longitudinal clinical decline in atypical early Alzheimer's disease	Katsumi | Howe | Eckbo | Wong | Quimby | Hochberg | McGinnis | Putcha | Touroutoglou | Dickerson	**Katsumi, Yuta**
34	Reduced coupling between cerebrospinal fluid flow and global brain activity is linked to cortical tau and atrophy	Han | Lee | Chen | Ziontz | Ward | Landau | Baker | Harrison | Jagust	**Han, Feng**
35	Cognitive decline and Alzheimer's disease clinical status in Down syndrome are better distinguished by amyloid and neurofibrillary tau compared to age	Zammit | Schworer | Betthauser | Hartley | Laymon | Tudorascu | Cohen | Johnson | Converse | Minhas | Zaman | Ances | Mathis | Klunk | Handen | Christian | Alzheimer's Biomarker Consortium - Down Syndrome	**Zammit, Matt**
36	Early Aβ and tau-seeded functional networks derived in young adults reflect patterns of tau deposition and accumulation	Fonseca | Harrison | Chadwick | Ziontz | Baker | Jagust	**Fonseca, Corrina**
37	Gray matter GABA and Glutamate reflect amyloid beta burden in cognitively healthy individuals	Schreiner | Kirchner | Van Bergen | Gietl | Buck | Hock | Prüssmann | Henning | Unschuld	**Unschuld, Paul**
38	Amyloid PET scan reader agreement in IDEAS: expert readers vs local clinician readers	Windon | Siegel | Zeltzer | Hanna | Carrillo | Hillner, | Iaccarino | La Joie | March | Perez | Mundada | Arora | Buckley | Bullich | Sherwin | Gatsonis | Rabinovici	**Windon, Charles**
39	Validation of a novel visual read interpretation of flortaucipir PET for identification of participants with high tau burden: Results from I7E-AV-A26 reader study	Tunali | Iaccarino | Wang | Arora | Lu | Shcherbinin | Pontecorvo	**Tunali, Ilke**
40	Longitudinal multicenter head-to-head harmonization of tau-PET	Lussier | Silva do Amaral | Povala | Negrini | Pascual | Gordon | Lowe | Oh | Soleimani-	**Lussier, Firoza**

	tracers: an overview of the HEAD study	Meigooni | Klunk | Tudorascu | Rosa-Neto | Baker | Pascoal	
41	Clinical phenotype and plasma biomarker associations of non-Alzheimer's hippocampal atrophy	Asken | Wang | McFarland | Barker | Adjouadi | Velez Uribe | Rosselli | Crocco | Armstrong | Curiel Cid | Vaillancourt | Loewenstein | Duara | Smith	**Asken, Breton**
42	Synaptic loss in relapsing and progressive multiple sclerosis: an in vivo exploratory study using SV2A-PET	Soleimani-Meigooni | Giorgio | Abdelhak | Cordano | Chen | Toueg | Weimer | Zinnhardt | Baker | Janabi | Green | Jagust | Rabinovici	**Soleimani-Meigooni, David**
43	[18F]-PI-2620 tau PET signal across the aging and Alzheimer's disease clinical spectrum	Young | Vossler | Romero | Smith | Park | Trelle | Winer | Wilson | Zeineh | Sha | Khalighi | Morales | Anders | Zaharchuk | Henderson | Andreasson | Wagner | Poston | Davidzon | Mormino	**Young, Christina**
44	Amyloid-induced hyperconnectivity drives tau spreading across connected brain regions in Alzheimer's disease	Roemer | Wagner | Steward | Biel | Dewenter | Dennecke | Gross | Zhu | Zheng | Dehsarvi | Dichgans | Ewers | Brendel | Franzmeier	**Roemer, Sebastian Niclas**
45	A visual-read algorithm for tau pathology using [18F]RO948	Smith | Garibotto | Hägerström | Jögi | Ohlsson | Tonietto | Janelidze | Stomrud | Klein | Hansson	**Smith, Ruben**
46	Establishing the interchangeability between CSF and PET for identifying patients with Alzheimer's disease pathology who are suitable for amyloid targeting therapies	Burnham | K Arora | Iaccarino | Kennedy | Kotari | Wijayawardana | Lu | Pontecorvo | Quevenco | Dell' Agnello | Neff | Petronzi | Viollet | Wang	**Burnham, Samantha**
47	Exploring A-T+ within the AT(N) framework	Lopresti | Cohen | Gogola | Ikonomovic | Snitz | Mason | Minhas | Matan | McGeown | Cieply | Chiang | Pascoal | Reese | Matela | Karikari | Sweet | Berman | Kofler | Lopez | Villemagne	**Lopresti, Brian**
48	Sex-specific synergistic interaction between Aβ and p-tau predicts faster tangle accumulation in females	Wang | Therriault | Servaes | Tissot | Rahmouni | Macedo | Fernandez-Arias | Mathotaarachchi | Benedet | Stevenson | Ashton | Lussier | Pascoal | Zetterberg | Rajah | Blennow | Gauthier | Rosa-Neto	**Wang, Yi-Ting**
49	Comparison of visual interpretation and quantitation in detecting amyloid pathology using florbetapir F-18 PET imaging: Results from nuclear medicine physicians or radiologists practicing at community healthcare settings	Wang | Lu | Iaccarino | Arora | Morris | Kim | Kennedy | Kotari | Burnham | collins | Pontecorvo	**Wang, Jian**
50	Parental history of memory impairment predicts β-amyloid burden and positivity in a preclinical population	Seto | Hohman | Mormino | Papp | Amariglio | Rentz | Johnson | Schultz | Sperling | Buckley | Yang	**Seto, Mabel**
51	A head-to-head comparison between plasma p-tau217 and tau-PET for predicting future cognitive decline among cognitively unimpaired individuals	Ossenkoppele | Salvado | Pichet-Binette | Therriault | Jonaitis | Bourgeat | Doré | Masters | Johnson | Villeneuve | Rosa-Neto | Rowe | Hansson	**Ossenkoppele, Rik**

52	Comparison of amyloid PET and plasma biomarkers in predicting future memory decline among cognitively normal individuals	Bilgel | An | Walker | Moghekar | Ashton | Kac | Karikari | Blennow | Zetterberg | Thambisetty | Resnick	**Bilgel, Murat**
53	Confocal microscopy assessment of flortaucipir binding by a fluorescence analog compound T726 shows 4RT overlap in frontotemporal lobar degeneration	Gatto | Youssef | Reichard | Whitwell | Josephs	**Gatto, Rodolfo**
54	Correlative histopathological evaluation of basal ganglia iron deposition and tau and PiB positron emission tomography in Alzheimer's disease and frontotemporal lobar degeneration	Gatto | Carlos | Reichard | Lowe | Whitwell | Josephs	**Gatto, Rodolfo**
55	Unraveling Alzheimer's disease heterogeneity: a comparative analysis using hydra and chimera	An | Sotiras | Gordon	**An, Zhaoqi**
56	Prevalence of Alzheimer's disease pathology in studies of memory and aging	McKay | Millar | Barthelémy | Benzinger | Morris | Bateman | Schindler | Gordon	**McKay, Nicole**
57	Depression in amyloid-positive individuals is associated with a faster rate of tau accumulation on longitudinal positron-emission tomography	Talmasov | Johnson | Lao | Marder | Miller	**Talmasov, Daniel**
58	Chronic neuroinflammation in older adults with persistent Long COVID: the preliminary findings of [18F]FEPPA PET imaging	Kim | Taboada | Liu | Maciarz | Armstrong | Palekar | Weisenbach	**Kim, Min-Jeong**
59	PET staging of tauopathy using amygdala	Hanseeuw | Rubinstein | Schultz | Buckley | Properzi | Farrell | Gatchel | Amariglio | Beiser | Seshadri | Marshall | Sperling | Jacobs | Johnson	**Hanseeuw, Bernard**
60	Discovery and optimization of [18F]ACI-15916, a promising PET tracer for the diagnosis of Parkinson's disease and other a-synucleinopathies	Vokali | Molette | Ravache | Delgado | Kocher | Pittet | Vallet | Luthi-Carter | Pfeifer | Kosco-Vilbois | Capotosti	**Vokali, Efthymia**
61	Clinical relevance of visually positive amyloid-PET burden in the occipital lobe	Collij | Smith | Palmqvist | Strandberg | Ossenkoppele | Hansson	**Collij, Lyduine**
62	Tau-PET subtypes show distinct profiles of cerebrospinal fluid biomarkers, neurodegeneration, and cognition in a large single-site cohort	Collij | Mastenbroek | Pichet Binette | Smith | Palmqvist | Mattsson-Carlgren | Strandberg | Ossenkoppele | Vogel | Hansson	**Collij, Lyduine**
63	ER176 neuroinflammatory PET profiles and relationships with flortaucipir tau PET in progressive apraxia of speech	Satoh | Utianski | Duffy | Clark | Botha | Lowe | Josephs | Whitwell	**Satoh, Ryota**
64	Aβ and tau associations with sex and affected parent's sex in preclinical Alzheimer's disease	Ourry | St-Onge | Mohammediyan | Yakoub | Soucy | Poirier | Breitner | Villeneuve	**Ourry, Valentin**

65	Differential association between plasma biomarkers and established biomarkers of Alzheimer's disease	Bluma | Chiotis | Bucci | Savitcheva | Matton | Kivipelto | Jeromin | De Santis | Di Molfetta | Ashton | Blennow | Zetterberg | Nordberg	**Bluma, Marina**
66	PiB PET demonstrates early, elevated amyloid striatal binding compared to florbetapir in Down syndrome	McLachlan | Rouanet | Garimella | Price | Tudorascu | Laymon | Keator | Kreisl | Klunk | Handen | Fryer | Zaman | Head | Mapstone | Bettcher | LeMerise | McVea | DiFillipo | Zammit | Hartley | Christian | Investigators	**McLachlan, Max**
67	Data-driven disease progression modelling consistently reveals an occipital amyloid-β subtype in two independent cohorts	Mastenbroek | Collij | Young | Vogel | Salvadó | den Braber | Visser | Gispert | van der Flier | Strandberg | Smith | Palmqvist | Mattson-Carlgren | Oxtoby | Barkhof | Ossenkoppele | Hansson	**Mastenbroek, Sophie**
68	Mid-life perceived discrimination and late-life Alzheimer's disease pathology and cognition in African American and non-Hispanic White populations	Royse | Snitz | Saeed | Reese | Lopresti | Karikari | Kamboh | Villemagne | Reis | Lopez | Cohen	**Royse, Sarah**
69	Comparison of amyloid positivity and global cortical SUVR between black and white non-Hispanic participants in the GAP Bio-Hermes study	Wolz | Hughes | Manber | Mohs | Dwyer | Beauregard	**Wolz, Robin**
70	APOE, ABCA7, and KIF13B associations with earlier onset of amyloid positivity from over 4000 harmonized Positron Emission Tomography images	Castellano | Wang | Archer | Cody | Harrison | Wu | Durant | Janve | Engelman | Jagust | Albert | Johnson | Resnick | Sperling | Bigel | Saykin | Vardarajan | Mayeux | Betthauser | Dumitrescu | Mormino | Mormino | Hohman | Koran	**Castellano, Tonnar**
71	Neuroinflammation in patients with mild cognitive impairment and Alzheimer's Disease	Kandimalla | Lee | Min | Botha | Graff-Radford | Jones | Vemuri | Kantarci | Knopman | Jack | Petersen | Lowe	**Kandimalla, Mahathi**
73	Elevated amyloid-ß and tau burden is associated with accelerated cognitive decline on a digital clock drawing test in preclinical AD	Fu | Robinson | Rodriguez Alonso | Francis Malave | Jutten | Del Carmen Montenegro | Thibault | Penney | Davis | Sperling | Johnson | Price | Rentz	**Fu, Jessie Fanglu**
74	Significance of a positive tau PET scan with a negative amyloid PET scan	Robinson | Lee | Min | Przybelski | Josephs | Jones | Graff-Radford | Boeve | Knopman | Jack. Jr. | Petersen | Machulda | Fields | Lowe	**Robinson, Carling**
75	Lower locus coeruleus function in associated with greater cognitive variability in preclinical Alzheimer's disease	Juneau | Baillet | Wiklund | Riphagen | Prokopiou | Papp | Jutten | Rentz | Sperling | Johnson | Jacobs	**Juneau, Truley**
76	Associations between regional tau pathology and cognitive decline across the AD continuum differ by sex	Singleton | Mattsson-Carlgren | Pichet Binette | Stomrud | Strandberg | Ossenkoppele | Hansson	**Singleton, Ellen**
77	Dynamic brain states are associated with Alzheimer's pathology and cognition	Adams | Kark | Chappel-Farley | Escalante | Stith | Rapp | Yassa	**Adams, Jenna**
78	Imaging synaptic density across the Alzheimer's disease continuum with [18]F-SynVestT-1	Giorgio | Soleimani-Meigooni | Chen | Toueg | Weimer | Zinnhardt | Baker | Janabi | Rabinovici | Jagust	**Giorgio, Joseph**

79	Data-driven analysis of 10,361 amyloid-PET scans from the IDEAS study reveals two primary axes of variation	Giorgio | Mundada | Blazhenets | Mejia Perez | Schonhaut | Carrillo | Hanna | Gatsonis | March | Apgar | Siegel | Hillner | Whitmer | Jagust | Rabinovici | La Joie	**Giorgio, Joseph**
80	Lower locus coeruleus structural integrity is associated with greater intraindividual cognitive variability in older individuals	Wiklund | Van Egroo | Juneau | Riphagen | Papp | Jutten | Rentz | Sperling | Johnson | Jacobs	**Wiklund, Emma**
81	Precuneus fMRI activity is associated with future Aβ burden in cognitively normal older APOE4 carriers	Maass | Molley | Binette | Vockert | Marquardt | Kreissl | Remz | Rajah | Villeneuve	**Maass, Anne**
82	PI-2620 binding in cognitively normal older adults including SuperAgers	Maass | Garcia-Garcia | Molley | Behrenbruch | Schuhmann-Werner | Vockert | Rullmann | Hochkeppler | Fischer | Svenja Schwarck | Baldauf | Schulze | Stephens | Patt | Barthel | Sabri | Duezel | Kreissl	**Maass, Anne**
83	Early phase amyloid PET as a surrogate marker of brain metabolism in cases of cognitive impairment	Aye | Melzer | Keenan | Croucher | Tippett | Anderson | Le Heron	**Aye, William**
84	Unlocking tau PET accessibility: a machine learning-based prediction of tau pathology from plasma, MRI and clinical variables	Karlsson | Vogel | Strandberg | Arvidsson | Åström | Seidlitz | Bethlehem | Stomrud | Ossenkoppele | Ashton | Blennow | Palmqvist | Smith | Janelidze | Pichet Binette | Mattson-Carlgren | Hansson	**Karlsson, Linda**
85	Amyloid and tau burden relate to longitudinal changes in performance of everyday activities as measured using the performance-based Harvard Automated Phone Task	Dubbelman | Diez Palacio | Gonzalez | Amariglio | Becker | Chhatwal | Gatchel | Johnson | Locascio | Udeogu | Wang | Papp | Properzi | Rentz | Schultz | Sperling | Vannini | Marshall	**Dubbelman, Mark**
86	In vivo structural integrity of the hypothalamus and the spatiotemporal evolution of Alzheimer's disease	Baillet | Betthauser | Salmon | Jacobs	**Baillet, Marion**
87	Cross-sectional comparison of extra-cerebral binding trends in [F-18]MK6240 PET images	McVea | DiFilippo | McLachlan | Betcher | Johnson | Betthauser | Christian	**McVea, Andrew**
88	Tau accumulation in Down Syndrome after onset of amyloid positivity	McVea | DiFilippo | Max McLachlan | Betcher | Zammit | Betthauser | Converse | Murali | Stone | Hartley | Johnson | Tudorascu | Laymon | Cohen | Minhas | Mathis | Ances | Zaman | Klunk | Handen | Christian | Investigators	**McVea, Andrew**
89	Greater locus coeruleus activity and locus coeruleus-amygdala hypoconnectivity during high arousal conditions are related to elevated concentrations of plasma p-tau231 in older individuals	Prokopiou | Van Egroo | Riphagen | Ashton | Janelidze | Sperling | Johnson | Blennow | Hansson | Zetterberg | Jacobs	**Prokopiou, Prokopis**
90	Establishing tau-PET cut-points for cognitive diagnosis with [F-18]PI-2620	Tennant | Wheeler | Lee | Terner | Raman | Rissman | Christian | Petersen | Lee | Cohen | Ances | Zhou | Zhang | Nandy | Yaffe | O'Bryant | Braskie	**Tennant, Victoria**

91	Plasma ADRD biomarkers predict longitudinal declines in intra-network functional brain connectivity	Dark | Shafer | Cordon | An | Lewis | Moghekar | Landman | Resnick | Walker	**Dark, Heather**
92	The role of frontoparietal control network and default mode network functional connectivity in cognitive resilience in preclinical Alzheimer's disease	Boyle | Shirzadi | Coughlan | Seto | Properzi | Klinger | Yuan | Scanlon | Jutten | Papp | Amariglio | Rentz | Chhatwal | Buckley | Sperling | Schultz	**Boyle, Rory**
93	Disrupted sleep and 24-hour rhythms are associated with 18F-PI-26260 tau PET in aging and neurodegenerative disease	Winer | Romero | Vossler | Young | Smith | Anders | Pacheco Morales | Davidzon | Henderson | Poston | Zeitzer | Mormino	**Winer, Joseph**
94	Cortical and substantia nigra 18F-PI-2620 tau PET are associated with cognitive and motor impairment in Lewy body disease	Winer | Vossler | Young | Romero | Smith | Shahid | Abdelnour | Wilson | Anders | Pacheco Morales | Davidzon | Mormino | Poston	**Winer, Joseph**
95	Predictability of amyloid-PET status with plasma phospho-Tau217 in adults with Down syndrome	Bettcher | Janelidze | McLachlan | Zammit | McVea | DiFilippo | Betthauser | Laymon | Tudorascu | Cohen | Garimella | Price | Keator | Brickman | Lao | Klunk | Rosas | Zaman | Hartley | Head | Mapstone | Krinsky-McHale | Johnson | Lai | Ances | Handen | Hansson | Christian | Alzheimer Biomarkers Consortium – Down Syndrome	**Bettcher, Brecca**
96	Locus coeruleus metabolism relates to Alzheimer's disease pathology in amyloid-positive symptomatic individuals	Koops | Dutta | Becker | van Egroo | Hanseeuw | Sperling | Johnson | Jacobs	**Koops, Elouise**
97	Correlating in vivo amyloid beta centiloid values with neuropathological burden: Insights from Down syndrome and Alzheimer's disease cohorts	Liou | Ikonomovic | Handen | Christian | Mapstone | Head | Tudorascu | Brickman | Price | Laymon | Rosas | Zaman | Hartley | Lai | Kofler | Ibrahim | Villemagne | Cohen	**Liou, Jr-Jiun**
98	Visualization of endogenously generated Dutch-type Abeta oligomers that dysregulate presynaptic neurotransmission in the absence of detectable inflammation	Gandy | Castranio | Varghese | Argyrousi | Tripathi | Glabe | Levy | Wang | Zhang | Lubell | Guerin | Rahimipour | Dickstein | Arancio | Ehrlich	**Gandy, Sam**
99	[18F]PI-2620 tau-PET binding patterns in American football players with suspected Chronic Traumatic Encephalopathy	Mejia Perez | Mosaheb | Schonhaut | Blazhenets | McKee | Stein | Farris | Mez | Stephens | Mueller | Keegan | La Joie | Rabinovici | Alosco	**Mejia Perez, Jhony**
100	Regional amyloid-β burden in Lewy Body Disease	Vossler | Abdelnour | Young | Winer | Smith | Smith | Shahid | Wilson | Davidzon | Mormino | Poston	**Vossler, Hillary**
101	Pathology-weighted connectivity with medial parietal lobe drives neocortical tau accumulation	Ziontz | Fonseca | Giorgio | Harrison | Jagust	**Ziontz, Jacob**
102	18F-MK-6240 Tau PET visual read algorithm for Alzheimer's disease: diagnostic accuracy and comparison with automated-quantitative Braak stage analysis	Provost | Soucy | Haeger | Macedo | Rahmouni | Stevenson | Servaes | Therriault | Arias | Rosa-Neto	**Provost, Karine**

103	Evaluating CenTauRz harmonization of matched FTP and MK6240 tau PET images: the HEAD Study	Minhas | Delbene | Luo | Reese | Gogola | Villemagne | Dore | Lopresti | Laymon | Lussier | Bauer-Negrini | Povala | Cohen | Crainiceanu | Pascual | Gordon | Lowe | Oh | Soleimani-Meigooni | Klunk | Rosa-Neto | Baker | Pascoal | Tudorascu	**Minhas, Davneet**
104	Characterizing the relationship between the functional connectome and tau PET in preclinical Alzheimer's disease	Abuwarda | Trainer | Ju | Constable | Fredericks	**Abuwarda, Hamid**
105	Estimating time-to-tau as a function of Aβ pathology in Alzheimer's disease using [18F]MK6240 and [18F]NAV4694 PET	Budd Haeberlein | Leuzy | Mathotaarachchi | Insel | Schöll | Moscoso | Villemagne | Doré | Rowe	**Budd Haeberlein, Samantha**
106	Neuroinflammation potentiates the effect of amyloid-β on longitudinal tau accumulation	Rahmouni | Wang | Therriault | Servaes | Tissot | Macedo | Arias-Fernandez | Kunach | Stevenson | Hosseini | Hall | Trudel | Jia | Gauthier | Zimmer | Benedet | Pascoal | Rosa-Neto	**Rahmouni, Nesrine**
107	Association between plasma pTau epitopes and synaptic density measured with [C-11]UCB-J PET	Yang | DiFilippo | Ma | Wilson | Thor | Pasquesi | Barnhart | Engle | Betthauser | Ashton | Johnson | Christian | Zetterberg | Bendlin	**Yang, Kao Lee**
108	"Treatment Related Amyloid Clearance" (TRAC): a framework to characterize a new biomarker state in the era of anti-amyloid therapies	La Joie | Sexton | Cummings | Galasko | Ikonomovic | Landau | Llibre-Guerra | Mummery | Ossenkoppele | Price | Risacher | Smith | Van Dyck | Carrillo	**La Joie, Renaud**
109	Alzheimer's disease biological PET staging using plasma p217+tau	Feizpour | Doré | Krishnadas | Bourgeat | Doecke | Saad | Triana-Baltzer | Laws | Shishegar | Huang | Fowler | Ward | Masters | Fripp | Kolb | Villemagne | Rowe	**Rowe, Christopher**
110	Plasma p-tau217 outperforms [18F]FDG-PET in identifying biological Alzheimer's disease in atypical and early-onset dementia	Quispialaya | Joseph Therriault | Aliaga | Benedet | Ashton | Karikari | Macedo | Rahmouni | Stevenson | Tissot | Arias | Wang | Hosseini | Jean-Claude | Pascoal | Gauthier | Gilfix | Vitali | Soucy | Zetterberg | Blennow | Zimmer | Rosa-Neto	**Quispialaya, Kely**
111	A-T+ PET participants in preclinical AD: clinical progression and concordance with fluid biomarkers	Yakoub | St-Onge | Fajardo | Mohammediyan | Dery | Sylvain | Tremblay-Mercier | Remz | Gonneaud | Vogel | Soucy | Pichet-Binette | Villleneuve | Research Group	**Yakoub, Yara**
112	Neighborhood disadvantage and the association between imaging biomarkers of Alzheimer's disease and cognition in a cohort of diverse older adults	Fan | Royse | Snitz | Reese | Karikari | Pascoal | Shaaban | Roush | Potopenko | Cisneros | Kotulsky | Kamboh | Lopresti | Villemagne | Lopez | Becker | Cohen	**Fan, Erica**
113	Longitudinal association of mid-life ten year cardiovascular disease risk score with blood biomarkers of Alzheimer's disease and neurodegeneration: Heart SCORE Brain Study	Saeed | Chang | Swanson | Villemagne | Snitz | Royse | Lopresti | Kip | Reese | Gogola | Pascoal | Kamboh | Blennow | Zetterberg | Karikari | Lopez | Reis | Cohen	**Saeed, Anum**
114	Comparison of FDG-PET in individuals with down syndrome and dominantly inherited Alzheimer's	Abdelmoity | Wisch | Gordon | Flores | Roman | Handen | Christian | Head | Mapstone | Hartley | Rafii | Lee | Krinsky-McHale | Lai | Rosas |	**Abdelmoity, Omar**

	disease: genetic forms with elevated production of amyloid	Zaman | Schmitt | Ptomey | Bateman | Benzinger | Ances	
115	Deep learning-based partial volume correction for tau PET imaging	Gong | Lois | Thibault | Tiss | Jang | Becker | Price | El Fakhri | Johnson	**Gong, Kuang**
116	Plasma levels of an N-terminal tau fragment predict core AD and neurodegenerative biomarkers in autosomal dominant Alzheimer's disease	Schultz | Liu | Ostaszewski | Anderson | Karch | Cruchaga | Gordon | Benzinger | Hassenstab | Morris | Perrin | Goate | Allegri | Barthelemy | Berman | Chui | Farlow | Fox | Day | Jucker | Jack | Koeppe | Lee | Levey | Levin | Martins | Mori | Noble | Rosa-Neto | Salloway | Sanchez | Schofield | McDade | Sperling | Selkoe | Bateman | Chhatwal	**Schultz, Stephanie**
117	Increased CSF GAP-43 is associated with accelerated tau accumulation and spread in Alzheimer's disease	Franzmeier | Dehsarvi | Steward | Biel | Dewenter | Römer | Wagner | Brendel | Ewers | Moscoso | Blennow | Zetterberg | Schöll	**Franzmeier, Nicolai**
118	Investigating the impacts of tau status in Alzheimer's disease by using [18F]Florzolotau tau cutoff	Huang | Lin | Huang | Hsu | Chang | Huang | Hsiao	**Huang, Shao-Yi**
119	Study of reference regions in the quantitation of [18F]Florzolotau tau PET imaging	Huang | Lin | Lin | Huang | Hsu | Chang | Huang | Hsiao	**Lin, Jyh-Ruei**
120	Assessing the efficacy of BETTH-derived tau thresholds to predict cognitive decline	Gogola | Lopresti | Snitz | Tudorascu | Minhas | Dore | Ikonomovic | Shaaban | Kofler | Matan | Bourgeat | Mason | Rowe | Aizenstein | Mathis | Klunk | Lopez | Cohen | Villemagne	**Gogola, Alexandra**
121	Assessing the correlations between imaging and plasma biomarkers within the AT(N) framework	Gogola | Cohen | Zeng | Lopresti | Snitz | Tudorascu | Minhas | Ikonomovic | Pascoal | Kofler | Matan | Mason | Aizenstein | Mathis | Klunk | Zetterberg | Blennow | Lopez | Villemagne | Karikari	**Gogola, Alexandra**
122	The effect of microglial activation on brain atrophy across the Alzheimer's disease continuum	Povala | Bellaver | Lukasewicz Ferreira | Ferrari-Souza | Schaffer Aguzzoli | Teixeira Leffa | Zalzale | Soares | Lussier | Negrini | Rohden | Benedet | Stevenson | Rahmouni | Tissot | Therriault | Servaes | Cohen | Klunk | Villemagne | Zatt | R Zimmer | Karikari | Rosa-Neto | A Pascoal	**Povala, Guilherme**
123	Disentangling the relationships between tau-PET, amyloid-β-PET, hippocampal subfield volumes, and memory: a longitudinal study	Aumont | Bedard | Bussy | Fernandez Arias | Therriault | Rahmouni | Stevenson | Tissot | Servaes | C. Macedo | Gauthier | M. Chakravarty | Rosa-Neto	**Aumont, Etienne**
124	Tau-PET Overlap Index; associations with Braak Stage and quantitative NFT measurements	Lee | Min | Moloney | Mester | Lund | Ghatamaneni | Senjem | Nguyen | Graff-Radford | Schwarz | Gunter | Kantarci | Boeve | Vemuri | Jones | Knopman | Jack | Petersen | Murray | Lowe	**Lowe, Val**
125	Tau-PET spatial extent for predicting cognitive decline within tau-positive individuals	Coomans | van Tol | Groot | van der Flier | Pijnenburg | van de Giessen | Ossenkoppele	**Coomans, Emma**
126	Association of sex and cerebral beta-amyloid with cortical gray matter brain age in cognitively impaired older adults	Li | Son | Chen | Wang | Aizenstein | Hong | Roh | Cho | Hong | Nam | Park | Kim | Lee | Choi | Moon | Seo | Choi | Kim | Wu	**Li, Jinghang**

127	Will cerebral glucose metabolism measured using [18F]FDG PET substitute tau PET in clinical studies?	Edison	**Edison, Paul**
128	CSF sTREM2 is associated with neuroprotective microglial states early in Alzheimer's disease and deleterious effects later in the disease trajectory	Edison	**Edison, Paul**
129	The Mobile Toolbox for assessing cognition remotely: associations with amyloid and tau deposition in cognitively unimpaired older adults	Jutten | Burling | Fu | Properzi | Amariglio | Papp | Marshall | Price | Johnson | Sperling | Rentz	**Jutten, Roos**
130	Characterizing multi-site harmonized amyloid and tau PET across the Alzheimer's continuum	Cody | Johns | Carlson | Younes | Young | Mukherjee | Trittschuh | Gibbons | Dumitrescu | Archer | Durant | Nakano | Klinedinst | Choi | Lee | Scollard | Mez | Saykin | Crane | Cuccaro | Toga | Tosun | Hohman | Mormino	**Cody, Karly**
131	Characterization of tau PET accumulation relative to duration of entorhinal tau positivity	Cody | Langhough | Heston | Teague | Christian | Johnson | Betthauser	**Cody, Karly**
132	Harmonization of multi-scanner PET data with ComBat: application to 18F-AV1451 data acquired on a Siemens ECAT HR+ PET and a GE Discovery MI PET/CT Scanner	Lois Gomez | Diez-Palacio | Price | Johnson	**Lois Gomez, Cristina**
133	Longitudinal white matter degeneration is associated with higher subsequent amyloid load across the Alzheimer's disease continuum	Burton | Blujus | Oh	**Burton, Courtney**
134	Multimodal analysis of tau epicenters in heterogeneous Alzheimer's disease variants	Trainer | Vin | Xu | Chase | O'Dell | Toyonaga | Tun | Li | Ju | Mecca | van Dyck | Fredericks	**Trainer, Anne**
135	A pretrained foundation model for learning representation of regional tau accumulation pattern and its downstream applications	Sohn | Song | Seong	**Sohn, JunYoung**
136	[18F]RO-948 Tau PET retention and correlation with fluid biomarkers in the early AD continuum	Shekari | González Escalante | Milà-Alomà | Falcon | López-Martos | Sánchez-Benavides | Brugulat-Serrat | Niñerola-Baizán | J. Ashton | K. Karikari | Lantero-Rodriguez | Snellman | Ortiz | Tonietto | Borroni | Klein | Minguillón | Fauria | Perissinotti | Molinuevo | Zetterberg | Blennow | Grau-Rivera | Suárez-Calvet | Gispert	**Shekari, Mahnaz**
137	Baseline plasma GFAP predicts longitudinal tau-PET uptake in Braak staging continuum	Jia | Rahmouni | Tissot | Servaes | Therriault | Cassa Macedo | Fernandez-Arias | Wang | Lussier | Kunach | Gauthier | Benedet | Ashton | Zetterberg | Pascoal | Blennow | Rosa-Neto	**Jia, Wan Lu**
138	Plasma NfL correlates to grey matter and white matter atrophy ambivalent to amyloid status in older adults	Hall | Rahmouni | Macedo | Servaes | Therriault | Fernandez-Arias | Trudel | Stevenson | Gauthier | Sanjeewa | Lussier | Pascoal | Benedet | Ashton | Zetterberg | Blennow | Rosa-Neto	**Hall, Brandon**

139	Astrocyte reactivity influences cognitive decline in individuals across the Alzheimer's disease continuum	Bellaver | Povala | Ferreira | Bauer-Negrini | Lussier | Leffa | Ferrari-Souza | Zalzale | Soares | Rohden | Aguzzoli | Abbas | Benedet | Ashton | Tissot | Therriault | Servaes | Stevenson | Rahmouni | Hong | Rho | Karim | Zimmer | Zetterberg | Blennow | Villemagne | Klunk | Lopez | Tudorascu | Slachevsky | Rosa-Neto | Cohen | Karikari | Son | Pascoal	**Bellaver, Bruna**
140	Elevated Plasma Ptau-181 is associated with congestive heart failure	Tanner | Wiedner | Himali | Ramos-Cejudo | Beiser | Seshadri | Javier Aparicio | Himali	**Tanner, Jeremy**
141	Regional cell-type proportions are associated with AD pathological changes	Kang | Ottoy | Soucy | Massarweh | Black | Rosa-Neto | Goubran	**Kang, Min Su**
142	Quantitative Gradient Recalled Echo (qGRE) MRI detects neuronal loss and iron accumulation in nucleus basalis of Meynert in preclinical and mild Alzheimer's disease	Kothapalli | Milchenko | Benzinger | Goyal | Eldeniz | Marcus | Morris | Yablonskiy | Raichle	**Kothapalli, Satya VVN**
143	Head-to-head analysis of [18F]MK6240 and [18F]Flortaucipir standardized update values (SUVs): the HEAD Study	Tsai | Tissot | Tudorascu | Rosa-Neto | Gordon | Pascual | Lowe | Soleimani-Meigooni | Oh | Klunk | Jagust | Pascoal | Baker	**Tsai, Hsin-Yeh**
144	Association between oxygen extraction fraction, tau, and amyloid pathology, and cognitive status in Alzheimer's disease: implications for advanced neuroimaging techniques	Hosseini | Servaes | Therriault | Tissot | Rahmouni | Macedo | Lussier | Stevenson | Wang | Fernandez-Arias | Socualaya | Aumont | Stevenson | Gauthier | Cho | Zhuang | Wang | Rudko | Pascoal | Rosa-Neto	**Hosseini, Seyyed Ali**
145	Association of plasma pTau epitopes with mesial temporal lobe cortical thinning	Trudel | Rahmouni | Macedo | Therriault | Servaes | Wang | Fernandez-Arias | Hall | Stevenson | Sanjeewa | Gauthier | Benedet | Ashton | Zetterberg | Blennow | Lussier | Tharick | Karikari | Rosa-Neto	**Trudel, Lydia**
146	Specific tau networks are associated with different cognitive domains in the elderly	Nayak | Hojjati | Ozoria-Blake | Razlighi	**Nayak, Siddharth**

HAI 2024 PROGRAM

Wednesday, January 17, 2024		
07:30 am – 08:15 am	Check-in	
07:30 am – 08:15 am	Breakfast	
08:15 am – 08:25 am	Welcome Notes	Keith Johnson, Massachusetts General Hospital
08:25 am – 08:30 am	Alzheimer's Association ISTAART Intro	Maria Carillo, Alzheimer's Association
08:30 am – 09:35 am	**SESSION I: Tracer Discovery and Biomarker Optimization**	**Julie Price, Massachusetts General Hospital, Boston, MA, United States** **Sandra Sanabria Bohorquez, Genentech, South San Francisco, CA, United States**
08:30	Intro	Chairs
08:35	Discovery and preclinical development of [18F]ACI-19626, a first-in-class TDP-43 PET tracer	**Efthymia Vokali**, AC Immune SA, EPFL Innovation Park, Building B, 1015, Lausanne, Switzerland
08:50	Bridging the gap between SUVR and DVR for [18F]MK6240 by correcting for tracer clearance in tissue: a simulation study	**Praveen Honhar**, Yale PET Center, Radiology and Biomedical Imaging, Yale University, New Haven, CT, United States
09:05	PET Spatial extent as a sensitive beta-amyloid biomarker in preclinical Alzheimer's disease	**Michelle E. Farrell**, Massachusetts General Hospital, Harvard Medical School, Boston, MA, United States
09:20	Optimizing the detection of whole-brain tau-related cognitive decline in mild cognitive impairment	**Sylvia Villeneuve**, Department of Psychiatry, Faculty of medicine, McGill University, Montreal, QC, Canada
09:35 am – 10:00 am	**Keynote: Targets and radioligands for PET imaging of neuroinflammation**	**Paolo Zanotti-Fregonara, NIH, Bethesda, MD, United States**
10:00 am – 10:25 am	Discussion	
10:25 am – 10:55 am	**Break/Poster Session Break/Poster Session**	

Wednesday, January 17, 2024		
01	Longitudinal synaptic loss follows tau PET Braak staging in vivo and supports local neurodegeneration by tau accumulation in stages III-VI	**Greet Vanderlinden**, Nuclear Medicine and Molecular Imaging, Imaging Pathology, KU Leuven, Leuven, Belgium
02	Plasma Aβ42/40 ratio, GFAP, and NfL across the neurodegenerative diseases: cross-sectional and longitudinal study in a large multi-center cohort	**Hyemin Jang**, Samsung medical center, Seoul, South Korea
03	Publicly Available Software and FTP calibration data for CenTauR tau PET standardization	**Christopher Schwarz**, Mayo Clinic, Rochester, MN, US
04	The impact of metabolic health on the relationship of obesity with and Alzheimer's and vascular markers	**Eun Hye Lee**, Department of Neurology, Samsung Medical Center, Sungkyunkwan University School of Medicine, Seoul, South Korea
05	Distinct effects of cholesterol profile components on amyloid and vascular burdens	**Sung Hoon Kang**, Department of Neurology, Korea University Guro Hospital, Korea University College of Medicine, Seoul, South Korea
06	Amyloid pet positivity in Korean Dementia syndromes: in relation to diagnosis, age, and Apoe genotypes	**Min Young Chun**, Department of Neurology, Samsung Medical Center, Sungkyunkwan University School of Medicine, Seoul, South Korea
07	Toward more representative estimates of the effect of tau on cognition	**C. Elizabeth Shaaban**, University of Pittsburgh, Pittsburgh, PA, US
08	Examination of synaptic density and neurofibrillary tau tangle burden in cognitively unimpaired and impaired older adults	**Alexandra DiFilippo**, University of Wisconsin-Madison Waisman Center, Madison, WI, US
09	Association between plasma P-tau and cognition in the Alzheimer's disease spectrum	**Jaime Fernandez**, Translational Neuroimaging Laboratory, McGill Research Centre for Studies in Aging, Montreal, QC, CA
10	The role of biofluid markers in predicting near-term cognitive impairment	**Sylvia Villeneuve**, McGill University, Montreal, QC, CA
11	Factors explaining tau onset age and time from tau onset to dementia	**Margo Heston**, Center for Health Disparities Research, University of Wisconsin School of Medicine and Public Health, Madison, WI, US

Wednesday, January 17, 2024		
12	Evaluation of ComBat as a harmonization technique for reducing across-tracer variance in regional amyloid PET analyses	**Braden Yang**, Mallinckrodt Institute of Radiology, Washington University in St. Louis, St. Louis, MO, US
13	Neurophysiological changes related to amyloid and tau pathology are associated with longitudinal cognition and MCI progression	**Jonathan Gallego Rudolf**, Douglas Mental Health University Institute, Montreal, QC, CA
14	Tau and Amyloid associations with sustained attention and episodic memory performance in clinically unimpaired older adults	**America Romero**, Department of Neurology and Neurological Sciences, Stanford University School of Medicine, Stanford, CA, US
15	Sex differences in the relationships between 24-h rest-activity patterns and plasma markers of Alzheimer's disease pathology	**Maxime Van Egroo**, Faculty of Health, Medicine and Life Sciences, School for Mental Health and Neuroscience, Alzheimer Centre Limburg, Maastricht University, Maastricht, The Netherlands
16	NODDI-derived measures of microstructural integrity in medial temporal lobe white matter pathways are associated with Alzheimer's disease pathology	**Dana Parker**, Department of Neurobiology and Behavior, University of California, Irvine, Irvine, CA, US
17	Longitudinal hippocampal volume trajectories and their relationships with β-amyloid, tau, cerebrovascular, and cognition in a baseline cognitively unimpaired sample	**Lianlian Du**, Wisconsin Alzheimer's Institute, University of Wisconsin-Madison School of Medicine and Public Health, Madison, WI, US
18	Beyond quantity: fill states as a biomarker for the degree of pathology and neurodegeneration across the Alzheimer's disease continuum.	**Gerard N Bischof**, Multimodal Imaging Laboratory (MMNI), University of Cologne, Faculty of Medicine and University Hospital Cologne, Department of Nuclear Medicine, Cologne, GERMANY, Cologne, Germany
19	Successful aging reflects anterior cingulate preservation but not tau accumulation rate	**Stefania Pezzoli**, University of California, Berkeley, Berkeley, CA, US
21	Distinct microbial species less abundant in Alzheimer's disease patients associate negatively with cerebrospinal fluid biomarkers of Alzheimer's disease	**Jea Woo Kang**, Wisconsin Alzheimer's Disease Research Center, University of Wisconsin School of Medicine and Public Health, Madison, WI, US

Wednesday, January 17, 2024		
22	Amyloid quantification is dependent on scanner: a head-to-head comparison of 18F-NAV4694 Centiloid measurements between three PET/CT scanners	**Ashley Gillman**, Health and Biosecurity, Commonwealth Scientific and Industrial Research Organisation, Brisbane, Australia
23	Neuroinflammation follows and outstrips tau progression patterns in primary 4R tauopathies	**Maura Malpetti**, University of Cambridge, Cambridge, United Kingdom
24	Relationship between enlarged perivascular space and beta-amyloid deposition among cognitively normal ADNI participants	**Jeongchul Kim**, Deaprtment of Radiology, Wake Forest School of Medicine, Winston Salem, NC, US
25	Examining inter- and intra-subject variability in digital clock drawing test performance in cognitively normal older adults	**Marina Rodríguez Alonso**, Athinoula A. Martinos Center for Biomedical Imaging, Charlestown, MA, US
26	Evaluating bidirectional effects of amyloid and tau on functional brain networks in preclinical Alzheimer's disease	**Peter Millar**, Washington University in St. Louis, St. Louis, MO, US
27	Tau propagates along principal axes of functional and structural brain organization in Alzheimer's disease	**Julie Ottoy**, Sunnybrook Research Institute, University of Toronto, Toronto, ON, Canada
28	X-ray based amyloid index as a quantitative biomarker for neurodegenerative diseases	**Karthika Suresh**, Division of Imaging, Diagnostics, and Software Reliability, Office of Science and Engineering Laboratories, Center for Devices and Radiological Health, Food and Drug Administration, Silver Spring, MD, US
29	An artificial neural network for PET brain amyloid imaging	**Mike Georgiou**, Dept. of Radiology, University of Miami Miller School of Medicine, Miami, FL, US
30	Predicting regional tau burden using structural connectivity from individualized epicenters	**Christopher Brown**, University of Pennsylvania, Philadelphia, PA, US
31	Microglia density across different clinical Alzheimer's disease variants	**Patrick Lao**, Columbia University, New York, NY, US
32	The TSPO circadian pattern: a [11C]ER176 test-retest study	**Quentin Finn**, Nantz National Alzheimer Center, Houston MEthodist Neurological and Research Institute, Houston, TX, US

Wednesday, January 17, 2024		
33	Tau PET signal within the default mode network predicts longitudinal clinical decline in atypical early Alzheimer's disease	**Yuta Katsumi**, Frontotemporal Disorders Unit, Department of Neurology, Massachusetts General Hospital and Harvard Medical School, Boston, MA, US
34	Reduced coupling between cerebrospinal fluid flow and global brain activity is linked to cortical tau and atrophy	**Feng Han**, Helen Wills Neuroscience Institute, University of California, Berkeley, Berkeley, CA, US
35	Cognitive decline and Alzheimer's disease clinical status in Down syndrome are better distinguished by amyloid and neurofibrillary tau compared to age	**Matt Zammit**, University of Wisconsin-Madison, Madison, WI, US
36	Early Aβ and tau-seeded functional networks derived in young adults reflect patterns of tau deposition and accumulation	**Corrina Fonseca**, Helen Wills Neuroscience Institute, University of California, Berkeley, Berkeley, CA, US
37	Gray matter GABA and Glutamate reflect amyloid beta burden in cognitively healthy individuals	**Paul Unschuld**, Institute for Regenerative Medicine, University of Zurich, Zurich, CH
38	Amyloid PET scan reader agreement in IDEAS: expert readers vs local clinician readers	**Charles Windon**, Memory and Aging Center, UCSF Weill Institute for Neurosciences, University of California San Francisco, San Francisco, CA, US
39	Validation of a novel visual read interpretation of flortaucipir PET for identification of participants with high tau burden: results from I7E-AV-A26 reader study	**Ilke Tunali**, Eli Lilly and Company, Indianapolis, IN, US
40	Longitudinal multicenter head-to-head harmonization of tau-PET tracers: an overview of the HEAD study	**Firoza Lussier**, Department of Psychiatry, University of Pittsburgh, Pittsburgh, PA, US
41	Clinical phenotype and plasma biomarker associations of non-Alzheimer's hippocampal atrophy	**Breton Asken**, University of Florida, Gainesville, FL, US
42	Synaptic loss in relapsing and progressive multiple sclerosis: an in vivo exploratory study using SV2A-PET	**David Soleimani-Meigooni**, Memory and Aging Center, Weill Institute of Neurosciences, University of California, San Francisco, San Francisco, CA, US

Wednesday, January 17, 2024		
43	[18F]-PI-2620 tau PET signal across the aging and Alzheimer's Disease clinical spectrum	**Christina Young**, Department of Neurology and Neurological Sciences, Stanford University School of Medicine, Palo Alto, CA, US
44	Amyloid-induced hyperconnectivity drives tau spreading across connected brain regions in Alzheimer's disease	**Sebastian Niclas Roemer**, University Hospital, LMU Munich, Munich, Germany
45	A Visual-read algorithm for tau pathology using [18F]RO948	**Ruben Smith**, Clinical Memory Research Unit, Department of Clinical Sciences, Lund University, Lund, Sweden
46	Establishing the interchangeability between CSF and PET for identifying patients with Alzheimer's disease pathology who are suitable for amyloid targeting therapies	**Samantha C Burnham**, Eli Lilly and Company, Indiana, IN, US
47	Exploring A-T+ within the AT(N) framework	**Brian Lopresti**, Department of Radiology, University of Pittsburgh School of Medicine, Pittsburgh, PA, US
48	Sex-specific synergistic interaction between Aβ and p-tau predicts faster tangle accumulation in females	**Yi-Ting Wang**, Translational Neuroimaging Laboratory, McGill Research Centre for Studies in Aging, Montreal, QC, CA
49	Comparison of visual interpretation and quantitation in detecting amyloid pathology using florbetapir F-18 PET imaging: results from nuclear medicine physicians or radiologists practicing at community healthcare settings	**Jian Wang**, Eli Lilly and Company, Indianapois, IN, US
50	Parental history of memory impairment predicts β-amyloid burden and positivity in a preclinical population	**Mabel Seto**, Harvard Aging Brain Study, Department of Neurology, Massachusetts General Hospital, Boston, MA, US
51	A head-to-head comparison between plasma p-tau217 and tau-PET for predicting future cognitive decline among cognitively unimpaired individuals	**Rik Ossenkoppele**, Clinical Memory Research Unit, Department of Clinical Sciences in Malmö, Lund University, Lund, Sweden., Lund, Sweden
52	Comparison of amyloid PET and plasma biomarkers in predicting future memory decline among cognitively normal individuals	**Murat Bilgel**, Laboratory of Behavioral Neuroscience, National Institute on Aging, Baltimore, MD, US

Wednesday, January 17, 2024		
53	Confocal microscopy assessment of flortaucipir binding by a fluorescence analog compound T726 Shows 4RT overlap in frontotemporal lobar degeneration	**Rodolfo Gatto**, Department of Neurology, Mayo Clinic, Rochester, MN, US
54	Correlative histopathological evaluation of basal ganglia iron deposition and tau and PiB Positron Emission Tomography in Alzheimer's disease and frontotemporal lobar degeneration	**Rodolfo Gatto**, Department of Neurology, Mayo Clinic, Rochester, MN, US
55	Unraveling Alzheimer's disease heterogeneity: a comparative analysis using HYDRA AND CHIMERA	**Zhaoqi An**, Mallinckrodt Institute of Radiology (MIR) at Washington University School of Medicine in St. Louis, St. Louis, MO, US
56	Prevalence of Alzheimer's disease pathology in studies of memory and aging	**Nicole McKay**, Washington University School of Medicine, St. Louis, MO, US
57	Depression in amyloid-positive individuals is associated with a faster rate of tau accumulation on longitudinal positron-emission tomography	**Daniel Talmasov**, Columbia University Medical Center, New York, NY, US
58	Chronic neuroinflammation in older adults with persistent Long COVID: the preliminary findings of [18F]FEPPA PET imaging	**Min-Jeong Kim**, Department of Psychiatry and Behavioral Health, Stony Brook University School of Medicine, Stony Brook, NY, US
59	PET staging of tauopathy using amygdala	**Bernard Hanseeuw**, Mass General Brigham, Boston, MA, US
60	Discovery and optimization of [18F]ACI-15916, a promising PET tracer for the diagnosis of Parkinson's disease and other a-synucleinopathies	**Efthymia Vokali**, AC Immune SA, EPFL Innovation Park, Building B, 1015, Lausanne, CH
61	Clinical relevance of visually positive amyloid-PET burden in the occipital lobe	**Lyduine Collij**, Clinical Memory Research Unit, Clinical Sciences Malmö, Lund University, Lund, Sweden
62	Tau-PET subtypes show distinct profiles of cerebrospinal fluid biomarkers, neurodegeneration, and cognition in a large single-site cohort	**Lyduine Collij**, Clinical Memory Research Unit, Clinical Sciences Malmö, Lund University, Lund, Sweden
63	ER176 neuroinflammatory PET profiles and relationships with flortaucipir tau PET in progressive apraxia of speech	**Ryota Satoh**, Mayo Clinic, Rochester, MN, US

Wednesday, January 17, 2024		
64	Aβ and tau associations with sex and affected parent's sex in preclinical Alzheimer's disease	**Valentin Ourry**, Department of Psychiatry, Faculty of Medicine, McGill University, Montreal, Quebec, Canada., Montreal, QC, CA
65	Differential association between plasma biomarkers and established biomarkers of Alzheimer's disease	**Marina Bluma**, Division of Clinical Geriatrics, Center for Alzheimer Research, Department of Neurobiology, Care Sciences and Society, Karolinska Institutet, Stockholm, Sweden
66	PiB PET demonstrates early, elevated amyloid striatal binding compared to florbetapir in Down syndrome	**Max McLachlan**, University of Wisconsin - Madison, Madison, WI, US
67	Data-driven disease progression modelling consistently reveals an occipital amyloid-β subtype in two independent cohorts	**Sophie Mastenbroek**, Department of Radiology and Nuclear Medicine, Vrije Universiteit Amsterdam, Amsterdam University Medical Center, location VUmc, Amsterdam, the Netherlands., Amsterdam, The Netherlands
68	Mid-life perceived discrimination and late-life Alzheimer's disease pathology and cognition in African American and non-Hispanic White populations	**Sarah Royse**, Department of Radiology, University of Pittsburgh, Pittsburgh, PA, US
69	Comparison of amyloid positivity and global cortical SUVR between black and white non-Hispanic participants in the GAP Bio-Hermes study	**Robin Wolz**, IXICO, London, United Kingdom
70	APOE, ABCA7, and KIF13B associations with earlier onset of amyloid positivity from over 4000 harmonized Positron Emission Tomography images	**Tonnar Castellano**, Vanderbilt Memory and Alzheimer's Center, Department of Neurology, Vanderbilt University Medical Center, Nashville, TN, US
71	Neuroinflammation in patients with mild cognitive impairment and Alzheimer's Disease	**Mahathi Kandimalla**, Department of Radiology, Mayo Clinic, Rochester, MN, US
73	Elevated amyloid-ß and tau burden is associated with accelerated cognitive decline on a digital clock drawing test in preclinical AD	**Jessie Fanglu Fu**, Athinoula A. Martinos Center for Biomedical Imaging, Charlestown, MA, US
74	Significance of a positive tau PET scan with a negative amyloid PET scan	**Carling Robinson**, Department of Radiology, Mayo Clinic, Rochester, MN, US

Wednesday, January 17, 2024		
75	Lower locus coeruleus function in associated with greater cognitive variability in preclinical Alzheimer's disease	**Truley Juneau**, Gordon Center for Medical Imaging, Department of Radiology, Massachusetts General Hospital, Boston, MA, US
76	Associations between regional tau pathology and cognitive decline across the AD continuum differ by sex	**Ellen Singleton**, Clinical Memory Research Unit, Department of Clinical Sciences Malmö, Lund University, Sweden, Lund, Sweden
77	Dynamic brain states are associated with Alzheimer's pathology and cognition	**Jenna Adams**, Department of Neurobiology & Behavior, University of California, Irvine, Irvine, CA, US
78	Imaging synaptic density across the Alzheimer's disease continuum with [18]F-SynVestT-1	**Joseph Giorgio**, Helen Wills Neuroscience Institute, University of California Berkeley, Berkeley, CA, US
79	Data-driven analysis of 10,361 amyloid-PET scans from the IDEAS study reveals two primary axes of variation	**Joseph Giorgio**, Helen Wills Neuroscience Institute, University of California Berkeley, Berkeley, CA, US
80	Lower locus coeruleus structural integrity is associated with greater intraindividual cognitive variability in older individuals	**Emma Wiklund**, Department of Radiology, Massachusetts General Hospital, Harvard Medical School, Boston, MA, US
81	Precuneus fMRI activity is associated with future Aβ burden in cognitively normal older APOE4 carriers	**Anne Maass**, Division of Nuclear Medicine, Department of Radiology & Nuclear Medicine, Faculty of Medicine, Otto von Guericke University Magdeburg, Magdeburg, Germany
82	PI-2620 binding in cognitively normal older adults including SuperAgers	**Anne Maass**, German Center for Neurodegenerative Diseases, Magdeburg, Germany, Magdeburg, Germany
83	Early phase Amyloid PET as a surrogate marker of brain metabolism in cases of cognitive impairment	**William Aye**, New Zealand Brain Research Institute, Christchurch, NZ
84	Unlocking rau PET accessibility: a machine learning-based prediction of tau pathology from plasma, MRI and clinical variables	**Linda Karlsson**, Clinical Memory Research Unit, Department of Clinical Sciences in Malmö, Lund University, Lund, Sweden, Lund, Sweden
85	Amyloid and tau burden relate to longitudinal changes in performance of everyday activities as measured using the performance-based Harvard Automated Phone Task	**Mark Dubbelman**, Department of Neurology, Massachusetts General Hospital, Harvard Medical School, Boston, MA, US

Wednesday, January 17, 2024		
86	In vivo structural integrity of the hypothalamus and the spatiotemporal evolution of Alzheimer's disease	**Marion Baillet**, Faculty of Health, Medicine and Life Sciences, School for Mental Health and Neuroscience, Alzheimer Centre Limburg, Maastricht University, Maastricht, The Netherlands
87	Cross-sectional comparison of extra-cerebral binding trends in [F-18]MK6240 PET images	**Andrew McVea**, University of Wisconsin - Madison, Madison, WI, US
88	Tau accumulation in Down Syndrome after onset of amyloid positivity	**Andrew McVea**, University of Wisconsin - Madison, Madison, WI, US
89	Greater locus coeruleus activity and locus coeruleus-amygdala hypoconnectivity during high arousal conditions are related to elevated concentrations of plasma p-tau231 in older individuals	**Prokopis Prokopiou**, Gordon Center for Medical Imaging, Department of Radiology, Massachusetts General Hospital, Boston, MA, US
90	Establishing tau-PET cut-points for cognitive diagnosis with [F-18]PI-2620	**Victoria R. Tennant**, 1. Imaging Genetics Center, Mark and Mary Stevens Neuroimaging and Informatics Institute, Keck School of Medicine, University of Southern California, Los Angeles, CA, US
91	Plasma ADRD biomarkers predict longitudinal declines in intra-network functional brain connectivity	**Heather Dark**, Laboratory of Behavioral Neuroscience, National Institute on Aging, Intramural Research Program, Baltimore, MD, US
92	The role of frontoparietal control network and default mode network functional connectivity in cognitive resilience in preclinical Alzheimer's disease	**Rory Boyle**, Massachusetts General Hospital, Harvard Medical School, Boston, MA, US
93	Disrupted sleep and 24-hour rhythms are associated with 18F-PI-26260 tau PET in aging and neurodegenerative disease	**Joseph Winer**, Department of Neurology and Neurological Sciences, Stanford University, Stanford, CA, US
94	Cortical and substantia nigra 18F-PI-2620 tau PET are associated with cognitive and motor impairment in Lewy body disease	**Joseph Winer**, Department of Neurology and Neurological Sciences, Stanford University, Stanford, CA, US
95	Predictability of amyloid-PET status with plasma phospho-Tau217 in adults with Down syndrome	**Brecca Bettcher**, University of Wisconsin-Madison School of Medicine and Public Health and Waisman Center, Madison, WI, US

Wednesday, January 17, 2024		
96	Locus coeruleus metabolism relates to Alzheimer's disease pathology in amyloid-positive symptomatic individuals	**Elouise A Koops**, Gordon Center for Medical Imaging, Department of Radiology, Massachusetts General Hospital, Harvard Medical School, Boston, MA, US
97	Correlating in vivo amyloid beta centiloid values with neuropathological burden: insights from Down syndrome and Alzheimer's disease cohorts	**Jr-Jiun Liou**, University of Pittsburgh, Pittsburgh, PA, US
98	Visualization of endogenously generated Dutch-type abeta oligomers that dysregulate presynaptic neurotransmission in the absence of detectable inflammation	**Sam Gandy**, Icahn School of Medicine, New York, NY, US
99	[18F]PI-2620 tau-PET binding patterns in American football players with suspected Chronic Traumatic Encephalopathy	**Jhony Mejia Perez**, Memory and Aging Center, Department of Neurology, University of California, San Francisco, San Francisco, CA, US
100	Regional amyloid-β burden in Lewy Body Disease	**Hillary Vossler**, Department of Neurology and Neurological Sciences, Stanford University School of Medicine, Stanford, CA, US
101	Pathology-weighted connectivity with medial parietal lobe drives neocortical tau accumulation	**Jacob Ziontz**, Helen Wills Neuroscience Institute, University of California, Berkeley, Berkeley, CA, US
102	18F-MK-6240 Tau PET visual read algorithm for Alzheimer's disease: diagnostic accuracy and comparison with automated-quantitative Braak stage analysis	**Karine Provost**, Centre Hospitalier de l'Université de Montréal, Montreal, QC, CA
103	Evaluating CenTauRz harmonization of matched FTP and MK6240 tau PET images: the HEAD Study	**Davneet Minhas**, University of Pittsburgh, Pittsburgh, PA, US
104	Characterizing the relationship between the functional connectome and tau PET in preclinical Alzheimer's disease	**Hamid Abuwarda**, Department of Neurology, Yale School of Medicine, New Haven, CT, US
105	Estimating time-to-tau as a function of Aβ pathology in Alzheimer's disease using [18F]MK6240 and [18F]NAV4694 PET	**Samantha Budd Haeberlein**, Enigma Biomedical USA, Knoxville, TN, US
106	Neuroinflammation potentiates the effect of amyloid-β on longitudinal tau accumulation	**Nesrine Rahmouni**, McGill University, Montreal, QC, CA

Wednesday, January 17, 2024		
107	Association between plasma pTau epitopes and synaptic density measured with [C-11]UCB-J PET	**Kao Lee Yang**, Wisconsin Alzheimer's Disease Research Center, University of Wisconsin, Madison, WI, US
108	"Treatment Related Amyloid Clearance" (TRAC): a framework to characterize a new biomarker state in the era of anti-amyloid therapies	**Renaud La Joie**, Memory and Aging Center, Department of Neurology, University of California, San Francisco, San Francisco, CA, US
109	Alzheimer's disease biological PET staging using plasma p217+tau	**Christopher Rowe**, The Florey Institute of Neuroscience and Mental Health, The University of Melbourne, Melbourne, Australia
110	Plasma p-tau217 outperforms [18F]FDG-PET in identifying biological Alzheimer's disease in atypical and early-onset dementia	**Kely Quispialaya**, Translational Neuroimaging Laboratory, The McGill University Research Centre for Studies in Aging, Douglas Hospital, McGill University, Montreal, Canada., Montréal, QC, CA
111	A-T+ PET participants in preclinical AD: Clinical progression and concordance with fluid biomarkers	**Yara Yakoub**, Douglas Mental Health University Institute, Montreal, QC, CA
112	Neighborhood disadvantage and the association between imaging biomarkers of Alzheimer's disease and cognition in a cohort of diverse older adults	**Yara Yakoub**, Douglas Mental Health University Institute, Montreal, QC, CA
113	Longitudinal association of mid-life ten year cardiovascular disease risk score with blood biomarkers of Alzheimer's disease and neurodegeneration: Heart SCORE Brain Study	**Anum Saeed**, University of Pittsburgh, Pittsburgh, PA, US
114	Comparison of FDG-PET in individuals with Down Syndrome and Dominantly Inherited Alzheimer Disease: genetic forms with elevated production of amyloid	**Omar Abdelmoity**, Washington University in St. Louis, St. Louis, Missouri, St. Louis, MO, US
115	Deep learning-based partial volume correction for tau PET imaging	**Kuang Gong**, Department of Biomedical Engineering, University of Florida, Gainesville, FL, US
116	Plasma levels of an N-terminal tau fragment predict core AD and neurodegenerative biomarkers in autosomal dominant Alzheimer's disease	**Stephanie Schultz**, Massachusetts General Hospital, Boston, MA, US

Wednesday, January 17, 2024		
117	Increased CSF GAP-43 is associated with accelerated tau accumulation and spread in Alzheimer's disease	**Nicolai Franzmeier**, Institute for Stroke and Dementia Research (ISD), University Hospital, LMU Munich, Germany, Munich, Germany
118	Investigating the impacts of tau status in Alzheimer's disease by using [18F]Florzolotau tau cutoff	**Shao-Yi Huang**, Department of Medical Imaging and Radiological Sciences, Chang Gung University, Taoyuan, TW
119	Study of reference regions in the quantitation of [18F]Florzolotau tau PET imaging	**Jyh-Ruei Lin**, Medical Imaging & Radiological Sciences and Healthy Aging Research Center, Chang Gung University, Taoyuan, TW
120	Assessing the efficacy of BETTH-derived tau thresholds to predict cognitive decline	**Alexandra Gogola**, Department of Radiology, University of Pittsburgh School of Medicine, Pittsburgh, PA, US
121	Assessing the correlations between imaging and plasma biomarkers within the AT(N) framework	**Alexandra Gogola**, Department of Radiology, University of Pittsburgh School of Medicine, Pittsburgh, PA, US
122	The effect of microglial activation on brain atrophy across the Alzheimer's disease continuum	**Guilherme Povala**, University of Pittsburgh, Pittsburgh, PA, US
123	Disentangling the relationships between tau-PET, amyloid-β-PET, hippocampal subfield volumes, and memory: a longitudinal study	**Etienne Aumont**, NeuroQAM Research Centre, Université du Québec à Montréal (UQAM), Montréal, QC, CA
124	Tau-PET Overlap Index; associations with Braak Stage and quantitative NFT measurements	**Val Lowe**, Department of Radiology, Mayo Clinic, Rochester, MN, US
125	Tau-PET spatial extent for predicting cognitive decline within tau-positive individuals	**Emma Coomans**, Alzheimer Center Amsterdam, Neurology, Vrije Universiteit Amsterdam, Amsterdam UMC location VUmc, Amsterdam, The Netherlands
126	Association of sex and cerebral beta-amyloid with cortical gray matter brain age in cognitively impaired older adults	**Jinghang Li**, Department of Bioengineering, University of Pittsburgh, Pittsburgh, PA, US
127	Will cerebral glucose metabolism measured using [18F]FDG PET substitute tau PET in clinical studies?	**Paul Edison**, Imperial College London, London, United Kingdom
128	CSF sTREM2 is associated with neuroprotective microglial states early in	**Paul Edison**, Imperial College London, London, United Kingdom

Wednesday, January 17, 2024		
	Alzheimer's disease and deleterious effects later in the disease trajectory	
129	The Mobile Toolbox for assessing cognition remotely: associations with amyloid and tau deposition in cognitively unimpaired older adults	**Roos Jutten**, Department of Neurology, Massachusetts General Hospital, Harvard Medical School, Boston, MA, US
130	Characterizing multi-site harmonized amyloid and tau PET across the Alzheimer's continuum	**Karly Cody**, Department of Neurology and Neurological Sciences, Stanford University, Stanford, CA, United States, Stanford, CA, US
131	Characterization of tau PET accumulation relative to duration of entorhinal tau positivity	**Karly Cody**, Department of Medicine, University of Wisconsin, Madison, WI, United States, Madison, WI, US
132	Harmonization of multi-scanner PET data with ComBat: application to 18F-AV1451 data acquired on a Siemens ECAT HR+ PET and a GE Discovery MI PET/CT Scanner	**Cristina Lois Gomez**, Massachusetts General Brigham, Boston, MA, US
133	Longitudinal white matter degeneration is associated with higher subsequent amyloid load across the Alzheimer's disease continuum	**Courtney Burton**, Memory and Aging Program, Butler Hospital, Providence, RI, US
134	Multimodal analysis of tau epicenters in heterogeneous Alzheimer's disease variants	**Anne Trainer**, Yale School of Medicine, New Haven, CT, US
135	A pretrained foundation model for learning representation of regional tau accumulation pattern and its downstream applications	**JunYoung Sohn**, Junyoung Sohn, Seoul, South Korea
136	[18F]RO-948 Tau PET retention and correlation with fluid biomarkers in the early AD continuum	**Mahnaz Shekari**, BarcelonaBeta Brain Research Center (BBRC), Pasqual Maragall Foundation, Barcelona, ES
137	Baseline plasma GFAP predicts longitudinal tau-PET uptake in Braak staging continuum	**Wan Lu Jia**, Translational Neuroimaging Laboratory, The McGill University Research Centre for Studies in Aging, Montreal, QC, CA
138	Plasma NfL correlates to grey matter and white matter atrophy ambivalent to amyloid status in older adults	**Brandon Hall**, McGill University, Montreal, QC, CA

Wednesday, January 17, 2024		
139	Astrocyte reactivity influences cognitive decline in individuals across the Alzheimer's disease continuum	**Bruna Bellaver**, Department of Psychiatry, University of Pittsburgh, Pittsburgh, PA, 15213, United States, Pittsburgh, PA, US
140	Elevated Plasma Ptau-181 is associated with congestive heart failure	**Jeremy Tanner**, University of Texas Health San Antonio - Biggs Institute, San Antonio, TX, US
141	Regional cell-type proportions are associated with AD pathological changes	**Min Su Kang**, Artificial Intelligence and Computational Neurosciences lab, Sunnybrook Research Institute, University of Toronto, Toronto, ON, Canada
142	Quantitative Gradient Recalled Echo (qGRE) MRI detects neuronal loss and iron accumulation in nucleus basalis of Meynert in preclinical and mild Alzheimer's disease	**Satya VVN Kothapalli**, Department of Radiology, Washington University in St. Louis, St. Louis, MO, US
143	Head-to-head analysis of [18F]MK6240 and [18F]Flortaucipir standardized update values (SUVs): the HEAD Study	**Hsin-Yeh Tsai**, Lawrence Berkeley National Laboratory, Berkeley, CA, US
144	Association between oxygen extraction fraction, tau, and amyloid pathology, and cognitive status in Alzheimer's disease: implications for advanced neuroimaging techniques	**Seyyed Ali Hosseini**, Translational Neuroimaging Laboratory, McGill Research Centre for Studies in Aging, McGill University, Montreal, QC, Canada, Montréal, QC, CA
145	Association of plasma pTau epitopes with mesial temporal lobe cortical thinning	**Lydia Trudel**, McGill University, Montreal, QC, CA
146	Specific Tau networks are associated with different cognitive domains in the elderly	**Siddharth Nayak**, Department of Radiology, Weill Cornell Medicine, New York, NY, US
10:55 am – 12:40 pm	**SESSION II: Tau PET Harmonization**	**Bradley Christian, University of Wisconsin, Madison, WI, United States** **Christopher Schwarz, Mayo Clinic, Rochester, MN, United States**
10:55	Introduction	Chairs
11:00	Universal scale for tau PET based on head-to-head data: the HEAD study	**Guilherme Bauer-Negrini**, Department of Psychiatry, University of Pittsburgh, Pittsburgh, PA, United States
11:15	Preliminary evaluation of CenTauR regions of interest with Flortaucipir-PET images and testing in PET-to-autopsy cohort	**Leonardo Iaccarino**, Eli Lilly and Company, Indianapolis, IN, United States

Wednesday, January 17, 2024		
11:30	Harmonizing tau PET in Alzheimer's disease: the CenTauR scale and the Joint Propagation Model	**Antoine Leuzy**, Clinical Memory Research Unit, Department of Clinical Sciences, Lund University, Lund, Sweden
11:45	Improving the associations between [18F]MK6240 and [18F]FTP in target regions	**Cécile Tissot**, Lawrence Berkeley National Laboratory, Berkeley, CA, United States
12:00	Elimination of putative off-target signal in the reference region for tau PET harmonization	**Emily Olafson**, Research and Early Development (gRED), Genentech, South San Francisco, CA, United States
12:15 pm – 12:40 pm	Discussion	
12:40 pm – 01:40 pm	Lunch break	
01:40 pm – 02:10 pm	**Keynote: A new era in AD therapeutic trials: translating hope into impact**	**Cath Mummery**, University College London, London, United Kingdom
02:10 pm – 02:20 pm	Keynote Discussion	
02:20 pm – 04:05 pm	**SESSION III: Modeling, the Real-world, and Natural History**	**Suzanne Baker, Lawrence Berkeley National Laboratory, Berkeley, CA, United States** **Pedro Rosa Neto, McGill University, Montreal, QC, Canada**
02:20	Introduction	Chairs
02:25	On fitting the Jack model to biomarker data	**Terry Therneau**, Department of Quantitative Health Sciences, Mayo Clinic, Rochester, MN, United States
02:40	Validation of sampled iterative local approximation for individualized estimates of tau PET onset age	**Jordan Teague**, Department of Medicine, University of Wisconsin, Madison, WI, United States
02:55	Quantitative analysis of amyloid-PET from real-world practice: lessons learned from processing the IDEAS dataset	**Renaud La Joie**, Memory and Aging Center, Department of Neurology, University of California, San Francisco, San Francisco, CA, United States
03:10	Parahippocampal tau-PET as a biomarker of the transition from rhinal to neocortical tauopathy	**Emma Thibault**, Massachusetts General Hospital, Boston, MA, United States

Wednesday, January 17, 2024		
03:25	Unraveling the early trajectory of cortical tau accumulation using 18F-MK6240	**Vincent Dore,** The Australian eHealth Research Centre, CSIRO, Melbourne, Australia
03:40 pm – 04:05 pm	Discussion	
04:05 pm – 04:35 pm	**Break/Poster Session**	
04:35 pm – 06:05 pm	**SESSION IV: Neuropathology - Part I**	**Milos Ikonomovic, University of Pittsburgh, Pittsburgh, PA, United States** **Melissa Murray, Mayo Clinic, Rochester, MN, United States**
04:35	Introduction	Chairs
04:40	Mature tangle scores strongly correlate with tau-PET and structural MRI measures	**Christina M. Moloney**, Department of Neuroscience, Mayo Clinic, Jacksonville, FL, United States
04:55	Neuropathologic characterization of FDG-PET and MRI-based AD subtypes	**Sophia Wheatley**, Division of Clinical Geriatrics, Department of Neurobiology, Care Sciences and Society, Center for Alzheimer Research, Karolinska Institutet, Stockholm, Sweden
05:10	Flortaucipir PET relationships to pathologically determined Braak neurofibrillary tangle stage and Thal β-amyloid phase in aging and Alzheimer's disease	**Jennifer Whitwell**, Mayo Clinic, Rochester, MN, United States
05:25	Development and validation of a novel tau summary measure: Tau Heterogeneity Evaluation in Alzheimer's Disease (THETA) score	**Robel K. Gebre**, Department of Radiology, Mayo Clinic, 55905, Rochester, MN, United States
05:40	Transmembrane protein 106B is one of the potential off-target binding substrates of tau PET tracers	**Ryuichi Harada**, Division of Pharmacology, Faculty of Medicine, Tohoku Medical and Pharmaceutical University, Sendai, Japan
05:40 pm – 06:05 pm	Discussion	
06:05 pm –	Welcome Reception	

Wednesday, January 17, 2024		
08:00 pm		

Thursday, January 18, 2024		
07:30 am – 08:30 am	Breakfast	
07:45 am – 08:15 am	Breakfast with A Mentor	
08:30 am – 10:00 am	**SESSION V: Neuropathology - PART II**	**Teresa Gomez Isla, Massachusetts General Hospital, Boston, MA, United States** **Laetitia Lemoine, Invicro, London, United Kingdom**
08:30	Introduction	Chairs
08:35	Pathologic correlations of [18F]-Flortaucipir imaging in mixed Lewy body and Alzheimer's disease	**Cinthya Aguero**, MassGeneral Institute for Neurodegenerative Disease, Charlestown, MA, United States
08:50	Flortaucipir PET relationships to pathologically determined Braak neurofibrillary tangle stage and Thal β-amyloid phase in aging and Alzheimer's disease	**Jennifer Whitwell**, Mayo Clinic, Rochester, MN, USA
09:05	Correlating hippocampal volume with neuropathological burden in neurodegenerative diseases using 7T postmortem MRI	**Jr-Jiun Liou**, University of Pittsburgh, Pittsburgh, PA, United States
09:20	Multimodal genetic analysis of brain amyloidosis	**Ting-Chen Wang**, Vanderbilt Memory and Alzheimer's Center, Department of Neurology, Vanderbilt University Medical Center, Nashville, TN, United States
09:35 am – 10:00 am	Discussion	
10:00 am – 10:30 am	Poster Session	

Thursday, January 18, 2024		
10:30 am – 12:00 pm	**SESSION VI: Early Amyloid and Tau Effects and Mod Pre-clinical AD**	**Annie Cohen, University of Pittsburgh, Pittsburg, PA, United States** **Gil Rabinovici, University of California, San Francisco, CA, United States**
10:30	Introduction	Chairs
10:35	Reduced tau accumulation mediates the protective effects of physical activity on prospective cognitive decline in preclinical Alzheimer's disease	**Wai-Ying Wendy Yau**, Department of Neurology, Massachusetts General Hospital, Boston, MA, United States
10:50	Speech patterns during memory recall relates to early tau burden across adulthood	**Christina Young**, Department of Neurology and Neurological Sciences, Stanford University School of Medicine, Palo Alto, CA, United States
11:05	Default mode network connectivity tracks with amyloid age and predicts conversion to amyloidosis, mild cognitive impairment and dementia across the Alzheimer's disease spectrum	**Nick Corriveau-Lecavalier**, Mayo Clinic, Rochester, MN, United States
11:20	Higher locus coeruleus integrity and cognitive reserve attenuate tau-related cognitive decline in older adults	**Lukas Heinrich**, Department of Radiology, Massachusetts General Hospital / Harvard Medical School, Boston, MA, United States
11:35 am – 12:00 pm	Discussion	
12:00 pm – 01:00 pm	Lunch break	
01:00 pm – 02:30 pm	**SESSION VII: Associations with longitudinal Tau PET**	**Elizabeth Mormino, Stanford University, Palo Alto, CA, United States** **Susan Landau, University of California, Berkeley, CA, United States**
01:00	Introduction	Chairs

Thursday, January 18, 2024		
01:05	Large-sample, longitudinal tau-PET in sporadic early-onset Alzheimer's disease: findings from the LEADS Consortium	**Daniel Schonhaut**, University of California, San Francisco, San Francisco, CA, United States
01:20	Associations between CSF alpha-synuclein pathology and longitudinal Aβ- and tau-PET	**Alexa Pichet Binette**, Clinical Memory Research Unit, Department of Clinical Sciences Malmö, Lund University, Lund, Sweden
01:35	Baseline PET predictors of neocortical tau accumulation and cognitive decline in the A4 study	**Justin Sanchez**, Massachusetts General Hospital/Harvard Medical School, BOSTON, MA, United States
01:40	A meta-analysis of sex differences in longitudinal tau-PET in clinically normal adults	**Gillian Coughlan**, Department of Neurology, Massachusetts General Hospital, Harvard Medical School, Boston, MA, United States
02:05 pm – 02:30 pm	Discussion	
02:30 pm – 03:00 pm	**Keynote: Fluid and PET imaging markers for Alzheimer's disease and neuronal synuclein disease**	**Oskar Hansson, Lund University, Lund, Sweden**
03:00 pm – 03:10 pm	Keynote Discussion	
03:10 pm – 03:40 pm	Poster Session	
03:40 pm – 05:25 pm	**SESSION VIII: Clinical and Biological Heterogeneity**	**Tobey Betthauser, University of Wisconsin, Madison, WI, United States** **Heidi Jacobs, Massachusetts General Hospital, Boston, MA, United States**
03:40	Introduction	Chairs
03:45	Heterogeneity of amyloid-PET-negative patients with a clinical diagnosis of sporadic early-onset AD: an FDG-PET study in the LEADS cohort	**Julien Lagarde**, Department of Neurology, University of California, San Francisco, San Francisco, CA, United States

Thursday, January 18, 2024		
04:00	The importance of AT(N)-V imaging biomarkers differs in diverse populations	**Karin Meeker**, Washington University School of Medicine, Saint Louis, MO, United States
04:15	The POINTER Imaging baseline cohort: Associations between neuroimaging biomarkers, cardiovascular health and cognition	**Theresa Harrison**, University of California Berkeley, Berkeley, CA, United States
04:30	Identification of genetic risk loci and polygenic prediction for β-amyloid deposition in East Asian Population	**Jun Pyo Kim**, Samsung Medical Center, Seoul, South Korea
04:45	Braak discordant cases in a large multi-site harmonized tau PET dataset	**Viktorija Smith**, Department of Neurology and Neurological Sciences, Stanford University, Stanford, CA, United States
05:00 pm – 05:25 pm	Discussion	
05:25 pm – 07:30 pm	Networking Reception	

Friday, January 19, 2024		
07:30 am – 08:30 am	Breakfast	
07:45 am – 08:15 am	Breakfast with A Mentor	
08:30 am – 09:10 am	ISTAART	
09:10 am – 10:40 am	**SESSION IX: New Methods for Plasma**	**Suzanne Schindler, Washington University, St Louis, MO, United States** **Tommy Karikari, University of Pittsburgh, Pittsburg, PA, United States**
09:10	Introduction	Chairs
09:15	Plasma Aβ42/Aβ40 is an Early Marker of Amyloidosis in Clinically Unimpaired Older Adults	**Alexandra N. Trelle**, Neurology & Neurological Sciences, Stanford University School of Medicine, Stanford, CA, United States

Friday, January 19, 2024		
09:30	A highly accurate blood test for Alzheimer's disease pathology has performance equivalent or superior to clinically used cerebrospinal fluid tests	**Gemma Salvadó**, Clinical Memory Research Unit, Department of Clinical Sciences Malmö, Faculty of Medicine, Lund University, Lund, Sweden
09:45	Associations of C2N plasma Aβ42/40 and p-tau217 and subsequent amyloid PET change	**Petrice Cogswell**, Mayo Clinic, Rochester, MN, United States
10:00	Plasma p-tau212 is increased in CSF amyloid positive and [18F]flutemetamol PET negative cognitively impaired individuals	**Przemyslaw Kac,** The Sahlgrenska Academy at the University of Gothenburg, Mölndal, Sweden
10:15 am – 10:40 am	Discussion	
11:10 am – 11:40 am	**Keynote: The multiple neurodegenerative pathologies of the aging brain**	**Johannes Attems, Newcastle University, Newcastle Upon Tyne, United Kingdom**
11:40 am – 11:50 am	Keynote Discussion	
11:50 am – 02:30 pm	**SESSION X: Plasma Applications**	**Henrik Zetterberg, University of Gothenburg, Sweden** **Keith Johnson, Massachusetts General Hospital, Boston, MA, United States**
11:50	Introduction	Chairs
11:55	Plasma GFAP mediates the relationship between amyloid and tau PET in individuals with Down Syndrome	**Anna Boerwinkle**, Department of Neurology, Washington University in St. Louis, Saint Louis, MO, United States
12:10	Association of plasma GFAP with FDG, PiB and tau PET across aging and the Alzheimer's disease continuum	**Ellen Dicks**, Department of Neurology, Mayo Clinic, Rochester, MN, United States
12:25	Relationships between PET and blood plasma biomarkers in corticobasal syndrome	**Neha Atulkumar Singh**, Department of Neurology, Mayo Clinic, Rochester, MN, United States
12:40	Evaluating the impact of racialization on imaging and plasma biomarkers	**Alexandra Gogola**, Department of Radiology, University of Pittsburgh School of Medicine, Pittsburgh, PA, United States
12:55	Lunch	

Friday, January 19, 2024		
01:45	Plasma, MRI, and PET biomarker-based risk prediction of dementia in the context of health-related comorbidities and demographic factors: A preliminary exploration	**Marc Rudolph**, Wake Forest School of Medicine, Winston-Salem, NC, United States
02:00	Longitudinal change of cerebral amyloid and tau and its association with plasma biomarkers in preclinical Alzheimer's disease.	**Alfonso Fajardo-Valdez**, Douglas Mental Health University Institute, Centre for Studies on the Prevention of Alzheimer's Disease(StoP-AD), Montreal, QC, Canada
02:15	Proteome-wide analyses Identifies Plasma Immune Regulators of Amyloid-beta progression	**Michael R. Duggan**, Laboratory of Behavioral Neuroscience, National Institute on Aging, National Institutes of Health, Baltimore, MD, United States
02:30 pm – 02:55 pm	Discussion	
02:55 pm – 03:10 pm	**Awards Ceremony**	
03:10 pm – 03:15 pm	Concluding Notes	HAI2024 Executive Committee

HAI 2024 ABSTRACTS

Wednesday, January 17, 2024 - 08:30 am - 09:35 am

Podium Session

SESSION I: Tracer Discovery and Biomarker Optimization

CHAIRS: Julie Price, Sandra Sanabria Bohorquez

Wednesday, January 17, 2024		
08:30 am - 09:35 am	**SESSION I: Tracer Discovery and Biomarker Optimization**	**Julie Price, Massachusetts General Hospital, Boston, MA, United States** **Sandra Sanabria Bohorquez, Genentech, South San Francisco, CA, United States**
08:30	Introduction	Chairs
08:35	Discovery and preclinical development of [18F]ACI-19626, a first-in-class TDP-43 PET tracer	Vokali | Dreyfus | Chevalier | Afroz | Charmey | Clavel | Rathnam | Melly | Jaquier | Kroth | Luthi-Carter | Pfeifer | Kosco-Vilbois | Seredenina
08:50	Bridging the gap between SUVR and DVR for [18F]MK6240 by correcting for tracer clearance in tissue: A simulation study	Mohanraj | Carson | Hillmer | Honhar
09:05	PET Spatial extent as a sensitive beta-amyloid biomarker in preclinical Alzheimer's disease	Farrell | Thibault | Becker | Price | Hanseeuw | Buckley | Jacobs | Chen | Sperling | Johnson
09:20	Optimizing the detection of whole-brain tau-related cognitive decline in mild cognitive impairment	St-Onge | Pichet Binette | Chapleau | Breitner | Villeneuve
09:35	KEYNOTE: Targets and radioligands for PET imaging of neuroinflammation	Paolo Zanotti-Fregonara
9:35	Discussion	

Discovery and preclinical development of [18F]ACI-19626, a first-in-class TDP-43 PET tracer

Efthymia Vokali[1], Nicolas Dreyfus[1], Elodie Chevalier[1], Tariq Afroz[1], Dorian Charmey[1], Mathieu Clavel[1], Monisha Rathnam[1], Tania Melly[1], Thomas Jaquier[1], Heiko Kroth[1], Ruth Luthi-Carter[1], Andrea Pfeifer[1], Marie Kosco-Vilbois[1], Tamara Seredenina[1]

1AC Immune SA, EPFL Innovation Park, Building B, 1015, Lausanne, Switzerland

Background: Intracellular aggregation of TDP-43 is found as primary neuropathology in amyotrophic lateral sclerosis (ALS), limbic-predominant age-related TDP-43 encephalopathy (LATE), in 50% of patients with frontotemporal dementia (FTD), and is present as co-pathology in other neurodegenerative diseases, including Alzheimer's disease (AD). Sensitive fluid or imaging biomarkers of TDP-43 pathology are currently not available. Direct detection of TDP-43 aggregates holds promise for unraveling the pathobiology of disease and for improved diagnosis, patient stratification and assessment of therapeutic efficacy in clinical trials.

Methods: Using our Morphomer® small molecule library of brain-penetrant and beta sheet binding compounds, initial hits were identified using patients' brain material. Radiobinding and autoradiography assays were used to assess binding affinity and target engagement on FTLD-TDP brain samples, and selectivity over other aggregation-prone proteins on AD and Parkinson's disease (PD) tissue. Brain pharmacokinetic profiles were obtained in mice, followed by assessment of brain uptake, distribution and washout for selected 18F radiolabeled compounds in non-human primates (NHP).

Results: Rational drug design and medicinal chemistry optimization enabled the development of the TDP-43 tracer, ACI-19626. This compound has high affinity binding (low nM Kd) for human brain-derived aggregated TDP-43 and can differentiate FTLD-TDP type A and B patient samples from age-matched controls. ACI-19626 displays selectivity for TDP-43 over Abeta, Tau and alpha-synuclein aggregates, and no binding to common off-target proteins, including monoamine oxidase A and B. In NHPs, [^{18}F]ACI-19626 has a rapid brain uptake and fast and complete washout, a profile suitable for brain PET imaging.

Conclusions: [^{18}F]ACI-19626 was identified as a potential first-in-class TDP-43 PET tracer and selected for evaluation in a First-in-Human study based on its excellent affinity, selectivity and pharmacokinetic properties. [^{18}F]ACI-19626 has the potential to detect and monitor the progression of TDP-43 pathology in brains of living patients with TDP-43 proteinopathies such as ALS, FTLD-TDP, AD and LATE.

Keywords: TDP-43, PET tracer, FTLD-TDP, ALS, biomarker

Bridging the gap between SUVR and DVR for [18F]MK6240 by correcting for tracer clearance in tissue: A simulation study

Prastik Mohanraj[1], Richard E Carson[1], Ansel T Hillmer[1], Praveen Honhar[1]

[1]*Yale PET Center, Radiology and Biomedical Imaging, Yale University, New Haven, CT, United States*

SUVR is a biased estimator for *DVR* due to time dependent effects of tracer clearance, confounding its interpretation as a measure of target concentration and posing challenges for data harmonization across different *SUVR* time-windows. Recently, a method that corrects this bias in *SUVR*-without need for PET data outside *SUVR* time-window, was developed for tracers well-described by one-tissue or simplified reference region-based kinetic models[1]. The correction takes the form:

$SUVR_C = SUVR/[1-\beta_{ref}/k_{2,ref}+SUVR\ \beta_t/(k_{2,ref}\ R_1)]$

($SUVR_C$:corrected *SUVR*, $k_{2,ref}$: population-based k_2 parameter of the reference region,[β_{ref}, β_t]: clearance rates of the tracer from the reference and target tissues,R_1=1). This work adapts the correction for [^{18}F]MK6240–correcting the *SUVR* acquired at different time-windows to the corresponding SRTM2 *DVR* value(ref=Cerebellum).

Based on data from Guehl et al.[2], simulated plasma input functions (with different tracer clearance rates during *SUVR* window[β]) and time activity curves (TACs) were generated to approximate kinetics in different brain regions and MCI/AD individuals. TACs corresponding to a higher binding potential(BP_{ND}) for misfolded tau were also generated by varying k_3/k_4 ratio to [1-2.25] times the mean values reported in Guehl et al[2]. *SUVR* measurements across different time-windows showed a mean positive bias ([10-20]% of SRTM2 *DVR*) in the temporal lobe and hippocampus which was significantly reduced in magnitude ([2-7]%,p<0.00001,paired *t*-test for bias magnitude) by $SUVR_C$(Fig1). Similar performance for $SUVR_C$ was observed for simulations with higher BP_{ND}(Fig2). Finally, 20 replicates for simulations computing the Cohen's *d* value for the group difference between a baseline-tau cohort(*n*=36, *SUVR* time-window=110-130 min) and a higher-tau cohort(*n*=36, *SUVR* time-window=70-90 min) showed that the Cohen's *d* value for *SUVR* was [30-60]% lower that than the corresponding values for *DVR*; this bias was reduced significantly for $SUVR_C$(Fig3). $SUVR_C$ can, therefore, help harmonize multi-center *SUVR* values acquired across different time-windows.

[1]: Honhar, P.et al. *JCBFM* 2023.In Press.https://doi.org/10.1177/0271678X231196804

[2]: Guehl, N.et al. *EJNMMI* 2019.46(10):2099-2111

SUVR Time-Window: 70-90 min

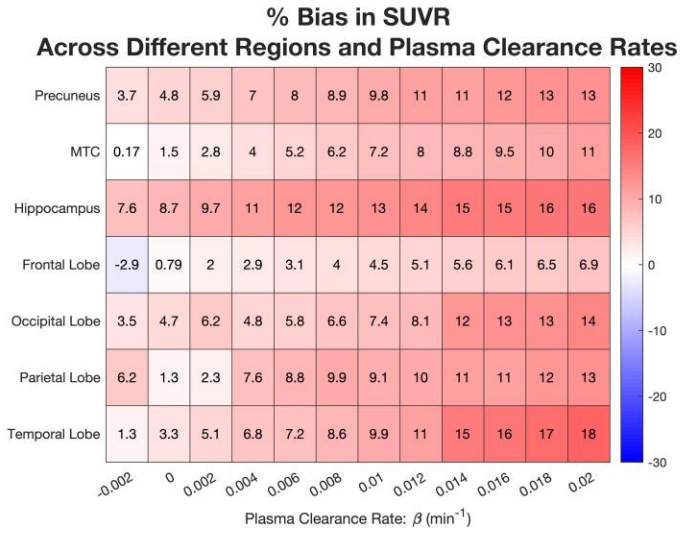

Region	Mean +/– Std
Hippocampus	12.4% +/– 2.8%
Temporal Lobe	9.9% +/– 5.5%

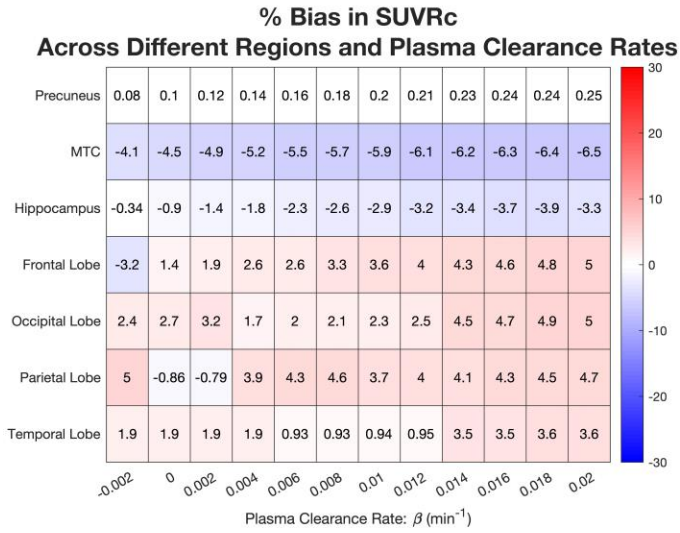

Region	Mean +/– Std
Hippocampus	–2.5% +/– 1.1%
Temporal Lobe	2.1% +/– 1.1%

SUVR Time-Window: 110-130 min

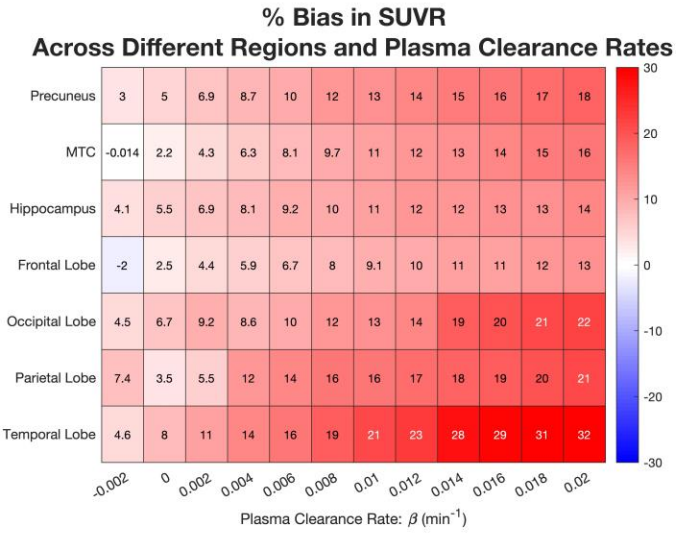

Region	Mean +/– Std
Hippocampus	9.9% +/– 3.2%
Temporal Lobe	19.6% +/– 9.1%

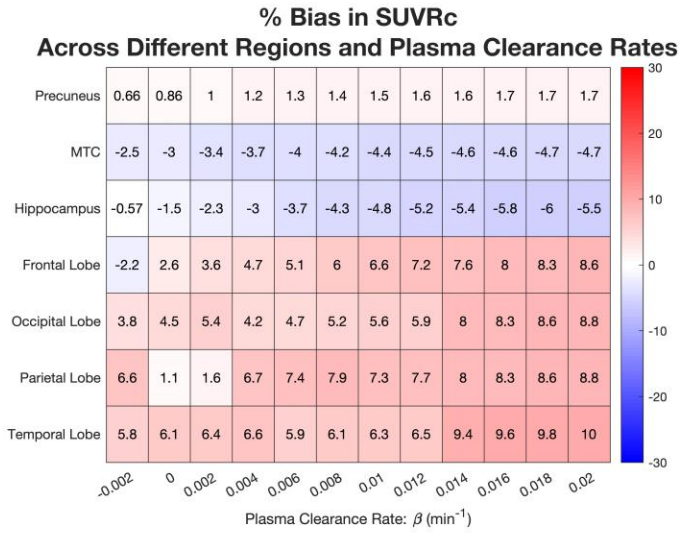

Region	Mean +/– Std
Hippocampus	–4.0% +/– 1.8%
Temporal Lobe	7.4% +/– 1.7%

Fig 1: Heatmaps quantifying the bias in *SUVR* (left column) and corrected *SUVR* (right column) for time-windows corresponding to 70-90 min (top row) and 110-130 min (bottom row) in simulations of [^{18}F]MK6240 across multiple brain regions and tracer clearance rates in plasma during the *SUVR* time window (β). Overall, corrected *SUVR* shows much lesser bias and also a lower variability in the bias in all regions. MTC: Mesial Temporal Cortex.

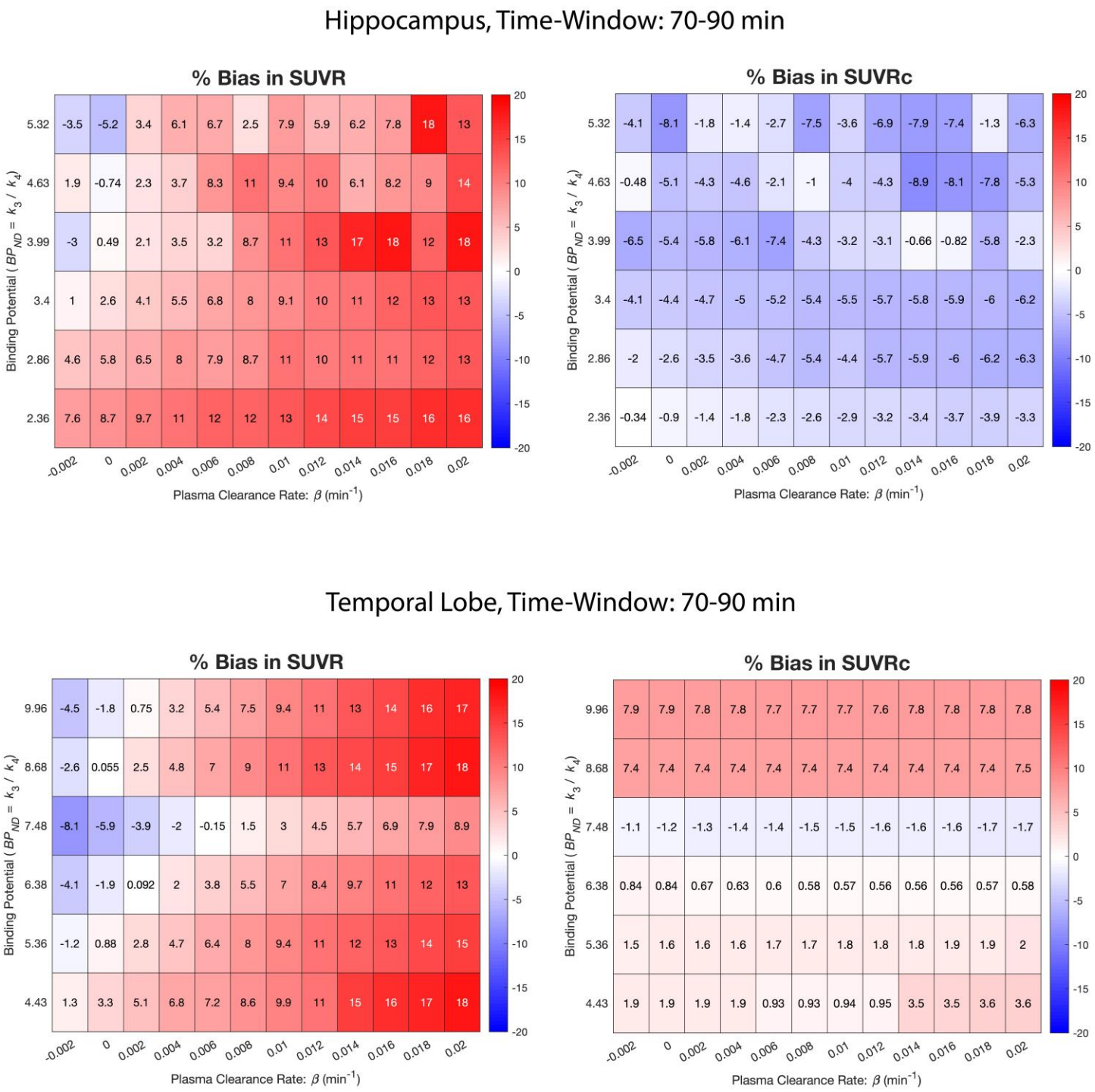

Fig 2: Heatmaps quantifying the bias in *SUVR* (left column) and corrected *SUVR* (right column) for the hippocampus (top) and temporal lobe (bottom). The simulations were performed over varying levels of tracer clearance rate in plasma during *SUVR* time window (β, x-axis) and binding potential levels (BP_{ND}, y-axis).

Cohen's *d* of group differences between cohorts of baseline tau binders (*SUVR* Time Window: 110-130 min) and high tau binders (*SUVR* Time Window: 70-90 min)

Temporal Lobe

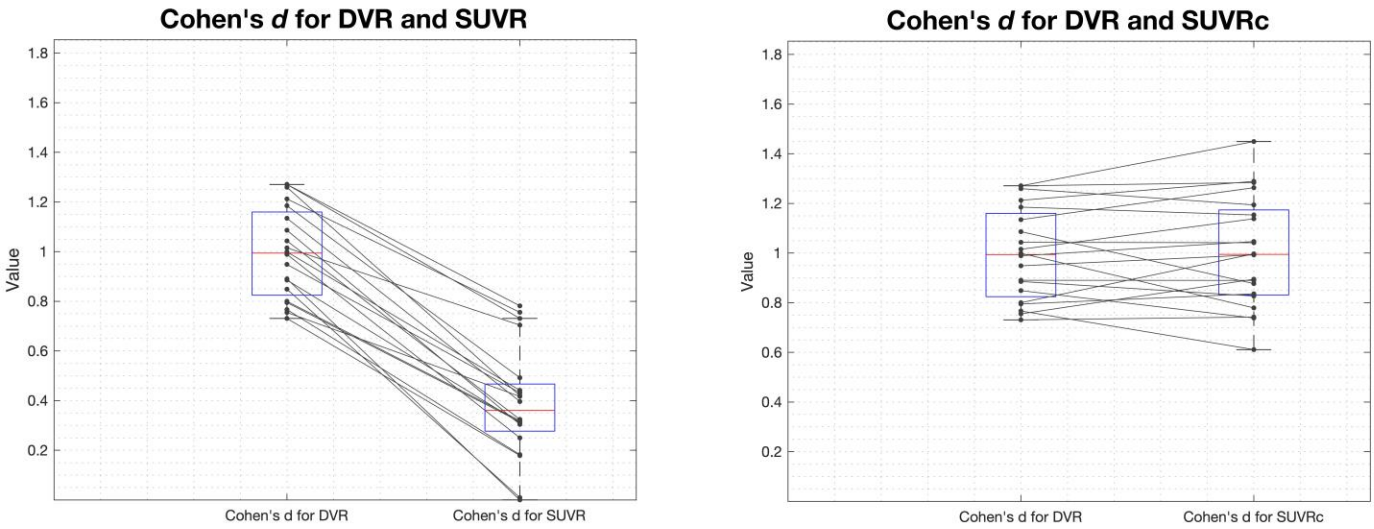

Hippocampus

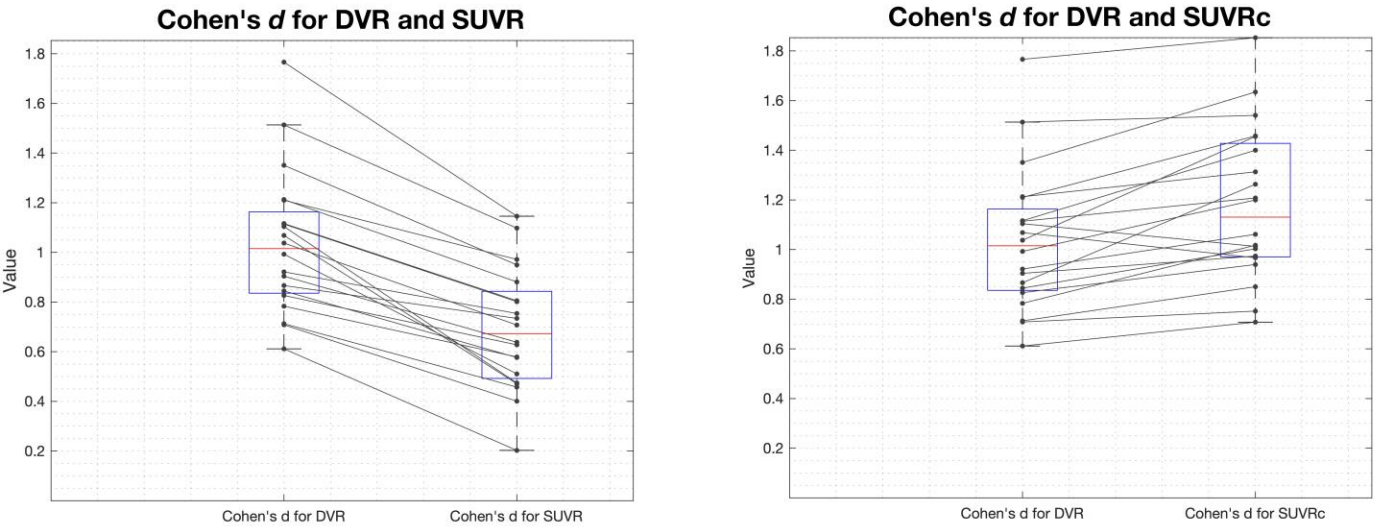

Fig 3: Simulations (20 replicates) showing Cohen's *d* effect size measure for SRTM2 *DVR* (gold standard), *SUVR* and corrected *SUVR* in the temporal lobe (top) and hippocampus (bottom). Cohen's *d* was computed across baseline (based on Guehl et al. [2], n=36 per replicate, *SUVR* time-window: 110-130 min) and high-tau (n=36 per replicate, *SUVR* time-window: 70-90 min) binders. Results show that the effect sizes are much lesser for *SUVR* but can be recovered by using corrected *SUVR*.

Keywords: SUVR bias, Tau PET quantification, Semi-Quantitative PET, [18F]MK6240, Tissue Clearance Correction

Farrell, Michelle

PET Spatial extent as a sensitive beta-amyloid biomarker in preclinical Alzheimer's disease

Michelle E. Farrell[1], Emma Thibault[1], J. Alex Becker[1], Julie C. Price[1], Bernard J. Hanseeuw[1,3], Rachel F. Buckley[1,2,4], Heidi I.L. Jacobs[1], Charles Chen[1], Reisa A. Sperling[1,2], Keith A. Johnson[1,2]

[1]*Massachusetts General Hospital, Harvard Medical School, Boston, MA, United States*
[2]*Brigham & Women's Hospital, Harvard Medical School, Boston, MA, United States*
[3]*Cliniques Universitaires Saint-Luc, Université Catholique de Louvain, Brussels, Belgium*
[4]*Florey institute of Neuroscience and Mental Health, Melbourne, Australia*

Background: Recent anti-Aβ trials suggest that intervention may be most successful when applied early in preclinical AD, when Aβ is spreading but tau pathology remains limited. Since Aβ is often not yet widespread throughout the neocortex during this early stage, standard Aβ-PET measures of average neocortical burden may be suboptimal. We developed a spatial extent-based Aβ-PET metric to sensitively measure spreading Aβ and tested its meaningfulness in preclinical AD for predicting Aβ-related tau proliferation and cognitive decline.

Methods: We included 261 clinically-normal older adults from the Harvard Aging Brain Study (HABS) with longitudinal Pittsburgh Compound-B (PIB)-PET, cognition, and flortaucipir (FTP)-PET. Neocortical (NEO) Aβ was quantified using average DVR (AVG) and spatial extent (EXT), the proportion of NEO with elevated PIB (Figure1). We evaluated the relationship between AVG and EXT and used linear mixed-effects models to assess each metric's prediction of future change in cognition (Preclinical Alzheimer's Cognitive Composite: PACC) and tau proliferation (FTP SUVR) in the medial temporal lobe (MTL) and temporal neocortex (TEMP).

Results: EXT began rising above its detection threshold (Figure2) before AVG, and identified which AVG- participants would become AVG+ in the next 5 years with 95% sensitivity and 99% specificity. Elevated PIB was detected throughout the neocortex (widespread EXT) at moderate AVG (1.44DVR/62CL), resulting in the classification of 3 phases (Figure2B): EXT-, EXT+ (spreading Aβ) and EXT++ (widespread Aβ). Baseline EXT was a stronger predictor of change in PACC and both MTL and TEMP FTP SUVR than AVG (Figure3A), with differences from EXT- detected in both EXT+ and EXT++ individuals (Figure3).

Conclusion: Our spatial extent-based metric was more sensitive to early Aβ deposits and may be more salient to Aβ's role in preclinical AD than a conventional neocortical average. While replication is needed, the spreading EXT+ phase may be an ideal target for prevention trials.

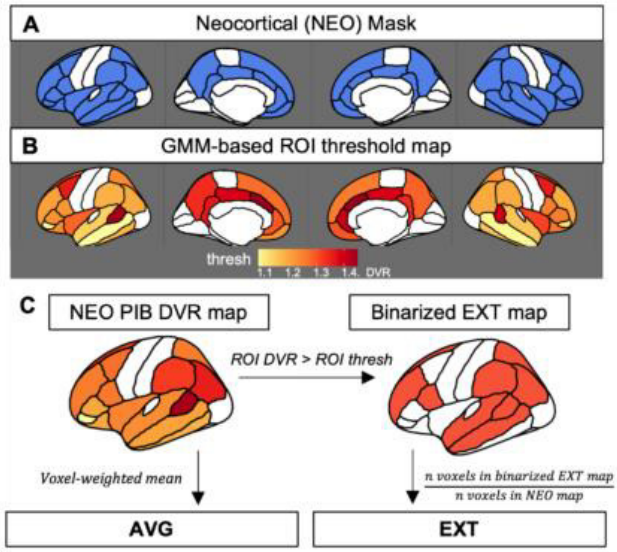

Figure 1. Approach. A) AVG and EXT metrics were computed within a set of Desikan-Killiany neocortical ROIs typically used for measures of global Aβ burden. B) We derived separate signal-to-noise thresholds for Aβ positivity in each ROI using gaussian mixture modeling. C) The 42 Desikan-Killiany atlas ROIs in the NEO aggregate vary greatly in size (~60-2000 voxels), so computation of both AVG and EXT were weighted by the number of voxels in each ROI. For AVG, the voxel-weighted average is computationally the same as computing the average DVR across the NEO mask, as is conventional. EXT was computed as the total number of voxels in ROIs above their own threshold, divided by the total number of voxels in the NEO mask. EXT therefore provides a measure of the proportion of the neocortex with elevated PIB signal.

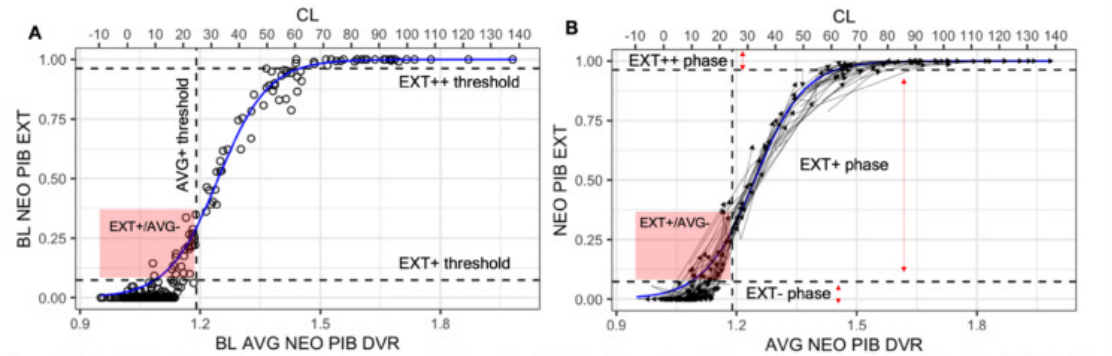

Figure 2. AVG vs EXT as Aβ metrics. The relationship between AVG (x-axis) and EXT (y-axis) are shown both cross-sectionally at baseline (A) and longitudinally (B). The AVG detection threshold is represented with the dashed vertical line at 1.19DVR/24CL. The detection threshold for EXT (EXT+ threshold), lower dashed horizontal line) was set at 7.3% EXT, derived longitudinally as the point beyond which EXT continued increasing, with no negative slopes regressing back towards EXT=0. Individuals were considered EXT- below 7.3%, representing either no Aβ or insufficient Aβ to differentiate from random PIB elevations due to noise. A total of 26 individuals were EXT+/AVG- at baseline (red box), suggesting EXT allows for detection of Aβ before AVG. Longitudinal PIB data was available in 20 EXT+/AVG- participants, and all 20 continued increasing in EXT and AVG, with 19/20 (95%) reaching AVG+ within the next five years. This provides confirmation that EXT reliably detects early Aβ below traditional AVG PET thresholds. The second dashed horizontal line (EXT++ threshold, EXT= 96.3%) represents when individuals reach widespread NEO Aβ, derived longitudinally as the the point beyond EXT change over time was no longer significant (p>.05). On average, individuals reached widespread EXT++ at 1.44DVR/62CL, after which AVG continued increasing. These thresholds were used to define three stages of neocortical amyloidosis: EXT- , EXT+ (spreading phase), EXT++ (widespread phase). EXT and AVG burden were highly correlated in the EXT+ phase (r=.97,p,<.001), suggesting low to moderate AVG burden is primarily a reflection of how far Aβ has spread while higher burden reflects a combination of widespread EXT and increasing concentration.

A

Outcome	metric	β	SE	t	p	η^2
PACC	EXT	-0.073	0.008	-8.788	<.001	.26
	AVG	-0.069	0.008	-8.430	<.001	.24
MTL	EXT	0.010	0.003	3.318	0.001	.09
	AVG	0.007	0.003	2.477	0.015	.05
TEMP	EXT	0.016	0.003	6.019	<.001	.29
	AVG	0.013	0.003	4.799	<.001	.18

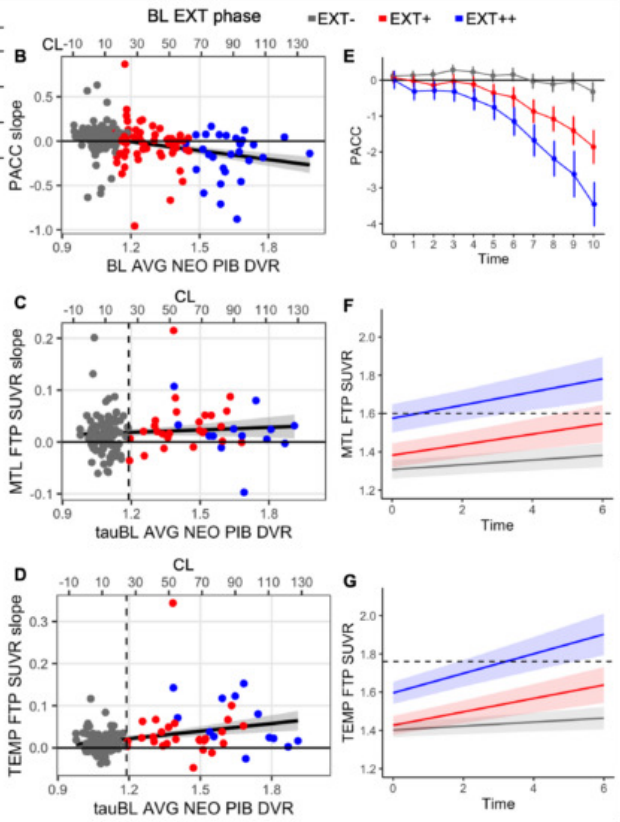

Figure 3. Baseline Aβ EXT vs. AVG as predictors of future change in cognition and tau. A) Linear mixed effect models results are tabulating testing baseline AVG and EXT as predictors of PACC, MTL FTP SUVR and TEMP FTP SUVR over time. All models include baseline age, sex, education, age*time as covariates and the random intercept and slope. AVG and EXT were standardized relative to their own baseline distribution (mean, standard deviation) to allow for comparison of *β* and *SE* estimates, but partial η^2 provides directly comparable effect sizes. EXT had a larger effect size than AVG for all three outcomes, but the largest improvement was for TEMP FTP SUVR. B-E) To demonstrate why the effect size of the association between continuous baseline EXT and change over time in PACC and MTL/TEMP FTP SUVR was higher than with AVG despite hitting ceiling at moderate AVG burden, scatterplots are shown depicting the association between the magnitude of baseline AVG burden and extracted slopes for PACC (B), MTL FTP SUVR (C), and TEMP FTP SUVR (D) with points colored by baseline EXT phase. While each outcome changed in conjunction with EXT phase (also shown in E-G), there was no association between the magnitude of AVG burden and cognitive decline/tau proliferation once individuals reached widespread Aβ in the EXT++ phase. E-G) Estimated marginal means for the average HABS participant (73.7 year old male with 15.8 years of education) are shown from LME models using baseline EXT phase rather than continuous EXT for each outcome measure. E) While PACC decline was strongest in EXT++ participants and EXT+ participants after 5 years, a more subtle difference between the EXT+ and EXT- groups was detectable after 2 years of follow-up. The EXT- group exhibited a practice effect, while the EXT+ did not show any increase in PACC performance at follow-up due to prior exposure. This is consistent with prior evidence that emerging Aβ impairs learning and demonstrates that prevention trials targeting early Aβ in EXT+ individuals may still be able to observe treatment effects on cognition over a reasonably short trial interval. F,G) The EXT+ and EXT++ group exhibited significant increases in MTL and TEMP FTP SUVR relative to the EXT- group but at changed at a similar rate. EXT+ and EXT++ groups instead differed in their tau level at baseline, with EXT++ individuals already exhibiting higher tau.

Keywords: early detection, prevention, tau, cognition, subthreshold

Optimizing the detection of whole-brain tau-related cognitive decline in mild cognitive impairment

Frédéric St-Onge[1,2], Alexa Pichet Binette[3], Marianne Chapleau[4], John CS Breitner[2,5], Sylvia Villeneuve[2,5,6]

[1]*Integrated Program in Neuroscience, Faculty of medicine, McGill University, Montreal, QC, Canada*
[2]*Research Center of the Douglas Mental Health University Institute, Montreal, QC, Canada*
[3]*Clinical Memory Research Unit, Department of Clinical Sciences, Lund, Sweden*
[4]*Faculty of medicine, University of California San Francisco, San Francisco, CA, United States*
[5]*Department of Psychiatry, Faculty of medicine, McGill University, Montreal, QC, Canada*
[6]*McConnell Brain Imaging Centre, Montreal Neurological Institute, Montreal, QC, Canada*

Background: Mild cognitive impairment (MCI) represents a critical stage in the clinical development of Alzheimer's disease (AD). At this point, tau pathology is often apparent in brain regions outside the medial temporal lobe. Yet, studies associating cognition and tau pathology are often restricted to regional measures like a temporal meta-ROI. As an alternative, we examined two different regional threshold methods and their association with cognitive impairment.

Methods: We investigated 132 Aβ+ ADNI participants with MCI having at least one Aβ and one tau-PET scan. We graded whole-brain tau deposition using spatial extent indices (SEIs) that counted the number of brain regions with tau deposition that exceeded specific thresholds. We compared two thresholding methods: Gaussian Mixture Models (GMM) based on the full ADNI cohort (n=832) or >2 SD from cognitively unimpaired (CU) Aβ- participants (Fig.1). Using four composite measures of performance and decline in memory, executive performance, language and visuospatial abilities, we also compared the gain in variance explained by each SEI method against a classical temporal meta-ROI.

Results: Thresholds derived from CU Aβ- participants were more strongly associated than GMM thresholds with outliers in the distribution of tau SUVR (Fig 1). However, the GMM SEI explained more variance in executive functioning performance both at baseline ($Z = -3.105$, $p < 0.001$) and decline ($Z = -1.701$, $p = 0.04$); and also in language performance at baseline ($Z = -1.795$, $p = 0.04$) (Fig 2) compared to the temporal meta-ROI. The SEI derived from CU Aβ- participants did not explain more variance than the GMM-SEI.

Conclusions: Multi-domain deficits in MCI occur with tau spreading outside of the temporal lobe. Shifting away from continuous temporal meta-ROI and CU Ab- threshold methods for GMM-based spatial extent index approaches could help optimize the detection of cognitive deficits in MCI.

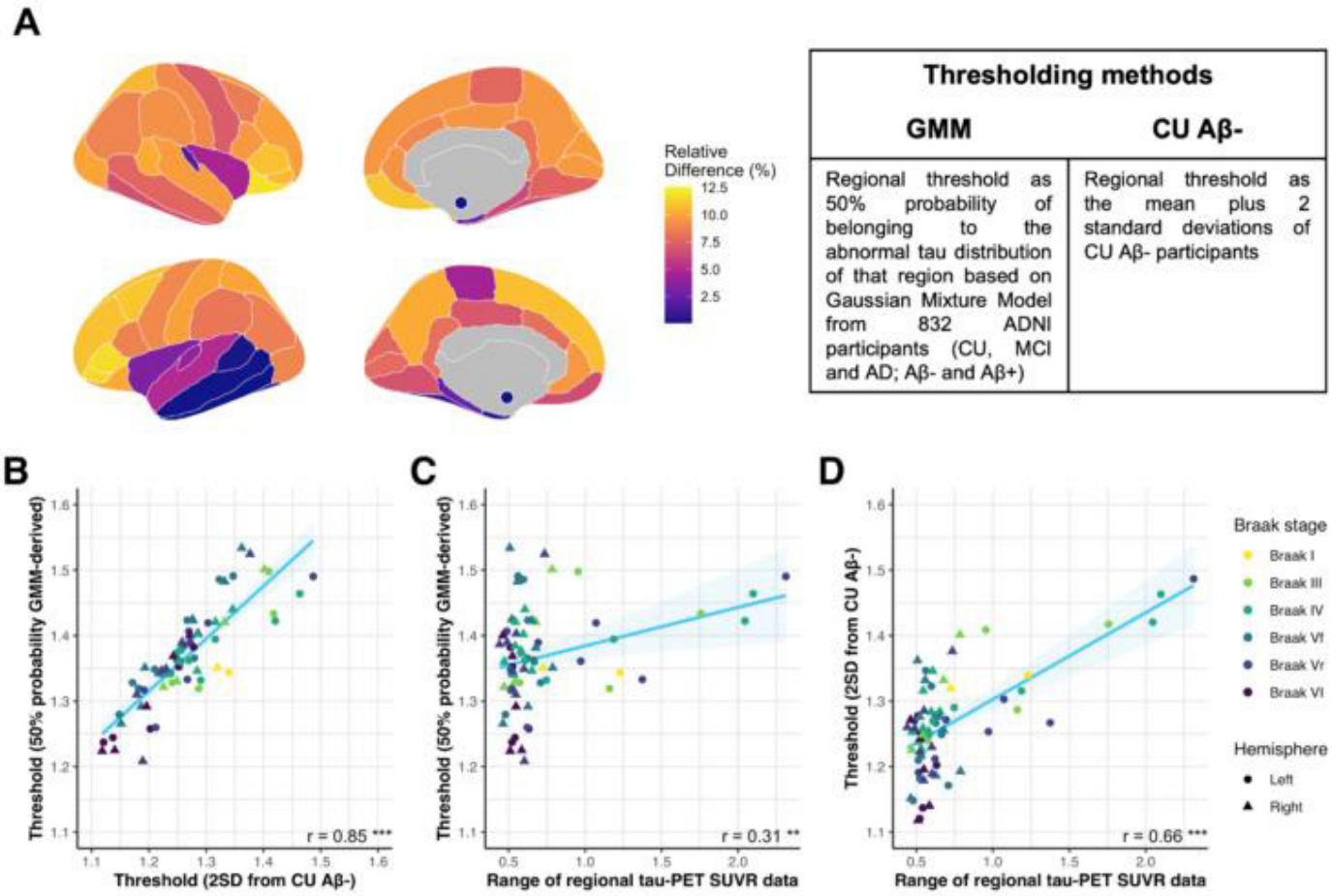

Figure 1 – Comparison of spatial extent approaches. *A) The percent difference in thresholds for tau-PET positivity across brain regions derived from applying GMM on the whole ADNI sample or by a criterion of > 2SD from the mean of CU Aβ- participants. Thresholds from the GMM approach averaged 0.10 SUVR higher than the 2SD method. The small sphere in the medial view of the brain represents the amygdala. B) Correlation between thresholds from the GMM and the 2SD CU Aβ- methods. C) Correlation between the regional thresholds derived from the GMM and the range (max-min) of SUVR values in all regions. D) Correlation between the regional thresholds derived from the 2SD CU Aβ- method and the range (min-max) of SUVR values in all regions. In all three panels, each point corresponds to a brain region, with the colour representing their Braak stage and the shape, the left or the right hemisphere (** : P < 0.01, *** P < 0.001).*

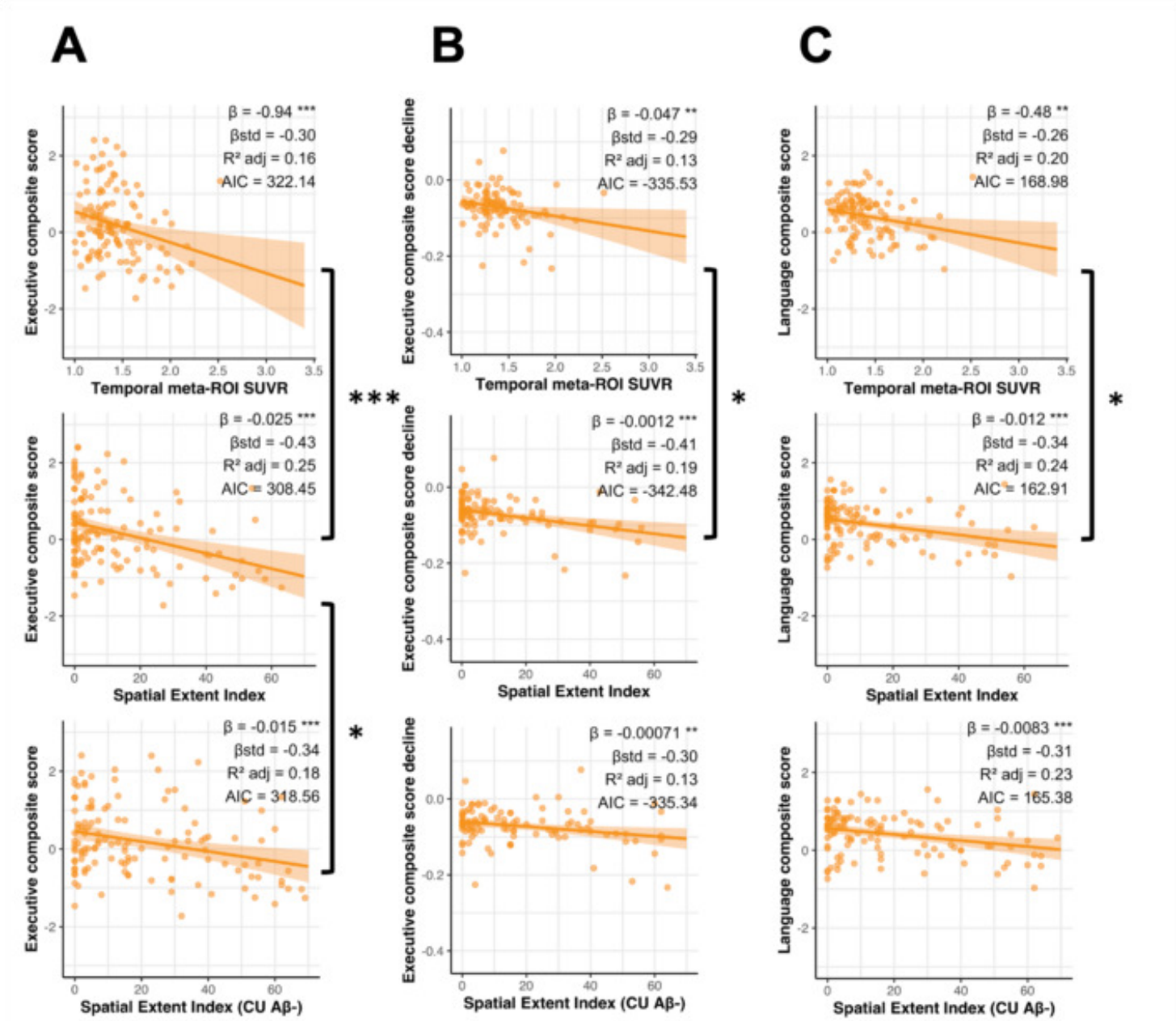

Figure 2 – Comparison of tau quantification approaches on association with cognition. *Association between temporal meta-ROI SUVR (top row), spatial extent index derived from GMM (middle row) and spatial extent index derived from CU Aβ- thresholds (bottom row) with (A) Executive composite at baseline, (B) Executive composite score decline and (C) Language composite score at baseline. Simple and standardized β coefficients, adjusted R^2 and AIC, controlled for age sex and education, are shown on the graphs. The P-value of models are indicated next to the simple beta coefficients. (** : P < 0.01, *** P < 0.001) Results remained significant after a multiple comparison false discovery rate (FDR) correction.*

Keywords: Tau-PET, whole-brain, Mild cognitive impairment, cognitive impairment

KEYNOTE: Targets and radioligands for PET imaging of neuroinflammation

Paolo Zanotti-Fregonara

NIH, Bethesda, MD, United States

This methodological talk will provide an overview of some of the most commonly used PET radioligands to image neuroinflammation, and the challenges associated with their use. The 18-kDa Translocator (TSPO) protein has been synonymous with imaging inflammation for decades.

TSPO expression is associated with activated microglia but is also present in activated astrocytes and endothelial cells. One of the main challenges in TSPO imaging is the presence of the rs6971 polymorphism. This polymorphism causes a single amino acid substitution in the TSPO protein, which affects the binding affinity of the radioligands. Consequently, inter-subject comparisons in PET studies cannot assume that binding affinity is consistent across all subjects. Efforts are underway to synthesize radioligands that are insensitive to the rs6971 polymorphism.

Cyclooxygenase-1 and 2 (COX-1 and COX-2) are enzymes involved in the production of prostaglandins, which play a role in inflammation. While COX-1 is constitutively expressed in the brain, COX-2 is induced by inflammatory stimuli. This talk will present two new radioligands for COX-1 and COX-2 developed at the NIH, and their initial validation in humans.

Paolo Zanotti Fregonara, MD, PhD, is a nuclear medicine physician who works as a Staff Scientist in the Molecular Imaging Branch of the National Institute of Mental Health in Bethesda, Maryland.

Dr. Zanotti earned his MD degree from the University of Milan, Italy, and his PhD from the University of Paris, France. He has held clinical and academic positions in France and in the United States, as an Assistant and Associate Professor of Biophysics and Nuclear Medicine at the Universities of Paris and Bordeaux, and as the Director of the PET core at Houston Methodist Research Institute in Houston, Texas.

Dr. Zanotti specializes in PET kinetic modeling and dosimetry.

His kinetic modeling research focuses on the validation of new radioligands using animal models, in healthy volunteers, and in patients with brain or peripheral diseases. In particular, he has worked on the initial validation of inflammation radioligands for various targets such as TSPO, COX-1, and COX-2, the methodology for radioligand quantification, and subsequent clinical application in patients with neuropsychiatric diseases.

In dosimetry, his work led to the establishment of new standard values for fetal 18F-FDG dosimetry.

Wednesday, January 17, 2024 - 10:25 am - 10:55 am

Break/Poster Session

Board #	Poster Title	Authors	Presenter
01	Longitudinal synaptic loss follows tau PET Braak staging in vivo and supports local neurodegeneration by tau accumulation in stages III-VI	Vanderlinden | Koole | Vandenbulcke | Van Laere	**Vanderlinden, Greet**
02	Plasma Aβ42/40 ratio, GFAP, and NfL across the neurodegenerative diseases: cross-sectional and longitudinal study in a large multi-center cohort	Jang | Kim | Shin | Yoo | Lee | Yun | Na | Kim | Blennow | Zetterberg | Seo	**Jang, Hyemin**
03	Publicly Available Software and FTP calibration data for CenTauR tau PET standardization	Schwarz | Przybelski | Prakaashana | Doré | Villemagne | Leuzy | Senjem | Lowe | Gunter | Kantarci | Vemuri | Graff-Radford | Petersen | Knopman | Jack	**Schwarz, Christopher**
04	The Impact of Metabolic Health on the relationship of Obesity with and Alzheimer's and Vascular Markers	LEE | Yoo | Kim | Cheon | Kwak | Kim | Ryu | Chang | Jang | Kim | Kim | Na | Kang | Seo	**Lee, Eun Hye**
05	Distinct effects of cholesterol profile components on Amyloid and Vascular burdens	Kang | Yoo | Kim | Seo	**Kang, Sung Hoon**
06	Amyloid pet positivity in Korean Dementia Syndromes: In Relation to Diagnosis, age, and Apoe Genotypes	Chun | Jang | Yun | Kim | Woo | Seo	**Chun, Min Young**
07	Toward more representative estimates of the effect of tau on cognition	Shaaban | Wu | Kunicki | Chasioti | Tommet | Rich | Oh | Karikari | Cohen | Lopresti | Villemagne | Glymour | Jones	**Shaaban, C. Elizabeth**
08	Examination of synaptic density and neurofibrillary tau tangle burden in cognitively unimpaired and impaired older adults	DiFilippo | Jonaitis | Ennis | McLachlan | McVea | Bettcher | Pasquesi | Davenport-Sis | Schulz | Thor | Grover | Barnhart | Engle | Betthauser | Johnson | Bendlin | Christian	**DiFilippo, Alexandra**
09	Association between Plasma P-tau and Cognition in the Alzheimer's Disease Spectrum	Fernandez | Therriault | Macedo | Servaes | Wang | Rahmouni | Aumont | Hosseini | Tissot | Mathotaarachchi | Stevenson | Stevenson | Pascoal | Ashton | Lessa | Karikari | Triana-Baltzer | Kolb | Zetterberg | Blennow | Rosa-Neto	**Fernandez, Jaime**

Board #	Poster Title	Authors	Presenter
10	The Role of Biofluid Markers in Predicting Near-term Cognitive Impairmen	Yakoub | Ashton | Karikari | Strikwerda-Brown | St-Onge | Ourry | Schöll | Geddes | Ducharme | Rosa-Neto | Soucy | Breitner | Zetterberg | Blennow | Poirier | Villeneuve | Prevent-AD research group	**Villeneuve, Sylvia**
11	Factors explaining tau onset age and time from tau onset to dementia	Heston | Teague | Ruiz de Chavez | Morse | Deming | Cody | Langhough | Zuelsdorff | Betthauser	**Heston, Margo**
12	Evaluation of ComBat as a harmonization technique for reducing across-tracer variance in regional amyloid PET analyses	Yang | Earnest | Kumar | Gordon | Sotiras	**Yang, Braden**
13	Neurophysiological changes related to Amyloid and Tau Pathology are associated with Longitudinal Cognition and Mild Cognitive Impairment Progression	Gallego Rudolf | Wiesman | Baillet | Villeneuve	**Gallego Rudolf, Jonathan**
14	Tau and Amyloid associations with sustained attention and episodic memory performance in clinically unimpaired older adults	Romero | Winer | Tran | Rathmann-Bloch | Park | Schwartz | Miller | Anders | Morales | Wilson | Trelle | Andreasson | Davidzon | Mormino | Wagner	**Romero, America**
15	Sex differences in the relationships between 24-h rest-activity patterns and plasma markers of Alzheimer's disease pathology	Van Egroo | Beckers | Ashton | Blennow | Zetterberg | Jacobs	**Van Egroo, Maxime**
16	NODDI-derived measures of microstructural integrity in medial temporal lobe white matter pathways are associated with Alzheimer's disease pathology	Parker | Adams | Kim | McMillan | Yassa	**Parker, Dana**
17	Longitudinal hippocampal volume trajectories and their relationships with β-amyloid, tau, cerebrovascular, and cognition in a baseline cognitively unimpaired sample	Du | Betthauser | Jonaitis | Stephenson | Hermann | Rivera | Larget | Chappell | Cadman | Rowley | Eisenmenger | Johnson | Langhough	**Du, Lianlian**
18	Beyond Quantity: fill states as a biomarker for the degree of pathology and neurodegeneration across the Alzheimer's disease continuum	Doering | Hoenig | Giehl | Andrassy | Bader | Bauer | Dzialas | Elmenhorst | Emert | Frensch | Jäger | Jessen | Krapf | Kroll | Lerche | Lothmann | Matusch | Neumaier | Onur | Ramirez | Richter | Sand | Tellmann | Theis | Zeyen | van Eimeren | Drzezga | Bischof	**Bischof, Gerard**

Board #	Poster Title	Authors	Presenter
19	Successful aging reflects anterior cingulate preservation but not tau accumulation rate	Pezzoli | Giorgio | Chen | Harrison | Jagust	**Pezzoli, Stefania**
21	Distinct microbial species less abundant in Alzheimer's disease patients associate negatively with cerebrospinal fluid biomarkers of Alzheimer's disease	Kang | Khatib | Dilmore | Heston | Ulland | Johnson | Asthana | Carlsson | Chin | Blennow | Zetterberg | Knight | Kaddurah-Daouk | Rey | Bendlin	**Kang, Jea Woo**
22	Amyloid quantification is dependent on scanner: a head-to-head comparison of 18F-NAV4694 Centiloid measurements between three PET/CT scanners	Gillman | Bourgeat | Cox | Li | Villemagne | Fripp | O'Keefe | Huang | Krishnadas | Feizpour | Williams | Bozinovski | Rowe | Doré	**Gillman, Ashley**
23	Neuroinflammation follows and outstrips tau progression patterns in primary 4R tauopathies	Malpetti | Römer | Harris | Gross | Gnörich | Stephens | Mueller | Koglin | Levin | Höglinger | Brendel | Franzmeier	**Malpetti, Maura**
24	Relationship between enlarged perivascular space and beta-amyloid deposition among cognitively normal ADNI participants	Kim | Hudson | Yuan | Lipford | Lyu | Whitlow	**Kim, Jeongchul**
25	Examining inter- and intra-subject variability in digital clock drawing test performance in cognitively normal older adults	Rodríguez Alonso | Fu | Robinson | Francis Malave | Jutten | Del Carmen Montenegro | Thibault | Penney | Davis | Sperling | Price | Rentz | Johnson	**Rodríguez Alonso, Marina**
26	Evaluating bidirectional effects of amyloid and tau on functional brain networks in preclinical Alzheimer's disease	Millar | Singhe | Macharia | Metcalf | Roman | Morris | Benzinger | Gordon | Ances	**Millar, Peter**
27	Tau propagates along principal axes of functional and structural brain organization in Alzheimer's disease	Ottoy | Tan | Kang | Bezgin | Lussier | Pascoal | Rahmouni | Stevenson | Soucy | Gauthier | Bernhardt | Black | Rosa-Neto | Goubran	**Ottoy, Julie**
28	X-ray based amyloid index as a quantitative biomarker for neurodegenerative diseases	Suresh | Dahal | Badano	**Suresh, Karthika**
29	An artificial neural network for PET brain amyloid imaging	Georgiou | Zhao | Deana | Sfakianaki | Curiel Cid | Loewenstein	**Georgiou, Mike**
30	Predicting regional tau burden using structural connectivity from individualized epicenters	Brown | Das | Nasrallah | Detre | Yushkevich | McMillan | Wolk	**Brown, Christopher**

Board #	Poster Title	Authors	Presenter
31	Microglia density across different clinical Alzheimer's disease variants	Lao | Johnson | Smith | Guzman | Okafor | Houlihan | Heuer | Rossano | Talmasov | Chikwem | Dass | Noble | Kreisl | De Jager | Small	**Lao, Patrick**
32	The TSPO circadian pattern: a [11C]ER176 test-retest study	Finn | Zanotti Fregonara | Appleton | Yu | Fujita | Masdeu | Pascual	**Finn, Quentin**
33	Tau PET signal within the default mode network predicts longitudinal clinical decline in atypical early Alzheimer's disease	Katsumi | Howe | Eckbo | Wong | Quimby | Hochberg | McGinnis | Putcha | Touroutoglou | Dickerson	**Katsumi, Yuta**
34	Reduced coupling between cerebrospinal fluid flow and global brain activity is linked to cortical tau and atrophy	Han | Lee | Chen | Ziontz | Ward | Landau | Baker | Harrison | Jagust	**Han, Feng**
35	Cognitive decline and Alzheimer's disease clinical status in Down syndrome are better distinguished by amyloid and neurofibrillary tau compared to age	Zammit | Schworer | Betthauser | Hartley | Laymon | Tudorascu | Cohen | Johnson | Converse | Minhas | Zaman | Ances | Mathis | Klunk | Handen | Christian | Alzheimer's Biomarker Consortium - Down Syndrome	**Zammit, Matt**
36	Early Aβ and tau-seeded functional networks derived in young adults reflect patterns of tau deposition and accumulation	Fonseca | Harrison | Chadwick | Ziontz | Baker | Jagust	**Fonseca, Corrina**
37	Gray matter GABA and Glutamate reflect amyloid beta burden in cognitively healthy individuals	Schreiner | Kirchner | Van Bergen | Gietl | Buck | Hock | Prüssmann | Henning | Unschuld	**Unschuld, Paul**
38	Amyloid PET scan reader agreement in IDEAS: expert readers vs local clinician readers	Windon | Siegel | Zeltzer | Hanna | Carrillo | Hillner, | Iaccarino | La Joie | March | Perez | Mundada | Arora | Buckley | Bullich | Sherwin | Gatsonis | Rabinovici	**Windon, Charles**
39	Validation of a novel visual read interpretation of flortaucipir PET for identification of participants with high tau burden: Results from I7E-AV-A26 reader study	Tunali | Iaccarino | Wang | Arora | Lu | Shcherbinin | Pontecorvo	**Tunali, Ilke**
40	Longitudinal multicenter head-to-head harmonization of tau-PET tracers: an overview of the HEAD study	Lussier | Silva do Amaral | Povala | Negrini | Pascual | Gordon | Lowe | Oh | Soleimani-Meigooni | Klunk | Tudorascu | Rosa-Neto | Baker | Pascoal	**Lussier, Firoza**

Board #	Poster Title	Authors	Presenter
41	Clinical phenotype and plasma biomarker associations of non-Alzheimer's hippocampal atrophy	Asken | Wang | McFarland | Barker | Adjouadi | Velez Uribe | Rosselli | Crocco | Armstrong | Curiel Cid | Vaillancourt | Loewenstein | Duara | Smith	**Asken, Breton**
42	Synaptic loss in relapsing and progressive multiple sclerosis: An in vivo exploratory study using SV2A-PET	Soleimani-Meigooni | Giorgio | Abdelhak | Cordano | Chen | Toueg | Weimer | Zinnhardt | Baker | Janabi | Green | Jagust | Rabinovici	**Soleimani-Meigooni, David**
43	[18F]-PI-2620 tau PET signal across the aging and Alzheimer's Disease clinical spectrum	Young | Vossler | Romero | Smith | Park | Trelle | Winer | Wilson | Zeineh | Sha | Khalighi | Morales | Anders | Zaharchuk | Henderson | Andreasson | Wagner | Poston | Davidzon | Mormino	**Young, Christina**
44	Amyloid-induced hyperconnectivity drives tau spreading across connected brain regions in Alzheimer's disease	Roemer | Wagner | Steward | Biel | Dewenter | Dennecke | Gross | Zhu | Zheng | Dehsarvi | Dichgans | Ewers | Brendel | Franzmeier	**Roemer, Sebastian Niclas**
45	A Visual-read Algorithm for Tau Pathology using [18F]RO948	Smith | Garibotto | Hägerström | Jögi | Ohlsson | Tonietto | Janelidze | Stomrud | Klein | Hansson	**Smith, Ruben**
46	Establishing the interchangeability between CSF and PET for identifying patients with Alzheimer's disease pathology who are suitable for amyloid targeting therapies	Burnham | K Arora | Iaccarino | Kennedy | Kotari | Wijayawardana | Lu | Pontecorvo | Quevenco | Dell' Agnello | Neff | Petronzi | Viollet | Wang	**Burnham, Samantha**
47	Exploring A-T+ within the AT(N) framework	Lopresti | Cohen | Gogola | Ikonomovic | Snitz | Mason | Minhas | Matan | McGeown | Cieply | Chiang | Pascoal | Reese | Matela | Karikari | Sweet | Berman | Kofler | Lopez | Villemagne	**Lopresti, Brian**
48	Sex-specific synergistic interaction between Aβ and p-tau predicts faster tangle accumulation in females	Wang | Therriault | Servaes | Tissot | Rahmouni | Macedo | Fernandez-Arias | Mathotaarachchi | Benedet | Stevenson | Ashton | Lussier | Pascoal | Zetterberg | Rajah | Blennow | Gauthier | Rosa-Neto	**Wang, Yi-Ting**
49	Comparison of visual interpretation and quantitation in detecting amyloid pathology using florbetapir F-18 PET imaging: Results from nuclear medicine physicians or radiologists practicing at community healthcare settings	Wang | Lu | Iaccarino | Arora | Morris | Kim | Kennedy | Kotari | Burnham | collins | Pontecorvo	**Wang, Jian**

Board #	Poster Title	Authors	Presenter
50	Parental history of memory impairment predicts β-amyloid burden and positivity in a preclinical population	Seto | Hohman | Mormino | Papp | Amariglio | Rentz | Johnson | Schultz | Sperling | Buckley | Yang	**Seto, Mabel**
51	A head-to-head comparison between plasma p-tau217 and tau-PET for predicting future cognitive decline among cognitively unimpaired individuals	Ossenkoppele | Salvado | Pichet-Binette | Therriault | Jonaitis | Bourgeat | Doré | Masters | Johnson | Villeneuve | Rosa-Neto | Rowe | Hansson	**Ossenkoppele, Rik**
52	Comparison of amyloid PET and plasma biomarkers in predicting future memory decline among cognitively normal individuals	Bilgel | An | Walker | Moghekar | Ashton | Kac | Karikari | Blennow | Zetterberg | Thambisetty | Resnick	**Bilgel, Murat**
53	Confocal Microscopy Assessment of Flortaucipir Binding by a Fluorescence Analog Compound T726 Shows 4RT Overlap in Frontotemporal Lobar Degeneration	Gatto | Youssef | Reichard | Whitwell | Josephs	**Gatto, Rodolfo**
54	Correlative Histopathological Evaluation of Basal Ganglia Iron Deposition and Tau and PiB Positron Emission Tomography in Alzheimer's Disease and Frontotemporal Lobar Degeneration	Gatto | Carlos | Reichard | Lowe | Whitwell | Josephs	**Gatto, Rodolfo**
55	Unraveling alzheimer's disease heterogeneity: a comparative analysis using hydra and chimera	An | Sotiras | Gordon	**An, Zhaoqi**
56	Prevalence of Alzheimer's disease pathology in studies of memory and aging	McKay | Millar | Barthelémy | Benzinger | Morris | Bateman | Schindler | Gordon	**McKay, Nicole**
57	Depression in amyloid-positive individuals is associated with a faster rate of tau accumulation on longitudinal positron-emission tomography	Talmasov | Johnson | Lao | Marder | Miller	**Talmasov, Daniel**
58	Chronic neuroinflammation in older adults with persistent Long COVID: the preliminary findings of [18F]FEPPA PET imaging	Kim | Taboada | Liu | Maciarz | Armstrong | Palekar | Weisenbach	**Kim, Min-Jeong**
59	PET staging of tauopathy using amygdala	Hanseeuw | Rubinstein | Schultz | Buckley | Properzi | Farrell | Gatchel | Amariglio | Beiser |	**Hanseeuw, Bernard**

Board #	Poster Title	Authors	Presenter
		Seshadri | Marshall | Sperling | Jacobs | Johnson	
60	Discovery and optimization of [18F]ACI-15916, a promising PET tracer for the diagnosis of Parkinson's disease and other a-synucleinopathies	Vokali | Molette | Ravache | Delgado | Kocher | Pittet | Vallet | Luthi-Carter | Pfeifer | Kosco-Vilbois | Capotosti	**Vokali, Efthymia**
61	Clinical relevance of visually positive amyloid-PET burden in the occipital lobe	Collij | Smith | Palmqvist | Strandberg | Ossenkoppele | Hansson	**Collij, Lyduine**
62	Tau-PET subtypes show distinct profiles of cerebrospinal fluid biomarkers, neurodegeneration, and cognition in a large single-site cohort	Collij | Mastenbroek | Pichet Binette | Smith | Palmqvist | Mattsson-Carlgren | Strandberg | Ossenkoppele | Vogel | Hansson	**Collij, Lyduine**
63	ER176 neuroinflammatory PET profiles and relationships with flortaucipir tau PET in progressive apraxia of speech	Satoh | Utianski | Duffy | Clark | Botha | Lowe | Josephs | Whitwell	**Satoh, Ryota**
64	Aβ and tau associations with sex and affected parent's sex in preclinical Alzheimer's disease	Ourry | St-Onge | Mohammediyan | Yakoub | Soucy | Poirier | Breitner | Villeneuve	**Ourry, Valentin**
65	Differential association between plasma biomarkers and established biomarkers of Alzheimer's disease	Bluma | Chiotis | Bucci | Savitcheva | Matton | Kivipelto | Jeromin | De Santis | Di Molfetta | Ashton | Blennow | Zetterberg | Nordberg	**Bluma, Marina**
66	PiB PET demonstrates early, elevated amyloid striatal binding compared to florbetapir in Down syndrome	McLachlan | Rouanet | Garimella | Price | Tudorascu | Laymon | Keator | Kreisl | Klunk | Handen | Fryer | Zaman | Head | Mapstone | Bettcher | LeMerise | McVea | DiFillipo | Zammit | Hartley | Christian | Investigators	**McLachlan, Max**
67	Data-driven disease progression modelling consistently reveals an occipital amyloid-β subtype in two independent cohorts	Mastenbroek | Collij | Young | Vogel | Salvadó | den Braber | Visser | Gispert | van der Flier | Strandberg | Smith | Palmqvist | Mattson-Carlgren | Oxtoby | Barkhof | Ossenkoppele | Hansson	**Mastenbroek, Sophie**
68	Mid-life perceived discrimination and late-life Alzheimer's disease pathology and cognition in African American and non-Hispanic White populations	Royse | Snitz | Saeed | Reese | Lopresti | Karikari | Kamboh | Villemagne | Reis | Lopez | Cohen	**Royse, Sarah**

Board #	Poster Title	Authors	Presenter
69	Comparison of amyloid positivity and global cortical SUVR between black and white non-Hispanic participants in the GAP Bio-Hermes study	Wolz | Hughes | Manber | Mohs | Dwyer | Beauregard	**Wolz, Robin**
70	APOE, ABCA7, and KIF13B associations with earlier onset of amyloid positivity from over 4000 harmonized Positron Emission Tomography images	Castellano | Wang | Archer | Cody | Harrison | Wu | Durant | Janve | Engelman | Jagust | Albert | Johnson | Resnick | Sperling | Bigel | Saykin | Vardarajan | Mayeux | Betthauser | Dumitrescu | Mormino | Mormino | Hohman | Koran	**Castellano, Tonnar**
71	Neuroinflammation in patients with mild cognitive impairment and Alzheimer's Disease	Kandimalla | Lee | Min | Botha | Graff-Radford | Jones | Vemuri | Kantarci | Knopman | Jack | Petersen | Lowe	**Kandimalla, Mahathi**
73	Elevated amyloid-ß and tau burden is associated with accelerated cognitive decline on a digital clock drawing test in preclinical AD	Fu | Robinson | Rodriguez Alonso | Francis Malave | Jutten | Del Carmen Montenegro | Thibault | Penney | Davis | Sperling | Johnson | Price | Rentz	**Fu, Jessie Fanglu**
74	Significance of a positive tau PET scan with a negative amyloid PET scan	Robinson | Lee | Min | Przybelski | Josephs | Jones | Graff-Radford | Boeve | Knopman | Jack. Jr. | Petersen | Machulda | Fields | Lowe	**Robinson, Carling**
75	Lower Locus Coeruleus function in associated with greater cognitive variability in preclinical Alzheimer's disease	Juneau | Baillet | Wiklund | Riphagen | Prokopiou | Papp | Jutten | Rentz | Sperling | Johnson | Jacobs	**Juneau, Truley**
76	Associations between regional tau pathology and cognitive decline across the AD continuum differ by sex	Singleton | Mattsson-Carlgren | Pichet Binette | Stomrud | Strandberg | Ossenkoppele | Hansson	**Singleton, Ellen**
77	Dynamic brain states are associated with Alzheimer's pathology and cognition	Adams | Kark | Chappel-Farley | Escalante | Stith | Rapp | Yassa	**Adams, Jenna**
78	Imaging synaptic density across the Alzheimer's disease continuum with [18]F-SynVestT-1	Giorgio | Soleimani-Meigooni | Chen | Toueg | Weimer | Zinnhardt | Baker | Janabi | Rabinovici | Jagust	**Giorgio, Joseph**
79	Data-driven analysis of 10,361 amyloid-PET scans from the IDEAS study reveals two primary axes of variation	Giorgio | Mundada | Blazhenets | Mejia Perez | Schonhaut | Carrillo | Hanna | Gatsonis | March | Apgar | Siegel | Hillner | Whitmer | Jagust | Rabinovici | La Joie	**Giorgio, Joseph**

Board #	Poster Title	Authors	Presenter
80	Lower locus coeruleus structural integrity is associated with greater intraindividual cognitive variability in older individuals	Wiklund | Van Egroo | Juneau | Riphagen | Papp | Jutten | Rentz | Sperling | Johnson | Jacobs	**Wiklund, Emma**
81	Precuneus fMRI activity is associated with future Aβ burden in cognitively normal older APOE4 carriers	Maass | Molley | Binette | Vockert | Marquardt | Kreissl | Remz | Rajah | Villeneuve	**Maass, Anne**
82	PI-2620 binding in cognitively normal older adults including SuperAgers	Maass | Garcia-Garcia | Molley | Behrenbruch | Schuhmann-Werner | Vockert | Rullmann | Hochkeppler | Fischer | Svenja Schwarck | Baldauf | Schulze | Stephens | Patt | Barthel | Sabri | Duezel | Kreissl	**Maass, Anne**
83	Early phase Amyloid PET as a Surrogate Marker of Brain Metabolism in Cases of Cognitive Impairment	Aye | Melzer | Keenan | Croucher | Tippett | Anderson | Le Heron	**Aye, William**
84	Unlocking Tau PET Accessibility: a Machine Learning-based Prediction of Tau Pathology from Plasma, MRI and Clinical Variables	Karlsson | Vogel | Strandberg | Arvidsson | Åström | Seidlitz | Bethlehem | Stomrud | Ossenkoppele | Ashton | Blennow | Palmqvist | Smith | Janelidze | Pichet Binette | Mattson-Carlgren | Hansson	**Karlsson, Linda**
85	Amyloid and tau burden relate to longitudinal changes in performance of everyday activities as measured using the performance-based Harvard Automated Phone Task	Dubbelman | Diez Palacio | Gonzalez | Amariglio | Becker | Chhatwal | Gatchel | Johnson | Locascio | Udeogu | Wang | Papp | Properzi | Rentz | Schultz | Sperling | Vannini | Marshall	**Dubbelman, Mark**
86	In vivo structural integrity of the hypothalamus and the spatiotemporal evolution of Alzheimer's disease	Baillet | Betthauser | Salmon | Jacobs	**Baillet, Marion**
87	Cross-sectional comparison of extra-cerebral binding trends in [F-18]MK6240 PET images	McVea | DiFilippo | McLachlan | Betcher | Johnson | Betthauser | Christian	**McVea, Andrew**
88	Tau accumulation in Down Syndrome after onset of amyloid positivity	McVea | DiFilippo | Max McLachlan | Betcher | Zammit | Betthauser | Converse | Murali | Stone | Hartley | Johnson | Tudorascu | Laymon | Cohen | Minhas | Mathis | Ances | Zaman | Klunk | Handen | Christian | Investigators	**McVea, Andrew**

Board #	Poster Title	Authors	Presenter
89	Greater locus coeruleus activity and locus coeruleus-amygdala hypoconnectivity during high arousal conditions are related to elevated concentrations of plasma p-tau231 in older individuals	Prokopiou | Van Egroo | Riphagen | Ashton | Janelidze | Sperling | Johnson | Blennow | Hansson | Zetterberg | Jacobs	**Prokopiou, Prokopis**
90	Establishing tau-PET cut-points for cognitive diagnosis with [F-18]PI-2620	Tennant | Wheeler | Lee | Terner | Raman | Rissman | Christian | Petersen | Lee | Cohen | Ances | Zhou | Zhang | Nandy | Yaffe | O'Bryant | Braskie	**Tennant, Victoria**
91	Plasma ADRD biomarkers predict longitudinal declines in intra-network functional brain connectivity	Dark | Shafer | Cordon | An | Lewis | Moghekar | Landman | Resnick | Walker	**Dark, Heather**
92	The role of frontoparietal control network and default mode network functional connectivity in cognitive resilience in preclinical Alzheimer's disease	Boyle | Shirzadi | Coughlan | Seto | Properzi | Klinger | Yuan | Scanlon | Jutten | Papp | Amariglio | Rentz | Chhatwal | Buckley | Sperling | Schultz	**Boyle, Rory**
93	Disrupted sleep and 24-hour rhythms are associated with 18F-PI-26260 tau PET in aging and neurodegenerative disease	Winer | Romero | Vossler | Young | Smith | Anders | Pacheco Morales | Davidzon | Henderson | Poston | Zeitzer | Mormino	**Winer, Joseph**
94	Cortical and substantia nigra 18F-PI-2620 tau PET are associated with cognitive and motor impairment in Lewy body disease	Winer | Vossler | Young | Romero | Smith | Shahid | Abdelnour | Wilson | Anders | Pacheco Morales | Davidzon | Mormino | Poston	**Winer, Joseph**
95	Predictability of amyloid-PET status with plasma phospho-Tau217 in adults with Down syndrome	Bettcher | Janelidze | McLachlan | Zammit | McVea | DiFilippo | Betthauser | Laymon | Tudorascu | Cohen | Garimella | Price | Keator | Brickman | Lao | Klunk | Rosas | Zaman | Hartley | Head | Mapstone | Krinsky-McHale | Johnson | Lai | Ances | Handen | Hansson | Christian | Alzheimer Biomarkers Consortium – Down Syndrome	**Bettcher, Brecca**
96	Locus coeruleus metabolism relates to Alzheimer's disease pathology in amyloid-positive symptomatic individuals	Koops | Dutta | Becker | van Egroo | Hanseeuw | Sperling | Johnson | Jacobs	**Koops, Elouise A**
97	Correlating in vivo amyloid beta centiloid values with neuropathological burden: Insights	Liou | Ikonomovic | Handen | Christian | Mapstone | Head | Tudorascu | Brickman |	**Liou, Jr-Jiun**

Board #	Poster Title	Authors	Presenter
	from Down syndrome and Alzheimer's disease cohorts	Price | Laymon | Rosas | Zaman | Hartley | Lai | Kofler | Ibrahim | Villemagne | Cohen	
98	Visualization of endogenously generated Dutch-type Abeta oligomers that dysregulate presynaptic neurotransmission in the absence of detectable inflammation	Gandy | Castranio | Varghese | Argyrousi | Tripathi | Glabe | Levy | Wang | Zhang | Lubell | Guerin | Rahimipour | Dickstein | Arancio | Ehrlich	**Gandy, Sam**
99	[18F]PI-2620 tau-PET binding patterns in American football players with suspected Chronic Traumatic Encephalopathy	Mejia Perez | Mosaheb | Schonhaut | Blazhenets | McKee | Stein | Farris | Mez | Stephens | Mueller | Keegan | La Joie | Rabinovici | Alosco	**Mejia Perez, Jhony**
100	Regional amyloid-β burden in Lewy Body Disease	Vossler | Abdelnour | Young | Winer | Smith | Smith | Shahid | Wilson | Davidzon | Mormino | Poston	**Vossler, Hillary**
101	Pathology-weighted connectivity with medial parietal lobe drives neocortical tau accumulation	Ziontz | Fonseca | Giorgio | Harrison | Jagust	**Ziontz, Jacob**
102	18F-MK-6240 Tau PET visual read algorithm for Alzheimer's disease: diagnostic accuracy and comparison with automated-quantitative Braak stage analysis	Provost | Soucy | Haeger | Macedo | Rahmouni | Stevenson | Servaes | Therriault | Arias | Rosa-Neto	**Provost, Karine**
103	Evaluating CenTauRz harmonization of matched FTP and MK6240 tau PET images: the HEAD Study	Minhas | Delbene | Luo | Reese | Gogola | Villemagne | Dore | Lopresti | Laymon | Lussier | Bauer-Negrini | Povala | Cohen | Crainiceanu | Pascual | Gordon | Lowe | Oh | Soleimani-Meigooni | Klunk | Rosa-Neto | Baker | Pascoal | Tudorascu	**Minhas, Davneet**
104	Characterizing the relationship between the functional connectome and tau PET in preclinical Alzheimer's disease	Abuwarda | Trainer | Ju | Constable | Fredericks	**Abuwarda, Hamid**
105	Estimating time-to-tau as a function of Aβ pathology in Alzheimer's disease using [18F]MK6240 and [18F]NAV4694 PET	Budd Haeberlein | Leuzy | Mathotaarachchi | Insel | Schöll | Moscoso | Villemagne | Doré | Rowe	**Budd Haeberlein, Samantha**
106	Neuroinflammation potentiates the effect of amyloid-β on longitudinal tau accumulation	Rahmouni | Wang | Therriault | Servaes | Tissot | Macedo | Arias-Fernandez | Kunach | Stevenson | Hosseini | Hall | Trudel | Jia |	**Rahmouni, Nesrine**

Board #	Poster Title	Authors	Presenter
		Gauthier | Zimmer | Benedet | Pascoal | Rosa-Neto	
107	Association between plasma pTau epitopes and synaptic density measured with [C-11]UCB-J PET	Yang | DiFilippo | Ma | Wilson | Thor | Pasquesi | Barnhart | Engle | Betthauser | Ashton | Johnson | Christian | Zetterberg | Bendlin	**Yang, Kao Lee**
108	"Treatment Related Amyloid Clearance" (TRAC): a framework to characterize a new biomarker state in the era of anti-amyloid therapies	La Joie | Sexton | Cummings | Galasko | Ikonomovic | Landau | Llibre-Guerra | Mummery | Ossenkoppele | Price | Risacher | Smith | Van Dyck | Carrillo	**La Joie, Renaud**
109	Alzheimer's Disease biological PET staging using plasma p217+tau	Feizpour | Doré | Krishnadas | Bourgeat | Doecke | Saad | Triana-Baltzer | Laws | Shishegar | Huang | Fowler | Ward | Masters | Fripp | Kolb | Villemagne | Rowe	**Rowe, Christopher**
110	Plasma p-tau217 outperforms [18F]FDG-PET in identifying biological Alzheimer's disease in atypical and early-onset dementia	Quispialaya | Joseph Therriault | Aliaga | Benedet | Ashton | Karikari | Macedo | Rahmouni | Stevenson | Tissot | Arias | Wang | Hosseini | Jean-Claude | Pascoal | Gauthier | Gilfix | Vitali | Soucy | Zetterberg | Blennow | Zimmer | Rosa-Neto	**Quispialaya, Kely**
111	A-T+ PET participants in preclinical AD: Clinical progression and concordance with fluid biomarkers	Yakoub | St-Onge | Fajardo | Mohammediyan | Dery | Sylvain | Tremblay-Mercier | Remz | Gonneaud | Vogel | Soucy | Pichet-Binette | Villleneuve | Research Group	**Yakoub, Yara**
112	Neighborhood disadvantage and the association between imaging biomarkers of Alzheimer's disease and cognition in a cohort of diverse older adults	Fan | Royse | Snitz | Reese | Karikari | Pascoal | Shaaban | Roush | Potopenko | Cisneros | Kotulsky | Kamboh | Lopresti | Villemagne | Lopez | Becker | Cohen	**Fan, Erica**
113	Longitudinal Association of Mid-Life Ten Year Cardiovascular Disease Risk Score with Blood Biomarkers of Alzheimer's Disease and Neurodegeneration: Heart SCORE Brain Study	Saeed | Chang | Swanson | Villemagne | Snitz | Royse | Lopresti | Kip | Reese | Gogola | Pascoal | Kamboh | Blennow | Zetterberg | Karikari | Lopez | Reis | Cohen	**Saeed, Anum**
114	Comparison of FDG-PET in individuals with Down Syndrome and Dominantly Inherited Alzheimer Disease: genetic forms with elevated production of amyloid	Abdelmoity | Wisch | Gordon | Flores | Roman | Handen | Christian | Head | Mapstone | Hartley | Rafii | Lee | Krinsky-McHale | Lai | Rosas | Zaman | Schmitt | Ptomey | Bateman | Benzinger | Ances	**Abdelmoity, Omar**
115	Deep learning-based partial volume correction for tau PET imaging	Gong | Lois | Thibault | Tiss | Jang | Becker | Price | El Fakhri | Johnson	**Gong, Kuang**

Board #	Poster Title	Authors	Presenter
116	Plasma levels of an N-terminal tau fragment predict core AD and neurodegenerative biomarkers in autosomal dominant Alzheimer's disease	Schultz | Liu | Ostaszewski | Anderson | Karch | Cruchaga | Gordon | Benzinger | Hassenstab | Morris | Perrin | Goate | Allegri | Barthelemy | Berman | Chui | Farlow | Fox | Day | Jucker | Jack | Koeppe | Lee | Levey | Levin | Martins | Mori | Noble | Rosa-Neto | Salloway | Sanchez | Schofield | McDade | Sperling | Selkoe | Bateman | Chhatwal	**Schultz, Stephanie**
117	Increased CSF GAP-43 is associated with accelerated tau accumulation and spread in Alzheimer's disease	Franzmeier | Dehsarvi | Steward | Biel | Dewenter | Römer | Wagner | Brendel | Ewers | Moscoso | Blennow | Zetterberg | Schöll	**Franzmeier, Nicolai**
118	Investigating the impacts of tau status in Alzheimer's disease by using [18F]Florzolotau tau cutoff	Huang | Lin | Huang | Hsu | Chang | Huang | Hsiao	**Huang, Shao-Yi**
119	Study of reference regions in the quantitation of [18F]Florzolotau tau PET imaging	Huang | Lin | Lin | Huang | Hsu | Chang | Huang | Hsiao	**Lin, Jyh-Ruei**
120	Assessing the efficacy of BETTH-derived tau thresholds to predict cognitive decline	Gogola | Lopresti | Snitz | Tudorascu | Minhas | Dore | Ikonomovic | Shaaban | Kofler | Matan | Bourgeat | Mason | Rowe | Aizenstein | Mathis | Klunk | Lopez | Cohen | Villemagne	**Gogola, Alexandra**
121	Assessing the correlations between imaging and plasma biomarkers within the AT(N) framework	Gogola | Cohen | Zeng | Lopresti | Snitz | Tudorascu | Minhas | Ikonomovic | Pascoal | Kofler | Matan | Mason | Aizenstein | Mathis | Klunk | Zetterberg | Blennow | Lopez | Villemagne | Karikari	**Gogola, Alexandra**
122	The effect of microglial activation on brain atrophy across the Alzheimer's disease continuum	Povala | Bellaver | Lukasewicz Ferreira | Ferrari-Souza | Schaffer Aguzzoli | Teixeira Leffa | Zalzale | Soares | Lussier | Negrini | Rohden | Benedet | Stevenson | Rahmouni | Tissot | Therriault | Servaes | Cohen | Klunk | Villemagne | Zatt | R Zimmer | Karikari | Rosa-Neto | A Pascoal	**Povala, Guilherme**
123	Disentangling the relationships between tau-PET, amyloid-β-PET, hippocampal subfield volumes, and memory: a longitudinal study	Aumont | Bedard | Bussy | Fernandez Arias | Therriault | Rahmouni | Stevenson | Tissot | Servaes | C. Macedo | Gauthier | M. Chakravarty | Rosa-Neto	**Aumont, Etienne**
124	Tau-PET Overlap Index; Associations with Braak Stage and Quantitative NFT Measurements	Lee | Min | Moloney | Mester | Lund | Ghatamaneni | Senjem | Nguyen | Graff-Radford | Schwarz | Gunter | Kantarci | Boeve | Vemuri | Jones | Knopman | Jack | Petersen | Murray | Lowe	**Lowe, Val**

Board #	Poster Title	Authors	Presenter
125	Tau-PET spatial extent for predicting cognitive decline within tau-positive individuals	Coomans | van Tol | Groot | van der Flier | Pijnenburg | van de Giessen | Ossenkoppele	**Coomans, Emma**
126	Association of Sex and Cerebral Beta-Amyloid with Cortical Gray Matter Brain Age in Cognitively Impaired Older Adults	Li | Son | Chen | Wang | Aizenstein | Hong | Roh | Cho | Hong | Nam | Park | Kim | Lee | Choi | Moon | Seo | Choi | Kim | Wu	**Li, Jinghang**
127	Will cerebral glucose metabolism measured using [18F]FDG PET substitute tau PET in clinical studies?	Edison	**Edison, Paul**
128	CSF sTREM2 is associated with neuroprotective microglial states early in Alzheimer's disease and deleterious effects later in the disease trajectory	Edison	**Edison, Paul**
129	The Mobile Toolbox for assessing cognition remotely: associations with amyloid and tau deposition in cognitively unimpaired older adults	Jutten | Burling | Fu | Properzi | Amariglio | Papp | Marshall | Price | Johnson | Sperling | Rentz	**Jutten, Roos**
130	Characterizing multi-site harmonized amyloid and tau PET across the Alzheimer's continuum	Cody | Johns | Carlson | Younes | Young | Mukherjee | Trittschuh | Gibbons | Dumitrescu | Archer | Durant | Nakano | Klinedinst | Choi | Lee | Scollard | Mez | Saykin | Crane | Cuccaro | Toga | Tosun | Hohman | Mormino	**Cody, Karly**
131	Characterization of tau PET accumulation relative to duration of entorhinal tau positivity	Cody | Langhough | Heston | Teague | Christian | Johnson | Betthauser	**Cody, Karly**
132	Harmonization of multi-scanner PET data with ComBat: application to 18F-AV1451 data acquired on a Siemens ECAT HR+ PET and a GE Discovery MI PET/CT Scanner	Lois Gomez | Diez-Palacio | Price | Johnson	**Lois Gomez, Cristina**
133	Longitudinal white matter degeneration is associated with higher subsequent amyloid load across the Alzheimer's disease continuum	Burton | Blujus | Oh	**Burton, Courtney**
134	Multimodal analysis of tau epicenters in heterogeneous Alzheimer's disease variants	Trainer | Vin | Xu | Chase | O'Dell | Toyonaga | Tun | Li | Ju | Mecca | van Dyck | Fredericks	**Trainer, Anne**

Board #	Poster Title	Authors	Presenter
135	A pretrained foundation model for learning representation of regional tau accumulation pattern and its downstream applications	Sohn | Song | Seong	**Sohn, JunYoung**
136	[18F]RO-948 Tau PET Retention and Correlation with Fluid Biomarkers in the Early AD Continuum	Shekari | González Escalante | Milà-Alomà | Falcon | López-Martos | Sánchez-Benavides | Brugulat-Serrat | Niñerola-Baizán | J. Ashton | K. Karikari | Lantero-Rodriguez | Snellman | Ortiz | Tonietto | Borroni | Klein | Minguillón | Fauria | Perissinotti | Molinuevo | Zetterberg | Blennow | Grau-Rivera | Suárez-Calvet | Gispert	**Shekari, Mahnaz**
137	Baseline plasma GFAP predicts longitudinal tau-PET uptake in Braak staging continuum	Jia | Rahmouni | Tissot | Servaes | Therriault | Cassa Macedo | Fernandez-Arias | Wang | Lussier | Kunach | Gauthier | Benedet | Ashton | Zetterberg | Pascoal | Blennow | Rosa-Neto	**Jia, Wan Lu**
138	Plasma NfL correlates to grey matter and white matter atrophy ambivalent to amyloid status in older adults	Hall | Rahmouni | Macedo | Servaes | Therriault | Fernandez-Arias | Trudel | Stevenson | Gauthier | Sanjeewa | Lussier | Pascoal | Benedet | Ashton | Zetterberg | Blennow | Rosa-Neto	**Hall, Brandon**
139	Astrocyte reactivity influences cognitive decline in individuals across the Alzheimer's disease continuum	Bellaver | Povala | Ferreira | Bauer-Negrini | Lussier | Leffa | Ferrari-Souza | Zalzale | Soares | Rohden | Aguzzoli | Abbas | Benedet | Ashton | Tissot | Therriault | Servaes | Stevenson | Rahmouni | Hong | Rho | Karim | Zimmer | Zetterberg | Blennow | Villemagne | Klunk | Lopez | Tudorascu | Slachevsky | Rosa-Neto | Cohen | Karikari | Son | Pascoal	**Bellaver, Bruna**
140	Elevated Plasma Ptau-181 is Associated with Congestive Heart Failure	Tanner | Wiedner | Himali | Ramos-Cejudo | Beiser | Seshadri | Javier Aparicio | Himali	**Tanner, Jeremy**
141	Regional cell-type proportions are associated with AD pathological changes	Kang | Ottoy | Soucy | Massarweh | Black | Rosa-Neto | Goubran	**Kang, Min Su**
142	Quantitative Gradient Recalled Echo (qGRE) MRI Detects Neuronal Loss and Iron Accumulation in Nucleus Basalis of Meynert in Preclinical and Mild Alzheimer's Disease	Kothapalli | Milchenko | Benzinger | Goyal | Eldeniz | Marcus | Morris | Yablonskiy | Raichle	**Kothapalli, Satya VVN**

Board #	Poster Title	Authors	Presenter
143	Head-to-head analysis of [18F]MK6240 and [18F]Flortaucipir standardized update values (SUVs): the HEAD Study	Tsai | Tissot | Tudorascu | Rosa-Neto | Gordon | Pascual | Lowe | Soleimani-Meigooni | Oh | Klunk | Jagust | Pascoal | Baker	**Tsai, Hsin-Yeh**
144	Association between Oxygen Extraction Fraction, Tau, and Amyloid Pathology, and Cognitive Status in Alzheimer's Disease: Implications for Advanced Neuroimaging Techniques	Hosseini | Servaes | Therriault | Tissot | Rahmouni | Macedo | Lussier | Stevenson | Wang | Fernandez-Arias | Socualaya | Aumont | Stevenson | Gauthier | Cho | Zhuang | Wang | Rudko | Pascoal | Rosa-Neto	**Hosseini, Seyyed Ali**
145	Association of plasma pTau epitopes with mesial temporal lobe cortical thinning	Trudel | Rahmouni | Macedo | Therriault | Servaes | Wang | Fernandez-Arias | Hall | Stevenson | Sanjeewa | Gauthier | Benedet | Ashton | Zetterberg | Blennow | Lussier | Tharick | Karikari | Rosa-Neto	**Trudel, Lydia**
146	Specific Tau networks are associated with different cognitive domains in the elderly	Nayak | Hojjati | Ozoria-Blake | Razlighi	**Nayak, Siddharth**

1 Longitudinal synaptic loss follows tau PET Braak staging in vivo and supports local neurodegeneration by tau accumulation in stages III-VI

Greet Vanderlinden[1], Michel Koole[1], Mathieu Vandenbulcke[2,3,4], Koen Van Laere[1,2,5]

[1]*Nuclear Medicine and Molecular Imaging, Imaging Pathology, KU Leuven, Leuven, Belgium*
[2]*Leuven Brain Institute, Leuven, Belgium*
[3]*Neuropsychiatry, Research Group Psychiatry, KU Leuven, Leuven, Belgium*
[4]*Department of Geriatric Psychiatry, University Hospitals UZ Leuven, Leuven, Belgium*
[5]*Division of Nuclear Medicine, University Hospitals UZ Leuven, Leuven, Belgium*

PET-based staging of tau accumulation in AD has high correspondence with pathology-based Braak classification. In aMCI, tau and synaptic density show a regional negative correlation, especially in the hippocampus in early stages. To assess whether longitudinal synaptic density loss follows tau seed-based distant spreading and/or local accumulation, we investigated their 2-year progression in vivo according to Braak staging.

Thirty aMCI patients (73±8yrs, 10M/20F, MMSE 21-30, 28 Aβ+/1Aβ-/1unknown) and 26 cognitively unimpaired subjects (CU) (69±9yrs, 14M/12F, MMSE 28-30, 4Aβ+/22Aβ-) underwent [^{18}F]MK-6240 and [^{11}C]UCB-J PET at baseline and 19 aMCI patients underwent 2-year follow-up imaging. [^{18}F]MK-6240 and [^{11}C]UCB-J SUVR was calculated (referenced to inferior cerebellar cortex and centrum semiovale, respectively) and PVC was applied.

Compared to CU, at baseline aMCI patients showed higher [^{18}F]MK-6240 binding in all 6 Braak stages (all $p \leq 0.03$), with largest effect size (ES) in early Braak I-III (medial temporal) regions, while [^{11}C]UCB-J binding was only significantly lower in Braak II (hippocampus) ($p=0.005$) (Fig1; Fig2A,B). Longitudinally, aMCI showed increased [^{18}F]MK-6240 binding in all Braak stages (all $p \leq 0.002$) except for Braak I-II showing a saturation effect. Homogeneous tau increases were present in Braak III-VI, consistent with the hypothesis that in late Braak stages, local replication is the main process controlling the rate of tau deposition. [^{11}C]UCB-J binding decreased significantly in all Braak regions (all $p \leq 0.006$), with largest ES in Braak I/II and smaller, homogeneous decreases in Braak III-VI (Fig1; Fig2C,D).

These findings show that tau accumulation reaches a plateau in early Braak stages already in the MCI stage of AD. Whereas synaptic density decreases up to 2 years later in the disease progression, it follows tau Braak stage progression with remarkable spatial accuracy and its homogeneous change at higher Braak stages is consistent with regional rather than distant effects.

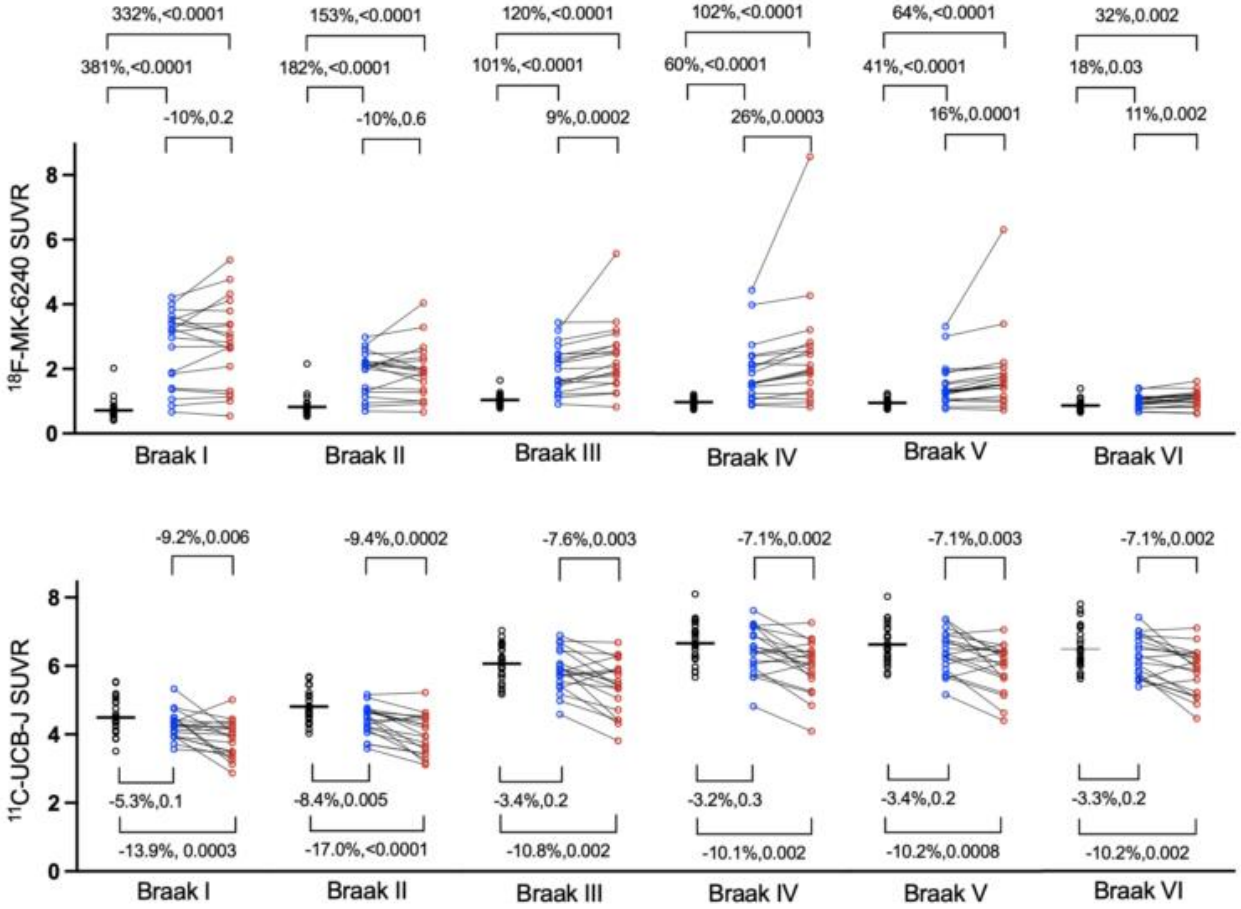

Figure 1. Volume-of-interest-based analysis.

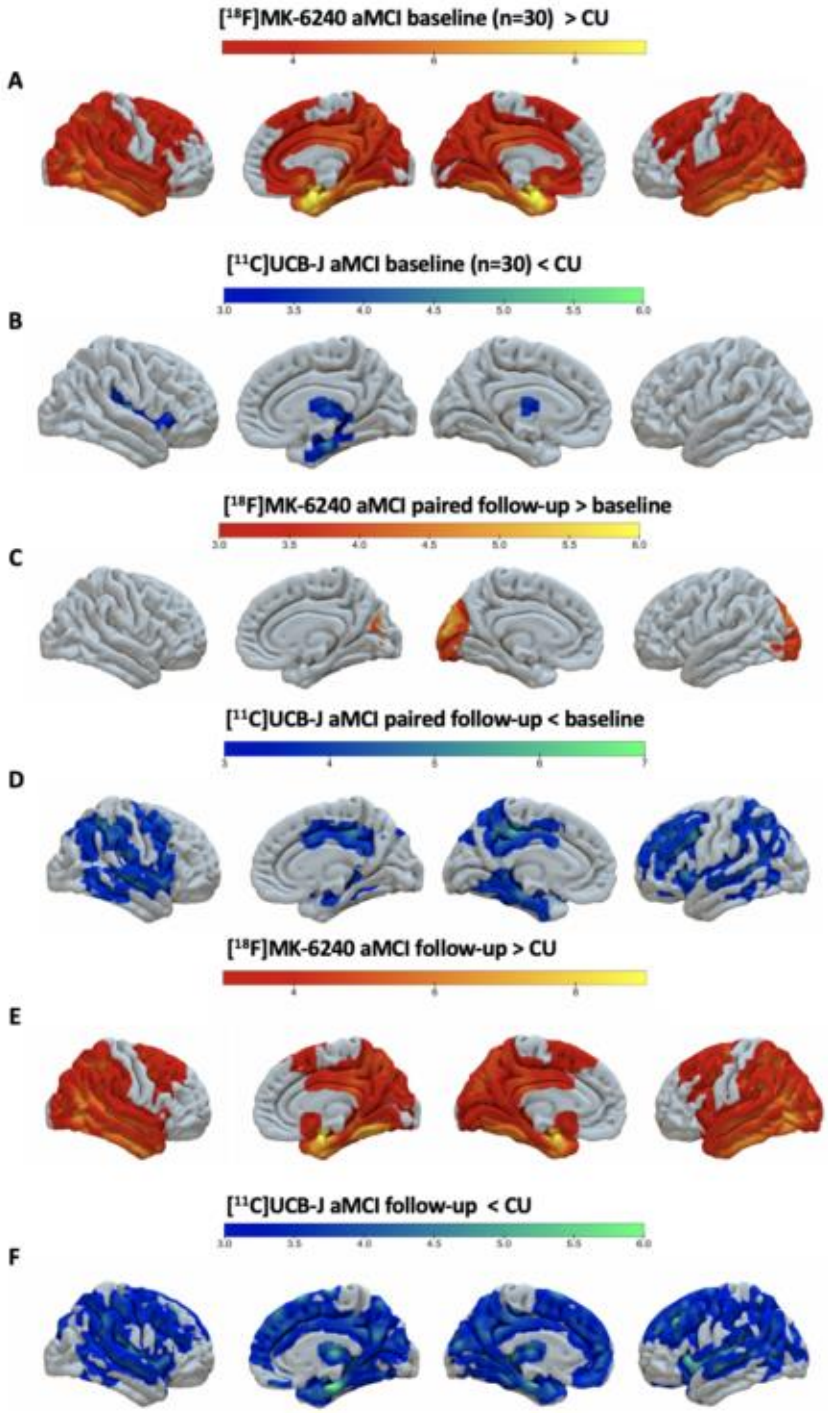

Figure 2. Voxel-based analysis.

Keywords: Tau, Synaptic Density, MCI

2 Plasma Aβ42/40 ratio, GFAP, and NfL across the neurodegenerative diseases: cross-sectional and longitudinal study in a large multi-center cohort

Hyemin Jang[2], Jun Pyo Kim[1], Daeun Shin[1], Heejin Yoo[1], Eun Hye Lee[1], Jihwan Yun[1], Duk L. Na[1], Hee Jin Kim[1], Kaj Blennow[3], Henrik Zetterberg[3], Sang Won Seo[1]

[1]*Samsung medical center, Seoul, South Korea*
[2]*Seoul National University Hospital, Seoul, South Korea*
[3]*Gothenberg University, Gothenberg, Sweden*

Background: We assessed the feasibility of plasma Ab42/Ab40, GFAP and Nfl determined using a SIMOA method as a useful biomarker of Abeta PET status in a large Korean cohort.

Methods: A total of 1878 participants belonging to five groups, Alzheimer's disease dementia (ADD, n=445), amnestic mild cognitive impairment (aMCI, n=695), cognitively unimpaired (CU, n=391), subcortical vascular cognitive impairment (SVCI, n=161), and frontotemporal dementia (FTD, n=79) were included in this study. Plasma Ab40, Ab42, GFAP and Nfl were quantitated using a single molecular array (SIMOA) method. We performed receiver operating characteristic (ROC) analysis to develop the cutoff of Ab42/Ab40, GFAP and Nfl and investigated its performance predicting centiloid-based PET positivity (PET+).

Results: Plasma Ab42/Ab40 were lower for PET+ individuals in ADD, aMCI, CU, SVCI and FTD ($p<0.001$). Plasma GFAP were higher for PET+ individuals in ADD, aMCI, CU, SVCI ($p<0.001$) and FTD ($p=0.0033$). Plasma Nfl were higher for PET+ individuals in aMCI and CU ($p<0.001$). In the group of CU, aMCI and ADD groups, plasma Ab42/Ab40 predicted PET+ with an area under the ROC curve (AUC) of 0.789 at a cutoff of 0.0058. When adding age, APOE4 and diagnosis, the AUC significantly improved to 0.869. In the same group, plasma GFAP and Nfl predicted PET+ with an AUC of 0.822 and 0.627 at a cutoff of 123.5 and 22.85, respectively.

Conclusion: Plasma Ab42/Ab40 and GFAP, as measured by SIMOA method, showed good discrimnating performance based on PET positivity.

Key words: Biomarker, Alzheimer's disease, Amyloid, Plasma, Ab42/Ab40, GFAP, Nfl, SIMOA

Keywords: Plasma biomarkers, Aβ42/40 ratio, GFAP, NfL, prognosis

3 Publicly available software and FTP calibration data for CenTauR tau PET standardization

Christopher G. Schwarz[1], Scott A. Przybelski[1], Carl M. Prakaashana[1], Vincent Doré[2], Victor L. Villemagne[3], Antoine Leuzy[4], Matthew L. Senjem[1], Val J. Lowe[1], Jeffrey L. Gunter[1], Kejal Kantarci[1], Prashanthi Vemuri[1], Jonathan Graff-Radford[1], Ronald C. Petersen[1], David S. Knopman[1], Clifford R. Jack[1]

[1]*Mayo Clinic, Rochester, MN, United States*
[2]*Austin Health, Melbourne, Australia*
[3]*University of Pittsburgh, Pittsburgh, PA, United States*
[4]*Lund University, Malmö, Sweden*

Background: The CenTauR project provides universal quantitative measurement scales and regions-of-interest (ROIs) for standardizing tau PET quantification across tracers and pipelines. It released ROIs for use with SPM8, but no public calibration datasets or software are available.

Methods: To create a dataset for calibrating arbitrary tau PET SUVR pipelines to CenTauR$_Z$ units, we sampled 100 participants from the Mayo Clinic Study of Aging and ADRC. This includes: 50 participants with clinical dementia with AD (confirmed amyloid positivity on Pittsburgh compound B) with exclusively amnestic phenotypes, and paired 3T T1-weighted MRI and Flortaucipir (FTP) PET; and 50 age-and-sex-matched amyloid-negative cognitively unimpaired participants. We de-identified and de-faced all images with *mri_reface* to allow easy-access public distribution.

We implemented the SPM8 "Centiloid standard" pipeline with the published CenTauR$_Z$ regression constants to compute CenTauR$_Z$ across this dataset. Next, we normalized the SPM8-based ROIs to higher resolution MNI152-nonlinear and Mayo Clinic Adult Lifespan Template (MCALT) spaces using SPM12. We implemented a SPM12-based pipeline that measures SUVR in MRI space with tissue-class masking and population-matched MCALT templates and priors. We calculated SUVR across the calibration dataset and calibrated the pipeline to CenTauR$_Z$ units using the measurements from the canonical SPM8 pipeline on the same images using Deming linear regression.

Results: Agreements between the proposed SPM12- and the standard SPM8-based pipelines were extremely high for all ROIs (R^2>0.98, Figure 1). The warped ROIs mapped well onto the higher-resolution template spaces (Figure 2).

Discussion: The FTP calibration dataset, automated software to compute CenTauR$_Z$ and SUVR for all tracers, and CenTauR ROIs in higher-resolution template spaces will be publicly available at https://www.gaain.org/centaur-project. The software will be updated to also compute CenTauR values when those regression constants are released. These tools will facilitate the development and calibration of alternative pipelines for measuring in universal CenTauR and CenTauR$_Z$ units.

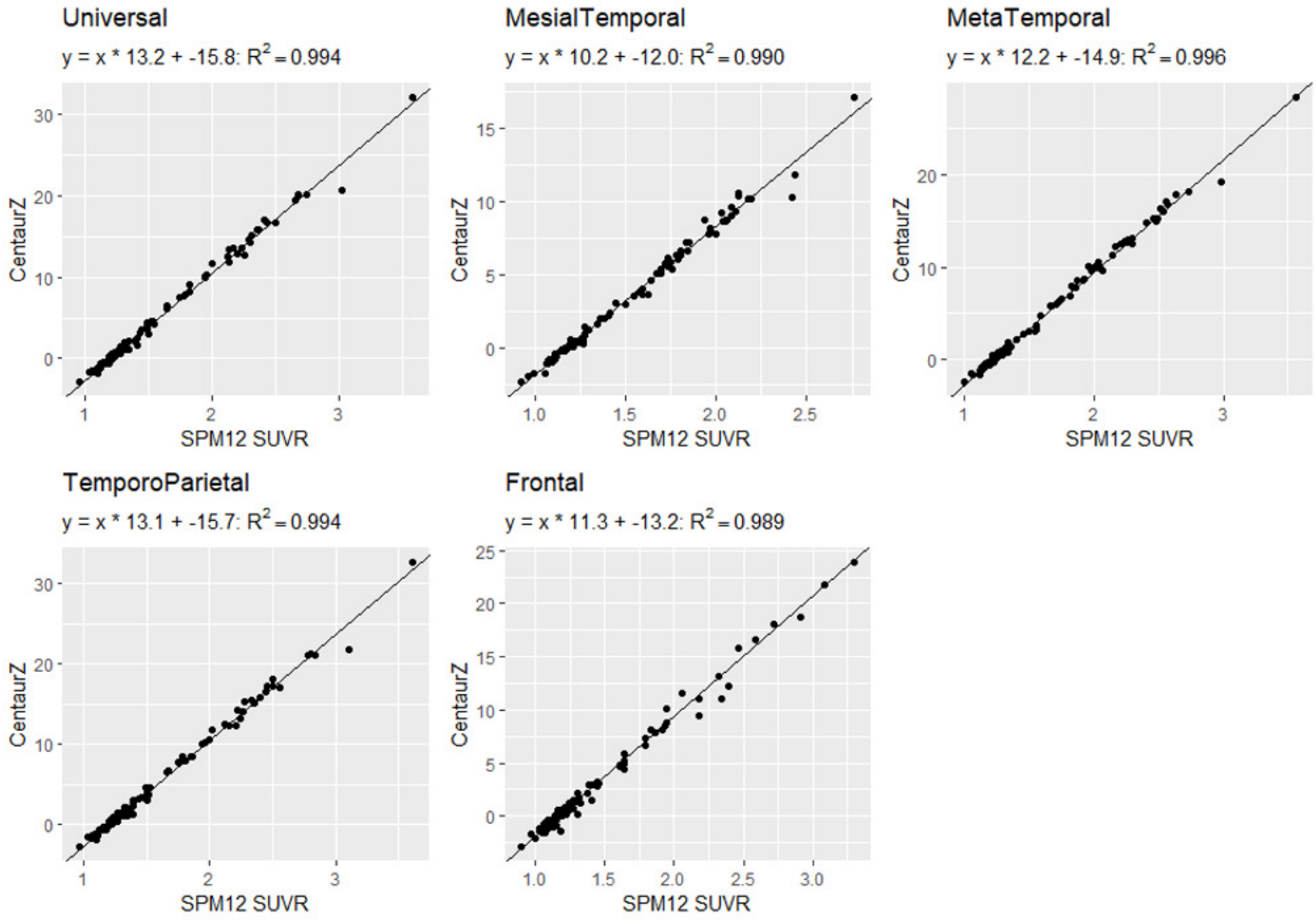

Figure 1: Calibration of our proposed SPM12-based pipeline to CenTauR$_Z$ units from the canonical SPM8 pipeline, using our proposed FTP calibration dataset. The Universal mask was constructed by the CenTauR project from the intersection of six tracer-specific masks. The additional 4 subregions were defined within the constraints of the universal mask: MesialTemporal: entorhinal, parahippocampus and amygdala; MetaTemporal: entorhinal, parahippocampus, amygdala, fusiform, inferior and middle temporal gyri; TemporoParietal: bankssts, cuneus, inferior-superior parietal, inferior-middle-superior temporal, istmuscingulate, lateral occipital, lingal, posterior cingulate, precuneus and superior marginal; Frontal: caudate middle frontal, precentral, rostral middle frontal, superior frontal. We share the dataset and both fully automated, pre-calibrated pipelines publicly on GAAIN.org.

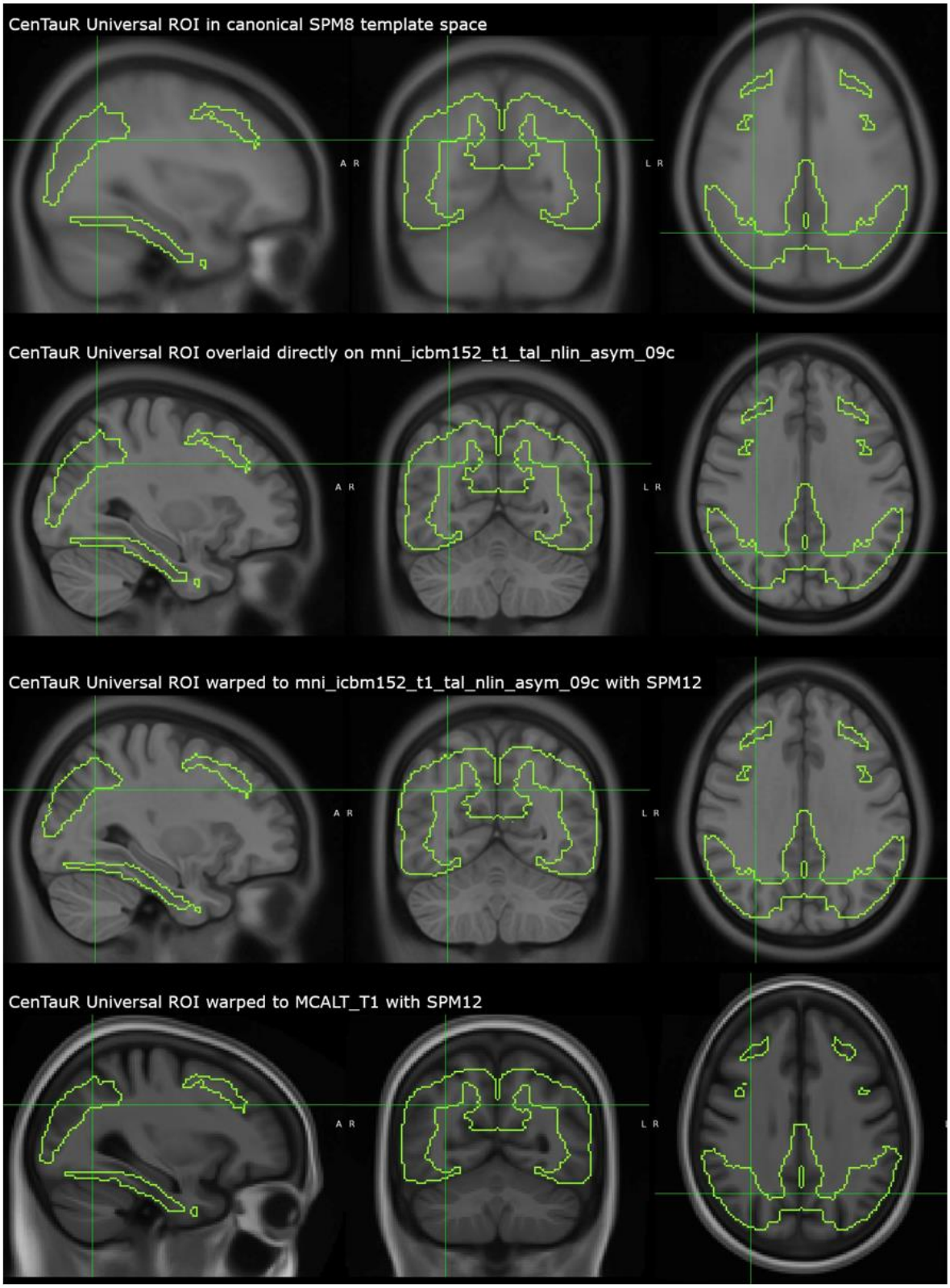

Figure 2: The original CenTauR ROIs are defined in SPM8's version of MNI template space. Used directly, they are incompatible with higher-dimensional MNI152 template spaces (localized more subcortically than intended). We warped them to MNI152-nonlinear and MCALT template spaces using SPM12, and we provide these files on GAAIN.org for use in pipelines with higher-dimensional spatial normalization.

Keywords: CenTauR,tau PET,Flortaucipir,standardization,harmonization

4 The impact of metabolic health on the relationship of obesity with and Alzheimer's and vascular markers

Eun Hye Lee[1], Heejin Yoo[1,2], Young Ju Kim[1,2], Bo Kyoung Cheon[1,2], Kichang Kwak[2], Yeo Jin Kim[3], Seungho Ryu[4], Yoosoo Chang[4], Hyemin Jang[1,2,5], Jun Pyo Kim[1], Hee Jin Kim[1,2,6,7], Duk L Na[1,2], Sung Hoon Kang[1,8], Sang Won Seo[1,2,6,7,9]

[1]*Department of Neurology, Samsung Medical Center, Sungkyunkwan University School of Medicine, Seoul, South Korea*
[2]*Alzheimer's Disease Convergence Research Center, Samsung Medical Center, Seoul, South Korea*
[3]*Department of Neurology, Kangdong Sacred Heart Hospital, Seoul, South Korea*
[4]*Center for Cohort Studies, Total Healthcare Center, Kangbuk Samsung Hospital, Sungkyunkwan University School of Medicine, Seoul, South Korea*
[5]*Neuroscience Center, Samsung Medical Center, Seoul, South Korea*
[6]*Department of Digital Health, SAIHST, Sungkyunkwan University, Seoul, South Korea*
[7]*Department of Health Sciences and Technology, SAIHST, Sungkyunkwan University,, Seoul, South Korea*
[8]*Department of Neurology, Korea University Guro Hospital, Korea University College of Medicine, Seoul, South Korea*
[9]*Department of Intelligent Precision Healthcare Convergence, Sungkyunkwan University, Suwon, South Korea*

We aimed to investigate the effect of metabolic health on the association between obesity and amyloid positivity or severe white matter hyperintensities (WMH).

We recruited 1,736 non-demented participants aged ≥55 years who underwent Aβ PET scan. They were categorized by BMI: <18.5kg/m2 (underweight); between 18.5kg/m2 and 25kg/m2 (normal weight); ≥25kg/m2 (obese). Each group was divided into metabolically healthy and unhealthy groups based on ATP-III criteria.
Aβ positivity was defined as Aβ PET centiloid>20. Severe WMH was defined as ≥10mm periventricular and ≥25mm deep WMH. Data on plasma glial fibrillary acidic protein (GFAP) levels, hippocampal volume (HV), and clinical dementia rating scale sum of boxes (CDR-SOB) were collected.
Logistic and linear regression analyses were performed using BMI status groups as predictors for Aβ positivity, severe WMH, and plasma GFAP, controlling for potential confounders. To examine the interaction between BMI status and metabolic healthiness, regression analyses were performed with an interaction term of BMI status*metabolic healthiness. Mediation analyses were performed to investigate the complex relationships among aforementioned factors.

Being underweight increased Aβ positivity risk (OR=2.37), whereas obesity decreased it (OR=0.63). The interaction was significant for obesity and metabolic healthiness on Aβ positivity (p for interaction<0.001), but not for underweight versus normal weight. For severe WMH, being underweight had no effect, but obesity increased odds (OR=1.69) without significant interaction between obesity and metabolic healthiness.
Being underweight predicted higher plasma GFAP (β=0.190, p=0.048), whereas obesity was associated with lower levels (β=-0.115, p=0.001) with no significant interaction between obesity and metabolic healthiness.
Mediated analyses of Aβ-positivity mediated pathways found that being underweight was associated with lower HV and higher CDR-SOB, while obesity showed the opposite effect.

The protective effects of obesity on Aβ positivity are different according to metabolic healthiness and being underweight is a risk factor for Aβ positivity regardless of metabolic healthiness.

Keywords: BMI, Metabolic health, Amyloid PET, Vascular marker, GFAP

5 Distinct effects of cholesterol profile components on Amyloid and Vascular burdens

Sung Hoon Kang[1,2], Heejin Yoo[2], Jun Pyo Kim[2], Sang Won Seo[2]

[1]*Department of Neurology, Korea University Guro Hospital, Korea University College of Medicine, Seoul, South Korea*
[2]*Department of Neurology, Samsung Medical Center, Sungkyunkwan University School of Medicine, Seoul, South Korea*

Background: Cholesterol plays important roles in β-amyloid (Aβ) metabolism and atherosclerosis. However, the relationships of plasma cholesterol levels with Aβ and cerebral small vessel disease (CSVD) burdens are not fully understood in Asians. Herein, we investigated the relationships between plasma cholesterol profile components and Aβ and CSVD burdens in a large, non-demented Korean cohort.

Methods: We enrolled 1,175 non-demented participants (456 with unimpaired cognition [CU] and 719 with mild cognitive impairment [MCI]) aged ≥ 45 years who underwent Aβ PET at the Samsung Medical Center in Korea. We performed linear regression analyses with each cholesterol (low-density lipoprotein cholesterol [LDL-c], high-density lipoprotein cholesterol [HDL-c], and triglyceride) level as a predictor and each image marker (Aβ uptake on PET, white matter hyperintensity [WMH] volume, and hippocampal volume) as an outcome after controlling for potential confounders.

Results: Increased LDL-c levels (β=0.014 to 0.115, *p*=0.013) were associated with greater Aβ uptake, independent of the *APOE* e4 allele genotype and lipid-lowering medication. Decreased HDL-c levels (β=−0.133 to −0.006, *p*=0.032) were predictive of higher WMH volumes. Increased LDL-c levels were also associated with decreased hippocampal volume (direct effect β=−0.053, *p*=0.040), which was partially mediated by Aβ uptake (indirect effect β=−0.018, *p*=0.006).

Conclusions: Our findings highlight that increased LDL-c and decreased HDL-c levels are important risk factors for Aβ and CSVD burdens, respectively. Furthermore, considering that plasma cholesterol profile components are potentially modified by diet, exercise, and pharmacological agents, our results provide evidence that regulating LDL-c and HDL-c levels is a potential strategy to prevent dementia.

Keywords: LDL-c, HDL-c, β-Amyloid-β (Aβ), white matter hyperintensity (WMH), hippocampal volume

6 Amyloid pet positivity in Korean Dementia Syndromes: in relation to diagnosis, age, and Apoe genotypes

Min Young Chun[1,2,3], Hyemin Jang[1], Jihwan Yun[1], Jun Pyo Kim[1], Sook-young Woo[4], Sang Won Seo[1]

[1]*Department of Neurology, Samsung Medical Center, Sungkyunkwan University School of Medicine, Seoul, South Korea*
[2]*Department of Neurology, Yonsei University College of Medicine, Seoul, South Korea*
[3]*Department of Neurology, Yongin Severance Hospital, Yonsei University Health System, Yongin, South Korea*
[4]*Biostatistics Team, Samsung Biomedical Research Institute, Seoul, South Korea*

Background: Ethnicity-specific characteristics of amyloid-β (Aβ) should be considered when recommending Aβ therapies for various populations. We aimed to investigate the prevalence of Aβ positivity (+) and longitudinal trajectories in dementia syndromes in the Korean population.

Methods: We included 6,634 participants with Aβ PET scans in Korea and followed 4,808 participants longitudinally. They were diagnosed with Alzheimer's disease-related cognitive impairment (ADCI), subcortical vascular cognitive impairments (SVCI), or frontotemporal dementia (FTD) and further categorized into three cognitive stages: cognitively unimpaired (CU), mild cognitive impairment (MCI), and dementia. We estimated Aβ (+) frequencies using the Clopper-Pearson method. Multivariable logistic regression assessed the odds of Aβ (+) in relation to age, sex, education, and *APOE* genotype.

Results: In the cross-sectional study, we found the odds of Aβ (+) among ADCI participants as follows: CU, 21.0 [95% CI 18.9–23.2]; MCI, 49.1 [47.3–50.9]; and dementia, 80.5 [78.3–82.5]. In SVCI, the odds were: CU, 20.0 [12.3–29.8]; MCI, 34.0 [28.2–40.0]; and dementia, 40.1 [34.2–46.2]. For FTD, the odds were 13.1 [8.6–18.9]. Additionally, among ADCI participants, Aβ (+) prevalence increased with age in the non-demented group (CU: odds 1.10; and MCI: 1.03) and decreased with age in the dementia group (odds 0.95). In contrast, SVCI and FTD had more Aβ (+) with increasing age. The *APOE* ε4 allele was a significant risk factor for Aβ (+) in all cognitive stages of ADCI and in the MCI and dementia groups of SVCI. In the longitudinal study involving ADCI participants, sex and *APOE* genotypes significantly affected Aβ (+) participants but not Aβ (−) participants, while education levels had an impact on both Aβ (+) and Aβ (−) participants.

Conclusions: Our results enhance understanding of Aβ (+) associations with age, sex, educational levels, and *APOE* genotype among the Korean population, suggesting ethnicity-specific applicability of Aβ-targeted treatments and prevention.

Keywords: Amyloid PET, Korean, Ethnicity, Cognitive trajectory

7 Toward more representative estimates of the effect of tau on cognition

C. Elizabeth Shaaban[1], Yingyan Wu[2], Zachary J. Kunicki[3], Danai Chasioti[4], Douglas Tommet[3], Adea Rich[3], Hwamee Oh[3], Thomas K. Karikari[1], Ann D. Cohen[1], Brian J. Lopresti[1], Victor L. Villemagne[1], M. Maria Glymour[5], Richard N. Jones[3]

[1]*University of Pittsburgh, Pittsburgh, PA, United States*
[2]*University of California, Los Angeles, Los Angeles, CA, United States*
[3]*Brown University, Providence, RI, United States*
[4]*Indiana University, Indianapolis, IN, United States*
[5]*Boston University, Boston, MA, United States*

Introduction: Alzheimer Disease (AD) clinical trial samples are highly selected. It is unknown if the hypothesized β-amyloid (Aβ), tau, and cognition relationships motivating current AD drug trials exist in community samples.

Methods: Using Alzheimer's Disease Neuroimaging Initiative (ADNI) data, we calculated linear regression coefficients and 95% confidence intervals for the association of plasma p-tau 181 with a composite memory score, ADNI-MEM, 2 years later (adjusting for baseline memory) across 3 Aβ PET-based inclusion criteria: TRAILBLAZER-ALZ trial (donanemab, set at Aβ>36 centiloids (CL)); ENGAGE/EMERGE trial (aducanemab, Aβ>25 CL based on the CL of a positive visual read); and Aβ only (Aβ=15-50 CL based on a balance of thresholds for detecting cognitive decline prior to tau-driven decline). Estimates were weighted to a population-representative US older adult sample using the Health and Retirement Study (HRS) / Aging, Demographics, and Memory Study (ADAMS) via inverse odds weights based on age, cognitive diagnosis, MMSE score, sex, education years, race/ethnicity, and *APOE4*.

Results: After weighting, the covariate balance plot showed evidence of covariate balance between ADNI and HRS ADAMS, with all weighted estimates except *APOE4* status falling within the |0.25| range. Greater P-tau 181 was associated with poorer memory 2 years later; effect sizes were small and statistically consistent across alternative Aβ inclusion criteria (weighted β = -0.0034 to -0.0007). Associations were only significant when the total sample was used suggesting this may be due to sample size.

Discussion: Effect size estimates for associations of tau with change in memory over two years were statistically consistent in the expected direction, but imprecise enough that no effects, or effects in the opposite direction, cannot be ruled out in the sample weighted to look more like the community. More testing is needed to confirm detection of these effects in a public health relevant general population of older adults.

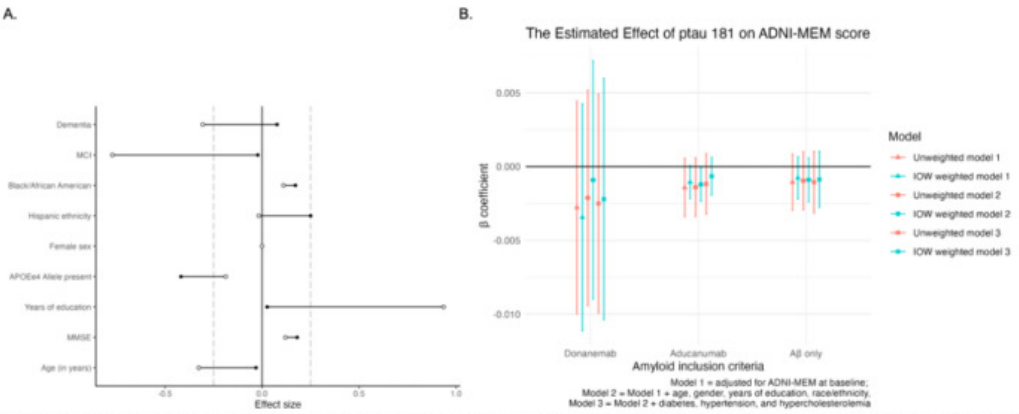

Figure 1. The left panel (A) shows the covariate balance plot, with the unfilled circles showing the unweighted standardized mean differences (Cohen's *d* for continuous variables or *h* for binary) between the HRS ADAMS and ADNI datasets. The filled black circles show the weighted standardized mean differences. Covariate balance can be inferred if all weighted standardized mean differences fall within |0.25|, which are indicated by the vertical dashed lines. The right panel (B) shows the weighted and unweighted regression coefficients and 95% confidence intervals for the association of plasma p-tau 181 with ADNI-MEM 24 months later across a range of Aβ inclusion criteria.

Table 1. Baseline characteristics for participants from survey weighted HRS ADAMS, unweighted ADNI, and inverse odds weighted ADNI data (N = 396 and N = 813 respectively)

	Dataset		
	HRS ADAMS, N = 396[1]	**unweighted ADNI**, N = 813[1]	**weighted ADNI**, N = 813[1]
Age	77.9 (4.9)	76.3 (4.7)	77.3 (4.6)
Female	239 (60.3%)	338 (41.6%)	447 (55.0%)
Years of education	12.2 (3.3)	15.4 (2.0)	12.5 (3.3)
Race			
White	357 (90.2%)	762 (93.7%)	768 (94.5%)
Black	32 (8.0%)	31 (3.8%)	36 (4.4%)
Other	7 (1.8%)	20 (2.5%)	9 (1.1%)
Ethnicity: Hispanic/Latino	17 (4.2%)	25 (3.1%)	12 (1.5%)
MMSE score	27.0 (3.7)	27.1 (3.2)	27.5 (3.0)
***APOE4* allele carrier**	114 (28.8%)	331 (40.7%)	272 (33.5%)
Aβ, centiloids		49.6 (46.4)	37.5 (38.2)
Cognitive diagnosis			
Normal	334 (84.2%)	300 (36.9%)	654 (80.4%)
Mild cognitive impairment	43 (10.8%)	350 (43.1%)	105 (13.0%)
Dementia	20 (4.9%)	163 (20.0%)	54 (6.6%)

[1]Mean (SD); n (%)

Table 2. Unweighted and population-weighted association of plasma p-tau 181 with memory 24 months later

		Unweighted				Weighted			
			95% confidence interval				95% confidence interval		
	Model	**Estimate**	**Low**	**High**	**p-value**	**Estimate**	**Low**	**High**	**p-value**
Donanemab (N=341)	**1**	-0.0028	-0.0100	0.0044	0.45	-0.0034	-0.0111	0.0043	0.38
	2	-0.0021	-0.0094	0.0052	0.57	-0.0009	-0.0090	0.0072	0.83
	3	-0.0025	-0.0099	0.0049	0.51	-0.0022	-0.0104	0.0060	0.60
Aducanumab (N=369)	**1**	-0.0014	-0.0034	0.0006	0.16	-0.0011	-0.0022	0.0001	0.07
	2	-0.0014	-0.0034	0.0006	0.17	**-0.0012**	**-0.0023**	**-0.0001**	**0.04**
	3	-0.0012	-0.0032	0.0009	0.26	-0.0007	-0.0019	0.0006	0.32
Aβ only (N=133)	**1**	-0.0008	-0.0022	0.0007	0.30	-0.0011	-0.0030	0.0009	0.28
	2	-0.0009	-0.0024	0.0006	0.24	-0.0010	-0.0029	0.0010	0.34
	3	-0.0009	-0.0028	0.0010	0.37	-0.0011	-0.0031	0.0010	0.33
Total analytic sample (N=813)	**1**	-0.0013	-0.0029	0.0003	0.12	**-0.0013**	**-0.0023**	**-0.0003**	**0.01**
	2	-0.0012	-0.0028	0.0004	0.13	**-0.0013**	**-0.0024**	**-0.0003**	**0.01**
	3	-0.0014	-0.0030	0.0002	0.10	**-0.0013**	**-0.0023**	**-0.0002**	**0.02**

P-tau 181 units = pg/mL. Models are linear regression models. Model 1=adjusted for ADNI-MEM score at baseline; Model 2=Model 1 + age, gender, years of education, race/ethnicity; Model 3 = Model 2 + diabetes, hypertension, and hypercholesterolemia. Bolded results are significant at α=0.05.

Keywords: amyloid, blood biomarkers, generalizability, population-level, tau

8 Examination of synaptic density and neurofibrillary tau tangle burden in cognitively unimpaired and impaired older adults

Alexandra DiFilippo[1], Erin Jonaitis[2], Gilda Ennis[2], Max McLachlan[1], Andrew McVea[1], Brecca Bettcher[1], Mary-Elizabeth Pasquesi[2], Nancy Davenport-Sis[2], Nicholas Schulz[2], Yer Thor[2], Ethan Grover[2], Todd Barnhart[2], Jonathan Engle[2], Tobey Betthauser[2], Sterling Johnson[2], Barbara Bendlin[2], Bradley Christian[1,2]

[1]*University of Wisconsin-Madison Waisman Center, Madison, WI, United States*
[2]*University of Wisconsin-Madison School of Medicine and Public Health, Madison, WI, United States*

Background: Neurofibrillary tau tangle (NFT) accumulation is a defining characteristic of Alzheimer's disease (AD), originating in the entorhinal cortex (ERC) before progressing into the hippocampus (Hp) and throughout temporal cortex. AD-associated synaptic loss initiates within the Hp and extends into the neocortex. While the accumulation of NFTs and loss of synapses both serve as robust indicators of cognitive impairment and neurodegeneration, the precise interplay between these factors remains poorly understood. In this study, we conducted PET imaging on older adults, with and without cognitive impairment, to investigate the relationship between NFT burden and synaptic density in regions exhibiting early-stage NFT pathology.

Methods: Cognitively unimpaired (n = 63) and impaired (n = 31) participants were recruited from the Wisconsin ADRC, Wisconsin Registry for Alzheimer's Prevention study, and community. Cognitive status was determined through consensus conference. Brain imaging included structural MRI (PET registration, *FreeSurfer* parcellation) and PET ([^{11}C]PiB: amyloid status, [^{18}F]MK-6240 $SUVR_{70\text{-}90,infCb}$: ROI NFT burden, [^{11}C]UCB-J $DVR_{LGA,Cb}$: Hp synaptic density). Pearson's correlation and linear model used for relationship analyses.

Results: Data from N = 94 participants (Table 1) showed ERC NFT and Hp synaptic density to be highly correlated ($r = -.44$, $p < .001$). A linear model showed a strong relationship between ERC NFT and Hp synaptic density ($R^2 = .19$, $p < .001$). A similar relationship between Hp NFT and Hp synaptic density was observed: $r = -.49$, $p < .001$; model $p < .001$, $R^2 = .24$.

Conclusions: In a sample of participants with and without cognitive impairment , a pronounced inverse relationship between NFT burden within regions of early tau accumulation in AD and hippocampal synaptic density was observed. Fully understanding the local effects of NFTs on synaptic density and cognition will assist in informing the neurotoxic effects of AD pathology and efficacy of therapeutic treatments.

Table 1

Participant demographics by cognitive status

	Cognitively Unimpaired	MCI	Dementia
Participants (n)	63	20	11
Sex (F, %)	42, 67%	6, 30%	3, 27%
Age (years)	69.6 (7.1)	73.2 (6.3)	78.6 (5.5)
A+* (n, %)	23, 36%	15, 75%	10, 91%

Note: Continuous variables presented as *mean (standard deviation)*. *A+ = amyloid positive if global [^{11}C]PiB DVR > 1.19.
Abbreviations: *MCI*, mild cognitive impairment.

Table 2

Synaptic density and neurofibrillary tau burden by cognitive status

	Cognitively Unimpaired	MCI	Dementia
[^{11}C]UCB-J Hp DVR	0.97 (0.05) [0.83 – 1.13]	0.92 (0.09) [0.79 – 1.16]	0.86 (0.09) [0.78 – 1.03]
[^{18}F]MK-6240 ERC SUVR	1.41 (0.56) [0.83 – 3.11]	1.83 (0.94) [0.89 – 4.07]	2.37 (0.83) [0.97 – 3.81]
[^{18}F]MK-6240 Hp SUVR	1.12 (0.39) [0.65 – 2.12]	1.27 (0.49) [0.67 – 2.22]	1.68 (0.60) [0.77 – 2.50]

Note: Data presented as mean *(standard deviation) [range]*. Abbreviations: *MCI*, mild cognitive impairment; *Hp*, hippocampus; *DVR*, distribution value ratio; *ERC*, entorhinal cortex; *SUVR*, standardized uptake value ratio.

Figure 1

Hp synaptic density with ERC (left) and Hp (right) tau burden

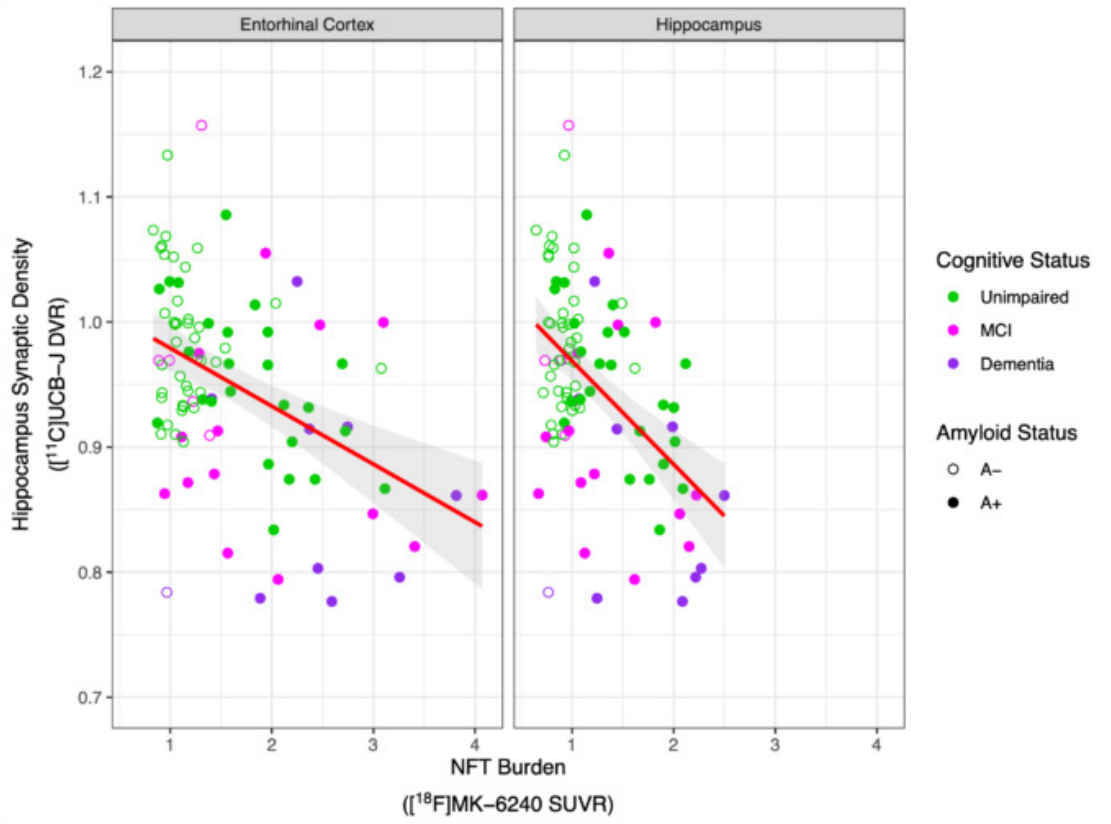

Note: Each datapoint depicts the ROI [18F]MK-6240 SUVR and corresponding Hp [11C]UCB-J DVR for each of the N=94 participants. The linear models are shown in red with the 95% confidence band shaded in grey. For ERC [18F]MK-6240 SUVR, the model is defined with intercept = 1.025, 95% CI [0.99, 1.06] and slope = -0.046, 95% CI [0.99, 1.06]. For Hip [18F]MK-6240 SUVR, the model is defined with intercept = 1.051, 95% CI [1.012, 1.091] and slope = -0.083, 95% CI [-0.113, -0.052].

Keywords: synaptic density, tau, PET

9 Association between plasma P-tau and cognition in the Alzheimer's disease spectrum

Jaime Fernandez[1,8], Joseph Therriault[1,8], Arthur Macedo[1,8], Stijn Servaes[1,8], Tina Wang[1,8], Nesrine Rahmouni[1,8], Etienne Aumont[1,8], Ali Hosseini[1,8], Cécile Tissot[1,2,8], Sulantha Mathotaarachchi[1,8], Jenna Stevenson[1,8], Alyssa Stevenson[1,8], Tharick Pascoal[1,8], Nicholas Ashton[1,8], Andrea Lessa[1,8], Thomas Karikari[1,8], Gallen Triana-Baltzer[1,8], Hartmuth Kolb[1,2,8], Henrik Zetterberg[1,8], Kaj Blennow[1,8], Pedro Rosa-Neto[1,8]

[1]*Translational Neuroimaging Laboratory, McGill Research Centre for Studies in Aging, Montreal, QC, Canada*
[2]*Lawrence Berkeley Laboratory, University of California, Berkeley, Berkeley, CA, United States*
[6]*Department of Psychiatry and Neurochemistry, Institute of Neuroscience and Physiology, The Sahlgrenska Academy, University of Gothenburg, Mölndal, Sweden*
[7]*King's College London, Institute of Psychiatry, Psychology and Neuroscience, Maurice Wohl Institute Clinical Neuroscience Institute, London, United Kingdom*
[8]*Neuroscience Biomarkers, Janssen Research & Development, La Jolla, CA, United States*
[9]*UK Dementia Research Institute at University College London, London, United Kingdom*
[10]*Hong Kong Center for Neurodegenerative Diseases, China, HK*
[8]*Department of Neurology and Neurosurgery, Faculty of Medicine, McGill University, Montreal, QC, Canada*
[9]*Wallenberg Centre for Molecular Medicine, University of Gothenburg, Gothenburg, Sweden*
[10]*Department of Neurology and Psychiatry, University of Pittsburgh School of Medicine, Pittsburgh, PA, United States*
[11]*NeuroQAM, Université du Quebec a Montréal, Montreal, QC, Canada*

Background: recent literature has unveiled the relationship between cognition and CSF p-tau biomarkers of Alzheimer's disease, but this relationship remains to be explored in detail in the most well-known plasma p-tau biomarkers.

Methods: we assessed 103 cognitively unimpaired (CU) older adults, and 40 cognitively impaired (CI), amyloid-β positive individuals. All participants had plasma assessments of p-tau181, p-tau217 and p-tau231, as well as amyloid-PET with [18F]AZD4694 and tau-PET with [18F]MK6240; and cognitive assessments including memory, executive function, language and visuospatial domains. We conducted regression analyses to explore the relationship between biomarkers and cognition. AUC values were also calculated for detection of cognitive impairment. Finally, we segregated participants into different profiles based on amyloid, p-tau and tau positivity and run tests to compare cognition across profiles.

Results: the relationship between p-tau biomarkers and cognition was strongest for p-tau217, particularly for memory. Plasma p-tau217 was superior than other p-tau biomarkers in detecting memory impairment, and at the level of tau PET. Memory impairment was already present in amyloid, p-tau217 or p-tau181 positive, but tau negative, subjects, as compared to subjects that were negative in all biomarkers.

Conclusions: plasma p-tau217 is revealed as a biomarker that is predominantly linked to memory impairment due to Alzheimer's disease.

Keywords: plasma p-tau, cognition, Alzheimer's disease, memory

10 The role of biofluid markers in predicting near-term cognitive impairment

Yara Yakoub[1], Nicholas J. Ashton[2], Thomas K. Karikari[2,3], Cherie Strikwerda-Brown[1,4], Frédéric St-Onge[1], Valentin Ourry[1], Michael Schöll[2], Maiya R. Geddes[1], Simon Ducharme[1], Pedro Rosa-Neto[1], Jean-Paul Soucy[1], John C.S. Breitner[1], Henrik Zetterberg[2], Kaj Blennow[2], Judes Poirier[1], Sylvia Villeneuve[1], for the Prevent-AD research group[1]

[1]*McGill University, Montreal, QC, Canada*
[2]*University of Gothenburg, Gothenburg, Sweden*
[3]*University of Pittsburgh, Pittsburgh, PA, United States*
[4]*The University of Western Australia, Perth, Australia*

Introduction: PET biomarkers have proven valuable for identifying cognitively unimpaired (CU) individuals who experience near-term clinical progression. Given the increasing enthusiasm about plasma biomarkers to detect Alzheimer's pathology, we assessed abnormal amyloid ($A\beta_{40/42}$) and tau (p-tau181) biomarkers in plasma ($A+T+_{plasma}$) in CU individuals as predictors of clinical progression to mild cognitive impairment (MCI). We then repeated these analyses using cerebrospinal fluid (CSF) and PET biomarkers.

Methods: We studied 293 participants from the PREVENT-AD cohort who had longitudinal cognitive follow-up (mean 7.7 years, range 1–10 years) and plasma biomarkers available when still CU. Cognition was measured annually using the RBANS. Plasma $A\beta_{42/40}$ concentrations were measured using ultrasensitive Simoa immunoassay, and plasma p-tau181 using an in-house Simoa platform (Gothenberg University). For 218 participants, plasma $A\beta_{42/40}$ was also analyzed using immunoprecipitation coupled with mass spectrometry (IP-MS). An overlapping 71 participants had $A\beta_{42/40}$ (meso scale discovery) and p-tau181 (Innotest enzyme-linked immunoassay) CSF data available, and 133 participants had Aβ (^{18}F-NAV4694) and tau (^{18}F-florbetapir) PET data.

Outcomes: Progression from CU to MCI and annual cognitive rate of change on the RBANS.

Results: The rate of progression from CU to MCI was 40.62% in $A+T+_{plasma}$ individuals when Aβ was measured with Simoa and 46.67% when measured using IP-MS; 55.56% in $A+T+_{CSF}$ and 90.00% in $A+T+_{PET}$ (Fig.1). Cox proportional hazard models indicated a faster progression rate in all A+T+ groups compared with their respective A-T- biomarker groups (Fig.2). Considering longitudinal RBANS scores, all A+T+ groups declined faster than the other groups (Fig.3).

Discussion: CU individuals classified as A+T+ based on plasma biomarkers are at increased risk of cognitive decline and clinical progression. Nevertheless, the progression rate in individuals classified with plasma was half the one found using PET suggesting that the latter remains the gold standard to identify presymptomatic pathological changes.

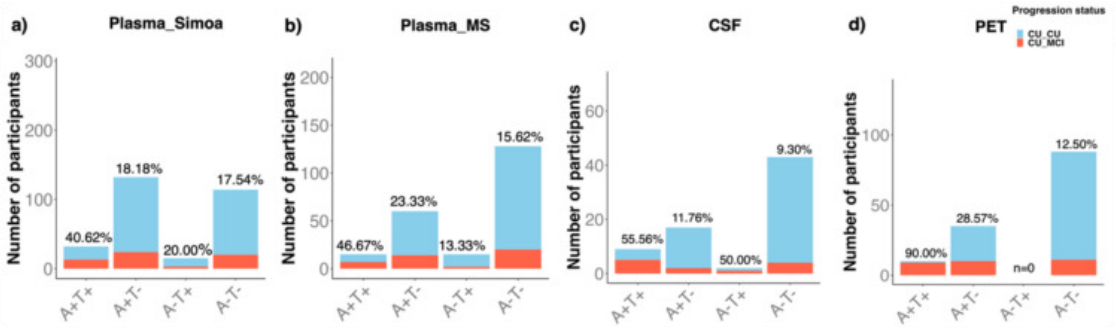

Figure 1. Bar graphs represent the proportion of MCI progressors across a) plasma $A\beta_{42/40}$ and p-tau181 measured using Simoa assay; b) plasma with $A\beta_{42/40}$ measured using mass spectrometry and plasma p-tau181 measured using Simoa; c) CSF; and d) PET biomarker profiles. *Notes*: The thresholds for Aβ and tau were based on independent cohorts when available ($A\beta_{42/40}$ and p-tau181plasma Simoa, CSF p-tau181) or derived using in-house methods. The results were similar if all thresholds of abnormality were set at the 35th percentile for Aβ and the 15th percentiles for tau. CU_CU: cognitively unimpaired older adults at the time of the biomarker measurement and remained cognitively unimpaired during follow-up; CU_MCI: cognitively unimpaired older adults at the time of the biomarker measurement, who progressed to MCI during follow-up.

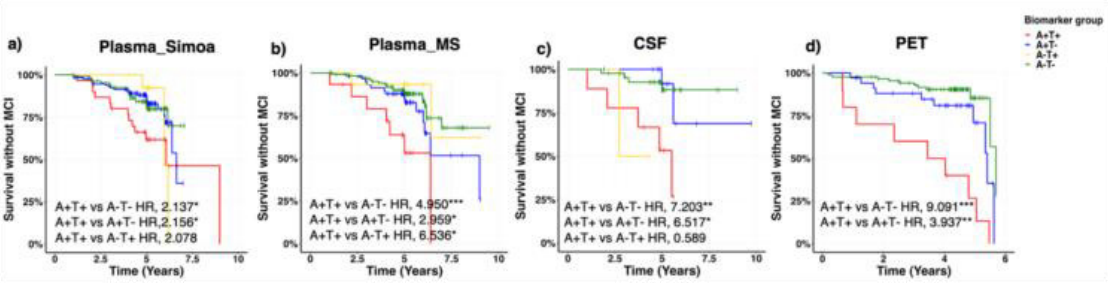

Figure 2. Cox proportional hazard models reflects the progression to MCI across a) plasma measured using Simoa assay; b) plasma with $A\beta_{42/40}$ measured using mass spectrometry; c) CSF; and d) PET biomarker profiles with risk table including the number of participants across the different biomarker groups at each time point. $^{*}P<0.05$, $^{**}P<0.01$, $^{***}P<0.001$

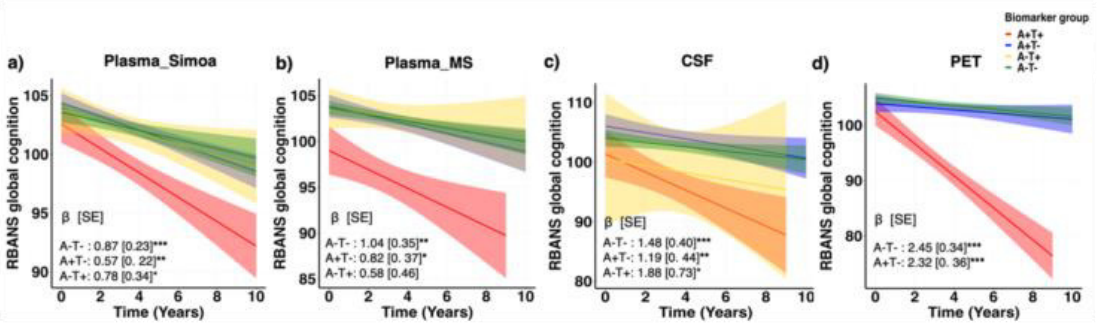

Figure 3. Longitudinal cognitive slopes for each biomarker group. Models included random slopes and intercepts for each participant and covariates of age, sex, and years of education. β estimates and SE are for the interaction between biomarker group and visit date, with A+T+ as the reference group. $^{*}P<0.05$, $^{**}P<0.01$, $^{***}P<0.001$

Keywords: plasma, CSF, PET, MCI, progression

11 Factors explaining tau onset age and time from tau onset to dementia

Margo B. Heston[1], Jordan Teague[2], Elena Ruiz de Chavez[2], Jacob Morse[2], Yuetiva K. Deming[2], Karly A. Cody[2], Rebecca E. Langhough[3], Megan L. Zuelsdorff[2,3], Tobey J. Betthauser[2,3]

[1]*Center for Health Disparities Research, University of Wisconsin School of Medicine and Public Health, Madison, WI, United States*
[2]*Wisconsin Alzheimer's Disease Research Center, University of Wisconsin School of Medicine and Public Health, Madison, WI, United States*
[3]*Wisconsin Alzheimer's Institute, University of Wisconsin School of Medicine and Public Health, Madison, WI, United States*

Background: Biomarker temporal models including sampled iterative local approximation (SILA) depict the hypothesized sequence of Alzheimer's disease (AD) and reveal variability in pathology and dementia onset age. The risk of earlier onset conferred by biological factors and social determinants of health remains unclear. We used SILA to generate person-level estimated tau onset age (ETOA) and time from T+ to dementia onset (TTD) to test whether biological risk factors and education were associated with younger ETOA and TTD.

Methods: 696 participants (Table 1) from the Alzheimer's Disease Neuroimaging Initiative with [^{18}F]flortaucipir scans processed by UC Berkeley were included in analyses. SILA was used to model longitudinal [^{18}F]flortaucipir meta-temporal SUVR (80-100 minutes post-injection; inferior cerebellum reference region) and estimate tau onset age (T+ SUVR>1.41 defined using Gaussian mixture modeling). Biological sex, number of *APOE*-ε4 alleles, *APOE*-by-sex interaction, and education were tested individually as ETOA predictors (log-rank test, Cox proportional hazards). A subset of 120 participants with ETOA at or before their last available PET measure were included to test whether the above factors and ETOA predicted TTD (CDR≥1).

Results: Median ETOA was 72.0 years old among T+ individuals. Female sex, higher *APOE*-ε4 allelic dose, and lower education were associated with earlier ETOA (Figure 1); female sex and higher *APOE*-ε4 allelic dose were associated with higher T+ risk. While *APOE*-by-sex was significantly associated with altered ETOA (Figure 1), T+ risk was primarily driven by *APOE* (Table 2). Median (95 CI%) TTD was 7.4 (5.96, 8.08) years (Figure 2). Only older ETOA was associated with shorter TTD.

Conclusions: *APOE*-ε4 carriage, education, and female sex were linked to earlier T+ onset. Earlier tau onset was linked to prolonged time to dementia onset. Future work will account for amyloid burden and onset age, and community-level exposure to socioeconomic disadvantage in additional cohorts.

Table 1. Participant demographics. Diagnosis at baseline is determined using scores from the Mini-Mental State Exam, CDR, and delayed paragraph recall from the Wechsler Memory Scale – Revised Logical Memory subscale, as well as reported impairment in cognitive functions and activities of daily living.

	ETOA Analysis	TTD Analysis
Characteristic	**N = 696**	**N = 120**
Age at baseline, *years*[1]	74 (7.7)	74 (7.7)
Diagnosis at baseline[2]		
Cognitively unimpaired	198 (28%)	12 (10%)
Subjective mild cognitive impairment	212 (31%)	15 (13%)
Early MCI	131 (19%)	28 (24%)
Late MCI	112 (16%)	41 (34%)
AD dementia	42 (6.0%)	23 (19%)
Unknown	1	1
Female sex[2]	359 (52%)	64 (53%)
APOE-ε4 allelic dose[2]		
0	402 (61%)	32 (28%)
1	211 (32%)	59 (52%)
2	48 (7.3%)	22 (19%)
Unknown	35	7
Education level[2]		
High school or less (≤12 years)	66 (9.5%)	13 (11%)
Some college (13-16 years)	303 (44%)	66 (55%)
Postgraduate	327 (47%)	41 (34%)
Race[2]		
White	636 (91%)	113 (94%)
Black	30 (4.3%)	4 (3.3%)
More than one	13 (1.9%)	2 (1.7%)
Asian	12 (1.7%)	
Unknown	3 (0.4%)	1 (0.8%)
Native American/Alaska Native	2 (0.3%)	

[1]Mean (SD), [2]n (%)

Table 2. Risk of tau positivity and dementia onset. Estimates were calculated using Cox proportional hazard models; *p*-values are calculated for contrast effects. Main effects of sex and *APOE*-ε4 allelic dose are reported from *APOE*-by-sex interaction model. Time to tau positivity event time was ETOA for T+ individuals and age at last PET observation (right censored) for individuals who were T- but could become T+. Event time for TTD was defined using dementia onset time – ETOA for individuals with dementia, and age at last CDR measurement – ETOA (right censored) for individuals with CDR < 1 across all observations.

	ETOA				TTD			
Predictor	**N (696)**	**HR**	**95% CI**	**p-value**	**N (120)**	**HR**	**95% CI**	**p-value**
Participant sex								
Female	359	—	—		64	—	—	
Male	337	1.06	0.55, 2.04	0.9	56	1.29	0.76, 2.19	0.3
APOE ε4 allelic dose								
0	402	—	—		32	—	—	
1	211	6.25	3.47, 11.3	<0.001	59	0.76	0.41, 1.41	0.4
2	48	11.7	5.35, 25.4	<0.001	22	0.81	0.39, 1.68	0.6
APOE-by-sex interaction		0.82	0.51, 1.34	0.4	—			
Education level								
High school or less (≤ 12 years)	66	—	—		13	—	—	
Some college (13-16 years)	303	1.21	0.68, 2.14	0.5	66	1.06	0.44, 2.54	0.9
Postgraduate education	327	0.62	0.34, 1.13	0.12	41	0.73	0.28, 1.90	0.5
Estimated age at tau onset, *years*	—							
40-60					12	—	—	
60-70					38	1.54	0.68, 3.50	0.3
70-80					47	4.19	1.75, 10.0	0.001
80+					23	17.4	5.78, 52.3	<0.001

HR, Hazard Ratio, *CI*, Confidence Interval.

Figure 1. Predictors of estimated tau onset age (ETOA; N=696; n=661 for *APOE*-ε4 allelic dose and *APOE*-by-sex models). Lines indicate ETOA calculated per group, with 95% confidence intervals included. Log-rank test *p*-values are reported for overall difference between groups. Event time was ETOA for T+ individuals and age at last PET observation (right censored) for individuals who were T- but could become T+.

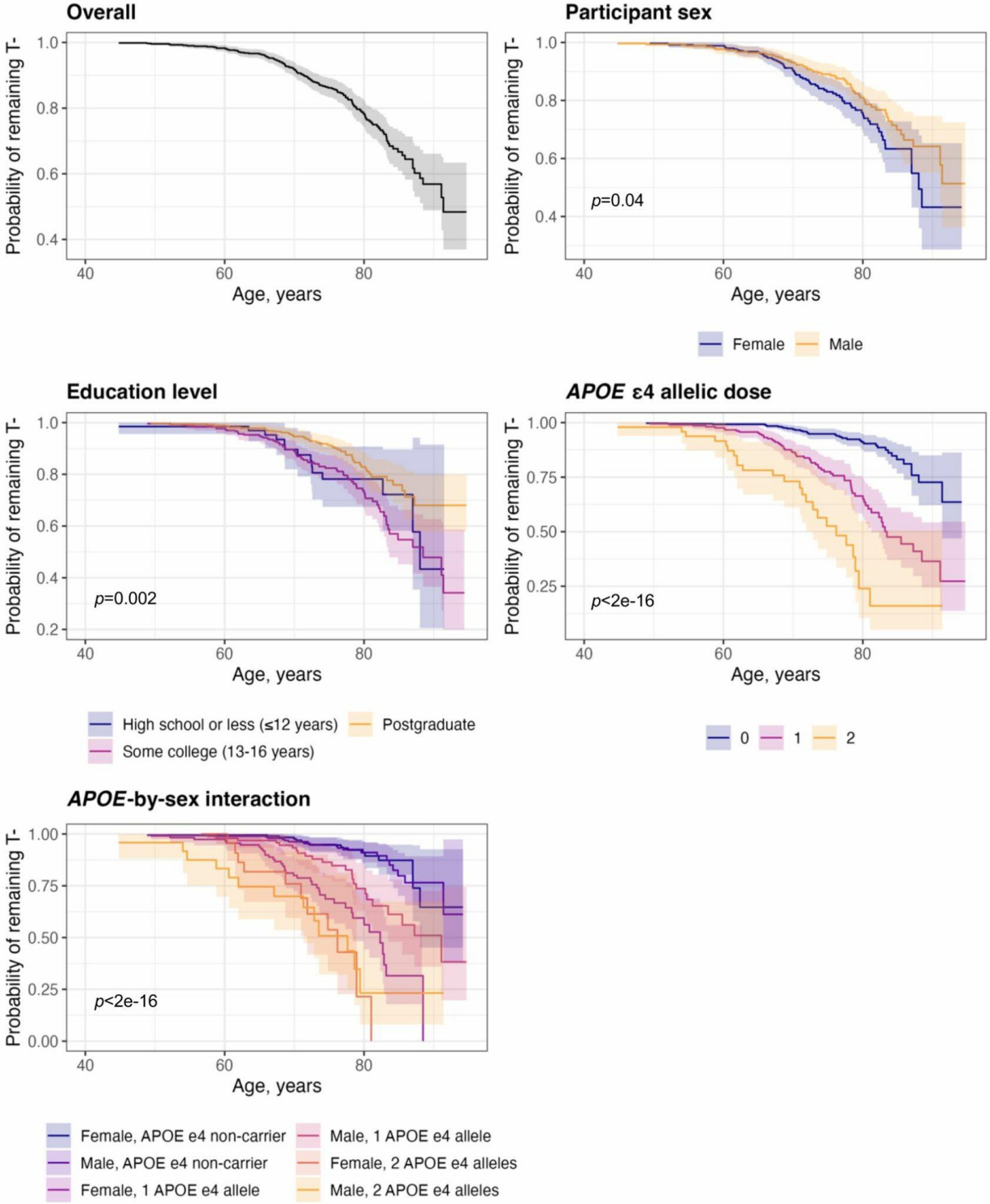

Figure 2. Predictors of TTD in the subset that had ETOA at or before the final available PET scan (n=120; n=113 for *APOE*-ε4 allelic dose model). Participants with dementia onset before ETOA (n=10) were excluded from analyses. Lines indicate time from ETOA (i.e., ETOA duration=0) to dementia onset (TTD calculated as dementia onset age – ETOA) calculated per group, with 95% confidence intervals included. Log-rank test *p*-values are reported for overall difference between groups. TTD event time was defined using dementia onset time minus ETOA for individuals with dementia, and age at last CDR measurement minus ETOA (right censored) for individuals with CDR < 1 across all observations.

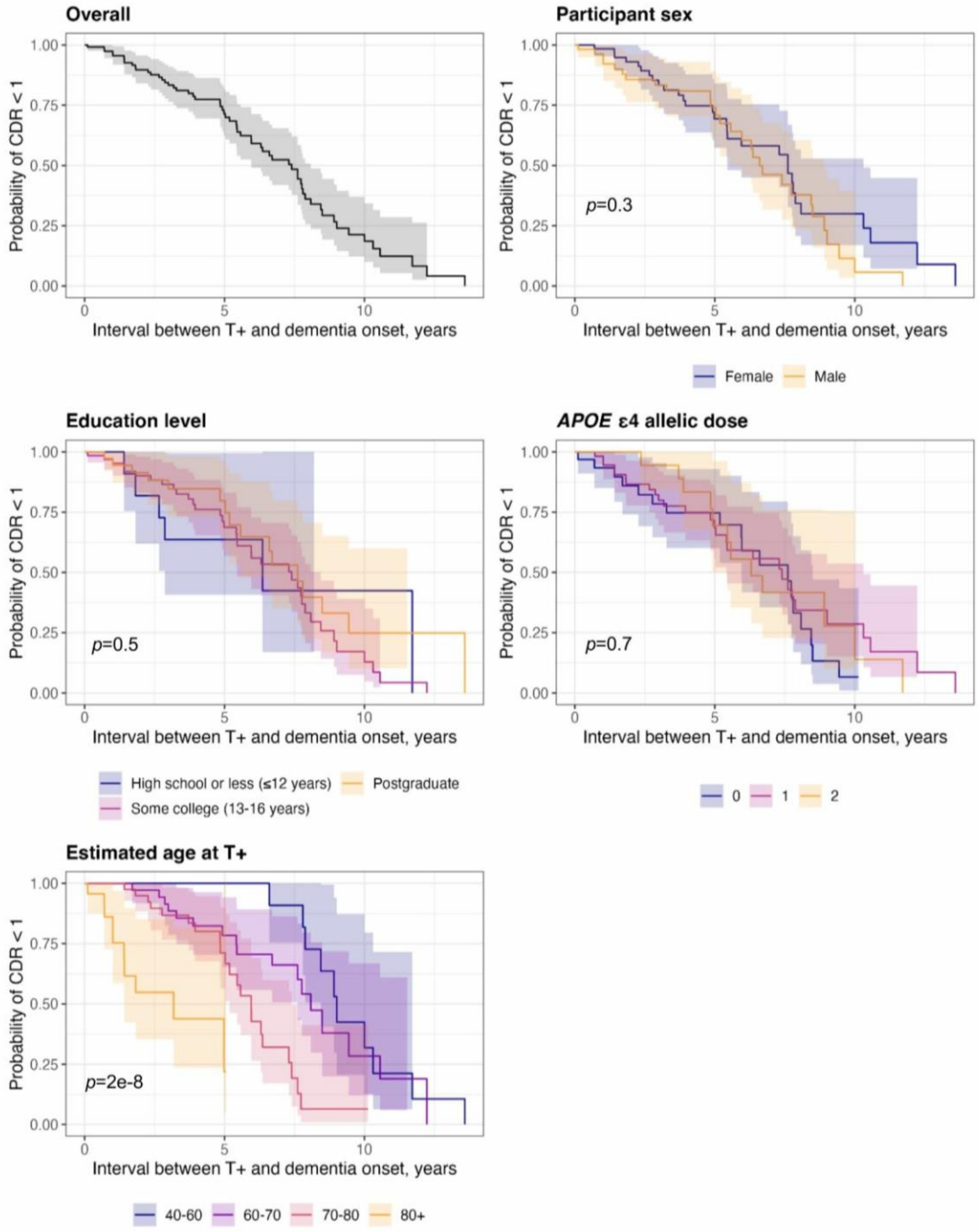

Keywords: temporal modeling, [18F]flortaucipir, dementia, risk factors, social determinants of health

12 Evaluation of ComBat as a harmonization technique for reducing across-tracer variance in regional amyloid PET analyses

Braden Yang[1], Thomas Earnest[1], Sayantan Kumar[1], Brian Gordon[1], Aristeidis Sotiras[1,2]

[1]*Mallinckrodt Institute of Radiology, Washington University in St. Louis, St. Louis, MO, United States*
[2]*Institute for Informatics, Data Science & Biostatistics, Washington University in St. Louis, St. Louis, MO, United States*

Background: Differences in amyloid PET radiotracer pharmacokinetics and binding properties lead to discrepancies in amyloid uptake measurements, which may adversely affect the statistical power of clinical trials that utilize multiple tracers to track brain amyloid deposition. To address this, the Centiloid scale was developed as a method of standardizing global amyloid SUVRs across tracers to a common scale. However, Centiloid has not been validated for regional SUVRs, and requires a calibration dataset to establish conversion equations. Alternatively, ComBat is a technique for reducing non-biological variance in a data-driven way, but this has not been validated for amyloid PET.

Objective: To evaluate the efficacy of ComBat to reduce tracer-specific biases in regional SUVRs of ^{18}F-Florbetapir (FBP) and Pittsburgh compound B (PiB) amyloid PET.

Methods: 113 FBP-PiB scan pairs, acquired within 90 days, were selected from 99 subjects from the OASIS-3 dataset. Regional SUVRs were extracted using the PET Unified Pipeline, which were converted to Centiloid using the OASIS-3 conversion equations. Additionally, ComBat models were trained on all remaining FBP (n=308) and PiB (n=636) baseline scans and applied to the 113 scan pairs. Three configurations of ComBat covariates were investigated: no covariates; linear age, sex, APOE-ε4; and non-linear age, sex, APOE-ε4. Intraclass correlation coefficient (ICC) and mean standardized absolute error (MsAE) were computed to measure absolute agreement of SUVRs across tracers.

Results: ComBat with no covariates performed better than Centiloid in increasing across-tracer agreement of regional SUVRs within the global summary region and did not significantly decrease tracer agreement in other cortical regions. All techniques failed to harmonize subcortical regions. Inclusion of covariates in ComBat modeling generally reduced agreement.

Conclusion: We successfully utilized ComBat, a fully data-driven technique, to harmonize regional amyloid PET SUVRs across FBP and PiB, which performed better than Centiloid within the global summary region and other cortical regions.

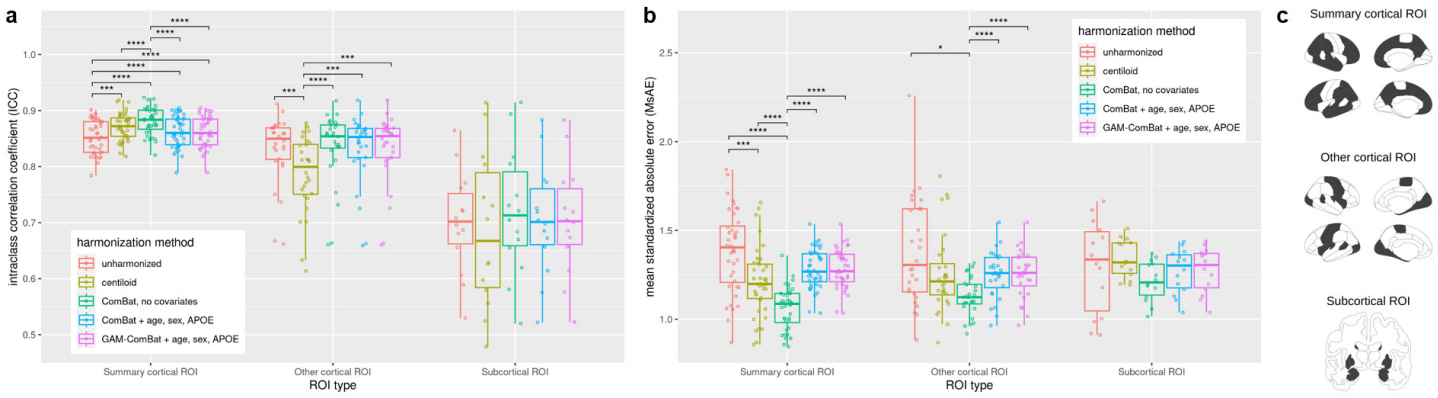

Figure 1. Regional ICC (*a*) and MsAE (*b*), grouped by region-of-interest (ROI) type. Bonferroni-corrected statistical significance of paired t-tests are indicated by asterisks (1 = p<0.05, 2 = p<0.01, 3 = p<0.001, 4 = p<1e-4). (*c*) Subgroupings of ROI, colored in gray. The summary cortical ROI are regions which compose the global summary meta-ROI, and includes frontal, parietal, and temporal regions. Other cortical ROI are regions in the cortex which are not part of the summary meta-ROI.

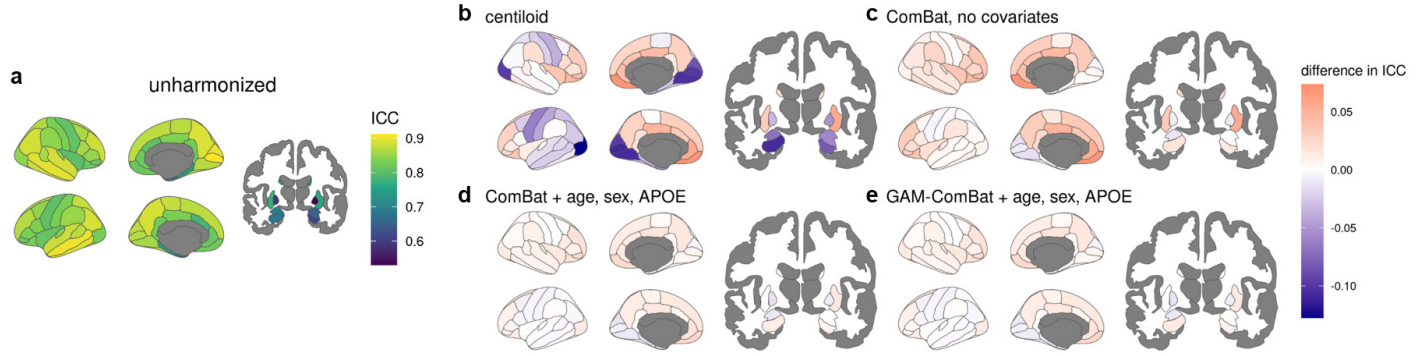

Figure 2. (*a*) Regional ICC plotted on the surface. Values closer to 1 indicate better agreement between tracer SUVRs. (*b*) - (*e*) Change in regional ICC of harmonized SUVRs compared to the ICC of the unharmonized SUVRs.

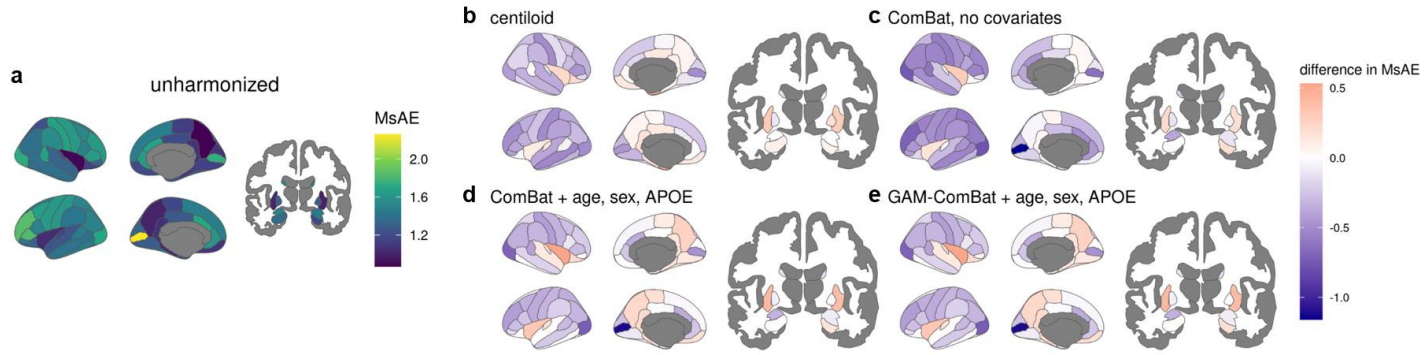

Figure 3. (*a*) Regional MsAE plotted on the surface. Smaller values indicate better agreement between tracer SUVRs. (*b*) - (*e*) Change in regional MsAE of harmonized SUVRs compared to the MsAE of the unharmonized SUVRs.

Keywords: amyloid PET, harmonization, Centiloid, ComBat

13 Neurophysiological changes related to amyloid and tau pathology are associated with longitudinal cognition and Mild Cognitive Impairment progression

Jonathan Gallego Rudolf[1,2], Alex Wiesman[2], Sylvain Baillet[2], Sylvia Villeneuve[1]

[1]*Douglas Mental Health University Institute, Montreal, QC, Canada*
[2]*Montreal Neurological Institute, Montreal, QC, Canada*

Alzheimer's Disease (AD) is defined by the pathological accumulation of amyloid-beta (Aβ) and tau in the brain. Regional deposition of these proteins is associated with changes in frequency-defined neurophysiological activity that can be detected using non-invasive magnetoencephalography (MEG). We examined whether neurophysiological activity alterations were associated with participants' demographic and clinical characteristics. We also addressed the utility of MEG for predicting progression of cognitively unimpaired individuals to mild cognitive impairment (MCI).

We used Positron Emission Tomography (PET) to measure the deposition of Aβ ([18F]NAV4694) and tau ([18F] Flortaucipir), Magnetic Resonance Imaging (MRI) to measure hippocampal volume and resting-state MEG to capture neurophysiological activity in a group of clinically unimpaired older adults with family history of AD (PREVENT-AD cohort; n=103). We implemented a multivariate partial least squares (PLS) analysis to test the association between imaging markers (i.e., neurophysiological activity and AD proteinopathy) and participants' clinical profiles (i.e., demographic-clinical variables and longitudinal cognition data). We then used logistic regression models to assess the added value of neurophysiological activity for predicting MCI progression (21 MCI progressors), as compared to established clinical, MRI, and PET imaging markers.

The PLS analysis identified a significant latent variable linking proteinopathy-related neurophysiological activity slowing to positive APOE ε4 status and longitudinal deficits across multiple cognitive domains. The logistic regression model that included demographic/clinical variables and MRI hippocampal volume had an AUC=0.830. Incorporating MEG spectral power features from temporal tau accumulating regions resulted in a considerable increase in accuracy (AUC=0.908), almost matching the accuracy provided by adding Aβ and tau PET (AUC=0.918).

Our results show that the neurophysiological changes linked to AD pathology are associated with longitudinal cognitive impairment. Neurophysiological activity features improve the accuracy for predicting MCI progression, contributing information beyond demographic/clinical variables and structural MRI and representing a more accessible and less invasive alternative than PET imaging.

Keywords: Neurophysiology, Amyloid, Tau, Cognition, Mild Cognitive Impairment progression

14 Tau and Amyloid associations with sustained attention and episodic memory performance in clinically unimpaired older adults

America Romero[1,2], Joseph R. Winer[1], Tammy T. Tran[2], Julia E. Rathmann-Bloch[2], Jennifer Park[1,2], Shawn T. Schwartz[2,3], Douglas S. Miller[2], David Anders[4], Aimara Morales[4], Edward N. Wilson[1,3], Alexandra N. Trelle[1], Katrin I. Andreasson[1,3], Guido A. Davidzon[4], Elizabeth C. Mormino[1,3], Anthony D. Wagner[2,3]

[1]*Department of Neurology and Neurological Sciences, Stanford University School of Medicine, Stanford, CA, United States*
[2]*Department of Psychology, Stanford University, Stanford, CA, United States*
[3]*Wu Tsai Neurosciences Institute, Stanford University, Stanford, CA, United States*
[4]*Department of Radiology, Stanford University School of Medicine, Stanford, CA, United States*

Background: Episodic memory in older adults is marked by high interindividual variability. It is unclear whether diminished attentional processes in aging and individual differences in sustained attention account for variability in memory performance, and subsequently, age-related diminished recall in unimpaired older adults. Amyloid beta (Aβ) and tau burden contribute to cognitive decline though the specific relationship between AD biomarkers and sustained attention has not received much investigation.

Methods: Clinically unimpaired older adults (N=65; 66-89 yrs, M=73.9 yrs) from the Stanford Aging and Memory Study (SAMS) or the Attention, Memory and Aging Study at Stanford (AMASS) completed the Gradual-Onset Continuous Performance Task (gradCPT) to assay between-person variability in sustained attention, along with neuropsychological tests of episodic memory (HVLT-R, BVMT-R, WMS-III LM). SAMS participants (N=25) completed a 18F-PI-2620 tau PET scan, with analyses focusing on volume-weighted mean SUVR within bilateral entorhinal cortex, amygdala, and inferior temporal gyrus. A comparison group of young adults (N=35; 18-35 yrs, M=24.3 yrs) completed the gradCPT.

Results: Older adults showed decreased sustained attention performance on gradCPT compared to young adults (accuracy: lower d', increased omission errors, increased median reaction time). Within the older adult group, increasing age was associated with lower accuracy (d') and increased reaction time variability (RTV). Analyses also revealed that Aβ+ older adults displayed increased RTV compared to Aβ- participants (**Figure 1**). GradCPT accuracy (d'), commission error rate, and RTV also predicted individual differences in episodic memory performance (**Figure 2**). Exploratory analyses on a subset of participants showed that 18F-PI-2620 uptake correlated with gradCPT commission error rate and RTV (**Figure 3**).

Conclusions: These findings raise the possibility that Aβ and tau accumulation explain between-person variability in attentional processes in older adults, with individual differences in sustained attention accounting for some of the variability in older adults' episodic memory performance.

Figure 1. GradCPT performance between younger and clinically unimpaired older adults, showing decreased accuracy (d'), increased omission errors, increased median reaction time. GradCPT performance within older adults, decreased d' and increased median reaction time with age. Aβ+ older adults displayed increased reaction time variability compared to Aβ- older adults.

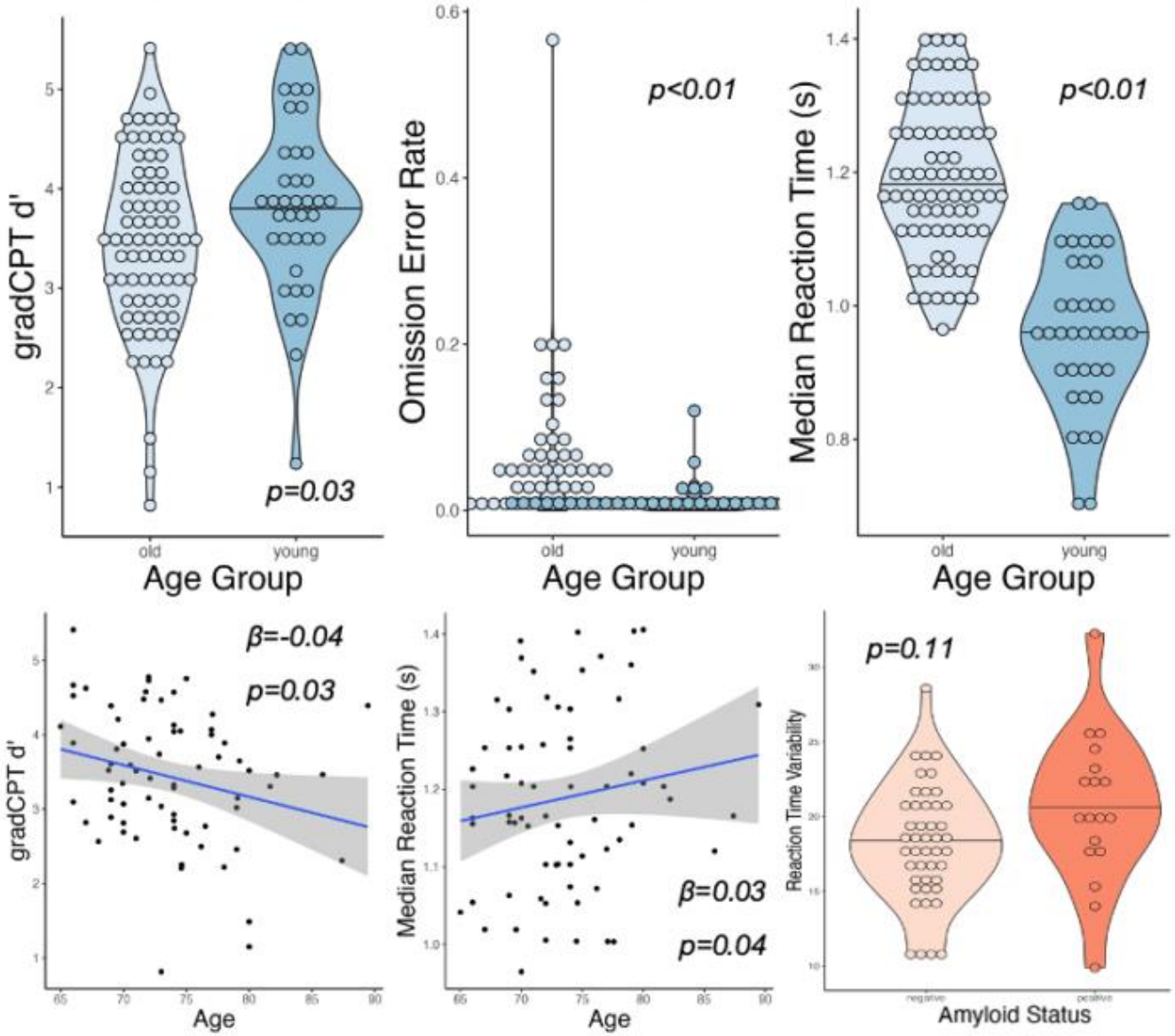

Figure 2. GradCPT accuracy (d'), commission error rate, and reaction time variability predicted individual differences in episodic memory performance.

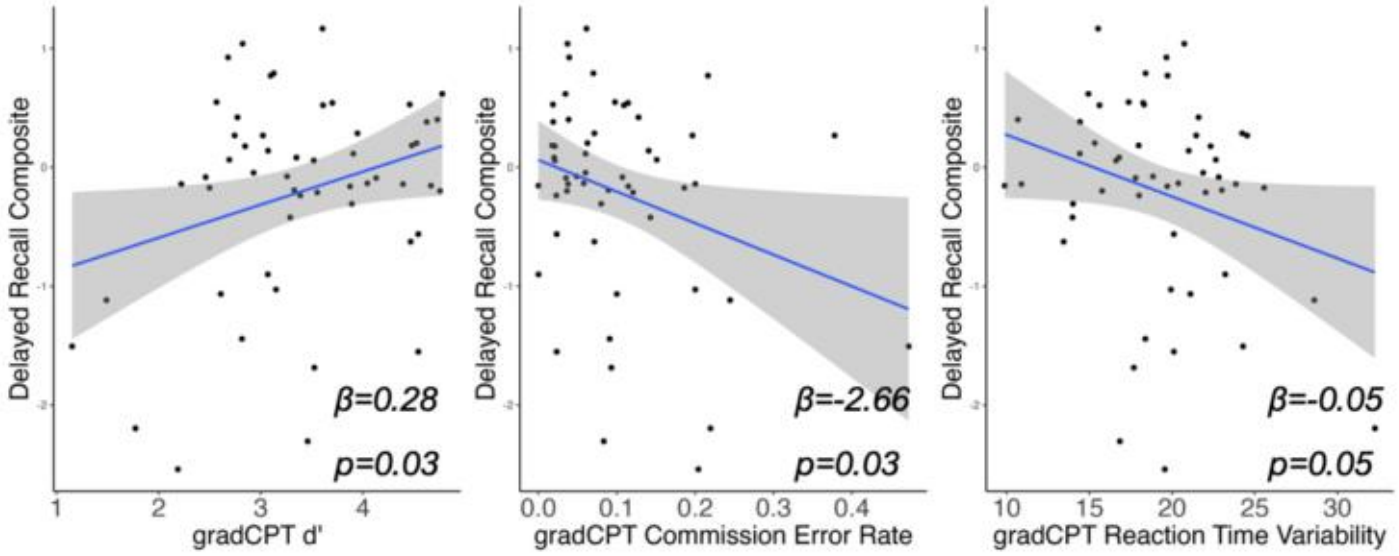

Figure 3. 18F-PI-2620 uptake — utilizing a composite volume-weighted value from the entorhinal cortex, amygdala, and inferior temporal gyrus — correlated with gradCPT commission error rate and reaction time variability.

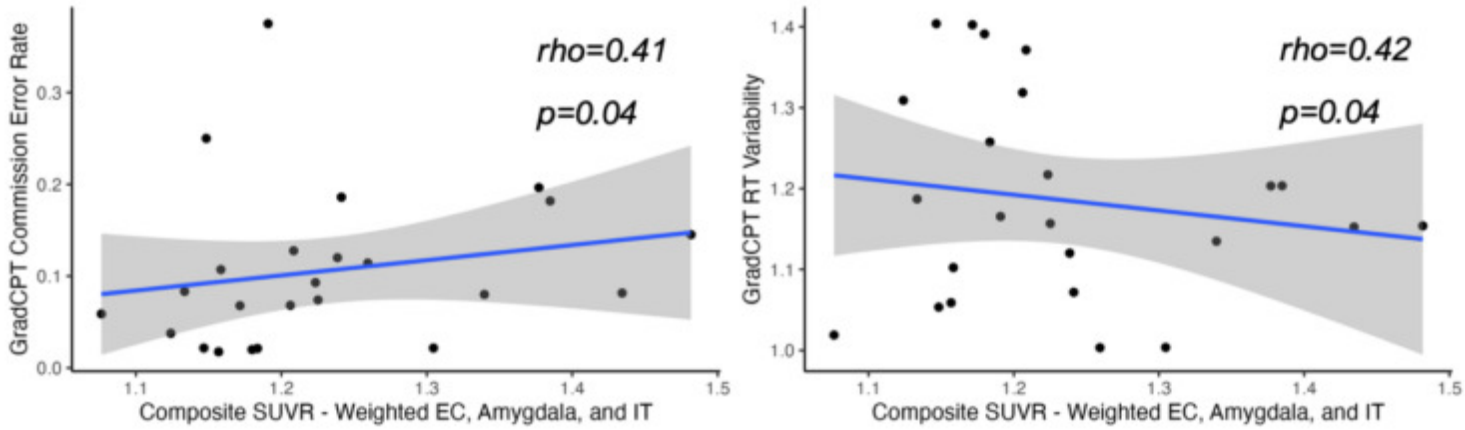

Keywords: sustained attention, episodic memory, tau PET

15 Sex differences in the relationships between 24-h rest-activity patterns and plasma markers of Alzheimer's disease pathology

Maxime Van Egroo[1], Elise Beckers[1,2], Nicholas Ashton[3,4,5,6], Kaj Blennow[3,7], Henrik Zetterberg[3,7,8], Heidi Jacobs[1,9]

[1]*Faculty of Health, Medicine and Life Sciences, School for Mental Health and Neuroscience, Alzheimer Centre Limburg, Maastricht University, Maastricht, The Netherlands*
[2]*Sleep and Chronobiology Lab, GIGA-Institute, CRC-In Vivo Imaging Unit, University of Liège, Liège, Belgium*
[3]*Department of Psychiatry and Neurochemistry, Institute of Neuroscience and Physiology, The Sahlgrenska Academy at the University of Gothenburg, Mölndal, Sweden*
[4]*Centre for Age-Related Medicine, Stavanger University Hospital, Stavanger, NO*
[5]*King's College London, Institute of Psychiatry, Psychology and Neuroscience, Maurice Wohl Institute Clinical Neuroscience Institute, London, United Kingdom*
[6]*NIHR Biomedical Research Centre for Mental Health and Biomedical Research Unit for Dementia at South London and Maudsley NHS Foundation, London, United Kingdom*
[7]*Clinical Neurochemistry Laboratory, Sahlgrenska University Hospital, Mölndal, Sweden*
[8]*Department of Neurodegenerative Disease, UCL Institute of Neurology, Queen Square, London, United Kingdom*
[9]*Gordon Center for Medical Imaging, Department of Radiology, Massachusetts General Hospital and Harvard Medical School, Boston, MA, United States*

Background: Although separate lines of research indicated a moderating role of sex in sleep-wake disruption and in the interindividual vulnerability to Alzheimer's disease (AD)-related processes, the investigation of sex differences in the interplay between sleep-wake dysregulation and AD pathology remains critically overlooked. Here, we examined sex-specific differences in the associations between circadian rest-activity patterns and novel AD-related plasma markers across the adult lifespan.

Methods: Ninety-seven cognitively unimpaired adults (mean age=60.73±14.33y., range=30–87y., 50 females, **Figure 1**) underwent 10 days of actigraphic recordings, and blood drawing. Standard non-parametric indices of 24-h rest-activity rhythm fragmentation (intradaily variability, IV) and stability (interdaily stability, IS) were computed. Plasma concentrations of neurofilament light chain (NfL), glial fibrillary acidic protein (GFAP), amyloid-$\beta_{42/40}$ ratio ($A\beta_{42/40}$), total tau, and tau phosphorylated at threonine 181 (p-tau_{181}) or 231 (p-tau_{231}) were measured using Single molecule array technology.

Results: Multiple linear regression models adjusted for age, sex, education, and body mass index showed that higher IV, indicating worse 24-h rest-activity rhythm fragmentation, was associated with higher plasma NfL (p<.0001), GFAP (p=.02), and at trend level with lower $A\beta_{42/40}$ ratio values (p=.053, **Figure 2**). Lower IS, reflecting more instability in the 24-h rest-activity rhythm, was related to higher plasma NfL (p=.02). Importantly, interaction models demonstrated that males were driving the relationships between IV and plasma NfL (p<.0001) or GFAP (p=.001), and revealed a male vulnerability on p-tau_{181} (IV: p<.0001; IS: p=.0004) and p-tau_{231} (IV: p=.0006; IS: p=.057, **Figure 3**). These associations remained unchanged when adding *APOE* ε4 carriership, depression, or self-reported symptoms of possible sleep apnea as additional covariates.

Conclusion: These findings suggest that the association between disrupted circadian rest-activity patterns and AD pathophysiological processes are more evident in cognitively unimpaired males. Our results have clinical implications for improved early detection and selection of at-risk individuals to be enrolled in preventive interventions.

Figure 1. Demographic characteristics, actigraphic variables, and plasma AD biomarkers in the whole study sample (*n* = 97), as well as stratified by sex.

	Whole sample (n = 97)	Females (n = 50)	Males (n = 47)
Demographic characteristics			
Age, years	60.73 ± 14.33 [30–87]	59.04 ± 14.23 [30–87]	62.53 ± 14.38 [31–85]
Education, years	14.49 ± 1.99 [10–20]	14.28 ± 2.11 [10–20]	14.72 ± 1.85 [10–20]
Ethnicity	Caucasian	Caucasian	Caucasian
Right-handed, *n* (%)	97 (100)	50 (100)	47 (100)
Body mass index, Kg/m²	24.51 ± 2.87 [17.56–31.71]	23.71 ± 3.15 [17.56–31.71]	25.04 ± 2.62 [19.71–30.04]
APOE ε4 carriers, *n* (%)[a]	33 (34.02)	14 (28.00)	19 (40.43)
Mini-Mental State Examination, score	28.98 ± 1.15 [26–30]	29.18 ± 1.00 [26–30]	28.77 ± 1.25 [26–30]
Hamilton Rating Scale for Depression, score	2.16 ± 2.42 [0–12]	2.36 ± 2.68 [0–12]	1.96 ± 2.12 [0–11]
Actigraphic variables			
Recording duration, days	9.81 ± 0.74 [7.07–12.07]	9.71 ± 0.58 [7.80–11.55]	9.90 ± 0.88 [7.07–12.07]
Actigraphic device wear ratio	1.00 ± 0.005 [0.97–1.00]	1.00 ± 0.005 [0.97–1.00]	1.00 ± 0.003 [0.99–1.00]
Intradaily variability	0.53 ± 0.16 [0.27–1.08]	0.48 ± 0.12 [0.27–0.77]	0.59 ± 0.19 [0.33–1.08]
Interdaily stability	0.63 ± 0.09 [0.43–0.83]	0.65 ± 0.09 [0.44–0.83]	0.61 ± 0.08 [0.43–0.77]
Plasma AD biomarkers			
NfL (pg/ml)[b]	18.61 ± 7.32 [6.56–43.43]	18.01 ± 6.77 [6.78–34.55]	19.23 ± 7.88 [6.56–43.43]
GFAP (pg/ml)[b]	152.90 ± 58.45 [53.79–389.32]	155.96 ± 60.32 [53.79–335.91]	149.14 ± 60.57 [75.32–389.32]
$A\beta_{40}$ (pg/ml)[b]	92.60 ± 11.49 [66.25–124.69]	91.38 ± 9.18 [73.66–119.15]	92.87 ± 13.17 [66.25–124.69]
$A\beta_{42}$ (pg/ml)[b]	8.34 ± 1.32 [3.32–11.02]	8.36 ± 1.24 [5.98–11.02]	8.34 ± 1.37 [3.32–10.81]
$A\beta_{42/40}$ ratio[b]	0.09 ± 0.01 [0.05–0.12]	0.09 ± 0.01 [0.06–0.12]	0.09 ± 0.01 [0.05–0.12]
Total tau (pg/ml)[c]	2.63 ± 0.87 [0.75–7.58]	2.68 ± 0.71 [0.75–4.01]	2.58 ± 1.02 [1.39–7.58]
p-tau_{181} (pg/ml)[c]	1.66 ± 0.75 [0.80–6.44]	1.48 ± 0.55 [0.80–3.15]	1.85 ± 0.89 [0.91–6.44]
p-tau_{231} (pg/ml)[b]	8.39 ± 3.80 [3.29–28.94]	7.75 ± 2.59 [3.81–16.34]	9.07 ± 4.68 [3.29–28.94]

[a] data missing for *n* = 1; [b] data missing for *n* = 5; [c] data missing for *n* = 11

Figure 2. Relationships between actigraphy-derived 24-h rest-activity rhythm fragmentation and plasma levels of neurofilament light chain (left, $t(86) = 4.31$, $p < .0001$), glial fibrillary acidic protein (middle, $t(86) = 2.36$, $p = .02$), and amyloid-beta$_{42/40}$ ratio (right, $t(86) = -1.96$, $p = .053$). Statistical models include covariates of age, sex, education, and body mass index. Red circles = female participants, blue circles = male participants.

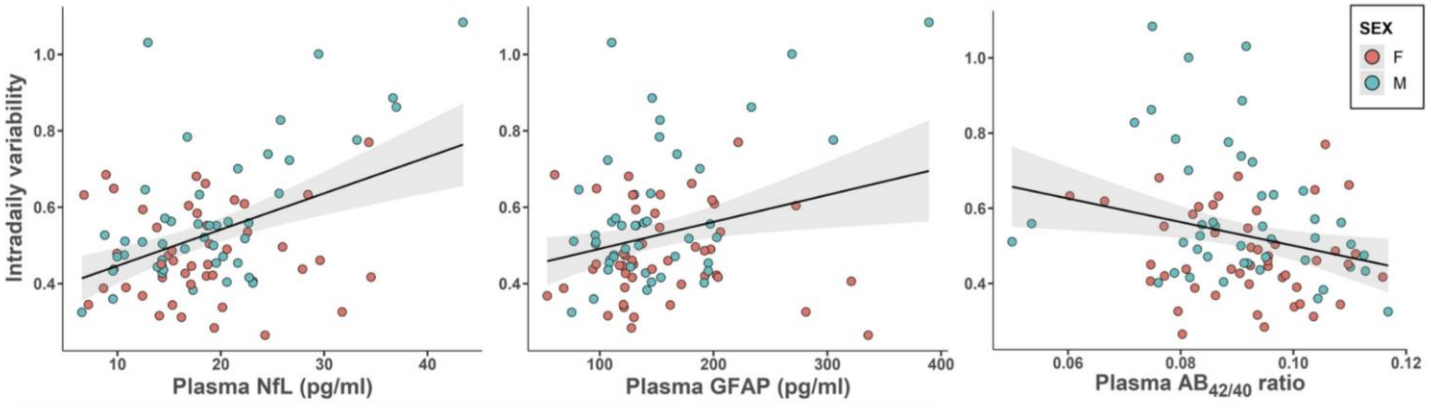

Figure 3. Sex-specific differences in the associations between actigraphy-derived 24-h rest-activity rhythm fragmentation (intradaily variability, IV) or stability (interdaily stability, IS) and plasma levels of neurofilament light chain ($t(85) = 4.14$, $p < .0001$), glial fibrillary acidic protein ($t(85) = 3.33$, $p = .001$), tau phosphorylated at threonine 181 (IV: $t(77) = 4.28$, $p < .0001$; IS: $t(77)=-3.67$, $p = .0004$), and tau phosphorylated at threonine 231 (IV: $t(83) = 3.57$, $p = .0006$; IS: $t(83) = -1.93$, $p = .057$). Statistical models include covariates of age, sex, education, and body mass index. Regression lines and associated 95% confidence interval for female and male participants are displayed in red and blue, respectively.

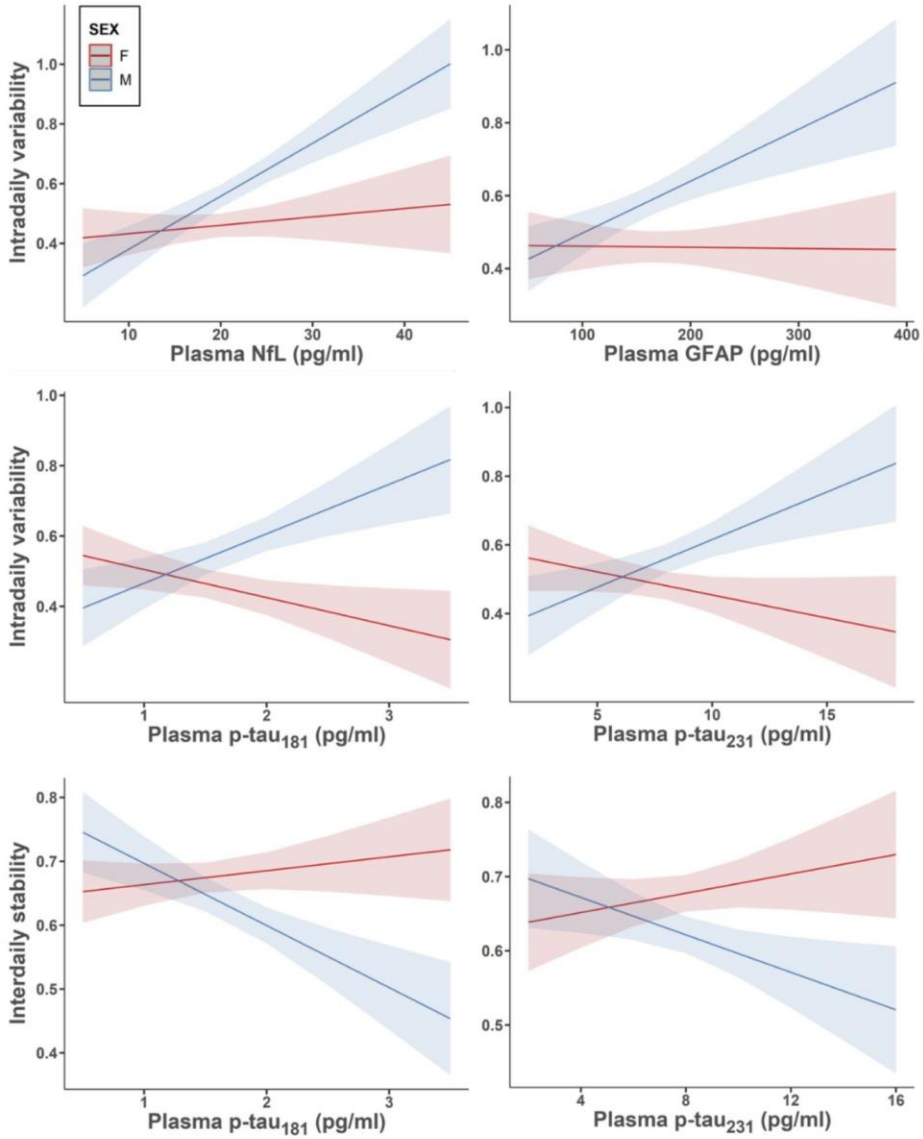

Keywords: 24-h rest-activity patterns, Actigraphy, Alzheimer's disease, Sex differences, Plasma biomarkers

16 NODDI-derived measures of microstructural integrity in medial temporal lobe white matter pathways are associated with Alzheimer's disease pathology

Dana Parker[1], Jenna Adams[1], Soyun Kim[1], Liv McMillan[1], Michael Yassa[1]

[1]*Department of Neurobiology and Behavior, University of California, Irvine, Irvine, CA, United States*

Introduction: Diffusion tensor imaging has been widely used to assess white matter (WM) changes in the early stages of Alzheimer's disease (AD), however, the tensor model is necessarily limited by its inability to detect diffusion alterations at a molecular level. A new method based upon multishell acquisition, Neurite Orientation Dispersion and Density Imaging (NODDI), can offer greater insights into microstructural features of WM change. We assessed whether NODDI-derived measures can better characterize medial temporal lobe (MTL) white matter damage due to tau and amyloid-beta pathology in AD compared to traditional tensor metrics.

Methods: 199 older adults from ADNI3 (121 cognitively normal and 78 cognitively impaired (MCI/AD) participants) received amyloid-beta (FBB or FBP) and tau (FTP) PET and multishell diffusion imaging. Global amyloid (centiloids) and tau SUVR (entorhinal, meta-temporal ROIs) were quantified. Standard diffusion tensor (fractional anisotropy, FA; mean diffusivity, MD) and NODDI metrics (Neurite Density Index, NDI; Orientation Dispersion Index; ODI) (**Fig1A**) were calculated for MTL WM tracts (**Fig1B**).

Results: NODDI measures in medial temporal tracts were more strongly correlated to cognitive performance and AD pathology than standard tensor measures. For NODDI metrics (**Fig2A**), entorhinal tau SUVR was strongly associated with NDI in the cingulum hippocampus ($r=-0.375$; $p<0.001$) and the uncinate ($r=-0.373$; $p<0.001$), and with ODI in the fornix ST ($r=-0.288$; $p=0.004$). Notably, ODI of the fornix ST showed a significant association in both tau ROIs (entorhinal $r=-0.288$; $p<0.001$; meta-temporal $r=-0.319$; $p<0.001$). For standard tensor measures (**Fig2B**), FA in any MTL tract was not significantly correlated with either tau or global amyloid-beta, while MD showed limited correlations between MTL tracts and pathology.

Discussion: NODDI metrics offer more sensitive insights about AD pathology-related MTL WM degeneration than standard tensor models.

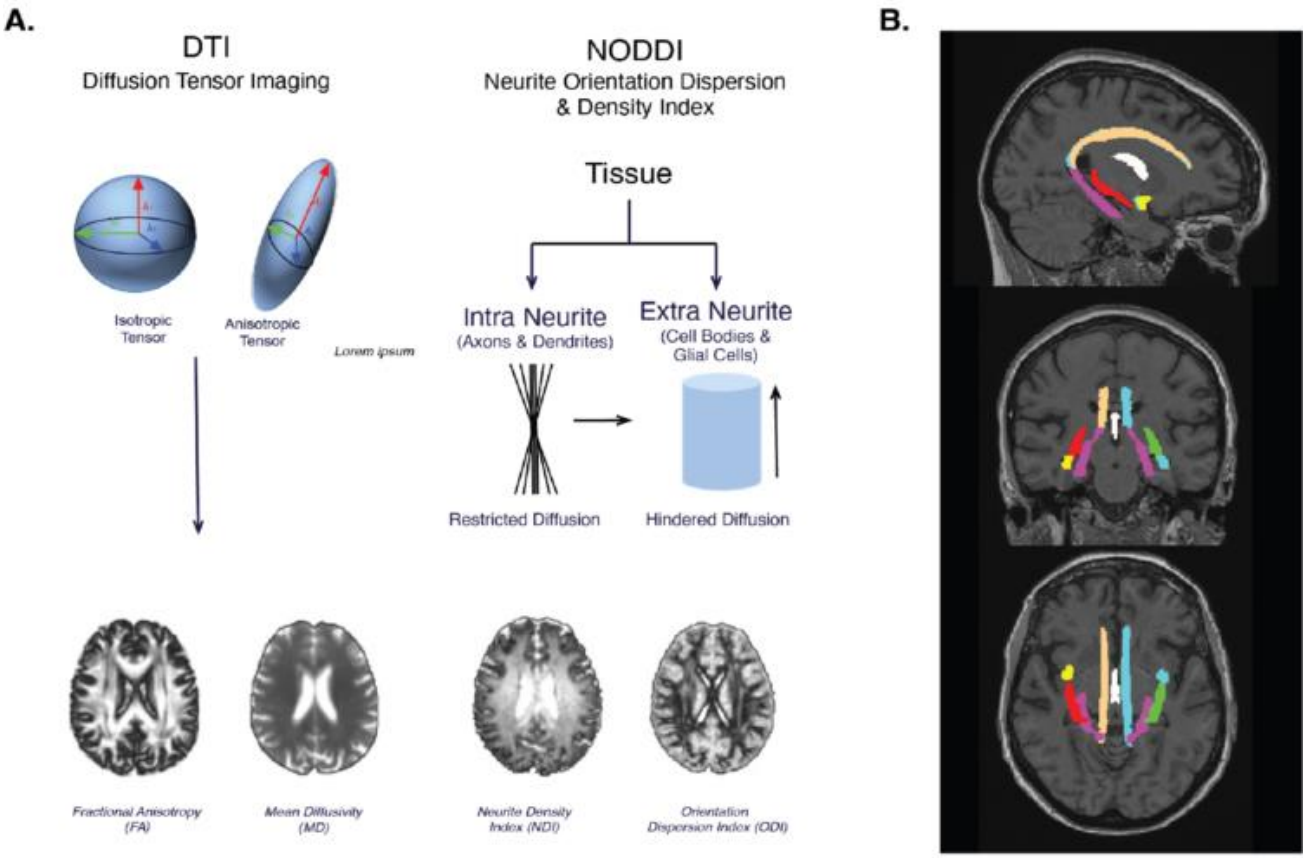

Figure 1: A. Overview of Diffusion Tensor imaging and overview of NODDI. B. Example of JHU WM Atlas ROIs

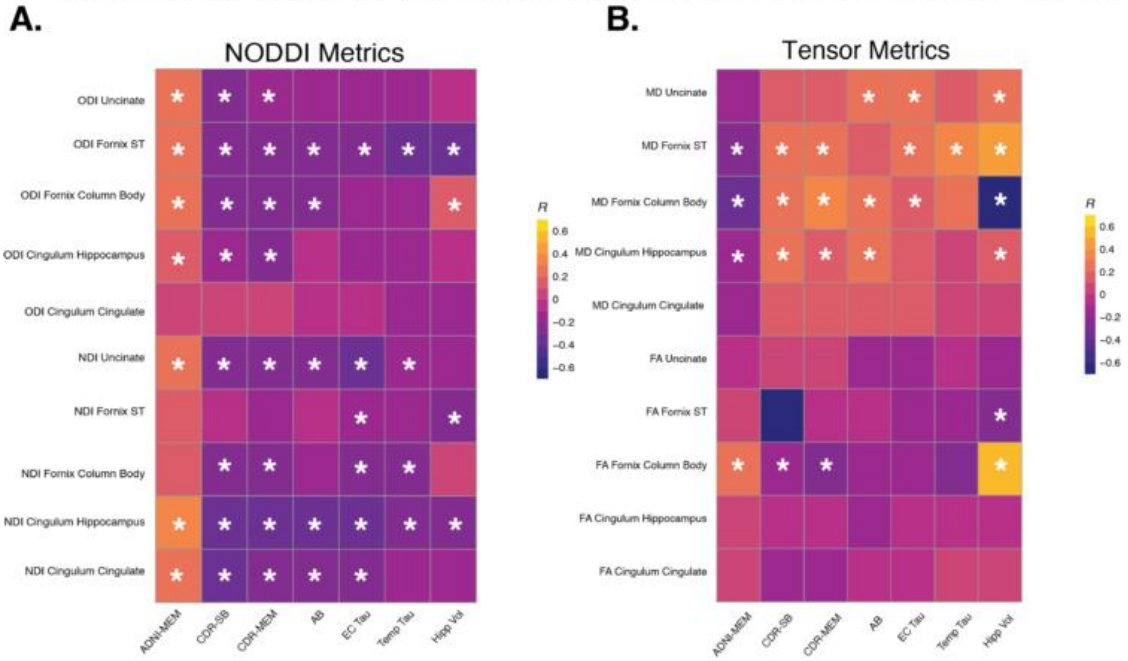

Figure 2: Correlation matrices between NODDI metrics (A) and tensor metrics (B) showing relationships between outcome measures and WM integrity of each ROI. NDI, neurite orientation index; ODI, * indicates p-value ≤ 0.05 after correction. Abbreviations: Fornix ST = Fornix Stria Terminalis, CDR-SB = Clinical Dementia Rating Scale Sum of Boxes, β-amyloid = Amyloid Beta, EC Tau = Entorhinal Tau, Temp Tau = Meta Temporal Tau, Hipp Vol = Hippocampal Volume.

Keywords: diffusion tensor imaging; Neurite Orientation Dispersion and Density Imaging; Alzheimer's disease; white matter; amyloid-beta; tau

17 Longitudinal hippocampal volume trajectories and their relationships with β-amyloid, tau, cerebrovascular, and cognition in a baseline cognitively unimpaired sample

Lianlian Du[1,2,3], Tobey Betthauser[1,2,3], Erin Jonaitis[1,2,3], Henry Stephenson[3], Bruce Hermann[1,4], Leonardo Rivera[2,3,5], Bret Larget[6], Rick Chappell[2,7], Robert Cadman[2,3], Howard Rowley[2,8], Laura Eisenmenger[8], Sterling Johnson[1,2,3,9], Rebecca Langhough[1,2,3]

[1]*Wisconsin Alzheimer's Institute, University of Wisconsin-Madison School of Medicine and Public Health, Madison, WI, United States*
[2]*Wisconsin Alzheimer's Disease Research Center, Madison, WI, United States*
[3]*Department of Medicine, University of Wisconsin-Madison School of Medicine and Public Health, Madison, WI, United States*
[4]*Department of Neurology, University of Wisconsin-Madison School of Medicine and Public Health, Madison, WI, United States*
[5]*Department of Medical Physics, University of Wisconsin-Madison School of Medicine and Public Health, Madison, WI, United States*
[6]*Department of Statistics, University of Wisconsin-Madison, Madison, WI, United States*
[7]*Department of Biostatistics and Medical Informatics, University of Wisconsin-Madison School of Medicine and Public Health, Madison, WI, United States*
[8]*Department of Radiology, University of Wisconsin School of Medicine and Public Health, Madison, WI, United States*
[9]*Madison VA GRECC, William S. Middleton Memorial Hospital, Madison, WI, United States*

Background: Reduced hippocampal volume (HV) associates with Alzheimer's disease (AD). Here we: 1) use Bayesian bent line regression models (BaBLR) and cluster analysis to characterize longitudinal patterns of HV change in a large, initially cognitively unimpaired (CU) sample; and 2) examine how baseline demographic, health characteristics, biomarkers and cognitive trajectories vary across these HV characteristics.

Methods: Data from initially CU participants were drawn from two late middle-aged cohorts (Wisconsin Registry for Alzheimer's Prevention and Wisconsin's Alzheimer's Disease Research Center; total N=1259). TICV -normalized HV was estimated using automated FSL-FIRST. Other biomarkers included PiB DVR, MK6240 SUVR and WMH (LST-LPA; SPM12). Biomarkers were converted to z-scores using a CU, amyloid negative subset. Posterior median estimated person-level CPs, slopes pre- and post-CP, and intercepts at CP for HV were extracted from BaBLR(age=time scale) and used to characterize HV trajectory groups (K-means clustering) and the estimated age at which each person would reach a HV z=-1.5("HV+"). We compared baseline demographic and health characteristics, biomarker positivity (in a subset) across HV groups using tests appropriate for the distribution of the data. Significant omnibus tests ($p<.05$) were followed with pairwise comparisons. Mixed effects models examined whether HV group or baseline HV+ duration modified Preclinical Alzheimer's Cognitive Composite (PACC3) trajectories.

Results: Cluster analysis identified 3 longitudinal HV profiles/groups: worst (earliest CP's and steepest slopes): n=120(9.5%); intermediate: n=705(56.0%); and best: n=434(34.5%); Figure1). HV groups differed in amyloid, tau and WMH(Table1). PACC3 decline was fastest in the worst HV group(Figure2); AICc model fits were substantially better using baseline HV+ chronicity (see Table2 and Figure2). At last visit, 83% of the worst HV group remained CU compared with 95% and 94% in the other two groups ($p<.0001$).

Conclusions: In this baseline CU sample, earlier and faster HV loss was associated with more abnormal biomarkers and faster cognitive decline.

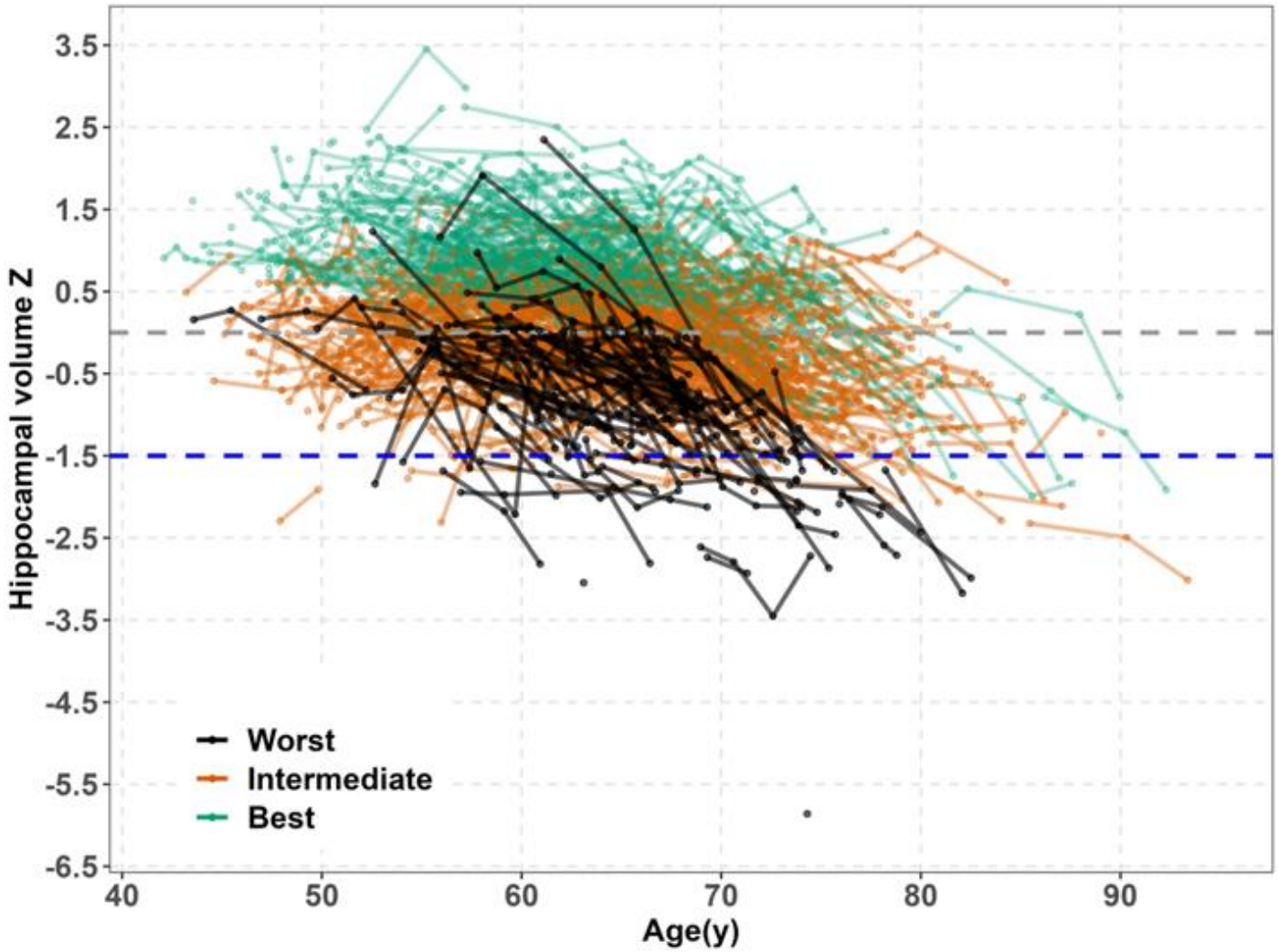

Fig. 1. Spaghetti plot of hippocampal volume among latent HV trajectory groups. MRI HV was estimated in cm^3 using the completely-automated FSL-FIRST algorithm on T1- weighted images. HV was normalized by total intracranial volume (TICV(L) = GM + WM + CSF volumes from SPM segmentation) and z-scores were computed using a regression-based approach in an amyloid negative and cognitively unimpaired subset (N = 417). Z-score = (Observed value – Predicted value)/ (Root mean squared error from CU, A-regression model that adjusted for TICV). The grey dashed line is z = 0. The blue dashed line is the abnormal HV threshold and represents 1.5 SD below the TICV-adjusted mean of the CU, A- subset. Posterior median estimated person-level CPs, slopes pre- and post-CP, and intercepts at CP for HV (fix and random effects) were extracted from BaBLR (age=time scale) to estimate age at which each person would reach a HV z=-1.5 ("HV+"). Du L, et al. doi:10.48550/arXiv.2211.09915

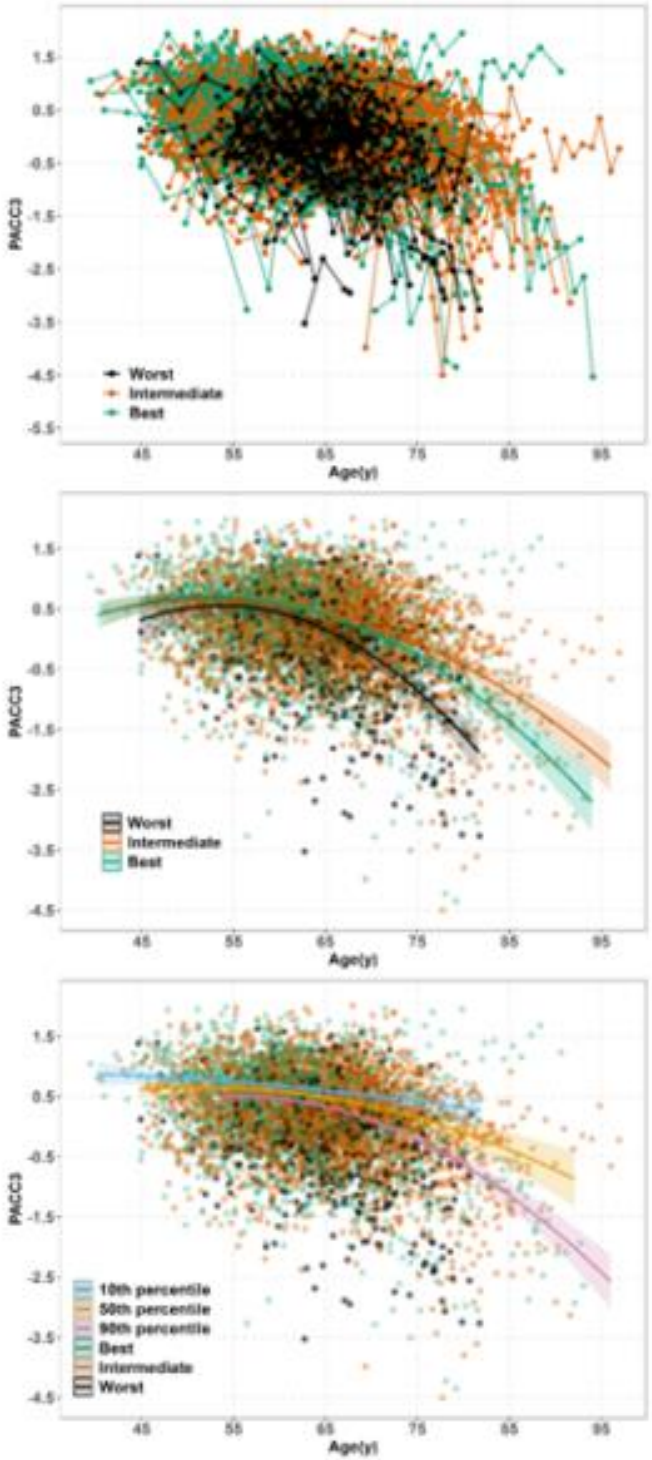

Fig. 2. PACC3 z-scores vs age. Top panel: spaghetti plots of observed PACC3 scores where each line represents a person's performance over time; colors indicate HV group. Middle and bottom panels: using output from Table 2, model 2 (middle) and model 3 (bottom), dots indicate observed values and lines represent estimated trajectories by HV group (middle) or baseline HV+ chronicity (bottom) from models including the HV*age^2 interactions. The full model for each panel was PACC3 ~ Age (up to cubic term) * HV characteristics (Cluster or HV+ Chronicity) + Gender + Education + Practice effect + random intercept + random slope; cubic terms were NS and were removed from models used. In the bottom panel, lines represent HV chronicity corresponding to the 10^{th}, 50^{th}, and 90^{th} centile of baseline HV chronicities (corresponding to values of -13.7, -1.22, and 14). For sphere of reference, the median chronicity value is 13.8, 0.37 and -7.07 in worst, intermediate and best group, respectively. The most parsimonious models are linear age*HV variable + quadratic age*HV variable + covariates. Model 2: Simple slopes shows the slope of worst group at age 60, 70, 80 is -0.039[-0.053, -0.026], -0.101[-0.118, -0.085] and -0.163[-0.197, -0.13], the intermediate group at age 60, 70 and 80 is -0.021[-0.027, -0.015], -0.051[-0.059, -0.044], -0.081[-0.094, -0.068], the best group at age 60, 70 and 80 is -0.029[-0.036, -0.022], -0.069[-0.079, -0.060] and -0.110[-0.127, -0.093]. The PACC3 diverged between worst and best, worst and intermediate group at age 60. Model 3: Simple slopes shows the slope of median chronicity in worst group at age 60, 70, 80 is -0.019[-0.029, -0.008], -0.061[-0.069, -0.053] and -0.103[-0.117, -0.089], the median chronicity in intermediate group at age 60, 70 and 80 is -0.017[-0.023, -0.010], -0.043[-0.051, -0.034], -0.068 [-0.084, -0.052], the median chronicity in best group at age 60, 70 and 80 is -0.016[-0.022, -0.010], -0.032[-0.043, -0.022] and -0.049[-0.067, -0.031].

Table 1 HIV trajectory group comparisons of sample characteristics, including demographic, health, and biomarker variables

	HIV Cluster/Group				
	Total (N=1259)	Worst (N=120)	Intermediate (N=705)	Best (N=434)	P value[c]
HIV Cluster Characteristics[a]					
Age at HIV baseline (years) (mean (SD))	61.34 (7.87)	63.44 (6.89)	62.28 (8.14)	59.23 (7.22)*#	<0.001
Age at most recent HIV (years) (mean (SD))	65.37 (8.25)	68.45 (5.23)	66.12 (8.39)*	63.29 (8.23)*#	<0.001
Total hippocampus volume z score (mean(SD))	0.17 (0.88)	-0.75 (1.01)	-0.20 (0.56)*	1.04 (0.51)*#	<0.001
Left hippocampus volume (mean (SD))	3.82 (0.47)	3.45 (0.51)	3.84 (0.35)*	4.22 (0.34)*#	<0.001
Right hippocampus volume (mean (SD))	3.95 (0.48)	3.62 (0.51)	3.76 (0.35)*	4.36 (0.37)*#	<0.001
TICV (mean (SD))	1.42 (0.14)	1.46 (0.19)	1.40 (0.14)*	1.44 (0.13)#	<0.001
HV_pred_at50 (mean (SD))	0.45 (0.71)	-0.08 (0.55)	0.09 (0.48)*	1.17 (0.45)*#	<0.001
HV_pred_at60 (mean (SD))	0.30 (0.66)	-0.35 (0.59)	0.02 (0.44)*	0.95 (0.41)*#	<0.001
HV_pred_at70 (mean (SD))	-0.11 (0.77)	-1.42 (0.75)	-0.30 (0.49)*	0.55 (0.47)*#	<0.001
HV_pred_at80 (mean (SD))	-1.14 (0.84)	-2.77 (0.90)	-1.22 (0.55)*	-0.56 (0.51)*#	<0.001
Estimated HV+ onset age (median [IQR])	83.81 [79.61, 98.55]	72.12 [68.88, 74.80]	82.43 [79.32, 85.95]*	87.67 [84.88, 91.33]*#	<0.001
HV+ chronicity at baseline HV (median [IQR])	25.56 [-30.22, -15.93]	-7.11 [-12.98, -2.08]	-21.09 [-27.42, -14.87]*	-29.63 [-33.72, -25.41]*#	<0.001
Demographics and Health Characteristics					
Gender Sex = M (%)	390 (31.0)	51 (42.5)	190 (27.0)*	149 (34.3)#	0.001
FamilyHistory = Y (%)	506 (42.8)	51 (43.2)	288 (43.5)	167 (41.4)	0.353
College =Y (%)	793 (67.1)	72 (61.0)	457 (66.0)	284 (71.8)	0.088
***APOE* e4 carriers = positive (%)**	463 (39.0)	53 (46.5)	245 (37.0)	165 (40.1)	0.134
Baseline health characteristics					
Age at baseline vital visit (mean (SD))	61.08 (7.85)	63.35 (6.83)	62.06 (8.08)	58.93 (7.25)*#	<0.001
BMI (median [IQR])	27.70 [24.34, 31.75]	27.87 [25.28, 30.61]	27.43 [24.22, 31.91]	28.08 [24.51, 31.96]	0.718
Obesity (BMI>30) (%)	430 (34.2)	38 (31.7)	235 (33.3)	157 (36.2)	0.514
CKD_EPI (median [IQR])	88.64 [76.29, 99.11]	86.16 [76.12, 97.36]	87.83 [75.45, 98.53]	90.09 [78.80, 100.30]#	0.011
Kidney Disease(%)	49 (4.1)	5 (4.4)	30 (4.5)	14 (3.3)	0.627
Systolic BP (mean (SD))	125.30 (16.37)	126.35 (17.70)	124.72 (16.09)	125.86 (16.55)	0.787
Diastolic BP (mean (SD))	77.02 (7.39)	74.42 (5.57)	76.72 (7.48)	77.91 (7.48)	0.066
Biomarker characteristics at baseline HV in subsets					
PET PiB[e]	N = 536	N=55 (10.2%)	N=368 (57.2%)	N=175 (32.5 %)	
Age at scan (mean(SD))	67.61 (7.43)	68.34 (5.53)	68.22 (7.48)	66.29 (7.72)#	0.017
PiB DVR[e] (median [IQR])	1.08 [1.04, 1.16]	1.09 [1.04, 1.44]	1.08 [1.04, 1.16]	1.07 [1.03, 1.15]	0.384
Estimated PiB+ at HV baseline (%)	77 (14.5%)	16 (29.1%)	38 (12.5%)*	23 (13.3%)*	0.005
EAOA (median [IQR])	58.61 [51.25, 62.88]	54.63 [48.89, 58.91]	60.14 [52.76, 65.78]	58.88 [51.06, 62.01]	0.29
MK6240 PET[f]	N=463	N=47 (10.2%)	N=269 (58.1%)	N=147 (31.7%)	
Age at scan (mean(SD))	68.08 (7.25)	67.90 (5.04)	68.81 (7.51)	66.81 (7.22)#	0.026
MTL z score (median [IQR])	0.09 [-0.58, 0.85]	0.45 [-0.41, 2.26]	0.01 [-0.68, 0.74] *	0.16 [-0.45, 0.90]	0.017
MTC z score (median [IQR])	0.13 [-0.55, 0.85]	0.60 [-0.34, 1.57]	0.05 [-0.67, 0.66] *	0.20 [-0.38, 0.95]	0.011
MTL+ (%)	71 (15.3)	15 (31.9)	33 (12.3)#	23 (15.6)*	0.003
MTC+ (%)	65 (14.0)	13 (27.7)	31 (11.5)#	21 (14.3)*	0.013
WMH[g]	N=775	N=78 (10.1%)	N=435 (56.1%)	N=262 (33.8%)	
Adjusted WMH (median [IQR])	0.48 [0.17, 1.48]	0.93 [0.43, 2.07]	0.44 [0.16, 1.45]*	0.46 [0.16, 1.25]*	0.002
Estimated WMH+ at HV baseline (%)	89 (11.5)	11 (14.1)	53 (12.2)	25 (9.5)	0.426
EWOA (median [IQR])	88.03 [71.47, 99.46]	76.57 [67.98, 99.42]	90.41 [71.78, 100.47]*	88.06 [71.96, 98.05]	0.039
Last cognitive status (%)					<0.001
Cognitively Unimpaired	1177 (93.5)	100 (83.3)	670 (95.0)*	407 (93.8)*	
MCI	66 (5.2)	12 (10.0)	21 (3.0)	13 (3.0)	
Impaired: Other	18 (1.4)	1 (0.8)	11 (1.6)	6 (1.4)	
Dementia	18 (1.4)	7 (5.8)	3 (0.4)	8 (1.8)	

[a]BMI = Body Mass Index, CKD_EPI = estimates Glomerular Filtration Rate (GFR) based on serum creatinine, TICV: Total intracranial volume, EWOA = Estimated WMH onset age, EAOA = Estimated amyloid onset age, MCI = Mild cognitive impairment, MTL = Medial temporal lobe composite, MTC = Meta-temporal composite (mid-to-late tau stage composite, based on Mayo meta-temporal composite) (Jack, Wiste, et al. 2018).
[b]Statistical tests: chi-square or Fisher's exact for categorical; analysis of variance (ANOVA) for continuous where mean (SD) reported, Kruskal-Wallis for continuous where median [Q1-Q3] reported and Likert-scale items. These values are nominal p-values only. Post-hoc pairwise group differences at unadjusted P < 0.05 noted in red symbol. * stands for significant difference compared to worst group, # means significant difference compared to intermediate group.
[c]MRI TIV-normalized HV was estimated in cm^3 using the completely-automated FSL-FIRST algorithm on T1- weighted images. Posterior median estimated person-level CPs, slopes pre- and post-CP, and intercepts at CP for HV were extracted from BaBLR (age-time scale) and used to estimate age at which each person would reach a HV z=-1.5 ("HV+"). HV_pred_at50, 60, 70, 80 were predicted HV at age 50, 60, 70 and 80 calculated using the fixed and random effects from BaBLR. The abnormal HV threshold represents 1.5 SD below the TICV-adjusted mean of the CU, A- subset. HV+ chronicity at baseline HV calculated as age at assessment - estimated onset age.
[d]Amyloid measures from positron emission tomography (PET) [C-11]Pittsburgh Compound B (PiB; n=538) scans included Global PiB DVR and proportion PiB+ (Global PiB DVR>1.16). Estimates use PiB DVR closest to the PiB+ threshold and SILA modeling as described in Betthauser et al., 2022.
[e][18F]-MK-6240 standardized uptake value ratio (SUVR; 70-90 min, cerebellum gray matter reference region) was used to assess tau burden in a medial temporal lobe composite (early tau stage composite, based on an average of the entorhinal cortex, hippocampus and amygdala) (Berron et al. 2021) and a temporal meta ROI encompassing the entorhinal cortex, amygdala, parahippocampal gyrus, fusiform gyrus, inferior and middle temporal gyri (Jack, Wiste, et al. 2018). Z score = ((Observed value – Mean value of CU, PET A-)/(Standard deviation of CU, PET A-)). The threshold for tau positivity was defined as z score = 1.5.
[f]Estimated TIV-normalized WMH lesion volume (WMH) was segmented and summed using the automated lesion prediction algorithm (LPA) pipeline from the Lesion Segmentation Tool (LST) version 1.2.3 for SPM12 in MATLAB (SPM12, MATLAB v.R2020a; MathWorks) from T1-weighted and T2-weighted FLAIR scans (n = 775); TIV-adjusted WMH >2.06=WMH+ used with SILA to estimate EWOA.

Table 2 LME output of PACC3

	Model 0			Model 1 (Age * HV Cluster)			Model 2 (Age * HV chronicity)		
Predictors	*Estimates*	*CI*	*p*	*Estimates*	*CI*	*p*	*Estimates*	*CI*	*p*
(Intercept)	0.24	0.18 – 0.30	**<0.001**	-0.02	-0.14 – 0.11	0.797	0.22	0.17 – 0.28	**<0.001**
c65age	-0.04	-0.05 – -0.04	**<0.001**	-0.07	-0.08 – -0.06	**<0.001**	-0.03	-0.04 – -0.02	**<0.001**
c65age^2	-0.00	-0.00 – -0.00	**<0.001**	-0.00	-0.00 – -0.00	**<0.001**	-0.00	-0.00 – -0.00	**<0.001**
gender f [Male]	-0.33	-0.41 – -0.26	**<0.001**	-0.32	-0.39 – -0.24	**<0.001**	-0.33	-0.40 – -0.26	**<0.001**
practice	0.08	0.07 – 0.09	**<0.001**	0.08	0.07 – 0.09	**<0.001**	0.09	0.08 – 0.10	**<0.001**
ed ba f [No BA]	-0.40	-0.47 – -0.33	**<0.001**	-0.39	-0.46 – -0.32	**<0.001**	-0.39	-0.46 – -0.32	**<0.001**
Cluster f [Intermediate]				0.28	0.16 – 0.40	**<0.001**			
Cluster f [Best]				0.25	0.12 – 0.38	**<0.001**			
c65age × Cluster f [Intermediate]				0.03	0.02 – 0.05	**<0.001**			
c65age × Cluster f [Best]				0.02	0.01 – 0.03	**0.001**			
Cluster f [Intermediate] × c65age^2				0.00	0.00 – 0.00	**0.002**			
Cluster f [Best] × c65age^2				0.00	0.00 – 0.00	**0.041**			
Chronicity z_hv=-1.5							-0.01	-0.01 – -0.01	**<0.001**
c65age × Chronicity z_hv =-1.5							-0.00	-0.00 – -0.00	**<0.001**
Chronicity z_hv=-1.5 × c65age^2							-0.00	-0.00 – -0.00	**<0.001**
Random Effects									
σ^2	0.14			0.14			0.14		
τ_{00}	0.31 $_{reggieid}$			0.30 $_{reggieid}$			0.30 $_{reggieid}$		
τ_{11}	0.00 $_{reggieid.c65age}$			0.00 $_{reggieid.c65age}$			0.00 $_{reggieid.c65age}$		
ρ_{01}	0.42 $_{reggieid}$			0.39 $_{reggieid}$			0.43 $_{reggieid}$		
ICC	0.73			0.72			0.73		
N	1178 $_{reggieid}$			1178 $_{reggieid}$			1178 $_{reggieid}$		
Observations	5345			5345			5345		
Marginal R^2 / Conditional R^2	0.275 / 0.803			0.296 / 0.803			0.334 / 0.817		
AIC	7623.6			7574.8			7536.1		
Log-likelihood	-3801.8			-3771.4			-3755.0		
AICc	7675.1			7681.0			7635.0		

Keywords: Hippocampal volume trajectories, β-amyloid, tau, cerebrovascular, cognitive unimpaired

18 Beyond quantity: fill states as a biomarker for the degree of pathology and neurodegeneration across the Alzheimer's disease continuum

Elena Doering[1,2], Merle C Hoenig[1,3], Kathrin Giehl[1,3], Gregory Andrassy[1], Abdelmajid Bader[4], Andreas Bauer[3,6], Verena Dzialas[1], David Elmenhorst[3], Johannes Emert[6,7], Silke Frensch[7], Elena Jäger[1], Frank Jessen[2,4], Philipp Krapf[6], Tina Kroll[3], Christoph Lerche[8], Julia Lothmann[1], Andreas Matusch[3], Bernd Neumaier[6,9,10], Özgür Onur[11], Alfredo Ramirez[2,12,13,14,15], Nils Richter[11,16], Frederik Sand[1], Lutz Tellmann[8], Hendrik Theis[1,11], Philipp Zeyen[4,6], Thilo van Eimeren[1,2,11], Alexander Drzezga[1,2,3], Gerard N Bischof[1,3]

[1]*Multimodal Imaging Laboratory (MMNI), University of Cologne, Faculty of Medicine and University Hospital Cologne, Department of Nuclear Medicine, Cologne, GERMANY, Cologne, Germany*
[2]*German Center for Neurodegenerative Diseases (DZNE), Bonn, Germany, Bonn, Germany*
[3]*Forschungszentrum Jülich, Institute of Neuroscience and Medicine - Molecular Organization of the Brain (INM-2), Jülich, Germany, Juelich, Germany*
[4]*University of Cologne, Faculty of Medicine and University Hospital, Department of Psychiatry, Cologne, Germany, Cologne, Germany*
[5]*University of Cologne, Faculty of mathematics and natural sciences, Cologne, Germany, Cologne, Germany*
[6]*Forschungszentrum Jülich, Institute of Neuroscience and Medicine – Nuclear Chemistry (INM-5), Jülich, Germany, Juelich, Germany*
[7]*Forschungszentrum Jülich, Institute of Neuroscience and Medicine - Imaging-Core-Facility (ICF), Jülich, Germany, Juelich, Germany*
[8]*Forschungszentrum Jülich, Institute of Neuroscience and Medicine – Medical Imaging Physics (INM-4), Jülich, Germany, Juelich, Germany*
[9]*University of Cologne, Faculty of Mathematics and Natural Sciences, Department of Nuclear Chemistry, Cologne, Germany, Cologne, Germany*
[10]*University of Cologne, Faculty of Medicine and University Hospital Cologne, Institute of Radiochemistry and Experimental Molecular Imaging, Cologne, Germany, Cologne, Germany*
[11]*University of Cologne, Faculty of Medicine and University Hospital, Department of Neurology, Cologne, Germany, Cologne, Germany*
[12]*Cluster of Excellence Cellular Stress Responses in Aging-associated Diseases (CECAD), University of Cologne, Cologne, Germany, Cologne, Germany*
[13]*Division of Neurogenetics and Molecular Psychiatry, Department of Psychiatry and Psychotherapy, University of Cologne, Medical Faculty, 50937 Cologne, Germany, Cologne, Germany*
[14]*Department for Neurodegenerative Diseases and Geriatric Psychiatry, University Hospital Bonn, Bonn, Germany, Bonn, Germany*
[15]*Department of Psychiatry and Glenn Biggs Institute for Alzheimer's and Neurodegenerative Diseases, San Antonio, TX, United States, San Antonio, TX, United States*
[16]*Forschungszentrum Jülich, Institute of Neuroscience and Medicine – Cognitive Neuroscience (INM-3), Jülich, Germany, Juelich, Germany*

The biomarker model of Alzheimer's disease (AD) suggests that *in vivo* markers of amyloid-beta (A), tau (T), and progressive neurodegeneration (N) capture the pathophysiological cascade of AD and aid in the clinical diagnosis of AD. While positron emission tomography (PET) biomarkers of AT(N) categorize AD based on mean signal in specific regions of interest (ROI), we were interested in whether the spatial extent of pathology and neurodegeneration (i.e., fill states) is superior to mean signal quantification for monitoring disease progression.

Data from the Tau Propagation over Time (T-POT) study were used. [C11]PIB-PET (A), [18F]AV1451 (T) and the perfusion phase of [18F]AV1451 scans (N) were pre-processed and z-standardized in a total of N=61 individuals with different cognitive status (i.e, subjective cognitive decline (N=27), mild cognitive impairment (N=27), patients clinically diagnosed with dementia of the AD type (N=7)), using a reference group of amyloid-negative cognitively

normal individuals (N=32). Fill states were determined as the percentage of abnormal voxels in modality-specific meta-regions. Standard-uptake value ratios (SUVR) were extracted in all meta-ROIs for comparison. We used statistical and machine learning methods to assess whether fill states or SUVR can distinguish between different clinical groups or levels of cognitive impairment. Fill states discriminated clinical groups better than SUVR (Figure 1A). Using machine learning classification, fill states outperformed SUVR in classifying cognitive impairment. In addition, fill states correlated more strongly with cognitive performance compared to SUVR. A combined approach of fill states and SUVR did not improve diagnostic accuracy over fill states alone. Fill states, which denote the spatial extent of ATN, offer clear clinical utility as a biomarker with superior diagnostic accuracy over traditional SUVR measures. Preliminary longitudinal follow-up (currently N=16; ~18 months) of this sample suggests higher sensitivity of fill states over SUVR to reflect changes in the ATN biomarker framework (Figure 1B).

Figure 1: Depicted are data from our baseline acquisition of participants (N=61) with subjective cognitive decline (SCD), mild cognitive impairment (MCI) and patients diagnosed with dementia of the Alzheimer's type (AD) in the T-POT Study (Figure 1A) Scale shows percentage of individuals who displayed abnormal voxel thresholds in meta-regions of typical pathology of amyloid (A) and tau (T) and neurodegeneration (N). Follow-up data after 18-months show (N=16) a typical increase of spatial extent in pathology (1B) in almost all modalities of ATN across diagnostic groups. We expect that by the time of HAI 2024 more data will be presented

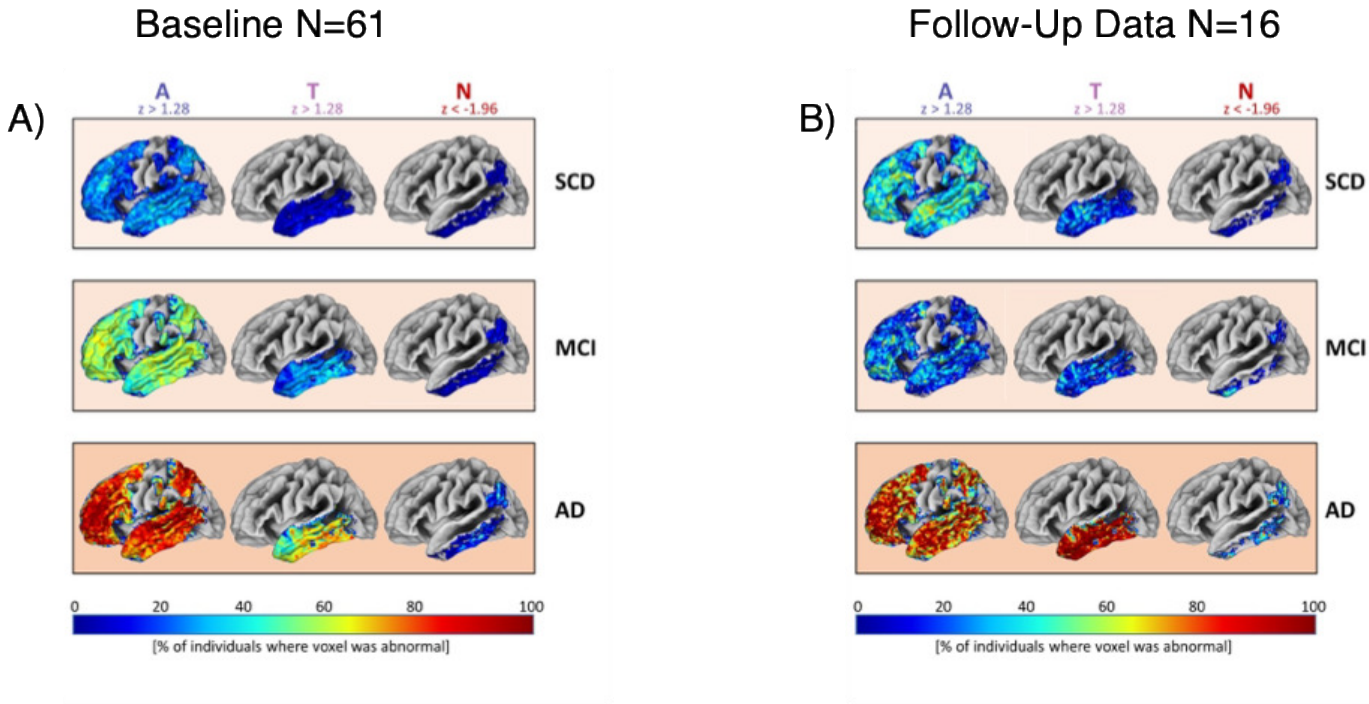

Keywords: In vivo PET, ATN, AD continiuum, machine learning, clinical

19 Successful aging reflects anterior cingulate preservation but not tau accumulation rate

Stefania Pezzoli[1,2], Joseph Giorgio[1,3], Xi Chen[1,2], Theresa M. Harrison[1], William J. Jagust[1,2]

[1]*University of California, Berkeley, Berkeley, CA, United States*
[2]*Lawrence Berkeley National Laboratory, Berkeley, CA, United States*
[3]*University of Newcastle, Newcastle, Australia*

Cross-sectional studies suggest successful aging (SA) is related to preservation of hippocampal volume and anterior cingulate and mid-cingulate cortical thickness compared to typical aging. In this study, we quantified SA using cognitive age gap (CAG, or cognitive age – chronological age), a continuous measure where lower scores indicate younger cognitive age. We examined relationships between CAG and longitudinal changes in cognition, brain structure, and tau, predicting that lower CAG would be associated with better longitudinal outcomes. A total of 109 cognitively normal older adults (70+ years old) underwent longitudinal β-amyloid (PiB) and tau (FTP) PET imaging, cognitive testing, and structural MRI scans. An age prediction model estimated participants' cognitive age from neuropsychological tests, and CAG was computed for each individual. Linear mixed-effects models were used to investigate longitudinal changes in 1) episodic memory (EM) and global cognition composite scores, 2) cingulate cortex atrophy (voxel-wise analysis in a cingulate cortex mask), 3) hippocampal atrophy (ROI analysis), and 4) entorhinal tau. CAG, Aβ-status, and entorhinal FTP uptake were included as predictors in all models. All analyses were adjusted for sex and years of education. We found a significant CAG x time interaction on 1) EM ($p=0.008$), and 2) global cognition ($p=0.03$) (Figure 1). There was also a significant entorhinal tau x time interaction for both EM ($p<0.001$) and global cognition ($p<0.001$). Voxel-wise analysis of cingulate cortex revealed regions where participants with lower CAG showed less longitudinal atrophy, specifically in the left anterior and mid-cingulate cortices (Figure 2). Longitudinal hippocampal atrophy and entorhinal tau accumulation did not vary by CAG (hippocampal atrophy: $p=0.55$, tau: $p=0.54$). In sum, younger cognitive age was associated with slower cognitive decline and cingulate brain atrophy, but not with tau accumulation or hippocampal atrophy rate. This suggests that different mechanisms may underlie SA and early Alzheimer's disease pathological changes.

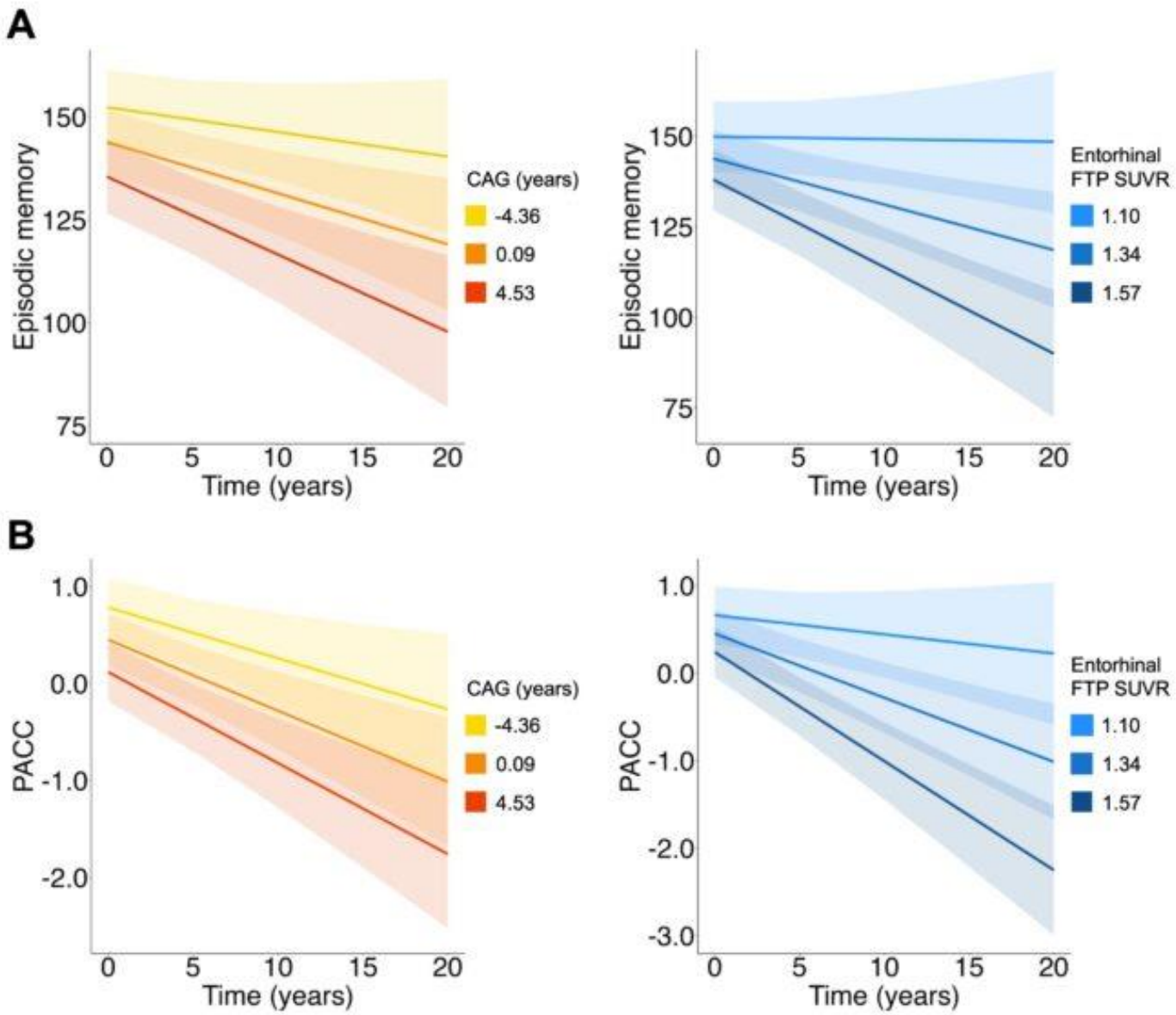

Figure 1 Linear mixed-effects models were used to predict longitudinal trajectories in cognitive decline. Lower cognitive age gap (CAG) scores and entorhinal FTP SUVR were independently associated with slower decline in A) an episodic memory composite score (CAG: β=-0.14, p=0.008, entorhinal FTP SUVR: β=-4.96, p<0.001) and B) in the Preclinical Alzheimer's Cognitive Composite (PACC) (CAG: β=-0.005, p=0.03, entorhinal FTP SUVR: β=-0.21, p<0.001). CAG and entorhinal FTP SUVR were included as a continuous variable in the models but represented as mean ±1 SD for visualization purposes.

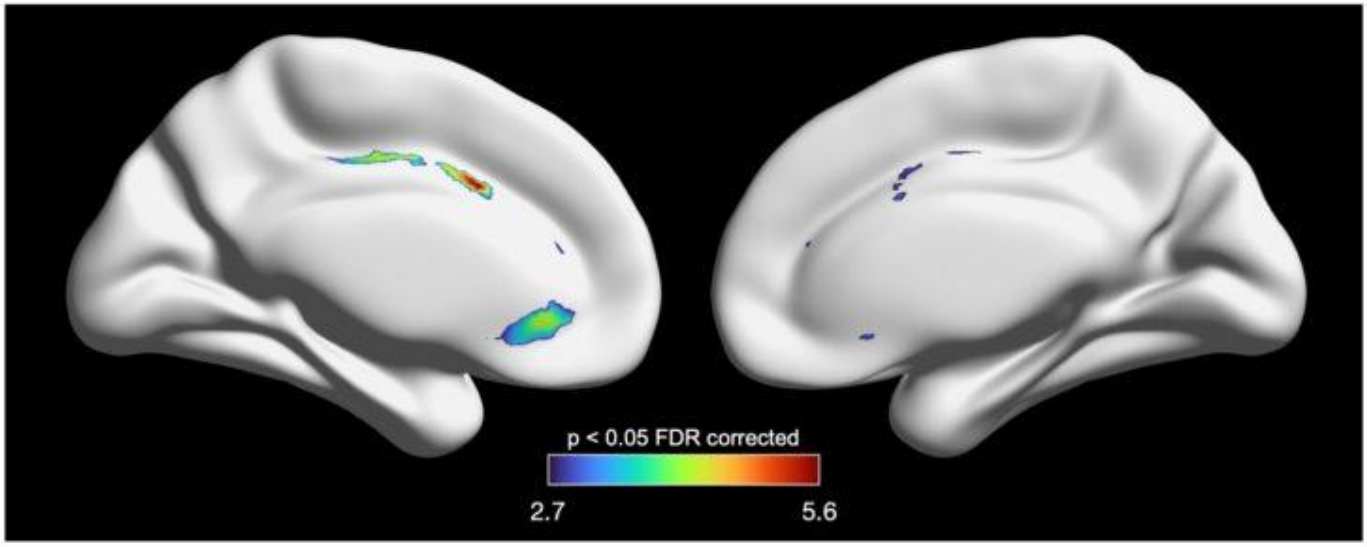

Figure 2 Results from voxel-wise linear mixed-effects models on a cingulate cortex mask. Lower cognitive age gap (CAG) scores were associated with slower atrophy progression mostly in the left anterior cingulate and mid-cingulate cortices. Color bar indicates z scores representing significant CAG x time interaction ($p<0.05$ FDR corrected for multiple comparisons).

Keywords: successful cognitive aging, Alzheimer's disease pathology, PET, longitudinal atrophy, cognitive decline

21 Distinct microbial species less abundant in Alzheimer's disease patients associate negatively with cerebrospinal fluid biomarkers of Alzheimer's disease

Jea Woo Kang[1], Lora A. Khatib[2], Amanda H. Dilmore[2], Margo B. Heston[1], Tyler K. Ulland[3], Sterling C. Johnson[1], Sanjay Asthana[1], Cynthia M. Carlsson[1], Nathaniel A. Chin[1], Kaj Blennow[4], Henrik Zetterberg[4], Rob Knight[2], Rima Kaddurah-Daouk[5], Federico E. Rey[6], Barbara B. Bendlin[1]

[1]*Wisconsin Alzheimer's Disease Research Center, University of Wisconsin School of Medicine and Public Health, Madison, WI, United States*
[2]*Department of Pediatrics, University of California San Diego, La Jolla, CA, United States*
[3]*Department of Pathology and Laboratory Medicine, University of Wisconsin-Madison, Madison, WI, United States*
[4]*Institute of Neuroscience and Physiology, The Sahlgrenska Academy at the University of Gothenburg, Mölndal, Sweden*
[5]*Duke University Medical Center, Durham, NC, United States*
[6]*Department of Bacteriology, University of Wisconsin-Madison, Madison, WI, United States*

Background: Evidence shows that gut microbiome alterations may contribute to the aggravation of Alzheimer's disease (AD). Differences in the gut microbiota composition and diversity between AD vs. control have been studied in age and sex-matched cohorts (n=25) using 16S rRNA sequencing. Here, we included 235 participants (Dementia-AD=24, Normal=211) whose diagnoses were determined by NIA-AA criteria and investigated the compositional differences in microbiota and their association with AD biomarkers.

Methods: Cerebrospinal fluid (CSF), PiB (Pittsburgh Compound-B) PET, and fecal samples were collected from participants enrolled in the Wisconsin Registry for Alzheimer's Prevention and Wisconsin Alzheimer's Disease Research Center studies. CSF biomarkers of AD, β-amyloid $(A\beta)_{42}/A\beta_{40}$ and phosphorylated-tau-181 (phospho-tau [181P]), were measured as part of the Roche NeuroToolKit (Roche Diagnostics International Ltd, Rotkreuz, Switzerland). Metagenomic sequencing was performed on fecal microbial genes as previously described. The differential abundance analysis was performed with the BIRDMAn pipeline. Spearman's rank correlation was used across participants matched with their CSF biomarkers to find novel associations between the microbiota composition and AD biomarkers and was adjusted for multiple testing.

Results: The differential abundance analysis showed that at genus and species levels, the top microbes more associated with AD vs. Normal were mostly *Fusobacterium* spp. and the bottom microbes less associated with AD vs. Normal were mostly *Clostridium* spp. *Fusobacterium nucleatum* was significantly and positively associated with neurofilament light chain levels in CSF (ρ=0.34). *Clostridium saccharobutylicum* was significantly and negatively associated with the neurodegeneration biomarker total tau (ρ=−0.37), the pre- and post-synaptic biomarkers alpha-synuclein and neurogranin (ρ=−0.32 and −0.33, respectively), and the tau pathology biomarker phosphorylated tau (ρ=−0.38) levels in CSF.

Conclusion: Individuals with AD have distinct microbial composition compared to cognitively normal individuals. Microbial species less abundant in AD were negatively associated particularly with CSF p-tau and t-tau.

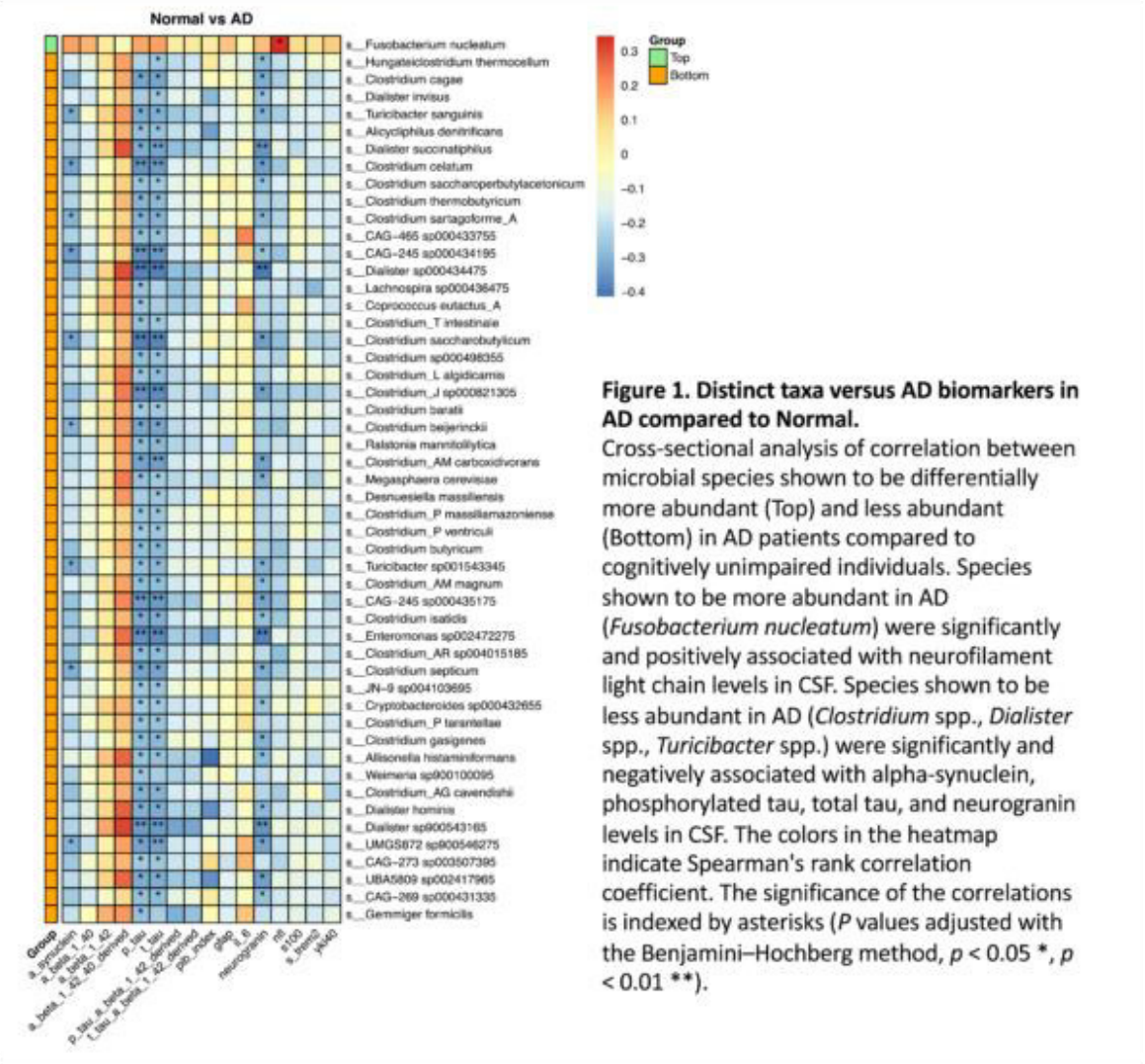

Figure 1. Distinct taxa versus AD biomarkers in AD compared to Normal.
Cross-sectional analysis of correlation between microbial species shown to be differentially more abundant (Top) and less abundant (Bottom) in AD patients compared to cognitively unimpaired individuals. Species shown to be more abundant in AD (*Fusobacterium nucleatum*) were significantly and positively associated with neurofilament light chain levels in CSF. Species shown to be less abundant in AD (*Clostridium* spp., *Dialister* spp., *Turicibacter* spp.) were significantly and negatively associated with alpha-synuclein, phosphorylated tau, total tau, and neurogranin levels in CSF. The colors in the heatmap indicate Spearman's rank correlation coefficient. The significance of the correlations is indexed by asterisks (*P* values adjusted with the Benjamini–Hochberg method, $p < 0.05$ *, $p < 0.01$ **).

Keywords: Alzheimer's disease, cerebrospinal fluid, gut microbiome

22 Amyloid quantification is dependent on scanner: a head-to-head comparison of 18F-NAV4694 Centiloid measurements between three PET/CT scanners

Ashley Gillman[1], Pierrick Bourgeat[1], Timothy Cox[1], Shenpeng Li[1], Victor L Villemagne[2,3], Jurgen Fripp[1], Graeme O'Keefe[3], Kun Huang[3], Natasha Krishnadas[4], Azadeh Feizpour[4], Rob Williams[5], Svetlana Bozinovski[3], Christopher C Rowe[3,4], Vincent Doré[1]

[1]*Health and Biosecurity, Commonwealth Scientific and Industrial Research Organisation, Brisbane, Australia*
[2]*Department of Psychiatry, University of Pittsburgh, Pittsburgh, PA, United States*
[3]*Department of Molecular Imaging & Therapy, Austin Health, Melbourne, Australia*
[4]*The Florey Institute of Neuroscience and Mental Health, The University of Melbourne, Melbourne, Australia*
[5]*Melbourne Brain Centre Imaging Unit, The University of Melbourne, Melbourne, Australia*

Background: Next-generation PET scanners possess superior resolution and sensitivity. Their use in research and clinics may affect Ab quantitation and have significant implications for longitudinal studies, including therapeutic trials. However, the effect of PET scanner on Centiloid remains relatively unexplored and is assumed to be minimized by harmonising PET resolutions. We compare paired Centiloid measurements between three PET/CT scanners.

Method: 37 AIBL participants underwent MPRAGE-MRI and ^{18}F-NAV4694 imaging on two scanners (Siemens Vision 600, Siemens mCT, Philips Gemini TF64) within a year. Centiloid was quantified using the standard SPM framework and corrected for expected accumulation between scans. We investigated difference in Centiloid and effectiveness of PET resolution harmonisation, i.e., smoothed to 6mm-equivalent point spread function using estimates from Hoffman phantom scans. Statistical significance was evaluated using empirical, one-sided, non-parametric bootstrap estimates.

Results: Figures below depict comparison results for the Vision~Gemini comparison with and without resolution harmonisation. Even with harmonisation, Vision Centiloid was found to be significantly higher than Gemini Centiloid (p=0.002); the difference followed a linear association with slope>1 (p=0.000). While the difference at 0CL was negligible, at 100CL (Gemini) corresponded to 112CL (Vision). Vision vs mCT Centiloid also indicated a Centiloid-dependent linear association with slope>1 that did not reach significance. Resolution harmonisation only reduced ~10% of scanner differences.

Conclusion: Results from different scanners yielded different Centiloid estimates, that were proportional to the participant's Ab levels. The standard resolution harmonisation procedure did not correct for scanner difference. For high-amyloid individuals, the measured difference between Vision/Gemini (12%) was greater than the expected annual accumulation rate and therefore relevant for longitudinal studies. The measured effect between scanners was linear, suggesting that scanner calibration methods are possible.

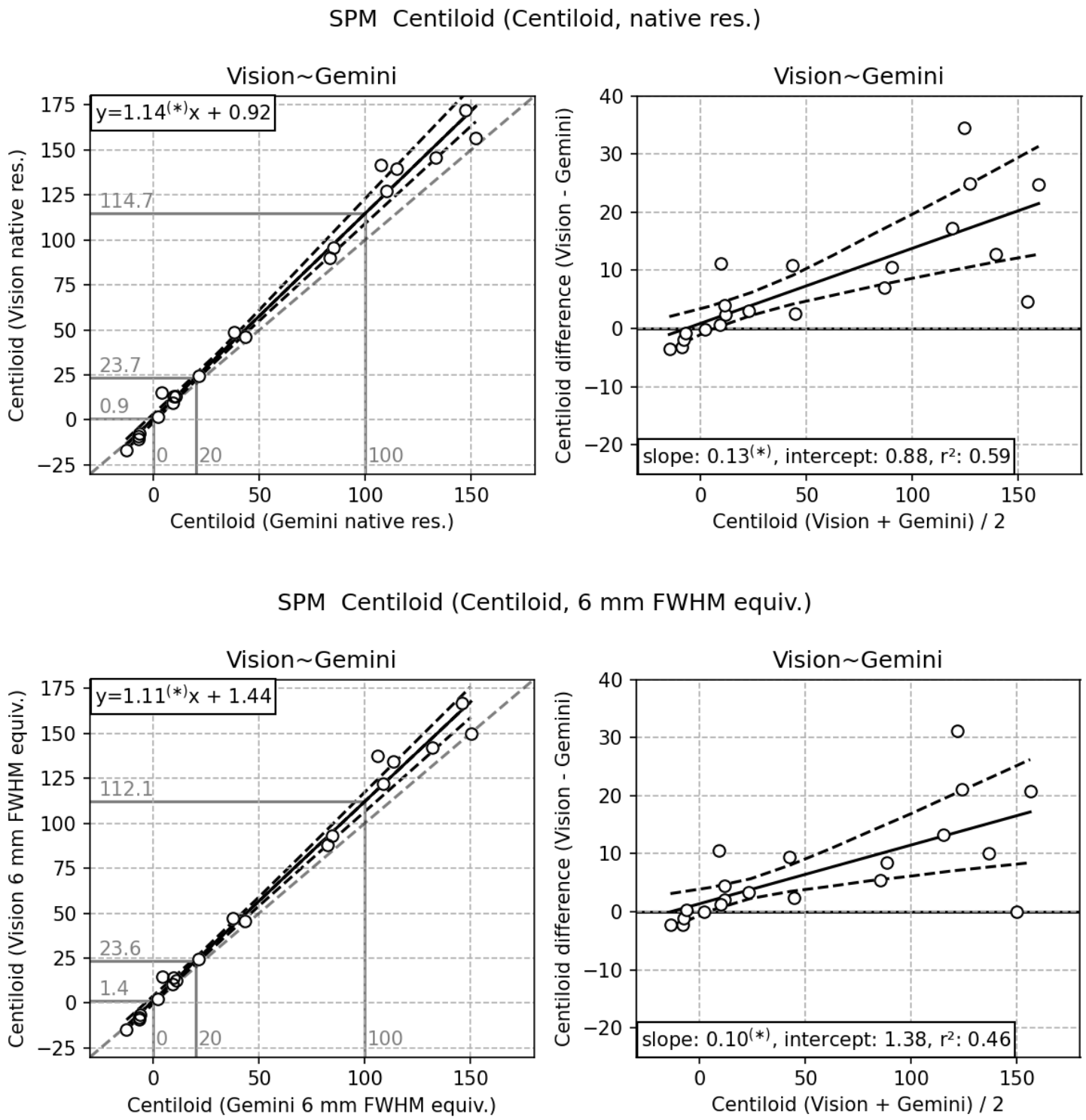

Vision~Gemini comparison at native (no harmonisation) and 6mm effective resolution: scatter and Bland-Altman plots with linear fit and confidence intervals. Asterisk indicates significant deviation from expected.

Keywords: Centiloid, harmonisation, quantification, 18F-NAV4694 PET, measurement error

23 Neuroinflammation follows and outstrips tau progression patterns in primary 4R tauopathies

Maura Malpetti[1], Sebastian Niclas Römer[2], Stefanie Harris[2], Mattes Gross[2], Johannes Gnörich[2], Andrew Stephens[3], Andre Mueller[3], Norma Koglin[3], Johannes Levin[2], Günter Höglinger[2], Matthias Brendel[2], Nicolai Franzmeier[2]

[1]*University of Cambridge, Cambridge, United Kingdom*
[2]*Ludwig-Maximilians-Universität LMU, Munich, Germany*
[3]*Life Molecular Imaging, Berlin, Germany*

Introduction: Preclinical, post-mortem and PET imaging studies have pointed to neuroinflammation as a key pathophysiological mechanism in degenerative tauopathies, including progressive supranuclear palsy (PSP) and corticobasal degeneration (CBD), and its role in accelerating disease progression. By combining PET markers for tau and microglial activation with resting-state fMRI-based connectivity, we aimed to test whether microglial activation (i) expands in similar spatial patterns as tau spreads across interconnected brain regions and (ii) follows or outstrips the spread of tau pathology.

Methods: We examined in vivo associations between tau aggregation and microglial activation in 31 patients with PSP and CBD, using 18F-PI-2620 (tau) PET and 18F-GE-180 (TSPO) PET to quantify regional levels of tau pathology and activated microglia, respectively. We determined tau epicenters as 5% of subcortical ROIs with highest tau PET signal and assessed the connectivity of tau epicenters to cortical ROIs using a 3T resting-state fMRI template derived from 69 age-matched healthy elderly controls (from the ADNI cohort).

Results: We found that higher regional TSPO PET signal covaries with elevated tau PET regional in patients with 4R tauopathies across brain regions that are functionally connected to each other (b=0.414, p<0.001, Figure 1A-B). Combining fMRI and TSPO PET, we found that microglial activation follows similar progression patterns as tau spreading and distributes primarily across brain regions strongly connected to individual tau epicenters (b=-0.594, p<0.001, Figure 1C). In these regions, microglial activation progression spatially outstrips tau spread detectable with 18F-PI-2620 PET (Figure 2).

Conclusions: Our findings indicate that microglial activation spatial expansion parallels and outstrips tau spreading across brain regions that are functionally connected to each other. The combination of tau and inflammation in vivo markers could support the development of immunomodulatory strategies for disease-modifying treatments in these conditions, alone or in conjunction with treatments targeting tau pathways.

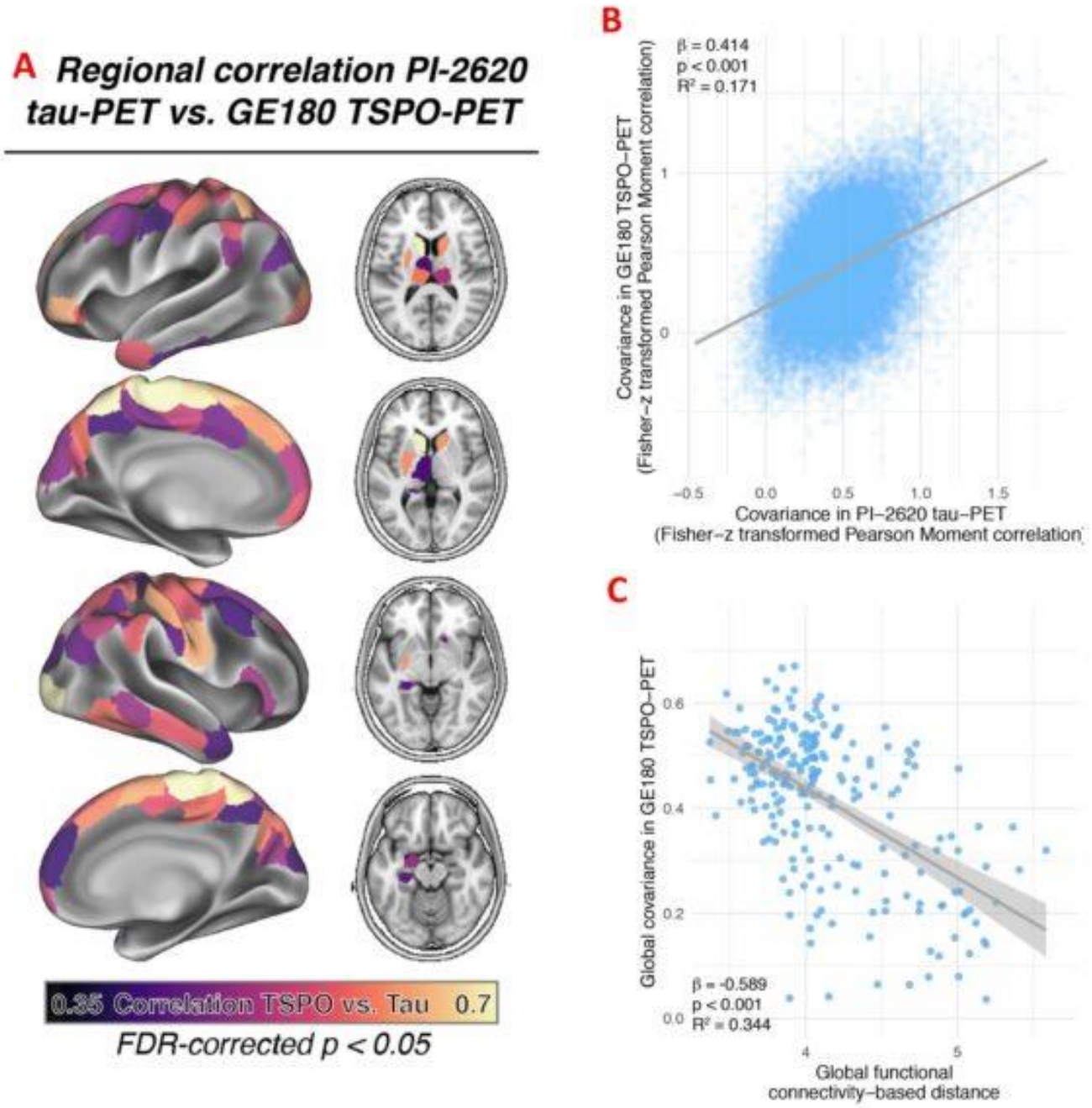

Figure 1. Association between TSPO PET, tau PET and progression patterns. Panel A: ROI-wise correlation between TSPO-PET and tau-PET across subjects, corrected for multiple comparisons (i.e. FDR, p<0.05). Panel B: association between covariance in PI-2620 tau-PET and covariance in GE180 TSPO-PET, showing that regions with correlated tau also show correlated neuroinflammation. Panel C: brain hubs (i.e. globally connected brain regions) are influential for brain wide neuroinflammation patterns: more globally connected regions (x-axis) showed higher global covariance in TSPO-PET.

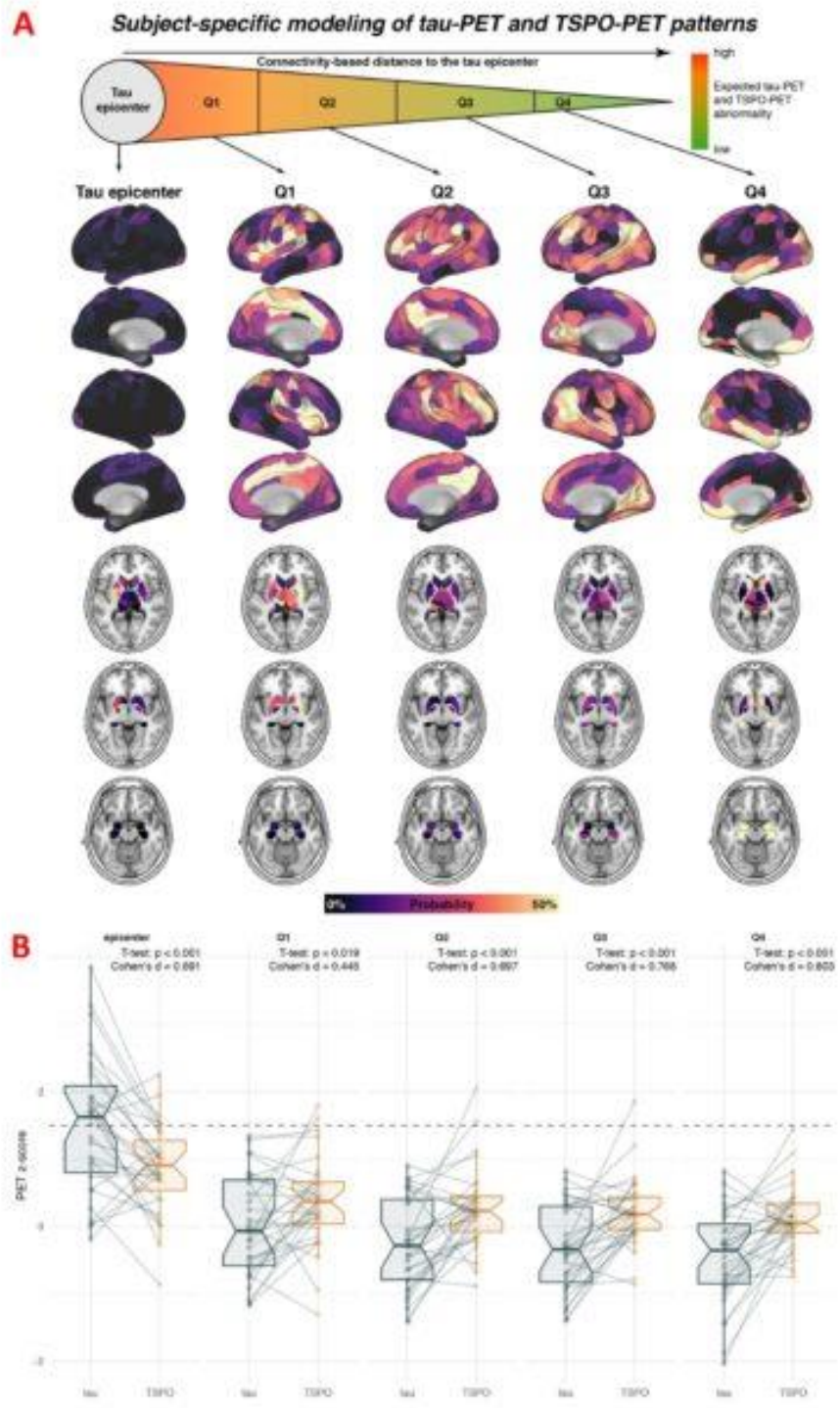

Figure 2. Microglial activation (TSPO PET) progression spatially outstrips tau spread detectable with PI-2620 PET. Panel A: using subject-level tau-PET data, we determined for each patient the subcortical tau epicenter, i.e., defined as 5% of ROIs with highest tau-PET SUVRs. The remaining regions of interest (ROIs) were grouped for each subject into quartiles, depending on connectivity strength to the subject-specific tau epicenter. Panel B: for each quartile we compared TSPO PET and PI2620 PET values. Within the tau epicenter, tau-PET z-scores were higher than TSPO-PET z-scores (Cohen's d=0.691, p<0.001). In contrast, TSPO-PET z-scores were higher than tau-PET z-scores across Q1/Q2/Q3/Q4 ROIs.

Keywords: Inflammation, tau, PET, connectivity, Progressive Supranuclear Palsy

24 Relationship between enlarged perivascular space and beta-amyloid deposition among cognitively normal ADNI participants

Jeongchul Kim[1], Jeremy Hudson[1], Hongyu Yuan[1], Megan Lipford[1], Qing Lyu[1], Chistopher Whitlow[1]

[1]*Deaprtment of Radiology, Wake Forest School of Medicine, Winston Salem, NC, United States*

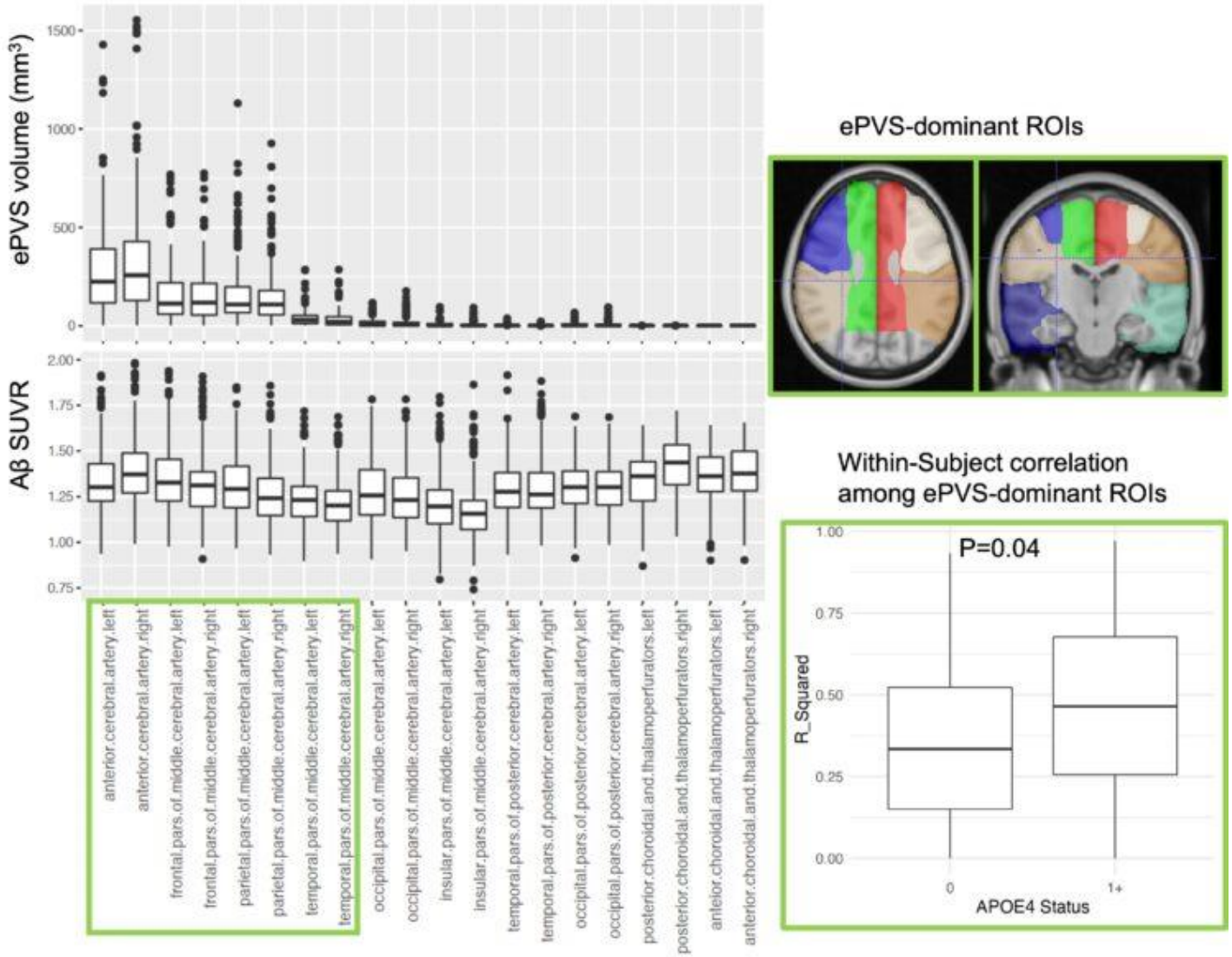

Figure. Distributions of ePVS and Aβ SUVR in the vascular territories (Left and Upper Right). Differences in within-subject correlation coefficients, r^2 (Lower Right) between APOE4 carriers and non-carriers.

Alzheimer's Disease (AD) is characterized by the accumulation of beta-amyloid (Aβ) plaques and tau tangles in the brain. The spatial distribution of Aβ varies in the brain and is influenced by factors such as the AD stage, the presence of the apolipoprotein E ε4 (APOE4) allele, and the degree of cerebral small vessel disease, such as enlarged perivascular spaces (ePVS). In our study involving 183 cognitively normal participants from ADNI, we explored the link between local ePVS and Aβ deposition based on the vascular territory. We used a public ePVS segmentation algorithm featuring a convolutional autoencoder and a U-shaped neural network, and determined ePVS volume with a threshold of 0.5 in a 0-1 range and a cluster size of 5 voxels. The vascular territory was defined a Digital 3D Brain MRI Arterial Territories Atlas for 32 brain subreigons. Though the whole-brain level correlation between total ePVS volume and gray matter Aβ SUVR was not significant, there were notable positive correlations

in the frontal pars of the left middle cerebral artery (r^2 =0.17, p=0.02) and the temporal pars of the left middle cerebral artery (r^2=0.21, p=0.003). Furthermore, within eight ePVS dominant vascular territories (highlighted in Figure), we found moderate-to-strong correlations between ePVS severity and Aβ SUVR, particularly in APOE4 allele carriers who showed stronger correlations than non-carriers. Our results suggest a potential association between ePVS presence, APOE4, and Aβ clearance at the vascular territory level, which might contribute to the varying Aβ patterns seen in AD.

Keywords: Beta-Amyloid, Perivascular Space, Small Vessel Diseases, Clearance, Alzheimer's Disease

25 Examining inter- and intra-subject variability in digital clock drawing test performance in cognitively normal older adults

Marina Rodríguez Alonso[2], Jessie Fanglu Fu[1,2], Talia Robinson[2], Adela Francis Malave[2], Roos J. Jutten[2], Grace Del Carmen Montenegro[2], Emma Thibault[2], Dana Penney[3], Randall Davis[4], Reisa A. Sperling[2], Julie C. Price[1,2], Dorene M. Rentz[2], Keith A. Johnson[2]

[1]*Athinoula A. Martinos Center for Biomedical Imaging, Charlestown, MA, United States*
[2]*Massachusetts General Hospital, Harvard Medical School, Boston, MA, United States*
[3]*Lahey Hospital and Medical Center, Burlington, MA, United States*
[4]*Massachusetts Institute of Technology, Cambridge, MA, United States*

Background: DCTclock™ (digital clock-drawing test) captures time-stamped coordinates during the clock-drawing process, generating composite scores as the sum of cognitive domain-specific subscores of Information Processing (**IP**), Drawing Efficiency (**DE**), Spatial Reasoning (**SR**), and Simple Motor (**SM**). Understanding DCTclock variability in cognitive normal older (**CN**) subjects without amyloid-β burden (**Aβ-**) is crucial for establishing inherent variability to detect early disease and cognitive changes with DCTclock. We aim to evaluate the inter- and intra-subject variability of DCTclock composite and domain-specific scores in Aβ- CN individuals and identify DCTclock domain-specific variability.

Methods: 135 CNs underwent baseline DCTclock and [^{11}C]PiB-PET (**Table.1**). Only Aβ- subjects (PiB-DVR < 1.19) were further analyzed. Longitudinal DCTclock performance was estimated as annual changes (DCTclock follow-up–DCTclock baseline/years). Subjects were classified as Normal (>75) or Abnormal (<60, **Fig.1A**) using baseline DCTclock composite scores based on FDA-approved cutoff for AD diagnosis. ANOVA and F-test compared mean and variance differences in DCTclock baseline and annual changes for composite and subscores between Normal and Abnormal groups, correcting for age, sex, education, handedness (significance= $p<0.05$). Visual observations of DCTclock qualitatively examined domains associated with low DCTclock scores.

Results: At baseline, the Abnormal group showed significantly lower DE and SR subscores, and higher variance in composite, DE, and SR subscores than the Normal group (**Fig.B-C, Table.1**). Longitudinally, no significant mean differences were observed in DCTclock subscores, however, DE and SR subscores exhibited higher variance in the Abnormal group than the Normal group (**Fig.D-F**, **Table.2**). Visually, over 60% of Abnormal group showed abnormalities in DE and SR domains (**Fig.1G**).

Conclusion: Our findings reveal significant inter- and intra-subject variability in DCTclock performance among Aβ- CN individuals, most evident on measures of visuospatial and executive function. These results provide basis for interpreting future studies of DCTclock performance variability in Aβ+ individuals to detangle test variability and early disease effects.

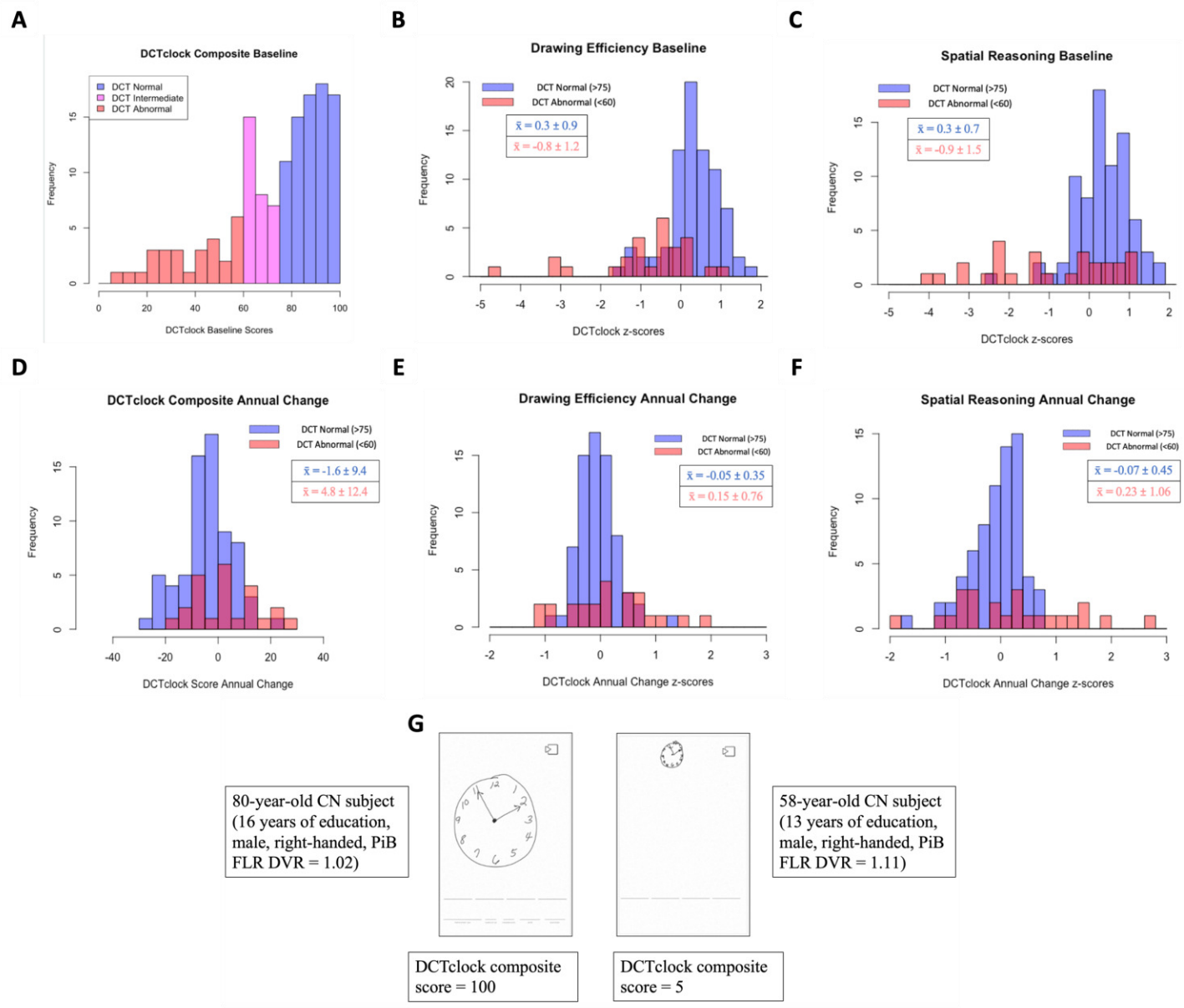

Figure1. Histograms for DCTclock composite score and domain-specific subscores at baseline and over time, and DCTclock examples in Aß- CN subjects. A) Histogram of DCTclock composite scores. Subjects who scored above 75 comprise the DCTclock Normal group and subjects who scored less than 60 comprise the DCTclock. Abnormal group based on the FDA-approved cutoff to aid AD diagnosis (DCTclock™). Baseline Drawing Efficiency **(B)** and Spatial Reasoning subscores **(C)**, yielded significantly lower mean (ANOVA) and higher variance (F-test) values in the Abnormal group relative to Normal group. **D)** Longitudinally, the Abnormal group showed significantly higher annual changes of DCTclock composite scores than the Normal group, potentially due to ceiling/flooring effects in DCTclock performance. With respect to Drawing Efficiency **(E)** and Spatial Reasoning subscores **(F)**, significantly higher variance was observed for the Abnormal group, while mean values were similar to those observed for the Normal group. **G) Examples of DCTclock drawing outcome** with a best achievable composite score of 100 (left, drawing time of 33s) and a poor DCTclock drawing outcome with a DCTclock composite score of 5 (right) for which worse performance in the Spatial Reasoning (off-centered vertical placement) and Drawing Efficiency (smaller drawing size and longer drawing time of 68s) domains were observed.

Characteristics for n= 105 cognitively normal participants with baseline DCTclock performance				
	DCT Normal (n = 78)	**DCT Abnormal (n= 27)**	**p (ANOVA)**	
Age, y	76 ± 5.56	82 ± 6.99	1.77e-06***	
Sex (% females)	64%	62%	0.2880	
Education, y	16.7 ± 2.47	15.3 ± 2.87	0.0202*	
Handedness (% right-handed)	85%	77%	0.0470*	
PiB FLR DVR	1.08 ± 0.04	1.07 ± 0.04	0.432	
PACC-5	0.38 ± 0.62 (-1.52 – 1.89)	-0.25 ± 0.72 (-1.98 – 1.02)	0.0518	
Time difference between DCTclock and PiB-PET (months)	16 ± 20	9 ± 22	N/A	
Baseline DCTclock Performance			**p (ANOVA)**	**p (F-test)**
DCTclock Composite Score (0-100)	88 ± 6.87 (75 – 100)	38 ± 15.4	<2e-16***	4.10e-05***
DCTclock Baseline Domain-Specific Subscores (z-scores)				
	DCT Normal	**DCT Abnormal**	**p (ANOVA)**	**p (F-test)**
Drawing Efficiency (DE) (e.g., total time, drawing size, noise)	0.43 ± 0.57 (-1.01 – 1.66)	-1.11 ± 1.27 (-4.98 – 0.97)	3.04e-11***	5.89e-06***
Information Processing (IP) (e.g., percent thinking time, latency)	0.27 ± 0.68 (-1.93 – 1.54)	-0.64 ± 1.40 (-4.16 – 1.51)	0.203	3.52e-06***
Simple Motor (SM) (e.g., oscillatory motion, speed)	0.27 ± 0.77 (-1.80 – 1.74)	-1.0 ± 1.37 (-4.95 – 0.95)	0.059	9.16e-05***
Spatial Reasoning (SR) (e.g., clockface circularity, clock component placement, horizontal/vertical placement)	0.45 ± 0.57 (-2.01 – 1.18)	-1.49 ± 1.59 (-4.15 – 0.63)	7.33e-05***	5.91e-08***

Table1. Demographics table of cognitively normal subjects without amyloid-β (Aß-) burden who completed a baseline DCTclock. All subjects underwent structural T1-weighted magnetic resonance imaging to generate regional parcellations using FreeSurfer and [^{11}C]Pittsburgh-Compound-B (**PiB**) PET imaging to estimate global Aß burden using distribution volume ratios (**DVR**, Logan graphical method, cerebellar gray matter reference) in a cortical composite of frontal, lateral, and retrosplenial regions (**FLR**). Aβ- CNs were classified as DCTclock normal (composite scores > 75, n = 78) and abnormal (composite scores < 60, n =27) based on FDA-approved dementia cutoff (Souillard-Mandar et al., 2021). All values in the table are expressed as mean ± deviation standard (min – max) when appropriate. ANOVA p-values for DCTclock composite scores and subscores were corrected for age, sex, education and handedness. Significance was assessed at p=0.05. *** = p<0.001, ** = p<0.01, * = p<0.05

DCT Normal = baseline composite scores > 75, **DCT Abnormal** = baseline composite scores < 60, **PiB** = [^{11}C]Pittsburgh-Compound-B, **FLR** = frontal, lateral, retrosplenial composite region for estimating global **Aß** burden, **PACC-5** = Preclinical Alzheimer's Cognitive Composite

Characteristics for n= 94 cognitively normal participants with longitudinal DCTclock performance				
	DCT Normal (n = 70)	**DCT Abnormal (n= 24)**	**p (ANOVA)**	
Age, y	76 ± 5.12	82 ± 6.36	2.34e-05***	
Sex (% females)	64%	70%	0.435	
Education, y	16.7 ± 2.50	15.2 ± 2.86	0.0235*	
Handedness (% right-handed)	88%	75%	0.0375*	
PiB FLR DVR	1.08 ± 0.04	1.07 ± 0.04	0.407	
PACC-5	0.38 ± 0.62 (-1.52 – 1.89)	-0.25 ± 0.72 (-1.98 – 1.02)	0.064	
Average annual follow up time difference (months)	16 ± 11	15 ± 8	N/A	
Annual Change DCTclock Performance			**p (ANOVA)**	**p (F-test)**
DCTclock Composite Score	-4 ± 9.61 (-25.1 – 20.1)	3.12 ± 12.2 (19.0 – 26.1)	0.00903**	0.078
DCTclock Annual Change Domain-Specific Subscores (z-scores)				
	DCT Normal	**DCT Abnormal**	**p (ANOVA)**	**p (F-test)**
Drawing Efficiency (DE) (e.g., total time, drawing size, noise)	0.43 ± 0.57 (-1.01 – 1.66)	-1.11 ± 1.27 (-4.98 – 0.97)	0.078	2.5e-07***
Information Processing (IP) (e.g., percent thinking time, latency)	0.27 ± 0.68 (-1.93 – 1.54)	-0.64 ± 1.40 (-4.16 – 1.51)	0.291	0.028
Simple Motor (SM) (e.g., oscillatory motion, speed)	0.27 ± 0.77 (-1.80 – 1.74)	-1.0 ± 1.37 (-4.95 – 0.95)	0.409	6.61e-04***
Spatial Reasoning (SR) (e.g., clockface circularity, clock component placement, horizontal/vertical placement)	0.45 ± 0.57 (-2.01 – 1.18)	-1.49 ± 1.59 (-4.15 – 0.63)	0.105	5.31e-10***

Table2. Demographics table of Aβ- cognitively normal subjects who completed at least one longitudinal DCTclock. Subjects were classified as DCTclock Normal (composite baseline scores > 75, n = 70) and Abnormal (composite baseline scores < 60, n =24) based on FDA-approved dementia cutoff (Souillard-Mandar et al., 2021). All values in the table are expressed as mean ± deviation standard (min – max) when appropriate. ANOVA p-values for DCTclock composite scores and subscores were corrected for age, sex, education and handedness. Significance was assessed at p=0.05. *** = p<0.001, ** = p<0.01, * = p<0.05

DCT Normal = baseline composite scores > 75, **DCT Abnormal** = baseline composite scores < 60, **PiB** = [^{11}C]Pittsburgh-Compound-B, **FLR** = frontal, lateral, retrosplenial composite region for estimating global Aß burden, **PACC-5** = Preclinical Alzheimer's Cognitive Composite

Keywords: Positron emission tomography, digital clock drawing test, Alzheimer's disease

26 Evaluating bidirectional effects of amyloid and tau on functional brain networks in preclinical Alzheimer's disease

Peter Millar[1], Nawang Singhe[2], Kiana Angela Macharia[1], Nicholas Metcalf[1], June Roman[1], John Morris[1], Tammie Benzinger[1], Brian Gordon[1], Beau Ances[1]

[1]*Washington University in St. Louis, St. Louis, MO, United States*
[2]*University of Minnesota, Minneapolis, MN, United States*

Background: There are conflicting reports regarding the effects of amyloid-β (Aβ) and tau on resting-state functional connectivity (RSFC) networks in cognitively unimpaired participants. One proposed model suggests that Aβ and tau have an interactive effect on RSFC, marked by hyper-connectivity with Aβ, then hypo-connectivity with tau. Although there is preliminary support for this model, independent validations and further characterizations of the effects of Aβ and tau on RSFC are needed.

Method: We analyzed RSFC, Aβ PET, and tau PET in cognitively unimpaired participants (Clinical Dementia Rating®: 0). RSFC was collected on two scanners in partly-overlapping samples (PETMR N: 190, Age: 46-91; TRIO N: 149, Age: 52-89). RSFC networks were defined using 298 regions of interest. Aβ was measured with PiB and AV-45 tracers, which were harmonized using a Centiloid conversion. Tau was measured with AV-1451 and was summarized in pre-defined regions. Relationships between Aβ, tau, and RSFC were tested with linear regression models, controlling for age, sex, education, and head motion, with a false discovery rate correction.

Result: We did not observe a bidirectional interaction effect in any of the hypothesized networks (default mode [DMN], salience [SAL], fronto-parietal [FPN]). Aβ was positively associated with RSFC, independent of tau, in the DMN and SAL, while tau was negatively associated with RSFC, independent of Aβ, in the SAL only. Exploratory analyses of FC within and between all networks did not identify clear patterns of interactive biomarker effects, nor consistent patterns of main effect relationships in the other networks.

Conclusion: These results do not support an interactive model of RSFC in preclinical AD. Inconsistencies with previous interactions may be driven by sample-specific or methodological differences, or the low reliability of FC and brain-behavior relationships. Prominent biomarker relationships in the DMN and SAL are consistent with regional overlap with Aβ deposition in early AD.

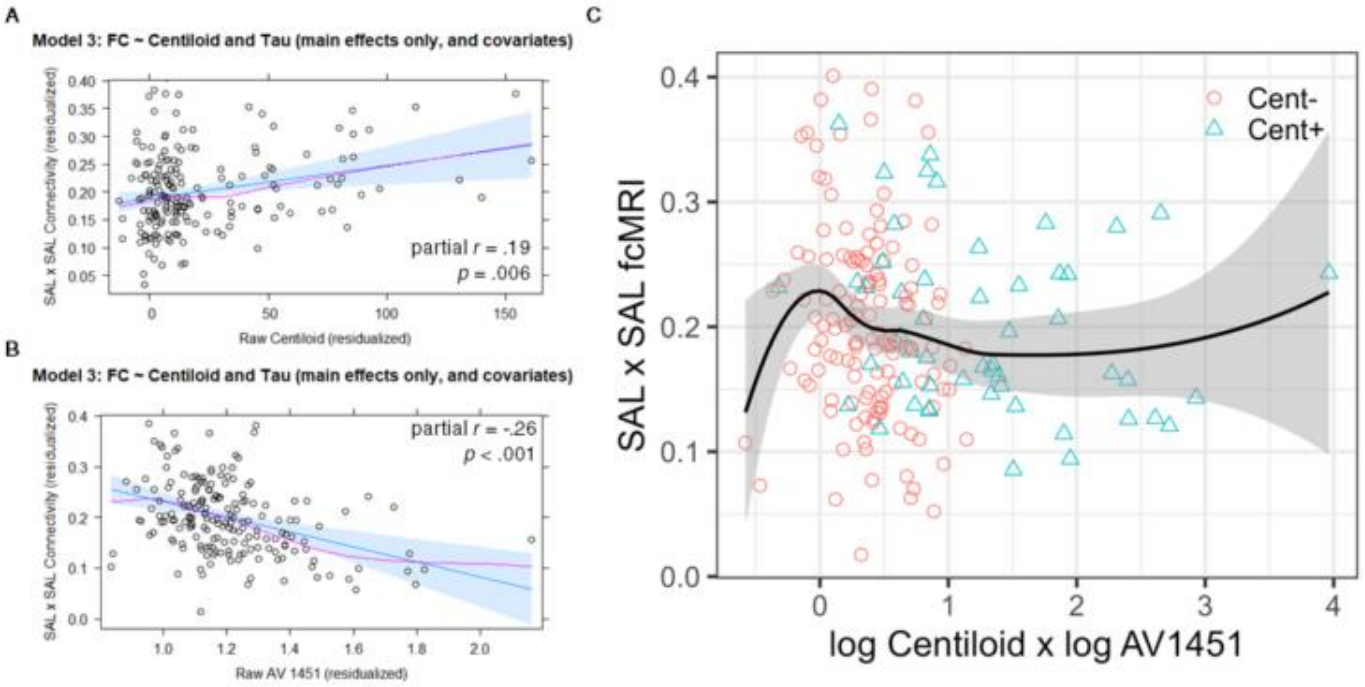

Figure 1. Visualization of SAL connectivity as a function of Amyloid PET (1A); and Tau PET (1B). Amyloid demonstrates a positive effect on SAL connectivity. In contrast, Tau demonstrates a negative effect on SAL connectivity. No evidence of bidirectional Amyloid * Tau interaction on SAL FC (1C).

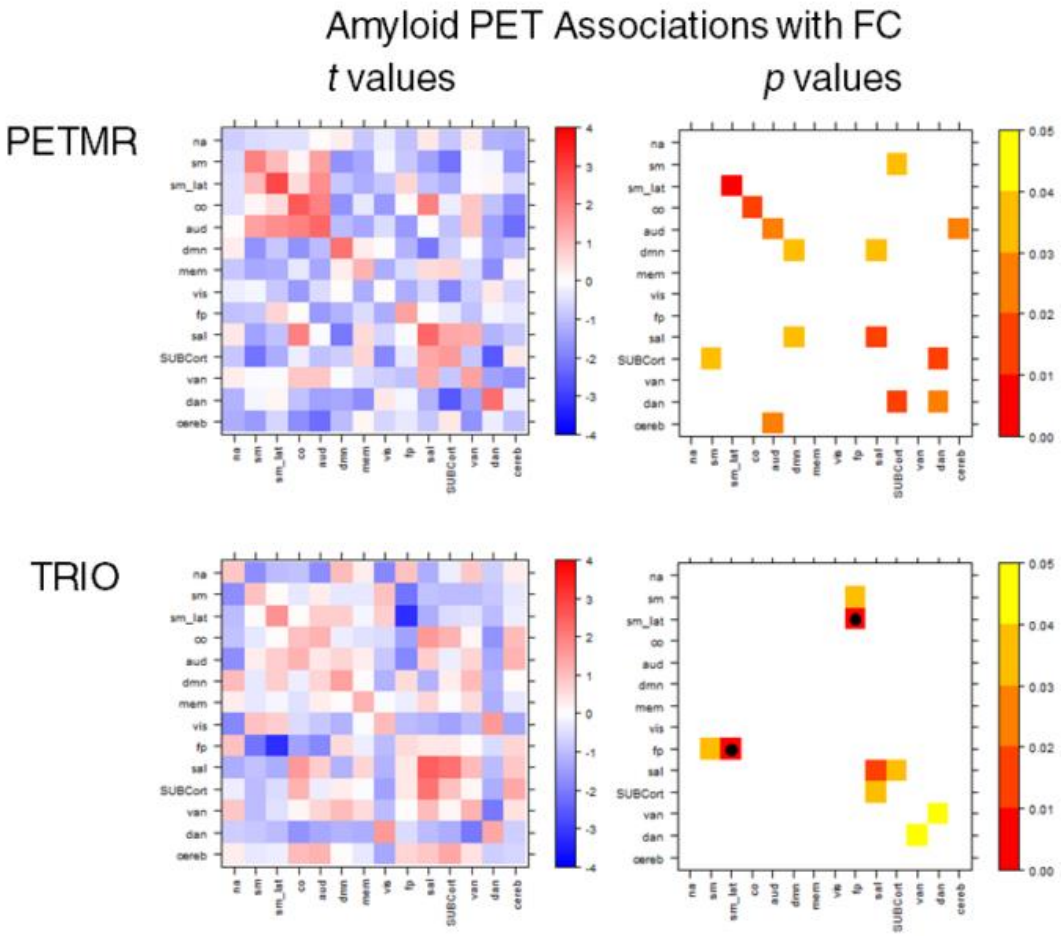

Figure 2. Amyloid-related hyper-connectivity in SAL consistently observed in both scanners, but does not survive correction for multiple comparisons. In the TRIO dataset, only one network (FP x SM_lat, black dot) maintained marginal significance after multiple comparisons correction.

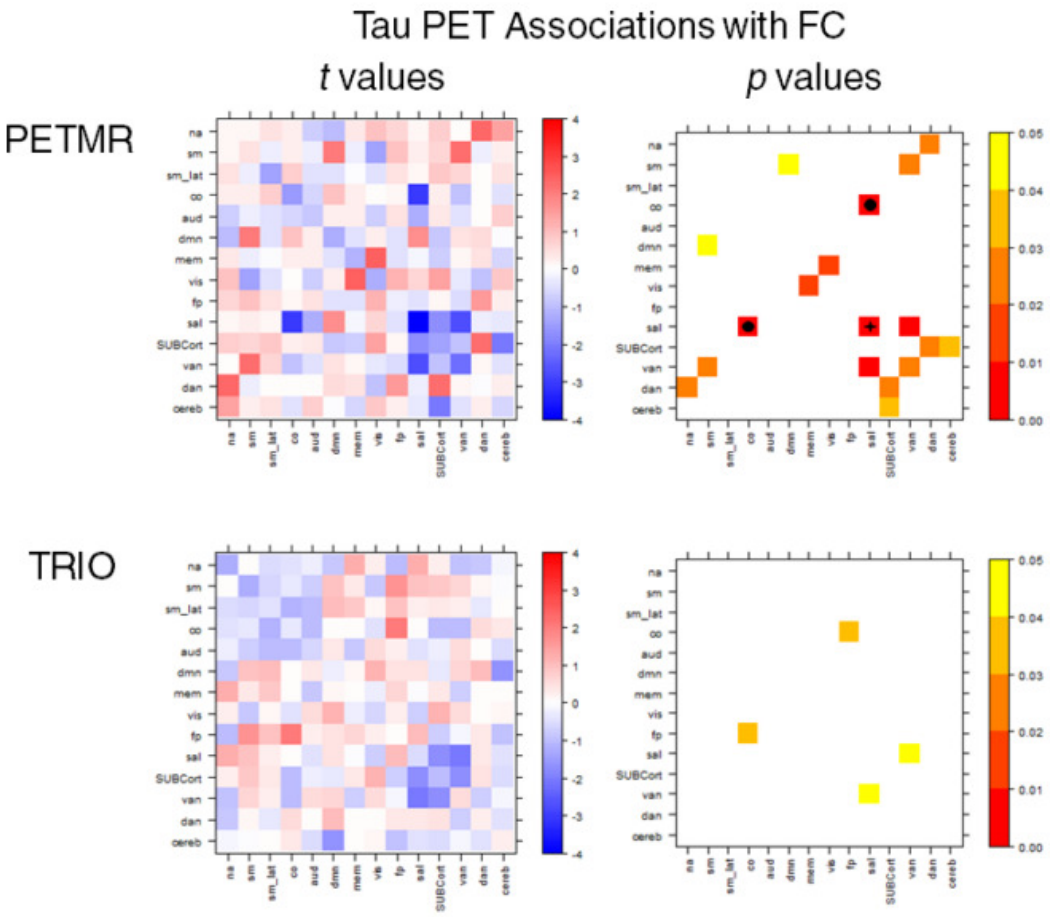

Figure 3. Tau-related hypo-connectivity between SAL & VAN consistently observed in both scanners, but does not survive correction for multiple comparisons. In the PETMR dataset, one network (SAL x CO, black dot) maintained marginal significance and one network (SAL x SAL, black star) maintained significance after multiple comparisons correction.

Keywords: resting-state functional connectivity, amyloid, tau

27 Tau propagates along principal axes of functional and structural brain organization in Alzheimer's disease

Julie Ottoy[1], Jazlynn Xiu Min Tan[1], Min Su Kang[1], Gleb Bezgin[2], Firoza Z. Lussier[3], Tharick A. Pascoal[3], Nesrine Rahmouni[4], Jenna Stevenson[4], Jean-Paul Soucy[5], Serge Gauthier[4], Boris C. Bernhardt[5], Sandra E. Black[1,6], Pedro Rosa-Neto[4], Maged Goubran[1,7,8]

[1]*Sunnybrook Research Institute, University of Toronto, Toronto, ON, Canada*
[2]*Neuroinformatics for Personalized Medicine lab, Montreal Neurological Institute, McGill University, Montreal, QC, Canada*
[3]*Department of Psychiatry, University of Pittsburgh, Pittsburgh, PA, CA*
[4]*Translational Neuroimaging laboratory, McGill Centre for Studies in Aging, McGill University, Montreal, QC, Canada*
[5]*Montreal Neurological Institute and Hospital, McGill University, Montreal, QC, Canada*
[6]*Department of Medicine (Division of Neurology), University of Toronto, Toronto, ON, Canada*
[7]*Department of Medical Biophysics, University of Toronto, Toronto, ON, Canada*
[8]*Physical Sciences Platform, Sunnybrook Research Institute, University of Toronto, Toronto, ON, Canada*

Introduction: Previous work has alluded to the effects of either functional or structural connectivity in driving tau propagation in Alzheimer's disease (AD). However, no studies have yet incorporated both functional and structural connectomes at the individual subject-level to model the effects of connectivity and network hubs on longitudinal tau spread. Here, we leveraged the connectome "gradient" space as a novel low-dimensional coordinate space that is sensitive to topographic changes in subject-specific connectomes for modeling tau spread.

Methods: 213 participants from the TRIAD cohort underwent diffusion-weighted MRI, rs-functional MRI, and ^{18}F-MK6240 tau-PET. Participants were grouped by disease stage: 103/35 Aβ-/+ cognitively normal and 75 cognitively impaired Aβ+. Eighty-seven participants had longitudinal tau-PET. We performed non-linear dimensionality reduction on the diffusion (structural) and rs-fMRI (functional) connectivity matrices to extract orthogonal components (gradients) explaining maximum variance per modality and disease stage. For each brain region, we then investigated the effect of baseline tau within highly connected (gradient-derived) hubs to that region on longitudinal Δtau spreading, as follows (**Fig. 1a**): $\Delta SUVR_{region}$ ~ baseline $SUVR_{region}$ + $SUVR_{functional\_hubs}$ + $SUVR_{structural\_hubs}$ + covariates (age, sex, APOE-ε4).

Results: Longitudinal tau accumulation in regions of early tau deposition (medial-temporal and lateral temporo-occipital cortices) was primarily facilitated by high tau deposition within their structural, but not functional, connected hubs (**Fig. 1b**). Conversely, tau accumulation in regions of the frontoparietal cortex was facilitated by high tau deposition within their functional, but not structural, connected hubs (**Fig. 1b**). Results were replicated irrespective of hub status and using two brain atlases. Using raw connectivity values instead did not yield accurate predictions.

Conclusion: Our unique approach demonstrates that subject-level gradients can predict future tau accumulation in AD. These findings suggest that high-tau hubs influence future tau accumulation in neighbouring regions, either through structural or functional connections, in a disease stage- and topographically-dependent manner.

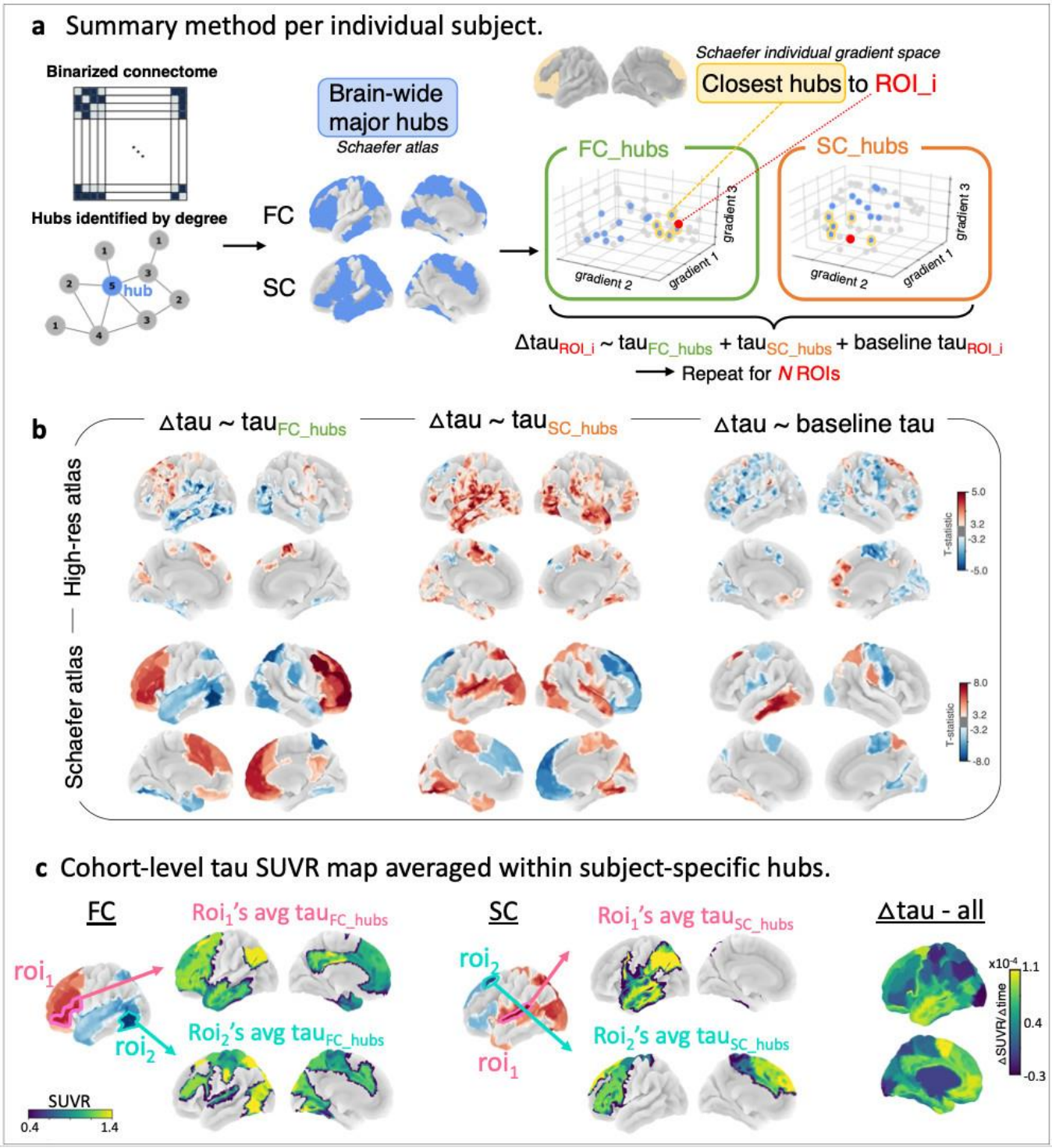

Figure 1. Tau within gradient-derived subject-specific hubs drives tau accumulation. **a**, Subject-specific hubs were identified (blue) based on degree extracted from the thresholded and binarized connectivity matrix, from which the top closest distance hubs (in gradient space) to each ROI was selected (yellow), for each participant. Tau was then averaged within each of these FC hubs (green) and SC hubs (orange). **b,** Regression results predicting tau accumulation, replicated for two different atlases. A positive t-statistic (red) within an ROI indicates a positive relationship between tau accumulation within the ROI and baseline tau within the ROI's hubs. **c,** Schematic showing that a positive t-statistic (from panel b) resulted from a relatively higher tau deposition within the ROI's hubs (see avg tau_{FC_hubs} and tau_{SC_hubs}) compared to tau within the ROI itself, while a negative t-statistic resulted from a relatively lower tau deposition within the ROI's hubs.

Keywords: Connectivity, gradients, tau, longitudinal, PET

28 X-ray based amyloid index as a quantitative biomarker for neurodegenerative diseases

Karthika Suresh[1,2], Eshan Dahal[1], Aldo Badano[1]

[1]*Division of Imaging, Diagnostics, and Software Reliability, Office of Science and Engineering Laboratories, Center for Devices and Radiological Health, Food and Drug Administration, Silver Spring, MD, United States*
[2]*Division of Biomedical Informatics, Research, and Biomarker Development, Office of Drug Evaluation Sciences, Office of New Drugs, Center for Drug Evaluation and Research, Food and Drug Administration, Silver Spring, MD, United States*

Background: Aggregation of innocuous proteins into insoluble, highly ordered fibrils is associated with numerous misfolding diseases including Alzheimer's and Parkinson's diseases. X-ray diffraction studies, super resolution microscopy, cryo-electron tomography and solid state nuclear magnetic resonance have given insights into the structure of protein aggregates in unprecedented detail at multiple scales. They have revealed a variety of structures including aggregates of amyloid-β, α-synuclein, tau and TDP-43 conforming to the cross-β fold. Here, we derive the X-ray based amyloid index based on cross-β signals to estimate regional aggregate load without defining a reference region and compare across different regions of interest.

Methods: X-ray scattering signals of oligomer and fibrillar aggregates were collected in pure form or after embedding in brain tissue phantoms or in sheep brain tissue using polychromatic or monochromatic X-ray source integrated with spectroscopic detectors. Region independent strategy for the assessment of aggregates load was established by normalizing the scattering profiles of different tissue regions with X-ray count at specific scattering angle unrelated to cross-β reflections. Amyloid index for normalized spectrum was defined as the ratio of AUP of knowledge based peak decomposed cross-β signal to the total spectrum AUP.

Results: Strong correlations were observed between AUPs of decomposed cross-β signals with ground truth values (Pearson correlation coefficient > 0.95). Protein aggregate level in brain tissue is governed the variations in amyloid index. The derived index metric avoided the selection of reference area and was independent of brain tissue region.

Conclusion: Our x-ray amyloid index based on cross-β signal is a metric for regional protein aggregate quantification which does not require the definition of target and reference regions and is independent of brain tissue region. Preliminary investigations from phantom and sheep brain studies suggest that this index can be a useful metric for assessing disease trajectories and monitoring targeted therapies.

Keywords: X-ray scattering, Amyloid index, cross-β, no-reference region, biomarker quantification

29 An artificial neural network for PET brain amyloid imaging

Mike Georgiou[1], Weizhao Zhao[1], Anthony Deana[1], Efrosyni Sfakianaki[1], Rosie Curiel Cid[1], David Loewenstein[1]

[1]*Dept. of Radiology, University of Miami Miller School of Medicine, Miami, FL, United States*
[2]*Dept. of Biomedical Engineering, University of Miami, Coral Gables, FL, United States*
[3]*Center of Cognitive Neuroscience and Aging, University of Miami Miller School of Medicine, Miami, FL, United States*

The purpose is to examine the feasibility of a deep learning (DL) artificial neural network (ANN) for classifying ^{18}F-florbetaben (FBB) PET/CT images based on quantitative analysis with SUV ratios (SUVr).

FBB images from 65 patients were visually interpreted and classified based on the brain amyloid plaque load (BAPL) scoring scheme as 27 BAPL=1, 20 BAPL=2 and 18 BAPL=3. The scans were quantitatively analyzed for regional amyloid plaque deposition of cortical regions, consisting of anterior cingulate gyrus, frontal lobe, occipital lobe, parietal lobe, posterior cingulate gyrus, and temporal lobe, using the Siemens syngo.via MI software. Whole cerebellum (WCER) was used for normalization. A deep learning ANN was applied with 6 inputs (SUVr values of the cortical regions), three hidden layers, and an output layer that can either classify the result based on BAPL category (1,2,3) or as normal vs. abnormal. A training function was created using MATLAB (learning rate 0.001, ReLU for internal activation and softmax for output activation). A user interface provided parameter-adjustable settings for testing, such as number of neurons in each layer and number of epochs, and supported output data collection (0 to 1 probability).

Using 64 neurons in each of the three hidden layers and 100,000 epochs, the system completed its training in 39 seconds. With all the data used for training and then randomly selecting cases for validation, the accuracy was 100% in categorizing the cases as BAPL 1,2,3 or as normal vs. abnormal. When training the system by first randomly removing cases used independently for validation, the accuracy for classification was 82% for the 3-BAPL classifier and 88% for the normal/abnormal classifier respectively. The accuracy improved using data augmentation with pseudo-cases.

This study demonstrated the potential of a DL ANN system for classifying FBB PET/CT cases into BAPL categories based on cortical regional SUVr analysis.

Keywords: Artificial Intelligence, amyloid brain analysis

30 Predicting regional tau burden using structural connectivity from individualized epicenters

Christopher Brown[1], Sandhitsu Das[1], Ilya Nasrallah[1], John Detre[1], Paul Yushkevich[1], Corey McMillan[1], David Wolk[1]

[1]*University of Pennsylvania, Philadelphia, PA, United States*

The factors that drive regional spread and heterogeneity of tau pathology across individuals with Alzheimer's disease (AD) remain poorly understood. Over the last several years studies have demonstrated the spread of tau pathology among functionally connected neurons. However, this work has defined group-level, canonical epicenters within typical and atypical AD using population-based connectomes. Here we identified individual-level epicenters of tau pathology and structural connectivity with these epicenters to predict regional tau burden. 183 participants from the Penn Aging Brain Cohort and ADNI with multi-shell diffusion MRI (dMRI) and AV1451 Tau PET within 18 months of each other were included in the present study. T1-weighted images were segmented using ANTS Multi-Atlas Joint Label Fusion pipeline. Tau PET and dMRI were both registered to T1-space using ANTS. Standard uptake value ratios (SUVR) were converted to Tau Positivity Indices (TPI) based on mixed-Gaussian models. We defined epicenters as the regions with the top 10% of TPI in each hemisphere. BEDPOSTX and PROBTRACKX2 were used for probabilistic tractography between all brain regions and structural connectivity distance ($Distance_{SC}$) of each region to tau epicenters was calculated and averaged for all epicenters. Linear mixed-modelling (Figure 1) including age, sex, education, race, and Epicenter TPI as fixed covariates and random slopes and intercepts demonstrated that regions with shorter $Distance_{SC}$ had higher TPI ($\beta_{unstand}$ = -0.077, 95% CI : [-0.11, -0.042], $p < 0.001$), with the full model explaining 68% of the regional variance in TPI ($\beta_{predict}$ = 1.013, $p < 0.001$). These models significantly outperformed those using Euclidean distance or a canonical epicenter in the entorhinal cortex (Figure 1). These results demonstrate that models using individualized epicenters and structural connectomes can account for a significant amount of regional heterogeneity in tau spread in Alzheimer's disease.

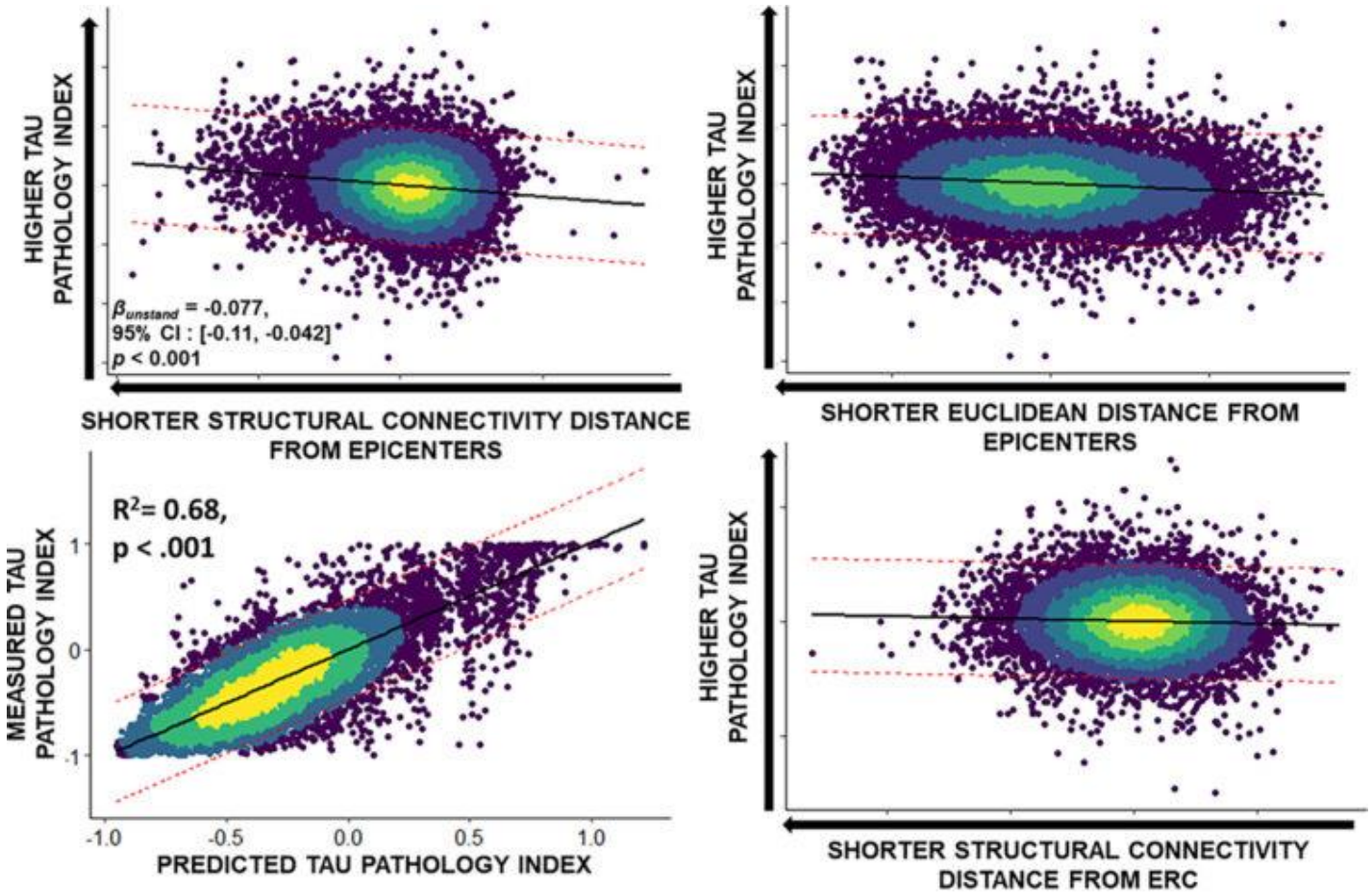

Figure 1. Structural Connectivity from Individualized Epicenters predicts Regional Tau Pathology. Prediction of regional tau pathology by structural connectivity distance from tau epicenters (top left) and comparison of predicted versus measured tau pathology (bottom left). Alternative models using Euclidean distance (top right) or distance from a canonical epicenter in the entorhinal cortex (bottom right) are also shown. Data points represent individual regions with density of points demonstrated by fill. Solid black lines are lines of linear best fit, while dashed red lines are the 95% prediction interval.

Keywords: Tau, dMRI, heterogeneity, PET, networks

31 Microglia density across different clinical Alzheimer's disease variants

Patrick Lao[1], Aubrey Johnson[1], Anna Smith[1], Diana Guzman[1], Amarachukwu Okafor[1], Hannah Houlihan[1], Lauren Heuer[1], Samantha Rossano[1,2], Daniel Talmasov[1], Ndubisi Chikwem[1], Dina Dass[1], James Noble[1], William Kreisl[1], Philip De Jager[1], Scott Small[1]

[1]*Columbia University, New York, NY, United States*
[2]*Life Molecular Imaging, New York, NY, United States*

Introduction: Microglia are inflammatory cells that surveil the brain, clearing Alzheimer's disease and related dementia (ADRD) pathology to prevent downstream neurodegeneration; however, there is evidence that microglia may also contribute to the aggregation and spreading of ADRD pathology, including tau tangles. AD and its variants are characterized by differential patterns of tau accumulation, following Braak staging in AD or a posterior distribution in posterior cortical atrophy (PCA). We hypothesized that translocator protein (TSPO) PET signal using a third-generation tracer, 11C-ER176, would follow a focal pattern that mirrors that of tau tangles.

Methods: Participants (69±7 years; 44% women; 18 amyloid-negative cognitively normal older adults (controls); 1 amyloid-positive MCI, 1 amyloid-positive AD; 3 amyloid-positive PCA) underwent amyloid PET (Florbetaben; visually determined positivity), tau PET (MK6240; 90-110min SUVR), and TSPO PET (ER176; 60-90min SUVR), as well as ADRC consensus diagnosis. Exploratory voxelwise analyses compared tau and TSPO between controls and all impaired participants as well as each variant.

Results: Impaired participants had widespread elevated tau and elevated TSPO in the occipital, temporal, and frontal cortices. The amyloid-positive MCI/AD group had widespread elevated tau across Braak regions and focal clusters of elevated TSPO in the frontal, temporal, parietal, and occipital cortices. In comparison, the amyloid-positive PCA group had more widespread elevated tau, which was highest in the occipital cortex, and more widespread focal clusters of elevated TSPO.

Conclusions: In a small subset of different clinical AD variants, evidence of elevated TSPO was present alongside elevated tau. Ongoing recruitment and longitudinal data collection, including within participants with logopenic variant of primary progressive aphasia, will further elucidate the spatial and temporal correspondence between tau and microglia across disease progression.

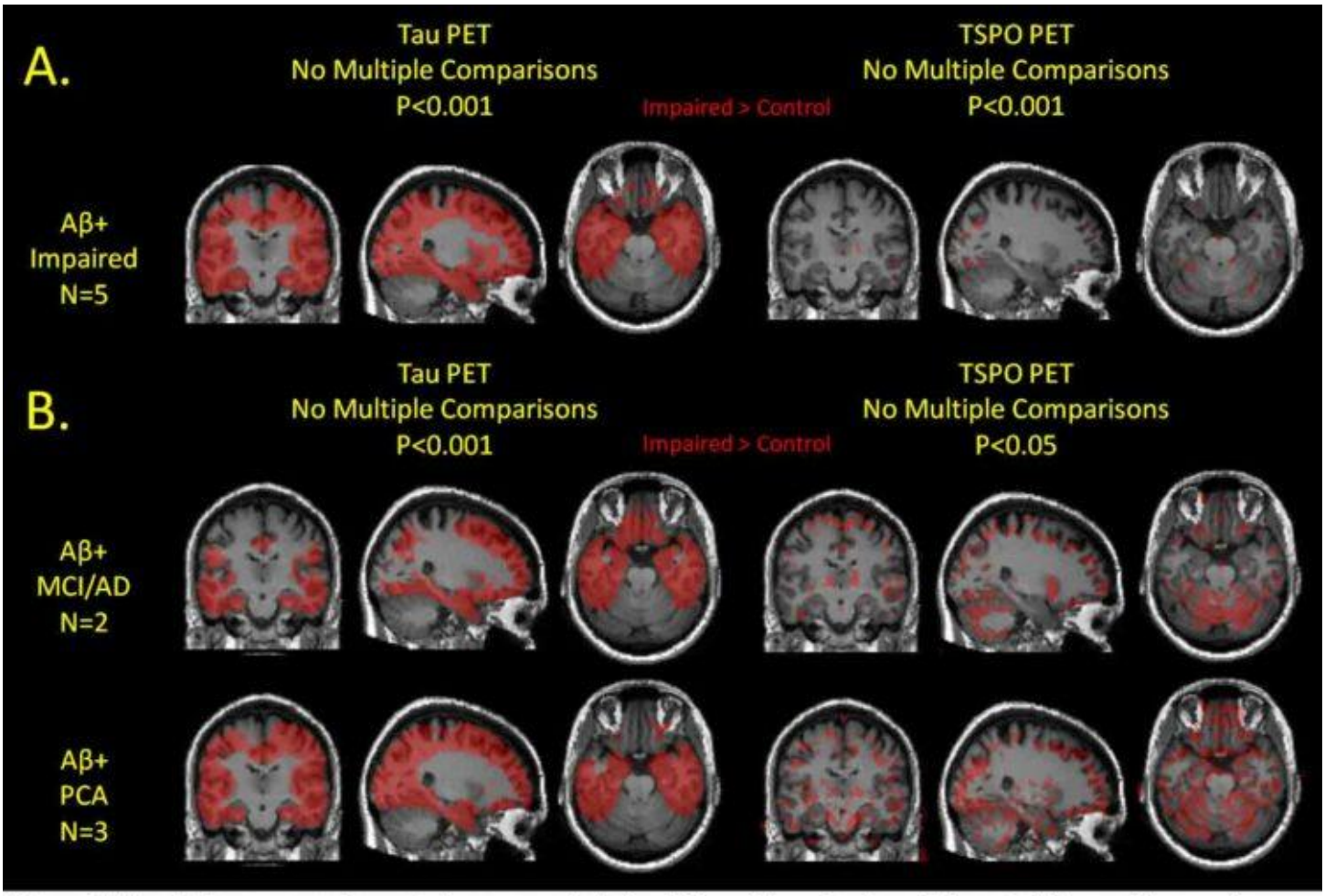

Figure 1. Voxelwise comparisons between controls (n=18) and impaired participants (A) as well as each variant (B). Clusters of red indicate greater tau (left) or TSPO (right) in impaired participants compared to controls. There were no clusters of greater tau or TSPO in controls. Note that clusters of elevated TSPO were present in the cerebellum, a validated TSPO pseudo-reference region for AD, in the smaller variant specific samples at a more liberal threshold that are minimized in the larger sample at a stricter threshold.

Keywords: Microglia, TSPO, tau, Alzheimer's disease, Posterior Cortical Atrophy

32 The TSPO circadian pattern: a [11C]ER176 test-retest study

Quentin Finn[1], Paolo Zanotti Fregonara[3], Johanna Appleton[1], Meixiang Yu[2,4], Masahiro Fujita[2,4], Joseph Masdeu[1,2], Belen Pascual[1,2]

[1]*Nantz National Alzheimer Center, Houston Methodist Neurological and Research Institute, Houston, TX, United States*
[2]*Weill Cornell Medicine, New York, NY, United States*
[3]*Molecular Imaging Branch, National Institute of Mental Health, National Institutes of Health, Bethesda, MD, United States*
[4]*Cyclotron and Radiopharmaceutical Core, Houston Methodist Research Institute, Houston, TX, United States*

Background: Mitochondrial translocator protein 18 kDa (*TSPO*) is a widely used marker of neuroinflammation. A possible circadian effect has been suggested in a [11C]PBR28 study. Unlike other *TSPO* tracers, [11C]ER176 has sufficient specific binding to image participants with any of the three *TSPO* genotypes, but its variability and reliability are unknown. We determined them in all *TSPO* genotypes by doing two [11C]ER176 scans in the same subject on the same day and an additional scan on a different day.

Methods: Seven healthy volunteers (age: 64.7±6.5 years, 3 female, HAB/MAB/LAB: 3/2/2) underwent 90-minute 11C-ER176 scans in the morning and afternoon. Ten subjects (62.8±5.5 years, 4 female, HAB/MAB/LAB: 6/2/2) (five of whom among the initial seven) had a retest scan on a different morning (104±121-day interval). Total distribution volume (VT) was calculated using an unconstrained two-tissue compartmental model and arterial input function. Outcome parameters were absolute variability (AV) and intraclass correlation coefficient (ICC).

Results: All same-day scans exhibited globally higher binding in the afternoon (average AV 23%); the increase tended to be higher in subjects with higher affinity (HAB/MAB/LAB: 28.5%/29.6%/8.5%); ICC was 0.91. For separate-day scans, average AV was 16.7%; ICC was 0.76. Removal of an outlying value decreased average AV to 13% and increased ICC to 0.92. Separate-day scans showed a small trend of increasing variability with affinity; average AV in HAB/MAB/LAB being 14.5%/11.7%/10%.

Conclusions: Previously only hinted at for *TSPO* tracers, our study clearly showed a circadian effect. [11C]ER176 uptake systematically increased in the afternoon compared to the morning. This effect increased variability and decreased reliability on same-day scans. Since [11C]ER176 uptake had a small variability and high reliability in scans obtained at the same time of day, clinical protocols should consider the impact of circadian variability on the reproducibility of studies performed with [11C]ER176 and other *TSPO* tracers.

Keywords: Neuroinflammation, ER176, PET, TSPO, Reliability

33 Tau PET signal within the default mode network predicts longitudinal clinical decline in atypical early Alzheimer's disease

Yuta Katsumi[1], Inola Howe[1], Ryan Eckbo[1], Bonnie Wong[1,2], Megan Quimby[1], Daisy Hochberg[1], Scott McGinnis[1,3], Deepti Putcha[1,2,3], Alexandra Touroutoglou[1,4,5], Brad Dickerson[1,2,4,5]

[1]*Frontotemporal Disorders Unit, Department of Neurology, Massachusetts General Hospital and Harvard Medical School, Boston, MA, United States*
[2]*Department of Psychiatry, Massachusetts General Hospital and Harvard Medical School, Boston, MA, United States*
[3]*Center for Brain Mind Medicine, Department of Neurology, Brigham & Women's Hospital, Boston, MA, United States*
[4]*Athinoula A. Martinos Center for Biomedical Imaging, Massachusetts General Hospital, Charlestown, MA, United States*
[5]*Alzheimer's Disease Research Center, Massachusetts General Hospital, Charlestown, MA, United States*

Identifying individuals with early stage Alzheimer's disease (AD) at greater risk of steeper clinical decline would allow professionals and loved ones to make better-informed medical, support, and life planning decisions. While recent research has started to demonstrate the clinical prognostic value of tau PET in typical late-onset amnestic AD, its utility in predicting clinical decline in individuals with atypical forms of AD remains unclear. Here, we examined the relationship between baseline tau PET signal and the rate of subsequent clinical decline in a sample of 48 $A^+/T^+/N^+$ patients with mild cognitive impairment or mild dementia due to AD with atypical clinical phenotypes: 16 Posterior Cortical Atrophy, 15 logopenic variant Primary Progressive Aphasia, and 17 amnestic syndrome with multi-domain impairment and age of onset < 65 years (**Table 1**). Baseline tau burden was measured with ^{18}F-Flortaucipir PET, whereas the rate of clinical decline was quantified as the annualized change in Clinical Dementia Rating Sum-of-Boxes scores (CDR-SB) from baseline to follow-up. Compared with amyloid-negative cognitively unimpaired controls, atypical early AD patients showed prominent baseline tau burden in the major nodes of the default mode network (DMN), including the angular gyrus, posterior cingulate cortex/precuneus, and lateral temporal cortex, with lesser involvement of the medial temporal lobe (**Fig. 1A**). Greater baseline tau in the broader DMN predicted faster clinical decline (**Fig. 1B**). Tau in the DMN was a stronger predictor of clinical decline than that in the other canonical networks (**Table 2**), which was supported by data-driven model selection that considers joint contributions of multiple networks (**Table 3**). These findings point to the role of DMN tau as an imaging biomarker to guide prognostication for patients with atypical early AD and their families and to inform the design of clinical trials, including potentially recruiting multiple clinical phenotypes of AD into a single trial.

Table 1. Demographic and clinical characteristics of the sample

	AD	Aβ- CU
n	48	24
Age (years)	64.1 ± 8.16	67.4 ± 4.9
Sex (M/F)	20/28	12/12
Education (years)	16.7 ± 2.46	#15.7 ± 2.3
MMSE at baseline	*23.57 ± 4.75	-
CDR at baseline	CDR 0 (n = 3) CDR 0.5 (n = 28) CDR 1 (n = 17)	CDR 0 (N = 24)
CDR-SB at baseline	3.5 ± 1.87	0
Baseline to follow-up (months)	14.55 ± 3.97	-
Global cortical amyloid (CL)	100.64 ± 26.37	6.63 ± 6.26

Note: CU = cognitively unimpaired. Data based on **n* = 21 and #*n* = 13.

Figure 1A. Atypical early AD is characterized by posterior cortical tau deposition, including the major nodes of the **default mode network (DMN)**

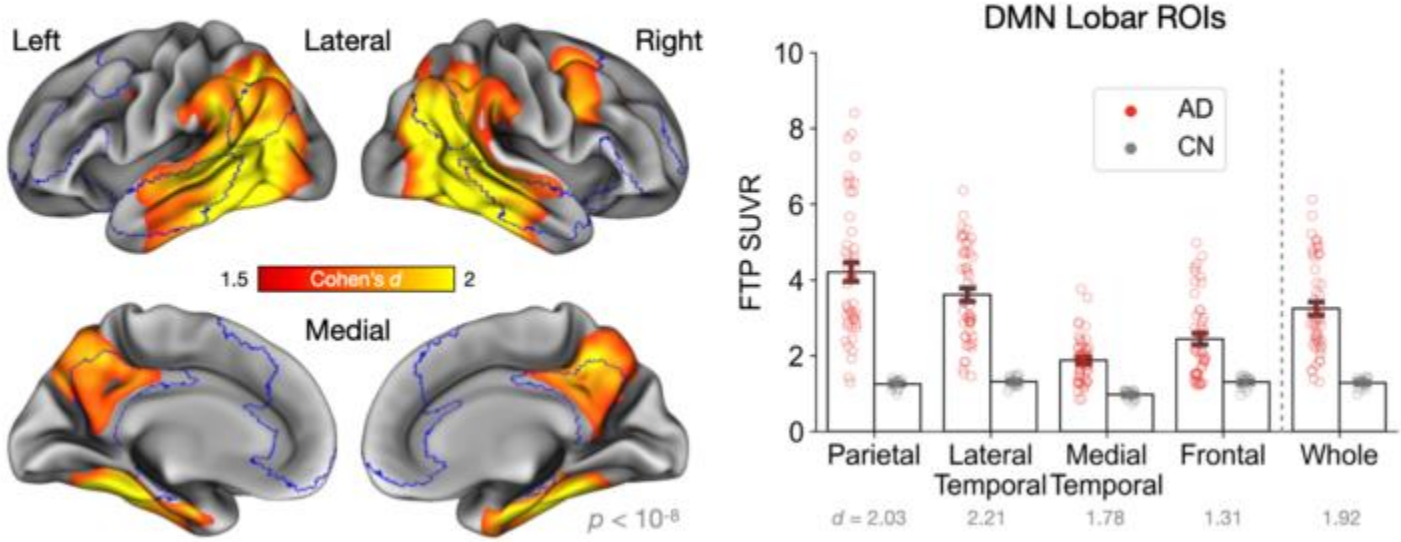

Figure 1B. Greater tau burden in the **DMN** at baseline predicts faster clinical decline in atypical early AD approximately one year later

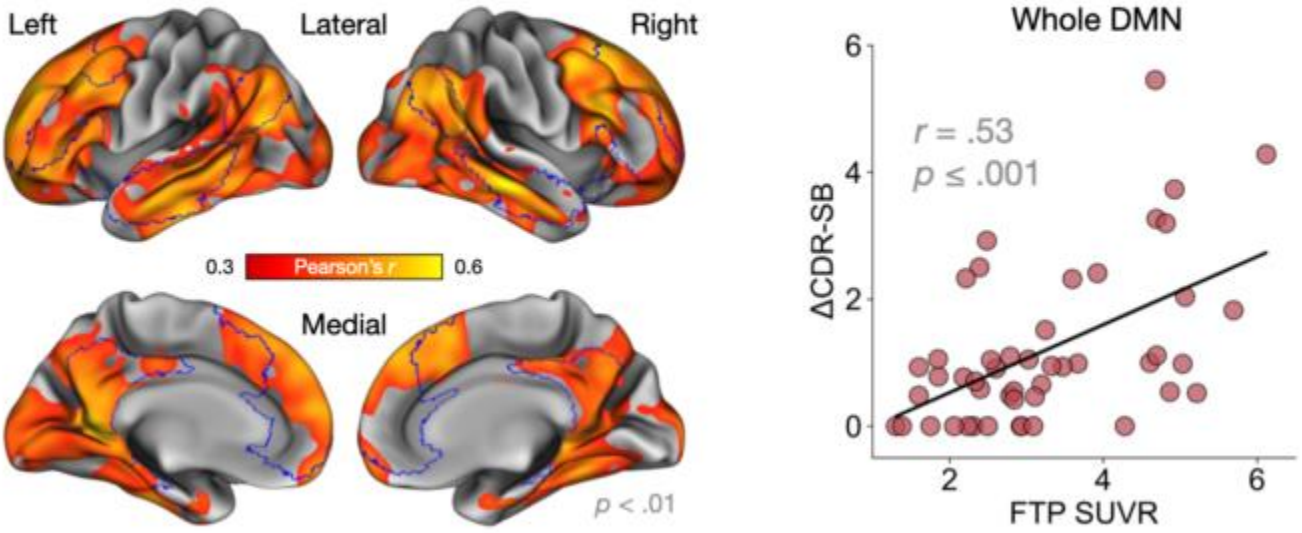

Table 2. Simple network multiple linear regression models reveal that baseline tau burden in the default mode network (DMN) is a stronger predictor of clinical decline than that in other canonical functional networks in atypical early AD.

Model	Age	Sex	Baseline CDR-SB	Default	Frontoparietal	Visual	Limbic	Dorsal Attention	Ventral Attention	Somatomotor	Adjusted R2	*p*	AIC
Basic	-0.07 (.63)	0.46 (.11)	**0.32 (.027)**	-	-	-	-	-	-	-	.10	.051	-1.40
Default	0.19 (.19)	0.16 (.53)	0.24 (.056)	**0.56 (<.001)**	-	-	-	-	-	-	.31	<.001	-12.84
Frontoparietal	0.21 (.17)	0.15 (.59)	0.23 (.077)	-	**0.54 (.002)**	-	-	-	-	-	.26	.0017	-9.87
Visual	-0.01 (.94)	0.34 (.23)	0.19 (.18)	-	-	**0.33 (.036)**	-	-	-	-	.17	.016	-4.38
Limbic	-0.01 (.91)	0.28 (.31)	**0.28 (.037)**	-	-	-	**0.37 (.011)**	-	-	-	.21	.0059	-6.80
Dorsal Attention	0.09 (.59)	0.30 (.31)	0.25 (.076)	-	-	-	-	0.32 (.068)	-	-	.15	.025	-3.17
Ventral Attention	0.15 (.37)	0.26 (.36)	**0.30 (.032)**	-	-	-	-	-	**0.40 (.024)**	-	.19	.011	-5.19
Somatomotor	0.03 (.84)	0.41 (.15)	**0.29 (.045)**	-	-	-	-	-	-	0.22 (.19)	.12	.050	-1.37

Note: The best performing model, defined as having the largest ΔAIC and ΔR^2 compared with the basic model, is highlighted in orange, where tau burden in the DMN is the only significant predictor in the model. AIC = Akaike information criterion.

Table 3. Data-driven model selection reveals that tau burden in the DMN alone provides sufficient explanatory power to predicting clinical decline in atypical early AD.

Age	Sex	Baseline CDR-SB	Default	Frontoparietal	Limbic	Ventral Attention	Visual	df	logLik	AICc	delta	weight
-	-	-	0.78	-	-	-0.44	0.29	5	-56.52	124.46	-	0.04
-	-	0.23	0.49	-	-	-	-	4	-57.92	124.77	0.30	0.03
-	-	-	0.42	-	-	-	0.24	4	-58.13	125.18	0.72	0.03
0.19	-	0.23	0.59	-	-	-	-	5	-56.92	125.26	0.79	0.03
-	-	0.25	1.14	-0.67	-	-	-	5	-57.08	125.58	1.12	0.02
-	-	0.17	0.42	-	-	-	0.17	5	-57.18	125.79	1.33	0.02
-	-	-	0.53	-	-	-	-	3	-59.64	125.82	1.36	0.02
-	-	0.21	0.75	-	-	-0.29	-	5	-57.20	125.82	1.36	0.02
-	-	0.14	0.74	-	-	-0.39	0.23	6	-55.91	125.86	1.40	0.02
-	-	-	0.62	-	0.21	-0.47	0.34	6	-55.92	125.88	1.42	0.02
0.18	-	-	0.51	-	-	-	0.24	5	-57.23	125.89	1.42	0.02
-	-	-	-	-	0.36	-	0.36	4	-58.51	125.94	1.48	0.02
-	-	-	1.07	-0.68	-	-	0.27	5	-57.27	125.97	1.50	0.02
-	-	0.19	1.14	-0.76	-	-	0.20	6	-56.07	126.20	1.73	0.02
0.19	-	0.18	0.52	-	-	-	0.17	6	-56.15	126.36	1.89	0.01
0.12	-	-	0.79	-	-	-0.37	0.28	6	-56.17	126.38	1.92	0.01
-	-	-	0.82	-	-	-0.33	-	4	-58.76	126.45	1.98	0.01

Note: Only the models with ΔAIC < 2 are shown (out of 256 models). The most parsimonious model, as defined by having the fewest predictors within two AIC points from the lowest AIC, is highlighted in orange, which has tau burden in the DMN as the sole predictor.

Keywords: Positron emission tomography, Clinical Dementia Rating Scale Sum of Boxes, prognostication, disease-modifying therapies, risk stratification

34 Reduced coupling between cerebrospinal fluid flow and global brain activity is linked to cortical tau and atrophy

Feng Han[1], JiaQie Lee[1], Xi Chen[1,2], Jacob Ziontz[1], Tyler Ward[1], Susan Landau[1], Suzanne Baker[2], Theresa Harrison[1], William Jagust[1,2]

[1]*Helen Wills Neuroscience Institute, University of California, Berkeley, Berkeley, CA, United States*
[2]*Lawrence Berkeley National Laboratory, Berkeley, CA, United States*

Background: The glymphatic system clears β-amyloid (Aβ) and tau through cerebrospinal fluid (CSF) movement. CSF inflow is coupled to global brain activity measured by global resting-state functional-MRI (gBOLD). Weaker coupling may reflect impaired glymphatic function and is associated with cognitive decline and Aβ load in early Alzheimer's disease (AD). Here we quantify glymphatic function with gBOLD-CSF coupling and investigate the role of glymphatic activity in tau pathology.

Method: We included 115 ADNI3 participants (72.5 ± 7.8 years; 60 females; 6 AD and 42 mild cognitive impairment) who underwent resting-state fMRI (rsfMRI; TR = 0.607s), tau-PET (flortaucipir), and amyloid-PET (florbetapir or florbetaben). These participants were classified into different sub-groups based on amyloid deposition (Aβ+: florbetapir > 1.11 SUVR; florbetaben > 1.08 SUVR) or diagnosis (cognitively impaired or unimpaired). CSF inflow signal was extracted at the bottom rsfMRI slice, and gBOLD signal was from gray matter. Correlation analysis between gBOLD-CSF coupling and tau load or cortical thickness was performed on the whole cohort and sub-groups. Predefined regions of interest (ROIs) included Braak ROIs and a meta-temporal ROI.

Result: CSF inflow and gBOLD were coupled. Each participant's coupling was quantified by the gBOLD-CSF cross-correlation at the negative peak (**Fig. 1**). Weaker coupling was correlated with more tau deposition and thinner cortices in Braak III-IV, V-VI, and meta-temporal ROI (but not in entorhinal cortex) in all participants, and the Aβ+ and Aβ+ impaired subgroups (**Fig. 2**&**3**). Tau deposition mediated the association between coupling and thickness across all and Aβ+ participants.

Conclusion: Coupling between gBOLD and CSF inflow is associated with tau deposition and cortical thickness across neocortex, especially in Braak V-VI ROIs. This effect is particularly evident in participants with elevated amyloid or cognitive impairment. These findings suggest that gBOLD-CSF coupling is important for tau clearance, likely through its association with the glymphatic system.

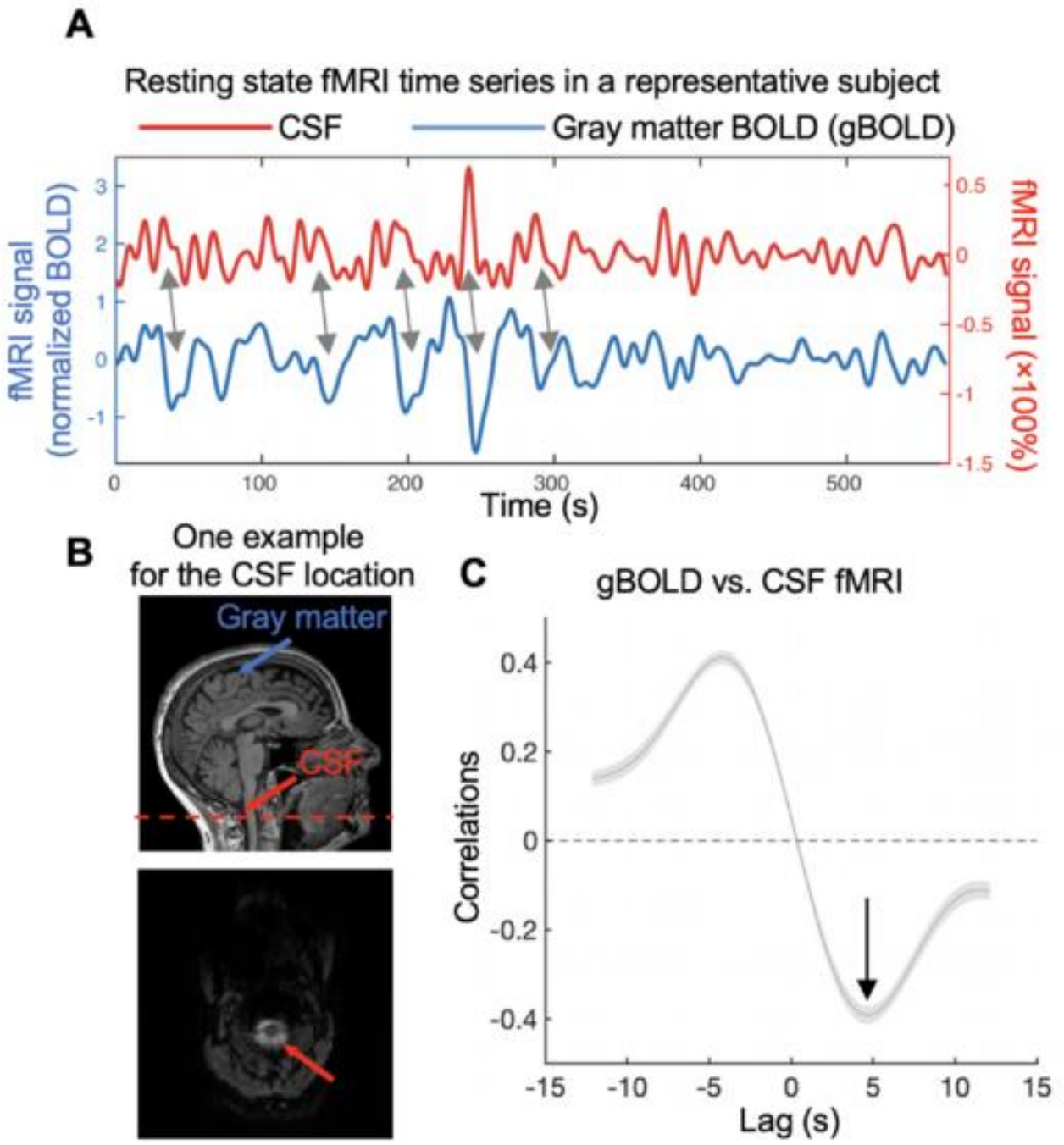

Fig. 1. Gray-matter rsfMRI (gBOLD) and CSF inflow signals are temporally coupled. (**A**) Coupled gBOLD and CSF changes (gray arrows) in a representative subject. (**B**) Upper: gBOLD was averaged across gray matter area; Lower: CSF inflow signal was extracted from the CSF region at the bottom slice of rsfMRI acquisition, corresponding to the red-dashed line on the T1-weighted image in the upper panel. (**C**) The mean gBOLD-CSF cross-correlation across all 115 subjects. The cross-correlation (r = - 0.34) at the +4.856-sec lag (black arrow; negative peak of the mean curve) was applied to quantify the BOLD–CSF coupling for each subject. Shaded region represents one standard error of mean (SEM).

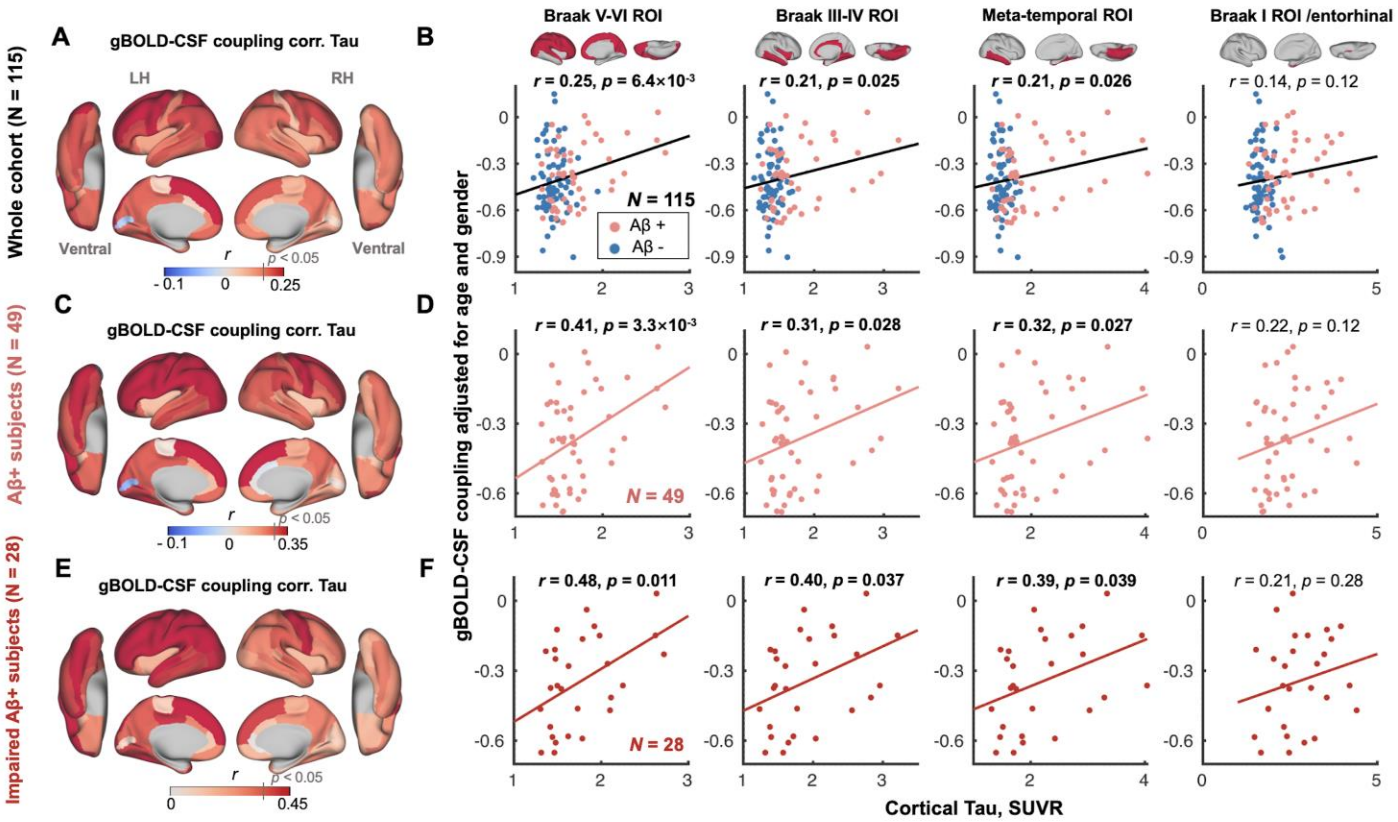

Fig. 2. gBOLD-CSF coupling is correlated with the cortical tau across the whole cohort and Aβ+ subjects. (**A**) gBOLD-CSF coupling was positively correlated with tau in most cortical regions across all subjects, i.e., subjects with weaker (less negative) coupling had more tau deposition. (**B**) gBOLD-CSF coupling (strength) significantly decreased with more tau deposition in Braak V-VI, Braak III-IV, and temporal meta-ROI across the whole cohort (all $r > 0.21$, all $p < 0.026$; N = 115). This association was similar, although not significant ($r = 0.14$, $p = 0.12$), for tau in Braak I (entorhinal cortex). (**C-F**) These associations between gBOLD-CSF coupling and regional tau were also evident among Aβ+ and/or specifically impaired Aβ+ subjects (all $r > 0.31$, all $p < 0.039$; in Braak V-VI, Braak III-IV, and temporal meta-ROI), but not for the rest of subjects. Aβ+: cortical AV45–Aβ > 1.11 SUVR or cortical FBB–Aβ > 1.08 SUVR. Impaired group: AD and MCI subjects. Each point represents one subject. The linear regression line was estimated based on the linear least-squares fitting (the same hereinafter unless noted otherwise).

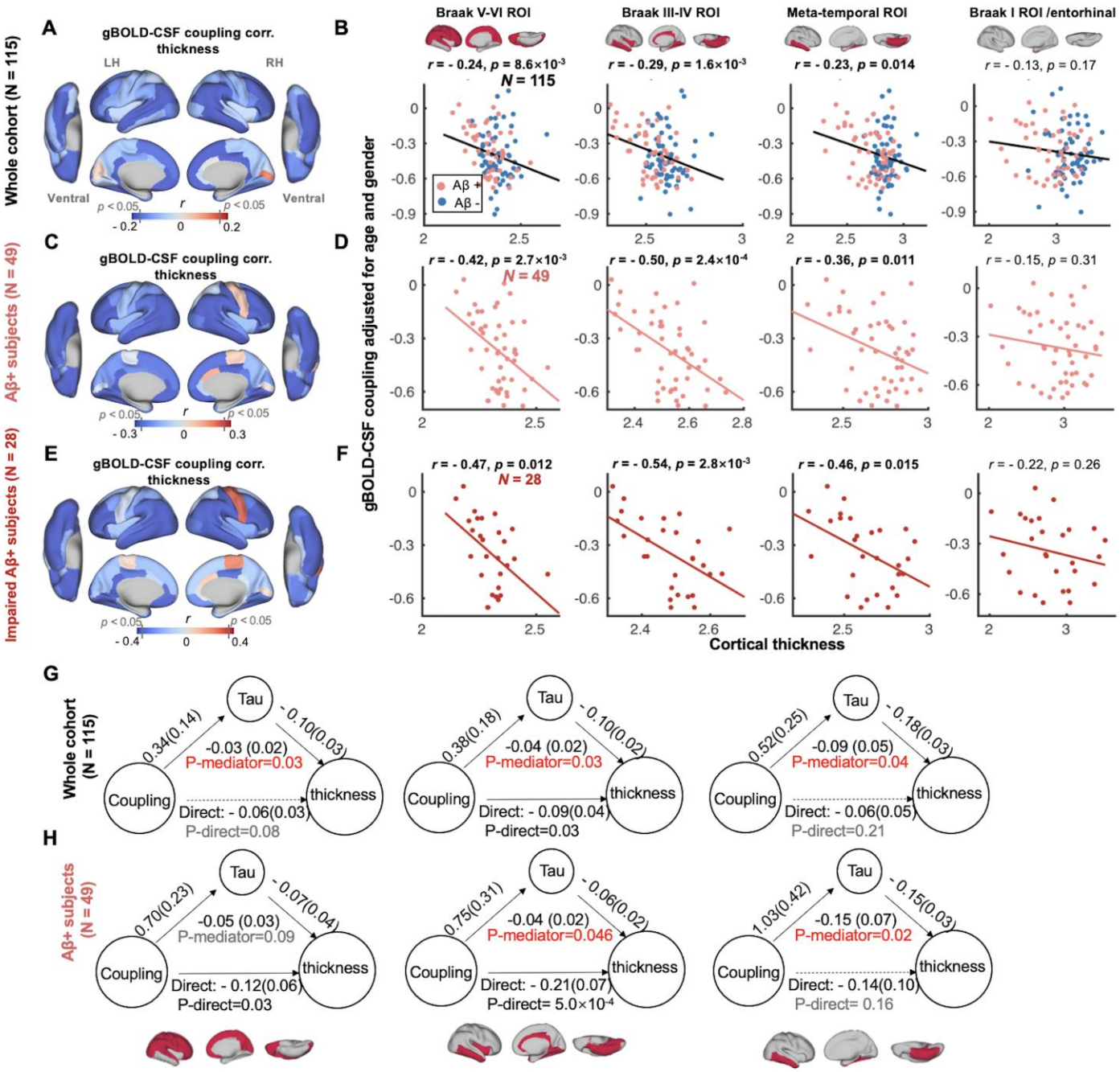

Fig. 3. gBOLD-CSF coupling is correlated with cortical thickness across the whole cohort and Aβ+ subjects, which is mediated by tau. (A) Subjects with weaker (less negative) gBOLD-CSF coupling had thinner cortices in the majority of brain regions, especially in the frontal, parietal, and temporal lobes, including default mode network (DMN) and fronto-parietal network (FPN). (B) The gBOLD-CSF coupling strength significantly decreased with thinner cortices in Braak V-VI, Braak III-IV, and temporal meta-ROIs across the whole cohort (all $r < -0.23$, all $p < 0.014$; $N = 115$). A similar but not significant coupling-thickness association was found in the entorhinal region ($r = -0.13$, $p = 0.17$). (C-F) Among Aβ+ subjects, particularly impaired Aβ+ ones, the coupling-thickness remained striking (all $r < -0.36$, all $p < 0.015$ in Braak V-VI, Braak III-IV, and temporal meta-ROI in D and F) while this was not the case in other participants. Each point represents one subject. (G-H) Across the entire cohort and Aβ+ subjects, tau mediated the significant association between gBOLD-CSF coupling and thickness throughout cortex, including Braak V-VI, Braak III-IV, and meta-temporal area ($p < 0.046$, except for the marginally significant relationship [$p = 0.090$] in Braak V-VI among the Aβ+ subjects).

Keywords: tau, cortical thickness, cerebrospinal fluid (CSF) flow, global brain activity, glymphatic function

35 Cognitive decline and Alzheimer's disease clinical status in Down syndrome are better distinguished by amyloid and neurofibrillary tau compared to age

Matt Zammit[1], Emily Schworer[1], Tobey Betthauser[1], Sigan Hartley[1], Charles Laymon[2], Dana Tudorascu[2], Ann Cohen[2], Sterling Johnson[1], Alexander Converse[1], Davneet Minhas[2], Shahid Zaman[3], Beau Ances[4], Chester Mathis[2], William Klunk[2], Benjamin Handen[2], Bradley Christian[1], The Alzheimer's Biomarker Consortium - Down Syndrome[1,2,3,4]

[1]*University of Wisconsin-Madison, Madison, WI, United States*
[2]*University of Pittsburgh, Pittsburgh, PA, United States*
[3]*University of Cambridge, Cambridge, United Kingdom*
[4]*Washington University in St. Louis, St. Louis, MO, United States*

Background: Characterization of cognitive decline following Alzheimer's disease (AD) biomarker emergence is necessary for clinical care in individuals with Down syndrome (DS). This study explores the relation between DS-specific cognitive measures with amyloid and tau PET.

Methods: 167 adults with DS underwent PiB and AV-1451 PET (N=92 with longitudinal data). Individuals were assessed using the modified Cued Recall Test (mCRT) and Down Syndrome Mental Status Examination (DSMSE). Clinical status (cognitively stable (CS), mild cognitive impairment (MCI) or dementia (DEM)) was determined from a consensus process independent of PET results. Amyloid burden was characterized using amyloid-positive (A+=18CL) chronicity (time-duration of A+), and tau burden was measured with SUVR across NFT stages of tau pathology. Age and chronicity were independently compared across groups categorized by clinical status using ANOVA with Tukey's HSD. Linear regression models (considering up to quadratic polynomials) were performed independently with mCRT and DSMSE scores against chronicity and NFT stage tau for the most recent timepoint while adjusting for sex and premorbid intellectual disability level.

Results: Individuals were distinguishable by age between CS and MCI/DEM, but not between MCI and DEM, while chronicity distinguished all groups (Fig.1). Negative associations ($p<.0001$) were observed between cognition and chronicity, and cognition and NFT stage tau. For all models, premorbid intellectual disability level as a covariate was significant, while sex was only significant for models evaluating DSMSE. Quadratic associations were observed for models assessing cognition vs. chronicity, while linear associations were observed for cognition vs NFT stage tau (Fig.2+3).

Discussion: A+ chronicity is an effective tool to classify individuals with DS based on their AD clinical status. Both amyloid and tau display significant negative associations with cognition in DS. These findings highlight the trajectory of cognitive decline following amyloid and tau emergence throughout AD progression in DS.

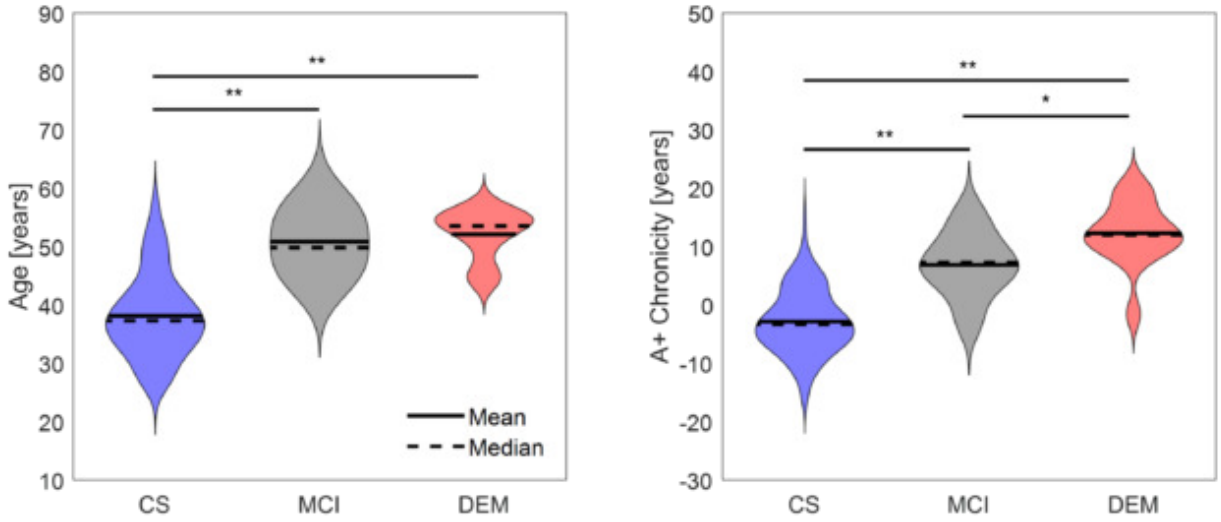

Significance: * .05; ** .0001. Adjusted for multiple comparisons using Tukey's HSD.

Fig 1. ANOVA comparisons between mean age and A+ chronicity categorized by clinical status (cognitively stable, mild cognitive impairment, dementia). A+ chronicity of 0 years indicates the threshold of A+ (18CL). Individuals with MCI had a mean age of 50.8(5.25) years and mean A+ chronicity of 6.84(5.37) years. Individuals with DEM had a mean age of 52.1(4.21) years and mean A+ chronicity of 12.3(5.30) years.

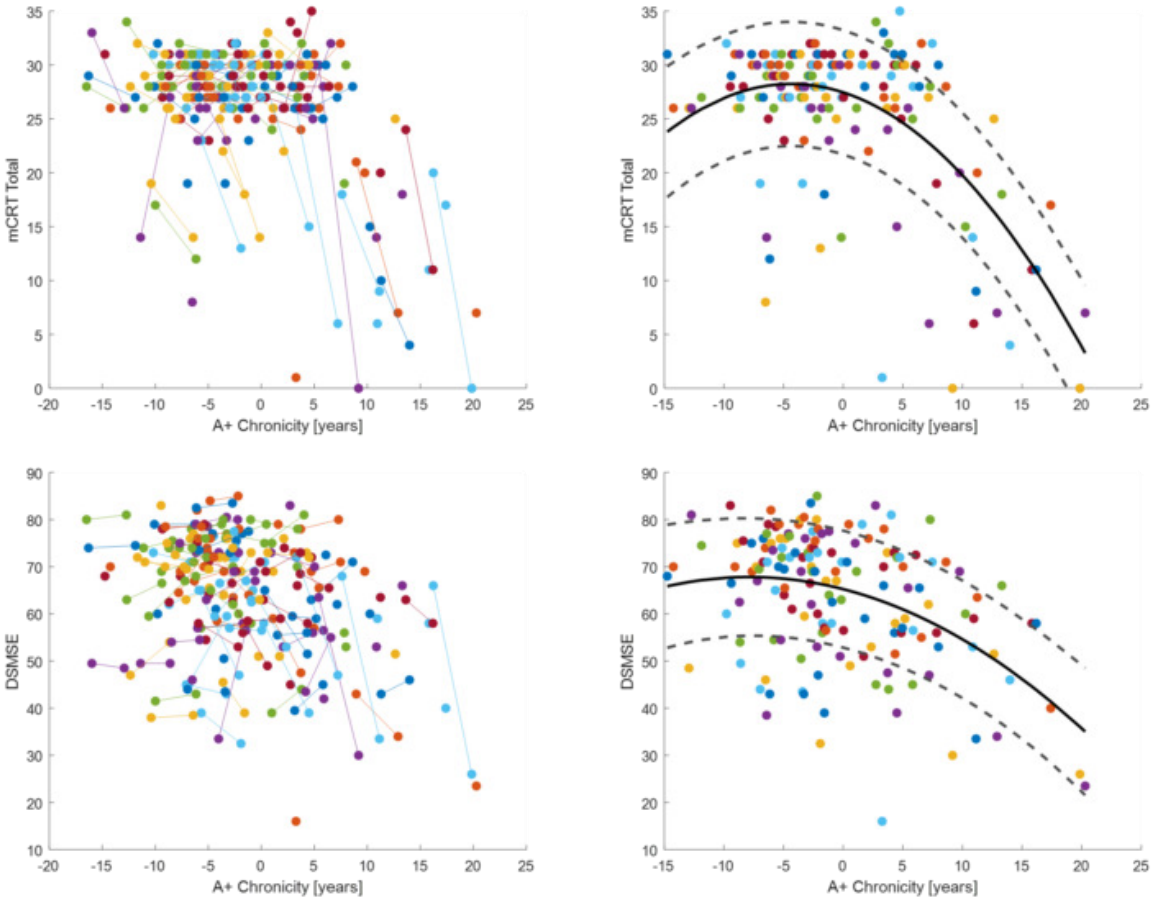

Fig 2. Negative associations between cognition (modified Cued Recall Test and Down Syndrome Mental Status Examination) and A+ chronicity. The left plots display results for all timepoints, where connected lines represent longitudinal data for each individual (represented as individual colors). The right plots display the regression fits between cognition and A+ chronicity for only the most recent timepoint. Dashed lines represent the standard error.

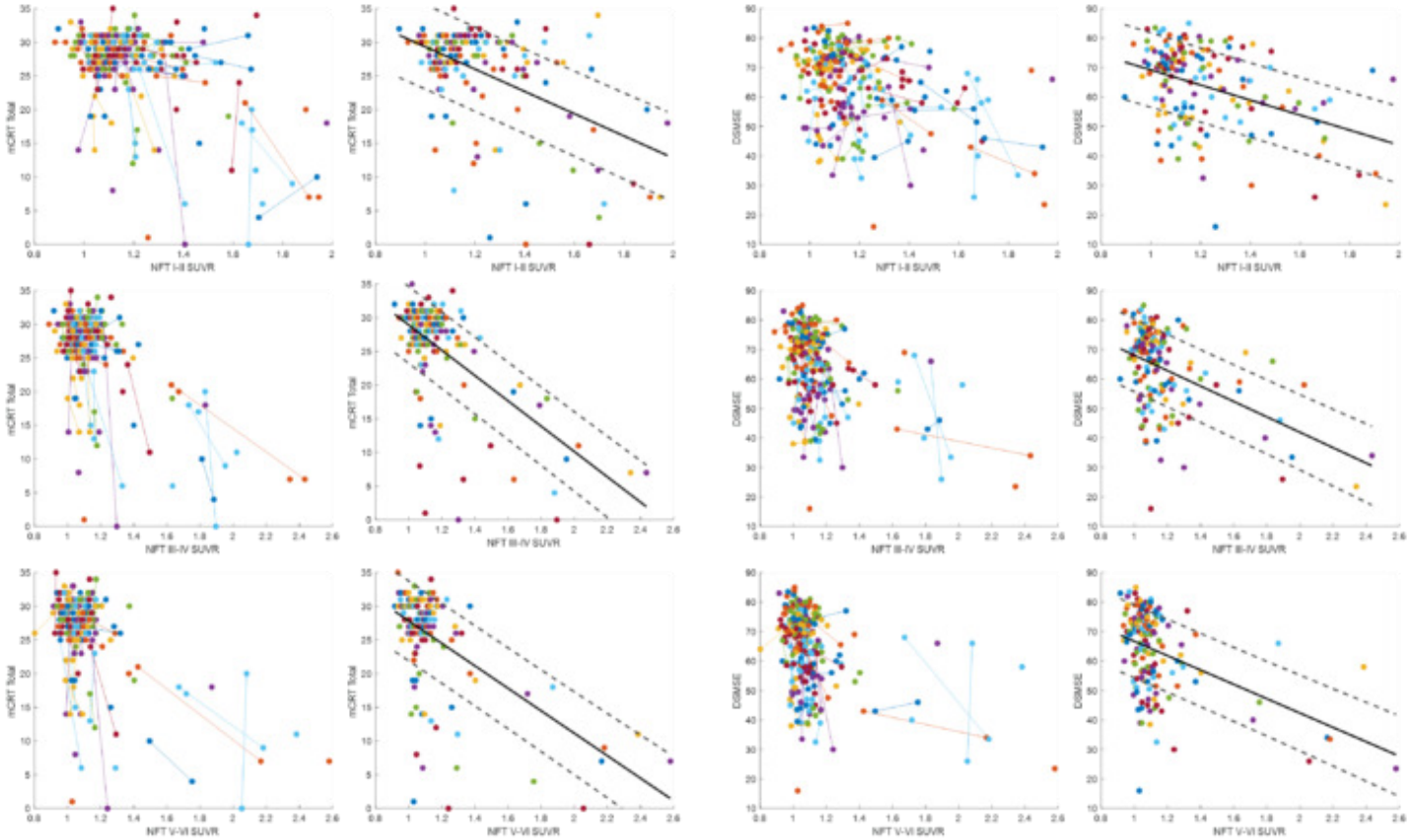

Fig 3. Negative associations between cognition (modified Cued Recall Test and Down Syndrome Mental Status Examination) and NFT stage tau. The left plots for each cognitive measure display results for all timepoints, where connected lines represent longitudinal data for each individual (represented as individual colors). The right plots for each cognitive measure display the regression fits between cognition and NFT stage tau for only the most recent timepoint. Dashed lines represent the standard error.

Keywords: Tau, Amyloid, Cognition, Down syndrome

36 Early Aβ and tau-seeded functional networks derived in young adults reflect patterns of tau deposition and accumulation

Corrina Fonseca[1], Theresa Harrison[1], Trevor Chadwick[1], Jacob Ziontz[1], Suzanne Baker[1], William Jagust[1,2]

[1]*Helen Wills Neuroscience Institute, University of California, Berkeley, Berkeley, CA, United States*
[2]*Lawrence Berkeley National Laboratory, Berkeley, CA, United States*

Background: Functional network interactions may drive Aβ and tau pathology accumulation in aging and AD. Here, we investigate how spatial patterns of functional networks connected to early Aβ and tau sites are associated with tau in cognitively healthy older adults (OA).

Methods: Voxel-wise PiB-PET and FTP-PET OA images were ordered by increasing global pathology burden and iteratively compared to a reference set of young adult (YA) PET images using a sliding window approach. Peak voxels of the earliest significant differences were used to create bilateral ROIs for both Aβ and tau. The ROIs were then used as seeds in a resting-state fMRI seed-to-voxel correlation analysis of 440 young adults from the Human Project. One-sample t-tests were used to construct FDR-corrected Aβ and tau-seeded networks (Figure 1). The networks were thresholded to the top 20% of connections, binarized, and applied to cross-sectional SUVR (n=178) and longitudinal SUVR slope (n=78) FTP-PET images. Repeated measures ANOVA and paired t-tests were used to compare mean FTP SUVR or slope within and outside of each network mask and the overlap between networks.

Results: Baseline FTP SUVR and slope were significantly greater within the Aβ and tau-seeded networks and the overlap compared to outside of the networks (Figure 2). The tau-seeded network had greater baseline FTP SUVR than the Aβ-seeded network. Lastly, there was greater baseline and longitudinal FTP in the overlapping regions compared to both the Aβ and tau-seeded networks.

Conclusions: Functional networks defined by putative Aβ and tau epicenters showed greater baseline and longitudinal tau accumulation compared to outside of these networks. The overlap between networks had the highest baseline tau and fastest rates of tau accumulation. Our results suggest that networks functionally connected to sites of early Aβ and tau interact in spatially overlapping regions, possibly conferring vulnerability to subsequent tau accumulation.

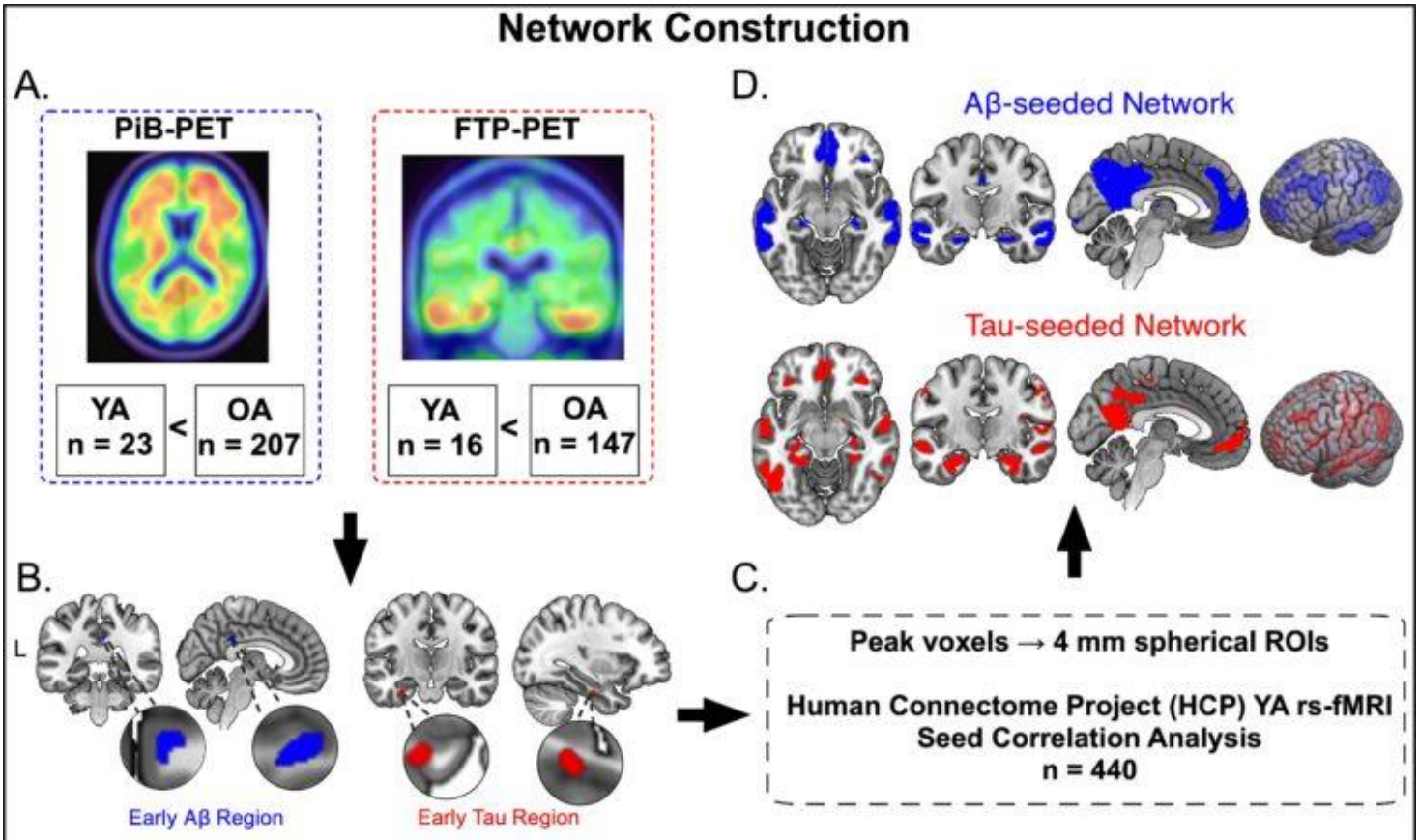

Figure 1. Network Construction. A) A sliding window t-test approach was performed iteratively comparing YA (aged < 35 years) and OA (aged 35+ years) PiB-PET and FTP-PET to identify the earliest regions of Aβ and tau deposition. B) At the eigth t-test comparison for PiB-PET, a significant cluster with a peak voxel (6,-37,33 mm) in the right posterior cingulate emerged. At the ninth t-test comparison for FTP-PET, a significant cluster with a peak voxel (-31,-14,-28 mm) emerged in the left entorhinal cortex. Significance thresholds for all t-tests were voxel uncorrected p <0.001 and cluster fwe-corrected p<0.05. C) Peak voxels from the PIB-PET and FTP-PET voxel-wise analyses were used to create 4 mm spherical ROIs. These ROIs were applied to resting-state fMRI data in 440 HCP YA and seed correlation analysis was performed to construct Aβ & tau-seeded networks. D) Then, the average FDR-corrected group SCA map was thresholded at the top 20% of connections and binarized to create a network mask for each network.

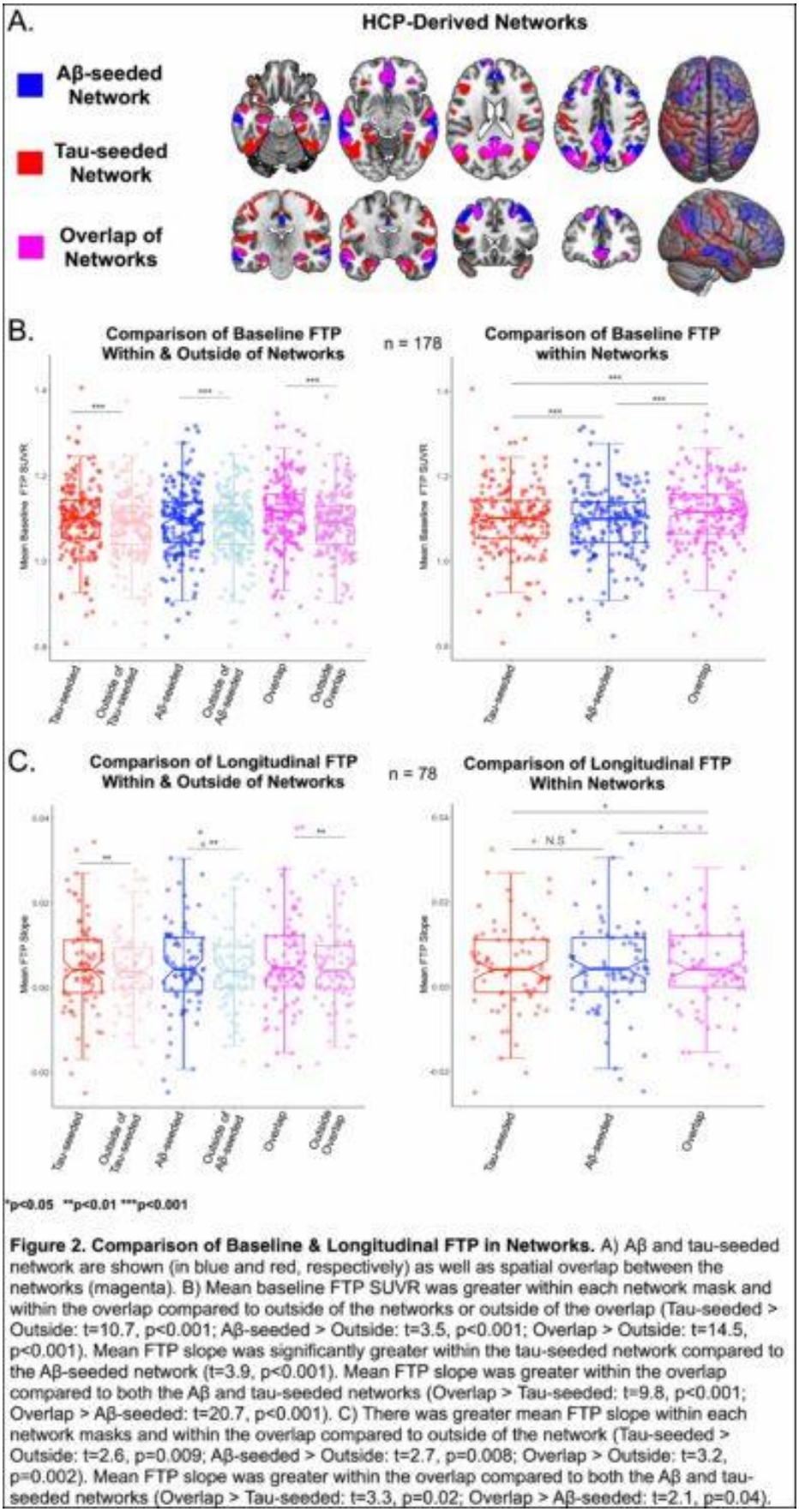

Figure 2. Comparison of Baseline & Longitudinal FTP in Networks. A) Aβ and tau-seeded network are shown (in blue and red, respectively) as well as spatial overlap between the networks (magenta). B) Mean baseline FTP SUVR was greater within each network mask and within the overlap compared to outside of the networks or outside of the overlap (Tau-seeded > Outside: t=10.7, p<0.001; Aβ-seeded > Outside: t=3.5, p<0.001; Overlap > Outside: t=14.5, p<0.001). Mean FTP slope was significantly greater within the tau-seeded network compared to the Aβ-seeded network (t=3.9, p<0.001). Mean FTP slope was greater within the overlap compared to both the Aβ and tau-seeded networks (Overlap > Tau-seeded: t=9.8, p<0.001; Overlap > Aβ-seeded: t=20.7, p<0.001). C) There was greater mean FTP slope within each network masks and within the overlap compared to outside of the network (Tau-seeded > Outside: t=2.6, p=0.009; Aβ-seeded > Outside: t=2.7, p=0.008; Overlap > Outside: t=3.2, p=0.002). Mean FTP slope was greater within the overlap compared to both the Aβ and tau-seeded networks (Overlap > Tau-seeded: t=3.3, p=0.02; Overlap > Aβ-seeded: t=2.1, p=0.04).

Keywords: Functional connectivity, amyloid, tau, networks

37 Gray matter GABA and Glutamate reflect amyloid beta burden in cognitively healthy individuals

Simon Schreiner[6], Thomas Kirchner[4], Jiri Van Bergen[1], Anton Gietl[1], Alfred Buck[3], Christoph Hock[1], Klaas P. Prüssmann[4], Anke Henning[4,5], Paul G. Unschuld[1,2]

[1]*Institute for Regenerative Medicine, University of Zurich, Zurich, CH*
[2]*Geriatric Psychiatry, University of Geneva, Geneva, CH*
[3]*Nuclear Medicine, University Hospital Zurich, Zurich, CH*
[4]*Institute for Biomedical Engineering, ETH Zurich, Zurich, CH*
[5]*Advanced Imaging Research Center, University of Texas Southwestern Medical Center, Dallas, TX, United States*
[6]*Department of Neurology, University Hospital Zurich, Zurich, CH*

Introduction: Gamma-hydroxy-butyric acid (GABA) and Glutamate are brain neurotransmitters with essential importance for cognitive processing. This study tested for relationships between gray-matter GABA, Glutamate, and brain ß-amyloid (Aß) burden before clinical manifestation of Alzheimer's disease (AD).

Methods: Thirty cognitively healthy adults (age 69.9±6 years) received high-resolution atlas-based ^{1}H-magnetic resonance spectroscopic imaging (MRSI) at ultra-high field strength of 7 Tesla (7T), for gray matter-specific assessment of brain GABA and Glutamate. Apolipoprotein-E-epsilon-4-allele (APOE4), Aß-burden and longitudinal memory-performance were assessed as indicators of the individual risk for AD.

Results: Higher gray matter GABA and Glutamate positively related to higher Aß-burden (β=0.60; p<0.03; β=0.64, p<0.01), with positive effect modification by APOE4 (p=0.03). GABA and Glutamate were negatively related to longitudinal change in verbal episodic memory performance (β=-0.48; p=0.02; β=-0.50; p=0.01).

Discussion: GABA and Glutamate neurotransmitter activities in the brain reflect early AD-pathology. They may represent promising biomarkers and possible therapeutic targets for preventive intervention.

Keywords: MRSI, PiB-PET, GABA, Glutamate, APOE4

38 Amyloid PET scan reader agreement in IDEAS: expert readers vs local clinician readers

Charles Windon[1], Barry A. Siegel[2], Ehud Zeltzer[1], Lucy Hanna[3], Maria C. Carrillo[4], Bruce E. Hillner,[5], Leonardo Iaccarino[6], Renaud La Joie[1], Andrew March[7], Jhony Mejia Perez[1], Nidhi Mundada[1], Anupa Arora[6], Christopher Buckley[8], Santiago Bullich[9], Paul Sherwin[8], Constantine Gatsonis[10], Gil Rabinovici[1]

[1]*Memory and Aging Center, UCSF Weill Institute for Neurosciences, University of California San Francisco, San Francisco, CA, United States*
[2]*Mallinckrodt Institute of Radiology, Washington University in St Louis, St. Louis, MI, United States*
[3]*Center for Statistical Sciences, Brown University School of Public Health, Providence, RI, United States*
[4]*Alzheimer's Association, Chicago, IL, United States*
[5]*Department of Medicine, Virginia Commonwealth University, Richmond, VA, United States*
[6]*Avid Radiopharmaceuticals, Philadelphia, PA, United States*
[7]*American College of Radiology, Reston, VA, United States*
[8]*GEHC, Marlborough, MA, United States*
[9]*Life Molecular Imaging GmbH, Berlin, Germany*
[10]*Department of Epidemiology and Biostatistics, Brown University School of Public Health, Providence, RI, United States*

Background: We examined accuracy of local radiologist and nuclear medicine physician interpretations of amyloid PET compared to expert readers across 17000 real world scans from IDEAS.

Method: Randomly selected amyloid PET/CT scans performed using one of three FDA-approved agents [^{18}F-Florbetaben (FBB), ^{18}F-Florbetapir (FBP), ^{18}F-Flutemetamol (FMM)] and previously interpreted by local readers from the Imaging Dementia - Evidence for Amyloid Scanning (IDEAS) study were assigned to vendor-selected panels of 3 expert readers for interpretation; 500 scans per agent and 1 panel per agent. Scans were stratified to match frequencies observed in the overall study by age, impairment level, interpretation result, and PET facility type.

Visual interpretations (positive or negative) were performed according to agent-specific validated interpretation criteria. Readers were blinded to clinical and demographic data. Cohen's kappa statistic with two-sided 95% confidence interval estimates examined agreement between local readers, expert panel, and individual expert readers.

Result: Median age for participants of 4489 interpreted scans was 75 (range 65-96); 51.4% were female, 60.5% MCI. Local readers interpreted 60.9% of scans positive and 39.1% negative (Table 1).

Across radiotracers, agreement between majority expert read and local readers was excellent (k coefficient 0.76; 95% CI 0.73 – 0.80, p<.0001) with 86.6% (791/913) agreement for positive scans and 90.9% (532/585) agreement for negative scans (Figure 1). Agreement by individual radiopharmaceuticals was good to excellent: k coefficient 0.78 (95% CI 0.72 – 0.83, p<.001) for FBB, k coefficient 0.72 (95% CI 0.66 – 0.78, p<.001) for FBP, and k coefficient 0.78 (95% CI 0.73 – 0.84) for FMM (Figure 1). Agreement varied between local readers and individual (good to excellent) (Figure 2).

Conclusion: We found good to excellent agreement between local readers and expert readers for combined scans and individual agents. Visual interpretation of Aβ PET can be performed in a clinical setting with high reliability.

Table 1. Demographic and Baseline Characteristics

Characteristic	*LMI, FBB (n=499)*	*Avid, FBP (n=500)*	*GEHC, FMM (n=498)*	*All Cases (n=1497)*
Age				
Mean (s.d.)	75.8 (6.4)	75.8 (6.3)	75.9 (6.4)	75.8 (6.4)
Median	75	75.5	75	75
Range (min-max)	65 - 96	65 - 93	65 - 94	65 - 96
Interquartile Range (25%-75%)	71 - 80	71 - 80	71 - 80	71 - 80
Gender, n(%)				
Male	238 (47.7)	247 (49.4)	243 (48.8)	728 (48.6)
Female	261 (52.3)	253 (50.6)	255 (51.2)	769 (51.4)
Race, n(%)				
American Indian / Alaskan native	1 (0.2)	1 (0.2)	1 (0.2)	3 (0.2)
Asian	10 (2.0)	12 (2.4)	9 (1.8)	31 (2.1)
Black or African American	13 (2.6)	12 (2.4)	29 (5.8)	54 (3.6)
White or caucasian	444 (89.0)	423 (84.6)	413 (83.0)	1280 (85.5)
Multiple races	1 (0.2)	2 (0.4)	1 (0.2)	4 (0.3)
Unknown or not reported	30 (6.0)	50 (10.0)	45 (9.0)	125 (8.4)
Ethnicity, n(%)				
Not Hispanic or Latino	437 (87.6)	432 (86.4)	439 (88.2)	1308 (87.4)
Hispanic or Latino	24 (4.8)	20 (4.0)	25 (5.0)	69 (4.6)
Not reported	11 (2.2)	18 (3.6)	12 (2.4)	41 (2.7)
Unknown	27 (5.4)	30 (6.0)	22 (4.4)	79 (5.3)
Level of Cognitive Impairment, n(%)				
MCI	302 (60.5)	302 (60.4)	301 (60.4)	905 (60.5)
Dementia	197 (39.5)	198 (39.6)	197 (39.6)	592 (39.5)
Local Scan Assessment, n(%)				
Positive	304 (60.9)	305 (61.0)	303 (60.8)	912 (60.9)
Negative	195 (39.1)	195 (39.0)	195 (39.2)	585 (39.1)
Type of Facility, n(%)				
Not based at a hospital	436 (87.4)	399 (79.8)	432 (86.7)	1267 (84.6)
Hospital based scanner	63 (12.6)	101 (20.2)	66 (13.3)	230 (15.4)

FBB - ^{18}F-Florbetaben
FBP -^{18}F-Florbetapir
FMM -^{18}F-Flutemetamol
GEHC – GE Healthcare
LMI – Life Molecular Imaging
MCI – mild cognitive impairment
s.d. – standard deviation

Figure 1. Interrater Agreement Between Majority Assessment Expert Panel and Local Readers

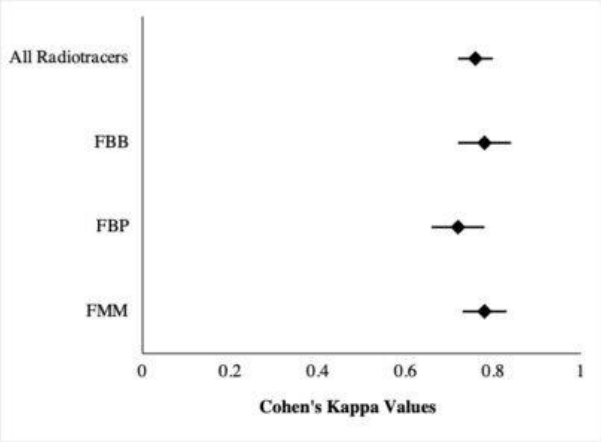

Forest plot displaying the Cohen's kappa values and respective 95% confidence intervals for all combined radiotracers and by individual radiotracers. Majority Assessment Defined as two out of three expert readers.

FBB - ^{18}F-Florbetaben
FBP -^{18}F-Florbetapir
FMM -^{18}F-Flutemetamol

Figure 2. Interrater Agreement Between Individual Expert Readers and Local Readers

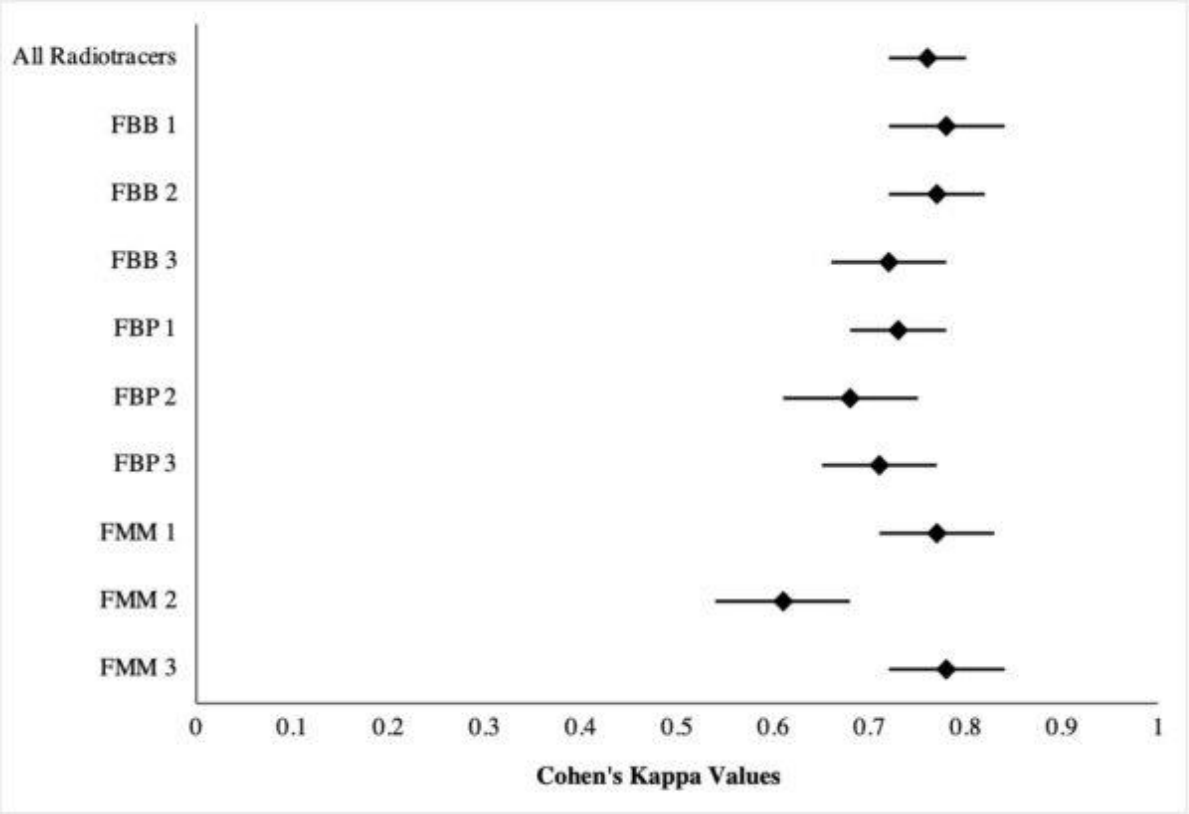

Forest plot displaying the Cohen's kappa values and respective 95% confidence intervals for all combined radiotracers and by individual expert readers for each radiotracer.

FBB - ^{18}F-Florbetaben
FBP -^{18}F-Florbetapir
FMM -^{18}F-Flutemetamol

Keywords: IDEAS, expert, local, interpretation

39 Validation of a novel visual read interpretation of flortaucipir PET for identification of participants with high tau burden: results from I7E-AV-A26 reader study

Ilke Tunali[1], Leonardo Iaccarino[1], Jian Wj Wang[1], Anupa K. Arora[1], Ming Lu[1], Sergey Shcherbinin[1], Michael Pontecorvo[1]

[1]*Eli Lilly and Company, Indianapolis, IN, United States*

Background: Patient stratification based on tau burden using flortaucipir F18 (FTP)-PET mainly relies on quantitation-based approaches. We previously developed a novel FTP-PET visual read method (**Fig. 1**, Iaccarino et al., ADPD 2023) to identify patients with Alzheimer's disease (AD) having high tau burden. Here we present results from an independent reader study validating the proposed method against the quantitation-based standard-of-truth.

Methods: Positive FTP-PET (**Fig. 1A**) baseline scans (N=140; 70 high tau and 70 non-high tau) from a subset of early symptomatic AD participants randomized into TRAILBLAZER-ALZ2 study (NCT04437511) were utilized. Five qualified imaging physicians were trained for the FTP-PET high tau visual read method and independently conducted reads to identify high tau scans, blinded to all quantitative and clinical information. Positive and negative percent agreement (PPA and NPA, respectively) between visual high tau reads and quantitation-based high tau (AD-signature SUVR>1.46) were assessed; success criteria were met if lower bounds of a two-sided 95% CI for PPA and NPA were ≥50% for at least three readers. Inter- and intra-reader reliability were assessed using Fleiss' Kappa and Cohen's Kappa (utilizing n=20 test-retest scans) scores.

Results: Patient demographics and clinical characteristics are presented in **Table 1**. The mean (SD) SUVR was 1.706 (0.201) and 1.178 (0.123) for high tau and non-high tau quantitation, respectively. The median PPA and NPA were 84.3% and 88.6%, respectively, with lower bounds of two-sided 95% CIs ≥50% for all readers (**Table 2**). Fleiss' Kappa point estimate was 0.8882 (95% CI: 0.8356–0.9409) and Cohen's Kappa point estimate was 0.9599 (95% CI: 0.9049–1.000), indicating almost perfect inter- and intra-reader agreement.

Conclusions: The FTP-PET high tau visual read method accurately identifies AD patients with quantitation-derived high tau burden. This method does not require advanced image processing steps and can be implemented with different standard imaging software.

A

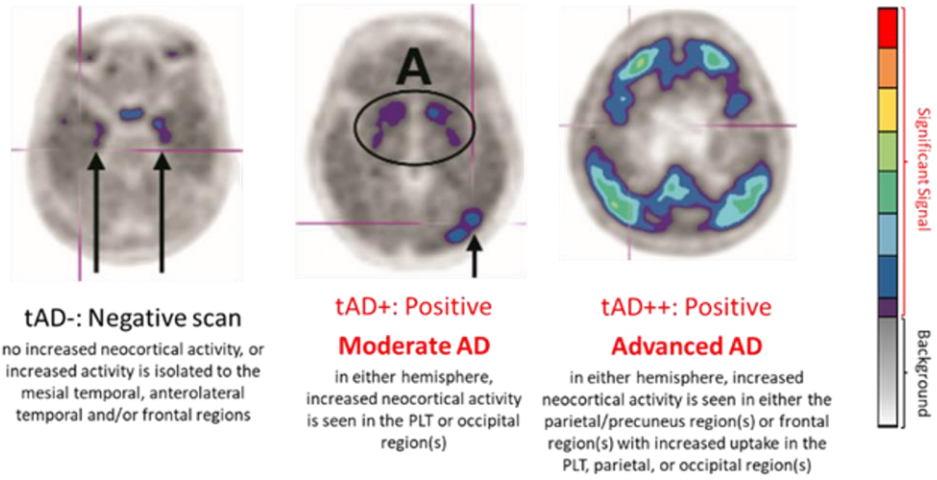

B

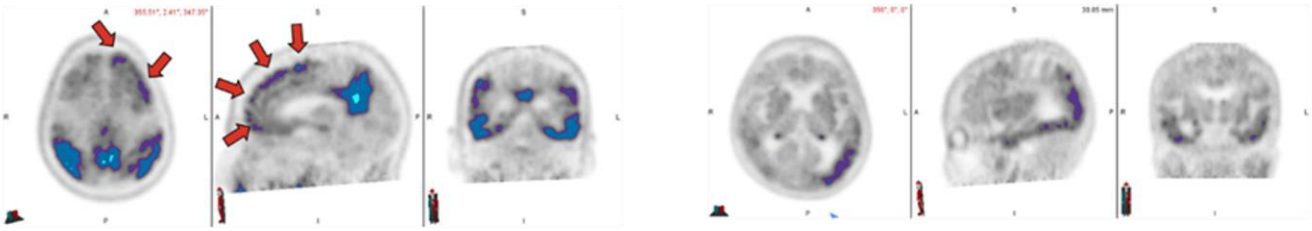

FTP scan consistent with high tau

After increasing the visual threshold to 2.80-times the average cerebellar count, neocortical activity was observed in multiple left frontal clusters.

FTP scan not consistent with high tau

After increasing the visual threshold to 2.80-times the average cerebellar count, neocortical activity is limited to temporal, parietal/occipital regions. No elevation in either of the frontal lobes is observed.

Figure 1. Interpretation of FTP-PET using novel high tau visual read method. **A)** Step 1: Interpret whether the FTP scan is positive using previously defined read methods (Fleisher et al., JAMA Neurol, 2020). Colorscale should be set such that a significant signal level is >1.65-times the average cerebellar count. Average cerebellar count is captured from a manually drawn 2D-ROI around cerebellum in the transverse plane. **B)** Step 2 (to be applied only if the Step 1 result is positive): Identify whether FTP scan is consistent with a high tau pattern. Colorscale should be set such that a significant signal level is >2.80-times the average cerebellar count. If a significant signal is observed anywhere in the neocortical grey matter of either frontal lobe hemisphere, irrespective of intensity or extent, the scan is considered as high tau. Examples of FTP scans consistent with high tau (left) and not consistent with high tau (right). All scans that were negative in Step 1 should be considered as not high tau. The FTP images used on this figure are for illustrative purposes only and were not included in the study cohort. Abbreviations: FTP, flortaucipir F 18; ROI, region of interest.

Table 1. Patient demographics and clinical characteristics (N=140)

	Non-High Tau Quantitation (SUVR ≤1.46) N=70	High Tau Quantitation (SUVR >1.46) N=70	Total N=140
Age (years)			
Mean (SD)	74.4 (5.7)	69.7 (6.6)	72.1 (6.6)
Median (min-max)	75.0 (70.0–78.8)	69.0 (65.0–74.8)	71.5 (67.0–78.0)
Sex			
Male	29 (41.4)	22 (31.4)	51 (36.4)
Race, n (%)			
White	61 (87.1)	68 (97.1)	129 (92.1)
Black or African American	1 (1.4)	1 (1.4)	2 (1.4)
Asian	8 (11.4)	1 (1.4)	9 (6.4)
Ethnicity, n (%)			
Not Hispanic or Latino	66 (95.7)	67 (97.1)	133 (96.4)
ApoE4 status, n (%)			
Carrier	49 (70.0)	47 (67.1)	96 (68.6)
Total MMSE score[1]			
Mean (SD)	23.5 (3.4)	20.5 (3.8)	22.0 (3.9)
Median (min-max)	23.0 (21.0–26.0)	20.0 (18.0–22.0)	22.0 (19.0–25.0)
FTP-PET visual read, n (%)			
τAD++[2]	66 (94.3)	69 (98.6)	135 (96.4)
AD-signature weighted neocortical SUVR			
Mean (SD)	1.178 (0.123)	1.706 (0.201)	1.442 (0.312)
Median (min-max)	1.132 (1.085–1.279)	1.644 (1.563–1.819)	1.455 (1.132–1.642)
Amyloid burden			
Mean Centiloid (SD)	97.3 (36.4)	110.0 (31.3)	103.7 (34.4)
Median Centiloid (min-max)	90.6 (73.4–113.7)	107.0 (91.0–132.5)	98.4 (80.1–125.3)

Abbreviations: AD, Alzheimer's disease; ApoE4, apolipoprotein E4; MMSE, mini mental state examination; SD, standard deviation; SUVR, standardized uptake value ratio.

[1]MMSE was missing for 2 participants (1 high tau quantitation and 1 non-high tau quantitation).

[2]τAD++ refers to advanced AD (**Fig. 1A**).

Table 2. High tau visual read agreement with standard-of-truth

	PPA (95% CI)	NPA (95% CI)	PPA and NPA Lower bound CI ≥50%
Reader 1	82.9% (72.4–89.9%)	90.0% (80.8–95.1%)	Yes
Reader 2	84.3% (74.0–91.0%)	88.6% (79.0–94.1%)	Yes
Reader 3	90.0% (80.8–95.1%)	87.1% (77.3–93.1%)	Yes
Reader 4	85.7% (75.7–92.1%)	87.1% (77.3–93.1%)	Yes
Reader 5	74.3% (63.0–83.1%)	91.4% (82.5–96.0%)	Yes

Abbreviations: CI, confidence interval; NPA, negative percent agreement; PPA, positive percent agreement.
All readers conducted reads on the same set of baseline tau-PET scans. Standard-of-truth was captured by the quantitation of tau-PET scans.

Keywords: Alzheimer's disease, flortaucipir-PET, high tau, simplified visual read

40 Longitudinal multicenter head-to-head harmonization of tau-PET tracers: an overview of the HEAD study

Firoza Lussier[1], Livia Silva do Amaral[1], Guilherme Povala[1], Guilherme Negrini[1], Belen Pascual[2], Brian Gordon[3], Val Lowe[4], Hwamee Oh[5], David Soleimani-Meigooni[6], William Klunk[1], Dana Tudorascu[1], Pedro Rosa-Neto[7], Suzanne Baker[8], Tharick Pascoal[1]

[1]*Department of Psychiatry, University of Pittsburgh, Pittsburgh, PA, United States*
[2]*Department of Neurology, Houston Methodist Research Institute, Houston, TX, United States*
[3]*Department of Radiology, Washington University in St. Louis, St. Louis, MO, United States*
[4]*Department of Radiology, Mayo Clinic, Rochester, MN, United States*
[5]*Department of Psychiatry, Brown University, Providence, RI, United States*
[6]*Memory and Aging Center, University of California San Francisco, San Francisco, CA, United States*
[7]*Translational Neuroimaging Laboratory, McGill University Research Centre for Studies in Aging, Montreal, QC, Canada*
[8]*Lawrence Berkeley National Laboratory, Berkeley, CA, United States*

Standardized tau pathology quantification in vivo is challenged by differences in binding characteristics between tau-PET tracers. The HEAD study aims to generate a leading, longitudinal head-to-head dataset of MK-6240, Flortaucipir, PI-2620, and RO948 tau-PET to harmonize these tracers' outcomes and develop tools for the generalization of findings across large studies and trials.

HEAD comprises ten acquisition sites across the US, Canada, and Europe, in which 620 cognitively unimpaired and impaired subjects will undergo tau-PET with at least 2 tracers, amyloid PET, MRI, blood collection, and standardized neuropsychological testing at baseline and 18-month follow-up. PET and MRI imaging parameters are based on ADNI4 protocols and neuropsychological testing employs the NACC Uniform Data Set. The National Centralized Repository for AD serves as the blood biorepository and the Laboratory of Neuroimaging provides a centralized database for imaging and neuropsychological data. PET data is reconstructed to maximize cross-scanner harmonization and is processed uniformly similarly to ADNI4 PET.

From January to October 2023, 282 participants were enrolled at 6 active sites, 25% of whom reflect underrepresented (racial, ethnic, or geographical) populations (**Figure 1**). Currently, 37% of subjects are amyloid-positive by visual rating. Head-to-head MK-6240 and Flortaucipir tau-PET is available for 190 participants with a mean acquisition interval of 27.2 days; PI-2620 and RO948 tau-PET are further acquired in a subset currently including 29 participants. **Figure 2** shows an example of these 4 tau-PET tracers in one subject. Preliminary data indicates significant associations of tau-PET Braak SUVRs with age and cognition but not with sex; this analysis was also run adjusting for site (**Figure 3**).

The HEAD study represents a continued effort in the optimization of AD imaging biomarkers. Further findings generated from this dataset will provide novel and crucial guidance on the use of tau-PET tracers in research, clinical trials, and prospectively in clinical practice.

Figure 1: HEAD Dataset Characteristics

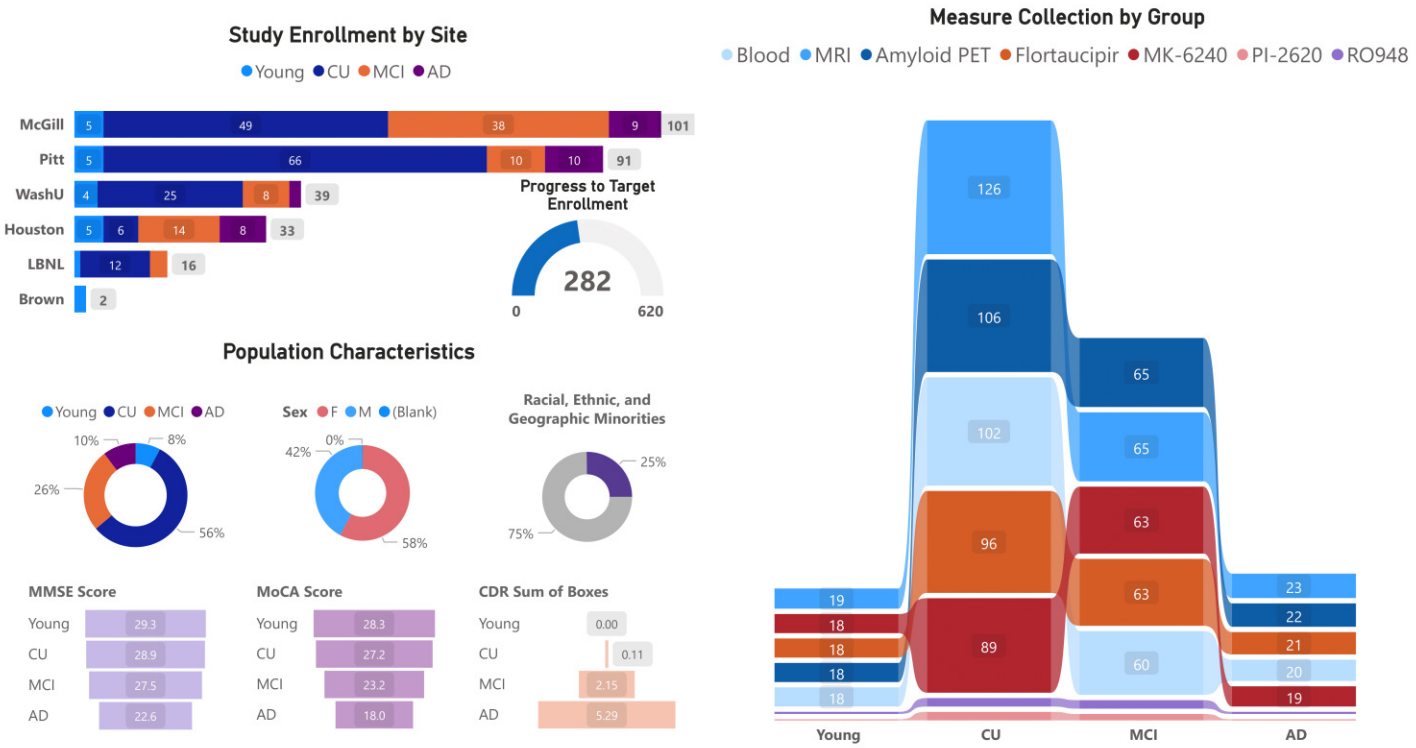

Figure 2: Head-to-head MK-6240, Flortaucipir, PI-2620, and RO948 tau-PET

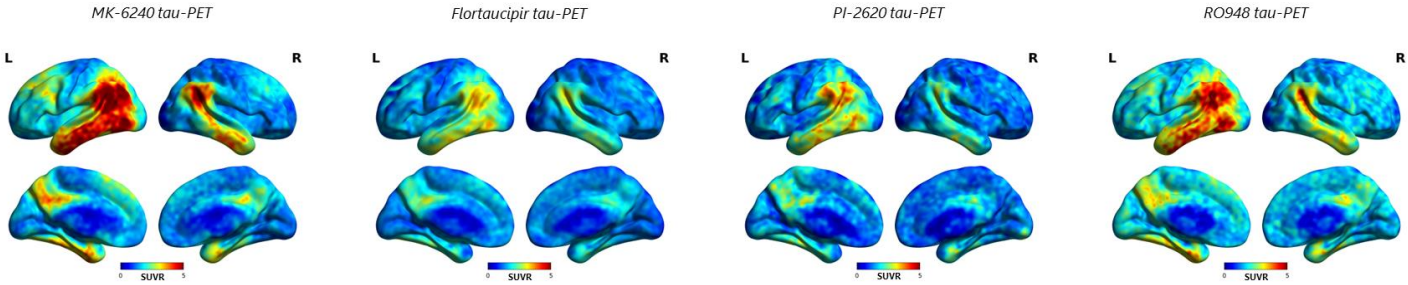

Subject is a 74-year-old White female; Aβ-positive on NAV4694 PET; Alzheimer's disease (global CDR = 2, MoCA = 13). All 4 tau-PET were acquired within 49 days.

Figure 3: Associations of Flortaucipir and MK–6240 Braak SUVR with MoCA, age, and sex

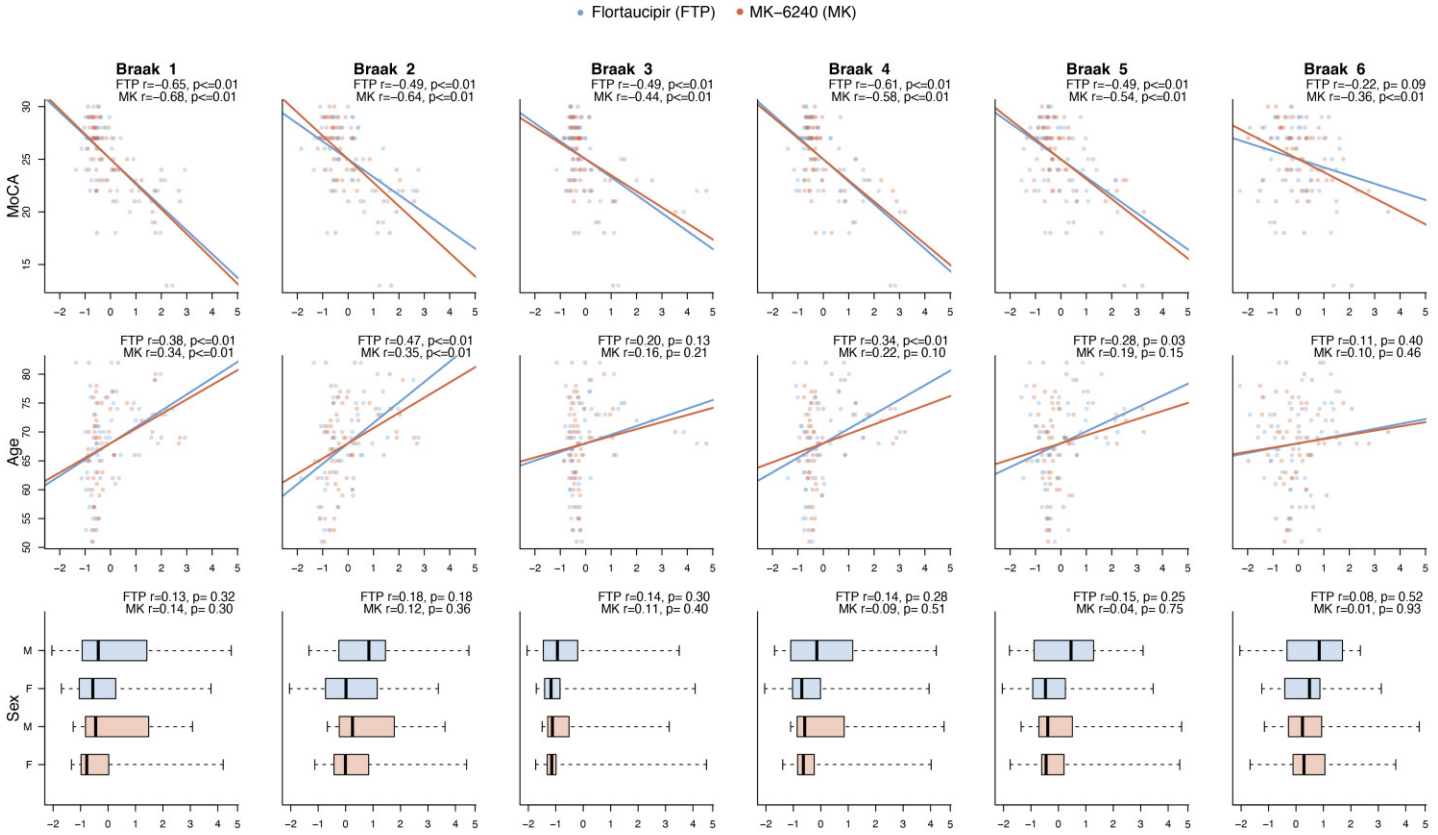

Note: Models were tested for adjustment for sites; significance remained unchanged.

Keywords: tau, harmonization, scale, Flortaucipir, MK6240

41 Clinical phenotype and plasma biomarker associations of non-Alzheimer's hippocampal atrophy

Breton Asken[1,2], Wei-en Wang[1,2], Karen McFarland[1,2], Warren Barker[2,6], Malek Adjouadi[2,3], Idaly Velez Uribe[2,4], Monica Rosselli[2,4], Elizabeth Crocco[2,5], Melissa Armstrong[1,2], Rosie Curiel Cid[2,5], David Vaillancourt[1,2], David Loewenstein[2,5], Ranjan Duara[2,6], Glenn Smith[1,2]

[1]*University of Florida, Gainesville, FL, United States*
[2]*1Florida Alzheimer's Disease Research Center, Gainesville, FL, United States*
[3]*Florida International University, Miami, FL, United States*
[4]*Florida Atlantic University, Boca Raton, FL, United States*
[5]*University of Miami, Miami, FL, United States*
[6]*Mount Sinai Medical Center, Miami, FL, United States*

Background: Alzheimer's disease (AD) is a common reason for hippocampal atrophy (HA). Age-related neuropathological changes (e.g., primary age-related tauopathy, aging-related tau astrogliopathy, limbic TDP43) may also contribute to HA in the absence of AD. We examined clinical diagnosis, APOE genotype, and plasma biomarker associations with non-AD HA.

Methods: 1Florida ADRC participants who completed MRI, blood draw, and Aβ-PET were classified on two biomarkers: 1) HA+ on volumetric MRI (0.5SD below normative reference) or HA-, 2) AD+ (positive Aβ-PET visual read and strongly positive Centiloids >50) or AD- (negative Aβ-PET visual read and strongly negative Centiloids <12). Our final study sample was 139 participants (age 70.7±8.5yrs, 58% female, education 15.8±3.4yrs, 46% Hispanic/Latino, 95% white; Table). Study groups were HA+/AD- (N=35), HA-/AD- (N=61), and HA+/AD+ (N=43). We used chi square and regression-based analyses to compare groups on clinical diagnosis, *APOE* e4 frequency, and plasma biomarkers (ALZPath pTau217, GFAP, NfL).

Results: The most common clinical diagnosis for HA+/AD- was amnestic MCI (50%). HA+/AD- were less likely than HA+/AD+ to have amnestic dementia (14% vs. 52%, p=.004) or be *APOE* e4 carriers (16% vs. 62%, p<.001), and were less likely than HA-/AD- to be clinically normal (8% vs. 33%, p=.02). HA+/AD- had significantly lower pTau217 and GFAP than HA+/AD+ (p's<.001, large effect), but significantly higher pTau217 than HA-/AD- (p=.006, large effect; Fig. 1A). Plasma pTau217 showed fair discrimination of HA+/AD- from HA-/AD- (AUC=0.73; Fig. 1B) and does not correlate with Centiloids in HA+/AD- (r=-.03, p=.85; Fig. 1C).

Conclusions Plasma pTau217 is increases in older adults with hippocampal atrophy despite absence of Aβ pathology on PET. Potential interpretations include a) pTau217 sensitivity to AD pathology preceding Aβ-PET detection or b) given existing HA, modestly elevated pTau217 might signal AD-like tau tangles without notable Aβ pathology (i.e., PART). Longitudinal work is needed to determine neuropathological correlates.

	Overall	Aβ-PET(-) with Hippocampal Atrophy *HA+ / AD-*	Aβ-PET(-) without Hippocampal Atrophy *HA- / AD-*	Aβ-PET(+) with Hippocampal Atrophy *HA+ / AD+*
N	139	35	61	43
Age, mean (SD)*	70.7 (8.5)	75.1 (7.6)	67.5 (8.1)	71.6 (8.2)
Sex, %female	58	47	56	69
Education, yrs	15.8 (3.4)	16.1 (4.1)	15.7 (3.0)	15.6 (3.2)
Race, %				
White	95	91	97	98
Black	4	9	2	2
Asian	1	0	2	0
Ethnicity, %Hispanic/Latino	46	29	54	50
HA Visual Rating (0-3), mean(SD)	1.5 (1.5)	2.1 (1.7)	0.5 (0.7)	2.5 (2.6)
Clinical Phenotype, %				
Clinically Normal	16	8	33	0
Amnestic MCI	39	50	33	38
Amnestic Dementia	22	14	5	52
Nonamnestic MCI/Dementia	10	17	9	7
Impaired – not MCI	13	11	21	2
***APOE* e4, %carriers**	33	14	24	62
Aβ-PET				
% positive	31	0.0	0.0	100.0
Centiloids, mdn (IQR)	2 (-5 – 65)	-4 (-12 – 3)	-3 (-7 – 4)	83 (66 – 95)
Plasma Biomarkers, mdn (IQR)				
pTau217	0.42 (0.27-0.92)	0.42 (0.32-0.55)	0.28 (0.23-0.32)	1.12 (0.85-1.57)
GFAP	163 (106-280)	155 (117-246)	108 (79-170)	302 (201-382)
NfL	12.9 (9.1-18.0)	15.0 (9.6-20.8)	10.3 (7.5-13.6)	15.7 (12.9-22.6)

*covariate in all analyses along with body mass index

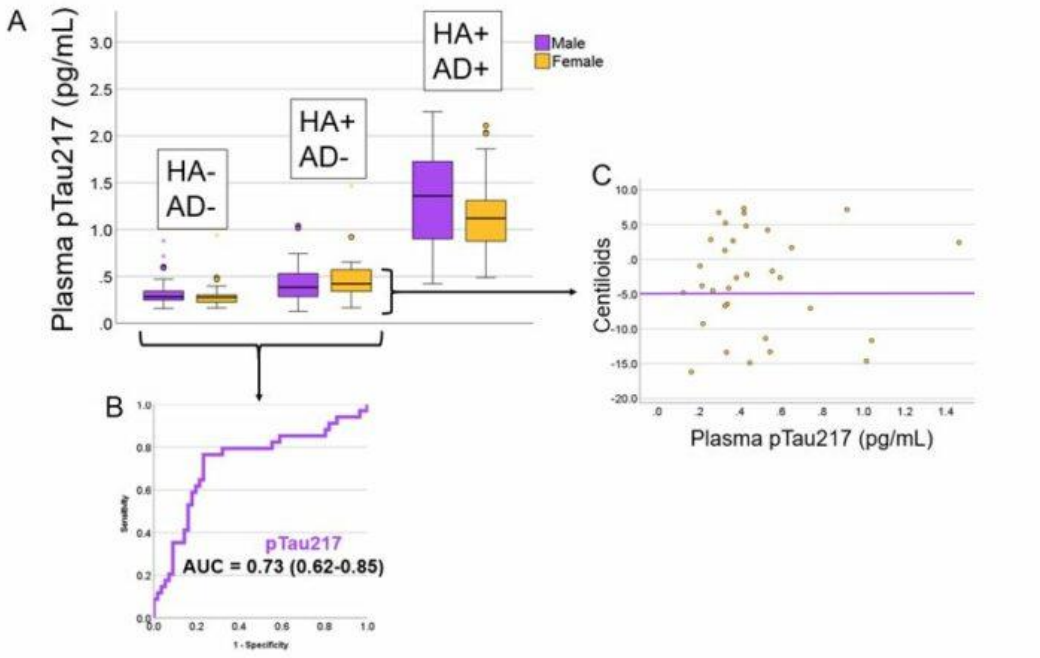

Figure: (A) Plasma pTau217 higher in participants with hippocampal atrophy (HA+) but strongly negative amyloid PET (AD-) compared to those without hippocampal atrophy. Concentrations were well below those observed in participants that were both HA+ and strongly positive on amyloid PET quantification (AD+). (B) Plasma pTau217 discriminated HA+ from HA- participants despite strongly negative amyloid PET in both groups. (C) Among the HA+ / AD- participants, there was no correlation between plasma pTau217 and amyloid burden (Centiloids).

Keywords: pTau217, amyloid, PART, hippocampal atrophy, plasma

42 Synaptic loss in relapsing and progressive multiple sclerosis: an in vivo exploratory study using SV2A-PET

David Soleimani-Meigooni[1], Joseph Giorgio[2,3], Ahmed Abdelhak[4], Christian Cordano[4], Xi Chen[2], Tyler Toueg[2], Robby Weimer[5], Bastian Zinnhardt[6], Suzanne Baker[7], Mustafa Janabi[7], Ari Green[4], William Jagust[2,7], Gil Rabinovici[1]

[1]*Memory and Aging Center, Weill Institute of Neurosciences, University of California, San Francisco, San Francisco, CA, United States*
[2]*University of California, Berkeley, Berkeley, CA, United States*
[3]*University of Newcastle, Callaghan, NSW, Australia*
[4]*Neuroimmunology and Glial Biology, Weill Institute of Neurosciences, University of California, San Francisco, San Francisco, CA, United States*
[5]*Genentech, Inc., South San Francisco, CA, United States*
[6]*Roche, Ltd., Basel, CH*
[7]*Lawrence Berkeley National Laboratory, Berkeley, CA, United States*

Background: Multiple sclerosis (MS) is a neurodegenerative disease associated with early and widespread synaptic loss in cortical gray matter, which dynamically changes and may be prominent in progressive disease phases. [^{18}F]SynVesT-1, which targets synaptic vesicle glycoprotein 2A (SV2A), could be used as an *in vivo* biomarker of synaptic changes in MS.

Methods: Eight relapsing MS (RMS) or progressive MS (PMS) participants, with brain MRI, neurological exam, and Expanded Disability Status Scale (EDSS) assessment, underwent [^{18}F]SynVesT-1 PET. We collected 90-minute dynamic PET data after injection of 5 mCi of [^{18}F]SynVesT-1. Participant whole-brain Distribution Volume Ratio (DVR) images were generated using a cerebellar grey matter reference region, with/without two-tissue compartment partial volume correction (PVC). Quantification was performed at *a priori* selected regions of interest. [^{18}F]SynVesT-1 DVR images from young healthy controls (YHC) and cognitively unimpaired older adults with negative [^{11}C]PiB amyloid-PET (OHC-) were available for comparison.

Results: MS participants were 53.3±10.3 years and 50% female. Five had RMS (mean EDSS 3.5±2). Three had PMS (mean EDSS 4.5±2). Visually, RMS had lower cortical tracer uptake than YHC and similar binding to OHC-. PMS had the lowest cortical tracer retention (**Figure 1**). Quantitatively, at the hippocampus, there was a significant effect of group (ANOVA F(3,19)=4.76, p=0.012), and *post hoc* Bonferroni test revealed that PMS had significantly lower tracer uptake (median 0.77, interquartile range [IQR] 0.63-0.91) than OHC- (median 0.96, IQR 0.94-1.08; p=0.010). There was a trend towards group differences at the parietal lobes (F(3,19)=2.63, p=0.080) and non-significant differences at other regions that suggested lower synaptic density in PMS compared to RMS and controls (**Figure 2A**). Non-PVC comparisons are also shown (**Figure 2B**).

Conclusions: We demonstrate the first *in vivo* application of SV2A-PET to estimate synaptic density changes in MS. MS patients could have widespread reduction in synaptic density, greatest in PMS.

Table 1: Participant characteristics

	Young Healthy Controls	Amyloid-neg. Older Healthy Controls	Multiple Sclerosis
N	7	8	8 (5 relapsing, 3 progressive)
Age, mean (SD)	26.1 (3.8)	78.6 (4.0)	53.3 (10.3)
Sex (% Female)	2 (29%)	4 (50%)	4 (50%)
Education, mean (SD)	18.7 (2.4)	17.9 (1.6)	NA
Race (% White)	3 (43%)	12 (88%)	8 (100%)

NA = Data not available, SD = Standard deviation.

Figure 1: Composite of [^{18}F]SynVesT-1 PET at level of medial temporal lobes and frontal/parietal lobes for young healthy controls, amyloid-negative older healthy controls, and MS patients.

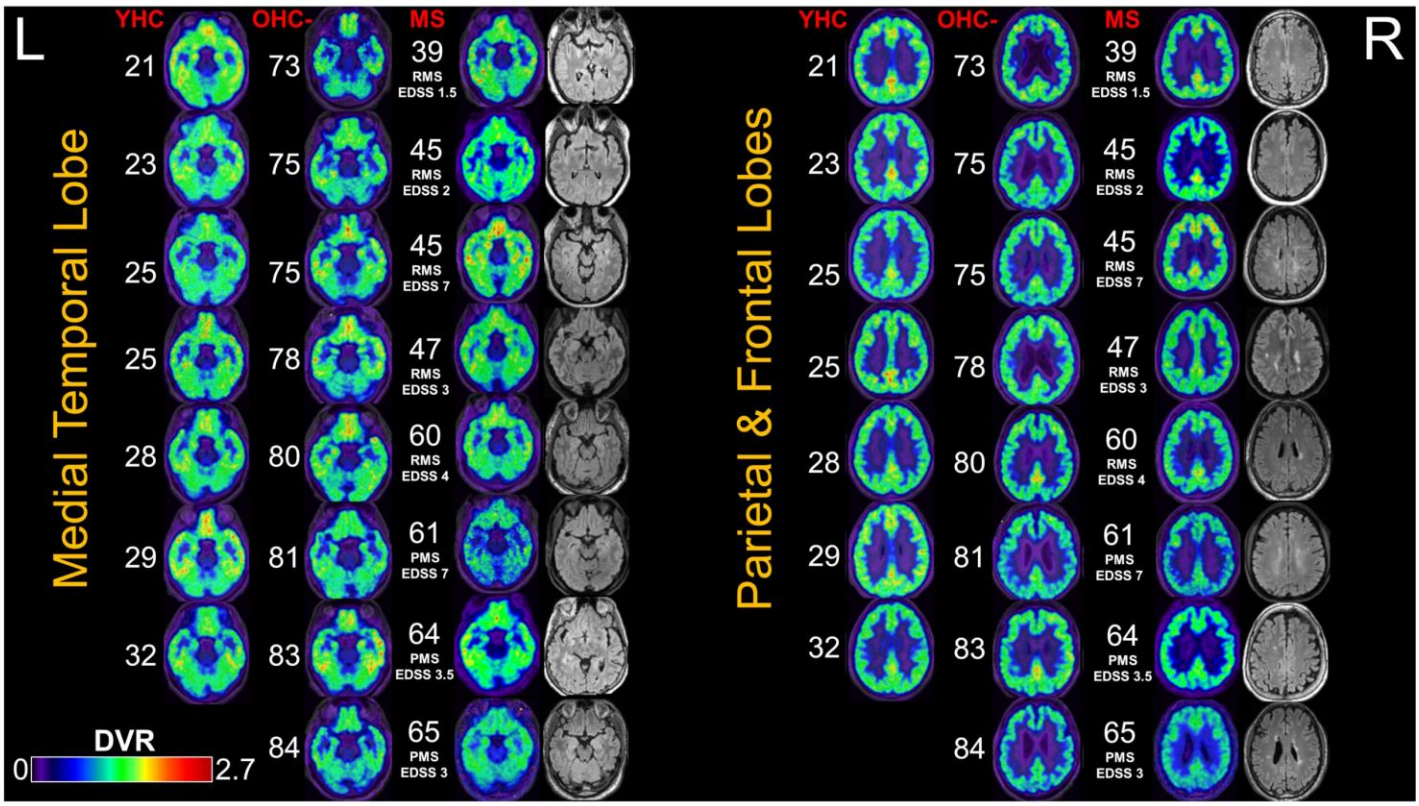

The number to the left of the image reflects the age of the participant. MS patients are also labeled with relapsing or progressive type and EDSS. FLAIR MRI images from the same axial level are shown for the MS patients. OHC- = Amyloid-negative older healthy control. PMS = Progressive multiple sclerosis. RMS = Relapsing multiple sclerosis. YHC = Young healthy control.

Figure 2: Quantification of tracer uptake at hippocampus, posterior cingulate, frontal, parietal, and temporal regions of interest in young healthy controls, amyloid-negative older healthy controls, and MS patients.

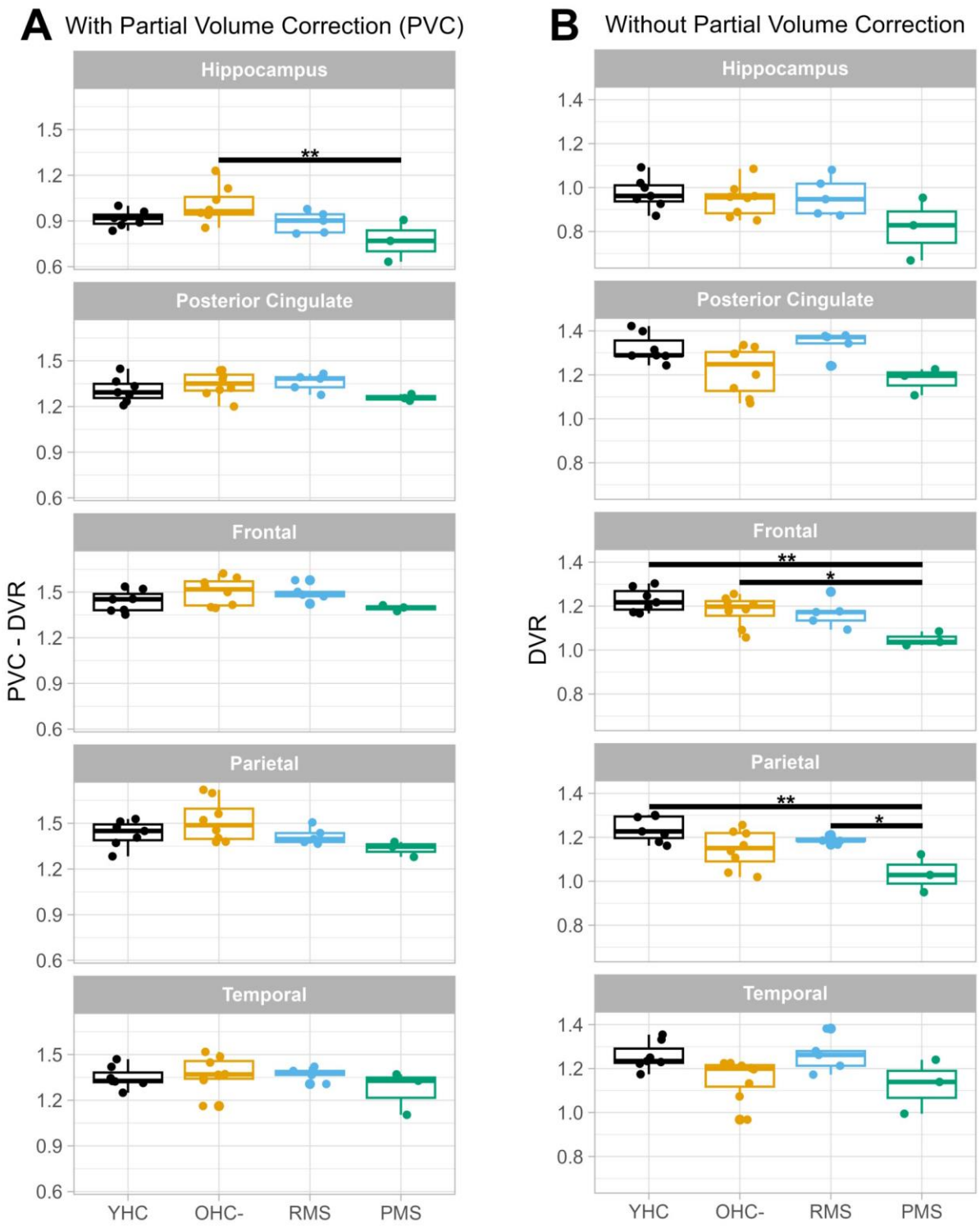

**p≤0.01, *p<0.05; OHC- = Amyloid-negative older healthy control. PMS = Progressive multiple sclerosis. RMS = Relapsing multiple sclerosis. YHC = Young healthy control.

Keywords: SV2A, [18F]SynVesT-1, synaptic density, synapse, multiple sclerosis

43 [18F]-PI-2620 tau PET signal across the aging and Alzheimer's disease clinical spectrum

Christina Young[1], Hillary Vossler[1], America Romero[1], Viktorija Smith[1], Jennifer Park[1], Alexandra Trelle[1], Joseph Winer[1], Edward Wilson[1], Michael Zeineh[2], Sharon Sha[1], Mehdi Khalighi[2], Aimara Morales[2], David Anders[2], Gregory Zaharchuk[2], Victor Henderson[1], Katrin Andreasson[1], Anthony Wagner[3], Kathleen Poston[1,4], Guido Davidzon[2], Elizabeth Mormino[1,4]

[1]*Department of Neurology and Neurological Sciences, Stanford University School of Medicine, Palo Alto, CA, United States*
[2]*Department of Radiology, Stanford University School of Medicine, Palo Alto, CA, United States*
[3]*Department of Psychology, Stanford University, Stanford, CA, United States*
[4]*Wu Tsai Neuroscience Institute, Stanford University, Palo Alto, CA, United States*

Background: 18F-PI-2620 is a novel second generation tau tracer that has shown promise in visualizing tau aggregates in Alzheimer's disease (AD).

Objective: To characterize 18F-PI-2620 signal across the healthy aging and Alzheimer's disease (AD) clinical spectrum, ranging from cognitively unimpaired (CU) to mild cognitive impairment (MCI) to dementia due to AD.

Methods: 18F-PI-2620 PET was used to examine tau burden in 91 participants (**Table 1**). SUVRs were examined in seven AD-relevant regions of interest (entorhinal, hippocampus, amygdala, inferior temporal, inferior parietal, precuneus, rostral middle frontal gyrus) as well as precentral gyrus, a region that is not impacted by tau until late in disease. Within CU individuals, associations between regional tau PET and CSF pTau181 were examined (**Table 2**). Associations between regional tau PET with amyloid status, age, and cognition were also examined across and within each diagnostic group (**Table 3**).

Results: As expected, tau positivity increased with disease severity such that SUVRs increased in a stepwise manner with increasing disease severity (**Figure 1**). Within cognitively unimpaired individuals, entorhinal, amygdala, and inferior temporal SUVR were significantly associated with CSF pTau181, validating detection of subtle elevations of tau in CU participants (**Figure 2**). Across a subset of participants with cognitive data, greater 18F-PI-2620 signal in all target regions was associated with worse memory, and greater signal in almost all target regions was significantly associated with worse executive functioning and language; there were no significant associations with visuospatial ability (**Figure 3**). With the 25 CU participants with cognitive data, greater 18F-PI-2620 signal was also associated with worse memory, executive functioning, and language though associations were weaker and more regionally dependent (**Figure 4**).

Conclusion: 18F-PI-2620 shows the expected elevations across the AD spectrum and is associated with cognitive deficits. This work provides further evidence that 18F-PI-2620 accurately captures tau aggregations in AD.

Table 1. Demographic Information of all participants across the AD clinical spectrum.

	A- CU (N=37)	A+ CU (N=27)	A+ MCI (N=11)	A+ AD (N=16)	Overall (N=91)
Age					
Mean (SD)	69.89 (7.98)	74.35 (6.57)	72.64 (10.16)	71.69 (7.96)	71.86 (7.97)
Median [Min, Max]	69.11 (41.45, 85.43)	74.56 (60.35, 91.54)	68.98 (56.33, 89.85)	74.22 (57.79, 81.22)	71.77 (41.45, 91.54)
Sex					
Female	21 (56.76 %)	18 (66.67 %)	4 (36.36 %)	9 (56.25 %)	52 (57.14 %)
Male	16 (43.24 %)	9 (33.33 %)	7 (63.64 %)	7 (43.75 %)	39 (42.86 %)

Amyloid status defined by amyloid PET and/or CSF.

Table 2. Demographic information of subset with CSF pTau-181.

	A- CU (N=26)	A+ CU (N=9)	Overall (N=35)
Age			
Mean (SD)	68.85 (4.84)	72.87 (4.98)	69.89 (5.12)
Median [Min, Max]	67.12 (61.70, 79.57)	74.37 (63.72, 78.16)	69.11 (61.70, 79.57)
Sex			
Female	12 (46.15 %)	4 (44.44 %)	16 (45.71 %)
Male	14 (53.85 %)	5 (55.56 %)	19 (54.29 %)
Years between CSF and Tau PET			
Mean (SD)	-0.67 (0.37)	-0.95 (0.53)	-0.74 (0.43)
Median [Min, Max]	-0.75 (-1.16, 0.02)	-1.02 (-1.76, -0.25)	-0.81 (-1.76, 0.02)
CSF pTau-181			
Mean (SD)	38.29 (10.95)	57.72 (19.88)	43.29 (15.98)
Median [Min, Max]	37.61 (12.70, 63.16)	55.46 (35.86, 90.96)	39.46 (12.70, 90.96)

Amyloid status defined by amyloid PET and/or CSF.

Table 3. Demographic information of subset with cognitive data.

	A- CU (N=10)	A+ CU (N=15)	A+ MCI (N=9)	A+ AD (N=9)	Overall (N=43)
Age					
Mean (SD)	71.13 (13.18)	74.44 (7.91)	71.55 (10.00)	75.01 (5.34)	73.18 (9.24)
Median [Min, Max]	71.48 (41.45, 85.43)	73.66 (60.35, 91.54)	68.98 (56.33, 89.85)	76.80 (62.34, 80.81)	73.40 (41.45, 91.54)
Sex					
Female	9 (90.00 %)	12 (80.00 %)	3 (33.33 %)	5 (55.56 %)	29 (67.44 %)
Male	1 (10.00 %)	3 (20.00 %)	6 (66.67 %)	4 (44.44 %)	14 (32.56 %)
Education					
Mean (SD)	17.00 (2.54)	18.07 (1.53)	16.44 (1.94)	17.78 (2.54)	17.42 (2.13)
Median [Min, Max]	18.00 (12.00, 20.00)	18.00 (16.00, 20.00)	16.00 (14.00, 20.00)	18.00 (14.00, 20.00)	18.00 (12.00, 20.00)
Memory Score					
Mean (SD)	0.10 (0.79)	-0.10 (0.87)	-2.36 (1.20)	-3.70 (0.33)	-1.05 (1.71)
Median [Min, Max]	0.29 (-1.22, 1.00)	0.17 (-2.16, 0.92)	-1.98 (-3.85, -1.01)	-3.66 (-4.12, -3.29)	-0.60 (-4.12, 1.00)
Missing	0 (0%)	2 (13.3%)	3 (33.3%)	3 (33.3%)	8 (18.6%)
Executive Function Score					
Mean (SD)	0.02 (0.43)	-0.21 (0.64)	-1.08 (0.89)	-1.51 (0.81)	-0.53 (0.88)
Median [Min, Max]	0.05 (-0.58, 0.85)	-0.07 (-1.58, 0.51)	-0.70 (-2.83, -0.48)	-1.63 (-2.31, -0.29)	-0.33 (-2.83, 0.85)
Missing	0 (0%)	4 (26.7%)	3 (33.3%)	3 (33.3%)	10 (23.3%)
Language Score					
Mean (SD)	-0.03 (0.39)	0.16 (0.88)	-0.98 (0.79)	-1.45 (1.23)	-0.44 (1.05)
Median [Min, Max]	0.03 (-0.73, 0.45)	0.20 (-1.25, 1.55)	-1.04 (-2.12, 0.02)	-0.89 (-3.35, -0.16)	-0.24 (-3.35, 1.55)
Missing	0 (0%)	0 (0%)	0 (0%)	1 (11.1%)	1 (2.3%)
Visuospatial Score					
Mean (SD)	-0.15 (0.25)	-0.14 (0.95)	0.09 (0.52)	-0.88 (2.50)	-0.23 (1.18)
Median [Min, Max]	-0.12 (-0.59, 0.19)	0.09 (-2.24, 0.78)	0.25 (-0.72, 0.63)	0.08 (-5.81, 0.78)	0.02 (-5.81, 0.78)
Missing	0 (0%)	2 (13.3%)	3 (33.3%)	3 (33.3%)	8 (18.6%)

Amyloid status defined by amyloid PET and/or CSF. Memory composite formed from z-score average of HVLT-R Delayed Recall, Craft Story Delayed Recall, Benson Figure Delayed Recall, and FCSRT Delayed Free Recall. Executive function composite formed from z-score average of Trails A, Trails B, Digit Span Forward, Digit Span Backward, Victoria Stroop Dot Time, Victoria Stroop Word Time, Victoria Stroop Color-Word Time, Coding, Clock - Command. Language composite formed from z-score average of Phonemic Fluency (F, L), Semantic Fluency (Animals, Vegetables), MINT, and Cookie Theft. Visuospatial composite formed from z-score average of JLO, Benson Figure Copy, Clock - Copy.

Figure 1. 18F–PI–2620 signal increases in an expected stepwise fashion with increasing disease severity. Significant differences between groups are shown with black lines and represent models accounting for age and sex.

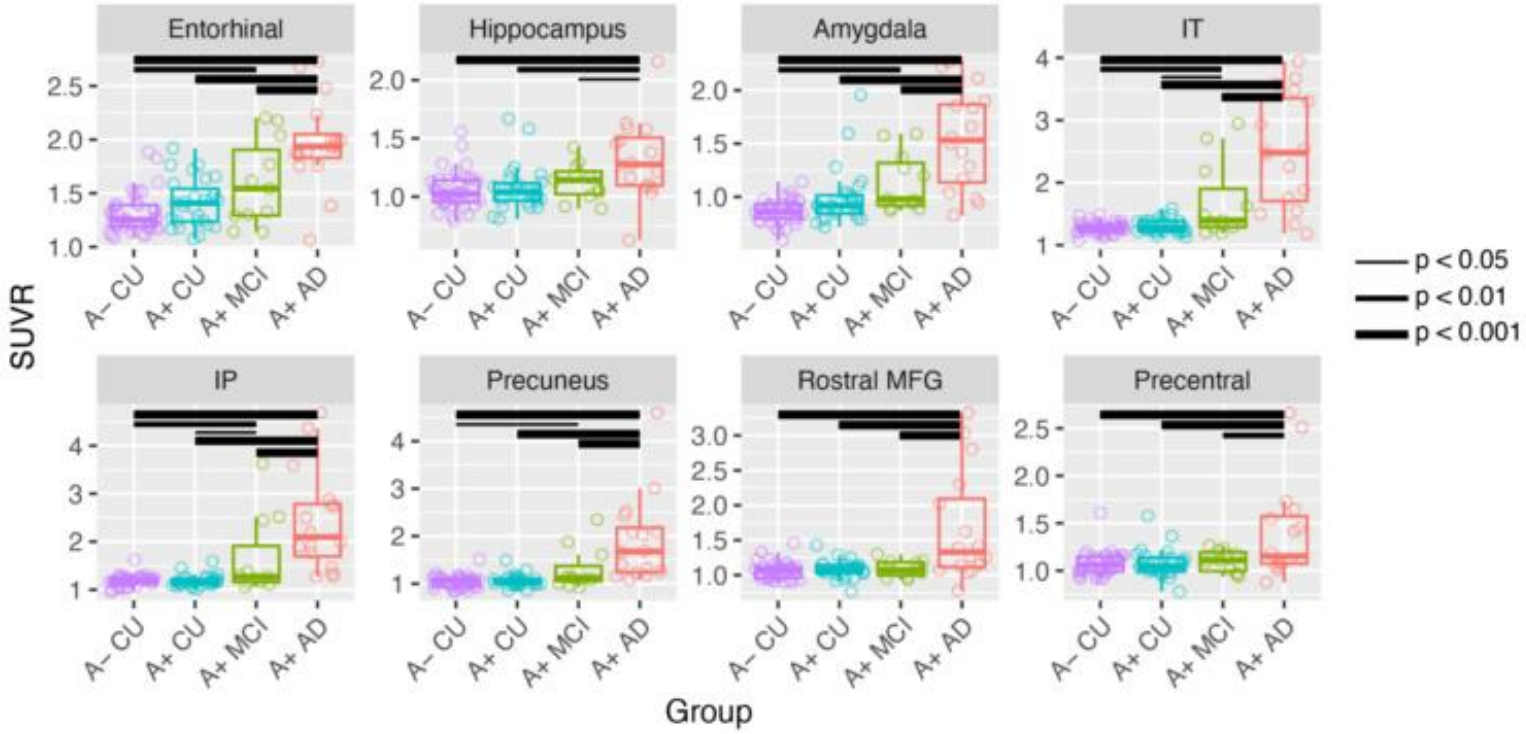

Figure 2. Association between tau SUVR and CSF pTau–181. Residuals shown account for age and sex.

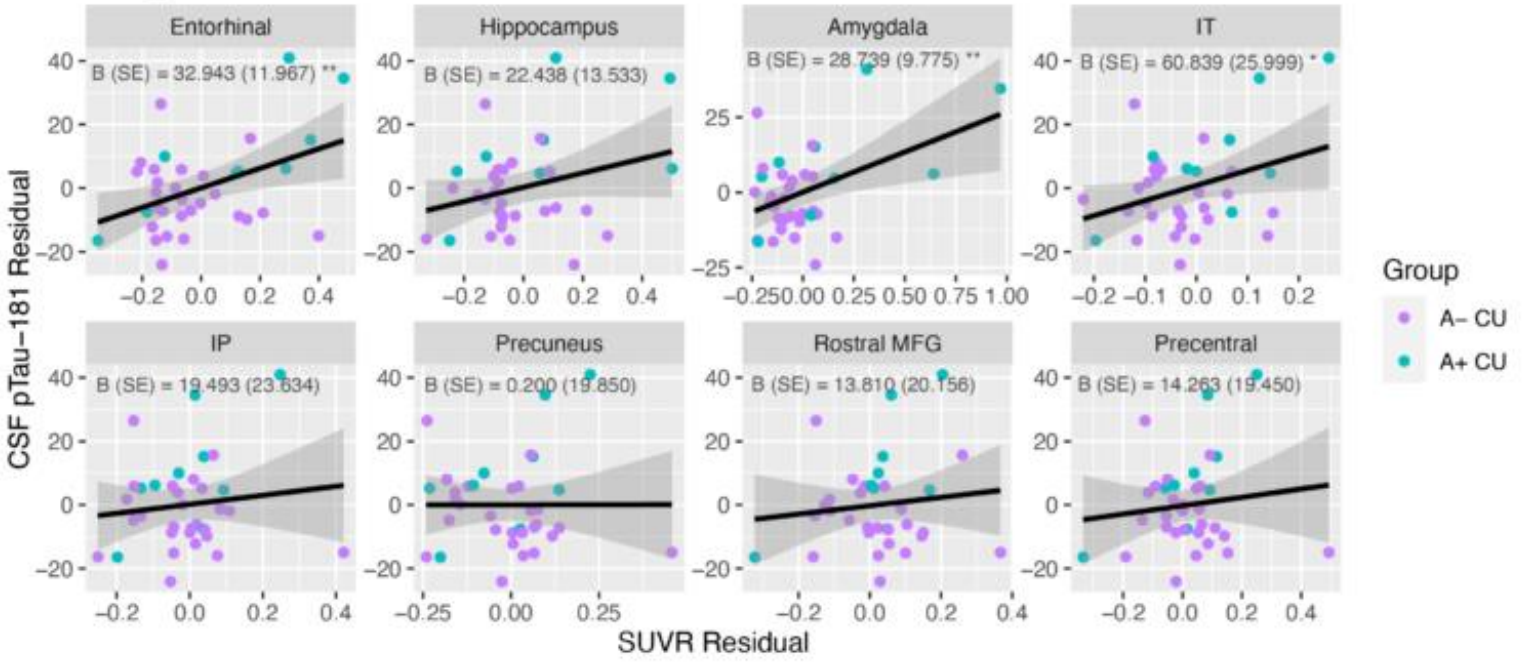

Figure 3. Association between tau SUVR and cognition in all participants. Residuals shown account for age, sex, and education.

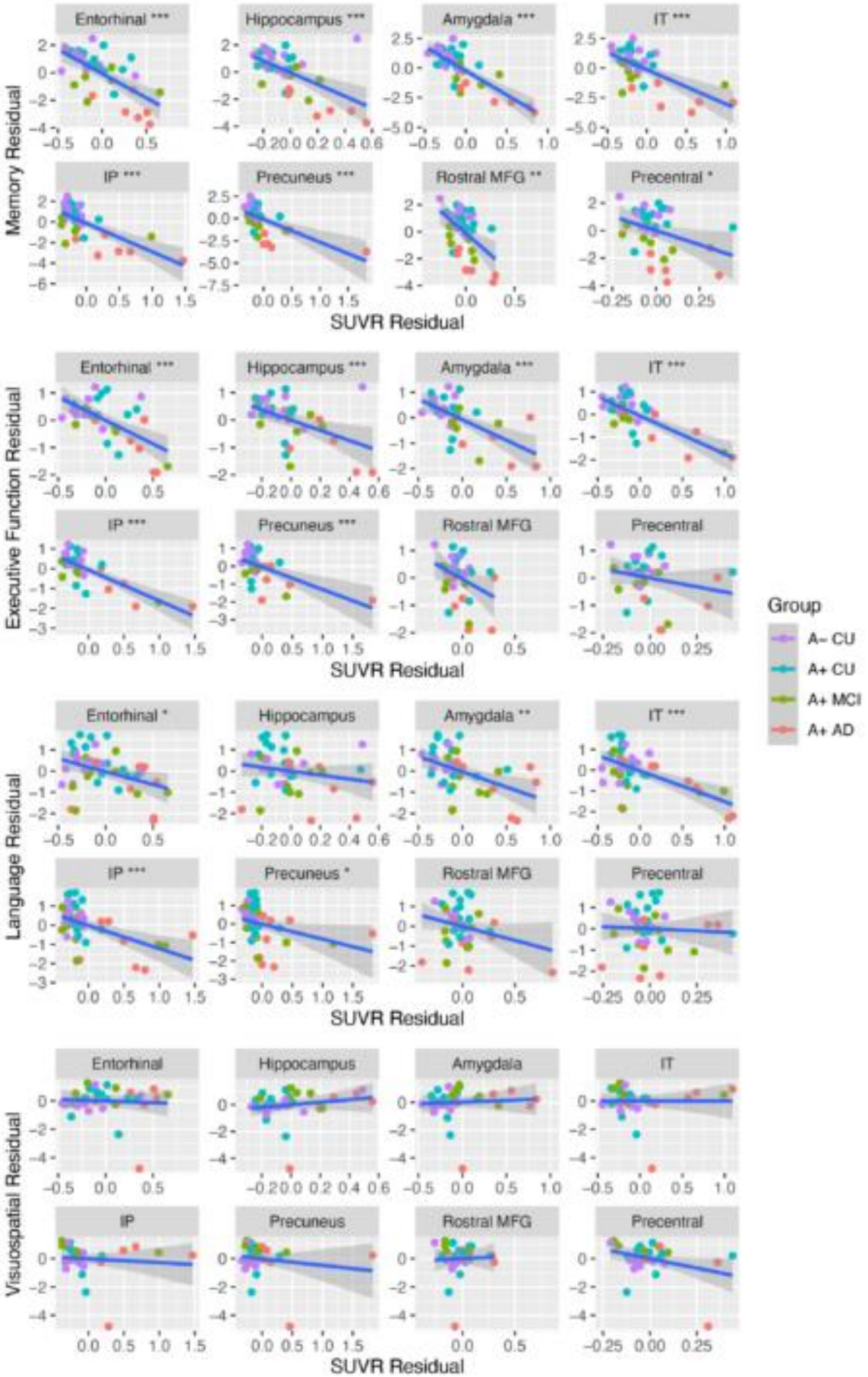

Figure 4. Association between tau SUVR and cognition in CU participants. Residuals shown account for age, sex, and education.

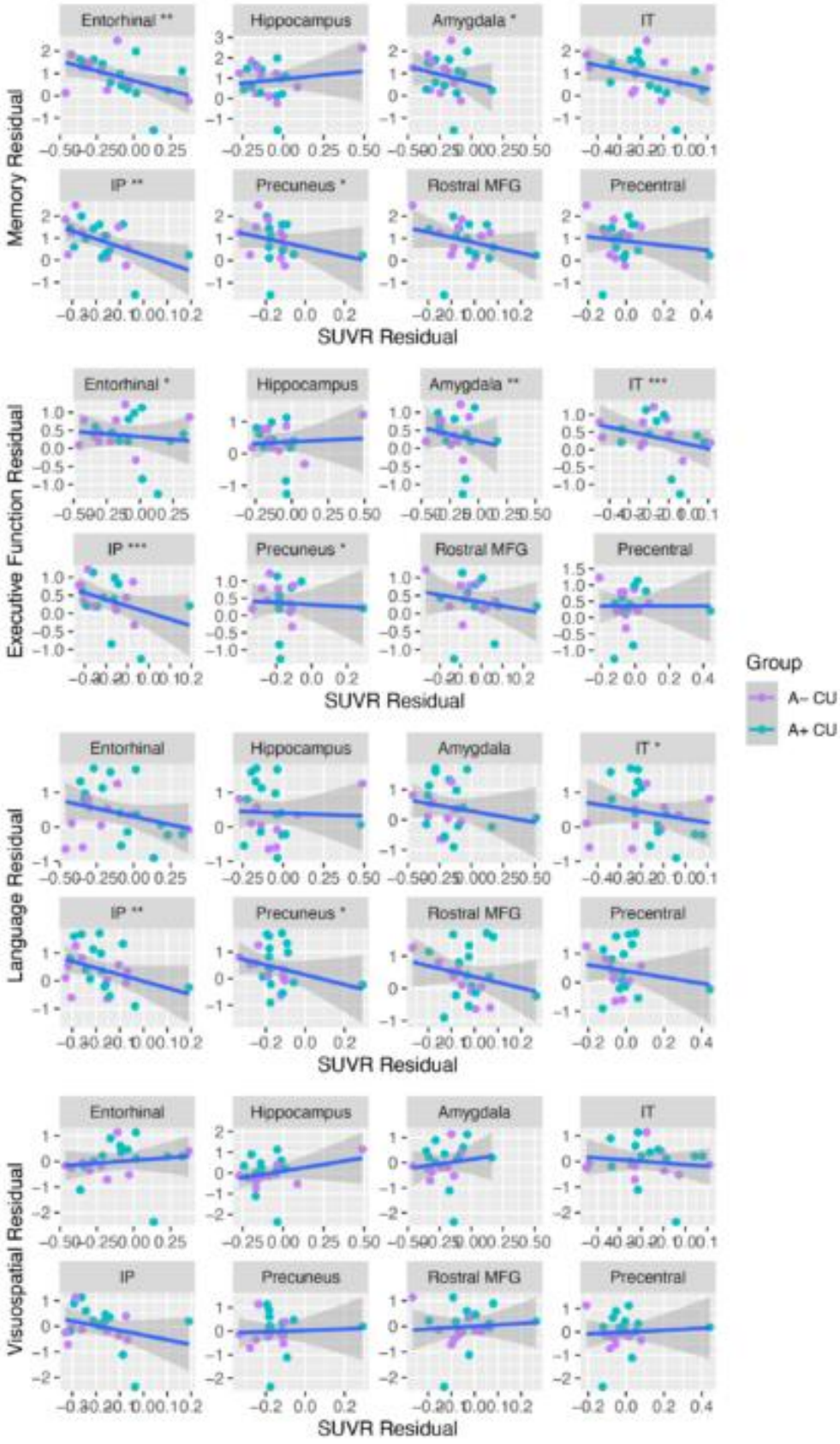

Keywords: 18F-PI-2620, tau PET, Alzheimer's disease

44 Amyloid-induced hyperconnectivity drives tau spreading across connected brain regions in Alzheimer's disease

Sebastian Niclas Roemer[1,2,3], Fabian Wagner[1,2], Anna Steward[1,2], Davina Biel[1,2], Anna Dewenter[1,2], Jannis Dennecke[1,2], Mattes Gross[1,2], Zeyu Zhu[1], Lukai Zheng[1], Amir Dehsarvi[1], Martin Dichgans[1], Michael Ewers[1], Matthias Brendel[1], Nicolai Franzmeier[1]

[1]*University Hospital, LMU Munich, Munich, Germany*
[2]*Institute for Stroke and Dementia Research (ISD), Munich, Germany*
[3]*Department of Neurology, University Hospital of Munich, LMU Munich, Munich, Germany, Munich, Germany*
[4]*Department of Nuclear Medicine, University Hospital of Munich, LMU Munich, Marchioninistraße 15, 81377 Munich, Germany, Munich, Germany*

Introduction: Alzheimer's disease (AD) is characterized by the accumulation of amyloid-beta (Ab) plaques, followed by the spreading of neurofibrillary tau pathology, ensuing neurodegeneration and cognitive decline. Preclinical and AD patient studies yielded converging evidence, that i) Ab plaques induce neuronal hyperexcitability in nearby neurons and that ii) tau spreads across connected neurons in an activity-dependent manner. Thus, we hypothesized that Ab induces a hyperexcitatory shift in neuronal activity, thereby causing transiently increased functional connectivity, which in turn accelerates the spread of tau across connected brain regions in AD.

Methods: We included 116 Ab-positive subjects across the preclinical to clinical AD spectrum plus 52 Ab-negative controls, all with baseline amyloid-PET, 3T resting-state fMRI and longitudinal Flortaucipir tau-PET data. PET data were parceled into 200 cortical ROIs of the Schaefer atlas, longitudinal tau-PET change rates were computed per ROI using linear mixed models. Resting-state fMRI connectivity was computed across the 200 ROIs. Tau epicenters were defined per subject as 5% of brain regions with highest baseline tau-PET SUVRs.

Results: Higher amyloid-PET (i.e. centiloid) is associated with increased connectivity of temporal-lobe tau epicenters to temporo-occipital and parietal regions (Fig.1), i.e. typical tau vulnerable regions. Higher connectivity of the tau epicenters to these brain regions predicted faster tau-PET increase over time (Fig.2). Mediation analysis revealed that Ab-associated connectivity increase to temporal, parietal and occipital brain regions mediated the association between higher amyloid-PET and faster tau-PET increase over time (Fig.3).

Discussion: We demonstrate a close link between Ab-associated connectivity increases and faster tau spread across connected regions in AD. These findings suggest that Ab promotes tau spreading via increasing neuronal activity and connectivity, hence Ab-associated neuronal hyperexcitability may be a promising target for attenuating tau spreading in AD.

Figure 1: ROI-wise association between average centiloid (target-Roi & tau-epicenter) und FC to tau-epicenter

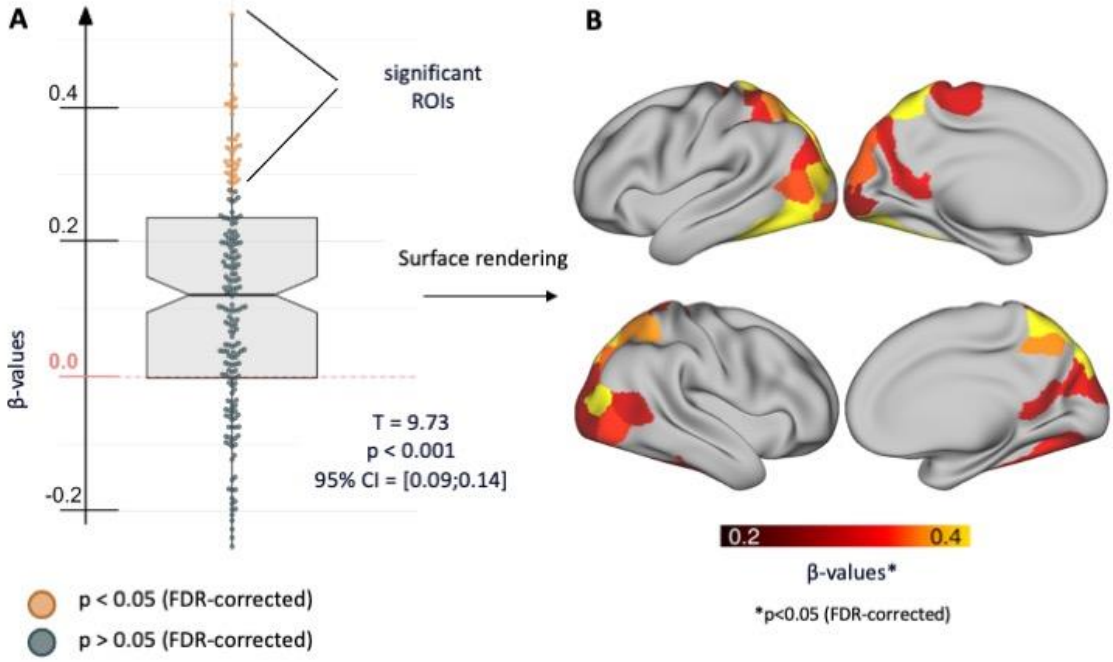

Figure 1: We used linear regression to determine whether regional amyloid-PET levels (i.e. centiloid) predict higher functional connectivity to the tau epicenter. The Boxplot (A) illustrates the distribution of standardized beta coefficients of this regression analysis. The distribution of standardized beta coefficients is significantly greater than zero ($p < 0.001$; 95% CI = [0.09-0.14]), showing that higher centiloid levels are linked to overall higher connectivity to the tau epicenter. Single ROIs with a significant correlation (FDR-corrected p-value < 0.05) are highlighted in yellow in the beeswarm panel (A) and plotted on the brain surface (B). Regression analyses are corrected for age, sex, diagnosis and mean head motion during the resting-state fMRI scan.

Figure 2: ROI-wise association between FC to tau-epicenter and tau-accumulation rates

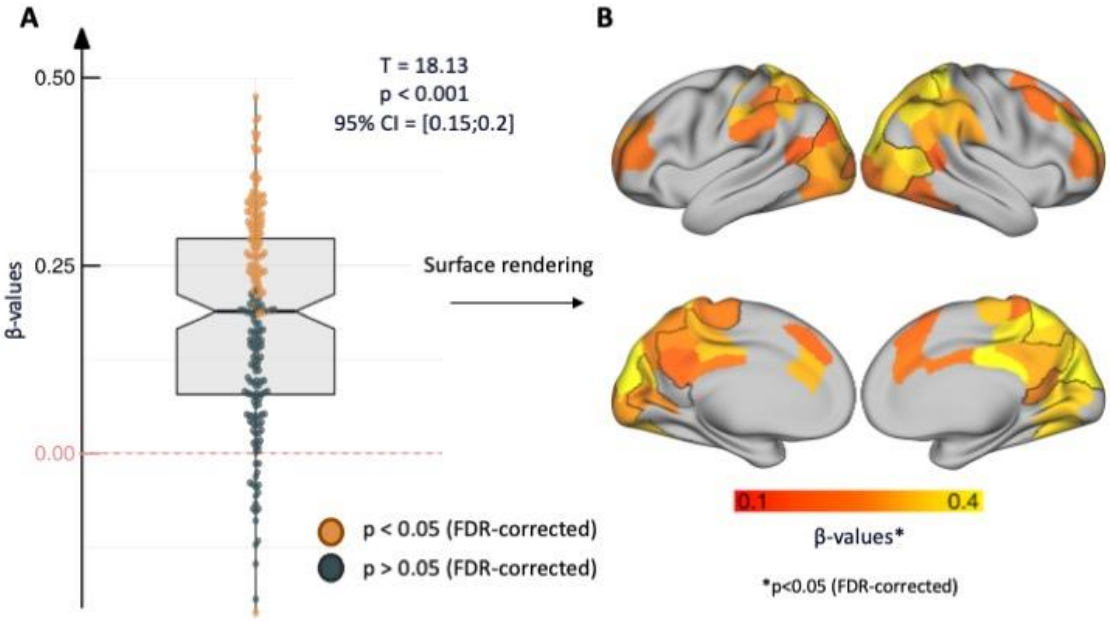

Figure 2: Using linear regression per ROI across subjects, we tested whether higher connectivity to the tau epicenter predicted faster tau accumulation rates (i.e. tau-PET SUVR annual change rate), indicative of connectivity-mediated tau spreading. The Boxplot/Beeswarm illustrates the distribution of standardized beta coefficients which are significantly greater than zero ($p < 0.001$; 95% CI = [0.15-0.2]), showing that higher connectivity to the epicenter is overall linked to faster tau accumulation. ROIs with a significant correlation (highlighted in yellow in panel A) are plotted on the brain surface (B). Black outlines indicate regions that showed a significant association between higher amyloid and higher connectivity to epicenters from Fig1, showing a substantial overlap with the regions highlighted in this figure.

Figure 3: ROI-wise mediation analysis

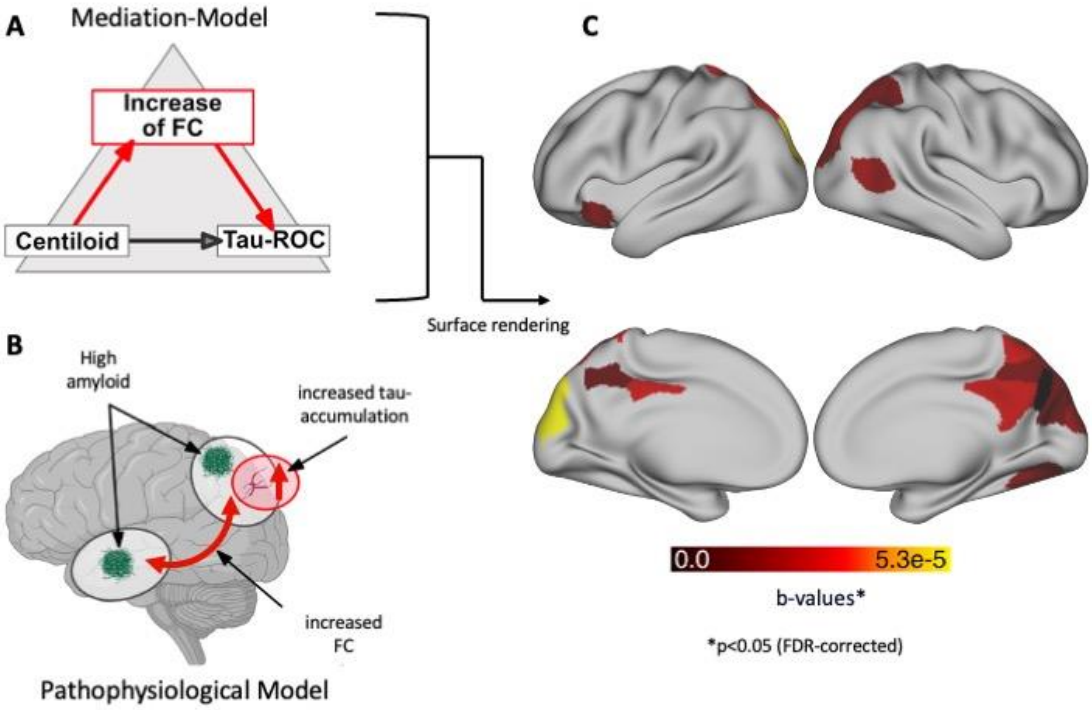

Figure 3: We performed bootstrapped mediation with 1000 iterations per ROI, to test whether the effect of amyloid on faster tau accumulation is explained by an amyloid-associated increase in connectivity (i.e. illustrated in panels A&B). Regions showing a significant mediation effect ($p<0.05$, FDR corrected) are plotted on the brain surface.

Keywords: Amyloid-PET, resting-state fMRI, longitudinal tau-PET, hyper-excitability

45 A visual-read algorithm for tau pathology using [18F]RO948

Ruben Smith[1,2,8], Valentina Garibotto[3], Douglas Hägerström[4], Jonas Jögi[5], Tomas Ohlsson[6], Matteo Tonietto[7], Shorena Janelidze[1], Erik Stomrud[1,8], Gregory Klein[7], Oskar Hansson[1,8]

[1]*Clinical Memory Research Unit, Department of Clinical Sciences, Lund University, Lund, Sweden*
[2]*Department of Neurology, Skåne University Hospital, Lund, Sweden*
[3]*Department of Nuclear Medicine and Molecular Imaging, Geneva University Hospital, University of Geneva, Geneva, CH*
[4]*Department of Neurophysiology, Skåne University Hospital, Lund, Sweden*
[5]*Skåne University Hospital, Department of Clinical Physiology and Nuclear Medicine, Lund, Sweden*
[6]*Department of Radiation Physics, Skåne University Hospital, Lund, Sweden*
[7]*F. Hoffmann-La Roche Ltd, Basel, CH*
[8]*Memory Clinic, Skåne University Hospital, Malmö, Sweden*

Objectives: To compare a visual read algorithm for [^{18}F]RO948 PET to quantitative measurements.

Methods: 1654 consecutively recruited patients in the BioFINDER-2 study, who underwent [^{18}F]RO948 PET scans were included, 754(46%) were Amyloid beta-positive. [^{18}F]RO948 PET scans were assessed by two reviewers, reaching a consensus visual read. Our algorithm was similar to the [^{18}F]MK6240 algorithm (Seibyl *et al J Nuclear Medicine* 2022), but allowed tau positivity based on a single region and using a cerebellar grey signal adjusted color scale. Scans were categorized: normal; early AD-pattern (temporal binding); late AD-pattern (temporal and other neocortical involvement); or inconclusive (Figure 1). The algorithm was compared to quantitative assessments in entorhinal (ERC) and temporal meta-ROIs as well as predicting plasma phospho-tau217 (pTau217) status. For inter-rater reliability 141 scans were assessed by an independent rater. To compare transferability of the visual read algorithm, 37 participants had head-to-head data for both [^{18}F]RO948 and [^{18}F]flortaucipir.

Results: 1092(66%) scans were read normal, 233(14%) early AD, 240(14.5%) late AD and 89(5%)inconclusive. Positive reads were associated with increased SUVRs and amyloid positivity, whereas 98.5% of normal visual reads had normal SUVRs (Figure 1). [^{18}F]RO948 visual reads had high concordance with increases in quantitative SUVRs, with accuracies of 93.8% [C.I. 92.5-94.9%] in ERC and 91.7% [C.I. 90.2-93.0%] in the temporal meta-ROI (Figure 2a-b). Inter-rater reliability was very good (Weighted Cohen's kappa 0.87 [C.I. 0.82-0.93]) and between-tracer concordance excellent (Weighted Cohen's kappa 0.94 [C.I. 0.86-1.00]). Visual reads and quantitative measurements had similar accuracies in predicting abnormal plasma pTau217 status (visual read 86.5% [C.I. 84.6-88.2%] and quantitative 84.8% [C.I. 82.8-86.6%]; Figure 2c-d).

Conclusions: Visual reads of [^{18}F]RO948 provides an easy method for assessing presence of tau in the brain. Visual reads exhibited a high accuracy to quantitative results, a very good inter-rater reliability and an excellent concordance between PET tracers.

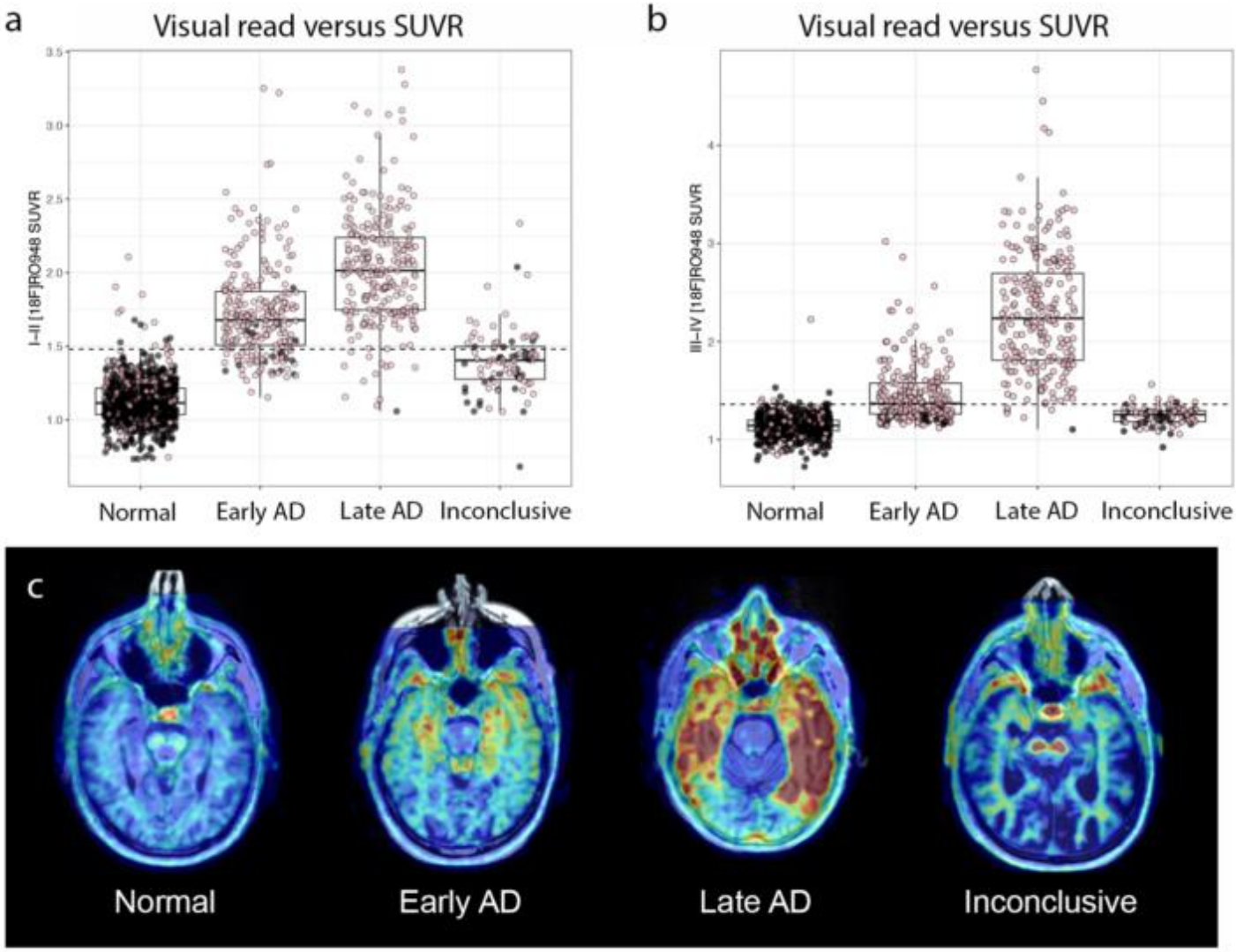

Figure 1. a-b) SUVR values in the a) entorhinal cortex and b) in a temporal meta-ROI in the different visual read categories. Pink dots indicate Aβ-positive and black dots Aβ-negative participants. Dashed lines represent quantitative cutoffs (1.48 in ERC and 1.36 in temporal meta-ROI). e) example images of the four visual read categories.
Aβ– = Aβ negative; Aβ+ = Aβ positive; ERC = entorhinal cortex.

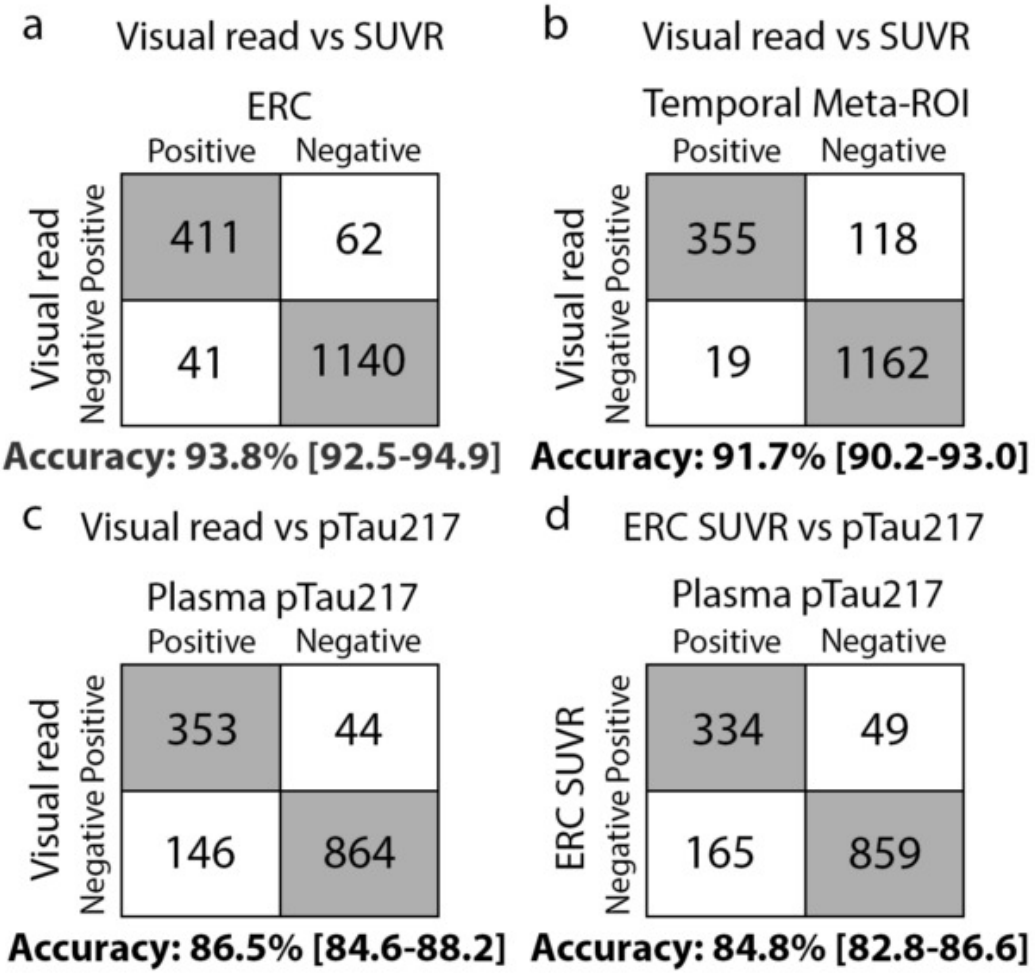

Figure 2. Accuracies for visual reads in predicting quantitative SUVRs in a) the entorhinal cortex (ERC) and b) a temporal meta-ROI. c) and d) shows the accuracies of visual reads (c) and ERC SUVRs (d) in predicting abnormal plasma pTau217. In c) and d) the number of included participants is (n=1407) since only participants having available data for all biomarkers (plasma pTau217, visual reads and quantitative SUVRs from ERC and the temporal meta-ROI) were included in the analysis.

Keywords: PET, tau, visual read, accuracy, RO948

46 Establishing the interchangeability between CSF and PET for identifying patients with Alzheimer's disease pathology who are suitable for amyloid targeting therapies

Samantha C Burnham[1], Anupa K Arora[1], Leonardo Iaccarino[1], Ian Kennedy[1], Vikas Kotari[1], Sameera R Wijayawardana[1], Ming Lu[1], Michael J Pontecorvo[1], Frances-Catherine Quevenco[2], Grazia Dell' Agnello[3], Michelle Neff[1], Nicole Chaves Petronzi[3], Sophie Viollet[4], Jian Wang[1]

[1]*Eli Lilly and Company, Indiana, IN, United States*
[2]*Eli Lilly and Company, Vernier, Geneva, CH*
[3]*Eli Lilly and Company, Sesto Fiorentino (FI), Italy*
[4]*Eli Lilly and Company, Neuilly sur Seine, France*

Background: Identifying patients who would benefit from novel disease modifying therapies (DMTs) for Alzheimer's disease (AD) is important. PET tracers are considered the gold standard for establishing the presence of AD pathology but are costly and not widely accessible. Thus, establishing the interchangeability between CSF and PET for patient identification may help overcome barriers to inequitable access for Alzheimer's DMTs.

Methods: Alzheimer's Disease Neuroimaging Initiative (ADNI) participants with MCI or AD dementia and available CSF data, amyloid-PET and/or tau-PET scans were included. CSF positivity was defined by respective label thresholds, PET positivity was defined by TRAILBLAZER-ALZ2 inclusion criteria. An additional early (temporal) tau-PET positivity criteria was considered. Agreement between CSF and PET (PPA, NPA), and the non-inferiority of CSF to amyloid-PET for patient identification were evaluated. Clinical/cognitive trajectories for tau-PET−/CSF± were calculated.

Results: Fujirebio-Lumipulse Aβ42/40 CSF (N=186/102 MCI/AD; mean age 72.9 years; 42.4% female and Roche-Elecsys P-tau181/Aβ42 CSF (152/99 MCI/AD; mean age 73.3 years, 41.0% female) were in agreement with amyloid-PET (98.3% PPA, 82.3% NPA and 91.4% PPA, 85.7% NPA, respectively). Both CSF assays were non-inferior to amyloid-PET for patient identification. Roche-Elecsys P-tau181/Aβ42 CSF (N=99/28 MCI/AD; mean age 71.0 years, 40.0% female) showed moderate agreement with tau-PET (98.0% PPA, 65.4% NPA) and high agreement with early temporal tau-PET (95.3% PPA, 77.8% NPA). A Youden's Index-based threshold for Roche-Elecsys P-tau181/Aβ42 CSF resulted in PPA and NPA >80% against tau-PET. Patients with CSF+/tau-PET− had faster clinical/cognitive decline than CSF−/tau-PET−.

Conclusions: Results support the hypothesis that approved CSF assays, used per label threshold, are interchangeable with amyloid-PET. CSF assays, per label threshold, likely identify individuals at an earlier disease stage than widespread neocortical tau-PET. Alternative thresholds for CSF assays, derived against tau-PET, may better align with widespread neocortical tau-PET. Further consideration of CSF strategies for tau is warranted, particularly given emerging tau-targeting therapies.

Figure 1: Study design

Selection criteria: Participants with MCI/dementia in ADNI with CE-marked CSF assay and amyloid and/or tau PET imaging (CSF draw and PET image within 6 months [amyloid-PET] or 8 months [tau-PET])

CSF stratification: Evaluated CSF with CE-marked Fujirebio Lumipulse Aβ42/40 or Roche Elecsys P-tau181/Aβ42, stratified using product label thresholds

PET stratification: Amyloid-PET visual read followed product label, amyloid-PET quantitation was stratified at 37 Centiloids[1], widespread neorcortical tau-PET stratification was based on a combination of visual read and quantitation[1], early (temporal) tau stratification was based on quantitation.[2]
Further details on PET image processing are available upon request.

Outcome measures: PPA, NPA, OPA, PPV, and NPV between CSF and PET stratification

Confidence intervals: Two-sided 95% CIs with Wilson score method were provided for all outcome measures, except for the non-inferiority test, which employed the sample-level bootstrap method to construct two-sided 95% CI

Additional outcome measures for tau: Additional analyses were undertaken to determine a Youden's Index-based threshold for Roche-Elecsys P-tau181/Aβ42 CSF against tau-PET as well as the longitudinal clinical/cognitive trajectories for tau-PET−/Elecsys CSF±

Additional outcome measure for amyloid: Additional analysis was undertaken to determine if CSF would be non-inferior to amyloid-PET quantitation: where the non-inferiority outcome is PPV_{c1r}-PPV_{c2r}[3]

PPV_{c1r}: PPV between amyloid-PET quantitation and amyloid-PET visual read
PPV_{c2r}: PPV between CSF and amyloid-PET visual read
Hypothesis: upper 95% confidence interval of PPV_{c1r}-PPV_{c2r} < 15%

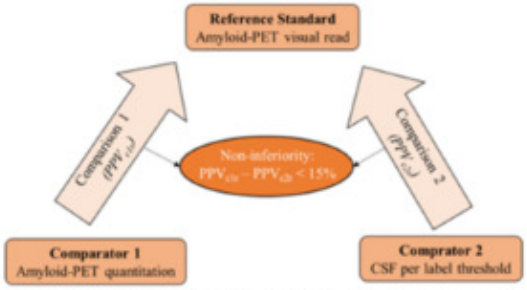

Abbreviations: Aβ, amyloid-beta; ADNI, Alzheimers Disease Neuroimaging Initiative; CSF, cerebrospinal fluid; MCI, mild cognitive impairment; NPA, negative percent agreement; NPV, negative predictive value; OPA, overall percent agreement; PET, positron emission tomography; PPA, positive percent agreement; PPV, positive predictive value.

References: 1. Sims JR, et al. *JAMA*. 2023; 330(6):512-527; 2. Kotari V, et. al. *Alzheimers Res Ther*. 2023; 15 (1):41; 3. Li M. *Statistics in Biopharmaceutical Research*. 2016;8(3):355-363.

Table 1: Agreement between CSF and PET

Reference standard	Amyloid-PET (n=288)	Amyloid-PET (n=251)	Tau-PET (n=127)	Early Tau-PET (n=127)
CSF assay (Label threshold)	Lumipulse Aβ42/40 (95% CI)	Elecsys P-tau181/Aβ42 (95% CI)	Elecsys P-tau181/Aβ42 (95% CI)	Elecsys P-tau181/Aβ42 (95% CI)
PPA	98.29 (95.08-99.42)	91.38 (86.26-94.71)	97.96 (89.31-99.64)	95.31 (87.10-98.39)
NPA	82.30 (74.24-88.24)	85.71 (76.20-91.83)	65.38 (54.33-74.99)	77.78 (66.09-86.27)
OPA	92.01 (88.30-94.62)	89.64 (85.26-92.83)	77.95 (69.98-84.28)	86.61 (79.61-91.47)
PPV	89.58 (84.46-93.16)	93.53 (88.79-96.35)	64.00 (52.70-73.94)	81.33 (71.07-88.54)
NPV	96.88 (91.21-98.93)	81.48 (71.67-88.44)	98.08 (89.88-99.66)	94.23 (84.36-98.02)

Abbreviations: CI, confidence interval; CSF, cerebrospinal fluid; NPA, negative percent agreement; NPV, negative predictive value; OPA, overall percent agreement; PET, positron emission tomography; PPA, positive percent agreement; PPV, positive predictive value.

Keywords: Amyloid-PET, tau-PET, CSF, concordance, Alzheimer's disease

47 Exploring A-T+ within the AT(N) framework

Brian Lopresti[1], Ann Cohen[2], Alexandra Gogola[1], Milos Ikonomovic[2], Beth Snitz[3], N. Scott Mason[1], Davneet Minhas[1], Cristy Matan[1], Patricia McGeown[3], Shannon Cieply[3], Ming-Hsuan Chiang[1], Tharick Pascoal[2], Alexandria Reese[1], Eunice Matela[3], Thomas Karikari[2], Robert Sweet[2,3,5], Sarah Berman[3,5], Julia Kofler[4], Oscar Lopez[2,3,5], Victor Villemagne[2]

[1]*Department of Radiology, University of Pittsburgh School of Medicine, Pittsburgh, PA, United States*
[2]*Department of Psychiatry, University of Pittsburgh School of Medicine, Pittsburgh, PA, United States*
[3]*Department of Neurology, University of Pittsburgh School of Medicine, Pittsburgh, PA, United States*
[4]*Department of Pathology, University of Pittsburgh School of Medicine, Pittsburgh, PA, United States*
[5]*Clinical and Translational Science Institute, University of Pittsburgh, Pittsburgh, PA, United States*

Introduction. The AT(N) framework allows a biological-based classification along the Alzheimer's disease (AD) spectrum. In this study we focused on participants classified as A-T+, defining T+ as high tau in the Meta-temporal (MT) region and investigating its relationship with clinical diagnosis and cognition.

Methods: 108 Pittsburgh ADRC participants with Aβ ([^{11}C]PiB) and tau ([^{18}F]FTP) PET scans were included. Centiloid <20 was used to define negative Aβ PET (Aβ–). The presence of neocortical tau was defined both visually and quantitatively in the MT region using a previously determined sensitivity threshold of >1.18 SUVR (Gogola et al., doi:10.2967/jnumed.123.265941, 2023). Participants were split into cognitively unimpaired (CU) and cognitively impaired (CI, including mild cognitive impairment and AD)

Results: 55/108 participants (51%) were classified as Aβ-, 14 (25%) of which (5 CU and 9 CI) exhibited high MT tau (>1.18 SUVR). There were discrepancies between visual and quantitative determinations of T+, with visual detecting two additional cortical T+ cases not captured by the MT region. Therefore, visual T+ classification was used for further analysis. Compared to A-T-, A-T+ presented significantly worse MMSE (27.8±2.9 vs 24.9±5.3, respectively, p=0.016). Further examination showed that only CU A-T+ presented worse MMSE compared to CU A-T- (27.3±0.6 vs 29.2±0.4, respectively, p=0.02), whereas no significant differences were observed between CI A-T+ and CI A-T- (24.0±6.1 vs 26.8±3.4, respectively, p=0.1), suggesting a non-AD condition in the latter.

Discussion: There are several potential conclusions to be drawn from this study: 1. A-T+ cases in this sample were more frequent than previously reported (25% of all Aβ– participants, and 13% of the entire sample); 2. Visual examination is an important complement to image quantification; 3. T+ in CU may indicate future cognitive decline. Further studies will examine cognitive trajectories and use plasma biomarkers to confirm A-T+ status.

Keywords: tau, amyloid, AT(N), cognition

48 Sex-specific synergistic interaction between Aβ and p-tau predicts faster tangle accumulation in females

Yi-Ting Wang[1,2], Joseph Therriault[1,2], Stijn Servaes[1,2], Cécile Tissot[1], Nesrine Rahmouni[1,2], Arthur Cassa Macedo[1,2], Jaime Fernandez-Arias[1,2], Sulantha Mathotaarachchi[1], Andréa Benedet[3], Jenna Stevenson[1,2], Nicholas Ashton[3], Firoza Lussier[4], Tharick Pascoal[4], Henrik Zetterberg[3], Maria Natasha Rajah[2], Kaj Blennow[3], Serge Gauthier[1,2], Pedro Rosa-Neto[1,2]

[1]*Translational Neuroimaging Laboratory, McGill Research Centre for Studies in Aging, Montreal, QC, Canada*
[2]*McGill University, Montreal, QC, Canada*
[3]*University of Gothenburg, Mölndal, Sweden*
[4]*University of Pittsburgh, Pittsburgh, PA, United States*

Background: Females are disproportionately affected by Alzheimer's disease (AD) dementia and present higher tau load compared to males. Previous literature has proposed that Aβ and phosphorylated-tau (p-tau) synergism accelerates tau tangle formation, yet the effect of biological sex in this process was overlooked.

Methods: We examined the neuroimaging and fluid biomarkers of 457 participants from the TRIAD and ADNI cohorts. Baseline neuroimaging assessment including Aβ-PET and tau-PET, and fluid biomarkers data were collected. Follow-up tau-PET imaging assessments were also conducted. We introduced the concept of amyloid tau phosphorylation index (ATP index), defined as the concentration of p-tau in the CSF divided by Aβ load, to investigate the effects of Aβ on tau phosphorylation and longitudinal tau progression.

Results: As shown in Figure 1, findings revealed that Aβ-positive (Aβ+) females presented higher CSF p-tau$_{181}$ concentrations as compared to Aβ+ males in both TRIAD *($P = 0.04$, Cohen's $d = 0.51$)* and ADNI cohort *($P = 0.027$, Cohen's $d = 0.41$)*. In addition, Aβ+ females also presented faster NFT accumulation compared to their male counterparts (TRIAD: $P = 0.026$; ADNI: $P = 0.049$). In line with this, the triple interaction between the female sex, Aβ and CSF p-tau$_{181}$ significantly predicts accelerated tau accumulation at the 2-year follow-up visit (Table 1). Similarly, the ATP index is positively correlated with tau accumulation in Aβ+ females (Figure 2), indicating that the higher p-tau levels triggered by Aβ plaques are linked to faster tangle accumulation.

Conclusions: Overall, this study proposes a sex-specific modulation of cortical Aβ on tau phosphorylation, and this consequently facilitates faster NFT progression seen in female individuals over time. This presents important clinical implications suggesting the early intervention targeting Aβ plaques and tau phosphorylation may be promising therapeutic strategies for females to prevent further accumulation and spread of tau aggregates.

Figure 1. Tau phosphorylation predicts faster tau accumulation in Aβ+ females

A) Aβ+ females presented higher CSF p-tau$_{181}$ concentrations as compared to Aβ+ males in both the TRIAD cohort ($P = 0.04$, *Cohen's d* = 0.51) and ADNI cohort ($P = 0.027$, *Cohen's d* = 0.41). B) Aβ+ females also presented faster NFT accumulation as compared to Aβ+ males (TRIAD cohort (1Y): $P = 0.026$, *Cohen's d* = 0.52; ADNI cohort (4Y): $P = 0.049$, *Cohen's d* = 1.14). C) In Aβ+ female subjects, baseline CSF p-tau$_{181}$ concentration was found to associate with the change in tau-PET meta-ROI SUVRs at 1-year (TRIAD: $P = 0.05$, $R^2 = 0.3$), 2-year (TRIAD: $P < 0.0001$, $R^2 = 0.73$; ADNI: $P = 0.0025$, $R^2 = 0.39$) and 4-year follow-up (ADNI: $P = 0.0014$, $R^2 = 0.84$) assessments. D) Voxel-based linear regression models demonstrated positive correlations between CSF p-tau$_{181}$ concentration and baseline tau-PET SUVR as well as longitudinal NFT accumulation in Aβ+ females. The models were corrected for age and *APOE ε4* carriage status, and for multiple comparisons using an FDR cluster threshold of $P < 0.001$.

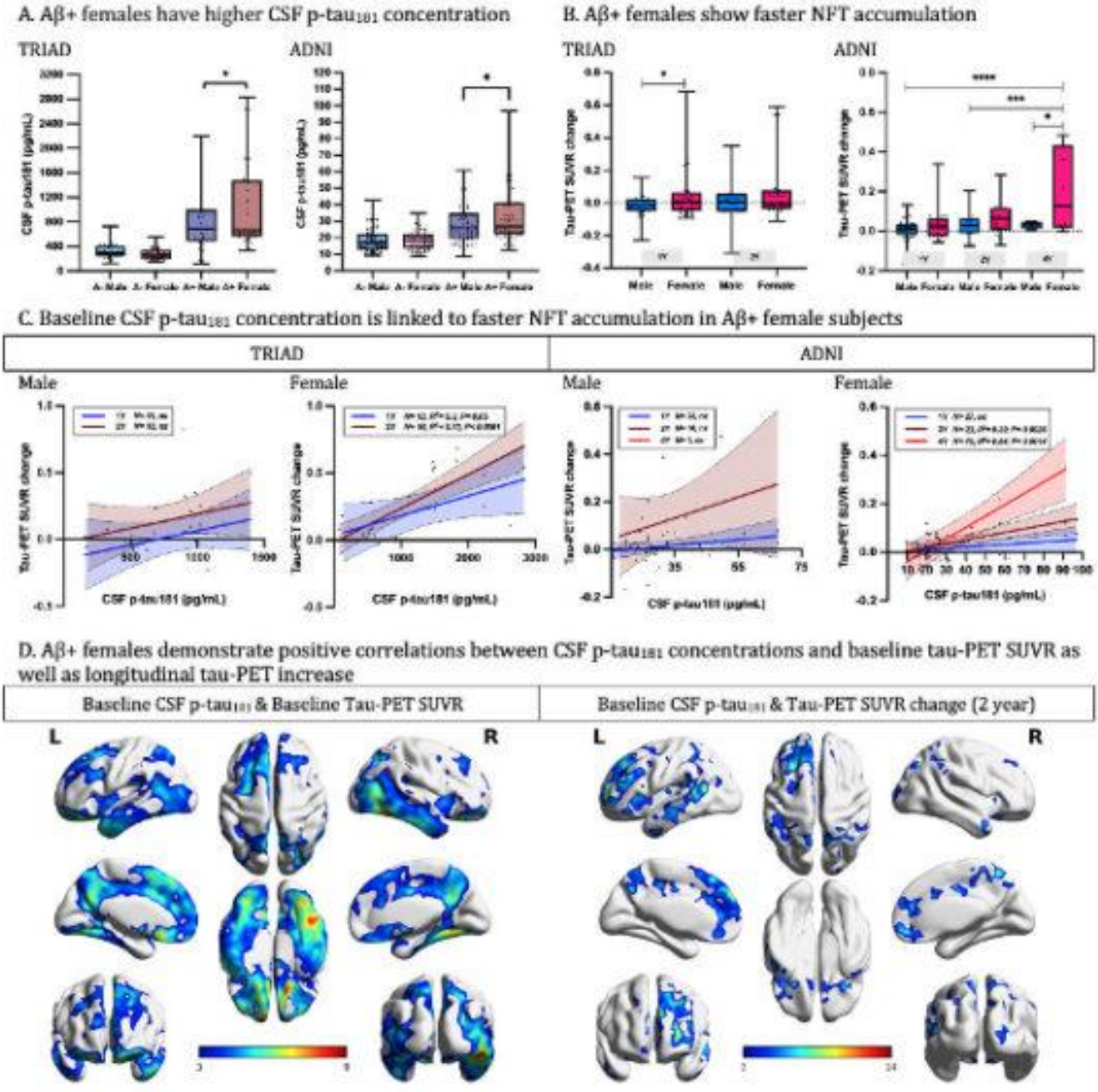

Table 1. Sex-specific modulation of Aβ on tau phosphorylation predicts faster tangle accumulation in female

Multivariate linear regression analyses unveiled that the triple interaction between the female sex, Aβ and CSF p-tau$_{181}$ was a significant predictor of accelerated tau accumulation throughout all Braak ROIs except for Braak II at the 2-year follow-up visit (Braak I: $P = 0.0067$, $t = 2.81$; Braak III: $P = 0.017$, $t = 2.45$; Braak IV: $P = 0.002$, $t = 3.17$; Braak V: $P = 0.006$, $t = 2.88$; Braak VI: $P = 0.0049$, $t = 2.93$). The models were corrected for age, *APOE ε4* carriage status, and pathological status to account for their potential influence.

	Braak I			**Braak II**		
	Est. (95% Conf. Int.)	t-stat	p-value	Est. (95% Conf. Int.)	t-stat	p-value
(Intercept)	0.32 (0.07, 0.58)	2.52	0.01	0.12 (-0.01, 0.25)	1.81	0.075
Age	0.03 (-0.03, 0.09)	1.02	0.31	-0.01 (-0.04, 0.02)	-0.55	0.58
APOE4 carriage status	-0.11 (-0.22, 0.01)	-1.86	0.068	0.00 (-0.06, 0.06)	0.02	0.99
Pathological status (A-T-)	-0.08 (-0.42, 0.27)	-0.44	0.66	-0.06 (-0.23, 0.12)	-0.66	0.51
Pathological status (A+T-)	-0.14 (-0.37, 0.08)	-1.29	0.2	-0.06 (-0.17, 0.06)	-0.98	0.33
Sex (Female)	-0.11 (-0.28, 0.05)	-1.39	0.17	0.00 (-0.08, 0.09)	0.08	0.94
Amyloid-PET	0.02 (-0.12, 0.16)	0.28	0.78	-0.01 (-0.08, 0.06)	-0.25	0.8
CSF p-tau$_{181}$	0.21 (0.01, 0.41)	2.11	0.039	0.06 (-0.04, 0.17)	1.26	0.21
Sex (Female) * Amyloid-PET * CSF p-tau$_{181}$	0.25 (0.07, 0.42)	2.81	0.0067	0.05 (-0.04, 0.14)	1.17	0.25
	Braak III			**Braak IV**		
	Est. (95% Conf. Int.)	t-stat	p-value	Est. (95% Conf. Int.)	t-stat	p-value
(Intercept)	0.47 (0.25, 0.68)	4.39	<0.0001	0.35 (0.19, 0.51)	4.29	<0.0001
Age	-0.04 (-0.09, 0.01)	-1.53	0.13	-0.03 (-0.07, 0.01)	-1.64	0.11
APOE4 carriage status	-0.02 (-0.11, 0.08)	-0.36	0.72	0.01 (-0.06, 0.09)	0.35	0.73
Pathological status (A-T-)	-0.37 (-0.66, -0.09)	-2.61	0.01	-0.24 (-0.46, -0.03)	-2.24	0.03
Pathological status (A+T-)	-0.38 (-0.56, -0.19)	-4.06	0.0002	-0.22 (-0.36, -0.07)	-3.05	0.003
Sex (Female)	-0.07 (-0.20, 0.07)	-1.0	0.32	-0.09 (-0.19, 0.01)	-1.74	0.09
Amyloid-PET	0.12 (0.01, 0.23)	2.12	0.04	0.01 (-0.07, 0.10)	0.29	0.77
CSF p-tau$_{181}$	-0.15 (-0.32, 0.02)	-1.76	0.08	0.10 (-0.03, 0.22)	1.52	0.13
Sex (Female) * Amyloid-PET * CSF p-tau$_{181}$	0.18 (0.03, 0.33)	2.45	0.017	0.18 (0.07, 0.29)	3.17	0.002
	Braak V			**Braak VI**		
	Est. (95% Conf. Int.)	t-stat	p-value	Est. (95% Conf. Int.)	t-stat	p-value
(Intercept)	0.29 (0.12, 0.45)	3.54	0.0008	0.26 (0.13, 0.40)	4.0	0.0002
Age	-0.05 (-0.09, -0.02)	-2.89	0.006	-0.05 (-0.08, -0.02)	-3.46	0.001
APOE4 carriage status	-0.03 (-0.10, 0.04)	-0.82	0.41	-0.03 (-0.09, 0.03)	-1.08	0.28
Pathological status (A-T-)	-0.22 (-0.43, 0.00)	-1.99	0.05	-0.18 (-0.36, 0.00)	-2.04	0.046
Pathological status (A+T-)	-0.21 (-0.35, -0.07)	-3.02	0.004	-0.20 (-0.31, -0.08)	-3.4	0.001
Sex (Female)	-0.08 (-0.18, 0.02)	-1.54	0.13	-0.11 (-0.20, -0.03)	-2.71	0.009
Amyloid-PET	0.08 (-0.01, 0.16)	1.74	0.09	-0.05 (-0.12, 0.03)	-1.28	0.21
CSF p-tau$_{181}$	-0.01 (-0.14, 0.12)	-0.13	0.89	0.23 (0.12, 0.33)	4.41	<0.0001
Sex (Female) * Amyloid-PET * CSF p-tau$_{181}$	0.16 (0.05, 0.28)	2.88	0.006	0.14 (0.04, 0.23)	2.93	0.0049

Figure 2. ATP index is positively correlated with tau accumulation in Aβ+ females

Aβ+ females display positive associations between ATP index and tau accumulation at the 1-year follow-up assessment (ATP index$_{181}$: $P = 0.0026$, $R^2 = 0.577$; ATP index$_{217}$: $P = 0.01$, $R^2 = 0.455$) and 2-year follow-up assessment (ATP index$_{181}$: $P = 0.0007$, $R^2 = 0.735$; ATP index$_{217}$: $P = 0.0009$, $R^2 = 0.725$). Aβ+ males also show positive associations between ATP index and tau accumulation at the 2-year follow-up assessment (ATP index$_{181}$: $P = 0.04$, $R^2 = 0.33$; ATP index$_{217}$: $P = 0.0144$, $R^2 = 0.435$).

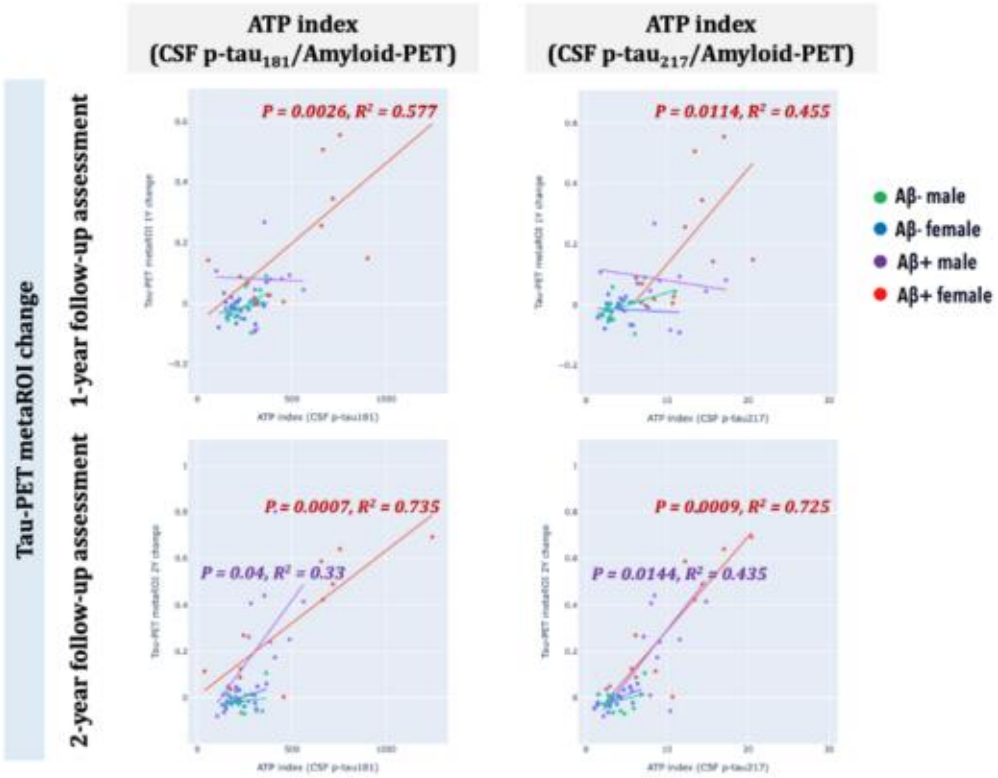

Keywords: Sex difference, Alzheimer's disease, Longitudinal tau progression, Tau phosphorylation

49 Comparison of visual interpretation and quantitation in detecting amyloid pathology using florbetapir F-18 PET imaging: Results from nuclear medicine physicians or radiologists practicing at community healthcare settings

Jian Wang[1], Ming Lu[1], Leonardo Iaccarino[1], Anupa Arora[1], Amanda Morris[1], Min Jung Kim[1], Ian Kennedy[1], Vikas Kotari[1], Samantha Burnham[1], Emily collins[1], Michael Pontecorvo[1]

[1]*Eli Lilly and Company, Indianapois, IN, United States*

Table 1.

Sample Demographics and Characteristics

	AV45-QP		AV45-A18		Overall	
	AB- (N=40)	AB+ (N=56)	AB- (N=222)	AB+ (N=383)	AB- (N=262)	AB+ (N=439)
Age (yr)						
Mean (SD)	77.2 (12.0)	76.7 (8.89)	71.4 (8.76)	73.6 (7.53)	72.3 (9.53)	74.0 (7.77)
Median [Min, Max]	78.0 [47.0, 103]	76.0 [55.0, 91.0]	73.0 [51.0, 91.0]	74.0 [50.0, 90.0]	73.0 [47.0, 103]	75.0 [50.0, 91.0]
Sex						
F	18 (45.0%)	30 (53.6%)	106 (47.7%)	193 (50.4%)	124 (47.3%)	223 (50.8%)
M	22 (55.0%)	26 (46.4%)	116 (52.3%)	190 (49.6%)	138 (52.7%)	216 (49.2%)
Race						
Black	3 (7.5%)	2 (3.6%)	1 (0.5%)	5 (1.3%)	4 (1.5%)	7 (1.6%)
White	37 (92.5%)	52 (92.9%)	150 (67.6%)	281 (73.4%)	187 (71.4%)	333 (75.9%)
Asian	0 (0%)	1 (1.8%)	1 (0.5%)	0 (0%)	1 (0.4%)	1 (0.2%)
Other	0 (0%)	0 (0%)	3 (1.4%)	0 (0%)	3 (1.1%)	0 (0%)
Missing	0 (0%)	1 (1.8%)	67 (30.2%)	97 (25.3%)	67 (25.6%)	98 (22.3%)
Ethnicity						
Hispanic or Latino	1 (2.5%)	3 (5.4%)	9 (4.1%)	21 (5.5%)	10 (3.8%)	24 (5.5%)
Not Hispanic or Latino	39 (97.5%)	53 (94.6%)	146 (65.8%)	265 (69.2%)	185 (70.6%)	318 (72.4%)
Missing	0 (0%)	0 (0%)	67 (30.2%)	97 (25.3%)	67 (25.6%)	97 (22.1%)
ApoE4 Status						
Carrier	1 (2.5%)	19 (33.9%)	0 (0%)	0 (0%)	1 (0.4%)	19 (4.3%)
Non-carrier	15 (37.5%)	7 (12.5%)	0 (0%)	0 (0%)	15 (5.7%)	7 (1.6%)
Missing	24 (60.0%)	30 (53.6%)	222 (100%)	383 (100%)	246 (93.9%)	413 (94.1%)
MMSE Score						
Mean (SD)	25.7 (6.21)	18.1 (8.48)	NA (NA)	NA (NA)	25.7 (6.21)	18.1 (8.48)
Median [Min, Max]	28.0 [0, 30.0]	19.0 [0, 29.0]	NA [NA, NA]	NA [NA, NA]	28.0 [0, 30.0]	19.0 [0, 29.0]
Missing	2 (5.0%)	15 (26.8%)	222 (100%)	383 (100%)	224 (85.5%)	398 (90.7%)
Centiloid						
Mean (SD)	6.90 (28.2)	80.1 (42.3)	-1.41 (22.4)	73.7 (36.2)	-0.143 (23.5)	74.5 (37.1)
Median [Min, Max]	1.23 [-41.8, 88.2]	75.5 [-10.4, 214]	-2.91 [-45.4, 88.9]	71.1 [-21.2, 215]	-1.52 [-45.4, 88.9]	72.5 [-21.2, 215]
Presentation Group						
NC	10 (25.0%)	1 (1.8%)	0 (0%)	0 (0%)	10 (3.8%)	1 (0.2%)
MCI	3 (7.5%)	1 (1.8%)	150 (67.6%)	185 (48.3%)	153 (58.4%)	186 (42.4%)
DEMENTIA	17 (42.5%)	53 (94.6%)	72 (32.4%)	198 (51.7%)	89 (34.0%)	251 (57.2%)
Missing	10 (25.0%)	1 (1.8%)	0 (0%)	0 (0%)	10 (3.8%)	1 (0.2%)

AV45-QP: NCT02107599 and NCT01946243; AV45-A18: NCT01703702; AB-: Amyloid negative by florbetapir PET visual assessment; AB+: Amyloid positive by florbetapir PET visual assessment; NC: Normal control; MCI: Mild cognitive impairment; MMSE Score: Mini-mental state examination total score

Figure 1. Study AV45-QP Distribution of Optimized Cutpoints in Centiloid

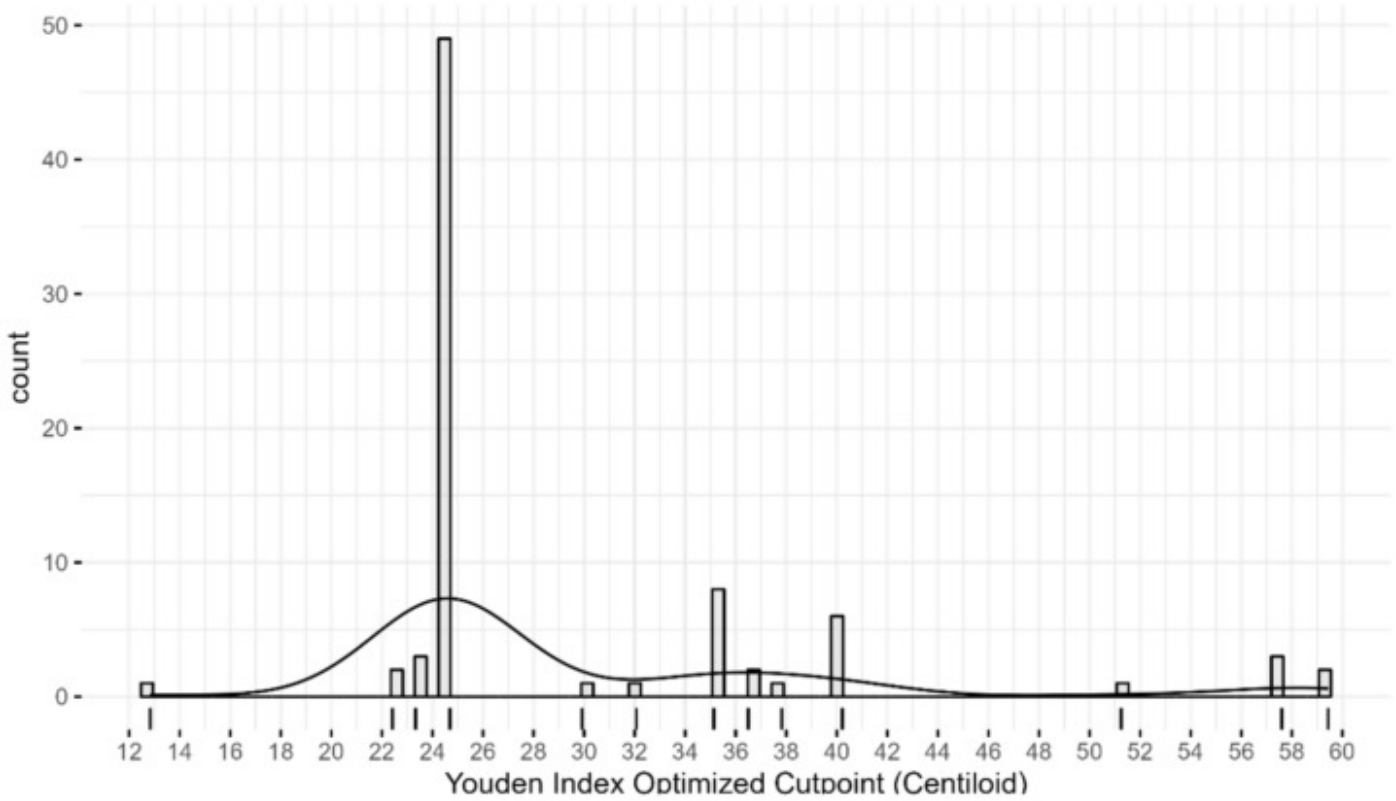

80 readers each visually read 96 scans in study AV45-QP. The read result (amyloid positive: AB+; amyloid negative: AB-) determined by each reader for each of the 96 scans was compared to a quantitative estimate of neuritic plaque density for that case. This comparison was done using the centiloid formula as shown by Navitsky et al. (2018). An Area Under the Curve (AUC) for Centiloid (CL) value vs visual read result was calculated for each reader. Youden's index was used to obtain the optimized quantitative threshold (cutpoint) value as centiloid that best matched the visual read result for each reader. The distribution of the cutpoints is plotted.

Table 2. Performance of Visual Interpretation and Quantitation Concordance

AV45-QP	Reader Level Summary Result
	96 scans each read by 80 readers
Optimal Cutpoint (Centiloid)	
Mean (SD)	29.7 (9.66)
Median [Min, Max]	24.7 [12.8, 59.4]
AUC	
Mean (SD)	0.893 (0.0354)
Median [Min, Max]	0.896 [0.759, 0.954]
Accuracy (%)	
Mean (SD)	86.0 (3.44)
Median [Min, Max]	86.5 [76.0, 92.7]
PPA (%)	
Mean (SD)	88.9 (5.77)
Median [Min, Max]	89.8 [71.2, 98.0]
NPA (%)	
Mean (SD)	83.4 (7.28)
Median [Min, Max]	84.0 [64.8, 100]
Cohen's Kappa	
Mean (SD)	0.708 (0.0710)
Median [Min, Max]	0.724 [0.527, 0.845]
AV45-A18	**Across Different Reader Result**
	605 scans read by 96 readers
Optimal Cutpoint (Centiloid)	31.7
AUC	0.97
Accuracy (%)	91.9
PPA (%)	90.86
NPA (%)	93.69
Cohen's Kappa	0.83

AV45-QP: NCT02107599 and NCT01946243; AV45-A18: NCT01703702; AUC: Area under the curve;

PPA: Positive percent agreement; NPA: Negative percent agreement

Background: Accurate detection of brain beta-amyloid plaque accumulation is critical for diagnosing Alzheimer's disease. In clinical trials employing florbetapir F-18 PET imaging to identify amyloid positive patients, the standard approach involves centralized visual interpretation and/or quantitation. However, in community healthcare settings, the conventional protocol relies on visual interpretation by local nuclear medicine physicians or radiologists (community readers). To investigate the relationship between florbetapir PET visual interpretation and quantitation, we analyzed data from two studies that employed community readers with limited experience in reading scans in their regular practice.

Methods: We obtained 701 florbetapir scans from AV45-QP (80 readers, 96 scans) and AV45-A18 (96 readers, 605 scans), and determined Youden-based Centiloid (CL) cut points (CP). Classification and agreement metrics, including area under ROC curve (AUC), accuracy, positive and negative percent agreements (PPA, NPA), and Cohen's Kappa were calculated.

Results: Sample demographics and characteristics are presented in Table 1. Figure 1 displays the distribution of CP from AV45-QP, with 49 of 80 readers having CP values between 24 and 25 CL, and most of the remaining readers having CP values between 20 and 40 CL. Readers with CP values beyond 20 and 40 CL range had minimal prior experience and below-average reading accuracy compared with pathology results. Table 2 illustrates performance at reader level (AV45-QP, median AUC 0.896, median Cohen's Kappa 0.724, median CP 24.7 CL) and across different readers (AV45-A18, AUC 0.97, Cohen's Kappa 0.83, CP 31.7 CL).

Conclusions: These results demonstrate a high concordance between quantitation and visual interpretation by community readers for florbetapir PET scans, both at the individual and across reader levels. The optimal CP ranges from a median of 24.7 CL (AV45-QP) to 31.7 CL (AV45-A18), aligning with estimates of CP in the literature that typically indicate clear amyloid positivity above 30 and clear negativity below 20.

Keywords: florbetapir, visual interpretation, quantitation, centiloid cutpoint, community readers

50 Parental history of memory impairment predicts β-amyloid burden and positivity in a preclinical population

Mabel Seto[1,2,3,6], Timothy Hohman[6], Elizabeth Mormino[7], Kathryn Papp[1,2,3], Rebecca Amariglio[1,2,3], Dorene Rentz[1,2,3], Keith Johnson[1,2,3,5], Aaron Schultz[1,4], Reisa Sperling[1,2,3], Rachel Buckley[1,2,3], Hyun-Sik Yang[1,2,3]

[1]*Harvard Aging Brain Study, Department of Neurology, Massachusetts General Hospital, Boston, MA, United States*
[2]*Center for Alzheimer Research and Treatment, Department of Neurology, Brigham and Women's Hospital, Boston, MA, United States*
[3]*Harvard Medical School, Boston, MA, United States*
[4]*Athinoula A. Martinos Center for Biomedical Imaging, Department of Radiology, Massachusetts General Hospital, Charlestown, MA, United States*
[5]*Department of Radiology, Massachusetts General Hospital, Boston, MA, United States*
[6]*Vanderbilt Memory and Alzheimer's Center, Vanderbilt University Medical Center, Nashville, TN, United States*
[7]*Department of Neurology and Neurological Sciences, Stanford University, Stanford, CA, United States*

Background: Alzheimer's disease (AD) is highly heritable, and previous studies suggest that a maternal history of AD confers a greater risk for AD than paternal history. The impact of parental history of dementia on AD endophenotypes among cognitively unimpaired individuals is not fully described. We examine the effects of parental history of dementia on brain amyloid levels and both subjective and objective measures of cognition.

Method: Measures of objective and subjective cognition (Preclinical Alzheimer's Cognitive Composite; Cognitive Function Index), *APOE*-ε4 genotype, β-amyloid (Aβ) PET, and self-reported parental history of memory impairment and AD dementia were obtained from 4,413 cognitively unimpaired individuals screening for the Anti-Amyloid Treatment in Asymptomatic Alzheimer's (A4) study (mean(SD); age=71.3(4.7), %male=40.7, %Non-Hispanic White=91.2). Aβ was measured with ^{18}F-florbetapir-PET using a mean neocortical composite referenced to whole cerebellum. Linear regression models assessed the association between parental history with cross-sectional cortical Aβ levels and cognition covarying for the participant's age, sex, and years of education where relevant.

Results: Parental history of memory impairment (one or both parents) was significantly associated with elevated neocortical Aβ ($p<0.001$). The association between Aβ and history in both parents remained significant when covarying for *APOE*-ε4 allele count ($p=0.002$). Mean amyloid levels were elevated in individuals with history in both parents (n=455, $p<0.001$) and in those with only maternal history (n=1772, $p<0.001$), compared to those with only paternal history (n=632) or no family history (n=1554). Regression models confirmed this finding: $\beta=0.03$, $p<0.001$ in individuals with maternal history, $\beta=0.01$, $p=0.1$ in individuals with paternal history. No associations with subjective or objective cognition were observed.

Conclusion: We confirm that self-reported parental history of dementia is associated with elevated brain amyloid independently of *APOE*-ε4 status in the A4 Study, with evidence that maternal history has a stronger impact on Aβ burden among asymptomatic older individuals.

Keywords: family history, PET, cognition, A4

51 A head-to-head comparison between plasma p-tau217 and tau-PET for predicting future cognitive decline among cognitively unimpaired individuals

Rik Ossenkoppele[1,2,3], Gemma Salvado[1], Alexa Pichet-Binette[1], Joseph Therriault[4,5], Erin Jonaitis[6,7], Pierrick Bourgeat[11], Vincent Doré[12,13], Colin Masters[15], Sterling Johnson[6,7], Sylvia Villeneuve[15,16], Pedro Rosa-Neto[4,5], Chistopher Rowe[13,14], Oskar Hansson[1,8]

[1]*Clinical Memory Research Unit, Department of Clinical Sciences in Malmö, Lund University, Lund, Sweden., Lund, Sweden*
[2]*Alzheimer Center Amsterdam, Neurology, Vrije Universiteit Amsterdam, Amsterdam UMC location VUmc, Amsterdam, The Netherlands., Amsterdam, The Netherlands*
[3]*Amsterdam Neuroscience, Neurodegeneration, Amsterdam, The Netherlands., Amsterdam, The Netherlands*
[4]*Translational Neuroimaging Laboratory, McGill Research Centre for Studies in Aging, Montreal, Quebec, Canada., Montreal, Canada*
[5]*Department of Neurology and Neurosurgery, Faculty of Medicine, McGill University, Montreal, Quebec, Canada., Montreal, Canada*
[6]*Wisconsin Alzheimer's Institute, School of Medicine and Public Health, University of Wisconsin-Madison, Madison., Wisconsin, United States*
[7]*Wisconsin Alzheimer's Disease Research Center, School of Medicine and Public Health, University of Wisconsin-Madison, Madison., Wisconsin, United States*
[8]*Memory Clinic, Skåne University Hospital, Malmö, Sweden., Malmö, Sweden*
[9]*Department of Neurology, Skåne University Hospital, Lund University, Lund, Sweden, Lund, Sweden*
[10]*Wallenberg Center for Molecular Medicine, Lund University, Lund, Sweden., Lund, Sweden*
[11]*CSIRO, Health & Biosecurity Flagship, The Australian eHealth Research Centre, Brisbane, Queensland, Australia, Brisbane, Australia*
[12]*Australian eHealth Research Centre, CSIRO, Melbourne, Victoria, Australia., Melbourne, Australia*
[13]*Department of Molecular Imaging & Therapy, Austin Health, Heidelberg, Victoria, Australia., Heidelberg, Australia*
[14]*The Florey Institute of Neuroscience and Mental Health, The University of Melbourne, Parkville, Victoria, Australia., Melbourne, Australia*
[15]*Douglas Mental Health University Institute, Centre for Studies on the Prevention of Alzheimer's Disease (StoP-AD), Montreal, Quebec, Canada., Montreal, Canada*
[16]*Department of Psychiatry, McGill University, Montreal, Quebec, Canada., Montreal, Canada*

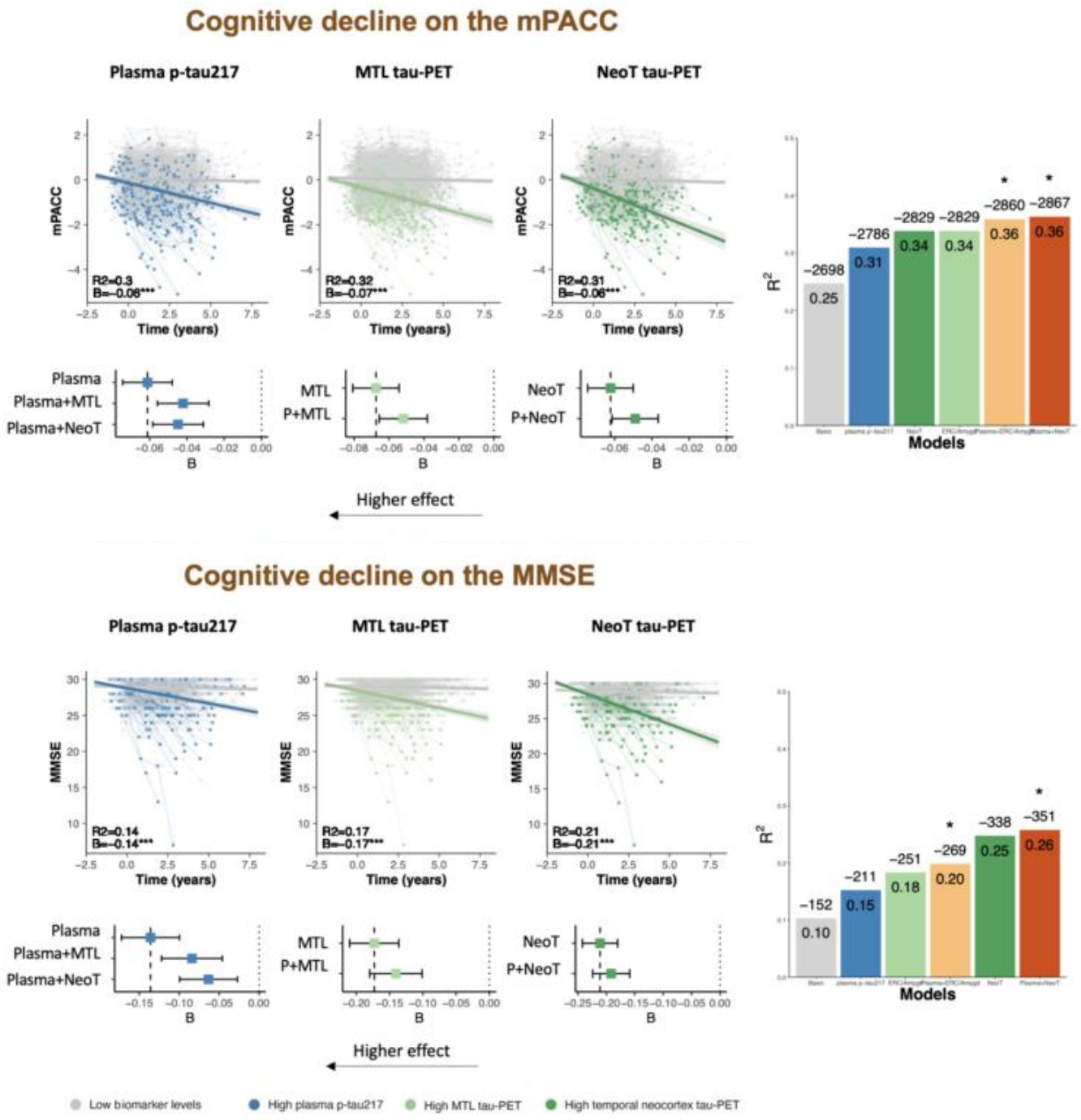

Objectives: An accurate prediction of Alzheimer's disease (AD) progression is important for patient management and optimization of participant selection for trials. Here, we compared and combined plasma p-tau217 and tau-PET measures for predicting longitudinal cognitive decline and clinical progression in cognitively unimpaired participants.

Methods: We included 1132 participants from seven independent cohorts (AiBL, BioFINDER-1, BioFINDER-2, TRIAD, ADC, PREVENT-AD and WRAP) with available plasma p-tau217 and tau-PET measures (measured less than one-year apart), being either amyloid-positive or amyloid-negative. Biomarker and cognitive data were z-scored by cohort using cognitively unimpaired CSF/PET amyloid-negative participants as reference for a unified analysis. We performed linear mixed models (for predicting cognitive decline on the mPACC and MMSE) and Cox-proportional hazards models (to assess progression to MCI or dementia), testing among both amyloid-negative and amyloid-positive individuals. We entered baseline plasma p-tau217, and tau-PET uptake in the medial

temporal lobe (MTL) or in the temporal neocortex individually, and also performed combined plasma/PET models. Age, sex, years of education and cohort were used as covariates.

Results: All individual tau biomarkers significantly predicted cognitive decline for both mPACC ($R^2_{p\text{-}tau217}$=0.27, $R^2_{MTL\text{-}tau}$=0.31, $R^2_{neotemporal\text{-}tau}$=0.28, Figure-1) and MMSE ($R^2_{p\text{-}tau217}$=0.12, $R^2_{MTL\text{-}tau}$=0.16, $R^2_{neotemporal\text{-}tau}$=0.19, Figure-2). The best model for predicting mPACC change included plasma p-tau217 and MTL tau-uptake (R^2=0.32, $p_{comparison}$<0.001), while for MMSE change included plasma p-tau217 and tau-uptake in the temporal neocortex (R^2=0.20, $p_{comparison}$≤0.007). Progression to MCI or dementia was also best predicted when including both plasma p-tau217 (HR[95%CI]=1.29[1.14,1.47], p<0.001) and MTL tau-uptake (HR[95%CI]=1.39[1.25,1.54], p<0.001, c-index=0.83). Analyses by individual cohorts showed similar trends.

Conclusions: Our data suggest that plasma p-tau217 is a suitable screening method for clinical trials in CU populations given its logistic advantages. In scenarios where a more refined prediction of cognitive decline is mandated, Tau-PET (preferably in a combined algorithm with plasma p-tau217) would be the methodology of choice.

Keywords: Tau PET, plasma p-tau, cognition, progression, cognitively unimpaired

52 Comparison of amyloid PET and plasma biomarkers in predicting future memory decline among cognitively normal individuals

Murat Bilgel[1], Yang An[1], Keenan Walker[1], Abhay Moghekar[2], Nicholas Ashton[3,4,5,6], Przemysław Kac[3], Thomas Karikari[3], Kaj Blennow[3,7], Henrik Zetterberg[3,7,8,9,10,11], Madhav Thambisetty[1], Susan Resnick[1]

[1]*Laboratory of Behavioral Neuroscience, National Institute on Aging, Baltimore, MD, United States*
[2]*Department of Neurology, Johns Hopkins University School of Medicine, Baltimore, MD, United States*
[3]*Department of Psychiatry and Neurochemistry, Institute of Neuroscience and Physiology, The Sahlgrenska Academy, University of Gothenburg, Mölndal, Sweden*
[4]*King's College London, Institute of Psychiatry, Psychology and Neuroscience, Maurice Wohl Clinical Neuroscience Institute, London, United Kingdom*
[5]*NIHR Biomedical Research Centre for Mental Health and Biomedical Research, Unit for Dementia at South London and Maudsley, NHS Foundation, London, United Kingdom*
[6]*Centre for Age-Related Medicine, Stavanger University Hospital, Stavanger, NO*
[7]*Clinical Neurochemistry Laboratory, Sahlgrenska University Hospital, Mölndal, Sweden*
[8]*Department of Neurodegenerative Disease, UCL Institute of Neurology, London, United Kingdom*
[9]*UK Dementia Research Institute at UCL, London, United Kingdom*
[10]*Hong Kong Center for Neurodegenerative Diseases, Clear Water Bay, HK*
[11]*Wisconsin Alzheimer's Disease Research Center, University of Wisconsin School of Medicine and Public Health, University of Wisconsin-Madison, Madison, WI, United States*

We examined whether amyloid PET or plasma biomarkers are better predictors of prospective longitudinal memory change among cognitively normal individuals.

We analyzed data collected over a mean of 6 years (764 visits) for 178 Baltimore Longitudinal Study of Aging participants who were cognitively normal at baseline (Table 1). Using cognitive data concurrent with and following baseline PET scan but excluding the last visit per participant, we modeled longitudinal memory score (mean of California Verbal Learning Test immediate and delayed recall *z*-scores) using a linear mixed effects model that included baseline age, age^2, sex, race, education, intracranial volume-adjusted bilateral hippocampal volume, baseline PET or plasma variable of interest, time from baseline, and interactions with time as independent variables. Each variable of interest (mean cortical PiB DVR; Quanterix Simoa plasma $A\beta_{42}/A\beta_{40}$, GFAP, NfL; U. Gothenburg Simoa plasma p-tau181 and p-tau231) was examined using a separate model. For plasma biomarkers, we additionally covaried for eGFR at baseline. Variables were *z*-scored using means and standard deviations calculated using the visit closest to age 70 per participant, enabling the computation of effect sizes that can be compared across variables. Using the fitted models, we predicted the memory score at the last visit and calculated the root mean square error.

For the term reflecting the association of the variable of interest with longitudinal change in memory, the variables with the greatest standardized effect sizes were PiB DVR and plasma $A\beta_{42}/A\beta_{40}$, with PiB DVR effect having a smaller standard error (Table 2 and Figure). PiB DVR yielded the lowest root mean square prediction error (0.74 vs. 0.766–0.781 for the plasma biomarkers).

These results suggest that among cognitively normal individuals, amyloid PET captures the magnitude of memory decline better than most plasma protein concentrations and allows for a more accurate prediction of future memory performance.

Table 1. Participant characteristics at baseline. Continuous variables are reported as median and interquartile range.

Characteristic	N = 176
Age (yr)	75 (69, 82)
Female	84 (48%)
Non-White	39 (22%)
Education (yr)	18 (16, 18)
ICV-adj. hippocampal volume (cm^3)	-0.22 (-0.70, 0.11)
Mean cortical PiB DVR	1.01 (0.99, 1.08)
$A\beta_{42}/A\beta_{40}$	0.050 (0.045, 0.055)
GFAP (pg/mL)	179 (131, 247)
NfL (pg/mL)	22 (17, 30)
p-tau181 (pg/mL)	7 (5, 11)
p-tau231 (pg/mL)	17 (13, 23)
eGFR (mL/min/1.73 m^2)	74 (63, 86)
Number of visits	4 (2, 6)
Duration of follow-up (yr)	6.1 (3.7, 8.9)

Table 2. Effect sizes for the terms reflecting the association of the *z*-scored variable with longitudinal change in memory. $A\beta_{42}/A\beta_{40}$ was negated to facilitate comparison.

Variable	Effect size	Standard Error	*p*-value
Mean cortical PiB DVR	-0.041	0.0069	4×10^{-9}
- $A\beta_{42}/A\beta_{40}$	-0.045	0.012	0.0001
GFAP	-0.026	0.0087	0.003
NfL	-0.0064	0.012	0.6
p-tau181	-0.028	0.0098	0.005
p-tau231	-0.025	0.0083	0.003

Figure. Estimated longitudinal memory trajectories from linear mixed effects models. Plots show the estimated trajectories for $z = \pm 1$ for each variable (i.e., one standard deviation above or below the mean) along with 95% confidence intervals. $A\beta_{42}/A\beta_{40}$ was negated to facilitate comparison.

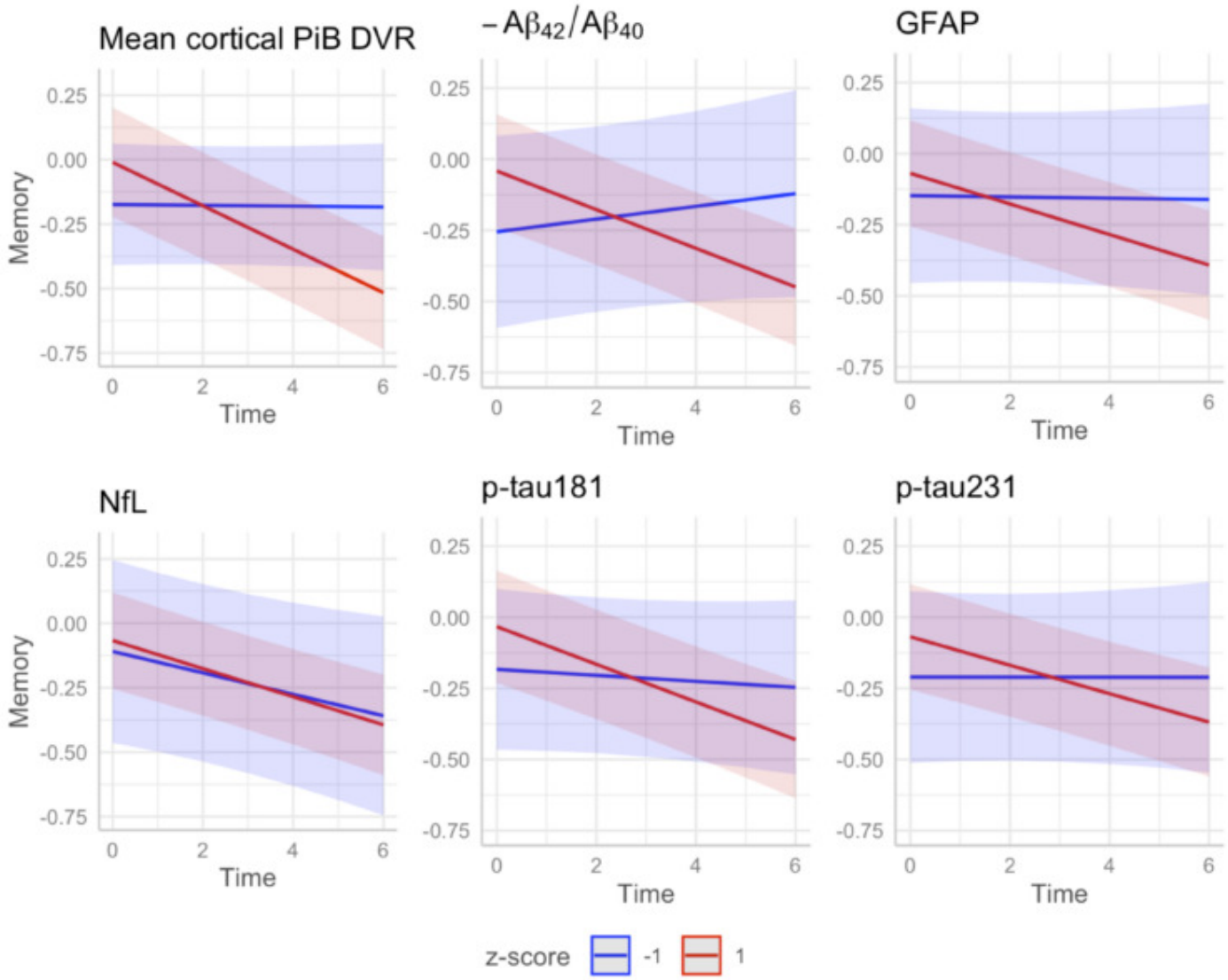

Keywords: Plasma, PiB, memory, cognitively normal, longitudinal

53 Confocal microscopy assessment of flortaucipir binding by a fluorescence analog compound T726 shows 4RT overlap in frontotemporal lobar degeneration

Rodolfo Gatto[1], Hossam Youssef[1], R. Ross Reichard[2], Jennifer Whitwell[3], Keith Josephs[1]

[1]*Department of Neurology, Mayo Clinic, Rochester, MN, United States*
[2]*Department of Laboratory Medicine and Pathology, Mayo Clinic, Rochester, MN, United States*
[3]*Department of Radiology, Mayo Clinic, Rochester, MN, United States*

Introduction: Flortaucipir was initially developed to measure in vivo tau burden in Alzheimer's disease (AD). In FTLD, however, significant intra and inter-subject variability and off-target binding have made interpretation difficult. Flortaucipir has a high affinity to the phosphorylated paired helical filaments (PHFs) of AD, but whether and how much uptake matches tau filaments and isoforms that define FTLD, remains unclear.

Objective: This study aims to use a fluorescence analog of flortaucipir to determine the degree to which flortaucipir binds to non-AD tau in FTLD.

Materials And Methods: We analyzed paraffin-embedded brain tissue from nine cases including one normal control, three with AD with low, intermediate, and high AD neuropathologic changes (LL, IL, and HL-AD, respectively), and five with FTLD-tau including two with progressive supranuclear palsy (PSP; 4RT), one with corticobasal degeneration (CBD; 4RT), one with globular glial tauopathy (GGT; 4RT), and one with Picks' disease (PiD; 3RT). Samples from the superior frontal and lateral temporal cortices, hippocampus, and basal ganglia were used for fluorescence staining. Each region was processed with TrueBlack Lipofuscin Autofluorescence Quencher (Biotium), and incubated with T726, a fluorescence analog of flortaucipir (Xia et al 2013; Wreng et al 2018). Samples were stained with beta-amyloid (BAM01; 6F/3D, Fisher), tau (PHF-1, Abcam), and 4RT (RD4, Millipore) antibodies. Imaging was completed by confocal microscopy (LSM 780, Zeiss).

Results: T726 showed significant overlap with PHF-1, but not with beta-amyloid, in the AD cases. Overlap was observed between T726 and 4RT in the PSP, CBD, and GGT cases with Pearson's colocalization coefficients in the superior frontal cortex of r= 0.62, 0.63, and 0.19 respectively. As expected, no 4RT was observed in PiD (r=0.045).

Conclusions: The findings suggest that a fraction of flortaucipir uptake observed in FTLD-tau may be due to the direct binding of the ligand to 4RT in FTLD.

Keywords: Frontotemporal Lobar Dementia, Flortaucipir, Confocal Microscopy, T726, 4RT

54 Correlative Histopathological evaluation of basal ganglia iron deposition and tau and PiB PET in Alzheimer's disease and frontotemporal lobar degeneration

Rodolfo Gatto[1], Arenn Carlos[1], R. Ross Reichard[2], Val Lowe[3], Jennifer Whitwell[3], Keith Josephs[1]

[1]*Department of Neurology, Mayo Clinic, Rochester, MN, United States*
[2]*Department of Laboratory Medicine and Pathology, Mayo Clinic, Rochester, MN, United States*
[3]*Department of Radiology, Mayo Clinic, Rochester, MN, United States*

Background: The role of iron in Alzheimer's disease (AD) and frontotemporal lobar degeneration (FTLD) has been the point of increasing debate. Relationships between iron and protein deposition in the basal ganglia in these diseases have not been fully elucidated.

Objective: The purpose of this study was to examine whether basal ganglia iron deposition is associated with beta-amyloid and tau burden measured by PET in AD and FTLD.

Material & Methods: Neuropathological samples were collected from two healthy controls, two cases with low and high AD neuropathologic changes (LL-AD and HL-AD respectively) and eight FTLD tauopathies, including progressive supranuclear palsy (PSP), corticobasal degeneration (CBD), Globular Glial Tauopathy (GGT), and Picks disease (PiD). All 12 cases had antemortem beta-amyloid (Pittsburgh Compound B) and tau (18F-flortaucipir) PET scans. The basal ganglia were stained for iron with Prussian blue (PB) and phosphorylated tau with AT8. Pathological burden was quantitated using digital pathology. Basal ganglia were subdivided into globus pallidum internus (GPi), globus pallidum externus (GPe), and putamen (Pu). Standardized uptake value ratios (SUVRs) from Tau-PET and PiB-PET in these regions were determined. Iron burden and PET SUVRs for each **(figure)** and all subregions were correlated.

Results: Basal ganglia SUVR from PiB-PET and Tau-PET were increased in HL-AD, but less in the FTLD cases compared to controls. Within the FTLD diagnoses, the greatest burden of basal ganglia iron was observed in PSP. For all basal ganglia regions combined (GPi + GPe + Pu) in the AD group, we found positive correlations between iron deposition and Tau-PET ($r=0.77$; $p < 0.0001$) and PiB-PET ($r= 0.38$; $p<0.01$). In FTLD, correlations for histopathological iron vs Tau-PET were ($r=0.58$; $p< 0.0001$) with PiB-PET ($r=0.53$; $p<0.0001$).

Conclusions: Our findings suggest that some PiB-PET and Tau-PET uptake in the basal ganglia in AD and FTLD may be related to iron deposition.

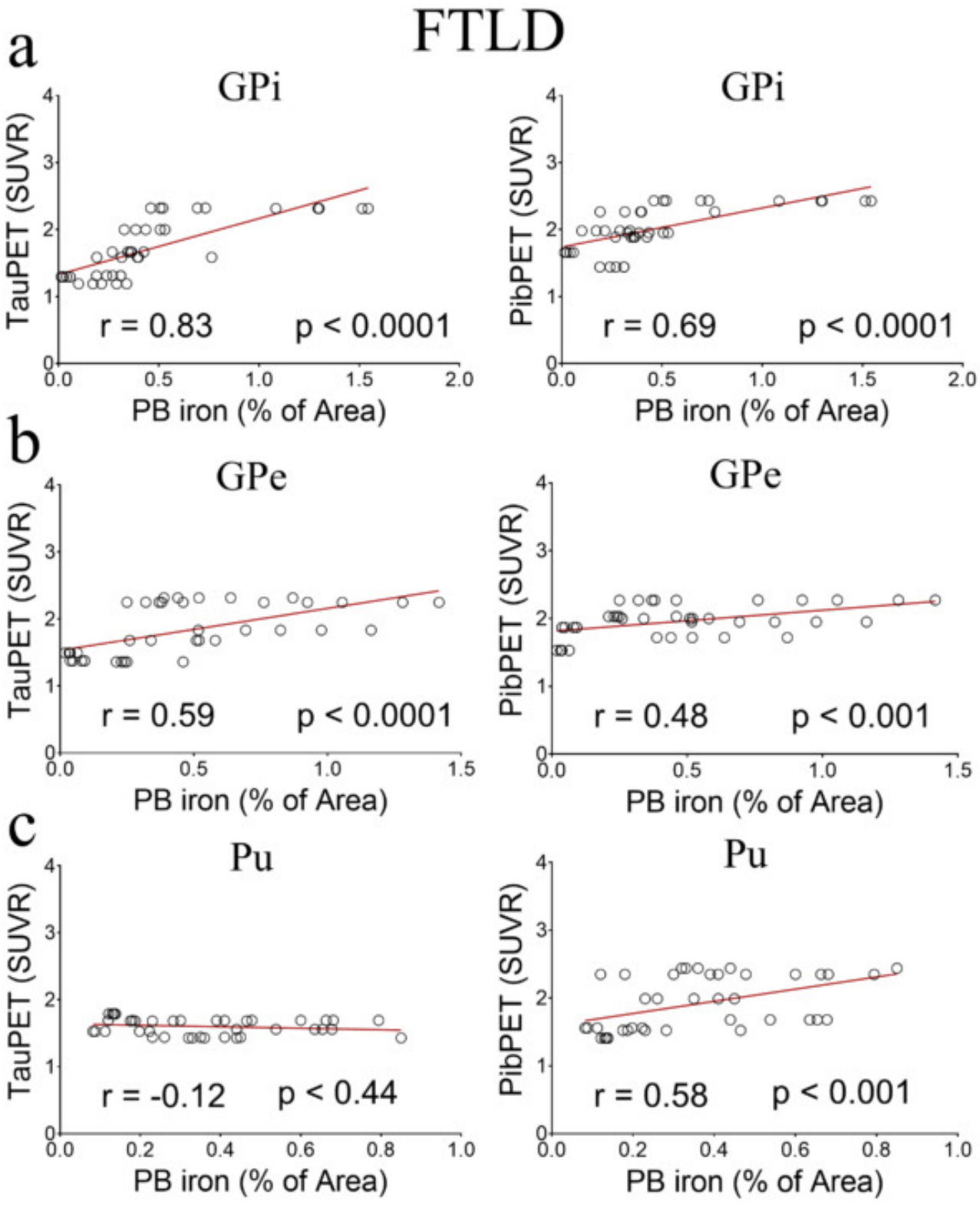

Keywords: Frontotemporal Lobar Degeneration, Tau-PET, PiB-PET, Iron Deposition, Basal Ganglia

55 Unraveling Alzheimer's disease heterogeneity: a comparative analysis using HYDRA AND CHIMERA

Zhaoqi An[1,2], Aristeidis Sotiras[1,2], Brian Gordon[1,2]

[1]*Mallinckrodt Institute of Radiology (MIR) at Washington University School of Medicine in St. Louis, St. Louis, MO, United States*
[2]*Devision of Computational and Data Sciences at Washington University in St. Louis, St. Louis, MO, United States*

Background: Alzheimer's Disease can present with heterogenous neurodegenerative patterns. In order to optimize clinical trials and personalized medicine, the identification and characterization of diverse pathological brain patterns associated with AD have become paramount. Optimal approaches to identify such heterogeneity are unknown.

Objective: The present study employed two distinct clustering approaches, namely HYDRA and CHIMERA, to delineate spatial patterns of brain atrophy attributable to AD. Methods were applied to MRI scans from the Open Access Series of Imaging Studies (OASIS-4) project.

Methods: HYDRA uses a convex polytope formed by multiple linear hyperplanes that correspond to various pathological patterns, capturing disease subtypes. CHIMERA assesses the pathological transition by transforming normal-control distribution to separate transformations matching the disease distribution. While both identify spatial patterns, the distinction lies in HYDRA's discriminative analysis of disease subtypes and CHIMERA's generative nature on disease progression through distribution matching.

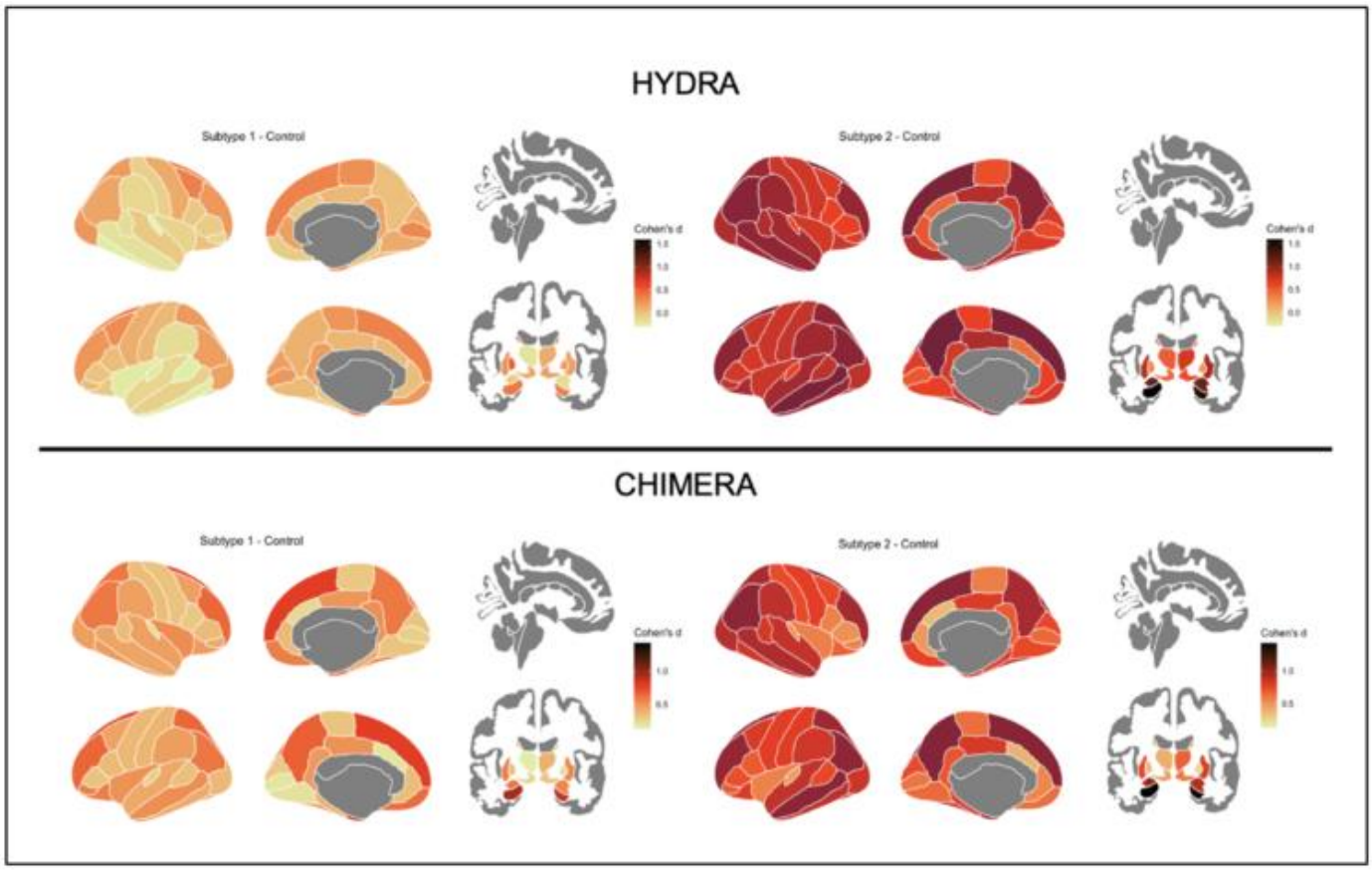

Figure 1.

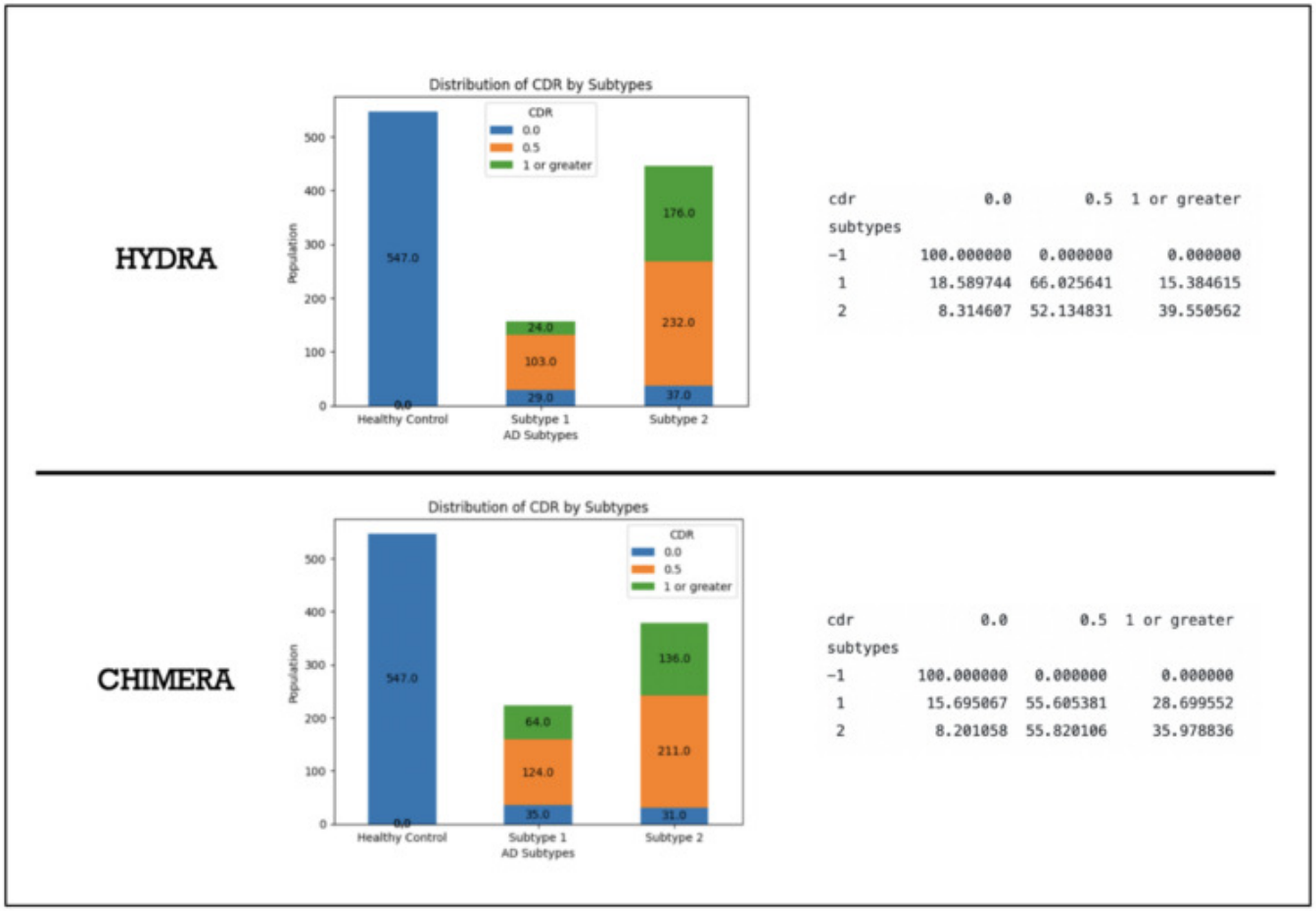

cdr	0.0	0.5	1 or greater
subtypes			
-1	100.000000	0.000000	0.000000
1	18.589744	66.025641	15.384615
2	8.314607	52.134831	39.550562

cdr	0.0	0.5	1 or greater
subtypes			
-1	100.000000	0.000000	0.000000
1	15.695067	55.605381	28.699552
2	8.201058	55.820106	35.978836

Figure 2.

Results: Both approaches identified two patterns, or subtypes (Figure 1) with similar CDR results (Figure 2). All subtypes demonstrate marked atrophy within the medial temporal areas, notably the hippocampus. Disparities are evident when assessing subtypes: Subtype-2 across both methods shows pronounced variations in regions such as superior frontal, middle temporal, parietal cortex, and precuneus, areas paramount in AD pathology. Conversely, HYDRA's Subtype-1 highlights subtle differences in temporal cortex relative to its Subtype-2. CHIMERA's Subtype-1, while mirroring its Subtype-2 pattern, is less intensified, suggesting an earlier AD stage. Collectively, these patterns concur with recognized AD neuropathological trajectories, pinpointing regions initially impacted in progression.

Conclusion: Our findings demonstrate data-driven approaches to derive clinically meaningful patterns of neurodegeneration. A parallel evaluation of both approaches accentuates the robustness of clustering techniques, revealing consistent and overlapping insights into the intricate pathological landscapes of AD. This convergence in findings bolsters confidence in the reliability of such analytical tools in AD research.

Keywords: Degenerative disorder, Alzheimer's Disease, Clustering, Classification

56 Prevalence of Alzheimer's disease pathology in studies of memory and aging

Nicole McKay[1], Peter Millar[1], Nicolas Barthelémy[1], Tammie Benzinger[1], John Morris[1], Randall Bateman[1], Suzanne Schindler[1], Brian Gordon[1]

[1]*Washington University School of Medicine, St. Louis, MO, United States*

Preclinical Alzheimer's disease (AD) describes a period prior to symptom onset during which pathology begins to accumulate. Recent development of neuroimaging and biofluid measures of AD pathology has allowed for *in vivo* quantification of preclinical pathological burden. Prior work estimated that by age 85, only one third of older adults remain free of amyloid and AD-related atrophy. Here, using complementary multimodal biomarkers of AD pathology, we aimed to reproduce and extend these estimates of preclinical AD prevalence in a cohort of cognitively unimpaired (Clinical Dementia Rating = 0) older adults (demographics in figure 1). We included neuroimaging derived measures of amyloid and neurodegeneration (cortical amyloid, cortical thickness, summary tau), as well as biofluid derived measures of non-specific AD pathology (amyloid42:40, phosphorylated-tau217, neurofilament light). Gaussian mixture modeling defined the probability of biomarker positivity, which we examined as a function of age (Figure 1). Our results reproduce and extend prior estimates of AD pathology in cognitively unimpaired older adults, confirming in our independent sample that AD pathology is present in cognitively unimpaired individuals. Cerebrospinal fluid-derived measures of amyloid peaked at a rate close to 60%, but all measures of amyloid and neurodegeneration were observed to rise to be present in at least 40% of cognitively unimpaired older adults. Unsurprisingly, tau was observed at the lowest rate, potentially reflecting its tight associated with cognitive impairment. It is important to note that cohorts examining sporadic AD recruit individuals with family histories of AD and therefore have higher rates than average populations of apolipoproteinvariant carriers, which may influence the rates of AD pathology. Nevertheless, characterizing the prevalence of preclinical AD is critical for understanding the pathophysiology of AD, may inform the design of clinical trials or interventions, and may also provide important context for furthering our understanding of cognition across older adulthood.

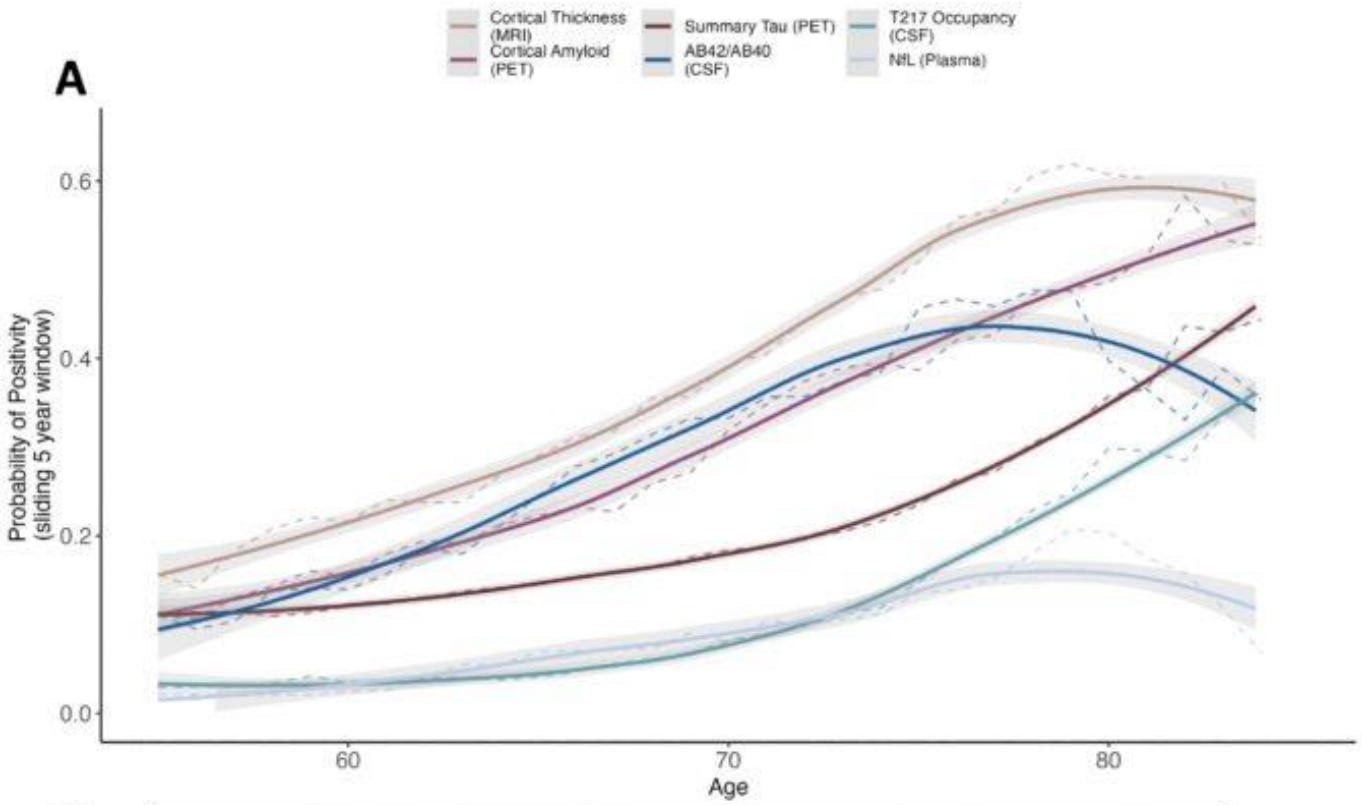

B

	Cortical Thickness (MRI)	Cortical Aβ (PET)	Summary Tau (PET)	Aβ42/Aβ40 (CSF)	Tau-217 Occupancy (CSF)	Neurofilament Light (Plasma)
n	2118	1202	630	1641	1544	1248
Age (SE)	70.56 (0.17)	69.28 (0.24)	70.45 (0.29)	68.96 (0.20)	68.75 (0.21)	68.81 (0.22)
Females (%)	1259 (66%)	756 (63%)	360 (57%)	954 (58%)	908 (59%)	727 (58%)
APOE-carriers (%)	1404 (34%)	392 (33%)	222 (35%)	559 (34%)	519 (34%)	426 (34%)
Positivity Value	2.37 (mm)	9.75 (Cent)	1.53 (SUVR)	0.07	0.10	24.04 pg/ml

Figure 1. Summary of Prevalence of Preclinical Alzheimer Disease Pathology in the Knight Alzheimer Disease Research Center Cohort. A: Prevalence plots representing the rates of amyloid and neurodegeneration related to preclinical Alzheimer disease in cognitively unimpaired (CDR = 0) older adults. **B:** A summary table showing demographics for each biomarker sample. Note, to maximize data points, all available samples were used for each independent biomarker. All individuals were aged between 50 and 90 years old. Positivity was determined using a Gaussian mixture modeling approach, where the cut-off represents the biomarker value where the probability of belonging to each distribution = 50%.

Keywords: preclinical, prevalence, CSF, MRI, PET

57 Depression in amyloid-positive individuals is associated with a faster rate of tau accumulation on longitudinal positron-emission tomography

Daniel Talmasov[1], Aubrey Johnson[1], Patrick Lao[1], Karen Marder[1], Jeffrey Miller[1]

[1]*Columbia University Medical Center, New York, NY, United States*

Background: Alzheimer's disease and depression are extremely common and highly comorbid. The mechanisms by which depression contributes to worsened outcomes in Alzheimer's disease dementia are poorly understood.

Methods: 355 participants in the Alzheimer's Disease Neuroimaging Initiative (ADNI) study had 2+ AV1451 scans, amyloid PET, and geriatric depression scale (GDS) scores taken between their first and last AV1451 scans. Of these, 214 participants were amyloid-positive and 141 were amyloid-negative. The yearly rate of tau accumulation (RTA) for each participant was modeled by fitting a regression line to all available measurements of AV1451 standardized uptake value ratios (SUVR) in the widely-used temporal meta-region of interest (ROI). Multivariable linear regression was used to model the effect of depressive symptoms (average GDS, log-transformed to account for skew inherent in the scale) on RTA. Explanatory models were ranked by Akaike's information criterion, comparing all possible models including variables GDS, amyloid status, APOE4 genotype, age, and sex.

Results: Higher GDS scores between scans were associated with higher RTA on univariable linear regression in all subjects (P = 0.01, ß = +3.28e-05 SUVR/year). The top explanatory model for RTA included factors for age (P < 0.001, ß = -3.53e-06), amyloid status (P<0.001, ß = +8.13e-05), and mean GDS score (P = 0.07, ß = +2.27e-05). Comparing amyloid-positive and amyloid-negative subjects in a multivariable model accounting for age and GDS score, GDS was associated with increased RTA in amyloid-positive (P = 0.03, ß = +4.1e-05 SUVR/year) but not amyloid-negative (P = 0.68) participants.

Conclusion: Depression is associated with higher rates of tau accumulation on longitudinal PET, an effect that appears to be specific to amyloid-positive individuals. These findings highlight a need for further studies to understand causal relationships and mechanisms underlying interactions between depression and the progression of Alzheimer's disease pathology.

Keywords: Depression, ADNI, Tau, AV1451, longitudinal

58 Chronic neuroinflammation in older adults with persistent Long COVID: the preliminary findings of [18F]FEPPA PET imaging

Min-Jeong Kim[1,2], Daniella Taboada[1], Yun-Hsin Liu[1], Jeremy Maciarz[1,3], Megan Armstrong[1,3], Nikhil Palekar[1,2], Sara Weisenbach[1,3]

[1]*Department of Psychiatry and Behavioral Health, Stony Brook University School of Medicine, Stony Brook, NY, United States*
[2]*Department of Neurology, Stony Brook University School of Medicine, Stony Brook, NY, United States*
[3]*McLean Hospital, Harvard Medical School, Belmont, MA, United States*

Introduction: After COVID-19 infection, approximately 5-30% of patients continue to have symptoms beyond four weeks ("Long COVID"). Persistent cognitive impairment and 'brain fog', chronic fatigue, and depression or anxiety are the most predominant symptoms. The underlying mechanism is unknown, but the most compelling hypothesis is the contribution of excessive neuroinflammation induced by a systemic inflammatory response or cytokine storm. We aimed to investigate the association between persistent Long COVID in older adults and neuroinflammation measured by [^{18}F]FEPPA PET targeting translocator protein (TSPO).

Methods: Older adults with persistent Long COVID for longer than six months (n=12) and healthy controls (n=6) were initially assessed with neuropsychiatric scales and cognitive testing batteries. [^{18}F]FEPPA PET scans were additionally obtained from three subjects with Long COVID (age 62-64 years, 3 females) and three controls (age 65-67 years, 2 females and 1 male) who had high-affinity binding to TSPO on genotype screening. After injection of [^{18}F]FEPPA, dynamic PET scans were acquired for 120 minutes with arterial blood sampling to measure input functions. Total distribution volume (V_T) was calculated using the two-tissue compartment model. The results were compared between the groups as well as with two other datasets of healthy individuals in the literature.

Results: Long COVID subjects showed a trend towards more depression, anxiety, fatigue, post-traumatic stress, sleep disturbance, and objective cognitive impairment than controls. The symptom duration of Long COVID varied from 8 months to 2 years. Long COVID subjects showed higher [^{18}F]FEPPA V_T in multiple brain regions compared to all different healthy control datasets, and the difference was even greater when compared to our own controls.

Conclusions: Older adults with persistent Long COVID showed a trend towards greater neuropsychiatric symptoms and cognitive impairment than controls. Our preliminary PET findings also suggest that persistent Long COVID in older adults will be associated with chronic neuroinflammation.

Keywords: COVID-19, Neuroinflammation, Aging, Neuropsychiatry, Cognitive impairment

59 PET staging of tauopathy using amygdala

Bernard Hanseeuw[1,2], Zoe Rubinstein[1], Aaron Schultz[1], Rachel Buckley[1], Michael Properzi[1], Michelle Farrell[1], Jennifer Gatchel[1], Rebecca Amariglio[1], Alexa Beiser[3], Sudha Seshadri[3], Gad Marshall[1], Reisa Sperling[1], Heidi Jacobs[1], Keith Johnson[1]

[1]*Mass General Brigham, Boston, MA, United States*
[2]*Cliniques Universitaires Saint-Luc, Brussels, Belgium*
[3]*Boston University, Boston, MA, United States*

Background: Previous tau-PET studies focused on entorhinal (tau-PET stage=1) or temporal neocortical regions (tau-PET stage≥3). Post-mortem studies define Braak-stage 2 as tau pathology in the medial temporal lobe, including hippocampus and amygdala, without neocortical tauopathy. Because most clinically normal (CN) older adults in tau-PET stage=1 do not progress rapidly, defining a tau-PET stage=2 may be critical for an early detection of progressive tauopathy. We investigated amygdala Flortaucipir data, as off-target binding blurs hippocampal signal.

Methods: ^{F18}-Flortaucipir tau-PET data were collected at Mass General Brigham (Boston, MA) in 590 CN individuals and 48MCI/AD patients. Gaussian mixture models defined thresholds for low (-) and high (+) tau-PET signal in three regions-of-interest: entorhinal cortex (EC), amygdala (AMYG), and inferior temporal (IT) neocortex. Tau-PET staging was proposed following the proportion of participants with positive signal in each region. Linear mixed-models with random intercept and slope predicted subsequent cognition (PACC5) with PET stages in CN. Similar models predicted subsequent neocortical tau accumulation in a subset of 167CN with longitudinal PET. Models were adjusted for age, sex, and education.

Results: Across the 638 participants, we observed 9.7% EC+ (n=62), 7.7% AMYG+ (n=49), 6.4% IT+ (n=41). Tau-PET staging classified 97.5% of participants, including 88.6% as stage=0 (EC-/AMYG-/IT-), 2.0% as stage=1 (EC+/AMYG-/IT-), 2.0% as stage=2 (EC+/AMYG+/IT-), and 4.9% as stage=3 (EC+/AMYG+/IT+). The proportion of MCI/AD and high-amyloid participants increased with stages (Table 1), with evidence that stage=2 individuals were mostly high-amyloid CN. In CN, higher tau-PET stages predicted faster cognitive decline, with stage=2 declining faster than stage=1 (p=0.05), and slower than stage=3 (p=0.03, Fig.1). Stage=2 CN also had faster neocortical tau accumulation than stage=0 individuals (p=0.04), with 50% stage=2 participants reaching stage=3 after an average three-year follow-up (Fig.2).

Conclusions: Amygdala tau-PET signal identifies clinically normal individuals at-risk for progressive tauopathy and cognitive decline before neocortical tauopathy is apparent.

Table 1: Characteristics of the participants

Mean value *(SD)*	All N=638	Stage 0 N=567	Stage 1 N=12	Stage 2 N=12	Stage 3 N=31	Two-tail p-value
Age at tau-PET Years	64.6 *(12.9)*	63.5 *(12.8)*	75.3* *(13.8)*	76.8* *(8.1)*	69.1* *(8.9)*	<0.001
Education Years	16.3 *(2.8)*	16.3 *(2.8)*	15.9 *(3.0)*	17.3 *(2.2)*	16.3 *(2.1)*	0.83
Female (%)	54.0%	55.2%	41.7%	66.7%	46.2%	0.21
E4 carriers (%)	25.7%	22.2%	8.3%	75.0%**	67.7%**	<0.001
% Clinically Impaired	7.5%	3.3%	8.3%	16.7%*	67.4%***	<0.001
% High-PiB individuals	19.8%	13.1%	16.7%	75.0%**	96.7%***	<0.001
Annual PACC5 change z-score/year	-0.06 *(0.10)*	-0.05 *(0.08)*	-0.08* *(0.09)*	-0.15** *(0.11)*	-0.23*** *(0.21)*	<0.001
Annual IT FTP change SUVr/year	0.009 *(0.011)*	0.007 *(0.007)*	0.015 *(0.009)*	0.017* *(0.009)*	0.041* *(0.012)*	<0.001
Cognitive Follow-up Years	6.3 *(4.0)*	6.3 *(4.0)*	5.9 *(4.1)*	5.0 *(3.5)*	7.3 *(4.4)*	0.30
PET Follow-up Years	3.6 *(1.5)*	3.7 *(1.5)*	3.4 *(0.6)*	2.5 *(0.4)*	2.7 *(1.4)*	0.17

* Significant difference versus Stage 0 (two-tail p<0.05 in post-hoc test comparing stages).
** Significant difference versus Stage 1 and 0 (two-tail p<0.05 in post-hoc test).
*** Significant difference versus Stage 2, 1, and 0 (two-tail p<0.05 in post-hoc test).
The four last lines are provided for CN only. These data are illustrated on Fig.1 and Fig.2

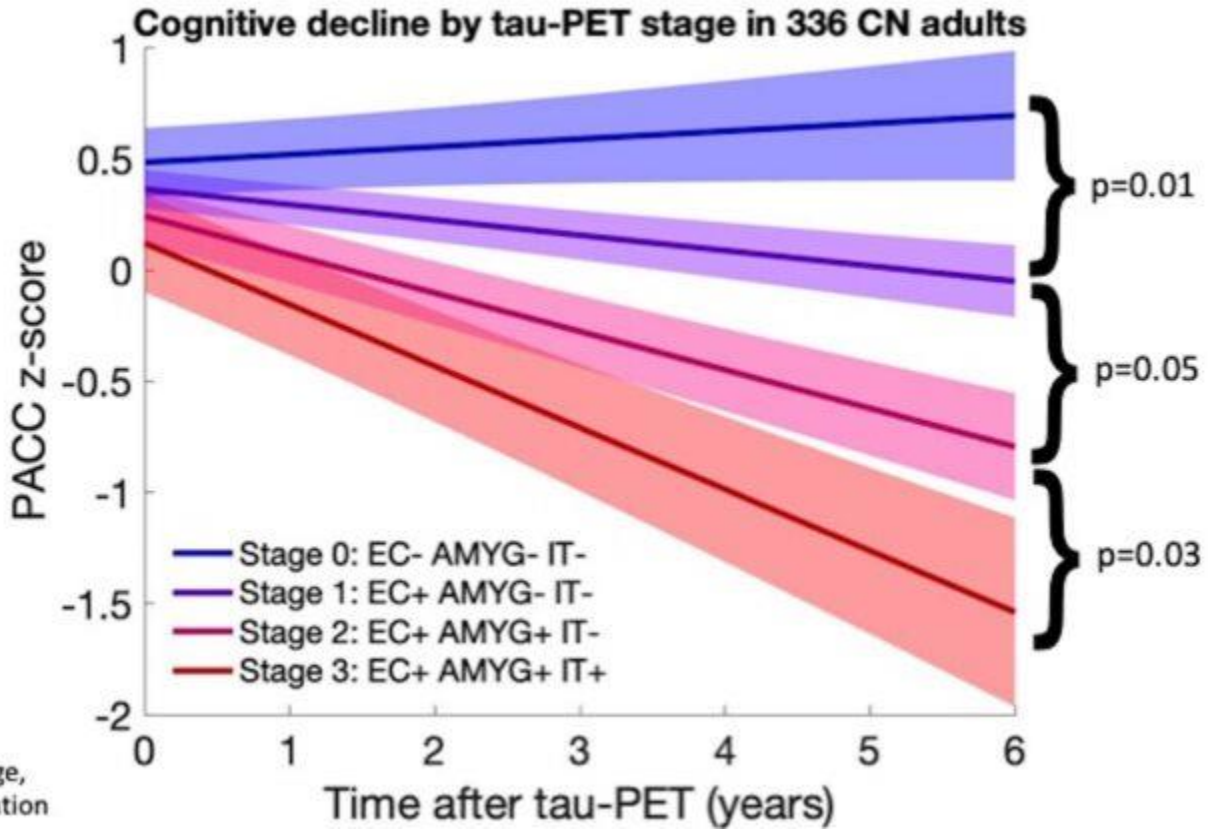

adjusted for age, sex, and education

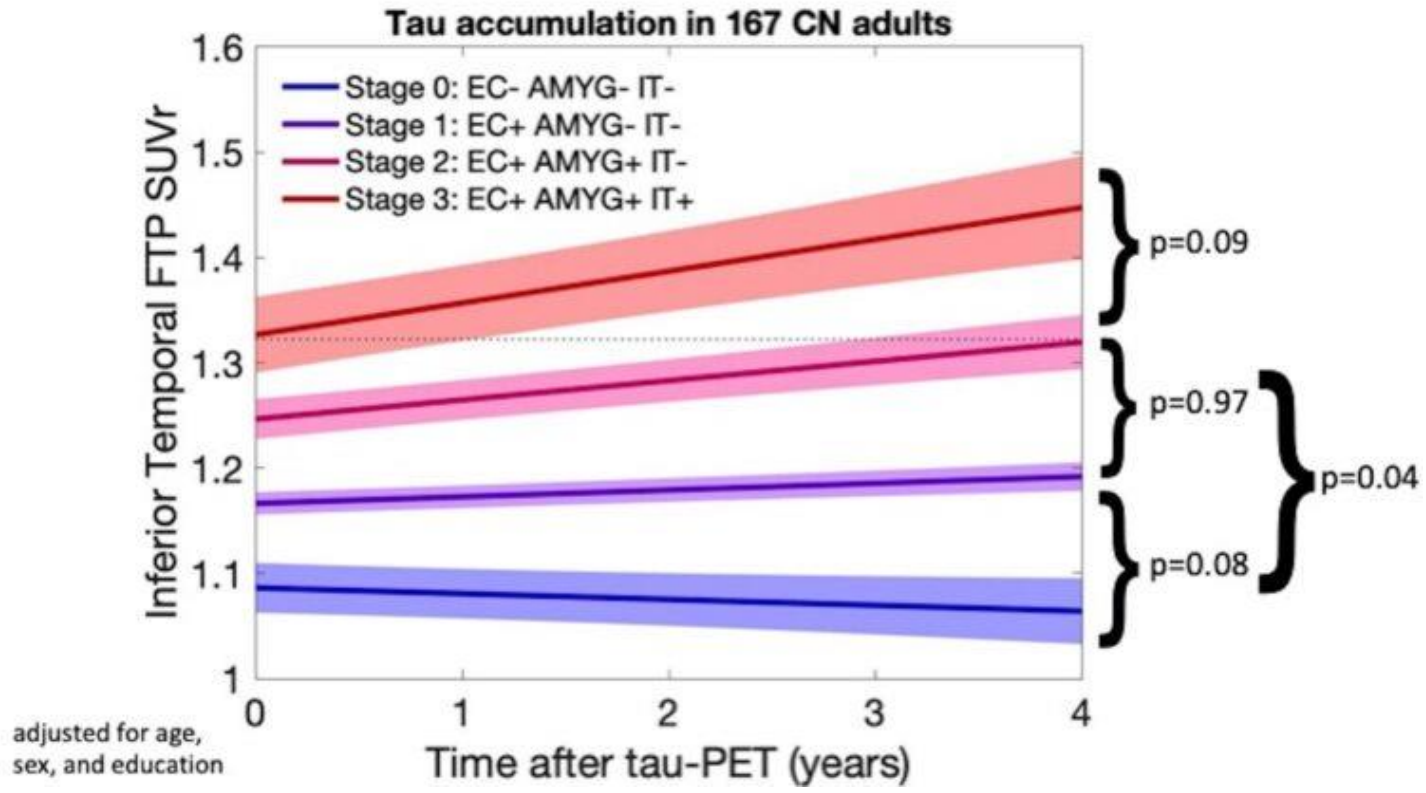

Keywords: Amygdala, tau-PET, Braak staging, cognitive decline

60 Discovery and optimization of [18F]ACI-15916, a promising PET tracer for the diagnosis of Parkinson's disease and other a-synucleinopathies

Efthymia Vokali[1], Jérôme Molette[1], Myriam Ravache[1], Christophe Delgado[1], Jacqueline Kocher[1], Laure Pittet[1], Coralie Vallet[1], Ruth Luthi-Carter[1], Andrea Pfeifer[1], Marie Kosco-Vilbois[1], Francesca Capotosti[1]

[1]*AC Immune SA, EPFL Innovation Park, Building B, 1015, Lausanne, CH*

Background: Progressive accumulation of a-synuclein (a-syn) inclusions is a hallmark of Parkinson's disease (PD) and other synucleinopathies that correlates with clinical manifestations. Imaging a-syn pathology in the brain using a PET tracer would transform diagnosis, patient recruitment and monitoring of therapeutic efficacy in clinical trials targeting a-syn.

Methods: Building on the discovery of ACI-12589, i.e., the first tracer detecting a-syn inclusions in patients, using our proprietary Morphomer® library of conformation-specific, brain-penetrant molecules, new compounds were identified with higher-affinity for pathological a-syn and displaying selectivity versus frequent co-pathologies. Affinity and target engagement were assessed using radiobinding and autoradiography on PD brain samples. The same techniques were used on AD brain samples to evaluate selectivity. Selected compounds were 18F-radiolabeled to determine brain pharmacokinetic (PK) properties in non-human primates (NHP).

Results: The newly identified ligand, ACI-15916, displayed significantly improved target occupancy on a-syn aggregates in brain samples from PD and other a-synucleinopathy cases in comparison to ACI-12589. Interestingly, ACI-15916 also detected smaller a-syn inclusions. ACI-15916 retained selectivity over Abeta and pathological Tau and demonstrated no off-target interactions, for example, no binding to MAO-A/B. Importantly, [^{18}F]ACI-15916 entered rapidly the brain of NHP and showed homogenous distribution, with fast and complete washout.

Conclusions: A promising new compound with improved binding properties, ACI-15916, has been identified. [^{18}F]ACI-15916 displays significantly higher specific binding to a-syn aggregates than [^{18}F]ACI-12589, while maintaining excellent selectivity and PK profiles. [^{18}F]ACI-15916 has the potential to detect a-syn pathology in brains of patients with synucleinopathies, including PD, and is being developed to enter soon the First-in-Human study

---

Keywords: a-synuclein, PET tracer, Parkinson's disease, a-synucleinopathies, biomarkers

61 Clinical relevance of visually positive amyloid-PET burden in the occipital lobe

Lyduine Collij[1,2], Ruben Smith[1], Sebastian Palmqvist[1], Olof Strandberg[1], Rik Ossenkoppele[1,3], Oskar Hansson[1]

[1]*Clinical Memory Research Unit, Clinical Sciences Malmö, Lund University, Lund, Sweden*
[2]*Radiology and Nuclear Medicine,Amsterdam UMC location VUmc, Amsterdam, The Netherlands*
[3]*Alzheimer Center Amsterdam, Neurology, Amsterdam UMC location VUmc, Amsterdam, The Netherlands*

Background: Amyloid-β (Aβ) in the occipital lobe is often omitted in PET assessments, both visually and quantitatively, while it might be clinically and biologically relevant. Here, we investigated whether subjects with occipital Aβ-PET burden differ in demographics, risk factors, and rates of Aβ- and tau-PET accumulation from Aβ-positive subjects without occipital uptake.

Methods: We included 1065 mostly pre-dementia (98.7%) participants from the BioFINDER-2 cohort with available [^{18}F]flutemetamol amyloid-PET regional visual read (VR), including the occipital lobe. Subjects were classified as Aβ-negative (Aβ-), occipital Aβ-positive (OCC+) or Aβ-positive without occipital uptake (Aβ+/OCC-). Baseline differences in demographics were assessed using chi-square and two-sample t-tests. Linear mixed models with random slope and intercept were used to determine regional differences in amyloid-PET and tau-PET over time. LMEs were corrected for age, sex, baseline diagnosis, and baseline Aβ-PET burden in case of the tau-PET model. Longitudinal PET analyses were FDR-corrected.

Results: Based on VR, 756 (71.0%) of participants were classified as Aβ-, 108 (10.1%) as OCC+, and 201 (18.9%) as Aβ+/OCC-. Isolated occipital positivity was rare, with the majority of OCC+ cases also visually classified as Aβ+ (103/108). OCC+ were less often *APOE*-ε4 carriers compared to Aβ+/OCC- (χ^2=100.4, p<0.001, **Table-1**), but did not significantly differ in age and sex. OCC+ had significantly higher baseline Aβ-PET burden, particularly in occipital and parietal regions but no faster Aβ-accumulation rate (**Figure-1**). OCC+ had significantly higher baseline tau-PET burden mainly in posterior regions. Moreover, OCC+ showed higher tau accumulation rates in the occipital, lateral parietal, superior frontal, and primary cortices, with a predilection towards the left hemisphere (**Figure-2**).

Conclusions: Visual positivity for occipital amyloid burden is associated with higher tau-PET burden and rate of accumulation, particularly in posterior regions. This suggests that occipital burden is of clinical relevance and could improve identification of subjects with faster disease progression.

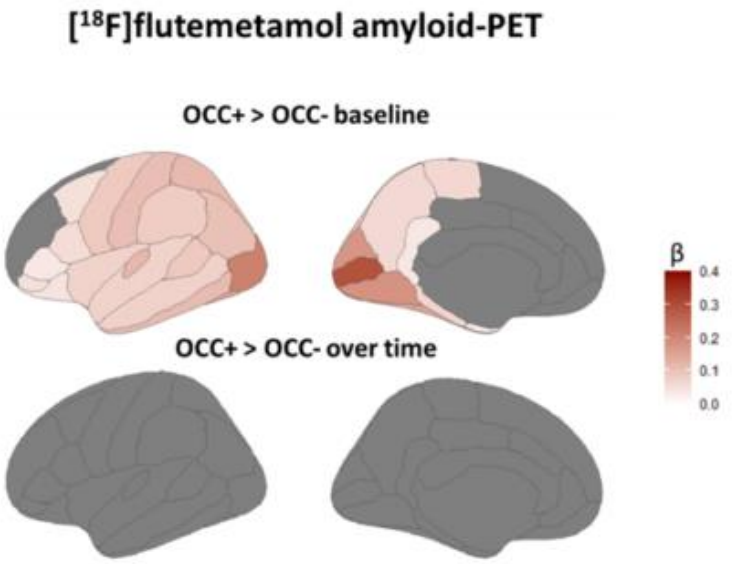

Figure 1. Higher [^{18}F]flutemetamol amyloid-PET burden in OCC+ group
Results of the linear mixed model, corrected for age, sex, and baseline cognitive status. OCC+ subjects showed higher baseline amyloid burden compared to Aβ+/OCC-, particularly in occipital regions and subsequently following in a gradient fashion towards frontal regions. However, no differences in rate of Aβ accumulation were observed. Only regions that survived FDR-correction are shown.

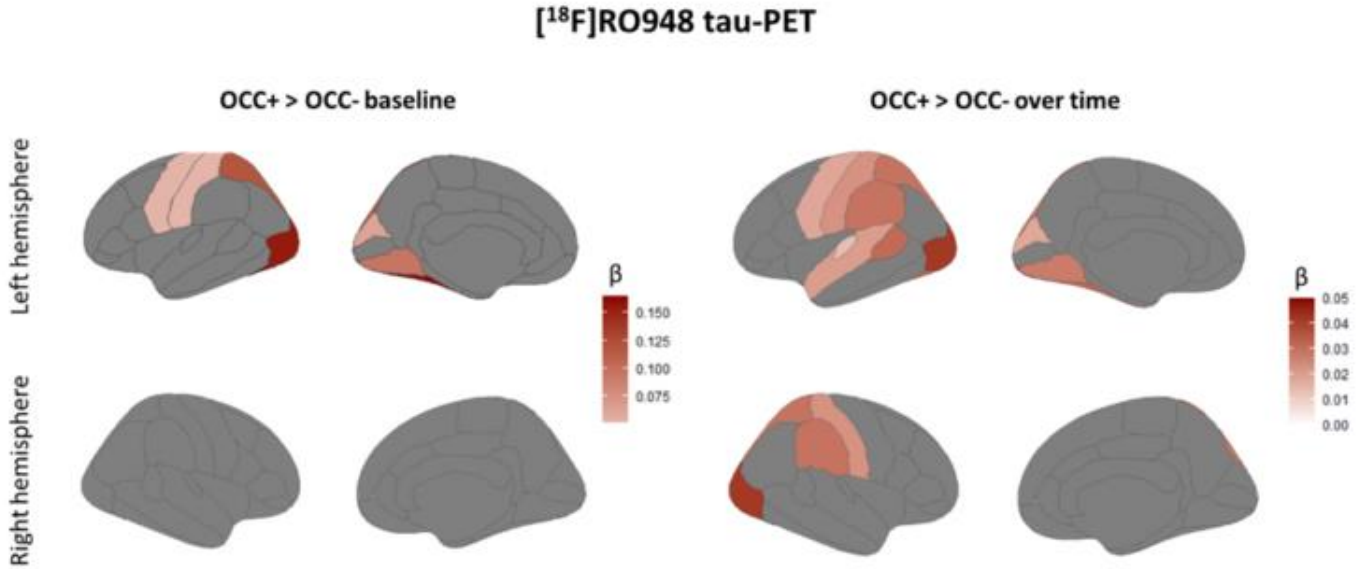

Figure 2. Higher [^{18}F]RO948 tau-PET burden in OCC+ group
Results of the linear mixed model, corrected for age, sex, baseline cognitive status, and baseline amyloid PET burden. OCC+ subjects showed higher baseline tau burden compared to Aβ+/OCC- in posterior regions. In addition, they showed higher tau accumulation rate, particularly in occipital, lateral parietal, superior frontal, and primary cortices. Also, higher tau burden and accumulation rate was more apparent for the left hemisphere. Only regions that survived FDR-correction are shown.

Keywords: Alzheimer's disease, Amyloid-beta, tau, PET imaging, occipital

62 Tau-PET subtypes show distinct profiles of cerebrospinal fluid biomarkers, neurodegeneration, and cognition in a large single-site cohort

Lyduine E. Collij[1,2], Sophie E. Mastenbroek[1,2], Alexa Pichet Binette[1], Ruben Smith[1], Sebastian Palmqvist[1], Niklas Mattsson-Carlgren[1], Olof Strandberg[1], Rik Ossenkoppele[1,3], Jacob W. Vogel[1], Oskar Hansson[1]

[1]*Clinical Memory Research Unit, Clinical Sciences Malmö, Lund University, Lund, Sweden*
[2]*Radiology and Nuclear Medicine,Amsterdam UMC location VUmc, Amsterdam, The Netherlands*
[3]*Alzheimer Center Amsterdam, Neurology, Amsterdam UMC location VUmc, Lund, The Netherlands*

Background: We previously identified four spatiotemporal subtypes of mixed 3R/4R tau deposition in Alzheimer's disease, as measured with PET[1]. Here, we investigated subtype differences in demographics, ancillary disease processes through CSF biomarkers, longitudinal atrophy patterns, and cognition.

Methods: We applied the previously established Subtype and Stage Inference (SuStaIn) model to 1252 BioFINDER-2 (BF2) participants with available [^{18}F]RO948 tau-PET. Linear models assessed subtype differences in CSF-biomarkers (corrected for $A\beta_{40}$ and log-transformed). Linear mixed models were used to determine regional subtype-differences in atrophy (gray-matter volume) and cognition (MMSE and ADAS-cog delayed recall) over time. Models included age, sex, and baseline diagnosis, TIV (atrophy) and level of education (cognition) as covariates and were FDR-corrected.

Results: The four previously identified tau-PET subtypes were replicated in BF2 (**Figure-1A**). Overall, 422 (33.7%) participants were assigned to a subtype (limbic: 254 (60.2%), MTL-sparing: 53 (12.6%), Posterior: 59 (13.9%), Lateral-Temporal: 56 (13.3%), **Table-1**). Participants classified to the Limbic-subtype were older (F=33.3, p<0.01), while Posterior-subtype participants were less often *APOE*-ε4 carriers (χ^2=119.83, p<0.001). Posterior and Lateral-temporal-subtype participants had higher temporal-tau compared to Limbic and MTL-sparing participants. Global tau-burden was lower in Limbic-subtype participants (**Table-1**). Lateral-Temporal-subtype participants had higher levels of NFL, YKL40, and NgN compared to Limbic-subtype participants (p_{FDR}<0.05, **Figure-1B**). Distinct patterns of cross-sectional and longitudinal regional gray matter volume reduction were observed across subtypes (**Figure-2**). Limbic-subtype and Lateral-Temporal-subtype participants performed worse on ADAS-cog delayed recall (β=-1.00, p_{FDR}<0.001) and MMSE (β=-1.01, p_{FDR}<0.05) compared to the MTL-sparing and Limbic-subtype over time, respectively.

Conclusions: In a large single-site dataset, we confirm and extend findings that spatiotemporal subtypes of tau burden are differentiated by demographics and risk-factors. Cortical atrophy patterns are mostly consistent with the distribution of tau burden. The Lateral-Temporal-subtype showed higher tau burden and increased CSF markers of neurodegeneration, in line with the volume loss and cognitive decline.

Table 1. Demographics

	No-subtype (*N*=830)	Limbic (*N*=254)	MTL-sparing (*N*=53)	Posterior (*N*=59)	Lateral-Temporal (*N*=56)	Overall (*N*=1252)
Age, y	64.5 (14.2)	73.7[a] (6.64)	67.7 (9.77)	70.8 (9.19)	73.8 (6.26)	67.2 (13.0)
Sex (F, %)	434 (52.3%)	133 (52.4%)	32 (60.4%)	39 (66.1%)	26 (46.4%)	664 (53.0%)
***APOE*-ε4 carrier**	327 (39.4%)	187 (73.6%)	38 (71.7%)	37[a,c,d] (62.7%)	41 (73.2%)	630 (50.3%)
Baseline cognitive status						
CU	557 (67.1%)	16 (6.3%)	5 (9.4%)	3 (5.1%)	0 (0%)	581 (46.4%)
SCD	193 (23.3%)	34 (13.4%)	2 (3.8%)	3 (5.1%)	5 (8.9%)	237 (18.9%)
MCI	71 (8.6%)	85 (33.5%)	19 (35.8%)	14 (23.7%)	16 (28.6%)	205 (16.4%)
Dementia	9 (1.1%)	119 (46.9%)	27 (50.9%)	39 (66.1%)	35 (62.5%)	229 (18.3%)
Tau-PET burden						
Braak I-IV	1.14 (0.09)	1.84[b,c] (0.63)	1.89[b,c] (0.41)	2.11[a,d] (0.58)	2.19[a,d] (0.61)	1.41 (0.52)
Braak I-VI	1.06 (0.08)	1.44[a,b,c] (0.40)	1.64[d] (0.38)	1.71[d] (0.43)	1.66[d] (0.48)	1.22 (0.34)
CSF biomarkers						
NfL	0.78 (0.27)	1.07 (0.23)	1.08 (0.20)	1.15 (0.26)	1.21 (0.27)[d]	0.89 (0.30)
NgN	1.60 (0.09)	1.75 (0.11)	1.76 (0.09)	1.77 (0.10)	1.82 (0.13)[d]	1.66 (0.12)
YKL40	0.91 (0.18)	1.07 (0.14)	1.05 (0.11)	1.07 (0.13)	1.13 (0.15)[d]	0.97 (0.18)

CU = cognitively unimpaired, SCD = subjective cognitive decline, MCI = mild cognitive impairment, MTL = medtial temporal lobe, CSF = cerebrospinal fluid

[a] $p_{FDR}<0.05$ compared to MTL-sparing subtype

[b] $p_{FDR}<0.05$ compared to Posterior

[c] $p_{FDR}<0.05$ compared to Lateral-temporal

[d] $p_{FDR}<0.05$ compared to Limbic subtype

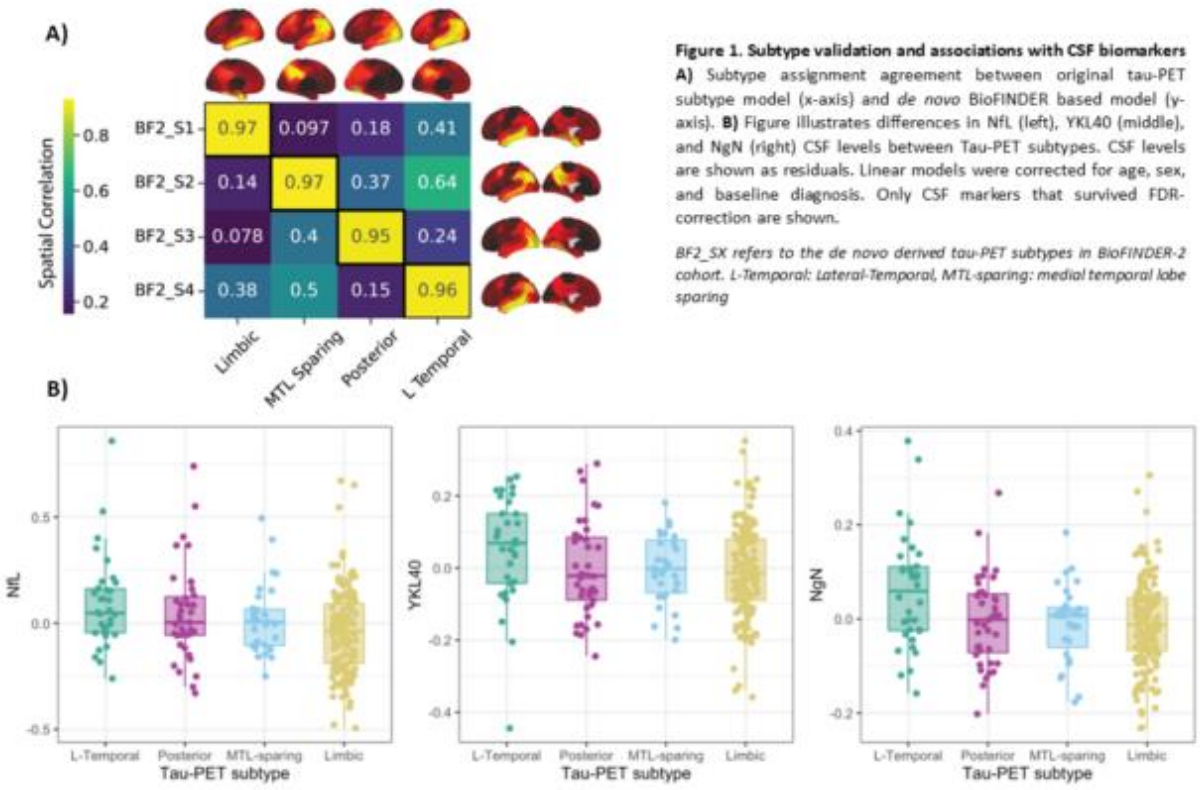

Figure 1. Subtype validation and associations with CSF biomarkers
A) Subtype assignment agreement between original tau-PET subtype model (x-axis) and *de novo* BioFINDER based model (y-axis). **B)** Figure illustrates differences in NfL (left), YKL40 (middle), and NgN (right) CSF levels between Tau-PET subtypes. CSF levels are shown as residuals. Linear models were corrected for age, sex, and baseline diagnosis. Only CSF markers that survived FDR-correction are shown.

BF2_SX refers to the de novo derived tau-PET subtypes in BioFINDER-2 cohort. L-Temporal: Lateral-Temporal, MTL-sparing: medial temporal lobe sparing

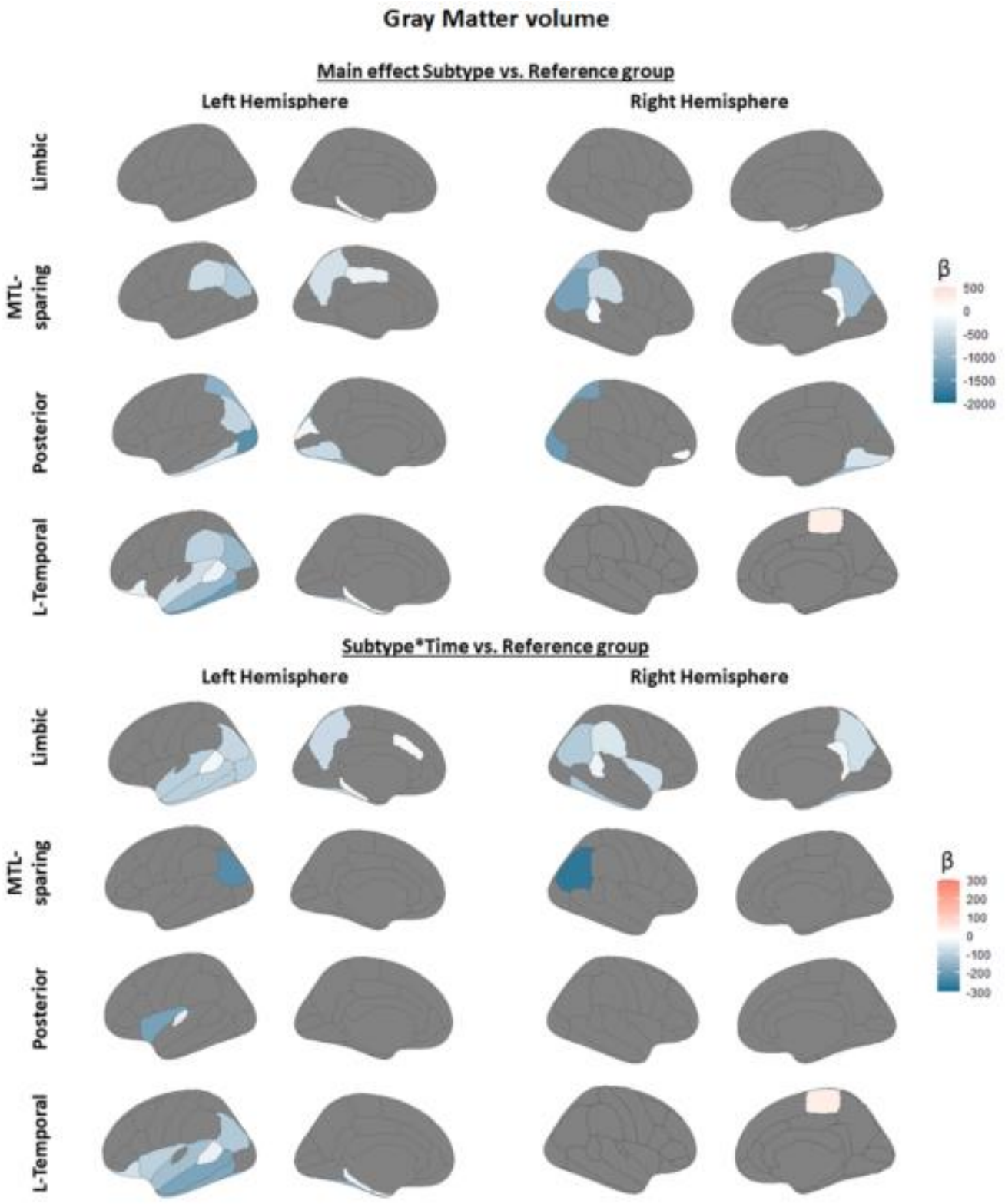

Figure 2. Baseline and longitudinal gray matter volume across Tau-PET subtypes
Figure illustrates regional differences in gray matter volume (derived from T1-weighted MR images processed with longitudinal FreeSurfer pipeline) between Tau-PET subtypes and the reference group, *i.e.,* participants assigned to no subtype. Top figure illustrates main effects of the Linear Mixed Effects model, while the bottom figure illustrates the interaction with time. LME model was corrected for age, sex, and baseline diagnosis. Only regions that survived FDR-correction are shown.

Keywords: Tau-PET, spatiotemporal subtypes, CSF biomarkers, atrophy, cognition

63 ER176 neuroinflammatory PET profiles and relationships with flortaucipir tau PET in progressive apraxia of speech

Ryota Satoh[1], Rene Utianski[1], Joseph Duffy[1], Heather Clark[1], Hugo Botha[1], Val Lowe[1], Keith Josephs[1], Jennifer Whitwell[1]

[1]*Mayo Clinic, Rochester, MN, United States*

Background: Progressive apraxia of speech (PAOS) is a neurodegenerative disorder that affects the planning or programming of speech. Patients with PAOS are likely to have underlying 4-repeat (4R) tauopathies such as progressive supranuclear palsy and corticobasal degeneration. Previous tau PET studies have shown increased signal in the precentral gyrus, supplementary motor area, and Broca's area in PAOS. This study aims to assess the neuroinflammatory profile in PAOS by using [^{11}C]-ER176 PET and to evaluate the relationship between neuroinflammation and tau uptake.

Methods: Nineteen PAOS patients and 22 cognitively and motorically normal controls underwent [^{11}C]-ER176 inflammatory PET and 3T MRI. Sixteen patients and 14 controls also underwent [^{18}F]-flortaucipir PET at the same visit. Standardized uptake value ratios (SUVRs) were calculated for inflammatory and tau PET images. Region-of-interest (ROI) and voxel-based analyses were performed to compare inflammatory SUVRs between PAOS and controls. Pearson's correlation coefficients were calculated to examine relationships between inflammatory and tau SUVRs across multiple cortical ROIs within each subject.

Results: ROI analysis showed greater inflammatory SUVRs in PAOS compared to controls in the precentral gyrus, supplementary motor area, putamen, pallidum, and subthalamic nucleus. Voxel-based analysis supported the ROI analysis and showed that PAOS had greater inflammatory SUVRs than controls in these same regions, plus superior, middle, and inferior frontal regions, with greatest uptake observed in the white matter (**Figure 1**). Inflammatory and tau SUVRs were positively correlated in the cortex in PAOS (median r=0.55) but not in controls (median r=0.15) (p<0.001). In PAOS subjects, higher correlation coefficients were associated with shorter disease duration (p<0.05).

Conclusions: ER176 PET detects neuroinflammation in frontal cortex and basal ganglia in PAOS, with neuroinflammation related to tau uptake particularly in the earlier phase of the disease.

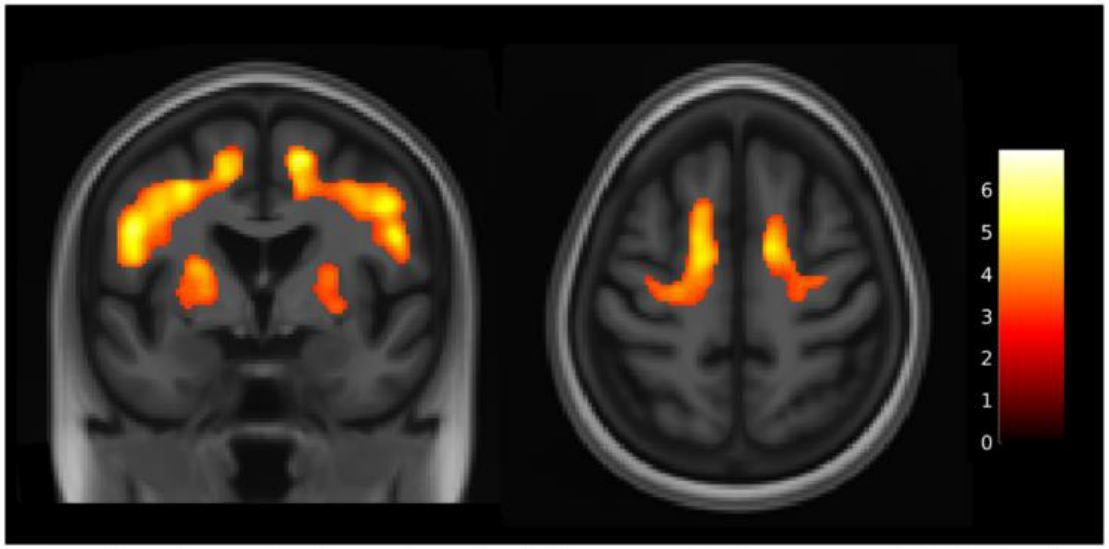

Figure 1 T-value map showing regions where inflammatory SUVR was greater in PAOS than in controls (FDR-corrected $p<0.05$).

Keywords: neuroinflammation, [11C]-ER176, tau, apraxia of speech, PAOS

64 Aβ and tau associations with sex and affected parent's sex in preclinical Alzheimer's disease

Valentin Ourry[1,2], Frédéric St-Onge[2,3], Bery Mohammediyan[1,2], Yara Yakoub[2,3], Jean-Paul Soucy[4], Judes Poirier[1,2], John C.S Breitner[1,2], Sylvia Villeneuve[1,2]

[1]*Department of Psychiatry, Faculty of Medicine, McGill University, Montreal, Quebec, Canada., Montreal, QC, Canada*
[2]*Douglas Mental Health University Institute, Montreal, Quebec, Canada., Montreal, QC, Canada*
[3]*Integrated Program in Neuroscience, Faculty of Medicine, McGill University, Montreal, Quebec, Canada., Montreal, QC, Canada*
[4]*McConnell Brain Imaging Center, Montreal Neurological Institute, McGill University, Montreal, Quebec, Canada., Montreal, QC, Canada*

Background and objectives: Women and individuals with a parental history of Alzheimer's disease (AD), particularly an affected mother, have increased risk of AD. However, the association between sex, or affected parent's sex, and preclinical AD biomarkers is uncertain. We examined: 1) whether sex or affected parent's sex predicted regional amyloid-beta (Aβ) or tau burden/accumulation; and 2) whether sex or affected parent's sex influenced association between Aβ and related regional tau.

Methods: We performed [18F]-NAV4694 and [18F]-AV1451 positron emission tomography on 238 older adults (age 68.3 ± 5.1 years, 69.7% female) from the PREVENT-AD cohort. All were cognitively unimpaired at baseline. Longitudinal scans were available for 106 (4.3 ± 0.4 years follow-up). We examined the association between sex or affected parent's sex and regional Aβ and tau burden and annual change. We then examined two-way interactions between Aβ and sex (or affected parent's sex) when predicting regional tau burden and annual change.

Results: Women had higher tau SUVR than men in Braak stages IV to VI. Women also showed faster accumulation of tau at Braak stage V. We observed interactions between Aβ and sex, or affected parent's sex, associated with baseline tau in Braak stages IV to VI. Association between amyloid and tau at these more advanced Braak stages appeared stronger in women and in persons with an affected father. Similar interactions were found between affected parent's sex and annual change in tau.

Discussion: Women and, surprisingly, individuals with an affected father showed more widespread tau associated with their Ab burden than did men or persons with an affected mother. We speculate that these groups may require a reduced Aβ to precipitate tau pathology, especially outside of the medial temporal lobe. Identifying specific vulnerabilities by sex or affected parent's sex may help to design personalized interventions for AD.

A

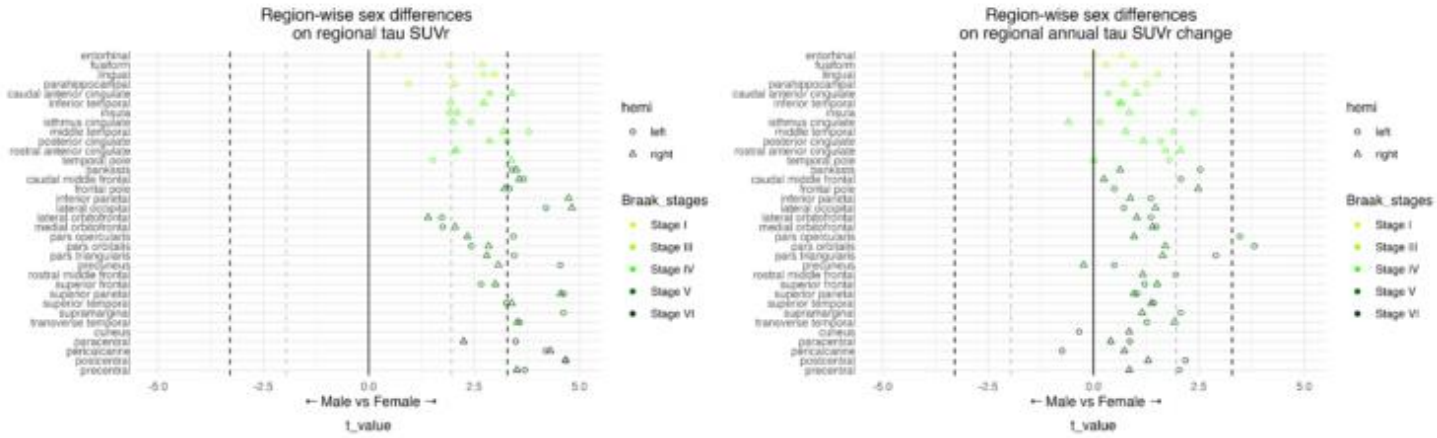
Region-wise sex differences
on regional tau SUVr
entorhinal
fusiform
lingual
parahippocampal
caudal anterior cingulate
inferior temporal
insula
isthmus cingulate
middle temporal
posterior cingulate
rostral anterior cingulate
temporal pole
bankssts
caudal middle frontal
frontal pole
inferior parietal
lateral occipital
lateral orbitofrontal
medial orbitofrontal
pars opercularis
pars orbitalis
pars triangularis
precuneus
rostral middle frontal
superior frontal
superior parietal
superior temporal
supramarginal
transverse temporal
cuneus
paracentral
pericalcarine
postcentral
precentral
-5.0
-2.5
0.0
2.5
5.0
← Male vs Female →
t_value
hemi
left
right
Braak_stages
Stage I
Stage II
Stage IV
Stage V
Stage VI
Region-wise sex differences
on regional annual tau SUVr change
entorhinal
fusiform
lingual
parahippocampal
caudal anterior cingulate
inferior temporal
insula
isthmus cingulate
middle temporal
posterior cingulate
rostral anterior cingulate
temporal pole
bankssts
caudal middle frontal
frontal pole
inferior parietal
lateral occipital
lateral orbitofrontal
medial orbitofrontal
pars opercularis
pars orbitalis
pars triangularis
precuneus
rostral middle frontal
superior frontal
superior parietal
superior temporal
supramarginal
transverse temporal
cuneus
paracentral
pericalcarine
postcentral
precentral
-5.0
-2.5
0.0
2.5
5.0
← Male vs Female →
t_value
hemi
left
right
Braak_stages
Stage I
Stage II
Stage IV
Stage V
Stage VI

B

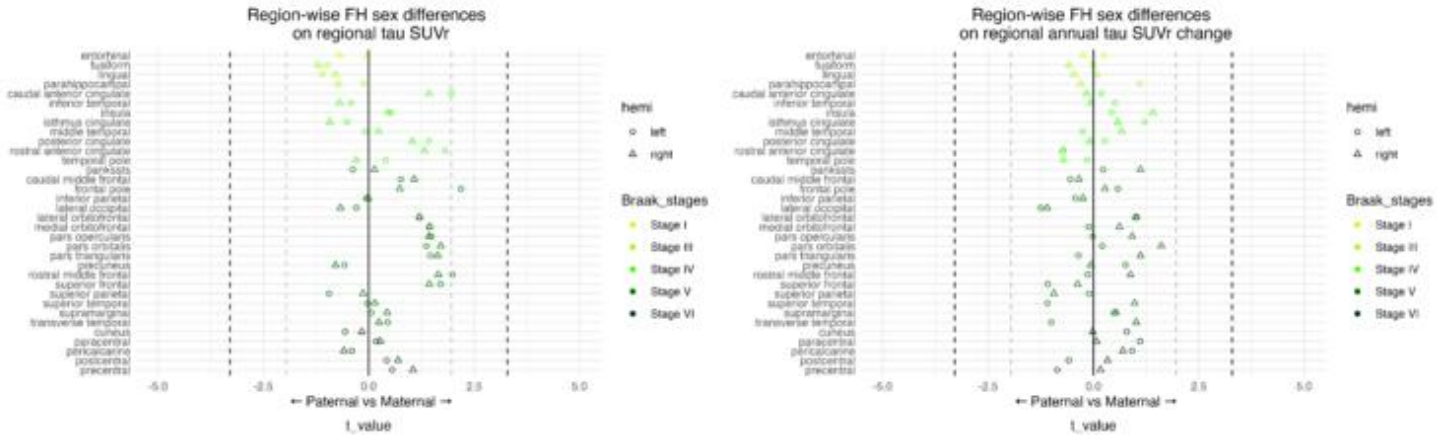
Region-wise FH sex differences
on regional tau SUVr
entorhinal
fusiform
lingual
parahippocampal
caudal anterior cingulate
inferior temporal
insula
isthmus cingulate
middle temporal
posterior cingulate
rostral anterior cingulate
temporal pole
bankssts
caudal middle frontal
frontal pole
inferior parietal
lateral occipital
lateral orbitofrontal
medial orbitofrontal
pars opercularis
pars orbitalis
pars triangularis
precuneus
rostral middle frontal
superior frontal
superior parietal
superior temporal
supramarginal
transverse temporal
cuneus
paracentral
pericalcarine
postcentral
precentral
-5.0
-2.5
0.0
2.5
5.0
← Paternal vs Maternal →
t_value
hemi
left
right
Braak_stages
Stage I
Stage II
Stage IV
Stage V
Stage VI
Region-wise FH sex differences
on regional annual tau SUVr change
entorhinal
fusiform
lingual
parahippocampal
caudal anterior cingulate
inferior temporal
insula
isthmus cingulate
middle temporal
posterior cingulate
rostral anterior cingulate
temporal pole
bankssts
caudal middle frontal
frontal pole
inferior parietal
lateral occipital
lateral orbitofrontal
medial orbitofrontal
pars opercularis
pars orbitalis
pars triangularis
precuneus
rostral middle frontal
superior frontal
superior parietal
superior temporal
supramarginal
transverse temporal
cuneus
paracentral
pericalcarine
postcentral
precentral
-5.0
-2.5
0.0
2.5
5.0
← Paternal vs Maternal →
t_value
hemi
left
right
Braak_stages
Stage I
Stage II
Stage IV
Stage V
Stage VI

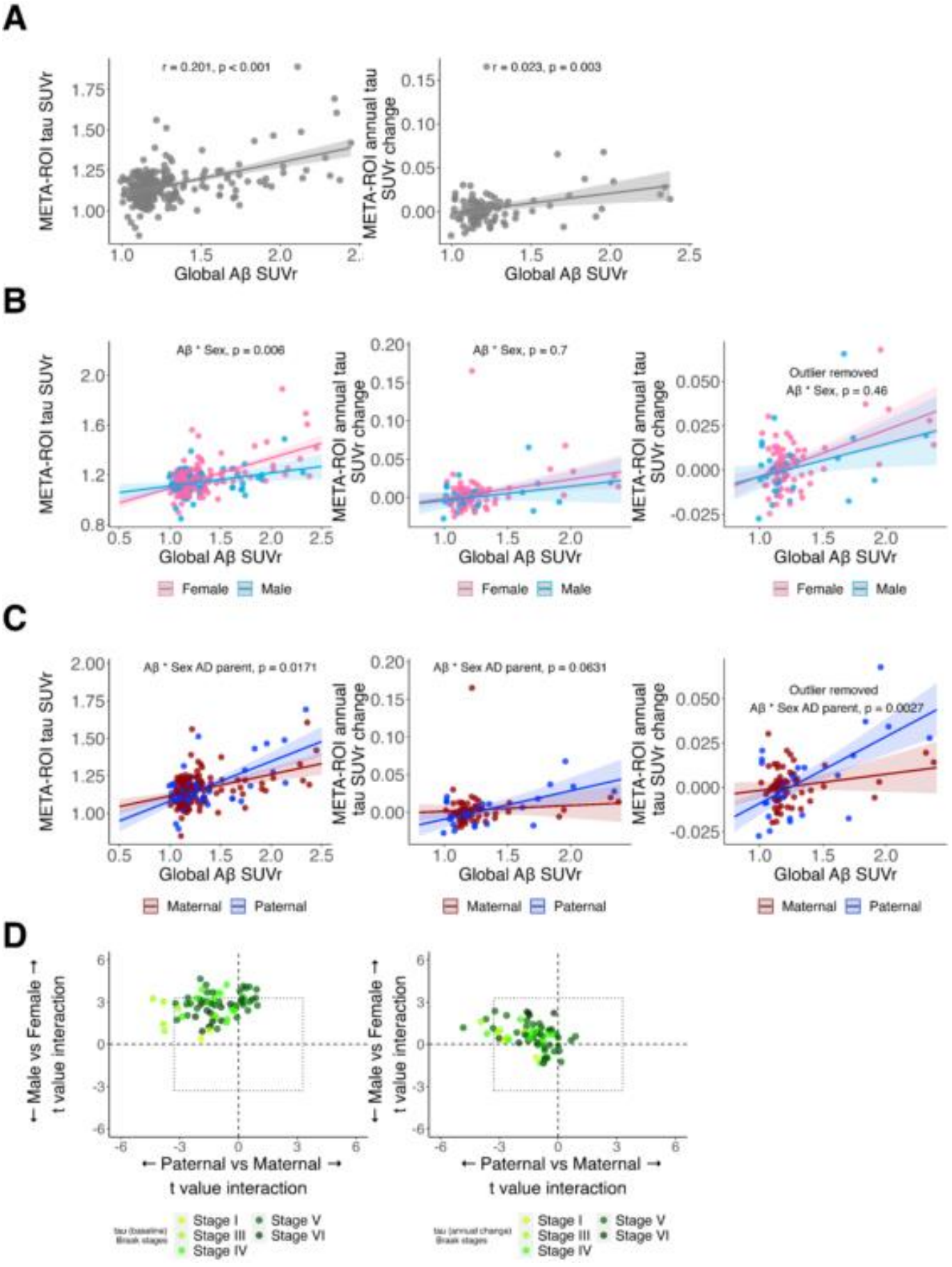
A
r = 0.201, p < 0.001
META-ROI tau SUVr
Global Aβ SUVr
r = 0.023, p = 0.003
META-ROI annual tau SUVr change
Global Aβ SUVr
B
Aβ * Sex, p = 0.006
META-ROI tau SUVr
Global Aβ SUVr
Female
Male
Aβ * Sex, p = 0.7
META-ROI annual tau SUVr change
Global Aβ SUVr
Female
Male
Outlier removed
Aβ * Sex, p = 0.46
META-ROI annual tau SUVr change
Global Aβ SUVr
Female
Male
C
Aβ * Sex AD parent, p = 0.0171
META-ROI tau SUVr
Global Aβ SUVr
Maternal
Paternal
Aβ * Sex AD parent, p = 0.0631
META-ROI annual tau SUVr change
Global Aβ SUVr
Maternal
Paternal
Outlier removed
Aβ * Sex AD parent, p = 0.0027
META-ROI annual tau SUVr change
Global Aβ SUVr
Maternal
Paternal
D
← Male vs Female →
t value interaction
← Paternal vs Maternal →
t value interaction
tau (baseline) Braak stages
Stage I
Stage III
Stage IV
Stage V
Stage VI
← Male vs Female →
t value interaction
← Paternal vs Maternal →
t value interaction
tau (annual change) Braak stages
Stage I
Stage III
Stage IV
Stage V
Stage VI

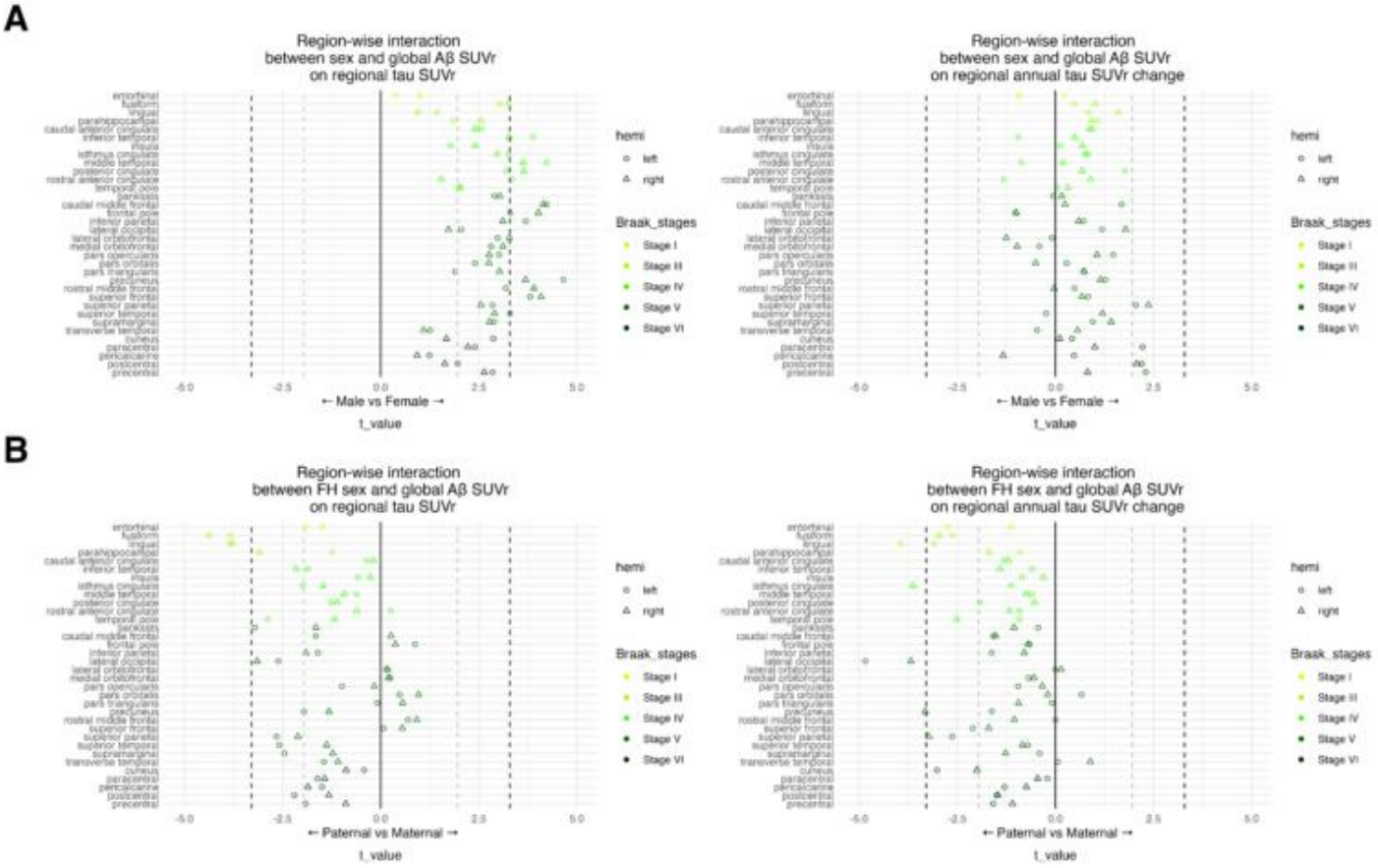

Keywords: sex, family history, amyloid, tau, Alzheimer's disease

65 Differential association between plasma biomarkers and established biomarkers of Alzheimer's disease

Marina Bluma[1], Konstantinos Chiotis[1], Marco Bucci[1], Irina Savitcheva[4], Anna Matton[1], Miia Kivipelto[1], Andreas Jeromin[5], Giovanni De Santis[3], Guglielmo Di Molfetta[3], Nicholas Ashton[3], Kaj Blennow[3], Henrik Zetterberg[3], Agneta Nordberg[1,3]

[1]*Division of Clinical Geriatrics, Center for Alzheimer Research, Department of Neurobiology, Care Sciences and Society, Karolinska Institutet, Stockholm, Sweden*
[2]*Theme Inflammation and Aging, Karolinska University Hospital, Stockholm, Sweden*
[3]*Department of Psychiatry and Neurochemistry, Institute of Neuroscience and Physiology, Sahlgrenska Academy, University of Gothenburg, Mölndal, Sweden*
[4]*Medical Radiation Physics and Nuclear Medicine, Karolinska University, Stockholm, Sweden*
[5]*ALZPath, Inc, Carlsbad, CA, United States*

Aims

Plasma biomarkers are poised for integration into screening for individuals at risk of Alzheimer's disease (AD). Yet, previous studies yielded contradictory results regarding their association with established biomarkers of AD pathology. This study aims to investigate the specific relationship between core AD biomarkers, such as amyloid PET, CSF pTau, brain atrophy, and the emerging plasma biomarkers pTau217,pTau181,pTau231, and GFAP.

Methods

Data consisted of the memory clinic patients (N=139) who underwent comprehensive clinical assessments at the Karolinska University Hospital, Stockholm,Sweden. We analyzed plasma pTau217,pTau181,pTau231,GFAP, CSF pTau181, [^{18}F]flutemetamol Aβ-PET, and visual ratings of global cortical (GCA) or mediotemporal (MTA) atrophy on MRI/CT scans. Individuals were categorized into groups of minimal, moderate (one scale abnormal) or severe (two scales abnormal) atrophy.

Results

We found significant positive associations between Aβ-PET and all plasma biomarkers (R^2=0.14-0.56); with the highest association observed for pTau217(R^2=0.56). Similarly, significant positive associations of lower magnitude were observed between plasma biomarkers and CSF pTau(R^2=0.09-0.26). After accounting for the influence of Aβ-PET on plasma biomarkers and CSF pTau, only plasma pTau217(R^2=.049) and pTau231(R^2=.024) remained significantly associated with CSF pTau. None of the plasma biomarkers could discriminate between minimal, moderate or severe atrophy groups(χ^2(2)=0.1-5.2). Dominance analysis showed that Aβ-PET was the best predictor of plasma biomarkers values, followed by CSF pTau. Aβ-PET and CSF pTau both explained the larger portion of variance in plasma pTau217 levels(~60%) and less variance in plasma GFAP (~30%),pTau181(~17%), and pTau231(~18%) levels .

Conclusions

Amyloid burden was the primary predictor for all plasma biomarkers. The effect of CSF pTau on GFAP and pTau181 was attenuated by the Aβ-PET levels, while pTau231 and pTau217 also reflected subtle changes in CSF pTau. Variance in plasma pTau217 levels appeared to be well explained by AD-related pathological changes, whereas none of the plasma biomarkers varied according to different levels of brain atrophy.

Keywords: Plasma, amyloid-PET, CSF, biomarkers, clinical patients

66 PiB PET demonstrates early, elevated amyloid striatal binding compared to florbetapir in Down syndrome

Max McLachlan[1], Jeremy Rouanet[2], Arun Garimella[3], Julie Price[3], Dana Tudorascu[4], Charles Laymon[4], David Keator[2], William Kreisl[5], William Klunk[4], Ben Handen[4], Tim Fryer[6], Shahid Zaman[6], Elizabeth Head[2], Mark Mapstone[2], Brecca Bettcher[1], Lisette LeMerise[1], Andrew McVea[1], Alexandra DiFillipo[1], Matthew Zammit[1], Sigan Hartley[1], Bradley Christian[1], Alzheimer Biomarkers Consortium — Down Syndrome Investigators[1,2,3,4,5,6]

[1]*University of Wisconsin - Madison, Madison, WI, United States*
[2]*University of California, Irvine, Irvine, CA, United States*
[3]*Massachusetts General Hospital Martinos Center, Harvard University, Boston, MA, United States*
[4]*University of Pittsburgh, Pittsburgh, PA, United States*
[5]*Columbia University Irving Medical Center, New York City, NY, United States*
[6]*University of Cambridge, Cambridge, United Kingdom*

Background: Individuals with Down syndrome (DS) carry a genetic risk for Alzheimer's Disease (AD) influenced by the elevated production of amyloid precursor protein. PET amyloid [^{11}C]PiB imaging of the DS population has revealed early detection of β amyloid plaques (Aβ) in the striatum, similar to autosomal dominant forms of AD. This work compares [^{11}C]PiB and [^{18}F]florbetapir (FBP) striatal uptake relative to the cortex in DS.

Methods: Participants from the ABC-DS study received PET imaging with either PiB or FBP, determined by study site (Table 1). Images were smoothed to 8 mm resolution, co-registered with participants' T1-weighted MRI, and normalized to a common DS MRI template space. $SUVR_{50\text{-}70min}$ images were created (whole cerebellum reference). ROIs were defined for anterior ventral striatum (AVS) and global cortex (CTX). SUVR was converted to approximate Centiloids (CL) for CTX (Klunk 2015) and AVS. Tracer cohorts were cross-sectionally age- and sex-matched (Table 1). The resulting subset was analyzed for differences in $SUVR_{AVS}/SUVR_{CTX}$ and fitted with a quadratic model: $CL_{AVS} \sim CL_{CTX} + CL_{CTX}^2 + Tracer$. The significance of model terms was evaluated with ANOVA.

Results: Figure 1 displays longitudinal $SUVR_{AVS}/SUVR_{CTX}$ for the entire cohort. 53 participants from each tracer cohort satisfied the match criteria (Figure 2). Welch's t-test for $(SUVR_{AVS}/SUVR_{CTX})^{PiB} - (SUVR_{AVS}/SUVR_{CTX})^{FBP}$ demonstrates a p-value = 2.34E-10, with an average difference of 0.218 [0.159,0.278]. ANOVA for the CL model revealed a p-value = 2.77E-12 for the tracer term significance. SUVR-based modeling replicates this significance.

Conclusion: The emergence of striatal amyloid deposition exhibits a strong dependence on PET imaging tracer. PiB shows significantly greater striatal uptake when scaled to the cortex compared to FBP. Early accumulation of diffuse Aβ plaques has been demonstrated in the striatum in adults with DS, which may suggest PiB has higher affinity for diffuse plaque than FBP. Further neuropathological investigation is needed to characterize these differences in DS.

	PiB	FBP
Entire Cohort		
Sample Size (n)	175	97
Average Age (yrs)	40.4 (SD = 9.3)	50.7 (SD = 7.0)
Participants with longitudinal scans	90 (32 months apart)	57 (16 months apart)
# with 2 scans	90	31
# with 3 scans	N/A	26
Sex (M/F)	93/82	62/35
Aβ +/-	45/130	72/25
Age- and Sex-matched Subset		
Subset Size (n)	53	53
Average Age (yrs)	47.6 (SD = 6.1)	47.6 (SD = 6.1)
Sex (M/F)	33/20	33/20
Aβ +/-	31/22	35/18

Table 1 – Participant demographics. Aβ positivity was determined based on the participant's most recent scan, using a threshold of 33 CL in the cortex for both tracers.

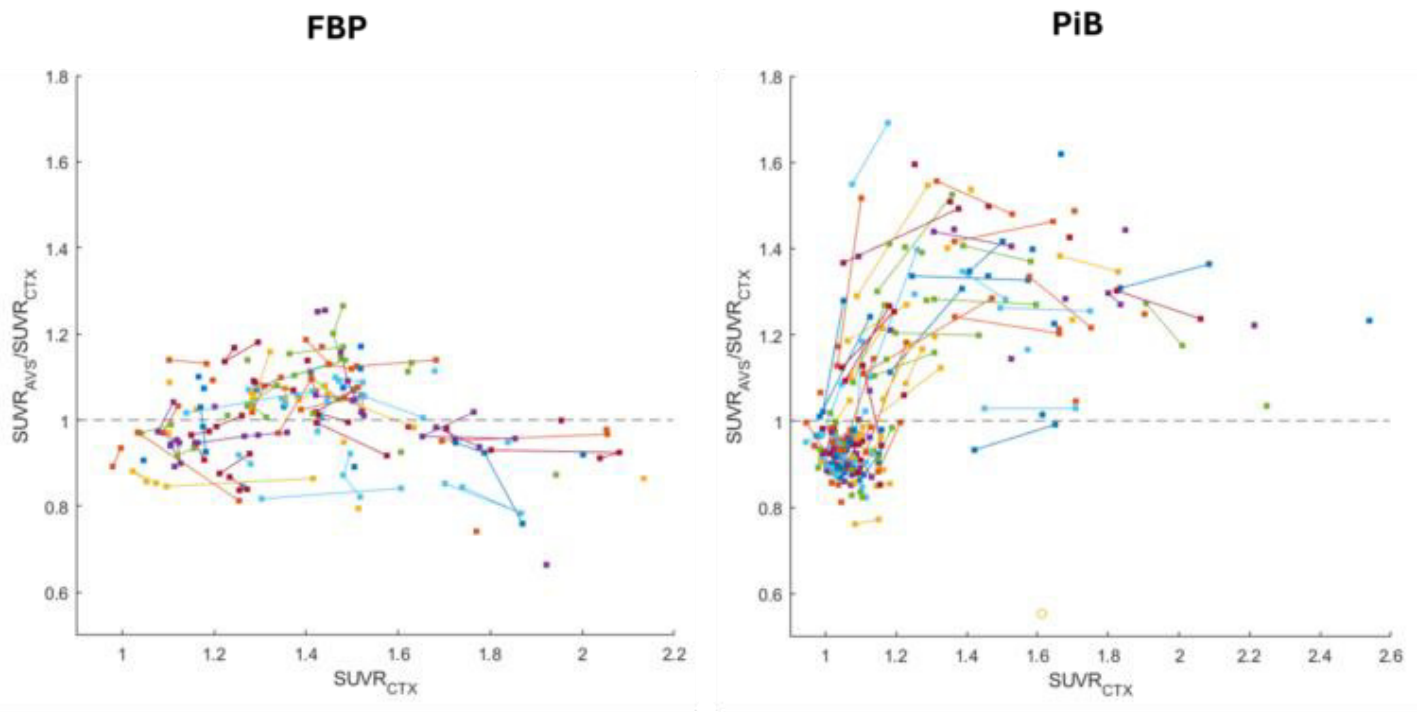

Figure 1 – Ratio of $SUVR_{AVS}/SUVR_{CTX}$ versus $SUVR_{CTX}$, separated by tracer cohort. Marker colors distinguish each participant, with lines connecting multiple timepoints of the same individual. Longitudinal FBP scans occurred 16 months apart, and longitudinal PiB scans occurred 32 months apart. The dashed line serves as a reference for a ratio of $SUVR_{AVS}/SUVR_{CTX} = 1$.

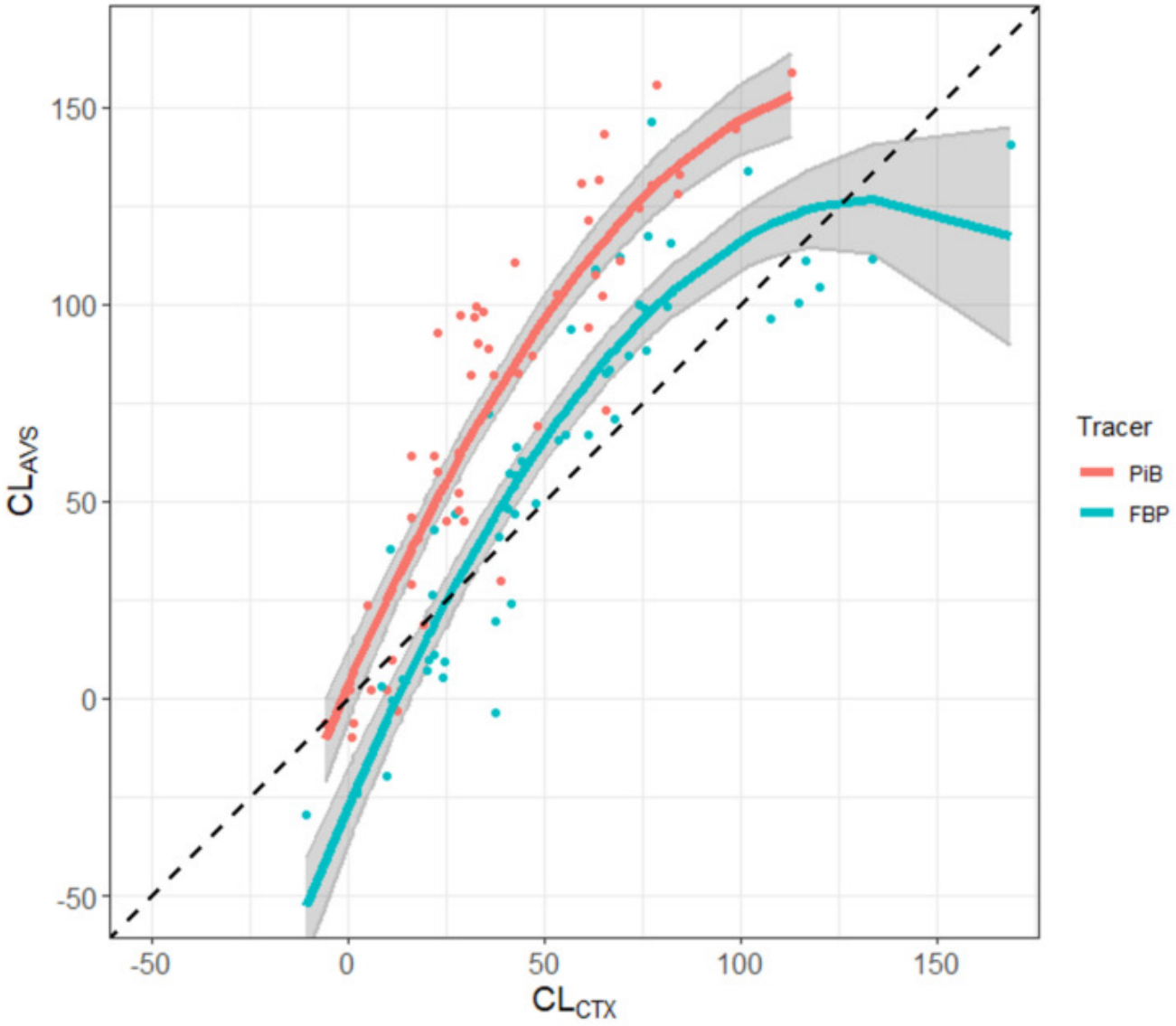

Figure 2 – Approximated CL_{AVS} compared to CL_{CTX} for 53 pairs of participants, matched by age and sex across tracer cohorts. A quadratic model of the form $CL_{AVS} \sim CL_{CTX} + CL_{CTX}^2 + Tracer$ was applied and overlayed with 95% confidence bands. The dashed line serves as a reference line of unity.

Keywords: Amyloid, Down syndrome, PET, striatum, Alzheimer's Disease

67 Data-driven disease progression modelling consistently reveals an occipital amyloid-β subtype in two independent cohorts

Sophie Mastenbroek[1,2,3], Lyduine Collij[1,2,3], Alexandra Young[4,5], Jacob Vogel[3,6], Gemma Salvadó[3], Anouk den Braber[7,8,9], Pieter Jelle Visser[7,8,10,11], Juan Domingo Gispert[12,13,14], Wiesje van der Flier[7,8,15], Olof Strandberg[3], Ruben Smith[3,16], Sebastian Palmqvist[3,17], Niklas Mattson-Carlgren[3,16,18], Neil Oxtoby[19], Frederik Barkhof[1,2,20], Rik Ossenkoppele[3,7,8], Oskar Hansson[3,17]

[1]*Department of Radiology and Nuclear Medicine, Vrije Universiteit Amsterdam, Amsterdam University Medical Center, location VUmc, Amsterdam, the Netherlands., Amsterdam, The Netherlands*
[2]*Amsterdam Neuroscience, Brain imaging, Amsterdam, the Netherlands., Amsterdam, The Netherlands*
[3]*Clinical Memory Research Unit, Lund University, Lund, Sweden., Lund, Sweden*
[4]*Department of Neuroimaging, Institute of Psychiatry, Psychological and Neuroscience, King's College London, UK., London, United Kingdom*
[5]*Centre for Medical Image Computing, Department of Computer Science, University College London, London, UK., London, United Kingdom*
[6]*Department of Clinical Science, SciLifeLab, Lund University, Lund, Sweden., Lund, Sweden*
[7]*Alzheimer Center Amsterdam, Neurology, Vrije Universiteit Amsterdam, Amsterdam UMC location VUmc, Amsterdam, The Netherlands., Amsterdam, The Netherlands*
[8]*Amsterdam Neuroscience, Neurodegeneration, Amsterdam, The Netherlands., Amsterdam, The Netherlands*
[9]*Department of Biological Psychology, Vrije Universiteit Amsterdam, Amsterdam, The Netherlands., Amsterdam, The Netherlands*
[10]*Alzheimer Center Limburg, School for Mental Health and Neuroscience, Maastricht University, Maastricht, The Netherlands., Maastricht, The Netherlands*
[11]*Department of Neurobiology, Care Sciences and Society, Division of Neurogeriatrics, Karolinska Institutet, Stockholm, Sweden., Stockholm, Sweden*
[12]*Barcelonaβeta Brain Research Center (BBRC), Pasqual Maragall Foundation, Barcelona, Spain., Barcelona, ES*
[13]*IMIM (Hospital del Mar Medical Research Institute), Barcelona, Spain., Barcelona, ES*
[14]*Centro de Investigación Biomédica en Red de Fragilidad y Envejecimiento Saludable, Instituto de Salud Carlos III, Madrid, Spain., Madrid, ES*
[15]*Epidemiology and Data Science, Vrije Universiteit Amsterdam, Amsterdam UMC location VUmc, Amsterdam, the Netherlands., Amsterdam, The Netherlands*
[16]*Department of Neurology, Skåne University Hospital, Lund, Sweden., Lund, Sweden*
[17]*Memory Clinic, Skåne University Hospital, Malmö, Sweden., Malmö, Sweden*
[18]*Wallenberg Center for Molecular Medicine, Lund University, Lund, Sweden., Lund, Sweden*
[19]*Centre for Medical Image Computing, Department of Computer Science, University College London, London, UK., London, United Kingdom*
[20]*Queen Square Institute of Neurology and Centre for Medical Image Computing, University College London, London, UK., London, United Kingdom*

Background: We previously applied the Subtype and Stage Inference (SuStaIn) algorithm to >3000 amyloid-PET scans and identified three subtypes of Aβ-deposition[1]. In the current study, we aimed to (i) improve generalizability of the model by enhancing harmonization and excluding subcortical regions and (ii) investigate the replicability of an early-Occipital subtype in an independent cohort.

Methods: For the discovery cohort, regional Aβ-PET SUVRs of 3009 pooled subjects from multiple cohorts were z-scored within each cohort and tracer and harmonized using ComBat. Mixture SuStaIn was used to assign each subject to a subtype and disease stage. The optimal number of Aβ-subtypes was determined with cross-

validation. Covariate-adjusted regression models compared subtypes on demographics. We repeated all previous steps in an independent validation cohort, comprising 1295 BioFINDER-2 subjects.

Results: In both cohorts, model fit improved substantially from a one- to two-subtypes model, but only slightly from two- to three-subtypes (**Figure-1**). We opted for reduced complexity by adopting the two-subtypes solution. In the discovery cohort (**Table-1**), 1165 (38.8%) subjects had detectable Aβ-pathology (stage>0) and confident subtype assignment (>0.5). Based on earliest abnormalities, a Parietal (*n*=958) and Occipital (*n*=207) subtype were identified **(Figure-2**). The three-subtypes model separated the Parietal into Parietal and Frontal subtypes. In the validation cohort (**Table-1**), 490 (38.4%) subjects had detectable Aβ-pathology and confident subtype assignment. The Occipital-subtype was replicated (*n*=23) (**Figure-2**). In addition, a Frontal-subtype (*n*=467) was observed, which was separated into Frontal and Parietal subtypes in the three-subtypes model. Subtype comparisons revealed distinct characteristics across subtypes (**Table-1**).

Conclusion: Using data-driven disease progression modelling, we consistently observed a more traditional (early frontal or parietal involvement) and atypical (early occipital involvement) spatial-temporal trajectory of Aβ-PET burden in two independent cohorts. While occipital amyloid is often disregarded in current guidelines and research, these results suggest that including occipital-Aβ may potentially render relevant prognostic information.

1. Collij LE, Salvadó G, Wottschel V, et al. Spatial-Temporal Patterns of β-Amyloid Accumulation: A Subtype and Stage Inference Model Analysis. Neurology. Apr 26 2022;98(17):e1692-e1703. doi:10.1212/wnl.0000000000200148

	Discovery cohort				Validation cohort			
	All (*N*=3009)	**Parietal subtype** (*n*=958)	**Occipital subtype** (*n*=207)	***p-value***	**All** (*N*=1295)	**Frontal subtype** (*n*=467)	**Occipital subtype** (*n*=23)	***p-value***
Diagnostic group, *n* (%)	**CU:** 1896 (63.0) **CI:** 2558 (37.0) **NA:** 1 (0.0)	**CU:** 384 (40.1) **CI:** 573 (59.8) **NA:** 1 (0.1)	**CU:** 122 (58.9) **CI:** 85 (41.1) **NA:** 0 (0.0)	.827	**CU:** 873 (67.4) **CI:** 378 (29.2) **NA:** 44 (3.4)	**CU:** 208 (44.6) **CI:** 237 (50.8) **NA:** 22 (4.7)	**CU:** 17 (53.9) **CI:** 3 (13.0) **NA:** 25 (5.1)	.066
Cohort, *n* (%)	**ABIDE:** 349 (11.6) **ADNI:** 1180 (39.2) **ALFA:** 358 (11.9) **OASIS:** 932 (31.0) **EMIF-AD:** 190 (6.3)	**ABIDE:** 140 (14.6) **ADNI:** 490 (51.1) **ALFA:** 64 (6.7) **OASIS:** 226 (25.6) **EMIF-AD:** 38 (4.0)	**ABIDE:** 26 (12.6) **ADNI:** 98 (47.3) **ALFA:** 35 (16.9) **OASIS:** 25 (12.1) **EMIF-AD:** 23 (11.1)	-	**BF-2:** 1295 (100.0)	**BF-2:** 467 (100.0)	**BF-2:** 23 (100.0)	-
Tracer, *n* (%)	**FBB:** 349 (11.6) **FLUT:** 548 (18.2) **FPIR:** 1540 (51.2) **PIB:** 572 (19.0)	**FBB:** 140 (14.6) **FLUT:** 102 (10.6) **FPIR:** 582 (60.8) **PIB:** 134 (14.0)	**FBB:** 26 (12.6) **FLUT:** 58 (28.0) **FPIR:** 109 (52.7) **PIB:** 14 (6.8)	-	**FLUT:** 1295 (100.0)	**FLUT:** 467 (100.0)	**FLUT:** 23 (100.0)	-
Age	68.7 (9.1)	72.0 (97.9)	70.9 (8.1)	.302	67.0 (13.1)	73.4 (7.7)	72.4 (11.1)	.671
Sex (male), *n* (%)	1451 (48.2)	484 (50.5)	94 (45.4)	.046*	623 (48.1)	230 (49.3)	12 (52.2)	.659
MMSE	27.9 (2.9)	26.6 (2.1)	27.3 (3.5)	.776	28.3 (1.9)	27.6 (2.1)	28.7 (2.1)	.189
***APOE*-ε4 carriers**, *n* (%)	1266 (42.1) **NA:** 14 (1.2)	613 (64.0) **NA:** 11 (1.1)	89 (43.0) **NA:** 3 (1.4)	.371	564 (43.5) **NA:** 68 (13.9)	288 (61.7) **NA:** 58 (12.4)	4 (17.3) **NA:** 68 (13.9)	.015*

Table 1. Population characteristics
Description of the discovery and validation cohorts used for SuStaIn modelling. Characteristics are shown for each cohort and for the subtypes (stage>0, subtype assignment >0.5) separately. *P*-values from regression models adjusted for age, sex, and SuStaIn stage are reported. * P < .05.

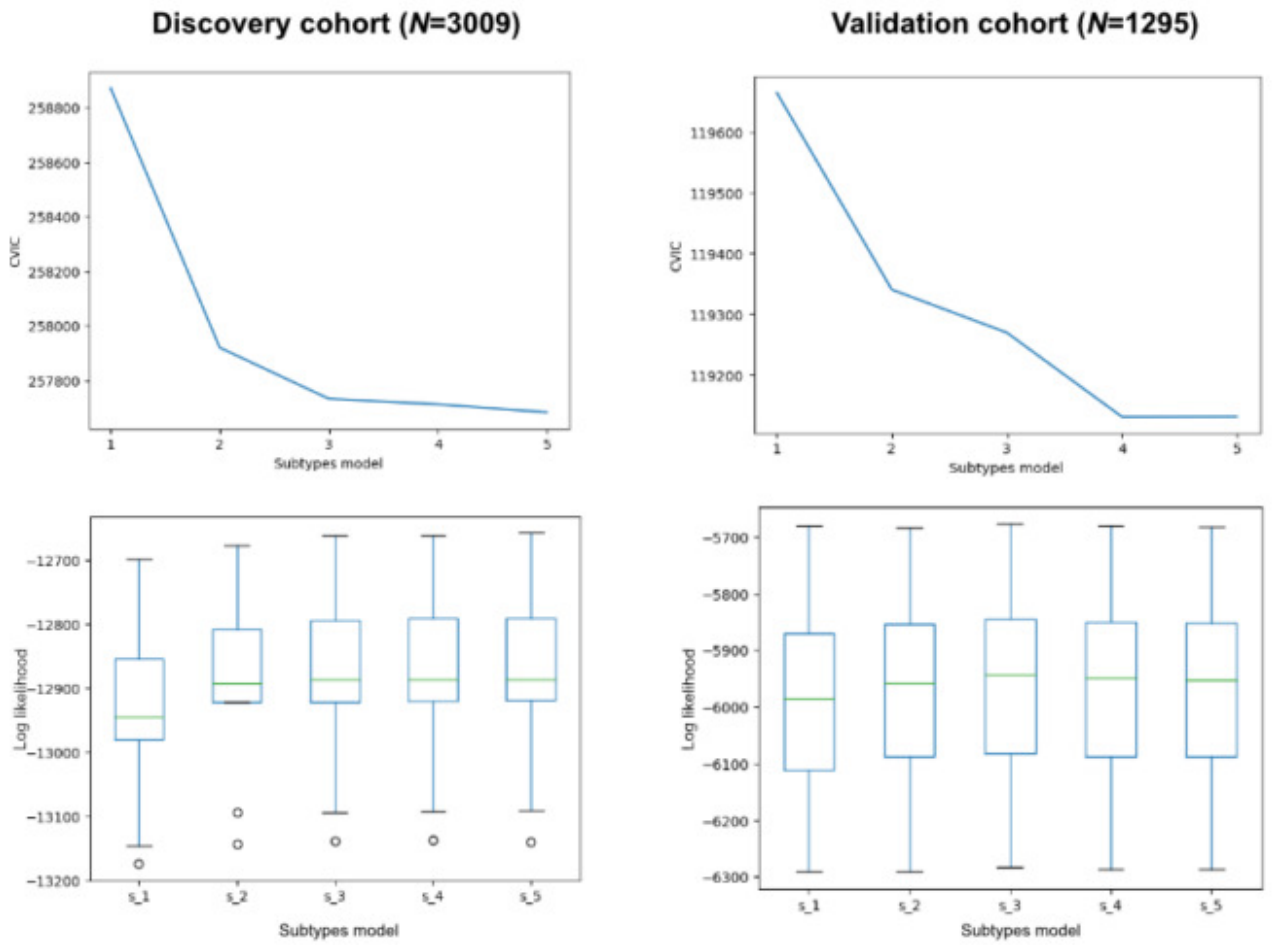

Figure 1. Model fit for up to 5 SuStaIn subtypes.
Model fit for SuStaIn models with varying number of subtypes. Cross-validation information criterion (CVIC) and) log-likelihood across 10-folds of cross-validation are shown for 1-5 subtypes. Substantial improved model fit can be appreciated from one to two and slight improvement from two to three.

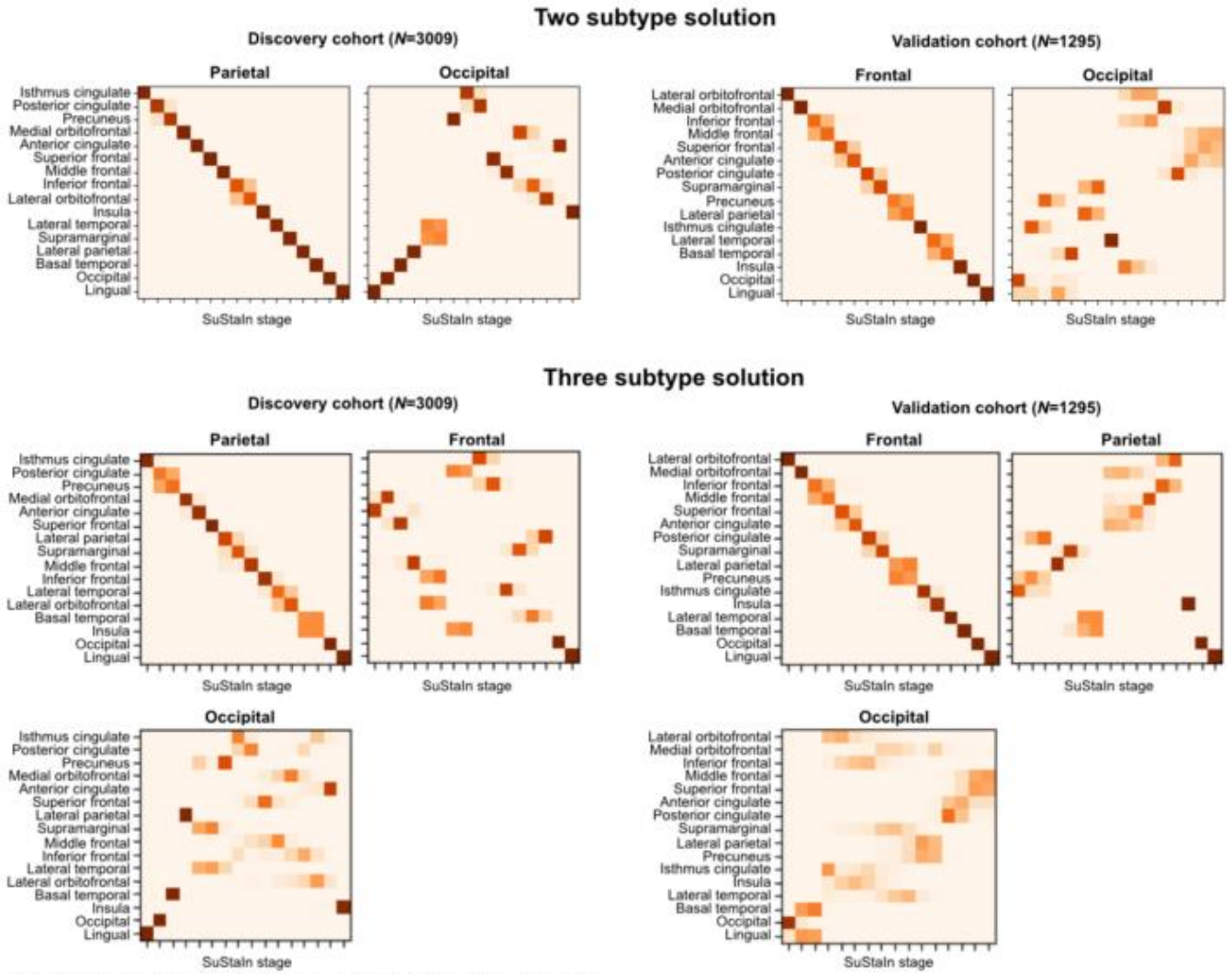

Figure 2. Spatiotemporal subtypes of amyloid deposition in two independent cohorts.
Representation of the two (top-row) and 3 (bottom-row) subtypes as identified by SuStaIn in the discovery cohort (left) and the validation cohort (right). Positional variance diagrams are shown, with darker colors indicating more model confidence. Each block or event represents one region to become abnormal on amyloid-PET. In the discovery cohort, the two-subtype model revealed a Parietal and Occipital subtype. The three-subtype model seemed to separate the Parietal subtype into Parietal and Frontal subtypes, while keeping the Occipital subtype. In the validation cohort, the two-subtype model showed that the Occipital subtype was replicated, while a Frontal instead of a Parietal subtype was observed. In the three-subtype model, the Frontal subtype was separated into a Frontal and Parietal subtype, similar to the discovery cohort. Exact regional can be appreciated in more detail in the figure.

Keywords: disease progression modelling, Subtype and Stage Inference, amyloid-β, Positron Emission Tomography

68 Mid-life perceived discrimination and late-life Alzheimer's disease pathology and cognition in African American and non-Hispanic White populations

Sarah Royse[1], Beth Snitz[2], Anum Saeed[3], Alexandria Reese[1], Brian Lopresti[1], Thomas Karikari[4], M Ilyas Kamboh[4,5,6], Victor Villemagne[4], Steven Reis[3], Oscar Lopez[2,4], Ann Cohen[4]

[1]*Department of Radiology, University of Pittsburgh, Pittsburgh, PA, United States*
[2]*Department of Neurology, University of Pittsburgh, Pittsburgh, PA, United States*
[3]*Heart and Vascular Institute, University of Pittsburgh, Pittsburgh, PA, United States*
[4]*Department of Psychiatry, University of Pittsburgh, Pittsburgh, PA, United States*
[5]*Department of Human Genetics, University of Pittsburgh, Pittsburgh, PA, United States*
[6]*Department of Epidemiology, University of Pittsburgh, Pittsburgh, PA, United States*

Introduction: Perceived discrimination in late life is associated with worse cognition, but its relationship to AD both across the lifespan and in promoting racialized group disparities is unknown. We interrogated associations of mid-life perceived discrimination with late-life AD pathology and cognition overall and between African American (AA) and non-Hispanic white (nHW) participants.

Methods: Participants in the Heart Strategies Concentration on Risk Evaluation (HeartSCORE) study completed the Everyday Discrimination Scale (EDS) between 2003-2005 (midlife: 45-59 years). From 2018-2023 (late-life: >65 years), a subset completed PET/MRI studies and neuropsychological assessments (N=141, 28% AA) and plasma biomarker assessments (N=129, 30% AA). Indices of Ab included global [^{11}C]PiB SUVR and plasma Ab42/40 ratio; tau was quantified using meta-temporal lobe [^{18}F]flortaucipir SUVR and plasma phosphorylated tau 181; measures of neurodegeneration were medial temporal lobe cortical thickness and plasma neurofilament light chain. MMSE, Long Delayed Recall, and Trail Making Test B assessed global cognition, episodic memory, and executive function, respectively. Linear models tested associations of mid-life EDS score with each late-life outcome overall, stratified by racialized group, and, if stratified results differed, with an EDS score-by-racialized group interaction. All models were adjusted for age, sex, racialized group, education, time between mid-life and late-life visits, mid-life hypertension and diabetes, and apolipoprotein-E4.

Results: Higher mid-life EDS score was associated with higher late-life Trail Making Test B score (*Table 1*). When stratified, this relationship was significant among AA, but not nHW, participants; the EDS score-by-racialized group interaction was significant (P=0.0006). All other associations of mid-life EDS score with late-life imaging, plasma, and cognition were non-significant (*Table 1*).

Discussion: More mid-life perceived discrimination was associated with worse late-life executive function only among AA participants. These results suggest that perceived discrimination may (1) have a long-term influence on cognition and (2) contribute to AD/dementia disparities through mechanisms outside the AT(N) framework.

Table 1. Associations between mid-life Everyday Discrimination Scale score and each late-life outcome

Late-life outcome	Overall β (P value)	African American β (P value)	Non-Hispanic white β (P value)
Imaging			
Global [^{11}C]PiB SUVR	0.04 (0.56)	0.04 (0.86)	0.03 (0.71)
Meta-temporal [^{18}F]FTP SUVR	0.03 (0.36)	0.18 (0.054)	–0.002 (0.95)
Medial temporal cortical thickness	–0.04 (0.68)	–0.13 (0.56)	–0.003 (0.98)
Plasma			
Aβ 42/40 ratio	–0.03 (0.73)	–0.53 (0.056)	0.03 (0.74)
Phosphorylated tau181	0.13 (0.55)	0.81 (0.22)	–0.08 (0.74)
Neurofilament light chain	0.20 (0.27)	0.59 (0.23)	0.17 (0.39)
Cognition			
MMSE	–1.75 (0.32)	–6.67 (0.10)	–0.24 (0.90)
Long Delayed Recall	–2.98 (0.32)	–6.91 (0.38)	–2.53 (0.44)
Trail Making Test B	0.40 (0.03)*	1.37 (0.01)*	0.06 (0.73)

*P value < 0.05

Note: all estimates adjusted for age, sex, racialized group (in overall model only), education, time between mid-life and late-life visits, mid-life hypertension and diabetes, and *APOE*4*

Abbreviations: Aβ = β–amyloid; FTP = flortaucipir; MMSE = Modified Mini Mental State Examination; PiB = Pittsburgh Compound-B; SUVR = standardized uptake value ratio

Keywords: racialization, perceived discrimination, cognition, imaging, plasma

69 Comparison of amyloid positivity and global cortical SUVR between black and white non-Hispanic participants in the GAP Bio-Hermes study

Robin Wolz[1], Lynne Hughes[2], Richard Manber[1], Richard Mohs[2], John Dwyer[2], Douglas Beauregard[2]

[1]*IXICO, London, United Kingdom*
[2]*Global Alzheimer's Platform Foundation, Washington, DC, United States*

Background: Improved enrollment of traditionally under-represented racial and ethnic groups is critical for Alzheimer's disease (AD) clinical trials.

The GAP Bio-Hermes study collected Florbetapir PET from 398 cognitively normal, 293 MCI and 254 mild AD participants across 16 US sites, recruiting 24% participants from traditionally underrepresented communities. At CTAD 2023 presented Bio-Hermes results show a significantly lower amyloid positive (Aβ+) rate in Black (N=103, 26% Aβ+) compared to White (N=727, 37% Aβ+) Non-Hispanic or Latino participants, despite comparable mix in diagnostic groups and lower mean MMSE in the Black population. No significant differences in global cortical SUVR were observed between the two racial groups.

Objectives: Further investigate amyloid PET differences between Black and White participants in Bio-Hermes to better understand relationship between Aβ+ status from visual read and quantitative SUVR.

Methods: Visual read was performed centrally through the VisQ process in the MIM Software, where global cortical area SUVR is considered by a reader to perform classification into Aβ+ or Aβ-. Here, we compare agreement between the visual reader and the previously proposed cut-off for Aβ+ from global cortical SUVR of 1.10 across the two racial groups.

Results: Results are presented in Figure 1: in both sub-populations, 93% of Aβ+ participants (per visual read), also exhibit SUVR ≥ 1.10. In Aβ- participants (per visual read), 76% of Black participants and 87% of White participants also exhibit SUVR < 1.10.

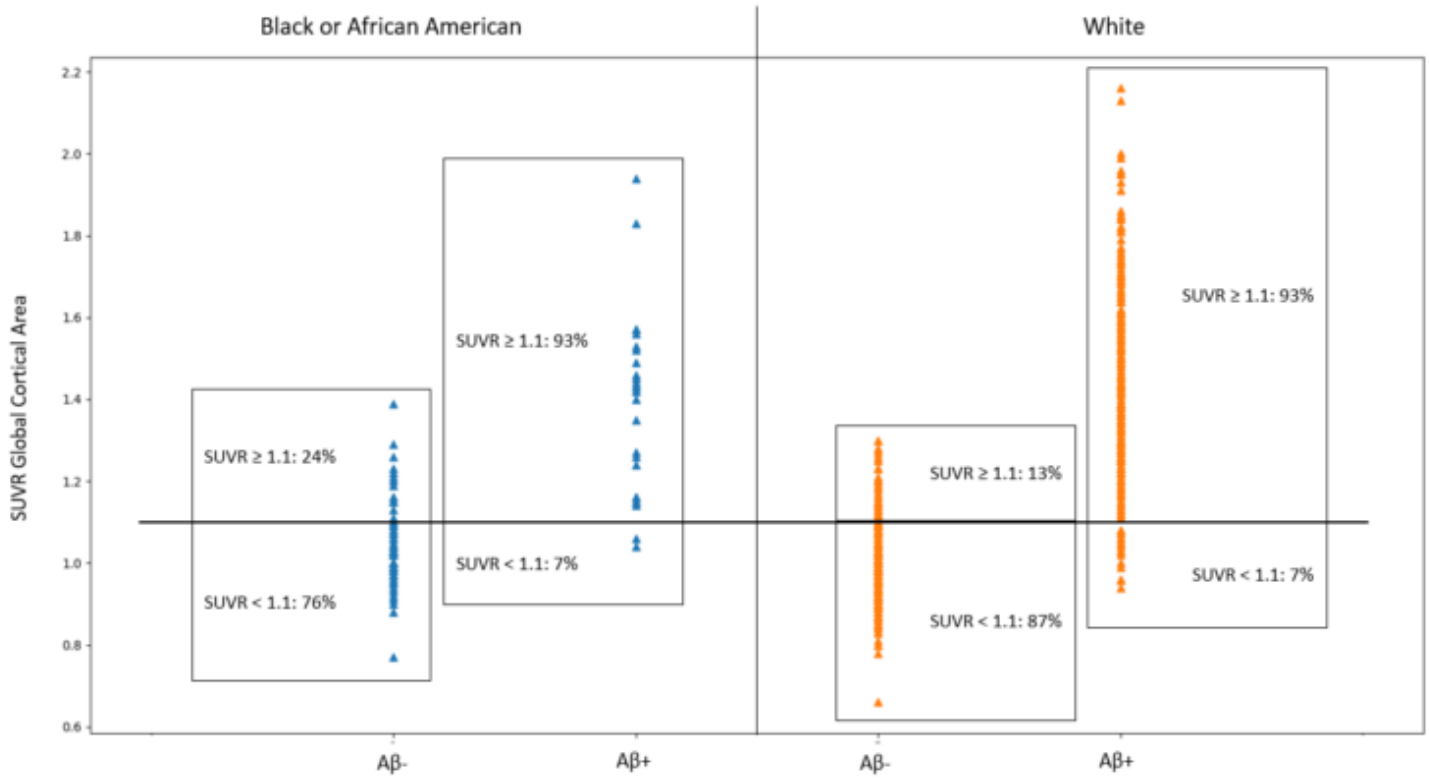

Conclusion:

A substantially higher disagreement of SUVR cut-off with visual read in Aβ- Black participants compared to White participants was observed. This suggests a potential difference in amyloid uptake patterns between the two populations is driving differences in Aβ+ rates as no differences in mean global SUVR was observed. In future work, regional SUVR analysis will be performed to further qualify these findings.

Keywords: Clinical trials, underrepresented populations, amyloid PET, SUVR

70 APOE, ABCA7, and KIF13B associations with earlier onset of amyloid positivity from over 4000 harmonized Positron Emission Tomography images

Tonnar Castellano[1,2], Ting Chen Wang[1,2], Derek Archer[1,2], Karly Cody[1,2], Theresa Harrison[1,2], Yiyang Wu[1,2], Alaina Durant[1,2], Vaibhav Janve[1,2], Corinne Engelman[1,2,3], William Jagust[1,2,3], Marilyn Albert[1,2], Sterling Johnson[1,2], Susan Resnick[1,2], Reisa Sperling[1,2], Murat Bigel[1,2], Andrew Saykin[1,2], Badri Vardarajan[1,2], Richard Mayeux[1,2], Tobey Betthauser[17,18], Logan Dumitrescu[1,2], Elizabeth Mormino[3], Emily Mormino[3], Timothy Hohman[1,2], Mary Ellen Koran[19]

[1]*Vanderbilt Memory and Alzheimer's Center, Department of Neurology, Vanderbilt University Medical Center, Nashville, TN, United States*
[2]*Vanderbilt Genetics Institute, Department of Neurology, Vanderbilt University Medical Center,, Nashville, TN, United States*
[3]*Department of Neurology and Neurological Sciences, Stanford University, Standford, CA, United States*
[4]*Helen Wills Neuroscience Institute, University of California, Berkeley, Berkeley, CA, United States*
[5]*Department of Population Health Sciences, University of Wisconsin, School of Medicine and Public Health, Madison, WI, United States*
[6]*Department of Neurology, Johns Hopkins University School of Medicine, Baltimore, MD, United States*
[7]*Alzheimer's Disease Research Center, University of Wisconsin School of Medicine and Public Health, Madison, WI, United States*
[8]*Laboratory of Behavioral Neuroscience, National Institute on Aging, National Institutes of Health,, Baltimore, MD, United States*
[9]*Department of Neurology, Massachusetts General Hospital, Boston, MA, United States*
[10]*Center for Alzheimer Research and Treatment, Department of Neurology, Brigham and Women's Hospital, Boston, MA, United States*
[11]*Department of Radiology and Imaging Sciences, Center for Neuroimaging, School of Medicine, Indiana University, Indianapolis, IN, United States*
[12]*Department of Medical and Molecular Genetics, School of Medicine, Indiana University, Indianapolis, IN, United States*
[13]*Department of Neurology, Columbia University Medical Center, New York, NY, United States*
[14]*Department of Neurology, The New York Presbyterian Hospital, New York, NY, United States*
[15]*Taub Institute for Research on Alzheimer's Disease and The Aging Brain, Columbia University Medical Center, New York, NY, United States*
[16]*The Institute for Genomic Medicine, Columbia University Medical Center, New York, NY, United States*
[17]*University of Wisconsin-Madison Alzheimer's Disease Research Center, Madison, WI, United States*
[18]*Department of Medicine, University of Wisconsin-Madison, Madison, WI, United States*
[19]*Department of Radiology, Standford University, Standford, CA, United States*

Introduction: The preclinical phase of Alzheimer's Disease (AD) is defined by the absence of clinical signs of AD in the presence of at least one biomarker of AD, including amyloid positivity on positron emission tomography (PET). This study aims to validate *APOE* associations with the estimated amyloid positivity onset age (EAOA) and explore other genetic factors associated with EAOA.

Methods: Data from six cohorts with amyloid PET and genetic data were analyzed. Overall, our data included 4221 non-Hispanic white people of which 57.6% were women. 86.7% were cognitively unimpaired at baseline scans. Amyloid PET data was harmonized using gaussian mixture models. Next**,** estimated age of amyloid onset (EAOA) was calculated using the sampled iterative local approximation (SILA) algorithm1 . A genome-wide association study was performed, covarying for the first three principal components, sex, and *APOE*4 status. Gene and pathway analyses were conducted using MAGMA. Finally, GNOVA was used to explore genetic correlations with complex traits.

Results: *APOE* e4 homozygotes converted to amyloid positivity nearly a decade before e3e4 heterozygotes and over two decades earlier than e3 homozygotes. APOE e2 carriers had slightly later EAOA than e3/e3 carriers. We identified a significant intronic SNP, rs12981369 with a positive relationship for EAOA ($\beta = 2.136$, $P = 9.27 \times 10–9$). Brain eQTL databases indicate associations between rs12981369 with the gene expression of ABCA7. Gene-level analyses revealed significant associations for *ABCA7*, *HMHA1*, *KIF13B*, TUBG1/COASY, and STOML2. No significantly enriched pathways were discovered.

Conclusion: This study reveals the role of *APOE*, *ABCA7*, and *KIF13B* on amyloid onset. In addition, we identified a novel variant on chromosome 19 correlated with later amyloid onset conversion. These findings highlight EAOA as a powerful endophenotype of AD and offer insights into potential drug-targetable pathways for early AD intervention.

Keywords: ABCA7, Age of Onset, Genetics, APOE, Endophenotype

71 Neuroinflammation in patients with mild cognitive impairment and Alzheimer's disease

Mahathi Kandimalla[1], Jeyeon Lee[1], Hoon-Ki Min[1], Hugo Botha[2], Jonathan Graff-Radford[2], David Jones[2], Prashanthi Vemuri[1], Kejal Kantarci[1], David Knopman[2], Clifford Jack[1], Ronald Petersen[2], Val Lowe[1]

[1]*Department of Radiology, Mayo Clinic, Rochester, MN, United States*
[2]*Department of Neurology, Mayo Clinic, Rochester, MN, United States*

Objective: Neuroinflammation leads to the direct demise of neurons, reduced synaptic activity, and suppression of neurogenesis in the hippocampus— making inflammation a critical factor in the progression of Alzheimer's Disease (AD). ER176 is a 3rd generation, PET neuroinflammation radiotracer that may help identify suitable candidates for specialized treatment when adversely impacted by neuroinflammation. ER176 has advantages over other radiotracers with its increased specific binding, reduced variability between subjects, capability to image low-affinity binders, and low radio metabolites entering the brain.

Methods: Participants were recruited from the Mayo Clinic Study of Aging. The study included four participant groups: cognitively unimpaired with normal amyloid (CU A-, n=19), cognitively unimpaired with high amyloid (CU A+, n=15), mild cognitive impairment with increased amyloid (MCI A+, n=8), and AD dementia (AD, n=6). We explored the variations in Neuroinflammation PET results among different groups.

Results: Neuroinflammation levels were higher in the MCI and AD patients compared to both CU groups. Group averages showed that inflammation locality (MCI in frontal lobe, thalamus, basal ganglia, temporal lobe, & the occipital lobe and AD in temporal lobe) levels varied between the different groups. A voxel-wise comparison using a two-sample t-test revealed that the MCI and AD groups exhibited greater neuroinflammation than the CU groups. No differences were seen between CU A- vs CU A+.

Conclusion: Our findings suggest that the progression of neuroinflammation aligns with cognitive decline rather than amyloid deposition alone. This insight underscores the potential utility of ER176 as a valuable diagnostic tool for identifying individuals who may benefit from targeted interventions addressing neuroinflammation in the context of AD.

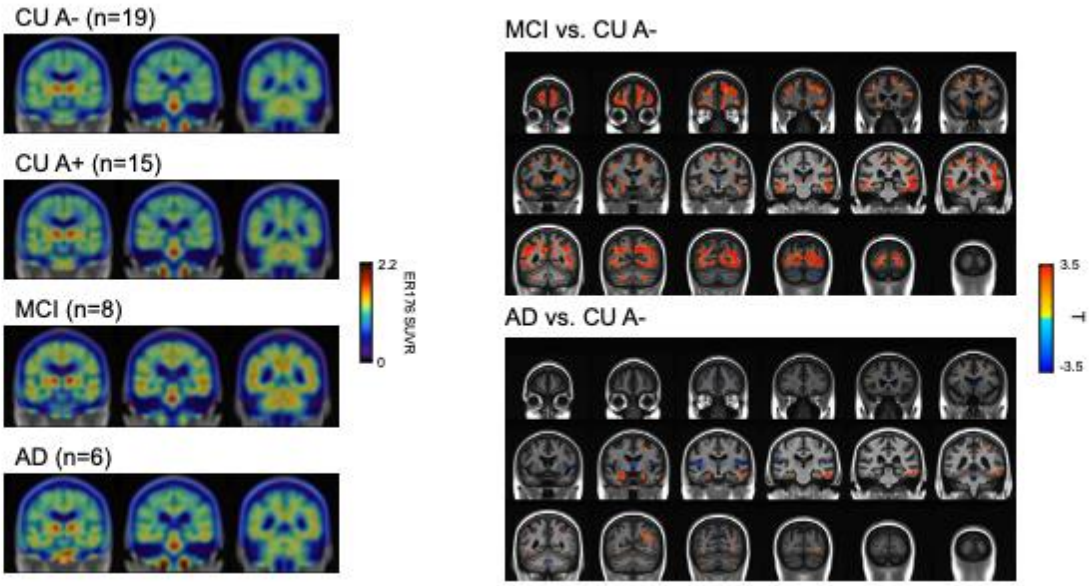

Keywords: Neuroinflammation, Alzheimer's Disease, PET Radiotracer, Mild Cognitive Impairment, Diagnostic Tool

73 Elevated amyloid-ß and tau burden is associated with accelerated cognitive decline on a digital clock drawing test in preclinical AD

Jessie Fanglu Fu[1,2], Talia Robinson[2], Marina Rodriguez Alonso[2], Adela Francis Malave[2], Roos J. Jutten[2], Grace A. Del Carmen Montenegro[2], Emma Thibault[2], Dana Penney[3], Randall Davis[4], Reisa A. Sperling[2], Keith A. Johnson[2], Julie C. Price[1,2], Dorene M. Rentz[2]

[1]*Athinoula A. Martinos Center for Biomedical Imaging, Charlestown, MA, United States*
[2]*Massachusetts General Hospital, Harvard Medical School, Boston, MA, United States*
[3]*Lahey Hospital and Medical Center, Burlington, MA, United States*
[4]*Massachusetts Institute of Technology, Cambridge, MA, United States*

Background: PET quantifies tau and amyloid-ß (**Aß**) pathology in preclinical AD. A 2-min digital clock-drawing test (**DCTclock™**) was developed to capture the clock-drawing outcome and processes, potentially more sensitive to excutive deficits in preclinical AD. The DCTclock composite score is the sum of subscores targeting multi-domain cognitive performance (i.e., Spatial Reasoning, Information Processing, Drawing Efficiency, and Simple Motor, **Table.1**). Using cross-sectional data, we previously showed worse performance in the Spatial Reasoning domain associated with high tau and Aß burden in cognitive normal order (**CN**) subjects. Here, we evaluate whether longitudinal DCTclock could capture subtle cognitive decline associated with Aß and tau burden in CN subjects.

Method: 204 CN subjects underwent baseline DCTclock, and at least one annual DCTclock follow-up (**Table.1**). Subjects underwent Ab PET ([^{11}C]PiB, n=204) and tau PET (Flortaucipir: n=146 or [^{18}F]MK-6240 (**MK**): n=40). Global Ab DVR was estimated in neocortical aggregate regions. Tau SUVR was estimated in the entorhinal and inferior temporal. PET outcomes used cerebellar gray-matter reference. Linear mixed effect models examined associations between longitudinal DCTclock and Ab or tau burden, correcting for age, sex, education and handedness.

Results: Higher baseline PiB uptake was associated with lower baseline and accelerated cognitive decline in DCTclock composite scores, and subscores targeting executive function (**Fig.1A-D, Table.2**). Higher Flortaucipir and MK uptake was specifically associated with accelerated cognitive decline in the Information Processing domain (**Fig.1E-H**). Higher inferior temporal MK uptake was also associated with accelerated cognitive decline in DCTclock composite scores (**Fig.1G-H**), despite smaller sample size than FTP.

Conclusion: Our results suggest that longitudinal DCTclock performance may capture subtle cognitive decline associated with early Ab and tau burden in preclinical AD. The DCTclock Information Processing subdomain (i.e., time spent thinking and latency between pen-strokes) may capture a greater thinking or cognitive effort, reflecting early changes in executive function in preclinical AD.

Table 1. Characteristics for n=204 cognitively normal participants with longitudinal DCTclock.			
		CN Aβ- (n=146)	**CN Aβ+ (n=58)**
Sex (%female)		57%	60%
Age, years		76.4 ± 8.8 (37 – 93)	78.4 ± 6.7 (59 – 94)
Education, years		16.3 ± 2.9 (8 – 20)	16.7 ± 3.0 (8 – 20)
Handedness (% right-handed)		80%	85%
PACC		0.11 ± 0.82 (-2.7 – 1.9)	-0.20 ± 0.76 (-2.6 – 1.5)
Baseline DCTclock composite scores			
Composite score (0-100)		73.5 ± 21.7 (5 – 100)	64.7 ± 22.8 (2 – 98)
Baseline DCTclock domain-specific subscores (z-scores)			
Drawing Efficiency (e.g., total time, drawing size)		0.03 ± 1.07 (-5.0 – 1.7)	-0.07 ± 1.20 (-4.6 – 1.8)
Information Processing (e.g., percent thinking time, latency)		0.03 ± 0.97 (-4.2 – 1.5)	-0.03 ± 1.10 (-3.6 – 1.7)
Simple Motor (e.g., oscillatory motion, speed)		-0.11 ± 1.15 (-4.7 – 1.8)	-0.29 ± 1.15 (-3.6 – 1.5)
Spatial Reasoning (e.g., clockface circularity, clock component placement)		-0.15 ± 1.26 (-4.2 – 1.2)	-0.44 ± 1.45 (-4.7 – 1.3)
DCTclock average longitudinal followup duration		16.5 ± 8.3 (5.5 – 56.6) months 1 followup: n = 50 2 followup: n = 39 3 followup: n = 38 4 followup: n =17 5 followup: n = 2	15.7 ± 7.7 (5.7 – 40.8) months 1 followup: n = 16 2 followup: n = 25 3 followup: n = 9 4 followup: n =5 5 followup: n = 1
PET imaging outcomes			
[^{11}C]PiB DVR (threshold = 1.19)	**Number of subjects**	n = 146	n = 58
	Time differences from baseline DCTclock	17 ± 21 months	16 ± 18 months
	Global FLR	1.08 ± 0.05 (0.98 – 1.18)	1.49 ± 0.21 (1.19 – 2.20)
Flortaucipir SUVR$_{75\text{-}105}$ (PVC)	**Number of subjects**	n = 107	n = 39
	Time differences from baseline DCTclock	12 ± 15 months	12 ± 9 months
	Entorhinal	1.33 ± 0.23 (0.78 – 2.00)	1.59 ± 0.39 (1.04 – 2.47)
	Inferior Temporal	1.46 ± 0.14 (1.14 – 1.82)	1.60 ± 0.22 (1.14 – 2.25)
[^{18}F]MK-6240 SUVR$_{90\text{-}110}$ (PVC)	**Number of subjects**	n = 26	n = 14
	Time differences from baseline DCTclock	0.2 ± 1.1 months	0 ± 0 months
	Entorhinal	0.88 ± 0.75 (0.21 – 4.00)	1.45 ± 0.78 (0.59 – 2.97)
	Inferior Temporal	1.07 ± 0.27 (0.68 – 2.00)	1.35 ± 0.95 (0.81 – 4.57)

*** Continuous values are expressed as mean ± standard deviation (min – max).**

DCTclock = digital clock drawing test. **CN** = cognitively normal. **Aβ** = amyloid-β. **PiB** = [^{11}C]Pittsburgh-Compound-B. **DVR** = distribution volume ratio (using Logan graphical method and cerebellar gray matter reference region). **SUVR** = standardized uptake value ratio (using cerebellar gray matter reference region). **FLR** = frontal, lateral temporal and retrosplenial composite region for estimating global Aβ burden. **PVC** = partial volume correction using geometric transfer matrix algorithm. **PACC** = preclinical Alzheimer's cognitive composite.

Table 2. Linear mixed effect model estimates for longitudinal DCTclock composite scores and subscores.

Predictors	Estimates [CI]			
DCTclock variables	**Composite Scores**	**Drawing Efficiency subscores**	**Information Processing subscores**	**Spatial Reasoning subcores**
Clinical Variables				
Age	-0.6 [-0.9 – -0.3] ***	N.S.	-0.02 [-0.04 – 0.01] **	-0.02 [-0.04 – 0.0] *
Sex	N.S.	N.S.	0.3 [0.08 – 0.6] *	N.S.
Education	1.7 [0.7 – 2.6] **	0.07 [0.03 – 0.1] **	0.06 [0.01 – 0.1] *	0.07 [0.02 – 0.1] **
Handedness	N.S.	N.S.	N.S.	N.S.
Time	-0.2 [-0.2 – -0.1] ***	N.S.	N.S.	N.S.
Global Aβ burden – [^{11}C]PiB				
Baseline PiB FLR	-21 [-35 – -7] **	N.S.	N.S.	-0.8 [-1.6 – -0.02] *
Time x PiB	-0.3 [-0.6 – -0.05] *	-0.02 [-0.03 – -0.00] *	-0.02 [-0.04 – -0.01] **	-0.02 [-0.05 – -0.00] *
Regional Tau burden – Flortaucipir (FTP)				
Time x FTP Inferior Temporal	N.S.	-0.02 [-0.05 – -0.00] *	-0.04 [-0.06 – -0.02] ***	N.S.
Time x FTP Entorhinal	N.S.	N.S.	-0.02 [-0.04 – -0.01] **	N.S.
Regional Tau burden – [^{18}F]MK-6240 (MK)				
Time x MK Inferior Temporal	-0.4 [-0.7 – -0.02] *	N.S.	-0.02 [-0.04 – -0.00] *	N.S.
Time x MK Entorhinal	N.S.	N.S.	N.S.	N.S.

***** = p<0.001, ** = p<0.01, * = p<0.05, CI = confidence interval, N.S. = not significant at p=0.05.**
Linear mixed model equation: **DCTclock ~ age + sex + education + handedness + PET*time, random=~1 + time|subject**, where time is time since DCTclock baseline. Only DCTclock domain-specific subscores that showed significant associations with PET imaging outcomes were included in the table. In linear mixed effect models with DCTclock and tau PET, baseline tau PET measures were not significantly associated with DCTclock scores.

DCTclock = digital clock drawing test. **CI** = 95% confidence interval. **PiB** = [^{11}C]Pittsburgh-Compound-B. **FLR** = frontal, lateral temporal and retrosplenial composite region for estimating global Aβ burden.

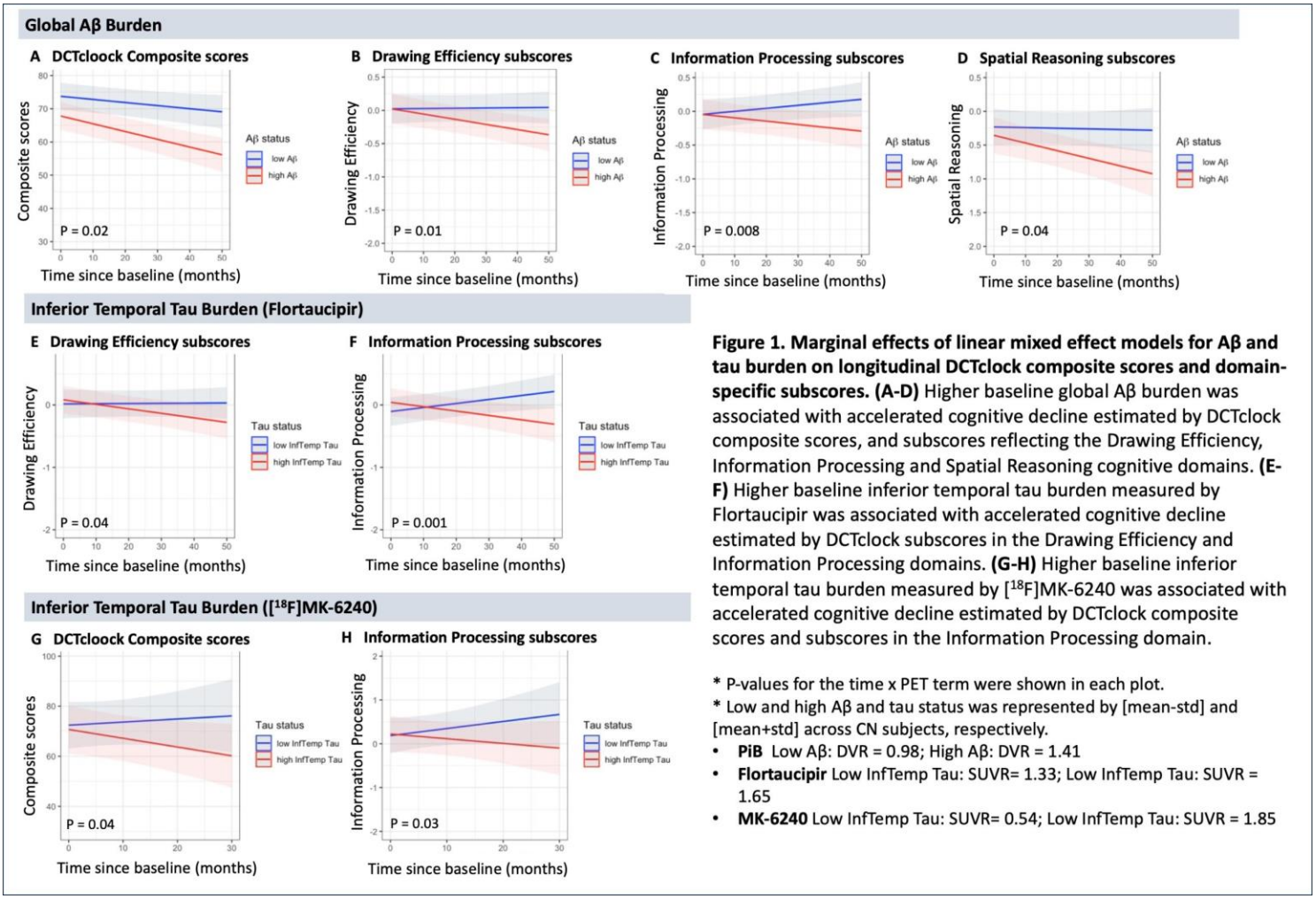

Figure 1. Marginal effects of linear mixed effect models for Aβ and tau burden on longitudinal DCTclock composite scores and domain-specific subscores. (A-D) Higher baseline global Aβ burden was associated with accelerated cognitive decline estimated by DCTclock composite scores, and subscores reflecting the Drawing Efficiency, Information Processing and Spatial Reasoning cognitive domains. **(E-F)** Higher baseline inferior temporal tau burden measured by Flortaucipir was associated with accelerated cognitive decline estimated by DCTclock subscores in the Drawing Efficiency and Information Processing domains. **(G-H)** Higher baseline inferior temporal tau burden measured by [^{18}F]MK-6240 was associated with accelerated cognitive decline estimated by DCTclock composite scores and subscores in the Information Processing domain.

* P-values for the time x PET term were shown in each plot.
* Low and high Aβ and tau status was represented by [mean-std] and [mean+std] across CN subjects, respectively.

- **PiB** Low Aβ: DVR = 0.98; High Aβ: DVR = 1.41
- **Flortaucipir** Low InfTemp Tau: SUVR= 1.33; Low InfTemp Tau: SUVR = 1.65
- **MK-6240** Low InfTemp Tau: SUVR= 0.54; Low InfTemp Tau: SUVR = 1.85

Keywords: Positron emission tomography, tau, digital clock drawing test, longitudinal analysis, Alzheimer's disease

74 Significance of a positive tau PET scan with a negative amyloid PET scan

Carling G. Robinson[1,7], Jeyeon Lee[6], Hoon-Ki Min[1], Scott A. Przybelski[4], Keith A. Josephs[3], David T. Jones[3], Jonathan Graff-Radford[3], Bradley F. Boeve[3], David S. Knopman[3], Clifford R. Jack. Jr.[1], Ronald C. Petersen[3], Mary M. Machulda[2], Julie Fields[2], Val J. Lowe[1]

[1]*Department of Radiology, Mayo Clinic, Rochester, MN, United States*
[2]*Deparment of Psychiatry and Psychology, Mayo Clinic, Rochester, MN, United States*
[3]*Department of Neurology, Mayo Clinic, Rochester, MN, United States*
[4]*Quantitative Health Sciences, Mayo Clinic, Rochester, MN, United States*
[5]*Department of Neuroscience, Mayo Clinic, Jacksonville, FL, United States*
[6]*Department of Biomedical Engineering, College of Medicine, Hanyang University, Seoul, South Korea*
[7]*Department of Psychological and Brain Sciences, Washington University in St. Louis, St. Louis, MO, United States*

Table 1. Characteristics of matched CU A-T- versus A-T+ (mean (SD) for continuous variables and count (%) for categorical variables).

	MCSA and ADRC with respective matches			MCSA only with respective matches		
	A-T- n = 196	A-T+ n = 98	P-value	A-T- n = 128	A-T+ n = 64	P-value†
Age, yrs	72.3 (11.2)	72.3 (11.3)	0.73	74.9 (10.1)	74.9 (10.1)	0.86
Males, no. (%)	126 (64%)	63 (64%)	1.00	80 (62%)	40 (62%)	1.00
Education, yrs	15.3 (2.6)	14.9 (2.4)	0.14	15.3 (2.4)	14.6 (2.1)	0.068
MMSE	28.7 (1.1)	27.1 (3.2)	<0.001	28.7 (1.0)	28.1 (2.0)	0.022
CDR SOB	0.0 (0.1)	1.3 (2.4)	<0.001	0.0 (0.2)	0.2 (0.7)	0.10
UPDRS Score	0.4 (1.4)	1.6 (3.9)	0.003	0.5 (1.4)	0.6 (1.7)	0.77
APOE e4 carriers, no. (%)	46 (25%)	12 (13%)	0.016	32 (27%)	6 (10%)	0.010
PiB SUVr	1.37 (0.07)	1.38 (0.07)	0.36	1.38 (0.07)	1.38 (0.06)	0.38
Tau SUVr	1.15 (0.07)	1.36 (0.09)		1.15 (0.07)	1.33 (0.04)	
APOE e4 carriers, no. (%)	46 (25%)	12 (13%)	0.016	32 (27%)	6 (10%)	0.010
Diagnosis						
Cognitively Unimpaired	196 (100%)	56 (57.1%)		128 (100%)	53 (82.8%)	
MCI		16 (16.3%)			9 (14.1%)	
Uncertain		5 (5.1%)			1 (1.6%)	
FTD		6 (6.1%)				
DLB		6 (6.1%)				
AD		1 (1.0%)				
Progressive Fluent Aphasia		2 (2.0%)				
Progressive Associative Agnosia		1 (1.0%)				
Logopenic Progessive Aphasia		2 (2.0%)				
Paraneoplastic		1 (1.0%)				
Dementia-Hard to Classify		1 (1.0%)			1 (1.6%)	
Prior Mental Deficit-Static		1 (1.0%)				

†P-values: Based on a conditional logistic model accounting for matching.

Table 2. Neuropsychological test scores (raw) for CU A-T- versus A-T+ (mean (SD) for continuous variables and count (%) for categorical variables).

	MCSA and ADRC with respective matches			MCSA only with respective matches		
	A-T- n = 196	A-T+ n = 98	P-value	A-T- n = 128	A-T+ n = 64	P-value†
Logical Memory I	26.0 (7.5)	18.4 (10.3)	<0.001	25.5 (7.5)	23.8 (8.0)	0.16
Logical Memory II	22.9 (8.3)	14.9 (9.9)	<0.001	22.3 (8.4)	19.0 (9.3)	0.022
AVLT Delayed Recall	8.7 (3.4)	7.1 (4.0)	0.004	8.5 (3.4)	7.3 (3.9)	0.040
Category Fluency (Animals)	20.1 (4.9)	17.9 (7.1)	0.005	19.9 (4.8)	19.9 (6.0)	0.94
Category Fluency (Vegetables)	12.4 (3.3)	11.2 (5.1)	0.021	12.2 (3.3)	12.7 (4.8)	0.41
*Trail Making Test A	35.3 (11.7)	46.4 (31.2)	<0.001	36.7 (12.4)	38.0 (18.5)	0.40
*Trail Making Test B	81.0 (40.5)	108.0 (71.9)	<0.001	84.7 (39.7)	96.0 (64.4)	0.12
Block Design	29.2 (9.3)	24.1 (10.9)	0.002	28.7 (9.4)	25.6 (10.2)	0.035

†P-values: Based on a conditional logistic model accounting for matching.

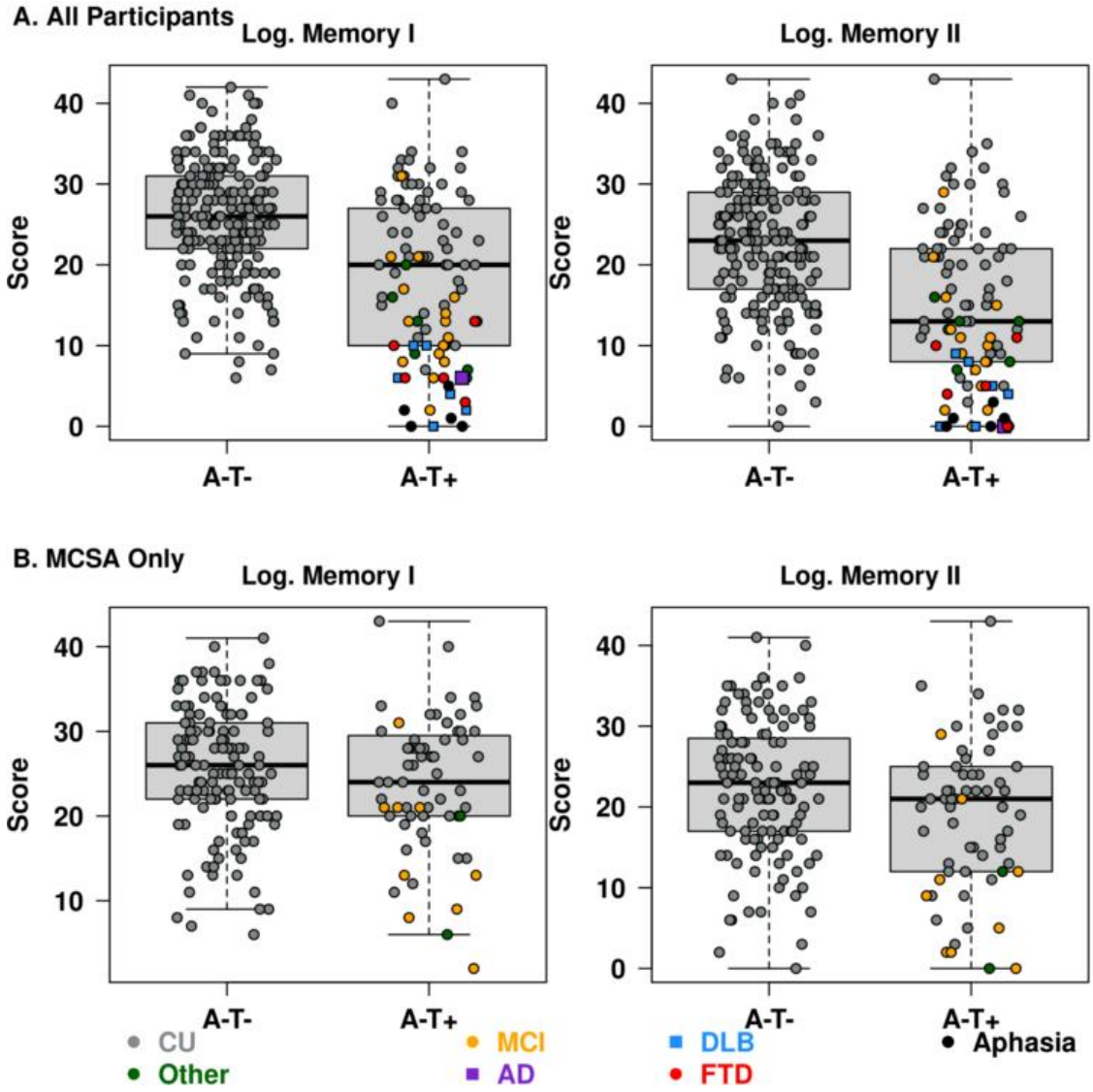

Introduction: The implications of positive tau positron emission tomography (T) with negative beta-amyloid positron emission tomography (A) are not well understood. A-T+ individuals have been described as belonging to the primary age-related tauopathy (PART) categorization, which is a neuropathological diagnosis delineated as mild/moderate tau deposition in the absence of beta-amyloid pathology. We investigated cognitive performance in participants who were T+ but A-.

Methods: We evaluated 98 participants from the Mayo Clinic Study of Aging (MCSA) and the Mayo Clinic Alzheimer's Disease Research Center (ADRC) who were positive for Flortaucipir (FTP) PET and negative for Pittsburgh compound-B (PiB) PET. Participants were classified as A- and T+ based on Standardized Uptake Value Ratios (SUVr) of FTP and PiB PET scans. The cutoff for tau positivity was greater than or equal to 1.29 and the cutoff for beta-amyloid negativity was less than 1.48. A-T+ participants were matched 2:1 to amyloid negative and tau negative cognitively unimpaired (CU) individuals from the MCSA. We compared cognitive test scores between different groups.

Results: The A-T+ group demonstrated lower performance than the A-T- group on the Mini Mental Status Exam (MMSE) ($p<0.001$), Wechsler Memory Scale-Revised Logical Memory I ($p<0.001$) and Logical Memory II ($p<0.001$), Auditory Verbal Learning Test (AVLT) delayed recall ($p=0.004$), category fluency (animals $p=0.005$; vegetables $p=0.021$), Trailmaking Test A and B ($p<0.001$), and others. There were no significant differences in demographic features or APOE genotype between CU A-T+ and CI A-T+.

Conclusions: Positive tau PET in the absence of beta-amyloid positivity is associated with lower cognitive performance. Determining if these participants truly reflect a PART diagnosis or other pathology will depend on future longitudinal neuroimaging and neuropathologic studies examining the presence of beta-amyloid in these participants later on in disease course.

Keywords: FTP-PET, tau, Alzheimers disease, cognition, amyloid PET

75 Lower Locus Coeruleus function in associated with greater cognitive variability in preclinical Alzheimer's disease

Truley Juneau[1], Marion Baillet[4], Emma Wiklund[1], Joost Riphagen[1], Prokopis Prokopiou[1], Kathryn Papp[3], Roos Jutten[3], Dorene Rentz[2,3], Reisa Sperling[2,3], Keith Johnson[1,3], Heidi Jacobs

[1]*Gordon Center for Medical Imaging, Department of Radiology, Massachusetts General Hospital, Boston, MA, United States*
[2]*Center for Alzheimer Research and Treatment, Department of Neurology, Brigham and Women's Hospital, Boston, MA, United States*
[3]*Department of Neurology, Massachusetts General Hospital, Boston, MA, United States*
[5]*Faculty of Health, Medicine and Life Sciences, School for Mental Health and Neuroscience, Alzheimer Centre Limburg, Maastricht University, Maastricht, The Netherlands*

Introduction: Increased intraindividual cognitive variability (IIV) has been linked to an increased risk of developing Alzheimer's Disease (AD). The neural underpinnings of IIV are unclear but are assumed to be related to dysregulation of the noradrenergic locus coeruleus (LC)-system reflected in a worse signal-to-noise signal processing in the brain. Given that the LC is also affected early in AD, we aimed to examine whether IIV is associated with LC function in the context of AD pathology.

Methods: We used data from cognitively normal older participants from the Harvard Aging and Brain study (N=128, Table 1) who performed a novel vs repeated face-name fMRI task and underwent Pittsburgh-Compound-B (beta-amyloid) PET imaging and serial annual cognitive testing. For each cognitive tests across various domains, each participant's coefficient of variation (CV) was calculated considering their within-subject mean and standard deviation in performance over time. Consistent with our previous work, LC function was determined by contrasting the BOLD fMRI signal in the LC during novel versus repeated face-name stimuli. Robust linear regression analyses associated the CV for each neuropsychological test with LC function (and its interaction with neocortical PiB) after adjusting for age, sex, and education.

Results: Higher LC function was associated with lower CV on the Buschke Selective Reminding Test (SRT) Delayed Recall (Figure 2). For our interactions with PiB, we found that the negative relationship between the CV on the Digit Symbol Substitution and Digit Span Forward and LC function were stronger at higher levels of neocortical PiB (Figure 3).

Conclusions: These findings indicate that lower activity of the LC during novelty, presumed to reflect less optimal synaptic signal-to-noise control, is associated with greater cognitive IIV in preclinical AD. In follow-up studies, we aim to replicate these findings for cognitive IIV on shorter time scales.

Keywords: Locus Coeruleus function, cognitive variability, beta-amyloid, Tau, preclinical Alzheimer's disease

76 Associations between regional tau pathology and cognitive decline across the AD continuum differ by sex

Ellen Singleton[1], Niklas Mattsson-Carlgren[1], Alexa Pichet Binette[1], Erik Stomrud[1], Olof Strandberg[1], Rik Ossenkoppele[1,2], Oskar Hansson[1]

[1]*Clinical Memory Research Unit, Department of Clinical Sciences Malmö, Lund University, Sweden, Lund, Sweden*
[2]*Alzheimer Center Amsterdam, Department of Neurology, Amsterdam Neuroscience, Vrije Universiteit Amsterdam, Amsterdam UMC, Amsterdam, the Netherlands, Amsterdam, The Netherlands*

Background: Female sex has been associated with faster tau accumulation over time and greater resilience in Alzheimer's disease. However, relatively few studies have examined the interaction between regional tau pathology and sex on cognitive decline in a large amyloid-positive cohort.

Methods: We included n=761 amyloid-positive participants from the Swedish BioFINDER-2 study who had undergone longitudinal tau PET and cognitive testing, of whom n=253 were cognitively unimpaired (CU A+) and n=508 were cognitively impaired (CI A+) (**Table 1**). [^{18}F]RO948-tau-PET SUVR within entorhinal, medial temporal, neocortical temporal, medial parietal, lateral parietal, occipital, frontal, anterior cingulate, insula and neocortical composite regions was quantified. Cognition was assessed with the mPACC5. Linear mixed models with random intercepts and slopes were fitted to assess the effect of the interaction between baseline tau and sex on cognition over time, adjusting for age, education and APOEe4 status.

Results: Models assessing the interaction between baseline tau and sex on cognitive decline showed significant *positive* associations in multiple tau regions in CU A+ and longitudinal mPACC5 (**Figure 1**), such that males with greater tau-PET burden had faster cognitive decline. However, the reverse was seen in CI A+, where significant *negative* associations between some tau regions and longitudinal mPACC5 were observed: females with greater tau-PET burden had faster cognitive decline (**Figure 1**). Examples of cognitive trajectories in males and females at different tau-PET levels are shown in **Figure 2**.

Discussion: Our results suggest that cognitively unimpaired A+ females exhibit greater cognitive resilience than males, while cognitively impaired A+ females exhibit less cognitive resilience in the face of tau pathology, and that these effects occur particularly at high levels of tau pathology.

Table 1. Demographic characteristics of the longitudinal dataset

	CU A+		CI A+		
	Female (N=134)	**Male (N=119)**	**Female (N=265)**	**Male (N=243)**	**p-value**
Age	72 (± 9.2)	73 (± 8.4)	73 (± 7.5)	74 (± 7.1)	0.859
Education	13 (± 3.5)	13 (± 3.9)	12 (± 4.1)	13 (± 4.4)	0.181
Diagnosis					
Normal	73 (54 %)	52 (44 %)	0 (0 %)	0 (0 %)	<0.001
SCD	61 (46 %)	67 (56 %)	0 (0 %)	0 (0 %)	
MCI	0 (0 %)	0 (0 %)	111 (42 %)	126 (52 %)	
AD	0 (0 %)	0 (0 %)	154 (58 %)	117 (48 %)	
MMSE	29 (± 1.2)	29 (± 1.5)	23 (± 4.4)	24 (± 4.4)	<0.001
mPACC5	-0.27 (± 0.80)	-0.35 (± 0.76)	-3.0 (± 1.5)	-2.9 (± 1.8)	<0.001
Tau PET cortical SUVR	1.1 (± 0.16)	1.1 (± 0.11)	1.5 (± 0.44)	1.4 (± 0.39)	<0.001
MRI cortical thickness	2.3 (± 0.079)	2.3 (± 0.084)	2.2 (± 0.097)	2.2 (± 0.10)	<0.001

CU=cognitively unimpaired, CI=cognitively impaired, A+=amyloid positive, SCD=subjective cognitive decline, MCI=mild cognitive impairment, AD=Alzheimer's disease, MMSE=mini mental state examination, mPACC5=modified preclinical Alzheimer's disease cognitive composite, PET=positron emission tomography, SUVR=standard uptake value ratio, MRI=magnetic resonance imaging. Mean(SD) are depicted unless otherwise specified.

Figure 1. Associations between the interaction between tau pathology and sex and longitudinal cognition across the AD clinical continuum

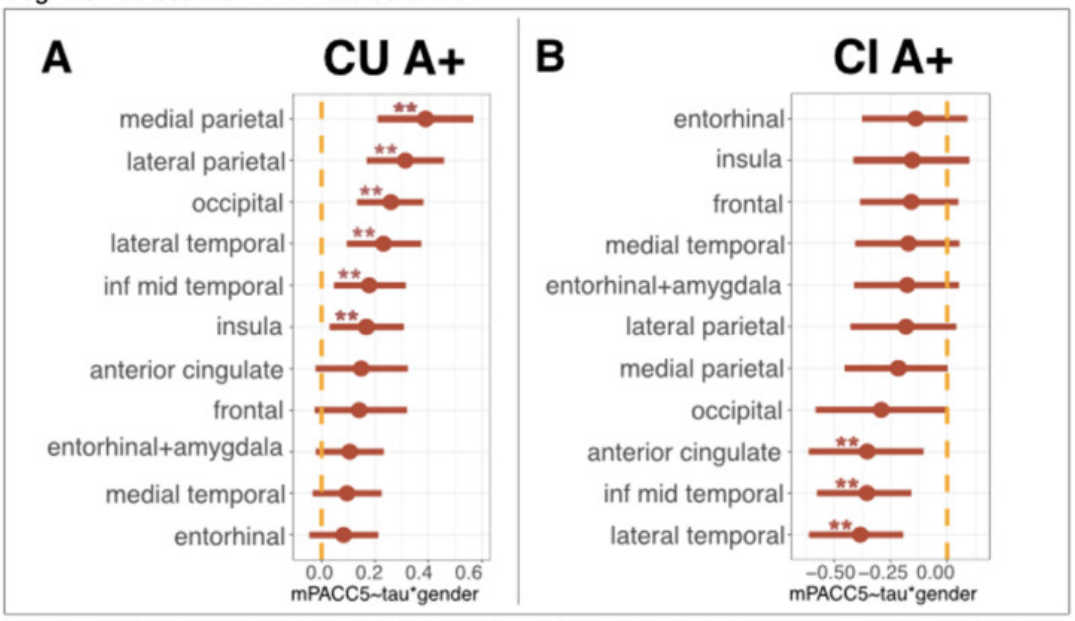

CU=cognitively unimpaired, *CI*=cognitively impaired, *A+*=amyloid positive, *mPACC5*=modified preclinical Alzheimer Cognitive Composite

Figure 2. Trajectories of cognitive decline per quartile of regional tau burden across the AD clinical continuum

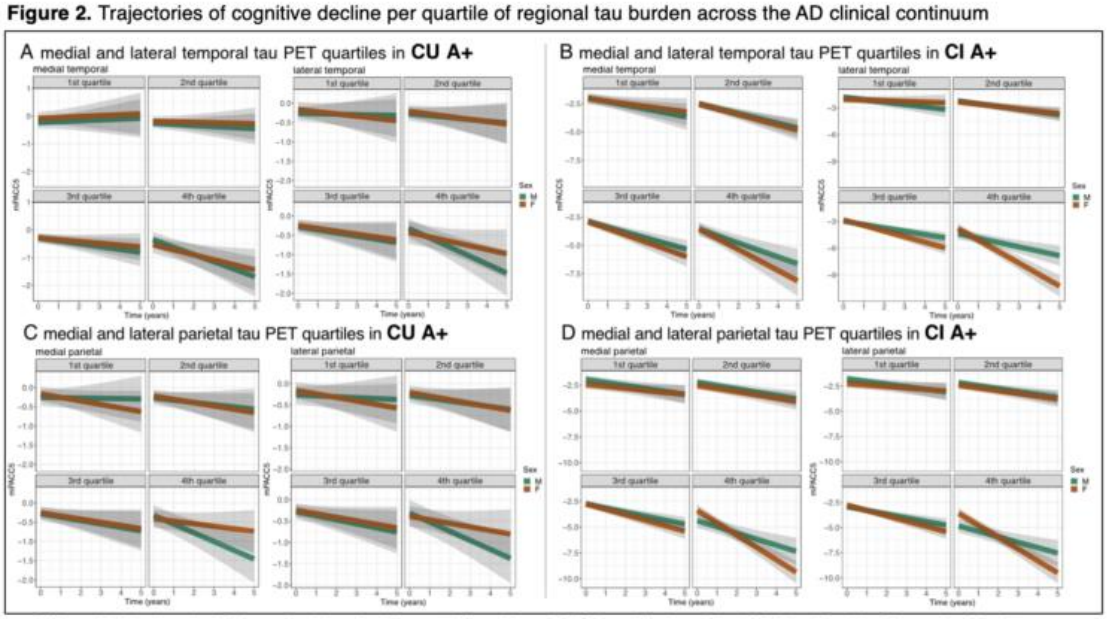

CU=cognitively unimpaired, *CI*=cognitively impaired, *A+*=amyloid positive, *mPACC5*=modified preclinical Alzheimer Cognitive Composite, M=males, F=females. Trajectories for the temporal regions (Panel A) and parietal regions (Panel C) in CU A+ and CI A+ (Panel B and D) are shown.

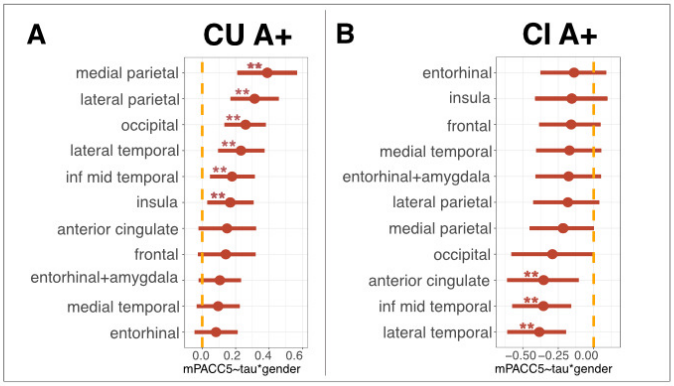

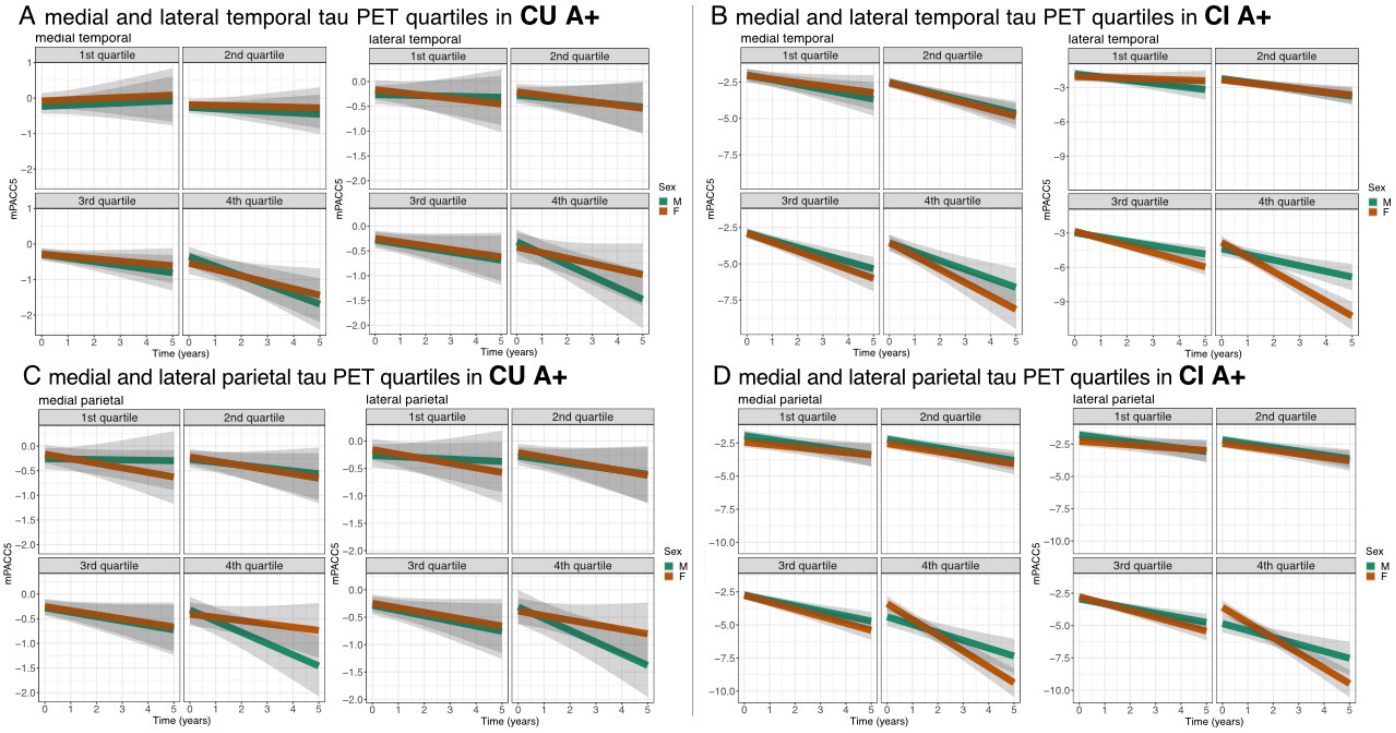

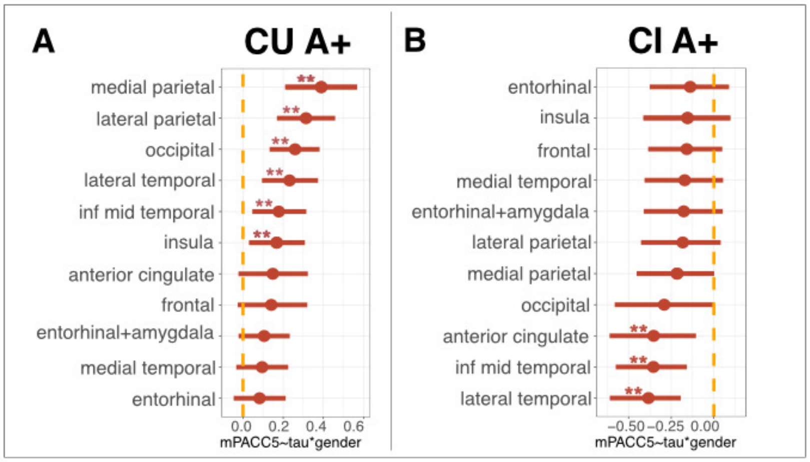

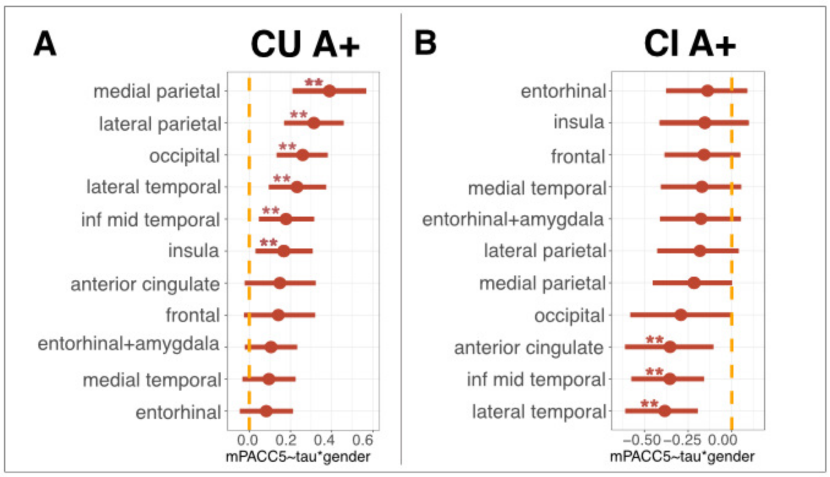

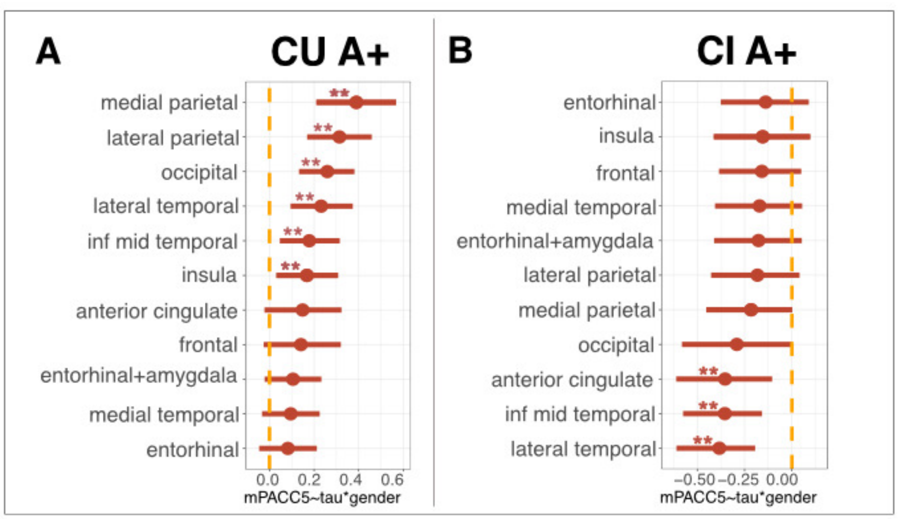

Keywords: tau PET, tau pathology cognition, longitudinal, sex, females, males

77 Dynamic brain states are associated with Alzheimer's pathology and cognition

Jenna Adams[1], Sarah Kark[1], Miranda Chappel-Farley[1], Yuritza Escalante[1], Lea Stith[1], Paul Rapp[2], Michael Yassa[1]

[1]*Department of Neurobiology & Behavior, University of California, Irvine, Irvine, CA, United States*
[2]*Department of Military and Emergency Medicine, Uniformed Services University, Bethesda, MD, United States*

Background: Dynamic and rapid reconfigurations of neural activation patterns that support cognition, known as brain states, may be vulnerable in Alzheimer's disease. Recent analytic advances applied to functional MRI now enable the moment-to-moment characterization of how brain states persist and transition across time, which provides richer information about neural dynamics than static functional connectivity metrics. We hypothesized that dysfunctional brain state persistence and transition patterns in older adults may reflect neurophysiological disruptions due to Alzheimer's pathology and be related to cognitive performance.

Methods: We analyzed 334 high-resolution resting-state functional MRI scans from ADNI3, spanning from cognitively unimpaired (n=188), mild cognitive impairment (n=115), and dementia (n=31) (mean age=73.9, 50.9% female). Dynamic brain states were derived with k-means clustering across all time points of the BOLD time series from 218 ROIs. Persistence of each brain state and transition probabilities between distinct states were quantified (**Fig1a**). Amyloid-beta and tau pathology were measured with FBP/FBB-PET (converted to Centiloids) and FTP-PET, respectively. Volume was extracted from FreeSurfer ROIs. Associations between brain states and regional pathology/volumes were conducted using sparse canonical correlations. Cognitive performance was assessed with MoCA and memory composite scores.

Results: We identified six distinct brain states, corresponding to patterns high or low coactivation resembling default mode, limbic, and visual networks (**Fig1b**). Higher limbic state persistence was associated with spatially specific patterns of tau pathology within medial and inferior temporal regions (r=0.23, p<0.001), amyloid-beta pathology in inferolateral and posterior occipital regions (r=0.18, p=0.006), and neurodegeneration in temporal and parietal regions (r=0.36, p<0.001) (**Fig2**). Higher persistence within and transitions to limbic states, at the expense of other brain states, was associated with worse MoCA and memory performance (**Fig3**).

Conclusions: Increased persistence and transitions into limbic brain states may reflect a pathological neurophysiological response during the development of Alzheimer's disease and contribute to cognitive deficits.

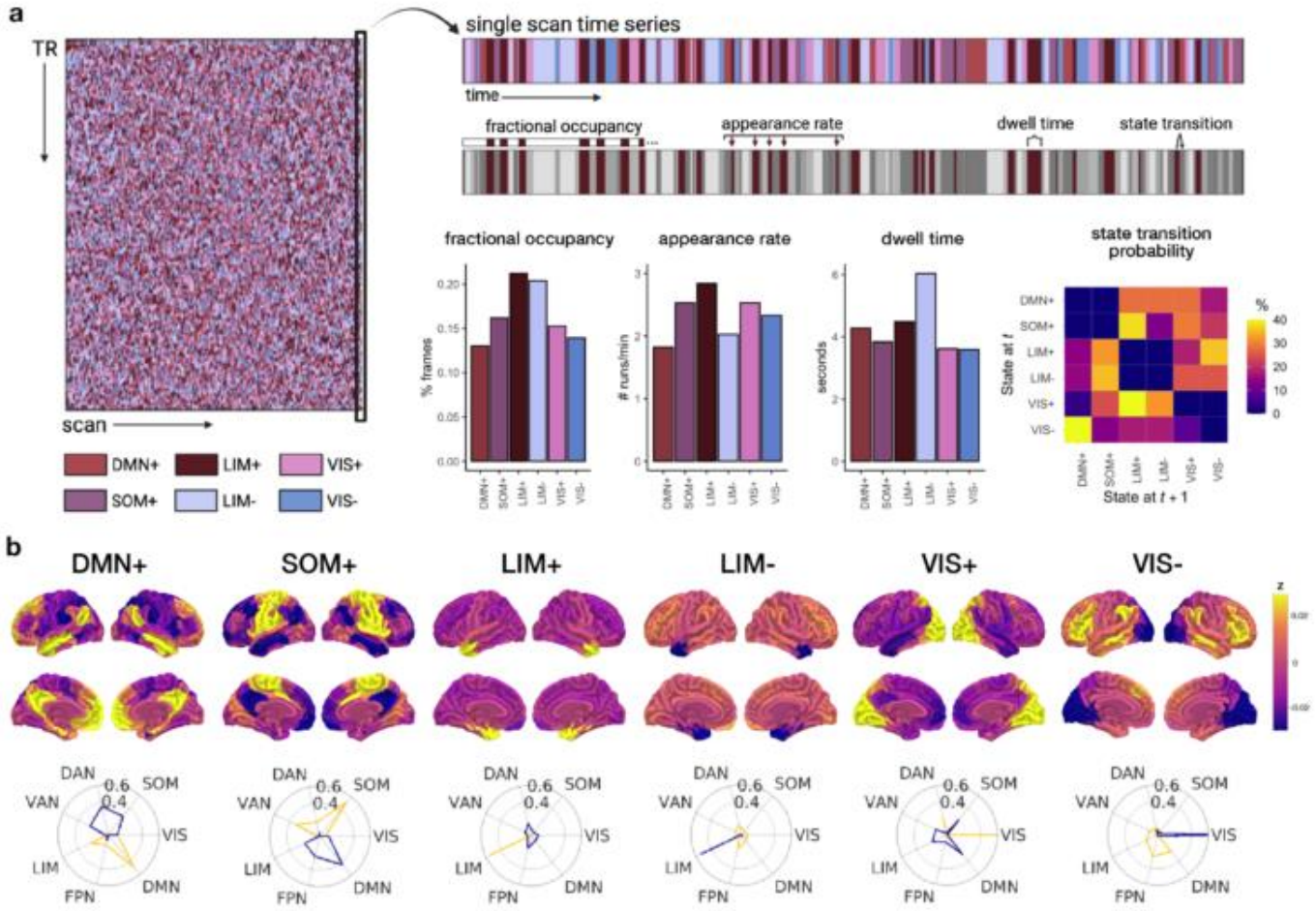

Figure 1. Visualization of brain states and derivation of brain state persistence features and transition probabilities. (a) Brain states were derived using a k-means clustering approach, in which each time point (TR, y-axis) of each scan (x-axis) was assigned to a state. For a single scan's time series, the progression of states can be represented over time (top right). We characterized three persistence features for each state: fractional occupancy, or the overall percentage of time spent in that state; appearance rate, or how often a state occurred per minute; and dwell time, or how long on average a state persisted in seconds. We also characterized state transition probability from each state at time *t* to the state at time point *t* + 1. (**a**) Six distinct brain states reflecting spatiotemporal patterns of whole brain coactivation were identified with a k-means clustering approach. The spatial pattern of coactivation in each brain state was compared to canonical resting state networks using cosine similarity, depicted in the polar plots in below each state. The outer circle boundary represents cosine similarity of 0.6, while the inner circle represents a cosine similarity value of 0.4. The resting state network with the most similar high amplitude (yellow, +) or low amplitude (blue, -) coactivation pattern was used to assign each brain state a name, however, brain states tend to reflect coactivation across resting state networks. DMN+, default mode network high amplitude state; SOM+, somatomotor network high amplitude state; LIM+, limbic network high amplitude state; LIM-, limbic network low amplitude state; VIS+, visual network high amplitude state; VIS-, visual network low amplitude state; DAN, dorsal attention network, DMN, default mode network, FPN, frontoparietal network, LIM, limbic network, SOM, somatomotor network; VAN, ventral attention network; VIS, visual network.

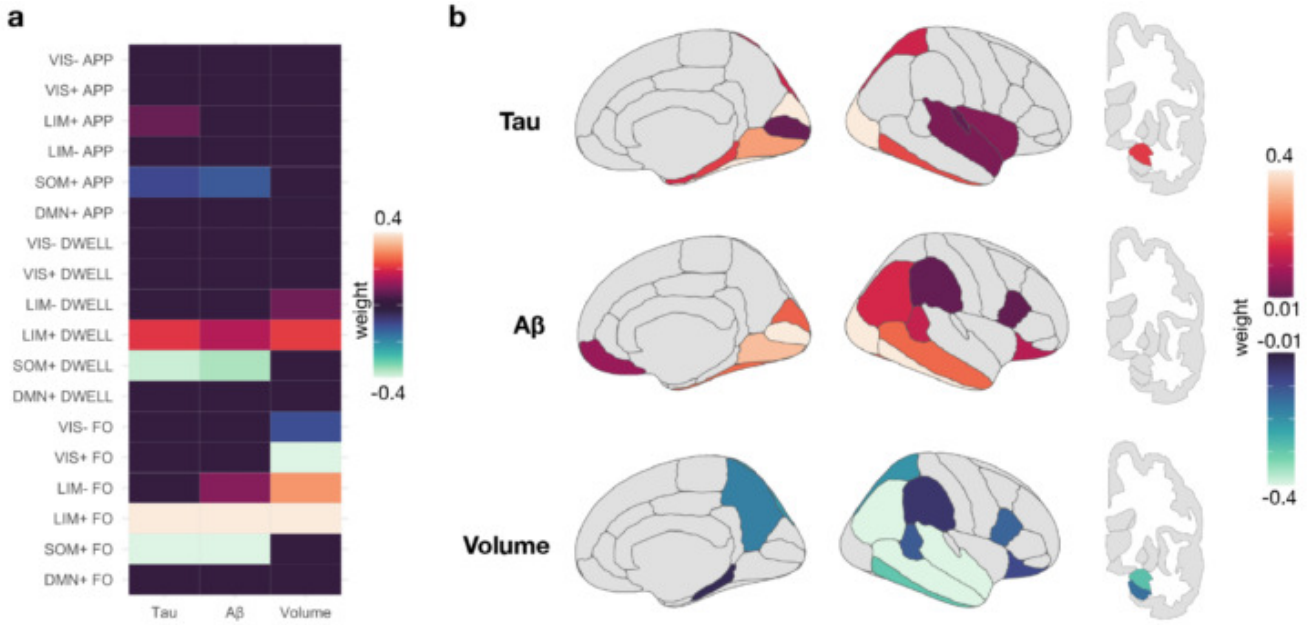

Figure 2. Associations between brain state persistence features and Alzheimer's disease neuropathology. To determine spatial patterns of tau, Aβ, and volume that reflected brain state persistence features, we conducted sparse canonical correlation analyses. Weight loadings for brain state persistence features are shown in **(a)**, with their associated spatial pattern rendered on brain images in **(b)**. Increased LIM+ state persistence (hot colors) and decreased SOM+/VIS+ state persistence (cool colors) were significantly associated with greater tau and Aβ deposition (hot colors) and decreased volume (cool colors) in regionally specific patterns mirroring known vulnerability. FO, fractional occupancy; DWELL, dwell time; APP, appearance rate.

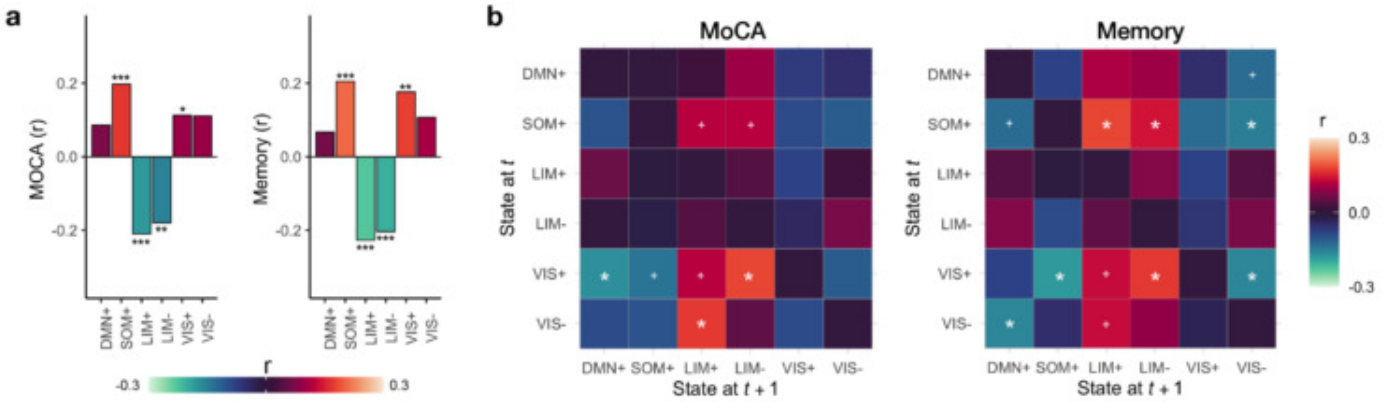

Figure 3. Associations between cognitive performance and brain states persistence and transitions. Cognitive performance was assessed with the Montreal Cognitive Assessment (MoCA) and an episodic memory composite score. **(a)** Associations between fractional occupancy of each state, a persistence feature representing the total percentage of time spent within that state, with cognitive outcomes. There was a significant negative correlation between LIM+/LIM- state fractional occupancy and MoCA/memory scores - higher LIM+/LIM- state fractional occupancy was associated with worse cognitive performance. In contrast, higher SOM+ and VIS+ state fractional occupancy was associated with better performance on the MoCA and memory composite. ***p<0.001 **p<0.01 *p<0.05 **(b)** Associations between cognitive performance and probability of transitions between distinct brain states from time *t* (y-axis) to time *t+1* (x-axis). Worse cognitive performance was associated with a greater probability of state transitions to LIM+/LIM- states, and a decrease in transitions to SOM+ and VIS+/VIS- states. Significance was corrected for multiple comparisons using FDR correction over 30 possible transitions. White asterisks represent p_{FDR}<0.05, and white crosses represent p_{unc}<0.05.

Keywords: brain states, amyloid-beta, tau, neurodegeneration, Alzheimer's disease

78 Imaging synaptic density across the Alzheimer's disease continuum with [18]F-SynVestT-1

Joseph Giorgio[1,2], David Soleimani-Meigooni[3], Xi Chen[1], Tyler Toueg[1], Robby Weimer[4], Bastian Zinnhardt[5], Suzanne Baker[6], Mustafa Janabi[6], Gil Rabinovici[3], William Jagust[1,6]

[1]*Helen Wills Neuroscience Institute, University of California Berkeley, Berkeley, CA, United States*
[2]*University of Newcastle, New South Wales, Australia*
[3]*Memory and Aging Center, Weill Institute for Neurosciences, University of California San Francisco, San Fransisco, CA, United States*
[4]*Genentech, San Fransisco, CA, United States*
[5]*Roche, Basal, CH*
[6]*Lawrence Berkeley National Laboratory, Berkeley, CA, United States*

Background: Progressive loss of synapses occurs throughout the Alzheimer's Disease (AD) continuum and is closely associated with cognitive impairment. Here, we investigate variation in synaptic density across ageing and AD using ^{18}F-SynVesT-1 PET, a ligand for SV2A.

Methods: 26 participants underwent ^{18}F-SynVesT-1 PET imaging to estimate synaptic density in-vivo. Participants were young adults (Y) (n=7; Age=26.1±3.8; Sex(F)=4), cognitively unimpaired older adults (OA) (n=13; Age=79.7±4.27; Sex(F)=7) or patients (AD) (n=6; Age=66.3±8.2; Sex(F)=1). Patients had MCI due to AD (n=1), AD dementia (n=3; all early-onset with age≤65), lvPPA(n=1), and PCA(n=1). We collected 90 min dynamic data after 5 mCi injection of tracer. Whole brain Distribution Volume Ratio images were generated using a cerebellar grey matter reference region. OA and AD groups also underwent tau and β-amyloid (Aβ) PET imaging (OA: ^{18}F-flortaucipir,^{11}C-PiB; AD: ^{18}F-PI-2620, ^{18}F-Florbetaben) and a visual assessment of tau and Aβ positivity for AD was determined by an expert reviewer (DSM). All AD patients were Aβ positive.

Results: We observed a significant effect of group (Y, OA, AD) on ^{18}F-SynVesT-1 PET uptake in four cortical regions: Hippocampus ($F(1,23)=4.35, p=0.025$); Temporal Lobe ($F(1,23)=7.95, p<0.05$(FWE)); Precuneus ($F(1,23)=11.7, p<0.05$(FWE)) and Parietal Lobe ($F(1,23)=13.9, p<0.05$(FWE))**.** Following partial volume correction (PVC), significant effects of group were observed in most regions with reductions for AD compared to OA in all regions: Hippocampus ($F(1,23)=4.76, p=0.019$); Temporal Lobe ($F(1,23)=2.46, p=0.1$); Precuneus ($F(1,23)=4.93, p<0.05$(FWE); Parietal Lobe ($F(1,23)=3.56, p=0.045$) (**Figure 1)**. Further, Aβ+ OA and AD showed a strong negative association between global Aβ (centiloids) and ^{18}F-SynVesT-1 PET uptake in the parietal lobe before and after PVC ($r(9)=-0.8, p=0.003$; PVC $r(9)=-0.61, p=0.045$) (**Figure 2**). Finally, visual inspection showed a mirroring of ^{18}F-SynVesT-1 and tau PET uptake that is characteristic of specific AD phenotypes (**Figure 3**).

Conclusion: ^{18}F-SynVesT-1 PET can capture age and AD related decreases in synaptic density across the cortex. Expected relationships between synaptic loss and tau parallels phenotypic variability.

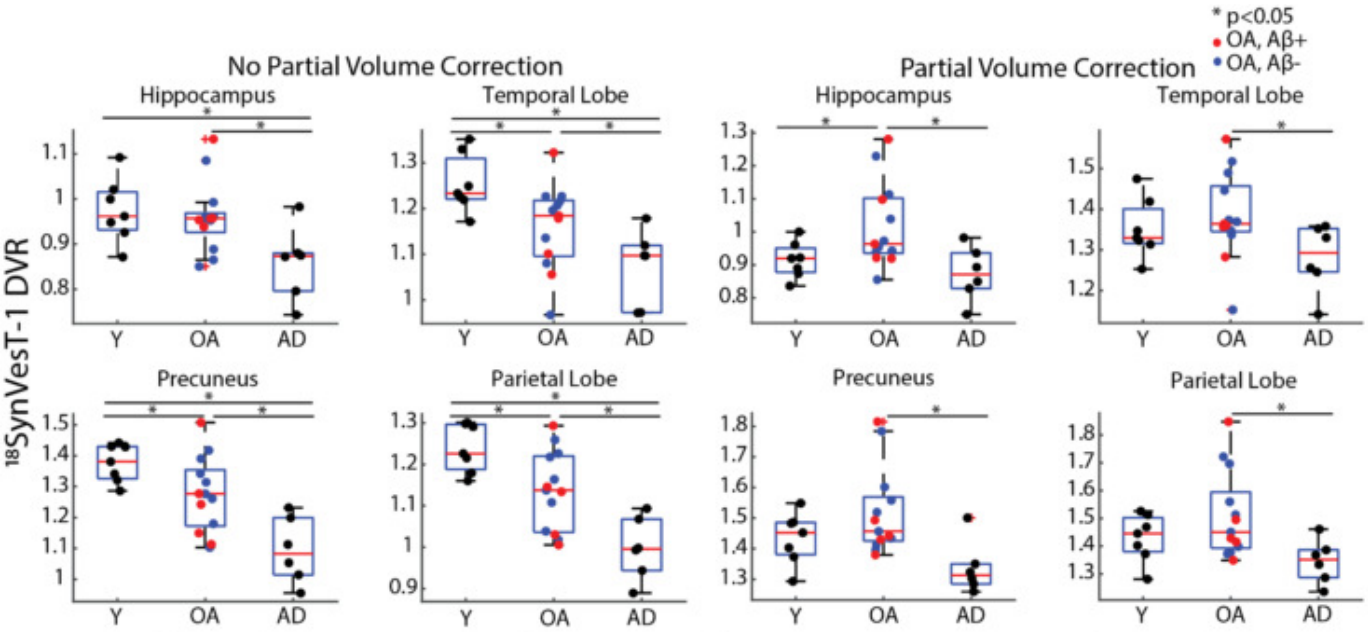

Figure 1. Distribution of 18F-SynVesT-1 PET for different groups. Differences in 18F-SynVesT-1 PET Distribution Volume Ratio (DVR) in four cortical regions of interest for young adults (Y), older adults (OA) and patients (AD) without partial volume correction (left) and with partial volume correction (right). *Indicates a significant ($p<0.05$) post-hoc test of difference between each group. Red + indicate outliers from the group distribution. All AD patients are Aβ positive.

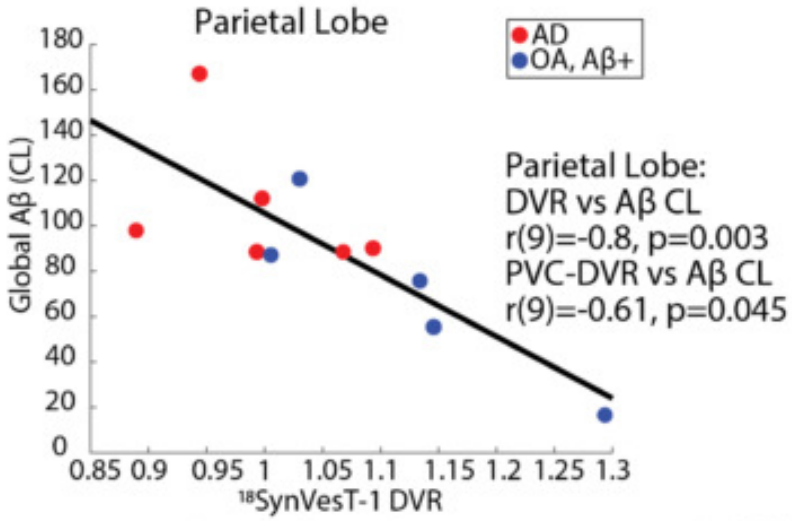

Figure 2. Correlation of parietal 18F-SynVesT-1 PET and global Aβ for Aβ positive individuals. Y-axis shows global Aβ in centiloids. X-axis shows parietal 18F-SynVesT-1 PET Distribution Volume Ratio (DVR). Blue and red dots show data for Aβ+ older adults (OA) and AD patients, respectively.

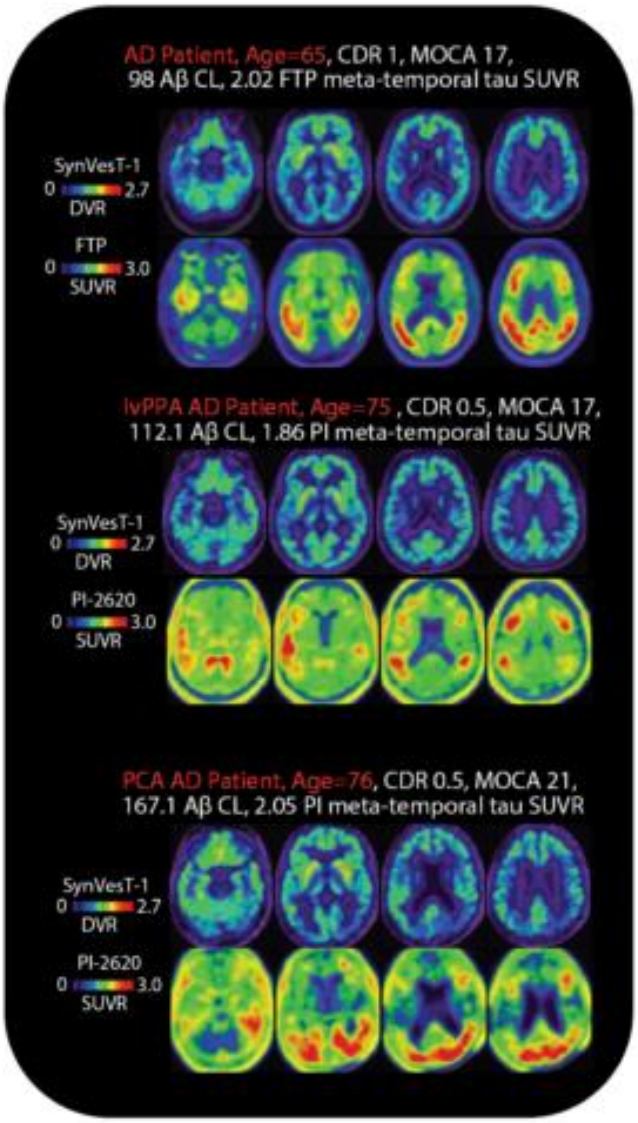

Figure 3. Relationship of 18F-SynVesT-1 and tau PET uptake. Each panel shows representative slices of 18F-SynVesT-1 (top row) and tau PET binding (bottom row) for three patients with different AD phenotypes: AD dementia (AD; top), logopenic variant primary progressive aphasia (lvPPA; middle) and posterior cortical atrophy (PCA).

Keywords: Synaptic Density, AD phenotypes, Multimodal PET

79 Data-driven analysis of 10,361 amyloid-PET scans from the IDEAS study reveals two primary axes of variation

Joseph Giorgio[1,2], Nidhi Mundada[3], Ganna Blazhenets[3], Jhony Mejia Perez[3], Daniel Schonhaut[3], Maria Carrillo[4], Lucy Hanna[5], Constantine Gatsonis[5,6], Andrew March[7], Charles Apgar[7], Barry Siegel[8], Bruce Hillner[10], Rachel Whitmer[9], William Jagust[1], Gil Rabinovici[3], Renaud La Joie[3]

[1]*Helen Wills Neuroscience Institute, University of California Berkeley, Berkeley, CA, United States*
[2]*University of Newcastle, New South Wales, Australia*
[3]*Memory and Aging Center, Weill Institute for Neurosciences, University of California San Francisco, San Fransisco, CA, United States*
[4]*Alzheimer's Association, Chicago, IL, United States*
[5]*Center for Statistical Sciences, Brown University School of Public Health, Providence, RI, United States*
[6]*Department of Biostatistics, Brown University School of Public Health, Providence, RI, United States*
[7]*Center for Research and Innovation, American College of Radiology, Reston, VI, United States*
[8]*Edward Mallinckrodt Institute of Radiology, Washington University School of Medicine, St Louis, MO, United States*
[9]*Department of Public Health Sciences and Neurology, University of California Davis, Davis, CA, United States*
[10]*Department of Medicine, Virginia Commonwealth University, Richmond, VI, United States*

Background: Variability in the regional distribution of Aβ-PET signal and its relation to clinical features is debated. We used data-driven approaches to uncover heterogeneity in cortical Aβ-PET signal from a large representative sample collected through the IDEAS study.

Methods: We analyzed cross-sectional Aβ-PET collected from 10,361 patients with MCI or mild dementia scanned in 295 PET facilities using one of the 3 FDA-approved tracers. Central image processing resulted in template-space SUVR images (reference: whole cerebellum) and centiloid (CL) values. Spatial independent component analysis was used to decompose SUVR volumes into 40 independent components. After excluding noise components, participants' scores were extracted for each of the remaining 11 grey matter (GM) components describing cortical and subcortical binding. K-means clustering was used on these GM component scores to assign each participant to different Aβ-PET clusters based on GM binding (**Figure1**).

Results: Three informative clusters of PET binding were estimated. Cluster 1: Aβ-(n=4729, CL mean=2±23) with low GM binding, and two Aβ+ clusters; Cluster 2(n=2484, CL mean=76±34) and Cluster 3(n=3148, CL mean=86±32). Subtracting average SUVR of Clusters 2 and 3 showed they differed along a posterior-anterior gradient with Cluster 2 showing an occipital predominant pattern. Principal component analysis conducted on the GM scores confirmed two dominant axes of variation separated the clusters, a Aβ- to Aβ+ axis and, an anterior-posterior axis (**Figure2).** Statistically significant but weak differences were observed between the two Aβ+ Clusters (2 vs 3); Visual Read (positive: 95% vs. 92%); Clinical Stage (dementia: 47% vs. 41%); Age (76.9±6.4 vs. 75.9±6.2) (**Figure3**).

Conclusion: Data driven classification of Aβ-PET reveals two primary axes reflecting Aβ load and anterior-posterior binding. Future work will apply new data to this model and investigate if this spatial variation in Aβ-PET is related to different neuropathological conditions (e.g., cerebral amyloid angiopathy) or longitudinal changes in pathology.

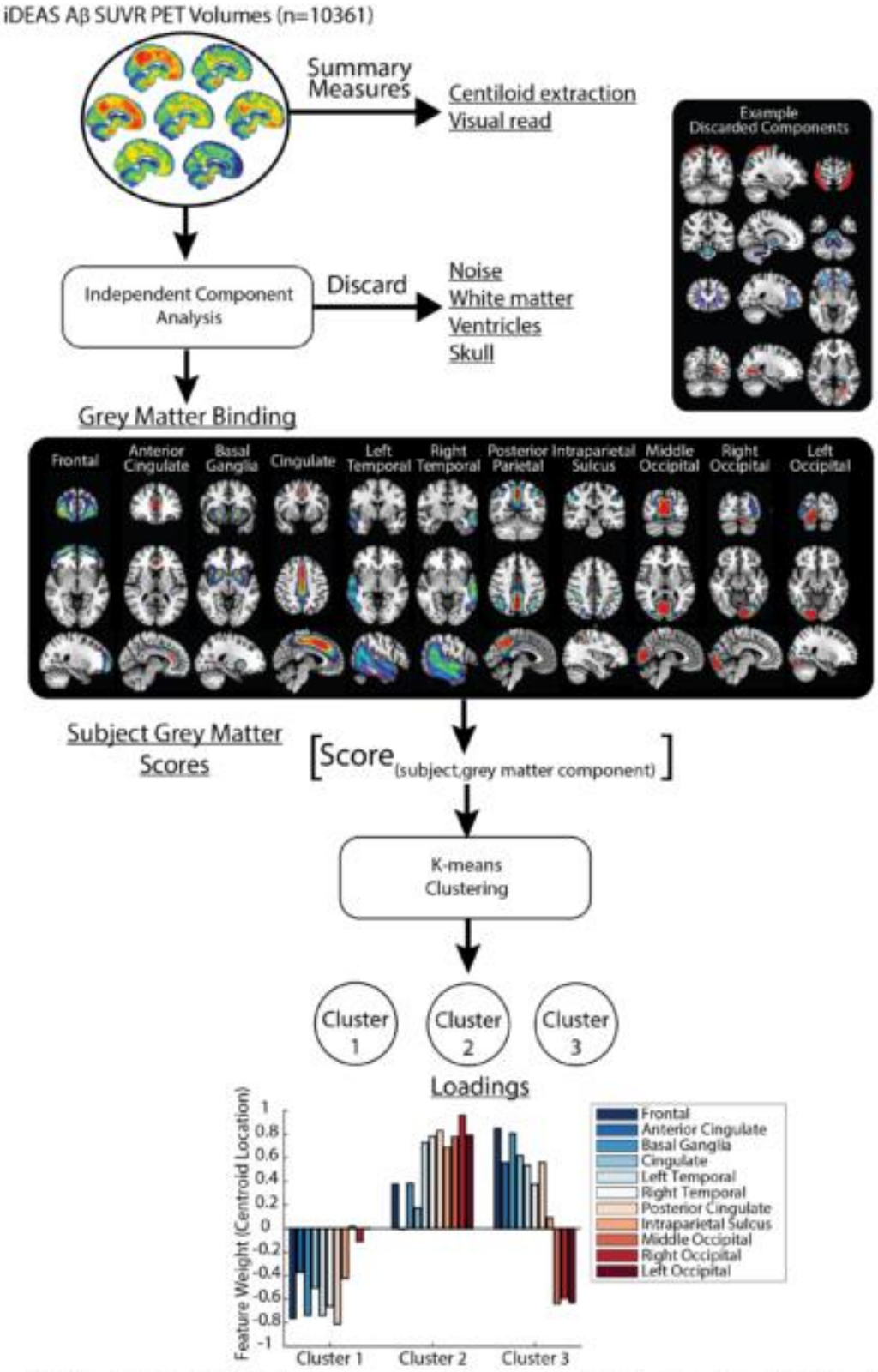

Figure 1 Analysis pipeline. 10,361 Aβ-PET images were processed into similar standardised uptake volume ratio (SUVR) volumes warped to Montreal Neurological Institute space. Initial summaries included a visual read for positivity at the imaging site and centralised extraction of centiloid values. These images were analysed using Independent Component Analysis to simultaneously extract subject values for cortical binding and remove signal of no interest (i.e. scanner noise, off target binding, reference regions and CSF). The brain maps on the right show examples of components of no interest that were discarded from analysis. The 11 grey matter binding components shown are selected for further analysis and a score for each component for each subject is extracted. Voxel values show heavily weighted positive voxels (Z>3.3) that contribute to the subject component score. Grey matter component scores are then clustered using k-means clustering with k=3. The bar chart in the bottom panel show the relative loadings (centroid location) of each of the grey matter components for each cluster.

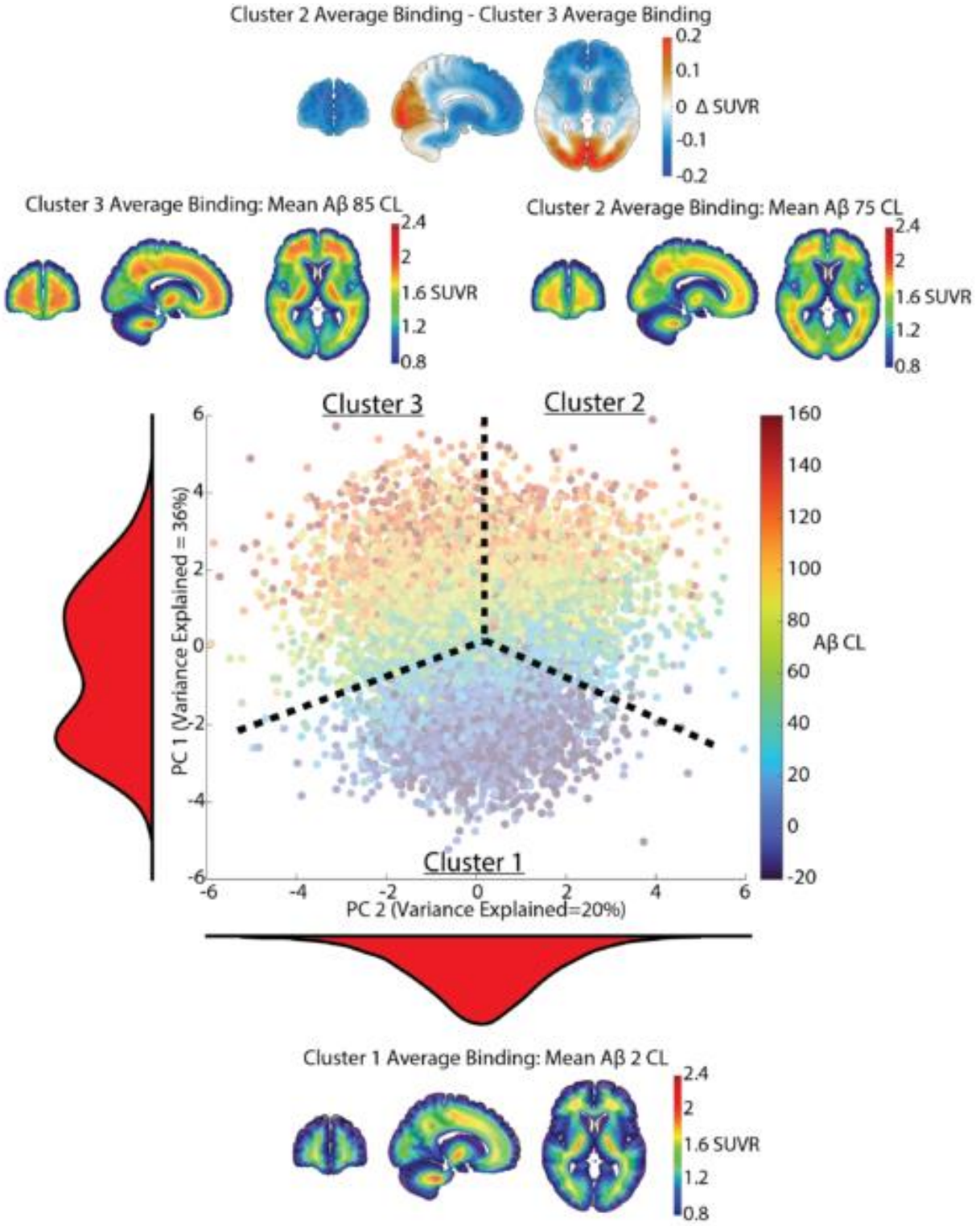

Figure 2 Spatial variation in Aβ-PET signal. Scatter plot shows each subject projected onto the two leading dimensions of grey matter binding. The y-axis shows the first principal component (PC) of grey matter binding which is related to global Aβ (colour scale of data points) that separates Cluster 1 from Clusters 2 and 3. The x-axis shows the second PC of grey matter binding which is related to an anterior to posterior (left to right) gradient. Histograms in red show the distribution of data points in the y and x axis (i.e., PC 1 and PC 2). Black dashed lines show the boundaries of each cluster. Average SUVR volumes for subjects assigned to each cluster are shown on the bottom, right and left for Clusters 1,2 and 3 respectively. The brain map in the top panel shows the difference between the average SUVR volume for Cluster 2 minus Cluster 3, highlighting a posterior-anterior gradient in average binding between the two clusters.

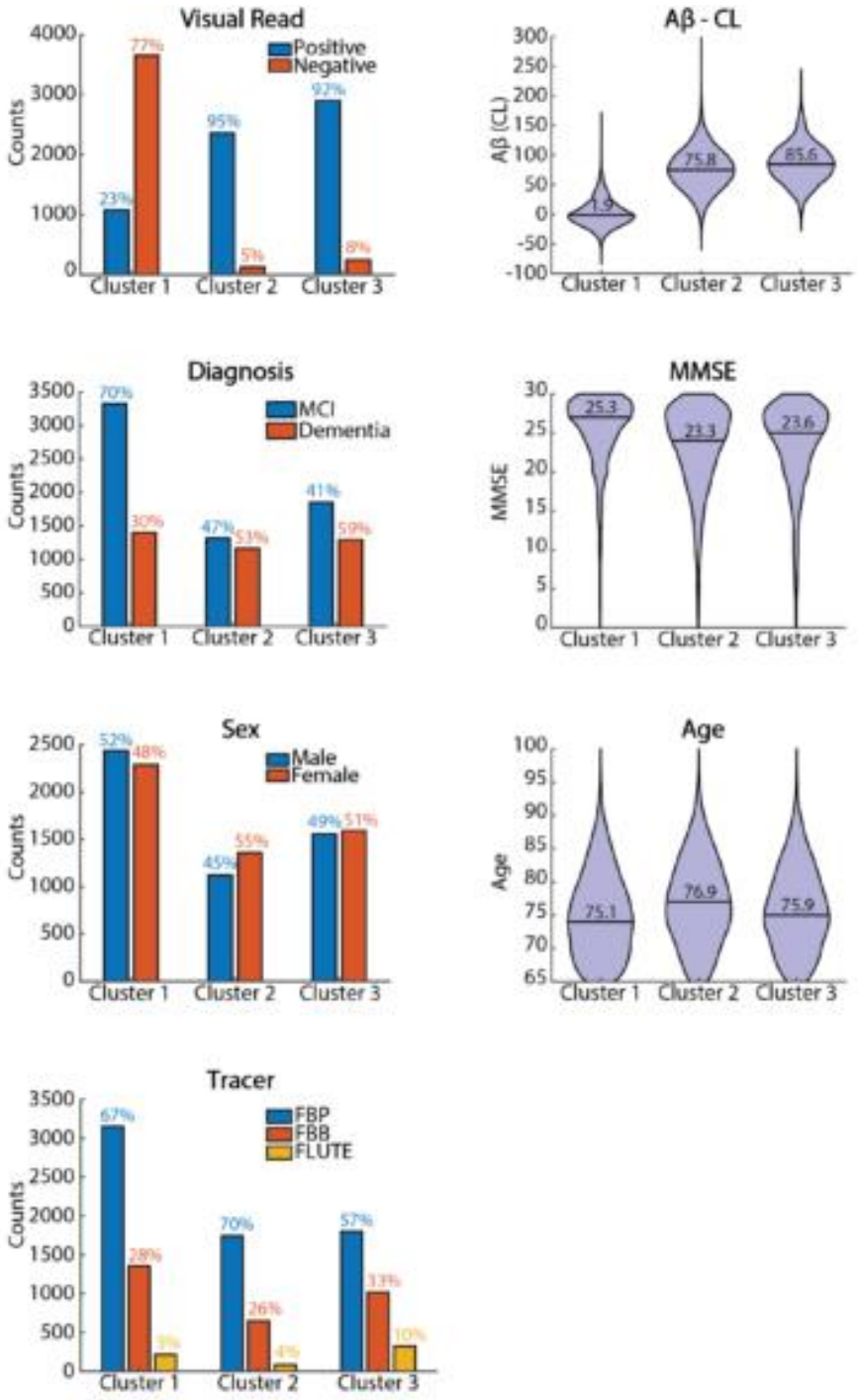

Figure 3 Distribution of demographic and clinical variables for each cluster. Proportions or averages for each variable within a cluster are shown in each panel. Significant and generally weak differences between Cluster 2 and Cluster 3 were observed for all variables. Visual Read (χ^2=17.3**, effect=0.06(VS)); Aβ centiloids (CL) (t=-11.1**, effect =-0.30(S)); Diagnosis (χ^2=18.3**, effect=0.06(VS)); MMSE (t=-2.3*, effect =-0.07(VS)); Sex (χ^2=9.8*, effect=0.04(VS)); Age (t=-5.9**, effect =0.16(S)); Tracer (χ^2=144.1**, effect=0.11(S)). Test statistics are either t values from independent sample t-tests (continuous variables) or Chi Square values from Chi Square tests (proportions). Effect sizes for independent sample t-tests are Cohen's d, for Chi Square tests on 2x2 contingency tables effect sizes are Phi, for Chi Square tests on 3x2 contingency tables effect sizes are Cramer's V. Values in parentheses next to effect sizes indicate the relative size of the effect. Effect sizes are- VS: Very Small; S: Small; M: Medium; L: Large; VL: Very Large. *p<0.05 ** p<0.001.

Keywords: Data-driven, amyloid PET, spatial variability, big data

80 Lower locus coeruleus structural integrity is associated with greater intraindividual cognitive variability in older individuals

Emma Wiklund[1], Maxime Van Egroo[3], Truley Juneau[1], Joost Riphagen[1], Kathryn Papp[4], Roos Jutten[2], Dorene Rentz[2,4], Reisa Sperling[2,4], Keith Johnson[1,2,4], Heidi Jacobs[1]

[1]*Department of Radiology, Massachusetts General Hospital, Harvard Medical School, Boston, MA, United States*
[2]*Department of Neurology, Massachusetts General Hospital, Harvard Medical School, Boston, MA, United States*
[3]*Faculty of Health, Medicine and Life Sciences, School for Mental Health and Neuroscience, Alzheimer Centre Limburg, Maastricht University, Maastricht, The Netherlands*
[4]*Center for Alzheimer Research and Treatment, Department of Neurology, Brigham and Women's Hospital, Harvard Medical School, Boston, MA, United States*

Introduction: Intraindividual variability in cognitive performance over multiple measurements has been linked to the structure and function of catecholaminergic systems, including the noradrenergic locus coeruleus (LC). Greater cognitive variability was associated with greater risk of Alzheimer's disease (AD). Here, we examined the associations between structural integrity of the LC, defined by LC MRI signal intensity, and intraindividual cognitive variability over multiple domains. Given that the LC is one of the first sites to accumulate tau, we also examined whether these relationships are moderated by AD pathology.

Methods: 173 older adults from the Harvard Aging Brain Study (**Figure 1**) underwent longitudinal cognitive evaluations, 3T LC MRI, PiB- and Flortaucipir-PET scans. For several cognitive tests, cognitive variability was defined by the intraindividual coefficient of variation (CV; SD/mean). LC MRI signal intensity was quantified by normalizing the LC to the pontine tegmentum and averaging clusters of 5 voxels with the highest intensities. PET measures were corrected for partial-volume effects. Robust linear regressions associated the CV and i) LC integrity and ii) LC integrity interacted with entorhinal tau or global amyloid (age, sex, education, and individual slope of performance as covariates).

Results: Lower LC integrity was associated with higher CV on the delayed recall of the Buschke Selective Reminding Test (p=0.02) (**Figure 2**). Interaction models demonstrated that this relationship is more strongly expressed at higher levels of amyloid or tau (**Figure 3**). Including individual slopes of longitudinal cognitive performance as confounding factor did not modify these relationships.

Conclusion: LC integrity may be a sensitive marker of intraindividual cognitive variability, particularly in those with elevated AD pathology. These findings have implications for the early detection of individuals at risk for cognitive decline. In the future, we aim to replicate these findings for cognitive data collected on shorter time scales.

Characteristics of Participants (N=173)	
Age (years)	72.74 (9.53)
Female (n, %)	103 (60%)
Education (years)	16.29 (2.88)
MMSE score	29.03 (1.27)
CDR Rating = 0 (n, %)	159 (92%)
Cognitive follow-up time (years)	4.06 (1.20)
LC integrity	1.33 (0.05)
Entorhinal FTP (SUVR, PVC)	1.36 (0.33)
Global PiB (DVR, PVC)	1.39 (0.39)

Figure 1. *Data is presented as numbers and (percentages) or means and (standard deviations). Missing data for MMSE (n=1) and CDR (n=3). Abbreviations: MMSE = Mini-Mental State Examination, CDR = Clinical Dementia Rating, LC= Locus Coeruleus; FTP = Flortaucipir; SUVR = Standardized Uptake Value Ratio; PVC = Partial Volume Correction; PiB = Pittsburgh compound B; DVR = Distribution Volume Ratio.*

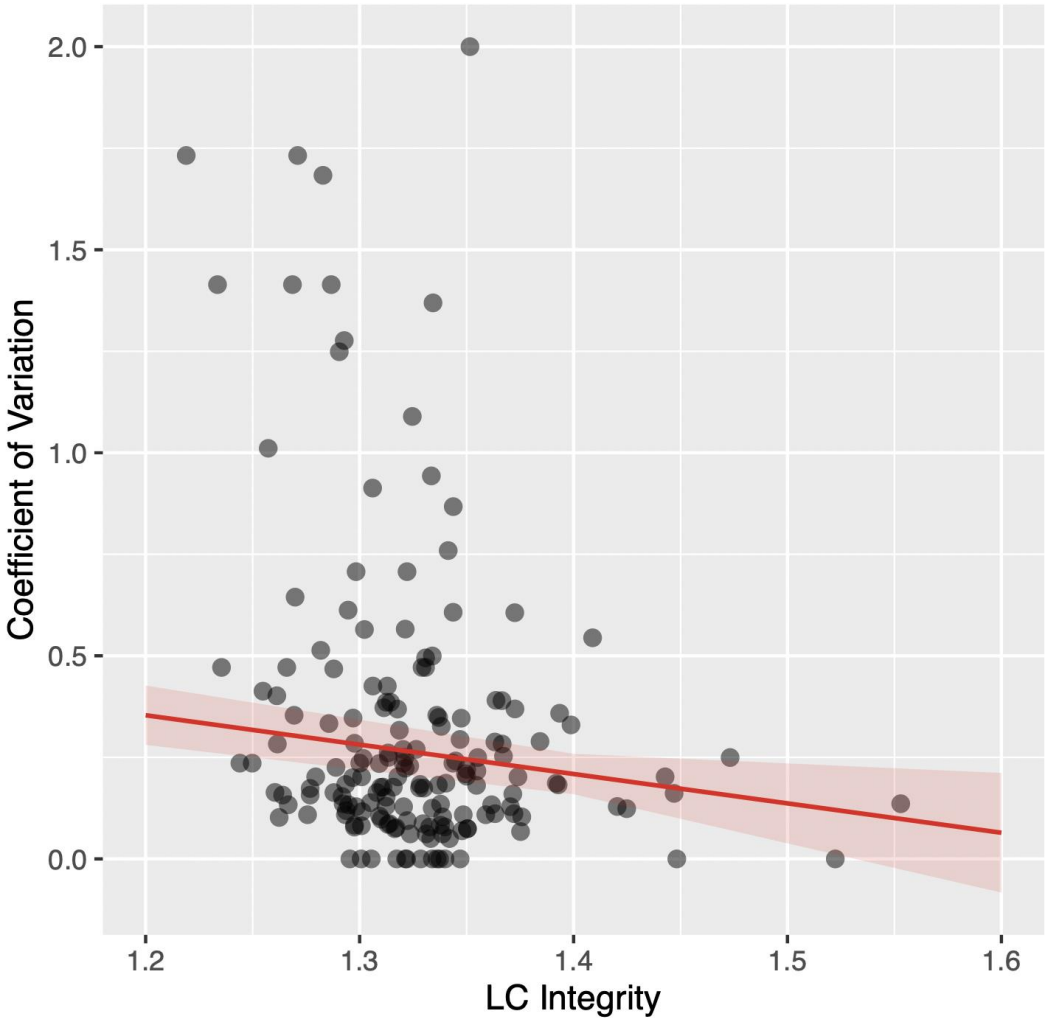

Figure 2. *Relationship between LC structural integrity and the intraindividual coefficient of variation for the delayed recall portion of the Buschke Selective Reminding Test. Abbreviations: LC= Locus Coeruleus.*

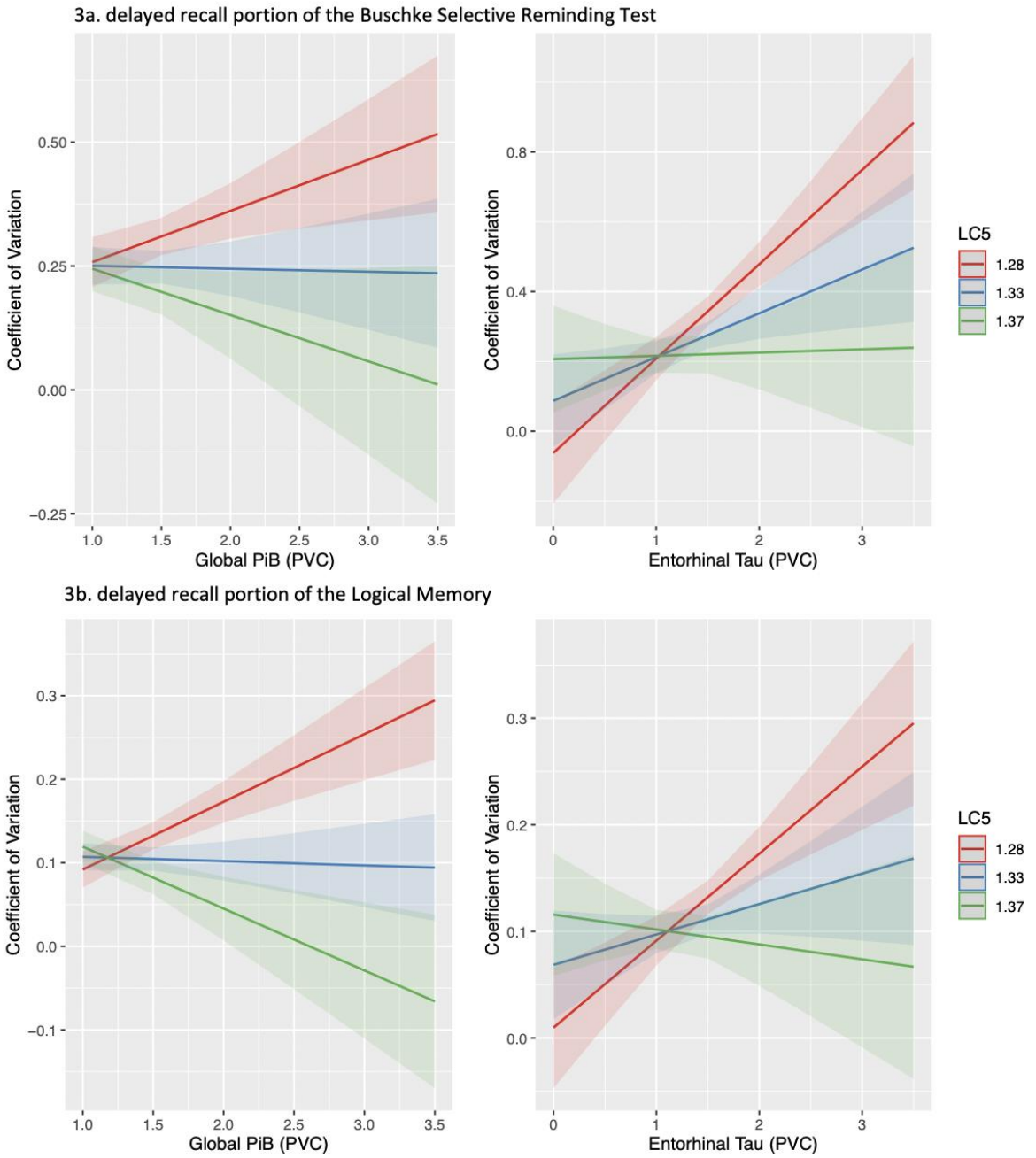

	Global PiB			EC Tau		
Cognitive Test	**Coefficient**	**T-Value**	**P-Value**	**Coefficient**	**T-Value**	**P-Value**
CAT2	-1.13	-3.84	<0.001	-0.66	-3.19	0.001
FAS	-1.49	-5.32	<0.001	-0.49	-2.54	0.02
FCSRT Free Recall	-1.42	-4.97	<0.001	-0.53	-2.49	0.02
Digit Symbol Substitution	-0.52	-2.61	0.009	-0.31	-2.14	0.03

Figure 3. a*: The relationship between LC structural integrity and the intraindividual coefficient of variation of the delayed recall portion of the Buschke Selective Reminding Test moderated by neocortical PiB (p= 0.04) or entorhinal Tau (p= 0.001). b: The relationship between LC structural integrity and the intraindividual coefficient of variation of delayed recall Logical Memory performance over time moderated by neocortical PiB (p <0.001) or entorhinal Tau (p <0.001). Table: Effect modification by neocortical PiB or entorhinal Tau on the relationships between LC structural integrity and the intraindividual coefficient of variation for additional cognitive tests. Abbreviations: LC = Locus Coeruleus; PVC = partial volume correction; PiB = Pittsburgh Compound B; EC = Entorhinal Cortex; FCSRT = Free and Cued Selective Reminding Test.*

Keywords: locus coeruleus structure, preclinical Alzheimer's disease, cognitive variability, beta-amyloid, tau

81 Precuneus fMRI activity is associated with future Aβ burden in cognitively normal older APOE4 carriers

Anne Maass[2], Eoin Molley[1,2], Alexa Pichet Binette[3], Niklas Vockert[2], Jonas Marquardt[2], Michael C Kreissl[1], Jordana Remz[4], Natasha Rajah[4,5,6], Sylvia Villeneuve[4]

[1]*Division of Nuclear Medicine, Department of Radiology & Nuclear Medicine, Faculty of Medicine, Otto von Guericke University Magdeburg, Magdeburg, Germany*
[2]*German Center for Neurodegenerative Diseases, Magdeburg, Germany*
[3]*Clinical Memory Research Unit, Faculty of Medicine, Lund University, Lund, Sweden*
[4]*Douglas Mental Health University Institute, McGill University, Montreal, QC, Canada*
[5]*Department of Psychiatry, McGill University, Montreal, QC, Canada*
[6]*Department of Psychology, Toronto Metropolitan University, Toronto, ON, Canada*

The precuneus is an early site of Aβ accumulation. Previous cross-sectional studies reported altered (often increased) precuneus fMRI activity in older adults with mild cognitive deficits or elevated Aβ. However, longitudinal studies in early AD-risk stages are lacking and the interaction with *APOE4* genotype is unclear.

In the PREVENT-AD cohort, we assessed how precuneus activity at baseline and its change over time relates to future Aβ (and tau) burden and to change in memory performance. We further studied how activity-pathology associations were modulated by *APOE4* genotype. We included 165 older adults (mean age: 63±4.4 years; 68% female; 66 *APOE4* carriers) who were cognitively normal at baseline and had a family history of AD. All participants performed task-fMRI at baseline, and tau-PET [^{18}F]flortaucipir and Aβ-PET [^{18}F]NAV4694 scans on average 5 years later (Fig.1). Longitudinal fMRI data were available for 151 participants. Regression models were used to test if precuneus activity predicts global NAV SUVR or entorhinal flortaucipir SUVR; age, sex, education and scan time difference were covariates.

Baseline precuneus activity during successful memory retrieval was associated with higher future Aβ burden (T=2.5, p=0.012). The interaction between *APOE4* genotype and baseline precuneus activity on Aβ was marginal (p=0.052). Subgroup analyses revealed that higher precuneus activity related to higher Aβ burden in *APOE4* carriers (r=0.30, p=0.018) but not non-carriers (r=.07, p>0.5, Fig.2). Longitudinally, we found an interaction with *APOE4* genotype (p=0.02); greater change in precuneus activity predicted higher Aβ in *APOE4* carriers (r=0.31, p=0.02) but not in non-carriers (r=-0.02, p>0.8). There were no effects of precuneus activity on tau burden. Finally, *APOE4* non-carriers with low baseline activity showed steepest increase (practice effects) in RBANS delayed memory over time. Our findings suggest that higher baseline precuneus activity and longitudinal increase in precuneus activity are associated with future Aβ burden in cognitively normal *APOE4* carriers.

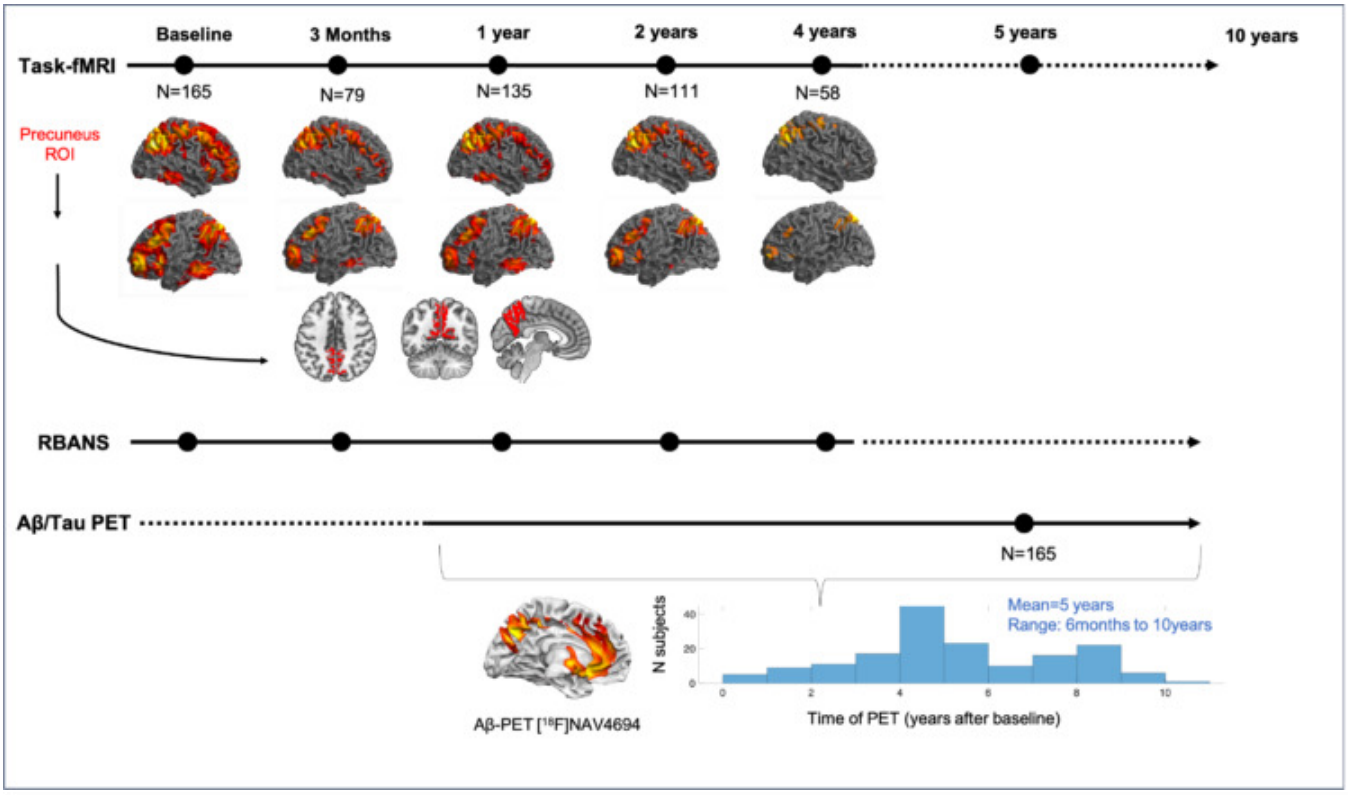

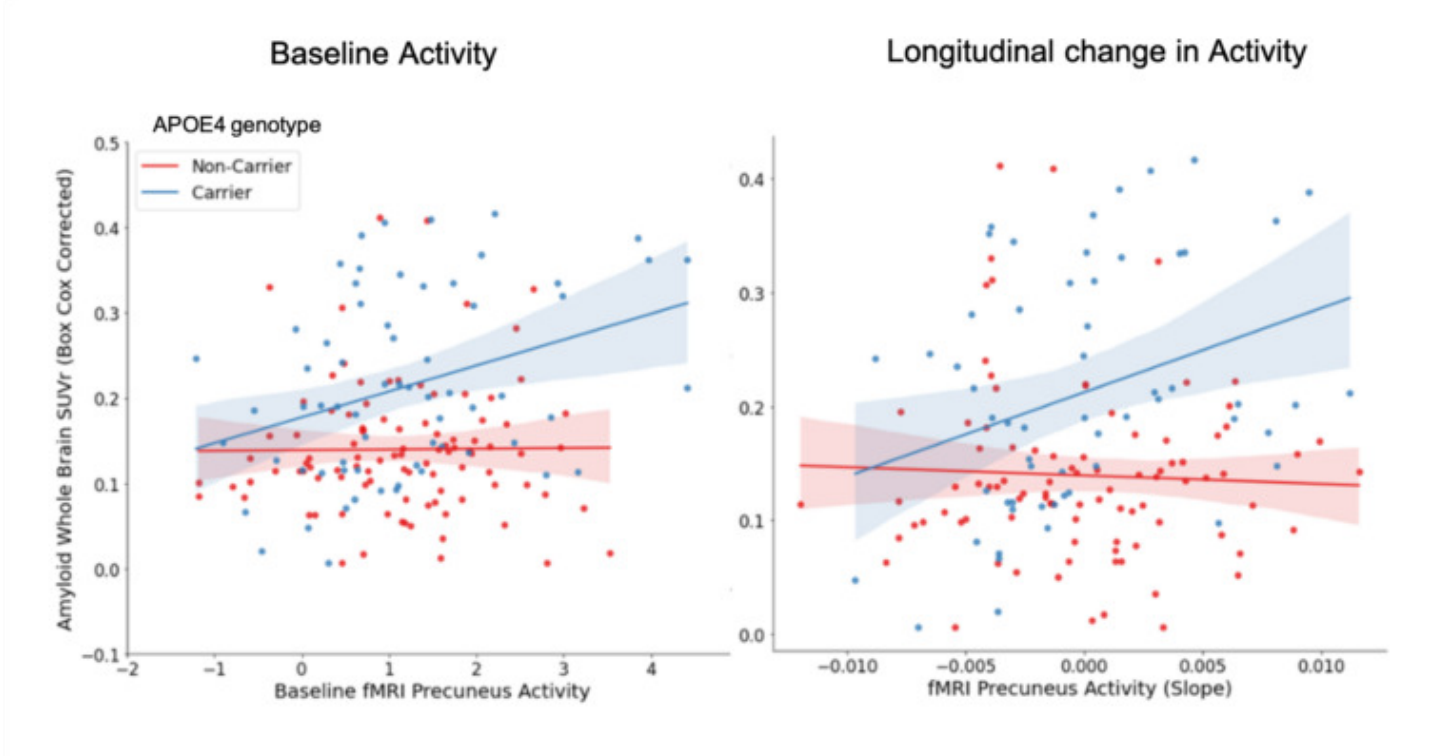

Keywords: precuneus, fmri, hyperactivity, APOE4, Amyloid

82 PI-2620 binding in cognitively normal older adults including SuperAgers

Anne Maass[1], Berta Garcia-Garcia[1,2], Eoin Molley[1,2], Niklas Behrenbruch[1], Beate Schuhmann-Werner[1,3], Niklas Vockert[1], Michael Rullmann[4], Anne Hochkeppler[1], Larissa Fischer[1], Svenja Svenja Schwarck[1,3], Kathrin Baldauf[1], Peter Schulze[1], Andrew W. Stephens[5], Marianne Patt[4], Henryk Barthel[4], Osama Sabri[4], Emrah Duezel[1,3], Michael C. Kreissl[1,2]

[1]*German Center for Neurodegenerative Diseases, Magdeburg, Germany, Magdeburg, Germany*
[2]*Division of Nuclear Medicine, Department of Radiology & Nuclear Medicine, Faculty of Medicine, Otto von Guericke University Magdeburg, Magdeburg, Germany*
[3]*Institute of Cognitive Neurology and Dementia Research, Otto-von-Guericke University Magdeburg, Magdeburg, Magdeburg, Germany*
[4]*Department of Nuclear Medicine, University of Leipzig, Leipzig, Germany*
[5]*Life Molecular Imaging GmbH, Berlin, Germany*

First-generation tau PET tracers showed frequent tracer binding in the medial temporal lobe in cognitively normal (CN) older adults that was related to worse memory performance and memory decline. However, these first-generation tau tracers suffered from off-target binding. 18F-PI-2620 is a next-generation tau tracer with high affinity to 3/4R tau in Alzheimer's disease and has been suggested to show less off-target binding and high sensitivity to early tau burden. In a novel aging and SuperAging cohort of CN, also including very old individuals (80 years and older) with superior memory performance, we use 18F-PI-2620 to assess early age- and AD-related tau pathology.

Here we report the first results of our ongoing study based on a subsample of 54 CN (mean age=72±8; 40%female, 14 subjects >79.5years) that underwent 60minuntes-dynamic PET scanning. Distribution Volume Ratio (DVR) images were created by means of Multilinear Reference Tissue Model2 using the inferior cerebellum as reference region. Voxel-wise and regional associations of tracer binding with age and memory performance were tested.

PI-2620 showed some degree of off-target binding in soft tissue/meninges, choroid plexus and basal ganglia (Fig.1A) and some white matter binding, which was increasing with younger age (Fig.1A/B). When covarying for global white matter uptake, older age related to higher 18F-PI-2620 binding in the anterior temporal lobe (Fig.1C). Of interest, higher tracer binding in a temporal lobe composite region related to worse episodic memory performance (Fig.2A). A preliminary analysis grouping individuals in SuperAgers based on their verbal memory performance (within range of 50-60 years old) versus typical older adults indicated lower temporal tracer binding in SuperAgers (Fig.2B).

In conclusion, less temporal lobe tau load relates to better episodic memory in older adutls including very old individuals with superior memory. In future work, we aim to study the factors underlying resistance or resilience against tau pathology.

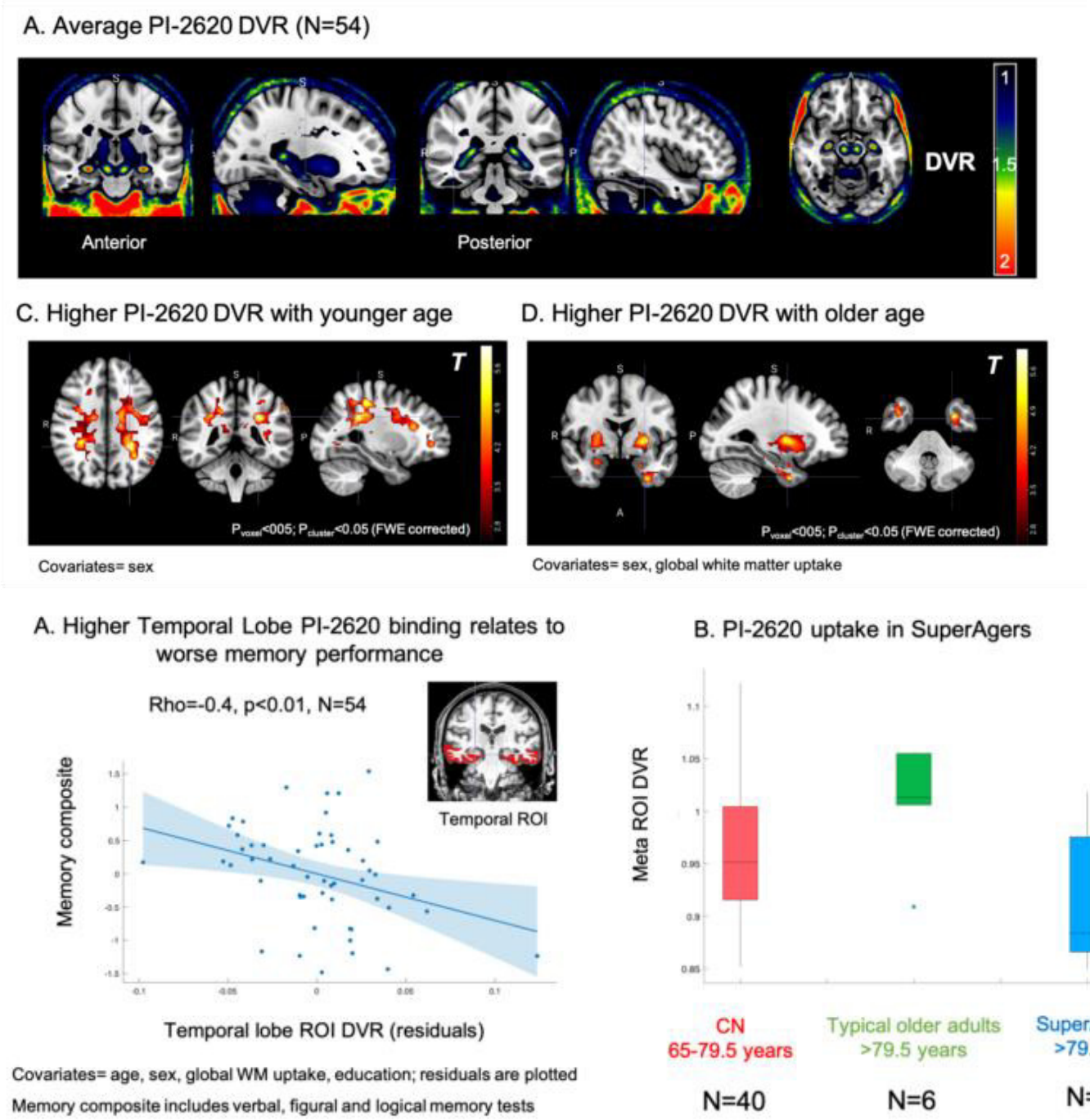

Keywords: PI-2620, successful aging, SuperAging, tau

83 Early phase amyloid PET as a surrogate marker of brain metabolism in cases of cognitive impairment

William Aye[1,2], Tracy Melzer[1,2,3], Ross Keenan[1,4], Matthew Croucher[8], Lynette Tippett[5,6], Tim Anderson[1,2,7], Campbell Le Heron[1,2,3,7]

[1]*New Zealand Brain Research Institute, Christchurch, NZ*
[2]*Department of Medicine, University of Otago, Christchurch, NZ*
[3]*School of Psychology, Speech, and Hearing, University of Canterbury, Christchurch, NZ*
[4]*Pacific Radiology, Christchurch, NZ*
[5]*School of Psychology, University of Auckland, Auckland, NZ*
[6]*Centre for Brain Research, Auckland, NZ*
[7]*Department of Neurology, Christchurch Hospital, Christchurch, NZ*
[8]*Department of Psychological Medicine, University of Otago, Christchurch, NZ*

In vivo neuroimaging techniques visualizing metabolic and cerebrovascular changes are vital in diagnosing many neurodegenerative disorders. The current gold standard, ^{18}F -Fluorodeoxyglucose (^{18}F-FDG) PET imaging, demonstrates regional metabolic deficits associated with particular causes of neurodegeneration, such as Alzheimer's disease and frontotemporal dementias.

However, emerging imaging modalities may provide alternatives to ^{18}F-FDG PET with unique advantages. PET radiological tracers binding to pathological proteins, such as amyloid-β (Aβ) and neurofibrillary tau, are increasingly used as molecular biomarkers for diagnosis. While these scans are usually read after ~90 min ("late-phase"), growing evidence suggests that the images acquired immediately after tracer injection provide cerebrovascular information analogous to ^{18}F-FDG PET. Another alternative – Arterial Spin Labelling (ASL) MRI – non-invasively and quantitatively measures cerebral perfusion, which is closely linked to metabolism.

We hypothesized that "early-phase" uptake of an Aβ PET tracer Florbetaben (FBB) would strongly correlate with ^{18}F-FDG and ASL MRI in individuals investigated for cognitive impairment (n=20). GE Discovery 690 PET/CT scanner acquired early-phase FBB and late-phase images 0-10 min and 90-110 min, respectively, after intravenous injection of 300 MBq ± 20% FBB. Participants also underwent ^{18}F-FDG PET, T1-weighted MPRAGE structural and arterial spin labeling (ASL) perfusion MRI.

Results from our pilot participants indicate visually striking similarities between early-phase FBB and ^{18}F-FDG, with high correlations between 95 cortical and subcortical structural regions ($r = 0.79$-0.92, $p<0.0001$), while showing significant, but lower correlations with ASL MRI ($r=0.30$-0.49, $p<0.001$). Validating this early-phase modality will permit simultaneous assessment of pathological protein status and regional brain metabolism, markedly increasing clinical utility.

Keywords: Early-phase PET, Cerebral Metabolism, Cognitive impairment, Neurodegenerative disorders, Cerebral Perfusion

84 Unlocking tau PET accessibility: a machine learning-based prediction of tau pathology from plasma, MRI and clinical variables

Linda Karlsson[1], Jacob Vogel[1,2], Olof Strandberg[1], Ida Arvidsson[3], Kalle Åström[3], Jakob Seidlitz[4], Richard A. I. Bethlehem[5], Erik Stomrud[1,6], Rik Ossenkoppele[1,7], Nicholas J. Ashton[8,9], Kaj Blennow[8,10], Sebastian Palmqvist[1,6], Ruben Smith[1,6], Shorena Janelidze[1], Alexa Pichet Binette[1], Niklas Mattson-Carlgren[1,6], Oskar Hansson[1,6]

[1]*Clinical Memory Research Unit, Department of Clinical Sciences in Malmö, Lund University, Lund, Sweden*
[2]*Department of Clinical Sciences, SciLifeLab, Lund University, Lund, Sweden*
[3]*Centre for Mathematical Sciences, Lund University, Lund, Sweden*
[4]*Penn/CHOP Lifespan Brain Institute, University of Pennsylvania, Philadelphia, PA, United States*
[5]*University of Cambridge, Department of Psychiatry, Cambridge Biomedical Campus, Cambridge, United Kingdom*
[6]*Memory Clinic, Skåne University Hospital, Malmö, Sweden, Malmö, Sweden*
[7]*Alzheimer Center Amsterdam, Department of Neurology, Amsterdam Neuroscience, Amsterdam UMC, Amsterdam, The Netherlands*
[8]*Department of Psychiatry and Neurochemistry, Institute of Neuroscience and Physiology, the Sahlgrenska Academy, University of Gothenburg, Mölndal, Sweden*
[9]*Institute of Psychiatry, Psychology and Neuroscience, Maurice Wohl Institute Clinical Neuroscience, King's College London, London, United Kingdom*
[10]*Clinical Neurochemistry Laboratory, Sahlgrenska University Hospital, Mölndal, Sweden*

Aims: Tau-PET is closely linked with clinical progression and provides important staging information in AD, but is expensive and not widely available in clinical settings. With emerging disease-modifying therapies for AD, accessible ways to estimate the load and distribution of tau pathology are becoming crucial. Here, we trained machine learning (ML) models to predict tau-PET outcomes from more accessible features only (clinical variables, plasma biomarkers and MRI).

Methods: The study included 1195 participants from the BioFINDER-2 (BF2) cohort, split into 80% train and 20% test sets. We created a rigorous ML pipeline that, with 10-fold cross-validation, evaluated different feature selection steps and estimators in a combined grid-search and Bayesian optimization set-up (Fig. 1). The three variable blocks (clinical, plasma and structural MRI) were used as features (together and separately) to predict two tau-PET characteristics: 1) tau load in the temporal cortex 2) hemispheric asymmetry of temporal tau load in tau positive participants (as an example of clinically-relevant spatial information).

Results: Feature combinations including plasma features (particularly plasma p-tau217) resulted in the best prediction of the tau load (Fig 2). The best performing model was a combination of plasma and MRI variables in a CatBoost regressor and achieved SUVR mean absolute error (MAE) = 0.160 and R-squared = 0.676 in the test set. For prediction of hemispheric asymmetry, models using MRI features performed best, and regions in the temporal lobe had the greatest contribution to the models (Fig 3). Top performance in the test set was laterality index MAE = 9.30 and R-squared = 0.316 in a SVR model including MRI and clinical variables.

Conclusions: From clinically accessible and non-invasive features, particularly plasma p-tau217 and structural MRI, we were able to predict the load and hemispheric asymmetry of pathological tau using standard ML techniques. Ongoing work involves validation in external cohorts.

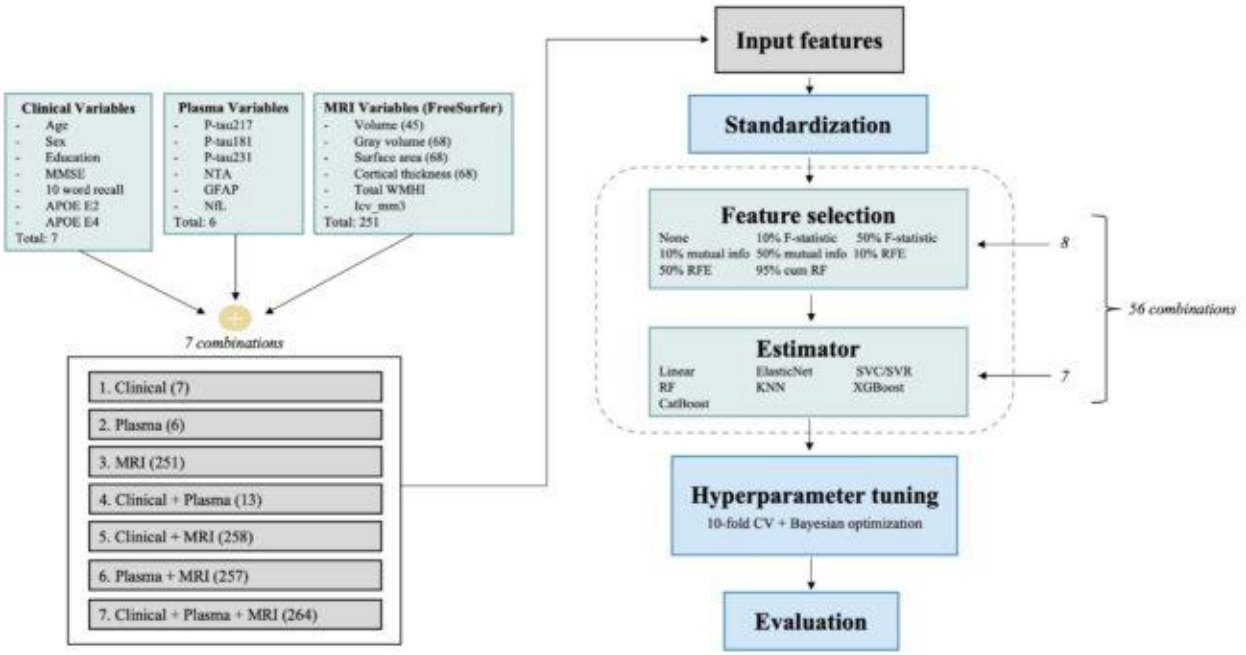

FIGURE 1: The pipeline created to compare combinations of input features in hyperparameter tuned machine learning estimators. Different blocks of variables (clinical, plasma and MRI) were tested separately and in combination as input features. The pipeline consisted of a combined grid search and Bayesian optimization approach to compare performance of different input features in hyperparameter tuned ML estimators. All tuning and evaluation was performed in the BioFINDER-2 training set with 10-fold cross-validation. The pipeline could handle different input and output variables, evaluation metrics and both regression and classification tasks.

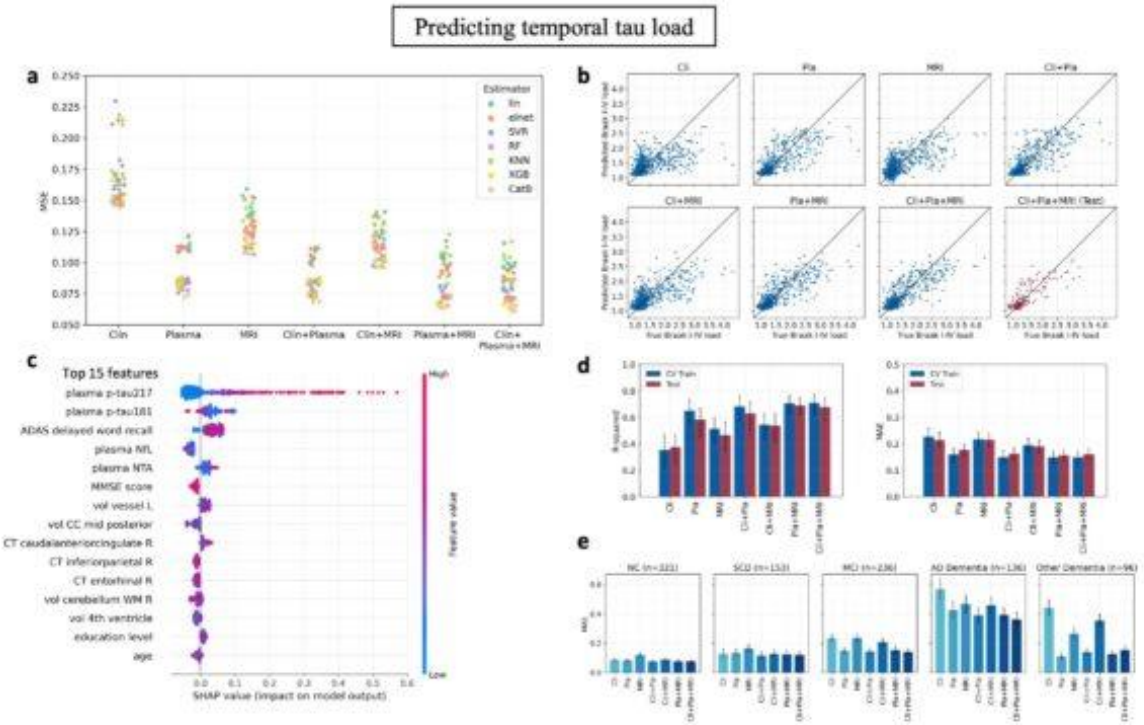

FIGURE 2: Plasma features are most informative for predicting temporal tau load. **a)** Mean squared error (MSE) results of all 56 feature selection + estimator combinations for the different input feature blocks when predicting temporal tau load. The blocks including plasma features consistently performed best. **b)** Scatter plots of true vs predicted Braak I-IV (temporal tau) load for the best pipeline combinations in a). **c)** top SHAP feature contributions in the model including all features. **d)** R-squared and mean absolute error (MAE) of best pipeline combinations in a). **e)** MAE performance of best pipeline combination in a) stratified by cognitive status.

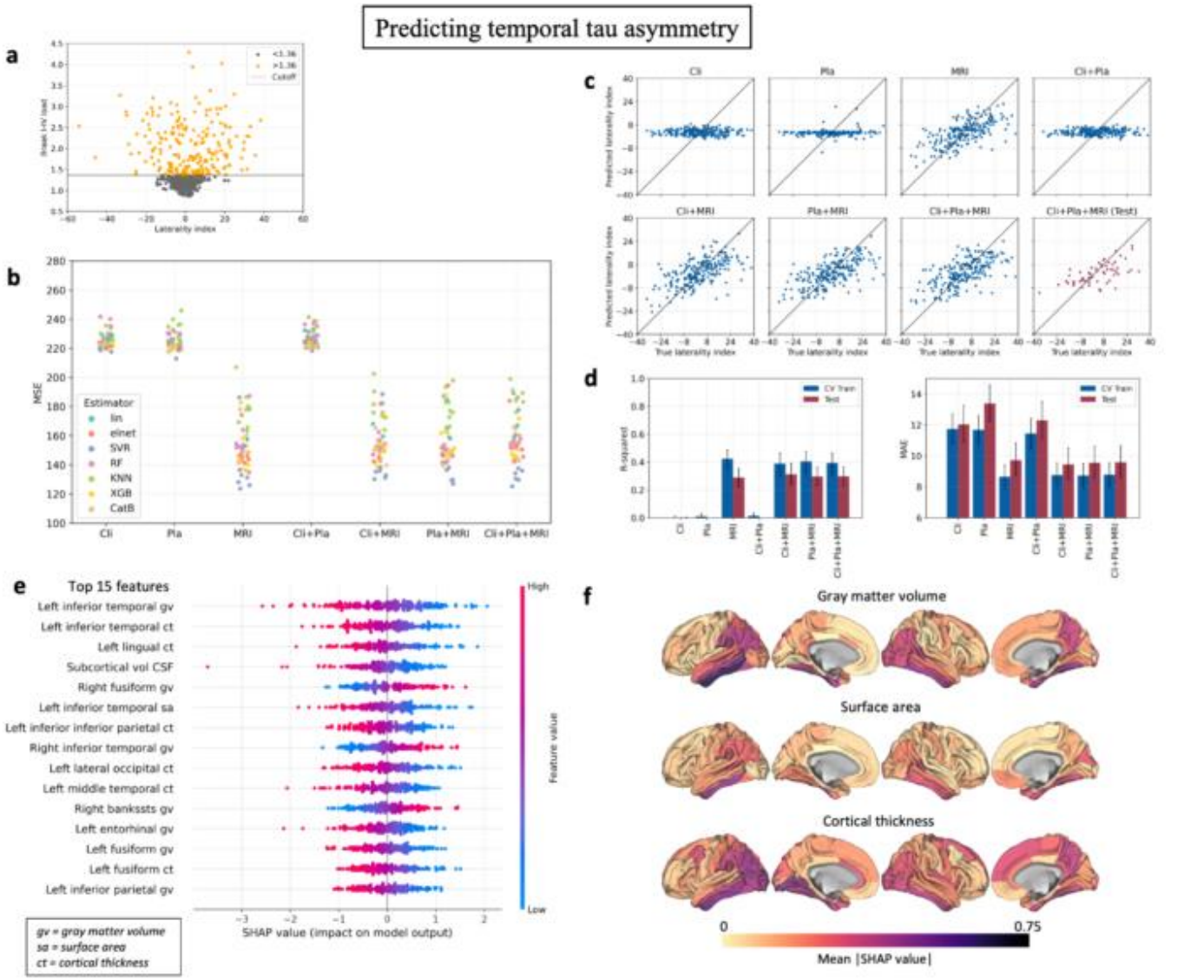

FIGURE 3: MRI features are most informative for predicting hemispheric asymmetry of temporal tau load. **a)** A dispersed asymmetry distribution was present in tau-positive individuals. **b)** Mean squared error (MSE) results of all 56 feature selection + estimator combinations for the different input feature blocks when predicting hemispheric asymmetry of temporal tau load. The blocks including MRI features consistently performed best. **c)** Scatter plots of true vs predicted laterality index (hemispheric asymmetry) for the best pipeline combinations in a). **d)** R-squared and mean absolute error (MAE) of best pipeline combinations in a). **e)** top SHAP feature contributions in the model including all features. **f)** SHAP feature contributions for MRI.

Keywords: tau-PET, machine learning

85 Amyloid and tau burden relate to longitudinal changes in performance of everyday activities as measured using the performance-based Harvard Automated Phone Task

Mark Dubbelman[1,2], Ibai Diez Palacio[3], Christopher Gonzalez[4], Rebecca Amariglio[1,2], J. Alex Becker[3], Jasmeer Chhatwal[1,2], Jennifer Gatchel[5,6], Keith Johnson[1,2,3], Joseph Locascio[1], Onyinye Udeogu[1], Sharon Wang[1], Kathryn Papp[1,2], Michael Properzi[1], Dorene Rentz[1,2], Aaron Schultz[1], Reisa Sperling[1,2], Patrizia Vannini[1,2], Gad Marshall[1,2]

[1]*Department of Neurology, Massachusetts General Hospital, Harvard Medical School, Boston, MA, United States*
[2]*Center for Alzheimer Research and Treatment, Department of Neurology, Brigham and Women's Hospital, Harvard Medical School, Boston, MA, United States*
[3]*Department of Radiology, Massachusetts General Hospital, Harvard Medical School, Boston, MA, United States*
[4]*Department of Psychology, Illinois Institute of Technology, Chicago, IL, United States*
[5]*Department of Psychiatry, Massachusetts General Hospital, Harvard Medical School, Boston, MA, United States*
[6]*Division of Geriatric Psychiatry, McLean Hospital, Harvard Medical School, Belmont, MA, United States*

Background: Changes in everyday functioning constitute a clinically meaningful outcome, even in early stages of Alzheimer's disease. We investigated how changes over time in everyday functioning relate to tau and amyloid burden as measured with positron emission tomography (PET) in cognitively unimpaired older adults.

Methods: Seventy-seven participants (72±6 years, 60% female) underwent Pittsburgh compound-B and flortaucipir PET at baseline and completed yearly assessments of the Harvard Automated Phone Task (APT; mean follow-up 2.0±0.9 years). Distribution volume ratios were computed for a cortical amyloid aggregate, and standardized uptake volume ratios for several temporal and frontal tau regions. The Harvard APT comprises three tasks to be completed through an automated phone system: prescription refill (APT-Script), primary care physician selection (APT-PCP), and money transfer (APT-Bank). Higher performance rates reflect better task performance. All participants were cognitively unimpaired at baseline. In separate linear mixed models, we used amyloid by time and tau by time interactions to predict changes in performance on the Harvard APT tasks. All models were adjusted for age, sex, and education. Three-way amyloid by tau by time interactions were also investigated.

Results: Global amyloid burden was associated with a decline in performance over time on APT-PCP, as were entorhinal and inferior temporal tau. Three-way interactions showed an association between amyloid and both entorhinal and precuneus tau and change over time on APT-PCP. Further, entorhinal tau was associated with a decline in performance over time on APT-Bank. Performance on APT-Script did not appear to relate to amyloid or tau. Table 1 displays all estimates.

Conclusion: Tau, specifically in early aggregating areas, and amyloid appear to be related to subtle changes over time in performance on a phone-based functional assessment. These results show that amyloid and tau burden are associated with measures of everyday functioning, even very early in the disease course.

Table 1. Estimates and 95% confidence intervals for interactions between time and ROIs, per APT task.

	APT-Script	APT-PCP	APT-Bank
Global amyloid	-0.010 [-0.022, 0.003]	**-0.008 [-0.014, -0.002]**	-0.006 [-0.016, 0.003]
Tau			
Entorhinal	-0.008 [-0.022, 0.005]	**-0.008 [-0.014, -0.001]**	**-0.010 [-0.020, -0.001]**
Inferior temporal	-0.005 [-0.020, 0.010]	**-0.005 [-0.009, -0.002]**	-0.008 [-0.020, 0.003]
Precuneus	-0.003 [-0.020, 0.015]	-0.004 [-0.013, 0.005]	-0.010 [-0.023, 0.003]
Posterior cingulate	0.0004 [-0.017, 0.018]	0.0002 [-0.009, 0.009]	-0.007 [-0.020, 0.006]
Supramarginal	-0.006 [-0.024, 0.011]	0.0003 [-0.009, 0.010]	-0.008 [-0.022, 0.005]
DLPF	-0.002 [-0.020, 0.015]	-0.001 [-0.010, 0.008]	-0.004 [-0.017, 0.010]
Tau by amyloid			
Entorhinal	-0.025 [-0.089, 0.040]	**-0.033 [-0.064, -0.001]**	0.026 [-0.023, 0.077]
Inferior temporal	0.092 [-0.026, 0.209]	-0.035 [-0.096, 0.025]	-0.031 [-0.123, 0.065]
Precuneus	0.033 [-0.132, 0.198]	**-0.093 [-0.179, -0.008]**	-0.086 [-0.212, 0.040]
Posterior cingulate	-0.052 [-0.201, 0.095]	**-0.079 [-0.158, -0.003]**	-0.068 [-0.187, 0.049]
Supramarginal	0.014 [-0.144, 0.174]	-0.060 [-0.141, 0.021]	-0.095 [-0.212, 0.025]
DLPF	-0.002 [-0.147, 0.145]	-0.049 [-0.125, 0.027]	0.017 [-0.105, 0.134]

All data are shown as estimate [95% confidence interval] and represent a time by ROI interaction. All models are adjusted for age, sex, and education. Significant results are shown in bold.

Abbreviations: APT, Automated Phone Task; DLPF, dorsolateral prefrontal; PCP, primary care physician; ROI, region of interest.

Keywords: everyday functioning, tau, amyloid, longitudinal, instrumental activities of daily living

86 In vivo structural integrity of the hypothalamus and the spatiotemporal evolution of Alzheimer's disease

Marion Baillet[1], Tobey Betthauser[2,3], Eric Salmon[4], Heidi Jacobs[1,5]

[1]*Faculty of Health, Medicine and Life Sciences, School for Mental Health and Neuroscience, Alzheimer Centre Limburg, Maastricht University, Maastricht, The Netherlands*
[2]*Wisconsin Alzheimer's Institute, School of Medicine and Public Health, University of Wisconsin-Madison, Madison, WI, United States*
[3]*Wisconsin Alzheimer's Disease Research Center, School of Medicine and Public Health, University of Wisconsin-Madison, Madison, WI, United States*
[4]*GIGA-CRC in Vivo Imaging, University of Liège, Liège, Belgium*
[5]*Gordon Center for Medical Imaging, Department of Radiology, Massachusetts General Hospital and Harvard Medical School, Boston, MA, United States*

Background: The posterior hypothalamus has been recently put forward as a critical site for Alzheimer's disease (AD) pathogenesis, as it encompasses several neuromodulatory nuclei that exhibit abnormal tau protein accumulation before any cortical deposition. Here, we aimed to investigate whether the structural integrity of the posterior hypothalamus is associated with tau accumulation in a group of cognitively unimpaired and impaired older individuals.

Methods: 51 cognitively normal (CN) individuals, 55 mild cognitive impairment (MCI) and 33 AD patients (mean [SD] age = 77.5 [7.5], 27 women; 73.9 [6.4], 25 women; 76.3 [7.4], 11 women; **Table 1**) from the ADNI3 dataset underwent longitudinal multimodal neuroimaging scans. The whole hypothalamus and its subunits, including the posterior region, were segmented on structural 3D T1-weighted images using a deep convolutional network algorithm (**Figure 1a**). Tau burden in the entorhinal cortex was measured with regional standardized uptake volume ratio (partial volume corrected) derived from [18F]Flortaucipir positron emission tomography (PET) images.

Results: AD patients exhibit lower posterior hypothalamic volume at baseline compared to CN participants and MCI patients (main effect of group, $p<0.0001$, adjusted for age and sex; **Figure 1b**). Linear mixed models revealed an overall loss of posterior hypothalamic volume over time (main effect of time, $p<0.0001$; **Figure 2a**) independently of age at baseline and sex. Crucially, lower posterior hypothalamic volume at baseline was associated with faster tau accumulation in the entorhinal cortex ($p=0.02$, adjusted for age at baseline and sex), which may be driven by MCI patients (interaction group*posterior hypothalamus, $p=0.08$, **Figure 2b**).

Conclusions: Our findings provide first evidence that the posterior hypothalamus may constitute a sensitive biomarker tightly linked to the earliest disease-related pathophysiological changes, and further highlight novel targets for the early detection of individuals at risk for neurodegeneration.

Table 1. Participants characteristics

Variables	Cognitively unimpaired participants	Mild cognitive impairment patients	Alzheimer's disease patients
N	51	55	33
Brain imaging follow-up duration (year)	2.8 ± 1.4	2.9 ± 1.5	1.5 ± 2.5
Demographic			
Age (years)	77.5 ± 7.5	73.9 ± 6.4	76.3 ± 7.4
Sex (n, %)			
Female	27 (53%)	25 (45%)	11 (33%)
Male	24 (47%)	30 (55%)	22 (67%)
Education (years)	16.6 ± 2.3	16.3 ± 2.7	16.1 ± 2.3
APOE ε4 carriers (n, %)†	16 (31%)	23 (42%)	19 (57%)
Structural brain imaging			
Whole hypothalamus volume (mm^3)‡	765.4 ± 71.7	769.2 ± 73.5	705.8 ± 83.7
Posterior hypothalamus volume (mm^3)‡	216.1 ± 27.9	222.1 ± 34.5	184.9 ± 40.3
Annual posterior hypothalamic loss (mm^3)	2.8 ± 0.7	2.5 ± 0.5	8.1 ± 3.0
Tau-PET imaging			
Tau-PET entorhinal cortex (SUVR PVC)	1.5 ± 0.4	2.1 ± 0.6	2.8 ± 0.8
Annual Tau-PET accumulation in entorhinal cortex (SUVR PVC)	0.02 ± 0.005	0.02 ± 0.009	0.06 ± 0.1

Mean ± standard deviation

†Missing values: 2 for mild cognitive impairment patients and 4 for Alzheimer's disease patients

‡Corrected for total intracranial volume

APOE: apolipoprotein E; SUVR: standardized uptake value ratio; PVC: partial volume corrected

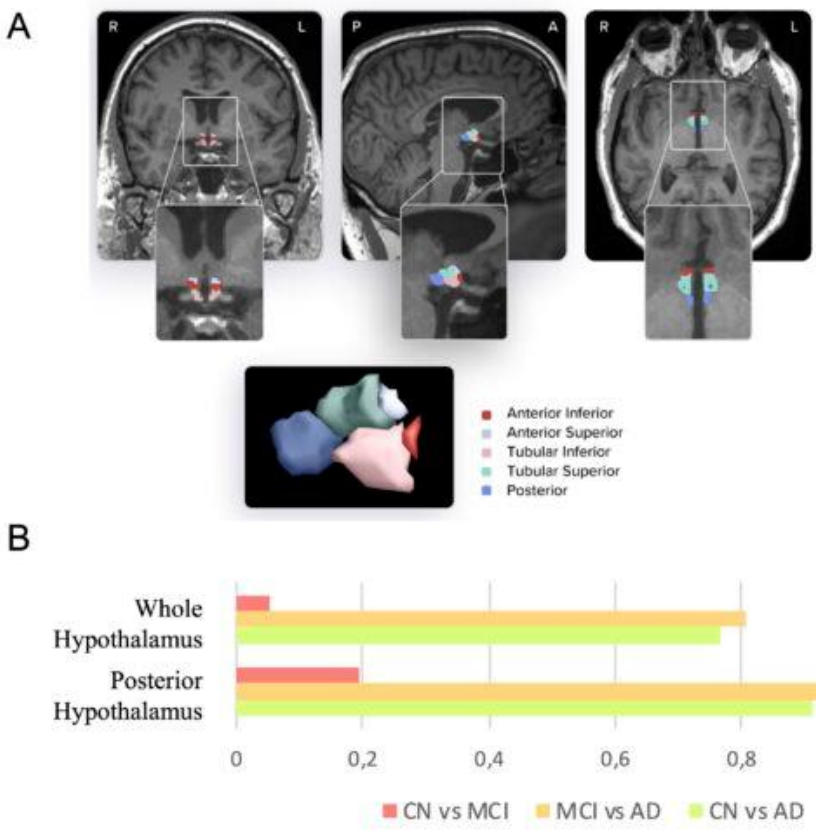

Figure 1. (A) Anatomical segmentation and parcellation of the hypothalamus in vivo and (B) Cohen's d measures between CN, MCI and AD patients for the whole hypothalamus and its posterior region at baseline

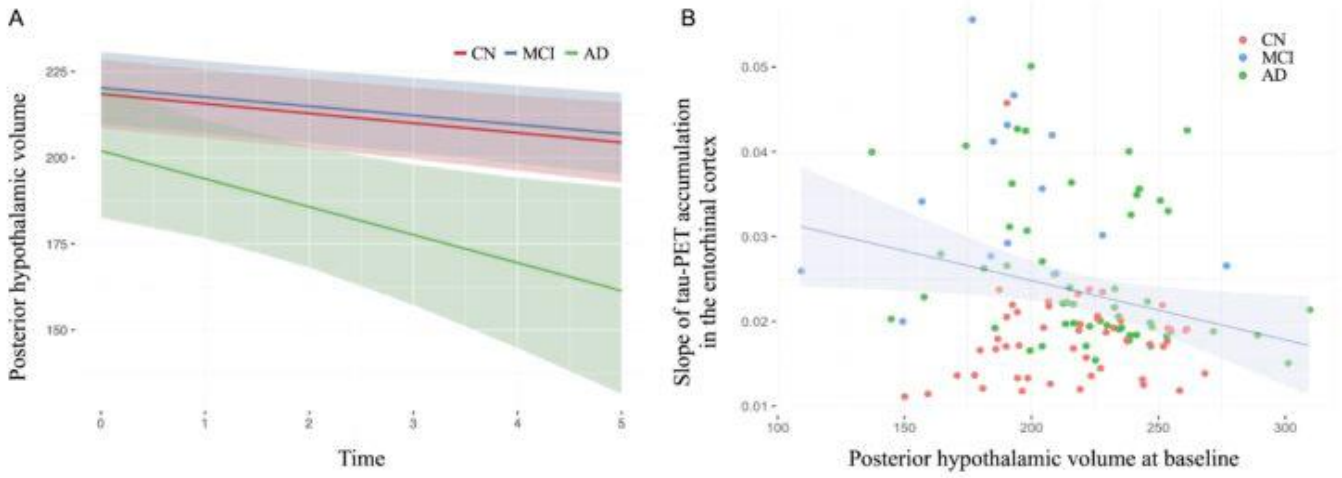

Figure 2. (A) Evolution of the posterior hypothalamic volume over time and (B) relationship between tau-PET accumulation in the entorhinal cortex over time and baseline posterior hypothalamic volume

Keywords: Hypothalamus, MRI, Tau, Alzheimer's disease

87 Cross-sectional comparison of extra-cerebral binding trends in [F-18]MK6240 PET images

Andrew McVea[1], Alexandra DiFilippo[1], Max McLachlan[1], Brecca Betcher[1], Sterling Johnson[1], Tobey Betthauser[1], Bradley Christian[1]

[1]*University of Wisconsin - Madison, Madison, WI, United States*

Background: [F-18]MK6240 is a PET radioligand that binds to tau aggregates in Alzheimer's disease. While MK6240 has reduced cortical off-target binding compared to other tau tracers, significant MK6240 signal is observed in the meninges and sinus. This extra-cerebral binding (ECB) can result in a spill-in effect where exterior brain regions see increased signal in reconstructed PET images. This study evaluates ECB in a large cohort to identify trends in this signal and establish SUVR thresholds for characterizing ECB signal.

Method: Participants were imaged at the University of Wisconsin–Madison on a Biograph mCT (n = 488) or ECAT HR+ (n = 475). PET images were smoothed using a $6mm^3$ gaussian kernel then processed using a standardized pipeline to generate SUVR images using the inferior cerebellar grey matter reference region. During QC MK6240 images were rated from 0-5 qualitatively ranking meningeal signal in relation to evaluating PET measures. This rating served as ground truth for deriving SUVR thresholds for Low (score of 0-1), Moderate (2-3) and High (4-5) ECB signal using ROC analysis.

Results: We did not observe significant differences in ECB signal between amyloid ($p_{meninges}$= 0.43, p_{sinus}= 0.95) or tau statuses ($p_{meninges}$= 0.18, p_{sinus}= 0.35). There was a significantly higher average SUVR in the meninges and sinus for female ($p_{meninges}$< 0.01, p_{sinus}< 0.01) and APOE4+ participants ($p_{meninges}$< 0.01, p_{sinus}= 0.05). No correlation between ECB and age ($p_{meninges}$= 0.89, p_{sinus}= 0.98) or cognitive status was observed ($p_{meninges}$= 0.20, p_{sinus}= 0.18). ROC analysis found an optimal SUVR cutoff of 1.10 for Moderate meningeal signal (Youden's: J = 0.67) and 1.41 for High (J = 0.78).

Conclusions: ECB is a highly variable factor in MK6240 imaging that can potentially bias tracer uptake outcomes. While we observed sex and risk factor differences, further work to identify the underlying sources and correct for ECB is ongoing.

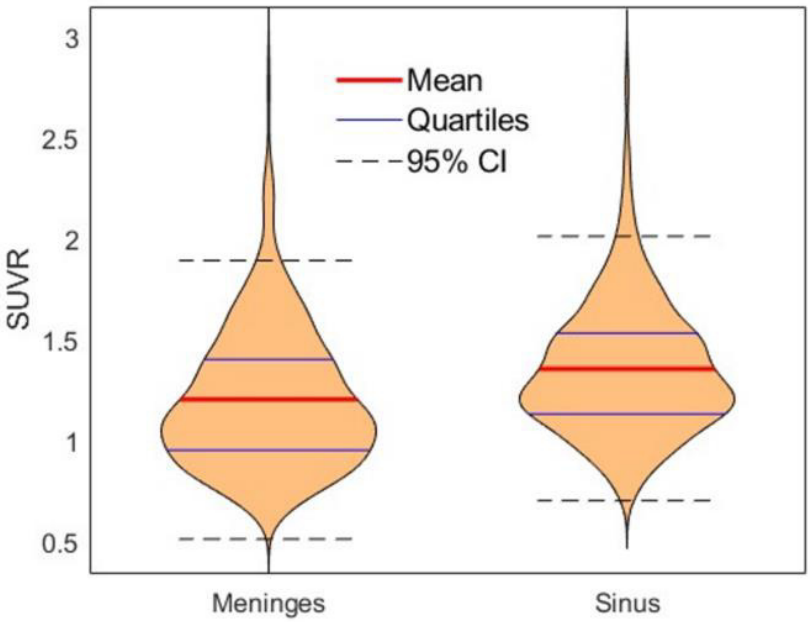

Fig. 1: Violin plots showing the distribution of meningeal and sinus SUVR ranging from 0.60 to 2.88 in the meninges and 0.70 to 2.90 in the sinus. On average there is higher binding in the sinus (1.35±0.33) compared to the meninges (1.20±0.34) in the scans observed.

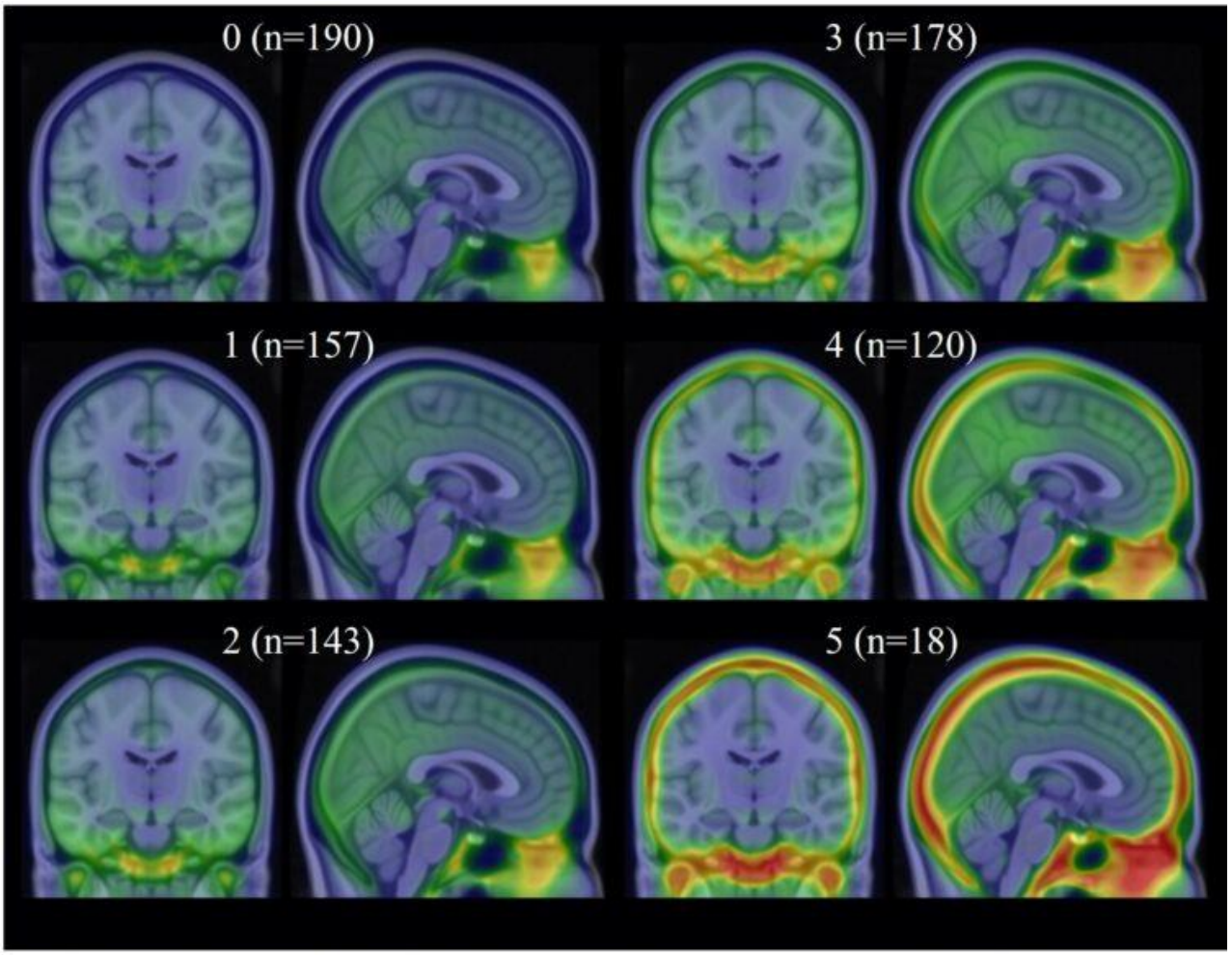

Fig. 2: Average images of the [F-18]MK6240 scans at our site based on visual rating of meningeal signal. Note that this rating system is just based on meningeal signal and not sinus signal unless there is signal spill-in from the sinus to the cortex observed.

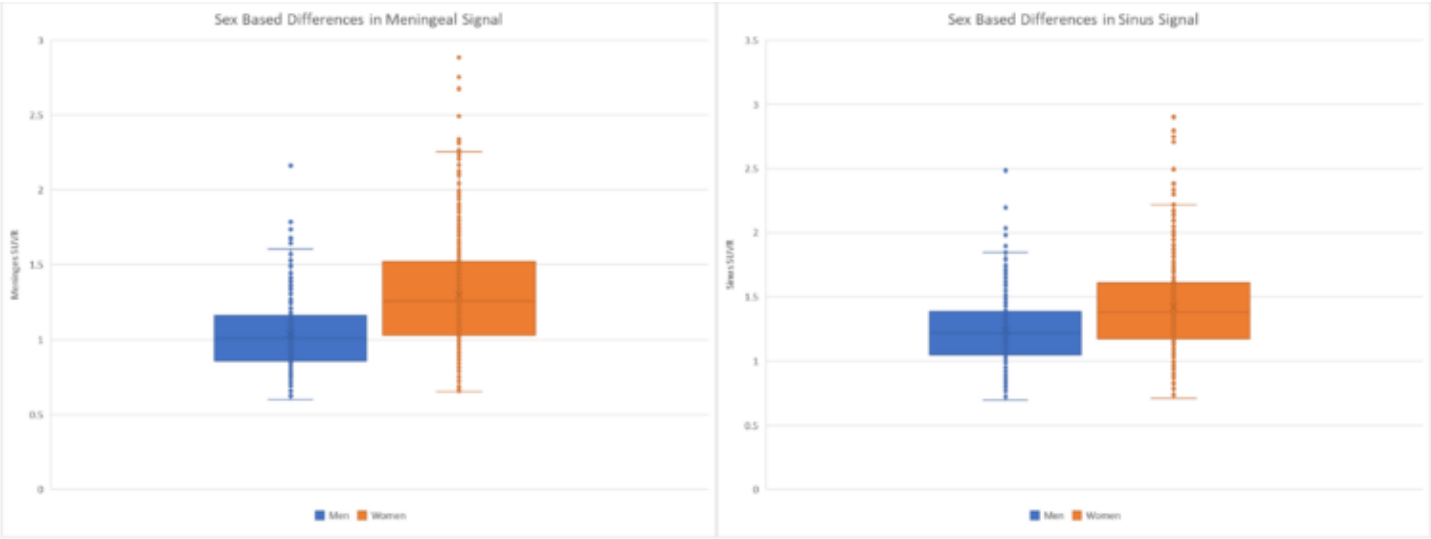

Fig. 3: Box plots showing the average meningeal (left) and sinus (right) SUVR for men and women. We observed significantly higher signal for women in both the meninges (1.30±0.36 vs. 1.04±0.23) and sinus (1.42±0.34 vs. 1.23±0.26) in our cohort.

Keywords: Extra-Cerebral Binding, Meninges, [F-18]MK6240, Sex and Age Differences, Off-target binding

88 Tau accumulation in Down Syndrome after onset of amyloid positivity

Andrew McVea[1], Alexandra DiFilippo[1], Max Max McLachlan[1], Brecca Betcher[1], Matthew Zammit[1], Tobey Betthauser[1], Alexander Converse[1], Dhanabalan Murali[1], Charles Stone[1], Sigan Hartley[1], Sterling Johnson[1], Dana Tudorascu[2], Charles Laymon[2], Ann Cohen[2], Davneet Minhas[2], Chester Mathis[2], Beau Ances[4], Shahid Zaman[3], William Klunk[2], Benjamin Handen[2], Bradley Christian[1], ABC-DS Investigators[1,2,3,4]

[1]*University of Wisconsin - Madison, Madison, WI, United States*
[2]*University of Pittsburgh, Pittsburgh, PA, United States*
[3]*University of Cambridge, Cambridge, United Kingdom*
[4]*Washington University in St. Louis, St. Louis, MO, United States*

Background: Alzheimer's Disease (AD) in Down syndrome (DS) has an increased prevalence tied to the triplication of chromosome 21 containing the amyloid precursor protein gene. In this study we compare the global tau burden of participants with DS delineated by amyloid chronicity.

Methods: Participants in the ABC-DS study with ≥1 [C-11]PiB scan for amyloid staging and ≥1 [F-18]AV1451 scan for tau were included (n= 169). Amyloid burden was determined using the amyloid load ($A\beta_L$) metric with values greater than 13.3$A\beta_L$ identified as Aβ(+). Amyloid data was input into the SILA model (Fig. 1) to find duration of amyloid positivity. Using this value we calculated participant age of Aβ(+) and amyloid chronicity values for the [F-18]AV1451 tau scans before creating five groups for comparison: Aβ(-) , Aβ(+) chronicity 0-5 years, 5-10 years, 10-15 years and >15 years. Tau images were processed using a uniform pipeline to calculate SUVR using the inferior cerebellar grey matter reference region. Global [F-18]AV1451 SUVR was quantified using the MeTeR ROI, defined by the mesial-temporal, temporoparietal and neocortical regions, to compare tauopathy between amyloid chronicity groups.

Results: With increasing amyloid chronicity, higher [F-18]AV1451 binding was observed in regions associated with tau deposition in AD (Fig. 2). In each amyloid chronicity group > 0, there was an increased average global [F-18]AV1451 SUVR compared to the previous group. Compared to the age < 0 group there were significant differences in global [F-18]AV1451 SUVR in the 0-5 year ($p= 0.03$) and all older groups ($p< 0.01$).

Conclusions: The onset of amyloid deposition in AD is a predictor of tau aggregation in the DS cohort with observable differences within years of amyloid positivity. However, the variability of accumulation rates of tau and amyloid in DS requires further investigation towards understanding the effect of genetic and lifestyle factors in this population.

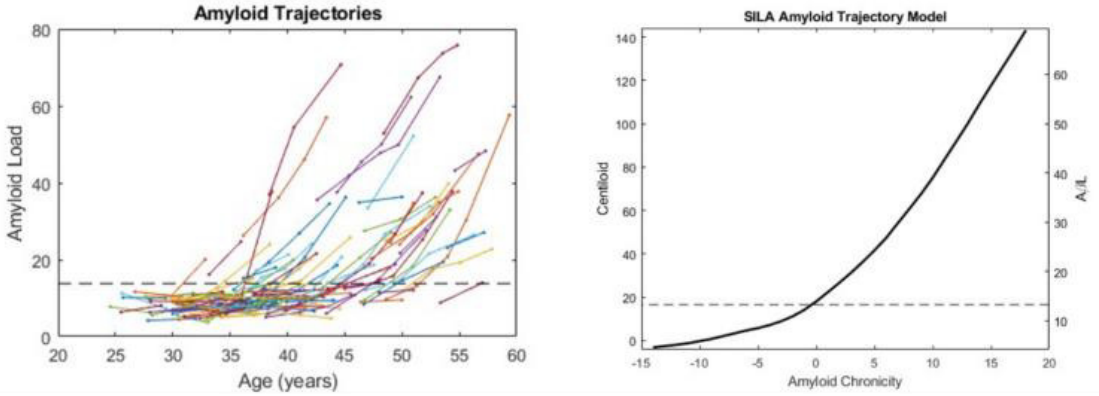

Fig. 1: Spaghetti plot (left) showing the amyloid trajectories of participants in our study with multiple [C-11]PiB scans. These data were then input into the Sampled Iterative Local Approximation (SILA) algorithm (Betthauser, 2021; Zammit 2023) to approximate at what time these participants would become amyloid positive. The SILA model fits the data to an average amyloid trajectory (right) shown in both centiloids and $A\beta_L$.

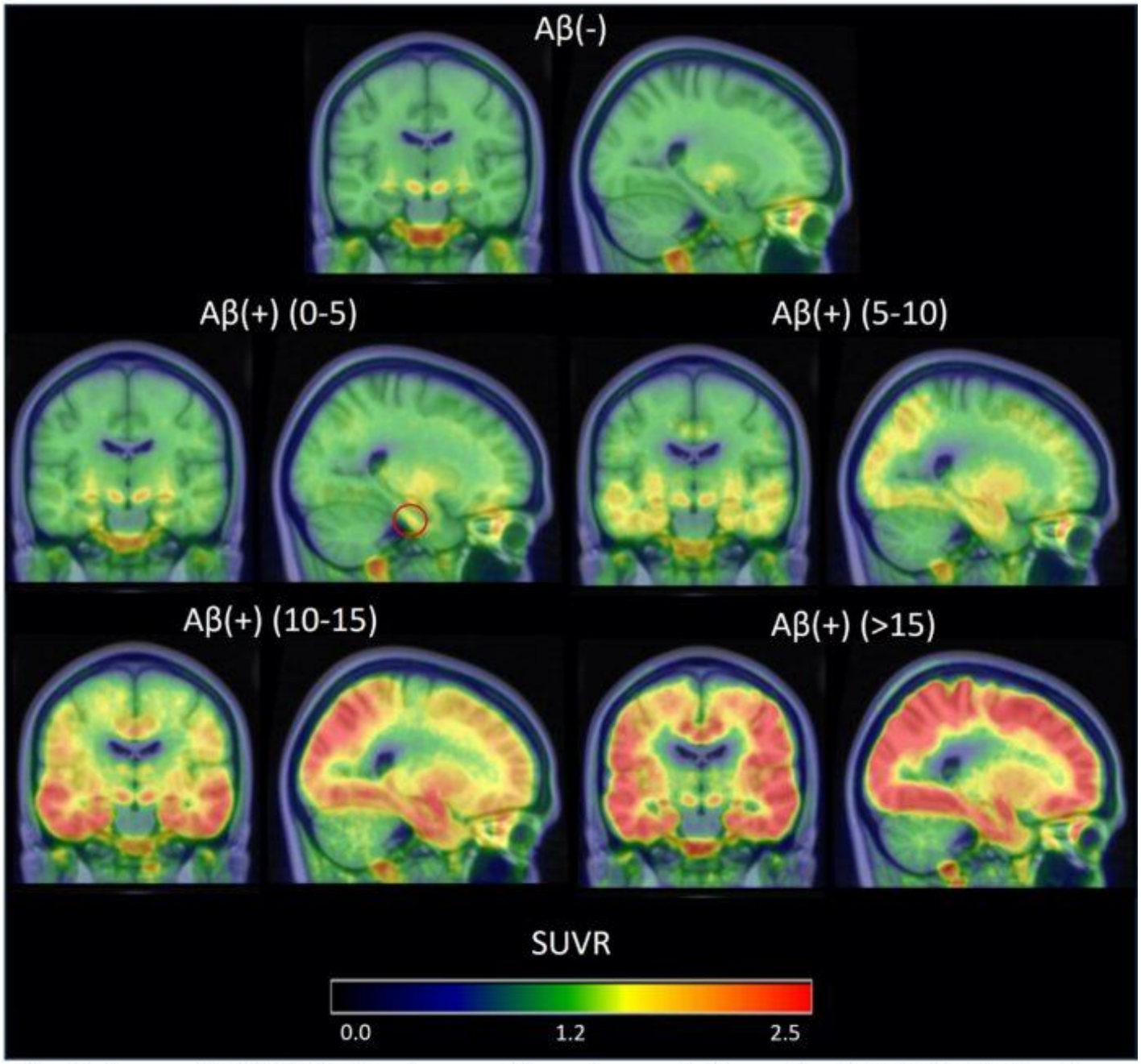

Fig. 2: Average [F-18]AV1451 tau images taken when amyloid negative, 0-5, 5-10, 10-15 and greater than 15 years after the point of amyloid positivity. Tau aggregation can be seen in the Braak I/II regions in the 0-5 year group (circled in red) before spreading throughout the mesial-temporal lobe and into the cortex in later time groups.

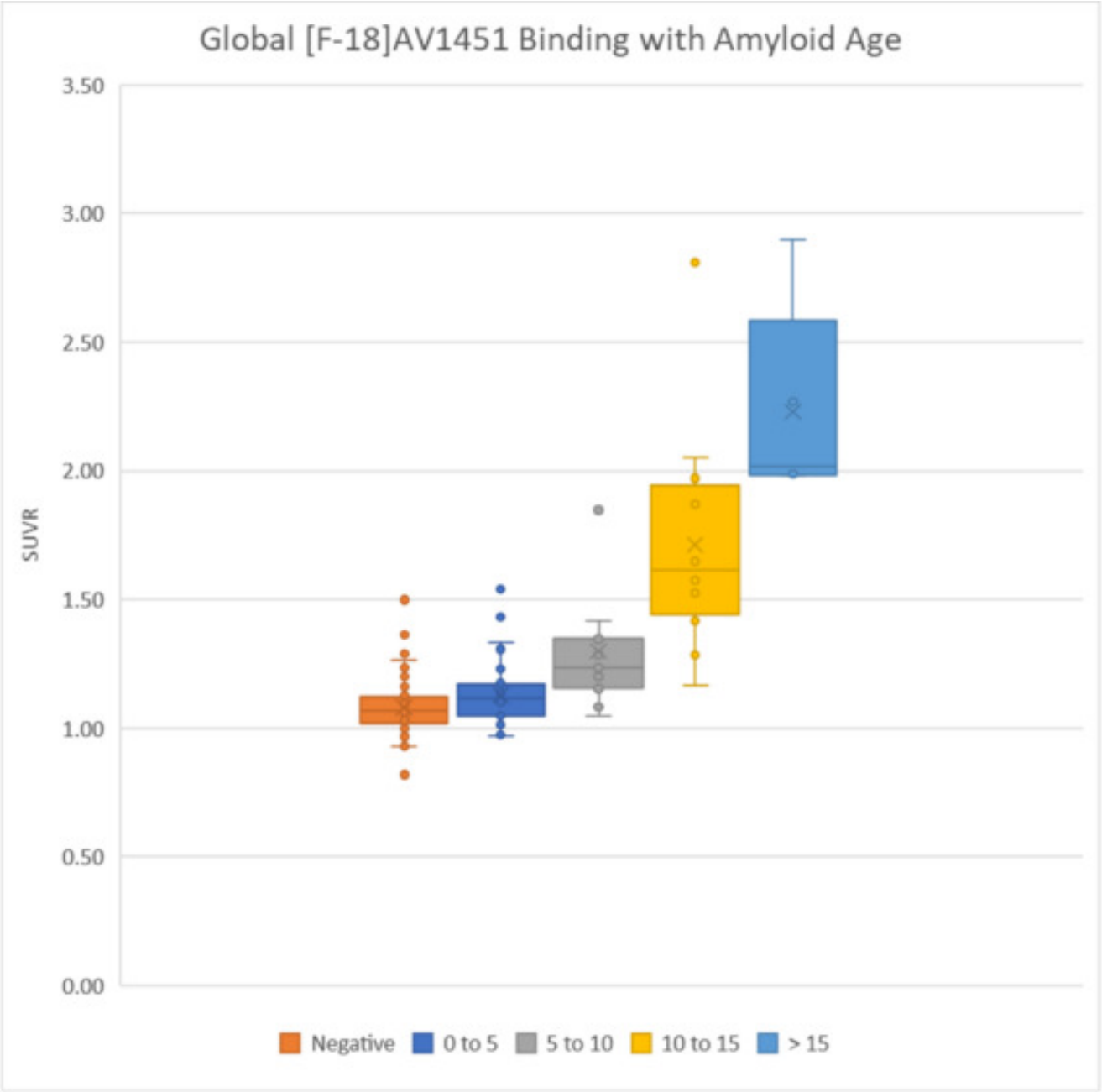

Fig. 3: Box plots showing increasing global [F-18]AV1451 SUVR with age after amyloid positivity. In total there were 200 tau scans across the five categories. Differences in SUVR between the amyloid negative group (1.08±0.09) and all of the positive groups have significant p-values: 0-5 years (1.13±0.12, p= 0.028), 5-10 years (1.30±0.22, p< 0.001), 10-15 years (1.71±0.41, p< 0.001), and >15 years (2.23±0.35, p= 0.003).

Keywords: Down Syndrome, tau, [F-18]AV1451, amyloid chronicity

89 Greater locus coeruleus activity and locus coeruleus-amygdala hypoconnectivity during high arousal conditions are related to elevated concentrations of plasma p-tau231 in older individuals

Prokopis Prokopiou[1,6], Maxime Van Egroo[1,2,6], Joost Riphagen[1,6], Nicholas Ashton[3,7,8,9], Shorena Janelidze[4], Reisa Sperling[5,6,10], Keith Johnson[1,6,10], Kaj Blennow[3,11], Oskar Hansson[4,12], Henrik Zetterberg[3,11,13,14,15], Heidi Jacobs[1,2,6]

[1]*Gordon Center for Medical Imaging, Department of Radiology, Massachusetts General Hospital, Boston, MA, United States*
[2]*Faculty of Health, Medicine and Life Sciences, School for Mental Health and Neuroscience, Alzheimer Centre Limburg, Maastricht University, Maastricht, The Netherlands*
[3]*Department of Psychiatry and Neurochemistry, Institute of Neuroscience and Physiology, The Sahlgrenska Academy at the University of Gothenburg, Mölndal, Sweden*
[4]*Clinical Memory Research Unit, Department of Clinical Sciences Malmö, Lund University, Lund, Sweden*
[5]*Center for Alzheimer Research and Treatment, Department of Neurology, Brigham and Women's Hospital, Boston, MA, United States*
[6]*Harvard Medical School, Boston, MA, United States*
[7]*Centre for Age-Related Medicine, Stavanger University Hospital, Stavanger, NO*
[8]*King's College London, Institute of Psychiatry, Psychology and Neuroscience, Maurice Wohl Institute Clinical Neuroscience Institute, London, United Kingdom*
[9]*NIHR Biomedical Research Centre for Mental Health and Biomedical Research Unit for Dementia at South London and Maudsley NHS Foundation, London, United Kingdom*
[10]*Department of Neurology, Massachusetts General Hospital, Boston, MA, United States*
[11]*Clinical Neurochemistry Laboratory, Sahlgrenska University Hospital, Mölndal, Sweden*
[12]*Memory Clinic, Skåne University Hospital, Malmö, Sweden*
[13]*Department of Neurodegenerative Disease, UCL Institute of Neurology, Queen Square, London, United Kingdom*
[14]*UK Dementia Research Institute at UCL, London, United Kingdom*
[15]*Hong Kong Center for Neurodegenerative Diseases, Clear Water Bay, Hong Kong, CN*

Introduction: The brainstem nucleus locus coeruleus (LC) is one of the first brain regions to accumulate hyperphosphorylated tau in the earliest stages of Alzheimer's disease (AD). Animal and human studies indicated that these early pathologic changes are associated with LC hypermetabolism and loss of noradrenergic projections to the cortex. Here, we investigated the relationships between LC activity or LC connectivity with the amygdala under different arousal levels and plasma markers of phosphorylated tau, including p-tau231, p-tau217, and p-tau181.

Methods: 79 cognitively unimpaired individuals underwent fasting blood draw and task-based 7T-fMRI, during which they were shown high- or low-arousing scenes. Plasma p-tau181 and p-tau231 were measured using in-house Simoa methods, and p-tau217 using MSD immunoassay. Averaged time-series from voxels within the LC were extracted using a cohort-specific 7T template of the LC. ROI-based fMRI analyses were performed to evaluate high>low arousal (h>l) LC activation and psychophysiological interactions analysis to evaluate LC connectivity with the amygdala. Age- and sex-adjusted associations between LC activity and p-tau were assessed using robust linear regression. P-values and 95% confidence intervals (CI) were evaluated using randomizations (n=2000).

Results: Greater h>l LC activity was associated with elevated p-tau181 (p=0.008-Fig.1B) and p-tau231 (p=0.03-Fig.1C). No significant associations were observed between LC-Amygdala connectivity (LAC)

and any p-tau biomarker (p>0.05–Fig.1D-F). LAC moderated the relationship between LC activity and p-tau231, whereby greater activity was related to higher p-tau231, particularly in lower LAC (Fig. 2C).

Conclusions: Our results suggest that LC dysfunction may relate to the early stages of AD pathology as detected in plasma tau markers in asymptomatic individuals. Notably, given that tau phosphorylation at threonine 231 is one of the earliest events in tau's phosphorylation cascade, our results suggest that LC hyperactivity associated with hypoconnectivity of the LC with its target regions may reflect processes related to early tau pathology.

Number of participants	79
Age (years)	61 [52, 70.5]
Sex, No. (%) = M	39 (49.36)
Education (years)	6 [4, 6]
MMSE (score)	29 [28, 30]
p-tau 231 (pg/mL)	8.47 [6.514, 9.705]
p-tau 217 (pg/mL)	0.25 [0.21, 0.29]
p-tau 181 (pg/mL)	1.67 [1.3, 1.9]

Table 1. Data are presented as medians [and interquartile ranges]. Abbreviations: (pg/mL) picogram per milliliter, Mini-Mental State Examination MMSE.

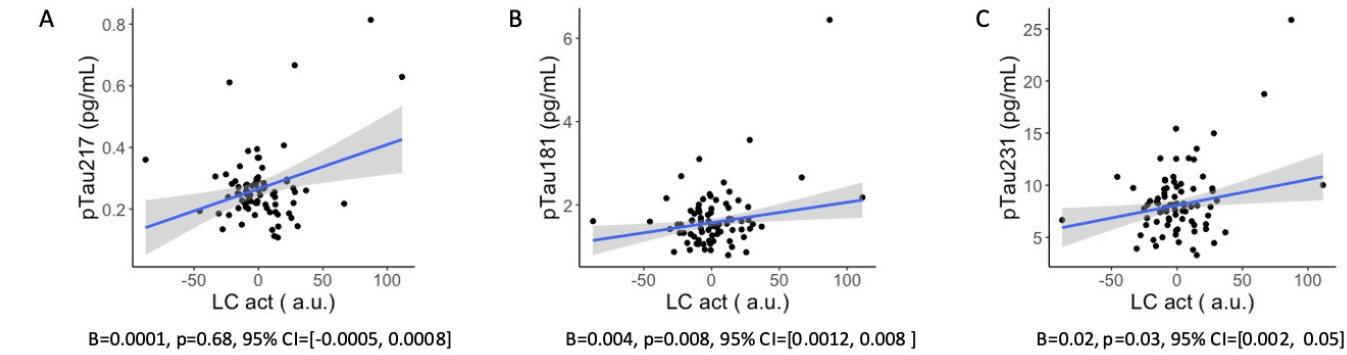

Fig. 1. Greater high> low arousal (h>l) LC activity was related to higher p-tau181 and p-tau231 (B-C). No associations between h>l LC activity and p-tau217 were observed (A). Similarly, no associations between LC-Amygdala connectivity and any biomarker were observed. Abbreviations: LC locus coeruleus, Amyg amygdala, a.u. arbitrary units.

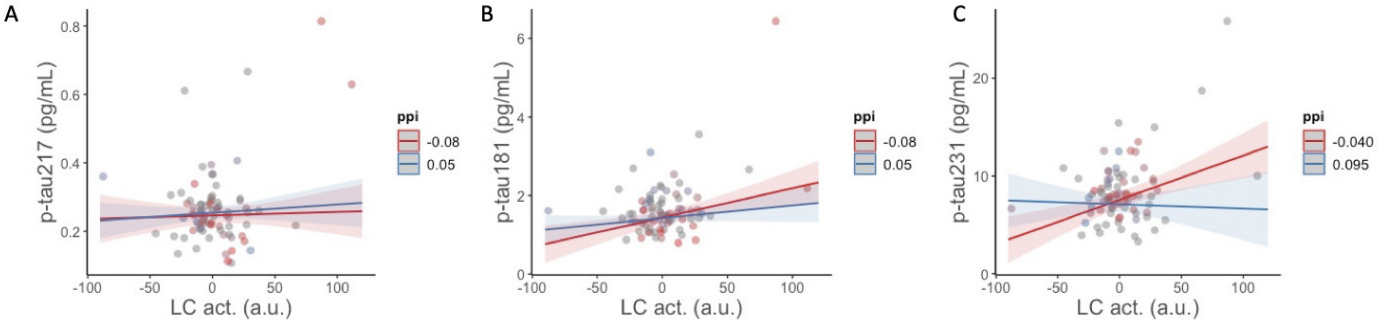

Fig. 2. Associations between two-way interactions between h>l LC activity by LC-Amygdala connectivity and p-tau. Greater LC activity was related to higher p-tau231, particularly at lower LC-Amygdala connectivity levels (C). No moderation effects were observed by LC-amygdala connectivity on the relationship between LC activity and p-tau217 or p-tau181(A-B). Abbreviations: LC locus coeruleus, Amyg amygdala, a.u. arbitrary units, ppi psychophysiological interactions.

Keywords: Locus coeruleus, plasma biomarkers, functional MRI, arousal, preclinical AD

90 Establishing tau-PET cut-points for cognitive diagnosis with [F-18]PI-2620

Victoria R. Tennant[1], Koral V. Wheeler[1], Noelle N. Lee[1], Jamie A. Terner[1], Rema Raman, Robert A. Rissman, Bradley T. Christian, Melissa Petersen, Joseph H. Lee, Annie Cohen, Beau Ances, Zhengyang Zhou, Fan Zhang, Rajesh R. Nandy, Kristine Yaffe, Sid E. O'Bryant, Meredith N. Braskie

[1]1. Imaging Genetics Center, Mark and Mary Stevens Neuroimaging and Informatics Institute, Keck School of Medicine, University of Southern California, Los Angeles, CA, United States
[2]University of California, San Diego, San Diego, CA, United States
[3]University of Pittsburgh School of Medicine, Pittsburgh, PA, United States
[4]Waisman Center, University of Wisconsin-Madison, Madison, WI, United States
[5]Washington University School of Medicine in St. Louis, St. Louis, MI, United States
[6]Columbia University Medical Center, New York, NY, United States
[7]Department of Psychiatry, Neurology, and Epidemiology and Biostatistics University of California San Francisco, San Francisco, CA, United States
[8]University of North Texas Health Science Center Fort Worth, Fort Worth, TX, United States

Background: [18F]-PI-2620 is a novel tau-PET radiotracer that has improved binding specificity to tau aggregates in Alzheimer's disease (AD). No studies have quantified tau cut-points for cognitive diagnosis with [18F]-PI-2620 standardized uptake value ratios (SUVR). Here we establish cut-points at which [18F]-PI-2620 regional SUVRs best discriminate between Aβ- cognitively unimpaired (CU) and 1) Aβ+ mild cognitive impairment (MCI) and 2) Aβ+ dementia in a multi-ethnic/racial cohort.

Methods: We scanned 217 older adults from the Health & Aging Brain Study-Health Disparities using [18F]-PI-2620-PET **(Table1).** We performed an AUC-ROC analysis using [18F]-PI-2620-SUVR signal in regions most often used in prior tau-PET cut-point research: entorhinal, middle temporal, inferior temporal, fusiform, parahippocampal, hippocampal, amygdala, and a combined temporal composite-ROI that included all regions. We tested a composite-ROI that included only regions that showed the most linear increase across cognitive diagnosis: entorhinal, parahippocampal, and amygdala. [18F]-PI-2620-SUVR cut-points were defined using two classification methods: **A)** an AUC-ROC curve analysis. The ROI-SUVR maximizing the Youden-Index identified the optimal region and cut-point and **B)** a calculation of two standard deviations above the mean (2SD+) in CU Aβ- participants only of the ROI-SUVR chosen in A.

Results: For the AUC-ROC method, the temporal composite best differentiated CU from AD and the entorhinal-parahippocampal-amygdala composite best differentiated CU from MCI **(Table2).** The AUC-ROC method was superior to the 2SD+ method when discriminating between disease states in the same regions. The Youden-Index was acceptable (>0.50) for both diagnostic comparisons using the AUC-ROC method, but only for CU vs AD using the 2SD+ method.

Conclusions: Although specificity was acceptable-to-excellent across all tests, sensitivity was low, suggesting that these cut-points could best be used to rule in pathological tau levels rather than to rule it out. Low sensitivity may arise from non-AD-related causes of cognitive decline that may occur even in Aβ+ participants.

Table 1. Participant Demographics

	Total (N=217)	CU (N=151)	MCI (N=41)	AD (N=25)
*All controls were Aβ- & all MCI & AD participants were Aβ+				
Age (years)				
Mean (SD)	66 (± 8.5)	65 (± 7.9)	70 (± 8.0)	69 (± 10)
Sex				
Male	93 (43 %)	60 (40 %)	20 (49 %)	13 (52 %)
Female	124 (57 %)	91 (60 %)	21 (51 %)	12 (48 %)
Ethnoracial Group				
Hispanic	50 (23 %)	35 (23 %)	10 (24 %)	5 (20 %)
Hispanic Black	1 (0 %)	0 (0 %)	0 (0 %)	1 (4 %)
non-Hispanic Black	75 (35 %)	50 (33 %)	15 (37 %)	10 (40 %)
non-Hispanic White	91 (42 %)	66 (44 %)	16 (39 %)	9 (36 %)
Education				
Mean (SD)	15 (± 3.4)	15 (± 3.2)	14 (± 3.3)	14 (± 4.5)
Global Aβ SUVR (18F-florbetaben)				
Mean (SD)	1.1 (± 0.20)	0.99 (± 0.046)	1.3 (± 0.19)	1.4 (± 0.24)

Table 2. Cut-point method results

	2 Standard Deviations		AUC-ROC	
	CU & MCI	CU & AD	CU & MCI	CU & AD
ROI	ERC-PHC-amygdala	Temporal composite	ERC-PHC-amygdala	Temporal composite
Cut-point	1.35	1.27	1.30	1.30
Sensitivity	49%	68%	66%	68%
Specificity	88%	95%	89%	98%
YI	0.36	0.63	0.55	0.66
AUC	--	--	0.78	0.83

***YI =** Youden Index, Temporal composite: volume weighted average FreeSurfer (v5.3.0) derived regions (with gray matter of posterior cerebellum as the reference region) of entorhinal, middle temporal, inferior temporal, fusiform, parahippocampal, hippocampus, amygdala. 1000 stratified bootstrap replicates were run to obtain A 95% confidence interval on the cut-points. All analyses were performed in R (Version 4.2.2), and ROC analyses were conducted using the "cutpointr" package.

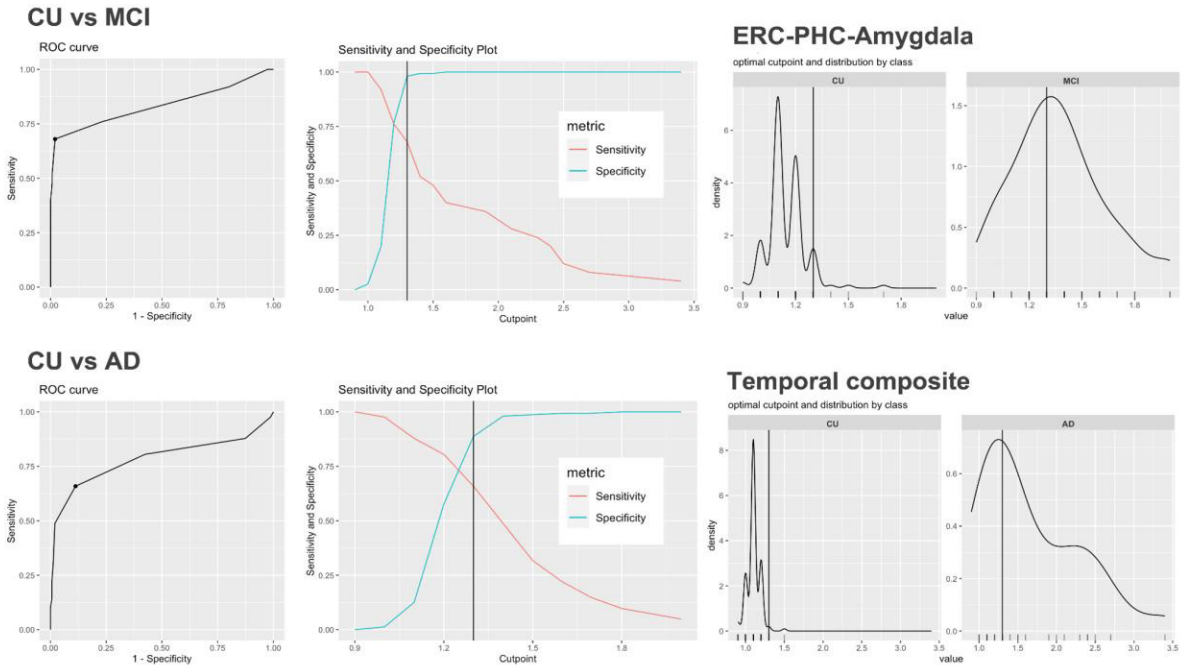

Keywords: biomarkers, Alzheimer's, tau, PET

91 Plasma ADRD biomarkers predict longitudinal declines in intra-network functional brain connectivity

Heather Dark[1], Andrea Shafer[1], Jenifer Cordon[1], Yang An[1], Alexandria Lewis[2], Abhay Moghekar[2], Bennett Landman[3,4], Susan Resnick[1], Keenan Walker[1]

[1]*Laboratory of Behavioral Neuroscience, National Institute on Aging, Intramural Research Program, Baltimore, MD, United States*
[2]*Department of Neurology, Johns Hopkins University School of Medicine, Baltimore, MD, United States*
[3]*Department of Electrical and Computer Engineering, Vanderbilt University, Nashville, TN, United States*
[4]*Department of Computer Science, Vanderbilt University, Nashville, TN, United States*

Background: Alzheimer's disease (AD) is neuropathologically defined by cortical amyloid-b (Ab) and tau which may contribute to alterations in large scale brain networks. Few studies have examined whether AD and neurodegenerative disease biomarkers measured in plasma predict changes in resting-state functional connectivity (rsFC). We examined whether plasma $A\beta_{42/40}$, phosphorylated tau (pTau-181), glial fibrillary acidic protein (GFAP), and neurofilament light chain (NfL) are related to changes in rsFC in cognitively unimpaired participants from the Baltimore Longitudinal Study of Aging.

Methods: Plasma biomarkers were measured with Quanterix SIMOA assays. Baseline was defined as the earliest visit with 3T resting-state fMRI scan and concurrent plasma biomarker measurement. Using a predefined cortical parcellation mask, intra-network connectivity from seven functional networks was extracted for each participant. Amyloid status (positive/negative) was defined using plasma $A\beta_{42/40}$, with the cutpoint determined based on optimal prediction of amyloid (PiB)-PET-positivity in a participant subset (n=212) (**Figure 1**). Linear mixed effects models adjusted for age, sex, race, education, gray matter volume, and time with covariate interactions were used to determine whether plasma biomarkers predicted changes in rsFC, and whether the magnitude of the biomarker-related rsFC changes differed by $A\beta_{42/40}$ status.

Results: Analyses (mean age±SD=65.57±16.14) included 494 participants (1171 visits; mean visits=2.37). Higher $A\beta_{42/40}$ and GFAP were associated with faster declines in rsFC within several networks (*P*-range=0.005-.04). Overall, plasma biomarker-rsFC associations differed by amyloid status. Among amyloid-positive participants, lower levels of $A\beta_{42/40}$ (*P*=0.03), and higher levels of GFAP, and NfL (**Figure 2**) were associated with faster declines in rsFC in the visual, dorsal and ventral attention, limbic, and frontoparietal networks (*P* range=<0.001-0.02). There were no statistically significant associations between plasma biomarkers and rsFC change among amyloid-negative participants.

Discussion: Those with AD pathological changes may be more susceptible to intra-network functional brain changes in the context of increased amyloidosis, astrogliosis, and axonal degeneration.

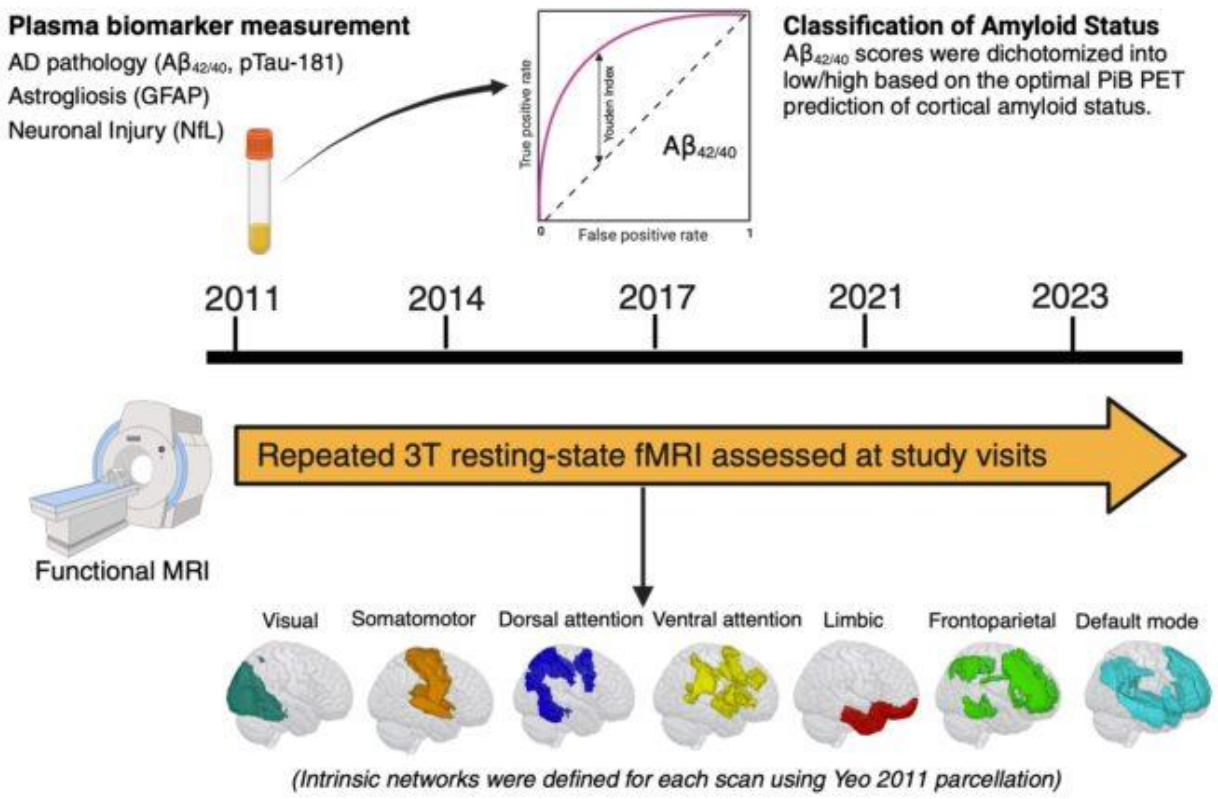

Figure 1. Study design

BLSA 3T resting-state functional (fMRI) scans were initiated in 2011. Baseline visits were considered the first visit for which participants had concurrent plasma biomarker measurement and 3T fMRI. From the baseline biomarker measurement, amyloid status (low versus high) was defined using an ROC analysis of $A\beta_{42/40}$ for optimal prediction of amyloid (PiB)-PET-positivity in BLSA participants (N=212). Finally, using a predefined cortical parcellation, seven intrinsic functional networks were derived for each resting-state fMRI scan. *Abbreviations*: Aβ: amyloid-β; fMRI: functional magnetic resonance imaginng; GFAP: glial fibrillary acidic protein; NfL: neurofilament light chain; pTau-181: tau phosphorylated at threonine-181. Figure created with BioRender.com.

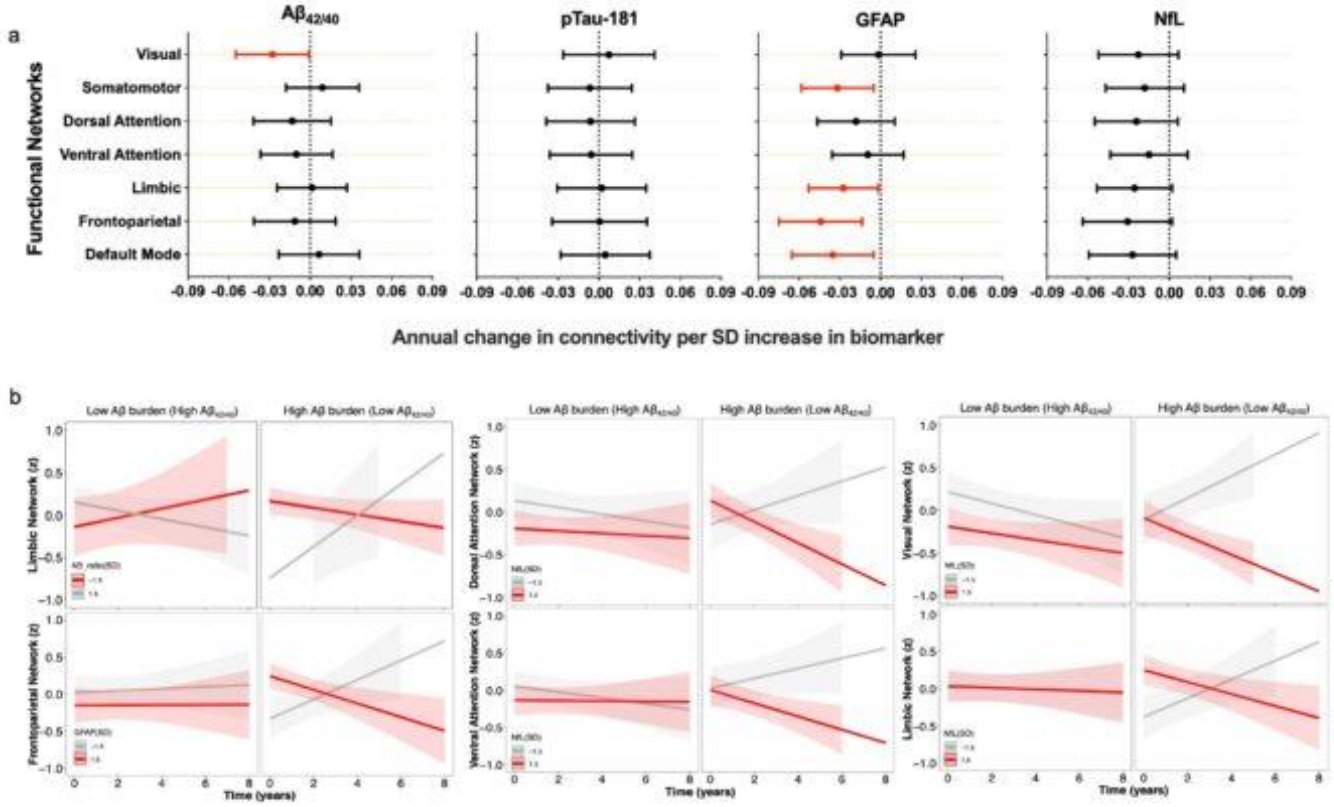

Figure 2. Relationship between baseline plasma biomarkers and longitudinal changes in resting-state functional connectivity

a. Results are derived from the linear mixed effects models (adjusted for age, sex, race, education, gray matter volume, and time with covariate interactions) that examined the relationship between baseline plasma biomarkers and changes in brain connectivity per functional network (*Plasma biomarker* × time). The x axis shows the difference in annual change in functional connectivity (β estimates) per standard deviation (SD) increase in baseline biomarker. Red bars reflect significant relationships between baseline biomarkers and change in brain connectivity, black bars reflect nonsignificant associations. **b.** Results are derived from adjusted linear mixed effects models that examined amyloid status (positive/negative) as a moderator of the association between baseline plasma biomarker levels and change in functional connectivity (*Plasma biomarker* × time × $A\beta_{42/40}$ status). For each figure, lines represent marginal effects from the following terms: $A\beta_{42/40}$ × time × $A\beta_{42/40}$ status; GFAP × time × $A\beta_{42/40}$ status; and NfL × time × $A\beta_{42/40}$ status. Red lines reflect high plasma biomarker level (+1.5 SD above the mean) and gray lines reflect low plasma biomarker level (-1.5 SD below the mean), except for the figure examining the $A\beta_{42/40}$ × time × $A\beta_{42/40}$ status interaction where red lines reflect -1.5 SD below the mean and gray lines reflect +1.5 SD above the mean.

Keywords: functional connectivity; plasma biomarkers; AB42/40 status

92 The role of frontoparietal control network and default mode network functional connectivity in cognitive resilience in preclinical Alzheimer's disease

Rory Boyle[1], Zahra Shirzadi[1], Gillian Coughlan[1], Mabel Seto[2], Michael Properzi[1], Hannah Klinger[1], Ziwen Yuan[1], Catherine Scanlon[1], Roos Jutten[1], Kathryn Papp[1,2], Rebecca Amariglio[1,2], Dorene Rentz[1,2], Jasmeer Chhatwal[1,2], Rachel Buckley[1,2], Reisa Sperling[1,2], Aaron Schultz[1]

[1]*Massachusetts General Hospital, Harvard Medical School, Boston, MA, United States*
[2]*Brigham and Women's Hospital, Harvard Medical School, Boston, MA, United States*

Background: Resting-state functional connectivity of the default mode (DMN) and frontoparietal control networks (FPCN) may support cognitive resilience (CR) to Alzheimer's disease (AD)-related pathology. The role of both networks in CR in the earliest stages of AD, prior to the onset of cognitive impairment, is unclear. We investigated whether these networks are associated with CR to AD biomarkers of β-amyloid (Aβ) and tau in cognitively unimpaired adults from the pre-randomization baseline dataset of the Anti-Amyloid Treatment in Asymptomatic Alzheimer's Disease (A4) study and its natural history observation arm, the Longitudinal Evaluation of Amyloid Risk and Neurodegeneration (LEARN) study.

Methods: In a cross-sectional dataset (n=1,641, mean age=71.57 years, 60% women; tau-PET subset n=420, mean age=71.87 years, 57% women, Table1), we examined independent effects of functional connectivity on cognition (Preclinical Alzheimer's Cognitive Composite) and moderation effects of connectivity on the relationship between AD pathology (global cortical Aβ[PiB]-PET, inferior temporal and entorhinal tau[FTP]-PET composite) and cognition, adjusting for covariates (age, sex, education, head motion, and scanner). Connectivity estimates of the DMN and FPCN were obtained using template-based rotation. Separate left and right-FPCN estimates allowed us to examine hemisphere specific effects.

Table 1. Descriptive statistics for A4 and LEARN cohorts.

	Full dataset				Tau-PET subset			
	Overall n = 1,641[1]	A4 n = 1,148[1]	LEARN n = 493[1]	p-value[2]	Overall n = 420[1]	A4 n = 365[1]	LEARN n = 55[1]	p-value[2]
Age	71.57 (4.74)	72.02 (4.83)	70.54 (4.36)	<0.001	71.87 (4.87)	72.20 (4.87)	69.65 (4.29)	<0.001
Gender				0.3				0.9
Male	661 (40%)	471 (41%)	190 (39%)		179 (43%)	156 (43%)	23 (42%)	
Female	980 (60%)	677 (59%)	303 (61%)		241 (57%)	209 (57%)	32 (58%)	
Education	16.61 (2.74)	16.57 (2.81)	16.70 (2.59)	0.3	16.20 (2.75)	16.14 (2.74)	16.64 (2.76)	0.3
*APOE*ε4 status				<0.001				<0.001
Non-ε4 carrier	848 (52%)	470 (41%)	378 (77%)		197 (47%)	156 (43%)	41 (75%)	
ε4 carrier	782 (48%)	668 (59%)	114 (23%)		219 (53%)	205 (57%)	14 (25%)	
Global cortical Aβ SUVr	1.23 (0.22)	1.33 (0.18)	0.99 (0.07)	<0.001	1.28 (0.20)	1.32 (0.18)	1.00 (0.06)	<0.001
Tau composite SUVr	1.21 (0.14)	1.22 (0.14)	1.12 (0.06)	<0.001	1.21 (0.14)	1.22 (0.14)	1.12 (0.06)	<0.001
Left FPCN FC	0.47 (0.07)	0.46 (0.07)	0.48 (0.07)	0.006	0.47 (0.07)	0.47 (0.07)	0.49 (0.06)	0.033
Right FPCN FC	0.49 (0.07)	0.49 (0.07)	0.50 (0.07)	0.002	0.50 (0.07)	0.49 (0.07)	0.51 (0.06)	0.044
DMN FC	0.59 (0.07)	0.58 (0.07)	0.59 (0.07)	0.4	0.59 (0.07)	0.59 (0.07)	0.61 (0.06)	0.087
PACC	-0.21 (2.62)	-0.41 (2.67)	0.24 (2.43)	<0.001	-0.45 (2.76)	-0.66 (2.73)	0.92 (2.60)	<0.001

[1] Mean (SD); n (%)
[2] Wilcoxon rank sum test; Pearson's Chi-squared test
Note: Global cortical Aβ SUVr = Mean standardized uptake value ratio across frontal, parietal, and temporal cortices; Tau composite SUVr = Mean standardized uptake value ratio across entorhinal and inferior temporal cortices. DMN FC = Default mode network functional connectivity; Left FPCN FC = Left frontoparietal control network functional connectivity; Right FPCN FC = Right frontoparietal control network functional connectivity.

Results: Functional connectivity of each network was positively associated with cognitive performance, independent of covariates and Aβ. Only left FPCN functional connectivity remained positively associated with cognition, independent of covariates, Aβ and tau in the tau-PET subset (Fig.1). We found significant three-way interactions between Aβ, tau, and connectivity in each network on cognition. These interactions showed a stronger negative association between tau and cognition at higher levels of Aβ in individuals with stronger connectivity (Fig.2).

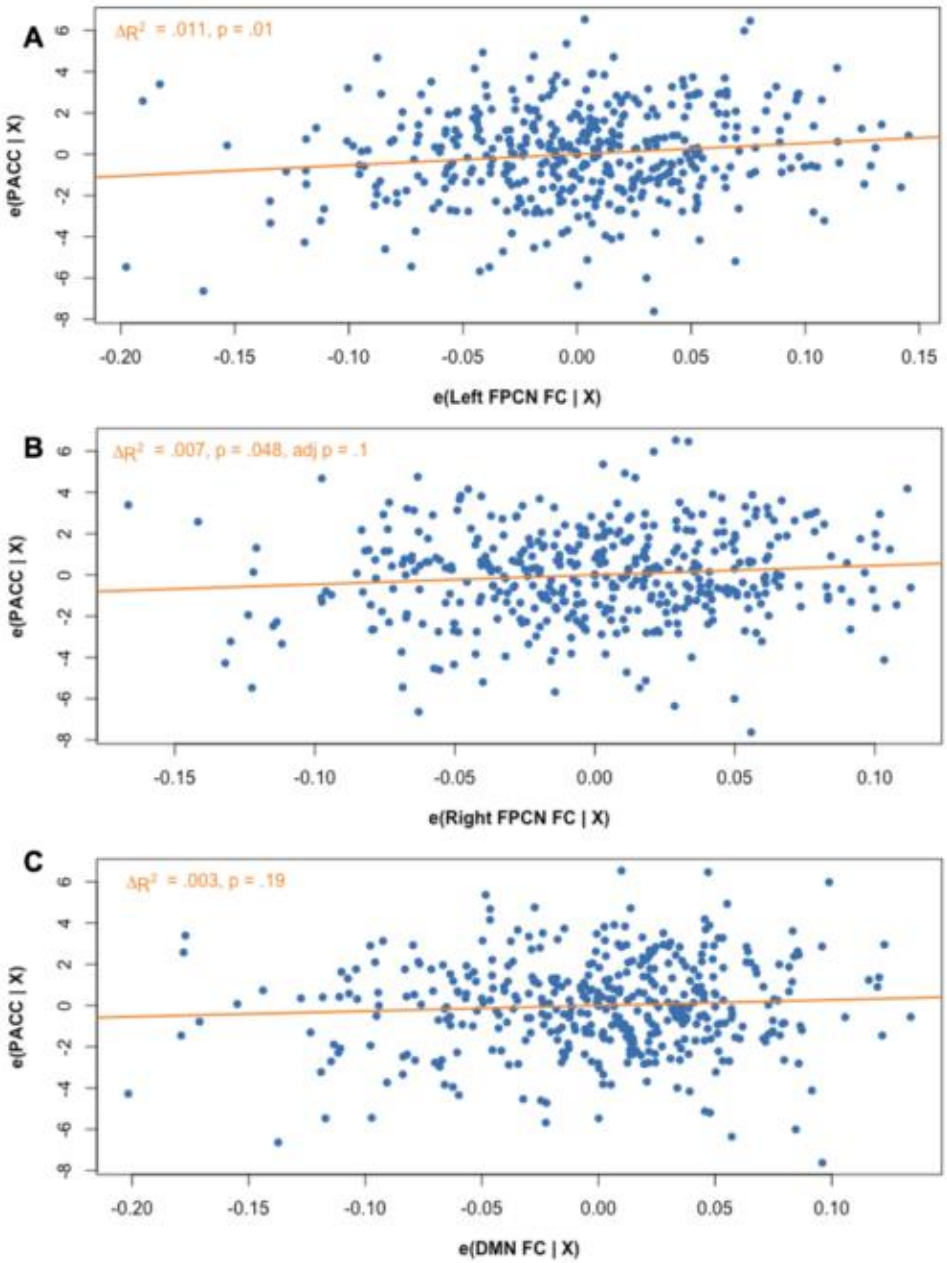

Figure 1. Added variable plots showing independent associations between functional connectivity of the A) Left FPCN, B) Right FPCN, and C) DMN and PACC, adjusting for covariates including age, gender, education, mean FWD, scanner, Aβ and tau (defined by X on the y-axis) in the tau-PET subsample.

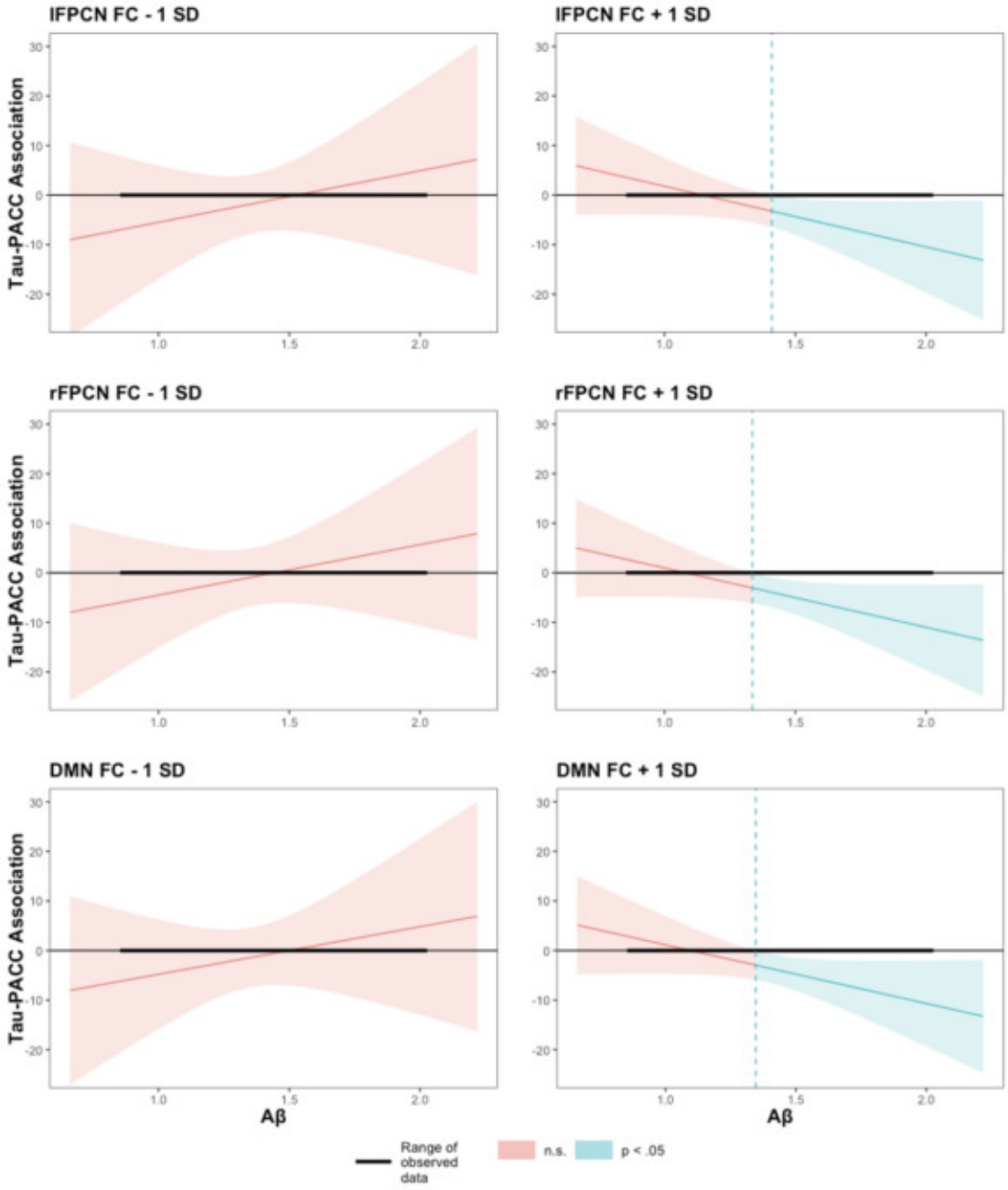

Figure 2. Johnson-Neyman plots of the tau x Aβ x FC interaction effect on PACC showing values of Aβ where the association between tau and PACC is significant at the lower and higher levels of functional connectivity.

Conclusion: Our results show that the reported CR effect of left-FPCN functional connectivity against AD pathology is evident in cognitively unimpaired individuals. Our results further suggest that this protective effect is attenuated at higher levels of AD pathology.

Keywords: Resilience, Connectivity, Amyloid, Tau, PET

93 Disrupted sleep and 24-hour rhythms are associated with 18F-PI-26260 tau PET in aging and neurodegenerative disease

Joseph Winer[1], America Romero[1], Hillary Vossler[1], Christina Young[1], Viktorija Smith[1], David Anders[2], Aimara Pacheco Morales[2], Guido Davidzon[2], Victor Henderson[1], Kathleen Poston[1], Jamie Zeitzer[3,4], Elizabeth Mormino[1]

[1]*Department of Neurology and Neurological Sciences, Stanford University, Stanford, CA, United States*
[2]*Department of Radiology, Stanford University, Stanford, CA, United States*
[3]*Department of Psychiatry and Behavioral Sciences, Stanford, CA, United States*
[4]*Sierra-Pacific Mental Illness Research, Education, and Clinical Center (MIRECC), Veterans Affairs Palo Alto Health Care System, Palo Alto, CA, United States*

Background: Disrupted sleep and fragmentation of sleep-wake rhythms are common in aging as well as neurodegenerative disease. Worsening sleep is associated with clinical decline, but the extent to which neuropathology may contribute to sleep impairment has not yet been examined across the spectrum of neurodegenerative disease.

Methods: 85 participants from the Stanford Alzheimer's Disease Center (ADRC) and the Stanford Aging and Memory Study (SAMS) were recruited for 14 days of at-home actigraphy (wrist-worn accelerometry) and ^{18}F-PI-2620 tau PET imaging. The cohort included cognitively normal older adults (healthy controls, HC), participants with Alzheimer's disease (AD), and participants with Lewy body disease (LBD). Actigraphy analyses focused on sleep efficiency and 24-hour activity fragmentation (intradaily variability). Tau burden was quantified as mean bilateral ^{18}F-PI-2620 SUVR within entorhinal cortex and inferior temporal cortex. Substantia nigra SUVR, reflecting neuromelanin binding, was used as a marker of nigral degeneration.

Results: In HC and participants with AD, greater entorhinal and inferior temporal ^{18}F-PI-2620 SUVR were associated with worse sleep efficiency and higher fragmentation of 24-hour activity (**Figure 1**). These associations were not present in participants with LBD, who had low ^{18}F-PI-2620 SUVR binding throughout cortex despite impaired sleep. However, across the full cohort, reduced substantia nigra ^{18}F-PI-2620 SUVR was associated with worse sleep efficiency (**Figure 2**). This association remained when adjusting for entorhinal SUVR.

Conclusions: These preliminary results confirm an association between tau burden and sleep disruption, extending this relationship to cognitively impaired individuals with AD. The novel association between ^{18}F-PI-2620-indexed nigral degeneration and sleep efficiency across disease etiologies is suggestive of mixed pathological contributions to sleep dysfunction in neurodegenerative disease.

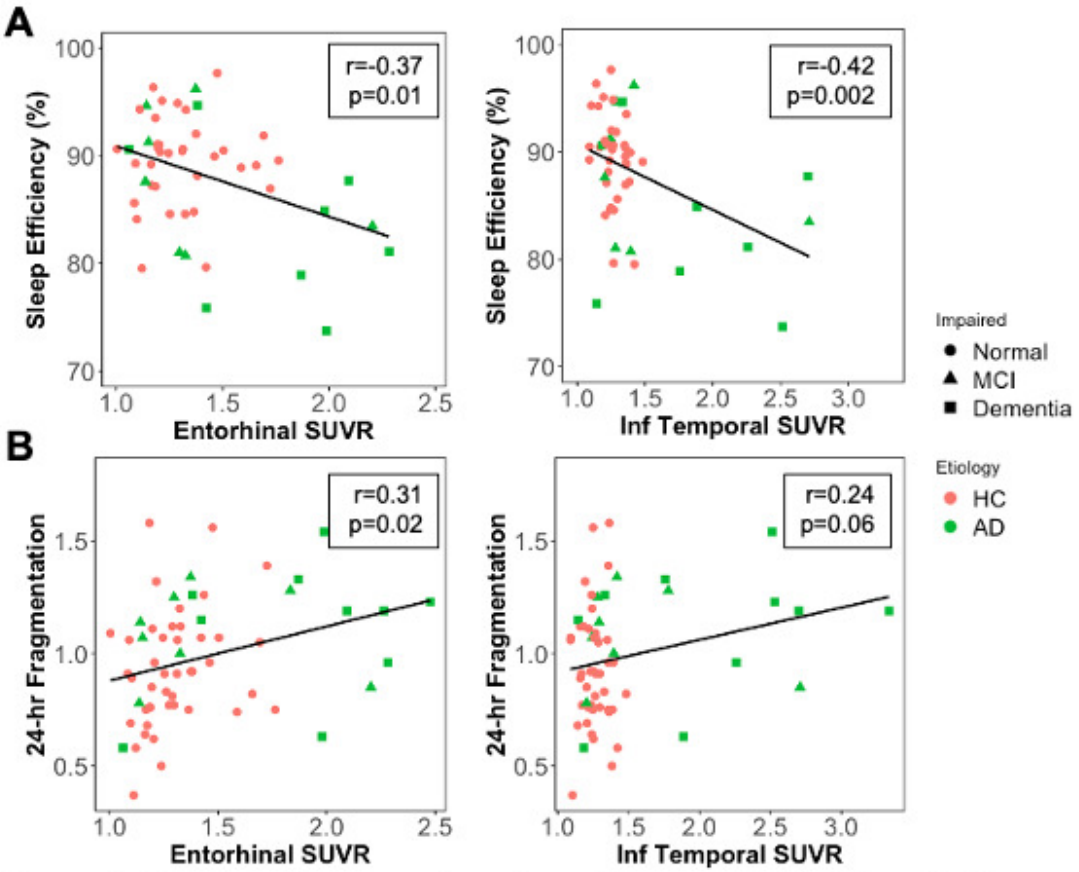

Figure 1. **A**) In healthy controls and participants with Alzheimer's disease, greater entorhinal and inferior temporal ^{18}F-PI-2620 SUVR are associated with worse sleep efficiency and **B**) greater fragmentation of 24-hour activity.

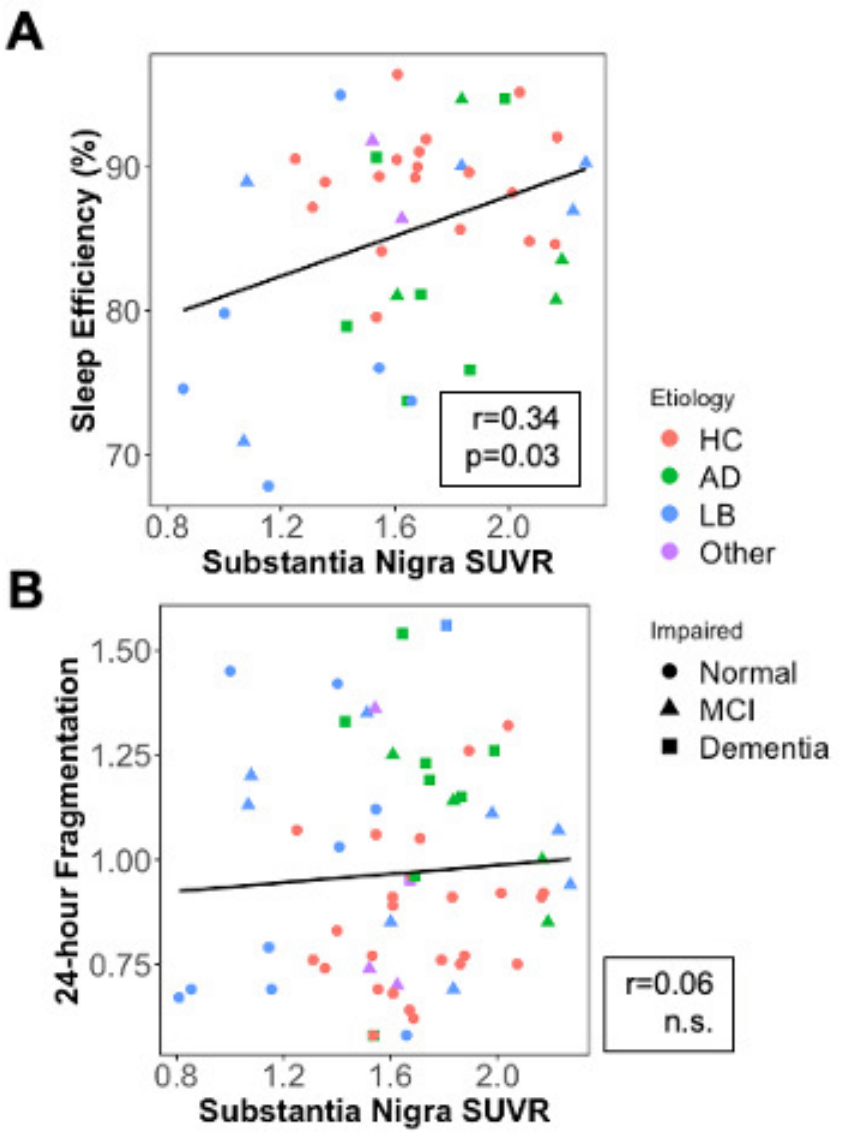

Figure 2. A) Reduced substantia nigra ^{18}F-PI-2620 SUVR is associated with worse sleep efficiency across all individuals. **B**) No association between substantia nigra SUVR and 24-hour fragmentation.

Keywords: sleep, aging, alzheimer's disease, lewy body disease, tau pet

94 Cortical and substantia nigra 18F-PI-2620 tau PET are associated with cognitive and motor impairment in Lewy body disease

Joseph Winer[1], Hillary Vossler[1], Christina Young[1], America Romero[1], Viktorija Smith[1], Marian Shahid[1], Carla Abdelnour[1], Edward Wilson[1], David Anders[2], Aimara Pacheco Morales[2], Guido Davidzon[2], Elizabeth Mormino[1], Kathleen Poston[1]

[1]*Department of Neurology and Neurological Sciences, Stanford University, Stanford, CA, United States*
[2]*Department of Radiology, Stanford University, Stanford, CA, United States*

Background: Co-pathology is frequent in neurodegenerative disease. Tau PET imaging may serve a dual role in Lewy body disease (LBD) by measuring tau aggregation as well as assessing dopaminergic loss attributed to binding to neuromelanin within substantia nigra (SN). We sought to characterize ^{18}F-PI-2620, a next generation PET tracer, in patients with LBD.

Method: 136 participants from the Stanford Alzheimer's Disease Center (ADRC) and the Stanford Aging and Memory Study (SAMS) were recruited for ^{18}F-PI-2620 PET scans. We compared ^{18}F-PI-2620 uptake within entorhinal cortex, inferior temporal cortex, precuneus, and lingual gyrus, as well as SN, across participants with Parkinson's disease (n=29), dementia with Lewy bodies (n=12), and Alzheimer's disease (n=25), in addition to cognitively normal older adults (n=70). Mean bilateral signal was extracted from cortical regions of interest in ^{18}F-PI-2620 SUVRs (inferior cerebellar gray reference) normalized to template space. Amyloid status was determined either by ^{18}F-florbetaben PET, CSF, or plasma (Lumipulse $A\beta_{42/40}$ assay). A subset of participants received cognitive testing and/or the MDS-UPDRS-III motor exam (off-medication).

Result: ^{18}F-PI-2620 uptake was low overall in LBD, although inferior temporal SUVR was significantly elevated in amyloid-positive relative to amyloid-negative LBD participants (**Figure 1**). Temporal ^{18}F-PI-2620 signal was not associated with memory in LBD, but parietooccipital signal was associated with worse performance in tests of executive function and attention (**Figure 2**). SN SUVR was significantly reduced in Parkinson's disease participants, and lower SN SUVR was associated with worse MDS-UPDRS-III score (**Figure 3**).

Conclusions: These findings suggest that cortical tau is low in LBD, but associated with cognitive function in LBD-relevant domains. Neuromelanin ^{18}F-PI-2620 signal within SN carries information about motor impairment. Cortical tau and SN binding represent two unique signals in the same PET image that may be informative in the context of LBD.

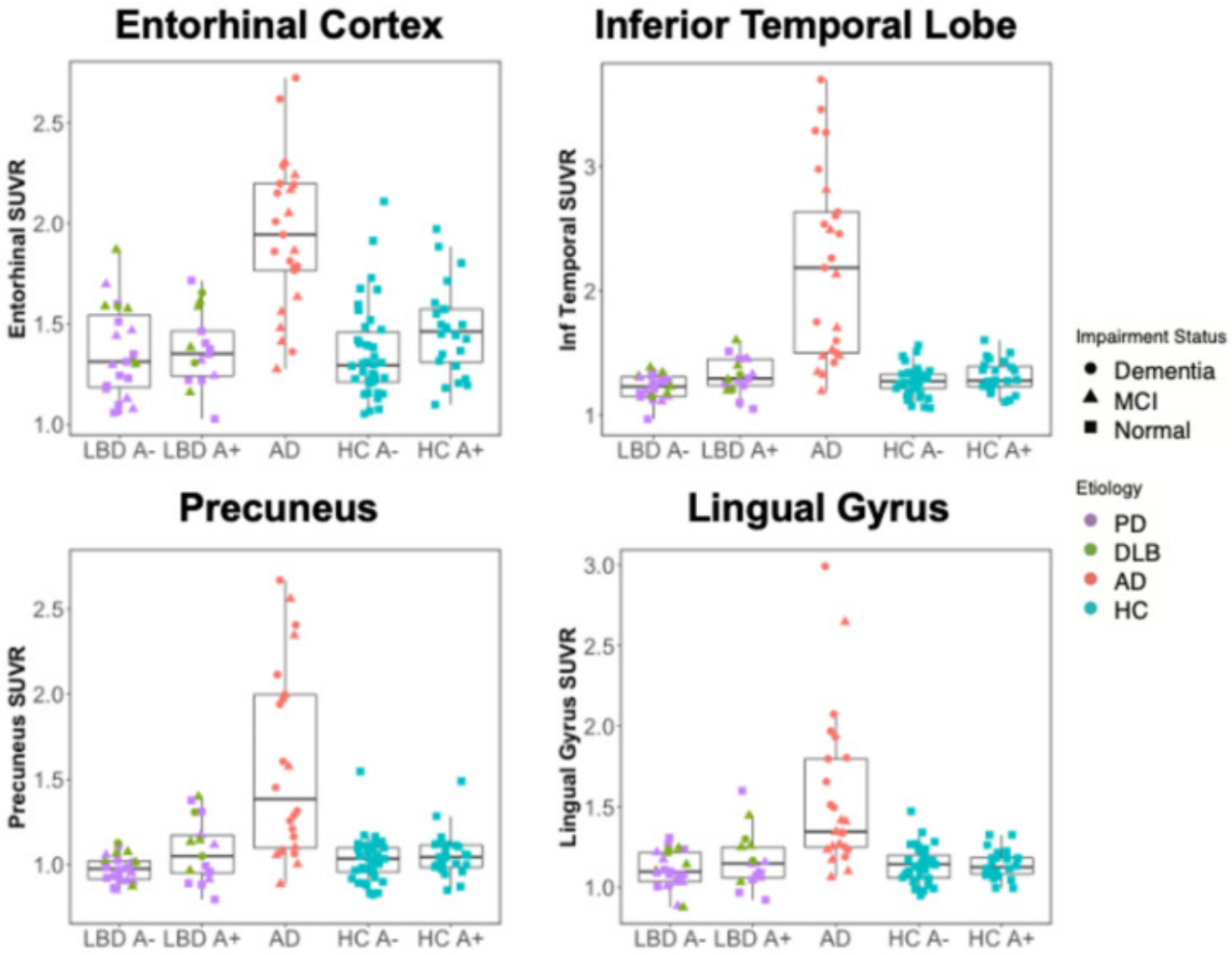

Figure 1 - Mean ^{18}F-PI-2620 SUVR within four regions of interest across Lewy body disease (Parkinson's disease & dementia with Lewy bodies), Alzheimer's disease, and healthy control participants split by amyloid status.

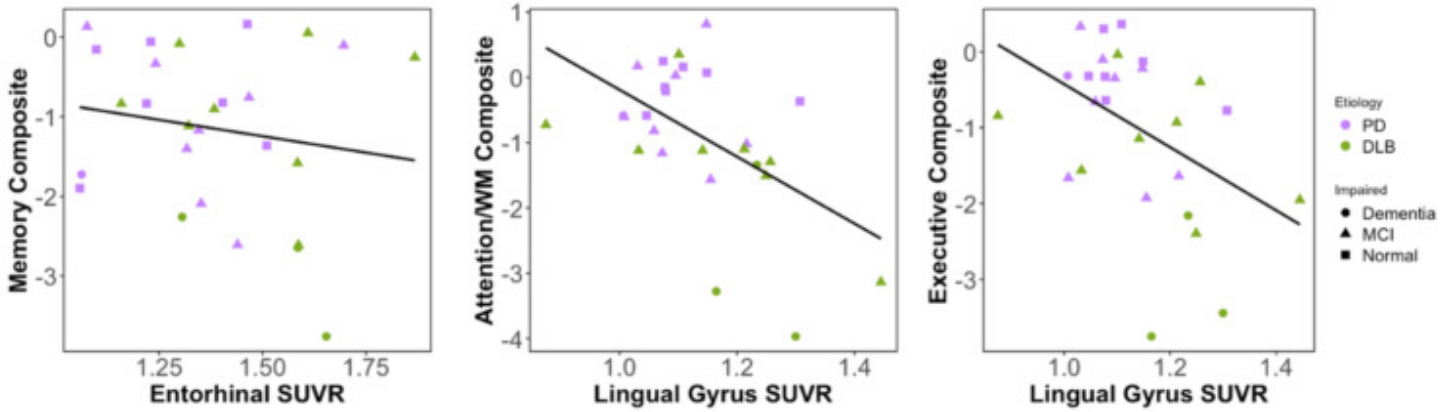

Figure 2 – In patients with Lewy body disease, memory performance is not associated with 18F-PI-2620 in temporal regions. Greater uptake within lingual gyrus is associated with worse performance in attention and working memory as well as executive function.

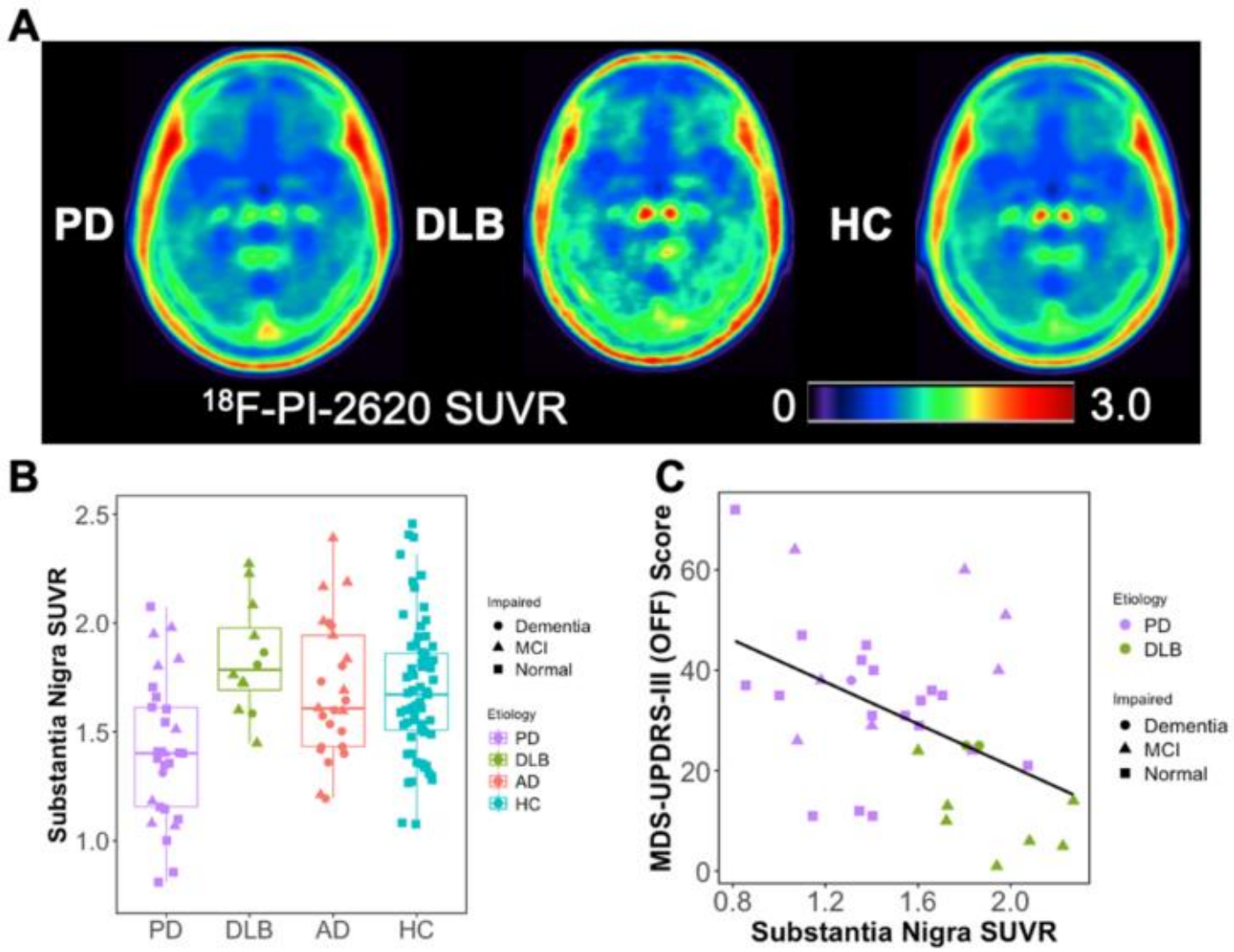

Figure 3 – (A) Mean SUVR images for Parkinson's disease, dementia with Lewy bodies, and healthy control groups. (B) Mean ^{18}F-PI-2620 SUVR within substantia nigra is lower in Parkinson's disease compared to all other groups. (C) Substantia nigra ^{18}F-PI-2620 SUVR is associated with worse motor impairment severity in patients with Lewy body disease.

Keywords: tau PET, lewy body disease, substantia nigra, alzheimer's disease, 18F-PI-2620

95 Predictability of amyloid-PET status with plasma phospho-Tau217 in adults with Down syndrome

Brecca Bettcher[1], Shorena Janelidze[9], Max McLachlan[1], Matthew Zammit[1], Andrew McVea[1], Alexandra H. DiFilippo[1], Tobey Betthauser[1], Charles Laymon[2], Dana Tudorascu[2], Annie Cohen[2], Arun Garimella[3], Julie Price[3], David Keator[4], Adam M. Brickman[5], Patrick Lao[5], William Klunk[2], Diana Rosas[3], Shahid Zaman[6], Sigan Hartley[1], Elizabeth Head[4], Mark Mapstone[4], Sharon Krinsky-McHale[7], Sterling Johnson[1], Florence Lai[3], Beau Ances[8], Benjamin Handen[2], Oskar Hansson[9], Bradley T. Christian[1], The Alzheimer Biomarkers Consortium – Down Syndrome[1,2,3,4,5,6,7,8,9]

[1]*University of Wisconsin-Madison School of Medicine and Public Health and Waisman Center, Madison, WI, United States*
[2]*University of Pittsburgh, Pittsburgh, PA, United States*
[3]*Massachusetts General Hospital, Harvard University, Boston, MA, United States*
[4]*University of California, Irvine, Irvine, CA, United States*
[5]*Columbia University Irving Medical Center, New York, NY, United States*
[6]*Cambridge University, Cambridge, United Kingdom*
[7]*New York State Institute for Basic Research in Developmental Disabilities, Staten Island, Staten Island, NY, United States*
[8]*Washington University, St. Louis, MO, United States*
[9]*Lund University, Lund, Sweden*

Background: Blood-based biomarkers able to detect Aβ neuropathology could serve as a cost-effective and noninvasive screening to include participants with Down syndrome (DS) in anti-amyloid clinical trials. Previous work (Janelidze, 2022) reports a strong correlation between plasma and PET biomarkers using pTau217 and [^{11}C]PiB. This work examines associations between plasma pTau217 accumulation and PET amyloid positivity, determined with [^{11}C]PiB and [^{18}F]florbetapir.

Methods: Participants were recruited from the Alzheimer Biomarkers Consortium – Down Syndrome (ABC-DS) study. Amyloid positivity was detected with PET imaging using [^{11}C]PiB or [^{18}F]florbetapir and a threshold of 18 Centiloids (CL). Plasma pTau217 concentration was measured on a Mesoscale Discovery platform (Lilly Research Laboratories). A robust norms approach derived plasma biomarker abnormality level used as reference for ROC analysis. Youden's Index was optimized to assess ptau217 sensitivity to PET A+ individuals. The time offset between PET amyloid positivity (18 CL) and ptau217 sensitivity was based on amyloid chronicity trajectories (Zammit 2023).

Results: Amyloid positive participants showed elevated pTau217 levels compared to amyloid negative participants (A+: 0.84 pg/ml, A-: 0.44 pg/ml, $p < 0.05$). pTau217 demonstrated a lack of sensitivity to amyloid positive individuals near the PET A+ threshold and greater variability with increasing amyloid burden (Figure 1). A robust norms approach identified a pTau217 threshold of 0.78 pg/ml. With this threshold, ROC analysis determined an optimal cutoff of 48.5 CL (AUC = 0.88, sensitivity = 0.89, specificity = 0.87) corresponding to a duration of ~6 years of PET amyloid positivity.

Conclusion: pTau217 exhibits sufficient discriminative properties between PET A+ and A- participants after reaching elevated amyloid levels of 48.5 CL or ~6 years PET A+. This work suggests that Aβ neuropathology detected by PET precedes plasma pTau217. Further investigation of the sample with 50 CL and greater is necessary due to the high variability exhibited in this group.

Table 1

Participant demographics by radiotracer

	[^{18}F]florbetapir	[^{11}C]PiB
Participants (n)	89	140
Age (years)	50 (8.5)	39 (6.7)
Amyloid + (CL > 18)	77	44
pTau217 (pg/ml)	0.87	0.51

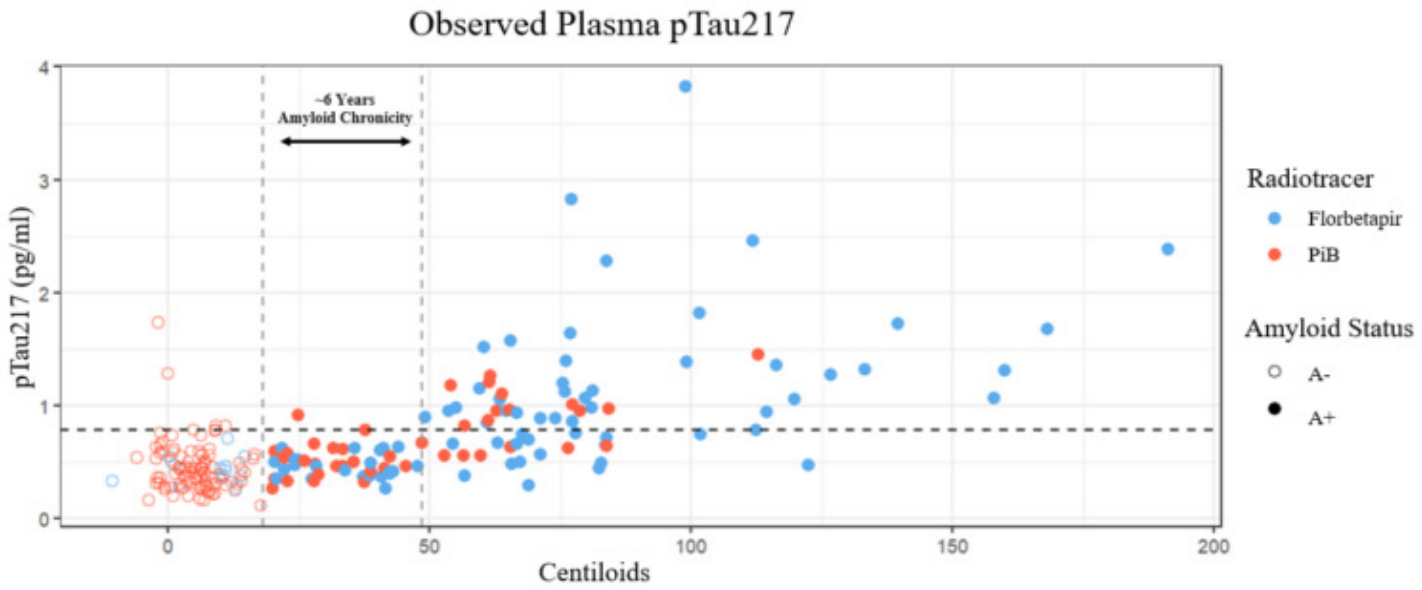

Figure 1: Plasma pTau217 plotted with respect to cortex CL value with one observation per participant. A robust norms approach identified a pTau217 threshold of 0.78 pg/ml. In this method, the 2.5th and 97.5th percentiles of amyloid negative individuals were computed. For observations in this range, the 97.5th percentile was again computed to derived biomarker threshold. Elevated pTau217 levels emerge around 48.5 CL, corresponding to an amyloid age of about 6 years.

Keywords: Amyloid, Plasma, PET

96 Locus coeruleus metabolism relates to Alzheimer's disease pathology in amyloid-positive symptomatic individuals

Elouise A Koops[1], Joyita Dutta[2], J Alex Becker[1], Maxime van Egroo[3], Bernard J Hanseeuw[1], Reisa A Sperling[4], Keith A Johnson[1,4], Heidi IL Jacobs[1,3]

[1]*Gordon Center for Medical Imaging, Department of Radiology, Massachusetts General Hospital, Harvard Medical School, Boston, MA, United States*
[2]*Department of Electrical and Computer Engineering, University of Massachusetts Amherst, Amherst, MA, United States*
[3]*Faculty of Health, Medicine and Life Sciences, School for Mental Health and Neuroscience, Alzheimer Center Limburg, Maatricht University, Maastricht, The Netherlands*
[4]*Department of Neurology, Brigham and Women's Hospital, Massachusetts General Hospital, Harvard Medical School, Boston, MA, United States*

Background: Higher cerebrospinal fluid noradrenergic metabolic turnover has been associated with higher levels of Alzheimer's disease pathology in cognitively impaired individuals. It remains unclear whether this is due to metabolic alterations in the locus coeruleus (LC), one of the first sites to accumulate tau, or dysfunction of adrenergic receptors in target regions of the LC. Here, we aimed to examine the relationship between LC metabolism measured with Positron Emission Tomography (PET) and beta-amyloid and tau pathology in individuals with cognitive impairment.

Methods: We investigated LC FDG-PET signal of 151 amyloid-positive, cognitively impaired participants from the ADNI-3 cohort (Table 1), using an MR joint-entropy-penalty algorithm to quantify PET signal within small brain regions. The LC was identified using our 7T MT-TFL template, registered to each T1. The FDG-PET signal was referenced to the pons, excluding the LC. Amyloid positivity was determined as a centiloid score 21, reflecting moderate neuritic plaques, on florbetaben and florbetapir PET scans. Multiple linear regressions investigated relationships between LC-FDG, global beta-amyloid and tau-burden (flortaucipir) in Braak stages, and cognition. Age and sex (and education) were included as covariates.

Results: Higher LC-FDG signal corresponded to higher amyloid burden (p=0.0112; Fig 1A), higher tau burden in Braak II (p=0.0096), III/IV (p=0.0023), and V/VI (p=0.0043) regions (Fig 1B), and worse cognition (p = 0.041) (Fig 2). Post-hoc assessments of the contributions of amyloid indicated a synergistic effect for Braak II (p=0.035) and at-trend level independence for higher Braak stages (III/IV: p=0.0515; V/VI: p=0.0643).

Conclusion: We observed that higher LC metabolism related to higher beta-amyloid and tau load in cortical regions implicated in Alzheimer's disease in individuals with cognitive impairment. In line with this, higher LC metabolism was associated with worse cognition. Future work will investigate these patterns in a cognitively healthy population and incorporate the accumulation and spread of tau.

Table 1. Characteristics of participants. Per diagnostic status, the mean and standard deviation are given for age, education level, MMSE score, amyloid burden, and LC metabolism. Percentages per biomarker group are depicted for Sex and CDR Sum of Boxes. Participants with a Tau-PET, Amyloid-PET, FDG-PET, and 3T-MRI scan obtained within 1 year were included. LC metabolism was extracted from FDG-PET scans with a 7T mask derived from a magnetization transfer-weighted turbo flash (MT-TFL) MRI sequence. Florbetaben and Florbetapir tracers were converted to centiloids to facilitate the integration of the results of these different tracers. For amyloid, the average amyloid-PET centiloid values were extracted from a composite mask of cortical regions comprising the frontal, parietal, temporal, and cingulate lobes. The sample consists of individuals with cognitive impairment (MCI or dementia). *Abbreviations: MMSE = Mini-Mental State Examination, LC = locus coeruleus, CDR Sum of Boxes = Clinical Dementia Rating Scale sum of boxes score, FDG-PET = [^{18}F]Fluordeoxyglucose Positron Emission Tomography, MRI = Magnetic Resonance Imaging.*

Characteristic	MCI, N = 114[1]	Dementia, N = 37[1]	p-value[2]
Age	72.58 (7.66)	73.80 (8.86)	0.4
Sex			0.4
Male	62 (54.39%)	24 (64.86%)	
Female	52 (45.61%)	13 (35.14%)	
Education (years)	16.38 (2.50)	15.95 (2.47)	0.4
MMSE	27.89 (1.82)	22.97 (2.62)	**<0.001**
Amyloid burden (CL)	90.27 (56.24)	130.19 (54.15)	**<0.001**
LC metabolism (SUVr)	0.82 (0.06)	0.84 (0.07)	0.12
CDR Sum of Boxes			**<0.001**
minor impairment	100 (94.34%)	7 (22.58%)	
very mild dementia	4 (3.77%)	4 (12.90%)	
mild dementia	2 (1.89%)	19 (61.29%)	
moderate dementia	0 (0.00%)	1 (3.23%)	
Unknown	8	6	

[1]Mean (SD); n (%)

[2]One-way ANOVA; Pearson's Chi-squared test; Kruskal-Wallis rank sum test

Figure 1. LC metabolism and AD pathology. An in-house developed LC mask primarily restricted to the rostral LC was used to extract the LC FDG-PET signal. The processing consisted of registering the FreeSurfer-processed T1 anatomical images to an MNI template, co-registering the T1 and the FDG-PET images, and MNI-based LC templates to T1-space. The FDG-PET images were referenced to the pontine signal minus the signal from the LC. The average signal from the LC was extracted from the MRI-PET joint entropy penalty deblurred FDG-PET images. (A) There was a significant association between LC metabolism and global cortical amyloid burden ($T = 2.57$, $p = 0.0112$), corrected for the effects of age and sex (n = 161). (B) In the individuals that were amyloid positive (n = 151), there was a positive association between LC metabolism and Tau-PET signal in Braak II (T = 2.63, p = 0.0096), Braak III/IV (T = 3.11, p = 0.0023) and Braak V/VI (T = 2.90, p = 0.0043) areas. Post-hoc assessment of the contributions of amyloid on this relationship showed an interaction with amyloid for the association between LC metabolism and Braak II Tau-PET signal ($T = 2.13$, $p = 0.035$) and at-trend level independence for the higher Braak stages (III/IV: $T = 1.96$, $p = 0.0515$; V/VI: $T = 1.87$, $p = 0.0643$). *Abbreviations: MNI = Montreal Neurological Institute, MCI = mild cognitive impairment, CL = Centiloids, SUVr = standardized uptake values referenced to the pons minus the LC, av1451 = [^{18}F]flortaucipir tracer.*

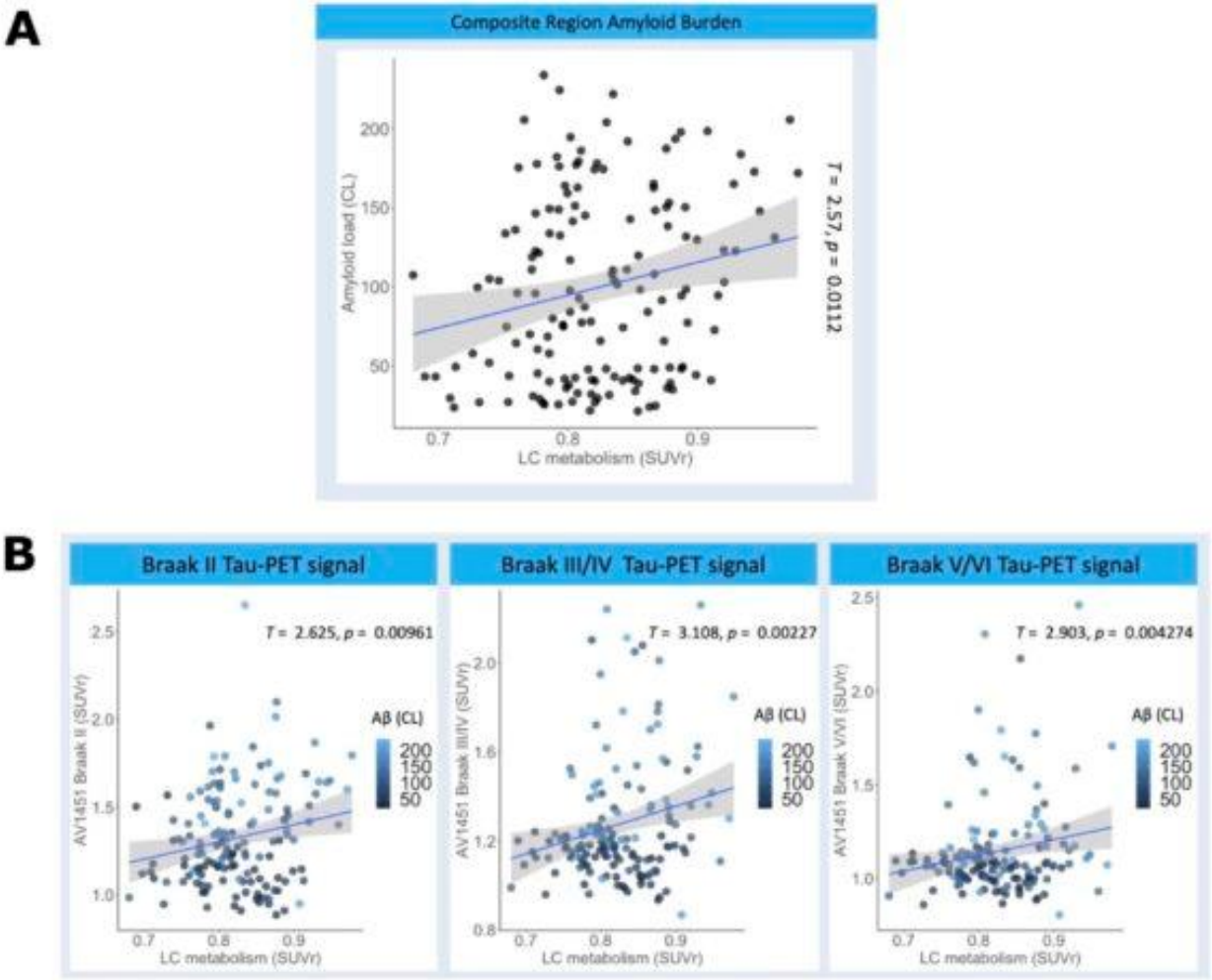

Figure 2. LC metabolism and cognition. In our sample of cognitively impaired individuals who are amyloid positive (n = 151), there was a significant association between LC metabolism and mPACC digits scores (T = -2.07, p = 0.041), corrected for the effects of age, sex, and education. Higher LC metabolism corresponded to worse cognition in amyloid-positive individuals with cognitive impairment. Post-hoc assessment of the contributions of amyloid on this relationship showed an interaction with amyloid for the association between LC metabolism and mPACC digit scores (T = -2.01, p = 0.046). The data points are shown colored for amyloid burden (in centiloids). *Abbreviations: mPACC = ADNI modified version of the Preclinical Alzheimer's Cognitive Composite.*

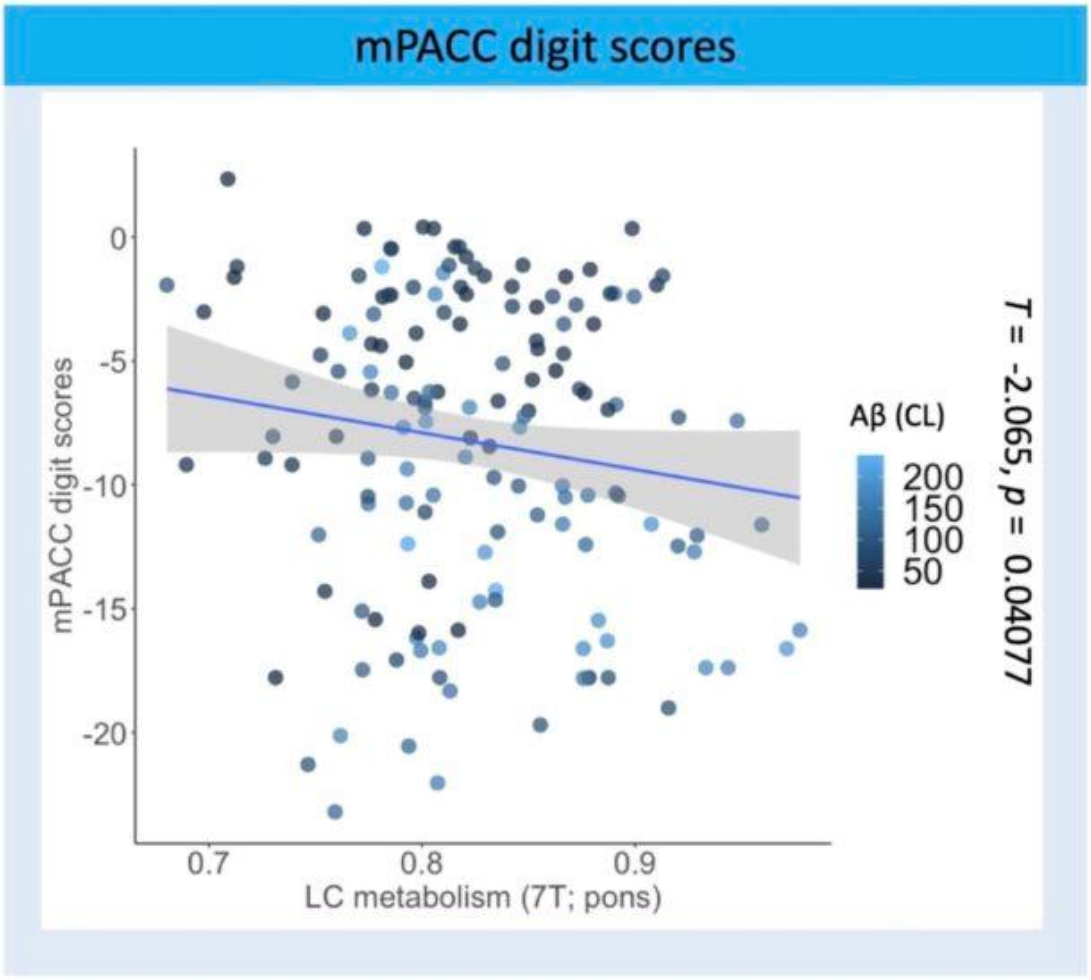

Keywords: locus coeruleus, amyloid, tau, PET, cognition

97 Correlating in vivo amyloid beta centiloid values with neuropathological burden: Insights from Down syndrome and Alzheimer's disease cohorts

Jr-Jiun Liou, Milos Ikonomovic, Benjamin Handen, Bradley Christian, Mark Mapstone, Elizabeth Head, Dana Tudorascu, Adam M Brickman, Julie Price, Charles Laymon, Diana Rosas, Shahid Zaman, Sigan Hartley, Florence Lai, Julia Kofler, Tamer Ibrahim, Victor L Villemagne, Ann Cohen

[1]*University of Pittsburgh, Pittsburgh, PA, United States*
[2]*University of Wisconsin-Madison, Madison, WI, United States*
[3]*Harvard University, Boston, MA, United States*
[4]*University of California, Irvine, Irvine, CA, United States*
[5]*Columbia University, New York, NY, United States*
[6]*University of Cambridge, Cambridge, United Kingdom*

Background: In Alzheimer's disease (AD), beta-amyloid deposition is associated with limbic-predominant age-related TDP-43 encephalopathy (LATE) pathology, but the association in Down syndrome (DS) has remained unexplored. People with DS are genetically predisposed to developing AD with beta-amyloid accumulating at earlier ages than late-onset AD, making them an ideal population with which to test this hypothesis. We examined if there was an association between beta-amyloid burden, as expressed in centiloid (CL) values, and postmortem AD and LATE neuropathology.

Methods: Six DS (4 demented + 1 MCI + 1 non-demented) and twelve AD (7 probable AD + 4 MCI + 1 normal) autopsy-confirmed cases were examined. In vivo 11C-Pittsburgh-compound-B (PiB) or 18F-florbetapir PET was obtained years before autopsy (mean interval 6.5±3.2 years). CL values were correlated with neuropathological findings (Thal phase, Braak stage, CERAD score, and LATE stage).

Results: Despite a significant age difference at the time of the PET scan between DS and AD groups (55.7±2.6 vs. 85.8±8.1 years, p<0.0001), there were no significant differences in beta-amyloid burden (82.4±46.8 vs. 58.0±52.1 CL, p=0.347). In the DS group, all DS individuals had CL>20, with 33% of cases displaying LATE+ and beta-amyloid burden significantly higher in LATE+ compared to LATE- cases (138.9 vs 54.2 CL, p=0.0062). In the AD group, no difference in CL was observed between LATE+ and LATE- cases (62.6 vs 51.6 CL, p=0.737); PiB+ cases (CL>20) exhibited significantly higher LATE stages than PiB- cases (1.500 vs. 0.250 stage, p=0.0323).

Discussion: We find correlations between beta-amyloid PET and postmortem AD neuropathologic change and that TDP-43 pathology is associated with high beta-amyloid burden in AD and DS irrespective of age. Future steps involve exploring other biomarkers, in vivo and ex vivo MRI alignment, as well as investigating brain atrophy and cortical thinning using ex vivo 7T MRI.

Keywords: Down syndrome, PiB, FBP, neuropathology, limbic-predominant age-related TDP-43 encephalopathy

98 Visualization of endogenously generated Dutch-type Abeta oligomers that dysregulate presynaptic neurotransmission in the absence of detectable inflammation

Sam Gandy[1], Emilie Castranio[1], Merina Varghese[1], Elentina Argyrousi[2], Kuldeep Tripathi[3], Charles Glabe[4], Efrat Levy[5], Minghui Wang[1], Bin Zhang[1], William Lubell[6], Brigitte Guerin[7], Shai Rahimipour[3], Dara Dickstein[8], Ottavio Arancio[2], Michelle Ehrlich[1]

[1]*Icahn School of Medicine, New York, NY, United States*
[2]*Vagelos College of Medicine at Columbia University, New York, NY, United States*
[3]*Bar Ilan University, Raman Gat, IL*
[4]*University of California, Irvine, CA, United States*
[5]*NYU & NKI, New York, NY, United States*
[6]*University of Montreal, Montreal, QC, Canada*
[7]*University of Sherbrooke, Sherbrooke, QC, Canada*
[8]*Uniformed Sciences University of the Health Sciences, Bethesda, MD, United States*

APPE693Q ("Dutch") transgenic mice develop aging-related learning deficits and accumulate endogenously generated nonfibrillar oligomeric Aβ (oAβ) and APP alpha-carboxy terminal fragments. The APPE693Q mutation disrupts amyloid fibril formation, and no plaques develop in these mice. In the current study, the aging-related accumulation of oAβ in APPE693Q mice was revealed by A11 immunohistochemistry and oligomer-specific azapeptide-FITC microscopy. The presynaptic termini of APPE693Q mice developed aging-related physiological abnormalities in posttetanic potentiation, synaptic fatigue, and synaptic vesicle replenishment. Using single-cell RNA sequencing, it was found that excitatory neurons exhibited the most altered transcriptomic profile, especially involving “protein translation” and “oxidative phosphorylation”. Microglial transcript analysis revealed no evidence of inflammation. The incomplete clinical response to fibrillar Aβ immunodepletion may be attributable, at least in part, to residual nonfibrillar oAβ that is undetectable by any currently available biofluid or neuroimaging biomarkers. The depletion and/or neutralization of nonfibrillar oAβ may be needed for complete elimination of Aβ toxicity. Dutch mice that accumulate nonfibrillar oAβ exclusively may be a useful experimental system for further characterization of the cyclicazaglycine peptide PET tracer Lys(64Cu/NOTA)1]-CP7 that shows robust PET signal from 44-day-old presymptomatic 5x FAD mice as reported by Habashi M, Vutla S, Tripathi K, *et al.* Early diagnosis and treatment of Alzheimer's disease by targeting toxic soluble Aβ oligomers. Proc Natl Acad Sci U S A. 2022 Dec 6;119(49):e2210766119. doi: 10.1073/pnas.2210766119. PMID: 36442093; PMCID: PMC9894226.

Keywords: Oligomer, amyloid, NOTA, cyclicazaglycine peptide PET tracer

99 [18F]PI-2620 tau-PET binding patterns in American football players with suspected Chronic Traumatic Encephalopathy

Jhony Mejia Perez[1], Sydney Mosaheb[2], Daniel Schonhaut[1], Ganna Blazhenets[3], Ann McKee[2], Thor D. Stein[2], Chad Farris[2], Jesse Mez[2], Andrew Stephens[4], Andre Mueller[4], Richard Keegan[4], Renaud La Joie[1], Gil D. Rabinovici[1,5], Michael L. Alosco[2]

[1]*Memory and Aging Center, Department of Neurology, University of California, San Francisco, San Francisco, CA, United States*
[2]*Boston University Chobanian & Avedisian School of Medicine, Boston, MA, United States*
[3]*Department of Nuclear Medicine, University of Freiburg Medical Center, Freiburg, Germany*
[4]*Life Molecular Imaging, Berlin, Germany*
[5]*Department of Radiology & Biomedical Imaging, University of California, San Francisco, San Francisco, CA, United States*

Background. Existing tau-PET tracers have yielded equivocal results in people with suspected CTE. We explored [^{18}F]PI-2620 as a putative *in vivo* biomarker of CTE pathology.

Methods. The sample included seven former American football players (ages 50-68) with 11+ years of football exposure who met Katz criteria for Traumatic Encephalopathy Syndrome due to Probable CTE (TES-CTE) at screening. β-amyloid status was determined in 6/7 participants via CSF p-Tau181/Aβ42 ratio (n=2) or [^{18}F]Florbetaben PET (n=4). All participants underwent [^{18}F]PI-2620 tau-PET imaging. PI-2620 data was averaged from 30-60min post-injection, co-registered to T1-MRIs, and referenced against inferior cerebellar cortex. SUVr images were visually interpreted by an expert blinded clinician. SUVr values were quantified in medial temporal lobe (MTL) and cortical regions-of-interest using Freesurfer7. Paired t-tests were performed between regions of interest to test if any region showed higher tau binding than the rest.

Results. The sample included males who played college (n=4), semi-professional (n=1) or professional tackle football (n=2). Three cases have been reviewed in diagnostic consensus (2 MCI, 1 dementia). One participant was β-amyloid PET positive (Table 1). Tau visual reads indicated elevated MTL PI-2620 binding in 2/7 participants (both amyloid negative, one MCI, one dementia), while remaining scans were visually negative (Figure 1). Region-of-interest analyses showed highest SUVr in the entorhinal cortex (mean=1.3, SD=0.1, FDR-corrected $P < 0.05$ in pairwise comparisons), while mean SUVr in remaining regions were 0.9-1.1 (Figure 2).

Conclusion. Elevated PI-2620 binding may occur in participants with suspected CTE in the MTL, especially the entorhinal cortex. Data collection is ongoing, including recruitment of additional cases and matched controls.

	Case 1	Case 2	Case 3	Case 4	Case 5	Case 6	Case 7
Demographics							
Age group	60-64	65-59	60-64	60-64	60-64	50-54	55-59
Racial identity	White	White	White	White	White	White	White
Education years	19	16	20	16	16	16	19
Athletics							
Total years of football	14	17	11	11	19	26	14
Diagnostic Characteristics							
Traumatic Encephalopathy Syndrome (TES)	No			Yes	Yes		
Level of CTE certainty	N/A			Possible	Probable		
Cognitive diagnosis	MCI			MCI	Dementia		
Montreal Cognitive Assessment (MoCA)	20/30	23/30	22/30	22/30	23/30	21/30	27/30
Cognitive Dementia Rating (CDR)	0.5			0.5	1.0		
Amyloid status							
Modality	CSF	PET		CSF	PET	PET	PET
Amyloid status for Alzheimer's Disease (AD)	Negative	Positive		Negative	Negative	Negative	Negative

Table 1. Sample characteristics of seven American football players with TES-CTE.
All participants met Katz criteria of Probable TES-CTE at screening. TES diagnoses of Table 1 are defined in consensus meetings integrating history and objective data from an in-person evaluation. Missing information is shaded in gray. Cases with missing diagnostic characteristics have not had a consensus meeting yet. Case 3 has a pending measurement of amyloid status.

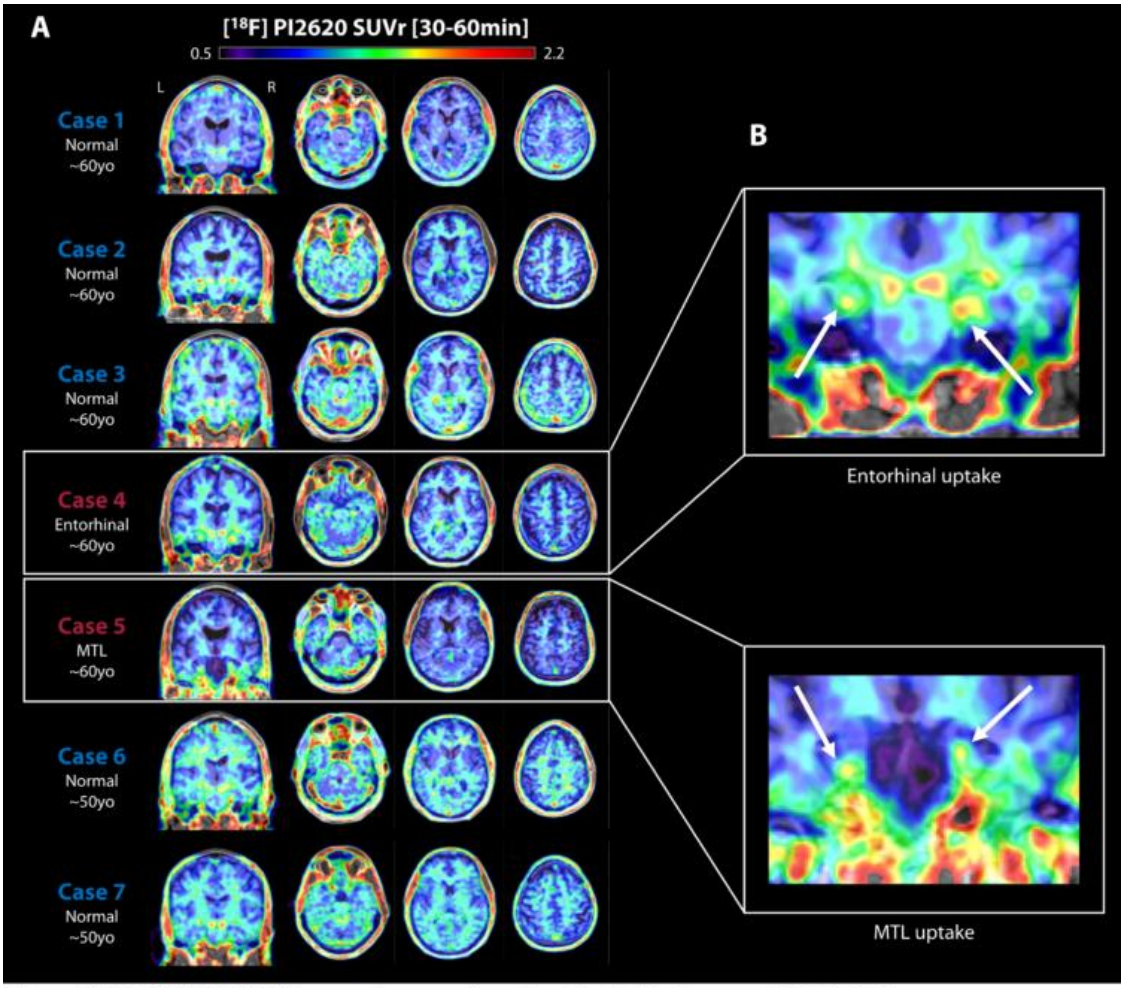

Figure 1. [18F]PI-2620 SUVr scans in seven American football players with TES-CTE.
A) Each row shows data from a single participant. Subjects are shown in order of study enrollment, and subject labels match those in Table 1. Image slices on the left show PI-2620 SUVr overlaid on native space MRIs in neurological orientation.
B) Close up views of the two participants with elevated MTL binding (white arrows).

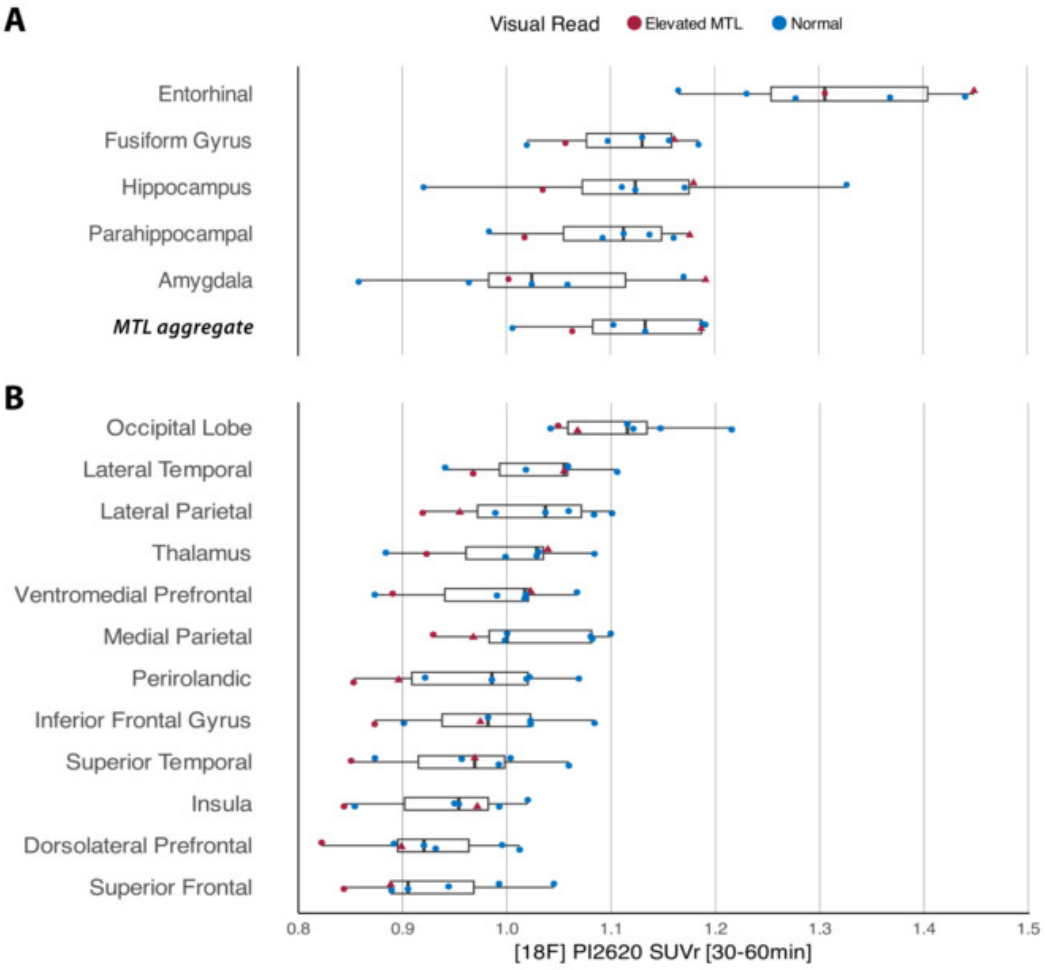

Figure 2. [^{18}F]PI-2620 SUVr in regions suggestive of CTE pathology.
Boxplots show mean SUVr values in medial temporal lobe (MTL; **panel A**) and FreeSurfer cortical (**panel B**) regions-of-interest across seven American football players (each point = one participant). Subjects visually read as having elevated MTL signal are shown in red (triangle = Case 4, circle = Case 5; see Figure 1), whereas those with no discernable signal aside from off-target binding are represented by blue circles. The ***MTL aggregate*** region in panel A combines data across the five MTL subregions shown, weighted by volume.

Keywords: Chronic Traumatic Encephalopathy, Traumatic Brain Injury, Tauopathies, PI-2620, Non-AD dementia

100 Regional amyloid-β burden in Lewy Body Disease

Hillary Vossler[1], Carla Abdelnour[1], Christina B. Young[1], Joseph Winer[1], Alena Smith[1], Viktorija Smith[1], Marian Shahid[1], Edward N. Wilson[1], Guido Davidzon[2], Elizabeth Mormino[1], Kathleen Poston[1]

[1]*Department of Neurology and Neurological Sciences, Stanford University School of Medicine, Stanford, CA, United States*
[2]*Department of Radiology, Stanford University School of Medicine, Stanford, CA, United States*

Background: Accurate assessment of *in vivo* amyloid-β burden in Lewy body disease (LBD) is crucial due to frequent occurrence of concomitant amyloidosis at autopsy. However, common regional definitions of amyloid deposition, including composite regions of interest defined by ADNI, exclude occipital lobe, which is a relevant region in LBD.

Objectives: (1) To determine whether LBD-spectrum participants (cognitively normal (CN), mild cognitive impairment (MCI), and dementia) have elevated amyloid-β burden in comparison to CN participants without a neurological disorder and Alzheimer's disease (AD) spectrum participants in frontal, cingulate, parietal, temporal, and occipital regions. (2) To examine changes in amyloid status (A+/A-) in LBD-spectrum participants when including and excluding occipital lobe.

Methods: We examined 256 participants (36-95 years old), who underwent Florbetaben PET (**Table 1**) and calculated SUVRs (whole cerebellum reference) for frontal, cingulate, parietal, temporal, and occipital regions. Amyloid-β burden in LBD-spectrum, CN, and AD spectrum participants were compared after controlling for age and sex **(Figure 2)**. We classified LBD-spectrum participants into A+ and A- based on Gaussian mixture modeling, including and excluding occipital lobe **(Figure 3)**.

Results: LBD-CU and LBD-MCI have comparable amyloid-β burden in all regions. LBD-CU and LBD-MCI have significantly lower amyloid-β burden compared to AD-MCI and AD-Dementia in all regions, except occipital lobe. LBD-Dementia has comparable amyloid-β burden to AD-MCI in all regions except occipital lobe, and significantly lower amyloid-β burden compared to AD-Dementia in occipital lobe. **(Figure 2; Table 2).** When examining amyloid status, including occipital region in the composite resulted in three LBD-spectrum participants (5%) switching from A- to A+ **(Figure 4).**

Conclusion: Our findings suggest that including occipital region might be relevant when assessing amyloid status in people across the LBD-spectrum with amyloid co-pathology. Accurate determination of amyloid-β burden in LBD holds prognostic significance, as concomitant amyloidosis has been associated with faster cognitive decline.

Table 1. Demographic characteristics of cohort.

	CN (N=150)	AD-MCI (N=24)	AD-Dementia (N=25)	LBD-CN (N=26)	LBD-MCI (N=23)	LBD-Dementia (N=8)	Overall (N=256)
Age							
Mean (SD)	71.8 (7.64)	72.9 (9.93)	70.6 (9.97)	70.0 (5.57)	72.3 (9.24)	69.0 (8.40)	71.6 (8.09)
Median [Min, Max]	72.0 [36.0, 92.0]	76.0 [45.0, 91.0]	74.0 [54.0, 89.0]	70.0 [60.0, 81.0]	73.0 [51.0, 95.0]	72.0 [57.0, 78.0]	72.0 [36.0, 95.0]
Sex							
Female	93 (62.0%)	7 (29.2%)	17 (68.0%)	12 (46.2%)	4 (17.4%)	3 (37.5%)	136 (53.1%)
Male	57 (38.0%)	17 (70.8%)	8 (32.0%)	14 (53.8%)	19 (82.6%)	5 (62.5%)	120 (46.9%)
Amyloid Status							
Negative	89 (59.3%)	6 (25.0%)	2 (8.0%)	18 (69.2%)	11 (47.8%)	2 (25.0%)	128 (50.0%)
Positive	61 (40.7%)	18 (75.0%)	23 (92.0%)	8 (30.8%)	12 (52.2%)	6 (75.0%)	128 (50.0%)
Centiloid (CL)							
Mean (SD)	28.5 (36.3)	72.0 (60.0)	105 (53.0)	19.4 (30.3)	31.5 (41.4)	64.6 (49.8)	40.5 (48.1)
Median [Min, Max]	15.0 [-10.0, 174]	85.5 [-12.0, 170]	102 [0, 216]	9.50 [-16.0, 129]	19.0 [-3.00, 164]	61.0 [4.00, 127]	17.5 [-16.0, 216]

Figure 2. Residual SUVRs by diagnosis. Significant differences between groups are shown with black lines and represent models accounting for age and sex.

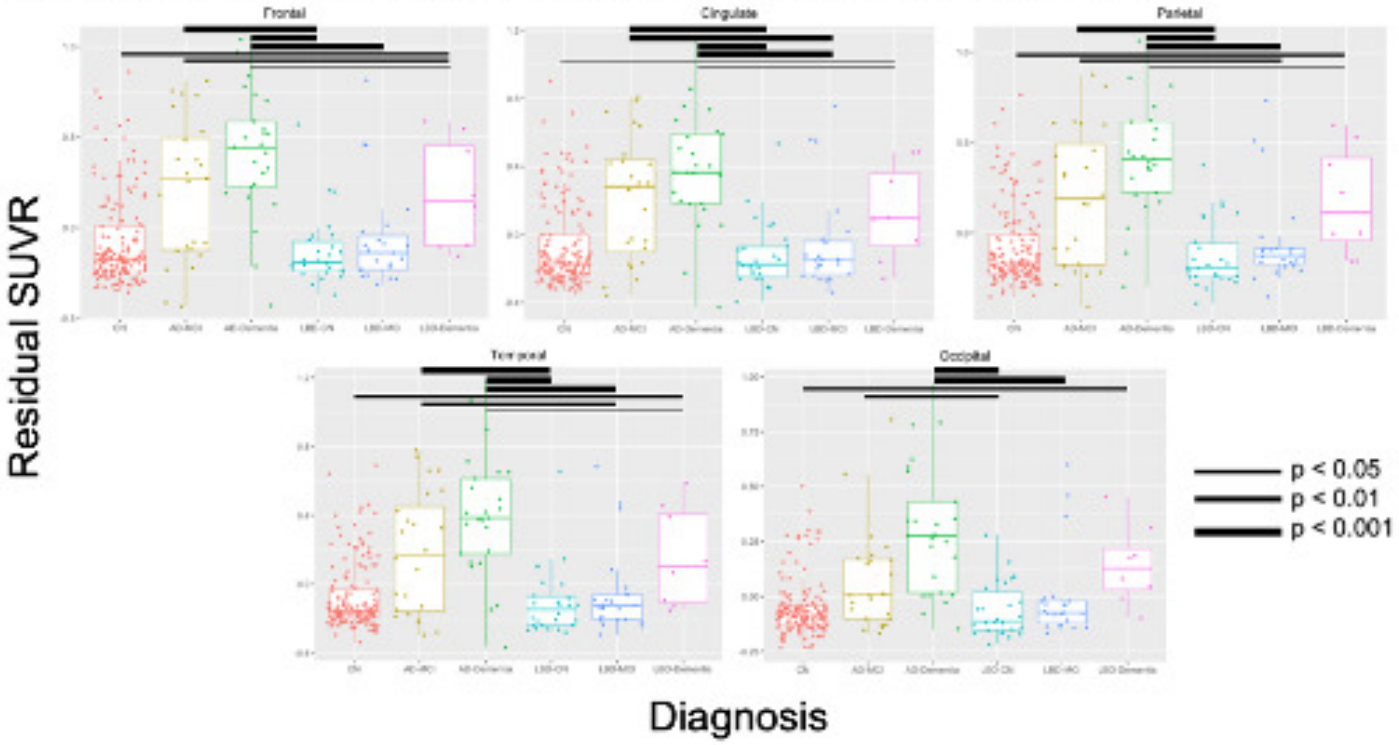

Table 2. Regional SUVR associations between LBD-spectrum and AD-spectrum participants. Each cell provides results from separate linear regression models with diagnosis predicting regional SUVRs, controlling for age and sex.

	Frontal	Cingulate	Parietal	Temporal	Occipital
LBD-CN vs. CN	-0.05 (0.06); p = 0.42	-0.05 (0.06); p = 0.38	-0.05 (0.05); p = 0.40	-0.28 (0.05); p = 0.59	-0.01 (0.04); p = 0.89
LBD-MCI vs. CN	0.02 (0.06); p = 0.77	0.02 (0.06); p = 0.78	0.04 (0.06); p = 0.54	0.03 (0.06); p = 0.65	0.05 (0.04); p = 0.21
LBD-Dementia vs. CN	**0.27 (0.10); p = 0.008**	**0.20 (0.10); p = 0.04**	**0.26 (0.09); p = 0.006**	**0.24 (0.09); p = 0.008**	**0.20 (0.06); p = 0.001**
LBD-CN vs. AD-MCI	**-0.33 (0.08); p < 0.001**	**-0.33 (0.08); p < 0.001**	**-0.32 (0.07); p < 0.001**	**-0.29 (0.07); p < 0.001**	**-0.13 (0.05); p = 0.007**
LBD-MCI vs. AD-MCI	**-0.26 (0.08); p = 0.001**	**-0.27 (0.08); p < 0.001**	**-0.24 (0.07); p = 0.002**	**-0.23 (0.07); p = 0.001**	-0.08 (0.05); p = 0.12
LBD-Dementia vs. AD-MCI	-0.01 (0.11); p = 0.90	-0.08 (0.11); p = 0.46	-0.01 (0.10); p = 0.89	-0.02 (0.10); p = 0.83	0.07 (0.07); p = 0.30
LBD-CN vs. AD-Dementia	**-0.54 (0.08); p < 0.001**	**-0.51 (0.08); p < 0.001**	**-0.56 (0.07); p < 0.001**	**-0.51 (0.07); p < 0.001**	**-0.36 (0.05); p < 0.001**
LBD-MCI vs. AD-Dementia	**-0.47 (0.08); p < 0.001**	**-0.44 (0.08); p < 0.001**	**-0.47 (0.08); p < 0.001**	**-0.45 (0.07); p < 0.001**	**-0.31 (0.05); p < 0.001**
LBD-Dementia vs. AD-Dementia	**-0.22 (0.11); p = 0.05**	**-0.25 (0.11); p = 0.02**	**-0.25 (0.10); p = 0.02**	**-0.24 (0.10); p = 0.02**	-0.15 (0.07); p = 0.28

Figure 3. Composite SUVR including and excluding the occipital region in all diagnoses. The two red vertical and horizontal lines indicate the cut points calculated from the Gaussion Mixture Models.

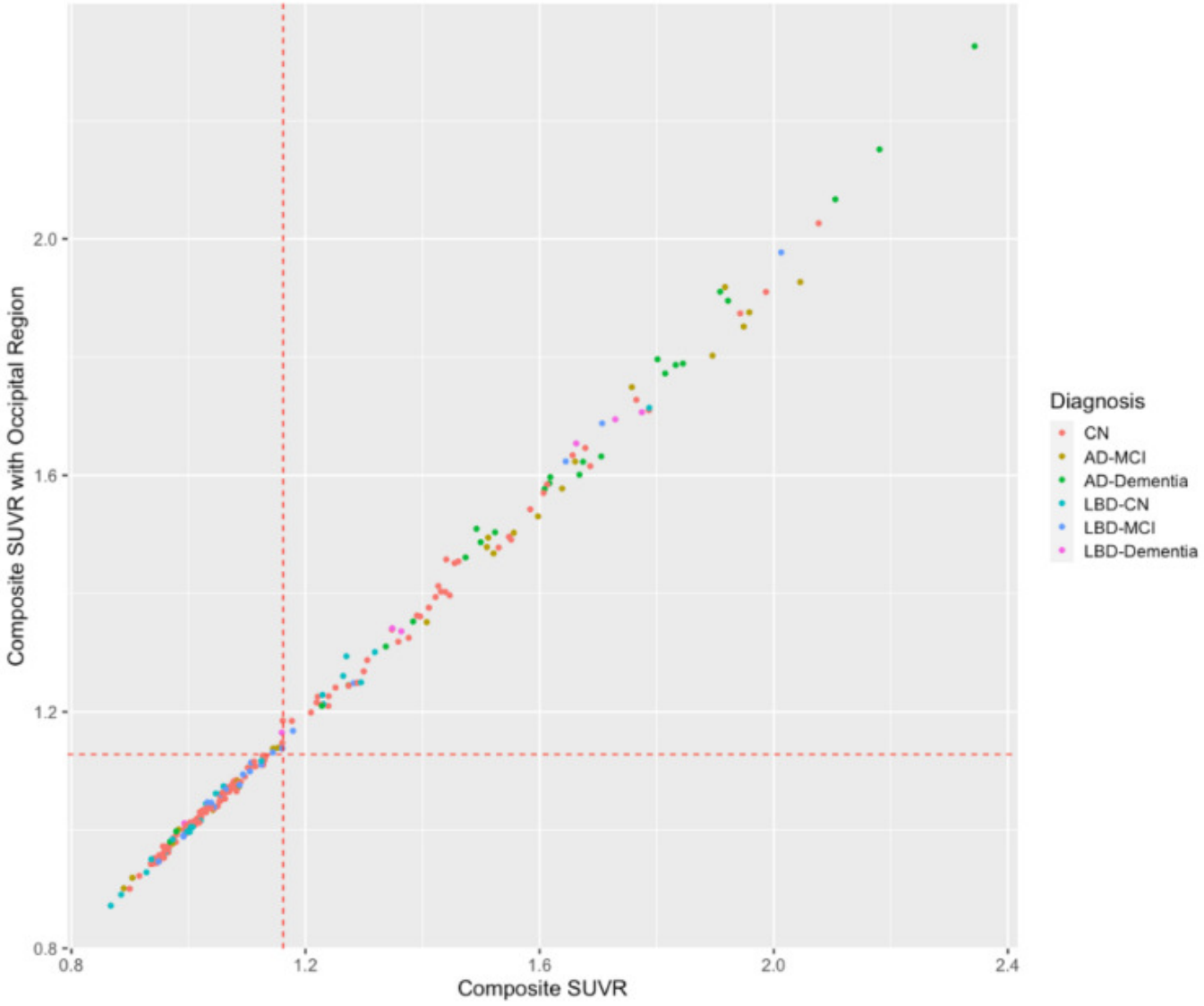

Figure 4. Discordant and concordant cases with both composite SUVRs in LBD-spectrum participants (N = 57).

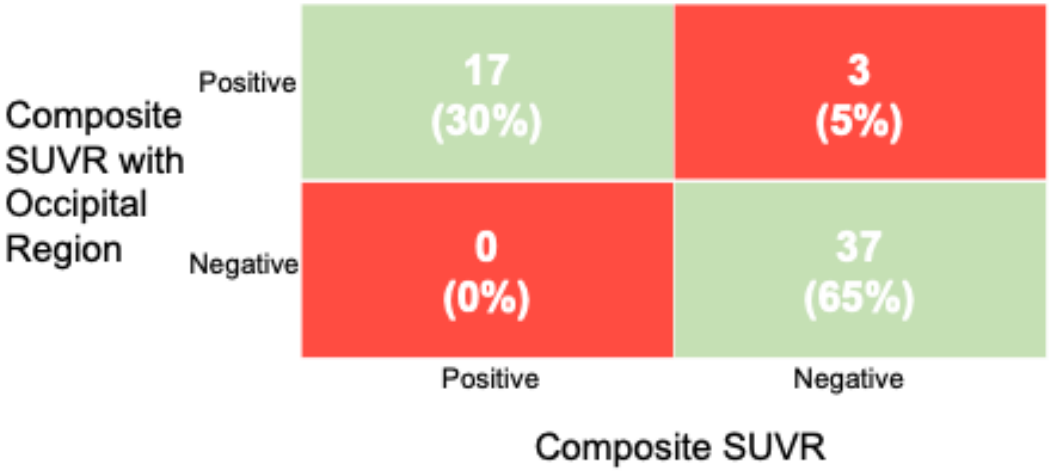

Keywords: Amyloid PET, Lewy Body Disease, Alzheimer's Disease, Co-pathology

101 Pathology-weighted connectivity with medial parietal lobe drives neocortical tau accumulation

Jacob Ziontz[1], Corrina Fonseca[1], Joseph Giorgio[1], Tessa Harrison[1], William Jagust[1,2]

[1]*Helen Wills Neuroscience Institute, University of California, Berkeley, Berkeley, CA, United States*
[2]*Lawrence Berkeley National Laboratory, Berkeley, CA, United States*

Background: Tau pathology is hypothesized to spread via structural and functional connections. Here, we investigate if baseline medial temporal tau and functional connectivity drive tau accumulation into tempoparietal neocortex.

Methods: 60 cognitively unimpaired older adults (M 77.5, SD 5.5 years) from the Berkeley Aging Cohort Study with rsfMRI, Aβ PET, and longitudinal tau PET were included. Resting state functional connectivity (rsFC) between Desikan-Killiany ROIs, PiB DVR, and FTP SUVR were computed at baseline. Regional rate of change in tau accumulation was computed using linear mixed effects models for ≥2 longitudinal time points, and voxelwise FTP slope images were created by fitting linear regressions at each voxel. We assessed the relationship between tau rate of change and pathology-weighted connectivity (PWC), defined as the interaction between seed tau, global Aβ, and seed-target rsFC strength.

Results: We examined whether PWC from hippocampus was associated with tau pathology accumulation in either precuneus or inferior temporal cortex (IT). Adjusting for age, sex, and choroid plexus FTP signal, tau accumulation in precuneus was associated with PWC from hippocampus, i.e. the three-way interaction between hippocampus-precuneus connectivity, baseline hippocampal tau, and global Aβ ($p < 0.001$; Figure 1). This effect was not significant using choroid plexus FTP signal in place of hippocampus ($p = 0.25$). The effect was specific to precuneus, as hippocampus-IT PWC was not associated with tau accumulation in IT ($p = 0.95$). Finally, voxelwise regression to predict FTP-slope maps revealed that hippocampus-precuneus PWC was strongly associated with tau accumulation in medial parietal lobe and temporal regions (Figure 2).

Conclusion: PWC from hippocampus to medial parietal lobe is strongly associated with rate of tau accumulation in key neocortical regions. This finding suggests that regions connected functionally and/or structurally are susceptible to connectivity-associated tau spread in the presence of seed tau pathology and cortical Aβ.

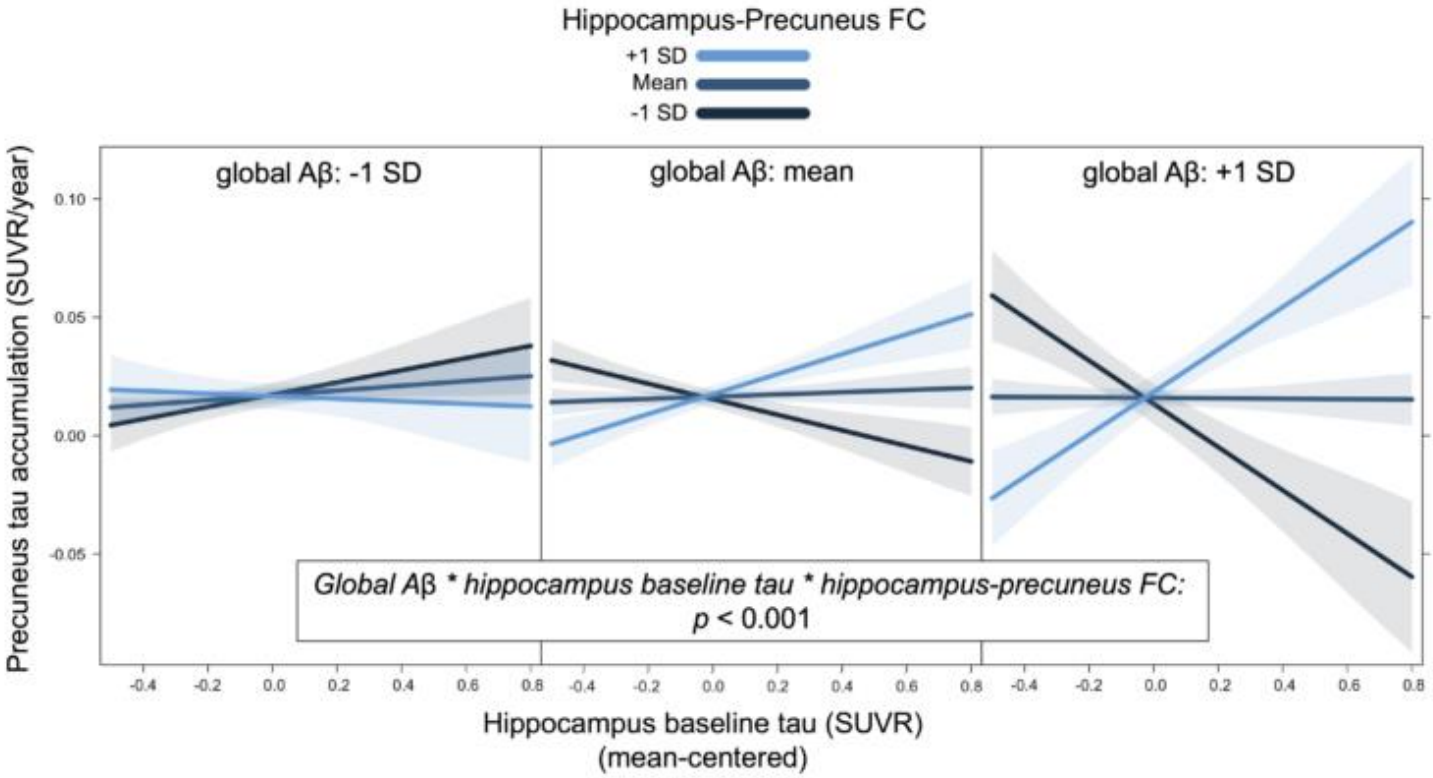

Figure 1. *Pathology-weighted connectivity with hippocampus is associated with rate of tau accumulation in precuneus.* Visualization of three-way interaction between global amyloid-beta (Aβ), baseline hippocampal tau, and hippocampus-precuneus resting state functional connectivity (FC) in linear regression model of precuneus tau accumulation. Adjusting for age, sex, and choroid plexus flortaucipir signal, the interaction of tau and Aβ pathology with connectivity between hippocampus and precuneus is strongly associated with the rate of change in tau pathology in precuneus.

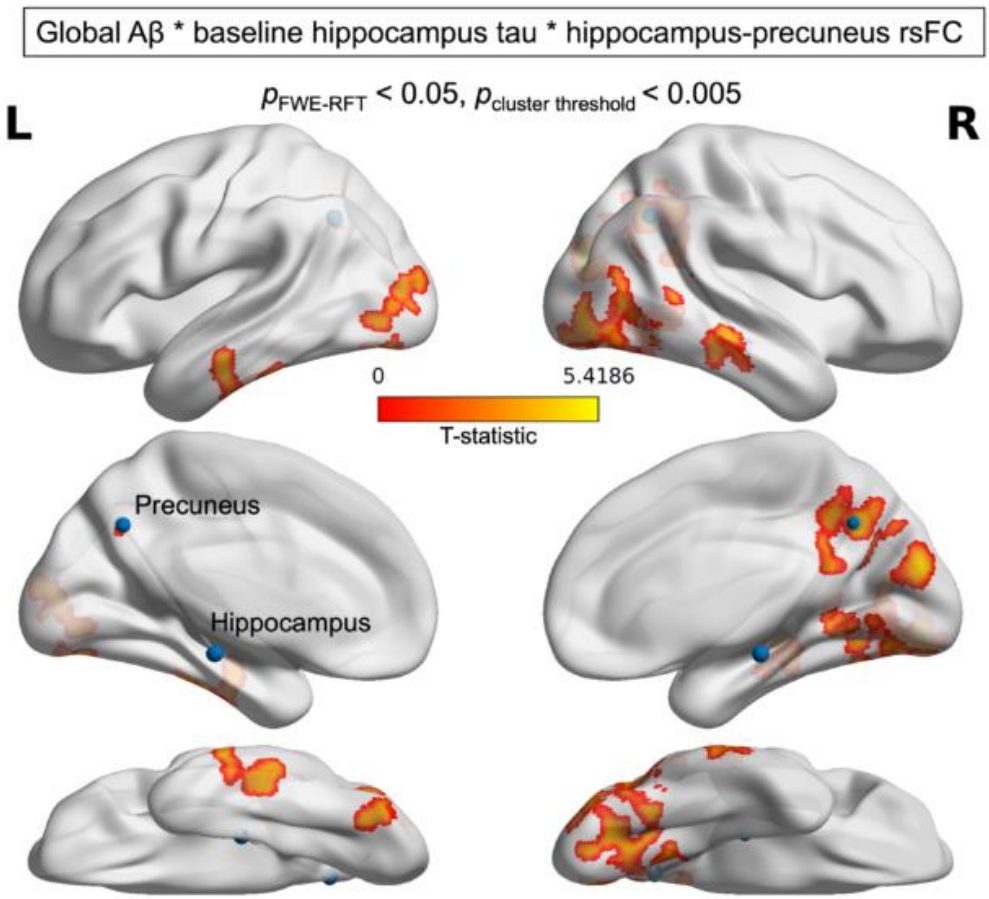

Figure 2. *Pathology-weighted connectivity between hippocampus and precuneus is associated with rate of tau accumulation in key neocortical regions.* Voxelwise association between tau rate of change and three-way interaction between global amyloid-beta (Aβ), baseline hippocampal tau, and hippocampus-precuneus resting state functional connectivity (rsFC). Adjusting for age and sex, the interaction of tau and Aβ pathology with connectivity between hippocampus and precuneus is strongly associated with the rate of change in tau pathology in cortical regions such as precuneus, as well as retrosplenial cortex, inferior temporal gyrus, and middle temporal gyrus. Spheres indicate center of ROIs used to compute FC. Significant voxels are corrected for multiple comparisons using a random field theory family-wise error (FWE-RFT) of $p < 0.05$ and a cluster threshold of $p < 0.005$.

Keywords: Connectivity, longitudinal, cogntitively unimpaired, tau, amyloid

102 18F-MK-6240 Tau PET visual read algorithm for Alzheimer's disease: diagnostic accuracy and comparison with automated-quantitative Braak stage analysis

Karine Provost[1], Jean Paul Soucy[1,2], Arlette Haeger[1,2], Arthur C Macedo[2], Nesrine Rahmouni[2], Jenna Stevenson[2], Stijn Servaes[2], Joseph Therriault[2], Jaime F Arias[2], Pedro Rosa-Neto[2]

[1]*Centre Hospitalier de l'Université de Montréal, Montreal, QC, Canada*
[2]*2 Montreal Neurological Institute, Montreal, QC, Canada*

Introduction: This study compares the diagnostic accuracy of Tau PET visual assessment of ^{18}F-MK-6240 with quantitative Braak stage for the diagnosis of Alzheimer's disease.

Methods: We included 140 participants (Table 1) who underwent ^{18}F -MK-6240 Tau PET at the MNI. Using a pre-defined visual interpretation algorithm (Figure 1) based on that of FDA-approved ^{18}F -Flortaucipir (Tauvid™), adapted to Braak-stages, three expert nuclear medicine physicians raters assigned a diagnostic category to PET scan images. The majority interpretation was compared to Braak-stage obtained by ROI-based quantification(Pascoal et al., 2020). Inter-rater reliability of visual reads was assessed using Fleiss' kappa and percent agreement with quantitative analysis. Diagnostic accuracy of visual read vs quantification was assessed based on a consensus clinical diagnosis.

Results: Inter-rater agreement was in the substantial range (κ=0.70, p<0.001 for all 3 raters; κ =0.64, p<0.001, κ =0.68, p<0.001 and κ =0.78, p<0.001 for reader pairs). The highest level of agreement was for Braak stages 0 and V-VI (κ =0.58 and 0.75, p<0.001). The majority visual read was concordant with Braak stage quantification in 57% of cases. A significant number (32%) of discordant cases were false positives on quantification due to off-target binding into ROIs, while 14% of cases were false-negative on quantification with Braak stage V-VI evident on visual assessment. Based on clinical diagnosis of Aβ+MCI/AD, visual read had a sensitivity of 94% and specificity of 59%, vs 98% and 50% for quantitative Braak stages using any Braak-stage >0. When using only Braak-stage≥3, sensitivity/specifity was 90%/71% for visual read, and 69%/88% for quantification. Examples of discordant cases (Figure 2) illustrate some potential advantages of using a visual read algorithm in conjunction with quantification.

Conclusion: ^{18}F -MK-6240 visual assessment has high inter-rater agreement, high sensitivity and improved specificity over the type of quantification we used for the diagnosis of Alzheimer's disease.

Table 1. Characteristics of study participants (n=140)

Age (years, mean (SD))	68.0 (12.4)
Sex (M/F)	62 / 78
Diagnosis (number of Aβ+)	
CN	23 (6)
SCI	4 (3)
MCI	67 (51)
AD	38 (33)
nonAD	8 (2)
MMSE (mean (SD))	25.4 (5.5)
CDR score (mean (SD))	0.5 (0.5)

CN: cognitively normal, SCI: subjective cognitive impairment, MCI: mild cognitive impairment, AD: Alzheimer's disease

Figure 1. Visual read interpretation algorithm for 18F-MK-6240

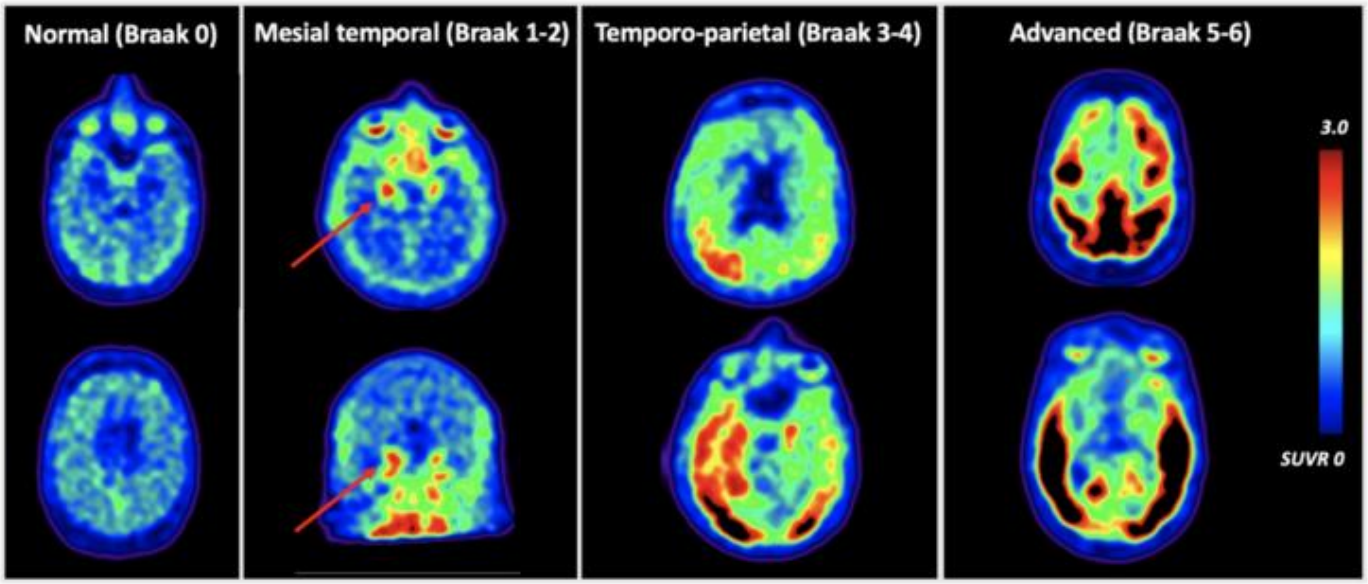

Figure 2. Example of discordant cases by quantitative Braak stage:
First row: (Q Braak VI) and visual interpretation (Braak 0, negative, all 3 raters). There is intense off-target binding in the skull/meninges which likely explains false-positive by quantitative analysis.
Second row: (Q Braak I-II) and visual interpretation (Braak V-VI) due to uptake in the pre-frontal cortex).
Third row: (Q Braak-I-II) and visual interpretation (Braak V-VI), with clear false-negative quantification due to technical error.

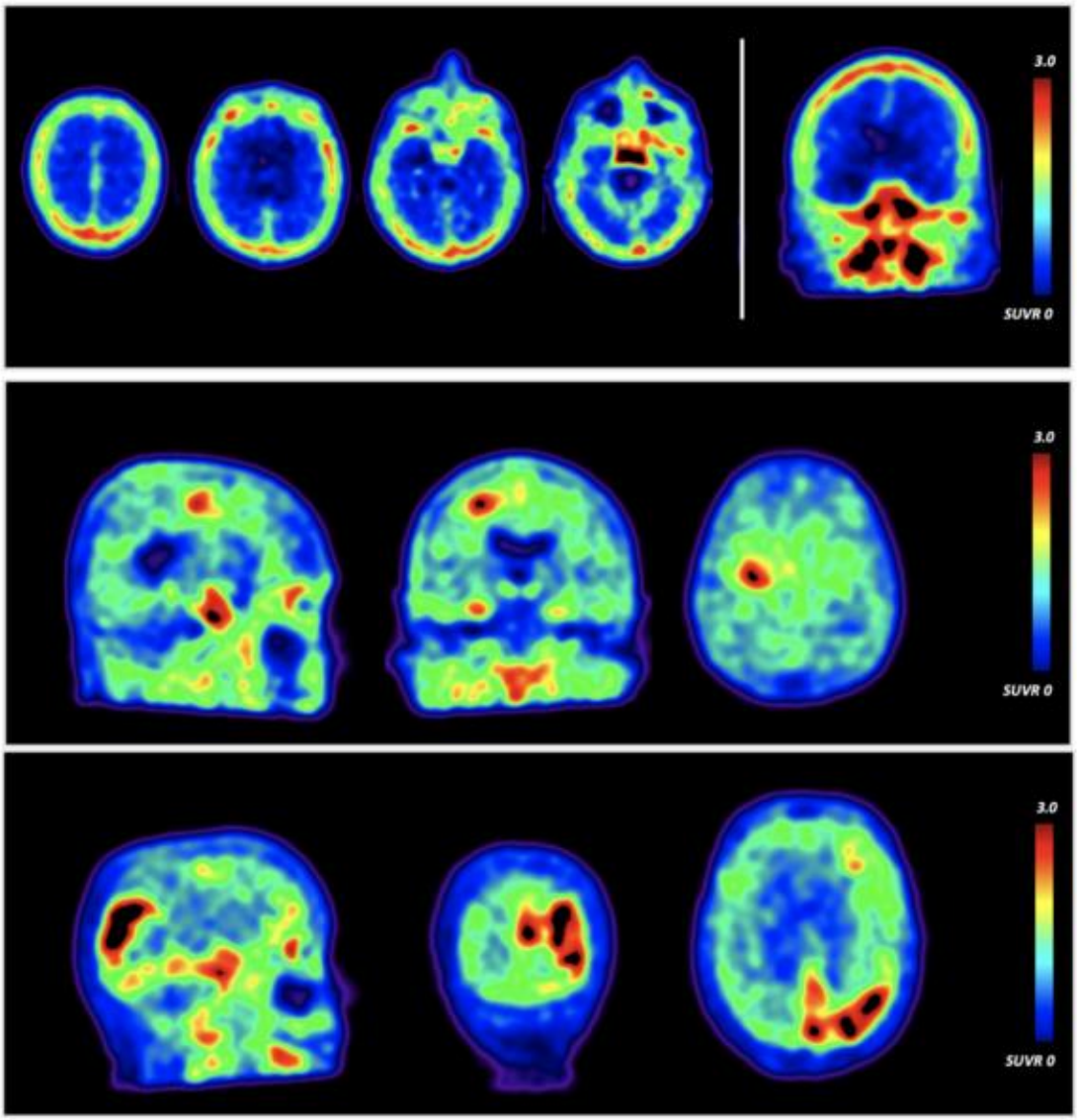

Keywords: Tau PET, visual read, PET, Alzheimer's

103 Evaluating CenTauRz harmonization of matched FTP and MK6240 tau PET images: the HEAD Study

Davneet Minhas[1], Alex Delbene[1], Weiquan Luo[1], Alexandria Reese[1], Alexandra Gogola[1], Victor Villemagne[1], Vincent Dore[2], Brian Lopresti[1], Charles Laymon[1], Firoza Lussier[1], Guilherme Bauer-Negrini[1], Guilherme Povala[1], Ann Cohen[1], Ciprian Crainiceanu[3], Belen Pascual[4], Brian Gordon[5], Val Lowe[6], Hwamee Oh[7], David Soleimani-Meigooni[8], William Klunk[1], Pedro Rosa-Neto[9], Suzanne Baker[10], Tharick Pascoal[1], Dana Tudorascu[1]

[1]*University of Pittsburgh, Pittsburgh, PA, United States*
[2]*Austin Health, Melbourne, Australia*
[3]*Johns Hopkins University, Baltimore, MD, United States*
[4]*Houston Methodist, Houston, TX, United States*
[5]*Washington University, St. Louis, MO, United States*
[6]*Mayo Clinic, Rochester, MN, United States*
[7]*Brown University, Providence, RI, United States*
[8]*University of California San Francisco, San Francisco, CA, United States*
[9]*McGill University, Montreal, QC, Canada*
[10]*Lawrence Berkeley National Laboratory, Berkeley, CA, United States*

Background: The CenTauR pipeline was developed to provide a consistent image processing method and positivity threshold across tau tracers. The objective of this work was to assess CenTauR$_Z$ as a method of harmonization for ^{18}F-flortaucipir (FTP) and ^{18}F-MK-6240 (MK) acquired in the same individuals.

Methods: 86 participants received T1 MR, amyloid PET, and FTP (80-100min) and MK (90-110min) tau PET imaging at 4 sites under the HEAD study. Tau PET images were processed using the SPM8-CenTauR pipeline. Universal CenTauR and subregion (Mesial Temporal, Meta Temporal, Temporo-Parietal [TP], and Frontal) SUVR outcomes were converted to CenTauR$_Z$ (CTRz) using published equations. Regional tau status was determined using a consistent threshold of 2 CTRz. Tau status agreement was assessed using Cohen's kappa.

Results: Demographics, outcomes, and kappa coefficients are presented in Table 1. Regional relationships between FTP and MK CTRz are presented in Figure 1. Discordant tau status cases (FTP-/MK+ or FTP+/MK-) were further categorized into mild (FTP and MK >1 and <3 CTRz) and severe (FTP or MK <1 or >3 CTRz). Universal, Meta, and TP severe discordant cases were exclusively FTP+/MK- (Figure 2). Mesial severe discordances were predominantly FTP-/MK+, with all such cases being female. Preliminary visual reads suggest elevated non-specific cortical retention in FTP may explain Universal FTP+/MK- discordances, and high neighboring meningeal off-target retention in MK may explain Mesial FTP-/MK+ discordances. Furthermore, 92.9% of severely discordant cases (13/14) were attributed to a single site and PET scanner from which 66.3% of scans were acquired (57/86).

Conclusions: These results suggest a z-score scale is insufficient to account for all differences in tau imaging studies. Harmonization efforts should consider a non-linear relationship between FTP and MK and address tracer-specific and individual variability in off-target retention profiles. Ongoing work will also examine scanner-specific differences affecting tau quantification and harmonization.

Table 1. Demographics and amyloid and tau PET outcomes with tau PET status agreement

Cog Status	N	Age (SD)	F (%)	PiB/NAV4694 Centiloid CL (SD)	PiB/NAV4694 Centiloid A+ (>24CL)	FTP CTRz Mean (SD) Universal	FTP CTRz Mean (SD) Mesial	FTP CTRz Mean (SD) Meta	FTP CTRz Mean (SD) TP	FTP CTRz Mean (SD) Frontal	MK6240 CTRz Mean (SD) Universal	MK6240 CTRz Mean (SD) Mesial	MK6240 CTRz Mean (SD) Meta	MK6240 CTRz Mean (SD) TP	MK6240 CTRz Mean (SD) Frontal	Tau PET Status (Pos/Neg) Percent Agreement (Kappa) Universal	Mesial	Meta	TP	Frontal
YC	15	22.7 (1.0)	9 (60%)	-0.9 (2.9)	0%	-0.2 (1.5)	-1.0 (1.3)	-0.7 (1.4)	-0.1 (1.5)	0.2 (1.6)	0.3 (1.1)	-0.4* (0.9)	-0.4 (1.1)	0.4 (1.1)	0.4 (1.2)	93.3% (NA)	100% (NA)	100% (NA)	93.3% (NA)	86.7% (NA)
CU	33	66.8 (8.3)	23 (70%)	19.8 (31.2)	28%	1.1 (1.5)	0.6 (1.7)	0.5 (1.6)	1.2 (1.5)	1.2 (1.1)	1.2 (2.3)	1.2* (2.7)	0.5 (2.3)	1.2 (2.2)	0.8 (1.1)	84.8% (0.46)	87.9% (0.54)	97.0% (0.84)	81.8% (0.40)	84.8% (0.46)
MCI	29	71.9 (5.5)	12 (41%)	56.4 (47.1)	68%	4.1 (5.7)	3.9 (4.5)	4.3 (6.1)	4.1 (5.9)	2.0 (3.1)	6.0* (9.0)	6.5*** (7.3)	6.3* (10.0)	5.9* (9.0)	3.2 (6.4)	93.1% (0.86)	82.8% (0.63)	89.7% (0.79)	86.2% (0.73)	79.3% (0.58)
AD	9	74.9 (6.4)	4 (44%)	91.6 (44.3)	89%	9.5 (6.5)	9.2 (5.8)	10.9 (7.9)	9.6 (6.5)	3.0 (2.6)	16.4** (11.2)	15.1** (9.0)	17.9** (12.4)	16.2** (11.2)	7.8** (6.2)	100% (1.00)	100% (1.00)	100% (1.00)	100% (1.00)	100% (1.00)
Total	86	61.7 (19.3)	48 (56%)	36.0 (45.8)	44%	2.7 (4.9)	2.3 (4.5)	2.7 (5.6)	2.8 (5.0)	1.5 (2.3)	4.3*** (8.0)	4.2*** (7.0)	4.1** (9.0)	4.2*** (7.9)	2.3* (4.8)	90.7% (0.79)	89.5% (0.77)	95.3% (0.88)	87.2% (0.71)	84.9% (0.65)
Excl. YC	71	69.9 (7.6)	39 (55%)	43.8 (46.8)	54%	3.4 (5.1)	3.0 (4.6)	3.4 (5.9)	3.4 (5.2)	1.7 (2.4)	5.1*** (8.5)	5.1*** (7.4)	5.1** (9.6)	5.0** (8.5)	2.7* (5.2)	90.1% (0.80)	87.3% (0.74)	94.4% (0.87)	85.9% (0.71)	84.5% (0.66)

* P<0.05, ** P<0.01, *** P<0.001 significant differences between MK6240 CTRz and FTP CTRz by cognitive status and CenTauR region.
Cohen's kappa was not calculated for YC due to 0 cases of positive agreement across all regions.
Kappa values are color coded as red for fair (0.21-0.40), orange for moderate (0.41-0.60), yellow for substantial (0.61-0.80), and green for almost perfect or perfect agreement (0.81-1.00)

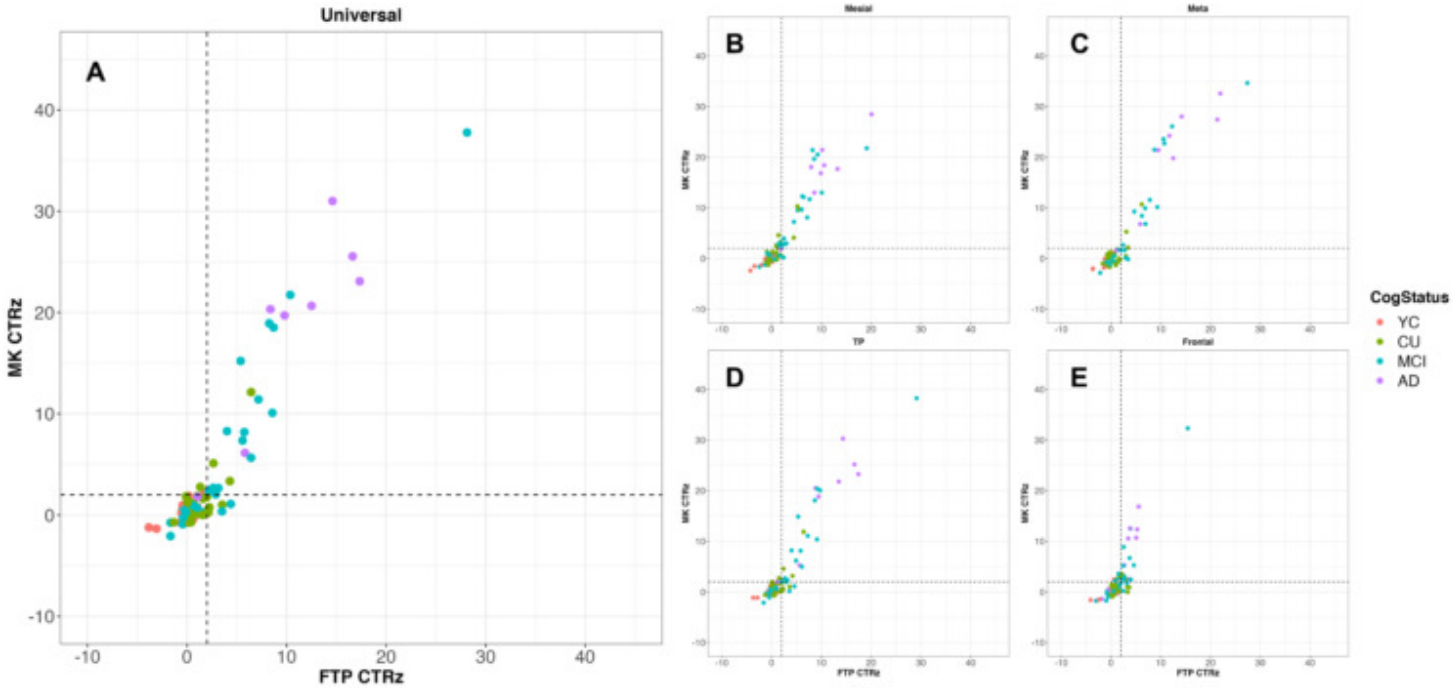

Figure 1. Relationship between MK CTRz and FTP CTRz for the (A) Universal CenTauR region and its constituent subregions: (B) Mesial Temporal, (C) Meta Temporal, (D) Temporo-Parietal (TP), and (E) Frontal.

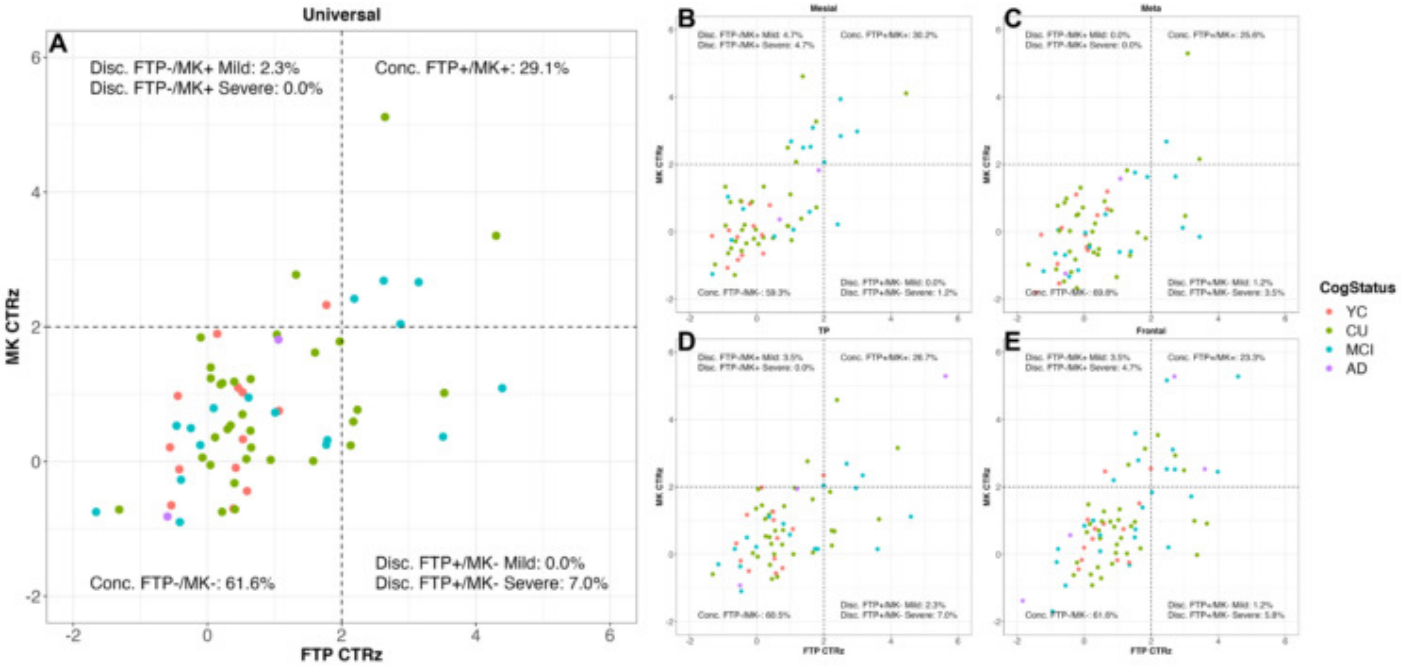

Figure 2. Concordant and discordant cases for the (A) Universal CenTauR region and its constituent subregions -- (B) Mesial Temporal, (C) Meta Temporal, (D) Temporo-Parietal (TP), and (E) Frontal -- around the 2 CTRz threshold. Individual cases with regional FTP and MK CTRz >2 CTRz were concordant positive (Conc. FTP+/MK+) and those with both tracers <2 CTRz concordant negative (Conc. FTP-/MK-). Discordant cases (Disc. FTP-/MK+ and Disc. FTP+/MK-) were classified as "Mild" if both FTP and MK were within 1 CTRz of the threshold, and "Severe" if either FTP or MK fell outside this 1-3 CTRz range. Percents of the study cohort belonging to each concordant and discordant classification are shown in their respective quadrants. Percents shown include cases outside the displayed -2 to 6 CTRz range.

Keywords: Flortaucipir, MK6240, CenTauR, PET, Harmonization

104 Characterizing the relationship between the functional connectome and tau PET in preclinical Alzheimer's disease

Hamid Abuwarda[1,2], Annie Trainer[1], Suyeon Ju[1], R. Todd Constable[3], Carolyn Fredericks[1]

[1]*Department of Neurology, Yale School of Medicine, New Haven, CT, United States*
[2]*Interdepartmental Neuroscience Program, Yale University, New Haven, CT, United States*
[3]*Department of Radiology and Biomedical Imaging, Yale School of Medicine, New Haven, CT, United States*

Amnestic Alzheimer's Disease (AD) is characterized by early disruptions in functional connectivity and progressive tau pathology, particularly in the Default Mode Network (DMN). Yet, the relationship between the functional connectome and tau is not fully understood. Our study aims to develop robust connectomic models to predict focal tau deposition to better understand functional connectivity changes in preclinical AD participants.

Methods. We used Connectome-based Predictive Modeling (CPM; identifies linear relationships) and Kernel Ridge Regression (KRR; identifies linear and nonlinear relationships) on baseline tau PET (FTP) and resting-state fMRI (rsfMRI) from the Anti-Amyloid in Asymptomatic Alzheimer's disease (A4) study, a clinical trial of cognitively unimpaired adults (aged 65-85) with elevated amyloid PET. Using rsfMRI (t=6.5 min, n=394), we predicted contemporaneous focal FTP binding (standardized uptake value ratio (SUVR)) in regions implicated in early-stage AD, and a previously-described meta-ROI. As a standard of comparison, we compared tau model performances to CPM and KRR models predicting RAVLT memory scores in the Human Connectome Project - Aging, a healthy aging cohort (aged 36-100, n=566) using Spearman's correlations.

Results. CPM models best predicted tau in posterior cingulate (r=0.30) and precuneus (r=0.23) regions, but minimally predicted parahippocampal tau, entorhinal tau, and cortical amyloid (r≈0.05-0.06). KRR models did not outperform CPM models for tau (Δr=-0.01-0.02), but KRR models did outperform CPM models for memory in HCP-A (Δr=0.05-0.09).

Conclusions. Using the functional connectome, we can predict a portion of the variance in focal tau PET within early-stage AD regions, particularly in DMN parietal regions. Incorporating nonlinear effects did not increase predictive power of focal tau, whereas it did for memory performance, suggesting the relationship between focal tau and the connectome is predominantly linear in preclinical AD populations. Future work will assess the networks underpinning our most successful models and externally validate these results in a separate at-risk AD cohort.

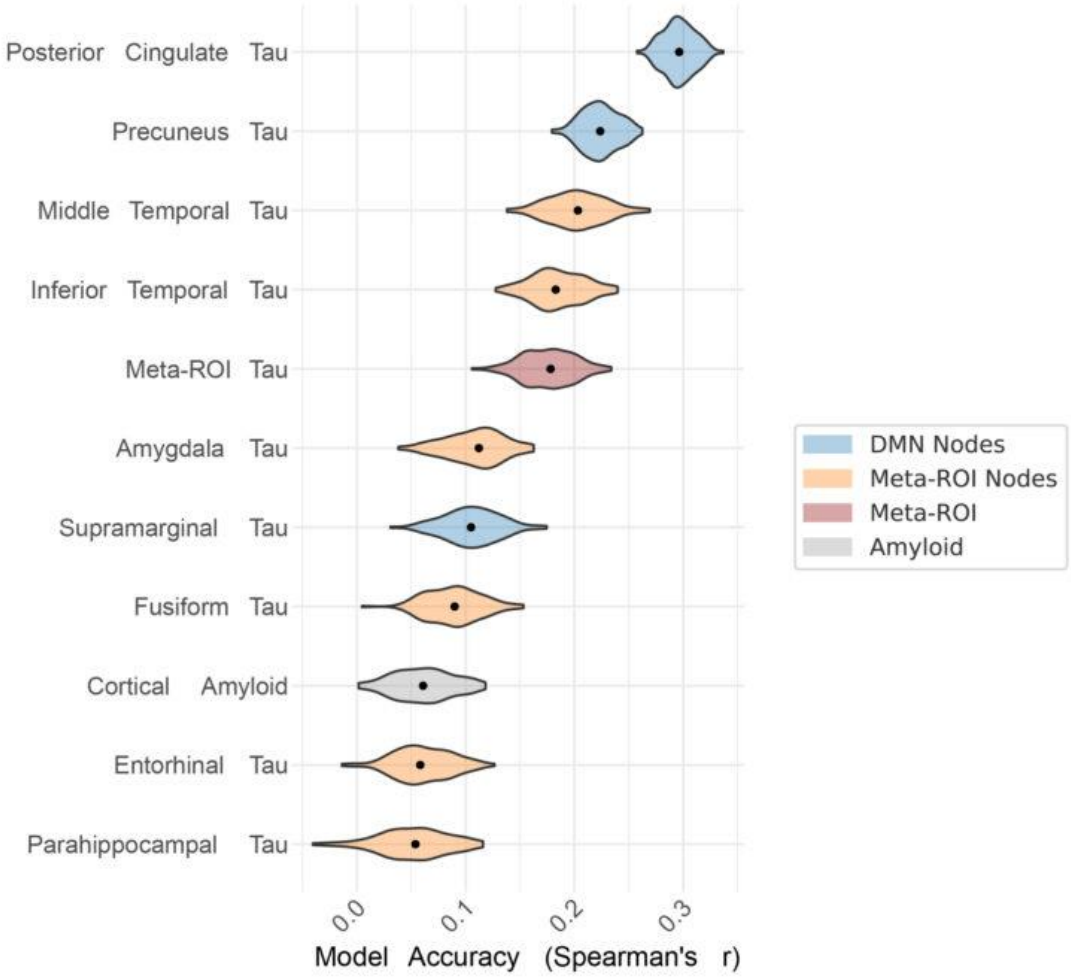
Posterior Cingulate Tau
Precuneus Tau
Middle Temporal Tau
Inferior Temporal Tau
Meta-ROI Tau
Amygdala Tau
Supramarginal Tau
Fusiform Tau
Cortical Amyloid
Entorhinal Tau
Parahippocampal Tau
0.0
0.1
0.2
0.3
Model Accuracy (Spearman's r)
DMN Nodes
Meta-ROI Nodes
Meta-ROI
Amyloid

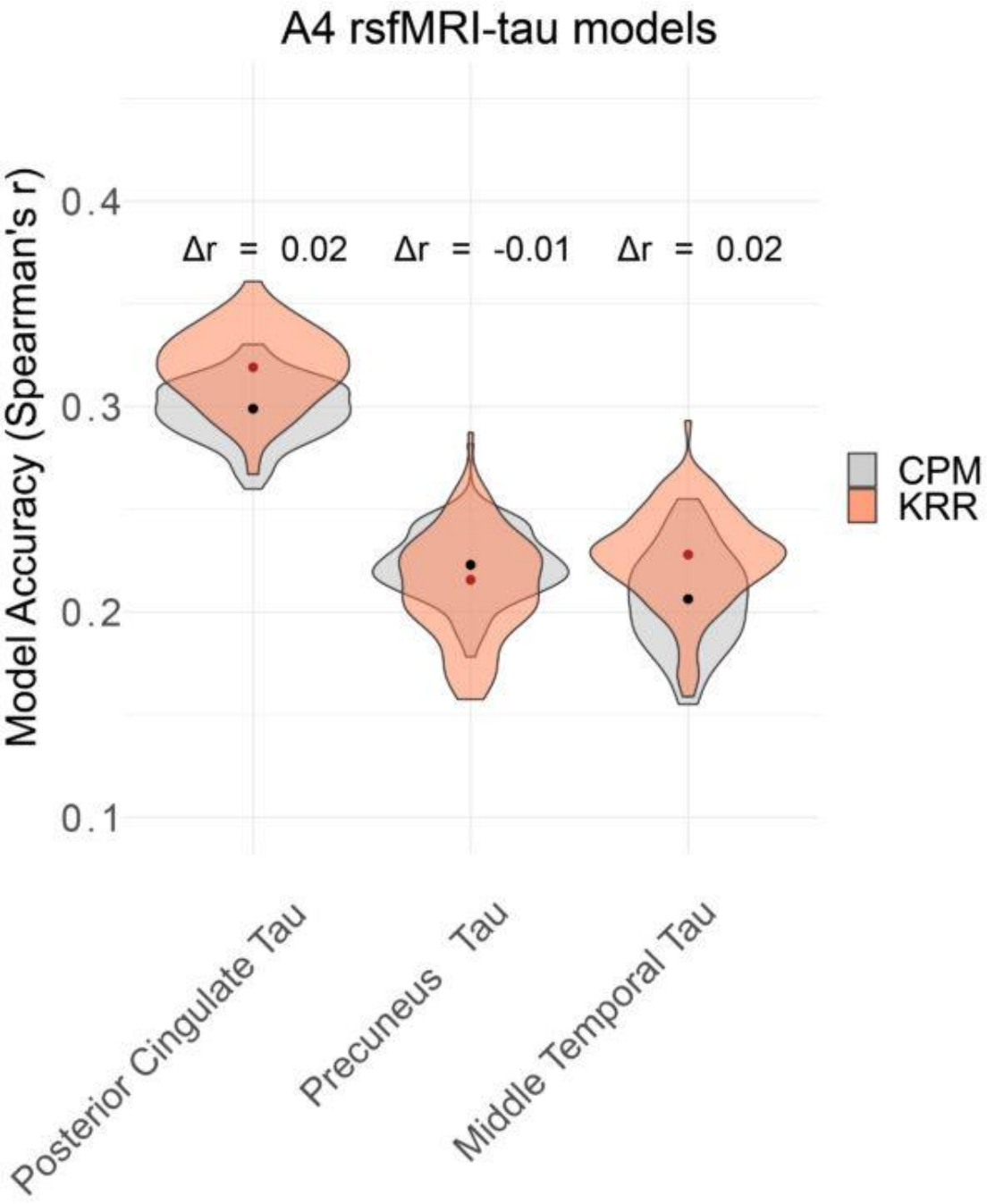
A4 rsfMRI-tau models
Model Accuracy (Spearman's r)
0.4
0.3
0.2
0.1
Δr = 0.02
Δr = -0.01
Δr = 0.02
CPM
KRR
Posterior Cingulate Tau
Precuneus Tau
Middle Temporal Tau

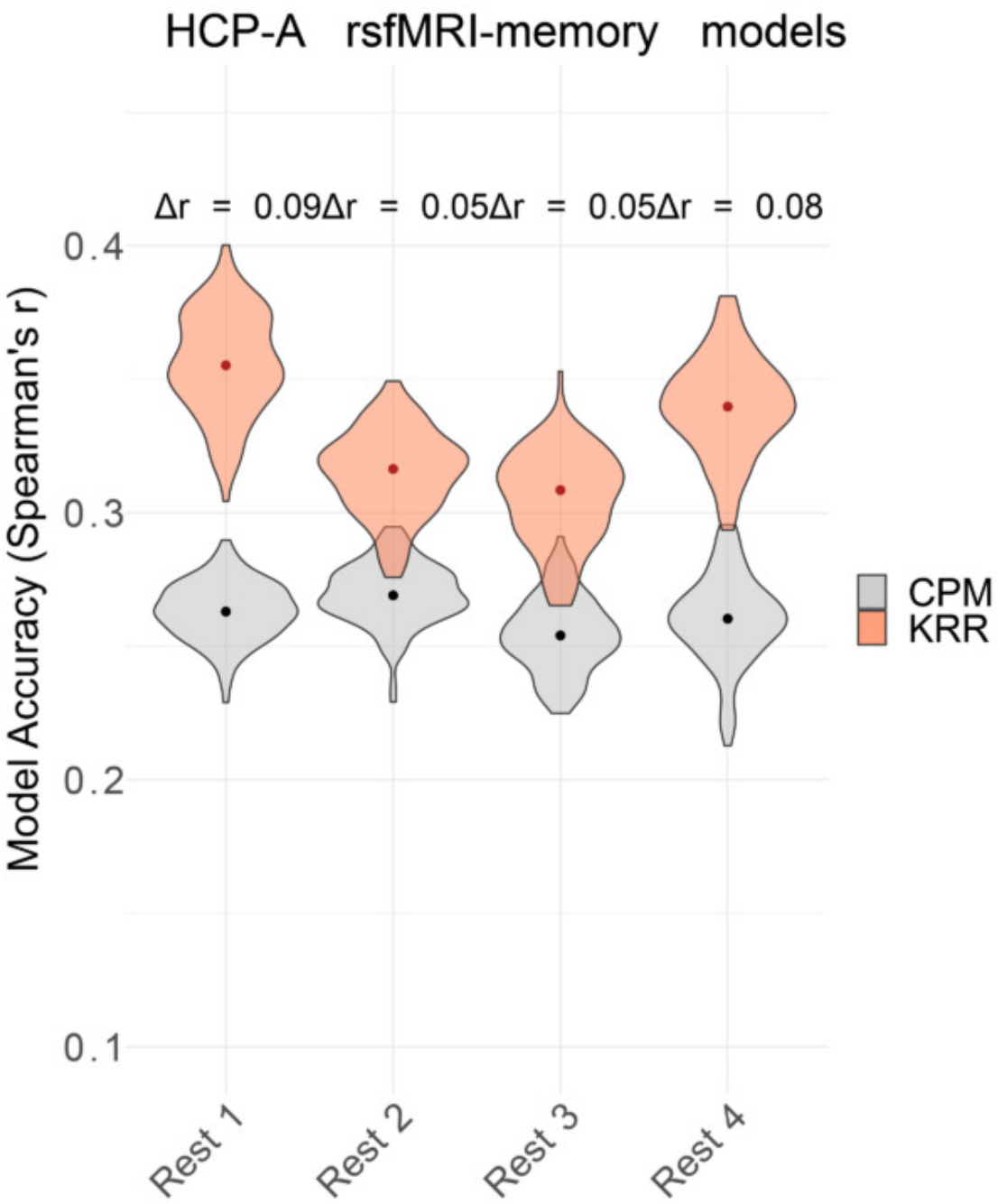

Keywords: Functional connectome, predictive modeling, tau PET

105 Estimating time-to-tau as a function of Aβ pathology in Alzheimer's disease using [18F]MK6240 and [18F]NAV4694 PET

Samantha Budd Haeberlein[1], Antoine Leuzy[1], Sulantha Mathotaarachchi[1], Philip S. Insel[2], Michael Schöll[3,4,5], Alexis Moscoso[3,4], Victor L. Villemagne[6,7,8], Vincent Doré[8,9], Christopher C. Rowe[7,8,10]

[1]*Enigma Biomedical USA, Knoxville, TN, United States*
[2]*Department of Psychiatry and Behavioral Sciences, University of California, San Francisco, CA, United States*
[3]*Wallenberg Centre for Molecular and Translational Medicine, University of Gothenburg, Gothenburg, Sweden*
[4]*Department of Psychiatry and Neurochemistry, Institute of Physiology and Neuroscience, University of Gothenburg, Gothenburg, Sweden*
[5]*Dementia Research Centre, Institute of Neurology, University College London, London, United Kingdom*
[6]*Department of Neurology, University of Pittsburgh School of Medicine, Pittsburgh, PA, United States*
[7]*Florey Department of Neuroscience, University of Melbourne, Victoria, Australia*
[8]*Department of Molecular Imaging & Therapy, Austin Health, Victoria, Australia*
[9]*Health and Biosecurity Flagship, The Australian eHealth Research Centre, CSIRO, Victoria, Australia*
[10]*The Australian Dementia Network (ADNeT), Melbourne, Australia*

Objective: To describe the characteristics of the amyloid-β (Aβ) PET imaging agent [^{18}F]NAV4694 and the association between [^{18}F]NAV4694 retention and increases in tau pathology in Alzheimer's disease (AD).

Methods: Using longitudinal (~2 year follow-up) [^{18}F]NAV4694 (Aβ) and [^{18}F]MK6240 (tau) from the Australian Imaging Biomarkers and Lifestyle flagship study of ageing (AIBL), we will estimate the time course of Aβ and tau pathology across the clinical continuum of AD (Aβ- or Aβ+ cognitively unimpaired individuals [n=152], Aβ+ mild cognitive impairment [n=47] and AD dementia [n=33]) using two different model: ordinary differential equations and non-linear mixed-effects disease progression models. Standardized uptake value ratios (SUVR) for [^{18}F]NAV4694 and [^{18}F]MK6240 will be based on the cerebellar cortex and pons, respectively, with [^{18}F]NAV4694 Centiloids determined using the Computational Analysis of PET from AIBL (CapAIBL) pipeline. Time to both significant increases and positivity will be defined for tau as a function of [^{18}F]NAV4694 Centiloids using both voxel-wise and regional approaches.

Results: Table 1 provides demographic summary information for the AIBL cohort with longitudinal data. The proposed time course analyses will identify brain region specific [^{18}F]NAV4694 Centiloid values at which tau pathology begins to i) accumulate and ii) exceed thresholds for positivity.

Conclusion: This work is the first to describe the link between Aβ deposition measured using [^{18}F]NAV4694 and tau accumulation in AD. Knowledge of the temporal course of Aβ and tau will facilitate the delineation of critical periods suitable for intervention and facilitate appropriate trial design using anti-Aβ therapies.

Table 1. Participant characteristics

	CU	MCI	AD dementia
N	152	47	33
Age	75.9 (5.8)	74.6 (6.9)	70.1 (7.8)
Sex, N male (%)	76 (50.0%)	28 (60.0%)	16 (50.0%)
Education	15.0 (5.0)	13.0 (6.5)	10.0 (5.5)
APOE ε4 carriership	60 (40.0%)	28 (60.0%)	16 (50.0%)
MMSE	29.0 (1.0)	27.0 (2.0)	23.5 (5.0)
CDR-SOB	0.0 (0.0)	1.0 (1.0)	4.5 (2.5)
Centiloids	34.2 (48.8)	76.1 (58.3)	106.5 (44.1)
Follow-up duration, PET	2.1 (0.9)	1.9 (0.7)	1.9 (0.7)

Keywords: [18F]NAV4694, Amyloid, PET, Alzheimer

106 Neuroinflammation potentiates the effect of amyloid-β on longitudinal tau accumulation

Nesrine Rahmouni[1], Yi-Ting Wang[1], Joseph Therriault[1], Stijn Servaes[1], Cécile Tissot[1], Arthur C. Macedo[1], Jaime Arias-Fernandez[1], Peter Kunach[1], Jenna Stevenson[1], Ali Hosseini[1], Brandon Hall[1], Lydia Trudel[1], Wan Lu Jia[1], Serge Gauthier[1], Eduardo R. Zimmer[4], Andrea L. Benedet[3], Tharick A. Pascoal[2], Pedro Rosa-Neto[1]

[1]*McGill University, Montreal, QC, Canada*
[2]*University of Pittsburgh, Pittsburgh, PA, United States*
[3]*University of Gothenburg, Gothenburg, Sweden*
[4]*Universidade Federal do Rio Grande do Sul, Porto Alegre, Brazil*

Background: It has been proposed that microglia released proinflammatory factors reactive to amyloid plaques constitute an early event leading to tau pathology. Here we assessed how the rate of progression of tau-PET is affected by baseline levels of amyloid-β and neuroinflammation.

Methods: We included 86 individuals from TRIAD cohort. Neuroinflammation, tau tangle and amyloid-β (Aβ) deposition were assessed via [^{11}C]PBR28-PET, [^{18}F]MK6240-PET and [^{18}F]AZD4694-PET, respectively. Voxel and region of interest regression models evaluated the relationship between baseline levels of TSPO- and Aβ-PET on Tau-PET yearly change. An interaction model evaluated the association of TSPO- and Aβ-PET with tau-PET yearly change as the outcome across Braak regions. Comparison of models was made using the Akaike Information Criterion (AIC) and the models' goodness-of-fit was evaluated using R^2 analyses. Models used [^{18}F]MK6240-PET SUVR yearly change as the outcome and used as predictors [^{11}C]PBR28-PET SUVR in the precuneus and posterior cingulate and [^{18}F]AZD4694-PET SUVR in the neocortical region. All models were corrected for age and sex and RFT was used to correct for voxelwise multiple comparisons.

Results: Positive associations were found between baseline levels of TSPO- and Aβ-PET and yearly change of Tau-PET **(Fig.1).** Positive correlations were found between Aβ-PET SUVR in the neocortical regions and Tau-PET SUVR across all braak regions **(Fig.1A).** Positive correlations were found between TSPO-PET SUVR in the precuneus and posterior cingulate and Tau-PET SUVR in Braak regions III-IV-V-VI **(Fig.1B)**. The interaction between Aβ- and TSPO-PET predicting the yearly change in tau-PET is the model with the highest R^2 and the lowest AIC values in Braak regions III-IV-V-VI. **(Fig.2).**

Conclusion: These results support the hypothesis that microglial activation and Aβ aggregates facilities tau progression interactively. Our results also support the notion that microglial abnormalities might be an early upstream event, presumably before tangle formation.

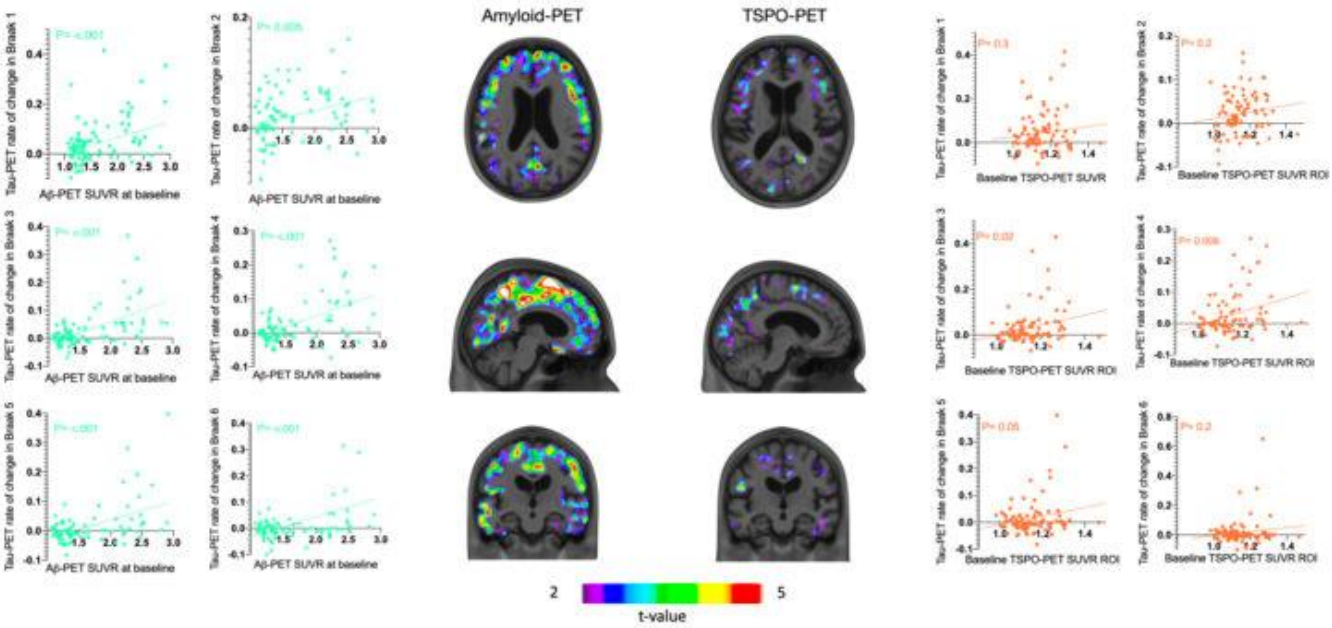

Figure 1: TSPO- and AB-PET baseline levels predict longitudinal increase of Tau-PET.
A. Voxel-based regression models evaluated the relationship between PET-uptake at baseline and the yearly change in Tau-PET.
B. Linear regression models using Pearson correlation coefficients evaluated the relationship between TSPO- and AB-PET SUVR with Tau-PET across Braak regions.

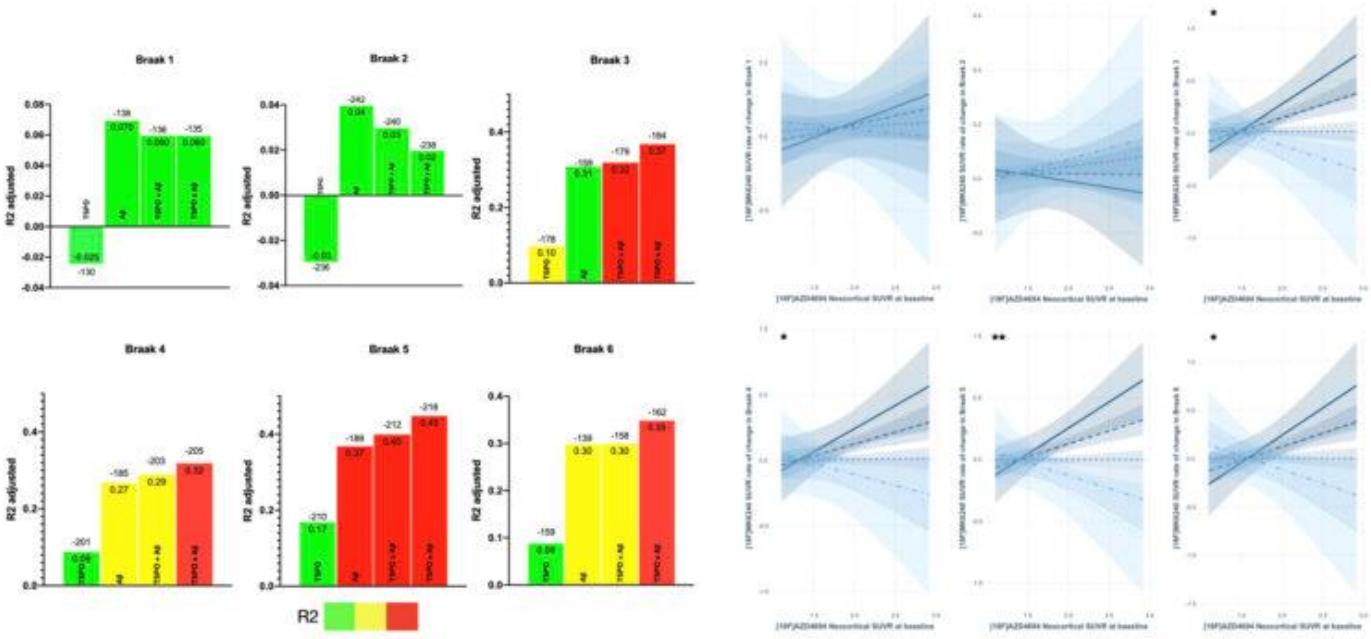

Figure 2: TSPO-PET potentiates the association between AB-PET and longitudinal Tau-PET change.
A. R^2 and AIC (above the bars) for different regression models with the yearly change in Tau-PET as the outcome, using amyloid-β-PET and TSPO-PET SUVR as predictors. All models included age and sex as covariates.
B. A linear regression interaction model evaluated the interaction between TSPO- and AB-PET with Tau-PET change as the outcome across braak regions.

Keywords: Inflammation, Biomarkers, PET-imaging, Alzheimer's disease, Tau

107 Association between plasma pTau epitopes and synaptic density measured with [C-11]UCB-J PET

Kao Lee Yang[1], Alexandra DiFilippo[2], Yue Ma[1], Rachael Wilson[3], Yer Thor[1], Mary-Elizabeth Pasquesi[1], Todd Barnhart[2], Jonathan Engle[2], Tobey Betthauser[1,3], Nicholas Ashton[4], Sterling Johnson[1,3,5], Bradley Christian[1,2], Henrik Zetterberg[1,4,6,7,8], Barbara Bendlin[1,3]

[1]*Wisconsin Alzheimer's Disease Research Center, University of Wisconsin, Madison, WI, United States*
[2]*Department of Medical Physics, University of Wisconsin, Madison, WI, United States*
[3]*Wisconsin Alzheimer's Institute, University of Wisconsin, Madison, WI, United States*
[4]*Department of Psychiatry and Neurochemistry, Institute of Neuroscience and Physiology, the Sahlgrenska Academy at the University of Gothenburg, Mölndal, Sweden*
[5]*Geriatric Research Education and Clinical Center, William S. Middleton Veterans Hospital, Madison, WI, United States*
[6]*Department of Neurodegenerative Disease, University College London Institute of Neurology, London, United Kingdom*
[7]*UK Dementia Research Institute at University College London, London, United Kingdom*
[8]*Hong Kong Center for Neurodegenerative Diseases, Hong Kong, CN*

Background: Tau hyperphosphorylation in Alzheimer's disease (AD) impairs axonal function, impacting transport of synaptic vesicles and potentially leads to synaptic dysfunction. Phosphorylated tau (pTau) highly colocalizes with synaptosomes in the entorhinal cortex (ERC) and hippocampus (Fein et al, 2008), and the presence of pTau may contribute to AD-related synaptic loss. However, the relationship between plasma pTau epitopes (181, 231, and 217) and synaptic density is unknown. Here, we present preliminary examinations of this relationship.

Methods: 12 participants (Table), recruited from the Wisconsin Registry for Alzheimer's Prevention study, underwent blood sampling for measurement of plasma pTau, our proposed metric for secreted tau, and [C-11]UCB-J PET imaging to assess synaptic density in regions known to show early AD tau accumulation. Synaptic density was quantified using [C-11]UCB-J $DVR_{LGA,\ Whole\ Cb}$, and regions of interest (ROIs; hippocampus, ERC, and fusiform gyrus) identified following *FreeSurfer* T1w-MRI parcellation. Plasma pTau181 and pTau231 were measured using a single molecule array (Simoa) assay on Quanterix. Plasma pTau217 was measured on the Quanterix HD-X platform using the ALZpath assay. We utilized Pearson correlation analysis to examine the strength and direction of the relationship between synaptic density and pTau epitopes.

Results: Plasma pTau epitopes negatively correlated with UCB-J DVR across all ROIs (Figure), but the effect sizes (magnitude of correlations) varied. Plasma pTau181 exhibited large and medium correlations in the hippocampus ($r = -0.59$), ERC ($r = -0.44$), and fusiform gyrus ($r = -0.45$). Plasma pTau231 and pTau217 showed medium and small correlations, respectively.

Conclusions: The large and moderate effect sizes for pTau181 and pTau231 underscores the potential impact of secreted pTau and pathological aggregation of tau on synaptic loss in regions vulnerable to tau tangle formation, particularly the hippocampus. Plasma analysis is ongoing in a larger sample of participants with [C-11]UCB-J PET to further elucidate these processes.

Table. Sample characteristics.

Characteristic	N = 12
Female, %	50 %
Race, *n*	
White	10
Black or African American	2
Age at synaptic PET scan, *years*	72.9 ± 5.37
Years between synaptic PET and blood draw	4.32 ± 2.18
Amyloid PET positive, %	66.7 %
Cognitive Status, *n*	
Unimpaired	9
MCI	2
Dementia	1
Plasma pTau levels, *pg/mL*	
pTau181	2.94 ± 1.03
pTau231	13.9 ± 5.24
pTau217	0.79 ± 0.47
[C-11]UCB-J DVR in ROIs	
Hippocampus	0.97 ± 0.08
Entorhinal Cortex	1.03 ± 0.15
Fusiform Gyrus	1.20 ± 0.11

Values are provided as mean±standard deviation unless noted otherwise.

Time between synaptic PET scan and the blood draw was calculated from taking the absolute value difference in age of the participant at the time of each procedure. Amyloid positivity was determined through [C-11]PiB PET scans with DVR ≥ 1.19 across 8 bilateral regions known to have amyloid plaque accumulation: medial orbital frontal, anterior cingulate, posterior cingulate, precuneus, angular, supramarginal, superior temporal and middle temporal gyri (Sprecher et al, 2015). Abbreviations: PET = positron emission tomography; MCI = mild cognitive impairment; pTau = phosphorylated tau; pTau181 = tau phosphorylated at amino acid residue 181; pTau231 = tau phosphorylated at amino acid residue 231; pTau217 = tau phosphorylated at amino acid residue 217; DVR = distribution volume ratio; ROIs = regions of interest.

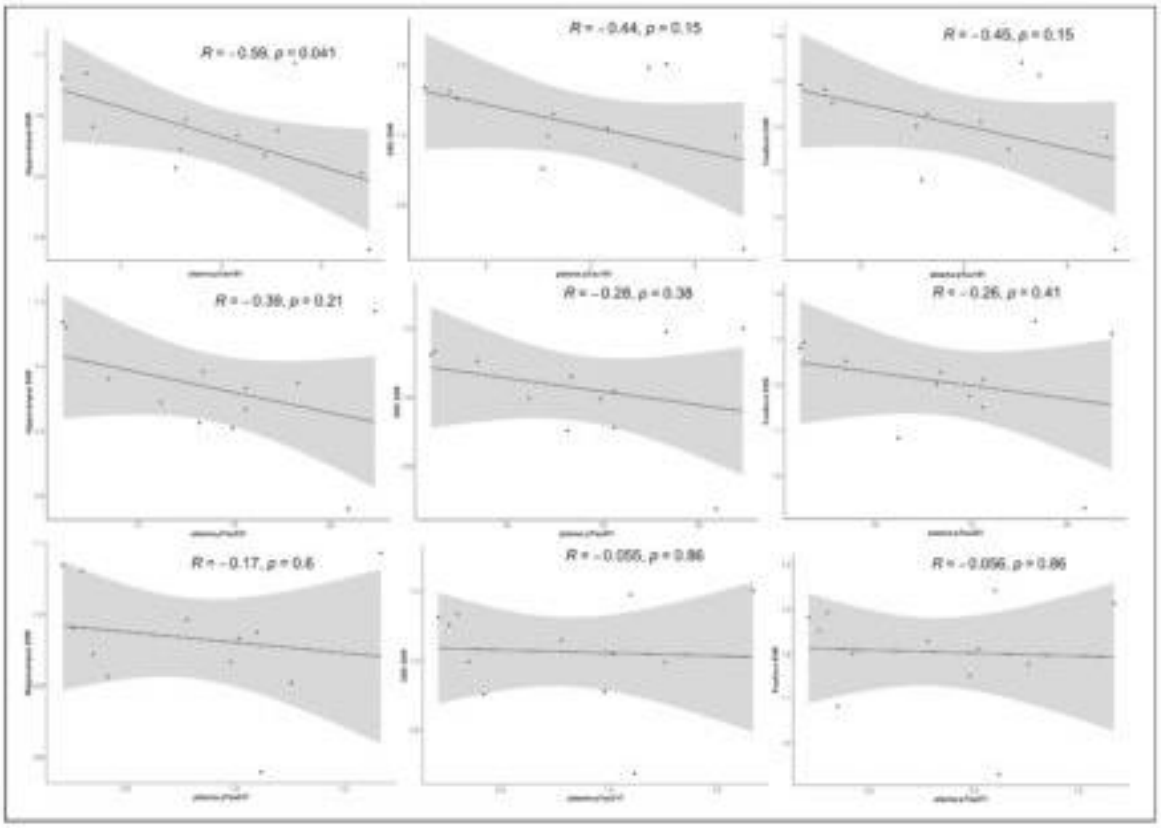

Figure. Correlations between plasma pTau epitopes and synaptic density.
This figure displays the relationship between [C-11]UCB-J DVR in the hippocampus (left column), entorhinal cortex (ERC; middle column) and fusiform gyrus (right column) with pTau181 (top row), pTau231 (middle row), and pTau217 (bottom row). Plasma pTau181 was significantly negatively correlated with hippocampus DVR. Though not significant, all other relationships were in the negative direction suggesting that higher plasma pTau concentrations associated with lower synaptic density.

Keywords: plasma, synapses, UCB-J PET, hippocampus

108 "Treatment Related Amyloid Clearance" (TRAC): a framework to characterize a new biomarker state in the era of anti-amyloid therapies

Renaud La Joie[1], Claire Sexton[2], Jeffrey L Cummings[3], Douglas Galasko[4], Milos Ikonomovic[5,6,7], Susan M Landau[8], Jorge Llibre-Guerra[9], Catherine Mummery[10], Rik Ossenkoppele[11], Julie Price[12], Shannon L Risacher[13,14], Ruben Smith[15,16], Christopher H. Van Dyck[17,18,19,20], Maria C. Carrillo[2]

[1]*Memory and Aging Center, Department of Neurology, University of California, San Francisco, San Francisco, CA, United States*
[2]*Alzheimer's Association, Chicago, IL, United States*
[3]*Chambers-Grundy Center for Transformative Neuroscience, Pam Quirk Brain Health and Biomarker Laboratory, Department of Brain Health, School of Integrated Health Sciences, University of Nevada, Las Vegas, Las Vegas, NV, United States*
[4]*Shiley-Marcos Alzheimer's Disease Research Center, Department of Neurosciences, University of California, San Diego, San Diego, CA, United States*
[5]*Department of Neurology, University of Pittsburgh, Pittsburgh, PA, United States*
[6]*Department of Psychiatry, University of Pittsburgh, Pittsburgh, PA, United States*
[7]*Geriatric Research Education and Clinical Center, VA Pittsburgh Healthcare System, Pittsburgh, PA, United States*
[8]*Hellen Wills Neuroscience Institute, University of California, Berkeley, Berkeley, CA, United States*
[9]*Department of Neurology, Washington University in St Louis, St Louis, MO, United States*
[10]*Dementia Research Centre, National Hospital for Neurology and Neurosurgery, University College London, London, UK*
[11]*Department of Neurology and Alzheimer Center, VU University Medical Center, Neuroscience Campus Amsterdam, Amsterdam, The Netherlands*
[12]*Massachusetts General Hospital/Harvard Medical School, Charlestown, MA, United States*
[13]*Department of Radiology and Imaging Sciences, Indiana University School of Medicine, Indianapolis, IN, United States*
[14]*Indiana Alzheimer's Disease Research Center, Indianapolis, IN, United States*
[15]*Clinical Memory Research Unit, Lund University, Lund, Sweden*
[16]*Department of Neurology, Skåne University Hospital,, Lund, Sweden*
[17]*Alzheimer's Disease Research Unit, Yale University School of Medicine, New Haven, CT, United States*
[18]*Department of Psychiatry, Yale University School of Medicine, New Haven, CT, United States*
[19]*Department of Neuroscience, Yale University School of Medicine, New Haven, CT, United States*
[20]*Department of Neurology, Yale University School of Medicine, New Haven, CT, United States*

Background. Amyloid-targeting therapies impact amyloid-PET levels. In many cases, PET signal drops below a positivity threshold: the amyloid biomarker is "negative". With the FDA approval of anti-amyloid therapies, there is a need to better define this new group of patients with treatment-induced changes in amyloid biomarkers to standardize research and ultimately improve patient care and management. This framework aims to standardize biomarker-based classification and data reporting for clinical trials and ongoing observational studies that enroll patients treated with anti-amyloid therapies.

Methods. The Alzheimer's Association gathered a group of expert clinicians and scientists to summarize the current knowledge on patients with amyloid biomarkers impacted by anti-amyloid therapies, identify gaps in knowledge, and make recommendations on the naming and operationalization of this entity in future studies.

Results. We suggest referring to this new biomarker state as "Treatment Related Amyloid Clearance" (TRAC). We propose a three-tier system (Figure 1) that complements the Revised Criteria for Diagnosis and Staging of Alzheimer's Disease ("AT(N) framework") to distinguish patients with: a negative amyloid-PET after treatment, i.e. full TRAC or A-(TRAC); a significant but incomplete reduction of amyloid-PET, i.e. partial TRAC or A+(TRAC); no

significant effect on amyloid-PET, i.e. A+(no TRAC). The specific approach to distinguish full versus partial TRAC is to be determined by investigators but we recommend using thresholds in the 15-25 CL range based on existing literature. We encourage investigators to report clinical, neuropathological, and other biomarker outcomes for these different tiers of patients.

Conclusions. This classification is originally meant to be based on amyloid-PET, as PET has been used as a gold standard and surrogate marker in trials. However, future versions of this framework might be based on fluid biomarkers to define these groups. Feedback from the broader community is sought to finalize workgroup recommendations.

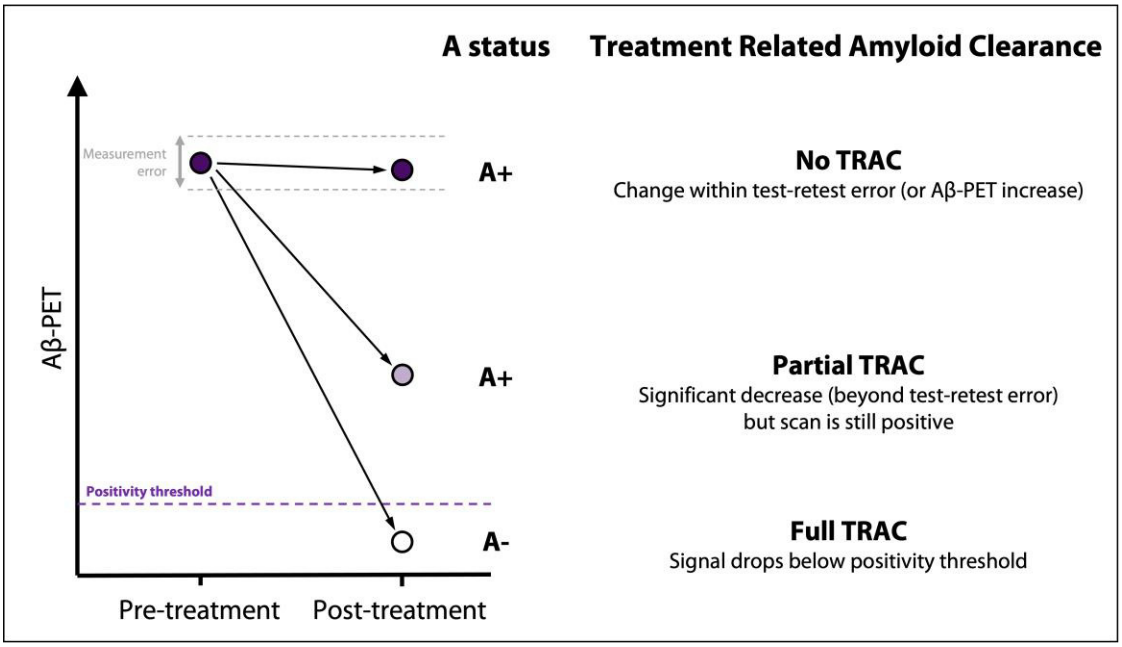

Keywords: Clinical trials, amyloid-PET, treatment, centiloids, AT(N)

109 Alzheimer's disease biological PET staging using plasma p217+tau

Azadeh Feizpour[1,2], Vincent Doré[2,3], Natasha Krishnadas[1,2], Pierrick Bourgeat[4], James D. Doecke[4], Ziad S. Saad[5], Gallen Triana-Baltzer[5], Simon M. Laws[6], Rosita Shishegar[3], Kun Huang[2], Christopher Fowler[1], Larry Ward[1], Colin L. Masters[1], Jurgen Fripp[4], Hartmuth C. Kolb[5], Victor L. Villemagne[2,7], Christopher C. Rowe[1,2,8]

[1]*The Florey Institute of Neuroscience and Mental Health, The University of Melbourne, Melbourne, Australia*
[2]*Department of Molecular Imaging & Therapy, Austin Health, Melbourne, Australia*
[3]*The Australian e-Health Research Centre, CSIRO, Melbourne, Melbourne, Australia*
[4]*The Australian e-Health Research Centre, CSIRO, Brisbane, Brisbane, Australia*
[5]*Neuroscience Biomarkers, Janssen Research and Development, La Jolla, CA, United States*
[6]*Centre of Excellence for Alzheimer's Disease Research and Care, School of Medical and Health Sciences, Edith Cowan University, Joondalup, Australia*
[7]*Department of Psychiatry, University of Pittsburgh, Pittsburgh, PA, United States*
[8]*Florey Department of Neuroscience and Mental Health, The University of Melbourne, Melbourne, Australia*

Background: Plasma phospho-tau biomarkers, such as p217+tau, excel at identifying Alzheimer's Disease (AD) neuropathology. However, questions remain regarding their capacity to inform AD biological PET stages at group level and maintain the same precision at individual patient level.

Method: Participants included 274 cognitively unimpaired (CU) and 225 cognitively impaired (CI) individuals, with plasma p217+tau Simoa® assay, ^{18}F-MK6240 tau PET (T) and ^{18}F-NAV4694 Aβ PET (A) data. Biological PET stages were defined based on the draft NIA-AA Revised Criteria (July 2023): Initial (A+T-), Early (A+$T_{MTL\ ONLY}$), Intermediate (A+$T_{MODERATE\ neocortical}$), and Advanced (A+$T_{HIGH\ neocortical}$). We used thresholds for A+ and T_{HIGH} of 25 Centiloid and 80 Centaur (2.68 SUVR), respectively. Adding an A-T- stage for comparison, we assessed the performance of p217+tau in discriminating between these stages at the group level using Receiver Operating Characteristic (ROC) analysis and at the individual level using logistic regression.

Results: Plasma p217+tau concentrations increased across the stages, with significant differences between them all, except for the Initial and Early stages. Screening for Advanced (*vs.* lower stages), combined Intermediate/Advanced (*vs.* lower stages), or all stages (*vs.* A-T-), p217+tau showed good group-level discriminations (AUC 0.91, 0.92 and 0.92; CI only: AUC 0.84, 0.89, 0.93, respectively). At the individual level, the likelihood of PET stage *vs.* p217+tau level (Figure 1) showed good discrimination of A-T- vs any A+ stage and of combined Intermediate/Advanced disease stage vs lower stages in the CI.

Conclusion: In addition to accurately screening for A+ individuals, plasma p217+tau shows promise for separating persons with either Intermediate or Advanced stage AD from those at a lower stage.

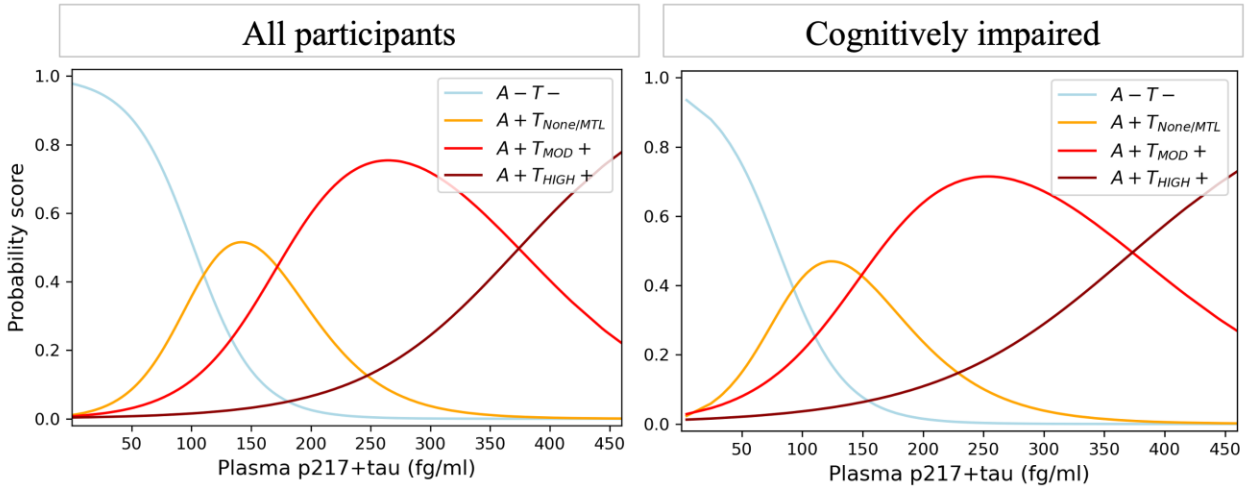

Logistic regression probability scores vs. plasma p217+tau concentration values. Cognitively unimpaired and cognitively impaired combined, on the left. Cognitively impaired-only on the right. Probability score: likelihood of a PET stage at any given p217+tau value.

Keywords: Plasma phospho-tau, Neuroimaging, Disease staging, Tau, Amyloid

110 Plasma p-tau217 outperforms [18F]FDG-PET in identifying biological Alzheimer's disease in atypical and early-onset dementia

Kely Quispialaya[1,3,4], Joseph Joseph Therriault[1,2,3], Antonio Aliaga[1,11], Andrea L. Benedet[1,7], Nicholas J. Ashton[7,8], Thomas K. Karikari[7,13], Arthur C. Macedo[1,2,3], Nesrine Rahmouni[1,3], Jenna Stevenson[1], Cécile Tissot[1,2], Jaime Fernandez Arias[1,2,3], Yi-Ting Wang[1,2,3], Seyyed Ali Hosseini[1,2,3], Bertrand Jean-Claude[4], Tharick Pascoal[13], Serge Gauthier[1,2,6], Brian M. Gilfix[5], Paolo Vitali[1], Jean-Paul Soucy[2,3], Henrik Zetterberg[7,9,14,15,16,17], Kaj Blennow[7,9], Eduardo R. Zimmer[1,10,11,12], Pedro Rosa-Neto[1,2,3,4,6]

[1]*Translational Neuroimaging Laboratory, The McGill University Research Centre for Studies in Aging, Douglas Hospital, McGill University, Montréal, QC, Canada*
[2]*Department of Neurology and Neurosurgery, McGill University, Montréal, QC, Canada*
[3]*Montreal Neurological Institute, Montréal, QC, Canada*
[4]*Department of Experimental Medicine, McGill University, Montréal, QC, Canada*
[5]*Department of Specialized Medicine, McGill University, Montréal, QC, Canada*
[6]*Department of Psychiatry, McGill University, Montréal, QC, Canada*
[7]*Department of Psychiatry and Neurochemistry, Institute of Neuroscience and Physiology, The Sahlgrenska Academy, University of Gothenburg, Mölndal, Sweden*
[8]*Wallenberg Centre for Molecular Medicine, University of Gothenburg, Gothenburg, Sweden*
[9]*Clinical Neurochemistry Laboratory, Sahlgrenska University Hospital, Mölndal, Sweden*
[10]*Department of Pharmacology, Universidade Federal do Rio Grande do Sul, Porto Alegre, Brazil*
[11]*Graduate Program in Biological Sciences: Biochemistry (PPGBioq) and Pharmacology and Therapeutics (PPGFT), Universidade Federal do Rio Grande do Sul, Porto Alegre, Brazil*
[12]*Brain Institute of Rio Grande do Sul, PUCRS, Porto Alegre, Brazil*
[13]*Department of Neurology and Psychiatry, University of Pittsburgh School of Medicine, Pittsburgh, PA, United States*
[14]*Department of Neurodegenerative Disease, UCL Institute of Neurology, Queen Square, London, UK., London, United Kingdom*
[15]*UK Dementia Research Institute at UCL, London, United Kingdom*
[16]*Hong Kong Center for Neurodegenerative Diseases, Clear Water Bay, Hong Kong, China*
[17]*Wisconsin Alzheimer's Disease Research Center, University of Wisconsin School of Medicine and Public Health, University of Wisconsin-Madison, Madison, WI, United States*

Objective: To compare the correspondence of an ultrasensitive plasma assay for p-tau217 and visual assessments of [18F]FDG-PET by expert raters with Alzheimer's disease (AD) pathological changes measured with CSF and amyloid-PET.

Methods: We conducted a retrospective analysis of individuals with atypical and/or early-onset dementia who were assessed at a specialized memory clinic. All participants underwent CSF evaluations to measure Aβ42, phosphorylated tau (P-tau181), and total tau levels, brain [18F]FDG-PET scans, plasma p-tau217, and amyloid-PET. The [18F]FDG-PET data were visually examined by two nuclear medicine experts to determine whether they were indicative of AD and CSF biomarker results were categorized as either AD biomarker positive or negative. Contingency analysis was performed to assess the relationships between the PET scan interpretations and CSF biomarker groupings. CSF biomarker groupings were treated as the reference standard.

Results: 75 subjects with early-onset or atypical dementia had CSF AD biomarker evaluations, amyloid-PET, [18F]FDG-PET ratings, and plasma p-tau217 assessments. Both [18F]FDG-PET and plasma p-tau217 had high levels of agreement with reference standard CSF AD biomarkers ([18F]FDG-PET: 69%; plasma p-tau217:81%). Although both biomarkers had similar specificity for AD ([18F]FDG-PET: 67%, plasma p-tau217 70%), plasma p-tau217 had higher sensitivity for abnormal CSF AD biomarkers (97%). Overall accuracy was also higher for plasma p-tau217 (AUC=83%, 95%CI = 0.74- 0.83). The same pattern of results was observed when using amyloid-PET as the

reference standard.

Discussion: Our study provides evidence that plasma p-tau217 has excellent diagnostic performance for AD in individuals with early-onset or atypical dementia evaluated in specialized settings. The topographical information from [^{18}F]FDG-PET may give complementary information.

Keywords: Alzheimer's disease, Plasma p-tau217, [18F]FDG-PET

111 A-T+ PET participants in preclinical AD: clinical progression and concordance with fluid biomarkers

Yara Yakoub[1,2], Frédéric St-Onge[1,2], Alfonso Fajardo[1,2], Bery Mohammediyan[1], Christine Dery[1], Elisabeth Sylvain[1], Jennifer Tremblay-Mercier[1], Jordana Remz[1], Julie Gonneaud[3], Jacob Vogel[4], Jean-Paul Soucy[5], Alexa Pichet-Binette[4], Sylvia Villleneuve[1,5,6], PREVENT-AD Research Group[1]

[1]*Douglas Mental Health University Institute, Montreal, QC, Canada*
[2]*Integrated Program in Neuroscience, Faculty of medicine, McGill University, Montreal, QC, Canada*
[3]*Normandie Univ, UNICAEN, INSERM, U1237, PhIND "Physiopathology and Imaging of Neurological Disorders", NeuroPresage Team, Caen, France*
[4]*Clinical Memory Research Unit, Department of Clinical Sciences Malmö, Lund, Sweden*
[5]*Montreal Neurological Institute, McGill University, Montreal, QC, Canada*
[6]*Department of Psychiatry, Faculty of medicine, McGill University, Montreal, QC, Canada*

Introduction: Amyloid-negative tau-positive PET (A-T+) participants have been reported in several studies. We assessed the prevalence and characteristics of A-T+ participants in a cohort of cognitively unimpaired individuals with a first-degree family history of AD dementia.

Methods: We studied 250 participants from the longitudinal PREVENT-AD cohort (mean cognitive follow-up = 7.73 years, SD = 1.72) who received an amyloid (^{18}F-NAV4694) and a tau (^{18}F-Flortaucipir) PET-scan. The amyloid-positivity threshold was 19 centiloids (SUVR=1.25) and tau positive threshold was set as 2SD above the mean of A- participants in a temporal meta-ROI (SUVR=1.27). Follow-up PET scans were available for 105 participants. We characterized A-T+ participants on clinical (age, sex, *APOE4* status, education, depression, apathy, anxiety, sleep), cognitive (RBANS, MMSE, ECoG) and fluid (CSF, plasma) measurements.

Results: In the PREVENT-AD cohort, only 3 (1.2%) of all studied participants were classified as A-T+ (see **Table 1** for participants characteristics). Participants 1 and 2 were positive based on plasma $A\beta_{42/40}$ and they had relatively low levels of tau binding that could represent early pathology. Participant 3 was also positive based on CSF and plasma, her Aβ-PET scan was classified as positive on visual read and became quantitatively positive at follow-up. Participant 3 had extensive unilateral tau binding at baseline that became bilateral at follow-up (**Figure 1**). **Figure 2** details the longitudinal cognitive trajectory of Participant 3. During the cognitive follow-up, participants 1 developed mild cognitive impairment and participant 3 developed dementia.

Conclusion: A-T+ individuals are rare in the PREVENT-AD cohort and the 3 A-T+ were classified as Aβ positive based on fluid biomarkers. One of the 3 A-T+ individuals showed a very fast clinical progression and a tau uptake pattern atypical of AD.

	PREVENT-AD	Participant 1	Participant 2	Participant 3
Demographics (n = 387)				
Age, at baseline	63.73 ± 5.23	62	73	63
Sex, F (%)	277 (71.58)	0	1	1
Education, years	15.45 ± 3.38	15 (-0.13)	19 (1.05)	11 (-1.32)
*APOE*4 carriers (%)	147 (37.98)	0	0	1
PET (n = 250)				
Aβ SUVR at BL	1.29 ± 0.30	1.21 (-0.26)	1.14 (- 0.50)	1.22 (-0.23)
Aβ SUVR at FU	1.32 ± 0.36	---	---	1.28 (-0.09)
Tau SUVR at BL	1.16 ± 0.12	**1.39 (1.94)**	1.32 (1.32)	**1.56 (3.37)**
Tau SUVR at FU	1.17 ± 0.16	---	------	**2.06 (5.49)**
CSF (n = 76)				
Aβ42/40	0.06 ± 0.02	NA	NA	**0.02 (-2.22)**
p-tau181 (pg/mL)	55.40 ± 22.97	NA	NA	79.16 (1.03)
Plasma (n = 374)				
Aβ42/40	0.07 ± 0.01	**0.04 (-2.22)**	0.06 (-0.51)	0.07 (-0.05)
p-tau181 (pg/mL)	7.09 ± 5.37	3.42 (-0.68)	6.53 (-0.10)	9.08 (0.37)
NfL(pg/mL)	16.43 ± 7.15	15.62 (-0.11)	20.47 (0.56)	20.97 (0.63)
GFAP (pg/mL)	107.46 ± 64.72	58.09 (-0.76)	78.53 (-0.45)	**336.41 (3.54)**
Cognitive scores (n = 387)				
RBANS at BL	102.41 ± 10.35	93 (-0.91)	93 (-0.91)	**86 (-1.59)**
RBANS at last clinical FU	99.74 ± 11.09	92 (-0.7)	96 (-0.34)	**65 (-3.13)**
MMSE at first PET visit	28.68 ± 1.43	**26 (-1.88)**	30 (0.92)	29 (0.22)
ECog at BL	1.18 ± 0.19	1.38 (1.12)	1 (-0.96)	1.13 (-0.26)
Neuropsychiatric factors (n = 339)				
Depression	1.56 ± 2.16	9 (3.45)	0 (-0.72)	0 (-0.72)
Apathy	26.17 ± 6.61	30 (0.58)	23 (-0.48)	28 (0.28)
Anxiety	2.79 ± 4.19	5 (0.53)	0 (-0.67)	7.37 (1.1)
Sleep measures (n = 230)				
PSQI	5.27 ± 3.22	5 (-0.08)	8 (0.85)	7 (0.54)
Sleep efficiency, %	86.7 ± 5.82	90.78 (0.7)	92.28 (0.96)	**73.38 (-2.29)**

Table 1. Mean ± standard deviation of the PREVENT-AD total cohort and the values and (z-score) of the 3 A-T+ participants across demographics, cognitive, and biomarker measurements. *Notes*: Aβ-PET SUVR represents amyloid index values; Tau-PET represents the average of the temporal meta-ROI (comprising the bilateral entorhinal cortex, amygdala, parahippocampal gyrus, fusiform gyrus, and inferior and middle temporal gyri). Values in bold represent z-scores below 1.5 SD. Depression is measured using geriatric depression scale; apathy is measured using apathy evaluation scale; and anxiety is measured using geriatric anxiety inventory. Clinical variables were acquired upon entry to the program. CSF, plasma, and sleep measurements reported in the table were taken closest to the first PET scan. RBANS scores from the baseline visit and the last time point are reported. A score of 100 represents the average of participants of the same age, and 15 points below the average represents 1.5 SD. ECog scores from the baseline visit are reported. Threshold for Aβ-PET = 1.25; Tau-PET = 1.27; CSF $A\beta_{42/40}$ = 0.061; CSF p-tau181 = 77 pg/mL; plasma $A\beta_{42/40}$ = 0.07; plasma p-tau181 = 9.27 pg/mL. *Abbreviations*: F = female; APOE = apolipoprotein-E genotype; PET = positron emission tomography; SUVR = Standardized Uptake Value Ratio; BL = baseline and refers to the first visit following the eligibility visit; FU = follow-up; CSF = cerebrospinal fluid; NfL = neurofilament light; GFAP = glial fibrilly acidic protein; RBANS = Repeatable Battery for the Assessment of Neuropsychological status; MMSE = Mini-Mental State Examination; ECog = Everyday Cognition scale; PSQI = Pittsburgh Sleep Quality Index.

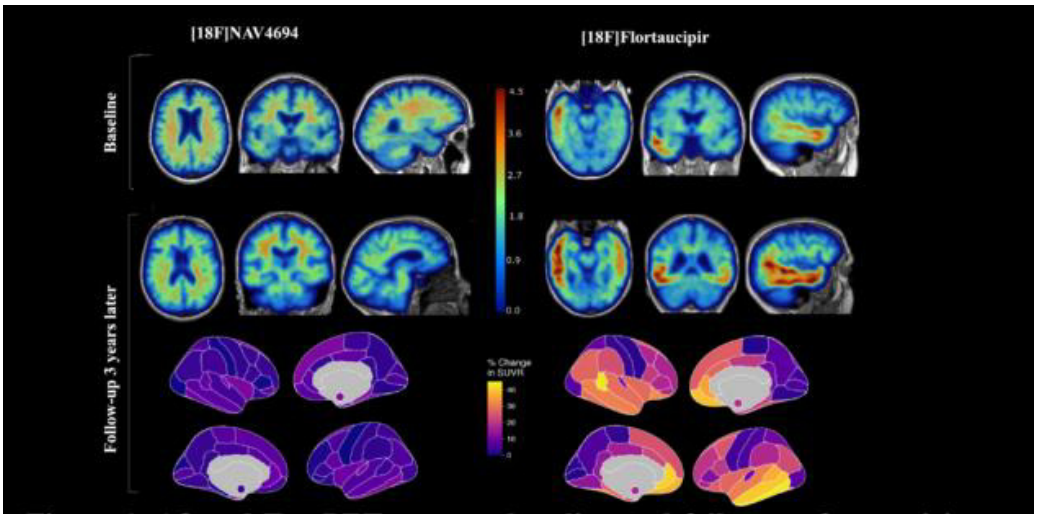

Figure 1. Aβ and Tau-PET scans at baseline and follow-up for participant 3. The left panel shows Aβ-PET scan at baseline and follow-up as well as the percentage of change in each region over the 3 year follow-up. The mean slope in Aβ-PET is 0.02 per year with a 5.44% difference in Aβ uptake between the two scans. The right panel shows tau-PET scan at baseline and follow-up, as the percentage of change in each region over the same follow-up length. The mean slope of tau is 0.1 (0.08) across regions with 19.96 % change between scans, exceeding 40% change in the right bankssts, frontalpole, left inferior temporal and rostral anterior cingulate regions. *Notes*: in both brain maps, bilateral amygdalae are represented by small colored circles in the medial view of the brain.

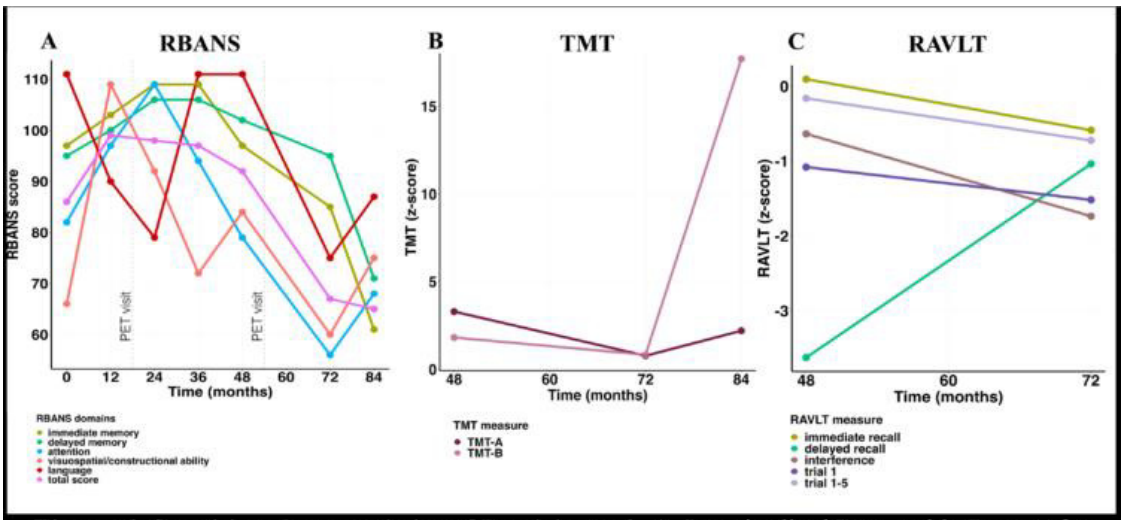

Figure. 2 Cognitive characteristics of Participant 3. A. Longitudinal Repeatable Battery for the Assessment of Neuropsychological Status (RBANS) domains (immediate memory, delayed memory, attention, visuospatial ability, and language subscales) and total score are presented. B. Trail Making Test scores with two parts: TMT-A (speed) and TMT-B (executive functioning) are presented, positive z-scores represents worse performance. C. Rey Auditory Verbal Learning Test scores and domains (immediate recall, delayed recall, interference, trial 1, and trial (1-5)), negative z-scores represents worse performance. Notes: Both TMT and RAVLT are shown in z scores. Dash lines in (A) represent the PET visits at baseline and at follow-up. This participant is now classified as having dementia.

Keywords: Tau, Amyloid, PET, Cognition, AD

112 Neighborhood disadvantage and the association between imaging biomarkers of Alzheimer's disease and cognition in a cohort of diverse older adults

Erica K. Fan[1,7], Sarah K. Royse[2], Beth E. Snitz[3], Alexandria C. Reese[2], Thomas K. Karikari[4], Tharick A. Pascoal[4], C. Elizabeth Shaaban[1], Rebecca E. Roush[3], Katey Potopenko[6], Geraldine Cisneros[6], Jay Kotulsky[6], M. Ilyas Kamboh[5], Brian J. Lopresti[2], Victor L. Villemagne[4], Oscar L. Lopez[3,4], James T. Becker[3,4,6], Ann D. Cohen[4]

[1]*Department of Epidemiology, University of Pittsburgh, Pittsburgh, PA, United States*
[2]*Department of Radiology, University of Pittsburgh, Pittsburgh, PA, United States*
[3]*Department of Neurology, University of Pittsburgh, Pittsburgh, PA, United States*
[4]*Department of Psychiatry, University of Pittsburgh, Pittsburgh, PA, United States*
[5]*Department of Human Genetics, University of Pittsburgh, Pittsburgh, PA, United States*
[6]*Department of Psychology, University of Pittsburgh, Pittsburgh, PA, United States*
[7]*School of Medicine, University of Pittsburgh, Pittsburgh, PA, United States*

Introduction: Neuroimaging biomarkers of Alzheimer's disease (AD) are well-validated in non-Hispanic White populations. However, it remains unclear if and how these biomarkers are associated with cognition in non-White populations disproportionately affected by systemic socioeconomic discrimination.

Methods: We investigated whether neighborhood disadvantage modifies associations of neuroimaging biomarkers with cognition in a diverse cohort of 198 adults ≥50 years, 50% of whom are Black. Outcomes included cognitive impairment and neuropsychological test scores representing different cognitive domains. Predictors were indices of neurodegeneration, vascular damage, and brain amyloid burden, quantified using MR-based indices of cortical thickness and white matter hyperintensities (WMH) and [^{11}C]PiB-PET, respectively. We measured neighborhood disadvantage using area deprivation index (ADI), a composite measurement of socioeconomic conditions within a given census tract.

Results: We found that Black participants have significantly lower ADI on average suggesting that ADI is an appropriate measure for neighborhood-level structural racism (Figure 1). In linear models, higher ADI, neurodegeneration, and WMH were separately associated with worse cognition. We found an ADI*neurodegeneration interaction on delayed recall memory (p=0.08, Figure 2). Neurodegeneration-positive participants had worse story delayed recall compared to neurodegeneration-negative regardless of ADI (β=-1.57, p=0.01). In neurodegeneration-negative participants, higher ADI was associated with worse delayed recall (β=-0.04, p=0.004): those with a high ADI exhibited low delayed recall, comparable to neurodegeneration-positive participants. ADI was not associated with cognition in neurodegeneration-positive participants. WMH and ADI interacted in models of impairment, visual memory, and visual copy (interaction p's<0.10, Figure 3). In those with high ADI, greater WMH was associated with worse cognition (β=-0.30, p=0.02) while participants with low ADI scored well regardless of WMH volume.

Discussion: Taken together, the relationship between neuroimaging biomarkers and cognition differs by neighborhood socioeconomic conditions, highlighting the need for clinical strategies that acknowledge structural disadvantage and informing potential changes in AD screening and diagnosis in disadvantaged neighborhoods.

Figure 1: ADI by racialization

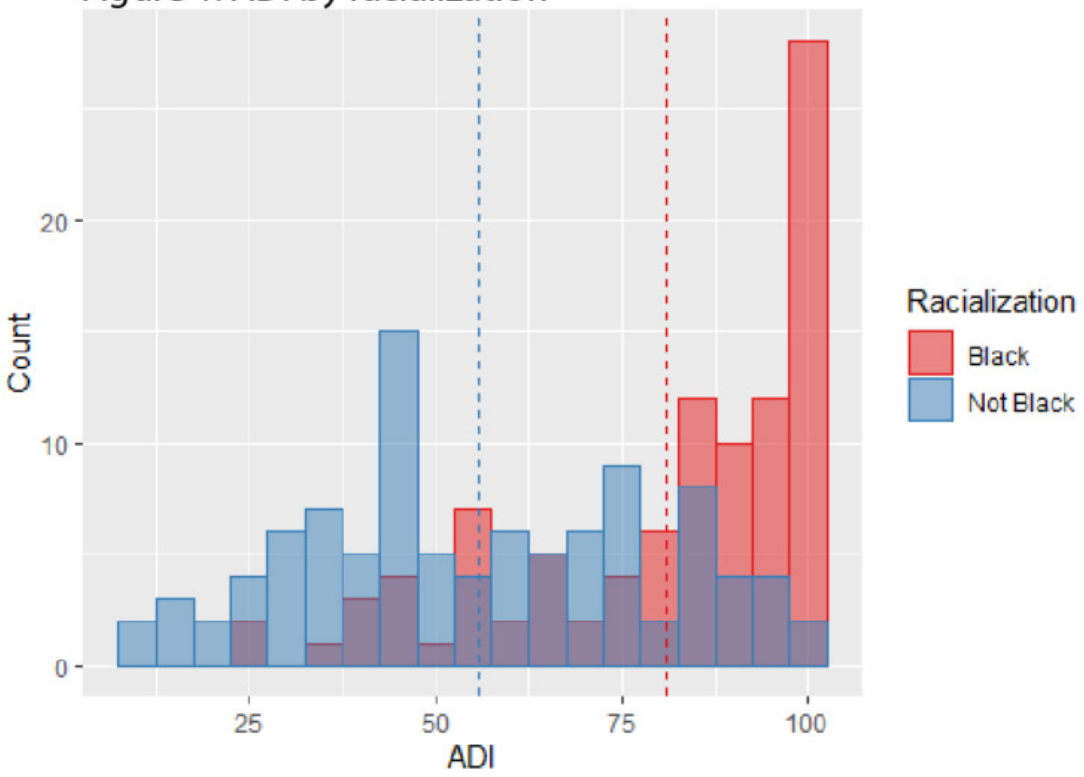

Figure 2: Interaction effect of ADI and N-status on delayed logical memory

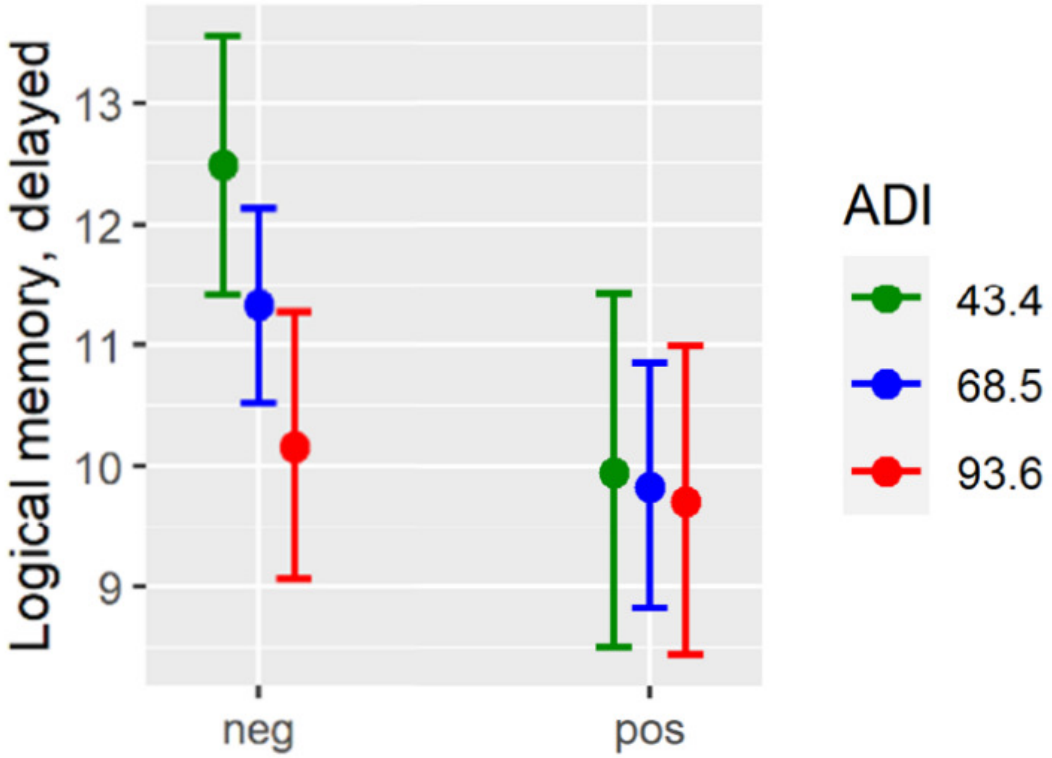

Figure 3: Interaction effect of WMH and ADI on impairment and Rey figure visual copy and memory

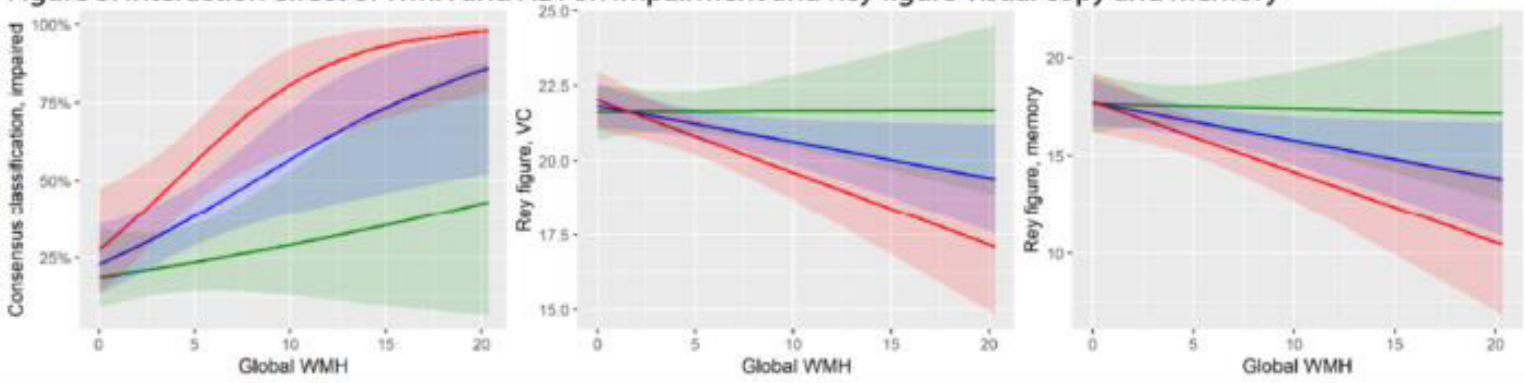

Keywords: biomarkers, cognition, census data, structural racism, epidemiology

113 Longitudinal association of mid-life ten year cardiovascular disease risk score with blood biomarkers of Alzheimer's disease and neurodegeneration: Heart SCORE Brain Study

Anum Saeed[1,2], Yue Fang Chang[1], Justin Swanson[3], Victor Villemagne[1], Beth Snitz[1], Sarah K. Royse[1], Brian Lopresti[1], Kevin Kip[1], Alexandria Reese[1], Alexandra Gogola[1], Tharick Pascoal[1,4], M. Ilyas Kamboh[1,4], Kaj Blennow[5], Henrik Zetterberg[5], Thomas Karikari[1,4], Oscar Lopez[1,4], Steven E. Reis[1,2], Ann D. Cohen[1]

[1]*University of Pittsburgh, Pittsburgh, PA, United States*
[2]*Heart and Vascular Institute, UPMC, Pittsburgh, PA, United States*
[3]*University of South Florida, Tampa, FL, United States*
[4]*Cognitive and Behavioral and Neurology Division, Pittsburgh, PA, United States*
[5]*University of Gothenburg, Gothenburg, Sweden*

Introduction: The role of Atherosclerotic cardiovascular disease (ASCVD) risk factors in preclinical Alzheimer's disease (AD) pathophysiology remains elusive. Here, we investigated relationships between mid-life 10-year ASCVD risk and late-life plasma and imaging AD biomarkers in a racially diverse cohort without dementia.

Methods: Participants enrolled in the Heart Strategies Concentrating on Risk Evaluation (Heart SCORE) study between 2003-2005 (mid-life) underwent brain PET scans for amyloid and tau [Pittsburgh Compound B (PiB) and Flortaucipir (FTP)], and collection of AD plasma biomarkers (SIMOA) of β-amyloid (Aβ42/40), tau (p-tau181, p-tau231), neurofilament light (NfL) and glial fibrillary acidic protein (GFAP) between 2020-22 (age >65 years, late-life). Mid-life 10-year ASCVD risk based on pooled cohort equations was categorized as borderline (5%-7.4%), intermediate (7.5%-19.9%), or high (≥20%). Blood biomarkers were log transformed and mean concentrations (±SD) calculated. Using linear regression, we determined associations between mid-life ASCVD risk (in continuous and categorical models) with late life biomarkers (beta coefficients±SE), stratified by racialization (self-identified White or Black).

Results: Compared to White participants (n=86), Black participants (n=37) had higher p-tau181 *(2.60±0.49 vs 2.85±0.68; p=0.02)* and p-tau231 *(1.99±0.59 vs 2.29±0.84; p=0.02)* while no statistically significant race-related differences were noted for Aβ42/40, GFAP and NfL.
Over a ~16y follow-up, midlife ASCVD risk was associated with late-life *NfL (2.45±0.69; p<0.001)*, p-tau181 *(2.64±0.83; p-0.002)* and p-tau231*(2.46±1.03; p=0.02)* but not Aβ42/40. When stratified by race, midlife ASCVD risk was only associated with late life NfL and p-tau181 in White participants but not those racialized as Black **(Table)**. No race-related differences were noted in PiB or FTP.

Conclusions: In this diverse non-demented cohort, we found differences in p-tau blood biomarkers between racialized groups. In addition, we found that ASCVD risk score in midlife may be an important predictor of future AD plasma biomarkers. However, its performance in ethnically different individuals warrants further investigation.

Table: Performance of mid-life atherosclerotic cardiovascular disease risk score with late-life plasma biomarkers of Alzheimer's disease and neurodegeneration in the Heart SCORE Brain Study

Model		Total Heart SCORE Brain Cohort (n=121)														
		GFAP			NfL			pTau181			pTau231			Ab42/40		
		b	*SE*	*p-value*	*b*	*SE*	*p-value*	*b*	*SE*	*p-value*	*b*	*SE*	*p-value*	*b*	*SE*	*p-value*
1	*Continuous*	0.50	0.84	0.56	**2.45**	**0.69**	**0.001**	**2.64**	**0.83**	**0.002**	**2.46**	**1.03**	**0.02**	0.01	0.38	0.99
2	*7.5% to <15%*	0.17	0.11	0.12	0.16	0.09	0.08	0.21	0.11	0.05	0.20	0.13	0.13	0.02	0.05	0.64
	>= 15%	-0.10	0.18	0.57	0.38	0.16	0.02	0.48	0.19	0.01	0.43	0.23	0.06	-0.05	0.08	0.58
		Self-identified White (n=84)														
		GFAP			NfL			pTau181			pTau231					
		b	*SE*	*p-value*	*b*	*SE*	*p-value*	*b*	*SE*	*p-value*	*b*	*SE*	*p-value*			
1	*Continuous*	0.08	0.10	0.41	**0.26**	**0.08**	**0.002**	**0.24**	**0.09**	**0.01**	0.18	0.11	0.09			
2	7.5% to<15%	0.18	0.14	0.18	0.15	0.11	0.18	0.14	0.12	0.23	0.07	0.14	0.64			
	>= 15%	0.10	0.26	0.70	0.57	0.21	0.01	0.49	0.23	0.03	0.34	0.27	0.21			
		Self-identified Black (n=37)														
		GFAP			NfL			pTau181			pTau231					
		b	*SE*	*p-value*	*b*	*SE*	*p-value*	*b*	*SE*	*p-value*	*b*	*SE*	*p-value*			
1	*Continuous*	0.01	0.12	0.93	0.17	0.10	0.12	0.14	0.15	0.37	0.18	0.19	0.34			
2	7.5% to<15%	0.12	0.20	0.55	0.15	0.17	0.39	0.21	0.25	0.41	0.32	0.31	0.32			
	>= 15%	-0.30	0.30	0.31	0.15	0.26	0.55	0.34	0.37	0.37	0.47	0.46	0.31			

**Regression coefficient was for 1SD (=0.0886) increment.*
Model 1= Continuous ASCVD risk score, Model 2= categories of ASCVD risk score
Abbreviations: atherosclerotic cardiovascular disease (ASCVD), plasma β-amyloid (Aβ) 42/40, tau (p-tau 181, 231), neurofilament light (NfL) and glial fibrillary acidic protein (GFAP)

Keywords: ASCVD risk, Alzheimer's disease biomarkers, plasma biomarkers, amyloid, tau

114 Comparison of FDG-PET in individuals with Down Syndrome and Dominantly Inherited Alzheimer Disease: genetic forms with elevated production of amyloid

Omar Abdelmoity[1], Julie Wisch[1], Brian Gordon[1], Shaney Flores[1], June Roman[1], Benjamin Handen[3], Bradley Christian[4], Elizabeth Head[2], Mark Mapstone[2], Sigan Hartley[4], Michael Rafii[5], Joseph Lee[6], Sharon Krinsky-McHale[7], Florence Lai[8], Diana Rosas[8], Shahid Zaman[9], Frederick Schmitt[10], Lauren Ptomey[11], Randall Bateman[1], Tammie Benzinger[1], Beau Ances[1]

[1]*Washington University in St. Louis, St. Louis, Missouri, St. Louis, MO, United States*
[2]*University of California, Irvine, Irvine, CA, Irvine, CA, United States*
[3]*University of Pittsburgh, Pittsburgh, PA, Pittsburgh, PA, United States*
[4]*University of Wisconsin, Madison, WI, Madison, WI, United States*
[5]*University of Southern California, Los Angeles, CA, Los Angeles, CA, United States*
[6]*Columbia University Irvin Medical Center, New York, NY, New York, NY, United States*
[7]*New York State Institute for Basic Research in Developmental Disabilities, Staten Island, NY, Staten Island, NY, United States*
[8]*Massachusetts General Hospital, Boston, MA, Boston, MA, United States*
[9]*University of Cambridge, Cambridge, UK, Cambridge, United Kingdom*
[10]*Sanders-Brown Center on Aging and the Kentucky Neuroscience Institute, Lexington, KY, Lexington, KY, United States*
[11]*University of Kansas Medical Center, Kansas City, KS, Kansas City, KS, United States*

Introduction: Fluorodeoxyglucose (FDG)-Positron Emission Tomography (PET) quantifies glucose metabolism, reflecting changes in neural activity. Two forms of genetically inherited Alzheimer Disease (AD) are Down Syndrome (DS) and Autosomal Dominant AD (ADAD). These forms provide models as to when an individual will develop AD. This study aimed to characterize brain glucose metabolism in genetically inherited AD groups.

Methods: This cross-sectional study included carriers of ADAD (N = 297) and familial controls (N = 199) enrolled in the Dominantly Inherited Alzheimer Network (DIAN) study and participants with DS (N = 76) enrolled in Alzheimer Biomarker Consortium-Down Syndrome (ABC-DS). Both FDG PET ([^{18}F]-FDG) and Amyloid PET ([^{11}C]-PiB or [^{18}F]-AV45) were acquired. We tested for group differences by form of AD and cognitive status using a summary region of FDG derived from the isthmus cingulate and inferior parietal normalized using the cerebellum. We evaluated changes in FDG-PET over time with respect to genetic form and amyloid using generalized additive models. Estimated years to symptom onset (EYO) was calculated based on parental age of onset for ADAD and age relative to 52.5 (previously published value) in DS.

Results: Participants with DS had lower FDG than controls or asymptomatic individuals with ADAD (Figure 1). Individuals with DS had significantly lower FDG than individuals with ADAD or controls at -20 EYO, while participants with ADAD had comparable FDG levels to controls until around -7 EYO (Figure 2). For all amyloid positive individuals (> 22.5 centiloids), amyloid was associated with a significant decline in FDG, even after correcting for age ($p = 0.02$) (Figure 3).

Conclusion: Low brain glucose metabolism in DS may initially reflect developmental differences rather than AD pathology. Preclinical AD pathology negatively associates with brain glucose metabolism in both DS and ADAD. FDG may have utility in identifying AD-related changes in ADAD at symptom onset.

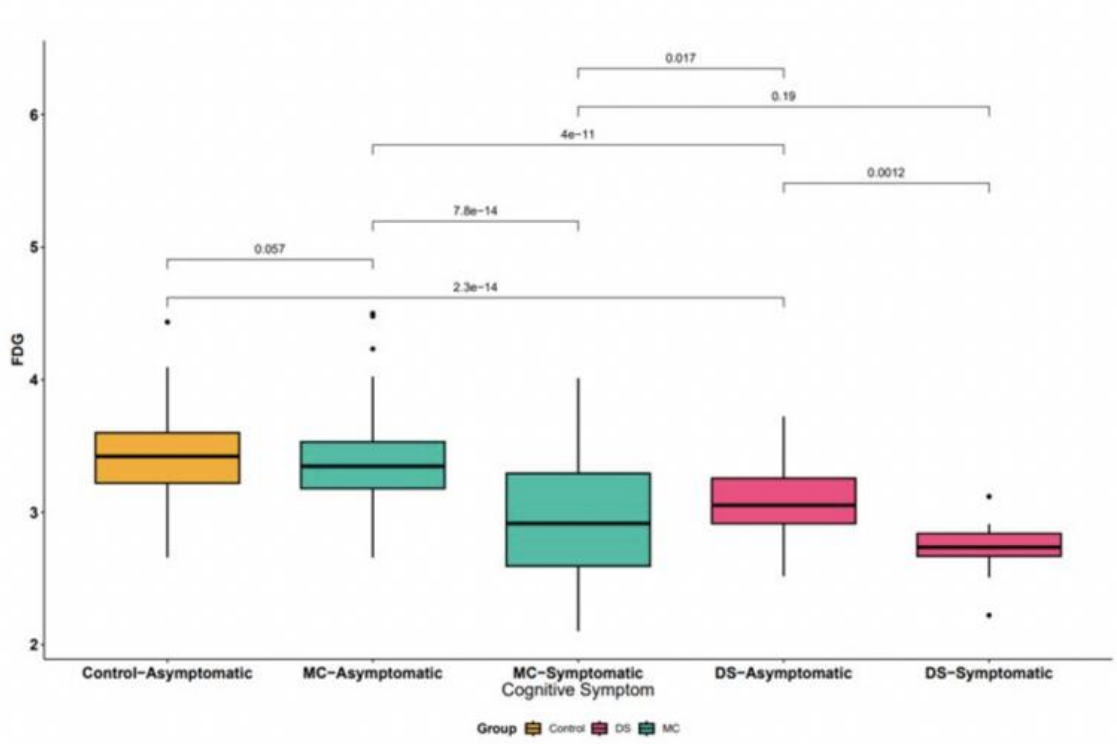

Figure 1. Summary FDG (Isthmus Cingulate & Inferior Parietal) differs by genetic group and cognitive status.

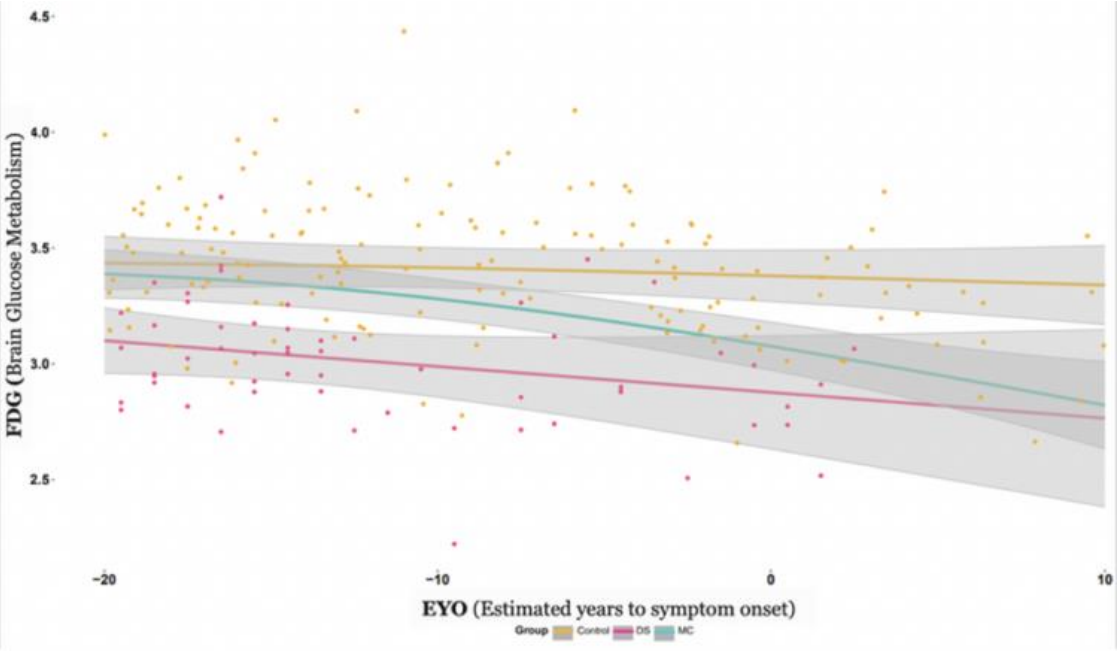

Figure 2. Nonlinear modeling of FDG over time shows that individuals with Autosomal Dominant Alzheimer Disease (ADAD) have comparable FDG levels to healthy controls until roughly 7 years prior to symptom onset (EYO). At this point, brain glucose metabolism rapidly declined. In contrast, individuals with Down Syndrome (DS) had persistently lower FDG as compared to controls. Around the time of symptom onset (EYO = 0) there was no difference in brain glucose metabolism in ADAD as compared to DS.

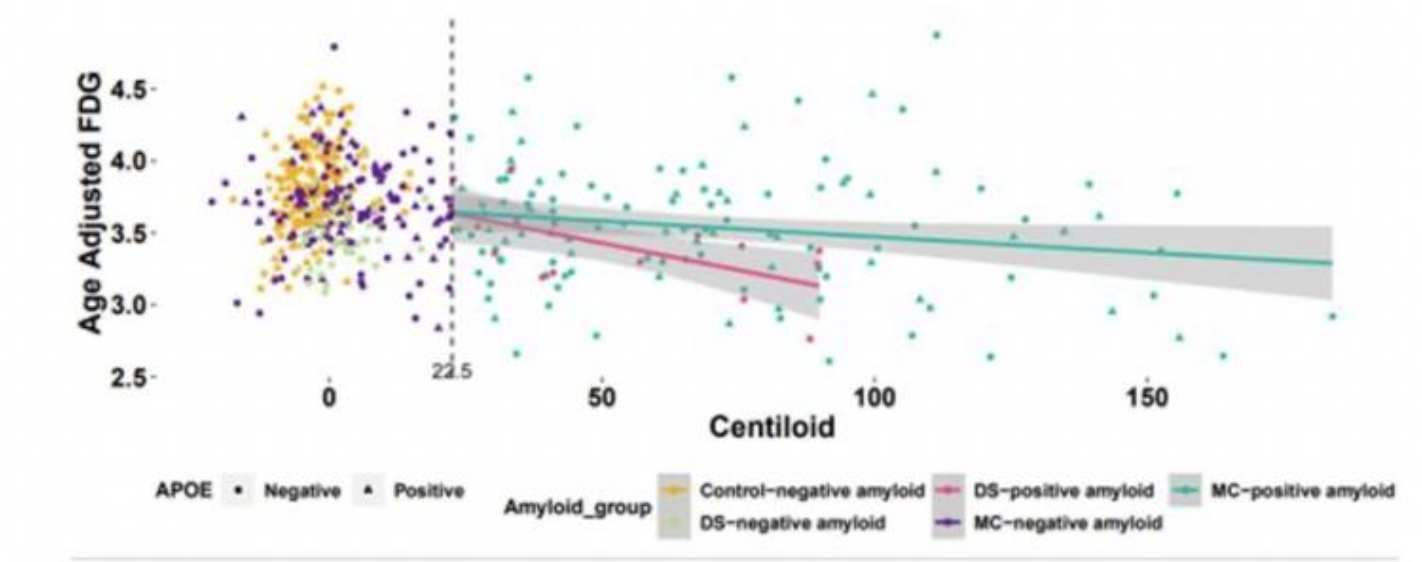

Figure 3. Increasing amyloid was negatively associated with brain glucose metabolism as measured by FDG for individuals with both Autosomal Dominant Alzheimer Disease (ADAD) as well as Down Syndrome (DS). This negative correlation persists even after controlling for age.

Keywords: Amyloid, Alzheimer's disease, FDG-PET, Down Syndrome, ADAD

115 Deep learning-based partial volume correction for tau PET imaging

Kuang Gong[1,2], Cristina Lois[2], Emma Thibault[2], Amal Tiss[2], Se-In Jang[2], Alex Becker[2], Julie Price[2], Georges El Fakhri[2], Keith Johnson[2]

[1]*Department of Biomedical Engineering, University of Florida, Gainesville, FL, United States*
[2]*Department of Radiology, Massachusetts General Hospital and Harvard Medical School, Boston, MA, United States*

Introduction: Due to partial volume effects (PVEs) caused by PET resolution limit, accurate recovery of tau retention patterns in thin cortical regions is difficult. This is especially true for early stages when the tau signal is weak. Furthermore, PVE is a confounding factor when assessing tau distribution in the trans-entorhinal cortex due to uptake in the meninges. In this work, we developed an unsupervised deep learning-based PVE correction method, named DIPRecon, to fully extract the pathophysiological information present in a tau scan.

Methods: For tau PET imaging, high-resolution training labels are difficult to obtain. We proposed an unsupervised learning framework, DIPRecon, where the patient's T1w MR image was utilized as the network input to provide the manifold constraint and the training objective function was solely constructed by the Poisson distribution assumption of PET raw data. Additionally, a kernel-method layer which utilized the MR image to provide nonlocal constraint, was embedded into the 3D U-net architecture to refine the final output. Data-driven event-by-event PET motion correction (MC) was embedded into the proposed framework. **Figure 1** shows the flowchart of the proposed network training procedure. To validate the effectiveness of the proposed method, one ^{18}F-MK-6240 dataset (70-90 min post-injection) of one AD patient acquired on the DMI PET/CT (GE) was utilized. The T1w MR image was acquired on the 3T Tim Trio (Siemens). FreeSurfer was used to identify the Braak stage-related cortices for quantification.

Results and Conclusions: Figure 2 shows three views of the results from different methods, the motion information derived and used in motion correction, and the regional quantification of different methods. Results show that the proposed DIPRecon method yielded increased tau cortical SUVR throughout the brain and significantly improved spatial resolution. In the future, we will perform more evaluations and group analyses based on datasets from different clinical groups.

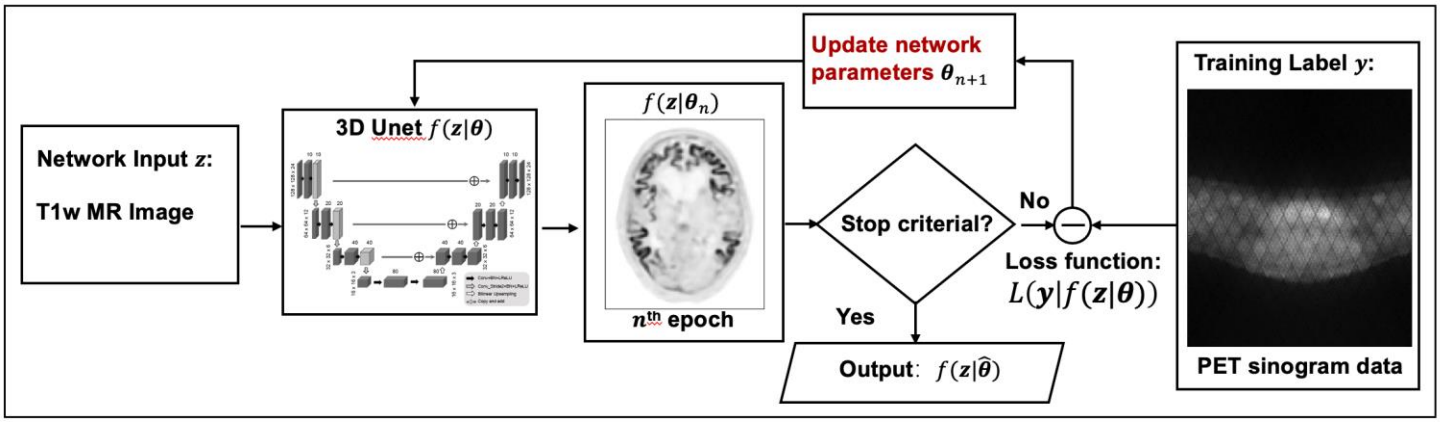

Figure 1. Flowchart of the proposed unsupervised deep learning-based partial volume correction method.

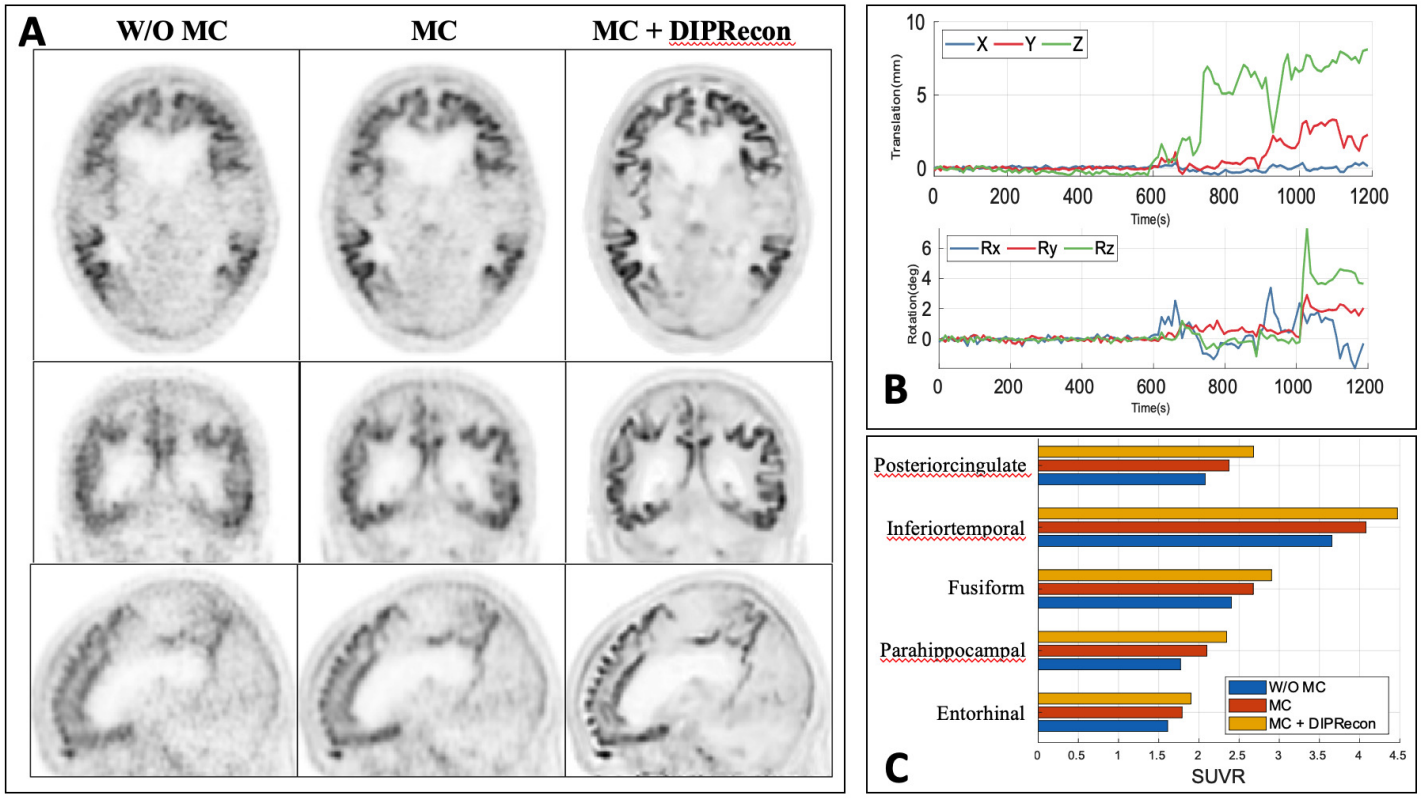

Figure 2. Results of the proposed method for one example 18F-MK-6240 dataset. (A) Visual comparison of images obtained with three different methods: original data (w/o MC), with motion correction (MC), and with the proposed method (MC+DIPRecon). (B) Derived rigid motion information for the whole 0-120 min dynamic scan. Data of 70-90 mins were used in this study; (C) Regional quantification for different methods.

Keywords: Partial volume correction, Tau PET imaging, Deep learning

116 Plasma levels of an N-terminal tau fragment predict core AD and neurodegenerative biomarkers in autosomal dominant Alzheimer's disease

Stephanie Schultz[1,2], Lei Liu[3,4], Beth Ostaszewski[3,4], Amirah Anderson[3,4], Celeste Karch[5], Carlos Cruchaga[5], Brian Gordon[5], Tammie Benzinger[5], Jason Hassenstab[5], John Morris[5], Richard Perrin[5], Alison Goate[6], Ricardo Allegri[7], Nicolas Barthelemy[5], Sarah Berman[8], Helena Chui[9], Martin Farlow[10], Nick Fox[11], Gregory Day[12], Mathias Jucker[14], Clifford Jack[15], Robert Koeppe[16], Jae-Hong Lee[17], Allan Levey[18], Johannes Levin[19], Ralph Martins[20], Hiroshi Mori[21], James Noble[22], Pedro Rosa-Neto[23], Steven Salloway[24], Rachel Sanchez[25], Peter Schofield[26], Eric McDade[5], Reisa Sperling[1,2,3], Dennis Selkoe[3,4], Randall Bateman[5], Jasmeer Chhatwal[1,2,3,4]

[1]*Massachusetts General Hospital, Boston, MA, United States*
[2]*Harvard Medical School, Boston, MA, United States*
[3]*Brigham and Women's Hospital, Boston, MA, United States*
[4]*Ann Romney Center for Neurologic Diseases, Boston, MA, United States*
[5]*Washington University in St. Louis School of Medicine, St. Louis, MO, United States*
[6]*Icahn School of Medicine at Mount Sinai, New York, NY, United States*
[7]*INEBA, Buenos Aires, AR*
[8]*University of Pittsburgh, Pittsburgh, PA, United States*
[9]*Keck School of Medicine, Los Angeles, CA, United States*
[10]*Indiana Alzheimer's Disease Research Center, Indianapolis, IN, United States*
[11]*Dementia Research Centre & UK Dementia Research Institute, UCL Institute of Neurology, London, United Kingdom*
[12]*Mayo Clinic, Jacksonville, FL, United States*
[13]*Universite College of Louvain, Brussels, Belgium*
[14]*German Center for Neurodegenerative Diseases, Tuebingen, Germany*
[15]*Mayo Clinic, Rochester, MN, United States*
[16]*University of Michigan, Ann Arbor, MI, United States*
[17]*University of Ulsan College of Medicine, Seoul, KP*
[18]*Emory, Atlanta, GA, United States*
[19]*German Center for Neurodegenerative Diseases, Munich, Germany*
[20]*Edith Cowan University, Joondalup, Australia*
[21]*Osaka City University Medical School, Osaka, Japan*
[22]*Columbia University, New York, NY, United States*
[23]*McGill University, Montreal, QC, Canada*
[24]*Butler Hospital, Providence, RI, United States*
[25]*Hospital Clínic de Barcelona, Barcelona, ES*
[26]*University of New South Wales, Sydney, Australia*

Background: Blood-based biomarkers that predict cognitive decline and AD pathology have the potential to accelerate AD therapeutic development and improve clinical care. Prior work suggests that plasma biomarkers of tau pathology (particularly post-translational modifications of tau) may be useful in diagnosis and risk stratification for AD-related neurodegeneration and cognitive decline. Levels of tau species lacking truncation of the N-terminal region, including plasma levels of N-terminal tau fragment 1 (NT1), have previously been shown to predict cognitive decline, neurodegeneration, and tau pathology in late-onset AD.

Methods: Here we examined NT1 as a possible predictor of cognitive (MMSE), clinical (Clinical Dementia Rating® Sum of Box [CDR-SB]), amyloid and tau (PiB-PET, CSF Ab42/40 and p-tau isoforms), and neurodegenerative (hippocampal volume and plasma NfL) trajectories in autosomal dominant AD (ADAD) using data from the Dominantly Inherited Alzheimer Network Observational Study (DIAN-Obs; Table 1). Plasma NT1 was measured using the Quanterix HD-X platform. PET, MRI, clinical, and biofluid measures were derived using previously

described procedures in DIAN-Obs.

Results: NT1 levels in mutation carriers (MC) increased across the disease continuum and become abnormal, compared to non-carriers, on average ~10 years before estimated symptom onset (EYO; Figure 1). Cross-sectionally and longitudinally, NT1 levels in MC were strongly associated with cognitive, clinical, tau, and neurodegeneration biomarkers, even after accounting for EYO (Figures 2-3). In contrast, NT1 levels were not associated with measures of beta-amyloid pathology after adjusting for EYO.

Conclusions: Plasma NT1 levels mirrored changes in clinical, cognitive, and neurodegenerative measures in ADAD, particularly in early symptomatic phases of disease. NT1 levels correlated with measures of tau, but were not strongly associated with measures of beta-amyloid pathology, unlike some previously studied tau measures. Together with supportive findings in sporadic AD, these results suggest that plasma NT1 may be a useful biomarker of AD-related tau pathology and neurodegeneration.

Table 1. Background Characteristics

Variable	N	Overall, N = 242[1]	Non-Carrier, N = 85[1]	Carrier, N = 157[1]	p-value[2]
Age (yrs)	242	40.8 (11.2)	41.8 (12.4)	40.2 (10.5)	0.5
Sex	242				0.064
Male		96 (40%)	27 (32%)	69 (44%)	
Female		146 (60%)	58 (68%)	88 (56%)	
APOE4	242				0.8
APOE4-		173 (71%)	60 (71%)	113 (72%)	
APOE4+		69 (29%)	25 (29%)	44 (28%)	
Education (yrs)	242	14.5 (2.9)	14.8 (2.2)	14.4 (3.2)	0.2
BMI	242	28.3 (5.9)	28.9 (6.4)	28.0 (5.6)	0.3
EYO (yrs)	242	-5.8 (11.4)	-5.5 (13.1)	-6.0 (10.4)	>0.9
CDR Global	242				<0.001
CDR 0		176 (73%)	85 (100%)	91 (58%)	
CDR 0.5		39 (16%)	0 (0%)	39 (25%)	
CDR 1+		27 (11%)	0 (0%)	27 (17%)	
Plasma NT1 (pg/ml)	242	8.6 (3.0)	7.9 (2.5)	8.9 (3.1)	0.019

[1]Mean (SD); n (%)

[2]Wilcoxon rank sum test; Pearson's Chi-squared test

Figure 1. Plasma NT1 increases with disease severity

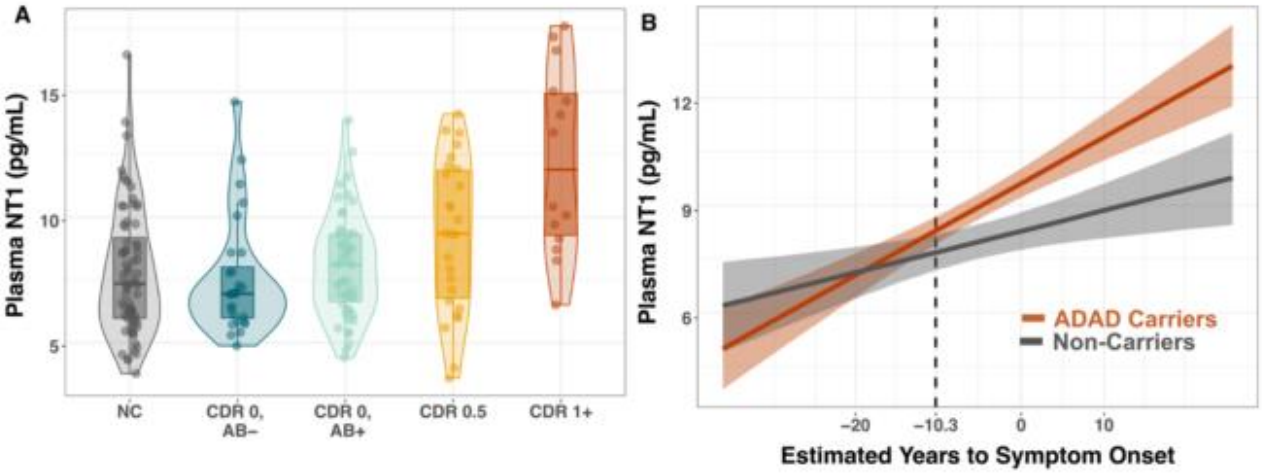

(A) Plasma NT1 levels were higher in ADAD mutation carriers (MC) compared to non-carriers (NC) (t[203] = -3, p = 0.007), specifically between NC and cognitively impaired MC groups (CDR1+; B[SE] = 4.33 [0.7], p < 0.0001). Within MC, plasma NT1 levels were higher within the CDR1+ group compared to the CDR0 groups (AB- group: B[SE] = 4.27 [0.9], p < 0.001; AB+ group: B[SE] = 3.96 [0.8], p < 0.001) and CDR0.5 group (B[SE] = 2.99 [0.8], p = 0.004). **(B)** Plasma NT1 levels increase in MC compared to NC as a function of EYO and become abnormal starting approximately 10 years before estimated symptom onset.

Figure 2. Plasma NT1 is associated with cognition, tau, and neurodegeneration

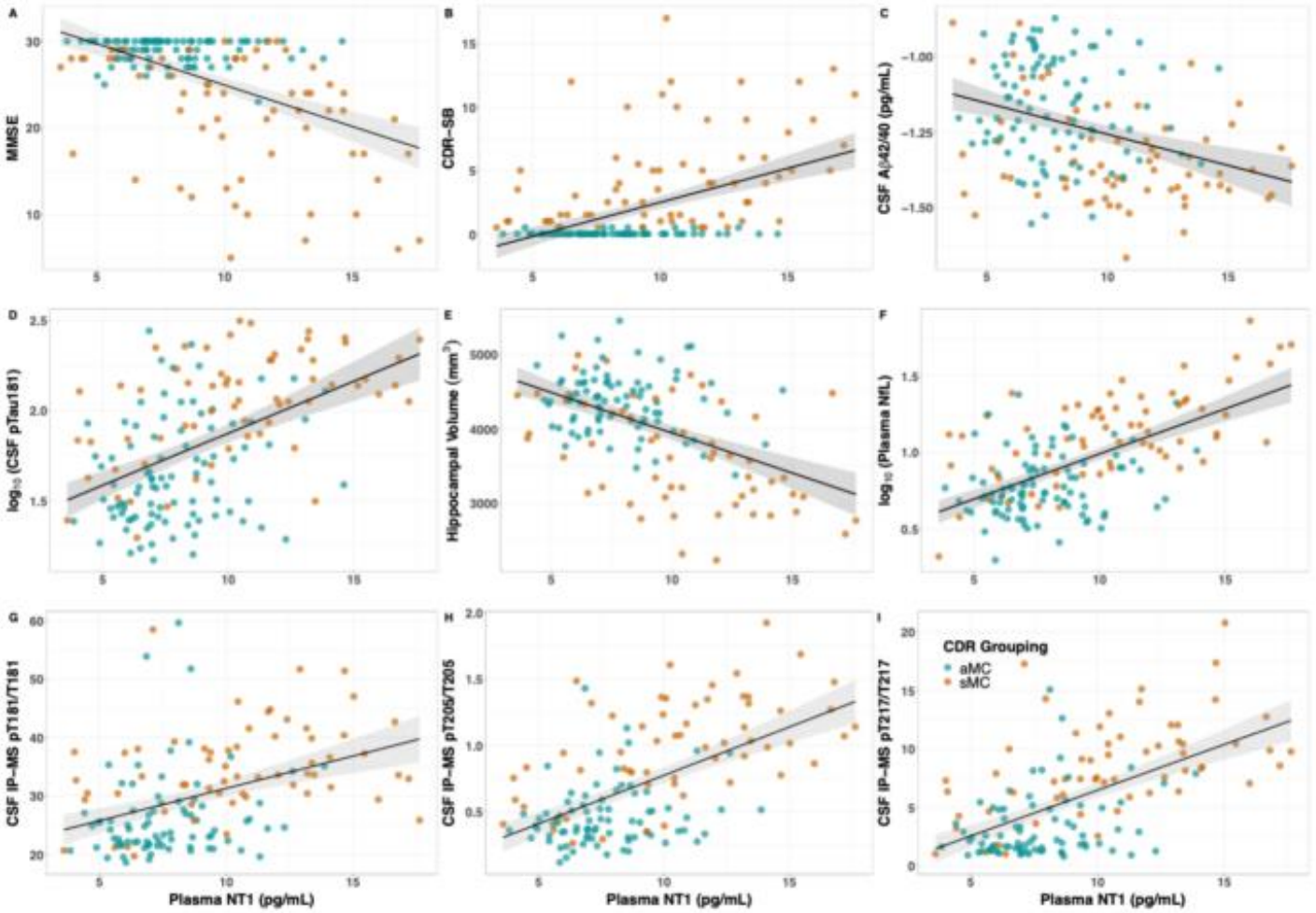

Linear regression models, adjusting for estimated years from symptom onset and sex were used to examine cross-sectional associations between plasma NT1 and MMSE (A), CDR-SB (B), CSF Aβ42/40 (C) and $\log_{10}$(pT181) (D), hippocampal volume (E), plasma $\log_{10}$(Neurofilament light) (F), and CSF pT181/T181 (G), pT205/T205 (H), and pT217/T217 (I) in asymptomatic (CDR = 0; blue) and symptomatic (CDR >0; orange) mutation carriers. Models examining MMSE and CDR-SB were additionally adjusted for years of education and model for hippocampal volume was additionally adjusted for total intracranial volume. Standardized coefficients and 95% CI are reported in Figure 3A.

Figure 3. Rate of change in NT1 is associated with rate of change in cognitive, pathologic, and neurodegeneration measures

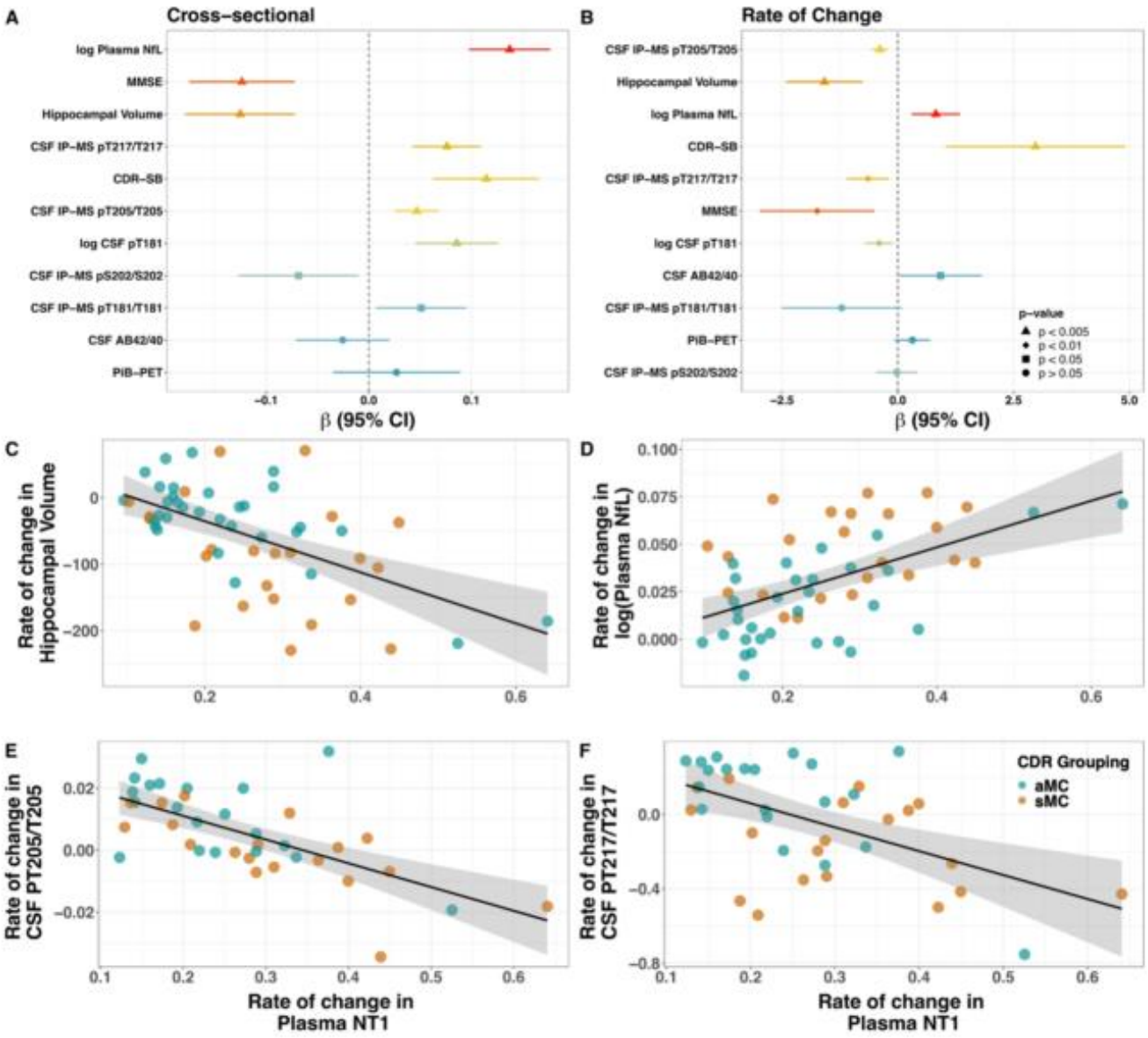

Standardized coefficients and 95% CI for covariate-adjusted cross-sectional (A) and longitudinal (B) associations between plasma NT1 and cognitive, clinical, and biomarker measures of interest. Associations between annualized rates of change for plasma NT1 and hippocampal volume (C), plasma NfL (D), CSF pT205/T205 (E), and CSF pT217/T217 (F).

Keywords: Plasma biomarkers, N-terminal tau fragment 1, Autosomal dominant Alzheimer's disease, longitudinal

117 Increased CSF GAP-43 is associated with accelerated tau accumulation and spread in Alzheimer's disease

Nicolai Franzmeier[1,2,3], Amir Dehsarvi[1], Anna Steward[1], Davina Biel[1], Anna Dewenter[1], Sebastian Niclas Römer[1], Fabian Wagner[1], Matthias Brendel[2,4], Michael Ewers[1,5], Alexis Moscoso[3], Kaj Blennow[3], Henrik Zetterberg[3], Michael Schöll[3]

[1]*Institute for Stroke and Dementia Research (ISD), University Hospital, LMU Munich, Germany, Munich, Germany*
[2]*Munich Cluster for Systems Neurology (SyNergy), Munich, Germany, Munich, Germany*
[3]*University of Gothenburg, The Sahlgrenska Academy, Institute of Neuroscience and Physiology, Department of Psychiatry and Neurochemistry, Gothenburg, Sweden*
[4]*Department of Nuclear Medicine, University Hospital, LMU Munich, Germany, Munich, Germany*
[5]*German Center for Neurodegenerative Diseases (DZNE), Munich, Germany, Munich, Germany*

Background: Preclinical studies found that tau spreads trans-synaptically in an activity-dependent manner, suggesting that synapses route tau spread in Alzheimer's disease (AD). Importantly, amyloid-beta (Ab) induces aberrant synaptic activity, which may accelerate trans-synaptic tau spread. In AD patients, we found previously that tau spreads from epicenters across functionally connected regions but it is unclear whether Ab-related synaptic changes accelerate tau spreading. The presynaptic growth-associated protein 43 (GAP-43) is implicated in synaptic plasticity and is increased in cerebrospinal fluid (CSF) in AD, suggesting that GAP-43 captures synaptic integrity deviations such as aberrant synaptic activity. We therefore tested whether higher GAP-43 is associated with faster Ab-related tau spread.

Methods: We included longitudinal [18F]Flortaucipir tau-PET, baseline [18F]Florbetapir amyloid-PET and CSF GAP-43 from 93 subjects (controls Ab-, n=54; cognitively normal/Mild Cognitive Impairment Ab+, n=33/21). To model connectivity-associated tau spread, we determined a connectivity template across 200 cortical regions (i.e., Schaefer atlas) using 3T resting-state fMRI in an independent control sample. Statistical models were controlled for age, sex and diagnosis.

Results: Higher CSF GAP-43 was associated with faster Ab-related tau-PET increase in pre-defined ROIs (centiloid x GAP-43 interaction, global/temporal-meta-ROI: b=0.0019/0.0028; p=0.009/0.007, Fig.1) as well as in the personalized Q1 ROI (b=0.0024; p=0.004) that summarizes regions most closely connected to tau epicenters with highest baseline tau-PET (Fig.2A). Importantly, the centiloid x GAP-43 interaction decreased across regions less strongly connected to tau epicenters (Q2/Q3/Q4: b=0.0017/0.0008/0.0002; p=0.009/0.080/0.344, Fig.2B-D, 3A). Further, we quantified subject-specific connectivity-associated tau spread (i.e., the regression-derived association between epicenter connectivity and tau-PET increase in remaining brain regions). Here, higher CSF GAP-43 was associated with a stronger association between Ab and connectivity-associated tau spread (centiloid x GAP-43 interaction, b=-0.0031; p=0.037, Fig.3B).

Conclusions: Higher CSF GAP-43 is associated with faster Ab-related tau spread across interconnected brain regions, rendering synaptic changes a potential target to attenuate tau spreading.

Figure 1:

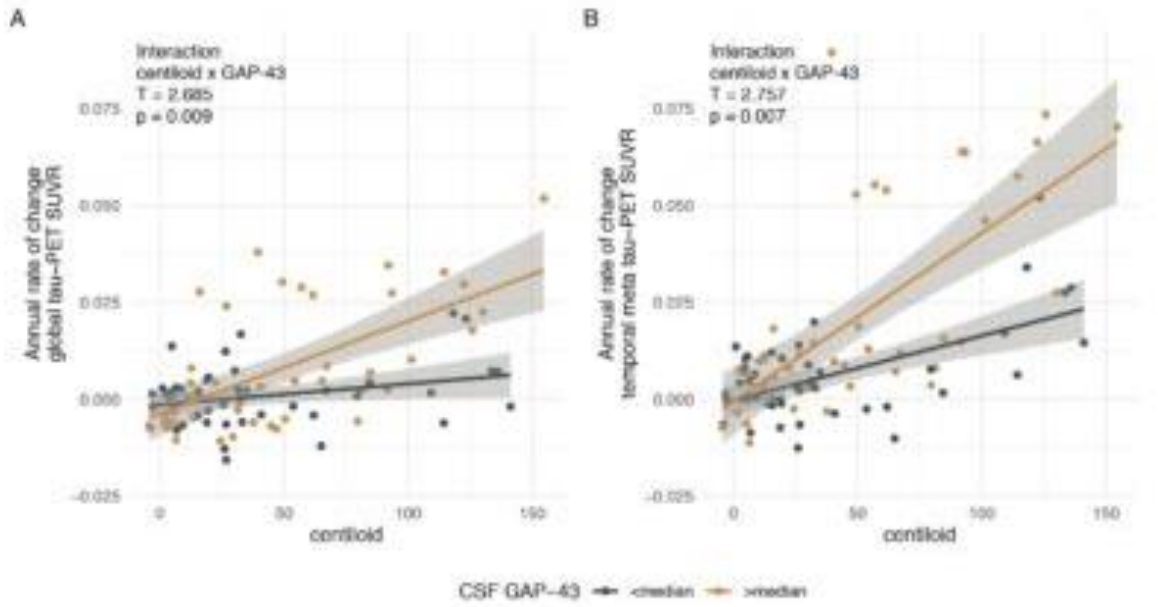

Scatterplots illustrating the interaction between amyloid-PET (i.e., centiloid) and CSF GAP-43 on tau-PET changes in a global cortical ROI (A) as well as a temporal-meta ROI (B). Regression models were controlled for age, sex and diagnosis. Note that interactions were computed using continuous GAP-43 measures, and that the median split was performed only for visualization.

Figure 2:

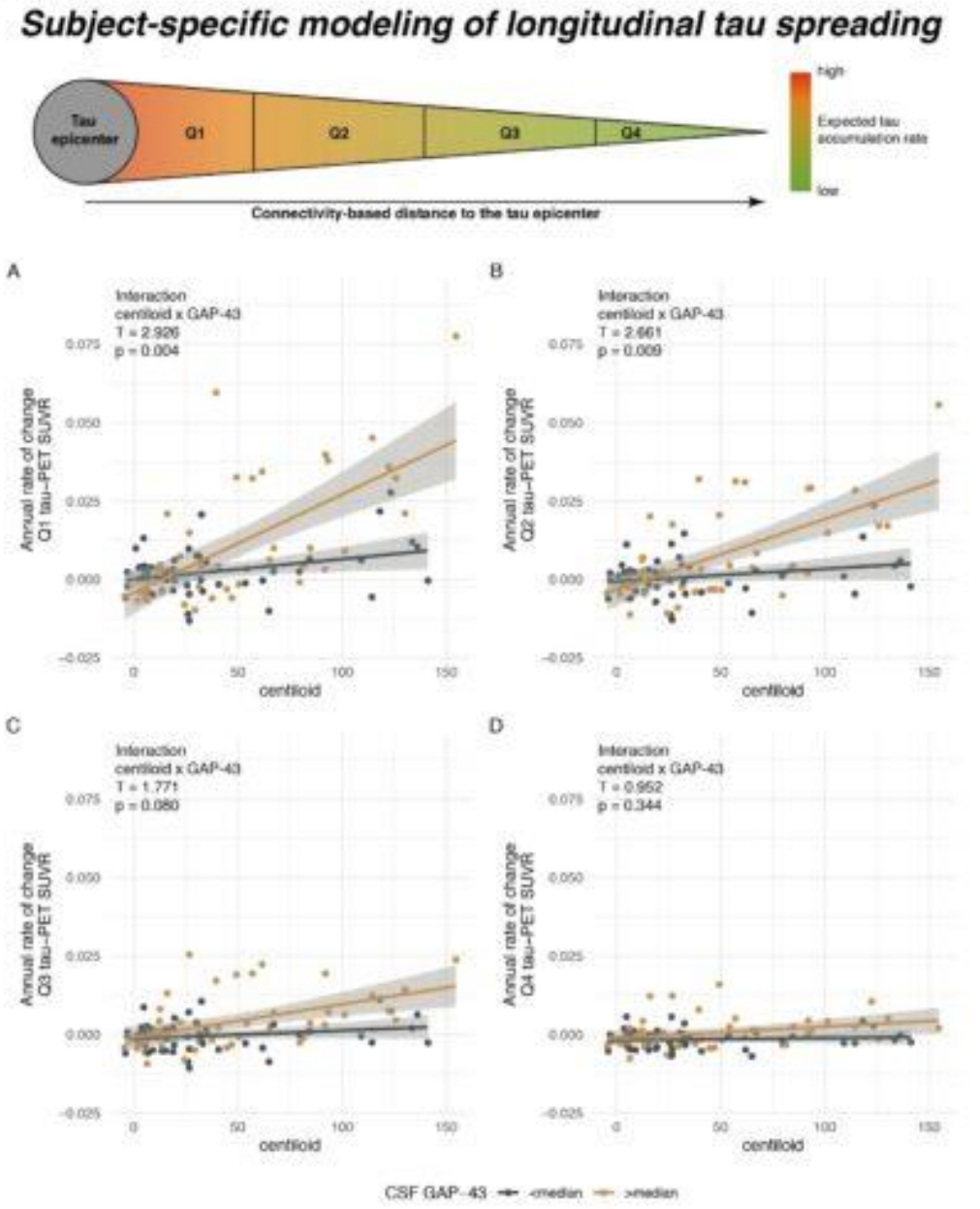

Scatterplots illustrating the interaction between amyloid-PET (i.e., centiloid) and CSF GAP-43 on tau-PET changes in connectivity-derived ROIs, ranging from regions that are closely connected to subject-specific tau epicenters (Q1, Panel A) to regions that are less strongly connected to subject-specific tau epicenters (Q2-Q4, Panels B-D). Tau epicenters were defined as 5% of brain regions with highest baseline tau-PET SUVRs. Connectivity was derived using a connectome template based on 3T multi-band resting-state fMRI data from cognitively normal Aβ- controls. Regression models were controlled for age, sex and diagnosis. Note that interactions were computed using continuous GAP-43 measures, and that the median split was performed only for visualization.

Figure 3:

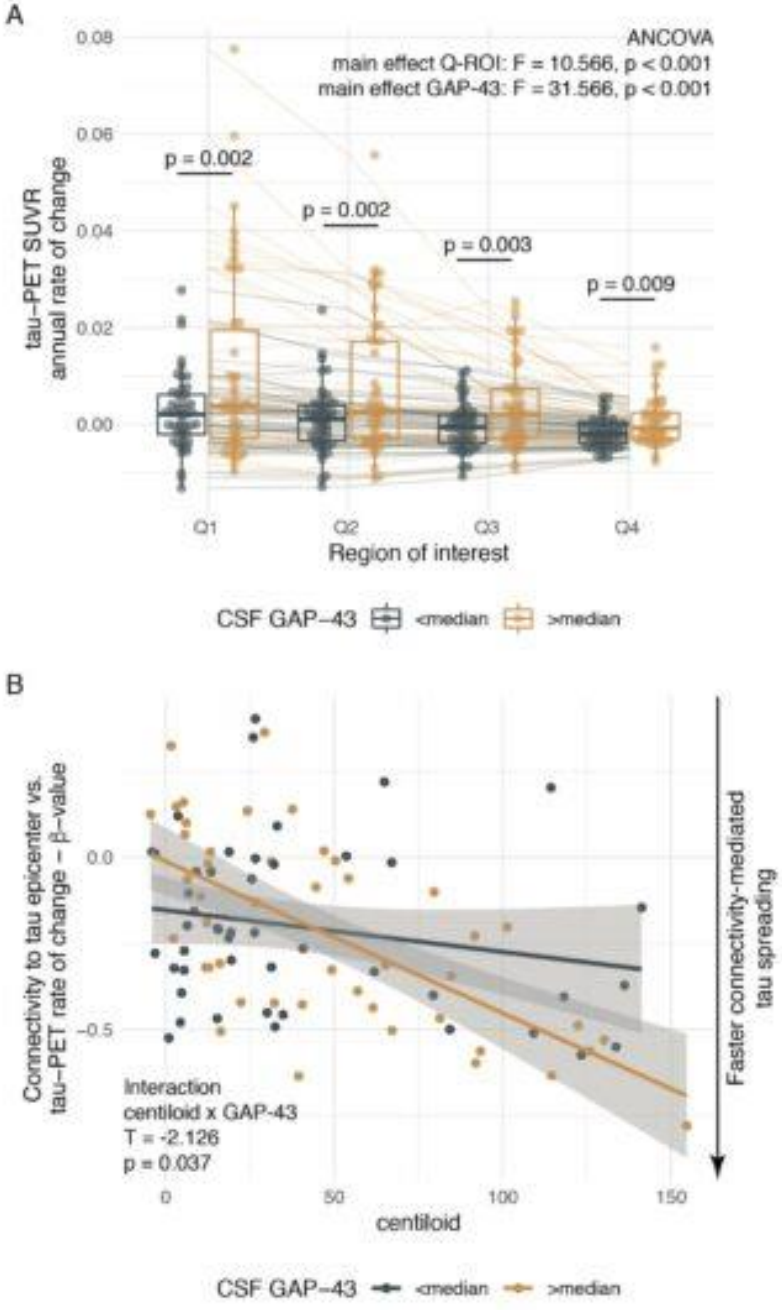

Boxplots illustrating the effect of GAP-43 levels on tau-PET increase in Q1-Q4 ROIs (A). Scatterplot (B), illustrating the interaction between amyloid-PET (i.e., centiloid) and CSF GAP-43 on connectivity-based tau spreading (y-axis). Regression and ANCOVA models were controlled for age, sex and diagnosis. Note that interactions for Panel B were computed using continuous GAP-43 measures, and that the median split was performed only for visualization.

Keywords: Tau spreading, amyloid, synaptic changes, GAP-43

118 Investigating the impacts of tau status in Alzheimer's disease by using [18F]Florzolotau tau cutoff

Shao-Yi Huang[1], Kun-Ju Lin[1,2,3], Chin-Chang Huang[4], Jung-Lung Hsu[4], Chiung-Chih Chang[5], Kuo-Lun Huang[4], Ing-Tsung Hsiao[1,2,3]

[1]*Department of Medical Imaging and Radiological Sciences, Chang Gung University, Taoyuan, TW*
[2]*Medical Imaging & Radiological Sciences and Healthy Aging Research Center, Chang Gung University, Taoyuan, TW*
[3]*Molecular Imaging Center and Nuclear Medicine, Chang Gung Memorial Hospital, Taoyuan, TW*
[4]*Neurology, Chang Gung Memorial Hospital, Taoyuan, TW*
[5]*Neurology, Chang Gung Memorial Hospital, Kaohsiung, TW*

Purpose: This work aims to derive tau cutoff based on a novel tau PET tracer [^{18}F]Florzolotau to classify individuals along AD continuum, and also to investigate the influences of tau status (positive/negative) among disease groups.

Methods: A total of 40 NC, 90 MCI, 90 AD were recruited from Chang Gung Memorial Hospital, Taiwan. All subjects underwent T1-MRI, [^{18}F]AV45, [^{18}F]Florzolotau and neuropsychological testing. SUVr was generated using cerebellar crus as the reference region for tau PET, and the whole cerebellum for amyloid PET. Subjects were classified by different combinations of amyloid and tau status. A cut-point of mcSUVR≧1.11 was defined as amyloid positive, while tau cutoffs were determined by two common methods using SUVr in Temporal-composite-VOI: (1) the mean+2SD of NC(A-) and (2) the ROC analysis with Youden index between NC(A-) and AD(A+). SUVr in different VOIs were compared among disease groups (NC, MCI, AD with A+/- and T+/-). MMSE difference between disease groups were expressed by effect size with Cohen's d method.

Results: The derived tau SUVr thresholds were 1.33 for mean+2SD and 1.25 for ROC analysis. Higher tau positive subjects in MCI(A-), MCI(A+), and AD(A+) were observed by using ROC analysis (Figure.1). SUVr in the temporal-composite VOI were higher in T+ group than those in T- group (MCI(A-T+):1.49±0.05; AD(A+T-):1.14±0.10). There is an incremental increase in SUVr along AD disease progression with tau positivity cutoffs derived from both methods. Lower MMSE was observed in T+ group, and also mean+2SD method showed larger effect size between T+ and T- group (Figure.2).

Conclusions: A conservative tau SUVr cutoff of 1.33 was derived from the mean+2SD method, while the tau cutoff was 1.25 by ROC analysis. Nevertheless, both methods showed comparable results but higher MMSE discrepancy between T+ and T- when using tau cutoff derived from mean+2SD.

Tau positive subjects (%)	NC A-	NC A+	MCI A-	MCI A+	AD A+
Mean+2SD (1.33)	5%	33%	3%	53%	78%
ROC (1.25)	5%	33%	8%	64%	82%

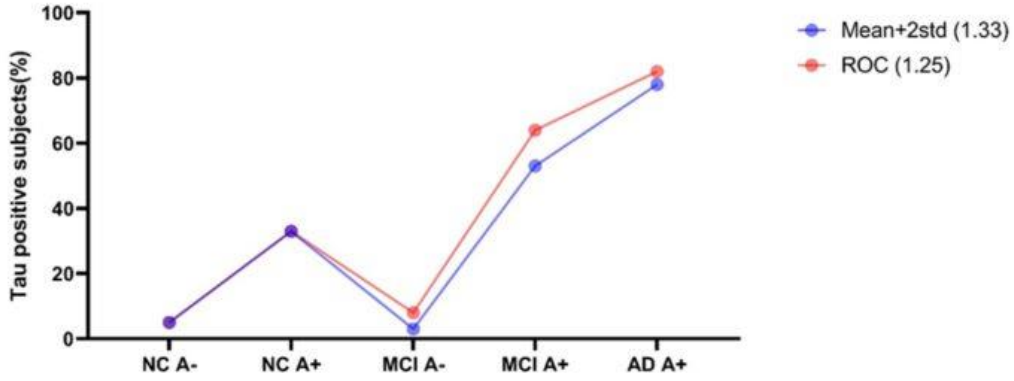

Figure. 1 Percentage of Tau positive subjects in different disease groups by using cut-offs derived from Mean+2SD of NC(A-) (blue line) and ROC between NC(A-) and AD(A+) (red line), respectively.

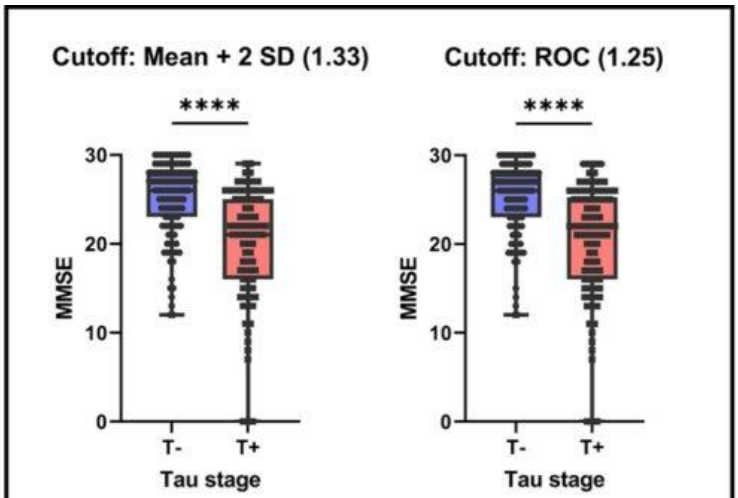

Comparison pair	Cohen's d	
	mean+2SD (1.33)	ROC (1.25)
AD(A+T+) vs NC(A-T-)	-2.23	-2.20
T+ vs T-	-0.93	-0.90

Figure.2 The two box-plot displays MMSE comparison between T- and T+ group using cut-offs derived from Mean+2SD (left) and ROC method (right), respectively. Lower table shows effect size (Cohen's d) in MMSE of AD(A+T+) vs NC(A-T-) and T+ vs T- groups.

Keywords: [18F]Flortaucipir, Tau PET, Alzheimer's disease, Tau positivity, Cutoff

119 Study of reference regions in the quantitation of [18F]Florzolotau tau PET imaging

Shao-Yi Huang[1,2], Jyh-Ruei Lin[1,2], Kun-Ju Lin[1,2,3], Chin-Chang Huang[4], Jung-Lung Hsu[4], Chiung-Chih Chang[5], Kuo-Lun Huang[4], Ing-Tsung Hsiao[1,2,3]

[1]*Department of Medical Imaging and Radiological Sciences, Chang Gung University, Taoyuan, TW*
[2]*Medical Imaging & Radiological Sciences and Healthy Aging Research Center, Chang Gung University, Taoyuan, TW*
[3]*Molecular Imaging Center and Nuclear Medicine, Chang Gung Memorial Hospital, Taoyuan, TW*
[4]*Neurology, Chang Gung Memorial Hospital, Taoyuan, TW*
[5]*Neurology, Chang Gung Memorial Hospital, Kaohsiung, TW*

Aim: This work aims to investigate the performance of different reference regions (RR) including cerebellar crus, eroded subcortical white matter (WM), modified PERSI (mPERSI) based on the work of Tagai et al. using the cross-sectional and longitudinal analysis in [^{18}F]Florzolotau PET images.

Methods: Two cohorts were studied in this work. Cohort 1 included healthy control (HC, n=17), mild cognitive impaired (MCI) subjects (MCI, n=20), AD subjects (n=23) and PSP subjects (n=14). Cohort 2 included 40 MCI and AD subjects with two PET scans (baseline and follow-up). All PET images were processed using the PMOD 4.2 software including MR-based spatial normalization, and intensity normalization to generate SUVr images using four RRs (cerebellar crus / WM / mPERSI using individual WM (mPERSI(WM)) and individual gray matter (mPERSI(GM))). Cross-sectional analysis was performed in cohort 1, and the group SUV difference of the four RR's was compared for stability of the reference values. To study the diagnostic power of different RR's, the SUVr effect size based on Cohen's d method between groups based on the four RR's was compared. The longitudinal analysis was performed in the cohort 2 for the annual SUVr change rates (ACR) in AD from the four RR's.

Results: In the cross-sectional analysis, no significant reference SUV difference was found among all groups, while larger variation were observed from cerebellar crus and mPERSI (GM), especially in AD group. Among all RR's, WM has the highest effect size in AD and PSP (Table.1). In the longitudinal analysis, WM also shows best performance for higher average ACR and smaller variation (Figure.1).

Conclusions: In summary, WM RR exhibited higher diagnostic power and effectiveness in detecting longitudinal change for [^{18}F]Florzolotau imaging. Future work should include more disease types and clinical performance vs SUVr using different reference regions.

Table.1 The effect sizes from Cohen's d methods for SUVr derived from different reference regions between disease groups for AD (A) and PSP (B) in different brain regions.

(A) NC/MCI/AD

MCI vs NC				AD vs NC				AD vs MCI			
Braak stage	I/II	III/IV	V/VI	Braak stage	I/II	III/IV	V/VI	Braak stage	I/II	III/IV	V/VI
Cerebellar crus	1.17	1.52	1.30	Cerebellar crus	1.66	2.52	2.19	Cerebellar crus	0.39	1.62	1.50
WM	**1.71**	1.55	1.41	WM	**1.74**	**3.24**	2.60	WM	0.30	1.61	1.43
mPERSI(WM)	**1.56**	1.50	1.32	mPERSI(WM)	**1.58**	**3.82**	3.26	mPERSI(WM)	0.18	**1.76**	**1.66**
mPERSI(GM)	0.85	1.17	0.80	mPERSI(GM)	1.37	2.19	1.88	mPERSI(GM)	0.51	1.74	1.62

(B) NC/PSP

PSP vs NC				
Subcortical regions	Pallidum	Midbrain	Substantia nigra	Subthalamic nucleus
Cerebellar crus	0.72	1.11	0.16	1.30
WM	**2.12**	**1.48**	**0.98**	**1.76**
mPERSI(WM)	**1.60**	**1.28**	**0.81**	**1.51**
mPERSI(GM)	1.04	1.09	0.41	1.28

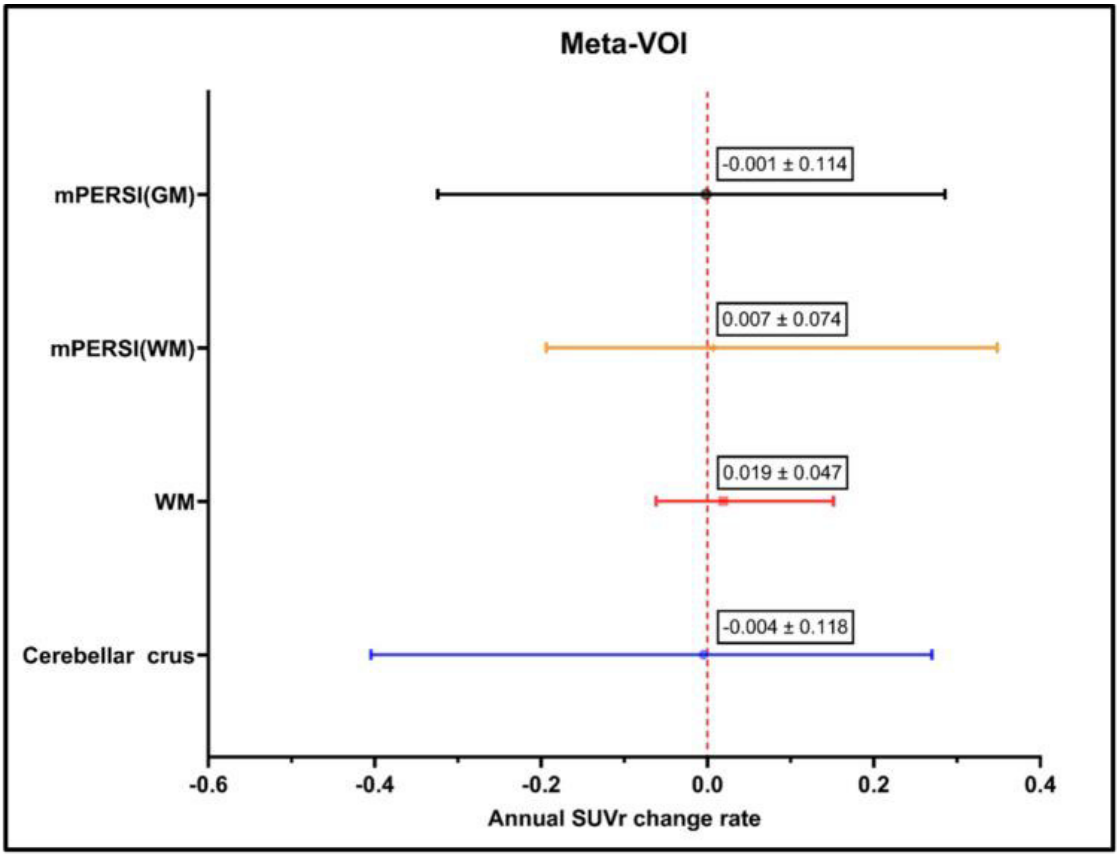

Figure 1. Annual SUVr change rate with mean and range within Meta-VOI by using different reference regions (cerebellar crus, WM, mPERSI(WM) and mPERSI(GM)).

Keywords: [18F]Florzolotau, Tau PET, Reference region, Progressive supranuclear palsy, Alzheimer's disease

120 Assessing the efficacy of BETTH-derived tau thresholds to predict cognitive decline

Alexandra Gogola[1], Brian Lopresti[1], Beth Snitz[3], Dana Tudorascu[2], Davneet Minhas[1], Vincent Dore[4,5], Milos Ikonomovic[3,6], C. Elizabeth Shaaban[7], Julia Kofler[8], Cristy Matan[1], Pierrick Bourgeat[5], N Scott Mason[1], Christopher Rowe[4], Howard Aizenstein[2], Chester Mathis[1], William Klunk[2], Oscar Lopez[3], Ann Cohen[2], Victor Villemagne[2,4]

[1]*Department of Radiology, University of Pittsburgh School of Medicine, Pittsburgh, PA, United States*
[2]*Department of Psychiatry, University of Pittsburgh School of Medicine, Pittsburgh, PA, United States*
[3]*Department of Neurology, University of Pittsburgh School of Medicine, Pittsburgh, PA, United States*
[4]*Department of Molecular Imaging & Therapy, Austin Health, Melbourne, Australia*
[5]*CSIRO Health & Biosecurity, Brisbane, Australia*
[6]*Geriatric Research Education and Clinical Center, VA Pittsburgh Healthcare System, Pittsburgh, PA, United States*
[7]*Department of Epidemiology, University of Pittsburgh School of Public Health, Pittsburgh, PA, United States*
[8]*Department of Pathology, University of Pittsburgh, Pittsburgh, PA, United States*

Background: Tau PET thresholds should detect early tau deposition and predict cognitive decline. We evaluated the relationships between the BETTH-derived sensitivity and specificity tau thresholds (Gogola et al, doi:10.2967/jnumed.123.265941, 2023) and cognitive changes in non-demented participants.

Methods: FTP scans from 314 non-demented participants (age 73.17.1 years) were processed and sampled to obtain regional SUVR values. Three cognitive measures were assessed: Clinical Dementia Rating Scale Sum of Boxes (CDR_SoB), Logical Memory (LM), and Mini Mental State Examination (MMSE). Cognitive measures collected at the time of scanning were considered timepoint 0 (T0) and the most recently collected measures were considered timepoint 1 (T1). To evaluate the thresholds, SUVRs were split into below (T-) and above (T+) threshold groups before assessment using both sensitivity (SEN) and specificity thresholds (SPC). Regression models between SUVR and change in cognitive measure, adjusted for age, gender, years of education, APOE status, Centiloids, cortical thickness and T0 cognitive score, were evaluated.

Results: The regression model R^2, regional p- and full-model p-values are shown in Table 1. While each composite region was included in at least one significant regression model, only Inferior Temporal, Lateral Temporal, Mesial Temporal, and Meta Temporal were significant factors within the models. Further, two composite region's sensitivity thresholds were consistently significantly associated ($p < 0.05$) with all three cognitive measures: Lateral Temporal and Meta Temporal. (Figure 1).

Conclusions: The superior performance of the Lateral Temporal and Meta Temporal regions in all three cognitive measures indicate that cognitive decline is associated with cortical tau deposition. Moreover, their SEN thresholds were the best overall predictor of cognitive measure change, suggesting that they are the optimal regions and thresholds to apply in clinical diagnosis and therapeutic trials. Further work will assess the Lateral Temporal and Meta Temporal SEN thresholds in relation to cognitive decline within the AT(N) framework.

Table 1. R^2 and p-values for T+ FTP SUVR regression models with decline in CDR_SoB, LM and MMSE in non-demented individuals (adjusted for age, gender, years of education, APOE status, Centiloids and cortical thickness)

			R^2	Region p-value	Model p-value
CDR_SoB	SEN	Amygdala	0.10	6.15E-01	3.20E-02*
		Inferior Temporal	0.21	7.21E-02	2.21E-04***
		Lateral Occipital	0.10	3.52E-01	1.84E-02*
		Lateral Temporal	0.17	3.52E-02*	8.01E-04***
		Mesial Temporal	0.18	8.58E-02	1.36E-03**
		Meta Temporal	0.12	3.98E-02*	7.04E-03**
	SPC	Amygdala	-0.15	7.15E-01	7.82E-01
		Inferior Temporal	0.22	1.51E-01	1.00E-01
		Lateral Occipital	0.57	1.54E-01	1.18E-01
		Lateral Temporal	0.18	1.55E-01	2.04E-01
		Mesial Temporal	0.08	2.14E-01	1.91E-01
		Meta Temporal	0.06	8.18E-01	4.17E-01
LM	SEN	Amygdala	0.06	1.30E-01	1.49E-01
		Inferior Temporal	0.11	2.68E-02*	2.82E-02*
		Lateral Occipital	0.05	3.64E-01	1.63E-01
		Lateral Temporal	0.12	2.96E-02*	1.84E-02*
		Mesial Temporal	0.04	4.74E-02*	2.15E-01
		Meta Temporal	0.09	3.75E-02*	4.47E-02*
	SPC	Amygdala	-0.13	5.36E-01	6.79E-01
		Inferior Temporal	-0.08	4.91E-01	6.34E-01
		Lateral Occipital	-0.15	6.38E-01	6.51E-01
		Lateral Temporal	0.09	9.89E-01	3.66E-01
		Mesial Temporal	0.10	6.51E-02	1.82E-01
		Meta Temporal	0.02	4.21E-01	4.86E-01
MMSE	SEN	Amygdala	0.03	8.25E-02	2.50E-01
		Inferior Temporal	0.17	6.13E-06****	1.32E-03**
		Lateral Occipital	0.00	3.61E-01	4.24E-01
		Lateral Temporal	0.20	3.40E-07****	1.35E-04***
		Mesial Temporal	0.17	1.74E-05****	1.81E-03**
		Meta Temporal	0.18	1.46E-06****	4.16E-04***
	SPC	Amygdala	0.28	6.56E-01	6.93E-02
		Inferior Temporal	0.20	2.34E-02*	1.21E-01
		Lateral Occipital	0.64	6.87E-02	7.81E-02
		Lateral Temporal	0.25	3.83E-02*	1.30E-01
		Mesial Temporal	0.17	1.89E-03**	4.42E-02*
		Meta Temporal	0.02	4.21E-01	4.86E-01

*$p < 0.05$, **$p < 0.01$, ***$p < 0.001$, ****$p < 0.0001$

Figure 1. T+ (SEN) FTP SUVR predicted decline in CDR_SoB, LM, and MMSE in non-demented individuals (adjusted for age, gender, years of education, APOE status, Centiloids. cortical thickness, and T0 cognitive score)

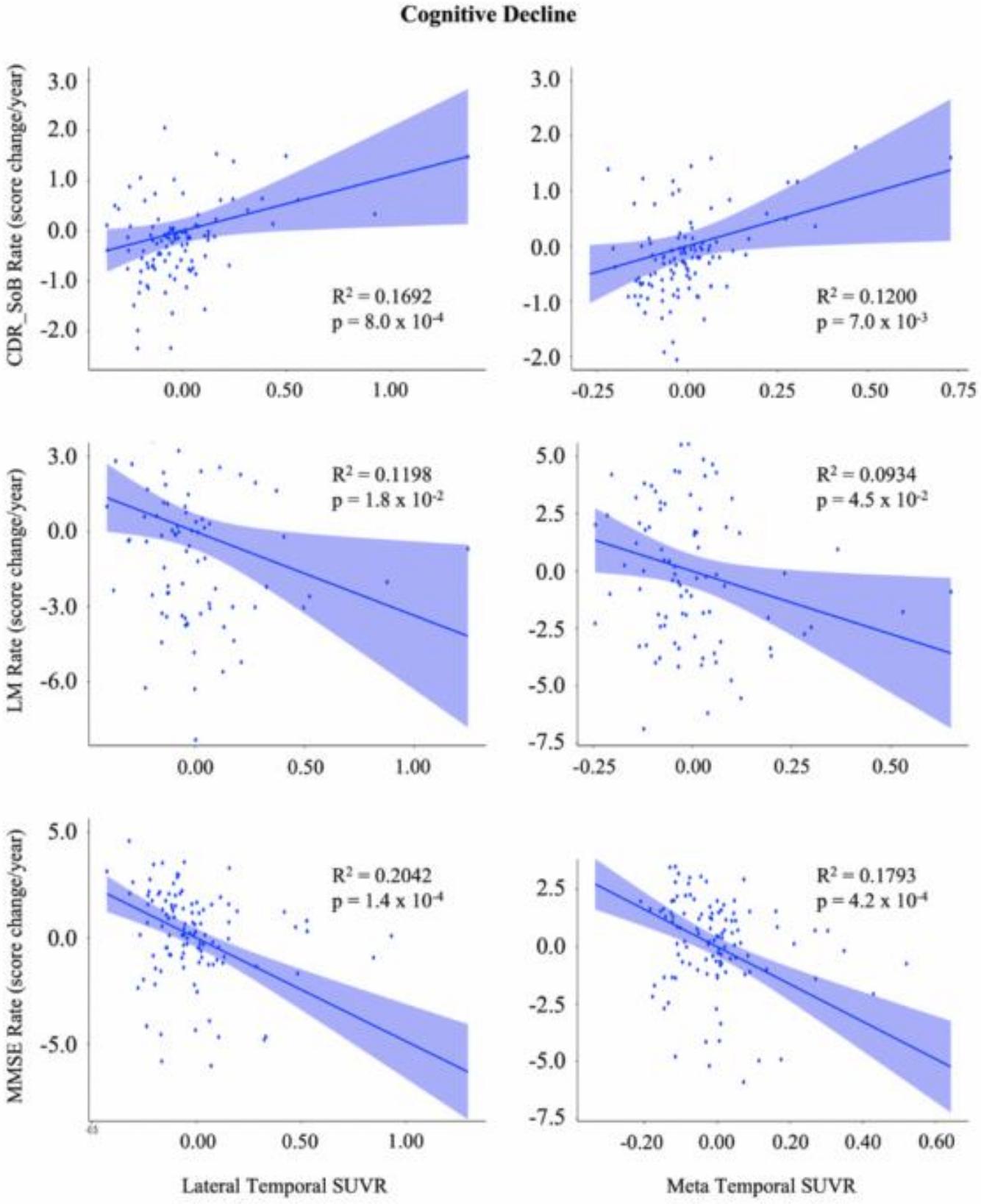

Keywords: Tau, PET, Cognition, Thresholds

121 Assessing the correlations between imaging and plasma biomarkers within the AT(N) framework

Alexandra Gogola[1], Ann Cohen[2], Xuemei Zeng[2], Brian Lopresti[1], Beth Snitz[3], Dana Tudorascu[2], Davneet Minhas[1], Milos Ikonomovic[3,4], Tharick Pascoal[2], Julia Kofler[5], Cristy Matan[1], N Scott Mason[1], Howard Aizenstein[2], Chester Mathis[1], William Klunk[2], Henrik Zetterberg[6], Kaj Blennow[6], Oscar Lopez[3], Victor Villemagne[2], Thomas Karikari[2,6]

[1]*Department of Radiology, University of Pittsburgh School of Medicine, Pittsburgh, PA, United States*
[2]*Department of Psychiatry, University of Pittsburgh School of Medicine, Pittsburgh, PA, United States*
[3]*Department of Neurology, University of Pittsburgh School of Medicine, Pittsburgh, PA, United States*
[4]*Geriatric Research Education and Clinical Center, VA Pittsburgh Healthcare System, Pittsburgh, PA, United States*
[5]*Department of Pathology, University of Pittsburgh, Pittsburgh, PA, United States*
[6]*Department of Psychiatry and Neurochemistry, Institute of Neuroscience and Physiology, University of Gothenburg, Mölndal, Sweden*

Background: Given the increasing usage of plasma biomarkers for Alzheimer's disease (AD) studies, it is necessary to better understand relationships between plasma biomarker and PET and MR imaging outcomes, particularly within the AT(N) framework.

Methods: We evaluated plasma samples from 233 subjects (age 74.05.9y) who underwent 3T MR and both [^{11}C]PiB and [^{18}F]flortaucipir (FTP) PET imaging. SUVR values were calculated for Global PiB, Amygdala FTP, and Meta-Temporal FTP. An AD signature cortical thickness (CT) composite was derived from MR images using FreeSurfer 7.1.1, Blood samples were processed and sampled to obtain measures of plasma Aβ42, Aβ40, p-tau181, p-tau231 and neurofilament light (NfL). Imaging outcomes were split into infra (-) and supra (+) threshold groups using 1.35 SUVR for Global PiB, 1.3 SUVR for Amygdala FTP, 1.18 SUVR for Meta-Temporal FTP, and 2.7 mm for CT. Plasma Aβ was expressed as Aβ42/Aβ40 ratio while p-tau181, p-tau231 and NfL were log-transformed to normally distribute the data. Simple regression models between continuous variables of each imaging-derived measure and all plasma biomarkers were evaluated.

Results: Full group regression model R^2 and regional p-values are shown in Table 1, suprathreshold regressions are shown in Table 2. Full Global PiB and Amygdala FTP were significantly associated with all plasma biomarkers while CT was associated with NfL, p-tau181, and p-tau231. Meta-Temporal FTP was associated with Aβ42/Aβ40. Additionally, A+Global PiB was significantly associated with Aβ42/Aβ40; (N+) CT with NfL; T+ Amygdala FTP with Aβ42/Aβ40, p-tau181, and p-tau231; and T+ Meta-Temporal FTP with p-tau181 (Figure 1).

Conclusions: The significant associations between suprathreshold imaging and plasma biomarkers suggests that, in A+, T+, or (N+) both capture abnormal AD pathophysiology. Further, the absence of an association in the infrathrehold cases supports that the suprathreshold associations are not artifactual. Future work will explore plasma thresholds and concordance between imaging and plasma AT(N).

Table 1. R^2 and p-values for regressions models between imaging and plasma biomarkers

		R^2	p-value
Global PiB	Aβ42/Aβ40	0.092	1.49E-06*
	NfL_ln	0.018	2.27E-02*
	p-tau181_ln	0.041	1.06E-03*
	p-tau231_ln	0.043	8.58E-04*
CT	Aβ42/Aβ40	0.006	1.24E-01
	NfL_ln	0.067	3.57E-05*
	p-tau181_ln	0.027	6.75E-03*
	p-tau231_ln	0.035	2.55E-03*
Amygdala FTP	Aβ42/Aβ40	0.026	7.39E-03*
	NfL_ln	0.018	2.24E-02*
	p-tau181_ln	0.033	3.18E-03*
	p-tau231_ln	0.013	4.29E-02*
Meta Temporal FTP	Aβ42/Aβ40	0.015	3.27E-02*
	NfL_ln	-0.003	5.35E-01
	p-tau181_ln	0.002	2.40E-01
	p-tau231_ln	-0.001	3.95E-01

* $p < 0.05$

Table 2. R^2 and p-values for imaging-derived A+, T+, and N+ regression models with A, T, and N plasma measures

		R^2	p-value
Global PiB	Aβ42/Aβ40	0.124	1.02E-02*
	NfL_ln	-0.009	4.38E-01
	p-tau181_ln	0.001	3.10E-01
	p-tau231_ln	0.001	3.12E-01
CT	Aβ42/Aβ40	0.017	1.47E-01
	NfL_ln	0.097	5.28E-03*
	p-tau181_ln	-0.015	9.03E-01
	p-tau231_ln	-0.012	6.77E-01
Amygdala FTP	Aβ42/Aβ40	0.141	5.46E-03*
	NfL_ln	0.019	1.79E-01
	p-tau181_ln	0.137	6.57E-03*
	p-tau231_ln	0.101	1.58E-02*
Meta Temporal FTP	Aβ42/Aβ40	0.000	3.16E-01
	NfL_ln	0.002	2.76E-01
	p-tau181_ln	0.053	1.69E-02*
	p-tau231_ln	0.009	1.82E-01

* $p < 0.05$

Figure 1. Significant associations between imaging-derived A+, T+, and N+ regression models with A, T, and N plasma measures

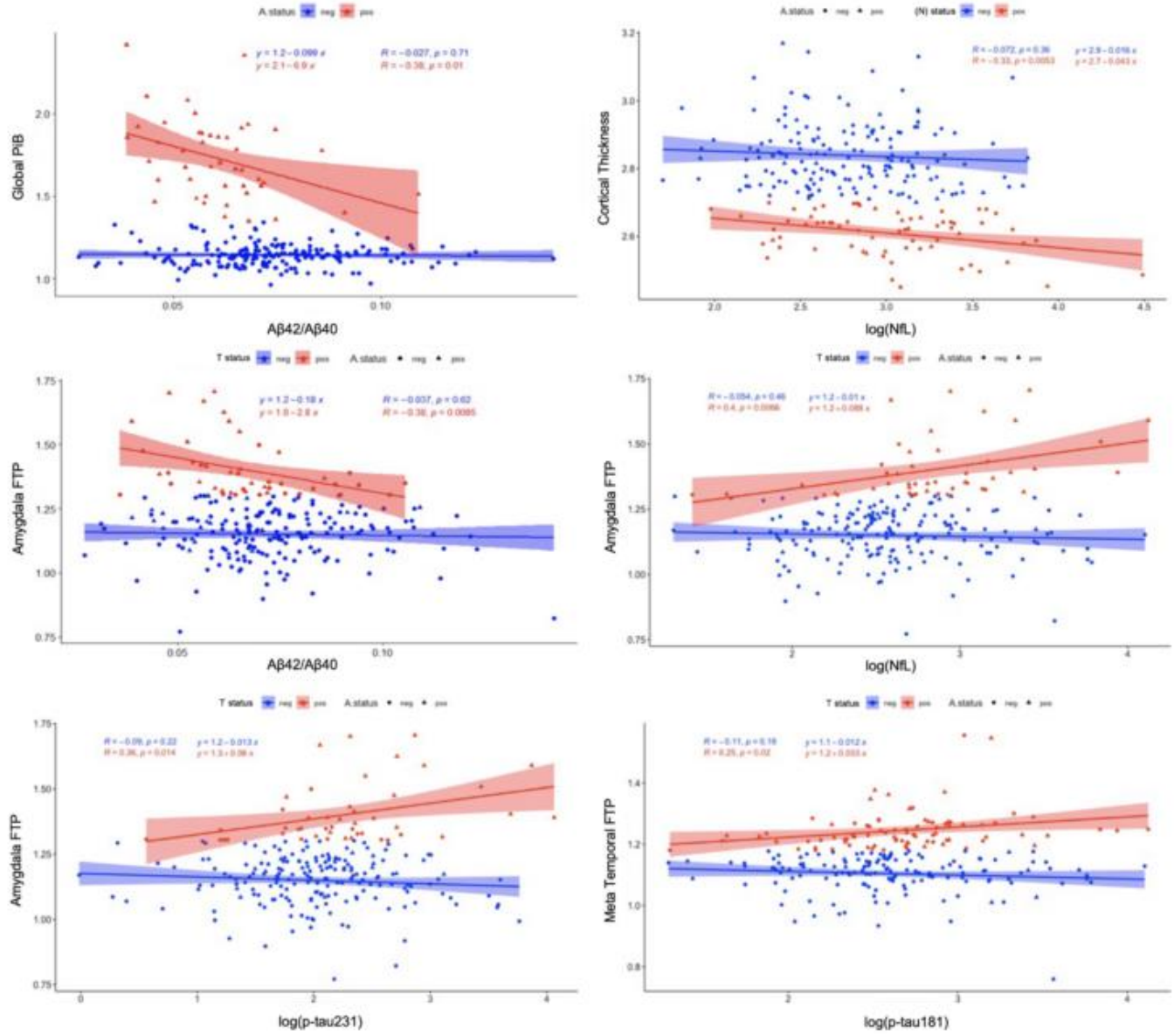

Keywords: PET, plasma, biomarkers, AT(N)

122 The effect of microglial activation on brain atrophy across the Alzheimer's disease continuum

Guilherme Povala[1], Bruna Bellaver[1], Pamela Lukasewicz Ferreira[1], Joao Pedro Ferrari-Souza[5], Cristiano Schaffer Aguzzoli[1], Douglas Teixeira Leffa[1], Hussein Zalzale[1], Carolina Soares[1], Firoza Lussier[1], Guilherme Negrini[1], Francieli Rohden[1], Andréa Benedet[2], Jenna Stevenson[3], Nesrine Rahmouni[3], Cécile Tissot[3], Joseph Therriault[3], Stijn Servaes[3], Ann Cohen[1], William Klunk[1], Victor Villemagne[1], Bruno Zatt[4], Eduardo R Zimmer[5], Thomas Karikari[1,2], Pedro Rosa-Neto[3], Tharick A Pascoal[1]

[1]*University of Pittsburgh, Pittsburgh, PA, United States*
[2]*University of Gothenburg, Molndal, Sweden*
[3]*Translational Neuroimaging Laboratory, Montréal, QC, Canada*
[4]*Universidade Federal de Pelotas, Pelotas, Brazil*
[5]*Universidade Federal do Rio Grande do Sul, Porto Alegre, Brazil*

Objective: To investigate the influence of microglial activation on cross-sectional and longitudinal brain atrophy, and future cognitive decline in Alzheimer's disease continuum.

Methods: We investigated 124 individuals from the TRIAD cohort with measures of brain voxel-based morphometry, microglial activation (MA) [11C]PBR28 PET, tau [18F]MK6240 PET, Aβ [18F]AZD4694 PET, and CDR sum of boxes. We performed regional-wise partial correlation analysis to investigate the association between MA and brain density. We calculated the rate of change (RoC) for the longitudinal analyses. We applied the principal component analysis for MA and brain density RoC in the longitudinal analysis.

Results: Regional-wise analysis reveals a mix of positive and negative associations for cognitively unimpaired (CU) individuals (Fig. 1A). When divided by amyloid-β (Aβ) status, Aβ- individuals exhibit only positive associations. In contrast, Aβ+ individuals demonstrate only negative associations (Figs. 1B, C). In CU Aβ+ individuals, we observed a synergistic association between MA and tau pathology, leading to future brain atrophy and cognitive decline (Figs. 1D, E). Next, we performed the same analysis for the CI Aβ+ individuals (Fig. 2A). In early Braak stages, we found only positive associations between MA and brain atrophy (Fig. 2B), while in late Braak stages, only negative associations were apparent (Fig. 2C). The interaction of MA and tau pathology synergistically predicted longitudinal brain atrophy and cognitive decline in CI individuals (Fig. 2D, E).

Conclusion: Our study found waves of positive and negative associations between MA and brain density modulated by Aβ in the early stages of the disease and by tau in the later stages. Furthermore, the interaction of MA with tau seems decisive for longitudinal brain atrophy and future cognitive decline in both the early and late stages of the disease.

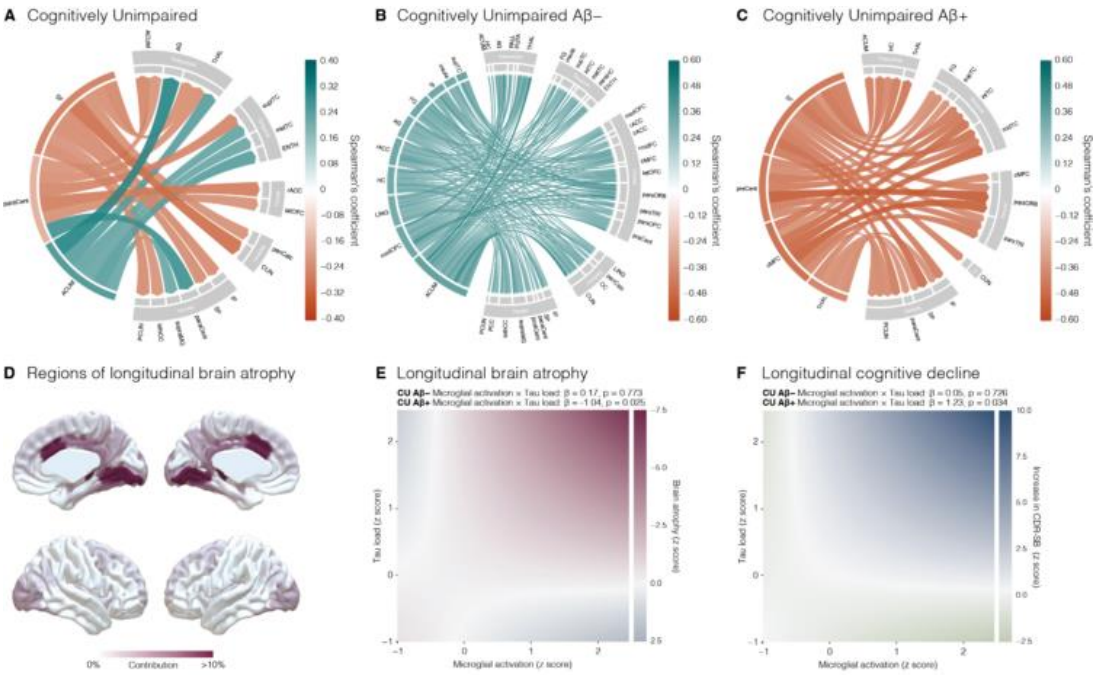

Figure 1. Amyloid-β (Aβ)-dependent effects of microglial activation effects on brain atrophy in cognitively unimpaired (CU) individuals. a-c Circos plots showing the statistically significant regional connections between microglial activation and brain atrophy in (**a**) CU individuals (n = 90), (**b**) CU Aβ- (n = 49) and (**c**) CU Aβ+ (n = 31). **d-f** Microglial activation interacts with tau load to predict longitudinal brain atrophy and cognitive decline only in the presence of Aβ. **d** Brain maps showing the regions with more pronounced longitudinal brain atrophy in CU Aβ+ individuals (n = 48). **e** Continuous association between tau load, microglial activation, and longitudinal brain volume for CU Aβ- (n = 29) and CU Aβ+ (n = 19) individuals adjusted for age and sex. **f** Continuous association between tau load, microglial activation, and longitudinal changes in CDR sum of boxes for CU Aβ- (n = 27) and CU Aβ+ (n = 17) individuals adjusted for age and sex.

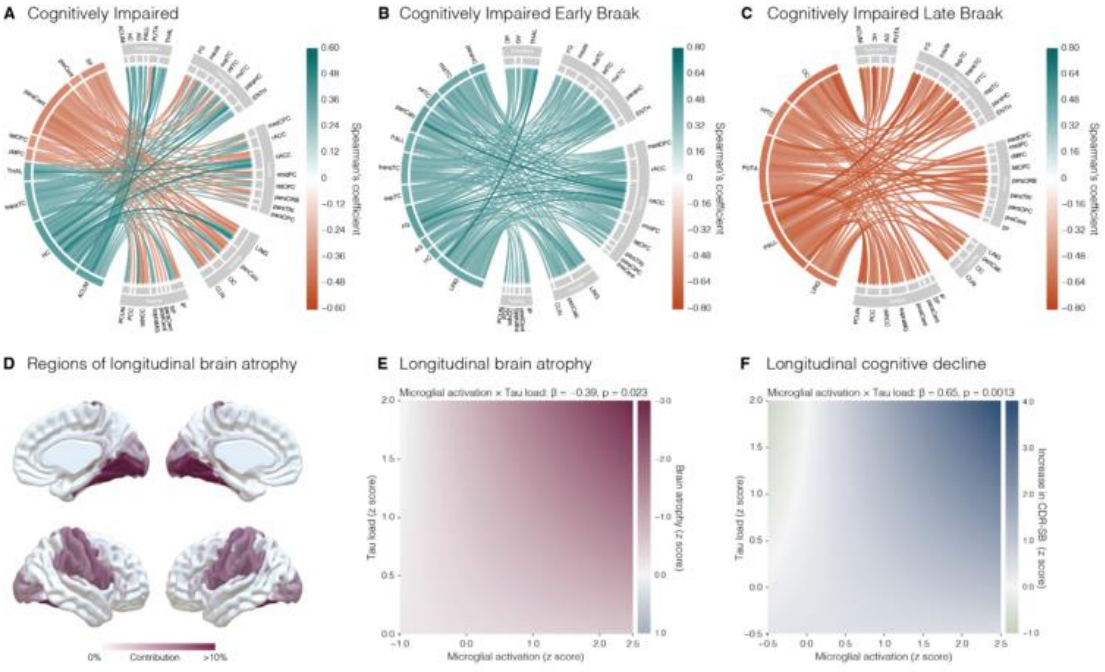

Figure 2. Tau load determines the dual effect of microglial activation in cognitively impaired (CI) individuals. a-c Circos plots showing the statistically significant regional connections between microglial activation and brain atrophy in (**a**) CI individuals (n = 54), (**b**) CI early Braak stages (n = 36) and (**c**) CI late Braak stages (n = 18). **d-f** Microglial activation interacts with tau load to predict longitudinal brain atrophy and cognitive decline. **d** Brain maps showing the regions with more pronounced longitudinal brain atrophy in CI individuals (n = 28). **e** Continuous association between tau load, microglial activation and longitudinal brain volume adjusted for age and sex (n = 28). **f** Continuous association between tau load, microglial activation, and longitudinal changes in CDR sum of boxes adjusted for age and sex (n = 26).

Keywords: Alzheimer's Disease, Inflammation, Microglial Activation, Brain Atrophy

123 Disentangling the relationships between tau-PET, amyloid-β-PET, hippocampal subfield volumes, and memory: a longitudinal study

Etienne Aumont[1,2,3], Marc-Andre Bedard[1,2,3,4], Aurelie Bussy[4,5,6], Jaime Fernandez Arias[2,3,4], Joseph Therriault[2,3,4], Nesrine Rahmouni[2,3,4], Jenna Stevenson[2,3,4], Cecile Tissot[2,3,4], Stijn Servaes[2,3,4], Arthur C. Macedo[2,3,4], Serge Gauthier[2,3,4], Mallar M. Chakravarty[4,5,6], Pedro Rosa-Neto[2,3,4]

[1]*NeuroQAM Research Centre, Université du Québec à Montréal (UQAM), Montréal, QC, Canada*
[2]*McGill University Research Centre for Studies in Aging, McGill University, Montréal, QC, Canada*
[3]*Montreal Neurological Institute, McGill University, Montréal, QC, Canada*
[4]*Department of neurology and neurosurgery, McGill University, Montréal, QC, Canada*
[5]*Cerebral Imaging Center, Douglas Research Center, Montréal, QC, Canada*
[6]*Computational Brain Anatomy (CoBrALab) Laboratory, Montréal, QC, Canada*

Cross-sectional studies have highlighted the interrelatedness among key Alzheimer's Disease (AD) features, including tau and amyloid β pathology, hippocampal atrophy and memory. We aimed to provide deeper insights into these relationships, by employing a longitudinal framework to examine correlations among these variables.

A cohort of 180 subjects (mean age: 70.1) underwent structural MRI, Tau-PET using [18F]MK6240, and Amyloid-PET using [18F]AZD4694. Among them, 101 were rescanned after 2 years. Utilizing MAGeT-Brain, we segmented the hippocampi into subfields: 1) dentate gyrus and CA4 (DG/CA4), 2) CA2 and CA3 (CA2/CA3), 3) CA1, 4) strata radiatum, lacunosum, and moleculare (SRLM), and 5) subiculum. Memory assessment involved the Rey Auditory verbal Learning Test (RAVLT) – delayed recall. We analyzed hippocampal subfield volumes, Braak I, II, and III tau SUVR, global amyloid β SUVR, RAVLT, and their respective rates of change over the study 2 year duration.

Our cross-sectional analyses indicated significant correlations among subfield volumes, tau SUVR, global amyloid β SUVR, and memory. Longitudinal analyses, however, demonstrated that only the rate of change in Braak II SUVR was significantly and negatively correlated with CA1, DG/CA4, and subiculum, as well as the RAVLT rate of change. Two mediation analyses, using either baseline or rate of change measures, indicated that CA1, DG/CA4, and subiculum did not mediate the association between Braak II tau and RAVLT.

It can be concluded that the rate of change in Braak II tau is the best predictor of both, hippocampal subfield atrophy and memory decline. Conversely, cross-sectional analyses do not provides with a good insight into the relationships between tau, amyloid β, hippocampal subfield volumes, and memory. This underscores the importance to consider hippocampal tau accumulation over time when considering hippocampal atrophy and memory decline.

Keywords: Hippocampus, Hippocampal subfields, Tau-PET, Memory, Longitudinal

124 Tau-PET Overlap Index; associations with Braak Stage and quantitative NFT measurements

Jeyeon Lee[1,2], Hoon-Ki Min[1], Christina Moloney[1], Carly Mester, Emily Lund, Sujala Ghatamaneni, Matthew Senjem, Aivi Nguyen, Jonathan Graff-Radford, Christopher Schwarz, Jeffrey Gunter, Kejal Kantarci, Bradley Boeve, Prashanthi Vemuri, David Jones, David Knopman, Clifford Jack, Ronald Petersen, Melissa Murray, Val Lowe

[1]*Department of Radiology, Mayo Clinic, Rochester, MN, United States*
[2]*Hanyang University, Seoul, South Korea*
[3]*Neuroscience, Mayo Clinic, Jacksonville, FL, United States*
[4]*Department of Health Sciences Research, Mayo Clinic, Rochester, MN, United States*
[5]*Information Technology Mayo Clinic, Rochester, MN, United States*
[6]*Laboratory Medicine and Pathology, Mayo Clinic, Rochester, MN, United States*
[7]*Department of Neurology, Mayo Clinic, Rochester, MN, United States*

Introduction: A reliable method to detect early tau accumulation in tau positron emission tomography (tau-PET) is crucial. We hypothesized that identifying voxels with stable signal serially will increase confidence that tau-PET signal represents tau neuropathology.

Methods: This study included 26 participants who had at least two serial tau-PETs and autopsy. We designed the "overlap index" (OI) method to detect spatially identical, voxel-wise standardized-uptake-value-ratio (SUVR) elevation when seen sequentially in serial tau-PET(*1*). We tested the association of META-OI and standard META-ROI SUVR with neuropathological Braak stage. Associations with quantitative immunohistochemical neurofibrillary tangle (NFT) were also tested. The minimum quantitative NFT detectability was determined by the point where the regression line of each tau-PET measure intersects with each threshold level (i.e., 0.5 for OI and 1.29 for SUVR). Association of regional OI and SUVR with the %NFT burden measured on immunohistochemistry was tested for the amygdala, hippocampus, parahippocampal gyrus, fusiform, superior temporal, and middle temporal cortex.

Results: Overlap index improved Braak stage detection in 5/26 (19%) participants and 3/11 (27%) early Braak stage (I-IV) participants (Figure 1). OI values increased earlier (lower %NFT) than SUVR value across six brain regions in quantitative NFT assessment suggesting that the estimated minimum detectability of the OI measure was significantly lower than that of SUVR (p=0.036) (Figure 2).

Discussion: OI could be a more sensitive measurement for detection of early Braak stage and NFT signal elevation than standard SUVR ROI measures. Early detection of NFT will be important in early AD treatment trials.

1. Lee J, Burkett BJ, Min HK, et al. The Overlap Index as a Means of Evaluating Early Tau PET Signal Reliability. *J Nucl Med.* 2022;63:1748-1753.

Figure 1. Tau-PET and Braak Stage.

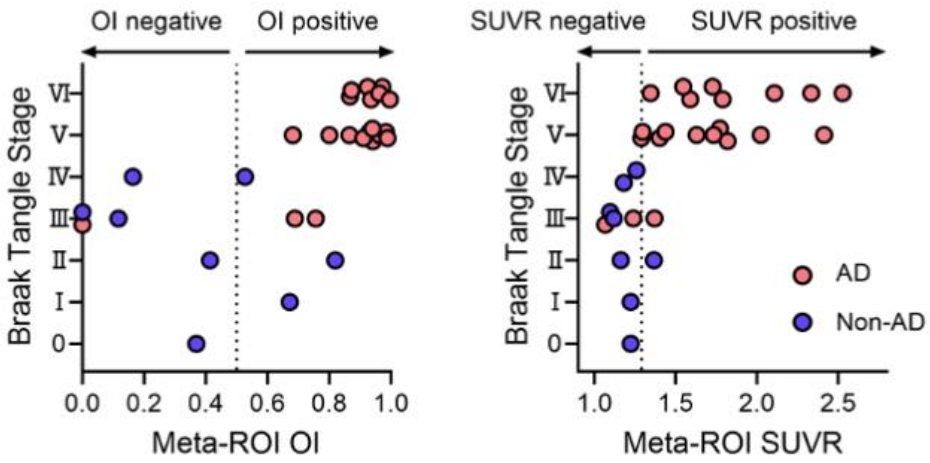

Figure 1. Plots of META-ROI OI and META-ROI SUVR vs Braak tangle stage are shown. Vertical dotted lines represent respective cut points of 0.5 for OI and 1.29 for SUVR. Neuropathologic diagnosis is show in blue or red.

Figure 2. Tau-PET and %tau (NFT) burden.

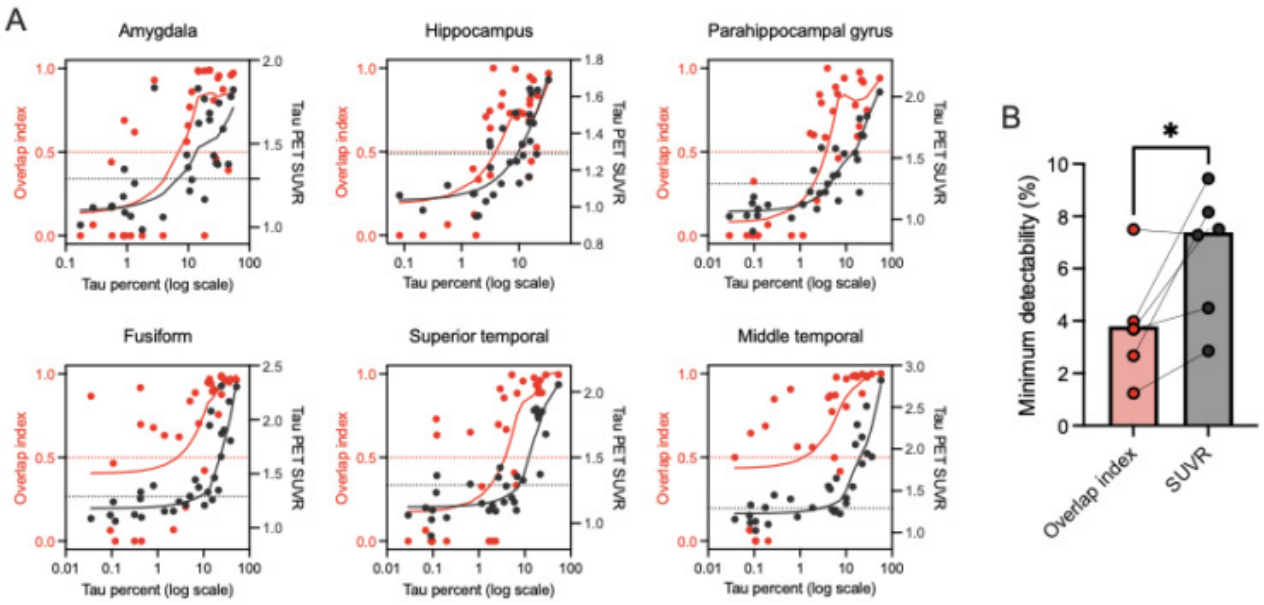

Figure 2. (A) Association of OI and SUVR with the %tau burden measured on immunohistochemistry is shown for the amygdala, hippocampus, parahippocampal gyrus, fusiform, superior temporal, and middle temporal cortex. The red and black dotted horizontal lines depict the threshold level for OI (=0.5) and SUVR (=1.29), respectively. (B) The minimum detectability was determined by the point where the regression line of each measure intersects with the threshold level. * $p<0.05$, paired t-test.

Figure 1. Tau-PET and Braak Stage.

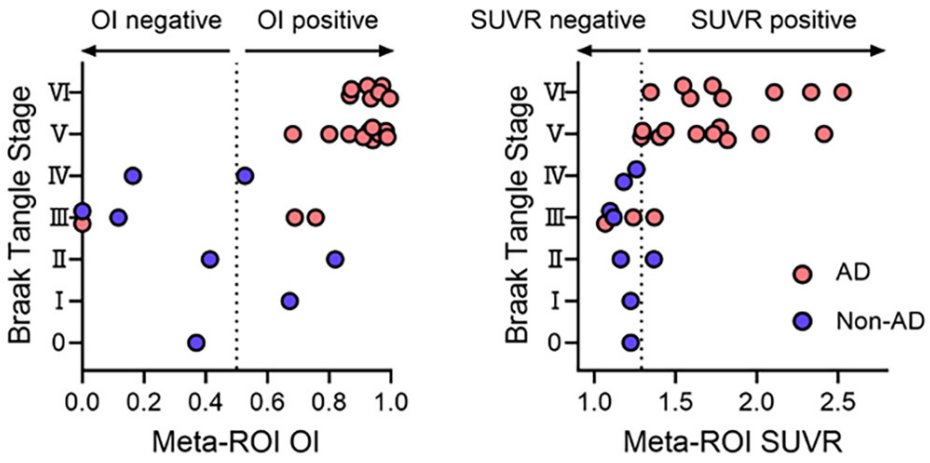

Figure 1. Plots of META-ROI OI and META-ROI SUVR vs Braak tangle stage are shown. Vertical dotted lines represent respective cut points of 0.5 for OI and 1.29 for SUVR. Neuropathologic diagnosis is show in blue or red.

Keywords: PET, tau imaging, neuropathology, Overlap Index, Braak stage

125 Tau-PET spatial extent for predicting cognitive decline within tau-positive individuals

Emma Coomans[1,2], Bastiaan van Tol[1,2], Colin Groot[1,2], Wiesje van der Flier[1,2], Yolande Pijnenburg[1,2], Elsmarieke van de Giessen[3,4], Rik Ossenkoppele[1,2,5]

[1]*Alzheimer Center Amsterdam, Neurology, Vrije Universiteit Amsterdam, Amsterdam UMC location VUmc, Amsterdam, The Netherlands*
[2]*Amsterdam Neuroscience, Neurodegeneration, Amsterdam, The Netherlands*
[3]*Radiology & Nuclear Medicine, Vrije Universiteit Amsterdam, Amsterdam UMC location VUmc, Amsterdam, The Netherlands*
[4]*Amsterdam Neuroscience, Brain Imaging, Amsterdam, The Netherlands*
[5]*Clinical Memory Research Unit, Lund, Sweden*

Background: In 2020, a visual read method for [^{18}F]flortaucipir received FDA-approval, thereby facilitating the clinical implementation of tau-PET. However, among tau-positive scans large variation exists in the number of voxels exceeding the FDA-approved threshold. Tau-PET visual read has already demonstrated high diagnostic value for Alzheimer's disease dementia, and we hypothesize that the extent of tau-positive voxels additionally yields important prognostic information.

Methods: We included participants from the Amsterdam Dementia Cohort (ADC, n=151) and the Alzheimer's Disease Neuroimaging Initiative (ADNI, n=781) who underwent tau-PET and had at least one MMSE measurement available (**Table-1**). First, tau-PET scans were visually read according to FDA-approved guidelines using non-intensity normalized, unitless images. Second, for tau-positive scans only (since variance in cognition in tau-negative individuals may be unrelated to tau) we calculated global and temporal meta-region spatial extent as the percentage of tau-positive voxels within a global and temporal meta-region mask (**Figure-1**). To compare the prognostic performance of spatial extent with that of more established metrics, we additionally included global and temporal meta-region SUVR. We performed age-, sex- and education-adjusted linear models between tau-PET spatial extent or SUVR (predictors) and concurrent MMSE or MMSE rate of change (outcomes).

Results: Within tau-positive individuals, spatial extent expectedly increased from cognitively unimpaired to mildly impaired to dementia stages (**Figure-1**). In both cohorts, spatial extent predicted concurrent MMSE (ADC: $stdB_{[global]}$=-0.47, $stdB_{[temporal]}$=-0.39; ADNI: $stdB_{[global]}$=-0.54, $stdB_{[temporal]}$=-0.47, all p<0.001) and MMSE rate of change (ADC: $stdB_{[global]}$=-0.64, $stdB_{[temporal]}$=-0.56; ADNI: $stdB_{[global]}$=-0.53, $stdB_{[temporal]}$=-0.57, all p<0.001; **Table-2**). When comparing spatial extent models with SUVR models, we consistently observed higher adjusted R^2-values and lower AICc-values for spatial extent models (**Table-2**).

Discussion: Within visually tau-positive individuals, tau-PET spatial extent predicted cognitive decline and outperformed established SUVR parameters. Tau-PET spatial extent may supplement the diagnostic information already provided by visual read with a more refined prediction of future cognitive decline.

Table 1 Demographics

	Amsterdam Dementia Cohort (ADC)		Alzheimer's Disease Neuroimaging Initiative (ADNI)	
	Tau-PET negative	Tau-PET positive	Tau-PET negative	Tau-PET positive
N	66	85	631	150
Age	67.0 ± 7.7	64.6 ± 7.2	72.8 ± 8.1	74.9 ± 7.8
Sex, n female (%)	27 (40.9)	44 (51.8)	332 (52.6)	79 (52.7)
Education, y	12.4 (2.8)	12.3 ± 3.1	16.5 ± 2.5	15.8 ± 2.3
APOE E4 status, n carrier (%)	28 (45.9)	56 (70.0)	158 (30.6)	85 (69.7)
Aβ-status, n positive (%)	27 (40.9)	85 (100.0)	180 (29.9)	137 (97.9)
Diagnosis				
CU, n (%)	54 (81.8)	6 (7.1)	402 (63.7)	24 (16.0)
MCI, n (%)	2 (3.0)	10 (11.8)	194 (30.7)	69 (46.0)
AD dementia, n (%)	10 (15.2)	69 (81.2)	35 (5.5)	57 (38.0)
MMSE				
Concurrent MMSE	25.1 ± 4.4	22.7 ± 4.2	28.6 ± 1.9	25.2 ± 4.1
N with longitudinal MMSE, n (%)	61 (92.4)	68 (80.0)	475 (75.3)	109 (72.7)
Annual rate of change in MMSE	-0.25 ± 1.3	-2.0 ± 2.1	-0.23 ± 1.1	-1.89 ± 2.4

All participants had at least one MMSE measurement available measured within 1-year from tau-PET. Education was missing for n=1 ADC participant. APOE E4 status was missing for n=10 ADC participants and for n=142 ADNI participants. Aβ-status was missing for n=38 ADNI participants.

Figure 1 Tau-PET spatial extent methodology

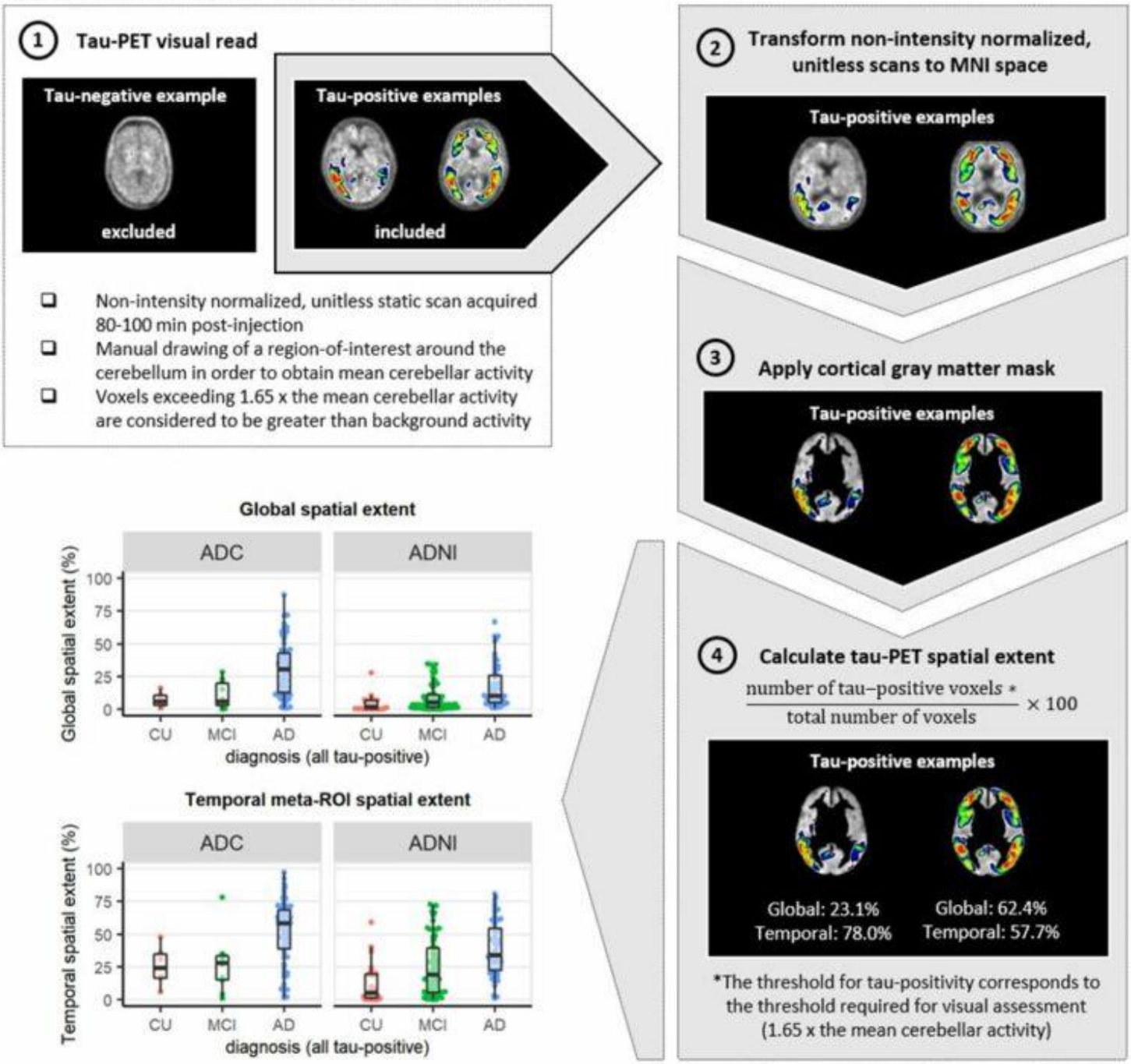

Table 2 Tau-PET spatial extent versus tau-PET SUVR for predicting concurrent MMSE and MMSE rate of change within visually tau-positive individuals

			Spatial Extent			SUVR		
			StdB [95% CI]	R^2	AICc	StdB [95% CI]	R^2	AICc
ADC	Concurrent MMSE	Global	-0.47 [-0.23, -0.72]	0.16	234.0	-0.40 [-0.15, -0.65]	0.12	238.5
		Temporal	-0.39 [-0.18, -0.61]	0.15	235.7	-0.22 [0.01, -0.44]	0.05	244.7
	MMSE rate of change	Global	-0.64 [-0.38, -0.90]	0.27	179.8	-0.63 [-0.34, -0.92]	0.22	184.1
		Temporal	-0.56 [-0.35, -0.78]	0.29	178.2	-0.48 [-0.22, -0.73]	0.17	188.5
ADNI	Concurrent MMSE	Global	-0.54 [-0.39, -0.69]	0.28	384.1	-0.52 [-0.36, -0.68]	0.25	390.2
		Temporal	-0.47 [-0.32, -0.62]	0.24	391.9	-0.45 [-0.30, -0.60]	0.22	395.6
	MMSE rate of change	Global	-0.53 [-0.32, -0.75]	0.17	295.9	-0.47 [-0.27, -0.66]	0.14	300.1
		Temporal	-0.57 [-0.39, -0.75]	0.26	284.8	-0.47 [-0.26, -0.69]	0.17	296.9

All analyses were performed within visually tau-positive participants. All participants had concurrent MMSE available measured within 1-year from tau-PET. MMSE rate of change was missing for n=17 (20.0%) ADC participants and n=41 (27.3%) ADNI participants.

Keywords: Alzheimer's disease, tau, positron emission tomography, prognosis

126 Association of sex and cerebral beta-amyloid with cortical gray matter brain age in cognitively impaired older adults

Jinghang Li[1], Sang Joon Son[2], Chang-Le Chen[1], Linghai Wang[1], Howard Aizenstein[1,3], Chang Hyung Hong[2], Hyun Woong Roh[2], Yong Hyuk Cho[2], Sunhwa Hong[2], You Jin Nam[2], Bumhee Park[4], Na-Rae Kim[4], Dong Yun Lee[4], Jin Wook Choi[5], So Young Moon[9], Sang Woon Seo[6], Seong Hye Choi[7], Eun-Joo Kim[8], Minjie Wu[3]

[1]*Department of Bioengineering, University of Pittsburgh, Pittsburgh, PA, United States*
[2]*Department of Psychiatry, Ajou University School of Medicine, Suwon, South Korea*
[3]*Department of Psychiatry, University of Pittsburgh, Pittsburgh, PA, United States*
[4]*Department of Biomedical Informatics, Ajou University School of Medicine, Suwon, South Korea*
[5]*Department of Radiology, Ajou University School of Medicine, Suwon, South Korea*
[6]*Department of Neurology, Samsung Medical Centre, Sungkyunkwan University School of Medicine, Seoul, South Korea*
[7]*Departmenti of Neurology, Inha University School of Medicine, Inchon, South Korea*
[8]*Department of Neurology, Pusan National University Hospital, Busan, South Korea*
[9]*Department of Neurology, Ajou University School of Medicine, Suwon, South Korea*

Background: MRI-derived brain age metrics, reflecting the varying rates of brain aging among individuals, offer insights into neurodevelopment and neurodegeneration . In this study, we employed a deep learning based conditional variational autoencoder (cVAE) and aimed to uncover the normative cortical brain aging patterns and explore their links to cognitive performances and other Alzheimer's disease (AD) biomarkers in an ongoing dementia brain imaging study.

Method & Results: The cVAE model was trained on cortical thickness maps from T1-weighted images while conditioned on chronological age. Specifically, the model was first trained on a cognitively normal dataset (CamCAN) that consists of 665 subjects spanning ages from 18 to 86 years. Subsequently, we conducted the model inference on a separate dementia dataset that is a part of an ongoing Biobank Innovations for Chronic Cerebrovascular Disease with Alzheimer's Disease Study (BICWALZS) including 643 participants with ages ranging from 49 to 87 years and cognitive conditions ranging from subjective memory impairment (SMI) to severe dementia. We found that the elevated brain age gap was positively correlated with amyloid standardized uptake value ratio (SUVR) and clinical dementia rating (CDR) (figure 1). Additionally, our analysis revealed gender differences in cortical aging within this dementia dataset; women appeared younger than men in the cortical brain age (figure 2). Finally, we demonstrated variations in the brain age gap among different dementia diagnoses including those with SMI, mild cognitive impairment (MCI), AD, vascular dementia (VD), and other types of dementia (figure 3).

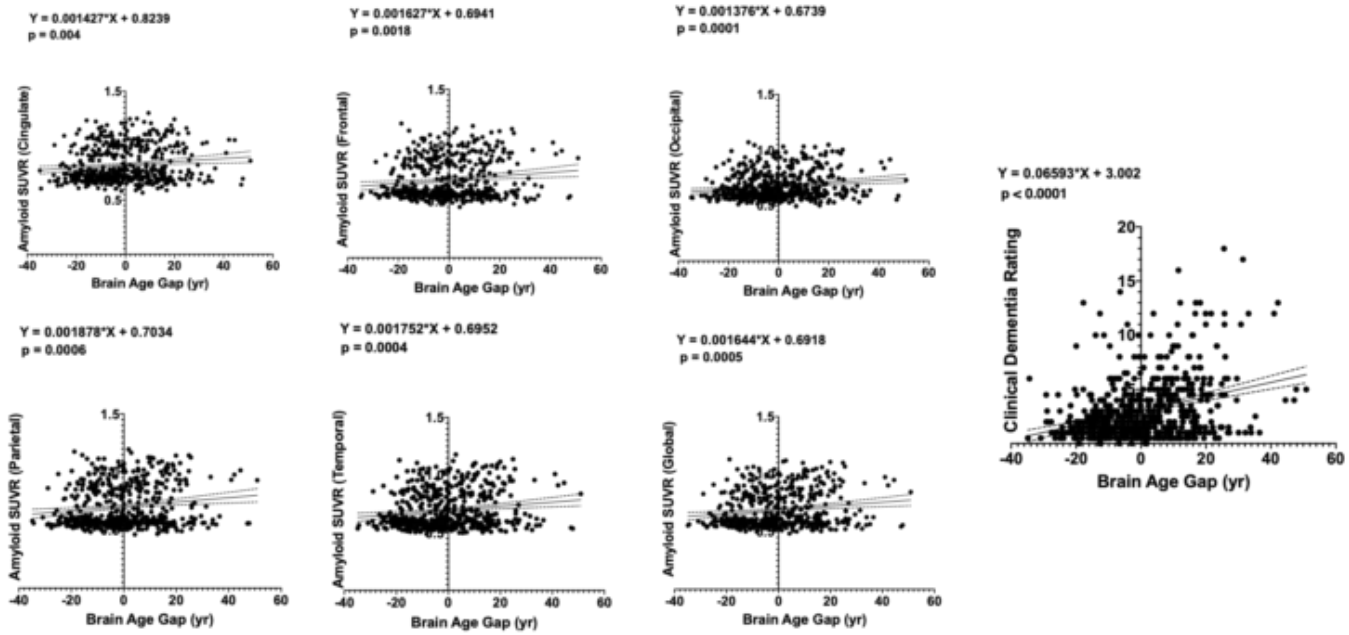

Figure 1. Association of brain age gap with reginal amyloid deposition and clinical dementia rating

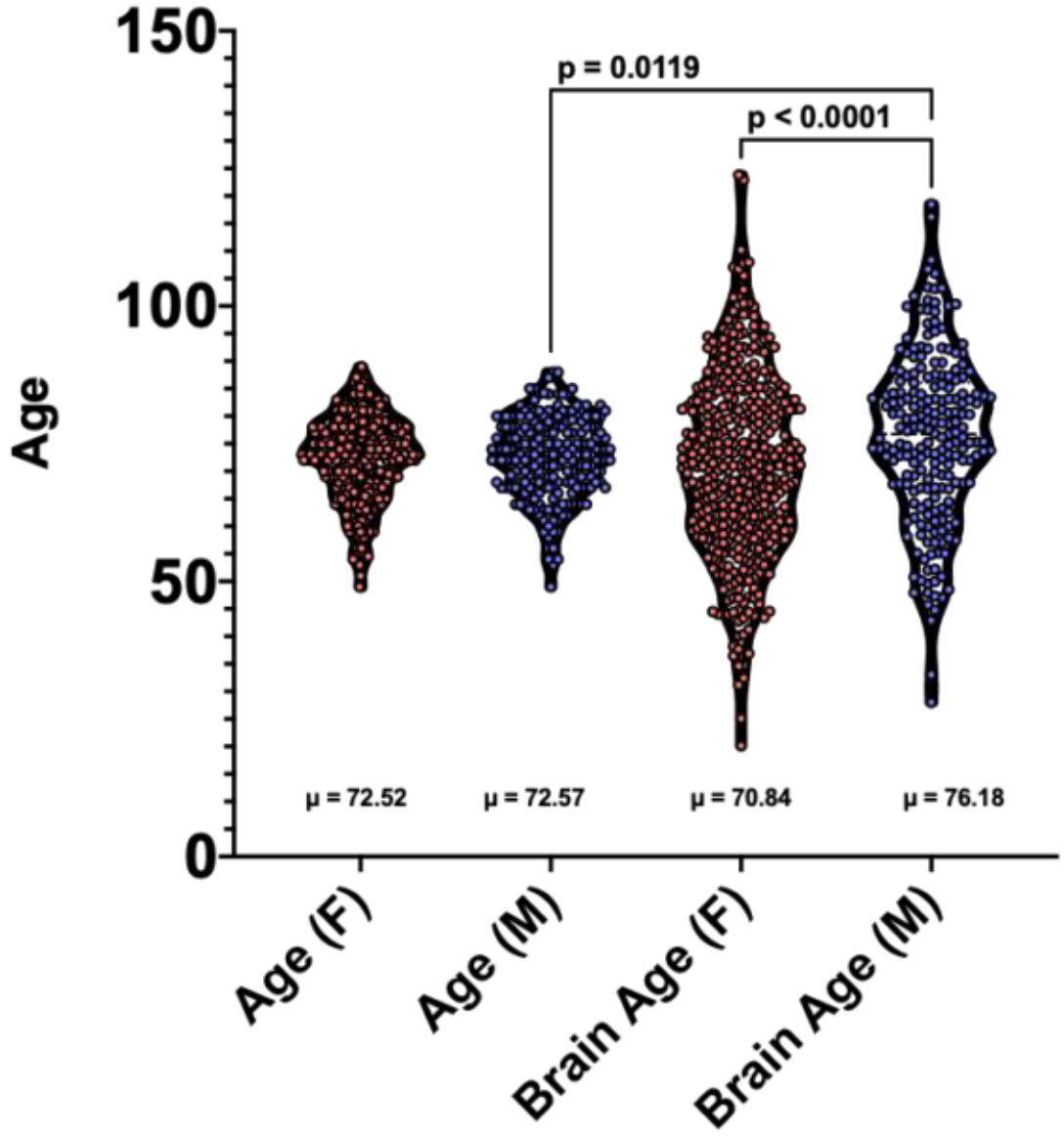

Figure 2. Sex differences in cortical brain age.

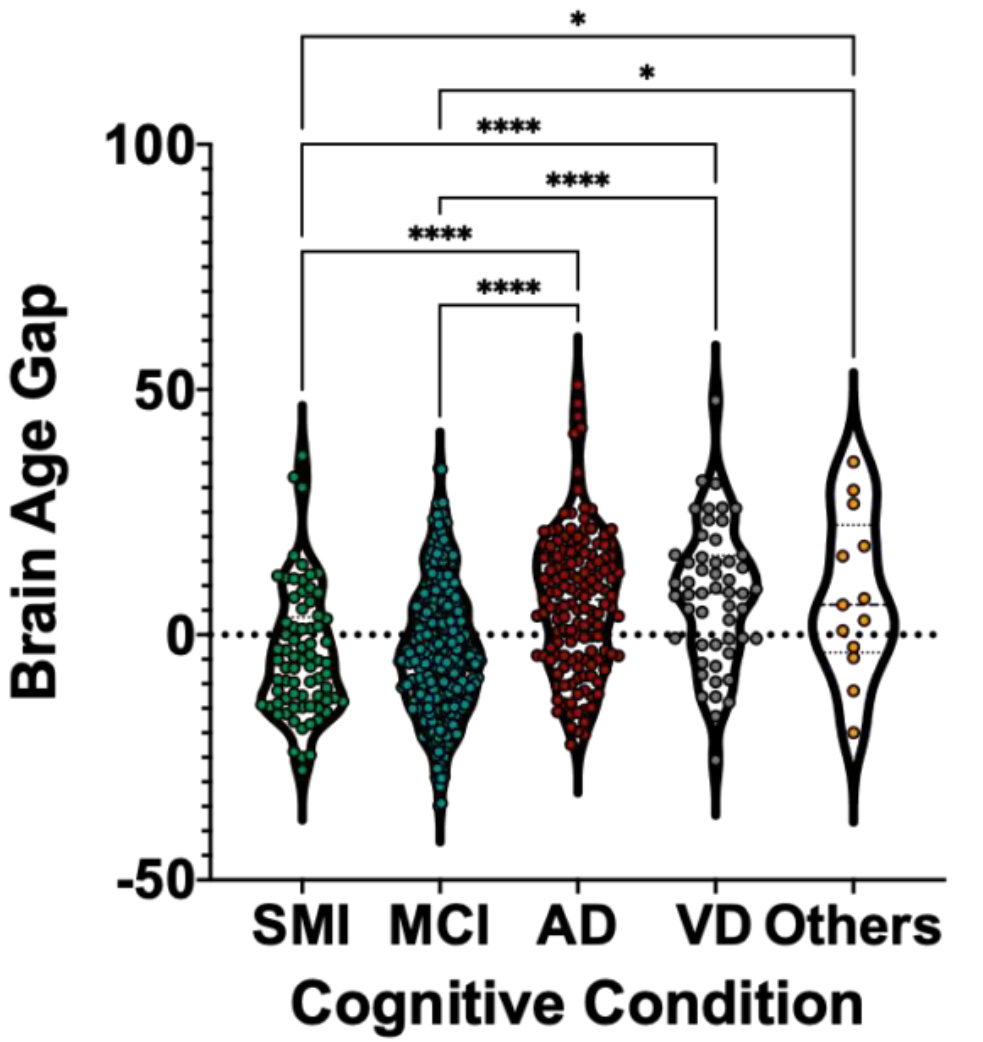

Figure 3. Brain age gap across cognitive conditions. (****p<0.0001, *p=0.025)

Conclusion

Our study employed a cVAE model to predict brain age based on cortical morphologies and identified that the elevated brain age gap was positively associated with amyloid uptake and dementia severities. Furthermore, we uncovered variations in brain age gap among different dementia diagnoses and gender-related difference in which females exhibited a younger cortical brain age than males.

Keywords: Deep learning, Brain Age, Dementia, Sex Differences

127 Will cerebral glucose metabolism measured using [18F]FDG PET substitute tau PET in clinical studies?

Paul Edison

[1]Imperial College London, London, United Kingdom

It is suggested that tau aggregation could mirror hypometabolism in Alzheimer's disease (AD). However, the pathophysiological processes underlying these changes are different, and we propose that these two hallmarks have different trajectories in AD. In this study, we tested whether glucose metabolism, using fluorodeoxyglucose ([18F]FDG)-positron emission tomography (PET), could replace tau-PET in clinical studies. We performed quantitative analysis of [18]FDG-PET and [18F]AV1451-PET along with MRI in 371 subjects. Initially, the standard uptake value ratio images were created for each subject. Single-subject statistical parametric maps were then created to assess individual uptake compared to the controls at a voxel level. Novel measurements of global tau load and global hypometabolism, which is a reflection of the global pathological changes, were then estimated by multiplying the volume of the individual statistical t-map with the intensity. Correlation analysis and linear models were then performed to evaluate the relationship between these pathological changes. Voxel-wise group and region-of-interest level analyses were also performed. There was adissociation between global cerebral glucose hypometabolism and global tau in amyloid-positive AD and amyloid-negative mild cognitive impairment (MCI) ($p>0.05$). Global hypometabolism was only associated with global cortical tau in amyloid-positive MCI when controlled for age. Voxel-level single subject tau load was a better predictor of neuropsychological performance, baseline Alzheimer's disease assessment scale-cognitive (ADAS-Cog) 13 score, and ADAS-Cog 13 one-year change compared with regional and global hypometabolism. This study suggests that global tau deposition does not mirror global hypometabolism. This may be due to the influence of other pathologies in the Alzheimer's trajectory affecting glucose metabolism. Additionally, single-subject global tau load better predicts cognitive deterioration than glucose metabolism. Hence, these two processes should be evaluated independently in observational and therapeutic intervention studies.

Keywords: FDG, Tau, glucose metabolism

128 CSF sTREM2 is associated with neuroprotective microglial states early in Alzheimer's disease and deleterious effects later in the disease trajectory

Harry Crook1D, Malak Wahdan1D, Nicholas R Livingston1, Sanara Raza1, Joseph Nowell1, Paul Edison1, 2*

[1]Imperial College London, London, United Kingdom

Introduction: Triggering receptor expressed on myeloid cells 2 (TREM2) is an immune receptor which regulates several microglial functions. The role of TREM2 in Alzheimer's trajectory is still being debated.

Methods: Here we investigated the influence of cerebrospinal fluid (CSF) soluble TREM2 (sTREM2) on neuropathological substrates during the Alzheimer's disease (AD) trajectory.

Results: CSF sTREM2 levels did not differ between AD, mild cognitive impairment (MCI) and cognitively normal subjects. CSF sTREM2 was positively associated with CSF total-tau and phosphorylated-tau181 across groups; and was also positively associated with CSF Aβ42 in amyloid-positive participants in each group. Early and late stages of the AD trajectory showed contrasting associations between CSF sTREM2 and neuroimaging markers.

Discussion: sTREM2 was associated with the deposition of amyloid and tau aggregation. Opposing correlations of CSF sTREM2 and neuroimaging markers between early versus late-stage AD suggests that sTREM2 may represent pro- and anti-inflammatory microglial proliferation/activation within the AD trajectory.

Keywords: sTREM, amyloid, Tau, CSF

129 The Mobile Toolbox for assessing cognition remotely: associations with amyloid and tau deposition in cognitively unimpaired older adults

Roos Jutten[1], Jessa Burling[1], Jessie Fu[2], Michael Properzi[1], Rebecca Amariglio[1,3], Kate Papp[1,3], Gad Marshall[1,3], Julie Price[2], Keith Johnson[2], Reisa Sperling[1,3], Dorene Rentz[1,3]

[1]*Department of Neurology, Massachusetts General Hospital, Harvard Medical School, Boston, MA, United States*
[2]*Department of Radiology, Massachusetts General Hospital, Harvard Medical School, Boston, MA, United States*
[3]*Department of Neurology, Brigham and Women's Hospital, Harvard Medical School, Boston, MA, United States*

Background: Remote, smartphone-based cognitive assessments such as the Mobile Toolbox (MTB) can facilitate the detection of subtle cognitive changes due to early Alzheimer's disease (AD) pathology. Here, we investigated the associations between the MTB and amyloid-β (Aβ) and tau deposition on positron emission tomography (PET) imaging in cognitively unimpaired (CU) older adults.

Methods: N=80 CU older adults from four affiliated observational cohort-studies completed the MTB at home on their personal device. A subset (n=64) had Aβ PET ([^{11}C]Pittsburgh-Compound-B) and n=35 also underwent tau PET with [^{18}F]flortaucipir (FTP) and n=26 with [^{18}F]MK-6240 (Table 1). The MTB includes six measures of fluid cognition, comprising episodic memory (Picture Sequence Memory and Face-Name Associative Memory Exam [FNAME]), executive functions (EF) and processing speed (Dimensional Change Card Sort [DCCS], Flanker, Memory for Sequences, Number-Symbol Match), and two measures of crystallized cognition (Spelling and Vocabulary). Linear regression models correcting for age, sex and education examined associations between MTB measures and global Aβ burden (DVR) and tau deposition (SUVR, PVC) in tau-relevant regions (entorhinal and inferior-temporal, and a neocortical composite of inferior-temporal, fusiform, middle-temporal, and inferior-parietal tau). Models were performed separately for each tau tracer and for the normalized SUVR values (z-scores) in a combined FTP+MK-6240 sample.

Results: No MTB measures were associated with global Aβ deposition. Lower Number-Symbol Match scores were associated with greater entorhinal tau in the FTP subset only. Lower FNAME and DCCS scores were associated with greater inferior-temporal tau in the combined tau sample. Associations between MTB measures and tau were consistent in the neocortical composite region (Table 2).

Conclusion: Preliminary findings suggest that MTB measures may capture subtle deficits in memory, EF and processing speed associated with tau deposition in CU older adults. Data collection and tau data harmonization is ongoing to further examine whether MTB measures can detect AD-related cognitive decline.

Table 1. Demographic, clinical and PET imaging characteristics for the Mobile Toolbox study sample.	
Total sample (N=80)	
Age, mean (SD)	70.6 (9.29)
Female, n (%)	50 (62.5%)
Years of education, mean (SD)	16.7 (2.52)
Race, AS / B / W, n (%)	2 (2.5%) / 10 (12.5%) / 68 (85.0%)
Ethnicity, H / NH, n (%)	5 (6.3%) / 75 (93.8%)
Preclinical Alzheimer's Cognitive Composite z-score, mean (SD)	0.00 (0.705)
Subset with PiB PET (n=65)	
Age, mean (SD)	71.7 (9.64)
Female, n (%)	38 (58.5%)
Years of education, mean (SD)	16.5 (2.60)
PiB DVR, Global FLR, mean (SD) [min, max]	1.22 (0.26), [0.98, 2.27]
PiB DVR Group (DVR threshold = 1.19), Ab-/Ab+ (%)	46 (70.8%) / 19 (29.2%)
Subset with FTP PET (n=35)	
Age, mean (SD)	74.9 (7.99)
Female, n (%)	21 (58.3%)
Years of education, mean (SD)	16.4 (2.96)
PiB Group (DVR threshold = 1.19), Ab-/Ab+ (%)	24 (68.5 %) / 11 (31.5%)
Entorhinal tau (SUVR, PVC), mean (SD) [min, max]	1.38 (0.36), [0.73, 2.11]
Inferior temporal tau (SUVR, PVC), mean (SD) [min, max]	1.57 (0.29), [1.22, 2.93]
Subset with MK6240 PET (n=26)	
Age, mean (SD)	64.6 (7.73)
Female, n (%)	18 (66.7%)
Years of education, mean (SD)	16.8 (2.11)
PiB Group (DVR threshold = 1.19), Ab-/Ab+/Unknown (%)	16 (59.3%) / 6 (22.2%) / 5 (18.5%)
Entorhinal tau (SUVR, PVC), mean (SD) [min, max]	0.95 (0.69), [0.21, 3.04]
Inferior temporal tau (SUVR, PVC), mean (SD) [min, max]	1.12 (0.16), [0.87, 1.54]

Abbreviations: PiB = [11C]Pittsburgh-Compound-B; DVR = distribution volume ratio; SUVR = standardized uptake value ratio (using cerebellar gray matter reference region); FLR = frontal, lateral temporal and retrosplenial composite region; FTP =[18F]flortaucipir; MK6240= [18F]MK-6240; PVC = partial volume correction using geometric transfer matrix algorithm.

Table 2. Estimates obtained from linear regression models examining associations between Mobile Toolbox measures and tau deposition.												
Entorhinal tau (SUVR, PVC)												
	Picture Sequence Memory			**FNAME**			**Flanker**			**DCCS**		
	Beta	*95%CI*	*P-value*	*Beta*	*95%CI*	*P-value*	*Beta*	*95%CI*	*P-value*	*Beta*	*95%CI*	*P-value*
FTP (n=35)	-0.04	-0.40 – 0.31	0.805	-0.15	-0.51 – 0.21	0.402	0.05	-0.35 – 0.44	0.819	-0.05	-0.34 – 0.24	0.723
MK (n=26)	-0.16	-0.52 – 0.21	0.388	-0.15	-0.60 – 0.30	0.495	-0.30	-0.65 – 0.06	0.095	-0.28	-0.76 – 0.19	0.231
FTP + MK (n=61)	-0.15	-0.46 – 0.15	0.316	-0.08	-0.38 – 0.22	0.603	-0.14	-0.47 – 0.18	0.385	-0.19	-0.48 – 0.10	0.199
	Memory for Sequences			**Number-Symbol Match**			**Spelling**			**Vocabulary**		
	Beta	*95%CI*	*P-value*	*Beta*	*95%CI*	*P-value*	*Beta*	*95%CI*	*P-value*	*Beta*	*95%CI*	*P-value*
FTP (n=35)	0.01	-0.36 – 0.37	0.971	**-0.34**	**-0.67 – -0.02**	**0.040**	0.03	-0.40 – 0.45	0.896	0.04	-0.45 – 0.52	0.877
MK (n=26)	-0.07	-0.46 – 0.33	0.724	-0.10	-0.49 – 0.29	0.605	0.12	-0.32 – 0.56	0.571	0.30	-0.04 – 0.64	0.177
FTP + MK (n=61)	-0.01	-0.32 – 0.29	0.934	-0.29	-0.59 – -0.00	0.050	0.15	-0.17 – 0.48	0.350	0.24	-0.08 – 0.57	0.138
Inferior-temporal tau (SUVR, PVC)												
	Picture Sequence Memory			**FNAME**			**Flanker**			**DCCS**		
	Beta	*95%CI*	*P-value*	*Beta*	*95%CI*	*P-value*	*Beta*	*95%CI*	*P-value*	*Beta*	*95%CI*	*P-value*
FTP (n=35)	-0.05	-0.39 – 0.28	0.754	-0.30	-0.64 – 0.04	0.078	0.31	-0.33 – 0.95	0.327	-0.27	-0.53 – 0.00	0.051
MK (n=26)	0.03	-0.33 – 0.39	0.857	-0.33	-0.75 – 0.10	0.124	-0.06	-0.43 – 0.30	0.716	-0.20	-0.67 – 0.28	0.404
FTP + MK (n=61)	-0.02	-0.29 – 0.24	0.873	**-0.30**	**-0.56 – -0.05**	**0.020**	0.10	-0.26 – 0.46	0.575	**-0.25**	**-0.50 – 0.00**	**0.049**
	Memory for Sequences			**Number-Symbol Match**			**Spelling**			**Vocabulary**		
	Beta	*95%CI*	*P-value*	*Beta*	*95%CI*	*P-value*	*Beta*	*95%CI*	*P-value*	*Beta*	*95%CI*	*P-value*
FTP (n=35)	-0.19	-0.54 – 0.16	0.282	-0.12	-0.45 – 0.22	0.484	-0.26	-0.64 – 0.11	0.160	-0.20	-0.63 – 0.24	0.359
MK (n=26)	0.02	-0.40 – 0.36	0.911	-0.09	-0.46 – 0.29	0.631	0.14	-0.29 – 0.57	0.509	0.09	-0.26 – 0.44	0.612
FTP + MK (n=61)	-0.12	-0.38 – 0.15	0.380	-0.12	-0.39 – 0.15	0.392	-0.08	-0.36 – 0.20	0.551	-0.07	-0.34 – 0.21	0.631
Neocortical tau composite (SUVR, PVC)												
	Picture Sequence Memory			**FNAME**			**Flanker**			**DCCS**		
	Beta	*95%CI*	*P-value*	*Beta*	*95%CI*	*P-value*	*Beta*	*95%CI*	*P-value*	*Beta*	*95%CI*	*P-value*
FTP (n=35)	-0.05	-0.38 – 0.29	0.783	-0.31	-0.65 – 0.02	0.067	0.20	-0.44 – 0.85	0.525	-0.23	-0.50 – 0.04	0.091
MK (n=26)	-0.02	-0.38 – 0.34	0.907	-0.37	-0.79 – 0.05	0.079	-0.07	-0.44 – 0.29	0.680	-0.29	-0.76 – 0.18	0.218
FTP + MK (n=61)	-0.04	-0.30 – 0.22	0.765	**-0.33**	**-0.58 – -0.08**	**0.011**	0.06	-0.30 – 0.42	0.754	**-0.27**	**-0.52 – -0.01**	**0.039**
	Memory for Sequences			**Number-Symbol Match**			**Spelling**			**Vocabulary**		
	Beta	*95%CI*	*P-value*	*Beta*	*95%CI*	*P-value*	*Beta*	*95%CI*	*P-value*	*Beta*	*95%CI*	*P-value*
FTP (n=35)	-0.23	-0.58 – 0.12	0.182	-0.10	-0.44 – 0.24	0.558	-0.32	-0.69 – 0.05	0.087	-0.27	-0.70 – 0.16	0.204
MK (n=26)	-0.24	-0.61 – 0.13	0.198	-0.24	-0.61 – 0.12	0.178	-0.07	-0.50 – 0.37	0.753	-0.01	-0.36 – 0.34	0.960
FTP + MK (n=61)	-0.24	-0.50 – 0.03	0.076	-0.17	-0.44 – 0.10	0.202	-0.21	-0.48 – 0.07	0.137	-0.15	-0.42 – 0.12	0.277

Note. No correction for multiple testing was applied for these preliminary analyses, table shows nominal P-values. SUVR = standardized uptake value ratio (using cerebellar gray matter reference region); FTP =[18F]flortaucipir; MK = [18F]MK-6240; PVC = partial volume correction using geometric transfer matrix algorithm. Neocortical tau composite includes inferior-temporal, fusiform, middle-temporal, and inferior-parietal tau.

Keywords: Cognition, remote assessment, positron emission tomography, tau

130 Characterizing multi-site harmonized amyloid and tau PET across the Alzheimer's continuum

Karly Cody[1], Emily Johns[1], Mackenzie Carlson[1], Kyan Younes[1], Christina Young[1], Shubhabrata Mukherjee[2], Emily Trittschuh[2], Laura E. Gibbons[2], Logan Dumitrescu[3], Derek Archer[3], Alaina Durant[3], Connie Nakano[2], Brandon Klinedinst[2], Seo-Eun Choi[2], Michael Lee[2], Phoebe Scollard[2], Jesse Mez[4], Andrew Saykin[5], Paul K. Crane[2], Michael Cuccaro[6], Arthur W. Toga[7], Duygu Tosun[8], Timothy Hohman[3], Elizabeth Mormino[1]

[1]*Department of Neurology and Neurological Sciences, Stanford University, Stanford, CA, United States*
[2]*Department of Medicine, University of Washington, Seattle, WA, United States*
[3]*Vanderbilt Memory and Alzheimer's Center, Vanderbilt Genetics Institute, Department of Neurology, Vanderbilt University Medical Center, Nashville, TN, United States*
[4]*Department of Neurology, Boston University School of Medicine, Boston, MA, United States*
[5]*Department of Radiology and Imaging Sciences, Indiana University School of Medicine, Indianapolis, IN, United States*[6]*Department of Human Genetics, University of Miami, Miami, FL, United States, Miami, FL, United States*
[7]*Alzheimer's Disease Research Center, Keck School of Medicine, University of Southern California, Los Angeles, CA, United States*
[8]*Department of Radiology, University of California, San Francisco, CA, United States*

Objectives: This study leverages large-scale harmonized PET data from the AD Sequencing Project-Phenotype Harmonization Consortium (ADSP-PHC) to 1) characterize the prevalence of amyloid and tau positivity; 2) examine the associations of amyloid and early tau to memory performance.

Methods: Participants (N=6347; 72.0±5.9 years) from A4 (n=3944), ADNI (n=1661), and NACC (n=742) who underwent amyloid PET imaging were included in this study. A subset of individuals also underwent tau PET imaging (n=1260). Amyloid (Florbetapir, Florbetaben, and PiB) PET and tau (FTP and MK6240) PET scans were quantified separately for each radiotracer as SUVRs using MRI-free pipelines. Amyloid SUVRs were translated to Centiloids (CL) and regional tau positivity (NFT+/-) was quantified hierarchically in terms of Braak NFT staging. We examined the correspondence between CL bins and PET-based NFT staging. Among those unimpaired (CU) at baseline with available harmonized memory scores, we examined cross-sectional associations between PET measures and memory.

Results: Incrementally higher baseline CL levels were seen across clinical diagnostic groups (Fig. 1A). In the subset with both amyloid and tau PET imaging, 1178 (93.5%) participants showed a hierarchical pattern of tau spread consistent with Braak staging. Among those that followed the hierarchical pattern of NFT deposition, the spatial extent of NFT+ increased with both CL level and clinical disease severity (Fig. 1B-D). Linear regressions indicated independent effects of CL and age on cross-sectional memory among CU. In the CU subset with tau, CL, NFT I/II+, and age each had independent associations with cross-sectional (Fig. 2). The associations of CL and NFT I/II with lower memory scores did not differ by education, sex, or *APOE* genotype.

Discussion: This study of large-scale harmonized PET and cognitive data recapitulates A/T associations with memory established in smaller studies, validating these methods and providing support for using these harmonized endophenotypes in work towards novel genetic discoveries.

Table 1. ADSP Baseline Amyloid PET Characteristics

Characteristic	Overall N = 6,347	Clinical Diagnosis CU N = 5,219	MCI N = 814	Dementia N = 314
Cohort				
A4	3,944 (62%)	3,944 (76%)	0 (0%)	0 (0%)
ADNI	1,661 (26%)	666 (13%)	718 (88%)	277 (88%)
NACC	742 (12%)	609 (12%)	96 (12%)	37 (12%)
Amyloid Tracer				
FBB	422 (7%)	239 (5%)	133 (16%)	50 (16%)
FBP	5,697 (90%)	4,875 (93%)	598 (73%)	224 (71%)
PIB	228 (4%)	105 (2%)	83 (10%)	40 (13%)
Age at amyloid PET (years)	72.0 (5.9)	71.6 (5.3)	73.0 (7.8)	75.2 (8.0)
Sex				
Female	3,639 (57%)	3,167 (61%)	346 (43%)	126 (40%)
Male	2,708 (43%)	2,053 (39%)	468 (57%)	187 (60%)
APOE4 status[a]				
e4 noncarrier	3,769 (63%)	3,248 (66%)	416 (54%)	105 (35%)
e4 carrier	2,232 (37%)	1,688 (34%)	351 (46%)	193 (65%)
Education (years)[b]	16.5 (2.7)	16.6 (2.7)	16.2 (2.7)	15.8 (2.7)
Centiloids (CL)	24 (40)	18 (35)	40 (47)	76 (47)
CL Bins				
<10	3,045 (48%)	2,718 (52%)	290 (36%)	37 (12%)
10-24	1,046 (16%)	937 (18%)	95 (12%)	14 (4%)
25-49	807 (13%)	677 (13%)	101 (12%)	29 (9%)
50-74	614 (10%)	440 (8%)	115 (14%)	59 (19%)
75-99	432 (7%)	261 (5%)	104 (13%)	67 (21%)
≥100	403 (6%)	186 (4%)	109 (13%)	108 (34%)
Age at tau PET (years)	73.1 (7.0)	72.6 (6.5)	74.5 (8.0)	74.2 (8.1)
Tau TRACER				
FTP	1,177 (93%)	835 (93%)	286 (96%)	56 (92%)
MK	83 (7%)	65 (7%)	13 (4%)	5 (8%)
Hierarchical NFT positivity[c]				
Tau -	890 (71%)	691 (77%)	180 (60%)	19 (31%)
I/II	109 (9%)	78 (9%)	27 (9%)	4 (7%)
III	25 (2%)	20 (2%)	4 (1%)	1 (2%)
IV	40 (3%)	26 (3%)	10 (3%)	4 (7%)
V	50 (4%)	18 (2. %)	22 (7%)	10 (16%)
VI	64 (5%)	16 (2%)	29 (10%)	19 (31%)
Discordant	82 (6%)	51 (6%)	27 (9%)	4 (7%)

Values are shown as n (%) or Mean (SD).

[a]N=346 individuals were missing genetic data

[b]N=7 individuals were missing education data

[c]Tau PET positivity was quantified in regions corresponding to NFT Braak staging (e.g. NFT I-VI) and individuals were assigned a hierarchical PET-based NFT stage, where later stages could only be achieved if the individual was tau positive in previous stages. Individuals who did not follow the hierarchical staging were classified as Braak discordant.

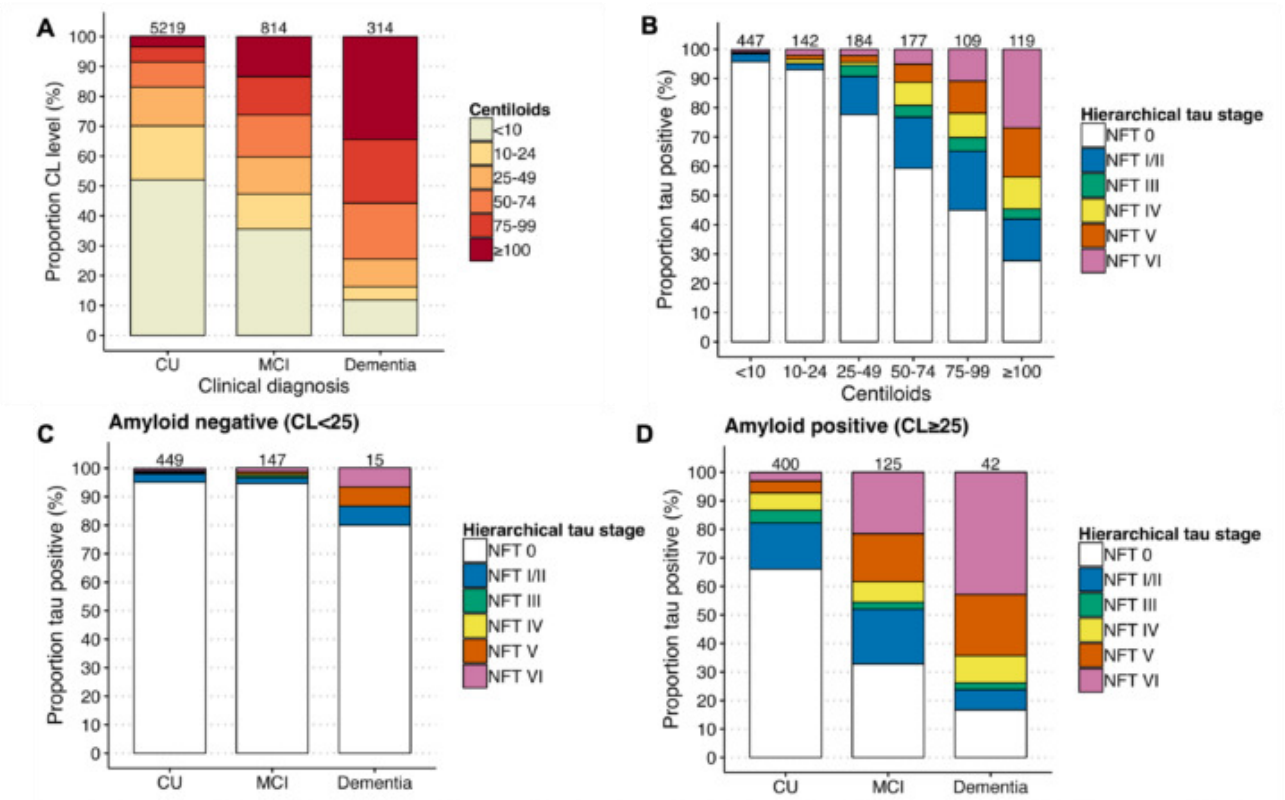

Figure 1. Baseline CL and hierarchical NFT stage distributions. Stacked bar plots of the percentage of CL bins across (A) diagnostic groups as well as the percentage of NFT stage tau positive subjects across (B) CL bins and (C-D) amyloid-based clinical groups.

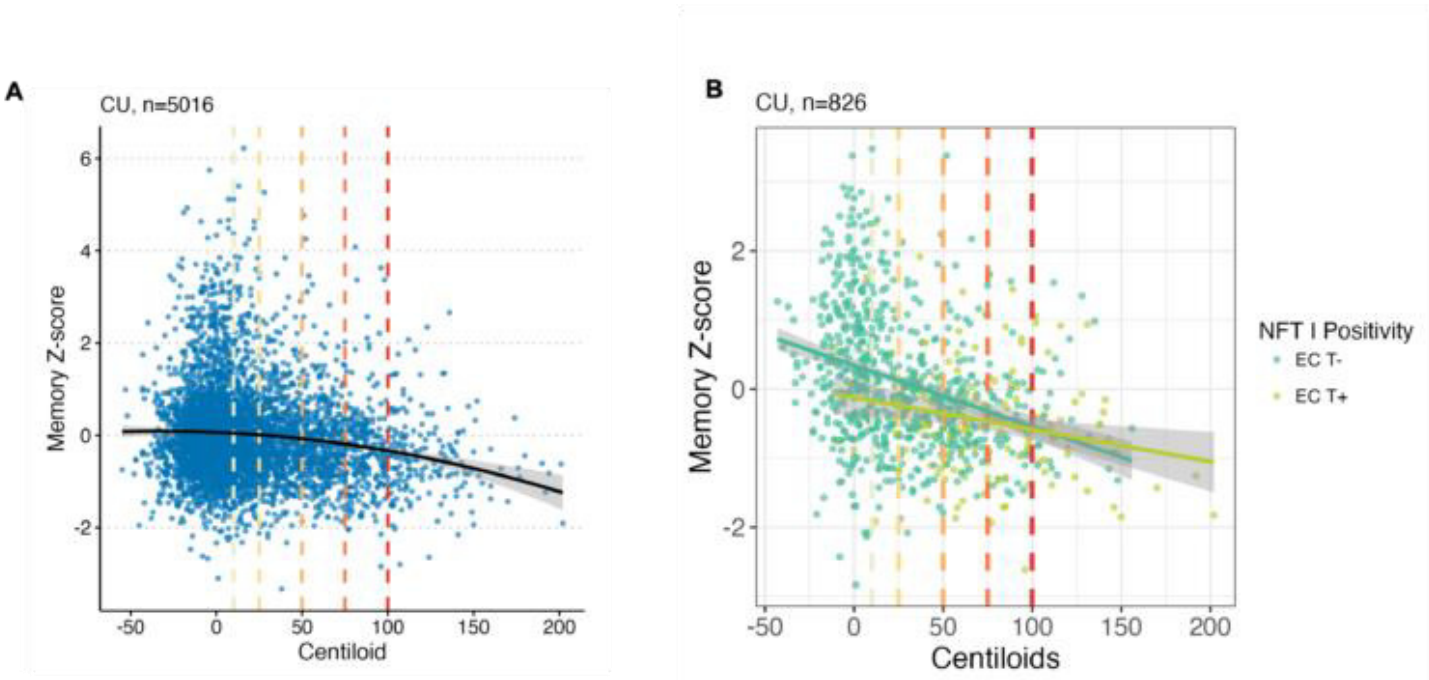

Figure 2. Effects of amyloid and tau on cross-sectional memory in unimpaired participants. (A) Memory scores are plotted against Centiloid levels with mean curves and 95% confidence intervals represented by the shaded region. (B) Memory scores plotted against Centiloid levels with mean curves for entorhinal tau positive and negative groups. The vertical dashed lines indicate the thresholds for CL bins.

Keywords: Amyloid, tau, PET, harmonization

131 Characterization of tau PET accumulation relative to duration of entorhinal tau positivity

Karly Cody[1,2], Rebecca Langhough[1], Margo Heston[1], Jordan Teague[1], Bradley Christian[1], Sterling Johnson[1], Tobey Betthauser[1]

[1]*Department of Medicine, University of Wisconsin, Madison, WI, United States*
[2]*Department of Neurology and Neurological Sciences, Stanford University, Stanford, CA, United States*

Objective: This work examined longitudinal tau PET (^{18}F-MK-6240) relative to age, amyloid duration, and entorhinal tau (EC) duration to better understand neurofibrillary tangle (NFT) spatial accumulation in Alzheimer's disease.

Methods: Participants (N=647; Table 1) from the Wisconsin Registry for Alzheimer's Prevention and WADRC underwent serial amyloid and tau PET imaging. Amyloid burden was quantified from global cortical ^{11}C-PiB $DVR_{(0-70)}$. Tau burden was quantified in regions corresponding to Braak NFT stages using ^{18}F-MK-6240 $SUVR_{(70-90)}$. Sampled iterative local approximation (SILA) was used to model longitudinal PiB and EC ^{18}F-MK-6240 trajectories and estimate biomarker positive onset ages and time. Longitudinal ^{18}F-MK-6240 uptake was assessed for relationships with age, A+ duration, EC T+ duration as well as patterns and timing of spatial tau spread relative to PET-based NFT stages.

Results: Increasing ^{18}F-MK-6240 SUVRs were associated with older age, longer A+ duration, and longer EC T+ duration (Fig. 1A-C). Analyses comparing age, A+ duration and EC T+ duration as predictors of regional ^{18}F-MK-6240 SUVR indicated that EC T+ duration accounted for significantly more variance in latent tau accumulation than both A+ duration and age (Fig. 1A-C; R^2 EC T+ time models > R^2 A+ time models > R^2 age models). Estimates of the average time from A+ onset to regional NFT T+ indicated that among A+ individuals, EC T+ (NFT I) occurred in the first decade of A+ (6.9±0.8years after A+ onset; Fig 2A). As a function of years of EC T+, regional T+ followed the expected spatiotemporal pattern (II-VI) as time from EC T+ onset increased (Fig 2B) ranging from 5.4±0.3years for NFT II+ to 13.5±0.3years for NFT VI+.

Conclusions: Temporal modeling of tau PET imaging demonstrates the spatiotemporal pattern of NFT accumulation. Time estimates of the onset and spread of tau outside the EC which will help inform clinical trial design.

Table 1. Participant Characteristics

Characteristic	Overall N = 647	Clinical Status: Normal N = 585	Clinical Status: MCI N = 49	Clinical Status: Dementia N = 13	p-value[a]
Cohort					<0.001
ADRC	198 (31%)	161 (28%)	27 (55%)	10 (77%)	
WRAP	449 (69%)	424 (72%)	22 (45%)	3 (23%)	
Age at tau PET (years)	67.52 (7.35)	67.08 (7.35)	70.89 (5.81)	74.81 (6.05)	<0.001
Sex					0.3
Female	425 (67%)	389 (68%)	29 (59%)	7 (54%)	
Male	212 (33%)	186 (32%)	20 (41%)	6 (46%)	
***APOE*e4 carriage**[b]	241 (41%)	203 (38%)	29 (64%)	9 (69%)	<0.001
Equivalent Centiloids at tau PET	21.13 (36.22)	16.06 (30.53)	63.60 (47.31)	88.86 (52.25)	<0.001
Global PiB DVR at tau PET	1.19 (0.24)	1.15 (0.21)	1.47 (0.32)	1.64 (0.35)	<0.001
A+ at tau PET	193 (30%)	148 (25%)	34 (69%)	11 (85%)	<0.001
Estimated age of A+ onset (years)[c]		61.92 (8.34)	58.44 (7.11)	58.68 (9.69)	0.032
Num. MK-6240 Scans					0.034
1	431 (67%)	379 (65%)	40 (82%)	12 (92%)	
2	201 (31%)	192 (33%)	8 (16%)	1 (7.7%)	
3	15 (2.3%)	14 (2.4%)	1 (2.0%)	0 (0%)	
EC T+ at tau PET	120 (19%)	82 (14%)	27 (55%)	11 (85%)	<0.001
Estimate age of EC T+ onset (years)[d]		65.27 (7.84)	62.98 (6.14)	63.94 (7.06)	0.2

Values are shown as n (%) or Mean (SD).

Abbreviations: MCI, mild cognitive impairment; PET, positron emission tomography; PiB, Pittsburg Compound B; A+, amyloid positive; EC T+, entorhinal tau positive

[a] Fisher's exact test (categorical variables) and Kruskal-Wallis rank sum test (continuous variables)

[b] N=595 had complete genetic information (n,missing=52)

[c] A+ onset age was estimated using the sampled iterative local approximation algorithm (SILA) and is shown only for those that became A+ (Global PiB DVR >1.16) over the course of the study (N=193)

[d] EC T+ onset age was estimated using SILA and is shown only for those that became EC T+ (Entorhinal MK-6240 SUVR >1.27) over the course of the study (N=120)

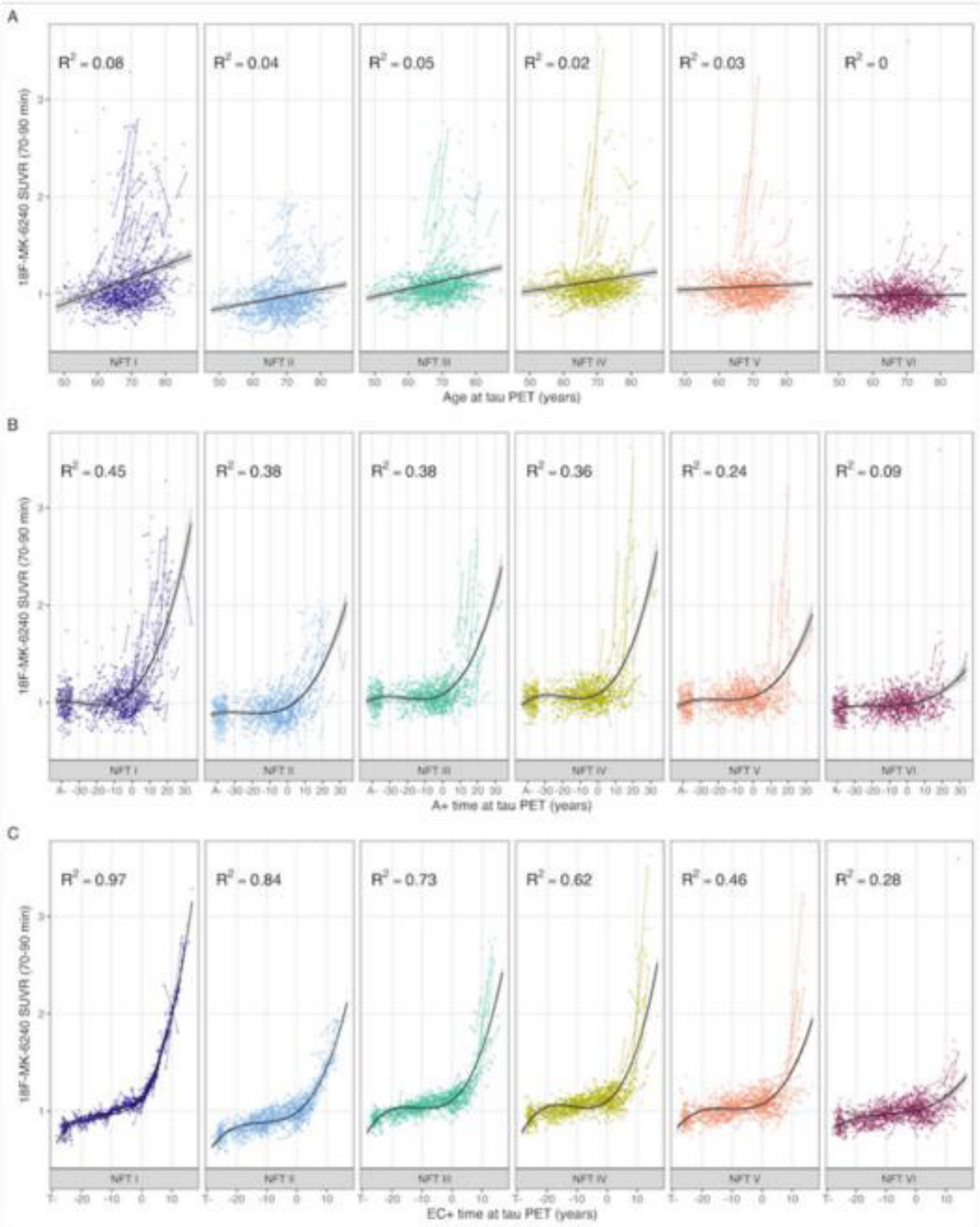

Figure 1. MK-6240 PET SUVR by (**A**) age at tau PET scan, (**B**) SILA estimated amyloid (A+) duration, (**C**) SILA estimated entorhinal (EC) tau duration. We compared model fit (Akaike Information Criterion (AICc) and R^2 values) for regression models using either age (mean-centered), SILA estimated A+ duration or SILA estimated EC T+ duration as predictors of MK-6240 SUVR across NFT regions of interest. For each predictor, models started with cubic polynomials, removing non-significant higher order terms sequentially. Lines indicate models of best fit, with the shaded regions indicating the 95% confidence interval.

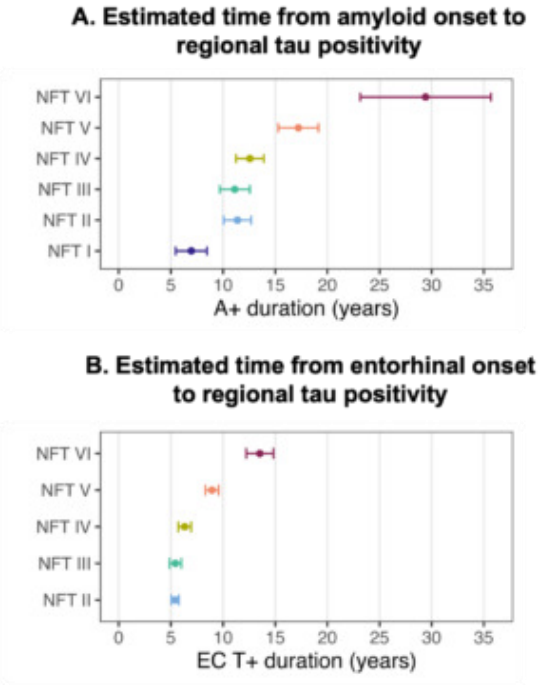

Figure 2. Estimated time to regional tau positivity from amyloid onset (A) and entorhinal tau onset (B) among amyloid positive individuals (n,ppts=212; n,scans=301). A summary of predicted amyloid duration and tau duration at regional tau positivity, including predicted 95% confidence intervals (Wald interval based on the delta method). On average, the magnitude of NFT regional tau changes along both the amyloid timeline and entorhinal tau timeline followed the stereotypical pattern of tau accumulation, with considerably less variability in regional tau positivity estimates along the entorhinal tau timeline. The average time from amyloid onset (A+ duration=0) to NFT I (entorhinal tau) positivity occurred in the first decade of amyloid accumulation. The average time from entorhinal tau onset (EC T+ duration=0) to tau spread outside of the medial temporal lobe ranged from 5.4±0.29 years to NFT III, 6.3±0.31 years to NFT IV, 8.9±0.29 years to NFT V, and 13.5±0.29 years to NFT VI).

Keywords: Tau, PET

132 Harmonization of multi-scanner PET data with ComBat: application to 18F-AV1451 data acquired on a Siemens ECAT HR+ PET and a GE Discovery MI PET/CT Scanner

Cristina Lois Gomez[1], Ibai Diez-Palacio[1], Julie C. Price[1], Keith A. Johnson[1]

[1]*Massachusetts General Brigham, Boston, MA, United States*

Background: The quantitative performance of PET scanners depends on factors like detector hardware and image reconstruction protocols. In studies involving multiple scanners, systematic quantitative inter-scanner variability hampers the ability to compare and combine data, and harmonization methods are needed to maximize study power. A common harmonization method in neuroimaging PET applies smoothing of data to match the lowest-resolution camera in the study. This degrades the quality of the data and may potentially cause a loss of relevant biological information.

ComBat is a harmonization method developed to remove batch effects in genomics [1] that has recently been applied to neuroimaging (cortical thickness [2], DTI [3]) with good results.

Aim: To apply ComBat to ^{18}F-AV1451 data and evaluate its potential for harmonization of multi-scanner PET neuroimaging data.

Methods: ^{18}F-AV1451 data were acquired in two cohorts of cognitively normal subjects (n=88/cohort) using two different scanners: a Siemens ECAT HR+ PET (HR+), and a GE Discovery-MI (GE-DMI) PET/CT. Our standard ^{18}F-AV1451 protocols were followed (HR+: OSEM 16s4i, 5mm Gaussian filter; GE-DMI: OSEM 16s5i, with PSF and TOF, no filter). Brain region segmentations were generated using FreeSurfer, and SUVR values were calculated (cerebellar grey reference). ComBat harmonization was applied to ROI SUVR data, including age and amyloid as covariates, and inter-scanner differences were analyzed.

One individual was sequentially scanned in both cameras and regional differences were evaluated before and after harmonization.

Results and Conclusions: ComBat efficiently removed the multi-scanner effects for SUVR regional data (Fig. 1), while maintaining biological variations (age, amyloid). Preliminary results of the individual scanned in both cameras showed ComBat reduced scanner-related SUVR differences (Table 1). ComBat is a promising harmonization method, but further validation is still needed.

[1] Johnson et al. *Biostatistics (2007)* 8, 118–127.

[2] Fortin et al. NeuroImage (2018) 167, 104-120.

[3] Fortin et al. NeuroImage (2017) 161, 149-170.

	Cohort 1	Cohort 2
Scanner	HR+	GE-DMI
N	86	86
Age (years)	59.7 ± 9.2	60.0 ± 9.6
Sex (F/M)	52/34	52/34
FLR PiB DVR	1.1 ± 0.1	1.1 ± 0.2
MMSE	29 ± 1	29 ± 1

Table 1. Subject demographics. Two cohorts of cognitively normal subjects with similar age, sex, and amyloid distributions, were scanned in two different scanners: HR+ or GE DMI. Data are expressed as mean ± standard deviation. F: female; M: male; FLR PiB DVR: distribution volume values obtained with 11C-Pittsburgh compound B in a large, amyloid susceptible cortical aggregate region (FLR); MMSE: Mini-Mental State Examination score.

	NOT Harmonized			ComBat Harmonized		
Brain Region	SUVR GE-DMI	SUVR HR+	% SUVR difference	SUVR GE-DMI	SUVR HR+	% SUVR difference
Amygdala	1.160	1.224	5.21	1.194	1.190	0.39
Hippocampus	1.396	1.402	0.41	1.694	1.583	7.06
Entorhinal	1.022	1.032	0.99	1.059	1.090	2.78
Inf. Parietal	1.136	1.080	5.24	1.218	1.212	0.53
Inf. Temporal	1.241	1.210	2.56	1.047	1.029	1.76
Mid.Temporal	1.193	1.118	6.71	0.991	1.014	2.27
AVERAGE			3.52			2.47

Table 2. Example regional SUVR values obtained for one individual scanned sequentially in the GE-DMI and HR+ cameras, before and after ComBat harmonization. Percentage SUVR absolute differences between cameras are reduced after ComBat harmonization.

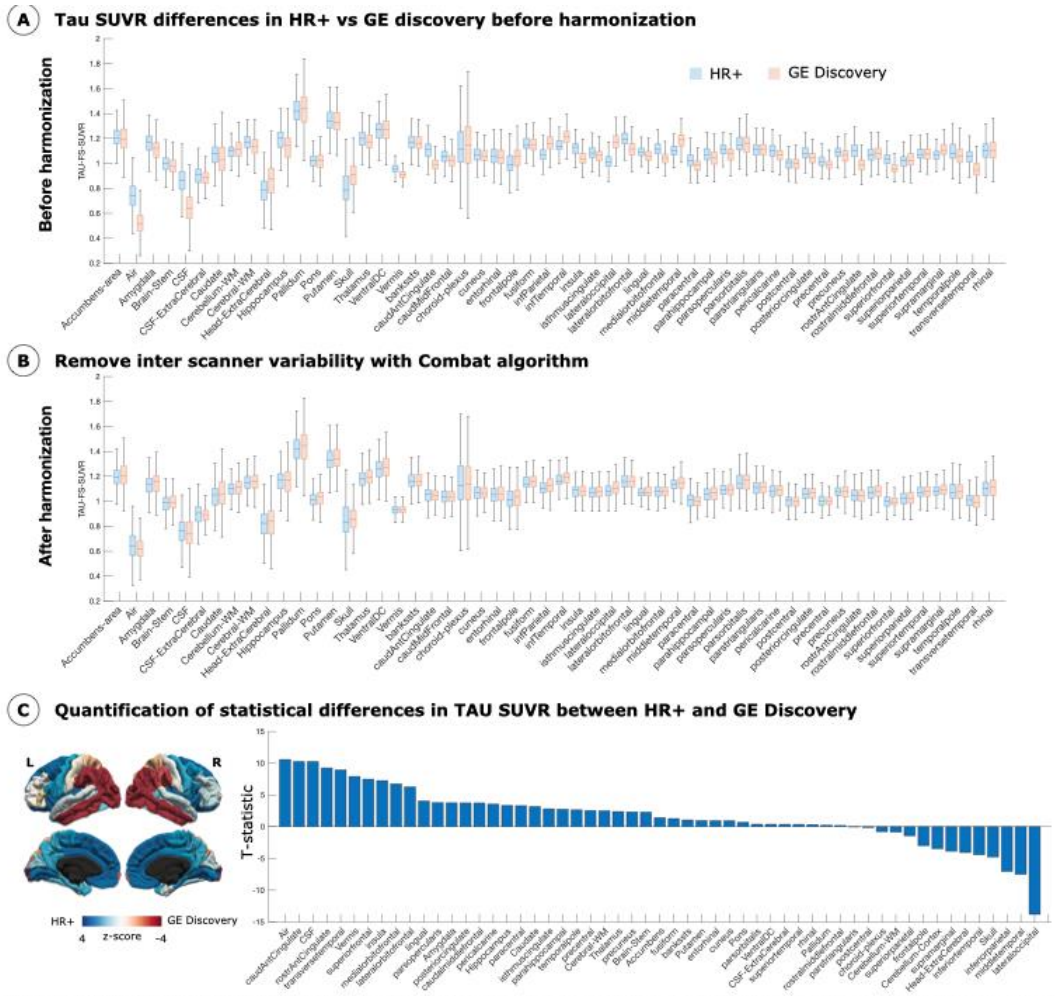

Fig 1. Regional 18F-AV1451 SUVR values obtained in two cohorts of cognitively normal subjects. Each cohort was scanned in a different scanner (HR+ or GE Discovery-MI). (A) Regional SUVR values before harmonization. (B) Regional SUVR values after ComBat harmonization, showing reduced inter-scanner variability. (C) Quantification of the regional SUVR differences obtained between HR+ and GE-DMI scanners.

Keywords: Harmonization, PET, inter-scanner variability

133 Longitudinal white matter degeneration is associated with higher subsequent amyloid load across the Alzheimer's disease continuum

Courtney Burton[1], Jenna Blujus[2], Hwamee Oh[2,3,4]

[1]*Memory and Aging Program, Butler Hospital, Providence, RI, United States*
[2]*Department of Cognitive, Linguistic, and Psychological Sciences, Brown University, Providence, RI, United States*
[3]*Department of Psychiatry and Human Behavior, Warren Alpert Medical School, Brown University, Providence, RI, United States*
[4]*Carney Institute for Brain Science, Brown University, Providence, RI, United States*

Background: Neuritic plaques with fibrillar beta-amyloid (Aβ) peptides and tau-protein neurofibrillary tangles have been associated with subsequent white matter integrity (WMI) loss. Recent studies suggest that WMI loss could also lead to increased Aβ deposition. In the current study, we examined whether longitudinal WMI loss would be associated with greater Aβ deposition at a later timepoint.

Methods: A total of 221 participants (138 cognitively normal [CN], 57 patients with mild cognitive impairment, and 26 patients with dementia) were selected from the ADNI database, given the availability of two timepoints of diffusion-weighted MRI (dMRI) data and one timepoint of Aβ PET data collected within one year of the second dMRI timepoint. The dMRI data were processed using FSL's FDT and TBSS pipelines to quantify the degree of fractional anisotropy (FA) and create annualized FA change maps to measure voxel-wise WMI change over time. Global amyloid SUVR values were converted to the Centiloid scale. The associations between longitudinal WMI change and Aβ pathology were assessed by FSL's randomise with cluster-level correction, controlling for age and sex. These voxel-wise analyses were performed first for the whole sample and separately for CN only.

Results: Across the whole sample, greater WMI loss was associated with higher global Aβ load across white matter tracts, including frontal, parietal, and temporal areas, as well as corpus callosum (Figures 1&2). Within CN individuals, the relationship between WMI loss and Aβ load was restricted within the body of corpus callosum.

Conclusions: Greater white matter degeneration across the brain was associated with higher Aβ load detected at a subsequent time point. Future studies are warranted to examine the regional association between white matter degeneration and amyloid accumulation, as well as the mediating factors of this relationship.

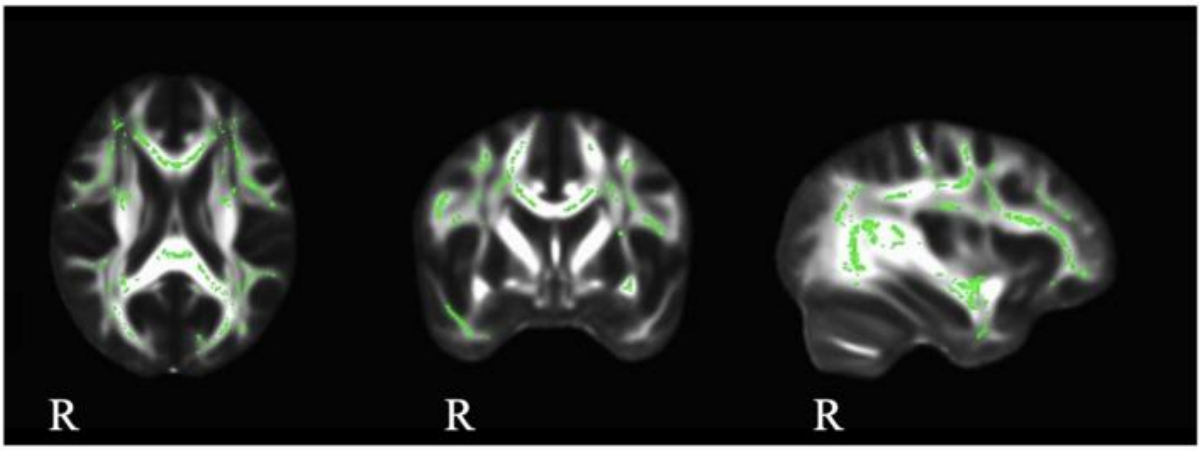

Figure 1. The associations between longitudinal WMI change, which was quantified by annualized FA ([FA Session 2 - FA Session 1]/years), and subsequent amyloid pathology, controlling for age and sex. Green-colored regions indicate greater WMI loss over two timepoints, in association with higher global amyloid load.

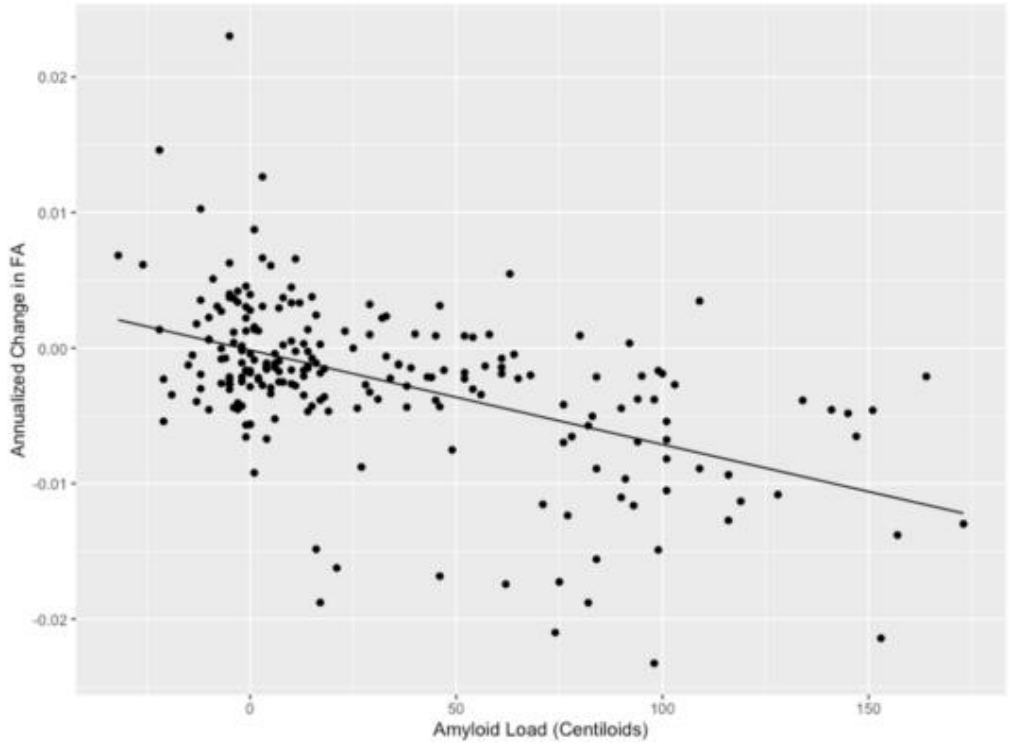

Figure 2. A scatterplot visualizing the significant associations between longitudinal WMI changes and subsequent amyloid pathology, controlling for age and sex. The y axis represents the average values within the significant cluster (green-colored regions) identified in Figure 1; negative values indicate WMI loss over time, while positive values indicate gain. The x axis indicates subsequent global amyloid load on the Centiloid scale.

Keywords: amyloid PET, longitudinal DTI, white matter integrity, cognitively normal, Alzheimer's disease continuum

134 Multimodal analysis of tau epicenters in heterogeneous Alzheimer's disease variants

Anne Trainer[1], Raina Vin[1], Wanwan Xu[1], Alison Chase[1], Ryan S O'Dell[1], Takuya Toyonaga[1], Samantha Tun[1], Joyce Li[1], Suyeon Ju[1], Adam P Mecca[1], Christopher H van Dyck[1], Carolyn A Fredericks[1]

[1]*Yale School of Medicine, New Haven, CT, United States*

Background: Tau spread in the brain is well-characterized in amnestic Alzheimer's disease (AD). However, it is undefined in clinically heterogeneous rare variants of AD: logopenic variant primary progressive aphasia (lvPPA) and posterior cortical atrophy (PCA). Moreover, the association between this tau spread and the functional architecture of the brain remains unclear. We used multimodal imaging and analyses to characterize this structure-function relationship in a heterogeneous cohort.

Methods: Functional resting state and task-based images and 18F-MK-6240 tau PET scans were acquired from 12 participants with early-stage clinically heterogeneous AD (5 lvPPA, 5 PCA, 2 amnestic). We identified three local maxima of tau SUVR for each participant (Fig. 1a) and derived each epicenter's functional connectivity (FC) in 1000 healthy controls using Neurosynth (Fig. 1b). Four regions of interest were then selected: temporo-parieto-occipital junction, inferior parietal lobule, posterior cingulate, and medial prefrontal cortex-anterior cingulate. We computed the node strength of each (Fig. 2) (globally and within-hemisphere) and evaluated their association with tau deposition and TALSA task performance.

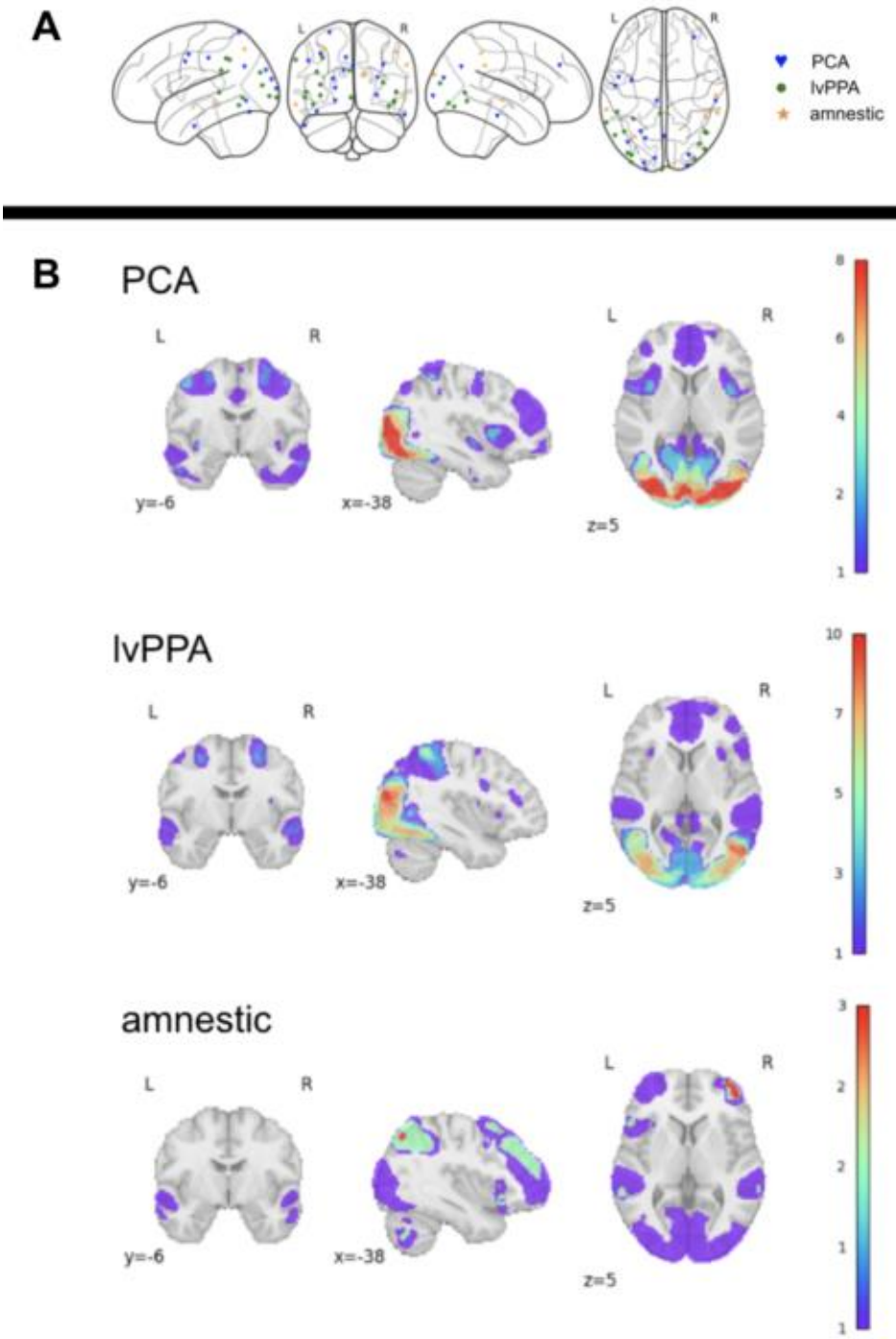
A
L
R
L
R
PCA
lvPPA
amnestic
B
PCA
L
R
y=-6
x=-38
L
R
z=5
8
6
4
2
1
lvPPA
L
R
y=-6
x=-38
L
R
z=5
10
7
5
3
1
amnestic
L
R
y=-6
x=-38
L
R
z=5
3
2
2
1
1

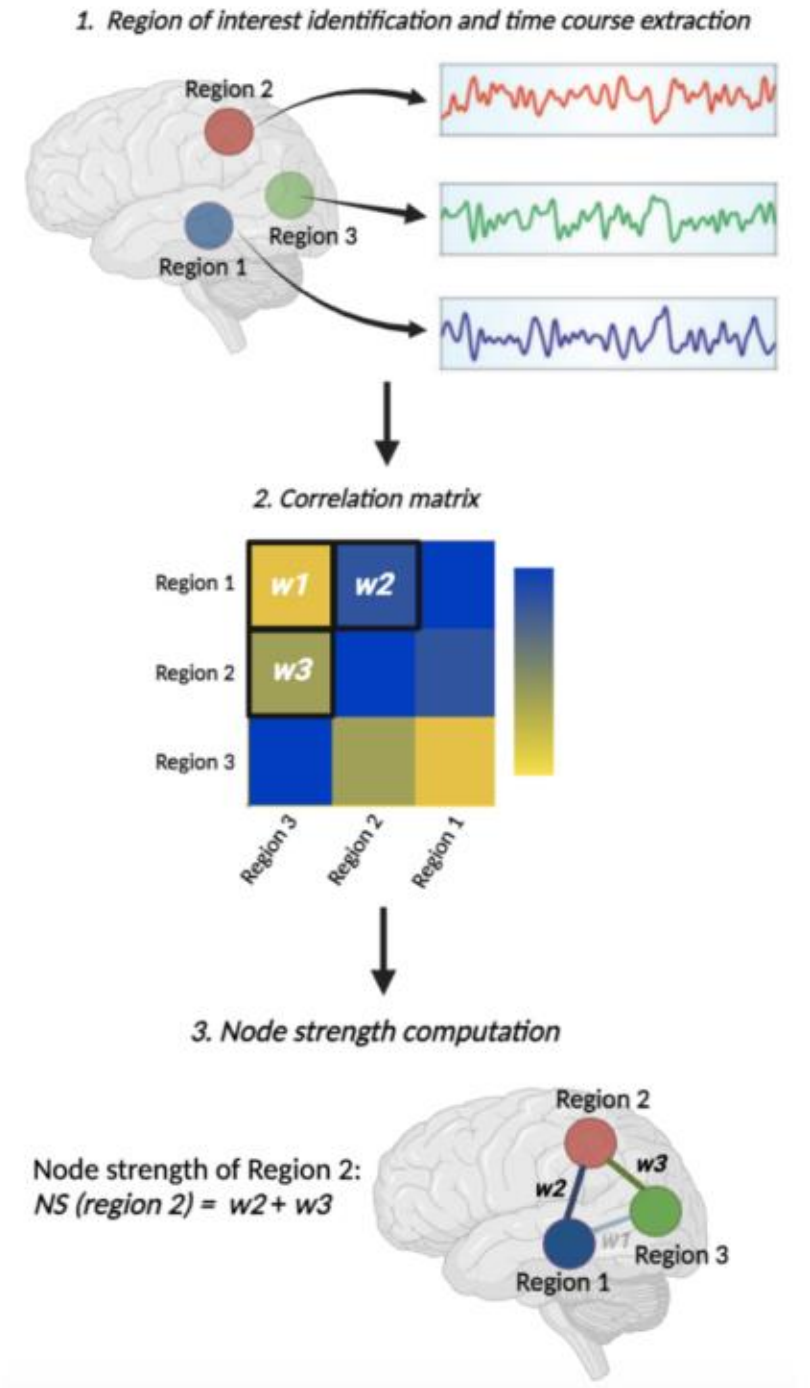

Results: High tau burden was found in diagnosis-specific regions: posterior temporoparietal and temporooccipital regions (lvPPA), bilateral parietooccipital cortex, frontal eye fields, and fusiform gyrus (PCA), and posterior temporoparietal regions (amnestic). Epicenter-derived FC maps highlighted language and visuospatial processing networks. In particular, the right inferior parietal lobule exhibited greater deviations in functional node strength (whole-brain and within-hemisphere) at higher tau levels (Figure 3A). Moreover, node strength deviations of the left and right inferior parietal lobule were negatively correlated with TALSA task performance (Figure 3B).

A Structure (tau) – function (node strength) correlations

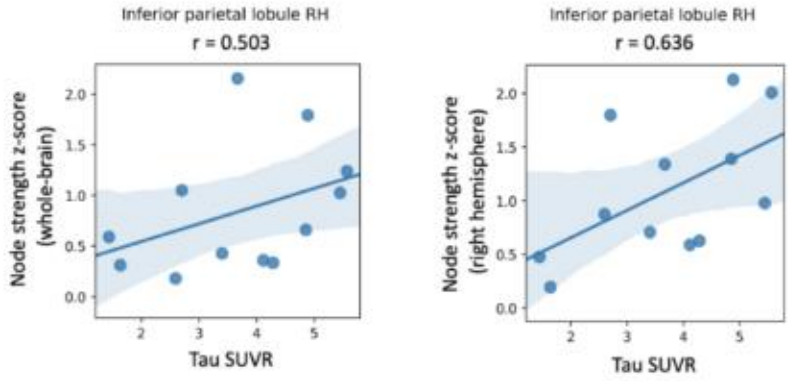

B Node strength – task performance correlations

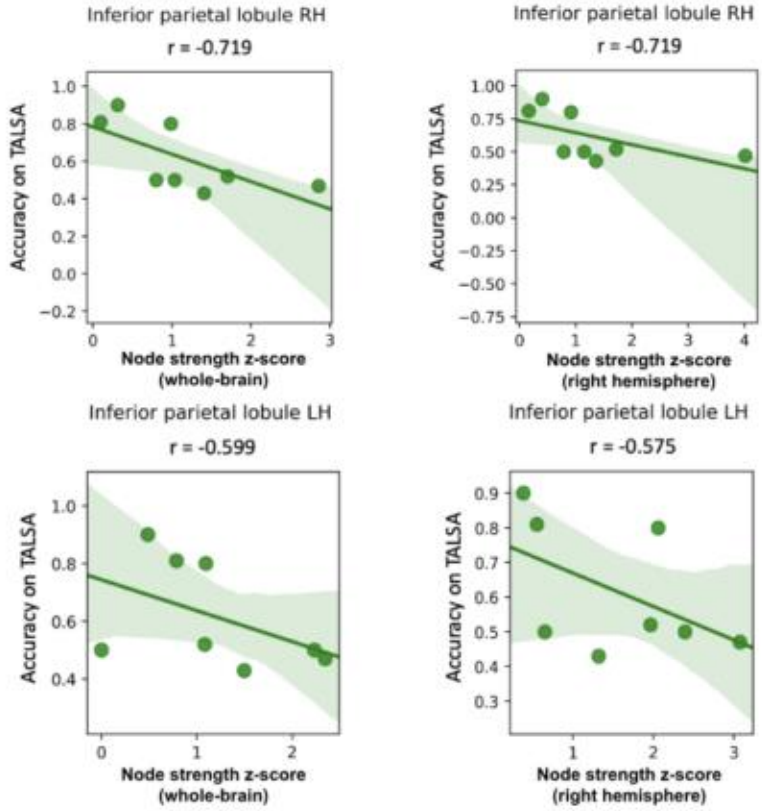

Conclusions: Findings suggest that the identified tau epicenters shape network connectivity and task performance. Future directions include collecting longitudinal tau PET to assess the extent of tau spread along established functional connections and broader circuits. This work could provide indications for patient-specific biomarkers of expected disease spread and effect in heterogeneous AD.

Keywords: tau PET, multimodal, functional MRI, atypical Alzheimer's, epicenters

135 A pretrained foundation model for learning representation of regional tau accumulation pattern and its downstream applications

JunYoung Sohn[1], Yeonghun Song[2], Joonkyung Seong[3]

[1]*Junyoung Sohn, Seoul, South Korea*
[2]*Yeonghun Song, Seoul, South Korea*
[3]*Joonkyung Seong, Seoul, South Korea*
[4]*ADNI, Los Angeles, CA, United States*

The aim of this study is to develop a pretrained foundation model for representing regional tau accumulation pattern. The vision transformer (ViT) model was adopted to our problem setting: regional tau SUVR values were mapped onto the cortical surface, each of which hemisphere samples cortical tau SUVR values from 642 vertices. For training the foundation model, a total of 1068 tau PET images was used from the ADNI dataset, and a separate set of 150 images was used for external validation with finetuning.

The pretrained foundation model can be used for various downstream applications with task-specific purposes. In our study, we demonstrated the efficacy of the proposed foundation model using three different applications: group comparison of regional encoding vectors, amyloid-positivity classification, and individualized functional covariance network (FCN) analysis. First, we conducted permutation-based statistical group comparison of regional embedding vectors for each pair of three groups (Figure1).

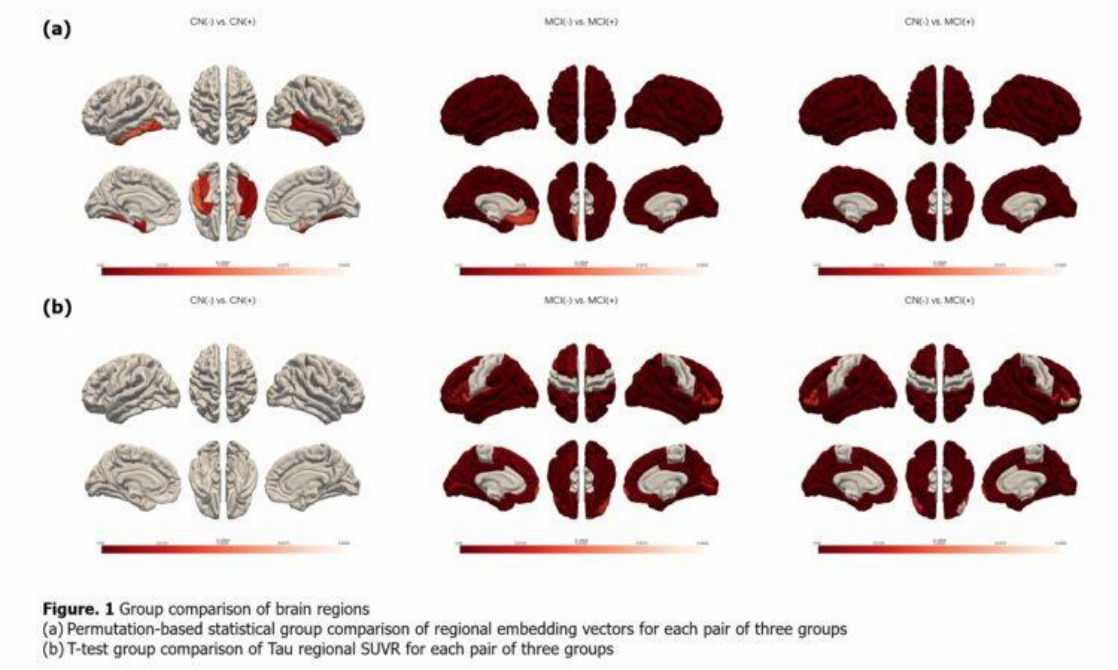

Figure. 1 Group comparison of brain regions
(a) Permutation-based statistical group comparison of regional embedding vectors for each pair of three groups
(b) T-test group comparison of Tau regional SUVR for each pair of three groups

Even using small number of patients in each group, the statistical power is significantly improved using regional embedding vectors instead of using scalar SUVR values. Second, a classifier was trained by finetuning the foundation model using the validation dataset (Figure2).

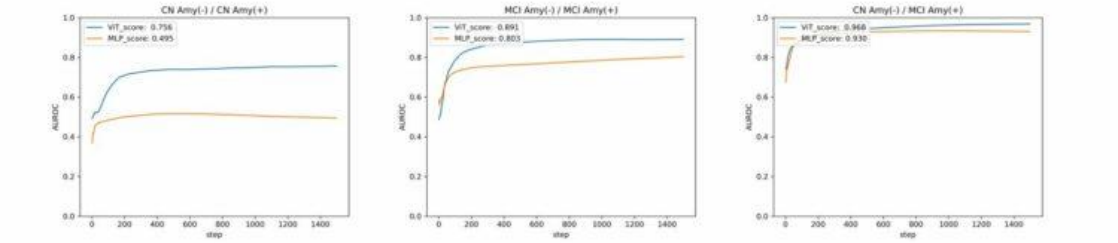

Figure. 2 Classification task AUROC score of pretrained ViT model and MLP model with same dataset

The classification AUROC scores of the finetuning model was 0.756, 0.891, 0.968, while a baseline, well-defined machine learning model has the score of 0.495, 0.803, 0.930 respectively. Third, the attention mechanism in the ViT model can be used as an individualized FCN that encodes a regional association of tau accumulation pattern between every possible region pair. We constructed such attention network for each individual in the validation dataset, and performed network-based analysis (Figure3).

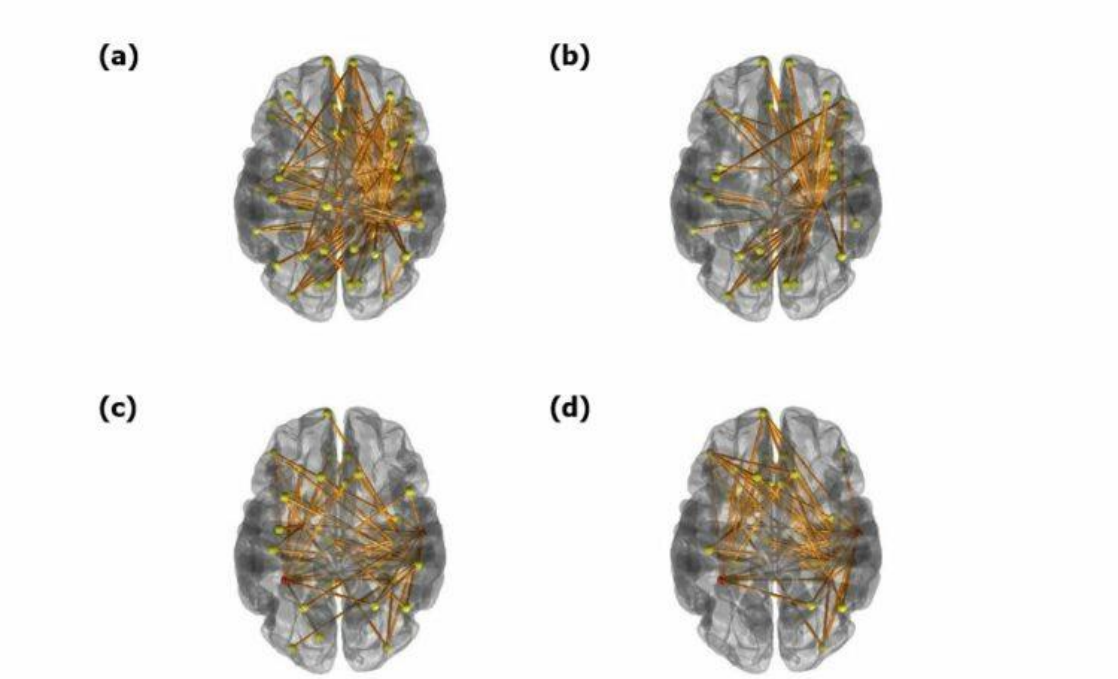

Figure. 3 Network-based analysis with attention network for each individual in the validation dataset
(a) Network-based statistic result between CN amyloid negative and CN amyloid positive
(b) Network-based statistic result between CN amyloid negative and MCI amyloid positive
(c) Cluster-based statistic result with MMSE score
(d) Cluster-based statistic result with Tau global SUVR

In summary, the proposed tau transformer model pretrained using large tau PET datasets learned context-aware representation of regional tau accumulation pattern, and could be used as a foundation model that can be finetuned using a small-size dataset for various downstream applications.

Keywords: foundation model, transformer, tau PET, deep learning

136 [18F]RO-948 tau PET retention and correlation with fluid biomarkers in the early AD continuum

Mahnaz Shekari[1,2,3], Armand González Escalante[1,2,3], Marta Milà-Alomà[1,2,4], Carles Falcon[1,2,5], David López-Martos[1,2], Gonzalo Sánchez-Benavides[1,2,4], Anna Brugulat-Serrat[1,2,4,6], Aida Niñerola-Baizán[5,7], Nicholas J. Ashton[9,10,11,12], Thomas K. Karikari[9,13], Juan Lantero-Rodriguez[9], Anniina Snellman[9,14], Paula Ortiz[1,2], Matteo Tonietto[8], Edilio Borroni[8], Gregory Klein[8], Carolina Minguillón[1,2,4], Karine Fauria[1,4], Andrés Perissinotti[5,7], José Luis Molinuevo[1,15], Henrik Zetterberg[16,17,18,19], Kaj Blennow[16,17], Oriol Grau-Rivera[1,2,4,20], Marc Suárez-Calvet[1,2,4,20], Juan Domingo Gispert[1,2,3,5]

[1]Barcelonaβeta Brain Research Center (BBRC), Pasqual Maragall Foundation, Barcelona, ES
[2]IMIM (Hospital del Mar Medical Research Institute), Barcelona, ES
[3]Universitat Pompeu Fabra, Barcelona, ES
[4]Centro de Investigación Biomédica en Red de Fragilidad y Envejecimiento Saludable (CIBERFES), Instituto de Salud Carlos III, Madrid, ES
[5]Centro de Investigación Biomédica en Red de Bioingeniería, Biomateriales y Nanomedicina (CIBERBBN), Instituto de Salud Carlos III,, Madrid, ES
[6]Global Brain Health Institute, San Francisco, CA, United States
[7]Nuclear Medicine Department, Hospital Clínic, Barcelona, ES
[8]Pharma Research and Early Development, FHoffmann-La RocheLtd., Basel, CH
[9]Department of Psychiatry and Neurochemistry, Institute of Neuroscience and Physiology, University of Gothenburg, Mölndal, Sweden
[10]Wallenberg Centre for Molecular and Translational Medicine; University of Gothenburg, Gothenburg, Sweden
[11]King's College London, Institute of Psychiatry, Psychology & Neuroscience, Maurice Wohl Clinical Neuroscience Institute, London, United Kingdom
[12]NIHR Biomedical Research Centre for Mental Health & Biomedical Research Unit for Dementia at South London & Maudsley NHS Foundation, London, United Kingdom
[13]Department of Psychiatry, University of Pittsburgh,, Pittsburgh, PA, United States
[14]Turku PET Centre, University of Turku, Turku, FI
[15]Lundbeck, Copenhagen, DK
[16]Department of Psychiatry and Neurochemistry, Institute of Neuroscience and Physiology, University of Gothenburg, Mölndal, Sweden
[17]Clinical Neurochemistry Laboratory, Sahlgrenska University Hospital, Mölndal, Sweden
[18]Department of Neurodegenerative Disease, UCL Institute of Neurology, Queen Square, London, United Kingdom
[19]K Dementia Research Institute at UCL, London, United Kingdom
[20]Servei de Neurologia, Hospital del Mar, Barcelona, ES

Background: In this study, we evaluated association between tau PET with AD biomarkers and cognition and explored biological mechanisms associated with elevated tau in cognitively unimpaired(CU) individuals.

Method: Ninety-nine CU individuals from ALFA+ cohort had [^{18}F]RO-948 and two longitudinal [^{18}F]flutemetamol PET, T1-weighted MRI, CSF, and plasma biomarkers. Longitudinal changes in cognition measured using the PACC and domain-specific composites(Table1). Participants were categorized into AT stages using pre-established CSF cut-offs(Table1). [^{18}F]RO-948 SUVR was measured in entorhinal(BraakI/II), limbic(BraakIII/IV), and neocortical(BraakV/VI) regions using the inferior cerebellum as reference. Regional positivity thresholds per Braak region were calculated as mean+2SD of the A-T- group. [^{18}F]flutemetamol PET scans were quantified in Centiloid(CL). Associations between [^{18}F]RO-948 SUVRs and AD biomarkers(Figure1) were assessed using Pearson correlations. Receiver Operating Curve(ROC) analyses were conducted to determine the capacity of biomarkers to predict BraakI/II positivity. In those with CL>12 for tau-PET positivity, differences in non-core AD fluid biomarkers(Figure1-D), longitudinal cognition, and ΔCL/year were sought between tau BraakI/II positive and

negative individuals. FDR-corrected p-values<0.05 were considered significant.

Results: Ten cases(10.10%) were positive in BraakI/II. Following a hierarchical pattern, five were positive for BraakIII/IV and one for BraakV/VI. However, one subject did not follow the pattern and was positive only in Braak III/IV. Fluid biomarkers presented correlations with tau PET SUVR in all Braak stages (Figure1) and predictive capacity for tau-PET positivity in BraakI/II (Figure2). In individuals with CL>12, BraakI/II positives had higher levels of CSF-GFAP(p=0.003), CSF-NFL(p=0.04), CSF-neurogranin(p=0.03) and presented declines in attention (Figure1-D).

Conclusion: Early in the AD *continuum*, [^{18}F]RO-948 PET conformed to the Braak hierarchical model. CSF and plasma biomarkers showed moderate associations with tau PET SUVR but a good capacity to predict tau PET positivity in BraakI/II. Tau-PET positivity in this region was associated with higher astrogliosis, neurodegeneration, and cognitive decline compared to tau-PET negatives with similar levels of amyloid deposition.

Demographic and biomarkers	Total	A-T-	A+T-	A+T+	A-T+
N	99	27	33	28	9
Age, mean (SD) [58 to 70.46], y	65.01±4.93	64.26±4.97	65.12±4.95	66.32±5.59	64.22±3.03
Sex, N (%), F	57 (57.58%)	14 (14.14%)	21 (21.21%)	18 (18.18%)	3 (3.03)
APOE-ε4, N (%), carriers	63 (63.64%)	12 (12.12%)	26 (26.26%)	19 (19.19%)	4 (4.04%)
CSF ptau181/Aβ42 N	0.020±0.013 90	0.009±0.002 27	0.020±0.007 28	0.03763±0.012 26	0.009±0.002 9
CSF ptau181/Aβ40 N	0.001±0.0003 90	0.0008±0.0002 27	0.0010±0.0001 28	0.0014±0.0003 26	0.0010±0.00009 9
CSF $A\beta_{42/40}$, mean (SD), pg/mL N	0.07±0.03 90	0.09±0.01 27	0.05±0.01 28	0.04±0.01 26	0.11±0.02 9
CSF p-Tau_{181}, mean (SD), pg/mL N	20.80±9.67 90	13.75±4.67 27	16.29±4.56 28	31.22±9.07 26	25.97±4.64 9
Centiloid N	22.51±26.25 90	0.93±8.30 26	25.81±21.33 33	46.84±20.55 23	-6.23±6.76 6
Annual rate of change (ΔCL/year) N	2.95±2.47 90	0.71±1.63 26	3.71±1.87 33	4.77±1.85 23	0.54±1.21 6
Z-scored longitudinal changes at attention composite, mean (SD) N	0.04±0.50 91	0.21±0.54 27	-0.02±0.45 30	-0.10±0.44 24	0.18±0.64 9
Z-scored longitudinal changes at memory composite, mean (SD) N	0.03±0.38 91	0.12±0.36 27	0.08±0.42 30	-0.10±0.36 24	-0.06±0.35 9
Z-scored longitudinal changes at executive composite, mean (SD) N	-0.07±0.46 91	-0.07±0.44	-0.04±0.38 30	-0.13±0.60 24	-0.02±0.37 9
Z-scored longitudinal changes at language composite mean (SD) N	-0.03±0.86 91	0.24±0.89 27	-0.42±0.79 30	0.02±0.75 24	0.19±0.85 9
Z-scored longitudinal changes at visual composite N	-0.04±0.68 91	0.02±0.69 27	0.02±0.66 30	-0.15±0.72 24	0.00±0.66 9
Z-scored PACC longitudinal changes at PACC N	0.05±0.38 91	0.19±0.39 27	-0.09±0.36 30	0.06±0.36 24	0.08±0.34 9

Table1. Demographic, CSF Aβ42/40, CSF ptau181, and cognition information of the participants. PACC: Preclinical Alzheimer's Cognitive Composite. CSF values were measured using RocheNTK. The Roche NeuroToolKit is a panel of robust prototype assays used for investigational purposes only and not approved for clinical use.

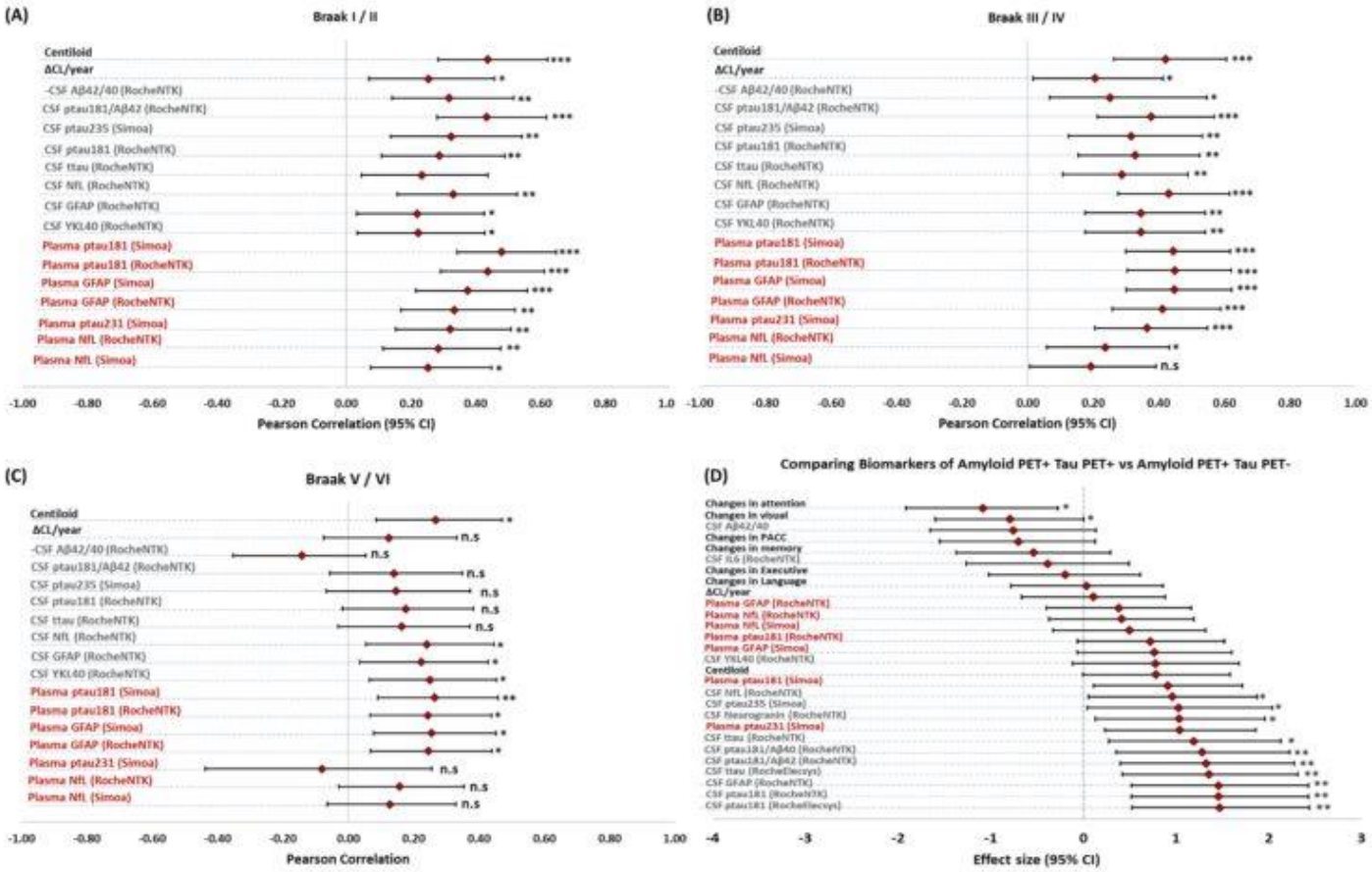

Figure 1. Correlation coefficients (95% Confidence interval) between BraakI/II (panel A), BraakIII/IV (Panel B), and BraakV/VI (Panel C) SUVRs and fluid biomarkers. Panel D represents the effect size for comparing each biomarker and longitudinal changes in cognitive measures in PET-based A+ BraakI/II + vs A+ BraakI/II – stages. It should be noted that the correlation between SUVR and fluid biomarkers was statistically significant for all Braak stages, except BraakV/VI and CSF Aβ42/40 and Centiloid. CSF and blood-based biomarkers were measured with different assays including in-house SIMOA and Roche NTK.

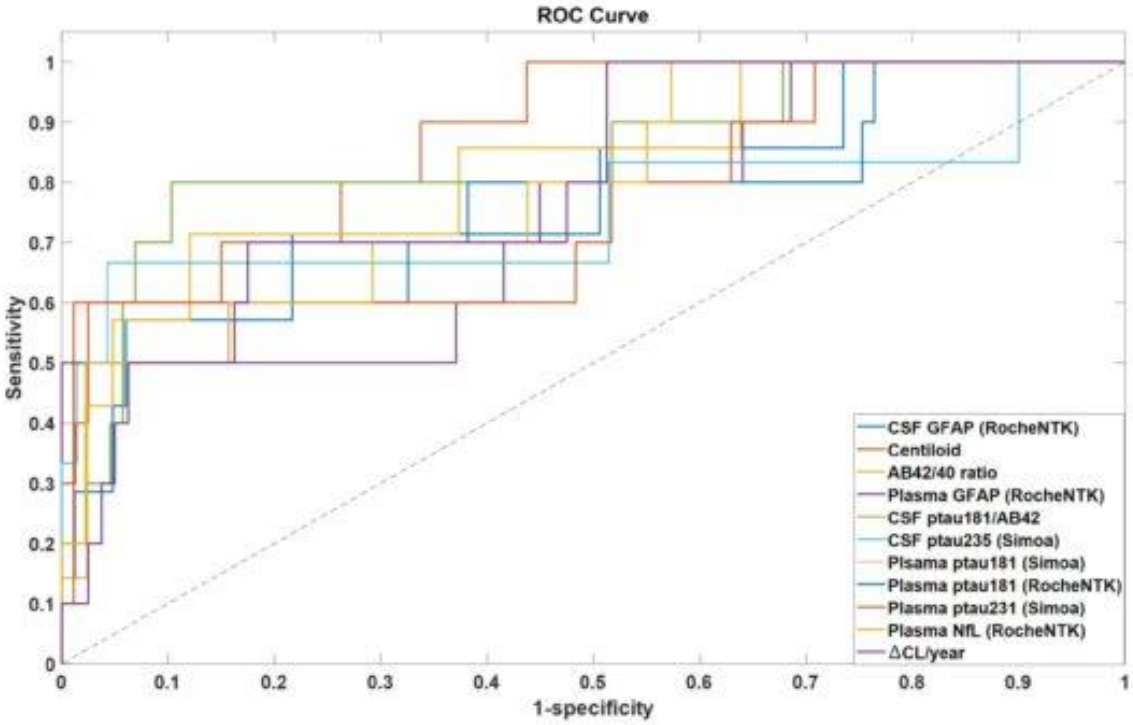

Biomarker	AUC	95% CI	p
Centiloid	**0.87**	**0.76-0.98**	**6.02e-5**
CSF Ptau181/AB42	0.83	0.62-1	0.001
CSF AB42/40 ratio	0.82	0.64-1	0.002
Plasma ptau181 (Simoa)	**0.81**	**0.66-0.96**	**0.0006**
Plasma ptau181 (RocheNTK)	**0.76**	**0.56-0.95**	**0.004**
Plasma ptau231 (Simoa)	**0.76**	**0.57-0.95**	**0.003**
Plasma NfL (RocheNTK)	**0.79**	**0.63-0.94**	**0.001**
ΔCL/year	**0.79**	**0.66-0.94**	**0.001**
CSF Ptau235 (Simoa)	0.75	0.66-0.94	0.008
CSF GFAP (RocheNTK)	0.77	0.65-0.94	0.009
Plasma GFAP (RocheNTK)	**0.74**	**0.56-0.92**	**0.005**

Figure2. ROC results for predicting Braak I/II tau Pet positivity and the corresponding area under the curve for each biomarker. It should be noted that age, APOE-e4, and sex were included in all ROC models.

Keywords: Tau PET, AD, Plasma biomarker, CSF biomarkers, Quantification

137 Baseline plasma GFAP predicts longitudinal tau-PET uptake in Braak staging continuum

Wan Lu Jia[1,2,3,4,5], Nesrine Rahmouni[1,4,5], Cecile Tissot[1,4,5], Stijn Servaes[1,4,5], Joseph Therriault[1,4,5], Arthur Cassa Macedo[1,4,5], Jaime Fernandez-Arias[1,4,5], Yi-Ting Wang[1,4,5], Firoza Z. Lussier[6], Peter Kunach[1,4,5], Serge Gauthier[4,5,12], Andrea L. Benedet[4,5,12], Nicholas J. Ashton[7,8,12], Henrik Zetterberg[10,11], Tharick A. Pascoal[6], Kaj Blennow[7,10], Pedro Rosa-Neto[4,5,12]

[1]*Translational Neuroimaging Laboratory, The McGill University Research Centre for Studies in Aging, Montreal, QC, Canada*
[2]*Department of Family Medicine, McGill University, Montreal, QC, Canada*
[3]*Division of Geriatric Medicine, Montreal, QC, Canada*
[4]*McGill University, Montreal, QC, Canada*
[5]*Department of Neurology and Neurosurgery, McGill University, Montreal, QC, Canada*
[6]*University of Pittsburg, Pittsburgh, PA, United States*
[7]*Department of Psychiatry and Neurochemistry, Institute of Neuroscience and Physiology,, Molndal, Sweden*
[8]*Wallenberg Centre for Molecular and Translational Medicine; University of Gothenburg,, Gothenburg, Sweden*
[9]*University of Gothenburg, Gothenburg, Sweden*
[10]*Clinical Neurochemistry Laboratory, Sahlgrenska University Hospital, Molndal, Sweden*
[11]*Institute of Neuroscience and Physiology, Sahlgrenska Academy, University of Gothenburg, Molndal, Sweden*
[12]*Douglas Mental Health Research Institute, Montreal, QC, Canada*

Background: Glial fibrillary acidic protein (GFAP) is a reactive astrogliosis biomarker, shown to increase in individuals with preclinical Alzheimer's disease (AD). First thought to be a great marker of amyloid-β (Aβ) pathology, recent post-mortem research has linked it to tau accumulation. We previously confirmed the independent associations of plasma GFAP with imaging markers of AD along the disease spectrum. Here we investigate the associations of baseline plasma GFAP in patients with longitudinal imaging, at 12 to 48 months of follow-up.

Methods: 66 individuals from TRIAD cohort underwent [^{18}F]MK6240 tau-PET, [^{18}F]AZD4694 Aβ-PET and plasma GFAP assessment using an in-house assay, at baseline and follow-up. Linear regression models evaluated the relationship between PET tracers and plasma GFAP. All models were corrected for age and sex. Linear regression models with [^{18}F]MK6240 tau-PET rate of change as the outcome was adjusted for [^{18}F]MK6240-PET rate of change and vice-versa. All models were corrected for age and sex.

Results: Baseline levels of plasma GFAP were significantly associated with [^{18}F]MK6240 tau-PET SUVR rate of change at higher levels of Braak staging in Braak stages III (R = 0.254, $p = 0.002$), IV (R = 0.248, $p = 0.002$), V (R = 0.33, $p < 0.001$), and VI (R = 0.364, $p < 0.001$) (Figure 1).

Figure 1 – [18F]MK6240 SUVR rate of change according to baseline plasma GFAP in the Braak staging continuum

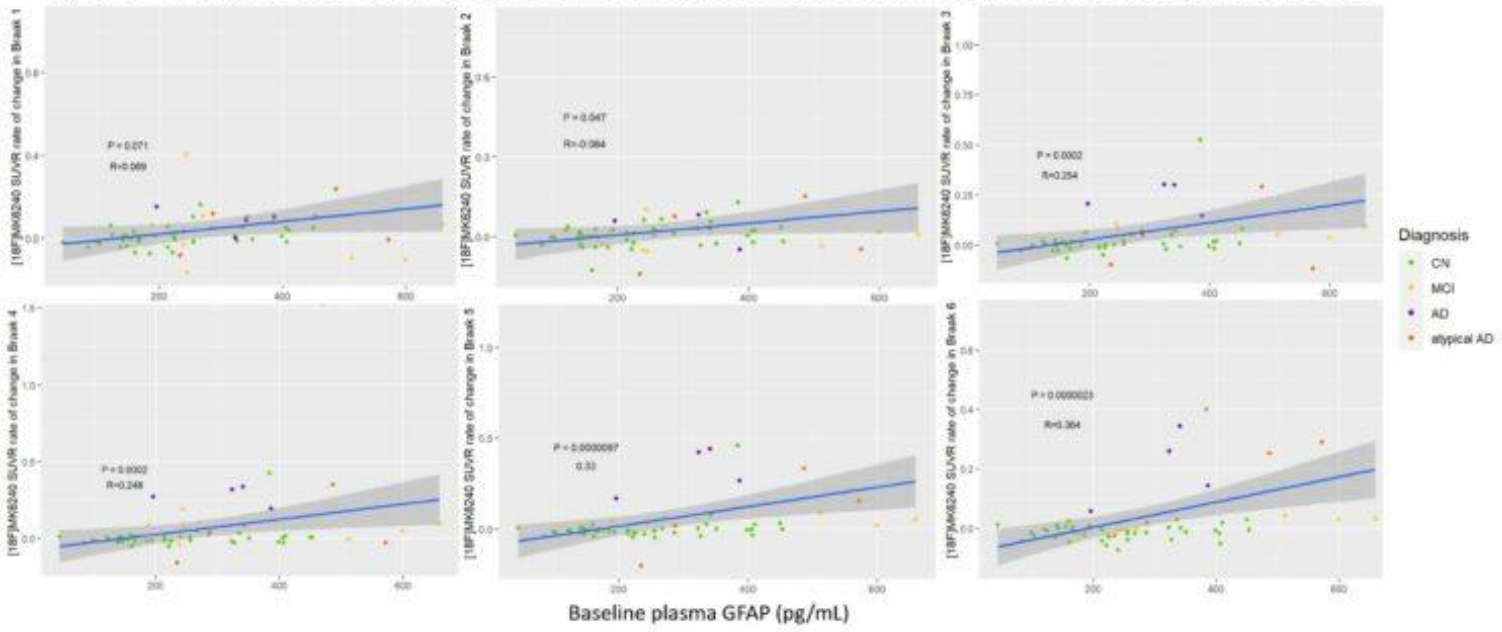

Conclusion: Our findings indicate that plasma GFAP predicts the longitudinal [^{18}F]MK6240 SUVR rate of change. Higher correlations and statistical significance were present later in the progression of AD pathology by Braak staging.

.

Keywords: Alzheimer's disease, PET imaging, GFAP, longitudinal tau-PET, plasma biomarkers

138 Plasma NfL correlates to grey matter and white matter atrophy ambivalent to amyloid status in older adults

Brandon Hall[1], Nesrine Rahmouni[1], Arthur Macedo[1], Stijn Servaes[1], Joseph Therriault[1], Jaime Fernandez-Arias[1], Lydia Trudel[1], Jenna Stevenson[1], Serge Gauthier[1], Sulantha Sanjeewa[1], Firoza Lussier[3], Tharick Pascoal[3], Andrea Benedet[2], Nicholas Ashton[2], Henrik Zetterberg[2], Kaj Blennow[2], Pedro Rosa-Neto[1]

[1]*McGill University, Montreal, QC, Canada*
[2]*University of Gothenburg, Gothenburg, Sweden*
[3]*University of Pittsburg, Pittsburg, PA, United States*

Introduction: The significance of plasma neurofibrillary light chain (pNfL) as a biomarker in Alzheimer's disease (AD) is a topic of ongoing debate. We assessed the relationship between pNfL and longitudinal atrophy in a meta-ROI of AD-relevant regions (entorhinal, fusiform, inferior temporal, middle temporal, parahippocampal gyri) and subcortical white matter (WM), combined with amyloid-PET and tau-PET imaging and cognitive assessments.

Methods: We sampled 210 participants age 50+ from the TRIAD cohort with longitudinal data for cognition and T1-weighted MRI, amyloid PET (F^{18}-NAV4694), and tau PET (F^{18}-MK6240) (125 female, 86 amyloid-positive, 124 amyloid-negative, age 69.7±6.7). SUVR was calculated for amyloid PET with a cerebellar grey matter reference region and an inferior cerebellar grey matter for tau PET. Thresholds of 1.55 (amyloid) and 1.24 (tau) SUVR defined positivity. FreeSurfer 7 derived volumes from T1 MRI. pNfL measured by Simoa assay. With R 4.0.3, we correlated pNfL with longitudinal atrophy in a) meta-ROI regions b) cerebral white matter, covarying for sex, age, APOE genotype, time between scans, amyloid SUVR, and tau SUVR. Additionally, baseline pNfL was correlated to follow-up global CDR score.

Results: See **Table 1** for linear regression results. In amyloid-negative participants, higher pNfL correlated with greater atrophy in WM, plus entorhinal, inferior temporal, and parahippocampal gyri, with trends in the fusiform and middle temporal gyri. In amyloid-positive participants, higher pNfL correlated with greater atrophy in the fusiform gyrus. See **Fig** 1 for comparison of the meta-ROI regions. Higher pNfL predicted higher follow-up CDR score at in the amyloid-negative group ($t = 3.7$, $p < 0.001$).

Conclusions: While increased pNfL correlates with greater atrophy in AD-relevant regions, correlations are stronger in amyloid-negative participants, which suggests that it is not specific to AD pathology. This is further suggested by pNfL's positive correlation with greater WM atrophy and higher CDR in amyloid-negative, not amyloid-positive, participants.

Region of Interest	Amyloid positive		Amyloid negative	
	t- value	p-value	t- value	p-value
Entorhinal	-0.4	0.7	-2.7	0.008 **
Fusiform	-2.2	0.03 *	-1.8	0.07 .
Inferior temporal	-0.5	0.6	-2.7	0.009 **
Middle temporal	-0.9	0.3	-1.9	0.05 .
Parahippocampal	-1.1	0.3	-2.4	0.02 *
Cerebellar White Matter	0.6	0.6	-2.2	0.03 *

Table 1. Displays the test statistic (t-value) and significance level (p-value) for the linear regressions of pNfL ~ longitudinal atrophy in each region of interest.
p < 0.1: .
p < 0.05: *
p < 0.01 **
p < 0.001***

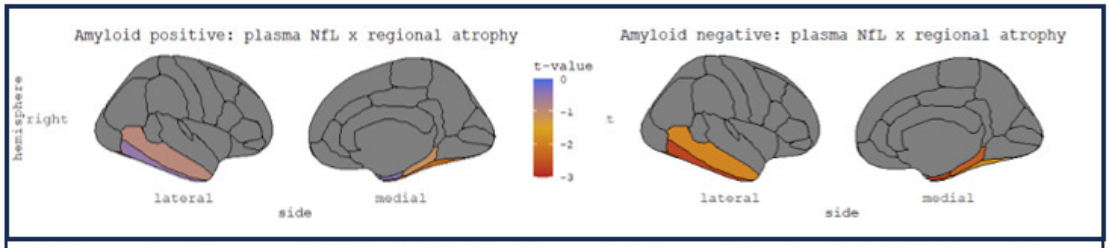

Fig 1 A comparison of the t-scores of pNfL's statistical relationship to atrophy in the meta-ROI regions. On the left is the map of the amyloid-positive relationships On the right is the maps of the amyloid-negative relationships.

Keywords: PET, plasma, neurofibrillary light chain, Alzheimer's, longitudinal

139 Astrocyte reactivity influences cognitive decline in individuals across the Alzheimer's disease continuum

Bruna Bellaver[1], Guilherme Povala[1], Pamela Ferreira[1], Guilherme Bauer-Negrini[1], Firoza Lussier[1], Douglas Leffa[1], João Pedro Ferrari-Souza[2], Hussein Zalzale[1], Carolina Soares[1], Francieli Rohden[1], Cristiano Aguzzoli[1], Sarah Abbas[1], Andréa Benedet[3], Nicholas Ashton[3], Cécile Tissot[4], Joseph Therriault[4], Stijn Servaes[4], Jenna Stevenson[4], Nesrine Rahmouni[4], Chang Hyung Hong[5], Hyun Woong Rho[5], Helmet Karim[1], Eduardo Zimmer[2], Henrik Zetterberg[3], Kaj Blennow[3], Victor Villemagne[1], William Klunk[1], Oscar Lopez[1], Dana Tudorascu[1], Andrea Slachevsky[6], Pedro Rosa-Neto[4], Ann Cohen[1], Thomas Karikari[1], Sang Joon Son[5], Tharick Pascoal[1]

[1]*Department of Psychiatry, University of Pittsburgh, Pittsburgh, PA, United States*
[2]*Graduate Program in Biological Sciences: Biochemistry, Universidade Federal do Rio Grande do Sul, Porto Alegre, Brazil*
[3]*Department of Psychiatry and Neurochemistry, The Sahlgrenska Academy at the University of Gothenburg, Mölndal, Sweden*
[4]*Translational Neuroimaging Laboratory, McGill University Research Centre for Studies in Aging, Alzheimer's Disease Research Unit, Douglas Research Institute, Le Centre intégré universitaire de santé et de services sociaux (CIUSSS) de l'Ouest-de-l'Île-de-Montréal; Department of Neurology and Neurosurgery, Psychiatry and Pharmacology and Therapeutics, McGill University, Montreal, QC Canada*
[5]*Department of Psychiatry, Ajou University School of Medicine, Suwon, South Korea*
[6]*Neurological Sciences, School of Medicine, University of Chile, Santiago, Chile*

Background: We recently have shown that GFAP is key to unleashing Aβ effects on tau phosphorylation in preclinical Alzheimer's disease (AD). However, the influence of astrocyte reactivity across the whole AD continuum is still underexplored. Here we investigated whether astrocyte reactivity influences tau pathology and cognition in individuals across the AD continuum.

Methods: We assessed 1,349 individuals across the aging and AD continuum four cohorts (TRIAD, BICWALZ, Pittsburgh and Chile) with Aβ (plasma or PET), plasma p-tau217, GFAP, and cognitive assessments. Individuals were classified as positive (Ast+) or negative (Ast-) for astrocyte reactivity and p-tau positivity using a cutoff based on plasma GFAP of younger Aβ- individuals and plasma p-tau217. Lowess method accounting for age and sex was used to model the trajectories of plasma p-tau as a function of Aβ burden. Cohen's *d* corrected for age and sex was used to estimate effect sizes between groups.

Results: Across the entire population, plasma p-tau217 levels increased as a function of Aβ mainly in Ast+ individuals following a sigmoid shaped curve trajectory (**Fig. 1A**) that was potentiated by APOEε4 carriership (**Fig. 1B**). The frequency of P-tau+ individuals was the highest in A+/Ast+: 35.2% of CU; 76.8% of CI (**Fig. 1C**). Cohen's *d* analysis revealed that the co-occurrence of A+/Ast+/Ptau+ presented the largest magnitude of effect on MMSE (Cohen's *d* = -0.84;**Fig. 1D**).

Conclusions: Astrocyte reactivity influences tau phosphorylation in CU and CI individuals, which was potentiated by APOEε4. The presence of astrocyte reactivity seems to have a detrimental effect on cognition in individuals Aβ and p-tau positive. Overall, our findings suggest that the co-presence of astrocyte reactivity, in addition to the

classical AD markers, is a predictor of cognitive deterioration.

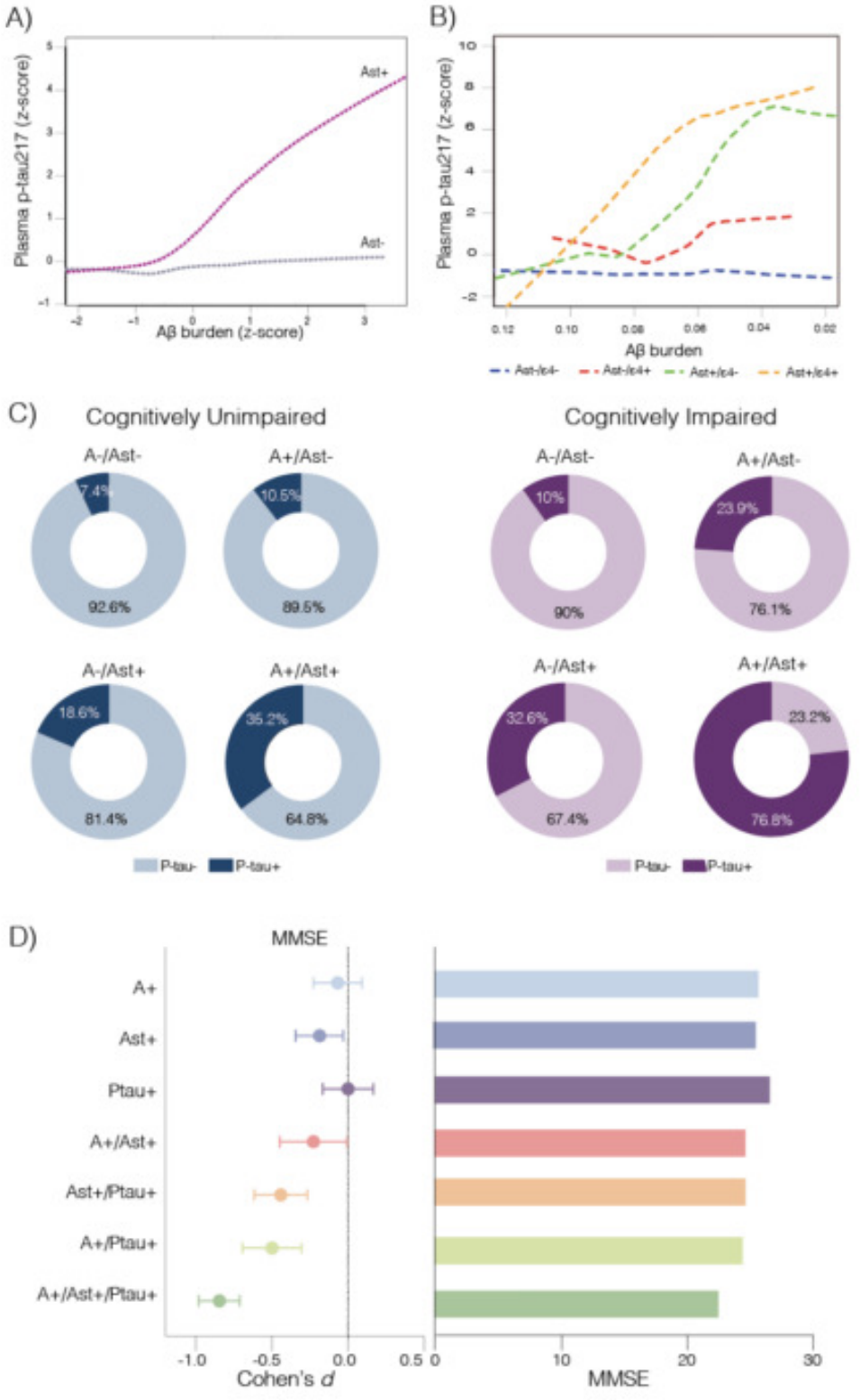

Figure 1. A) Robust local weighted regressions show that plasma p-tau217 increases as a function of Aβ burden mainly Ast+ individuals across aging and AD continuum, with B) an effect of APOEε4 carriership. C) Distribution of T+ individuals in CU and CI individual according to A/Ast groups. D) Cohen's d analysis accounting for age, sex and years of education shows the effect sizes of Aβ, Ast, and Ptau on MMSE.

Keywords: fluid biomarkers, GFAP, Alzheimer's disease, cognition

140 Elevated plasma Ptau-181 is associated with congestive heart failure

Jeremy Tanner[1], Crystal Wiedner[1], Dibya Himali[2], Jaime Ramos-Cejudo[3], Alexa Beiser[2], Sudha Seshadri[1], Hugo Javier Aparicio[2], Jayandra Himali[1]

[1]*University of Texas Health San Antonio - Biggs Institute, San Antonio, TX, United States*
[2]*Boston University, Boston, MA, United States*
[3]*New York University, New York, NY, United States*

Background: While plasma p-tau biomarkers are promising diagnostic tools for widespread clinical use, recent studies have raised concerns regarding the effect of medical comorbidities, such as cardiovascular disease(CVD), on plasma p-tau specificity. We sought to determine the association between plasma p-tau181 and prevalent and incident CVD outcomes in the Framingham Heart Study(FHS).

Methods: FHS is a community-based longitudinal cohort study with deep-phenotyping of CVD. P-tau181 levels were measured from stored samples of 2543 participants predominantly cognitively unimpaired from 2011-2014 (Offspring and Omni Cohorts, age 71±8, 55% female, 22% APOE4+, p-tau181 median 2.29,Q1-Q3[1.70-3.28]) using Quanterix Simoa. P-tau181 levels were analyzed as a binary predictor (highest quintile vs remainder). CVD outcomes (binary:yes/no) included coronary heart disease, congestive heart failure(CHF), stroke/TIA, and peripheral arterial disease. Multivariate logistic regressions were performed to assess the association between p-tau181 and each prevalent CVD outcome adjusting for age, sex, cohort, eGFR, and BMI. Cox regression models were performed to assess the association between p-tau181 and incident CVD outcomes adjusting for similar covariates after a median follow-up of 7.0 years [5.8-7.6], excluding participants with the respective CVD outcome at baseline.

Results: At baseline, elevated p-tau181 was associated with prevalent CHF(OR 1.73; 95%CI[1.01-2.97]; **Table 1**). Longitudinally, elevated p-tau181 was associated with greater future risk of developing CHF(HR 1.54[1.02-2.32];**Table 2**). There was no association between p-tau181 level and other CVD outcomes in cross-sectional or longitudinal analyses.

Conclusions: Elevated plasma p-tau181 levels are associated with prevalent and incident CHF in a community-based population. Prior studies have found greater amyloid in myocardial tissue and diastolic dysfunction in participants with AD, which warrants further evaluation. P-tau181 levels should be interpreted with caution in patients with CHF until the link between p-tau181 and CHF can be clarified. Studies to understand medical comorbidities that influence plasma AD biomarkers are necessary to enable appropriate clinical use.

Table 1. Association Between P-tau181 and Prevalent Cardiovascular Disease (CVD) Outcomes

Outcome	Number of Cases*	Odds Ratio	95% CI	*P*-Value
Coronary Heart Disease	273 (10.7%)	0.91	0.66 – 1.25	.56
Congestive Heart Failure	71 (2.8%)	1.73	1.01 – 2.97	**.045**
Stroke/Transient Ischemic Attack	81 (3.2%)	1.24	0.74 – 2.08	.41
Peripheral Arterial Disease	69 (2.7%)	1.19	0.69 – 2.07	.53

Multivariate logistic regression to assess the association between plasma p-tau181 (binary: highest quintile vs remaining quintiles) and each prevalent CVD outcome adjusting for co-variates of age, sex, cohort, eGFR, and BMI.
* Total participants: n=2543

Table 2. Association Between P-tau181 and Incident CVD Outcomes

Outcome	Number of Events*	Hazard Ratio	95% CI	*P*-Value
Coronary Heart Disease	78/2214	0.98	0.56 – 1.69	.93
Congestive Heart Failure	112/2416	1.54	1.02 – 2.32	**.04**
Stroke/Transient Ischemic Attack	71/2404	1.39	0.82 – 2.36	.23

Cox regression model to assess the association between plasma p-tau181 and each incident CVD outcome adjusting for co-variates of age, sex, cohort, eGFR, and BMI.

*To identify incident cases, participants with prevalent CVD at baseline evaluation were excluded (for example, participants with congestive heart failure at baseline were excluded from incident congestive heart failure analyses)

Keywords: Plasma p-tau, fluid, community-based

141 Regional cell-type proportions are associated with AD pathological changes

Min Su Kang[1,2], Julie Ottoy[1,2], Jean-Paul Soucy[3], Gassan Massarweh[3], Sandra Black[4], Pedro Rosa-Neto[5], Maged Goubran[1,2,6]

[1]*Artificial Intelligence and Computational Neurosciences lab, Sunnybrook Research Institute, University of Toronto, Toronto, ON, Canada*
[2]*LC Campbell Cognitive Neurology Unit, Hurvitz Brain Sciences Program, Sunnybrook Research Institute, University of Toronto, Toronto, ON, Canada*
[3]*McConnell Brain Imaging Centre, Montreal Neurological Institute and Hospital, McGill University, Montreal, QC, Canada*
[4]*Department of Medicine (Division of Neurology), University of Toronto, Toronto, ON, Canada*
[5]*Translational Neuroimaging laboratory, McGill Centre for Studies in Aging, Montreal, QC, Canada*
[6]*Department of Medical Biophysics, University of Toronto, Toronto, ON, Canada*

Background: Amyloid-beta (Aβ) and tau are thought to show stereotypical spatial patterns, suggesting regional or network vulnerability to Alzheimer's Disease (AD) pathogenesis. Numerous cell culture and animal model studies highlighted various cell types (ie. neurons, astrocytes, microglia, oligodendrocytes) to be important in Aβ/tau pathology. However, it remains unclear if the relationship between AD pathology and the proportion of the cell type varies depending on regions/networks, potentially playing a role in the emergence of vulnerability.

Methods: 255 participants (Aβ-: 32 Young and 103 CN; Aβ+: 41 CN, 44 MCI and 35 AD) from TRIAD underwent 3T-MRI, ^{18}F-AZD4694-PET and ^{18}F-MK6240-PET. Linear regressions were used to compare Aβ- and Aβ+ groups in Aβ-/tau-PET, adjusted for age, sex, education and APOEε4. The t-statistics from the comparison were correlated with the six (endothelial, neuron, astrocyte, microglia, oligodendrocyte, oligodendrocyte precursor) brain cell-type-proportion maps, estimated from the cell deconvolution of the Allen Human Brain Atlas, using 7-network Schaefer atlas. The ANOVA and post-hoc analyses evaluated whether the networks and cell type modulate the t-statistics and cell-type proportion relationship with FDR as the multiple comparisons tests.

Results: The spatial pattern of the astrocyte, neuron, or oligodendrocyte cell-type proportion was significantly associated with Aβ-PET t-statistics while the endothelial or oligodendrocyte cell-type proportion was significantly associated with tau-PET t-statistics (Figure1). The ANOVA revealed that the networks and cell types significantly interact on the relationship between cell-type proportions and Aβ ($F(30,528)=3.61$, $p<0.001$) or tau ($F(30,528)=2.11$, $p<0.001$) t-statistics (Figure2). The post-hoc analysis highlighted notable distinctions from the limbic network, where the relationship between Aβ t-statistics and neuronal or endothelial cell proportions appeared more positive while the association between tau t-statistics and neuronal or endothelial cell proportions displayed more negative.

Conclusion: Our study shows evidence to support that regional/network vulnerability to AD pathology may be associated with different proportions/densities of cell types.

Figure 1.

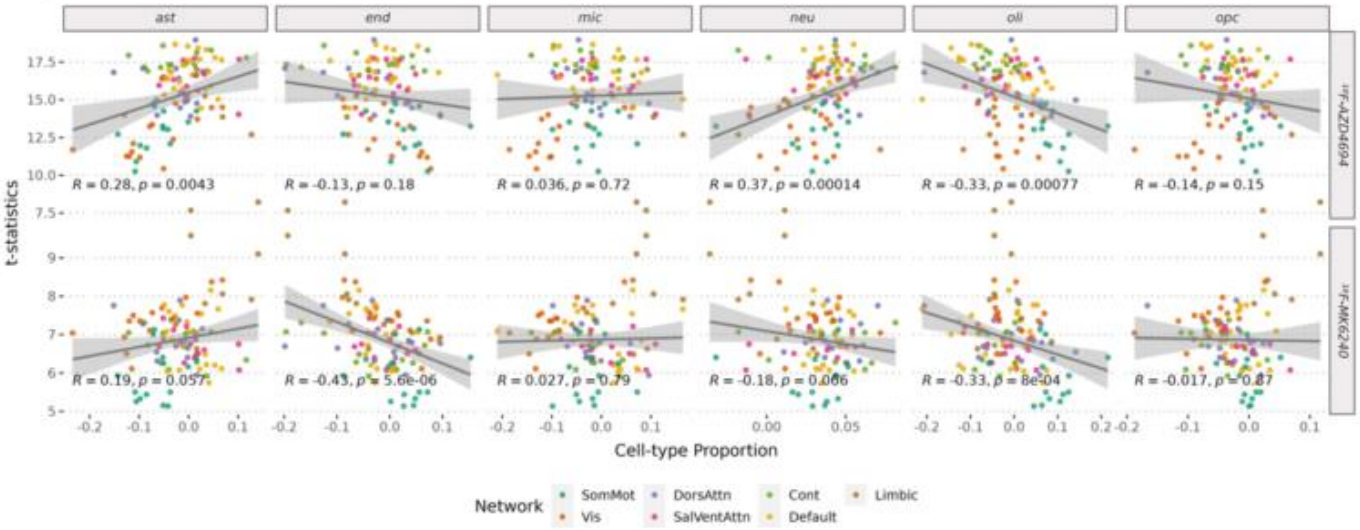

Figure 2.

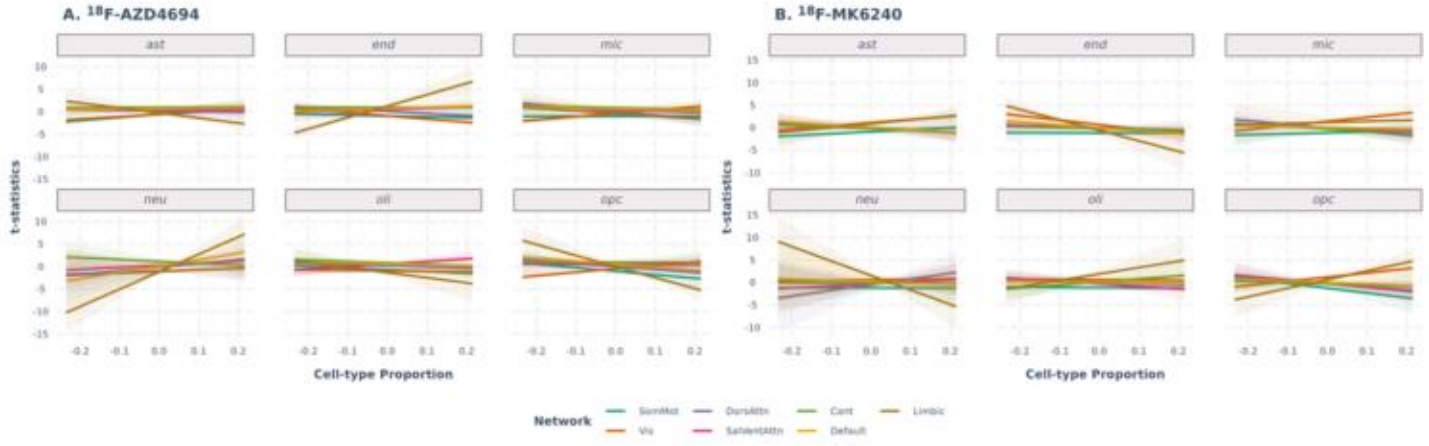

Keywords: imaging-transcriptomics,cell-type,PET,biomarkers,networks

142 Quantitative Gradient Recalled Echo (qGRE) MRI detects neuronal loss and iron accumulation in nucleus basalis of Meynert in preclinical and mild Alzheimer's disease

Satya VVN Kothapalli[1], Mikhail V. Milchenko[1], Tammie L. Benzinger[1,2], Manu S. Goyal[1,3], Cihat Eldeniz[1], Daniel S. Marcus[1], John C. Morris[2,3], Dmitriy A. Yablonskiy[1,2,4], Marcus E. Raichle[1,3,4]

[1]*Department of Radiology, Washington University in St. Louis, St. Louis, MO, United States*
[2]*Knight Alzheimer Disease Research Center, Washington University in St. Louis, St. Louis, MO, United States*
[3]*Department of Neurology, Washington University in St. Louis, St. Louis, MO, United States*
[4]*The Hope Center for Neurological Disorders, Washington University in St. Louis, St. Louis, MO, United States*

Postmortem and morphological assessments of nucleus basalis of Meynert (nbM) report that neurodegeneration is moderate in normal aging and severe in early Alzheimer's disease (AD). Thus, detection of microstructural changes in the nbM could serve as diagnostic of early AD. However, assessing microstructural changes in nbM related to neurodegeneration using quantitative MRI methods facing challenges mostly due to its small size. Recently introduced high resolution quantitative gradient recalled echo (qGRE) MR method demonstrated in vivo sensitivity to pre-atrophic neurodegeneration (identified as Dark Matter (DM), i.e., regions of low qGRE R2t* metric) that related to normal ageing and early AD. Further, qGRE can also provide information on iron accumulation (regions of high R2t*).

The aim of this study is to investigate in vivo microstructural changes in nbM using qGRE metrics in asymptomatic and symptomatic AD brains as compared with normal ageing brains. A total of 86 participants were recruited from the Knight Alzheimer Disease Research Center, representing three groups: Healthy controls [HC; Clinical Dementia Rating® (CDR®)=0, amyloid β (Aβ)-negative), n=49]; Preclinical AD (PC; CDR=0, Aβ-positive, n=17); and mild AD (CDR=0.5 or 1, Aβ-positive, n=20). We found no significant difference in nbM volumes between groups but increased regions of DM and high R2t* in PC (mean DM=3.4%; mean R2t*=23.2±4.6s^{-1}) and mild AD (3.5%; 24.2±5.5s^{-1}) when compared with HC (0.8%; 21.7±4.4s^{-1}), indicating neuronal loss and iron accumulation. This leads to significant increased heterogeneity of R2t* (quantified by its standard deviation) in PC (p=0.0049) and mild AD (p=0.0024) groups compared with HC. Note that iron-related increased R2t* overpowers DM-decreased R2t*, hence increased mean R2t*. Importantly, STD of R2t* exhibited positive association with PET-defined mean cortical amyloid (r=0.36) and mean tauopathy (r=0.26).

In conclusion, qGRE MR is a promising tool in identifying pre-atrophic neurodegeneration and iron accumulation in nbM related to early AD.

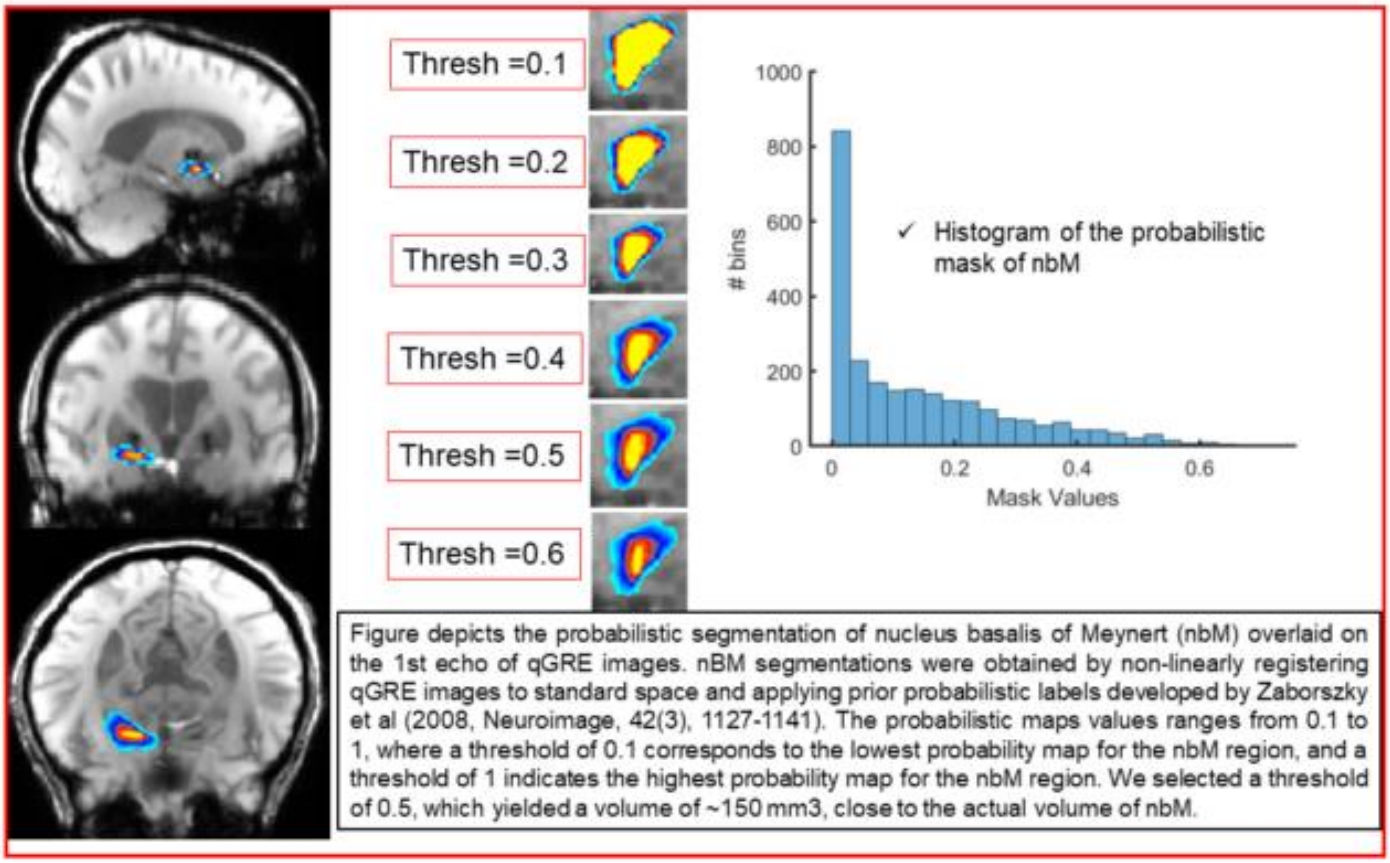

Figure depicts the probabilistic segmentation of nucleus basalis of Meynert (nbM) overlaid on the 1st echo of qGRE images. nBM segmentations were obtained by non-linearly registering qGRE images to standard space and applying prior probabilistic labels developed by Zaborszky et al (2008, Neuroimage, 42(3), 1127-1141). The probabilistic maps values ranges from 0.1 to 1, where a threshold of 0.1 corresponds to the lowest probability map for the nbM region, and a threshold of 1 indicates the highest probability map for the nbM region. We selected a threshold of 0.5, which yielded a volume of ~150 mm3, close to the actual volume of nbM.

Keywords: Alzheimer's Disease, Nucleus Basalis of Meynert, Quantitative Gradient Recalled Echo, Neuronal Loss, Iron Accumulation

143 Head-to-head analysis of [18F]MK6240 and [18F]Flortaucipir standardized update values (SUVs): the HEAD Study

Hsin-Yeh Tsai[1], Cécile Tissot[1], Dana L. Tudorascu[2], Pedro Rosa-Neto[3], Brian Gordon[4], Belen Pascual[5], Val Lowe[6], David Soleimani-Meigooni[7], Hwamee Oh[8], William Klunk[2], William Jagust[9], Tharick Pascoal[2], Suzanne Baker

[1]*Lawrence Berkeley National Laboratory, Berkeley, CA, United States*
[2]*University of Pittsburgh, Pittsburgh, PA, United States*
[3]*McGill University, Montreal, QC, Canada*
[4]*Washington University, Saint-Louis, MO, United States*
[5]*Houston Methodist Hospital, Houston, TX, United States*
[6]*Mayo Clinic, Rochester, MN, United States*
[7]*University of California, San Francisco, San Francisco, CA, United States*
[8]*Brown University, Providence, RI, United States*
[9]*University of California, Berkeley, Berkeley, CA, United States*

Background: [18F]Flortaucipir and [18F]MK6240 differ in binding characteristics, which makes harmonization across tracers complicated.

Objective: Evaluate correlations between standardized uptake value (SUV) of [18F]Flortaucipir and [18F]MK6240 and age in the reference, on- and off-target regions.

Methods: Participants (n=84 [HEAD Data Freeze 1.0], Table 1) received an amyloid-PET scan ([11C]PIB or [18F]NAV4694), an [18F]MK6240 scan (90-110 min post-injection) and [18F]Flortaucipir scan (80-100 min post-injection). Individual PET frames were realigned, averaged, and coregistered to a Freesurfer 7.1-segmented T1-MPRAGE. SUVs were calculated in the reference region (inferior cerebellar gray), on-target regions (entorhinal cortex [EC], hippocampus, Braak III/IV, Braak V/VI), and off-target regions (caudate, pallidum, putamen, thalamus, eroded white matter [WM]). We examined correlations between [18F]MK6240 and [18F]Flortaucipir SUVs as a function of diagnosis, amyloid status, and sex, as well as their associations with age.

Results: In the reference region, [18F]Flortaucipir has a higher coefficient of variation (CoV) and a significantly ($p=0.001$) higher mean (CoV=0.36, mean=0.47±0.17) than [18F]MK6240 (CoV=0.30, mean=0.39±0.12). Age significantly correlated with [18F]Flortaucipir in the reference region, all on-target and off-target regions except WM, and with [18F]MK6240 in EC, hippocampus, Braak III/IV, pallidum, putamen and thalamus ($p<0.01$). The correlations between [18F]Flortaucipir and [18F]MK6240 were significant in all regions (Figure 1, divided by diagnosis). When including interactions with sex, diagnosis and amyloid status in the model (Table 2), the resulting r2 values were higher, and sex (in comparison to amyloid status and diagnosis) most frequently contributed significantly to the model.

Conclusions: SUVs are highly correlated between tracers with a significant by-sex interaction. The higher [18F]Flortaucipir reference region SUV contributes to the tracer's narrower SUVR dynamic range.

Table 1: Demographics

	n	Sex F/M	Number of amyloid positive	Age (std)	[18F]Flortaucipir dose in mCi (std)	[18F]MK6240 dose in mCi (std)	Days between tau-PET scans (std)	Years Education (std)	MMSE (std)
Cognitively Unimpaired Young	13	6/7	0	22.7 (1.3)	8.6 (2.0)	4.7 (0.4)	14.5 (12.2)	15.5 (1.9) 2 missing	29.0 (1.2) 6 missing
Cognitively Unimpaired Old	37	24/1 3	5	68.0 (0.9)	7.0 (2.2)	4.5 (0.3)	14.5 (13.6)	15.9 (3.0) 8 missing	29.1 (0.9) 7 missing
Cognitively Impaired *	34	14/2 0	20	72.3 (5.6)	6.6 (2.2)	4.5 (0.4)	27.0 (28.8)	16.5 (4.4) 8 missing	27.0 (3.0) 8 missing

* Cognitively Impaired subjects are diagnosed as Mild Cognitive Impairment or Alzheimer's Disease by a clinician without the use of biomarkers

Figure 1: SUV [18F]Flortaucipir vs [18F]MK6240

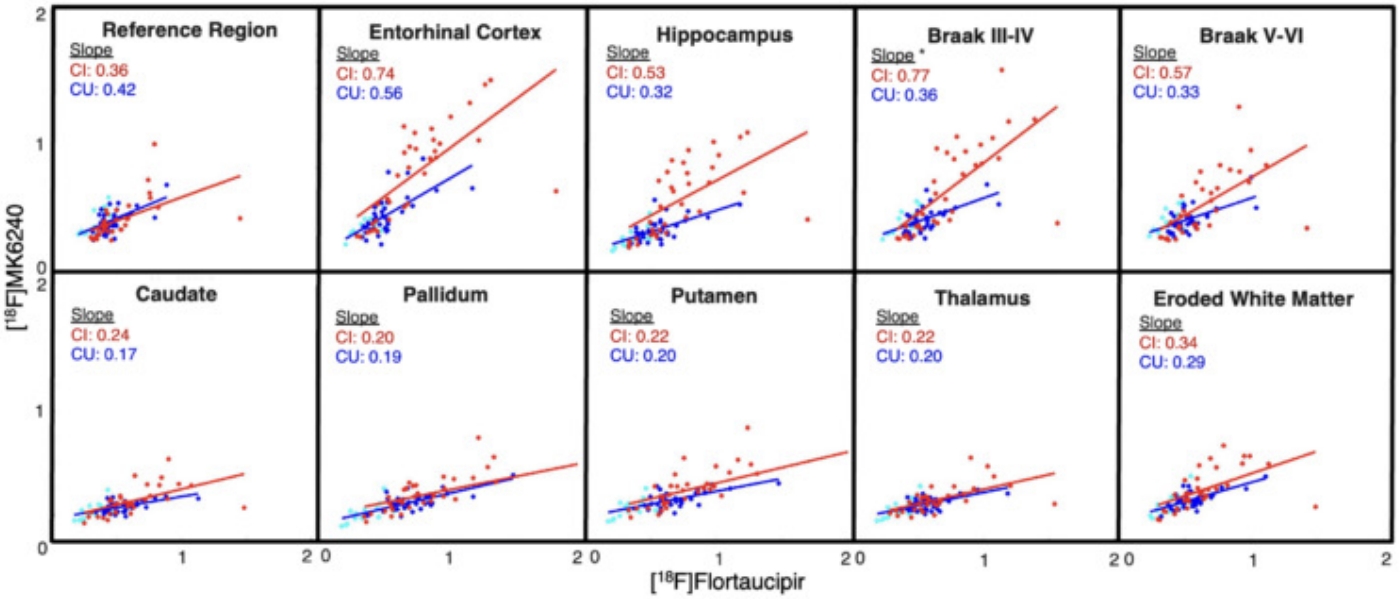

Slope values are fitted for the cognitively unimpaired group (CU; younger healthy controls are in light blue and older healthy controls are in dark blue) and the cognitively impaired group (CI; in red). No significant interactions by diagnosis except in Braak III-IV ($p<0.05$).

Table 2: Exploring the impact of diagnosis, amyloid status, and sex interactions on [^{18}F]Flortaucipir and [^{18}F]MK6240 correlations

Adjusted R^2	MK~1+FTP					
		+age	+age+FTP*diag +FTP*amy+FTP*sex			
	R^2	R^2	R^2	FTP*diag significance	FTP*amy significance	FTP*sex significance
Inferior cerebellar gray	0.28	0.32	0.47			p<0.001
Entorhinal Cortex	0.59	0.59	0.71		p<0.01	p<0.01
Hippocampus	0.45	0.45	0.61	p<0.01	p<0.001	p<0.01
Braak III/IV	0.52	0.52	0.59	p<0.05		p<0.05
Braak V/VI	0.39	0.40	0.45		p=0.05	
Caudate	0.35	0.34	0.44		p<0.05	p<0.01
Pallidum	0.44	0.45	0.57			p<0.001
Putamen	0.40	0.41	0.53			p<0.001
Thalamus	0.38	0.37	0.48			p<0.001
Eroded White Matter	0.38	0.37	0.50		p<0.05	p<0.001

MK = [^{18}F]MK6240 and FTP = [^{18}F]Flortaucipir
diag = diagnosis, cognitively unimpaired vs cognitively impaired (AD & MCI)
amy = amyloid, amyloid positive vs amyloid negative

Keywords: Tau-PET, SUV, reference region, Braak, Off-target

144 Association between oxygen extraction fraction, tau, and amyloid pathology, and cognitive status in Alzheimer's disease: implications for advanced neuroimaging techniques

Seyyed Ali Hosseini[1,2], Stijn Servaes[1,2], Joseph Therriault[1,2], Cécile Tissot[1,2], Nesrine Rahmouni[1,2], Arthur C. Macedo[1,2], Firoza Z. Lussier[3], Jenna Stevenson[1,2], Yi-Ting Wang[1,2], Jaime Fernandez-Arias[1,2], Kely Quispialaya Socualaya[1,2], Étienne Aumont[1,2], Alyssa Stevenson[1,2], Serge Gauthier[1,2], Junghun Cho[4], Hangwei Zhuang[5], Yi Wang[5], David Rudko[6,7,8], Tharick A. Pascoal[3], Pedro Rosa-Neto[1,2]

[1]Translational Neuroimaging Laboratory, McGill Research Centre for Studies in Aging, McGill University, Montréal, QC, Canada
[2]Department of Neurology and Neurosurgery, Faculty of Medicine, McGill University, Montréal, QC, Canada
[3]Department of Psychiatry and Neurology, University of Pittsburgh, Pittsburgh, Pennsylvania, United States
[4]Department of Biomedical Engineering, University at Buffalo, The State University of New York, New York, United States[5]MRI Research Institute, Departments of Radiology and Biomedical Engineering, Cornell University, New York, NY, United States
[6]Department of Neurology and Neurosurgery, McGill University, Montréal, QC, Canada
[7]McConnell Brain Imaging Centre, Montreal Neurological Institute and Hospital, Montréal, QC, Canada
[8]Department of Biomedical Engineering, McGill University, Montréal, QC, Canada

Aims: The Oxygen Extraction Fraction (OEF) provides a detailed metric, quantifying the proportion of oxygen utilized from blood during its course through the cerebral vasculature. In an era of cutting-edge neuroimaging advancements, this study is focused on clarifying the relationships between OEF values, tau and amyloid pathology, and cognitive status in Alzheimer's Disease (AD).

Methods: We assessed a cohort of 347 subjects, including young controls (Y: n=37), Cognitively-unimpaired older adults (CU_{65+}: n=182), individuals with Mild Cognitive-Impairment (MCI: n=80), and AD patients (n=48). All participants underwent the tau Positron emission tomography (PET), amyloid PET, and 3D gradient-recalled echo sequence Magnetic Resonance Imaging (MRI) scans. Using TRIAD cohort data, we crafted a robust OEF mapping pipeline. This process entailed phase unwrapping, background field removal techniques, and the inverse problem. Subsequently, OEF maps were adeptly aligned to the benchmark Montreal Neurological Institute (MNI_{152}) space, for Region-Of-Interest (ROI) and voxel-specific analyses. Using FreeSurfer, the images underwent segmentation into eighty-two regions, delineated in the MNI space. OEF images were blurred by 8mm for voxel-wise analysis.

Results: Most brain regions demonstrated a decreasing trend in OEF values transitioning from young to CN, MCI, and AD categories. Significant differences in OEF values were detected in multiple ROIs, inclusive of the right and left caudate, hippocampus, and both the precentral and caudal middle frontal regions. Age-associated OEF decrease was pronounced, emphasizing age's dominant role in influencing brain OEF levels. Additionally, OEF reductions were most apparent in (Amyloid positive – Tau Positive) A+T+ compared to (Amyloid Negative – Tau Negative) A-T- in the Cortex and White matter, suggesting that tau and amyloid pathology significantly influence OEF and therefore brain functionality.

Conclusions: This study underlines the impact of age, tau and amyloid pathology on MRI-determined OEF values and might enhance our understanding of cerebral metabolic changes in Alzheimer's Disease progression.

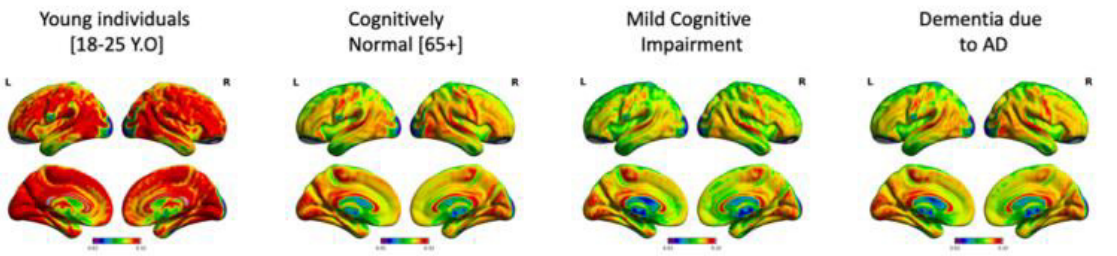

Figure1: Average OEF images

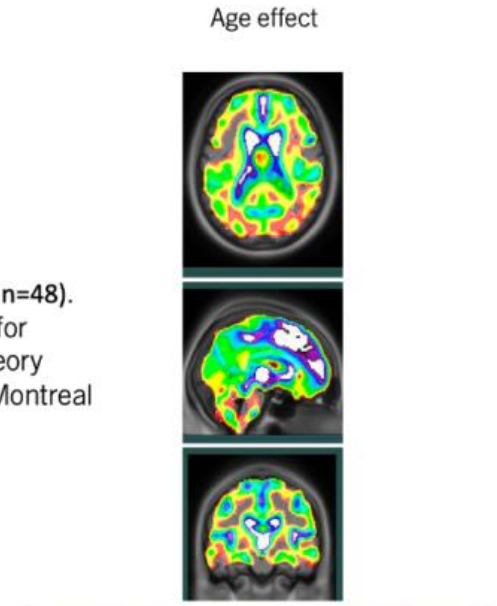

Model: OEF ~ tau + Amyloid + COV.

- COV : age, sex, Apoe4
- **(Y:** n=37), (CU_{65+}: n=182), (MCI: n=80), and (AD: n=48).
- T-statistical parametric maps were corrected for multiple comparisons using a random field theory cluster threshold of P < .001, overlaid on the Montreal Neurological Institute reference template.

Figure2. AGE related cortical Differences

ROI	Labels	Significant	p-value
R_caudate_mean	AD vs CN	TRUE	0.0004
R_transverse_temporal_mean	AD vs CN	TRUE	0.0022
L_cuadte_mean	AD vs CN	TRUE	0.0049
R_caudate_mean	CN vs MCI	TRUE	0.0083
R_hippocampus_mean	AD vs CN	TRUE	0.0094
R_transverse_temporal_mean	AD vs MCI	TRUE	0.0123
L_hippocampus_mean	AD vs CN	TRUE	0.0168
R_hippocampus_mean	AD vs MCI	TRUE	0.0183
L_transverse_temporal_mean	AD vs CN	TRUE	0.0201
L_caudal_middle_frontal_mean	AD vs MCI	TRUE	0.0250

Table 1. The Least Significant Difference (LSD) test in ANOVA between the groups

Keywords: Oxygen Extraction Fraction, Tau Pathology, Amyloid Pathology, Alzheimer's Disease, MRI

145 Association of plasma pTau epitopes with mesial temporal lobe cortical thinning

Lydia Trudel[1], Nesrine Rahmouni[1], Arthur C. Macedo[1], Joseph Therriault[1], Stjin Servaes[1], Yi-Ting Wang[1], Jaime Fernandez-Arias[1], Brandon Hall[1], Jenna Stevenson[1], Sulantha Sanjeewa[1], Serge Gauthier[1], Andrea L. Benedet[3], Nicholas J. Ashton[3], Henrik Zetterberg[3], Kaj Blennow[3], Firoza Lussier[2], Pascoal A. Tharick[2], Thomas K. Karikari[2], Pedro Rosa-Neto[1]

[1]*McGill University, Montreal, QC, Canada*
[2]*University of Pittsburgh, Pittsburgh, PA, United States*
[3]*University of Gothenburg, Gothenburg, Sweden*

Background: Brain atrophy is an important pathological process in Alzheimer's disease (AD) and is closely associated with the onset of cognitive impairment. Intracellular tau tangles have been linked to brain atrophy in AD. Recent high-performance biomarkers of phosphorylated tau (p-tau) in plasma are correlated with cerebral amyloid-β and tau and become abnormal early in the AD process. This study investigated the relationship between plasma tau biomarkers and cortical thickness in the parahippocampal and entorhinal regions, as they are vulnerable to insult during early tau pathology.

Methods: We studied 182 individuals from the TRIAD cohort (mean age = 69.5 ± 7.6, 111 women) with [^{18}F]MK6240-PET and plasma pTau181, pTau217, and pTau231 assessments, measured with Simoa assays. Brain thickness was extracted using FreeSurfer 7. Multiple linear regression analyses were used to assess the relationship between each plasma tau biomarker and bilateral parahippocampal and entorhinal thickness, controlling for age, sex and amyloid-β status.

Results: Of the biomarkers tested, only pTau217 correlated with cortical thickness, bilaterally for the entorhinal cortex and in the left parahippocampal region ($p < 0.01$) (**Figure 1, Figure 2**). A main effect of amyloid-β status was also observed in our models predicting the right parahippocampal and both entorhinal regions' thickness ($p < 0.05$). Finally, we observed a main effect of age on the right entorhinal thickness ($p < 0.05$). When assessing the relationship between plasma and PET biomarkers, we found that pTau217 levels correlated strongly with [18F]MK6240-PET signal ($r = 0.79$, $p < 0.0001$).

Conclusion: Our results suggest that plasma pTau217 is associated with brain atrophy in regions vulnerable in early AD.

Keywords: brain atrophy, Alzheimer's disease, parahippocampal regions, entorhinal cortex

146 Specific Tau networks are associated with different cognitive domains in the elderly

Siddharth Nayak[1], Seyed Hani Hojjati[1], Sindy Ozoria-Blake[1], Qolamreza R. Razlighi[1]

[1]*Department of Radiology, Weill Cornell Medicine, New York, NY, United States*

The relationship between tau deposition and cognitive decline in cognitively healthy individuals is still unclear. Recent studies have thrown light on the relationship between the specificity of Tau and human brain networks based on resting-state scans. Notably, the tau PET tracer ^{18}F-MK-6240 has shown favorable imaging characteristics to identify early tau deposition in aging. In this study, we evaluate the relationship between network-level Tau and cognition as measured across three cognitive domains: episodic memory, processing speed, and fluid reasoning in 124 cognitively normal healthy adults (68.62 ± 5.56 years). Network level Tau measurements were performed based on Schaefer's Atlas' parcellation of 7 functional networks: Visual, Somatomotor, Dorsal Attention network (DAN), Ventral Attention/Salience network (VAN), Limbic, Control network, and Default mode network. Higher tau in the functional networks was associated with poorer cognitive scores. Tau in the DMN ($t = -2.95$, $p = 0.005$) and Visual ($t = -2.62$, $p = 0.01$) network regions were related to accuracy scores in the episodic memory domain, while functional connectivity derived from the resting state scans of the DMN, and visual networks weren't predictive of the same. In addition, we found exploratory findings for the speed of processing domain and fluid reasoning domain for tau in VAN ($t = -2.45$, $p = 0.04$) and visual ($t = -2.15$, $p = 0.04$) networks, respectively. These findings suggest that Tau burden may affect other cognitive domains as well, not only memory. The findings reinforce the idea that early tau deposition in cognitively healthy individuals may provide insights into cognition across different domains, even in a sample of subjects with low amyloid-beta pathology.

Keywords: Tau, DMN, Salience, PET, fMRI

Wednesday, January 17, 2024 - 10:55 am - 12:40 pm

Podium Session

SESSION II: Tau PET Harmonization

CHAIRS: Bradley Christian, Christopher Schwarz

Wednesday, January 17, 2024		
10:55 am - 12:40 pm	SESSION II: Tau PET Harmonization	Bradley Christian, University of Wisconsin, Madison, WI, United States Christopher Schwarz, Mayo Clinic, Rochester, MN, United States
10:55	Introduction	Chairs
11:00	Universal scale for tau PET based on head-to-head data: the HEAD study	Bauer-Negrini | Povala | Lussier | Amaral | Bellaver | Lukasewicz Ferreira | Lowe | Soleimani-Meigooni | Oh | Cohen | Dore | Lopresti | Minhas | Tudorascu | Villemagne | Jagust | Klunk | Pascual | Gordon | Rosa-Neto | Zatt | Baker | Pascoal
11:15	Preliminary evaluation of CenTauR regions of interest with Flortaucipir-PET images and testing in PET-to-autopsy cohort	Iaccarino | Kotari | Kennedy | Shcherbinin | Pontecorvo
11:30	Harmonizing tau PET in Alzheimer's disease: the CenTauR scale and the Joint Propagation Model	Leuzy | Lau Raket | Villemagne | Klein | Tonietto | Olafson | Saad | Bullich | Lopresti | Sanabria Bohorquez | Boada | Charil | Collins | Collins | Cullen | Gunn | Higuchi | Hostetler | Hutchison | Iaccarino | Insel | Irizarry | Jack Jr | Jagust | Johnson | Karten | Marquié | Mathotaarachchi | Mintun | Ossenkoppele | Pappas | Petersen | Rabinovici | Rosa-Neto | Smith | Stephens | Whittington | Carillo | Pontecorvo | Budd Haeberlein | Dunn | Kolb | Sivakumaran | Rowe | Hansson | Doré
11:45	Improving the associations between [18F]MK6240 and [18F]FTP in target regions	Tissot | Tsai | Tudorascu | Rahmouni | Servaes | Therriault | Stevenson | Rosa-Neto | Gordon | Pascual | Lowe | Soleimani-Meigooni | Oh | Klunk | Jagust | Pascoal | Baker
12:00	Elimination of putative off-target signal in the reference region for tau PET harmonization	Olafson | Tonietto | Teng | Abramzon | Klein | Borroni | Stephens | Baker | de Crespigny | Sanabria Bohórquez
12:15	Discussion	

Universal scale for tau PET based on head-to-head data: the HEAD study

Guilherme Bauer-Negrini[1], Guilherme Povala[1], Firoza Lussier[1], Livia Amaral[1], Bruna Bellaver[1], Pamela Lukasewicz Ferreira[1], Val Lowe[2], David Soleimani-Meigooni[3], Hwamee Oh[4], Ann Cohen[1], Vincent Dore[5], Brian Lopresti[1], Davneet Minhas[1], Dana Tudorascu[1], Victor Villemagne[1], William Jagust[6], William Klunk[1], Belen Pascual[7], Brian Gordon[8], Pedro Rosa-Neto[9], Bruno Zatt[10], Suzanne Baker[6], Tharick Pascoal[1]

[1]*Department of Psychiatry, University of Pittsburgh, Pittsburgh, PA, United States*
[2]*Department of Radiology, Mayo Clinic, Rochester, MN, United States*
[3]*Memory and Aging Center, University of California San Francisco, San Francisco, CA, United States*
[4]*Department of Psychiatry and Human Behavior, Brown University, Providence, RI, United States*
[5]*Austin Health, Melbourne, Australia*
[6]*Lawrence Berkeley National Laboratory, Berkeley, CA, United States*
[7]*Department of Neurology, Houston Methodist Research Institute, Houston, TX, United States*
[8]*Department of Radiology, Washington University in Saint Louis, Saint Louis, MO, United States*
[9]*Translational Neuroimaging Laboratory, McGill University Research Centre for Studies in Aging, Douglas Research Institute, Montréal, QC, Canada*
[10]*Universidade Federal de Pelotas, Pelotas, Brazil*

Objective: The HEAD study was conceptualized under the assumption that a large head-to-head tau-PET dataset is required to provide robust anchor values across tracers. Here, we aim to demonstrate that anchoring tau tracer uptake values based on head-to-head acquisitions has the potential to produce an accurate universal tau-PET scale (Uniτ(tau)).

Methods: 101 individuals across the aging and AD spectrum (Training; HEAD data freeze 1.0:n=84, Testing; Pittsburgh dataset(Gogola *et al.*):n=15) with Flortaucipir/MK-6240-PET. SUVRs were processed to a common 6mm FWHM with inferior cerebellar gray as reference (Pascoal et al.). Uniτ explored two anchoring/harmonization steps. We generated three anchor values based on a reference ROI (meta-temporal), with the Young (<25 years) mean set to 0, 3SD>mean CU to 20, and the AD 95th percentile voxels to 100. We also tested linear/non-linear regressions for anchoring between tracers. We produced 3D images based on: (a)parameters generated by ROI analysis; and (b)anchoring equations optimized for each voxel. For testing, we used CenTauR ROIs (Villemagne *et al.*).

Results: Uniτ scale with 2 anchors produced similar estimates regardless of tracer in the training and testing datasets (Fig.1). A less accurate scaling in Frontal and Braak2 (not shown) ROIs supports high tracer correspondence for measuring tau tangles, but less so for non-specific/off-target signals. However, Uniτ 3-anchor-value model provided the most similar estimates. Fig.2 supports that a single equation has the potential to generate reasonably accurate 3D Uniτ images. Fig.3 shows that voxel-specific anchoring equations resulted in only minor improvements in the 3D Uniτ images.

Conclusion: These preliminary findings suggest that within-tracer anchoring of tau-PET extreme values is useful for harmonizing tau tracers without compromising their intrinsic properties at global, regional, and even voxel levels. Uniτ parameters are being refined using head-to-head data and will be made available in the future when generated using subsequent HEAD data freezes (n>300).

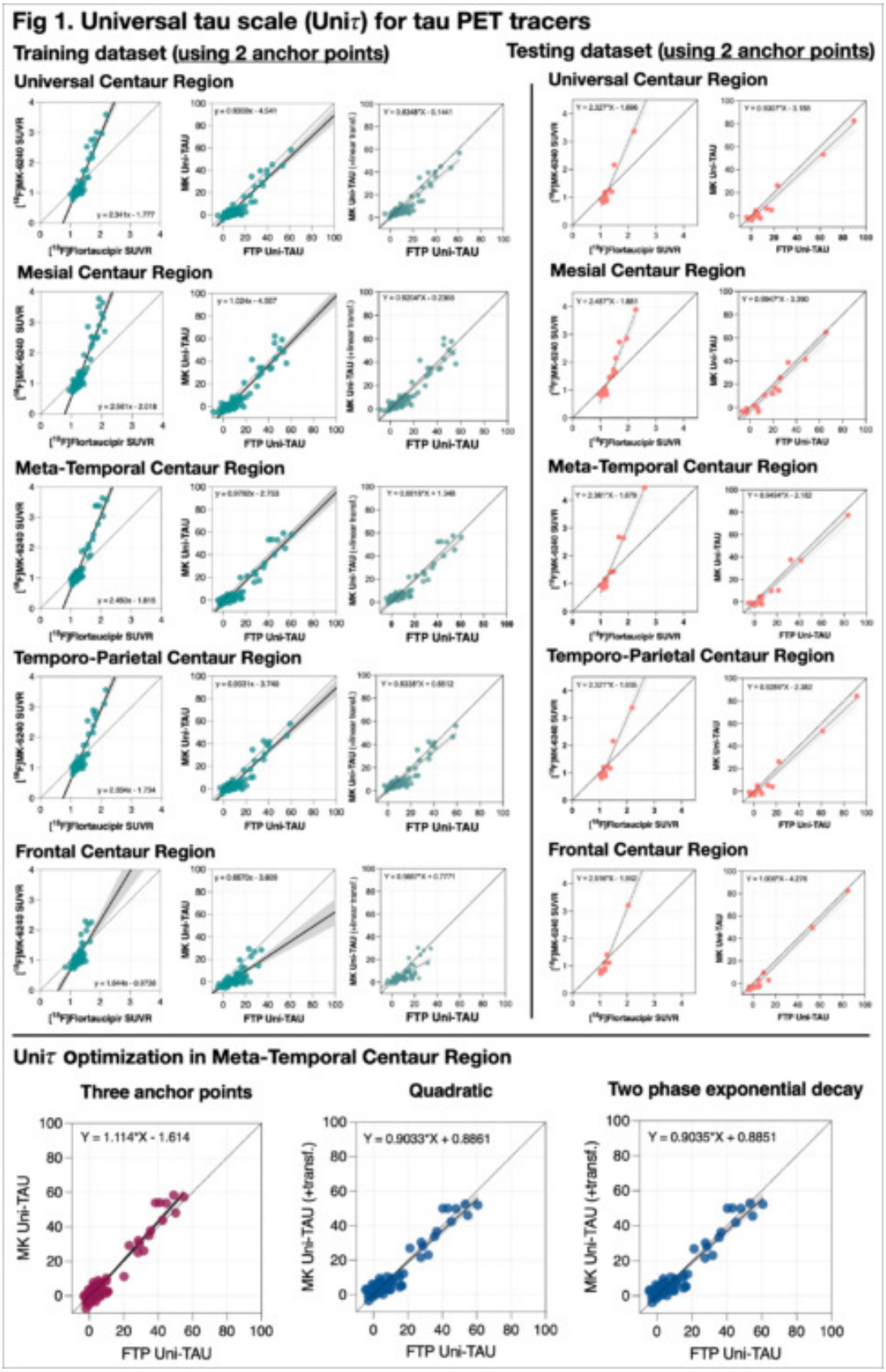
Fig 1. Universal tau scale (Uniτ) for tau PET tracers
Training dataset (using 2 anchor points)
Testing dataset (using 2 anchor points)
Universal Centaur Region
Mesial Centaur Region
Meta-Temporal Centaur Region
Temporo-Parietal Centaur Region
Frontal Centaur Region
[18F]MK-6240 SUVR
[18F]Flortaucipir SUVR
MK Uni-TAU
FTP Uni-TAU
MK Uni-TAU (+linear transf.)
Uniτ Optimization in Meta-Temporal Centaur Region
Three anchor points
Quadratic
Two phase exponential decay
Y = 1.114*X - 1.614
Y = 0.9033*X + 0.8861
Y = 0.9035*X + 0.8851
MK Uni-TAU (+transf.)

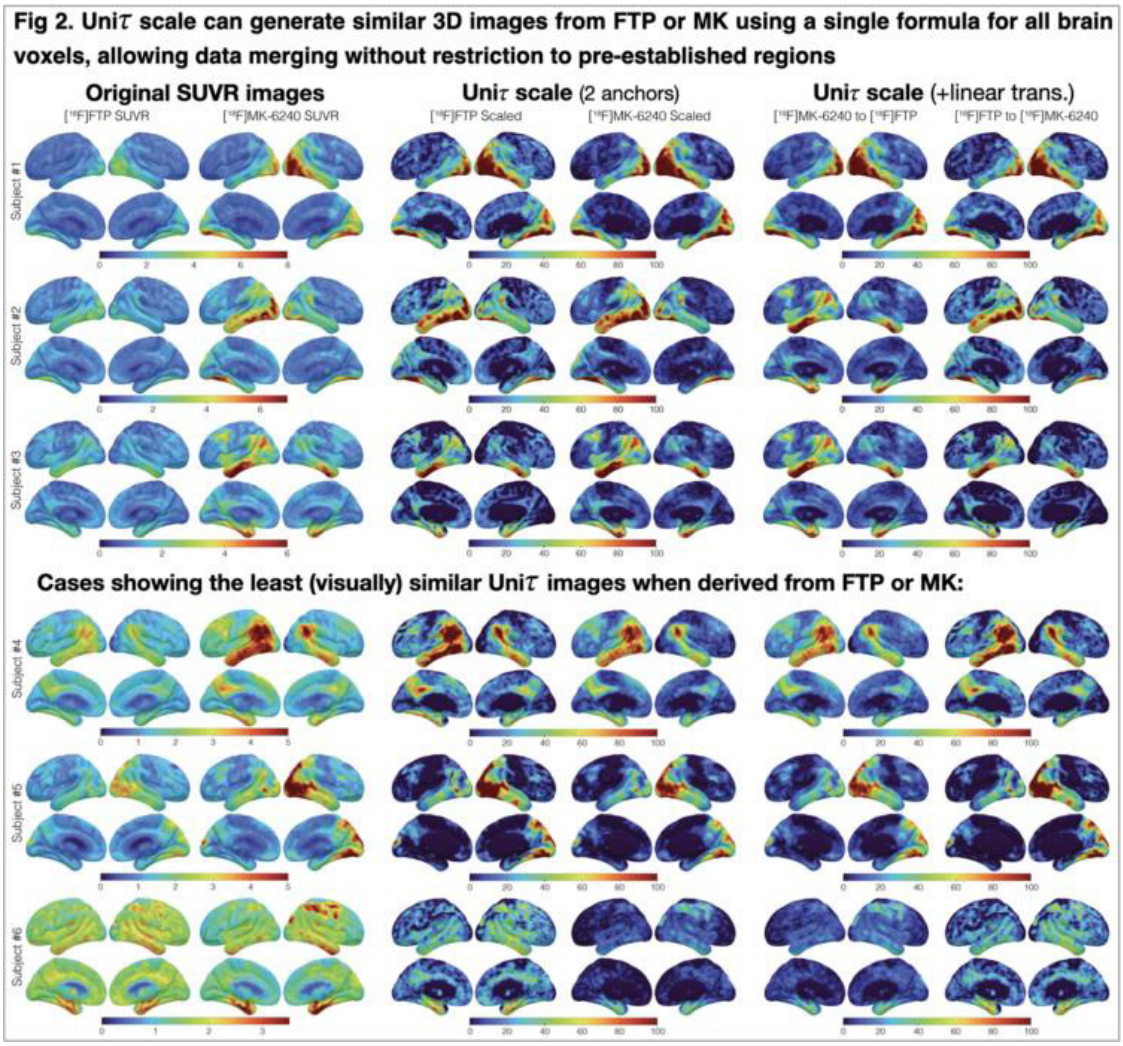
Fig 2. Uniτ scale can generate similar 3D images from FTP or MK using a single formula for all brain voxels, allowing data merging without restriction to pre-established regions
Original SUVR images
[18F]FTP SUVR
[18F]MK-6240 SUVR
Uniτ scale (2 anchors)
[18F]FTP Scaled
[18F]MK-6240 Scaled
Uniτ scale (+linear trans.)
[18F]MK-6240 to [18F]FTP
[18F]FTP to [18F]MK-6240
Subject #1
Subject #2
Subject #3
Cases showing the least (visually) similar Uniτ images when derived from FTP or MK:
Subject #4
Subject #5
Subject #6

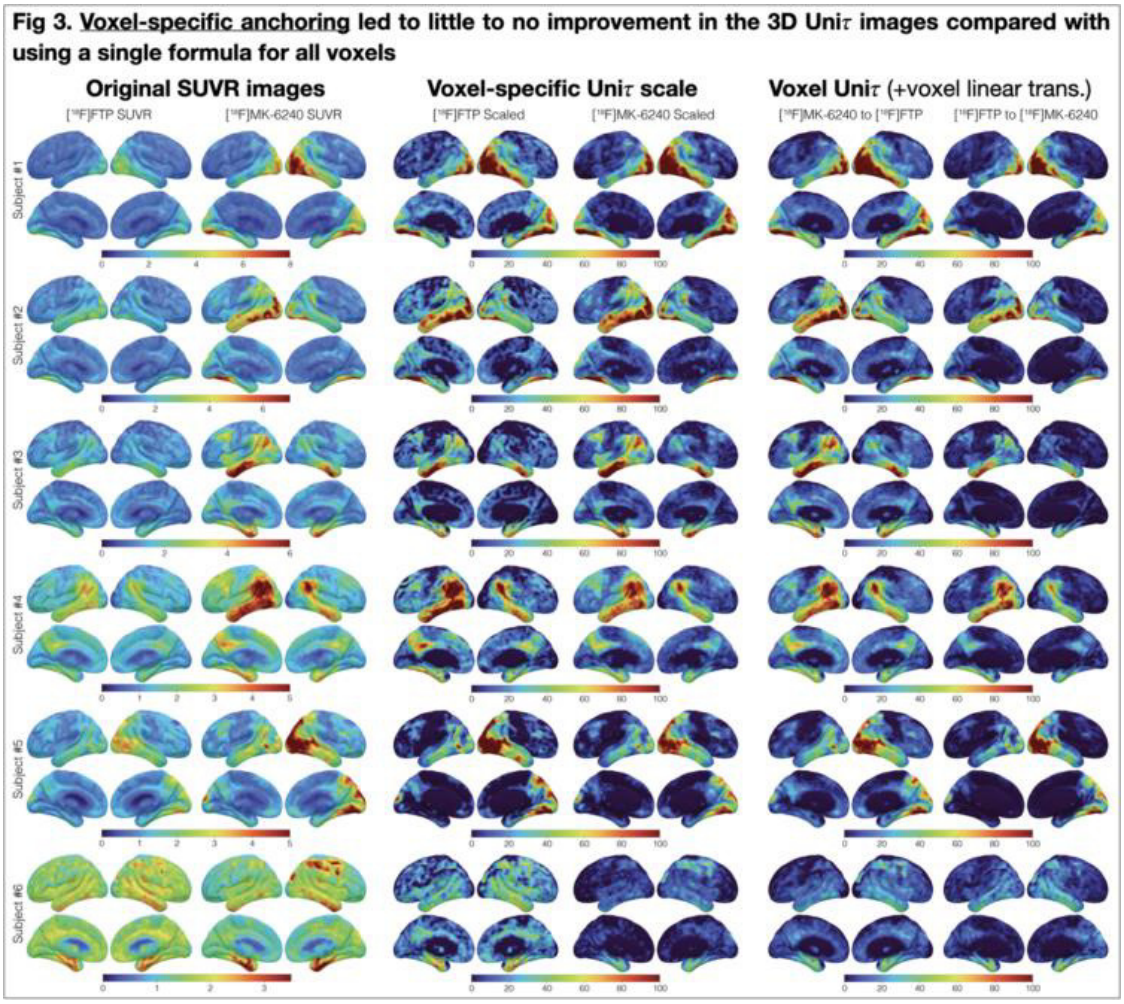

Keywords: tau-PET, harmonization, scale, head-to-head

Preliminary evaluation of CenTauR regions of interest with Flortaucipir-PET images and testing in PET-to-autopsy cohort

Leonardo Iaccarino[1], Vikas Kotari[1], Ian Kennedy[1], Sergey Shcherbinin[1], Michael Pontecorvo[1]

[1]*Eli Lilly and Company, Indianapolis, IN, United States*

Background: The CenTauR workgroup has recently distributed regions of interest (ROIs) that were created using data from six different tau-PET tracers (Villemagne et al., 2023), including both neocortical target and cerebellar cortex reference regions. In this study, we preliminarily evaluated Flortaucipir-PET quantitation performed with CenTauR ROIs compared to standard quantitation approaches.

Methods: We included baseline Flortaucipir-PET data from a clinically heterogeneous cohort of an observational study (A05E, NCT02016560) and from a PET-to-autopsy study (A16, NCT02516046) (see Figure 1 for a demographic summary). Dynamic flortaucipir-PET frames were motion corrected, acquisition time corrected, averaged, and, in the observational study, rigidly aligned to the subject's baseline MRI, and warped to standard space with MRI-based parameters. In the PET-to-autopsy study, lacking MRIs, PET images were aligned to a previously developed flortaucipir PET template. Using images from the observational study, we explored the relationship between CenTauR SUVrs (Universal ROI with CenTauR cerebellar cortex reference) and standard AD-signature weighted neocortical SUVr (Devous et al., 2018), with cerebellar crus [AD-SUVR-CC] or subject-specific white matter reference (AD-SUVr-PERSI, Southekal et al., 2018) The three SUVr measures were then evaluated on their ability to predict advanced Braak V/VI (B3) pathology at autopsy (A16 data), using Youden-index based study-specific cut-off thresholds.

Results: CenTauR SUVrs showed significant linear and positive associations with both AD-SUVR-CC and AD-SUVR-PERSI (R^2=0.983 and R^2=0.839, respectively, both $p<0.001$, see Figure 2). Sensitivity, Specificity and Accuracy were comparable between CenTauR SUVR and AD-SUVR-CC (71%/100%/82% and 79%/95%/85%, respectively), but higher with AD-SUVR-PERSI (84%/100%/90%) (see Figure 3).

Conclusions: CenTauR SUVr showed robust associations and similar performance when compared with standard Flortaucipir-PET quantitation, especially when using a cerebellar reference. These results indicate high correspondence between the Universal CenTauR and the AD-signature weighted neocortical target regions.

Figure 1. Demographic and Clinical Summary

	A05E	A16
N	217	60
Age mean(SD)	67.8 (14.5)	82.9 (9.4)
Sex N Female	109/217	33/60
Amyloid status N Positive/Negative*	84/133	52/8
Clinical Stage N(%)		
Cognitively Normal	73 (33.64%)	12 (20%)
Mild Cognitive Impairment	96 (44.24%)	1 (1.67%)
Dementia	48 (22.12%)	47 (78.33%)

Table showing demographic and clinical summary of included patients.

* Amyloid status for Study A05E was determined according to Florbetapir-PET visual reads. Amyloid status for Study A16 was determined according to CERAD scoring, with C2 or C3 considered positive.

Legend: SD=Standard Deviation

Figure 2. Associations between CenTauR SUVrs and AD-signature weighted Neocortical SUVrs

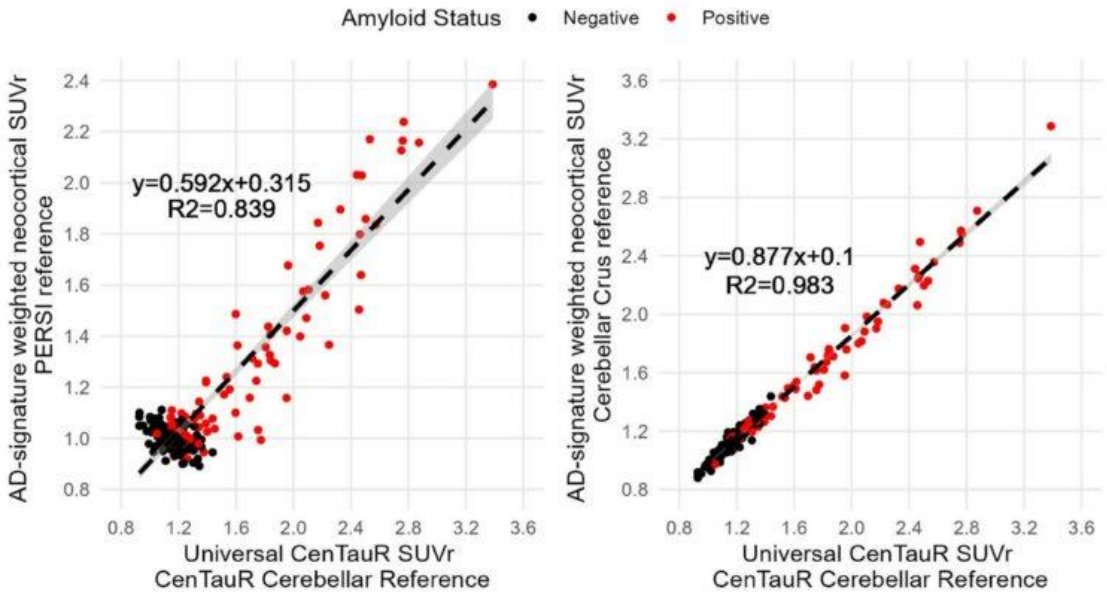

Figure showing associations between CenTauR SUVrs (Universal ROI target region and cerebellar reference region) and AD-signature weighted neocortical SUVRs with either subject-specific white matter PERSI reference (left) or cerebellar crus reference region (right). Amyloid Status was established through Florbetapir-PET visual read.

Legend: ROI: Region of Interest; PERSI = Parametric Estimation of Reference Signal Intensity; SUVr= Standardized Uptake Value ratio.

Figure 3. Diagnostic performance of the different SUVr measures predicting Braak V/VI

	AUC	Sensitivity	Specificity	Accuracy
AD-SUVr-PERSI	**0.910**	**84.2%**	**100%**	**90%**
AD-SUVr-CC	**0.905**	**78.9%**	**95.5%**	**85%**
CenTauR	**0.880**	**71.1%**	**100%**	**82%**

Figure showing diagnostic performance for the different SUVr metrics for the prediction of Braak V/VI at autopsy.

Legend: AD=Alzheimer's Disease; SUVr=Standardized Uptake Value ratio; PERSI= Parametric Estimation of Reference Signal Intensity; CC= Cerebellar Crus; AUC=Area Under the Curve

Keywords: PET, tau-PET, quantitation, centaur, autopsy

Harmonizing tau PET in Alzheimer's disease: the CenTauR scale and the Joint Propagation Model

Antoine Leuzy[1,2,3], Lars Lau Raket[1,4], Victor L Villemagne[5,6,7], Gregory Klein[8], Matteo Tonietto[8], Emily Olafson[9], Ziad Saad[11], Santiago Bullich[12], Brian Lopresti[13], Sandra Sanabria Bohorquez[9], Mercè Boada[14,15], Arnaud Charil[16], Emily C Collins[4], Jessica Collins[17], Nicholas Cullen[2], Roger N Gunn[18,19], Makoto Higuchi[20], Eric Hostetler[21], R Matthew Hutchison[17], Leonardo Iaccarino[4], Philip S Insel[22], Michael C Irizarry[16], Clifford R Jack Jr[23], William J Jagust[24], Keith A Johnson[25,26], Yashmin Karten[2], Marta Marquié[14,15], Sulantha Mathotaarachchi[3], Mark A Mintun[4], Rik Ossenkoppele[1,27], Ioannis Pappas[28,29], Ronald C Petersen[23], Gil D Rabinovici[30,31], Pedro Rosa-Neto[32,33], Ruben Smith[1,34], Andrew W Stephens[12], Alex Whittington[18], Maria C Carillo[35], Michael J Pontecorvo[4], Samantha Budd Haeberlein[3], Billy Dunn[36], Hartmuth C Kolb[11], Sudhir Sivakumaran[2], Christopher C Rowe[6,7,37], Oskar Hansson[1,38], Vincent Doré[7,39]

[1]*Clinical Memory Research Unit, Department of Clinical Sciences, Lund University, Lund, Sweden*
[2]*Critical Path for Alzheimer's Disease (CPAD) Consortium, Critical Path Institute, Tucson, AZ, United States*
[3]*Enigma Biomedical USA, Knoxville, TN, United States*
[4]*Eli Lilly and Company, Indianapolis, IN, United States*
[5]*Department of Neurology, University of Pittsburgh School of Medicine, Pittsburgh, PA, United States*
[6]*Florey Department of Neuroscience, University of Melbourne, Victoria, Australia*
[7]*Department of Molecular Imaging & Therapy, Austin Health, Victoria, Australia*
[8]*F. Hoffmann-La Roche Ltd, Basel, CH*
[9]*Clinical Imaging Group, Genentech, Inc., San Francisco, CA, United States*
[10]*Lawrence Berkeley National Laboratory, Berkeley, CA, United States*
[11]*Janssen Research & Development, San Diego, CA, United States*
[12]*Life Molecular Imaging GmbH, Berlin, Germany*
[13]*Department of Radiology, University of Pittsburgh School of Medicine, Pittsburgh, PA, United States*
[14]*Ace Alzheimer Center Barcelona, Universitat Internacional de Catalunya, Barcelona, ES*
[15]*Networking Research Center on Neurodegenerative Diseases (CIBERNED), Instituto de Salud Carlos III, Madrid, ES*
[16]*Eisai, Inc., Nutley, NJ, United States*
[17]*Biogen, Cambridge, MA, United States*
[18]*Invicro, London, United Kingdom*
[19]*Brain Sciences, Imperial College London, Hammersmith Hospital, London, United Kingdom*
[20]*Department of Functional Brain Imaging, Institute for Quantum Medical Science, National Institutes for Quantum Science and Technology, Chiba, Japan*
[21]*Merck & Co., Inc., West Point, PA, United States*
[22]*Department of Psychiatry and Behavioral Sciences, University of California, San Francisco, CA, United States*
[23]*Department of Neurology, Mayo Clinic, Rochester, MN, United States*
[24]*University of California Berkeley, Lawrence Berkeley National Laboratory, Berkeley, CA, United States*
[25]*Harvard Medical School, Department of Radiology, Boston, MA, United States*
[26]*Gordon Center for Medical Imaging, Massachusetts General Hospital, Boston, MA, United States*
[27]*Amsterdam University Medical Center, Neuroscience Campus Amsterdam, Alzheimercenter, Amsterdam, The Netherlands*
[28]*Department of Psychology, Helen Wills Neuroscience Institute, University of California, Berkeley, CA, United States*
[29]*Department of Neurology, VA Northern California Health Care System, Martinez, CA, United States*
[30]*Department of Neurology, Memory and Aging Center, Weill Institute for Neurosciences, University of California, San Francisco, CA, United States*
[31]*Department of Radiology & Biomedical Imaging, University of California,, San Francisco, CA, United States*
[32]*Translational Neuroimaging Laboratory, Department of Neurology and Neurosurgery, Faculty of Medicine, The McGill University Research Centre for Studies in Aging, McGill University, Montreal, QC, Canada*
[33]*Montreal Neurological Institute, McGill University, Montreal, QC, Canada*
[34]*Department of Neurology, Skåne University Hospital, Lund, Sweden*

[35]*Alzheimer's Association, Chicago, IL, United States*
[36]*Senior advisor to CPAD Consortium, Critical Path institute, Tucson, AZ, United States*
[37]*The Australian Dementia Network (ADNeT), Melbourne, Australia*
[38]*Memory Clinic, Skåne University Hospital, Lund, Sweden*
[39]*Health and Biosecurity Flagship, The Australian eHealth Research Centre, CSIRO, Victoria, Australia*

Objective: We tested a joint propagation model (JPM) to standardize tau PET SUVR values using a common scale (units of this scale named "CenTauRs" [CTR]). JPM is a nonlinear mixed-effects model that simultaneously models the relations between head-to-head and anchor point data, without the need for a reference tracer (Figure 1). The JPM was compared to a reference tracer based linear regression approach analogous to the one used in the Centiloid method for amyloid PET (Figure 1).

Methods: 117 individuals with head-to-head tau PET were included from five cohorts (Table 1): [18F]RO948 vs [18F]flortaucipir (BioFINDER-2, n=37, [18F]MK-6240 vs [18F]flortaucipir (University of Pittsburgh, n=15), [18F]GTP1 vs [18F]PI-2620 (Roche/Invicro, n=26), [18F]GTP1 vs [18F]MK-6240 (Roche/Invicro, n=22), and [18F]RO948 vs [18F]PI-2620 (Fundació ACE Healthy Brain Initiative (FACEHBI) study, n=17). Anchor point values (CTR-0 and CTR-100) were derived using an additional 325 individuals (Figure 2, see legend Table 1 for criteria): [18F]flortaucipir (BioFINDER-2, n=53); [18F]GTP1 (n=26); [18F]MK-6240 (AIBL, n=171); [18F]PI-2620 (Life Molecular Imaging, n=19); and [18F]RO948 (BioFINDER-2, n=64). We used a recently proposed global tau ROI as well as four subregions (Mesial Temporal, Meta Temporal, Temporo-Parietal and Frontal; Figure 1). To compare the performance of the JPM and the linear regression approach, 20 replications of 5-fold cross-validation analysis (100 evaluations) were performed.

Results: Using head-to-head data, strong linear associations were observed between tracers across all ROIs (Figure 3): [18F]RO948 vs [18F]flortaucipir (R2=0.977), [18F]MK-6240 vs [18F]flortaucipir (R2=0.985), [18F]GTP1 vs [18F]PI-2620 (R2=0.945), [18F]GTP1 vs [18F]MK-6240 (R2=0.928), [18F]RO948 vs [18F]PI-2620 (R2=0.903). Cross validation results comparing the JPM and the linear regression approach on the CTR scale showed that the JPM consistently resulted in lower mean square prediction error (mean 45.0 vs. 76.8).

Conclusion: While additional data and comparison to other methods is required, preliminary findings using the JPM support the idea of a standardized scale for tau PET.

Figure 1. Overview of the CenTauR ROIs, the JPM and the linear regression approach

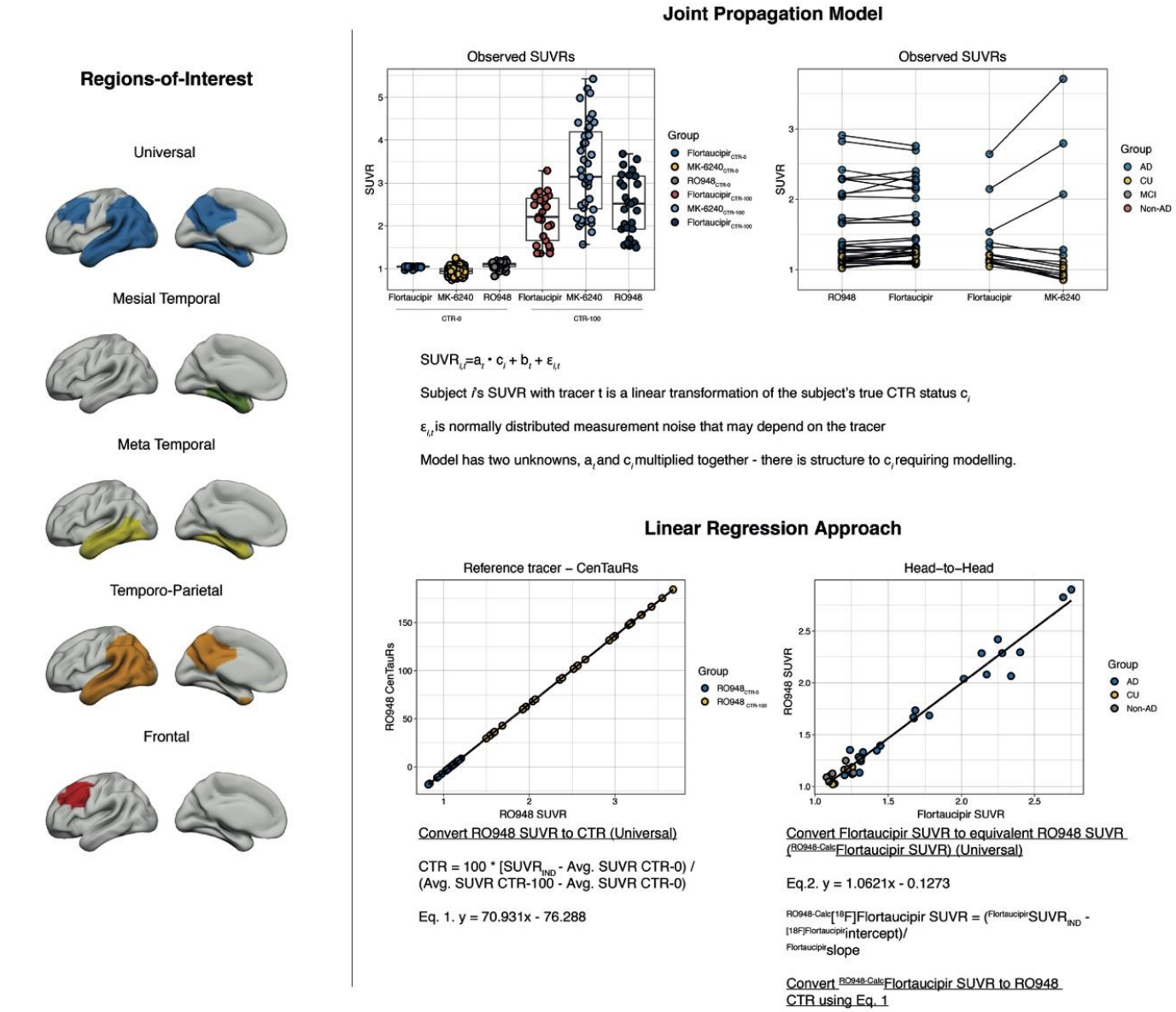

Figure 2. CenTauR values across regions of interest (ROIs) in anchor point and head-to-head cohorts

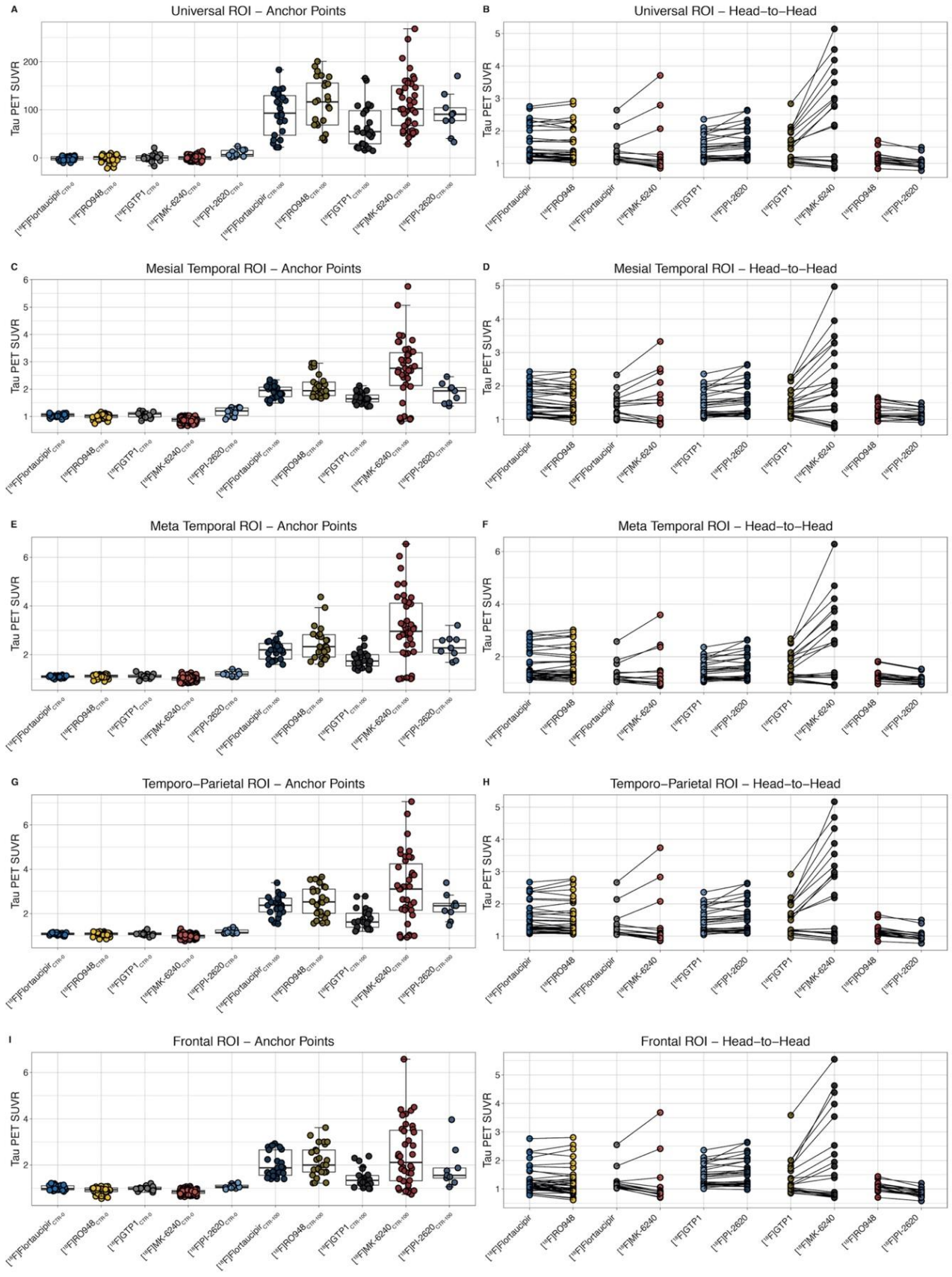

Figure 3. Associations between JPM-based CTR values across head-to-head cohorts

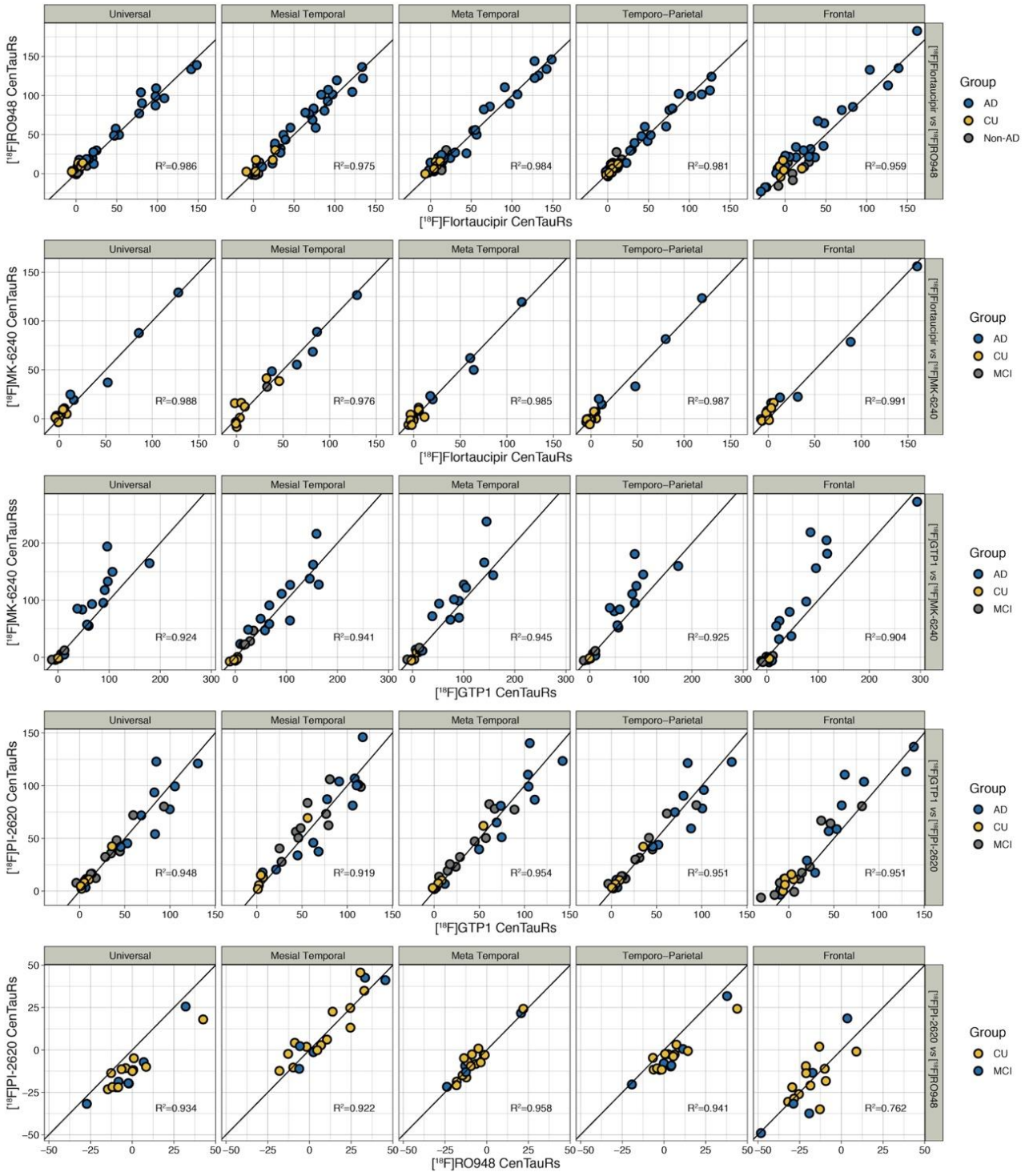

Table 1. Overview of head-to-head cohorts

	CU	MCI	AD	Non-AD
Cohort 1: [^{18}F]RO948 *vs* [^{18}F]flortaucipir (BioFINDER-2)				
N	5	-	24	8
Cohort 2: [^{18}F]MK-6240 *vs* [^{18}F]flortaucipir (University of Pittsburgh)				
N	9	1	5	-
Cohort 3: [^{18}F]GTP1 *vs* [^{18}F]PI-2620 (Roche/Invicro)				
N	5	10	12	-
Cohort 4: [^{18}F]GTP1 *vs* [^{18}F]MK-6240 (Roche/Invicro)				
N	5	3	14	-
Cohort 5: [^{18}F]RO948 *vs* [^{18}F]PI-2620 (FACEHBI)				
N	13	5	-	-

Criteria for the CTR-0 group were CU individuals who were negative on both amyloid (visual read and Centiloids <10, a cutoff associated with the absence of Aβ plaques) and tau PET (visual read). Criteria for the CTR-100 group were having a clinical diagnosis of AD dementia, age <75, MMSE >20 and being positive on both amyloid (visual read and Centiloids >50) and tau PET (visual read). Applying the anchor point criteria to different datasets available to the Working Group resulted in the following groups: [^{18}F]flortaucipir (n=29 CTR-0, n=25 CTR-100 [BioFINDER, Avid A05]); [^{18}F]RO948 (n=36 CTR-0, n=36 CTR-100 [BioFINDER-2]); [^{18}F]MK-6240 (n=120 CTR-0, n=39 CTR-100 [AIBL]); [^{18}F]GTP1 (n=7 CTR-0, n=19 CTR-100 [Roche/Invicro]); [^{18}F]PI-2620 (n=10 CTR-0, n=9 CTR-100 [Life Molecular Imaging]).

Keywords: Tau, PET, CenTauR, harmonization, Alzheimer

Improving the associations between [18F]MK6240 and [18F]FTP in target regions

Cécile Tissot[1], Hsin-Yeh Tsai[1], Dana L. Tudorascu[2], Nesrine Rahmouni[3], Stijn Servaes[3], Joseph Therriault[3], Jenna Stevenson[3], Pedro Rosa-Neto[3], Brian Gordon[4], Belen Pascual[5], Val Lowe[6], David Soleimani-Meigooni[7], Hwamee Oh[8], William Klunk[2], William Jagust[9], Tharick Pascoal[2], Suzanne Baker[1]

[1]*Lawrence Berkeley National Laboratory, Berkeley, CA, United States*
[2]*University of Pittsburgh, Pittsburgh, PA, United States*
[3]*McGill University, Montreal, QC, Canada*
[4]*Washington University, Saint-Louis, MO, United States*
[5]*Houston Methodist Hospital, Houston, TX, United States*
[6]*Mayo Clinic, Rochester, MN, United States*
[7]*University of California, San Francisco, San Francisco, CA, United States*
[8]*Brown University, Providence, RI, United States*
[9]*University of California, Berkeley, Berkeley, CA, United States*

Background: [18F]Flortaucipir (FTP) and [18F]MK6240 are widely used tau-PET tracers in Alzheimer's disease (AD). Each presents with different binding properties and regions of off-target signal. Our primary objective was to investigate whether the incorporation of regions of off-target signal covariates could enhance the correlation between these tracers within on-target regions.

Methods: We assessed 64 individuals from the HEAD dataset (9 young, 28 cognitively unimpaired elderlies and 27 cognitively impaired) with [18F]MK6240 and [18F]FTP. Images were acquired 80-100 ([18F]FTP) and 90-110-minutes ([18F]MK6240) post-injection, and underwent the same processing pipeline, using the inferior cerebellar grey (CG) as the reference region. Individuals where divided based on their Aβ-PET status. We first conducted linear models between tracers in Braak I to Braak VI, and we introduced different off-target regions to evaluate their potential impact on improving the correlations. Off-target regions were caudate, pallidum, putamen, thalamus, choroid plexus, the extracortical hotspot medial to the entorhinal cortex (entoech) and meninges for both [18F]FTP and [18F]MK6240.

Results: [18F]MK6240 and [18F]FTP SUVR in each Braak stage is significantly correlated with each other, with a lower R^2 value for Braak VI (Figure 1A). Interestingly, the slopes of Aβ positive individuals exhibited higher R^2 values than Aβ- in all Braak stages (Figure 1B). The addition of most off-target regions (both [18F]FTP and [18F]MK6240) significantly contributed to the model for different Braak ROIs (Figure 2). We observed the correcting for pallidum in Braak I and putamen in Braak II to VI resulted in the highest R^2 values, especially when including the interaction between on-target [18F]FTP and Aβ status.

Conclusion: In summary, these findings suggest that there is an opportunity to improve the correlation between [18F]MK6240 and [18F]FTP SUVRs by including an interaction with Aβ status and off-target regions. Adjusting for these factors can lead to more accurate harmonization between tau-PET tracers.

Figure 1

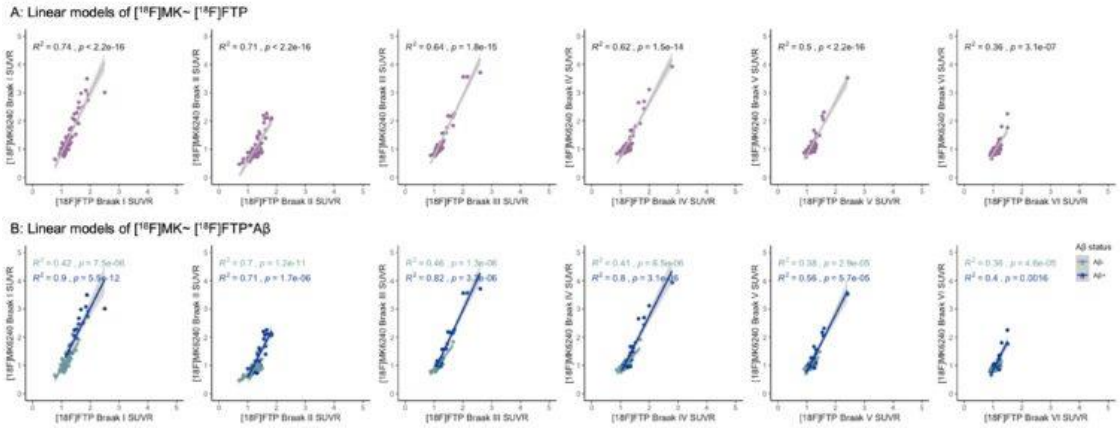

Figure2

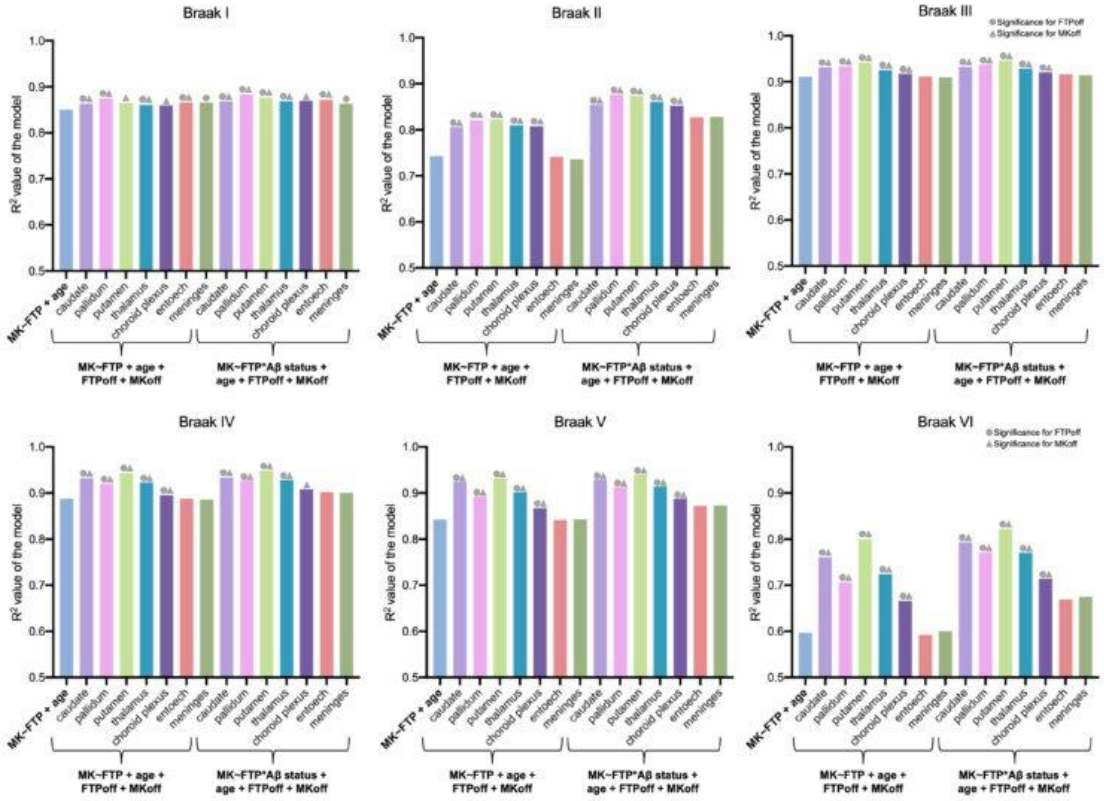

Keywords: tau-PET, harmonization, off-target, Braak

Elimination of putative off-target signal in the reference region for tau PET harmonization

Emily Olafson[1], Matteo Tonietto[2], Edmond Teng[1], Dan Abramzon[1], Gregory Klein[2], Edilio Borroni[2], Andrew Stephens[3], Suzanne Baker[4], Alex de Crespigny[1], Sandra Sanabria Bohórquez[1]

[1]*Research and Early Development (gRED), Genentech, South San Francisco, CA, United States*
[2]*Research and Early Development (pRED), Hoffmann-La Roche, Basel, CH*
[3]*Life Molecular Imaging, Berlin, Germany*
[4]*Cellular and Tissue Imaging, Lawrence Berkeley National Lab, Berkeley, CA, United States*

Introduction: Tau PET imaging is increasingly used in clinical trials of Alzheimer's disease (AD) as an enrichment tool and as a downstream pharmacodynamic biomarker. Several tau PET tracers have been developed, and uptake is generally correlated between tracers in regions with tau pathology. However, off-target signal is idiosyncratic to each tracer and may introduce noise into tracer conversion equations if not properly addressed. In this study, we evaluated whether removing putative off-target signal in the reference region improved correlations between [18F]GTP1, [18F]MK-6240, and [18F]PI-2620.

Methods: 27 subjects underwent [18F]GTP1 and [18F]PI-2620 PET imaging, and 22 subjects underwent [18F]GTP1 and [18F]MK-6240 PET imaging. Both cohorts included subjects ranging from cognitive normal amyloid negative (Aβ-) to AD Aβ+. Voxelwise SUV values in the reference region were transformed into z-scores for each subject for visual comparisons between tracers. The SUV ratio (SUVR) was used to quantify tau binding across 5 target regions using the inferior cerebellum as a reference region. Increasing proportions of high-intensity voxels, reflecting presumed off-target binding, were removed from each subject's reference region, and the relationship between tracer SUVRs was calculated using the coefficient of determination (R2).

Results: Mean z-score images in the reference region showed tracer-specific patterns that correspond to known off-target signal (Figure 1). Removing the highest intensity voxels from the cerebellum strengthened the association between [18F]GTP1 and [18F]PI-2620 for all target regions, but only improved the association between [18F]GTP1 and [18F]MK-6240 when the [18F]MK-6240 reference region was not modified (Figure 2). This method reduced the residual error in the conversion between [18F]GTP1 and [18F]PI-2620 (Figure 3).

Conclusion: Removing the highest intensity voxels in the reference region improved the head-to-head relationship between [18F]GTP1 and [18F]PI-2620. This methodology may improve cross-tracer harmonization by removing subject- and tracer-specific off-target signal.

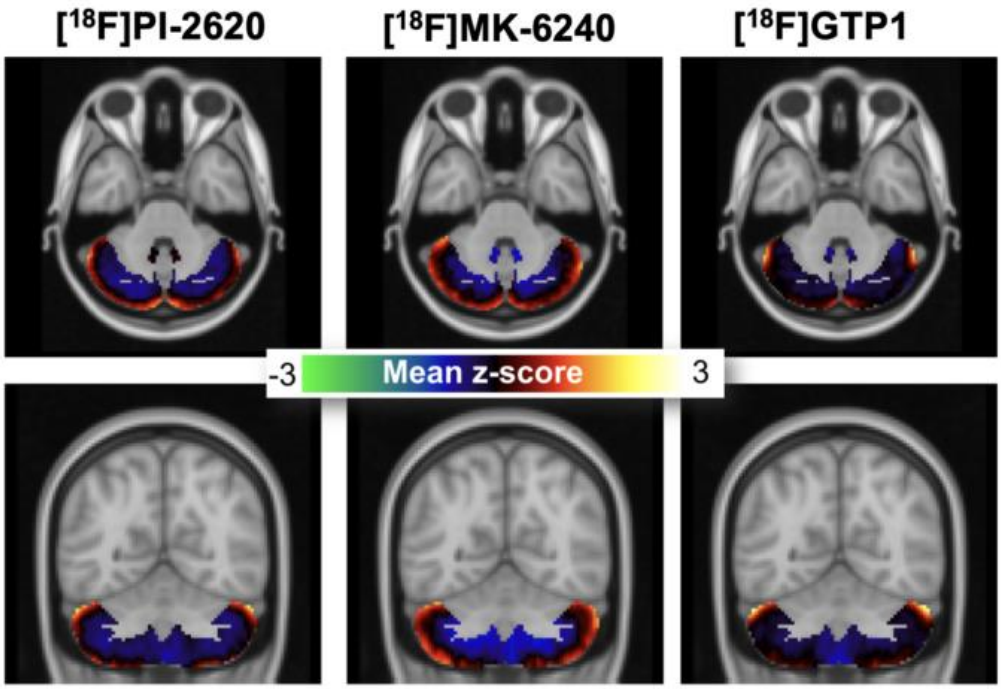

Figure 1. Higher z-scores are found in regions known to contribute to tracer-specific off-target signal (e.g. venous sinus, meninges). Voxelwise average cerebellar z-score images are displayed for each tracer, with horizontal (top) and coronal (bottom) views that emphasize the differences between each tracer.

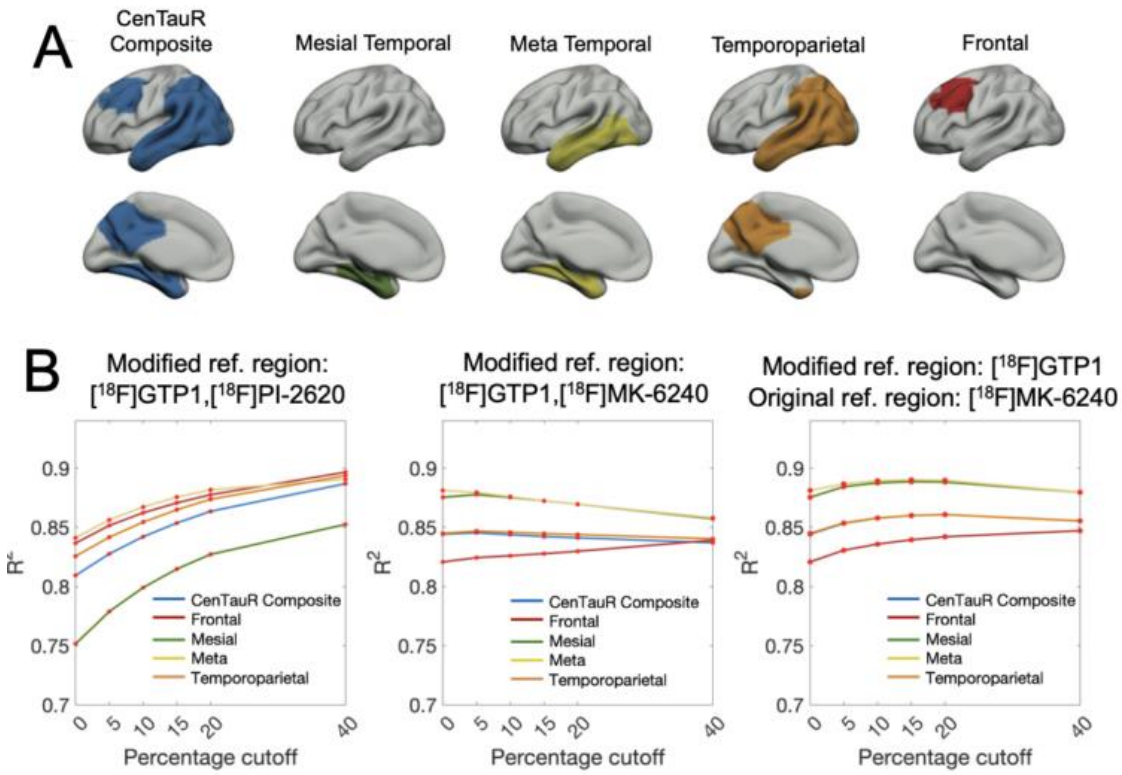

Figure 2. Effect of removing high-intensity voxels on head-to-head SUVR R^2 between tracers. A. Target regions of interest that capture shared AD pathology across. **B.** Removing the highest intensity voxels in the cerebellum for each subject increases the R^2 between [^{18}F]GTP1 and [^{18}F]PI-2620. Modifying the reference region of [^{18}F]GTP1 and [^{18}F]MK-6240 in this way does not improve the R^2 between [^{18}F]GTP1 and [^{18}F]MK-6240, but modifying only the [^{18}F]GTP1 reference region modestly improves the R^2.

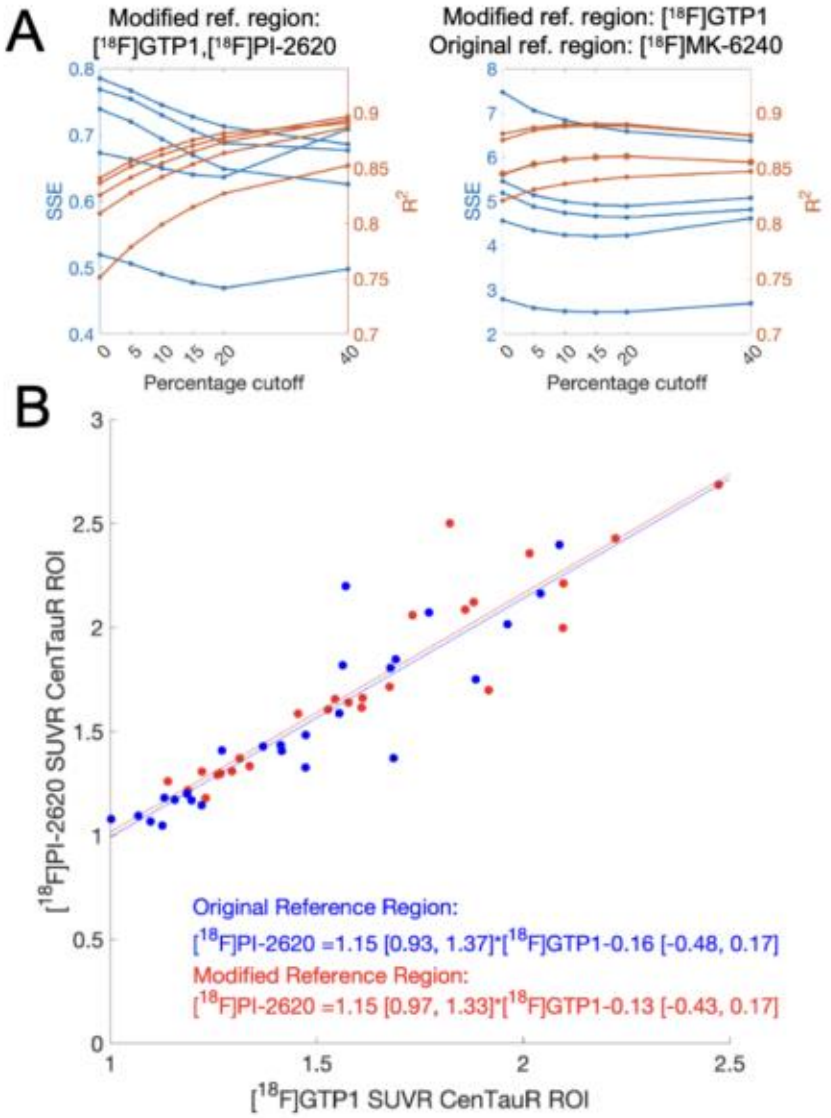

Figure 3. **A.** Sum of squared errors (SSE) and R^2 (same values as Figure 2B) are plotted with increasing percentage cutoffs, shown for all target regions. SSE reflects the distance between the data points and the line of best fit. **B.** Scatterplot of [^{18}F]GTP1 and [^{18}F]PI-2620 SUVRs using the original reference region (blue) and the modified reference region (red) with a cutoff of 20%. Linear coefficients and their 95% confidence intervals are written in blue and red text.

Keywords: tau PET, reference region, off-target binding, harmonization,

Wednesday, January 17, 2024 - 02:20 pm - 04:05 pm

KEYNOTE: A new era in AD therapeutic trials: translating hope into impact

Cath Mummery

University College London, London, United Kingdom

After a long, hard road, we now have early foundations on which to build effective treatments for Alzheimer's disease. Recent trials have shown that reducing amyloid in the brain can alter the course of disease, though initial results are modest.

I will discuss these findings and the role of PET and other markers in furthering our understanding of the building evidence; I'll discuss the challenges we face in implementing these new therapies and the lessons we need to learn. In parallel it is critical we continue to diversify our drug portfolio as we are likely to need to use drugs in combination to comprehensively treat AD. I'll discuss novel methods of targeting amyloid and tau that are showing promise in early trials, and the use of new biomarkers to provide evidence of biological effect.

Dr. Cath Mummery has been a consultant neurologist since 2002 and leads the cognitive disorders service at the National Hospital for Neurology and Neurosurgery. She is also Honorary Senior Clinical Research Fellow, Neurodegenerative Diseases at the University College London.

She studied medicine at UCH, trained in neurology at NHNN and Kings College Hospital, and gained a PhD in cognitive neurology at the Wellcome Department of Functional Imaging, UCL.

She is head of novel therapeutics at the Dementia Research Centre, UCL and has been senior investigator on over 20 early phase drug trials of disease modifying agents in dementias including genetic forms of Alzheimer's disease and frontotemporal dementia.

She is deputy director for the Leonard Wolfson Experimental Neurology Centre at NHNN, a unit dedicated to early phase trials in neurodegeneration.

Dr. Mummery was elected to the executive of the Association of British neurologists as services chair in 2017 and works closely with the Royal College of Physicians, sitting on the medical specialties board and chairing the joint clinical neurosciences committee.

As deputy director of the NHSE Neurosciences Clinical Reference Group, she is closely involved in work to enhance neurology care for patients.

Wednesday, January 17, 2024 - 02:20 pm - 04:05 pm

Podium Session

SESSION III: Modeling, the Real-world, and Natural History

CHAIRS: Suzanne Baker, Pedro Rosa-Neto

Wednesday, January 17, 2024		
02:20 pm - 04:05 pm	**SESSION III: Modeling, the Real-World, and Natural History**	**Suzanne Baker, Lawrence Berkeley National Laboratory, Berkeley, CA, United States** **Pedro Rosa Neto, McGill University, Montreal, QC, Canada**
2:20	Introduction	Chairs
2:25	On fitting the Jack model to biomarker data	Therneau | Cogswell | Lundt | Jack
2:40	Validation of sampled iterative local approximation for individualized estimates of tau PET onset age	Teague | Heston | Ruiz de Chavez | Navaratna | Cody | Morse | Deming | Langhough | Betthauser
2:55	Quantitative analysis of amyloid-PET from real-world practice: lessons learned from processing the IDEAS dataset	La Joie | Mundada | Blazhenets | Mejia Perez | Schonhaut | Zeltzer | Soleimani-Meigooni | Cho | Ranasinghe | Windon | Yadollahikhales | Iaccarino | Carrillo | Hanna | Gatsonis | March | Apgar | Siegel | Hillner | Whitmer | Rabinovici
3:10	Parahippocampal tau-PET as a biomarker of the transition from rhinal to neocortical tauopathy	Thibault | Farrell | Fu | Sanchez | Healy | Hanseeuw | Jacobs | Price | Becker | Sperling | Johnson
3:25	Unraveling the early trajectory of cortical tau accumulation using 18F-MK6240	Doré | Krishnadas | Bourgeat | Leuzy | Feizpour | Cox | Huang | Budd Haeberlein | Fripp | Villemagne | Rowe
3:40	Discussion	

On fitting the Jack model to biomarker data

Terry Therneau[1], Petrice Cogswell[2], Emily Lundt[1], Clifford Jack[2]

[1]*Department of Quantitative Health Sciences, Mayo Clinic, Rochester, MN, United States*
[2]*Department of Radiology, Mayo Clinic, Rochester, MN, United States*

A key question in Alzheimer's dementia research is understanding the evolution of the disease over time, via measured biomarkers. A popular conceptual model proposed by Jack () visualizes this as an overlapping cascade, with (continuous) marker A progressing from normal to abnormal, then B, C, etc. Statistically, each marker process k can be visualized as a generalized linear mixed effects model (GLME), but with unknown link function f_k that must also be estimated. A key challenge is that the underlying processes may evolve over 30-40 years, but we only see 2-8 years for any given subject.

Multiple approaches have been proposed which fit into this framework [Betthauser(2022), Bigel(2022), Li(2019), Koscik(2020), and Therneau (2021), among others] but the problem has proven challenging. We will compare several of these using imaging, plasma, and cognitive biomarkers from the Mayo Clinic Study of Aging, an age and sex stratified population sample of 18 years duration (5 years mean follow-up), augmented with targeted simulations. This points out strengths and weaknesses of currently proposed approaches.

An important way forward is to make use of within participant correlations of the estimated temporal shifts between multiple markers. Figure 1 shows a subset of per-participant trajectories from the MCSA for amyloid PET (PiB) SUVR, global cognition and memory z-scores, and p-tau217 ratio(C2N), and Figure 2 the same participants after left-right shifts to a common shape. Whereas amyloid PET and other biomarkers with a common baseline value can be modeled via simple left-right shifts, modeling of cognition required further adjustment for potential per-participant baselines. The correlations between shift parameters were .76 between amyloid PET and the ptau-217 ratio, .88 between the memory and global cognition scores, and .16-.2 between biomarker-cognition pairs. The correlation information substantially increases the precision of the estimated timing of per participant/biomarker progression over single outcome results.

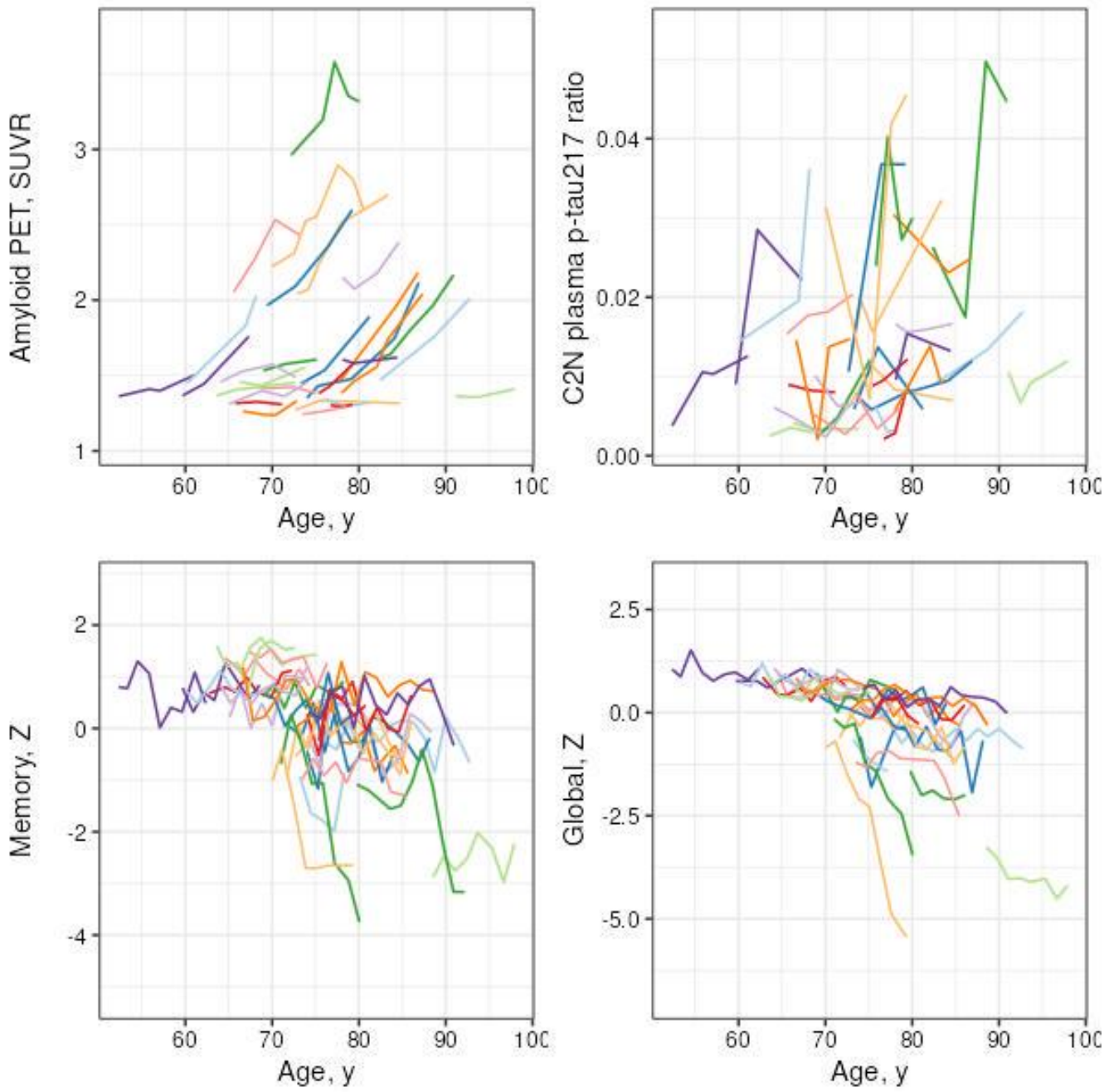
Amyloid PET, SUVR
3
2
1
60
70
80
90
100
Age, y
C2N plasma p-tau217 ratio
0.04
0.02
0.00
60
70
80
90
100
Age, y
Memory, Z
2
0
-2
-4
60
70
80
90
100
Age, y
Global, Z
2.5
0.0
-2.5
-5.0
60
70
80
90
100
Age, y

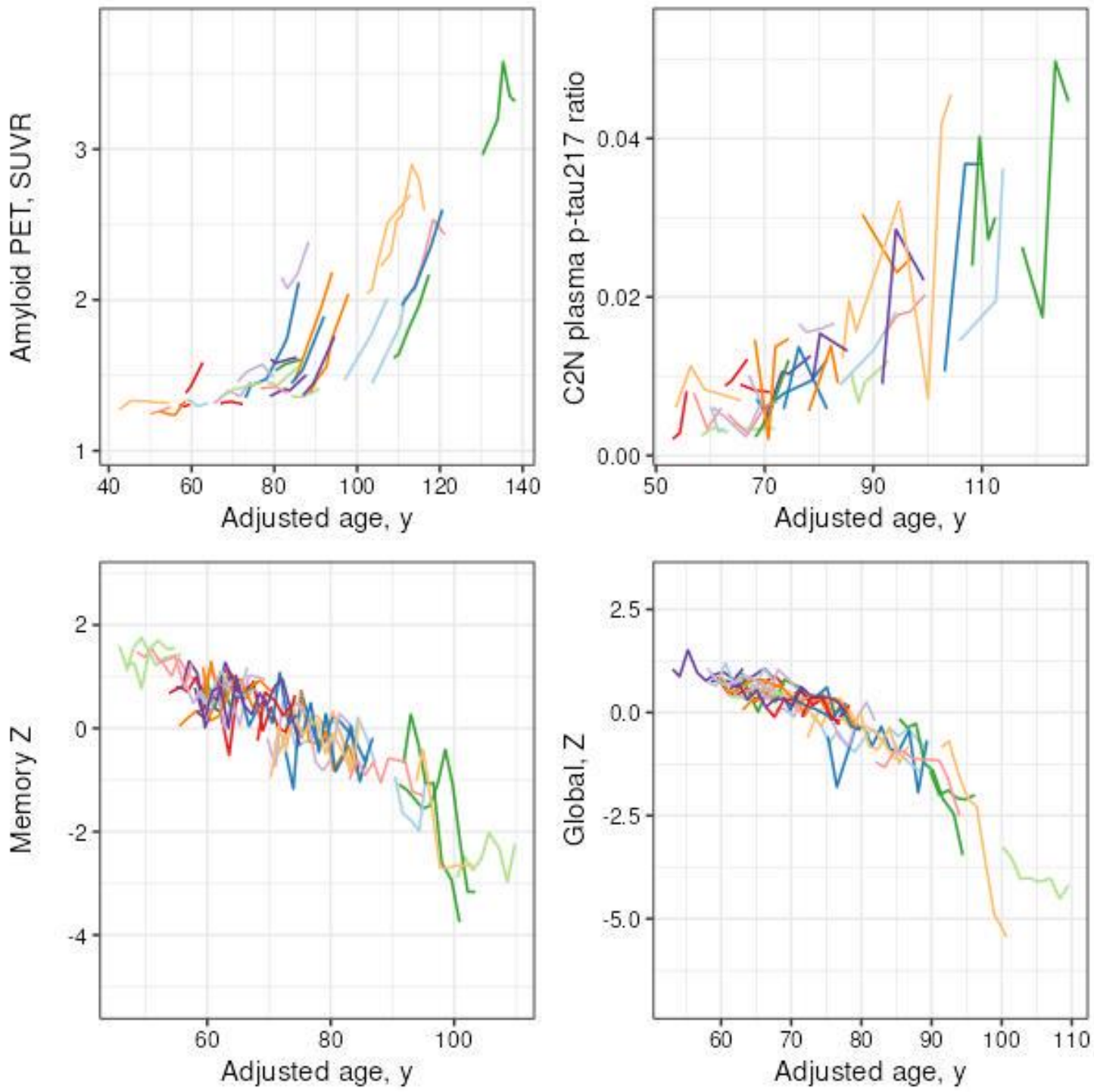

Keywords: biomarkers, modeling, timeline

Validation of sampled iterative local approximation for individualized estimates of tau PET onset age

Jordan Teague[1], Margo Heston[1], Elena Ruiz de Chavez[1], Ruvini Navaratna[1], Karly Cody[1,2], Jacob Morse[1], Yuetiva Deming[1], Rebecca Langhough[1], Tobey Betthauser[1]

[1]*Department of Medicine, University of Wisconsin, Madison, WI, United States*
[2]*Department of Neurology and Neurological Sciences, Stanford University, Stanford, CA, United States*

Background: Quantifying the time course of AD amyloid and tau pathology is essential to identifying optimal disease treatment and secondary prevention windows. Sampled iterative local approximation (SILA) is a temporal modeling method validated for amyloid PET and provides person-level estimated amyloid onset age. The goal of this work is to validate SILA to model longitudinal tau PET trajectories and generate person-level estimated tau onset age (ETOA).

Methods: N=348 participants (mean (SD) baseline age = 73.3 (7.0)) from the Alzheimer's Disease Neuroimaging Initiative (ADNI) with longitudinal [^{18}F]Flortaucipir (FTP) tau PET imaging were included. Data were processed by UC Berkeley, which included FreeSurfer ROI parcellation of T1-weighted MRI and generation of regional [^{18}F]FTP standard uptake volume ratios (SUVR; inferior cerebellar GM reference region; 80-100 min). Meta-temporal SUVR was averaged across amygdala, entorhinal, fusiform, inferior-temporal, and middle-temporal bilateral ROIs. Gaussian mixture modeling was applied to longitudinal SUVR data to establish a tau positivity (T+) threshold (SUVR>1.41) 2.5 SD above the mean of non-accumulators. Ten-fold cross validation was used to investigate forwards and backwards SUVR prediction and T+/- stratification accuracy. We also examined ETOA accuracy in observed T- to T+ converters.

Results: SILA converged on a solution for tau vs time (Figure 1). Residuals indicated no clear relationship with age, reference SUVR, or time to/from reference scan (Figure 2). Backwards prediction (RMSE=0.081) had a lower error than forwards prediction (RMSE=0.11) for SUVR prediction and T+/- stratification (0.96/0.92 accuracy, respectively). In a subset of T- to T+ converters, ETOA was within -0.13 (-3.12, 2.87) years of midpoint between the observed last negative and first positive scan (Table 1).

Conclusions: Tau PET is amenable to temporal modeling using SILA. SILA provides reasonable estimates of T+ onset age. Future work will validate SILA tau PET modeling with additional tracers and cohorts.

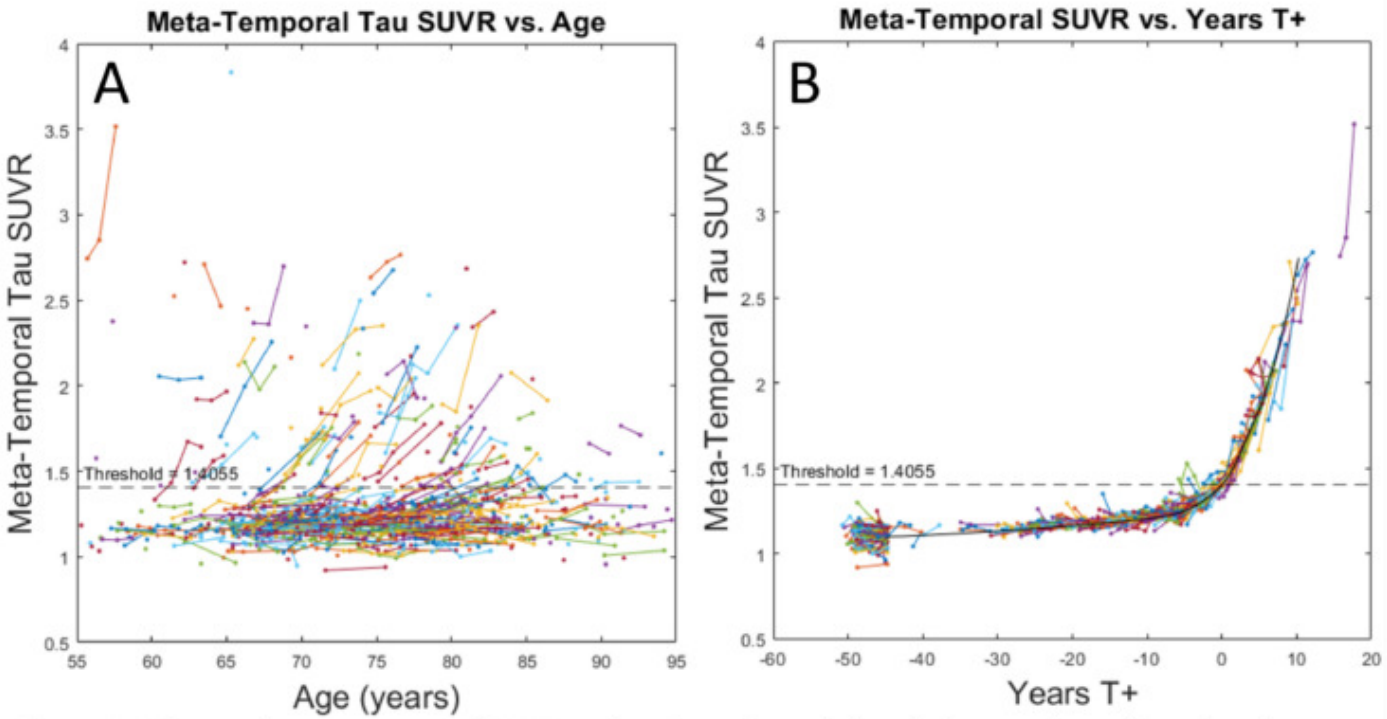

Figure 1. Observed meta-temporal SUVR as function of age (A) and observations aligned to the non-parametric tau vs time curve output from SILA (B) with last scan as the reference scan. The tau accumulator threshold is shown in a dashed line. SUVR thresholds were determined by gaussian mixture modeling.

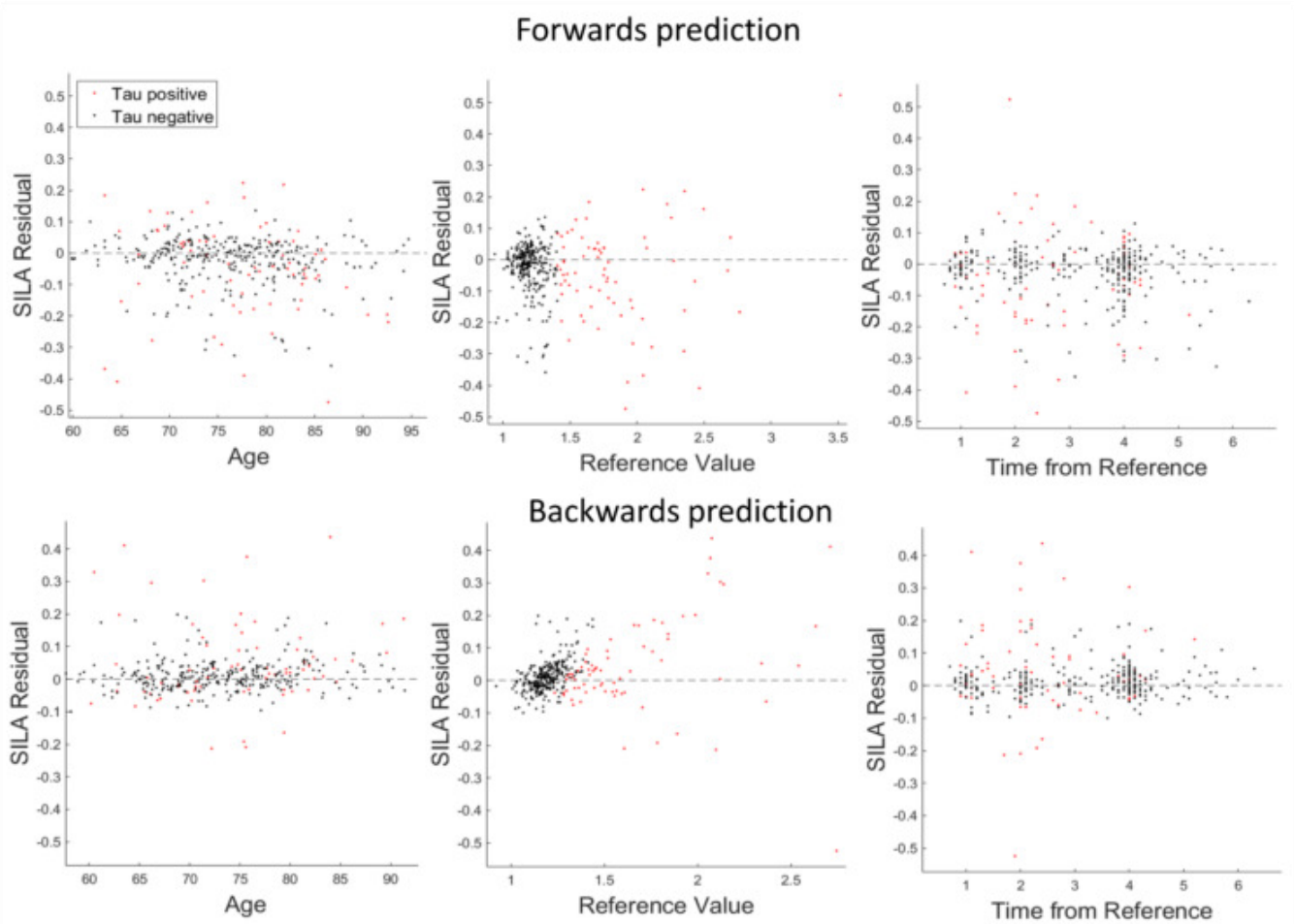

Figure 2. SUVR prediction residuals for forward and backward prediction for SILA as a function of age at the reference scan, reference SUVR value, and time from the reference scan for ADNI participants with two or more tau PET scans. Residuals are calculated using 10-fold cross-validation with either predicting a first scan SUVR from a last reference scan or predicting a last scan SUVR from a first reference scan.

Table 1. Summary Statistics

	Forward	Backward
SSQ	3.85	2.28
SSQ T+	2.01	1.61
SSQ T-	1.83	0.67
RMSE	0.11	0.081
Balanced accuracy	0.94	0.93
Accuracy	0.92	0.96
Conversion midpoint error, mean years (95% CI)	-0.125(-3.12,2.87)	0.185(-2.40, 2.77)

Keywords: Tau, PET, temporal modeling, tau onset, SILA

Quantitative analysis of amyloid-PET from real-world practice: lessons learned from processing the IDEAS dataset

Renaud La Joie[1], Nidhi Mundada[1], Ganna Blazhenets[1], Jhony Mejia Perez[1], Daniel Schonhaut[1], Ehud Zeltzer[1], David Soleimani-Meigooni[1], Hanna Cho[1], Kamalini Ranasinghe[1], Charles Windon[1], Golnaz Yadollahikhales[1], Leonardo Iaccarino[1,2], Maria C. Carrillo[3], Lucy Hanna[4], Constantine Gatsonis[4,5], Andrew March[6], Charles Apgar[7], Barry Siegel[8], Bruce Hillner[9], Rachel Whitmer[10,11], Gil D. Rabinovici[1,12]

[1]*Memory and Aging Center, Department of Neurology, University of California, San Francisco, San Francisco, CA, United States*
[2]*Eli Lilly and Company, Indianapolis, IN, United States*
[3]*Alzheimer's Association, Chicago, IL, United States*
[4]*Center for Statistical Sciences, Brown University School of Public Health US, Providence, RI, United States*
[5]*Department of Epidemiology, Brown University School of Public Health, Providence, RI, United States*
[6]*Center for Research and Innovation, American College of Radiology, Philadelphia, Pennsylvania, Philadelphia, PA, United States*
[7]*Center for Research and Innovation, American College of Radiology, Reston, Virginia, Reston, VA, United States*
[8]*Edward Mallinckrodt Institute of Radiology, Washington University School of Medicine, St Louis, MO, United States*
[9]*Department of Medicine, Virginia Commonwealth University, Richmond, VA, United States*
[10]*Division of Research, Kaiser Permanente, Oakland, CA, United States*
[11]*Department of Public Health Sciences, University of California, Davis, Davis, CA, United States*
[12]*Department of Radiology & Biomedical Imaging, University of California, San Francisco, San Francisco, CA, United States*

Background: We aimed to process scans from IDEAS, a large-scale, real-world study of amyloid-PET. Major challenges lie in scans being acquired on various PET/PET-CT/PET-MR scanners without standardization of acquisition or reconstruction protocols, and without MRI to preprocess data.

Methods: 18,295 Medicare beneficiaries with MCI or dementia underwent PET with [^{18}F]florbetapir, [^{18}F]florbetaben, or [^{18}F]flutemetamol at 343 facilities. Sites shared 10,700 raw scans with their visual interpretation (positive or negative) by local physicians. Scans were processed using a PET-only pipeline, which derives Centiloid based on a cortex-to-cerebellum tissue ratio in template space. Processed scans underwent standardized visual quality control by 2 raters (Fig 1a-b), and flagged scans were reviewed in a consensus meeting. Injected dose and time between tracer injection and PET acquisition were obtained from DICOM headers.

Results: 9,963 scans (93%) were successfully pre-processed with default parameters (Fig 1a) and 403 additional scans (4%) were included after manual intervention (Fig 1c). 339 scans (3%) were excluded because of technical artifacts or major lesions (Fig 1c). The final sample (n=10,361) is described in Table 1, with example scans in Fig 1d. Centiloids showed the expected bimodal distribution (Fig 2a) and differentiated visually positive from negative scans (AUC=0.913, Fig 2b). PET acquisition generally followed tracer-specific FDA recommendations for injected dose and acquisition time, but major variability was observed (Fig 2c). Centiloid values were higher in patients scanned at later time windows for [^{18}F]flutemetamol, resulting from known slow tracer kinetics (Fig 2c).

Conclusion: MRI-free, amyloid-PET quantification was feasible, with results conforming to expected Centiloid distribution and concordant with visual reads. However, greater standardization of PET acquisition time than is currently required by FDA labels will be needed to reliably quantify PET in clinical practice (e.g., to monitor response to therapy). The IDEAS dataset will be made available via the Global Alzheimer's Association Interactive Network.

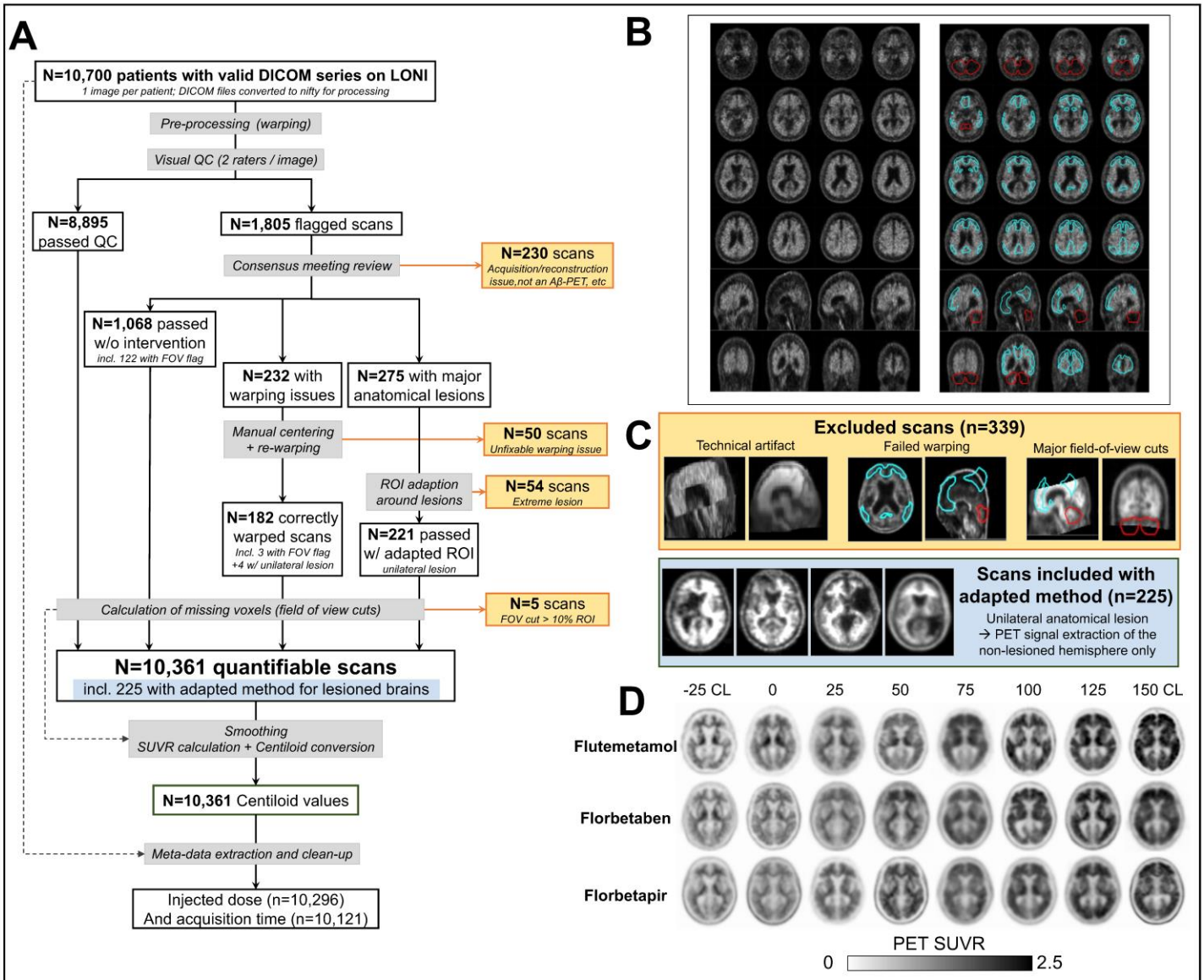

Figure 1. Overview of PET data processing and quality control.

A. Flowchart of scan quality control
B. Standard display used to perform visual quality control on 10,700 scans. Warped PET image is shown both without (left) and with (right) the cortical (cyan) and cerebellar (red) regions used for PET extraction and Centiloid calculation.
C. Examples of images that were excluded (yellow) or included with an adaptation of the extraction region (blue)
D. Images included in the final sample. For each tracer, random images were selected for a set of Centiloid values.

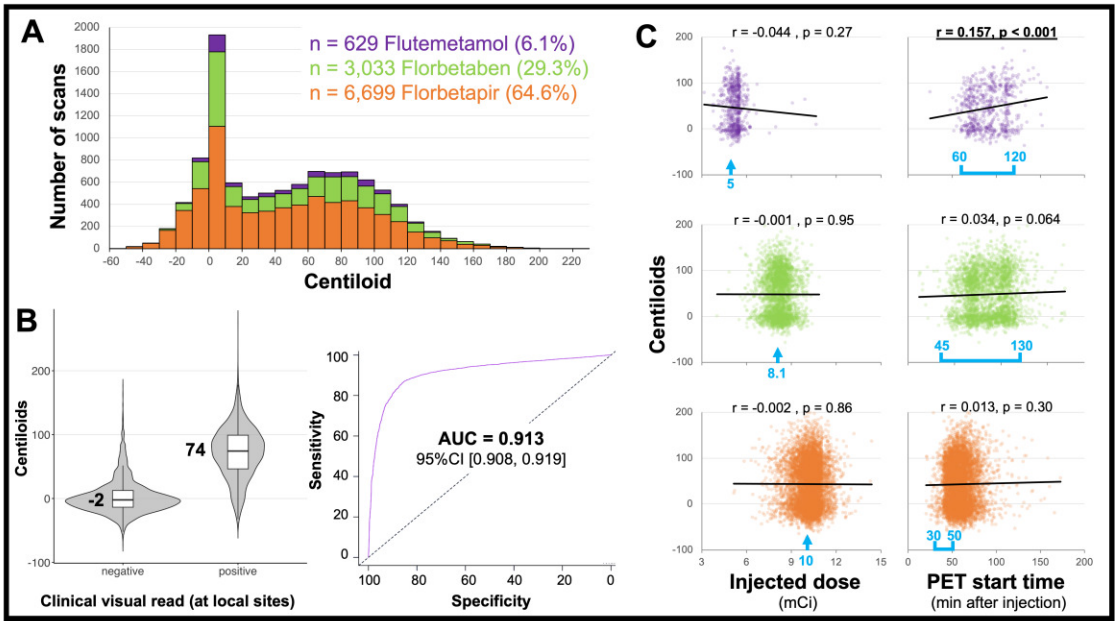

Figure 2. PET scans and Centiloid quantification in the final sample (n=10,361)

A. Histogram of Centiloid values in the whole sample
B. Relationship between Centiloid values and PET scan visual read performed at each site by a local radiologist. Median values are indicated.
C. Association of Centiloid values with injected radiotracer dose (left) and PET scan acquisition time (right) across tracers. Blue arrows, intervals, and numbers indicate the target dose and acquisition time window according to each radiotracer prescribing information.

		Patients with CL values	Whole IDEAS cohort
Variable	*Level*	*N=10,361*	*N=18,293*
Demographics			
Age	Median	75.0	75.0
	IQR (25%-75%)	71.0 - 80.0	71.0-80.0
Gender	Male / Female	49.4% / 50.6%	48.7% / 51.3%
Race	American Indian / Alaskan native	0.1%	0.1%
	Asian	1.8%	1.8%
	Black or African American	3.0%	3.5%
	Native Hawaiian or Pacific Islander	<0.1%	0.1%
	White or caucasian	88.0%	86.6%
	Multiple races	0.2%	0.2%
Ethnicity	Hispanic or Latino	4.3%	4.5%
Highest level of education	Did not complete high school	6.8%	7.1%
	High school	25.3%	26.3%
	Some college or associate degree	24.1%	23.3%
	Bachelor's degree	23.3%	23.3%
	Master's degree or Doctorate	20.6%	20.0%
Clinical			
Level of impairment	MCI / dementia	62.7% / 37.3%	60.5% / 39.5%
MMSE score	Median	26.0	26.0
	IQR (25%-75%)	22.0 - 28.0	22.0 - 28.0
Taking AD drugs at baseline (yes)		43.2%	42.9%
Leading suspected etiology is Alzheimer Disease (yes)		77.2%	77.0%

Table 1. Demographic and clinical characteristics of the final sample.

Keywords: Centiloids, quality control, real world implementation, harmonization, brain lesion

Parahippocampal tau-PET as a biomarker of the transition from rhinal to neocortical tauopathy

Emma Thibault[1], Michelle Farrell[1], Jessie Fanglu Fu[1], Justin Sanchez[1], Brian Healy[1,2], Bernard Hanseeuw[1,3], Heidi Jacobs[1,4], Julie Price[1], J. Alex Becker[1], Reisa Sperling[1,2], Keith Johnson[1,2]

[1]*Massachusetts General Hospital, Boston, MA, United States*
[2]*Brigham and Women's Hospital, Boston, MA, United States*
[3]*Université Catholique de Louvain, Brussels, Belgium*
[4]*Maastricht University, Maastricht, The Netherlands*

Background: Cerebral tau pathology accumulates in the medial temporal lobe (**MTL**) across the adult lifespan. The spread of tau pathology into the neocortex in the presence of amyloid-β (**Aβ**) pathology is believed to be a critical event in Alzheimer's disease pathogenesis. The anatomical transition between MTL and temporal neocortex involves the parahippocampal cortex (**PH**). We therefore tested whether PH may serve as an effective tau-PET biomarker of this critical transition period.

Methods: 268 clinically-normal individuals (Table 1) from the Harvard Aging Brain Study (HABS) underwent longitudinal [^{11}C]-Pittsburgh Compound-B (PiB, PiB-DVR>1.19 as PiB+) and Flortaucipir (FTP)-PET. We evaluated the spatiotemporal sequence of changes in FTP from rhinal (**RC**) to PH to neocortex (inferior temporal, **IT**) (**Fig.1**). A series of linear mixed effects models assessed this sequence using baseline FTP SUVR for each region to predict change over time in the subsequent region as a function of baseline PiB status (Time*FTP*PiBstatus). Models covaried for age and included random intercepts and slopes.

Results: All tau-to-tau interactions were only significant in the presence of elevated PiB (Fig.2). Higher baseline RC FTP SUVR was associated with accelerated change in PH FTP SUVR over time (Fig.2A). Baseline PH FTP was associated with accelerated IT FTP SUVR change over time (Fig.2B). Models testing the reverse order (RC~PH, PH~IT) were not significant. The direct association between baseline RC FTP and IT FTP change was significant (eta^2_{RC}=0.17), but the effect size for the association between baseline PH FTP and IT FTP change was higher (eta^2_{PH}=0.29).

Conclusions: This study provides in vivo PET evidence that PH FTP may represent an important transition point between age-related MTL tauopathy and AD-related neocortical tauopathy. Future studies with additional longitudinal data will evaluate whether PH may serve as an effective tau-PET biomarker to identify individuals on the cusp of neocortical tau proliferation.

	PIB- (N=197)	PIB+ (N=71)	Overall (N=268)
Age			
Mean (SD)	71.8 (9.38)	77.3 (6.63)	73.2 (9.05)
Sex			
F	118 (59.9%)	43 (60.6%)	161 (60.1%)
M	79 (40.1%)	28 (39.4%)	107 (39.9%)
Years Education			
Mean (SD)	16.0 (3.05)	16.4 (2.76)	16.1 (2.97)
Missing	2 (1.0%)	0 (0%)	2 (0.7%)
APOE Status			
e4-	157 (79.7%)	27 (38.0%)	184 (68.7%)
e4+	30 (15.2%)	41 (57.7%)	71 (26.5%)
Missing	10 (5.1%)	3 (4.2%)	13 (4.9%)
FLR DVR			
Mean (SD)	1.08 (0.0417)	1.47 (0.192)	1.19 (0.201)
Rhinal SUVR			
Mean (SD)	1.14 (0.101)	1.26 (0.160)	1.17 (0.129)
Parahippocampal SUVR			
Mean (SD)	1.10 (0.0712)	1.18 (0.118)	1.12 (0.0926)
Inferior Temporal SUVR			
Mean (SD)	1.17 (0.0700)	1.25 (0.135)	1.19 (0.0979)
Follow-up Time			
Mean (SD)	2.80 (2.25)	3.42 (2.35)	3.26 (2.33)

Table 1. Harvard Aging Brain Study (HABS) sample demographics at baseline. Subjects had up to 4 FTP scans, including 202 with 2+ scans (23.7% PIB+), 114 with 3+ scans (24.6% PIB+), and 14 with 4 scans (42.8% PIB+). PIB+/- groups did not differ in years of education or sex.

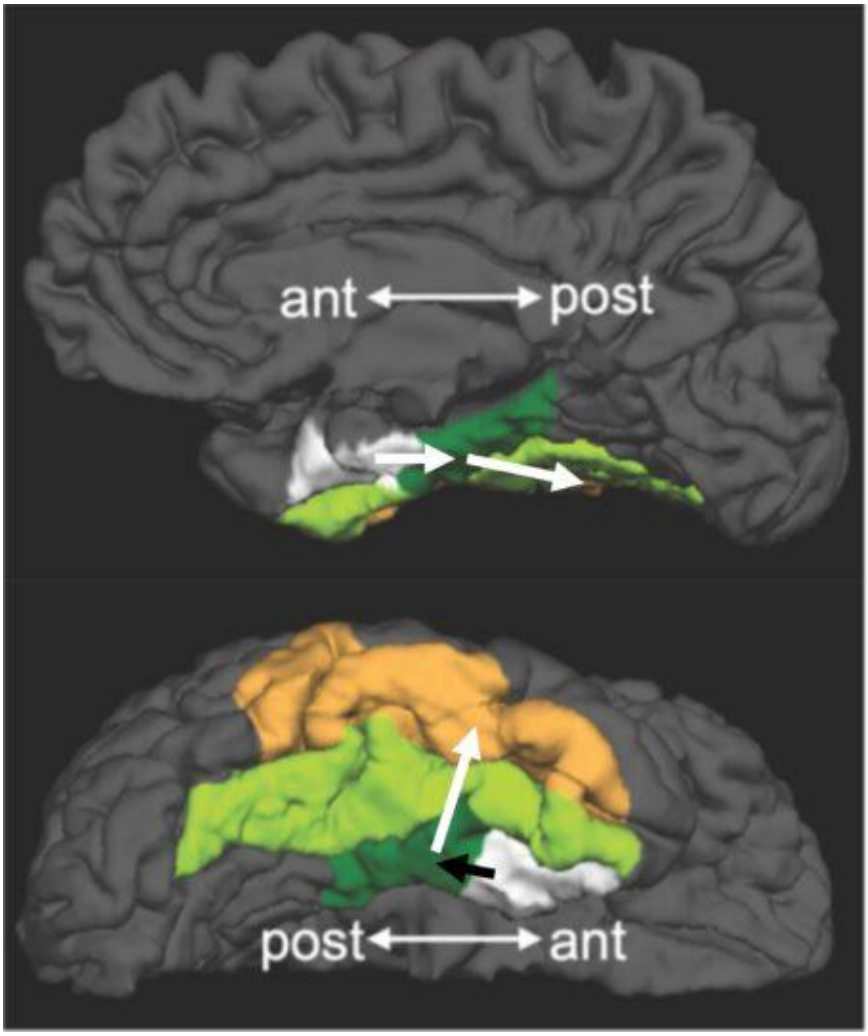

Figure 1. Anatomy of regions relevant to early tau stages. Regions were derived from the Desikan atlas, which is commonly used for tau PET quantification. Arrows on image indicate the hypothesized trajectory of tau spread. Parahippocampal (dark green) serves as an anatomical transition between the entorhinal (white) and neocortex (fusiform (light green) and inferior temporal (orange)). Inferior temporal is the most commonly used temporal neocortical region for tau PET. We included fusiform given its proximity to our regions of interest, but the associations were weaker so our analyses focused on RC, PH, and IT. Figure modified from Sanchez *et al.*, Sci Transl Med, 2021.

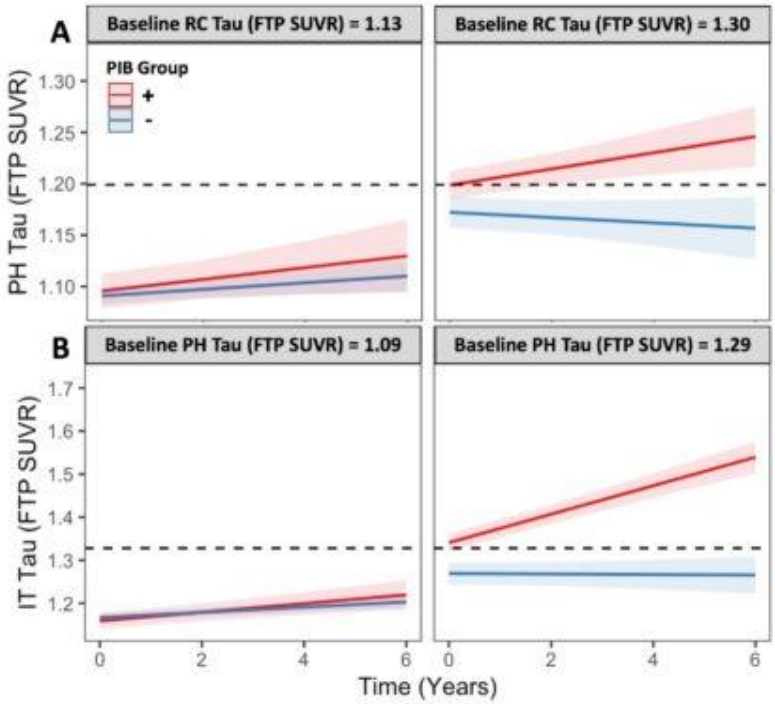

Figure 2. Elevated baseline regional tau predicts accumulation in spatiotemporally subsequent regions in individuals with Aβ. Data are estimated marginal means from linear mixed effects models at the average age of 73.2 years. Colors represent baseline PiB status determined using Gaussian Mixture Modeling (**GMM,** threshold=1.19 PiB DVR). **A)** Baseline RC FTP SUVR predicted PH FTP change over time as a function of baseline PiB status (PH FTP SUVR ~ Baseline RC SUVR*PiB Group*Time + Age; β=-0.047, *SE*=0.020, p=0.018, η^2=0.03). Marginal means are plotted side by side at two levels of baseline RC FTP SUVR representing the means of the RC+/RC- groups from a GMM (RC+/- threshold=1.36 FTP SUVR). The dashed line represents the GMM-derived PH threshold at 1.20 SUVR. Higher RC FTP (right) at baseline was associated with increasing PH FTP over time in PiB+ individuals, but no change was seen in PiB-. Lower RC FTP (left) was associated with a slight increase in PH FTP over time but did not reach the detection threshold and likely reflects noise. B) Similar results were observed for baseline PH FTP predicting IT FTP change over time (IT FTP SUVR ~ Baseline PH SUVR*PiB Group*Time + Age; β=-0.15, *SE*=0.023, p<0.001, η^2=0.29), with a high rate of change in IT FTP in PiB+ individuals with high baseline PH FTP. IT+/- GMM-derived threshold is represented as a dashed line at 1.33 SUVR.

Keywords: tau-PET, biomarker

Unraveling the early trajectory of cortical tau accumulation using 18F-MK6240

Vincent Doré[1,2], Natasha Krishnadas[2,3], Pierrick Bourgeat[1], Antoine Leuzy[4], Azadeh Feizpour[2,5], Tim Cox[1], Kun Huang[2], Samantha Budd Haeberlein[4], Jurgen Fripp[1], Victor Villemagne[2,6], Christopher Rowe[2,3,5]

[1]*The Australian eHealth Research Centre, CSIRO, Melbourne, Australia*
[2]*Department of Molecular Imaging & Therapy, Austin Health, Heidelberg, Australia*
[3]*Florey Department of Neurosciences & Mental Health, The University of Melbourne, Melbourne, Australia*
[4]*Enigma Biomedical Group, Toronto, ON, Canada*
[5]*Florey Institute of Neurosciences & Mental Health, Parkville, Australia*
[6]*Department of Psychiatry, University of Pittsburgh, Pittsburgh, PA, United States*

Tau PET is instrumental in tracking the longitudinal progression of Alzheimer's disease (AD). ^{18}F-MK6240 is a high affinity tracer targeting the 3R/4R paired helical filaments of tau in AD. We aimed to evaluate the early phase of the natural progression of tau accumulation using ^{18}F-MK6240.

219 participants: 97 cognitively unimpaired (CU) Aβ– (Centiloid<25CL), 55 CU Aβ+, 67 cognitively impaired Aβ+ (36 with mild cognitive impairment (MCI) and 31 with dementia) from the AIBL cohort were followed-up with ^{18}F-MK6240 PET over one to four years (median 2.2years). Temporo-parietal CenTauR (CTR) were generated using CapAIBL and CU CL<15, N=120 and AD (typical AD tau pattern, MMSE>24, CL>50 & age<75, N=39) as 0 and 100CTR anchored points. Abnormal level of tau was defined at 2 standard deviations above the CU Aβ- (13CTR). Linear ordinary differential equations (ODE) were employed to model the mean natural history of CTR based on tau accumulators (CTR>13 or CTR rate>0) only. Given the limited numbers of individuals with CTR>100, our analysis concentrated on the early phase of the tau accumulation (CTR<100, N=204).

Figure1A illustrates a linear relationship between the average and the rate of CTR, with a R^2 of 0.69. Tau accumulation spanned from 2.7CTR/yr at 13CTR to 16CTR/yr at 100CTR, with a standard deviation of the residuals at 2.1CTR/yr. Figure1B displays the individual's trajectories projected on the ODE model. We estimated that, on average it takes 11.7 (CI:[11.3-12.3]) years for an individual crossing 13CTR to reach 100CTR.

Longitudinal ^{18}F-MK6240 is a robust tool for estimating natural progression of tau accumulation. Our findings indicate that it typically takes around 12 years to reach the tau levels associated with mild AD once tau starts aggregating in the neocortex. These findings shed light into the initial stages of cortical tau accumulation, relevant for early diagnosis and therapeutic interventions in AD.

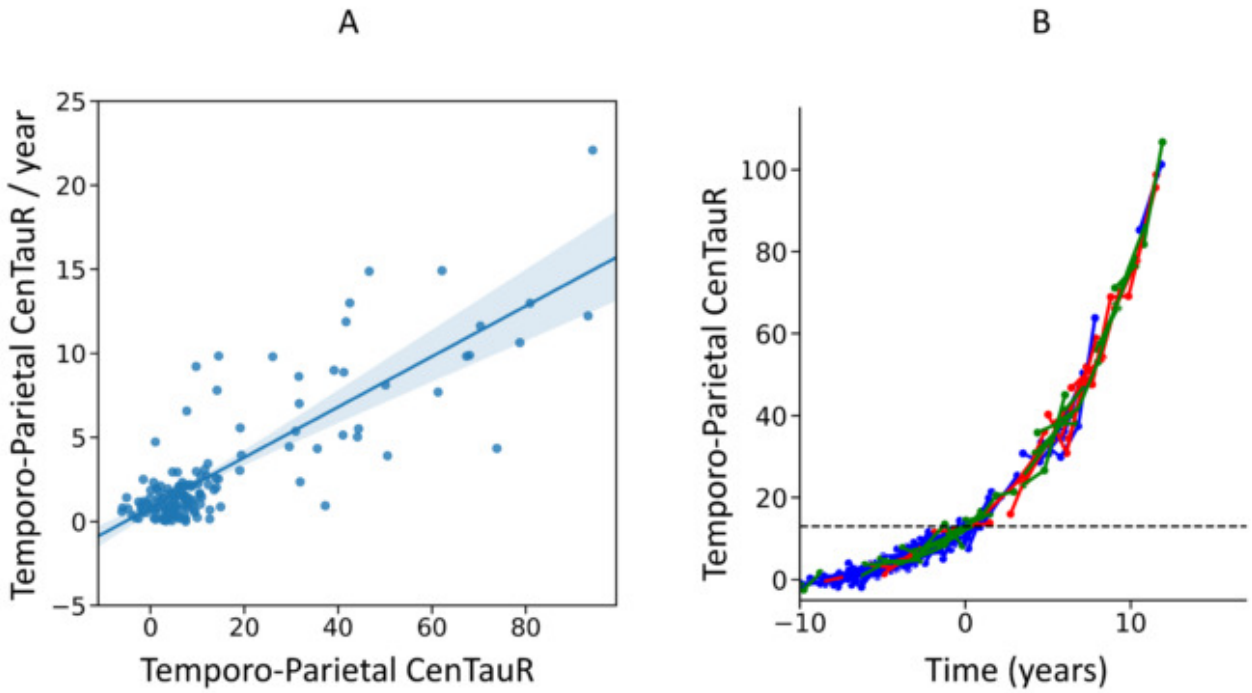

Figure 1: A shows the temporo-Parietal CenTauR rate as a function of the Temporo-Parietal CenTauR. A linear regression best describes the association (R^2=0.68). B) All the individuals were projected back on the mean ODE model. Color code is blue: (CU), green (MCI) and red (AD). Dash line corresponds to abnormal level of tau (13CTR).

Keywords: tau, accumulation, MK6240, CenTauR

Wednesday, January 17, 2024 - 04:35 pm - 06:05 pm

Podium Session

SESSION IV: Neuropathology - Part I

CHAIRS: Milos Ikonomovic, Melissa Murray

Wednesday, January 17, 2024		
04:35 pm - 06:05 pm	**SESSION IV: Neuropathology - Part I**	**Milos Ikonomovic, University of Pittsburgh, Pittsburgh, PA, United States** **Melissa Murray, Mayo Clinic, Rochester, MN, United States**
4:35	Introduction	Chairs
4:40	Mature tangle scores strongly correlate with tau-PET and structural MRI measures	Moloney | Wood | Rothberg | Tranovich | Przybelski | Hofrenning | Pottier | Petersen | Jack Jr | Dickson | Nguyen | Reichard | Vemuri | Lowe | Murray
4:55	Neuropathologic Characterization of FDG-PET and MRI -based AD Subtypes	Wheatley | Muehlboeck | Ferreira | Nordberg | Mohanty | Grothe | Westman
5:10	Development and Validation of a Novel Tau Summary Measure: Tau Heterogeneity Evaluation in Alzheimer's Disease (THETA) Score	Gebre | Rial | Raghavan | Wiste | Sparrman | Heeman | Costoya-Sánchez | Schwarz | Spychalla | Lowe | Graff-Radford | Knopman | Petersen | Schöll | Murray | Jack Jr | Vemuri
5:25	Transmembrane protein 106B is one of the potential off-target binding substrates of tau PET tracers	Harada | Yokoyama | Kudo | Iwata | Kudo | Furumoto | Okamura
5:40	Discussion	

Mature tangle scores strongly correlate with tau-PET and structural MRI measures

Christina M. Moloney[1], Ashley C. Wood[1], Darren M. Rothberg[1], Jessica F. Tranovich[1], Scott A. Przybelski[2], Ekaterina I. Hofrenning[2], Cyril Pottier[1], Ronald C. Petersen[3], Clifford R. Jack Jr[4], Dennis W. Dickson[1], Aivi T. Nguyen[5], R. Ross Reichard[5], Prashanthi Vemuri[4], Val J. Lowe[4], Melissa E. Murray[1,5]

[1]*Department of Neuroscience, Mayo Clinic, Jacksonville, FL, United States*
[2]*Department of Quantitative Health Sciences, Mayo Clinic, Rochester, MN, United States*
[3]*Department of Neurology, Mayo Clinic, Rochester, MN, United States*
[4]*Department of Radiology, Mayo Clinic, Rochester, MN, United States*
[5]*Department of Laboratory Medicine and Pathology, Mayo Clinic, Rochester, MN, United States*

Objectives: In Alzheimer's disease, neurofibrillary tangle maturity can be defined by three levels: pretangles, mature tangles, and ghost tangles. While tangle maturity is extensively characterized in pyramidal neurons of the hippocampus, these maturity levels are less well-characterized in the cortex. Our goal was to create a novel tangle maturity score to evaluate relationships between worsening tangle pathology with neuroimaging measures in the cortex.

Methods: Temporal cortex of cases with neuroimaging acquired within 3 years of death were stained with an early (AT8) and middling (PHF-1) tangle maturity marker (**Figure**). Digital pathology was performed on middle and superior temporal cortex (burden). These temporal cortices were semi-quantitatively scored for the presence of mild (0-4 tangles/1800x900μm^2), moderate (5-9 tangles/1800x900μm^2), and severe (10+ tangles/1800x900μm^2) tangle maturity levels. Neuroimaging measures included flortaucipir tau-PET standard uptake value ratio (SUVr) and structural MRI cortical thickness. SUVr was obtained by normalizing to cerebellar crus.

Results: AT8 and PHF-1 burden strongly correlated with higher tau-PET SUVr and lower cortical thickness in middle and superior temporal cortices (**Table 1**). Pretangle scores were not observed to significantly associate with neuroimaging measures and ghost tangles were not as readily identified by the antibodies (**Table 2**). Higher tau-PET SUVr in middle and superior temporal cortex correlated with a more severe mature tangle score in the associated region for AT8 and PHF-1. Lower middle and superior temporal cortical thickness correlated with a more severe mature tangle score in the associated region for AT8 and PHF-1.

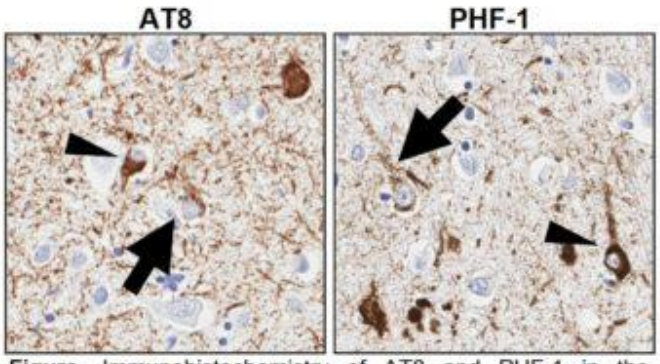

Figure. Immunohistochemistry of AT8 and PHF-1 in the superior temporal cortex. Arrow indicates pretangle, arrowhead indicates mature tangle.

Table 1. Spearman correlations of AT8 and PHF-1 burden.

Variable	AT8 Burden		PHF-1 Burden	
	Rho	p-value	Rho	p-value
Tau-PET (SUVr)				
Superior temporal cortex (n=28)	0.804	<0.001	0.793	<0.001
Middle temporal cortex (n=28)	0.812	<0.001	0.807	<0.001
MRI (cortical thickness)				
Superior temporal cortex (n=19)	-0.550	0.012	-0.644	0.002
Middle temporal cortex (n=19)	-0.642	0.002	-0.648	0.002

Data are presented as non-parametric Spearman correlation coefficient (rho) and significance (p-value). p<0.05 was considered statistically significant. Acronyms: SUVr, standard uptake value ratio

Table 2. Spearman correlations of AT8 and PHF-1 tangle maturity scores.

Variable	AT8 tangle maturity scores						PHF-1 tangle maturity scores					
	Pretangle		Mature Tangle		Ghost Tangle		Pretangle		Mature Tangle		Ghost Tangle	
	Rho	p-value	Rho	p-value	Rho	p-value	Rho	p-value	Rho	p-value	Rho	p-value
Tau-PET (SUVr)												
Superior Temporal (n=28)	0.365	0.057	0.741	<0.001	—	—	0.293	0.131	0.807	<0.001	—	—
Middle Temporal (n=28)	0.322	0.095	0.665	<0.001	—	—	0.343	0.074	0.759	<0.001	0.164	0.403
MRI (cortical thickness)												
Superior temporal cortex (n=19)	-0.063	0.799	-0.656	0.002	—	—	-0.063	0.799	-0.68	0.001	—	—
Middle temporal cortex (n=19)	-0.2	0.411	-0.581	0.009	—	—	-0.282	0.242	-0.676	0.001	—	—

Data are presented as non-parametric Spearman correlation coefficient (rho) and significance (p-value). p<0.05 was considered statistically significant. '—' indicates a relationship was not observed owing to the lack of appreciable ghost tangles. Acronyms: SUVr, standard uptake value ratio

Conclusions: The severity of pretangles may not be represented by neuroimaging biomarker changes to tau pathology. However, structural MRI and flortaucipir tau-PET changes may better reflect tau fibrillization in the form of mature tangles. Ongoing studies will extend these findings to other cortical areas and markers representing more advanced tangle maturity.

Keywords: Neuropathology, neurofibrillary tangle maturity, tau-PET, structural MRI

Neuropathologic characterization of FDG-PET and MRI -based AD subtypes

Sophia Wheatley[1], J-S Muehlboeck[1], Daniel Ferreira[1,2], Agneta Nordberg[1], Rosaleena Mohanty[1], Michel J. Grothe[3], Eric Westman[1,4]

[1]*Division of Clinical Geriatrics, Department of Neurobiology, Care Sciences and Society, Center for Alzheimer Research, Karolinska Institutet, Stockholm, Sweden*
[2]*Department of Radiology, Mayo Clinic, Rochester, MN, United States*
[3]*CIEN Foundation/Queen Sofia Foundation Alzheimer Center, Madrid, Spain*
[4]*Department of Neuroimaging, Centre for Neuroimaging Sciences, Institute of Psychiatry, Psychology and Neuroscience, King's College London, London, United Kingdom*

Background: Neurodegeneration-based subtypes of Alzheimer's disease (AD) have been observed using FDG-PET and MRI. Although neurodegeneration is downstream to AD and non-AD pathologies, whether neurodegeneration subtypes based on FDG-PET and MRI are similarly susceptible to copathologies is unclear. Therefore, this study's aim is to investigate the link between antemortem FDG-PET (hypometabolism) and MRI (atrophy) subtypes with postmortem neuropathologies.

Methods: The cohort for this study consisted of 68 clinically diagnosed MCI and AD individuals from the Alzheimer's Disease Neuroimaging Initiative with antemortem FDG-PET and MRI as well as postmortem neuropathological assessment. Subtyping into 'Limbic Predominant', 'Typical AD', or 'Hippocampal Sparing' subtypes was performed antemortem using a previously validated method based on the lower 25th and upper 75th percentiles of the hippocampus-to-cortex ratio in each modality. Regional brain maps with w-scores (age at scan, sex, education and *APOE* ε*4* carriership adjusted) were plotted relative to an amyloid-negative cognitively normal control group (n=176) (Figure 1). Antemortem clinical and demographic and postmortem neuropathological variables were assessed across subtypes with Kruskal-Wallis and chi-square tests.

Results: Hippocampal Sparing hypometabolism and atrophy subtypes were younger, had earlier age at onset and fewer *APOE* ε*4* carriers, whereas Limbic Predominant atrophy and hypometabolism subtypes were older and had later age at onset. The Limbic Predominant hypometabolism subtype had higher instances of TDP-43 inclusions, Hippocampal Sclerosis, and ageing-related tau astrogliopathy (ARTAG), but this co-pathology enrichment was not significant for the limbic-predominant atrophy subtype. The Hippocampal Sparing hypometabolism subtype showed more cerebral amyloid angiopathy (CAA) compared to Limbic Predominant hypometabolism, whereas the Hippocampal Sparing atrophy subtype was associated with greater neuronal loss in the substantia nigra than Limbic Predominant and Typical atrophy subtypes.

Conclusion: Antemortem hypometabolism and atrophy subtypes were differentially associated with neuropathologic comorbidities. Our findings highlight that through multimodal imaging subtyping, distinct differences in copathologies can be identified.

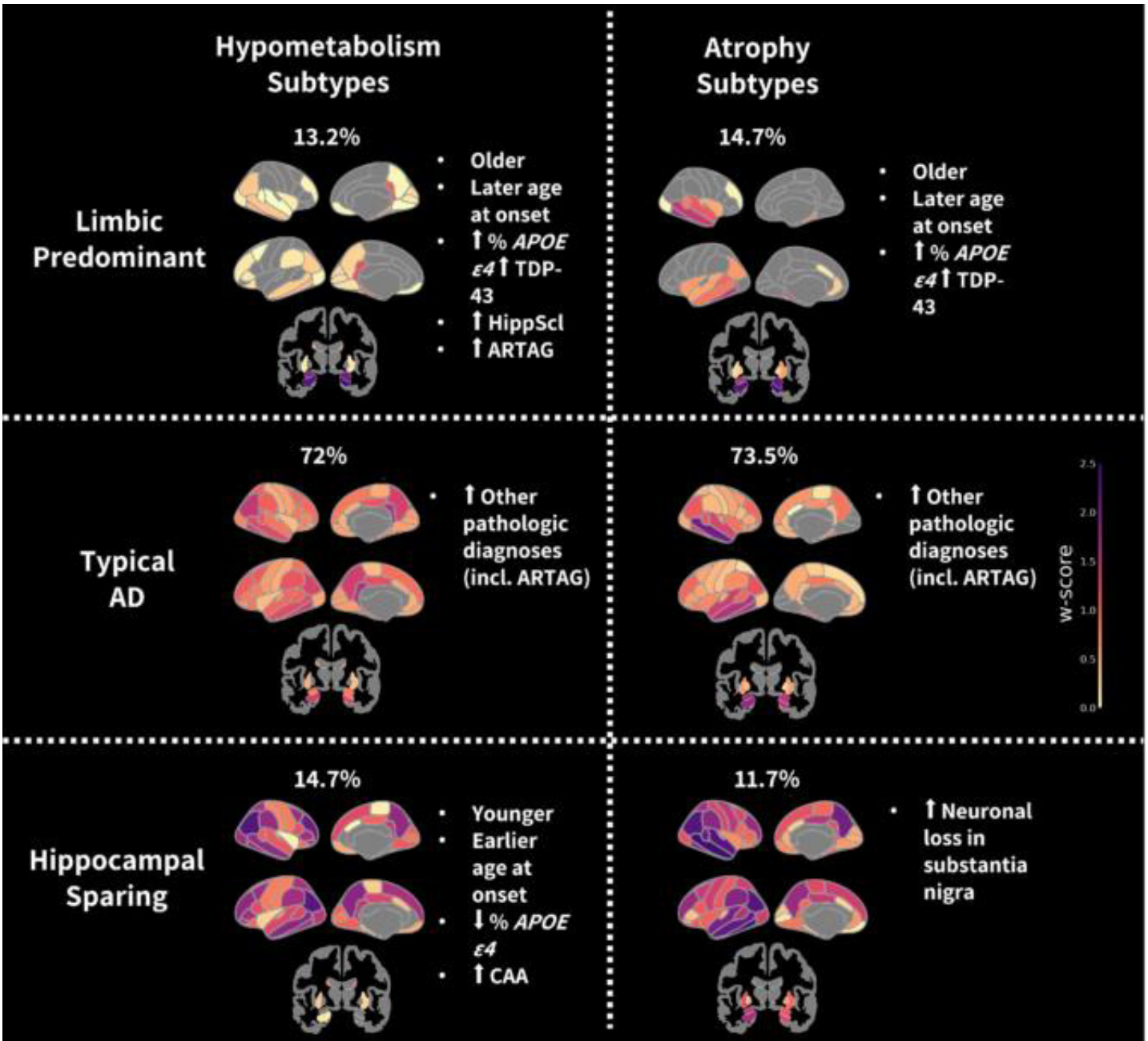

Figure 1: Antemortem FDG-PET and MRI-based subtypes' regional neurodegeneration maps and demographic, neuropathologic summaries. Regional w-score maps (adjusted for age at FDG-PET/MRI scan, sex, education and *APOE ε4* carriership) were plotted between the subtypes and cognitively unimpaired for: Hypometabolism subtypes from FDG-PET scans in left-hand column of figure and atrophy subtypes from MRI scans on the right-hand column. Demographic and neuropathologic summaries listed next to subtype. Legend shows w-score scales for brain maps ranging from 0-2.5, 0: indicating no difference compared to cognitively unimpaired and 2.5: greatest difference in hypometabolism/atrophy. *Abbreviations: TDP-43 : TAR DNA-binding protein 43, HippScl: Hippocampal Sclerosis, CAA: Cerebral amyloid angiopathy, ARTAG: Aging-related tau astrogliopathy.*

Keywords: Alzheimer's, neuropathology, FDG-PET, MRI, neuroimaging

Development and validation of a novel tau summary measure: Tau Heterogeneity Evaluation in Alzheimer's Disease (THETA) score

Robel K. Gebre[1], Alexis Moscoso Rial[2,3], Sheelakumari Raghavan[1], Heather J. Wiste[4], Kohl L Johnson Sparrman[1], Fiona Heeman[2,3], Alejandro Costoya-Sánchez[5,6,7], Christopher G. Schwarz[1], Anthony J. Spychalla[1], Val J. Lowe[1], Jonathan Graff-Radford[8], David S. Knopman[8], Ronald C. Petersen[4,8], Michael Schöll[2,3,9], Melissa E. Murray[10], Clifford R. Jack Jr[1], Prashanthi Vemuri[1]

[1]*Department of Radiology, Mayo Clinic, 55905, Rochester, MN, United States*
[2]*Department of Psychiatry and Neurochemistry, Institute of Neuroscience and Physiology, The Sahlgrenska Academy, University of Gothenburg, Gothenburg, Sweden*
[3]*Wallenberg Centre for Molecular and Translational Medicine, University of Gothenburg, Gothenburg, Sweden*
[4]*Department of Quantitative Health Sciences, Mayo Clinic, Rochester, MN, United States*
[5]*Universidade de Santiago de Compostela, Santiago de Compostela, Santiago, Spain*
[6]*Centro de Investigación Biomédica en Red sobre Enfermedades Neurodegenerativas (CIBERNED), Instituto de Salud Carlos III, Madrid, Spain*
[7]*Nuclear Medicine Department and Molecular Imaging Group, Instituto de Investigación Sanitaria de Santiago de Compostela (IDIS), Travesía da Choupana s/n, Santiago de Compostela, 15706, Santiago, Spain*
[8]*Department of Neurology, Mayo Clinic, 55905, Rochester, MN, United States*
[9]*Dementia Research Centre, Institute of Neurology, University College London, London, United Kingdom*
[10]*Department of Neuroscience, Mayo Clinic, Jacksonville, Jacksonville, FL, United States*

Introduction: Given the spatial heterogeneity of tau pathology in Alzheimer's disease (AD), we aimed to develop and validate a novel machine learning (ML) tau-PET quantification method that would map well to clinical and pathological indices of AD.

Methods: We included three independent cohorts: Mayo (N=1290, Histopathology N=90), ADNI (N=831), and OASIS-3 (N=430). Tau-PET scans were visually assessed by three raters following FDA-approved criteria for classifying tau positivity based on the density and distribution of the radiotracer [18F] flortaucipir. Regional standard uptake value ratio (SUVR) values were calculated using the cerebellar crus median as a reference. A ML model was trained on the Mayo data using SUVRs as input and tau status based on visual positivity as a binary target. The THETA score was calculated based on the contributions of the input SUVRs to the ML model predictions using SHAP (SHapley Additive exPlanations). The model predictions were compared to SUVR values of the meta-ROIs (MTL, NEO, and Temporal) using clinical (MMSE, CDR-SB) and pathological (Braak stages) indices of AD.

Results: The ML model predicted tau status with 95% accuracy on the Mayo test set and ≥87% on ADNI and OASIS-3. Compared to the meta-ROIs, THETA correlated better with MMSE and CDR-SB with the highest correction observed for Mayo (Spearman's $|rho| \geq 0.45$, $p<0.05$ vs $|rho| \leq 0.44$, $p<0.05$) (Fig. 1). The association of THETA with Braak staging was slightly better than the meta-ROIs ($rho=0.87$, $p<0.05$ for THETA vs $rho \leq 0.83$, $p<0.05$ for meta-ROIs) and it provided improved separation of clinical diagnostic groups (Fig. 2).

Conclusions: We developed a novel tau summary measure, THETA; validated it on three independent datasets; and provided analyses for better performance when compared to meta-ROIs. We demonstrate evidence that the adaptive consideration of participant-specific heterogenous tau deposition by THETA may provide a better estimate of the pathological tau burden.

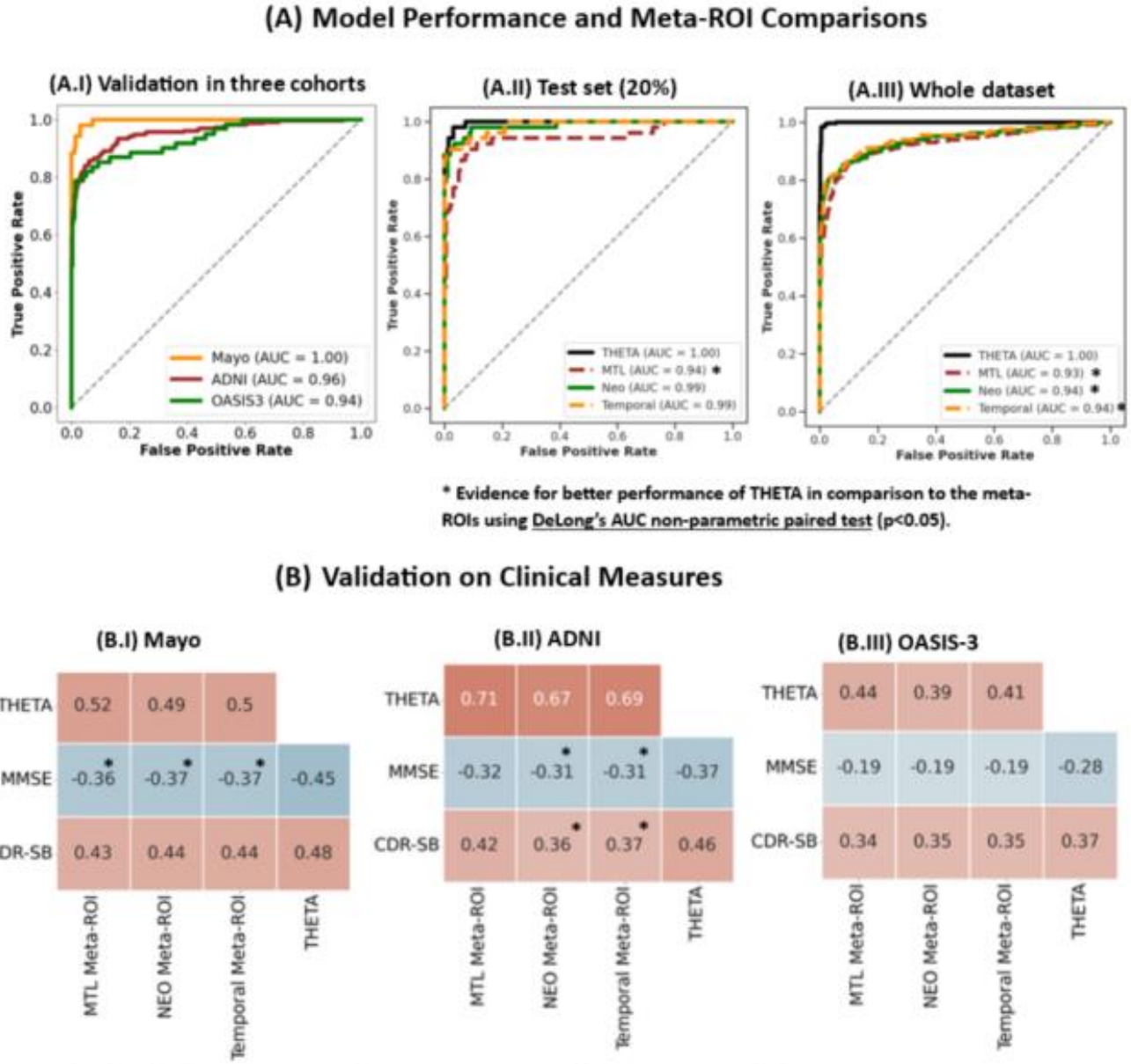

Figure 1. Figures under (A) illustrate the performance of the ML model for predicting tau status. The model was trained on the Mayo (80% training: 20% testing) and validated on ADNI and OASIS-3. (A.I) shows the model's performance in Mayo, ADNI, and OASIS-3 cohorts, while (A.II) and (A.III) illustrate the comparison of THETA to the meta-ROIs to classify tau positivity. Figures under (B) illustrate the comparison of the meta-ROIs and THETA to the clinical indices Mini-Mental State Examination (MMSE) and CDR-Sum of Boxes (CDR-SB). The meta-ROIs are medial temporal lobe (MTL), neocortical (NEO), and temporal.

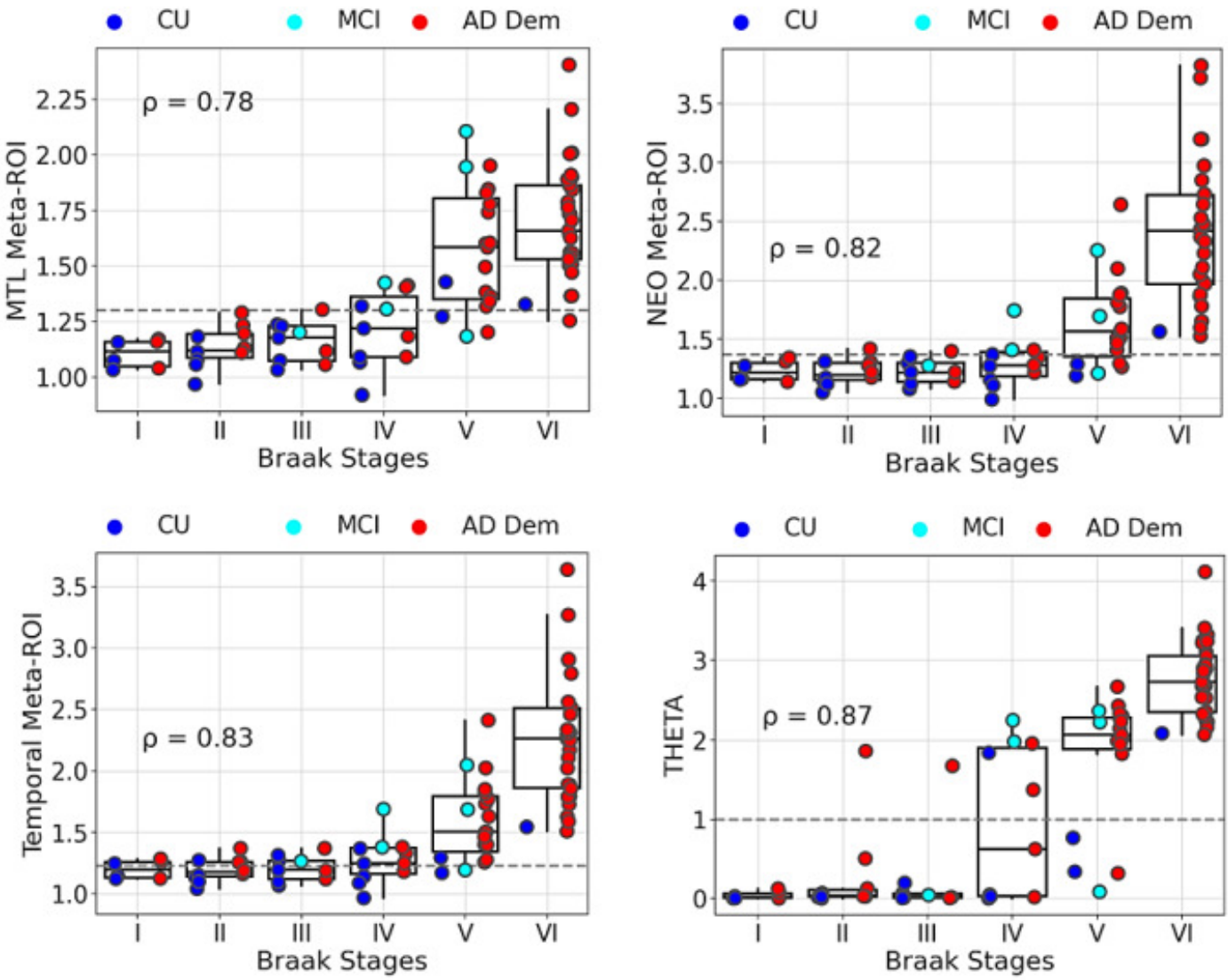

Figure 2. Association of meta-ROIs and THETA to Braak stages (I to VI). The SUVR cutoff points for each metric are shown by dotted lines (MTL at 1.30 SUVR, NEO at 1.37 SUVR, Temporal at 1.23 SUVR and, and THETA at 1.0). The diagnostic groups (CU, MCI, and AD Dementia) are shown in blue, cyan, and red respectively.

Keywords: Tau-PET, Machine learning, PET, Quantification, Validation

Transmembrane protein 106B is one of the potential off-target binding substrates of tau PET tracers

Ryuichi Harada[1,2,3], Yuka Yokoyama[2], Kaede Kudo[3], Ren Iwata[2], Yukitsuka Kudo[3], Shozo Furumoto[2], Nobuyuki Okamura[1]

[1]*Division of Pharmacology, Faculty of Medicine, Tohoku Medical and Pharmaceutical University, Sendai, Japan*
[2]*Cyclotron and Radioisotope Center, Tohoku University, Sendai, Japan*
[3]*Institute of Development, Aging and Cancer, Tohoku University, Sendai, Japan*

Background: Some tau PET tracers suffered from off-target binding to the choroid plexus (CP). Recent cryo-electron microscopy analyses and neuropathological researches revealed that a novel amyloid fibril of transmembrane protein 106B (TMEM106B) accumulated in various brain regions, including CP, of the neurodegenerative disease brains. The aim of this study was to evaluate the binding of tau PET tracers to TMEM106B aggregates in human brain tissues.

Methods: Tau PET tracers; such as [^{18}F]SNFT-1, [^{18}F]MK6240, [^{18}F]Flortaucipir, [^{18}F]PI-2620, and [^{18}F]PM-PBB3 were prepared using their respective precursors. In vitro autoradiography using each tau tracer was performed on hippocampal sections containing CP from human brains. Immunohistochemistry (IHC) with TMEM106B and tau were performed.

Results: A significant deposition of TMEM106B was confirmed in the CP of the hippocampal sections by IHC. In vitro autoradiography using the sections demonstrated that weak binding of [^{18}F]SNFT-1, [^{18}F]MK-6240, [^{18}F]PI-2620 were observed in the CP, which contained a high density of TMEM106B aggregates but not tau. [^{18}F]Flortaucipir showed mild binding and partially displaced by a MAO-A inhibitor, Clorygiline. On the other hand, [^{18}F]PM-PBB3 highly accumulated in the CP and the binding was displaced by unlabeled PM-PBB3, suggesting that the binding was specific. In addition, PM-PPB3 fluorescence staining was colocalized with TMEM106B IHC, which was similar to previously reported "Biondi ring tangles" in the CP.

Conclusions: Off-target binding of some tau PET tracers to CP observed in clinical PET might be due to the binding to TMEM106B aggregates. Further quantitative analyses were required to validate these findings.

Keywords: Tau PET tracers, Autoradiography, Off-target binding, TMEM106B

Thursday, January 18, 2024 - 08:30 am - 10:00 am

Podium Session

SESSION V: Neuropathology - PART II

CHAIRS: Teresa Gomez-Isla, Laetitia Lemoine, Laetitia Lemoine

Thursday, January 18, 2024		
08:30 am - 10:00 am	**SESSION V: Neuropathology - PART II**	**Teresa Gomez Isla, Massachusetts General Hospital, Boston, MA, United States** **Laetitia Lemoine, Invicro, London, United Kingdom**
08:30	Introduction	Chairs
08:35	Pathologic correlations of [18F]-Flortaucipir imaging in mixed Lewy body and Alzheimer's disease	Aguero | Scapellato | Klein | Lois | Ye | Kumar | Gomperts | Melloni | Gaona | Connors | Frosch | Gómez-Isla
08:50	Flortaucipir PET relationships to pathologically determined Braak neurofibrillary tangle stage and Thal β-amyloid phase in aging and Alzheimer's disease	Whitwell | Tosakulwong | Weigand | Schwarz | Senjem | Graff-Radford | Machulda | Kantarci | Knopman | Nguyen | Reichard | Dickson | Petersen | Lowe | Jack | Josephs
09:05	Correlating hippocampal volume with neuropathological burden in neurodegenerative diseases using 7T postmortem MRI	Liou | Ibrahim | Kofler
09:20	Multimodal genetic analysis of brain amyloidosis	Wang | Archer | Ali | Mormino | Buckley | Lee | Saykin | De Jager | Schneider | Bennett | Barnes | Vardarajan | Mayeux | Kunkle | Bush | Keene | Seshadri | Sperling | Vemuri | Ramanan | Schellenberg | Huentelman | Hamilton-Nelson | Pericak-Vance | Goate | Haines | Montine | Beecham | Cruchaga | Hohman | Dumitrescu
09:35	Discussion	

Pathologic correlations of [18F]-Flortaucipir imaging in mixed Lewy body and Alzheimer's disease

Cinthya Aguero[1,2], Margaret Scapellato[1,2], C. Zachary Klein[1,2], Cristina Lois[3,4], Rong Ye[1,2], Sunny Kumar[1,2], Stephen Gomperts[1,2], Alexandra Melloni[1,2,5], Angelica Gaona[1,2,5], Theresa Connors[1,2,5], Matthew P. Frosch[1,2,5], Teresa Gómez-Isla[1,2]

[1]*MassGeneral Institute for Neurodegenerative Disease, Charlestown, MA, United States*
[2]*Department of Neurology, Massachusetts General Hospital, Boston, MA, United States*
[3]*Department of Radiology, Massachusetts General Hospital, Boston, MA, United States*
[4]*Gordon Center for Medical Imaging, Division of Nuclear Medicine and Molecular Imaging, Massachusetts General Hospital, Boston, MA, United States*
[5]*C.S. Kubik Laboratory for Neuropathology, Massachusetts General Hospital, Boston, MA, United States*

Background: Multiple autopsy studies have demonstrated that dementia in most aged patients results from a brain multimorbidity rather than from one single disease. Dementia with Lewy bodies (DLB) is the second most common form of neurodegenerative dementia in older people after Alzheimer's disease (AD). However, many DLB cases also exhibit concomitant AD pathology. [^{18}F]-Flortaucipir PET imaging may help to more accurately discriminate between pure DLB and mixed DLB/AD cases with relevant diagnostic, prognostic and therapeutic implications in clinical practice. Neuroimaging-pathologic correlation studies are critical to correctly interpret *in vivo* [^{18}F]-Flortaucipir *positivity in the setting of mixed DLB and AD pathologies*.

Objective: To examine the correlation of *in vivo* [^{18}F]-Flortaucipir retention and tau and alpha-synuclein lesion burdens at autopsy in a cohort of 19 pathologically confirmed pure AD, DLB and mixed AD/DLB cases.

Methods: We quantified *in vivo* retention of [^{18}F]-Flortaucipir as standardized uptake value ratios (SUVRs) and performed quantitative measurements of tau and alpha-synuclein lesion burdens in postmortem brain samples containing multiple matching regions of interest (ROIs) from 3 AD, 7 DLB, and 9 mixed DLB/AD pathologically confirmed cases. They all underwent [^{18}F]-Flortuacipir PET imaging prior to death (with an average interval of $\pm$3.6 years).

Results: Quantification of tau burden in immunostained sections revealed a significant correlation between tau lesion load at postmortem and [^{18}F]-Flortaucipir-PET retention in matching ROIs in both pure AD (p=0.01) and mixed DLB/AD (p=0.02). As expected, no correlation was found between [^{18}F]-Flortaucipir-PET retention and postmortem alpha-synuclein lesion burden in matching ROIs in pure DLB and mixed DLB/AD cases.

Conclusion: Our results further favor the notion that [^{18}F]-Flortaucipir is a reliable biomarker for the *in vivo* detection and assessment of AD tau burden and may help to improve the accuracy of the clinical diagnosis and prognosis of DLB patients who harbor concomitant AD pathology in the brain.

Keywords: Flortaucipir, DLB, AD, Autoradiography

Flortaucipir PET relationships to pathologically determined Braak neurofibrillary tangle stage and Thal β-amyloid phase in aging and Alzheimer's disease

Jennifer Whitwell[1], Nirubol Tosakulwong[1], Stephen Weigand[1], Christopher Schwarz[1], Matthew Senjem[1], Jonathan Graff-Radford[1], Mary Machulda[1], Kejal Kantarci[1], David Knopman[1], Aivi Nguyen[1], Ross Reichard[1], Dennis Dickson[2], Ronald Petersen[1], Val Lowe[1], Clifford Jack[1], Keith Josephs[1]

[1]*Mayo Clinic, Rochester, MN, United States*
[2]*Mayo Clinic, Jacksonville, FL, United States*

Background and objective: [^{18}F]-Flortaucipir PET is considered an excellent biomarker of Alzheimer's disease. However, it is unknown how flortaucipir is associated with distribution of histopathologic tau and how associations are influenced by β-amyloid. We aimed to model relationships between flortaucipir PET and both Braak and Thal phase across different brain regions and determine optimum flortaucipir cut points to differentiate between AD neuropathologic change (ADNC) levels and primary age-related tauopathy (PART).

Methods: 181 participants who had undergone flortaucipir PET, died and undergone an autopsy were identified. Each case was assigned a Braak neurofibrillary tangle stage (0-VI), Thal phase (T0-T5), and were classified as not ADNC, low-intermediate ADNC, high ADNC and PART. Flortaucipir uptake was measured in nine regions selected to capture Braak stages (entorhinal, anterior hippocampus, fusiform, inferior temporal, superior frontal, precuneus, superior parietal, calcarine and motor cortex). Standardized uptake value ratios (SUVRs) were calculated with reference to cerebellar crus grey matter. Generalized additive models were fit to capture nonlinear relationships between SUVR and Thal phase/Braak stage. Area under the receiver operator characteristic curve analysis was used to identify optimum cut-points to separate ADNC levels.

Results: Mean flortaucipir uptake differences were greater with increasing Braak stage in all regions, although increasing uptake at low Braak stages in medial temporal regions was only observed in cases with high β-amyloid Thal phase (**Figure**). Mean flortaucipir uptake linearly increased with β-amyloid Thal phase in medial temporal and cortical regions (**Figure**). The highest flortaucipir uptake occurred with high ADNC, followed by low-intermediate ADNC, then PART. Entorhinal cortex provided the best differentiation between groups with greatest sensitivity and specificity to differentiate high ADNC from both PART and low-intermediate ADNC (**Table**).

Discussion: Spatial patterns of flortaucipir mirror histopathological tau distribution, are influenced by β-amyloid phase, and are useful for distinguishing different levels of ADNC and PART.

Figure: Estimated flortaucipir standardized uptake value ratios (SUVRs) within each Thal phase or Braak stage with all regions on the same SUVR axis.

ERC = entorhinal cortex; AHP = anterior hippocampus; FFG = fusiform gyrus; ITG = inferior temporal gyrus; SFG = superior frontal gyrus; PRCU = precuneus; SPG = superior parietal gyrus; CAL = calcarine; PrCG = precentral gyrus.

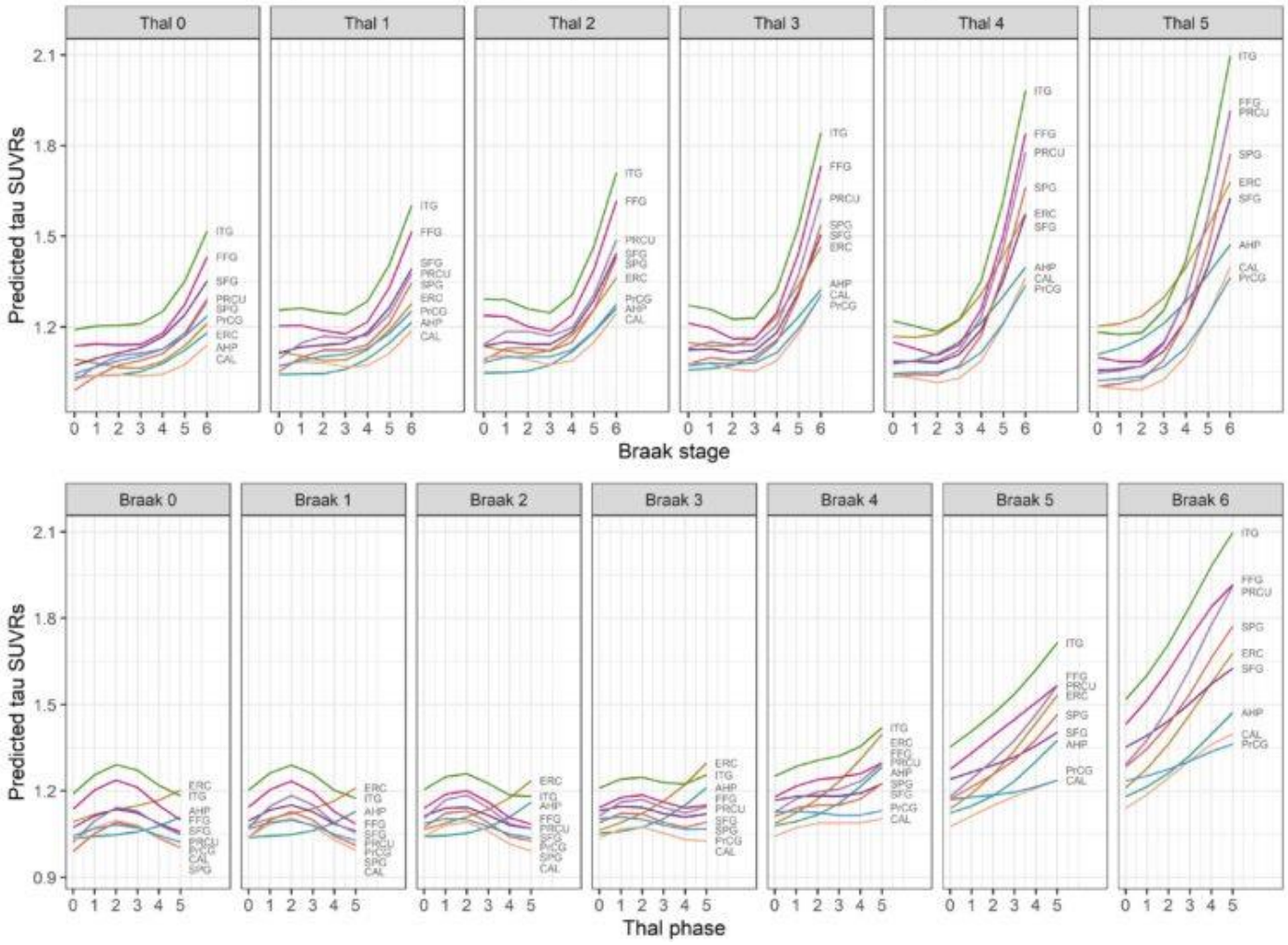

Table 1: Area under the receiver operator characteristic curve analysis to differentiate PART and ADNC levels

Region	High ADNC vs Low/Intermediate ADNC				High ADNC vs PART				Low/Intermediate ADNC vs PART			
	AUROC (95% CI)	Cut-off	Sens (%)	Spec (%)	AUROC (95% CI)	Cut-off	Sens (%)	Spec (%)	AUROC (95% CI)	Cut-off	Sens (%)	Spec (%)
Entorhinal cortex	0.89 (0.83, 0.95)	1.39	89	81	0.98 (0.96, 1.00)	1.28	100	91	0.72 (0.61, 0.83)	1.18	88	61
Fusiform	0.88 (0.82, 0.94)	1.45	93	77	0.95 (0.91, 0.99)	1.35	100	83	0.67 (0.57, 0.78)	1.23	83	48
Anterior HP	0.87 (0.80, 0.93)	1.25	85	78	0.94 (0.90, 0.98)	1.18	95	86	0.62 (0.51, 0.73)	1.16	92	37
Inferior temporal	0.89 (0.83, 0.95)	1.46	87	81	0.95 (0.91, 0.99)	1.35	92	90	0.68 (0.57, 0.78)	1.26	65	67
Superior frontal	0.79 (0.71, 0.87)	1.29	89	64	0.83 (0.76, 0.91)	1.23	85	74	0.58 (0.46, 0.69)	1.15	63	61
Precuneus	0.81 (0.73, 0.89)	1.34	91	68	0.88 (0.82, 0.94)	1.29	97	71	0.66 (0.55, 0.77)	1.20	85	52
Superior parietal	0.82 (0.74, 0.89)	1.26	89	70	0.87 (0.81, 0.93)	1.26	97	70	0.63 (0.52, 0.74)	1.12	63	65
Calcarine	0.76 (0.68, 0.85)	1.18	87	62	0.83 (0.76, 0.90)	1.12	82	78	0.61 (0.49, 0.72)	1.12	82	43
Precentral	0.72 (0.63, 0.81)	1.28	100	46	0.73 (0.64, 0.81)	1.34	98	42	0.51 (0.40, 0.62)	1.12	60	52

Area under the receiver operator curve (AUROC), Sensitivity, and Specificity (based on the Youden criteria maximizing the sum of sensitivity and specificity) are shown for each region. HP = hippocampus.

Keywords: Tau PET, AD, primary age-related tauopathy, pathology, neurofibrillary tangle

Correlating hippocampal volume with neuropathological burden in neurodegenerative diseases using 7T postmortem MRI

Jr-Jiun Liou[1], Tamer Ibrahim[1], Julia Kofler[1]

[1]*University of Pittsburgh, Pittsburgh, PA, United States*

Background: The hippocampus is among the earliest areas compromised in neurodegenerative diseases. In the context of limbic-predominant age-related TDP-43 encephalopathy (LATE), the severity of LATE can be categorized into three stages based on the distribution of TDP-43. This study aims to introduce a 7T postmortem MRI protocol that employs intact hemispheres embedded in agar, centers on Alzheimer's disease and Down syndrome, and investigates correlations between hippocampal volume and neuropathological burden including LATE pathology.

Methods: In this research, ex vivo postmortem MRI scans were conducted on formalin- or paraformaldehyde-fixed left hemispheres at 7T in a cohort of 77 autopsy cases. The hippocampus was manually segmented, and its volume was correlated with clinical data and neuropathological findings.

Results: The manually segmented ex vivo hippocampal volume exhibited a significant correlation with in vivo volume ($p=0.0066$). The hippocampal volume displayed a positive association with whole brain weight measured during autopsy ($p<0.001$) and a negative relationship with Thal phase ($p<0.0001$), Braak stage ($p=0.0005$), LATE pathology ($p<0.0001$), and dementia duration ($p=0.0064$). Notably, individuals with Down syndrome exhibited a significantly smaller hippocampal volume compared to non-Down syndrome cases ($p=0.0025$). In cases of Alzheimer's disease and Lewy body disease, a marked distinction was evident between LATE and non-LATE cases ($p<0.0001$). Furthermore, hippocampi in LATE stage 2 ($p<0.0001$) and stage 1 ($p=0.0494$) were notably smaller than those in stage 0. Additionally, the hippocampal volume was diminished in cases diagnosed with hippocampal sclerosis (HS) when compared to those without ($p=0.0091$), and the volume of LATE cases without HS was lower than that of non-LATE cases ($p=0.0125$).

Discussion: This study presents an innovative postmortem imaging protocol that harnesses the power of ultra-high field MRI, rendering acquisition in a mere three hours per brain feasible. It successfully demonstrates precise measurement of hippocampal volumes and their correlation with postmortem assessments of neuropathological burden.

Keywords: Pathology, hippocampus, limbic-predominant age-related TDP-43 encephalopathy, postmortem, MRI

Multimodal genetic analysis of brain amyloidosis

Ting-Chen Wang[1,2], Derek Archer[1,2], Muhammad Ali[3,4], Elizabeth Mormino[5], Rachel Buckley[6,7], Annie Lee[5], Andrew Saykin[8,9,10], Philip De Jager[11,12], Julie Schneider[13,14], David Bennett[15], Lisa Barnes[16], Badri Vardarajan[5], Richard Mayeux[5,17], Brian Kunkle[18], William Bush[19], C. Dirk Keene, Sudha Seshadri, Reisa Sperling, Prashanthi Vemuri, Vijay Ramanan, Gerard Schellenberg, Matt Huentelman, Kara Hamilton-Nelson, Margaret Pericak-Vance, Alison Goate, Jonathan Haines, Thomas Montine, Gary Beecham, Carlos Cruchaga, Timothy Hohman, Logan Dumitrescu

[1]*Vanderbilt Memory and Alzheimer's Center, Department of Neurology, Vanderbilt University Medical Center, Nashville, TN, United States*
[2]*Vanderbilt Genetics Institute, Vanderbilt University Medical Center, Nashville, TN, United States*
[3]*Department of Psychiatry, Washington University, St. Louis, MO, United States*
[4]*NeuroGenomics and Informatics, Washington University, St. Louis, MO, United States*
[5]*Department of Neurology, Columbia University Medical Center, New York, NY, United States*
[6]*Department of Neurology, The New York Presbyterian Hospital, New York, NY, United States*
[7]*Taub Institute for Research on Alzheimer's Disease and The Aging Brain, Columbia University Medical Center, New York, NY, United States*
[8]*The Institute for Genomic Medicine, Columbia University Medical Center, New York, NY, United States*
[9]*Department of Radiology and Imaging Sciences, Center for Neuroimaging, School of Medicine, Indiana University, Indianapolis, IN, United States*
[10]*Department of Medical and Molecular Genetics, School of Medicine, Indiana University, Indianapolis, IN, United States*
[11]*Research and Early Development, Biogen Inc, Cambridge, MA, United States*
[12]*Alzheimer's Therapeutic Research Institute, Keck School of Medicine, University of Southern California, San Diego, CA, United States*
[13]*Center for Translational and Computational Neuroimmunology, Department of Neurology, Columbia University Medical Center, New York, NY, United States*
[14]*Cell Circuits Program, Broad Institute, Cambridge, MA, United States*
[15]*Rush Alzheimer's Disease Center, Rush University Medical Center, Chicago, IL, United States*
[16]*Knight Alzheimer's Disease Research Center, Washington University, St. Louis, MO, United States*
[17]*Hope Center for Neurologic Diseases, Washington University, St. Louis, MO, United States*
[18]*Department of Genetics, Washington University School of Medicine, St. Louis, MO, United States*
[19]*John T MacDonald Foundation Department of Human Genetics, University of Miami, Miami, FL, United States*
[20]*John P. Hussman Institute for Human Genomics, University of Miami School of Medicine, Miami, FL, United States*
[21]*Department of Population and Quantitative Health Sciences, Institute for Computational Biology, Case Western Reserve University, Cleveland, OH, United States*
[22]*Department of Pathology, University of Washington, Seattle, WA, United States*
[23]*Department of Pathology, Stanford University, Stanford, CA, United States*
[24]*Department of Pathology and Laboratory Medicine, Perelman School of Medicine, University of Pennsylvania, Philadelphia, PA, United States*
[25]*Neurogenomics Division, Translational Genomics Research Institute, Phoenix, AZ, United States*
[26]*Ronald M Loeb Center for Alzheimer's Disease, Department of Neuroscience, Icahn School of Medicine at Mount Sina, New York, NY, United States*
[27]*Department of Neurology and Neurological Sciences, Stanford University, Stanford, CA, United States*
[28]*Framingham Heart Study, Framingham, MA, United States*
[29]*Boston University School of Medicine, Boston, MA, United States*
[30]*Department of Neurology, Harvard Medical School, Boston, MA, United States*
[31]*Brigham and Women's Hospital and Department of Neurology, Massachusetts General Hospital, Harvard Medical School, Boston, MA, United States*

[32]*Athinoula A. Martinos Center for Biomedical Imaging, Charlestown, MA, United States*
[33]*Department of Radiology, Mayo Clinic-Minnesota, Rochester, MN, United States*

Objectives: Recently, genome wide association studies (GWAS) on endophenotypes of Alzheimer's disease (AD), such as amyloid burden in the brain, have been utilized to elucidate the contribution of genetic variants and their associated molecular pathways to AD. We combine measures of brain amyloidosis from PET imaging and autopsy to overcome the sample size limitations of previous approaches and identify novel genetic drivers of disease.

Methods: Across 15 cohorts of aging and AD, amyloidosis status (positive/negative) was determined for each participant based on either *in vivo* amyloid PET imaging (N=7036, 35% amyloid positive, 53.67% female, age=71) or on Consortium to Establish a Registry for Alzheimer's Disease (CERAD) staging at autopsy (N=6519, 63.08% amyloid positive, 51.34% female, age at death=83). All participants were individuals of European ancestry. GWAS was performed within each modality and meta-analyzed. Covariates included age, sex, and principal components of genetic ancestry.

Results: We identified three known AD loci (*APOE*, *CR1*, and *BIN1*) and a novel locus on chromosome 17 (rs35635959, intergenic, MAF=0.27, OR=1.18, p= 1.47×10^{-8}). The gene-based MAGMA test excluding the *APOE* region identified significant associations between *COASY*, *PLEKHH3*, and *TUBG2* on chromosome 17 and amyloidosis. Brain eQTL databases indicate associations between rs35635959 with gene expression of *COASY* and *TUBG2*, both of which have evidence for differential expression in AD brains.

Conclusions: In the largest European GWAS of brain amyloidosis to date, our results replicate known brain amyloidosis loci, while indicating a potential novel locus on chromosome 17. Both our variant and gene level results implicate *TUBG2*, a gene involved in microtubule organization, as a high-quality candidate for future evaluation. Current efforts are seeking to replicate these novel effects in independent datasets.

Keywords: brain amyloidosis, PET imaging, autopsy, GWAS, chromosome 17

Thursday, January 18, 2024 - 10:30 am - 12:00 pm

Podium Session

SESSION VI: Early Amyloid and Tau Effects and Mod Pre-clinical AD

CHAIRS: Susan Landau, Elizabeth Mormino

Thursday, January 18, 2024		
10:30 am – 12:00 pm	**SESSION VI: Early Amyloid and Tau Effects and Mod Pre-clinical AD**	**Annie Cohen, University of Pittsburgh, Pittsburg, PA, United States** **Gil Rabinovici, University of California, San Francisco, CA, United States**
10:30	Introduction	Chairs
10:35	Reduced Tau Accumulation Mediates the Protective Effects of Physical Activity on Prospective Cognitive Decline in Preclinical Alzheimer's Disease	Yau | Kirn | Rabin | Properzi | Schultz | Rentz | Johnson | Sperling | Chhatwal
10:50	Speech patterns during memory recall relates to early tau burden across adulthood	Young | Smith | Karjadi | Ang | Insel | Henderson | Sumner | Poston | Au | Mormino
11:05	Default mode network connectivity tracks with amyloid age and predicts conversion to amyloidosis, mild cognitive impairment and dementia across the Alzheimer's disease spectrum	Corriveau-Lecavalier | Dicks | Martin | Lundt | Wiste | Gunter | Kamykowski | Senjem | Schwarz | Botha | Graff-Radford | Machulda | Fields | Boeve | Lowe | Knopman | Petersen | Jack | Jones
11:20	Higher locus coeruleus integrity and cognitive reserve attenuate tau-related cognitive decline in older adults	Heinrich | Riphagen | Koops | Papp | Rentz | Sperling | Johnson | Jacobs
11:35	Discussion	

Reduced tau accumulation mediates the protective effects of physical activity on prospective cognitive decline in preclinical Alzheimer's disease

Wai-Ying Wendy Yau[1,2], Dylan Kirn[1,2,3], Jennifer Rabin[4,5], Michael Properzi[1,6], Aaron Schultz[1,6], Dorene Rentz[1,2,3], Keith Johnson[1,2,3,6], Reisa Sperling[1,2,3], Jasmeer Chhatwal[1,2,3]

[1]*Department of Neurology, Massachusetts General Hospital, Boston, MA, United States*
[2]*Harvard Medical School, Boston, MA, United States*
[3]*Center for Alzheimer Research and Treatment, Department of Neurology, Brigham and Women's Hospital, Boston, MA, United States*
[4]*Harquail Centre for Neuromodulation and Hurvitz Brain Sciences Program, Sunnybrook Research Institute, Toronto, ON, Canada*
[5]*Division of Neurology, Department of Medicine, Sunnybrook Health Sciences Centre, University of Toronto, Toronto, ON, Canada*
[6]*Athinoula A. Martinos Center for Biomedical Imaging, Department of Radiology, Massachusetts General Hospital, Charlestown, MA, United States*

Background: Physical activity is a putative protective factor associated with reduced risk of dementia, including Alzheimer's disease (AD). Prior work from the Harvard Aging Brain Study (HABS) suggests that higher levels of physical activity in cognitively unimpaired individuals with elevated amyloid burden are associated with slower prospective cognitive decline. However, whether this protective effect on cognition in preclinical AD is mediated by altered trajectory of tau pathology is unclear.

Method: We examined 297 cognitively unimpaired at baseline older adults from HABS (Table 1). Baseline physical activity (mean steps per day) was measured using a waistband-mounted pedometer (HJ-720ITC; Omron Healthcare) worn over 7 consecutive days during waking hours. Using linear mixed effects models, we examined the interactive effects of baseline physical activity and amyloid PET burden (Pittsburgh Compound-B) on longitudinal cognitive decline (Preclinical Alzheimer Cognitive Composite-5) and longitudinal inferior temporal cortex (ITC) tau PET burden (Flortaucipir; subset n=170). We further investigated whether the interactive effects on cognition were mediated by changes in ITC tau.

Result: In a larger sample of HABS participants with up to 12 years of cognitive follow-up, we replicated the significant interaction between higher physical activity and elevated amyloid burden on slower prospective cognitive decline (β=0.09, t=3.5, p<0.001; Figure 1A). We further demonstrated a novel interactive effect on tau pathology, where higher physical activity was associated with reduced ITC tau accumulation in individuals with elevated baseline amyloid (β=-0.09, t=-3.2, p=0.002; Figure 1B). Importantly, moderated mediation analyses revealed that reduced tau accumulation fully mediated the effects of higher physical activity on slower cognitive decline in the setting of elevated amyloid (p<0.001, 93% mediated; Figure 2).

Conclusion: Our findings provide strong support for promoting physical activity as a lifestyle intervention, in conjunction with anti-amyloid therapy, to slow the onset and/or progression of tau pathology and cognitive decline in preclinical AD.

Table 1. Participant characteristics

Characteristic [N=297 except N=170 for tau PET subset]	
Age at baseline, yr, mean (SD)	72.5 (7.3)
Females, n (%)	177 (60)
Education, yr, mean (SD)	15.8 (3.0)
APOE ε4 carriers, n (%)	84 (29)
Mean steps per day (SD)	5755 (2958)
Baseline PiB PET FLR DVR, PVC, mean (SD)	1.38 (0.4)
β-Amyloid positive, n (%)	89 (30)
Baseline ITC tau PET SUVR, PVC, mean (SD)	1.46 (0.2)
# Longitudinal tau PET scans, mean (SD)	2.6 (0.6)
Duration of tau PET follow up, yr, mean (SD)	4.3 (1.6)
# Longitudinal PACC5 assessments, mean (SD)	7.6 (2.7)
Duration of cognitive follow up, yr, mean (SD)	6.7 (2.4)

APOE ε4 = apolipoprotein E ε4 allele; DVR = distribution volume ratio; FLR = frontal, lateral temporal and parietal, and retrosplenial regional uptake; ITC = inferior temporal cortex; PACC5 = Preclinical Alzheimer's Cognitive Composite-5; PET = positron emission tomography; PiB = Pittsburgh compound B; PVC = partial volume corrected; SUVR = standardized uptake value ratio.

Figure 1. High baseline physical activity was associated with A) slower prospective cognitive decline and B) reduced inferior temporal cortex (ITC) tau accumulation, in baseline cognitively unimpaired older adults with elevated amyloid burden. For visualization, predicted cognition (A) and ITC tau (B) trajectories based on different levels of baseline physical activity and amyloid are presented. Low and high physical activity levels are represented by 1 SD below and above the group mean (2800 steps per day and 8700 steps per day, respectively). Low and high amyloid are represented by the mean Pittsburgh compound-B distribution volume ratio (PiB DVR) of amyloid-negative (1.17) and amyloid-positive (1.86) participants respectively.

Aβ = β-amyloid; PACC5 = Preclinical Alzheimer's Cognitive Composite-5; PVC = partial volume corrected; SUVR = standardized uptake value ratio.

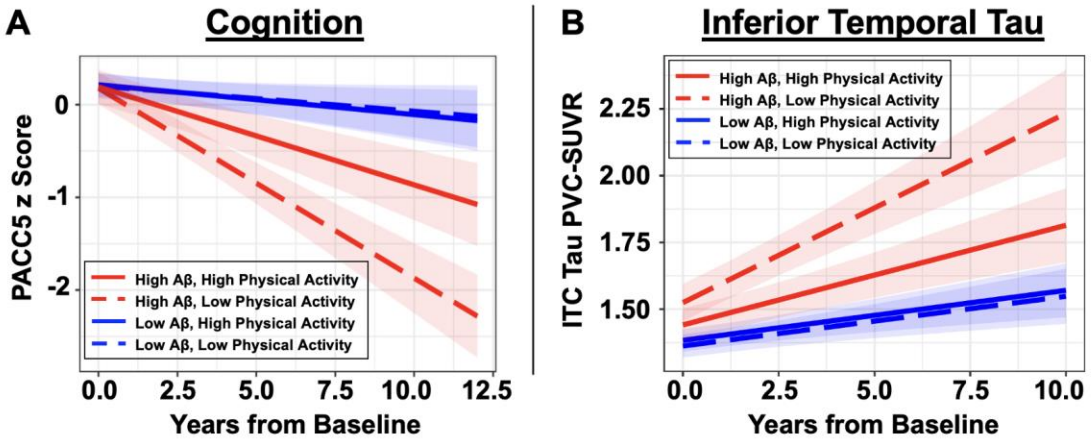

Figure 2. Reduced inferior temporal tau accumulation fully mediates the protective effects of high physical activity on slower cognitive decline in setting of high baseline amyloid burden (93% mediated).

Aβ = β-amyloid; ITC = inferior temporal cortex; PACC5 = Preclinical Alzheimer's Cognitive Composite-5.

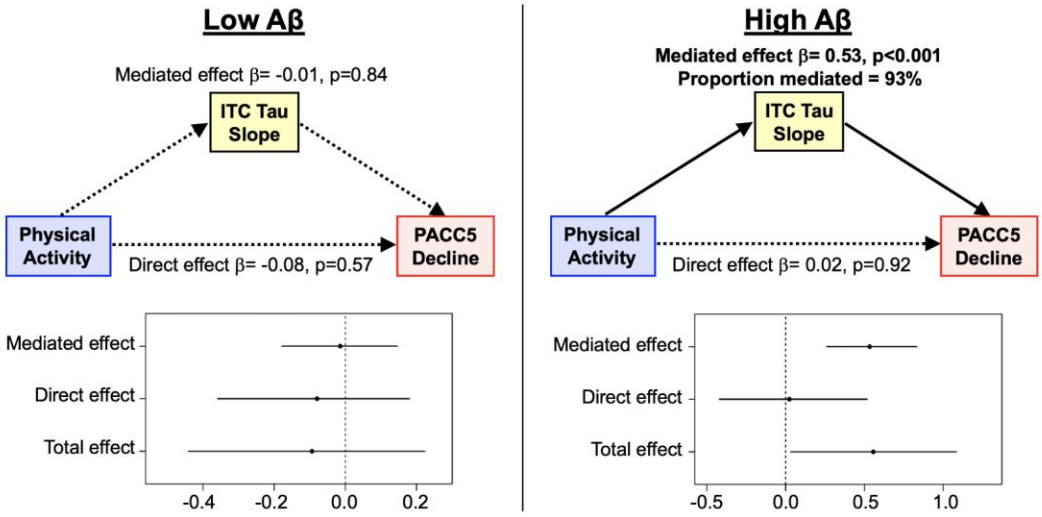

Keywords: Physical activity, amyloid PET, tau PET, preclinical Alzheimer's disease, cognition

Speech patterns during memory recall relates to early tau burden across adulthood

Christina Young[1], Victorija Smith[1], Cody Karjadi[2], Ting Fang Alvin Ang[2], Philip Insel[3], Victor Henderson[1,4], Meghan Sumner[5], Kathleen Poston[1,6], Rhoda Au[2], Elizabeth Mormino[1,6]

[1]*Department of Neurology and Neurological Sciences, Stanford University School of Medicine, Palo Alto, CA, United States*
[2]*Department of Anatomy & Neurobiology and Framingham Heart Study, Boston University Chobanian and Avedisian School of Medicine, Boston, MA, United States*
[3]*Department of Psychiatry, University of California San Francisco, San Francisco, CA, United States*
[4]*Department of Epidemiology and Population Health, Stanford University, Palo Alto, CA, United States*
[5]*Department of Linguistics, Stanford University, Palo Alto, CA, United States*
[6]*Wu Tsai Neuroscience Institute, Stanford University, Palo Alto, CA, United States*

Background: Early cognitive decline related to Alzheimer's disease pathology may manifest through subtle differences in speech.

Objective: To determine whether speech patterns during delayed recall of a story memory task relate to traditional neuropsychological scores, differ between those with normal (Aβ-) and abnormal (Aβ+) amyloid PET burden, and relate to regional tau PET signal.

Methods: We examined 238 cognitively unimpaired adults from the Framingham Heart Study, ranging from ages 32 to 75 years, who completed amyloid (Pittsburgh Compound B) and tau (Flortaucipir) PET imaging in addition to having an audio recorded neuropsychological assessment within 1 year of tau PET (**Figure 1; Table 1**). The delayed recall portion of the logical memory story memory task was transcribed, and neuropsychological delayed recall scores were compared to five speech markers: amount of time the participant spent speaking (i.e., total utterance time), total length of between-utterance pauses, number of between-utterance pauses, speech rate, and percentage of unique relative to total words spoken. We then examined how these speech markers related to global amyloid status (Aβ+ vs. Aβ-) and continuous regional tau signal controlling for age, sex, education, and amyloid status.

Results: All speech markers except for between-utterance pause time significantly correlated with delayed recall score though the shared variance was low (2-15%; **Figure 2**). Delayed recall score was not significantly different between Aβ+ and Aβ- groups (**Table 2**) and was not associated with regional tau signal (**Table 3**). However, longer and more between-utterance pauses as well as slower speech rate were associated with increased tau signal across entorhinal, amygdala, inferior parietal, and precuneus regions (**Figure 3; Table 3**).

Conclusion: Tau-associated changes in speech during delayed memory recall may emerge prior to tau associations with traditional delayed recall scores. Subtle speech changes during memory recall may reflect cognitive impairment associated with early Alzheimer's disease pathology.

Figure 1. Data Overview.

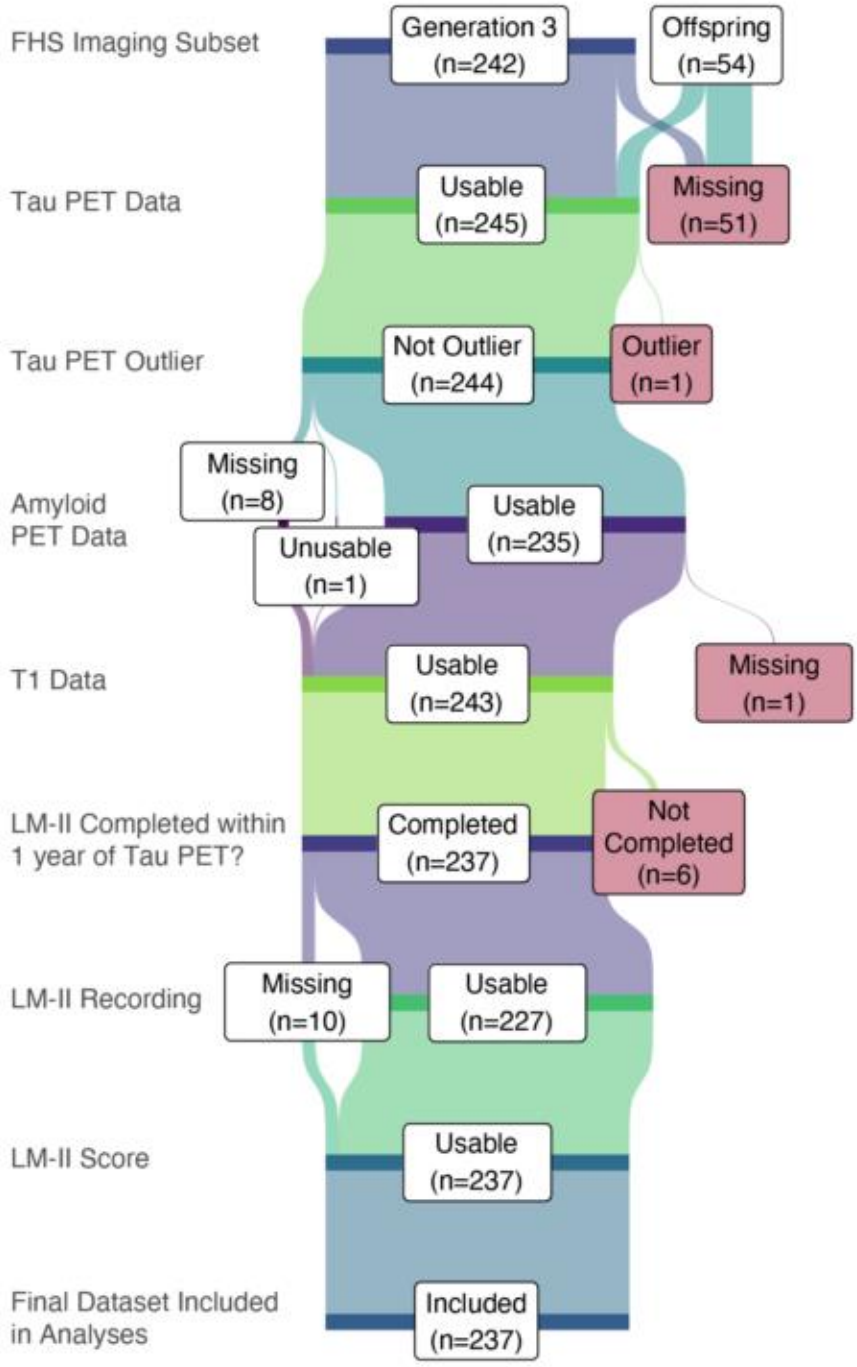

Figure 2. Correlations between speech markers extracted during logical memory (LM) delayed recall and LM (delayed recall scores (LM-II). Black font denotes significant associations; gray font denotes non-significant associations.

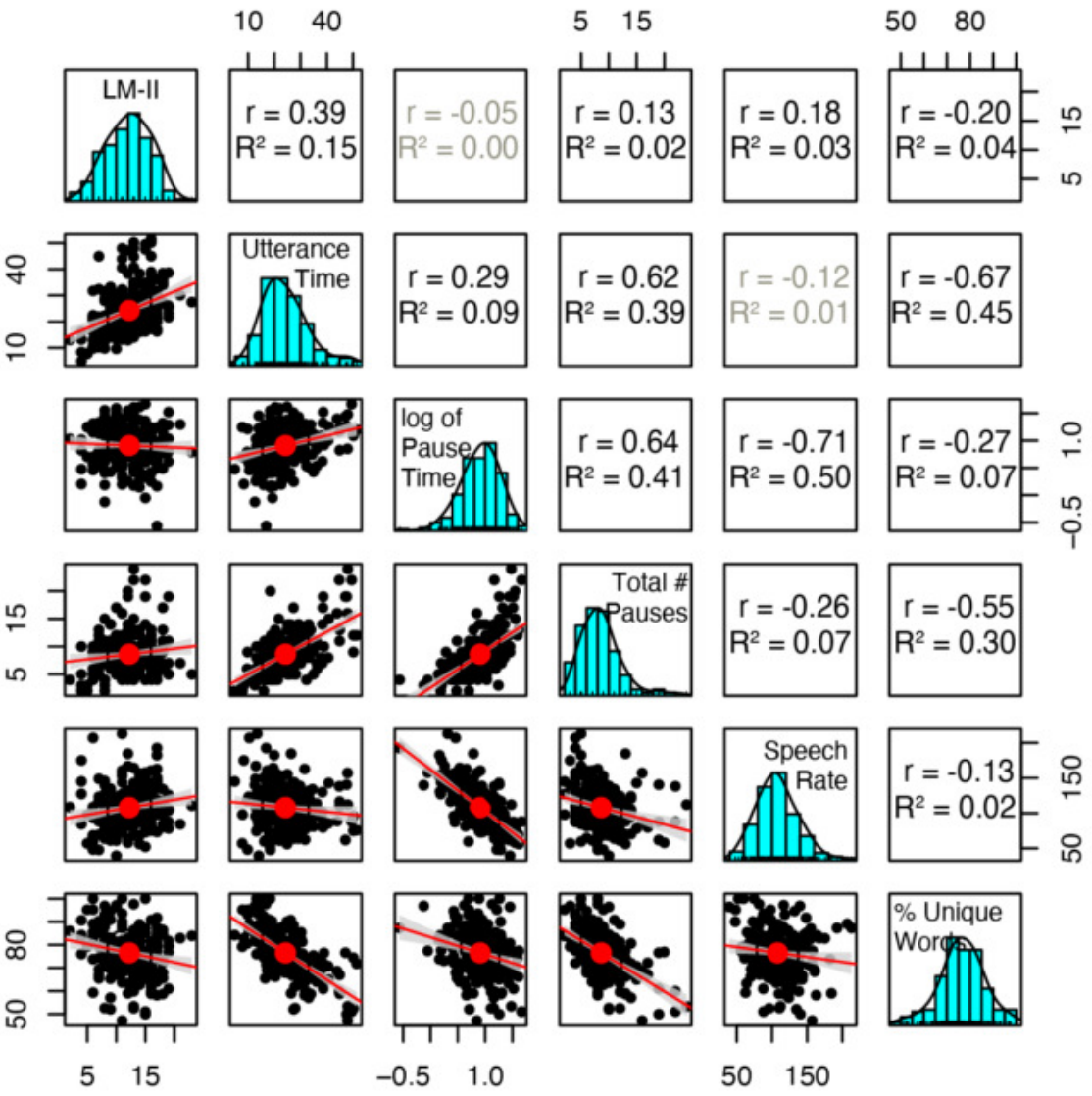

Figure 3. Associations between regional tau and (A) logical memory delayed recall (LM-II) scores, (B) total utterance time, (C) log of total between-utterance pause time, (D) number of between-utterance pauses, (E) speech rate (words per minute), and (F) percentage of unique words. Residuals after controlling for age, sex, education, and amyloid status are plotted on the x- and y-axes, and were calculated for visualization of the independent effects of regional tau PET on LM-II and speech metrics. Black boxes denote significant associations.

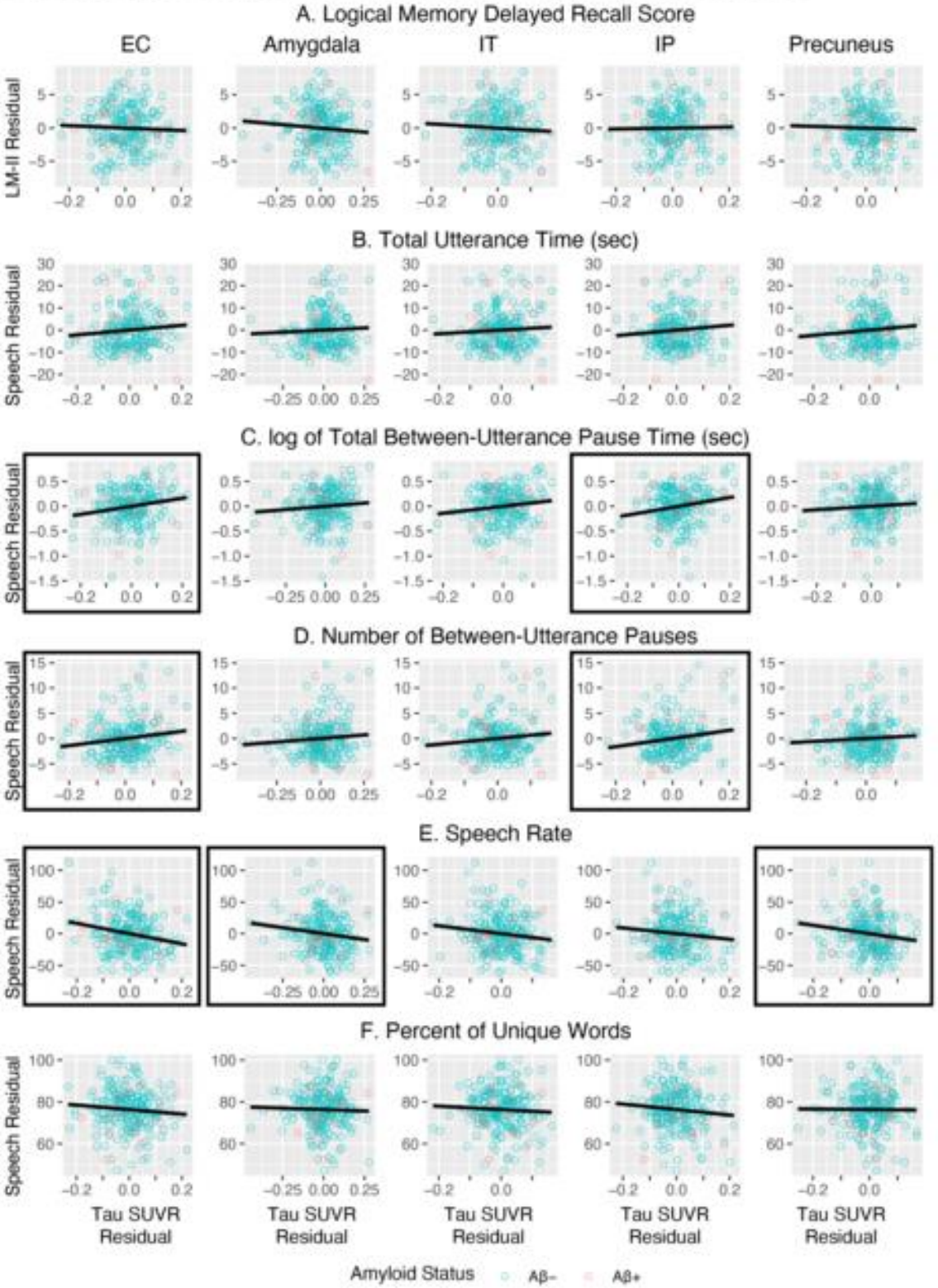

Table 1. Demographic and speech characteristics. Note: NP = neuropsychological assessment.

	n=237
Age at tau PET scan (years)	
Mean (SD)	55 (8)
Median (Min, Max)	55 (32, 75)
Sex	
Female, n (%)	121 (51.1%)
Male, n (%)	116 (48.9%)
Education	
High School or Less, n (%)	26 (11.0%)
Some College, n (%)	70 (29.5%)
College, n (%)	141 (59.5%)
Amyloid Status	
Aβ-, n (%)	210 (88.6%)
Aβ+, n (%)	18 (7.6%)
Unknown, n (%)	9 (3.8%)
Days between tau PET and amyloid PET	
Mean (SD)	0.4 (11.7)
Median (Min, Max)	0.0 (-62.8, 0.3)
Days between tau PET and closest NP	
Mean (SD)	-63.9 (55.8)
Median (Min, Max)	-47.8 (-327.8, -1.1)

Table 2. Amyloid status associations with logical memory (LM) delayed recall score and speech metrics. Each row represents a separate multiple regression model with amyloid status, age, sex, and education predicting logical memory or speech.

	Aβ+ vs. Aβ-	Age	Male vs. Female	Some College vs. HS or Less	College vs. HS or Less
Neuropsychological Score					
LM Delayed Recall Score	-0.908 (0.868); p = 0.297	-0.040 (0.029); p = 0.177	**-2.307 (0.451); p < 0.001**	1.115 (0.802); p = 0.166	**3.294 (0.749); p < 0.001**
Speech Metrics					
Utterance Time	2.490 (2.288); p = 0.278	0.120 (0.078); p = 0.129	**-3.848 (1.202); p = 0.002**	-0.720 (2.170); p = 0.740	1.857 (2.050); p = 0.366
Log of Between-Utterance Pause Time	-0.003 (0.094); p = 0.976	-0.001 (0.003); p = 0.665	0.012 (0.049); p = 0.807	-0.029 (0.089); p = 0.744	-0.096 (0.084); p = 0.255
# Between-Utterance Pauses	1.349 (0.967); p = 0.164	-0.025 (0.033); p = 0.455	-0.614 (0.508); p = 0.228	-1.152 (0.917); p = 0.211	-1.035 (0.867); p = 0.234
Speech Rate	-1.821 (7.844); p = 0.817	0.009 (0.269); p = 0.972	-3.776 (4.120); p = 0.360	-5.673 (7.442); p = 0.447	3.286 (7.029); p = 0.641
% Unique Words	-0.837 (2.509); p = 0.739	**-0.195 (0.086); p = 0.024**	1.588 (1.318); p = 0.230	2.232 (2.381); p = 0.349	0.733 (2.249); p = 0.745

Table 3. Regional tau associations with logical memory (LM) delayed recall score and speech metrics. Each cell provides results from separate multiple regression models with regional tau predicting LM or speech. Amyloid status was not significant in any model (effects not shown).

	Regional Tau PET					
	EC	Amygdala	IT	IP	Precuneus	Putamen
A. Controlling for age, sex, education, and amyloid status						
LM Delayed Recall Score	-1.991 (2.816); p = 0.480	-1.979 (2.012); p = 0.326	-3.161 (3.434); p = 0.358	1.134 (3.110); p = 0.716	-1.336 (3.313); p = 0.687	-0.586 (1.633); p = 0.720
Utterance Time	10.809 (7.446); p = 0.148	3.739 (5.424); p = 0.491	8.123 (9.179); p = 0.377	10.999 (8.183); p = 0.180	11.909 (8.717); p = 0.173	3.035 (4.356); p = 0.487
Log of Between-Utterance Pause Time	**0.815 (0.302); p = 0.008**	0.261 (0.222); p = 0.241	0.701 (0.374); p = 0.062	**0.893 (0.332); p = 0.008**	0.344 (0.359); p = 0.338	0.084 (0.179); p = 0.640
# Between-Utterance Pauses	**7.023 (3.126); p = 0.026**	2.752 (2.288); p = 0.230	6.376 (3.863); p = 0.100	**8.064 (3.429); p = 0.020**	3.261 (3.694); p = 0.378	1.696 (1.840); p = 0.358
Speech Rate	**-80.476 (25.060); p = 0.002**	**-37.159 (18.446); p = 0.045**	-61.112 (31.254); p = 0.052	-44.410 (28.013); p = 0.114	**-65.505 (29.683); p = 0.028**	-23.723 (14.866); p = 0.112
% Unique Words	-10.787 (8.175); p = 0.188	-2.665 (5.954); p = 0.655	-8.163 (10.072); p = 0.419	-13.175 (8.969); p = 0.143	-1.194 (9.603); p = 0.901	0.264 (4.784); p = 0.956

Keywords: Tau PET, Amyloid PET, speech, cognition, aging

Default mode network connectivity tracks with amyloid age and predicts conversion to amyloidosis, mild cognitive impairment and dementia across the Alzheimer's disease spectrum

Nick Corriveau-Lecavalier[1], Ellen Dicks[1], Peter Martin[1], Emily Lundt[1], Heather Wiste[1], Jeffrey Gunter[1], Michael Kamykowski[1], Matthew Senjem[1], Christopher Schwarz[1], Hugo Botha[1], Jonathan Graff-Radford[1], Mary Machulda[1], Julie Fields[1], Brad Boeve[1], Val Lowe[1], David Knopman[1], Ronald Petersen[1], Clifford Jack[1], David Jones[1]

[1]*Mayo Clinic, Rochester, MN, United States*

There exists a close biological interrelationship between large-scale functional dyshomeostasis and amyloid accumulation in Alzheimer's disease (AD). We assessed longitudinal patterns of default mode network (DMN) connectivity dynamics across the AD spectrum using task-free functional magnetic resonance imaging. We then examined their predictive value for conversion to amyloidosis, mild cognitive impairment (MCI) and dementia. This was done in 1451 individuals spanning the clinico-pathological spectrum of AD from Mayo Clinic research programs (ADRC, MCSA). All participants included for analysis were either amyloid-positive (A+) at baseline or converted from amyloid-negative (A-) to A+ over the time course of data collection. We leveraged quantile curves to generate age-adjusted connectivity *Z* scores for the posterior DMN (pDMN), anterior dorsal DMN (adDMN), ventral DMN (vDMN) and a global marker of DMN failure (network failure quotient; NFQ) based on a normative cohort of 758 A-T- cognitively unimpaired (CU) individuals. We then used a non-linear mixed effects model (Therneau et al., 2021) to calculate the "amyloid age" of participants, which measures their position in their amyloid progression trajectory based on their global amyloid-PET standard uptake ratio value adjusting for participant-specific covariates (age, sex, education, *APOE*). We used Bayesian mixed-effect modelling which showed decreases in pDMN and vDMN connectivity and increases in NFQ values with increasing amyloid age across the AD spectrum, while adDMN connectivity remained stable (Fig. 1). Survival analyses revealed that low connectivity across all metrics (pDMN, vDMN, adDMN, NFQ) predicted conversion to amyloidosis (i.e., A- to A+), low pDMN and vDMN connectivity predicted conversion from CU to MCI, and higher NFQ predicted conversion from CU or MCI to dementia (Fig. 2). We demonstrate that longitudinal DMN connectivity correlates with amyloid pathophysiology across the AD spectrum and predicts conversion to critical stages of the disease. Importantly, these abnormal connectivity changes precede amyloidosis detectable on imaging.

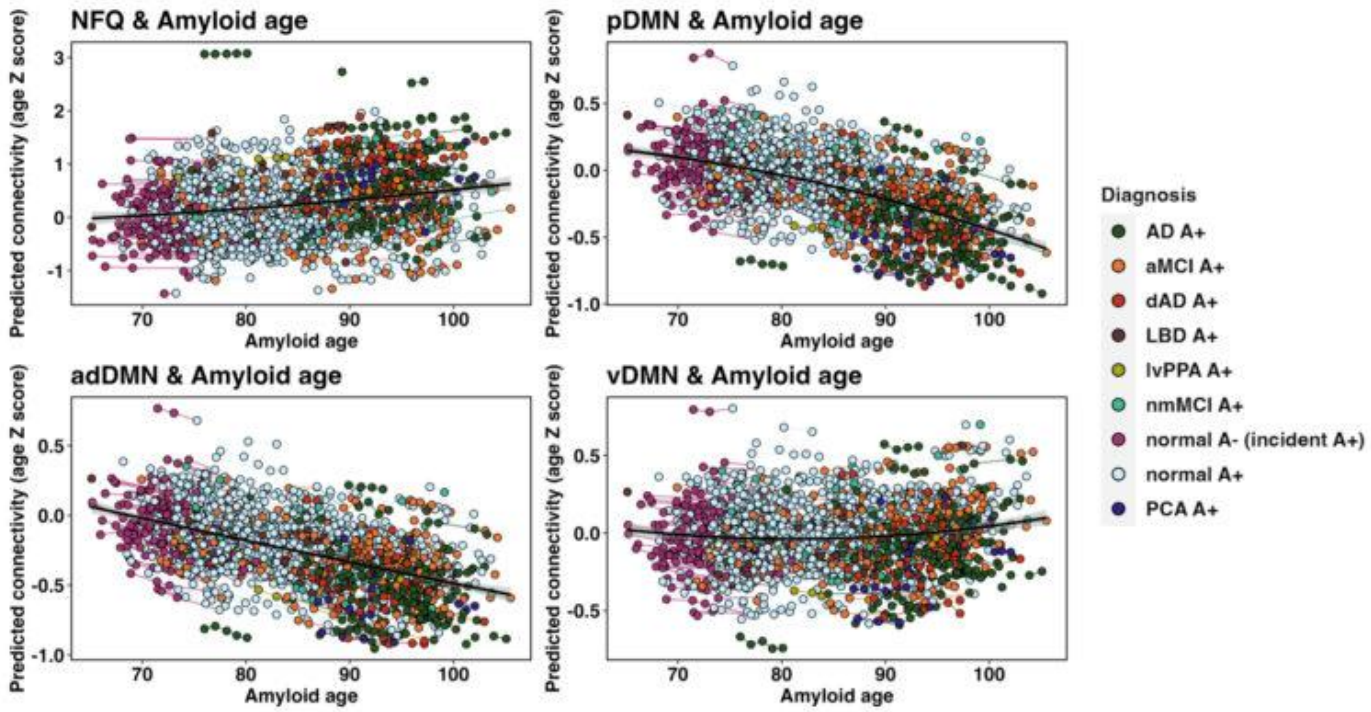

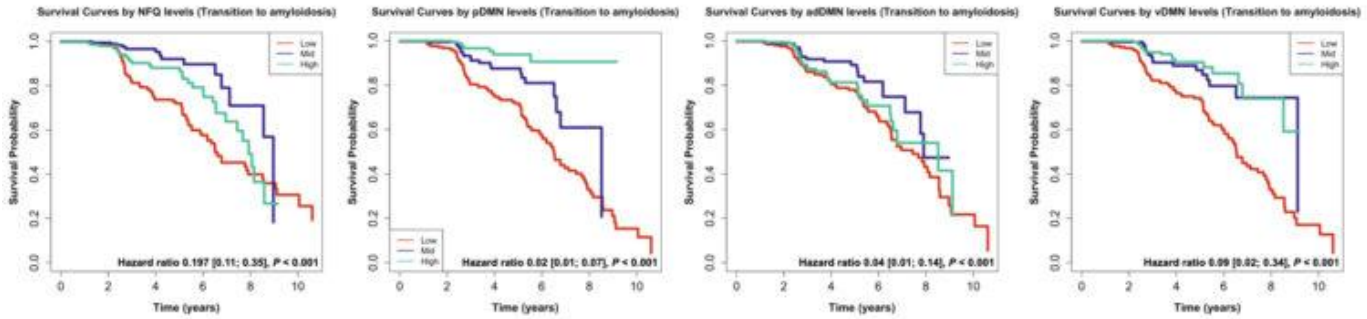

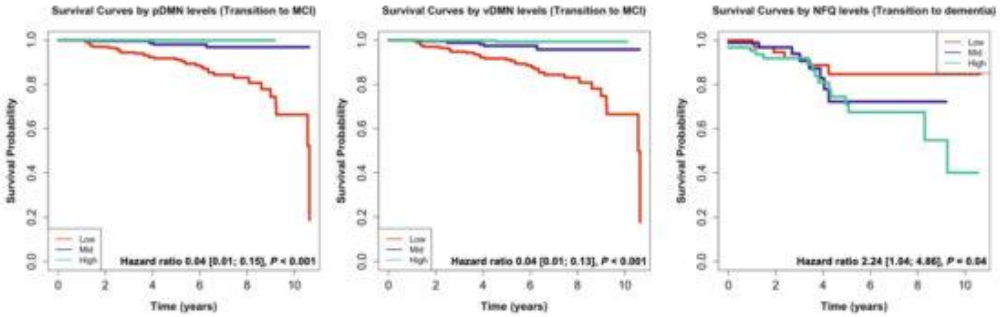

Keywords: Default mode network; Functional connectivity; Amyloidosis; Network failure quotient; Cascading network failure

Higher locus coeruleus integrity and cognitive reserve attenuate tau-related cognitive decline in older adults

Lukas Heinrich[1,2], Joost M Riphagen[1], Elouise A Koops[1], Kathryn V Papp[4], Dorene M Rentz[3,4], Reisa A Sperling[3,4], Keith A Johnson[1,3,4], Heidi IL Jacobs[1]

[1]*Department of Radiology, Massachusetts General Hospital / Harvard Medical School, Boston, MA, United States*
[2]*Faculty of Psychology and Neuroscience, Maastricht University, Maastricht, The Netherlands*
[3]*Department of Neurology, Massachusetts General Hospital/ Harvard Medical School, Boston, MA, United States*
[4]*Center for Alzheimer Research and Treatment, Department of Neurology, Brigham and Women's Hospital, Boston, MA, United States*

Background: The biological basis for cognitive reserve (CR) remains poorly understood. Previous research suggested that locus coeruleus (LC) integrity may contribute to the neural substrate providing CR, as demonstrated by positive associations between CR and MRI-based integrity of the LC, one of the first regions to accumulate tau pathology. We aimed to investigate whether higher MRI-based integrity of the LC allows the brain to withstand cognitive decline related to Alzheimer's disease pathology in individuals with higher cognitive reserve.

Methods: Individuals (n=190) with LC MRI, 18F-Flortaucipir (FTP-tau), and 11C-Pittsburgh Compound-B (PIB) PET were selected from the Harvard Aging Brain Study (Figure 1). Cognition over time was assessed using PACC5. For cognitive reserve, a composite score was constructed by z-scoring verbal IQ, years of education, and the inverse Hollingshead scale of occupational attainment. Multiple linear regression associated cognitive reserve and LC integrity. K-means cluster analysis was performed to group individuals based on cognitive reserve and entorhinal FTP or neocortical PIB. Linear mixed effects modeling evaluated the relationship between LC MRI-integrity and cognition over time across the cluster-derived tau-cognitive reserve groups (age and sex included as covariates).

Results: Higher cognitive reserve composite scores were associated with higher LC integrity. Cluster analysis identified three groups (Figure 2): high tau/high CR; low tau/high CR, and low tau/low CR. Similar clusters were identified using PIB. The high tau/high CR cluster showed less steep cognitive decline in a dose-response manner of LC integrity compared to steeper decline in individuals in the low tau/low CR (β = -2.69, df =103.7, $p < 0.001$) (Figure 3). This effect was not significant for amyloid-beta.

Conclusion: The study revealed that higher LC integrity may contribute to attenuated cognitive decline in individuals with higher CR and elevated entorhinal tau. Future research aims to extend this research to LC function and networks.

N	190
Demographics	
Age	72 (9.6)
Biological Sex(f)	110 (58%)
ApoE4-Carriers	47 (25%) / (9 missing)
MMSE	28.7 (1.6)
Years of Education	16.2 (3.0)
Hollingshead Score	25.4 (14)
Verbal IQ	121.9 (8.3)
PACC5 follow-up time	4.1 (1.2)
Clinical Characteristics	
PIB+	50 (26%) / (3 missing)
CDR: 0 / >0.5	173 (91%) / 17 (9%)

Figure 1 Demographics. *Abbreviations: SD = standard deviation, f = female, ApoE4 = apolipoprotein E4, MMSE = mini mental state examination, PIB+ = individuals with 11C-Pittsburgh Compound-B mean values above clinical cut off (>1.24), CDR = clinical dementia rating (0 = absent, 0.5 = mild, 1 = moderate, 2/3 = severe). Data is presented as means and (standard deviations), and counts and (percentages) for sex, ApoE4, PIB+ and CDR scores.*

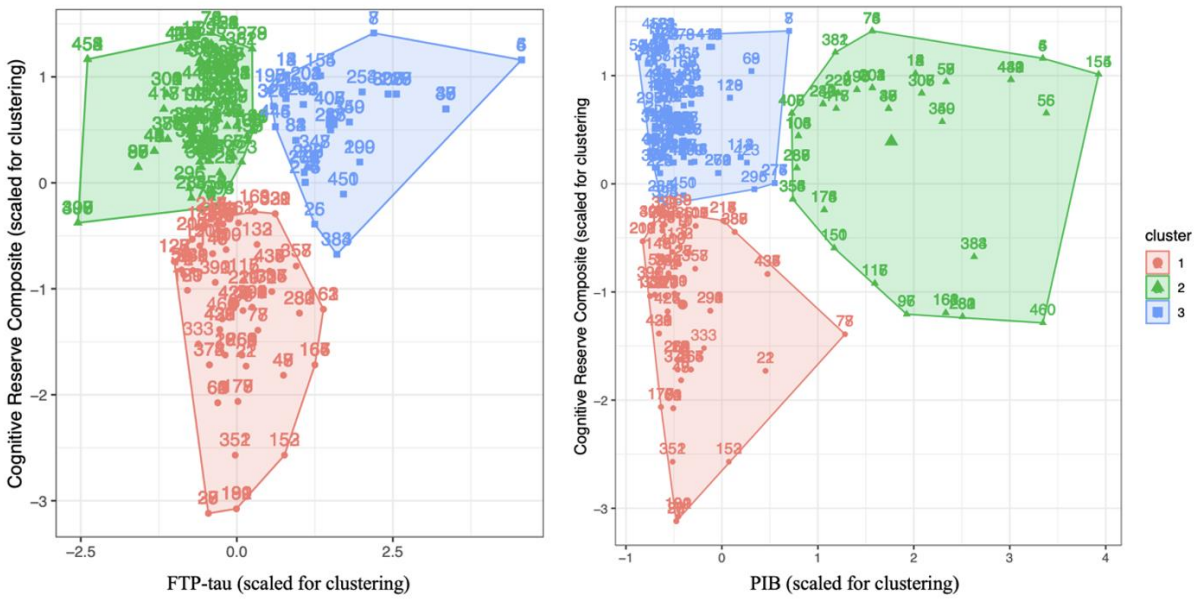

Figure 2 Illustration of grouping based on Hartigan-Wang cluster algorithm. *The clusters reflect three groups. On the left: Low tau/low CR (Cluster 1, red), low tau/high CR (Cluster 2, green), and high tau/high CR (Cluster 3, blue). On the right: Low PIB/ low CR (Cluster 1, red), high PIB/ high CR (Cluster 2, green), and low PIB/high CR (Cluster3, blue). Note that the units reflect scaled variables, as necessary for clustering.*

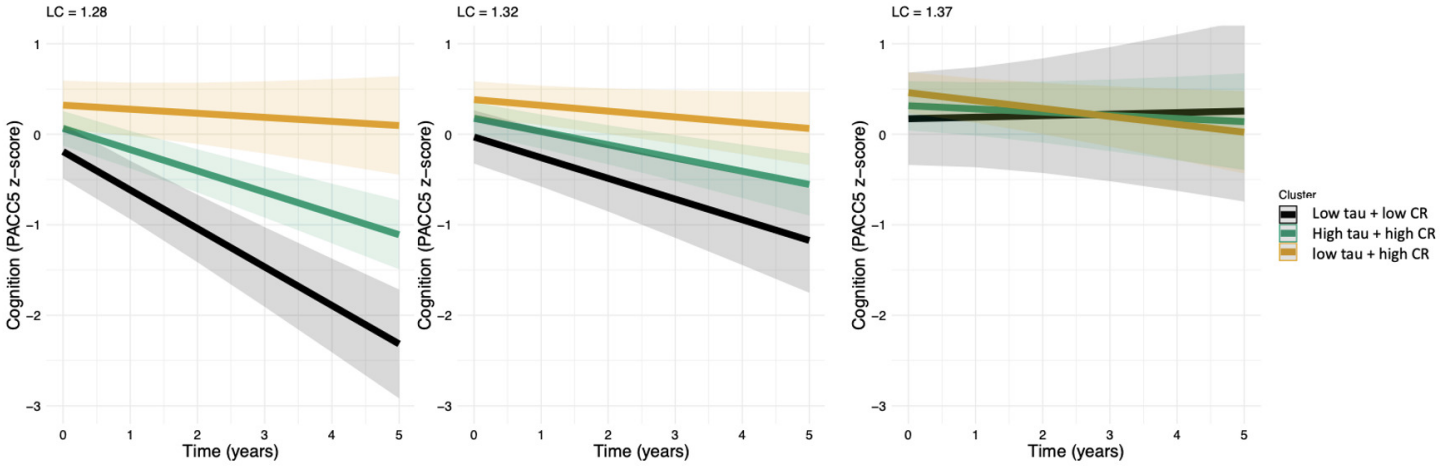

Figure 3 Effect of LC integrity on cognitive changes across the cluster groups of tau and cognitive reserve. *Cognitive performance does not differ when LC integrity is high (right panel). The high tau/high CR cluster showed less steep cognitive decline in a dose-response manner of LC integrity compared to steeper decline in individuals in the low tau/low CR. At lower levels of LC integrity, we see a differential effect that depends on tau burden and cognitive reserve. Note that LC integrity was used as a continuous variable in the analysis but is presented categorically for visualisation. LC values represent mean (LC = 1.32), and one standard deviation above and below the mean. Shaded areas represent confidence intervals.*

Keywords: cognitive reserve, locus coeruleus, amyloid-beta, tau, aging

Thursday, January 18, 2024 - 01:00 pm - 02:30 pm

Podium Session

SESSION VII: Associations with longitudinal Tau PET

CHAIRS: Ann Cohen, Gil Rabinovici

Thursday, January 18, 2024		
01:00 pm - 02:30 pm	**SESSION VII: Associations with longitudinal Tau PET**	**Elizabeth Mormino, Stanford University, Palo Alto, CA, United States** **Susan Landau, University of California, Berkeley, CA, United States**
01:00	Introduction	Chairs
01:05	Large-sample, longitudinal tau-PET in sporadic early-onset Alzheimer's disease: Findings from the LEADS Consortium	Schonhaut | Insel | Soleimani-Meigooni | Zeltzer | Windon | Mundada | Maiti | Shankar | Amuiri | Koeppe | Carrillo | Apostolova | Rabinovici | La Joie
01:20	Associations between CSF alpha-synuclein pathology and longitudinal Aβ- and tau-PET	Pichet Binette | Mammana | Wisse | Rossi | Strandberg | Janelidze | Palmqvist | Parchi | Hansson
01:35	Baseline PET predictors of neocortical tau accumulation and cognitive decline in the A4 study	Sanchez | Properzi | Schultz | Thibault | Becker | Shcherbinin | Kotari | Yaari | Sims | Sperling | Aisen | Johnson
01:50	A meta-analysis of sex differences in longitudinal tau-PET in clinically normal adults	Coughlan | Klinger | Boyle | Betthauser | Christenson | Healy | Jacobs | Jonaitis | Jack | Johnson | Langhough | Properzi | Rentz | Schultz | Seto | Johnson | Mielke | Sperling | Vemuri | Buckley
02:05	Discussion	

Large-sample, longitudinal tau-PET in sporadic early-onset Alzheimer's disease: findings from the LEADS Consortium

Daniel Schonhaut[1], Philip Insel[1], David Soleimani-Meigooni[1], Ehud Zeltzer[1], Charles Windon[1], Nidhi Mundada[1], Piyush Maiti[1], Ranjani Shankar[1], Alinda Amuiri[1], Robert Koeppe[2], Maria Carrillo[3], Liana Apostolova[4], Gil Rabinovici[1], Renaud La Joie[1]

[1]*University of California, San Francisco, San Francisco, CA, United States*
[2]*University of Michigan, Ann Arbor, MI, United States*
[3]*Alzheimer's Association, Chicago, IL, United States*
[4]*Indiana University, Indianapolis, IN, United States*

Introduction: Longitudinal tau-PET trajectories in early-onset Alzheimer's disease (EOAD, age-at-onset<65) have not been established and are needed to optimize tau-PET as an outcome measure in clinical trials. Here we model tau-PET accumulation in three meta-ROIs with high AD-tau burden in the Longitudinal Early-onset Alzheimer's Disease Study.

Methods: Longitudinal [^{18}F]Flortaucipir-PET (FTP) scans were acquired in 167 amyloid-PET-positive, sporadic EOAD patients with MCI or mild dementia due to AD (**Table 1**). FTP scans were normalized against inferior cerebellar GM, and mean SUVRs were calculated in three meta-ROIs comprising temporal (Jack et al., 2016), parietal, and frontal association cortices (**Figure 1A**). Linear mixed-effects models assessed baseline SUVR and rate-of-change differences between regions. Penalized cubic-spline regressions modeled rate-of-change by baseline SUVR associations within-region. The fitted spline functions defined first-order differential equations that were solved with Euler's modified method, yielding regional tau trajectories over time. An exhaustive search algorithm identified time lags between regional trajectories that best fit the baseline data.

Results: FTP SUVRs increased longitudinally in most patients, including those with lowest baseline values (**Figure 1B, 2A**). Baseline SUVRs were significantly higher in parietal (2.24±0.61, mean±SD) than temporal (2.10±0.47) regions, and lowest in frontal cortex (1.79±0.55; all Bonferroni-Holm-corrected $P<0.001$; **Figure 1C**). Conversely, annualized rates-of-change were highest in frontal (0.10±0.12), then temporal (0.09±0.12), then parietal (0.08±0.15) regions (Bonferroni-Holm-corrected $P<0.05$; **Figure 1D**). Baseline SUVR by rate-of-change associations were inverted U-shaped with peak accumulation near 1.9 SUVR (**Figure 2A,B**). Trajectory models showed parietal cortex leading the temporal meta-ROI by 0.6 years and the frontal meta-ROI by 5 years, with the full timecourse of FTP accumulation occurring over ~18 years from earliest detectable signal (**Figure 2C**).

Conclusions: Tau-PET in the frontal meta-ROI is lower than temporal or parietal signal at baseline but has faster prospective accumulation, suggesting this region could be optimal for trials in symptomatic EOAD patients.

Number of EOAD patients	167
Flortaucipir scans per patient	2.5 ± 0.7 (range: 2-4)
Years followed	1.8 ± 0.9
Inter-scan interval	1.3 ± 0.4
Sex	F: 94 (56%) M: 73 (44%)
Age at baseline	59.3 ± 4.1
APOE-ε4 alleles	0: 74 (47% of known) 1: 64 (41% of known) 2: 20 (13% of known) Not known: 9 (5%)
Baseline Amyloid-PET Centiloids	95.9 ± 25.9
Baseline CDR Sum of Boxes	3.7 ± 1.7
Baseline MMSE	21.8 ± 5.0

Table 1. Patient demographics. Values are reported as mean ± standard deviation across patients.

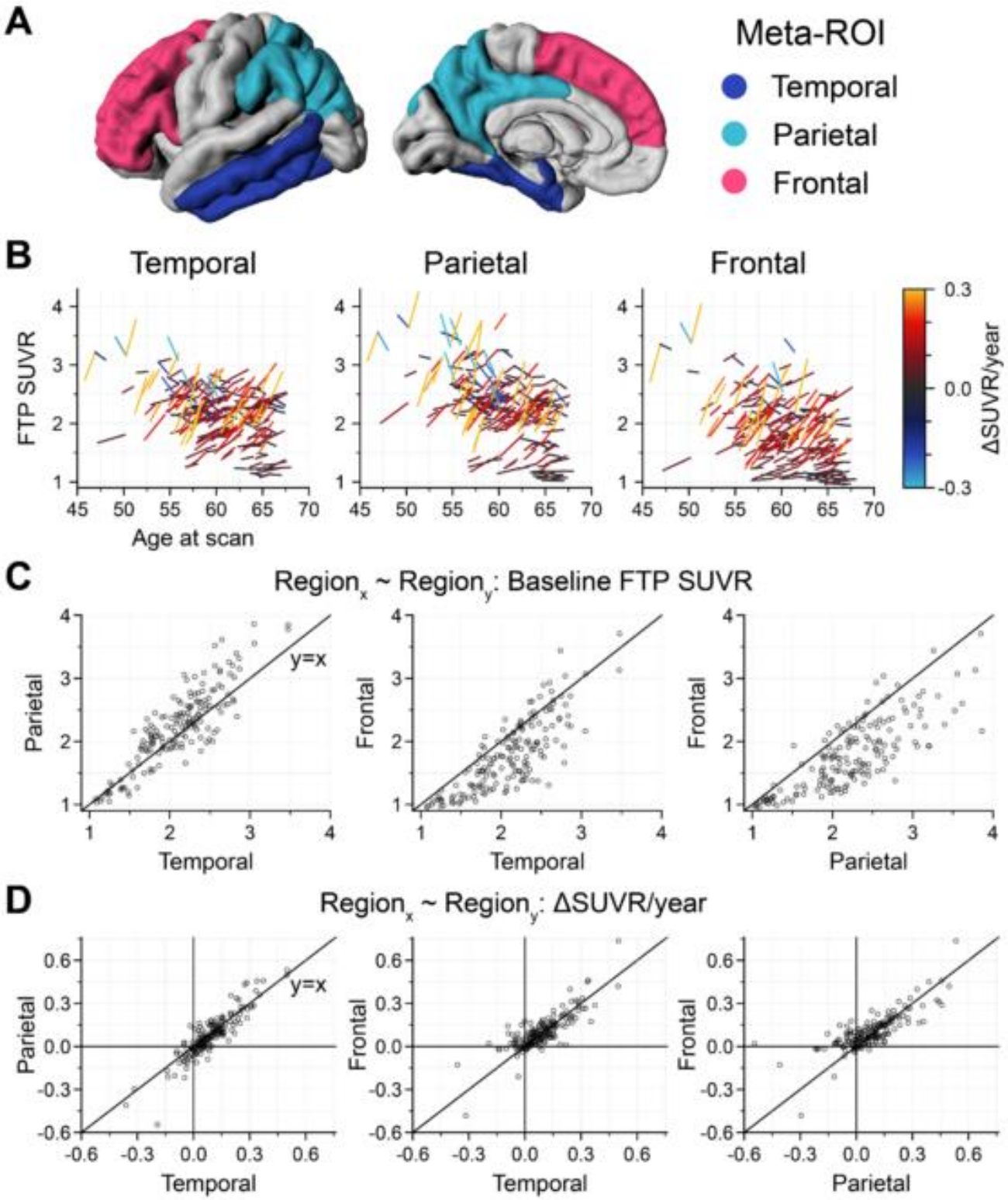

Figure 1. Baseline tau-PET and longitudinal rates-of-change in EOAD. (A) Bilateral meta-ROIs are shown in one hemishere for visual comparison. **(B)** Spaghetti plots show mean [18F]Flortaucipir SUVRs in 167 EOAD patients separated by age at scan. Lines connect visits within-patient, with line color indicating the annualized SUVR change between visits. **(C, D)** FTP SUVRs at baseline (**C**) and annualized SUVR rates-of-change (**D**) are compared between each pair of meta-ROIs (1 point = 1 patient).

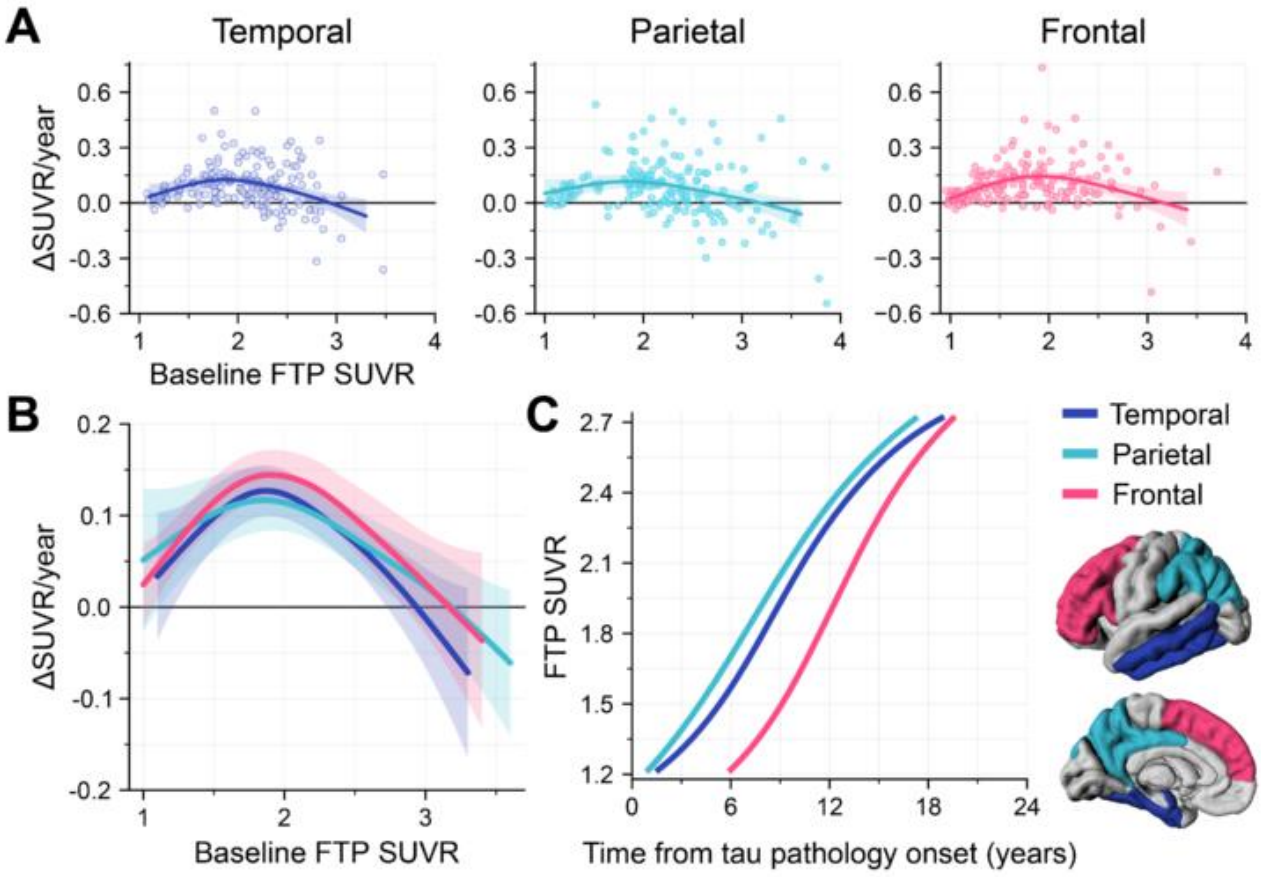

Figure 2. Longitudinal tau-PET trajectories in meta-ROIs. (A) Baseline [18F]Flortaucipir SUVRs are plotted against annualized change rates across 167 EOAD patients (1 point = 1 patient) in each meta-ROI. Cubic spline fits with 95% confidence intervals are shown. **(B)** Same cubic spline fits as in **A**, at higher scaling. **(C)** Estimated FTP accumulation trajectories from time of first detectable increase in the earliest meta-ROI.

Keywords: tau-PET, Flortaucipir, EOAD, longitudinal, LEADS

Associations between CSF alpha-synuclein pathology and longitudinal Aβ- and tau-PET

Alexa Pichet Binette[1], Angela Mammana[2], Laura Wisse[3], Marcello Rossi[2], Olof Strandberg[1], Shorena Janelidze[1], Sebastian Palmqvist[1,4], Piero Parchi[2,5], Oskar Hansson[1,4]

[1]*Clinical Memory Research Unit, Department of Clinical Sciences Malmö, Lund University, Lund, Sweden*
[2]*Istituto delle Scienze Neurologiche di Bologna (ISNB), Bologna, Italy*
[3]*Diagnostic Radiology Unit, Department of Clinical Sciences Lund, Lund University, Lund, Sweden*
[4]*Memory Clinic, Skåne University Hospital, Malmö, Sweden*
[5]*Department of Biomedical and Neuromotor Sciences, University of Bologna, Bologna, Italy*

Background: Experimental studies suggest that misfolded alpha-synuclein (α-syn) might interact with abnormal Aβ and tau aggregates in significant ways. However, longitudinal studies investigating such potential interactions in humans are lacking. Therefore, we analyzed longitudinal accumulation of Aβ and tau aggregates with PET in individuals with or without evidence of misfolded a-syn.

Methods: We included BioFINDER-2 participants (n=633) with baseline α-syn status (Negative or Positive) based on CSF seed amplification assay (Palmqvist et al, *Nature Medicine*, 2023), longitudinal Aβ- (flutemetamol) and tau-PET (RO948) (Table 1). Linear mixed effect models with random slope and intercept were fitted with longitudinal SUVR as outcome and the α-syn status*time as the main variable of interest. Statistical details are reported in Fig.1-2. Analyses were conducted in the whole sample (cognitively unimpaired and MCI participants) as well as in Aβ-negative or Aβ-positive subgroups (defined based on CSF Aβ42/40).

Table 1. Participants' characteristics

	α-syn negative (n=570)	α-syn positive (n=63)	p-value
Age (years)	65.08 ± 12.59	73.24 ± 7.34	<0.001
Sex M n (%M)	273 (48%)	43 (68%)	<0.001
Education (years)	12.78 ± 3.59	12.69 ± 3.51	0.89
APOEε4 carriers n (%)	267 (47%)	32 (51%)	0.93
Cognitive status Unimpaired: MCI	423:147	28:35	<0.001
Aβ status (based on CSF Aβ42/40) **Negative: Positive (% positive)**	383:187 (33%)	33:30 (48%)	0.03
Baseline Aβ-PET SUVR (flutemetamol; global neocortical ROI)	1.10 ± 0.31	1.22 ± 0.34	<0.001
Baseline tau-PET SUVR (RO948; temporal meta-ROI)	1.22 ± 0.26	1.21± 0.20	0.32
PET follow-up time	2.57 ± 0.98	2.61 ± 0.97	0.89

Data are presented as mean ± standard deviation unless specified otherwise. α-syn status was determined using a real-time, quaking-induced conversion assay (RT-QuIC; see Palmqvist et al, *Nature Medicine*, 2023). Abbreviations: Aβ= beta-amyloid; *APOE*ε4= apolipoprotein E genotype (carrying at least one ε4 allele); CSF= cerebrospinal fluid; M=male; MCI=mild cognitive impairment; PET= positron emission tomography; ROI=region of interest; SUVR= standardized uptake value ratio

Results: In the whole sample**,** α-syn positive participants had faster Aβ-PET SUVR increase in the global neocortical region (α-syn*time=0.03, p=0.004) compared to α-syn negative participants (Fig.1a). This increase was evident across many brain regions, particularly in lateral frontal and parietal regions (Fig.1b). There was no significant difference between α-syn positive and negative participants on tau-PET SUVR change over time, either in a temporal meta-ROI or in other brain regions (Fig.2). In participants who were Aβ-negative at baseline, there was a trend for faster Aβ-PET SUVR increase in the global neocortical region (α-syn*time=0.06, p=0.07), but not tau-PET. In Aβ-positive participants, no differences were found between α-syn positive and negative participants on longitudinal Aβ- nor tau-PET.

Figure 1. Effect of α-syn on longitudinal Aβ-PET

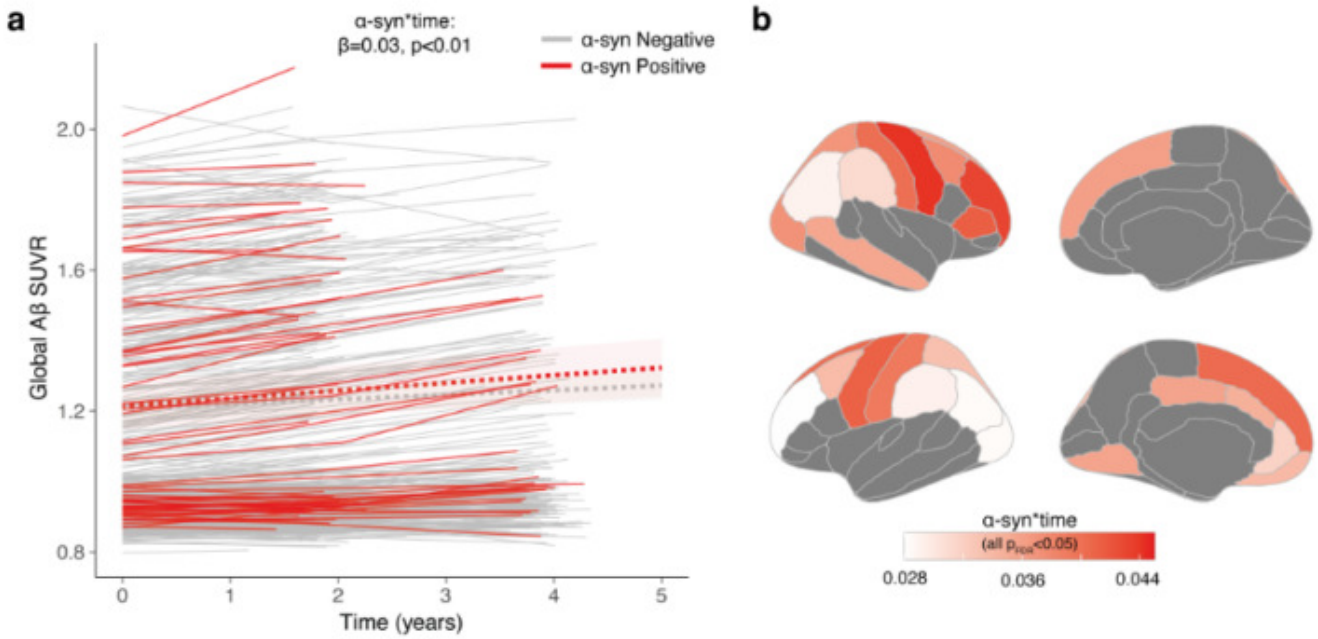

Linear mixed effect (LME) models investigating the effect of α-syn status on global neocortical Aβ (**a**), and on individual brain regions (**b**). LME models with random slope and intercept were fitted, including age, sex and cognitive status as covariates. In **a**, dashed lines correspond to the α-syn groups average from the fitted LME model. In **b**, colors correspond to the α-syn*time coefficient. Only regions significant at p_{FDR}<0.05 are depicted.
Of note, results remained the same when further adjusting for the CSF Aβ status, suggesting an effect of α-syn on change in Aβ-PET SUVR beyond the fact that α-syn positive participants are more Aβ-positive.
SUVR were generated using the whole cerebellum as reference region, but results were unchanged if using a composite reference region from the brainstem, eroded white matter and cerebellum.

Figure 2. Effect of α-syn on longitudinal tau-PET

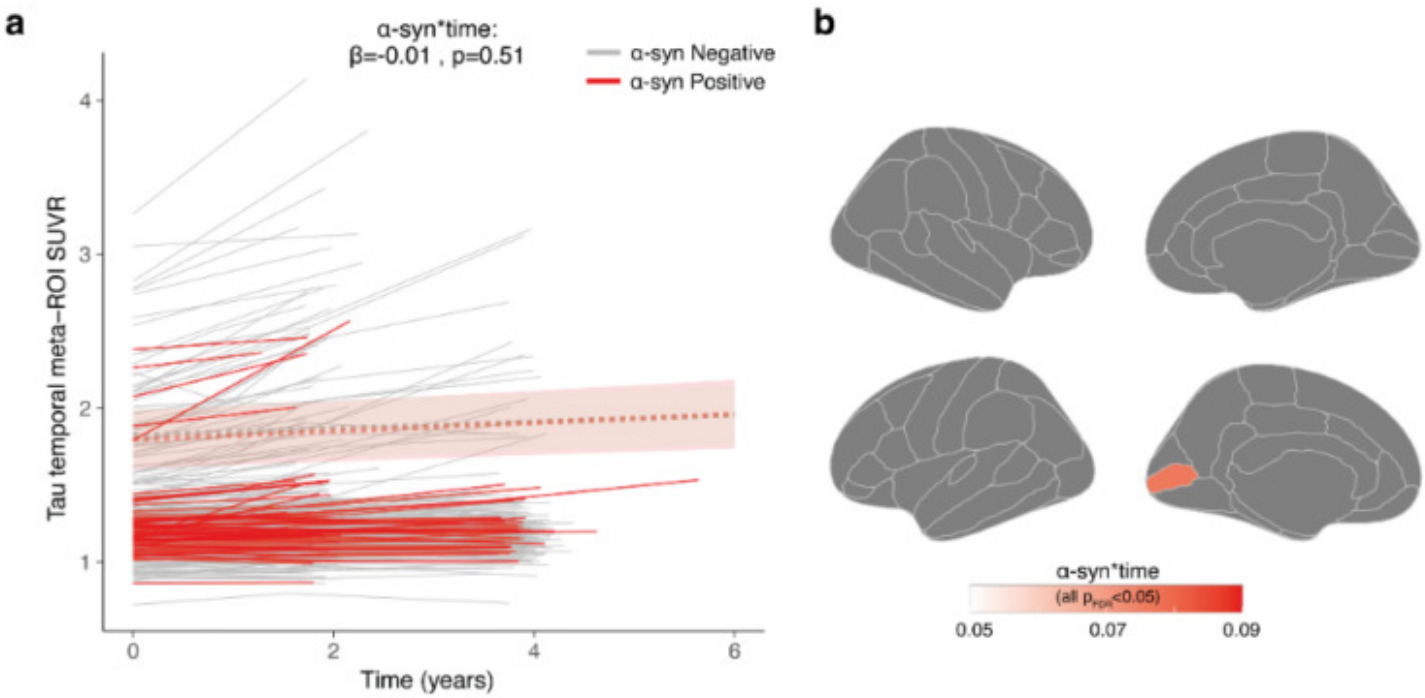

Linear mixed effect (LME) models investigating the effect of α-syn status on temporal meta-ROI tau (**a**), and on individual brain regions (**b**). LME models with random slope and intercept were fitted, including age, sex, cognitive status and baseline global Aβ-PET SUVR as covariates. In **a**, dashed lines correspond to the α-syn groups average from the fitted LME model. In **b**, colors correspond to the α-syn*time coefficient and the only significant region at $p_{FDR}<0.05$ was the left pericalcarine sulcus.
SUVR were generated using the inferior cerebellum cortex as reference region.

Conclusions: The presence of α-syn is associated with an increase of Aβ pathology over time, likely early on, as this was not the case in participants who were already Aβ-positive. The presence of α-syn was not associated with change in tau pathology over time.

Keywords: PET, Amyloid-beta, tau, alpha-synuclein, RT-QuIC

Baseline PET predictors of neocortical tau accumulation and cognitive decline in the A4 study

Justin Sanchez[1], Michael Properzi[1], Aaron Schultz[1], Emma Thibault[1], Alex Becker[1], Sergey Shcherbinin[2], Vikas Kotari[2], Roy Yaari[2], John Sims[2], Reisa Sperling[1], Paul Aisen[3], Keith Johnson[1]

[1]*Massachusetts General Hospital/Harvard Medical School, BOSTON, MA, United States*
[2]*Eli Lilly and Co, Indianapolis, IN, United States*
[3]*University of Southern California, San Diego, CA, United States*

Background: Cortical pathologic tau accumulation in Alzheimer's disease begins in the medial temporal lobe (MTL) and spreads to neocortex in association with cognitive decline. PET imaging measures that predict subsequent tau accumulation and cognitive decline would enable baseline screening to identify patients most likely to benefit from tau-targeted therapeutic strategies.

Methods: 258 participants from the A4 and LEARN studies who did not receive solanezumab were included in this study (Table 1). Participants underwent longitudinal tau (Flortaucipir) and amyloid-β (Florbetapir) PET and cognitive testing (PACC). Tau-PET was assessed in rhinal cortex (RC, MTL proxy), inferiortemporal cortex (IT, neocortex), and in surface vertices. Amyloid-β (Aβ) was measured in a neocortical aggregate region (FLR). Longitudinal data was modeled with subject-specific estimates of annualized change from LME models (baseline=first tau PET). Baseline PET measures were assessed in their ability to predict subsequent IT tau accumulation and cognitive decline using correlations and competitive models.

Results: Correlations between main variables of interest are shown in Figure 1. IT tau slope and PACC slope were associated with baseline PET predictors, whereas RC tau slope and Aβ slope were not. IT tau slope was positively correlated with RC tau slope and negatively correlated with PACC slope. In competitive models, RC tau was the strongest predictor of IT tau slope, explaining unique variance over baseline IT tau and Aβ (Fig. 2B). Surface-wide analyses confirmed that baseline MTL tau regions most strongly predicted IT tau accumulation (Fig. 2A). By contrast, baseline IT tau was the strongest predictor of PACC slope (Fig. 2D), with surface analyses confirming the strongest predictors with IT and nearby temporal neocortex (Fig 2C).

Conclusions: Baseline MTL tau outperformed other PET measures in predicting subsequent tau accumulation, whereas baseline IT tau predicted subsequent cognitive decline. Early intervention targeting MTL tau may prevent catastrophic tau accumulation in neocortex.

	LEARN	A4(placebo)	A4+LEARN
N	55	203	258
Longit. Tau	50 (90.9)	171 (84.2)	221 (85.7)
Longit. PACC	0 (0.0)	193 (95.1)	193 (74.8)
Years follow-up	3.4 ± 1.6 [0.0-5.5]	3.6 ± 1.9 [0.0-5.5]	3.6 ± 1.8 [0.0-5.5]
Age (Y)	69.7 ± 4.3 [65-84]	71.7 ± 4.9 [65-86]	71.3 ± 4.8 [65-86]
Females, N (%)	32 (58.2)	123 (60.6)	155 (60.1)
Education (Y)	16.6 ± 2.8 [12-26]	16.1 ± 2.8 [9-25]	16.2 ± 2.8 [9-26]
Aβ burden (FLR SUVr)	1.18 ± 0.07 [1.04-1.35]	1.48 ± 0.19 [1.10-2.23]	1.42 ± 0.21 [1.04-2.23]
MMSE	29.0 ± 1.0 [27-30]	28.6 ± 1.3 [24-30]	28.7 ± 1.3 [24-30]
APOEe4+ N (%)	14 (25.5)	119 (58.6)	133 (51.6)

Table 1: Demographics. Continuous variables: Mean +/- SD [range]. Categorical: N (%)

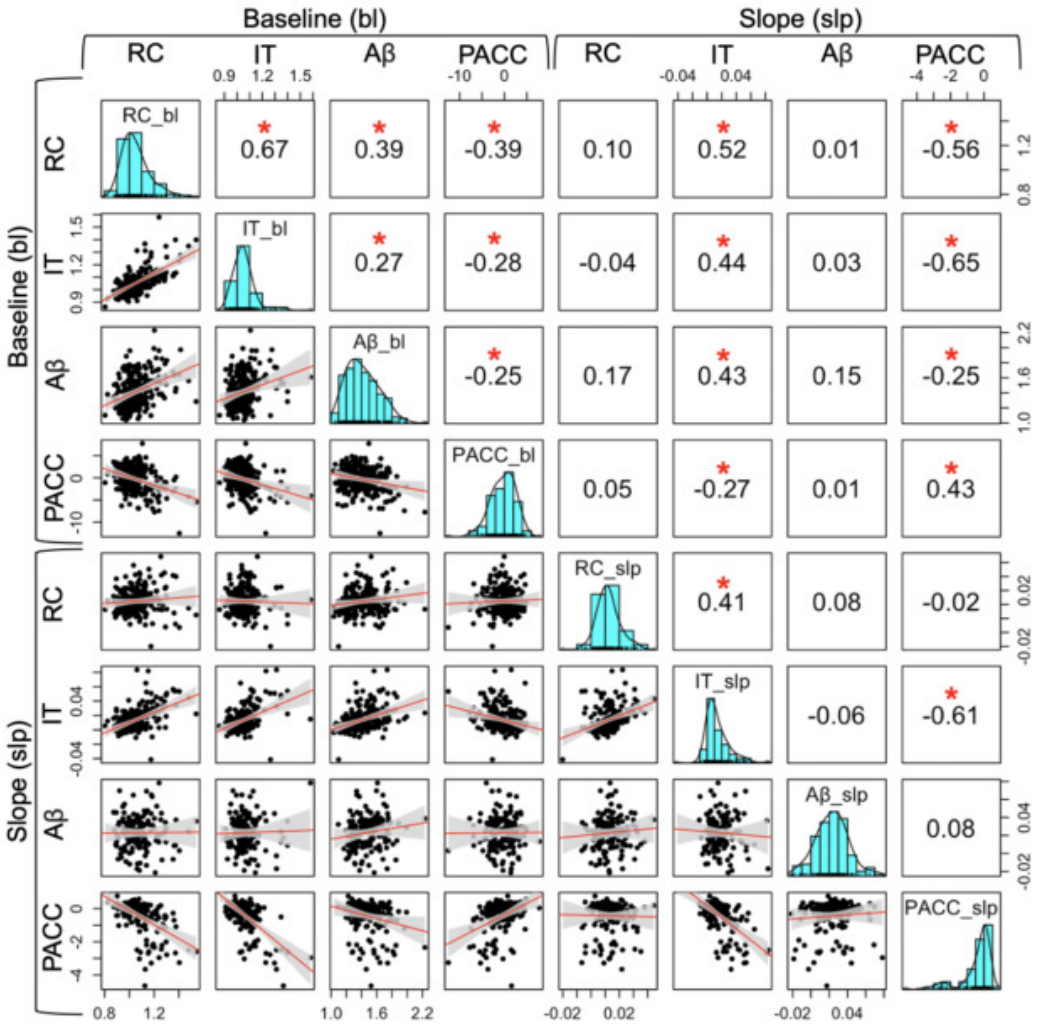

Figure 1: Correlations between PET surrogates and outcomes. RC=rhinal cortex tau; IT=inferior temporal cortex tau; Aβ = neocortical amyloid (Florbetapir SUVr), PACC=Preclinical Alzheimer Cognitive Composite. bl=baseline; slp=slope (i.e., annualized change rate). Bottom half of matrix shows scatter plot with linear model estimate (red) and 95% confidence interval overlay gray. Top half of matrix shows Pearson correlation; *indicates significant correlation after Bonferroni correction ($p<0.0018$).

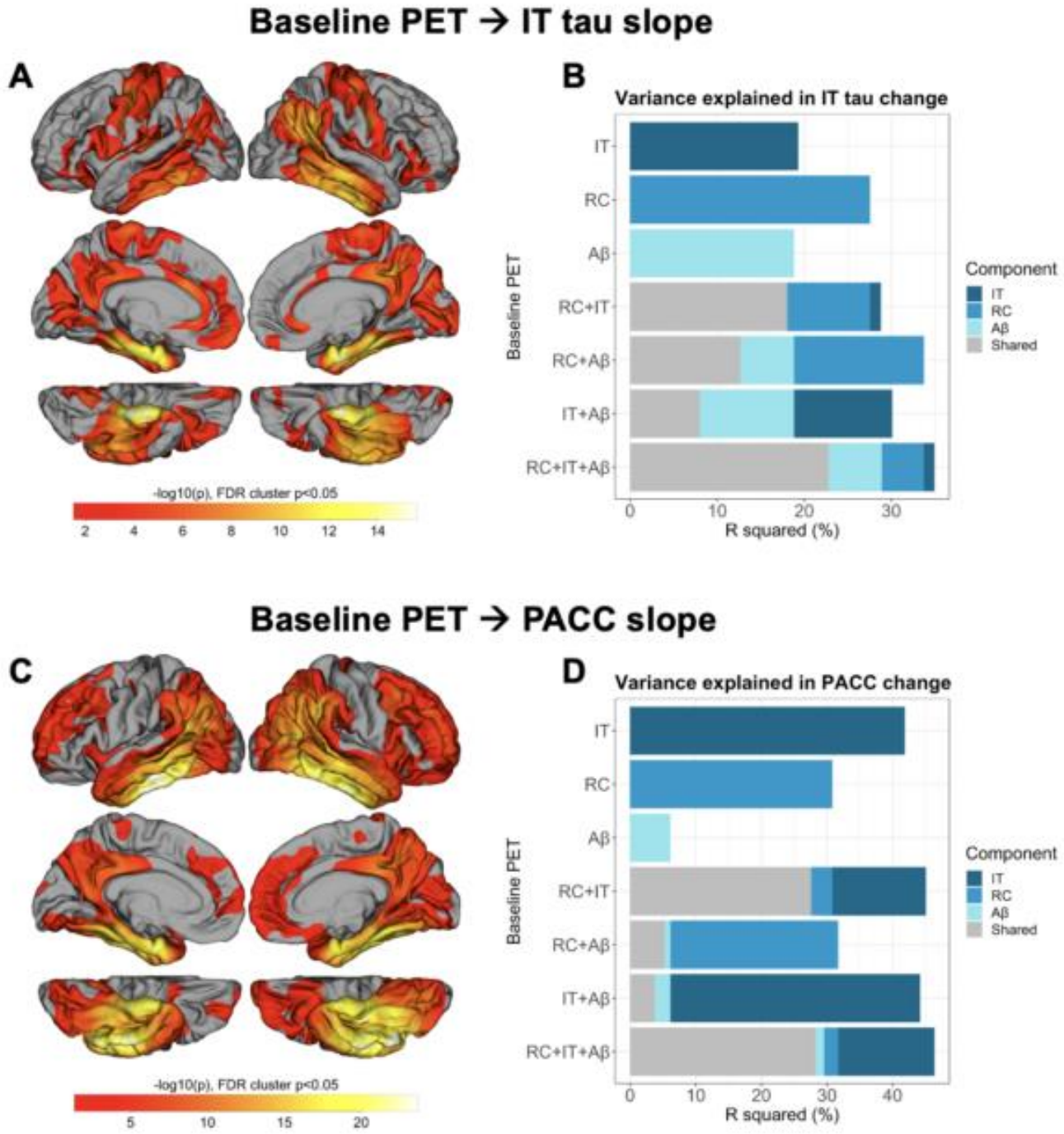

Figure 2: Baseline PET predicting subsequent change in IT tau, PACC. Surface maps (A,C) show correlations between vertex-wise baseline tau and subsequent change in IT tau (A) or PACC (C), as -log10(p) significant at $p<0.05$ after cluster-wise FDR correction. Bar plots show the proportion of variance in IT tau (B) or PACC (D) explained by baseline predictors, with color coding indicating shared vs. unique variance among predictors. RC=rhinal cortex tau; IT=inferior temporal cortex tau; Aβ =neocortical amyloid (Florbetapir SUVr), PACC=Preclinical Alzheimer Cognitive Composite.

Keywords: PET, MTL, tau, cognition, prediction

A meta-analysis of sex differences in longitudinal tau-PET in clinically normal adults

Gillian Coughlan[1], Hannah Klinger[1], Rory Boyle[1], Tobey Betthauser[2], Luke Christenson[3], Brian Healy[4], Heidi Jacobs[1], Erin Jonaitis[2], Clifford Jack[3], Keith Johnson[1], Rebecca Langhough[2], Michael Properzi[1], Dorene Rentz[1], Aaron Schultz[1], Mabel Seto[1], Sterling Johnson[2], Michelle Mielke[5], Reisa Sperling[1], Prashanthi Vemuri[3], Rachel Buckley[1]

[1]*Department of Neurology, Massachusetts General Hospital, Harvard Medical School, Boston, MA, United States*
[2]*Department of Medicine, University of Wisconsin-Madison, Madison, WI, United States*
[3]*Department of Radiology, Mayo Clinic Rochester, Rochester, MN, United States*
[4]*Harvard Public School of Health, Boston, MA, United States*
[5]*School of Medicine, Wake Forest University, Winston-Salem, NC, United States*

Cross-sectional sex differences in tau deposition are apparent in clinically normal older adults, particularly in the context of elevated β-amyloid (Aβ). However, the interpretation of cross-sectional studies on sex and tau deposition may be confounded by selective survival bias (i.e., excess dementia burden in women due to female longevity). To address this confound, we examined whether the longitudinal association between baseline Aβ status and regional tau differs between men and women.

1,286 clinically normal adults from four longitudinal cohorts including Alzheimer's Disease Neuroimaging Initiative, Harvard Aging Brain Study, Wisconsin Registry of Alzheimer's Prevention and Mayo Clinic Study of Aging (baseline age 70; 653 women [52%], 362 *APOE*ε4 carriers [32%]; Table) were scanned repeatedly with Aβ and tau-Positron Emission Tomography (PET). Time reflected years between baseline and final tau-PET (median time = 3 years[range 1-6]). Seven tau-PET SUVr regions of interest demonstrating cross-sectional sex differences were selected (entorhinal cortex, inferior temporal, rostral middle frontal, superior and inferior parietal lobule, temporal fusiform, and lateral occipital gyrus). For each cohort, random-effects models covarying baseline age*time, examined sex(men/women)* baseline Aβ(negative/positive)*time interactions on tau outcomes. Meta-analyses estimated the global fixed effect (β) and total heterogeneity across cohorts (t^2), with a Bonferroni corrected significance level (*p*=.013).

Among Aβ positive individuals, women exhibited significantly faster tau accumulation in the temporal fusiform gyrus(β=-.12[95%CI=-.17,-.06], t^2=.00 [SE=.004], *p*=.008) compared to men, with 0.13 SUVr annualised rate of change difference between the sexes. An uncorrected interaction was also observed in lateral occipital(β=-.16[95%CI=-.26,-.05], t^2=.00 [SE=.003],*p*=.018) and inferior temporal(β=-.14[95%CI=-.25,-.02], t^2=.00[SE=.003],*p*=.031) gyri.

Our results show that temporal fusiform tau accumulation is accelerated in Aβ positive women compared to Aβ positive men. These findings provide evidence of a sex-specific biological effect on regional tauopathy and provide an additional rationale for considering sex differences when designing anti-tauopathy clinical trials.

Table: Participant charateristics

	ADNI (n=226)		HABS (n=202)		WRAP (n=284)		MAYO (n=574)		Combined (n=1,286)
Characteristics	**Men**	**Women**	**Men**	**Women**	**Men**	**Women**	**Men**	**Women**	**Overall**
Total No. (%)	94 (42)	132 (58)	78 (40)	124(60)	63 (34)	121 (66)	298 (52)	276 (48)	1,286
Baseline tau-PET Age (S	74.3 (6.7)	72.5 (6.7)	74.9 (8.4)	72.2 (9.5)	67.6 (6.5)	67.4 (6.3)	67.4 (9.7)	66.7 (9.5)	70 (7.9)
APOE4 (%)	33 (35)	54 (41)	21 (27)	35 (28)	22 (35)	40 (33)	77 (26)	80 (29)	362 (32)
Aβ positive* (%)	24 (25)	41 (31)	20 (25.6)	22 (17.7)	12 (19)	16 (13)	89 (30)	82 (30)	306 (23)
Education (SD)	17.0 (2.4)	16.5 (2.4)	16.2 (3.2)	16.1 (2.7)	17.1 (2.2)	15.8 (2.4)	15.4 (3.2)	15 (3.5)	16.5 (2.7)
Tau-PET time (SD)	2.5 (1.4)	2.5 (1.4)	4.7 (1.7)	4.0 (1.4)	2.6 (0.9)	2.6 (0.9)	2.6 (1.5)	2.5 (1.4)	3.0 (1.3)

ADNI indicates, Alzheimer's Disease Neuroimaging Initiative; HABS, Harvard Aging Brain Study;
WRAP, Wisconsin Registry of Alzheimer's Prevention; MAYO: Mayo Clinic Study of Aging
*The Aβ positivity threshold was cohort specific

Figure 1. Sex Interaction With Aβ on Longitudinal tau-PET

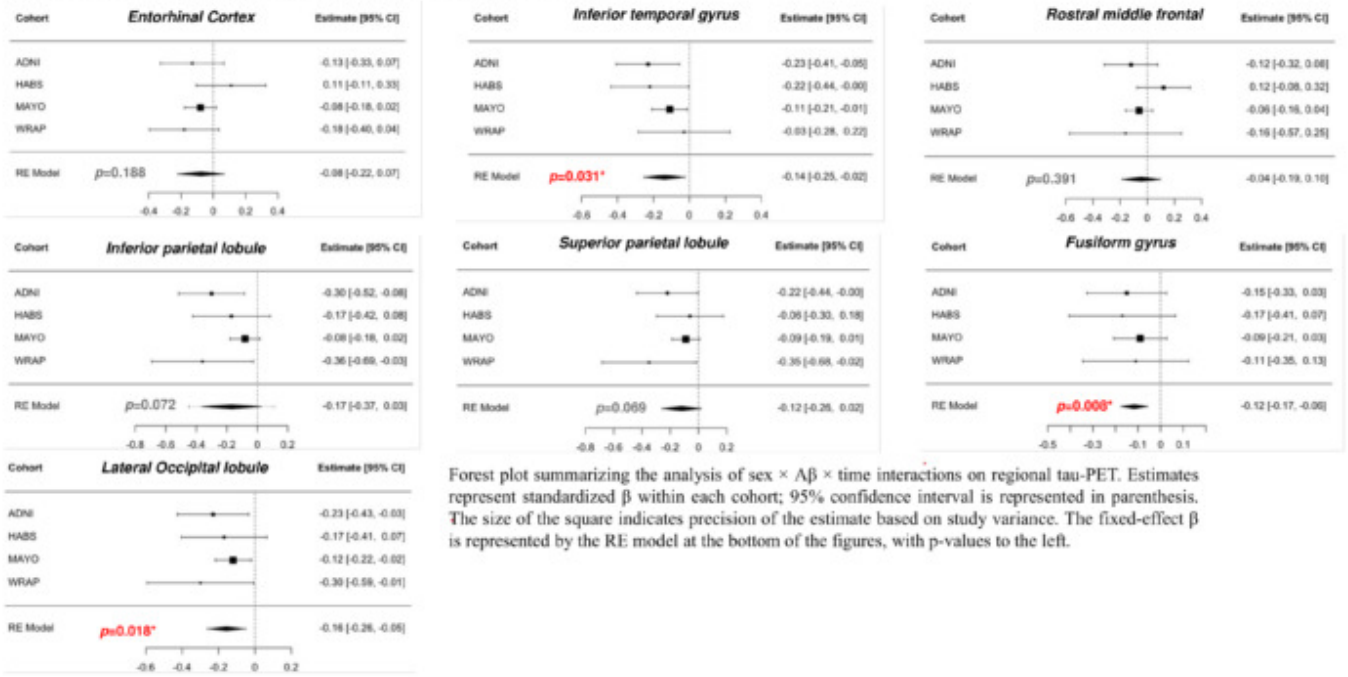

Forest plot summarizing the analysis of sex × Aβ × time interactions on regional tau-PET. Estimates represent standardized β within each cohort; 95% confidence interval is represented in parenthesis. The size of the square indicates precision of the estimate based on study variance. The fixed-effect β is represented by the RE model at the bottom of the figures, with p-values to the left.

Figure 2. Sex interaction With Aβ on Longitudinal Temporal Fusiform Tau-PET

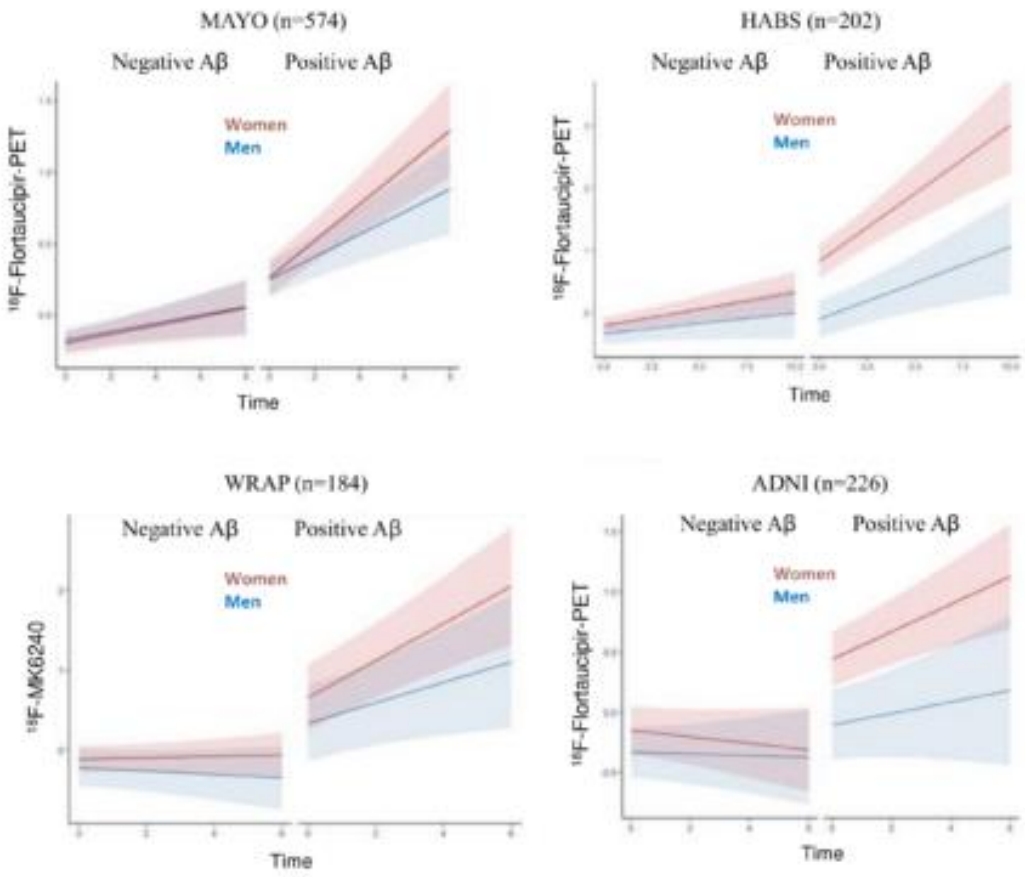

Keywords: Sex differences, tau-PET, preclinical Alzheimer's disease

KEYNOTE: Fluid and PET imaging markers for Alzheimer's disease and neuronal synuclein disease

Oskar Hansson

Lund University

There is need for biomarkers that improve the diagnostic work-up of neurodegenerative diseases, including Alzheimer's disease (AD) and Parkinson's disease (PD), which can be used in both clinical practice and trials. In this talk I will focus on recent advances in fluid and PET imaging biomarkers for tau pathology in AD. We have recently shown that certain blood-based markers (BBMs) for AD perform equivalent, or even superior, to FDA-approved CSF biomarkers to detect AD pathology in memory clinic cohorts. We also have data supporting the use of BBMs to improve the diagnostic work-up of AD in primary care, even when blood is analyzed prospectively in a biweekly manner. We further propose a two cut-point approach where BBMs can be used with high accuracy to identify those patients that are very likely to either have AD pathology or not (with negative and positive predictive values above 90%), but also an intermediate group where further testing is needed to confirm an AD diagnosis. The latter group is smaller (<10-20%) when using high-performing BBM tests.

I will also show data on the feasibility of using BBMs to detect individuals with preclinical AD, who are at clear increased risk of developing cognitive impairment and thereby suitable for inclusion in interventional trials.

Finally, I will discuss the potential use of novel seeding aggregation assays for α-synuclein pathology for early detection of Lewy body disease in the context of selecting appropriate participants for clinical trials and to improve the diagnostic and prognostic work-up in clinical practice.

Dr. Oskar Hansson gained his PhD in neurobiology in 2001 and his MD in 2005. He became senior consultant in neurology in 2012 at Skåne University Hospital, and full professor of neurology in 2017 at Lund University, Sweden. Dr. Hansson performs internationally recognized clinical and translational research focusing on the early phases of Alzheimer's and Parkinson's diseases.

His work on biomarkers has led to over 400 original peer-reviewed publications.
He heads the prospective and longitudinal Swedish BioFINDER studies (www.biofinder.se), where the research team focuses on the development of optimized diagnostic algorithms for early diagnosis, and also studies the consequences of different brain pathologies on cognitive, neurologic and psychiatric symptoms in healthy individuals and patients with dementia and parkinsonian disorders. Recently, the BioFINDER team has shown that Tau PET imaging can with high accuracy distinguish Alzheimer's from all other neurodegenerative diseases (JAMA, 2018), predict cognitive decline in cognitively normal individuals (Nature Medicine, 2022), and to detect different subtypes of Alzheimer's (Nature Medicine 2021). Dr. Hansson has also developed and validated blood-based biomarkers for early detection of Alzheimer's disease (Nature Medicine, 2020; JAMA, 2020, Nature Aging 2021, Nature Medicine 2021, Nature Medicine 2022) and markers for Lewy body disease (Nature Medicine 2023, Nature Medicine 2023).

He is the co-director of the strategic research area of neuroscience at Lund University, and responsible for research at the Memory Clinic at Skåne University Hospital.

Thursday, January 18, 2024 - 03:40 pm - 05:25 pm

Podium Session

SESSION VIII: Clinical and Biological Heterogeneity

CHAIRS: Tobey Betthauser, Heidi Jacobs

Thursday, January 18, 2024		
03:40 pm - 05:25 pm	**SESSION VIII: Clinical and Biological Heterogeneity**	**Tobey Betthauser, University of Wisconsin, Madison, WI, United States** **Heidi Jacobs, Massachusetts General Hospital, Boston, MA, United States**
03:40	Introduction	Chairs
03:45	Heterogeneity of amyloid-PET-negative patients with a clinical diagnosis of sporadic early-onset AD: an FDG-PET study in the LEADS cohort	Lagarde | Schonhaut | Maiti | Zhang | Soleimani-Meigooni | Zeltzer | Windon | Hammers | Dage | Nudelman | Eloyan | Koeppe | Carrillo | Touroutoglou | Vemuri | Dickerson | Apostolova | Rabinovici | La Joie | Consortium
04:00	The importance of AT(N)-V imaging biomarkers differs in diverse populations	Meeker | Ances | Wisch | Braskie | Toga | O'Bryant
04:15	The POINTER Imaging baseline cohort: Associations between neuroimaging biomarkers, cardiovascular health and cognition	Harrison | Ward | Taggett | Maillard | Vemuri | Lockhart | Jung | Lovato | Koeppe | Jagust | Masdeu | Oh | Gitelman | Aggarwal | Snyder | Baker | DeCarli | Landau
04:30	Identification of Genetic Risk Loci and Polygenic Prediction for B-amyloid Deposition in East Asian Population	Kim | Jung | Ali | Cruchaga | Kim | Won | Seo
04:45	Braak discordant cases in a large multi-site harmonized tau PET dataset	Smith | Carlson | Cody | Johns | Younes | Young | Mukherjee | Trittschuh | Gibbons | Dumitrescu | Archer | Durant | Nakano | Klinedinst | Choi | Lee | Scollard | Mez | Saykin | Crane | Cuccaro | Toga | Tosun | Hohman | Mormino
05:00	Discussion	

Heterogeneity of amyloid-PET-negative patients with a clinical diagnosis of sporadic early-onset AD: an FDG-PET study in the LEADS cohort

Julien Lagarde[1], Daniel Schonhaut[1], Piyush Maiti[1], Jiaxiuxiu Zhang[1], David Soleimani-Meigooni[1], Ehud Zeltzer[1], Charles Windon[1], Dustin Hammers[2], Jeffrey Dage[2], Kelly Nudelman[8], Ani Eloyan[3], Robert Koeppe[4], Maria Carrillo[5], Alexandra Touroutoglou[6], Prashanthi Vemuri[7], Bradford Dickerson[6], Liana Apostolova[2], Gil Rabinovici[1], Renaud La Joie[1], LEADS Consortium[9]

[1]*Department of Neurology, University of California, San Francisco, San Francisco, CA, United States*
[2]*Department of Neurology, Indiana University School of Medicine, Indianapolis, IN, United States*
[3]*Department of Biostatistics, Center for Statistical Sciences, Brown University, Providence, RI, United States*
[4]*Department of Radiology, University of Michigan, Ann Arbor, MI, United States*
[5]*Medical & Scientific Relations Division, Alzheimer's Association, Chicago, IL, United States*
[6]*Department of Neurology, Massachusetts General Hospital and Harvard Medical School, Boston, MA, United States*
[7]*Department of Radiology, Mayo Clinic, Rochester, Rochester, MN, United States*
[8]*Department of Medical and Molecular Genetics, Indiana University School of Medicine, Indianapolis, IN, United States*
[9]*NA, NA, United States*

Objectives In the Longitudinal Early-onset Alzheimer's Disease Study (LEADS), 25% of patients with clinically diagnosed early-onset AD are amyloid-PET-negative. We used FDG-PET to characterize the heterogeneity of hypometabolic profiles in these "EOnonAD" patients to identify underlying etiologies.

Methods (Figure 1): Seventy-four EOnonAD patients and 61 amyloid-PET-negative controls underwent FDG-PET 30-60 min post-injection. Pons-normalized SUVR images were warped to template space to compute age- and sex-adjusted W-score maps for each patient relative to controls. Patients were classified as having normal or hypometabolic FDG based on the proportion of GM voxels with W<-2 (threshold=2.3%, assuming normal distribution). We compared the clinical, MRI and biofluid characteristics of normal vs. hypometabolic EOnonAD groups. Finally, hierarchical clustering was performed in hypometabolic patients to identify subgroups based on regional profiles.

Results: Fifty-two EOnonAD patients (70%) had abnormal FDG scans. They were older (Figure 2A), more severely impairment across most cognitive domains (Figure 2B), and had lower cortical volume/thickness across multiple regions than patients with normal FDG (Figure 2C). They also had higher plasma GFAP and higher plasma and CSF levels of neurofilament light chain (NfL; Figure 2D). At the group level, hypometabolism was diffuse (Figure 3A), but hierarchical clustering identified three profiles: occipito-parietal (n=13), lateral frontal and parietal (n=17) and anterior temporal and orbitofrontal (n=22) (Figure 3B). Genetic testing identified two patients with FTLD-associated pathogenic variants (*MAPT* and *c9orf72*), both assigned to the orbitofrontal cluster.

Conclusions: Thirty percent of EOnonAD patients had normal FDG-PET and minimal clinical impairment, suggesting non-neurodegenerative etiologies. This interpretation is reinforced by other neurodegeneration biomarkers (i.e., structural MRI, NfL) being in the range of controls. EOnonAD patients with abnormal FDG showed heterogeneous hypometabolic patterns suggestive of multiple etiologies including Lewy body disease and Frontotemporal Lobar Degeneration. The characterization of these subgroups will be refined using longitudinal clinical and imaging data.

Figure 1: Study design

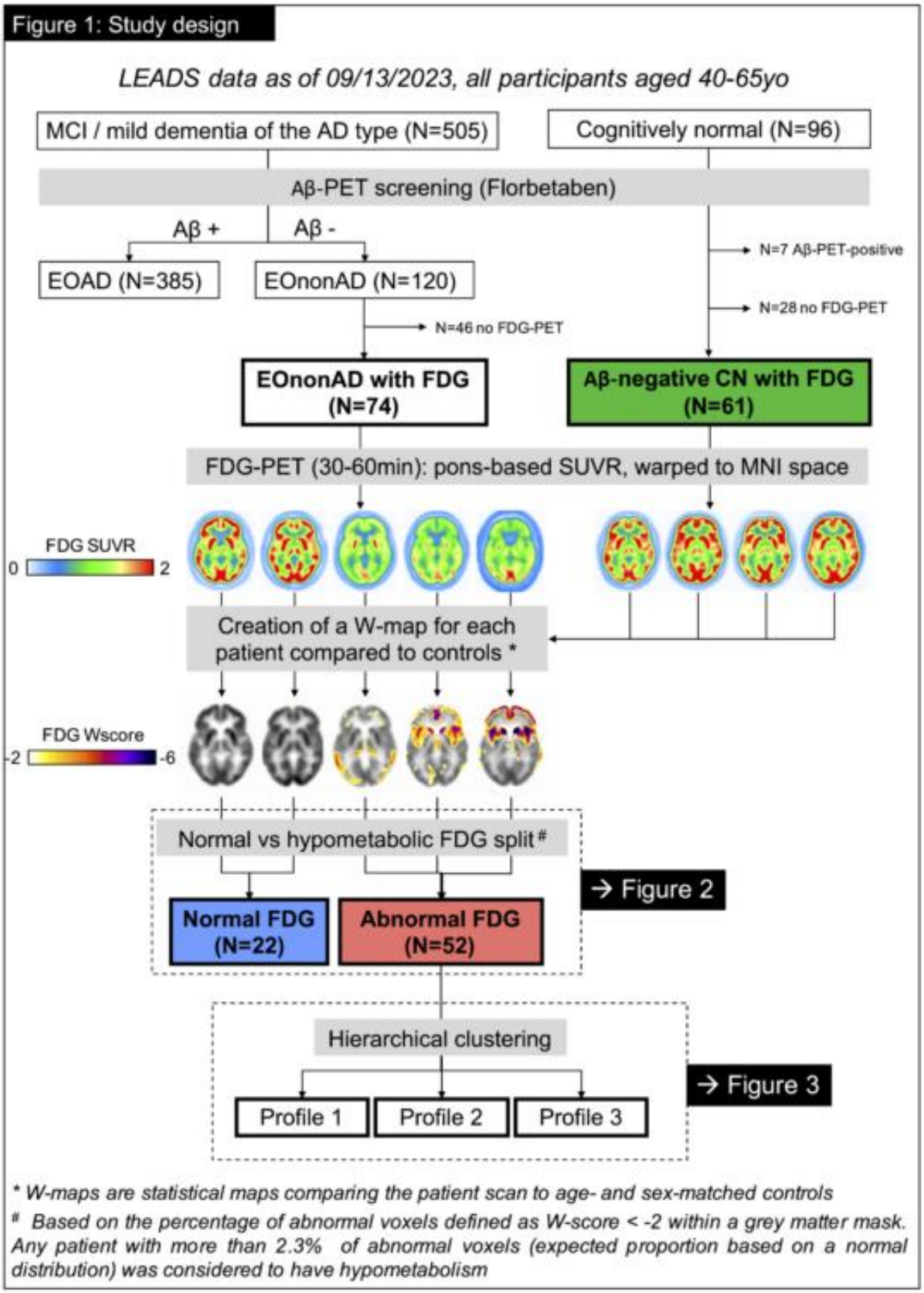

** W-maps are statistical maps comparing the patient scan to age- and sex-matched controls*

 # Based on the percentage of abnormal voxels defined as W-score < -2 within a grey matter mask. Any patient with more than 2.3% of abnormal voxels (expected proportion based on a normal distribution) was considered to have hypometabolism

Figure 2: Comparison of EOnonAD patients with hypometabolic vs normal FDG scans

A. General characteristics

		Controls (n=61)	EOnonAD		Normal vs Hypometabolic (Mann-Whitney or Fisher test, p)
			Normal FDG (N=22)	Hypometabolic FDG (N=52)	
Age: Mean (SD)		59 (5.4)	57.3 (6.4)	61.1 (5.1)	**0.015**
Sex: F (%)		39 (64%)	5 (23%)	23 (44%)	0.12
Genetics	ApoE: n e4 carriers (%)*	24 (41%)	8 (42%)	16 (39%)	0.78
	GRN/C9orf72/MAPT mutations	0/0/0	0/0/0	0/1/1 (R406W)	-
Clinical phenotype: Amnestic (%) / non-Amnestic		-	20 (91%) / 2	40 (77%) / 12	0.21
MMSE score: Mean (SD)		29.2 (1)	27.3 (2.5)	25.5 (4.5)	0.1
Amyloid PET Centiloid value: Mean (SD)		7.2 (6.8)	7 (8.9)	6.3 (9.7)	0.69

** 2 missing data in Controls and 14 in EOnonAD.*

B. Cognitive scores

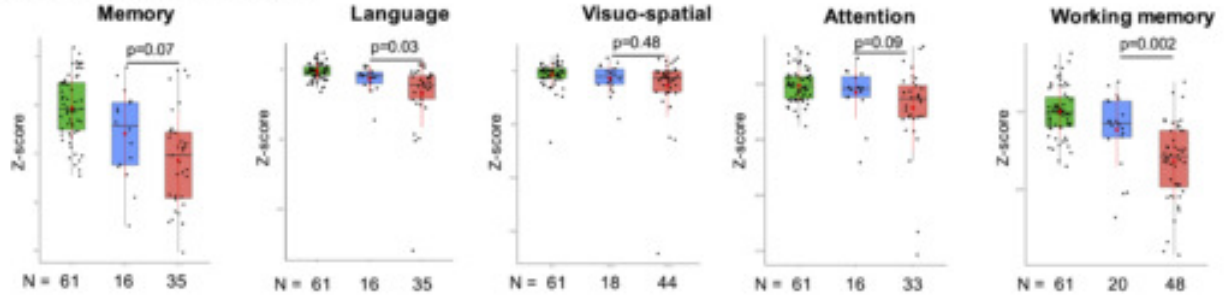

C. Structural MRI

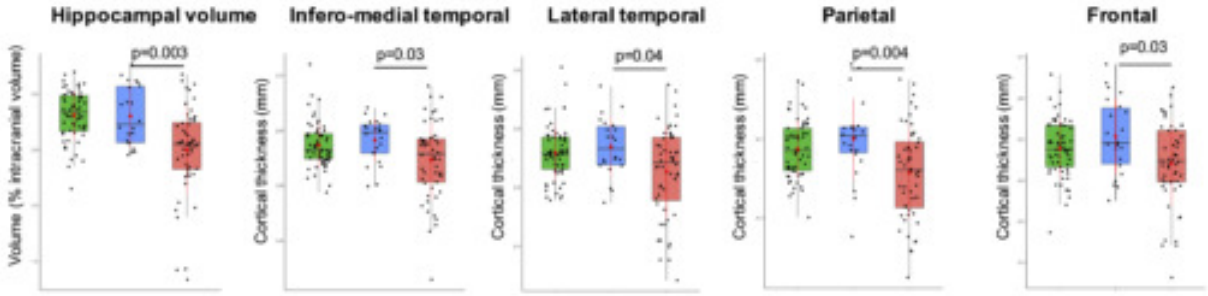

D. Fluid biomarkers

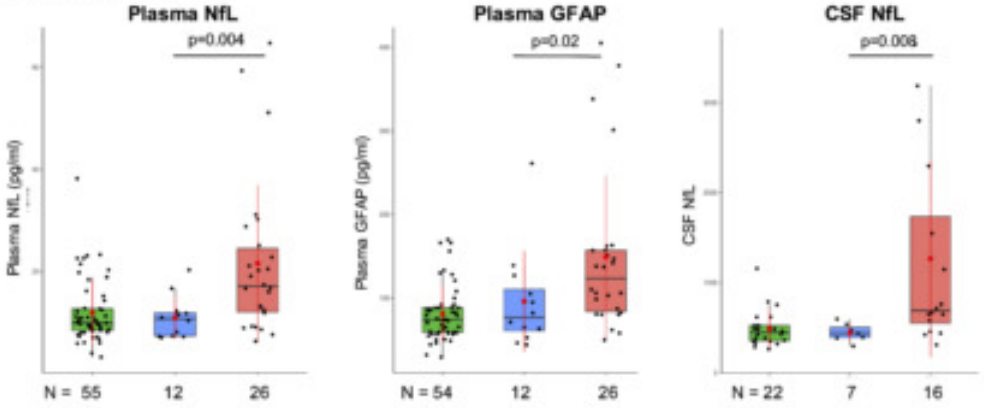

The p-values are for the comparison between EOnonAD patients with normal and hypometabolic FDG (uncorrected for multiple comparisons). The values for controls are provided for reference purposes.

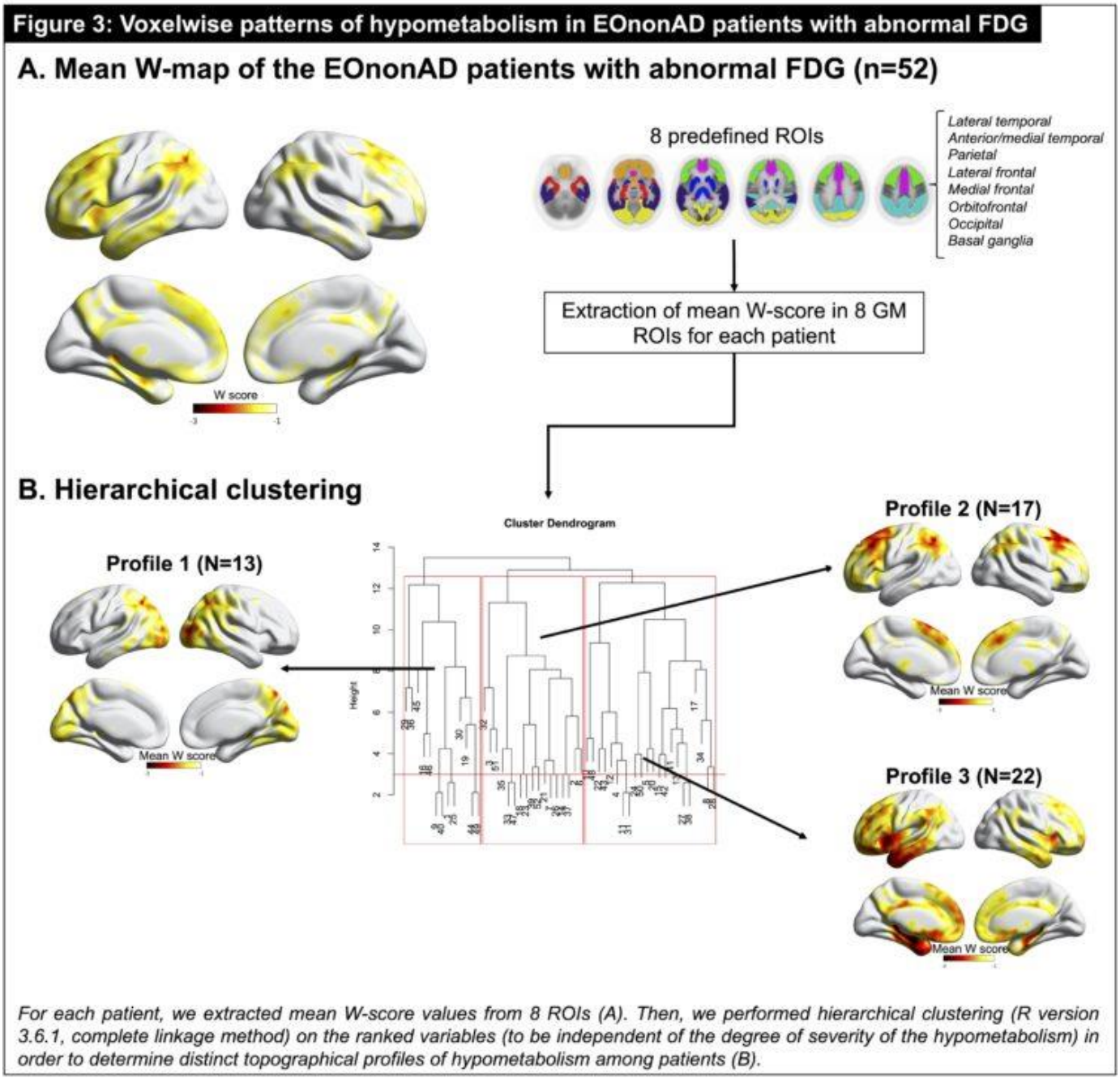

For each patient, we extracted mean W-score values from 8 ROIs (A). Then, we performed hierarchical clustering (R version 3.6.1, complete linkage method) on the ranked variables (to be independent of the degree of severity of the hypometabolism) in order to determine distinct topographical profiles of hypometabolism among patients (B).

Keywords: Early-onset AD, PET imaging, heterogeneity

The importance of AT(N)-V imaging biomarkers differs in diverse populations

Karin Meeker[1], Beau Ances[1], Julie Wisch[1], Meredith Braskie[3], Arthur Toga[3], Sid O'Bryant[2]

[1]*Washington University School of Medicine, Saint Louis, MO, United States*
[2]*University of North Texas Health Science Center, Fort Worth, TX, United States*
[3]*University of Southern California, Los Angeles, CA, United States*

Objectives: Investigations into the amyloid, tau, and neurodegeneration (ATN) framework, which is used to stage Alzheimer's disease (AD) and advance clinical trials, typically consist of clinic-based non-Hispanic White (NHW) populations. The present study sought to cross-sectionally characterize AT(N) and vascular (V) imaging markers (i.e., amyloid and tau positron emission tomography [PET], AD cortical thickness signature, and white matter hyperintensities), and determine the relative importance of each marker in predicting cognitive status in a large ethnically and racially diverse sample.

Methods: Data were obtained from the community-based Health and Aging Brain Study – Health Disparities (HABS-HD) and included Mexican Americans (MAs, n=231), African Americans (AAs, n=602), and NHWs (n=272). Group differences in AT(N)-V biomarkers were assessed using analysis of covariance. Age, sex, cognitive status (Clinical Dementia Rating Scale [CDR]), and years of education were included as covariates. Dominance analysis determined the relative 'importance' of each biomarker in predicting global cognitive status in the entire cohort and separately for each group.

Results: Tau was significantly greater in MAs compared to AAs (p<0.05) and NHWs (p<0.001), and in AAs compared to NHWs (p<0.001). AAs also had greater neurodegeneration compared to NHWs (p<0.001) and MAs (p<0.05). No other significant differences were observed (ps>0.05). In the entire cohort, V was the most important biomarker (as evidenced by greater R^2 values; see Figure 1) in predicting cognitive functioning. In MAs, V was the most important while in AAs, A was the most important. In NHWs T and V were of equal importance

Conclusions: The magnitude and overall contributions of AT(N)-V imaging biomarkers in clinical outcomes varies among ethno-racial groups. Possible differential effects of AD biomarkers should be considered in research, clinical trials, and response to treatment. A, T and N are differentially related to clinical outcomes among diverse populations.

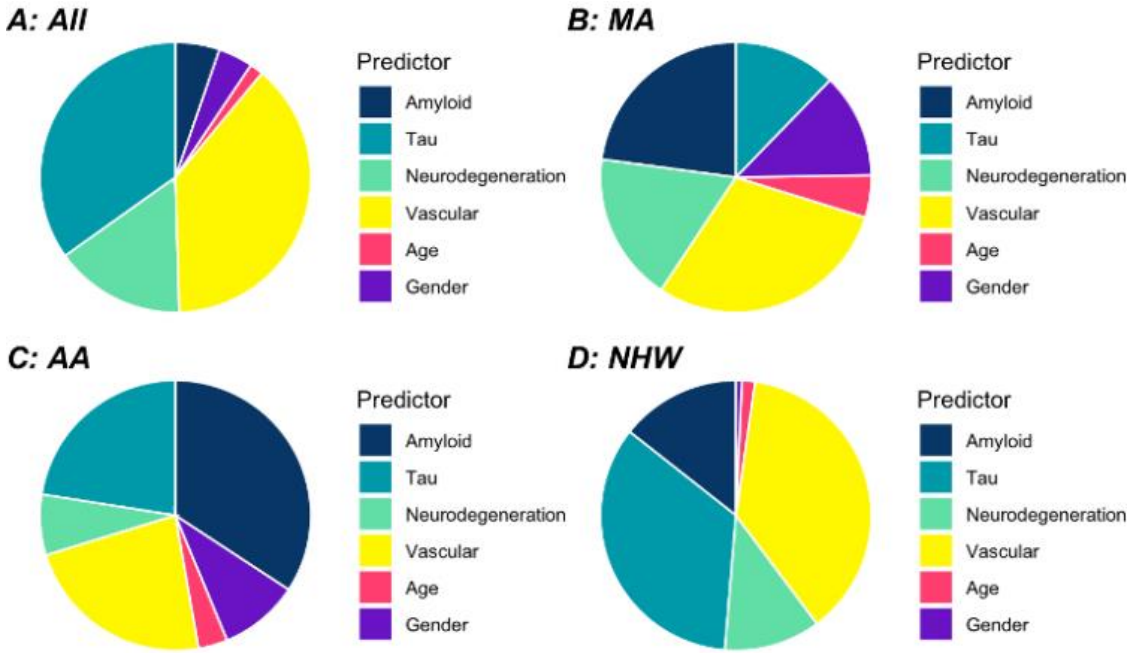

Keywords: Alzheimer's disease, imaging, biomarkers, disparities

The POINTER Imaging baseline cohort: Associations between neuroimaging biomarkers, cardiovascular health and cognition

Theresa Harrison[1], Tyler Ward[1], Jacinda Taggett[1], Pauline Maillard[2], Prashanthi Vemuri[3], Samuel Lockhart[4], Youngkyoo Jung[2], Laura Lovato[4], Robert Koeppe[5], William Jagust[1,6], Joseph Masdeu[7], Hwamee Oh[8], Darren Gitelman[9], Neelum Aggarwal[10], Heather Snyder[11], Laura Baker[4], Charles DeCarli[2], Susan Landau[1]

[1]*University of California Berkeley, Berkeley, CA, United States*
[2]*University of California Davis, Davis, CA, United States*
[3]*Mayo Clinic, Rochester, MN, United States*
[4]*Wake Forest University School, Winston-Salem, NC, United States*
[5]*University of Michigan, Ann Arbor, MI, United States*
[6]*Lawrence Berkeley National Laboratory, Berkeley, CA, United States*
[7]*Houston Methodist, Houston, TX, United States*
[8]*Brown University, Providence, RI, United States*
[9]*Advocate Aurora Health, Chicago, IL, United States*
[10]*Rush University Medical Center, Chicago, IL, United States*
[11]*Alzheimer's Association, Chicago, IL, United States*

Background: The U.S. Study to Protect Brain Health Through Lifestyle Intervention to Reduce Risk (U.S. POINTER) is a 2-year randomized controlled trial to evaluate the effect of lifestyle interventions in unimpaired older adults who are at risk for decline/dementia. Here we characterize the completed POINTER Imaging ancillary study baseline dataset (50% of trial participants) including relationships between demographics, cardiovascular health, multimodal neuroimaging and cognitive data.

Methods: Participants underwent baseline health and cognitive assessments, structural and diffusion-weighted MRI, [^{18}F]Florbetaben Aβ-PET and [^{18}F]MK6240 tau-PET. Framingham risk score (FRS) was used to quantify cardiovascular disease (CVD) risk. We examined associations between AD biomarkers (Aβ status, temporal tau), brain structure (whole cerebral volume, hippocampal volume), FRS, white matter measures (white matter hyperintensities [WMH] volume, global fractional anisotropy [FA] and free water [FW]) and cognitive domains (episodic memory [EM], executive function [EF], processing speed [PS]) adjusted for age, sex, education, and underrepresented group (URG) versus white status. Elastic net models predicting cognition were used to select and rank variables.

Results: 1052 participants enrolled in POINTER Imaging and 31% were from URG. Compared to Aβ-, Aβ+ (29%) participants were older, had lower EM performance, greater temporal tau, greater WMH, lower global FA and a trending lower proportion of URG individuals (Fig.1). AD pathology measures were related to EM, but not to EF or PS. WMH and FW were related to PS and FA was related to PS and EF (Fig.2). Brain structure and FRS were not related to cognition. Elastic net models supported these findings, reducing non-relevant predictor coefficients to zero (Table1).

Conclusions: In this heterogeneous, at-risk cohort, Aβ+ individuals had higher tau and evidence of white matter disease. CVD-related neuroimaging measures were better predictors of cognition compared to FRS. Drivers of cross-sectional cognition vary according to domain and regularized regression can help identify relevant predictors.

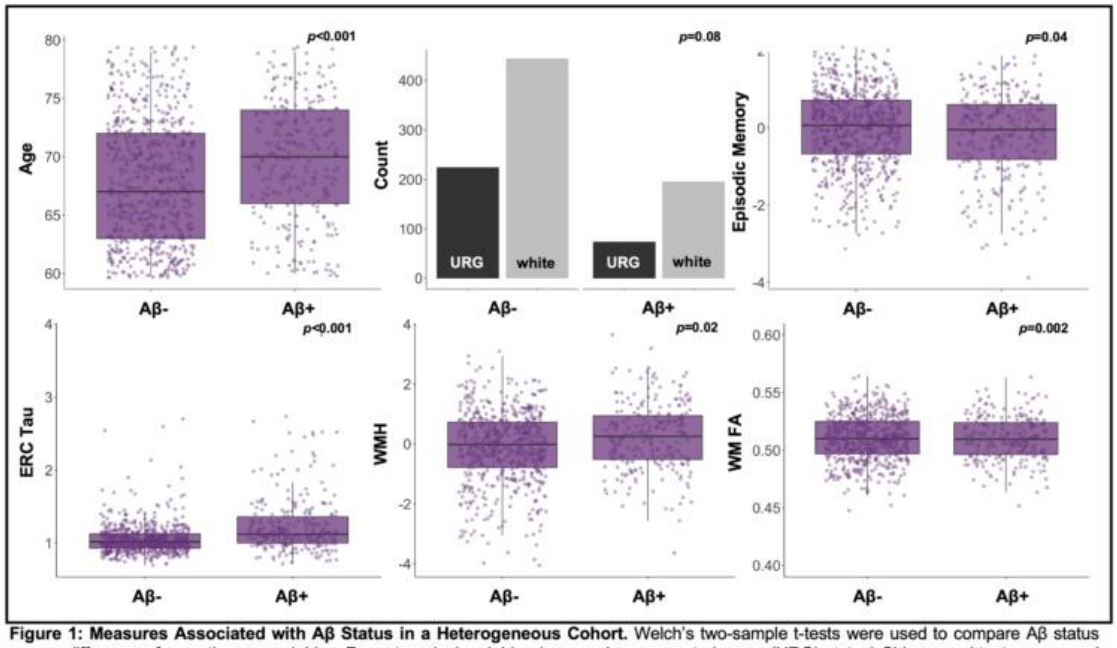

Figure 1: Measures Associated with Aβ Status in a Heterogeneous Cohort. Welch's two-sample t-tests were used to compare Aβ status groups differences for continuous variables. For categorical variables (e.g., underrepresented group (URG) status) Chi-squared tests were used to compare Aβ status groups. An individual was assigned to URG if they self-reported as mixed race or a race other than white.

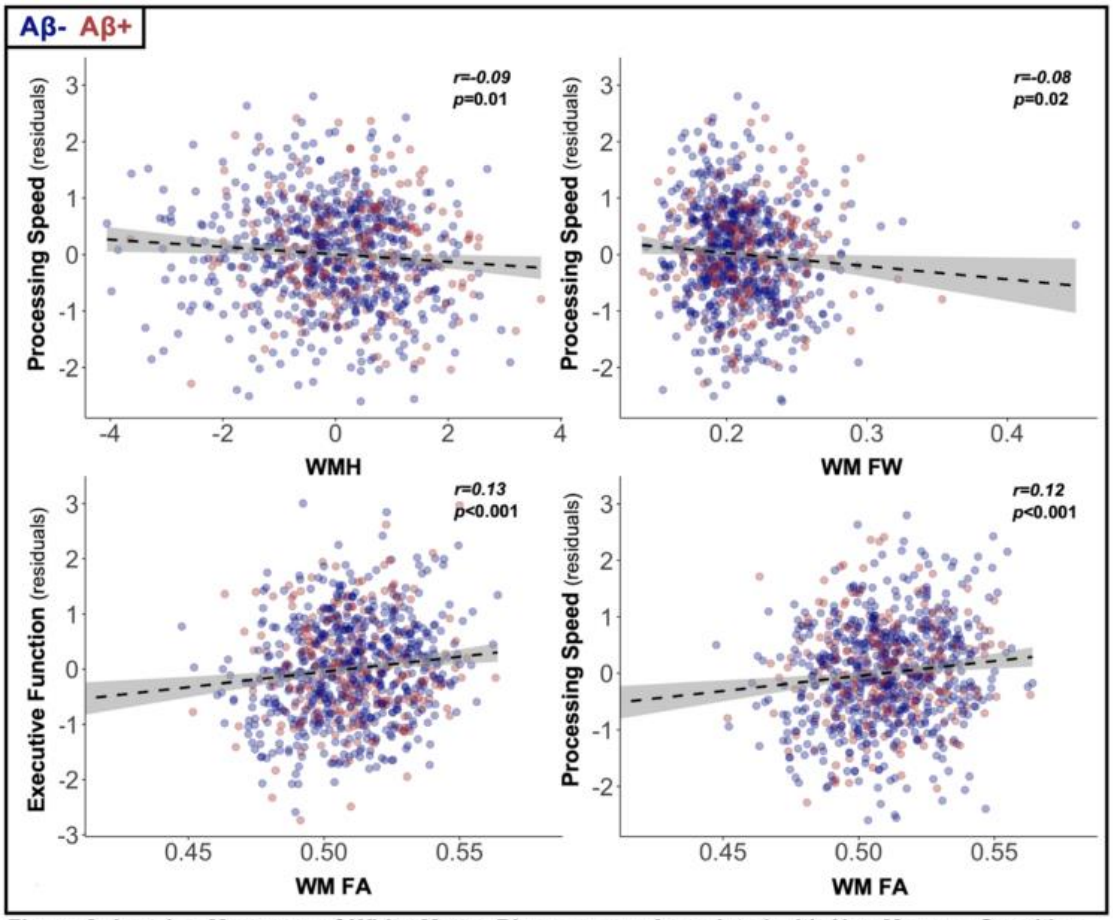

Figure 2: Imaging Measures of White Matter Disease were Associated with Non-Memory Cognition. Pearson correlations were used to relate neuroimaging measures of white matter disease to cognitive domain scores adjusted for age, sex, education and underrepresented group status.

Table 1: Elastic Net Regressions Predicting Cognitive Domain Scores

Predictor	Episodic Memory	Executive Function	Processing Speed
age	-0.020	-0.039	-0.047
edu	0.061	0.099	0.057
FRS	-0.013	-0.006	-0.005
global Aβ	.	0.270	.
ERC tau	-0.428	0.099	.
hippo. vol.	0.028	-0.131	.
cerebral vol.	.	-0.009	.
WMH	.	-0.057	-0.007
WM FA	0.080	10.160	5.924
WM FW	.	3.041	.
MSE:	*0.806*	*0.947*	*0.926*

edu=years of education; FRS=Framingham risk score; Aβ= beta amyloid; ERC=entorhinal cortex; hippo. vol.=hippocampal volume adjusted for intracranial volume; cerebral vol.= cerebral volume adjusted for intracranial volume; WMH=white matter hyperintensities volume log transformed and adjusted for intracranial volume; WM FA=white matter fractional anisotropy; WM FW=white matter free-water; MSE=mean squared error

Keywords: cohort heterogeneity, unimpaired, cardiovascular risk, MK6240, diffusion weighted imaging

Identification of genetic risk loci and polygenic prediction for β-amyloid deposition in East Asian population

Jun Pyo Kim[1], Sang-Hyuk Jung[2], Muhammad Ali[3], Carlos Cruchaga[3], Chi-Hun Kim[4], Hong-Hee Won[1], Sang Won Seo[1]

[1]*Samsung Medical Center, Seoul, South Korea*
[2]*University of Pennsylvania, Philadelphia, PA, United States*
[3]*Washington University, St. Louis, WA, United States*
[4]*Hallym University, Pyungchon, South Korea*

Introduction: Meta-analyses of genome-wide association studies have reported significant risk loci for clinical diagnosis of Alzheimer's disease. However, these studies were mostly based on the European population, and the β-amyloid (Aβ) status was not considered. We performed a meta-GWAS using East Asian genomics data and also performed polygenic prediction of Aβ status.

Methods: Genotype data of 3387 participants from a Korean consortium of 20 hospitals, who underwent amyloid PET were included in our analysis. Additionally, we utilized summary statistics from an amyloid PET GWAS using data from 498 East Asians in 9 international cohorts. We performed a meta-analysis to identify risk loci for cerebral Aβ deposition. We then calculated the polygenic risk score (PRS) using the PRScsx tool in an independent group of 325 Korean participants.

Results: We identified 16 SNPs showing genome-wide significant associations near *SORL1* (Fig1). The SNP rs76490923 (MAF in East Asians = 0.21) showed the most significant association (β(SE) -0.166(0.028), $p=2.46\times10^{-9}$). The subjects who carry the *APOE* ε4-allele and have high PRS (>75%ile) showed a highly increased risk (OR (95%CI) 27.7 (5.7-136.7)) of Aβ positivity compared to the lowest risk subjects who did not carry ε4-allele and had low PRS (<25%ile) (Table1). The high PRS group within the ε4 non-carriers also showed an increased risk of Aβ positivity (OR 3.1 (1.2-7.8)).

Discussion: While variants related to *SORL1* have not been identified in a recent multi-ethnic amyloid PET GWAS, our analysis in East Asians identified significant SNPs near *SORL1*. Previous studies might have undetected this association due to Europeans' low minor allele frequency (0.023). Our finding supports the importance of ethnic diversity, which has been increasingly recognized recently in AD genomics studies. Our findings also showed the value of polygenic risk prediction, which could effectively predict Aβ positivity independent of *APOE* ε4-carrier status.

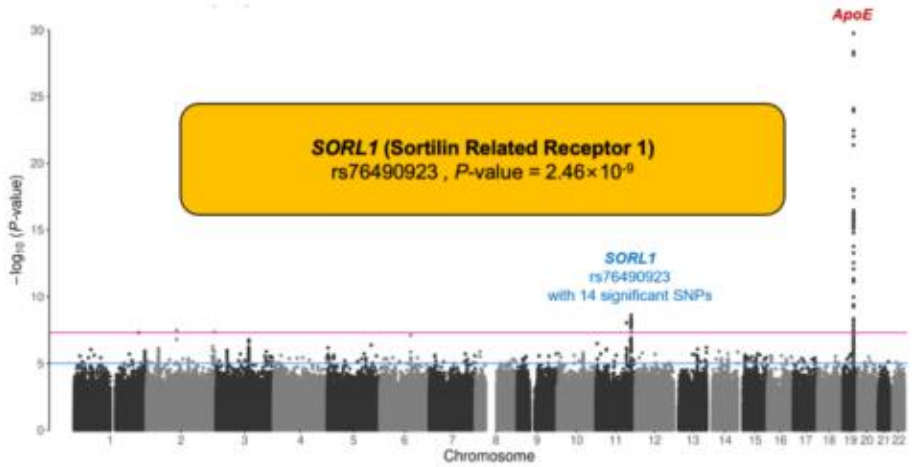

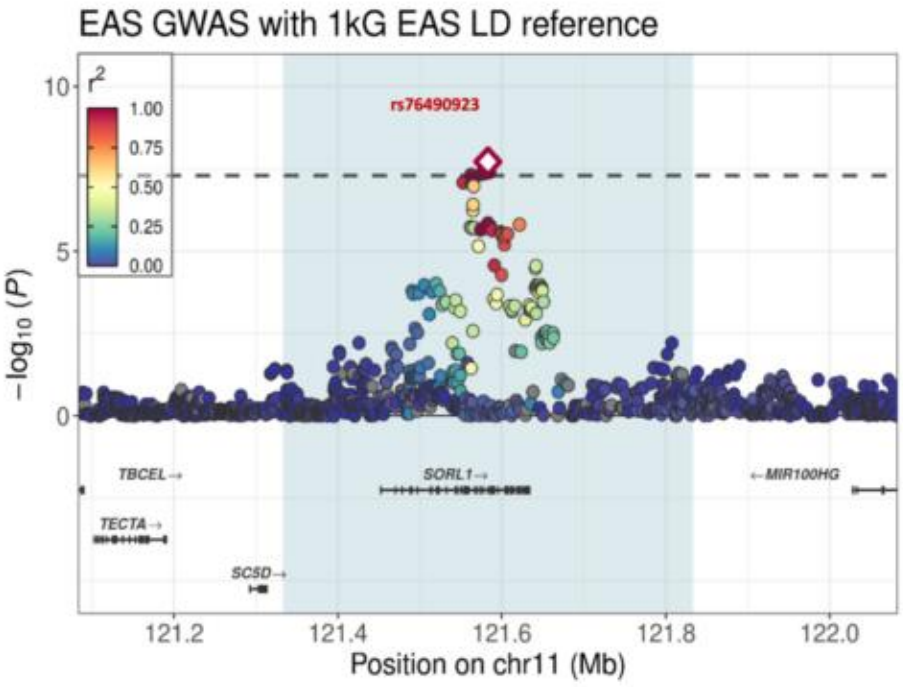

Fig1. A Manhattan plot of East Asian amyloid PET GWAS and the locus zoom plot for the SORL1 region

Table 1. Polygenic risk prediction of β-amyloid deposition

		Polygenic risk score (β-amyloid)					
ApoE	Geneβtic risk	Total no. of participants	No. of β-amyloid positivity (%)	OR (95% CI)	*P*-value	*P*-value for trend	*P*-value for interaction
Non-carrier	Low (0-25%)	44	18 (40.1%)	1 (reference)		<.001	0.471
	Intermediate (25-50%)	96	61 (63.5%)	**2.67 (1.21-5.88)**	0.015		
	High (75%-100%)	44	28 (63.6%)	**3.05 (1.20-7.80)**	0.020		
Carrier	Low (0-25%)	38	28 (73.7%)	**5.34 (1.86-15.29)**	0.002		
	Intermediate (25-50%)	66	58 (87.9%)	**15.55 (5.54-43.65)**	<.001		
	High (75%-100%)	37	35 (94.6%)	**27.71 (5.66-135.66)**	<.001		

β-amyloid positivity (visual) ~ Joint (PRS group + *ApoE* carrier) + Age + Sex + genetic PCs 1-5
Tool: PRScsx (Excluding *ApoE* region 44Mb-46Mb [GRCh38])

Keywords: Amyloid, Genome wide association study, Polygenic risk score, Asian, Ethnic diversity

Braak discordant cases in a large multi-site harmonized tau PET dataset

Viktorija Smith[1], Mackenzie L. Carlson[1], Karly Cody[1], Emily Johns[1], Kyan Younes[1], Christina B. Young[1], Shubhabrata Mukherjee[2], Emily Trittschuh[2,3,4], Laura E. Gibbons[2], Logan Dumitrescu[5], Derek Archer[5], Alaina Durant[5], Connie Nakano[2], Brandon Klinedinst[2], Seo-Eun Choi[2], Michael Lee[2], Phoebe Scollard[2], Jesse Mez[6], Andrew Saykin[7], Paul K. Crane[2], Michael Cuccaro[8,9], Arthur Toga[10,11], Duygu Tosun[12], Timothy Hohman[5], Elizabeth C. Mormino[1]

[1]*Department of Neurology and Neurological Sciences, Stanford University, Stanford, CA, United States*
[2]*Department of Medicine, University of Washington, Seattle, WA, United States*
[3]*Department of Psychiatry and Behavioral Sciences, University of Washington School of Medicine, Seattle, WA, United States*
[4]*VA Puget Sound Health Care System, GRECC, Seattle, WA, United States*
[5]*Vanderbilt Memory and Alzheimer's Center, Vanderbilt Genetics Institute, Department of Neurology, Vanderbilt University Medical Center, Nashville, TN, United States*
[6]*Department of Neurology, Boston University School of Medicine, Boston, MA, United States*
[7]*Indiana Alzheimer's Disease Research Center and the Department of Radiology and Imaging Sciences, Indiana University School of Medicine, Indianapolis, IN, United States*
[8]*The John P Hussman Institute for Human Genomics, The University of Miami Miller School of Medicine, Miami, FL, United States*
[9]*Dr. John T. MacDonald Foundation, Department of Human Genetics, University of Miami, Miami, FL, United States*
[10]*Alzheimer's Disease Research Center, Keck School of Medicine, University of Southern California, Los Angeles, CA, United States*
[11]*Laboratory of Neuroimaging, United StatesC Stevens Neuroimaging and Informatics Institute, Keck School of Medicine, University of Southern California, Los Angeles, CA, United States*
[12]*Department of Radiology and Biomedical Imaging, University of California San Francisco, San Francisco, CA, United States*

Objectives: This study leverages large-scale harmonized PET data from the Alzheimer's Disease Sequencing Project-Phenotype Harmonization Consortium to understand the prevalence and relevance of Braak staging "discordance".

Methods: We examined 1836 (71.7±7.45 years) unique participants from A4 (n=447), ADNI (n=944), WRAP (n=343) and NACC (n=102) who had harmonized baseline tau PET data (FTP and MK6240) quantified using MRI-free pipelines. Individuals were assigned a hierarchical PET-based Braak stage, where later stages could only be achieved if the individual was tau positive in previous stages. Individuals who did not follow the hierarchical pattern of tau accumulation were classified as Braak staging "discordant." Discordant cases underwent visual examination to classify subtypes of discordant patterns of tau accumulation. Associations with demographics and harmonized cognitive scores closest in time to tau PET were assessed across discordant subtypes.

Results: 1716/1836 (93.5%) followed a hierarchical Braak pattern of tau accumulation (Table 1), whereas 119/1836 (6.5%) were classified as Braak staging "discordant" (Table 2). Visual examination revealed five biologically plausible subgroups in 80/119 (67.2%) discordant cases: 1) subthreshold cases (39/119, 33.8%), 2) neocortical only (15/119, 12.6%), 3) asymmetrical left (7/119, 5.9%), 4) asymmetrical right (13/119, 10.9%), 5) other atypical (6/119, 5.0%). 39/119 (32.8%) were confirmed to have an image artifact. Age decreased with increasing Braak stage, whereas age in discordant subtypes was generally similar across all groups except for the amyloid positive neocortical only group who were older (Figure 1A, 2A). Cognitive scores (controlled for age, sex, and education) were lower with increasing Braak stages; in comparison to the later Braak stages, memory was relatively preserved in almost all discordant groups, language was preserved in the R>L group, and executive function was preserved in the sub-threshold group (Figure 1B-D, 2B-D).

Discussion: Large-scale harmonized PET data provides an opportunity to probe mechanisms that drive heterogeneity across individuals in tau spread.

Table 1: Demographics of cases classified across hierarchical PET-based Braak stage.

	T- (N=1337)	Braak I-II (N=140)	Braak III (N=35)	Braak IV (N=53)	Braak V (N=67)	Braak VI (N=84)	Overall (N=1716)
Cohort							
A4	298 (22.3%)	54 (38.6%)	17 (48.6%)	24 (45.3%)	16 (23.9%)	8 (9.5%)	417 (24.3%)
ADNI	672 (50.3%)	67 (47.9%)	10 (28.6%)	22 (41.5%)	45 (67.2%)	63 (75.0%)	879 (51.2%)
NACC	84 (6.3%)	3 (2.1%)	1 (2.9%)	3 (5.7%)	0 (0%)	8 (9.5%)	99 (5.8%)
WRAP	283 (21.2%)	16 (11.4%)	7 (20.0%)	4 (7.5%)	6 (9.0%)	5 (6.0%)	321 (18.7%)
Tau Tracer							
FTP	970 (72.6%)	121 (86.4%)	27 (77.1%)	46 (86.8%)	61 (91.0%)	71 (84.5%)	1296 (75.5%)
MK	367 (27.4%)	19 (13.6%)	8 (22.9%)	7 (13.2%)	6 (9.0%)	13 (15.5%)	420 (24.5%)
Age at Tau PET							
Mean (SD)	70.8 (7.5)	74.1 (6.5)	76.6 (6.3)	75.8 (5.9)	74.0 (6.2)	72.3 (7.7)	71.5 (7.5)
Median (Min, Max)	70.0 (48.1, 94.0)	73.3 (60.0, 92.0)	76.7 (58.5, 89.0)	76.0 (63.0, 94.0)	72.9 (63.0, 91.0)	71.3 (56.0, 90.0)	71.0 (48.1, 94.0)
Missing	0 (0%)	1 (0.7%)	0 (0%)	0 (0%)	0 (0%)	0 (0%)	1 (0.1%)
Sex							
Female	769 (57.5%)	89 (63.6%)	13 (37.1%)	27 (50.9%)	35 (52.2%)	45 (53.6%)	978 (57.0%)
Male	568 (42.5%)	50 (35.7%)	22 (62.9%)	26 (49.1%)	32 (47.8%)	39 (46.4%)	737 (42.9%)
Missing	0 (0%)	1 (0.7%)	0 (0%)	0 (0%)	0 (0%)	0 (0%)	1 (0.1%)
Amyloid Status GMM							
Negative	927 (69.3%)	32 (22.9%)	3 (8.6%)	4 (7.5%)	4 (6.0%)	8 (9.5%)	978 (57.0%)
Positive	394 (29.5%)	105 (75.0%)	31 (88.6%)	49 (92.5%)	61 (91.0%)	71 (84.5%)	711 (41.4%)
Missing	16 (1.2%)	3 (2.1%)	1 (2.9%)	0 (0%)	2 (3.0%)	5 (6.0%)	27 (1.6%)
Diagnosis group							
CN	1080 (80.8%)	97 (69.3%)	25 (71.4%)	32 (60.4%)	23 (34.3%)	19 (22.6%)	1276 (74.4%)
MCI	200 (15.0%)	32 (22.9%)	6 (17.1%)	12 (22.6%)	21 (31.3%)	30 (35.7%)	301 (17.5%)
MCI due to other etiology	19 (1.4%)	2 (1.4%)	0 (0%)	0 (0%)	1 (1.5%)	0 (0%)	22 (1.3%)
Dementia	32 (2.4%)	8 (5.7%)	4 (11.4%)	9 (17.0%)	22 (32.8%)	34 (40.5%)	109 (6.4%)
Dementia due to other etiology	1 (0.1%)	0 (0%)	0 (0%)	0 (0%)	0 (0%)	1 (1.2%)	2 (0.1%)
Missing	5 (0.4%)	1 (0.7%)	0 (0%)	0 (0%)	0 (0%)	0 (0%)	6 (0.3%)

Table 2: Demographics of discordant cases

	sub-threshold (N=39)	neocortical only (N=15)	L > R (N=7)	R > L (N=13)	other atypical (N=6)	image artifact (N=39)	Overall (N=119)
Cohort							
A4	13 (33.3%)	4 (26.7%)	3 (42.9%)	3 (23.1%)	2 (33.3%)	5 (12.8%)	30 (25.2%)
ADNI	19 (48.7%)	7 (46.7%)	3 (42.9%)	9 (69.2%)	2 (33.3%)	24 (61.5%)	64 (53.8%)
NACC	1 (2.6%)	2 (13.3%)	0 (0%)	0 (0%)	0 (0%)	0 (0%)	3 (2.5%)
WRAP	6 (15.4%)	2 (13.3%)	1 (14.3%)	1 (7.7%)	2 (33.3%)	10 (25.6%)	22 (18.5%)
Tau Tracer							
FTP	32 (82.1%)	11 (73.3%)	6 (85.7%)	12 (92.3%)	4 (66.7%)	29 (74.4%)	94 (79.0%)
MK	7 (17.9%)	4 (26.7%)	1 (14.3%)	1 (7.7%)	2 (33.3%)	10 (25.6%)	25 (21.0%)
Age at Tau PET							
Mean (SD)	74.6 (6.9)	73.5 (8.2)	74.8 (5.6)	75.4 (7.8)	75.1 (9.6)	72.2 (6.8)	73.8 (7.2)
Median (Min, Max)	74.8 (56.0, 90.0)	74.2 (60.0, 89.0)	75.0 (63.5, 81.4)	76.0 (59.5, 85.5)	78.4 (60.2, 84.7)	72.0 (59.6, 87.0)	73.8 (56.0, 90.0)
Sex							
Female	22 (56.4%)	8 (53.3%)	4 (57.1%)	6 (46.2%)	3 (50.0%)	23 (59.0%)	66 (55.5%)
Male	17 (43.6%)	7 (46.7%)	3 (42.9%)	7 (53.8%)	3 (50.0%)	16 (41.0%)	53 (44.5%)
Amyloid Status GMM							
Negative	10 (25.6%)	8 (53.3%)	1 (14.3%)	0 (0%)	2 (33.3%)	20 (51.3%)	41 (34.5%)
Positive	29 (74.4%)	7 (46.7%)	6 (85.7%)	13 (100%)	4 (66.7%)	18 (46.2%)	77 (64.7%)
Missing	0 (0%)	0 (0%)	0 (0%)	0 (0%)	0 (0%)	1 (2.6%)	1 (0.8%)
Diagnosis group							
CN	26 (66.7%)	11 (73.3%)	4 (57.1%)	7 (53.8%)	4 (66.7%)	27 (69.2%)	79 (66.4%)
MCI	11 (28.2%)	3 (20.0%)	2 (28.6%)	4 (30.8%)	2 (33.3%)	9 (23.1%)	31 (26.1%)
MCI due to other etiology	0 (0%)	0 (0%)	0 (0%)	2 (15.4%)	0 (0%)	0 (0%)	2 (1.7%)
Dementia	2 (5.1%)	1 (6.7%)	1 (14.3%)	0 (0%)	0 (0%)	3 (7.7%)	7 (5.9%)
Dementia due to other etiology	0 (0%)	0 (0%)	0 (0%)	0 (0%)	0 (0%)	0 (0%)	0 (0%)

Figure 1. (A) Age, (B) memory, (C) language, and (D) executive functioning differences between Braak staging groups and discordant groups in amyloid negative and amyloid positive participants. Right panels indicate significant differences between group pairs.

Figure 2. (A) Age, (B) memory, (C) language, and (D) executive functioning differences between Braak staging groups and discordant groups in amyloid positive participants only. Right panels indicate significant differences between group pairs.

Keywords: amyloid PET, tau PET, Braak staging

Friday, January 19, 2024 - 09:10 am - 10:40 am

Podium Session

SESSION IX: New Methods for Plasma

CHAIRS: Thomas Karikari, Suzanne Schindler

Friday, January 19, 2024		
09:10 am – 10:40 am	**SESSION IX: New Methods for Plasma**	**Suzanne Schindler, Washington University, St Louis, MO, United States** **Tommy Karikari, University of Pittsburgh, Pittsburg, PA, United States**
09:10	Introduction	Chairs
09:15	Plasma Aβ42/Aβ40 is an Early Marker of Amyloidosis in Clinically Unimpaired Older Adults	Trelle | Young | Vossler | Ramos Benitez | Romero | Park | Shahid | Corso | Skylar-Scott | Younes | Yutsis | Fredericks | Kerchner | Deutsch | Davidzon | Sha | Greicius | Longo | Henderson | Wyss-Coray | Andreasson | Poston | Wagner | Mormino | Wilson
09:30	A highly accurate blood test for Alzheimer's disease pathology has performance equivalent or superior to clinically used cerebrospinal fluid tests	Salvadó | Barthélemy | Schindler | He | Janelidze | Collij | Saef | Henson | Chen | Gordon | Benzinger | Morris | Mattsson-Carlgren | Palmqvist | Ossenkoppele | Stomrud | Bateman | Hansson
09:45	Associations of C2N plasma Aβ42/40 and p-tau217 and subsequent amyloid PET change	Cogswell | Wiste | Weigand | Therneau | Algeciras-Schimnich | Lowe | Graff-Radford | Schwarz | Senjem | Gunter | Vemuri | Knopman | Petersen | Jack Jr
10:00	Plasma p-tau212 is increased in CSF amyloid positive and [18F]flutemetamol PET negative cognitively impaired individuals	Kac | González-Escalante | Milà-Alomà | Ashton | Shekari | Turton | Harrison | Ortiz-Romero | Zetterberg | Gispert | Blennow | Suárez-Calvet | Karikari
10:15	Discussion	

Plasma Aβ42/Aβ40 is an early marker of amyloidosis in clinically unimpaired older adults

Alexandra N. Trelle[1], Christina B. Young[1], Hillary Vossler[1], Javier Ramos Benitez[1], America Romero[1], Jennifer Park[1], Marian Shahid[1], Nicole K. Corso[1], Irina Skylar-Scott[1], Kyan Younes[1], Maya V. Yutsis[1], Carolyn A. Fredericks[1], Geoffrey A. Kerchner[1], Gayle K. Deutsch[1], Guido Davidzon[2], Sharon J. Sha[1], Michael D. Greicius[1], Frank M. Longo[1], Victor W. Henderson[1], Tony Wyss-Coray[1], Katrin I. Andreasson[1], Kathleen L. Poston[1], Anthony D. Wagner[3], Elizabeth C. Mormino[1], Edward N. Wilson[1]

[1]*Neurology & Neurological Sciences, Stanford University School of Medicine, Stanford, CA, United States*
[2]*Radiology, Stanford University School of Medicine, Stanford, CA, United States*
[3]*Psychology, Stanford University, Stanford, CA, United States*

Background: Plasma $A\beta_{42}/A\beta_{40}$ is a sensitive and specific biomarker of brain amyloidosis in individuals along the Alzheimer's disease continuum.

Objective: To evaluate plasma $A\beta_{42}/A\beta_{40}$ as an early amyloid state marker in clinically unimpaired (CU) older adults.

Methods: Plasma $A\beta_{42}/A\beta_{40}$ was examined in two cohorts of older adults along the AD continuum (**Table 1**). The Discovery Cohort consisted of participants from the Stanford Alzheimer's Disease Research Center while the Validation Cohort included participants from the Stanford Aging and Memory Study (SAMS). Plasma $A\beta_{42}/A\beta_{40}$ was measured using the fully-automated and scalable Lumipulse immunoassays. A/T status were defined using CSF biomarkers and amyloid PET (^{18}F-florbetaben). Regression models evaluated change in plasma $A\beta_{42}/A\beta_{40}$, associations between baseline plasma $A\beta_{42}/A\beta_{40}$ with baseline cognition and with change in cognition over a follow-up period of up to 6 years.

Results: Plasma $A\beta_{42}/A\beta_{40}$ was lower in MCI and AD compared to CU and lower within clinical diagnostic groups positive for amyloid by CSF or PET (**Figure 1**). A/T classification showed lower plasma $A\beta_{42}/A\beta_{40}$ in A+T- at a level not significantly different from the A+T+ group. A similar pattern of results was observed in the Validation Cohort. Notably, in both cohorts approximately 17% of individuals were plasma positive but not CSF or PET positive, suggesting that plasma changes in amyloid are detectable before CSF and PET (**Table 2**). On follow-up, plasma $A\beta_{42}/A\beta_{40}$ remained stable in plasma amyloid-positive CU and clinically impaired (CI) groups (**Figure 2**). Plasma amyloid-positivity predicted future memory decline while plasma amyloid-negative groups remained stable (**Figure 3**). Finally, lower plasma $A\beta_{42}/A\beta_{40}$ was associated with worse performance on sensitive hippocampal-dependent memory tests in SAMS CU.

Conclusion: Plasma $A\beta_{42}/A\beta_{40}$ is an early state marker of amyloidosis related to memory performance in CU older adults.

Table 1: Discovery and Validation Cohort Demographics

Discovery Cohort				
	CU (N=217)	**MCI (N=63)**	**AD (N=58)**	**Overall (N=338)**
Age				
Mean (SD)	72.4 (8.15)	75.1 (7.56)	71.0 (9.76)	72.7 (8.42)
Sex				
M	81 (37.3%)	41 (65.1%)	26 (44.8%)	148 (43.8%)
F	136 (62.7%)	22 (34.9%)	32 (55.2%)	190 (56.2%)
Plasma Aβ42/40				
Mean (SD)	0.0911 (0.013)	0.0863 (0.013)	0.0816 (0.0091)	0.0885 (0.013)
Validation Cohort				
	CU (N=266)	**MCI (N=25)**	**AD (N=23)**	**Overall (N=314)**
Age				
Mean (SD)	69.4 (7.25)	71.7 (5.94)	71.3 (7.13)	69.7 (7.17)
Sex				
M	116 (43.6%)	11 (44.0%)	11 (47.8%)	138 (43.9%)
F	150 (56.4%)	14 (56.0%)	12 (52.2%)	176 (56.1%)
Plasma Aβ42/40				
Mean (SD)	0.0977 (0.012)	0.0878 (0.0097)	0.0824 (0.0082)	0.0958 (0.012)

Table

Table 2: Characteristics of Amyloid Concordance Groups

	Neg/Neg (N=134)	Plasma+/Neg (N=56)	Pos/Pos (N=130)	Plasma-/Pos (N=2)
Age				
Mean (SD)	68.6 (6.84)	70.9 (7.55)	71.2 (7.61)	72.6 (4.38)
Sex				
M	57 (42.5%)	24 (42.9%)	51 (39.2%)	1 (50.0%)
F	77 (57.5%)	32 (57.1%)	79 (60.8%)	1 (50.0%)
Diagnosis				
CU	124 (92.5%)	50 (89.3%)	81 (62.3%)	1 (50.0%)
MCI	8 (6.0%)	4 (7.1%)	19 (14.6%)	1 (50.0%)
AD	2 (1.5%)	2 (3.6%)	30 (23.1%)	0 (0%)
APOE ε4				
Non-Carrier	104 (77.6%)	36 (64.3%)	43 (33.1%)	0 (0%)
Carrier	15 (11.2%)	14 (25.0%)	76 (58.5%)	2 (100%)
Missing	15 (11.2%)	6 (10.7%)	11 (8.5%)	0 (0%)
Plasma Aβ42/40				
Mean (SD)	0.105 (0.00725)	0.0853 (0.00762)	0.0810 (0.00739)	0.0981 (0.00237)

1 Table

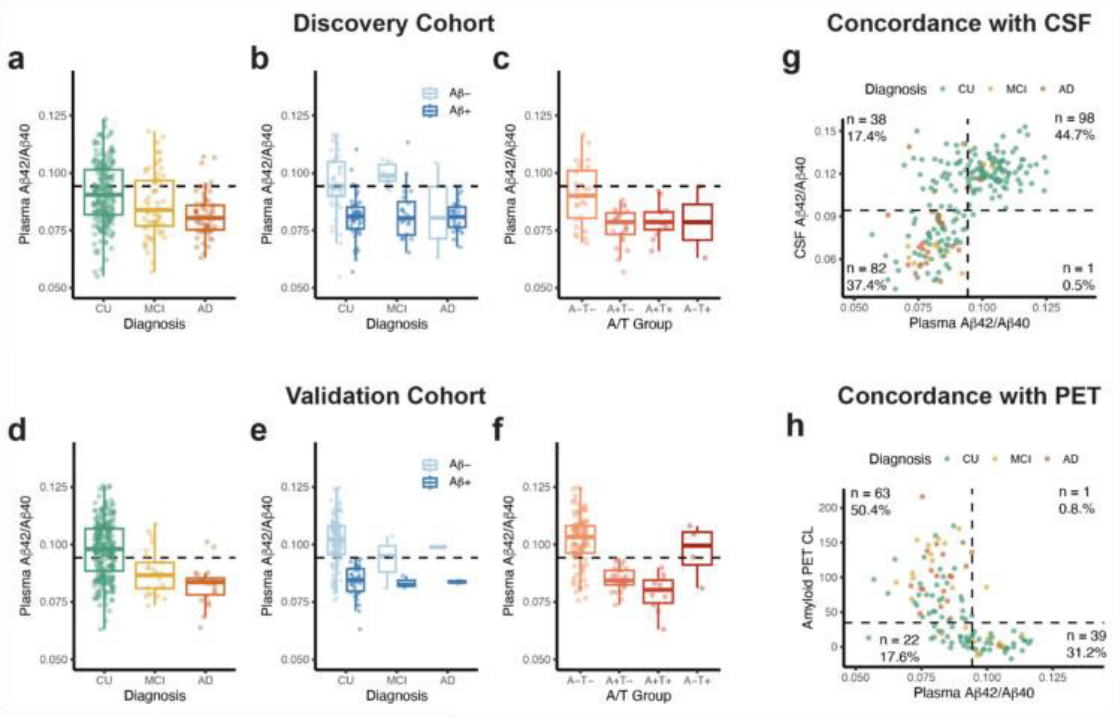

2 Figure

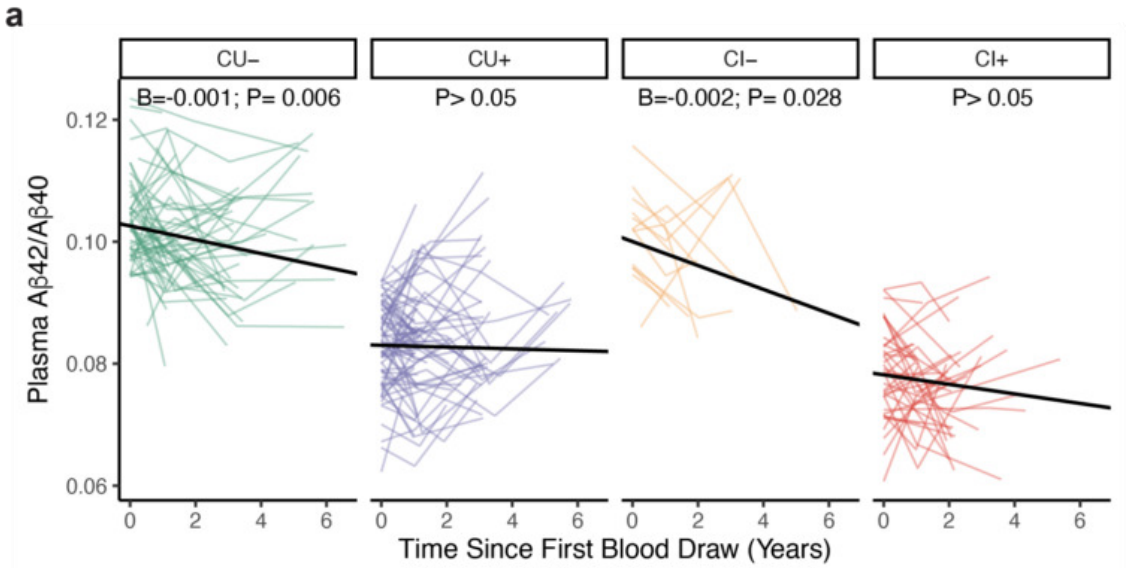

1 Figure

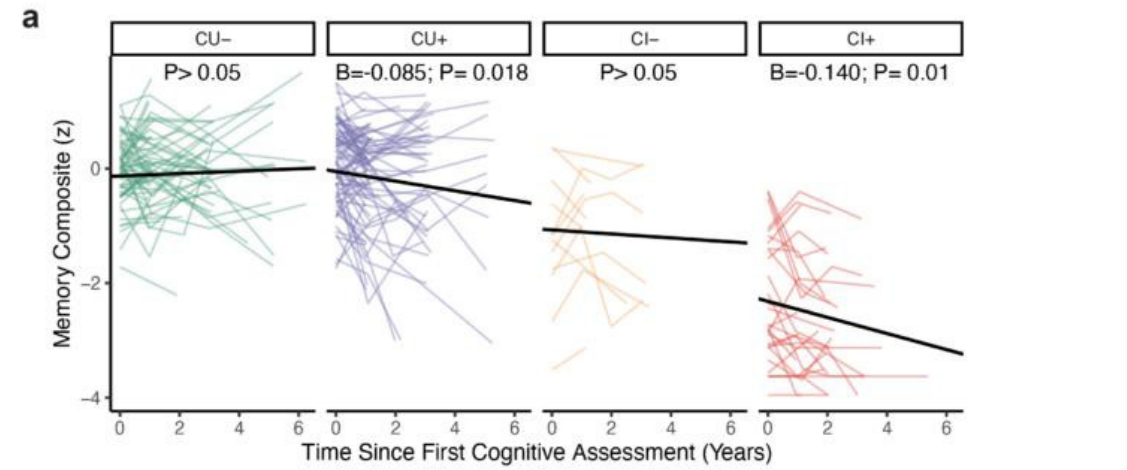

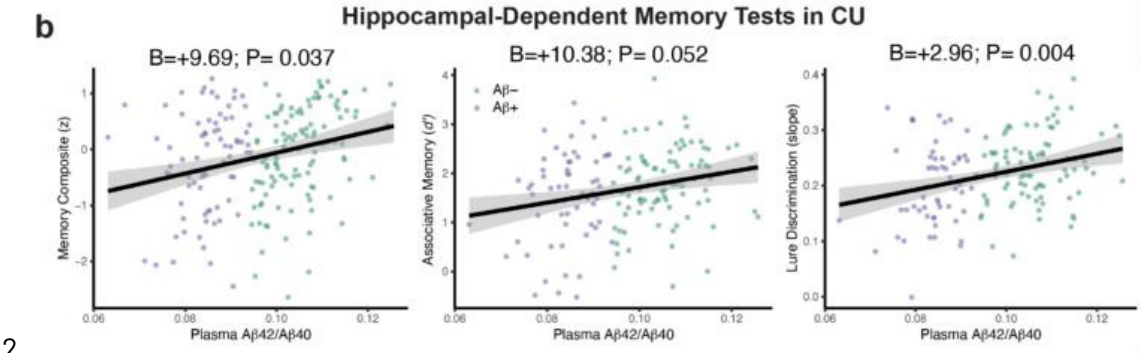

2 Figure 3

Table 2: Characteristics of Amyloid Concordance Groups

	Neg/Neg (N=134)	Plasma+/Neg (N=56)	Pos/Pos (N=130)	Plasma-/Pos (N=2)
Age				
Mean (SD)	68.6 (6.84)	70.9 (7.55)	71.2 (7.61)	72.6 (4.38)
Sex				
M	57 (42.5%)	24 (42.9%)	51 (39.2%)	1 (50.0%)
F	77 (57.5%)	32 (57.1%)	79 (60.8%)	1 (50.0%)
Diagnosis				
CU	124 (92.5%)	50 (89.3%)	81 (62.3%)	1 (50.0%)
MCI	8 (6.0%)	4 (7.1%)	19 (14.6%)	1 (50.0%)
AD	2 (1.5%)	2 (3.6%)	30 (23.1%)	0 (0%)
APOE ε4				
Non-Carrier	104 (77.6%)	36 (64.3%)	43 (33.1%)	0 (0%)
Carrier	15 (11.2%)	14 (25.0%)	76 (58.5%)	2 (100%)
Missing	15 (11.2%)	6 (10.7%)	11 (8.5%)	0 (0%)
Plasma Aβ42/40				
Mean (SD)	0.105 (0.00725)	0.0853 (0.00762)	0.0810 (0.00739)	0.0981 (0.00237)

Keywords: plasma amyloid, amyloid PET, hippocampal-dependent memory, clinically unimpaired

A highly accurate blood test for Alzheimer's disease pathology has performance equivalent or superior to clinically used cerebrospinal fluid tests

Gemma Salvadó[1], Nicolas R Barthélemy[2,3], Suzanne E Schindler[2,3,4], Yingxin He[2,3], Shorena Janelidze[1], Lyduine E Collij[1,5,6], Benjamin Saef[2], Rachel L Henson[2], Charles D Chen[7], Brian A Gordon[7], Tammie LS Benzinger[7], John C Morris[2,4], Niklas Mattsson-Carlgren[1,8,9], Sebastian Palmqvist[1,8], Rik Ossenkoppele[1,6,10], Erik Stomrud[1,8], Randall J Bateman[2,3,4], Oskar Hansson[1,8]

[1]*Clinical Memory Research Unit, Department of Clinical Sciences Malmö, Faculty of Medicine, Lund University, Lund, Sweden*
[2]*Department of Neurology, Washington University School of Medicine, Saint Louis, MO, United States*
[3]*The Tracy Family SILQ Center, Washington University School of Medicine, Saint Louis, MO, United States*
[4]*The Knight ADRC, Washington University School of Medicine, Saint Louis, MO, United States*
[5]*Dept. of Radiology and Nuclear Medicine, Amsterdam UMC, location VUmc, Amsterdam, The Netherlands*
[6]*Amsterdam Neuroscience, Brain Imaging, Amsterdam, Amsterdam, The Netherlands*
[7]*Department of Radiology, Washington University School of Medicine, Saint Louis, MO, United States*
[8]*Memory Clinic, Skåne University Hospital, Malmö, Sweden*
[9]*Wallenberg Center for Molecular Medicine, Lund University, Lund, Sweden*
[10]*Alzheimer Center Amsterdam, Neurology, Vrije Universiteit Amsterdam, Amsterdam UMC location VUmc, Amsterdam, The Netherlands*

Background: With the emergence of Alzheimer's disease (AD) disease-modifying therapies, identifying patients who could benefit from these treatments becomes critical. We evaluated whether a precise blood test could match established cerebrospinal fluid (CSF) tests in detecting amyloid plaques and tau tangles as measured by PET.

Methods: Plasma %p-tau217 (ratio of phosporylated-tau217 to non-phosphorylated tau) was analyzed by mass spectrometry in the BioFINDER-2 (n=1,422) and the Knight ADRC (n=337) cohorts. Matched CSF samples were analyzed with clinically used FDA-approved automated immunoassays for Aβ42/40 and p-tau181/Aβ42. We compared the accuracy of plasma %p-tau217 and the CSF biomarkers for detecting amyloid- (Centiloid≥37) and tau-pathologies (SUVR≥1.32), focusing on cognitively impaired individuals.

Results: Plasma %p-tau217 was non-significantly different to FDA-approved CSF tests in classifying amyloid-PET status, with an area-under-the-curve (AUC) for both cohorts between 0.96-0.98 in cognitively impaired ($p \geq 0.13$) and unimpaired individuals ($p \geq 0.46$, Figure 1A-B). Plasma %p-tau217 generally outperformed ($p \leq 0.002$) CSF tests in classification of tau-PET exhibiting AUCs around 0.90-0.98 (Figure 1C-D). In cognitively impaired sub-cohorts (BioFINDER-2: n=720; Knight ADRC: n=50), plasma %p-tau217 had an accuracy, positive predictive value and negative predictive value of 89-90% (BioFINDER-2) and 97-100% (Knight ADRC) for amyloid-PET, which were non-inferior to CSF tests ($p \geq 0.25$, Figure 2A and 2D). These statistics increased up to or above 95% when using a two cut-off approach remaining non-inferior than those of CSF biomarkers ($p \geq 0.65$, Figure 2B and 2E). For tau-PET status accuracy was 80-88% and around 94% for the single and two cut-off approaches, respectively, which were non-inferior ($p \geq 0.65$) or even superior to CSF tests ($p \leq 0.02$, Figure 3).

Conclusions: Blood plasma %p-tau217 demonstrates performance equivalent or superior to clinically used FDA-approved CSF tests in the detection of AD pathology as measured by PET. Use of high accuracy blood tests in clinical practice can improve access to accurate AD diagnosis and AD-specific treatments.

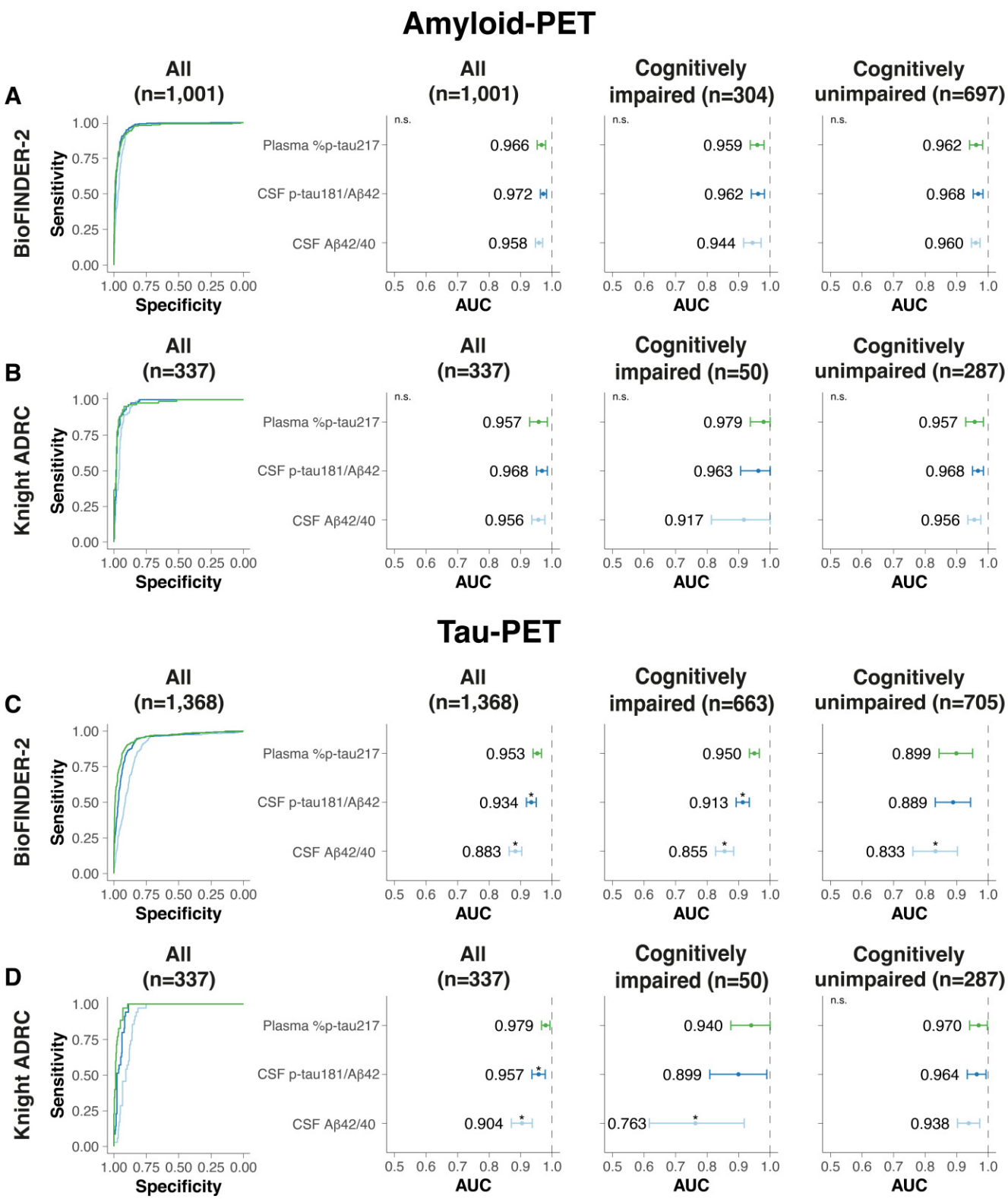

Figure 1: Concordance of fluid and imaging biomarkers of amyloid and tau pathologies
Concordance of fluid biomarkers with amyloid- and tau-PET positivity in BioFINDER-2 (A and C) and Knight ADRC (B and D) participants. ROC curves including all participants are included in the first row. AUCs for all, cognitively impaired and cognitively unimpaired groups are shown in the next three columns, respectively. Dots and error bars represent the actual AUC and 95%CI, respectively. Vertical dashed lines represent the maximal AUC value possible (1). Plots including n.s. in the upper left corner indicate not significant differences between plasma %p-tau217 AUCs and those of the CSF biomarkers. Asterisks represent statistically significant differences with plasma %p-tau217 AUCs. Amyloid-PET positivity was assessed as Centiloids≥37. Tau-PET positivity was assessed using previously validated in-house thresholds (SUVR>1.32 for both cohorts).
Abbreviations: Aβ, amyloid-β; AUC, area under the curve; CI, confidence interval; CSF, cerebrospinal fluid; ROC, receiver operating characteristic.

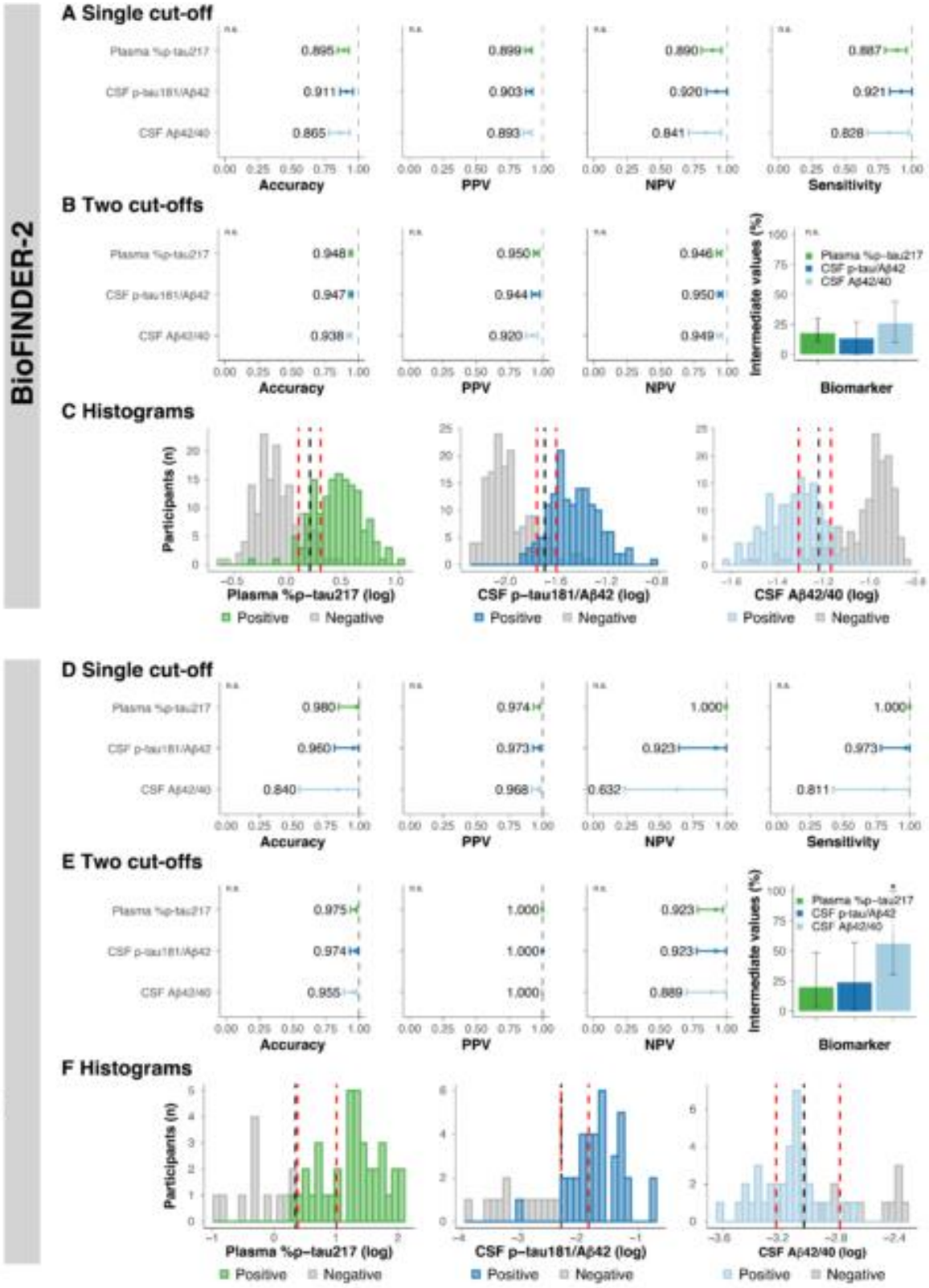

Figure 2: Comparison among fluid biomarkers on predicting amyloid-PET positivity in cognitively impaired patients
Prediction of amyloid-PET positivity in cognitively impaired participants from the BioFINDER-2 (A-C) and Knight ADRC (D-F) cohorts, using a single cut-off (A and D) and a two cut-offs (B and E) approaches, respectively. In the first approach, the threshold was calculated maximizing sensitivity fixing specificity at 90%. In the second approach, the lower threshold was obtained by maximizing specificity with sensitivity fixed at 95%, whereas the upper threshold was obtained by maximizing sensitivity while fixing specificity at 95%. Participants that fall between these two cut-offs were classified in the intermediate group. Dots and error bars represent the actual statistic and 95%CI, respectively. Vertical dashed lines represent the maximal statistical value possible (1). For the intermediate values plots, coloured bars represent the actual percentage and error bar the 95%CI. Plots including n.s. in the upper left corner indicate not significant differences between plasma %p-tau217 statistics and those of the CSF biomarkers. Asterisks represent statistically significant differences with plasma %p-tau217 statistics. Histograms (C and F) represent the distribution of the data coloured by the imaging biomarker status. Vertical black line represents the threshold derived from the first approach, and red lines represent the lower and upper thresholds from the second approach. Amyloid-PET positivity was assessed as Centiloids≥37.
Abbreviations: Aβ, amyloid-β; CI, confidence interval; CSF, cerebrospinal fluid; NPV, negative predictive value; PPV, positive predictive value.

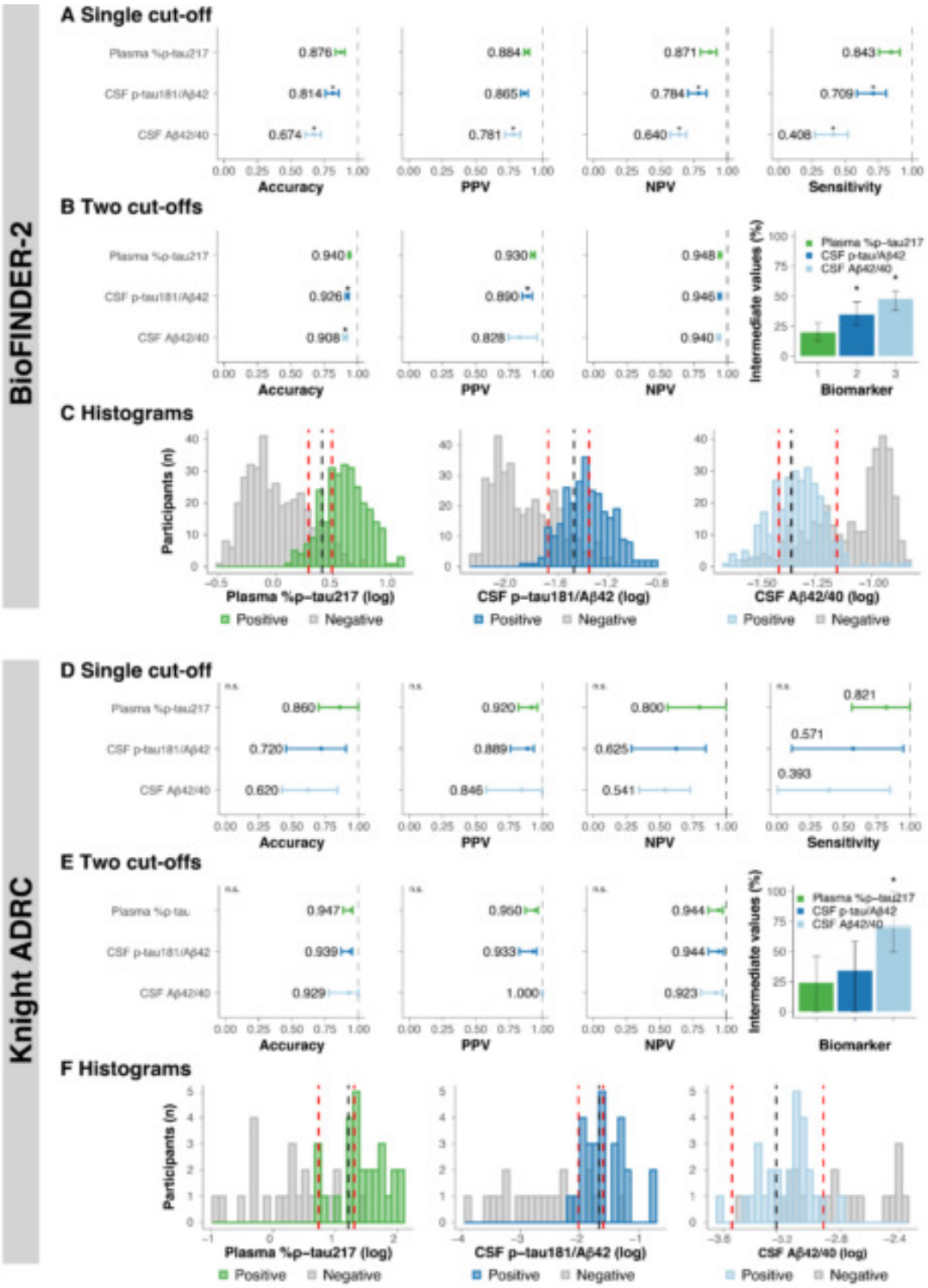

Figure 3: Comparison among fluid biomarkers on predicting tau-PET positivity in cognitively impaired patients
Prediction of tau-PET positivity in cognitively impaired participants from the BioFINDER-2 (A-C) and Knight ADRC (D-F) cohorts, using a single cut-off (A and D) and a two cut-offs (B and E) approaches, respectively. In the first approach, the threshold was calculated maximizing sensitivity fixing specificity at 90%. In the second approach, the lower threshold was obtained by maximizing specificity with sensitivity fixed at 95%, whereas the upper threshold was obtained by maximizing sensitivity fixing specificity at 95%. Participants that fall between these two cut-offs were classified in the intermediate group. Dots and error bars represent the actual statistic and 95%CI, respectively. Vertical dashed lines represent the maximal statistical value possible (1). For the intermediate values plots, coloured bars represent the actual percentage and error bar the 95%CI. Plots including n.s. in the upper left corner indicate not significant differences between plasma %p-tau217 statistics and those of the CSF biomarkers. Asterisks represent statistically significant differences with plasma %p-tau217 statistics. Histograms (C and F) represent the distribution of the data coloured by the imaging biomarker status. Vertical black line represents the threshold derived from the first approach, and red lines represent the lower and upper thresholds from the second approach. Tau-PET positivity was assessed using an in-house previously validated threshold (SUVR>1.32). Three individuals were excluded from the histograms in C (only for visualization purposes) due to very low values of plasma %p-tau217.
Abbreviations: Aβ, amyloid-β; CI, confidence interval; CSF, cerebrospinal fluid; NPV, negative predictive value; PPV, positive predictive value.

Keywords: Plasma biomarkers; head-to-head; amyloid-PET; tau-PET; prediction.

Associations of C2N plasma Aβ42/40 and p-tau217 and subsequent amyloid PET change

Petrice Cogswell[1], Heather Wiste[1], Stephen Weigand[1], Terry Therneau[1], Alicia Algeciras-Schimnich[1], Val Lowe[1], Jonathan Graff-Radford[1], Christopher Schwarz[1], Matthew Senjem[1], Jeffrey Gunter[1], Prashanthi Vemuri[1], David Knopman[1], Ronald Petersen[1], Clifford Jack Jr[1]

[1]*Mayo Clinic, Rochester, MN, United States*

Objective: The C_2N mass spectrometry assays consistently perform well in head-to-head comparisons of Alzheimer's disease plasma biomarker assays. Further validation is needed for use in clinical practice. We evaluated the association of plasma Aβ42/40 and p-tau217 with rates of amyloid PET change and progression from normal (A–) to abnormal (A+) amyloid PET among A– individuals without dementia.

Methods: We included 267 Mayo Clinic Study of Aging participants with C_2N plasma Aβ42/40, p-tau217 ratio (phosphorylated to non-phosphorylated), Amyloid Probability Score 2 (APS2) and serial amyloid PET (PiB) who were cognitively unimpaired (n=250) or had mild cognitive impairment (n=17) and had normal amyloid PET (SUVR≤1.48, Centiloid≤22) at baseline. Linear mixed effects models and Cox proportional hazards models were used to estimate associations with baseline plasma biomarkers and rate of amyloid PET change or progression from A– to A+ adjusting for age and sex.

Results: Participants were median age 71 (range 52–92) years, 47% female, and had median 7 (range 1–13) years from first to last PET scan. A doubling in p-tau217 ratio and 25 points higher APS2 were associated with a 0.3% (95% CI: 0.1–0.5%, p=0.002) and 0.4% (0.1–0.7%, p=0.005) increase in the annual rate of amyloid PET (Figures 1 and 2) and a 1.2 (1.0–1.4, p=0.05) and 1.3 (1.0–1.6, p=0.04) increase in the hazard of progression from A– to A+ (Figure 3), respectively. Aβ42/40 was not significantly associated with amyloid PET change or progression from A– to A+.

Conclusions: Evaluation of the ability of plasma biomarkers to predict future amyloid positivity in patients without dementia is important to inform the utility of plasma biomarkers as use as screening and prognostic tools. Findings in this study suggest that the C_2N plasma p-tau217 ratio and APS2 may be informative about amyloid progression.

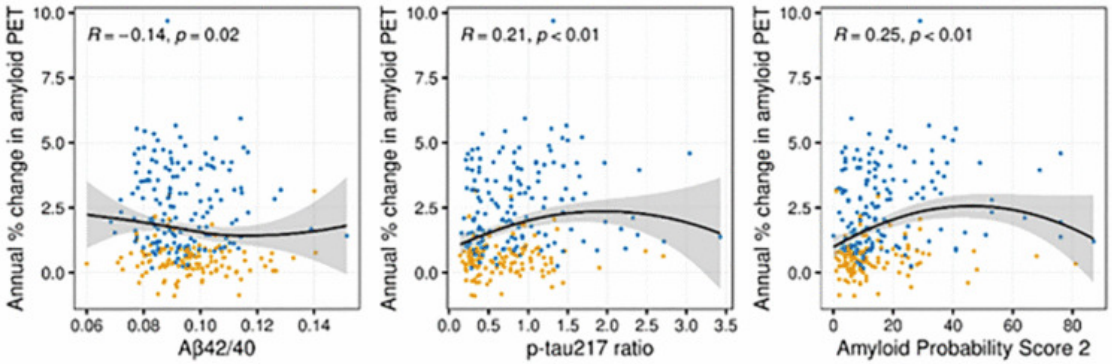

Figure 1: Annual rate of change (%) in amyloid PET vs. baseline plasma biomarkers. Annual % change in amyloid PET was estimated by fitting a separate linear regression model within each person with log(amyloid PET) as the outcome and time from first scan as the predictor. Scatter plots are shown with a nonparametric smoother line and points are colored by those that remained A- (orange) vs. those that progressed to A+ (blue) over follow-up. Spearman correlations show associations of annual % change in amyloid PET vs. plasma Aβ42/40, plasma p-tau217 ratio, and Amyloid Probability Score 2 (APS2), a score generated by C_2N via a statistical algorithm that uses both the plasma Aβ42/40 and p-tau217 ratio.

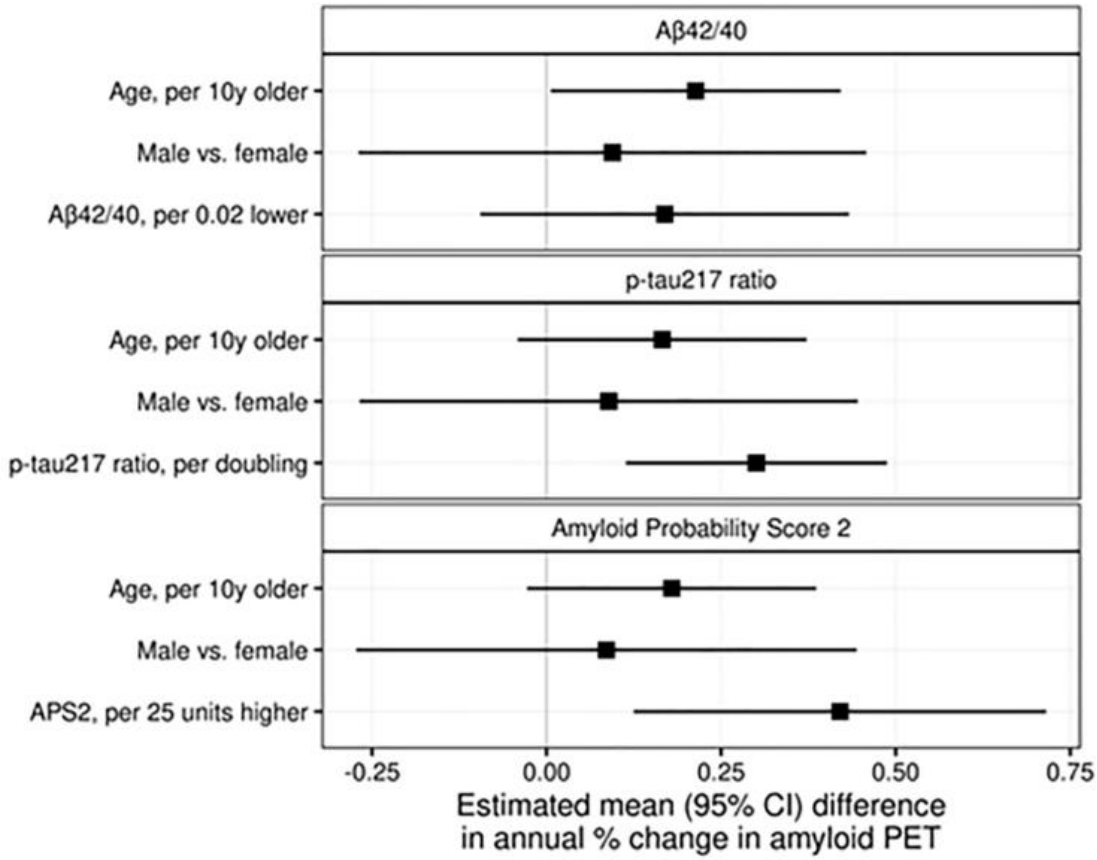

Figure 2: Forest plots of estimated difference in annual rate of change in amyloid PET (%) from linear mixed effects regression models with log(amyloid PET) as the outcome and baseline age, sex, and baseline plasma biomarker level as predictors for each plasma measure: Aβ42/40, p-tau217 ratio, and Amyloid Probabilty Score 2 (APS2).

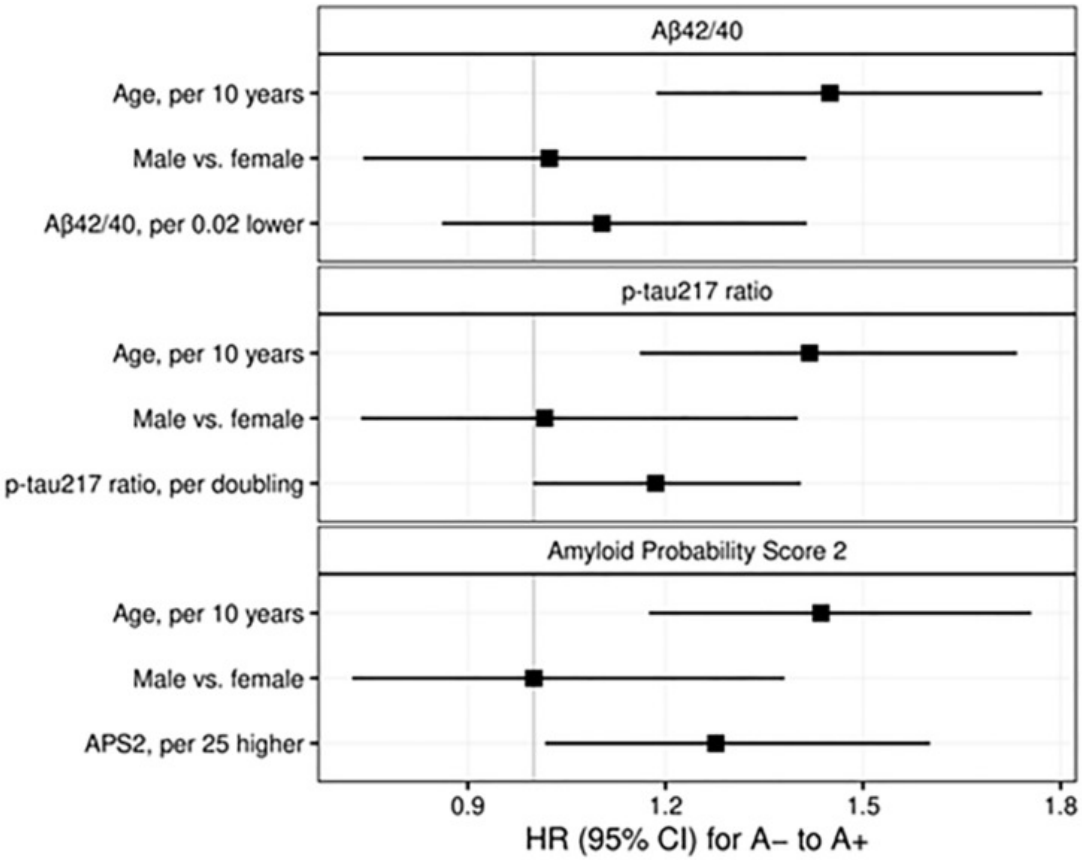

Figure 3: Forest plots of hazard ratios from Cox models with time from A- to A+ as the outcome and baseline age, sex, and baseline plasma biomarker level as predictors for each plasma measure: Aβ42/40, p-tau217 ratio, and Amyloid Probability Score 2 (APS2). A+ was defined as SUVR = 1.48 (Centiloid = 22).

Keywords: Plasma p-tau, plasma Aβ42/40, Amyloid Probability Score 2, amyloid PET, Alzheimer's disease

Plasma p-tau212 is increased in CSF amyloid positive and [18F]flutemetamol PET negative cognitively impaired individuals

Przemyslaw R. Kac[1], Armand González-Escalante[2,3,4], Marta Milà-Alomà[2,5], Nicholas J. Ashton[1,6,7,8], Mahnaz Shekari[2,3,4,5], Michael Turton[9], Peter Harrison[9], Paula Ortiz-Romero[2,3], Henrik Zetterberg[1,6,10,11,12,13], Juan Domingo Gispert[2,3,14], Kaj Blennow[1,15], Marc Suárez-Calvet[2,3,14,16], Thomas K. Karikari[1,17]

[1]*Department of Psychiatry and Neurochemistry, Institute of Neuroscience and Physiology, The Sahlgrenska Academy at the University of Gothenburg, Mölndal, Sweden*
[2]*Barcelonaβeta Brain Research Center (BBRC), Pasqual Maragall Foundation, Barcelona, Spain*
[3]*Hospital del Mar Research Institute, Barcelona, Spain*
[4]*Universitat Pompeu Fabra, Barcelona, Spain*
[5]*Centro de Investigación Biomédica en Red de Fragilidad y Envejecimiento Saludable (CIBERFES), Madrid, Spain*
[6]*Institute of Psychiatry, Psychology and Neuroscience, Maurice Wohl Clinical Neuroscience Institute, King's College London, London, United Kingdom*
[7]*UK NIHR Biomedical Research Centre for Mental Health and Biomedical Research Unit for Dementia at South London and Maudsley NHS Foundation, London, United Kingdom*
[8]*Centre for Age-Related Medicine, Stavanger University Hospital, Stavanger, Norway*
[9]*Bioventix Plc, Farnham, United Kingdom*
[10]*Department of Neurodegenerative Disease, Dementia Research Centre, UCL Institute of Neurology, Queen Square, London, United Kingdom*
[11]*UK Dementia Research Institute, University College London, London, United Kingdom*
[12]*Hong Kong Center for Neurodegenerative Diseases, HKCeND, Hong Kong, China*
[13]*School of Medicine and Public Health, University of Wisconsin-Madison, Madison, WI, United States*
[14]*Centro de Investigación Biomédica en Red Bioingeniería, Biomateriales y Nanomedicina, Madrid, Spain*
[15]*Clinical Neurochemistry Laboratory, Sahlgrenska University Hospital,, Mölndal, Sweden*
[16]*Servei de Neurologia, Hospital del Mar, Barcelona, Spain*
[17]*Department of Psychiatry, School of Medicine, University of Pittsburgh, Pittsburgh, PA, United States*

Recently published articles suggest that most plasma p-tau biomarkers (e.g., p-tau181, p-tau217 and p-tau231) have shown high accuracies for AD diagnosis; however, some of them appear to be increased earlier in the AD continuum than others. Blood biomarkers that can identify subtle elevations in amyloid-beta pathology among older adults without evidence of cognitive impairment would be ideal candidates for the recruitment and enrichment of participants with preclinical AD in clinical trials. Plasma p-tau212 is a novel, autopsy-confirmed blood biomarker that can discriminate subjective cognitive decline patients from AD patients in memory clinics. However, we evaluated the capacity of plasma p-tau212 to detect emerging amyloid-beta pathology in cognitively unimpaired individuals with abnormal levels of CSF Aβ42/40 ratio but remain normal for amyloid-beta PET.

In-house developed plasma p-tau212 Simoa immunoassay was used to measure p-tau212 levels in the ALFA+ cohort (n=311). N=268 participants had available [^{18}F]flutemetamol scans. Participants were classified as Aβ positive (A+) if CSF Aβ42/40<0.071. We further classified participants according to their CSF/PET Aβ status. The group with a low burden of Aβ pathology was defined as CSF Aβ42/40<0.071 and Aβ PET Centiloids<30 and was compared with CSF/PET Aβ negative (CSF Aβ42/40≥0.071 and Aβ PET Centiloids<30) and CSF/PET Aβ positive (CSF Aβ42/40<0.071 and Aβ PET Centiloids≥30).

In the low-burden Aβ pathology group, plasma p-tau212 concentration was significantly higher, reaching 35.6% mean-fold increase compared with the A- group. P-tau181 and p-tau231 levels were increased 14.7% and 30.5% respectively. Plasma p-tau212 had also higher than other biomarkers %mean-fold increases in the A+ PET positive group.

Increase of plasma p-tau212 before established Aβ PET positivity makes it a cost-effective and simple-to-

implement biomarker for population screening and clinical trial recruitment purposes. Further increase of p-tau212 in Aβ PET-positive participants suggests that this biomarker has utility for clinical monitoring of anti-amyloid therapies.

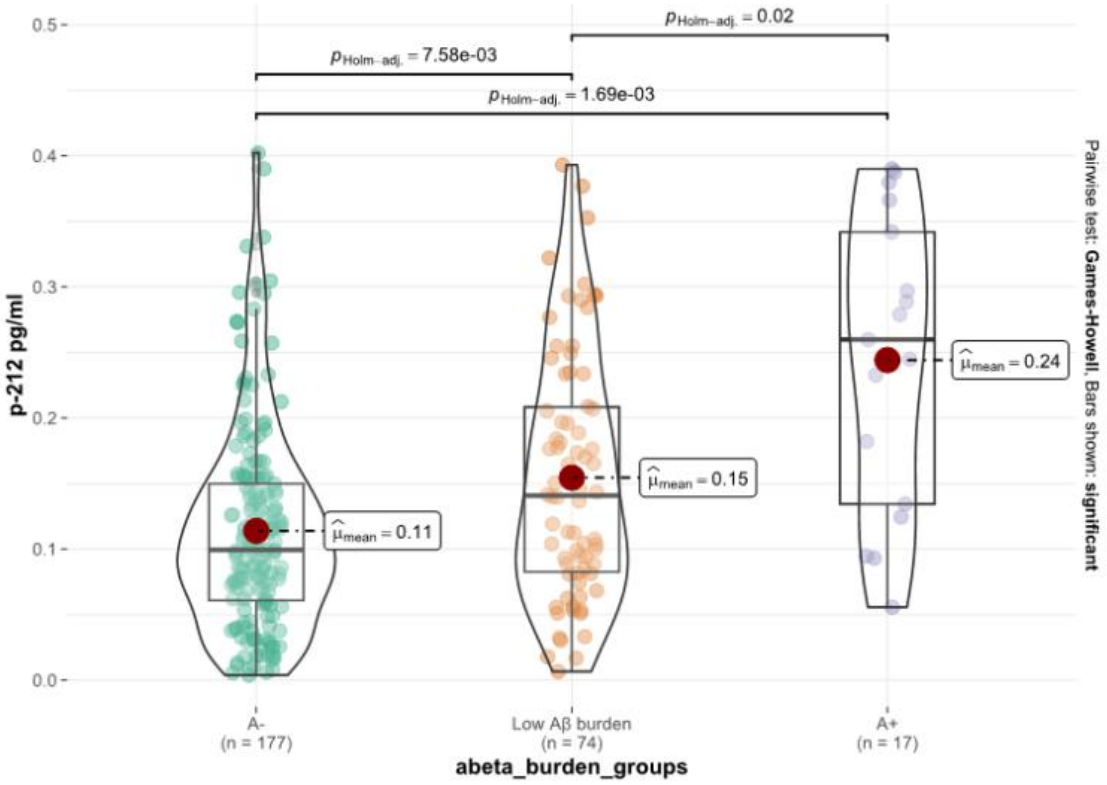

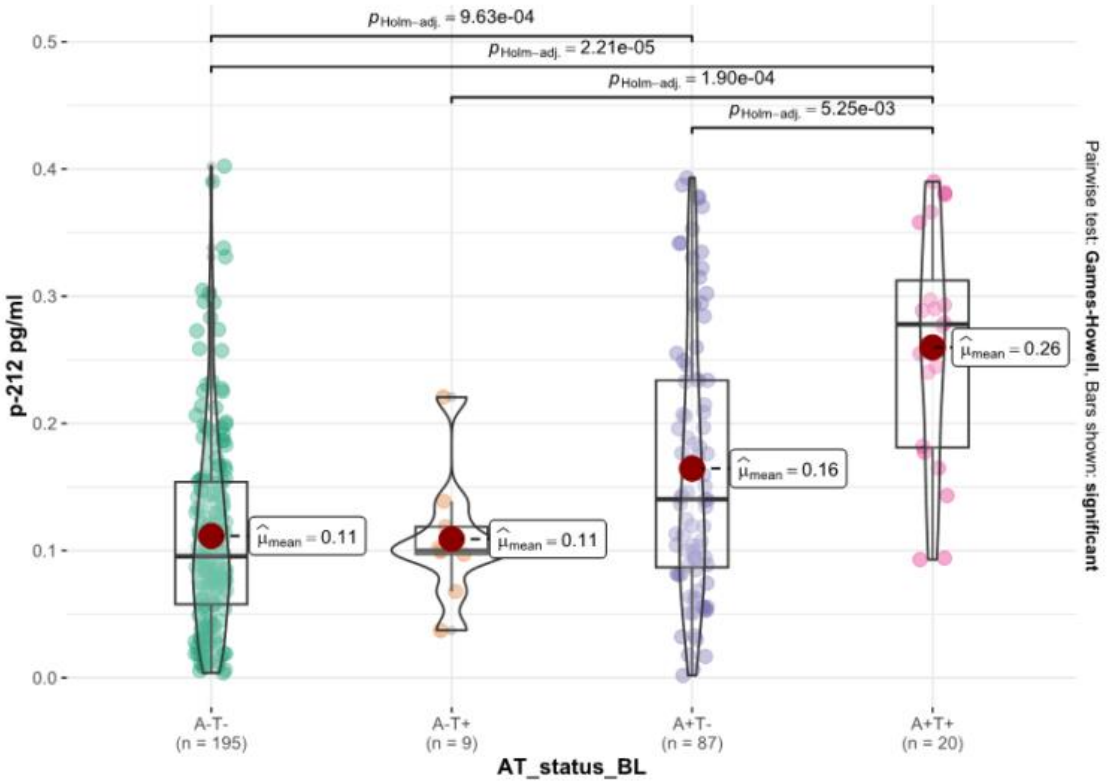

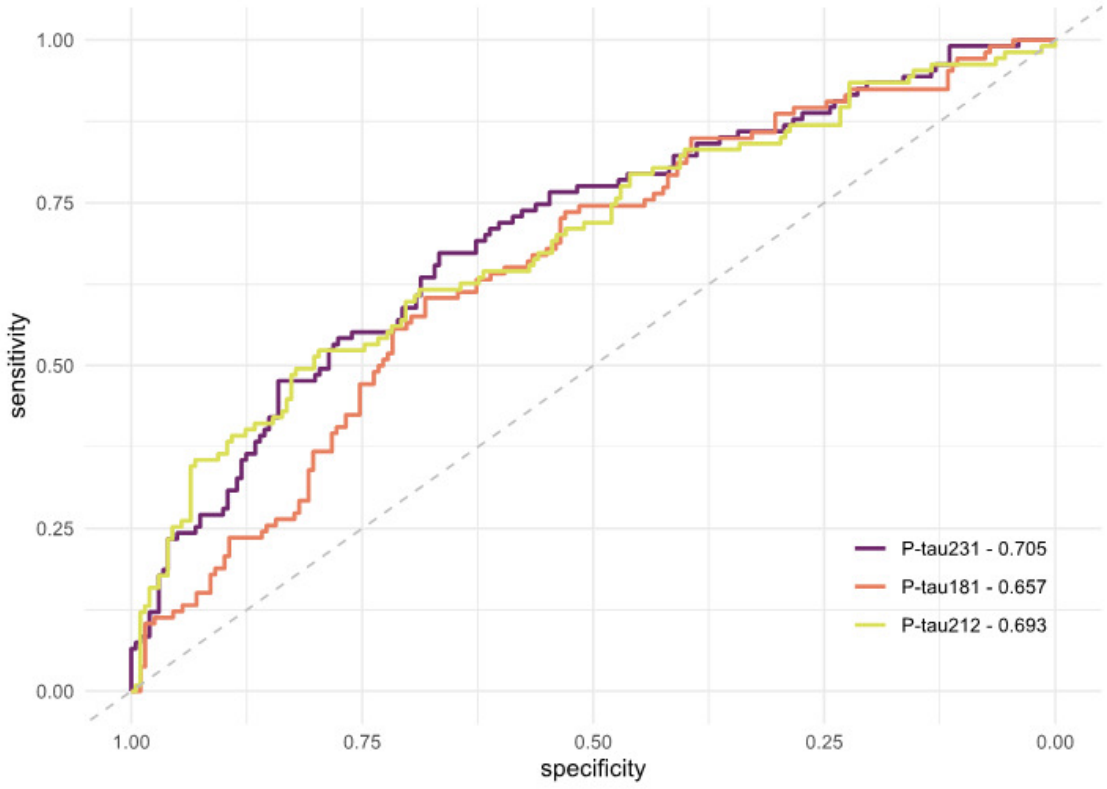

Keywords: Preclinical Alzheimer's Disease, p-tau212, [18F]flutemetamol, plasma,

KEYNOTE: The multiple neurodegenerative pathologies of the ageing brain

Johannes Attems

Newcastle University, Newcastle upon Tyne, United Kingdom

The defining neuropathological features of age associated neurodegenerative diseases are aggregations of misfolded proteins and the neuropathological diagnosis is based on the semiquantitative assessment of these misfolded proteins that constitute the neuropathological hallmark lesion for the respective disease: e.g. Alzheimer's disease (AD), amyloid-β (Aβ) hyperphosphorylated tau (tau); Lewy body diseases, α-synuclein (α-syn); frontotemporal lobar degeneration, tau or TDP-43 or ubiquitin or FUS.

In addition, cerebrovascular lesions are assessed for the diagnosis of cerebrovascular disease. However, in brains of elderly patients suffering from neurodegenerative diseases multiple pathologies are usually present and various amounts of neurodegenerative and cerebrovascular pathology are frequently seen even in brains of non-demented elderly. It does indeed become increasingly clear that the clinical picture of dementia in most aged patients results from multiple pathologies rather than from one single disease.

Importantly, these multiple pathologies are often not detected clinically, which has a detrimental impact on clinical studies since apparently homogeneous study cohorts (e.g. AD) are likely to be heterogeneous (e.g. AD only, AD and α-syn, AD and TDP-43), which in turn introduces a bias into therapeutic trials and biomarker/ imaging studies. Hence, wherever possible clinical studies should ideally involve neuropathological *postmortem* assessment to correlate clinical with neuropathological data as this will enable a more accurate stratification of clinical cohorts according to the presence of multiple pathologies. This is important in order to interpret clinical data on biomarkers and therapeutic effects.

Dr. Johannes Attems' research interest is neurodegenerative diseases of the ageing brain with a focus on clinico-neuropathological correlative studies.

Despite the categorization of age associated neurodegenerative diseases into specific subtypes, such as Alzheimer's disease and Lewy body diseases, it becomes more and more apparent that the ageing brain is characterized by the presence of multiple pathologies. Dr. Attems aims to evaluate the combined influence of these pathologies on the clinical syndrome as this might lead to the identification of new disease subtypes and thereby to the development of novel therapeutic strategies against age associated neurodegeneration.

Dr. Attems is Professor of Neuropathology at Newcastle University, Honorary Consultant Pathologist at Royal Victoria Infirmary, Newcastle and Director of the Newcastle Brain Tissue Resource.

He is Editor in Chief of **Acta Neuropathologica** and leads the Neurodegenerative Pathology Research Group.

Friday, January 19, 2024 - 11:50 am - 02:30 pm

Podium Session

SESSION X: Plasma Applications

CHAIRS: Keith Johnson, Henrik Zetterberg

Friday, January 19, 2024		
11:50 am - 02:30 pm	**SESSION X: Plasma Applications**	**Henrik Zetterberg, University of Gothenburg, Sweden** **Keith Johnson, Massachusetts General Hospital, Boston, MA, United States**
11:50	Introduction	Chairs
11:55	Plasma GFAP mediates the relationship between amyloid and tau PET in individuals with Down Syndrome	Boerwinkle | Wisch | Gordon | Flores | Kennedy | Roman | Nelson | Handen | Christian | Head | Mapstone | Klunk | Rafii | O'Bryant | Price | Schupf | Laymon | Krinsky-McHale | Lai | Rosas | Hartley | Zaman | Lott | Silverman | Brickman | Lee | Cohen | Schmitt | Ptomey | Ances
12:10	Association of plasma GFAP with FDG, PiB and tau PET across aging and the Alzheimer's disease continuum	Dicks | Schwarz | Fan | Barnard | Botha | Algeciras-Schimnich | Boeve | Corriveau-Lecavalier | Graff-Radford | Knopman | Lowe | Senjem | Vemuri | Petersen | Jack Jr. | Jones
12:25	Relationships between PET and blood plasma biomarkers in corticobasal syndrome	Singh | Alnobani | Graff-Radford | Machulda | Schwarz | Senjem | Jack, Jr | Lowe | Kanekiyo | Josephs | Whitwell
12:40	Evaluating the impact of racialization on imaging and plasma biomarkers	Gogola | Zeng | Saeed | Lopresti | Snitz | Tudorascu | Minhas | Ikonomovic | Kofler | Matan | Mason | Pascoal | Aizenstein | Mathis | Klunk | Zetterberg | Blennow | Lopez | Reis | Villemagne | Karikari | Cohen
12:55	Lunch	
01:45	Plasma, MRI, and PET biomarker-based risk prediction of dementia in the context of health-related comorbidities and demographic factors: a preliminary exploration	Rudolph | Rundle | Sutphen | Register | Hughes | Bateman | Whitlow | Solingapuram Sai | Dage | Russ | Mielke | Craft | Lockhart
02:00	Longitudinal change of cerebral amyloid and tau and its association with plasma biomarkers in preclinical AD	Fajardo-Valdez | Yakob | Javanray | St-Onge | Gallego-Rudolf | Qiu | Ourry | Remz | Saucy | Ashton | Zetterberg | Blennow | Poirier | Breitner | Villeneuve
02:15	Proteome-wide analyses Identifies Plasma Immune Regulators of Amyloid-beta progression	Duggan | Gomez | Bilgel | Chen | Hohman | Cordon | Castellano | Koran | Candia | Lewis | Moghekar | Ashton | Kac | Karikari | Blennow | Zetterberg | Thambisetty | Coresh | Resnick | Walker

Friday, January 19, 2024	
02:30	Discussion

Plasma GFAP mediates the relationship between amyloid and tau PET in individuals with Down Syndrome

Anna Boerwinkle[1,2], Julie Wisch[1], Brian Gordon[3], Shaney Flores[3], James Kennedy[1], June Roman[1], Brittany Nelson[1], Benjamin Handen[4], Bradley Christian[5], Elizabeth Head[6], Mark Mapstone[7], William Klunk[4], Michael Rafii[8], Sid O'Bryant[9], Julie Price[10], Nicole Schupf[11,12], Charles Laymon[13], Sharon Krinsky-McHale[14], Florence Lai[15], H. Diana Rosas[10,15], Sigan Hartley[16], Shahid Zaman[17,18], Ira Lott[19], Wayne Silverman[19], Adam Brickman[11,20,21], Joseph Lee[11,12], Annie Cohen[4], Frederick Schmitt[21], Lauren Ptomey[22], Beau Ances[1]

[1]*Department of Neurology, Washington University in St. Louis, Saint Louis, MO, United States*
[2]*McGovern Medical School at UTHealth Houston, Houston, TX, United States*
[3]*Department of Radiology, Washington University in St. Louis, Saint Louis, MO, United States*
[4]*Department of Psychiatry, University of Pittsburgh, Pittsburgh, PA, United States*
[5]*Department of Medical Physics and Psychiatry, University of Wisconsin, Madison, Madison, WI, United States*
[6]*Department of Pathology and Laboratory Medicine, University of California, Irvine, Irvine, CA, United States*
[7]*Department of Neurology, University of California, Irvine, Irvine, CA, United States*
[8]*Alzheimer's Therapeutic Research Institute, Keck School of Medicine, Los Angeles, CA, United States*
[9]*Institute for Translational Research, University of North Texas Health Science Center, Fort Worth, TX, United States*
[10]*Department of Radiology, Harvard Medical School, Massachusetts General Hospital, Charlestown, MA, United States*
[11]*Department of Neurology, Vagelos College of Medicine, Columbia University, New York City, NY, United States*
[12]*Department of Epidemiology, Vagelos College of Medicine, Columbia University, New York City, NY, United States*
[13]*Department of Radiology, University of Pittsburgh, Pittsburgh, PA, United States*
[14]*Department of Psychology, New York State Institute for Basic Research in Developmental Disabilities, Staten Island, NY, United States*
[15]*Department of Neurology, Harvard Medical School, Massachusetts General Hospital, Brigham and Women's Hospital, Boston, MA, United States*
[16]*Waisman Center, University of Wisconsin, Madison, WI, United States*
[17]*Cambridge Intellectual and Developmental Disabilities Research Group, University of Cambridge, Cambridge, United Kingdom*
[18]*Cambridgeshire and Peterborough Foundation NHS Trust, Cambridge, United Kingdom*
[19]*Department of Pediatrics, University of California Irvine School of Medicine, Irvine, CA, United States*
[20]*Taub Institute of Research on Alzheimer's disease and the Aging Brain, Vagelos College of Medicine, Columbia University, New York, NY, United States*
[21]*Sanders-Brown Center on Aging and the Kentucky Neuroscience Institute, Lexington, KY, United States*
[22]*University of Kansas Medical Center, Kansas City, KS, United States*

Introduction: Almost all individuals with Down Syndrome (DS) develop early-onset Alzheimer's disease (AD), but AD biomarker accumulation seems to occur more rapidly in DS. Plasma GFAP, a biomarker of astrocyte health and neuroinflammation, has been shown to partially mediate the relationship between amyloid and tau accumulation in sporadic AD. We aimed to assess the role of GFAP in AD progression in DS.

Methods: We included 348 participants with DS and 42 controls from the Alzheimer's Biomarker Consortium – Down Syndrome (ABC-DS) (**Table 1**). Amyloid PET was acquired using [^{11}C]-PiB or [^{18}F]-AV45, and amyloid-positive was defined as Centiloid > 22.5. Tau PET was acquired using [^{18}F]-AV1451, and tau-positive was defined as tau summary SUVR > 1.3. We assessed initial biomarker changes over estimated-years-to-symptom-onset (EYO), calculated as the participant's current age subtracted from 52.5 years, an average age of symptom onset in DS. We then compared plasma GFAP levels by amyloid-positivity (A-/A+) and tau-positivity (T-/T+) status. Finally, a mediation analysis measured whether plasma GFAP mediated the relationship between amyloid and tau PET measures.

Results: Amyloid PET accumulation began prior to other AD biomarker changes in individuals with DS at EYO = -16.4 and was closely followed by plasma GFAP at EYO = -14.3 (**Figure 1**). Tau PET elevation did not occur until EYO = -11.3. Plasma GFAP levels were significantly elevated in A+/T- and A+/T+ compared to A-/T- and controls (p-values < 0.001) (**Figure 2**). Finally, plasma GFAP partially mediated the relationship between PET amyloid and tau (15% of total effect, p = 0.034).

Conclusion: Overall, our results suggest neuroinflammation may contribute to the accelerated timeline between significant amyloid and tau accumulation in DS. This is an important consideration for future clinical trials and the treatment of AD in individuals with DS.

Table 1. Participant demographics

	Controls (n = 42)	Down syndrome (DS) (n = 348)	p-value
Age, years (mean [SD])	43.57 [12.5]	44.93 [9.7]	0.409
Female	33 (78.6%)	157 (45.1%)	**0.003**
Race			0.781
White	42 (100%)	334 (96%)	
Black or African American	0	4 (1.2%)	
Asian	0	5 (1.4%)	
Multi/Other	0	5 (1.4%)	
APOE ε4-positive	11 (26.2%)	81 (23.4%)	0.835
Consensus diagnosis			--
Asymptomatic	--	251 (72.1%)	
Symptomatic	--	41 (11.8%)	
No consensus	--	15 (4.3%)	
Down syndrome type			---
Full trisomy 21	--	303 (89.9%)	
Translocation	--	19 (5.6%)	
Mosaicism	--	15 (4.5%)	

Abbreviations: APOE = apolipoprotein E; DS = Down syndrome; SD = standard deviation

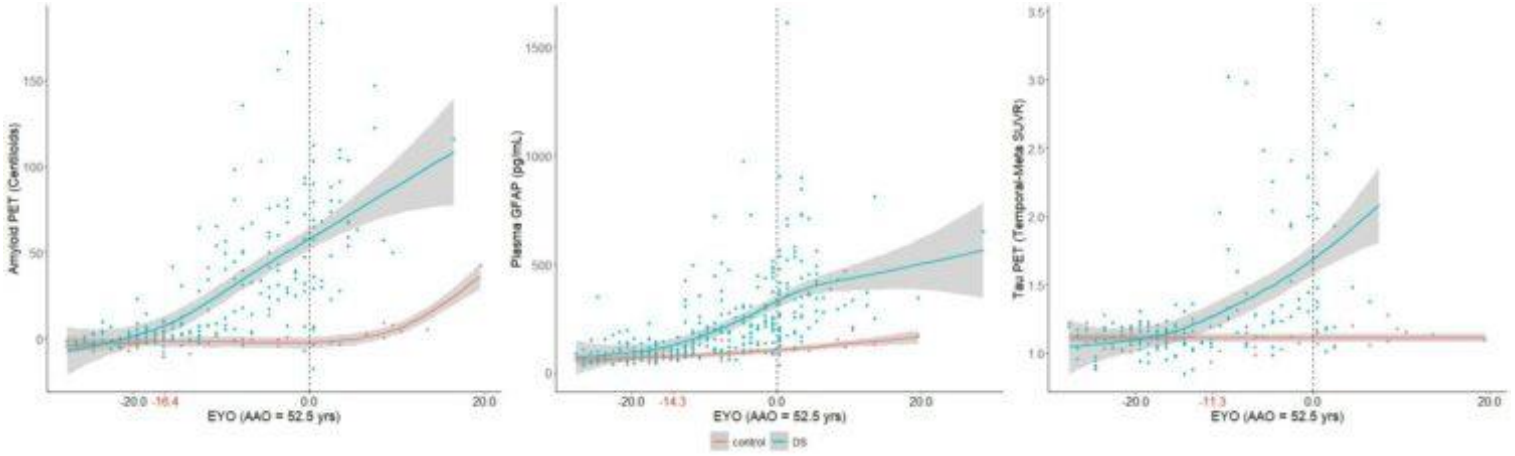

Figure 1

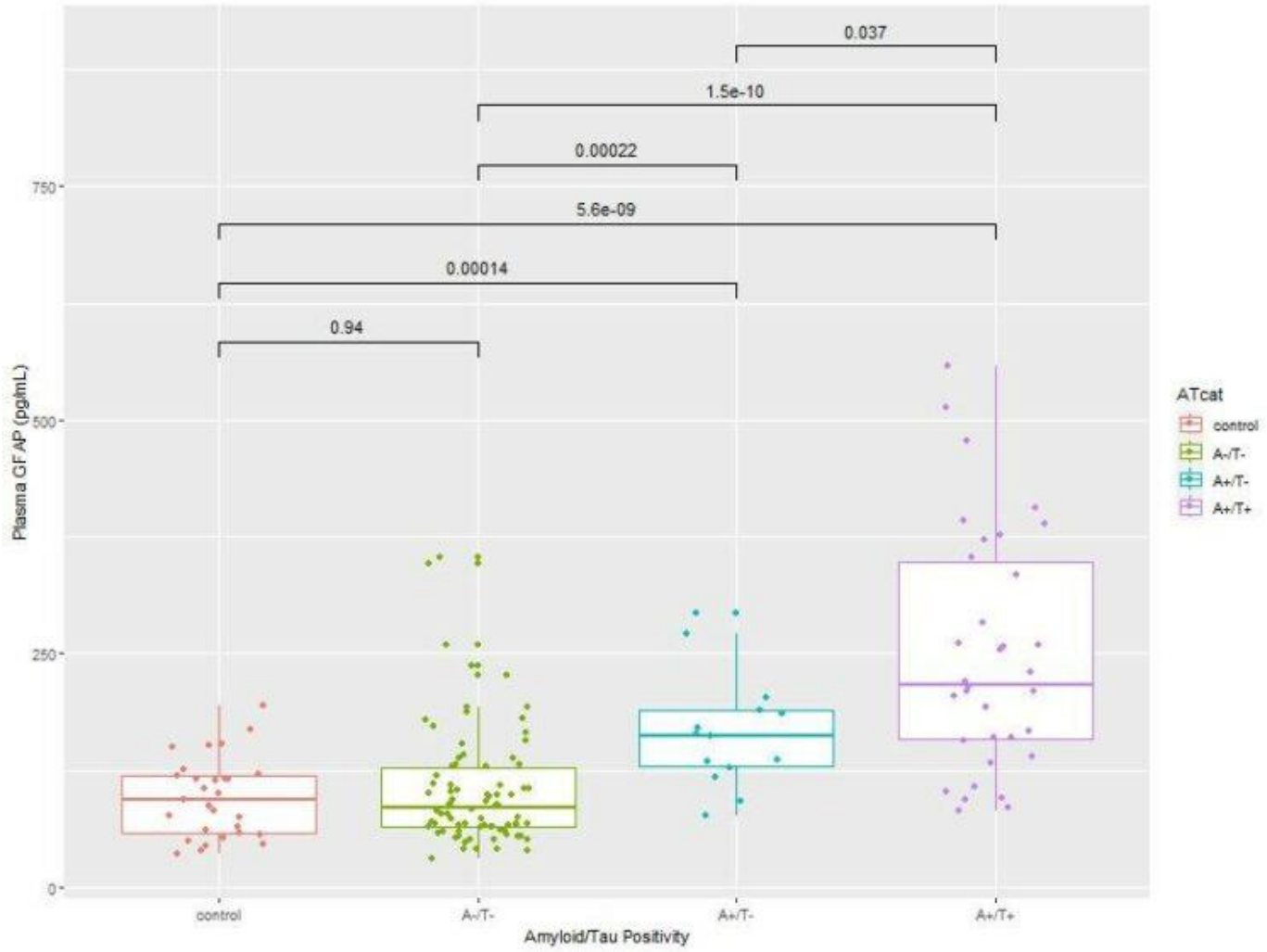

Figure 2

Keywords: Down syndrome, Alzheimer, GFAP, Amyloid, Tau

Association of plasma GFAP with FDG, PiB and tau PET across aging and the Alzheimer's disease continuum

Ellen Dicks[1,2], Christopher Schwarz[3], Winnie Fan[4], Leland Barnard[1], Hugo Botha[1], Alicia Algeciras-Schimnich[5], Bradley F. Boeve[1], Nick Corriveau-Lecavalier[1,6], Jonathan Graff-Radford[1], David S. Knopman[1], Val J. Lowe[3], Matthew L. Senjem[3,7], Prashanthi Vemuri[3], Ronald C. Petersen[1], Clifford R. Jack Jr.[3], David T. Jones[1]

[1]*Department of Neurology, Mayo Clinic, Rochester, MN, United States*
[2]*Alzheimer Center Amsterdam, Department of Neurology, Amsterdam Neuroscience, Vrije Universiteit Amsterdam, Amsterdam UMC, Amsterdam, The Netherlands*
[3]*Department of Radiology, Mayo Clinic, Rochester, MN, United States*
[4]*Department of Quantitative Health Sciences, Mayo Clinic, Rochester, MN, United States*
[5]*Department of Laboratory Medicine and Pathology, Mayo Clinic, Rochester, MN, United States*
[6]*Department of Psychiatry and Psychology, Mayo Clinic, Rochester, MN, United States*
[7]*Department of Information and Technology, Mayo Clinic, Rochester, MN, United States*

Plasma levels of glial fibrillary acidic protein (GFAP), a marker for astrocytosis, have been shown to increase with aging and to be elevated in Alzheimer's disease (AD) compared to controls. However, the relationship between plasma GFAP and imaging biomarkers remains poorly understood. Here, we assessed these associations in 218 cognitively unimpaired (CU) individuals with normal amyloid/tau-PET (A-T-) and 231 individuals on the AD continuum (80 CU A+T-, and 49 CU, 32 amnestic MCI 70 AD dementia who were all A+T+) from the ADRC/MCSA who had plasma GFAP and FDG/PiB/AV1451-PET within 6 months available. Meta-ROI SUVR values were calculated for each imaging modality. We first assessed the association between age and GFAP and used residuals for subsequent analyses. We then used regression models and estimated marginal means for the association between GFAP and meta-ROI SUVR across the AD continuum. GFAP levels were associated with age in all groups, except aMCI (Fig.1). Group comparisons showed increasing GFAP with more advancing disease stages (Fig.2). We found that higher GFAP was significantly associated with higher PiB-PET SUVR in CU A+T+ only (Fig.3A). Associations were stronger between tau-PET SUVR and advanced disease stages, with higher GFAP being significantly associated with higher SUVR in the aMCI and AD group (Fig.3B). Higher GFAP was significantly related to higher FDG-SUVR in CU A-T-, and this relationship gradually inverted across the AD continuum, with higher GFAP being related to lower FDG-SUVR in AD (Fig.3C). We found similar relationships for annual delta SUVR for all modalities in a subset of individuals with longitudinal FDG/PiB/AV1451-PET available. Our results show that GFAP in plasma is related to disease worsening and that levels are distinctly associated with several AD imaging biomarkers. Findings of a positive association between GFAP levels and FDG-PET SUVR in cognitively unimpaired groups suggest hypermetabolism in early AD stages.

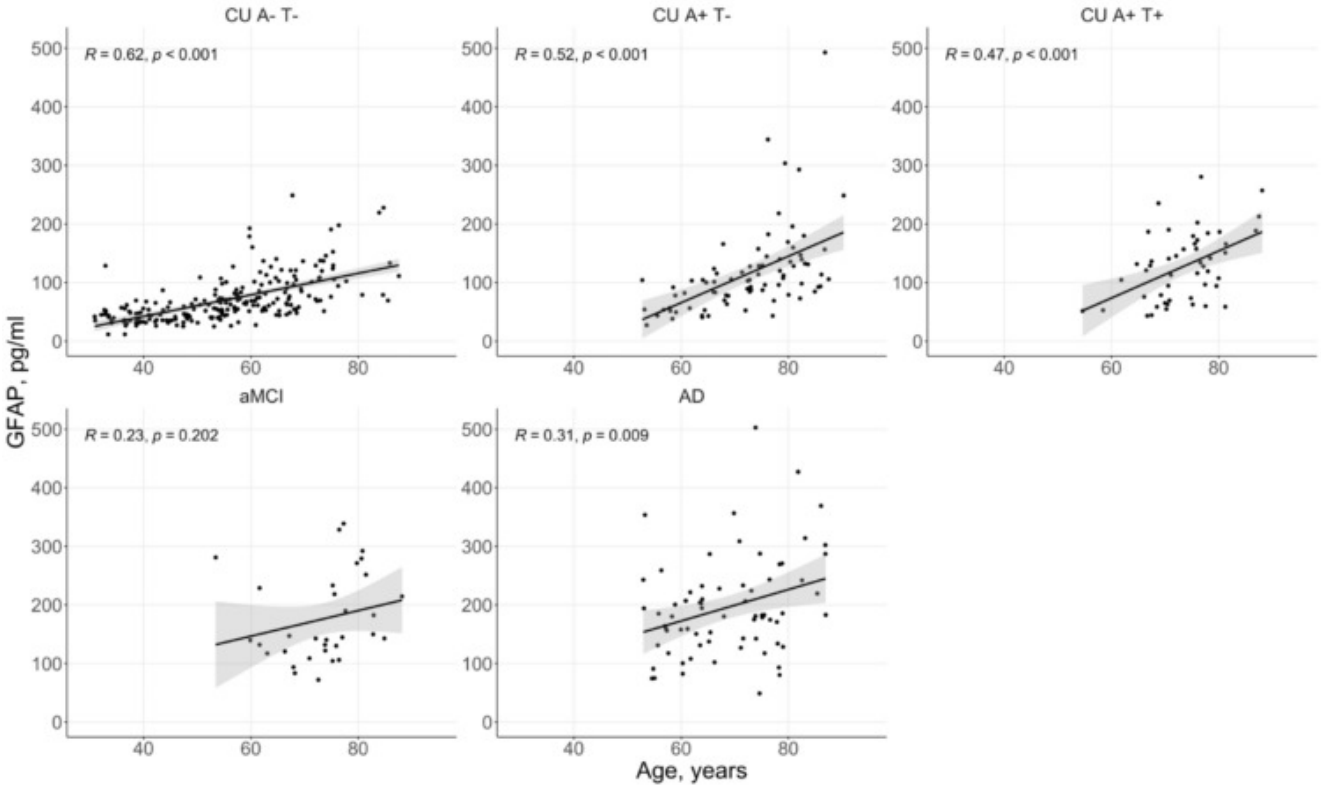

Figure 1. Relationship between aging and plasma GFAP levels across the AD continuum. Pearson's correlation coefficients are displayed. CU: cognitively unimpaired, A-/A+: amyloid negative/positive, T-/T+: tau negative/positive, aMCI: amnestic mild cognitive impairment, AD: Alzheimer's disease dementia.

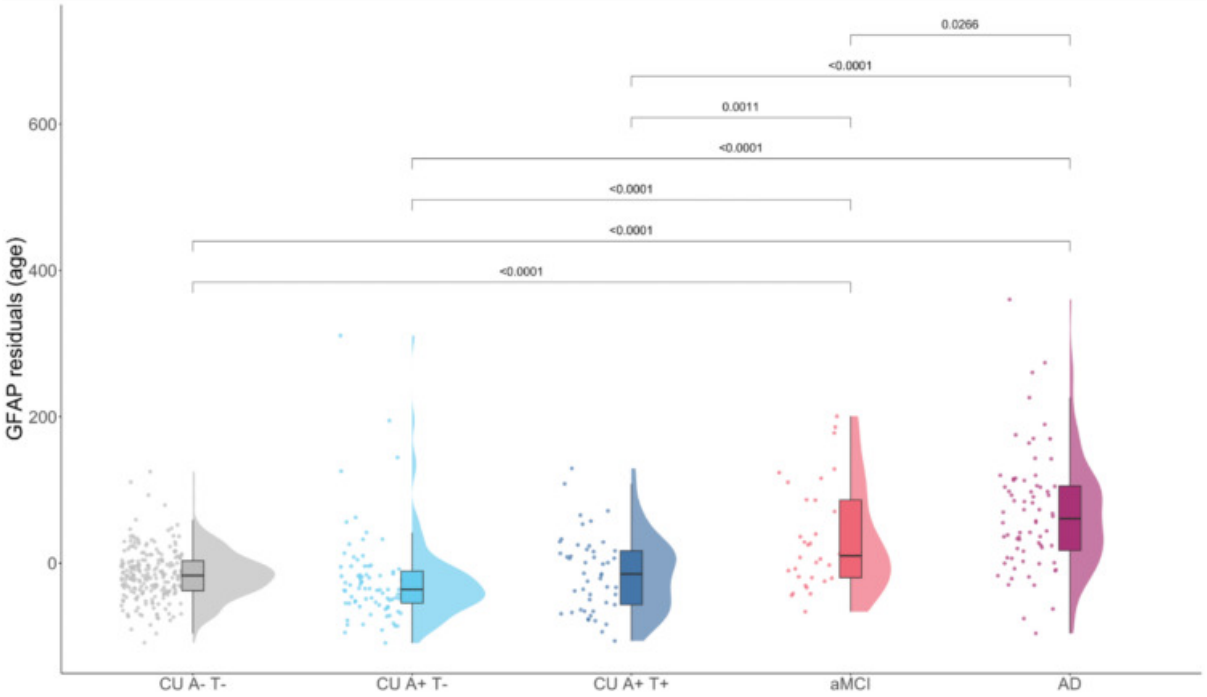

Figure 2. Comparison of GFAP residuals between groups. Residuals were computed by regressing GFAP plasma levels on age. Pairwise comparisons were performed using Tukey's test. CU: cognitively unimpaired, A-/A+: amyloid negative/positive, T-/T+: tau negative/positive, aMCI: amnestic mild cognitive impairment, AD: Alzheimer's disease dementia.

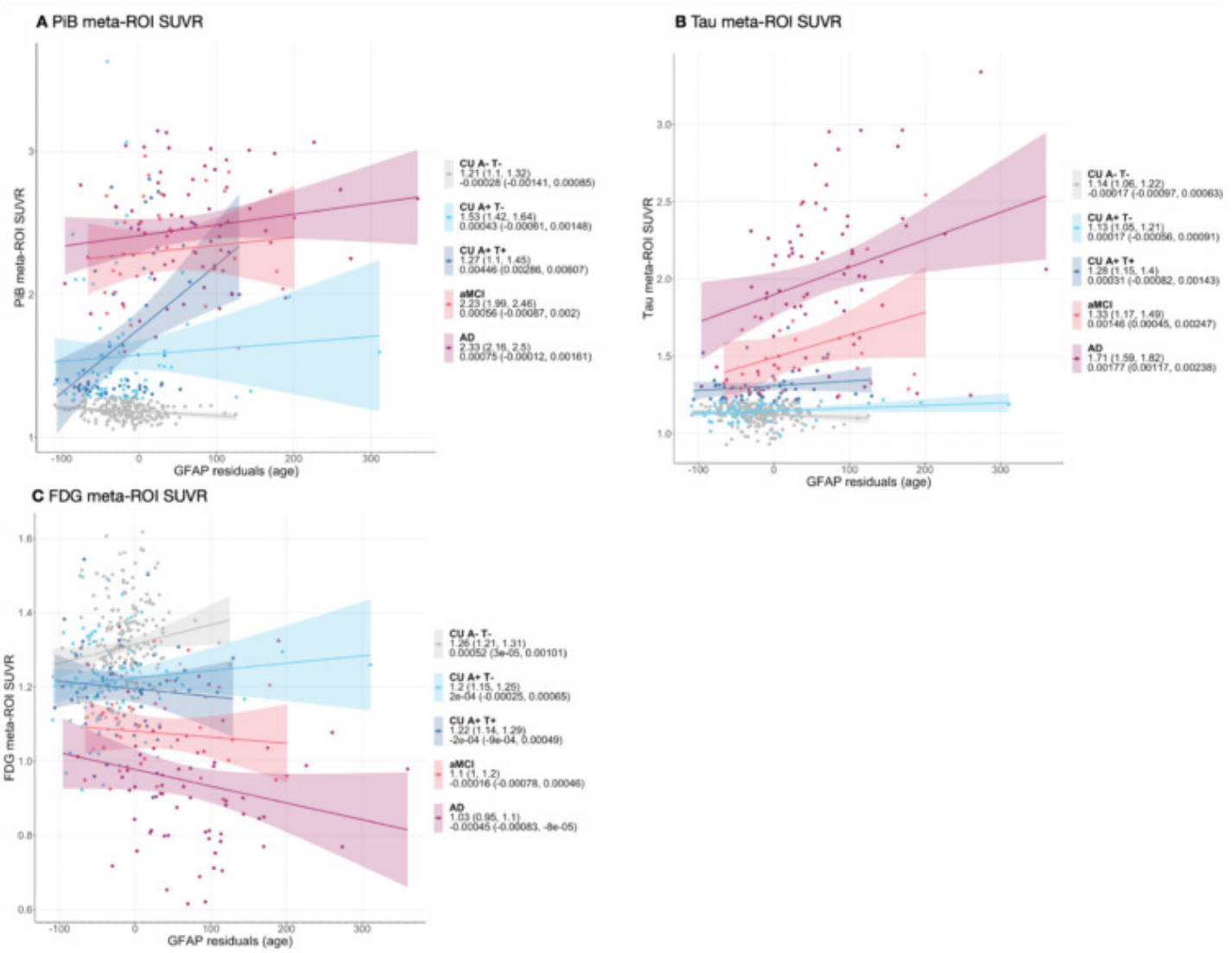

Figure 3. Relationship between GFAP residuals and PiB, tau and FDG meta-ROI SUVR across the AD continuum. Associations were estimated using linear regressions, including GFAP residuals, diagnosis and their interaction effect as predictors and the meta-ROI SUVR of the respective modality (PiB, tau, FDG) as the outcome. Results displayed are estimated marginal means and trends (95% confidence interval). Please note that trends were estimated for a 1-unit change in GFAP residuals (e.g. for CU A- T-, a 0.00028 decrease in PiB meta-ROI SUVR per 1 increase in GFAP residuals). CU: cognitively unimpaired, A-/A+: amyloid negative/positive, T-/T+: tau negative/positive, aMCI: amnestic mild cognitive impairment, AD: Alzheimer's disease dementia.

Keywords: Alzheimer's, FDG PET, PiB PET, AV1451 PET, plasma GFAP

Relationships between PET and blood plasma biomarkers in corticobasal syndrome

Neha Atulkumar Singh[1], Alla Alnobani[2], Jonathan Graff-Radford[1], Mary Machulda[3], Christopher Schwarz[4], Matthew Senjem[4], Clifford Jack, Jr[4], Val Lowe[4], Takahisa Kanekiyo[2], Keith Josephs[1], Jennifer Whitwell[4]

[1]*Department of Neurology, Mayo Clinic, Rochester, MN, United States*
[2]*Department of Neuroscience, Mayo Clinic, Jacksonville, FL, United States*
[3]*Department of Psychiatry & Psychology, Mayo Clinic, Rochester, MN, United States*
[4]*Department of Radiology, Mayo Clinic, Rochester, MN, United States*

Background: Corticobasal syndrome (CBS) is a progressive neurodegenerative syndrome that can result from several underlying neuropathologies, including Alzheimer's disease (AD). Little is known about the utility of blood plasma metrics to predict PET biomarker confirmed AD in CBS.

Methods: Eighteen CBS patients (8 PET Aβ+; 10 PET Aβ-) and 8 cognitively unimpaired Aβ- individuals (CU) were recruited by the Neurodegenerative Research group from the Department of Neurology, Mayo Clinic, Rochester, MN, underwent Aβ (Pittsburgh Compound-B) and tau (^{18}F-flortaucipir) PET and provided a blood sample. Blood plasma analysis was performed to assess p-tau 181, total tau, Aβ 42/40, neurofilament light chain (NfL) and glial fibrillary acidic protein (GFAP). Plasma concentrations were compared between Aβ-, and Aβ+ CBS and controls using Kruskal-Wallis corrected for multiple comparisons using Dunn's test, with effect size measured with area under the receiver operator characteristic curve (AUROC) analysis. Spearman correlations were calculated to assess relationships between plasma concentrations and Aβ and tau PET uptake.

Results: The CBS Aβ+ group showed reduced Aβ42/40 ratio, with elevated p-tau 181, GFAP and NfL plasma concentrations compared to CU, while the CBS Aβ- group only showed elevated NfL concentration compared to CU (Figure 1). Both p-tau 181 (AUROC=0.95) and GFAP (AUROC=0.91) plasma concentrations were able to differentiate CBS Aβ- from CBS Aβ+. Plasma p-tau 181 and GFAP concentrations showed a positive correlation to both Aβ and tau PET uptake, and the Aβ42/40 ratio showed a negative correlation to Aβ PET uptake (Figure 2). No correlations were observed between NfL and Aβ and tau PET.

Discussion: This study supports the use of plasma p-tau 181 and GFAP to detect AD in CBS, while NfL shows potential as a nonspecific disease biomarker of CBS regardless of underlying pathology. Plasma concentrations may potentially be incorporated in clinical trials targeting CBS patients with underlying AD.

Plasma level differences across groups

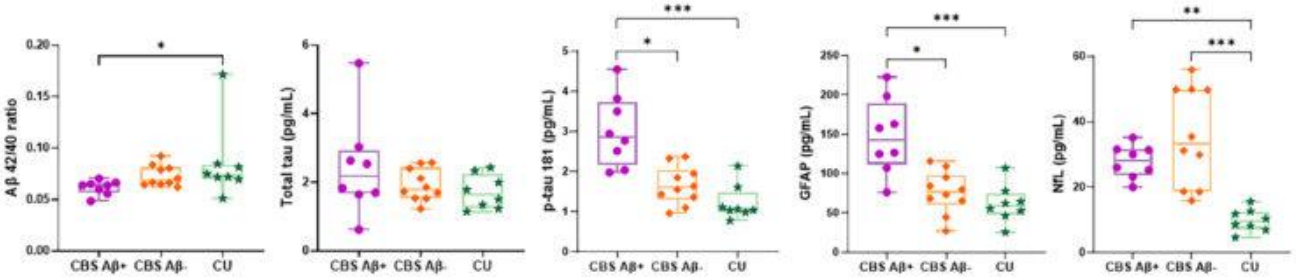

Figure 1: Difference in blood plasma biomarker levels between CBS Aβ-, CBS Aβ+ and CU. Group comparisons for assessing differences in plasma levels across the three groups using Kruskal-Walli's test corrected for multiple comparisons using Dunn's test

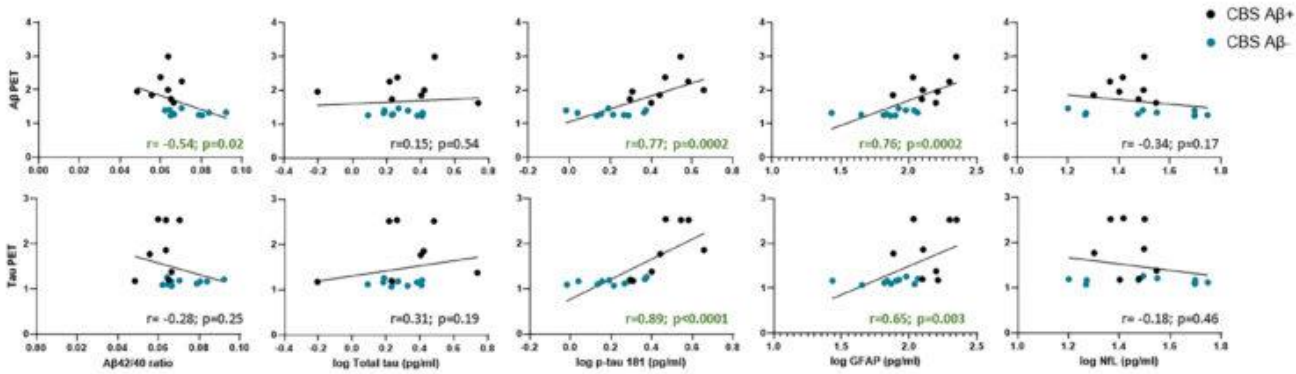

Figure 2: Spearman correlations between plasma biomarkers and PET uptake. These plots represent the relation between plasma biomarker concentrations and PET uptake. Here the analysis was done on the CBS group, however CBS Aβ- and CBS Aβ+ patients have been highlighted in different colours.

Keywords: Corticobasal syndrome, blood plasma biomarkers, PET uptake

Evaluating the impact of racialization on imaging and plasma biomarkers

Alexandra Gogola[1], Xuemei Zeng[2], Anum Saeed[3,4], Brian Lopresti[1], Beth Snitz[5], Dana Tudorascu[2], Davneet Minhas[1], Milos Ikonomovic[5,6], Julia Kofler[7], Cristy Matan[1], N Scott Mason[1], Tharick Pascoal[2], Howard Aizenstein[2], Chester Mathis[1], William Klunk[2], Henrik Zetterberg[8], Kaj Blennow[8], Oscar Lopez[5], Steven Reis[3,4], Victor Villemagne[2], Thomas Karikari[2,8], Ann Cohen[2]

[1]*Department of Radiology, University of Pittsburgh School of Medicine, Pittsburgh, PA, United States*
[2]*Department of Psychiatry, University of Pittsburgh School of Medicine, Pittsburgh, PA, United States*
[3]*Department of Medicine, University of Pittsburgh, Pittsburgh, PA, United States*
[4]*Heart and Vascular Institute, University of Pittsburgh Medical Center, Pittsburgh, PA, United States*
[5]*Department of Neurology, University of Pittsburgh School of Medicine, Pittsburgh, PA, United States*
[6]*Geriatric Research Education and Clinical Center, VA Pittsburgh Healthcare System, Pittsburgh, PA, United States*
[7]*Department of Pathology, University of Pittsburgh, Pittsburgh, PA, United States*
[8]*Institute of Neuroscience and Physiology, University of Gothenburg, Mölndal, Sweden*

Background: Imaging and plasma biomarkers are widely used in Alzheimer's disease (AD) observational studies and clinical trials. Due to the lack of racial or ethnic diversity in earlier studies, a more complete understanding of biomarker differences across racialized groups is needed. Further, results from the few previous studies have disagreed on both the magnitude and direction of AD biomarker differences in racialized groups. We evaluated differences in plasma Aβ42/Aβ40, p-tau181 and Aβ PET outcomes between participants racialized as either Black or African American (AA) or non-Hispanic white (NHW).

Methods: We evaluated 326 participants enrolled in observational studies at the University of Pittsburgh with PET imaging and plasma biomarker assessments including: Global PiB SUVR, plasma Aβ42/Aβ40 and p-tau181 (Simoa HD-X). Outlier analysis resulted in a total of 88 AA and 166 NHW participants. To further refine the comparison, AA and NHW participants were matched based on age, sex, and ApoE status, resulting in a matched set with 88 AA and 88 NHW participants. Group differences were assessed using t-tests.

Results: In both the full and matched sets, Aβ42/Aβ40 (Table 1) showed no differences between the AA and NHW groups ($p>0.05$) whereas a p-tau181 and Global PiB SUVRs revealed greater tau ($p<0.001$) and lower Aβ burden ($p<0.05$), respectively, in AA. (Figure 1)

Conclusions: In both the full and matched datasets, the AA and NHW groups showed significant differences in Global PiB SUVR and p-tau181 outcomes in opposite directions. As such, racialization should be given more consideration in AD clinical research, particularly when biomarker results are used for inclusion or exclusion criteria. Future work will explore the influence of racialization on other imaging and plasma biomarkers and their relationship with cognitive performance.

Table 1. T-test p-values between racialized groups for Global PiB SUVR, p-tau181, and Aβ42/Aβ40.

	p-value	AA	NHW
Full set		N = 88	N = 16
PiB	6.13E-04**	1.13±0.10	1.17±0.11
ptau181	2.65E-02*	2.68±0.49	2.54±0.47
Aβ42/Aβ40	3.39E-01	0.07±0.01	0.08±0.02
Matched set		N = 88	N = 88
PiB	6.71E-03**	1.13±0.10	1.17±0.10
ptau181	7.24E-04**	2.68±0.49	2.44±0.42
Aβ42/Aβ40	4.70E-01	0.07±0.08	0.08±0.02

* $p < 0.05$, ** $p < 0.01$

Figure 1. Boxplots of Aβ42/Aβ40, p-tau181, and Global PiB by racialized group.

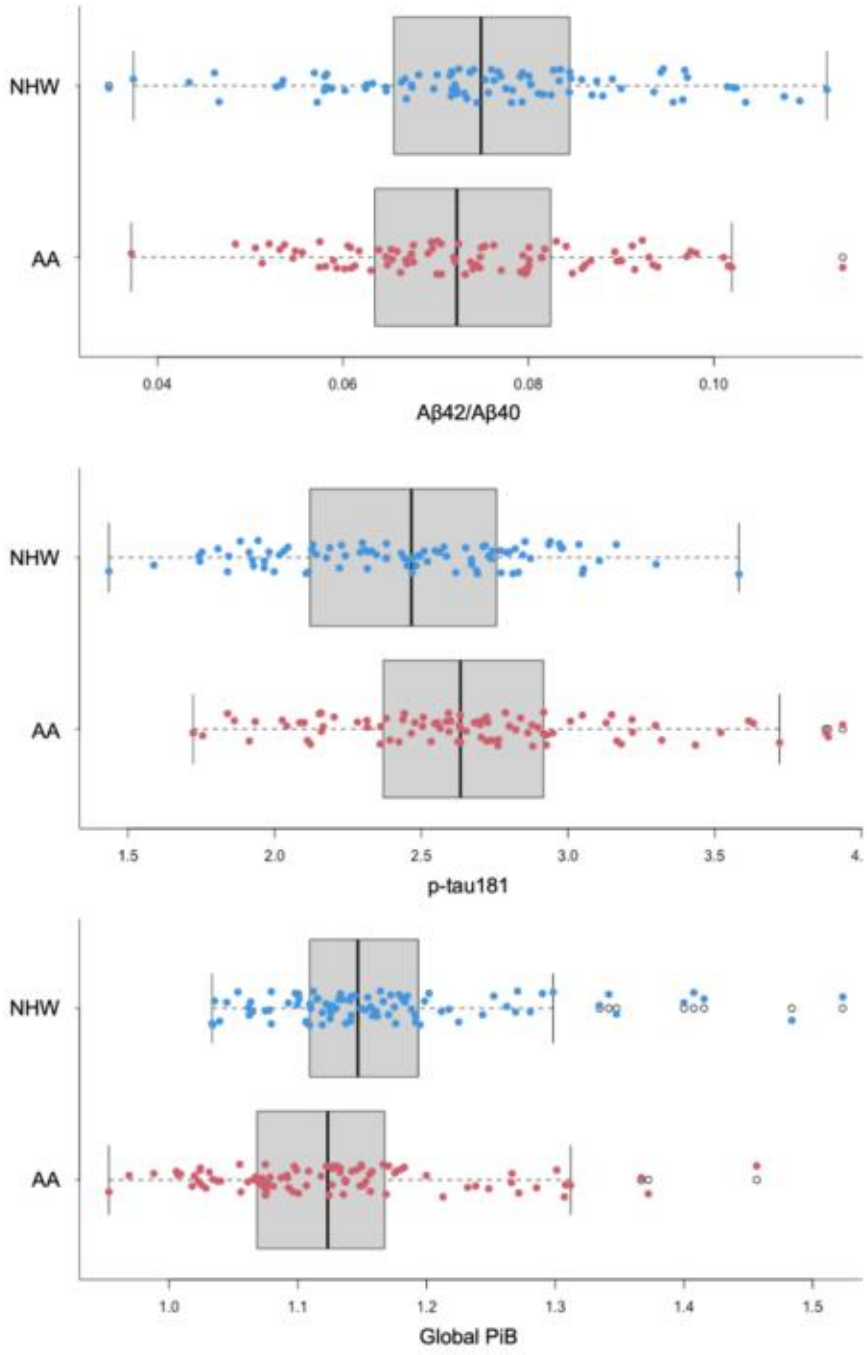

Keywords: Racialization, PET, plasma, biomarkers

Plasma, MRI, and PET biomarker-based risk prediction of dementia in the context of health-related comorbidities and demographic factors: a preliminary exploration

Marc Rudolph[1], Melissa Rundle[1], Courtney Sutphen[1], Thomas Register[1], Timothy Hughes[1], James Bateman[1], Christopher Whitlow[1], Kiran Solingapuram Sai[1], Jeffrey Dage[2], Kristen Russ[2], Michelle Mielke[1], Suzanne Craft[1], Samuel Lockhart[1]

[1]*Wake Forest School of Medicine, Winston-Salem, NC, United States*
[2]*2Indiana University School of Medicine, Indianapolis, IN, United States*

Background: Clinically meaningful biomarker-specific cut-points may serve as screening tools, inform diagnosis, and aid in early detection of individuals at risk of dementia. Here we incorporate *longitudinal* amyloid (Aβ) and baseline tau-PET deposition, evaluating modeling strategies to converge on a range of biomarker thresholds based on multimodal participant-level risk estimates applied to participants lacking PET data.

Method: Plasma (Quanterix SIMOA HD-X: Aβ42/40, GFAP, NfL, p-tau181) and neuroimaging (global PiB [Aβ] SUVr, CL); meta-temporal FTP (tau) SUVr; MRI total brain volume (BVOL), global white matter hyperintensity volume (WMH), diffusion-weighted fractional anisotropy (FA) and NODDI freewater (FW) biomarkers were acquired in participants with diagnosis of cognitively normal (NC; N=299), mild cognitive impairment (MCI; N=192) or dementia (DEM; N=65) from the Wake Forest ADRC (Table 1). Covariates included *APOE*-ε4 carrier status, demographics (age, sex, race, education), and cardiometabolic factors (estimated glomerular filtration rate [eGFR]; BMI). Gaussian-mixture models (GMM), ROC analysis, logistic regression, and random forest modeling were used in analyses.

Results: 12 Aβ-PET accumulators (>3CL/year; 4/12: ~33%) converted to Aβ-PET+ at ~2yr follow-up. Baseline Aβ and tau-PET deposition were positively associated (r^2=.58; p<.001; ~43% concordance at SUVr=1.21; Figure 1). An intermediate zone of 1.11-1.21 SUVr (Aβ: ~9.8-18.8 CL) captured ~58% & ~43% of Aβ-PET converters with Aβ & tau-PET and overlapped with (1) lower/upper bounds for p-tau181 (2.45-4.64 pg/mL) & GFAP (98.75-162.48 pg/mL), and (2) cut-points derived from logistic regression (AUC=.871-.966; Figure 2). Random forest-derived Shapley values highlight *participant-level* predictive features (not shown).

Conclusion: Univariate (GMM) and bivariate (ROC) cut-points identify Aβ+/tau+. Subthreshold Aβ & tau-PET (~1.07-1.21) captures Aβ accumulators/converters. Participants could be classified as Aβ-PET+, based on a combination of demographics, health-related information, and plasma and MRI biomarkers. Future work will focus on developing well-validated diagnostic prediction models to assess participant-level risk over biomarker-specific cut-points, leveraging interactive dashboards to aid real-time decision-making.

Table 1. Participant characteristics and summary statistics

	Overall, N = 556[1]	NC, N = 299[1]	MCI, N = 192[1]	DEM, N = 65[1]	p[2]	p-fdr[3]
Age	70 (63, 76)	68 (62, 73)	71 (65, 77)	73 (66, 78)	**<0.001**	**<0.001**
Female	369 (66%)	217 (73%)	116 (60%)	36 (55%)	**0.003**	**0.005**
Race					**0.027**	**0.036**
White	444 (80%)	243 (81%)	145 (76%)	56 (86%)		
Black	105 (19%)	51 (17%)	46 (24%)	8 (12%)		
Asian	5 (0.9%)	5 (1.7%)	0 (0%)	0 (0%)		
American-Indian	2 (0.4%)	0 (0%)	1 (0.5%)	1 (1.5%)		
Education (years)	16 (14, 18)	16 (14, 18)	16 (13, 18)	16 (13, 18)	**0.001**	**0.002**
APOE e4					**<0.001**	**<0.001**
CARRIER	182 (34%)	80 (28%)	69 (37%)	33 (53%)		
NONCARRIER	356 (66%)	210 (72%)	117 (63%)	29 (47%)		
Missing	18	9	6	3		
BMI	26.7 (24.1, 30.7)	26.6 (23.9, 30.9)	27.3 (24.8, 31.1)	25.5 (23.4, 28.5)	**0.021**	**0.03**
eGFR	75 (65, 86)	76 (65, 87)	75 (65, 85)	73 (65, 83)	0.5	0.5
Missing	146	88	48	10		
NfL (pg/mL)	14 (10, 20)	13 (9, 17)	15 (11, 21)	20 (15, 29)	**<0.001**	**<0.001**
GFAP (pg/mL)	118 (83, 168)	107 (76, 145)	118 (87, 184)	190 (149, 247)	**<0.001**	**<0.001**
Aβ42/40 (pg/mL)	.053 (.046,.060)	.055 (0.049,.062)	.051 (.044,.059)	.048 (.044,.053)	**<0.001**	**<0.001**
p-tau181 (pg/mL)	2.89 (2.18, 4.06)	2.58 (2.10, 3.37)	3.01 (2.17, 4.37)	4.77 (3.73, 6.33)	**<0.001**	**<0.001**
Aβ-PET (SUVr)	1.15 (1.07, 1.66)	1.10 (1.07, 1.17)	1.24 (1.10, 1.97)	2.07 (1.46, 2.21)	**<0.001**	**<0.001**
*N (IV1)**	140	76	44	20		
TAU-PET (SUVr)	1.18 (1.12, 1.46)	1.13 (1.10, 1.18)	1.28 (1.13, 1.43)	1.61 (1.20, 2.09)	**<0.001**	**0.002**
*N (IV1)**	41	16	14	11		
Accumulators	21 (3.8%)	9 (3.0%)	10 (5.2%)	2 (3.1%)	-	-
Aβ + Converter	7 (1.3%)	4 (1.3%)	3 (1.6%)	0 (0%)	-	-

[1] n (%); Median (IQR); [2] Pearson's Chi-squared tests; Kruskal-Wallis rank sum test; Fisher's exact test; [3] False discovery rate correction for multiple testing; * Scan included from initial visit 1 (IV1)

Figure 1. Amyloid accumulators and associations between Aβ and TAU-PET and plasma p-tau181 and GFAP and a comparison of cutoffs in the context of comorbidities

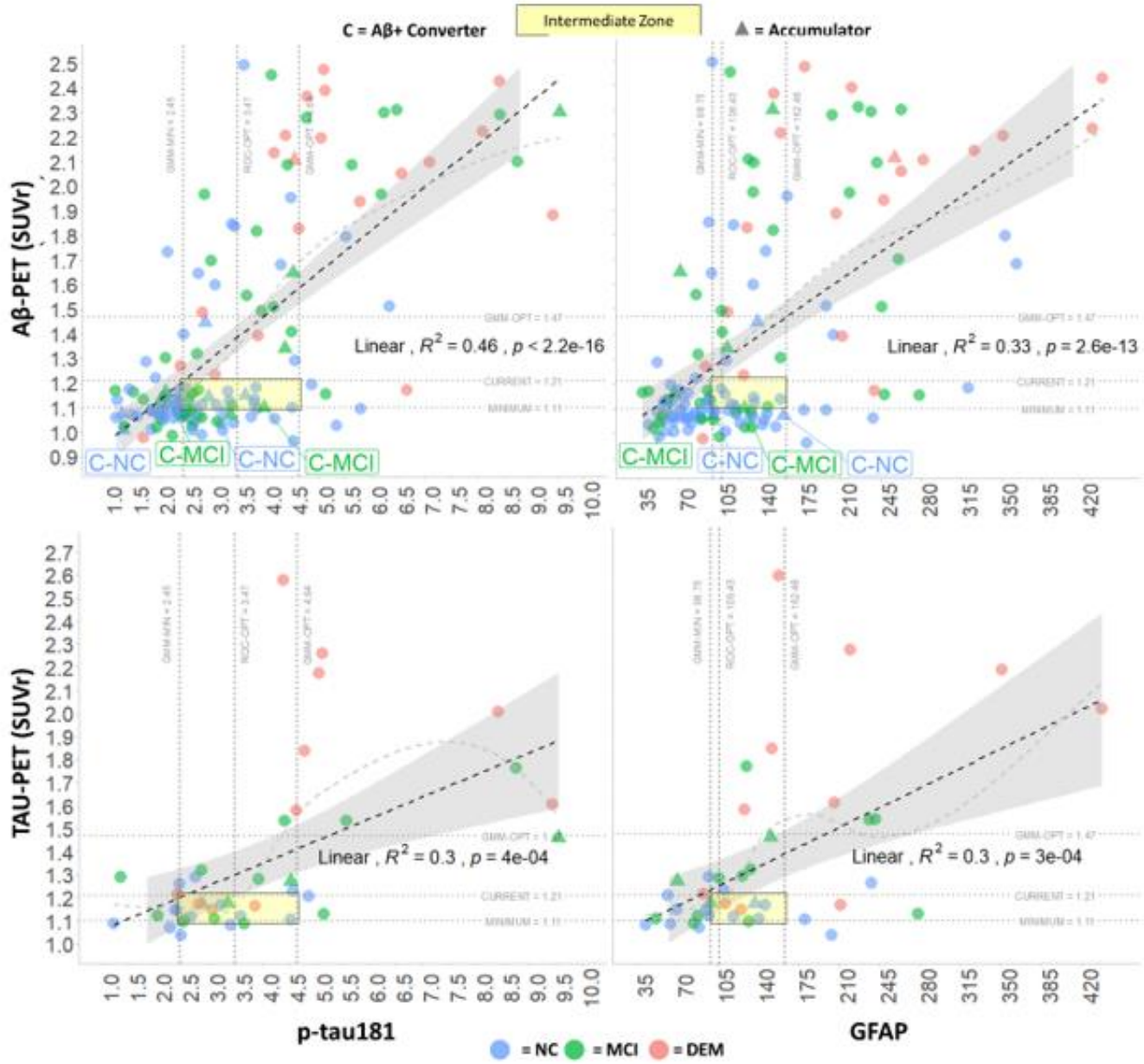

Note: Associations between Aβ- and TAU-PET and plasma p-tau181 and GFAP. Plasma specific cut-points are indicated by dashed lines and correspond to (1) an optimal and lower-bound threshold derived from gaussian-mixture modeling (GMM-OPT, GMM-MIN) or ROC-based analyses (Aβ-PET positivity ~ plasma). PET imaging cut-points are based on minimum and current *Aβ-PET* thresholds (SUVr ~= 1.11, 1.21) and a sample-derived optimal GMM threshold. The intersection of cut-points represents a potential intermediate zone (yellow box) sensitive to Aβ-PET accumulators and/or Aβ-PET converters. Accumulators (Triangles) are defined here by participants whose Aβ-PET values increase by greater than 3 centiloids following recommended pre- and post-processing procedures (Klunk, 2015). Participants who accumulate Aβ-PET over two-sessions and surpass a common threshold (SUVr = 1.21 Centiloids = ~18.8) are labelled Aβ-converters and are of particular interest. One participant, labelled an accumulator converted to Aβ-PET+ at follow up, fell slightly below the 1.11 threshold (SUVr = 1.075) and was plasma biomarker positive using GMM, & ROC-based (Aβ-PET positivity) cut-points. Abbreviations Aβ = Amyloid Beta; GFAP = Glial Fibrillary Acid Protein; NfL = Neurofilament Light-Chain

Figure 2. Multi-biomarker thresholds based on predicted probabilities from model classifying an individual as amyloid positive or negative in both training and test data sets

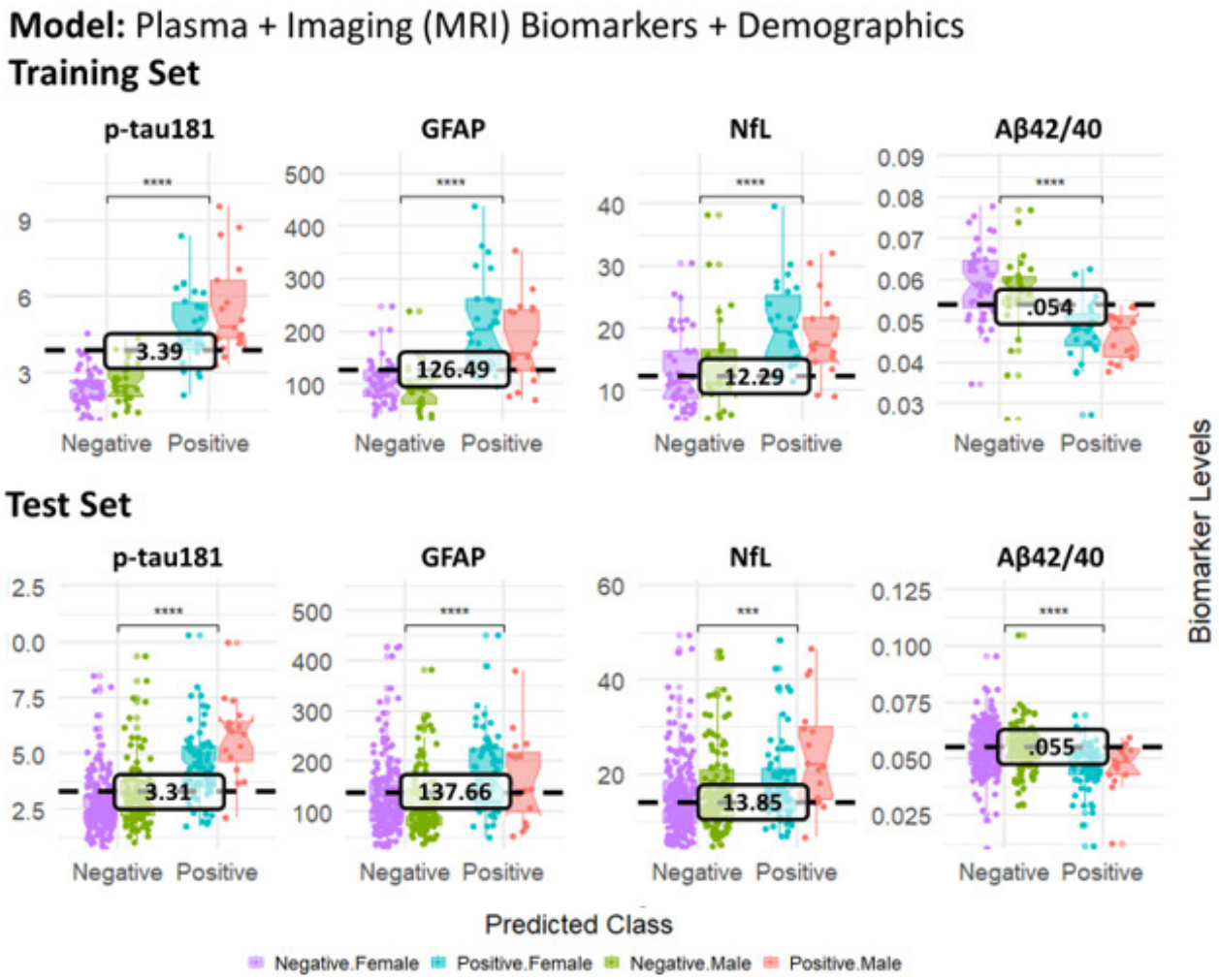

Note: The probability of being classified as Aβ-PET+ (e.g., predicted probabilities; SUVr >= 1.21) were extracted from logistic regression models and used in ROC analyses (e.g., here the outcome was *predicted* Aβ-PET+). The Youden index representing model-based cut-points are indicated by a black dashed line and labelled in black text. Predicted probabilities are further stratified by sex for visualization. Models were generated exclusively in the training set of participants with Aβ-PET data and applied to a test set of participants without Aβ-PET data who have not yet received a PET scan. Cutoffs represent the point that best separates participants predicted as Aβ-PET positive using a combination of plasma and/or imaging biomarkers with (as shown here) and without the addition of covariates and/or health-related factors. All cut-points fall within the intermediate zone illustrated in Figure 1. As expected, participants more likely to be classified as Aβ-PET+, based on a combination of demographics (age, sex, race, education) and health-related information (eGFR, BMI), APOE genotype, and plasma (p-tau181, GFAP, NfL, Aβ42/40) and MRI (BVOL, WMH, DTI FA, NODDI FW) biomarkers have poorer overall brain health (e.g., lower total grey matter brain volumes, higher WMH, and NODDI FW) and altered plasma biomarker levels. Clinical diagnosis (NC, MCI, DEM) was not used in any of the current models. *Abbreviations:* Aβ = Amyloid Beta; GFAP = Glial Fibrillary Acid Protein; NfL = Neurofilament Light-Chain; eGFR = Estimated Glomerular Filtration Rate; BVOL = Total Brain Volume; WMH = Global White Matter Hyperintensities; DTI = Diffusion-Tensor Imaging; FA = Fractional Anisotropy; NODDI = Neurite Orientation Dispersion and Density Imaging; FW = Freewater

Keywords: PET, Plasma, Biomarkers, Dementia, Risk

Longitudinal change of cerebral amyloid and tau and its association with plasma biomarkers in preclinical Alzheimer's disease

Alfonso Fajardo-Valdez[1], Yara Yakob[1], Mohammadali Javanray[1], Frédéric St-Onge[1], Jonathan Gallego-Rudolf[1], Ting Qiu[1], Valentin Ourry[1], Jordana Remz[1], Jean-Paul Saucy[2], Nicholas James Ashton[3], Henrik Zetterberg[3], Kaj Blennow[3], Judes Poirier[1], John C. Breitner[1], Sylvia Villeneuve[1]

[1]*Douglas Mental Health University Institute, Centre for Studies on the Prevention of Alzheimer's Disease(StoP-AD), Montreal, QC, Canada*
[2]*Montreal Neurological Institute, McGill University, Montreal, QC, Canada*
[3]*Department of Psychiatry and Neurochemistry, Institute of Neuroscience and Physiology,The Sahlgrenska Academy,University of Gothenburg, Gothenburg, Sweden*

Introduction: Amyloid-beta (Aβ) and tau biomarkers are typically dichotomized into positive (+) and negative (-) status to define individuals with Alzheimer's disease (AD) pathology. However, such AD proteinopathies start accumulating years before reaching clinically defined abnormality thresholds. We examined longitudinal Aβ and tau accumulation in cognitively unimpaired (CU) participants and assessed whether demographic and/or plasma measures were related to steeper Aβ and tau accumulation.

Methods: We studied 105 CU participants from the PREVENT-AD cohort[(1)] who underwent longitudinal Aβ and tau PET scans (mean time between scans = 4.33 years, 0.44 SD). Participants were labeled as Aβ+ if amyloid index SUVr > 1.25. We then calculated the annual rate of change (aRC) for Aβ and tau. Subjects were labeled as Aβ accumulators if aRC > 2.1 centiloids/year [(2)] and as tau accumulators if temporal meta-ROI[(3)] aRC surpassed the mean plus 2 SD from a group of young participants[(4)]. We then compared demographic/plasma information between Aβ and tau accumulators and non-accumulators and performed linear regression models between Aβ/tau aRC and demographic/plasma measures. Age and sex were included as covariates when not used as independent variables.

Results: Aβ positivity, *APOE*4 status, lower plasma $A\beta_{42/40}$ levels and higher ptau-181 and GFAP levels were all associated with faster Aβ-PET aRC (Fig. 2). Only GFAP levels were associated with faster tau-PET aRC. When participants were classified into Aβ and tau accumulators and non-accumulators, the Aβ accumulator group included more *APOE*4 carriers than the non-Aβ accumulator group, and individuals accumulating both pathologies had higher GFAP plasma values when compared to the other groups (Table 1).

Conclusions: Several demographic and plasma markers are associated with Aβ aRC. Increased plasma GFAP levels are closely related to faster aRC of both Aβ, and tau-PET. Therefore, GFAP might be an indicator of an accelerated Aβ/Tau accumulation pattern.

Table 1: Demographics and statistical comparisons per accumulator groups. Categorical variables were tested using Fisher's exact test and continuous variables using ANOVA. *Differences surviving FDR. Significant difference between [a]G1 vs G2; [b]G1 vs G3; [c]G1 vs G4; [d]G2 vs G4; and [e]G3 vs G4.

N = 105	Non-Aβ Acc / Non-Tau Acc (G1)	Aβ Acc / Non-Tau Acc (G2)	Non-Aβ Acc / Tau Acc (G3)	Aβ Acc / Tau Acc (G4)	Statistical Significance
Sample Size n (%)	59 (56.2)	12 (11.4)	17 (16.2)	17 (16.2)	$p < 0.001^{*}$
Sex n (%)	F: 40 (67.7)	F: 10 (83.33)	F: 14 (82.35)	F: 13 (76.47)	p = 0.59
Aβ+ n (%)	10 (16.94)	7 (58.33)	4 (23.52)	11 (64.7)	$p < 0.001^{*a, b, *c}$
ApoE4 Carrier n (%)	18 (30.51)	8 (66.67)	3 (17.65)	10 (58.82)	$p < 0.001^{*a,*c}$
Age (Mean ± SD)	66.95 ± 5.03	67.08 ± 4.93	67.06 ± 4.71	70.35 ± 4.08	p = 0.08
Education Years (Mean ± SD)	15.85 ± 3.75	14.08 ± 2.27	14.24 ± 2.66	15.29 ± 2.91	p = 0.18
$Aβ_{42/40}$ (Mean ± SD)	0.07 ± 0.02	0.06 ± 0.01	0.07 ± 0.02	0.07 ± 0.01	p = 0.71
pTau181 (Mean ± SD)	6.58 ± 3.51	7.2 ± 3.27	6.11 ± 2.63	7.25 ± 2.36	p = 0.70
NfL (Mean ± SD)	17.47 ± 6.36	16.17 ± 2.52	17.66 ± 6.72	19.08 ± 6.02	p = 0.65
GFAP (Mean ± SD)	100.77 ± 45.87	100.56 ± 27.44	126.23 ± 95.55	148.65 ± 41.37	$p = 0.011^{*c, d, *e}$

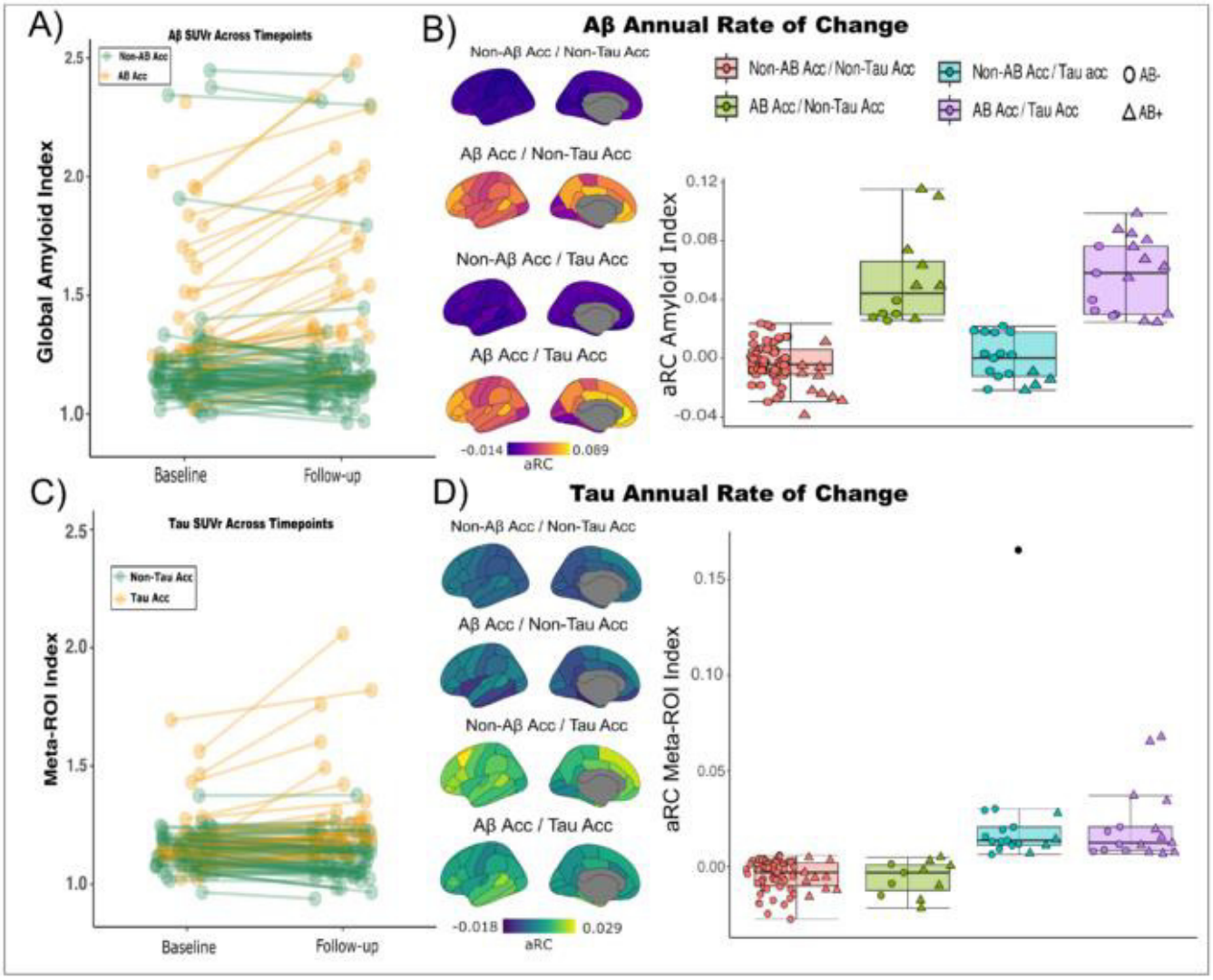

Figure 1. Spaghetti plots of PET global Aβ and meta-ROI tau in accumulator vs non-accumulator groups for baseline and follow-up sessions (A, C); Rate of change of global PET Aβ and Meta-ROI Tau across all four groups (B,D). Brain maps showing average aRC in each brain region per group. The black-colored dot in boxplots represents an extreme tau accumulator. This participant showed high levels of tau in both baseline and follow-up PET scans but was labeled as Aβ- and non-Aβ accumulator. A visual read nevertheless suggests focal amyloid binding. This participant was removed from the main analyses.

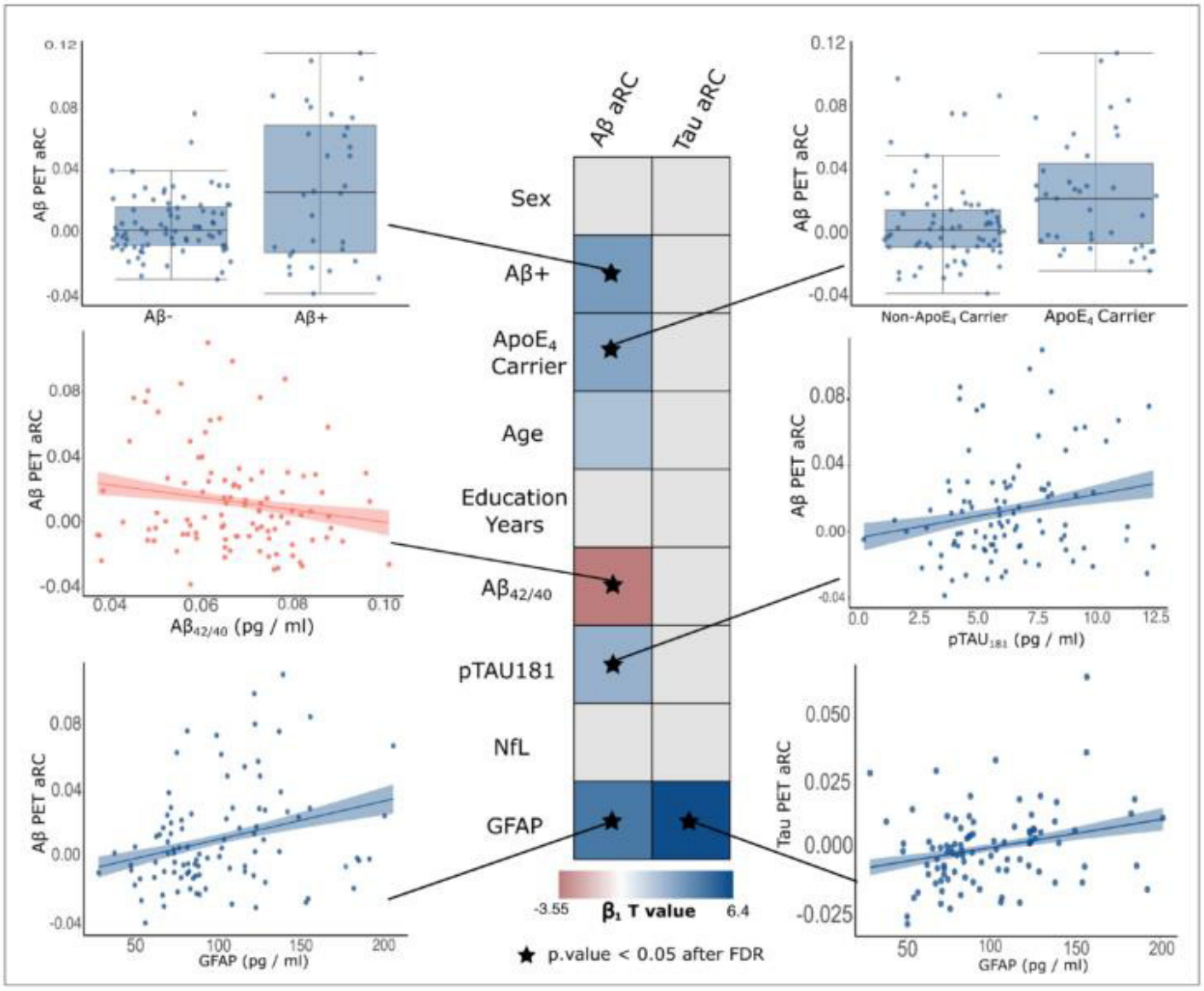

Figure 2. Association between plasma/demographics and Aβ/Tau aRC. Gray-colored cells depict non-significant associations, while red/blue coloured cells depict significant associations at an uncorrected p-value of 0.05. Colormap is proportional to the directionality and strength of the associations. Associations that remained significant after correction for multiple comparisons are marked with a star.

Keywords: PET, Amyloid, Tau, Rate of Change, Plasma

Proteome-wide analyses identifies plasma immune regulators of amyloid-beta progression

Michael R. Duggan[1], Gabriela T. Gomez[2], Murat Bilgel[1], Jingsha Chen[3], Timothy J. Hohman[4,5], Jenifer Cordon[1], Tonnar Castellano[6], Mary Ellen I. Koran[6], Julian Candia[7], Alexandria Lewis[2], Abhay Moghekar[2], Nicholas J. Ashton[8,9,10,11], Przemysław R. Kac[8], Thomas K. Karikari[8,12], Kaj Blennow[8,13,14,15], Henrik Zetterberg[8,13,16,17,18,19], Madhav Thambisetty[1], Josef Coresh[3], Susan M. Resnick[1], Keenan A. Walker[1]

[1]*Laboratory of Behavioral Neuroscience, National Institute on Aging, National Institutes of Health, Baltimore, MD, United States*
[2]*Department of Neurology, Johns Hopkins University School of Medicine, Baltimore, MD, United States*
[3]*Department of Epidemiology, Johns Hopkins University Bloomberg School of Public Health, Baltimore, MD, United States*
[4]*Vanderbilt Memory and Alzheimer's Center, Vanderbilt University Medical Center, Nashville, TN, United States*
[5]*Vanderbilt Genetics Institute, Vanderbilt University Medical Center, Nashville, TN, United States*
[6]*Department of Radiology and Radiological Sciences, Vanderbilt University Medical Center, Nashville, TN, United States*
[7]*Translational Gerontology Branch, National Institute on Aging, National Institutes of Health, Baltimore, MD, United States*
[8]*Department of Psychiatry and Neurochemistry, Institute of Neuroscience and Physiology, University of Gothenburg, Mölndal, Sweden*
[9]*King's College London, Institute of Psychiatry, Psychology and Neuroscience Maurice Wohl Institute Clinical Neuroscience Institute, London, United Kingdom*
[10]*NIHR Biomedical Research Center for Mental Health and Biomedical Research Unit for Dementia at South London and Maudsley NHS Foundation, London, United Kingdom*
[11]*Center for Age-Related Medicine, Stavanger University Hospital, Stavanger, Norway*
[12]*Department of Psychiatry, School of Medicine, University of Pittsburgh, Pittsburgh, PA, United States*
[13]*Clinical Neurochemistry Laboratory, Sahlgrenska University Hospital, Mölndal, Sweden*
[14]*ICM Institute, Pitié-Salpêtrière Hospital, Sorbonne University, Paris, France*
[15]*First Affiliated Hospital, University of Science and Technology of China, Anhui, China*
[16]*Department of Neurodegenerative Disease, University College London Institute of Neurology, London, United Kingdom*
[17]*UK Dementia Research Institute, University College London, London, United Kingdom*
[18]*Hong Kong Center for Neurodegenerative Diseases, Hong Kong, HK*
[19]*Wisconsin Alzheimer's Disease Research Center, University of Wisconsin School of Medicine and Public Health, University of Wisconsin-Madison, Madison, WI, United States*

While immune function is known to play a mechanistic role in Alzheimer's disease (AD), whether peripheral immune proteins influence the rate of amyloid-β (Aβ) progression remains unknown. In the Baltimore Longitudinal Study of Aging (n=196; mean follow-up: 5 years/3.8 scans), we identified 32 immunological proteins in plasma (out of 942) associated with rates of change in cortical Aβ, as measured with ^{11}C-PiB PET (**Figure 1A**). Longitudinal changes in a subset of these candidate proteins also predicted cortical Aβ progression (**Figure 1B**), and the mid- to late-life trajectory of one protein, CAT, was associated with late-life Aβ-positive status in the Atherosclerosis Risk in Communities (ARIC) study (**Figure 1C**). We showed that genetic variants associated with the plasma abundance of CAT and two additional candidate proteins (CD36 and KRT19) predicted rates of Aβ accumulation (**Figure 2A-F**). In addition to their associations with other AD-related phenotypes (tau PET, plasma AD biomarker changes) (**Figure 2G-H**), we showed that 28% of candidate proteins were related to mid-life (20-year) or late-life (8-year) dementia risk in ARIC (**Figure 2I**). Candidate proteins were enriched for atherogenic signaling pathways (**Figure 3A**), susceptible to regulation by key pro-inflammatory cytokines (e.g., TNF, IL1-b) (**Figure 3B**), and not highly expressed in CNS cells but differentially detected in AD brains (especially neurovascular cell types) (**Figure 3C**), suggesting these candidate proteins emanating from peripheral immune cells may be particularly important

drivers of Aβ neuropathology, potentially through interactions with neurovascular and meningeal cell types. Our findings reveal plasma proteins whose levels are associated with longitudinal Aβ accumulation, and identify specific immune mediators in circulation that may contribute to the progression of AD pathophysiology.

Figure 1

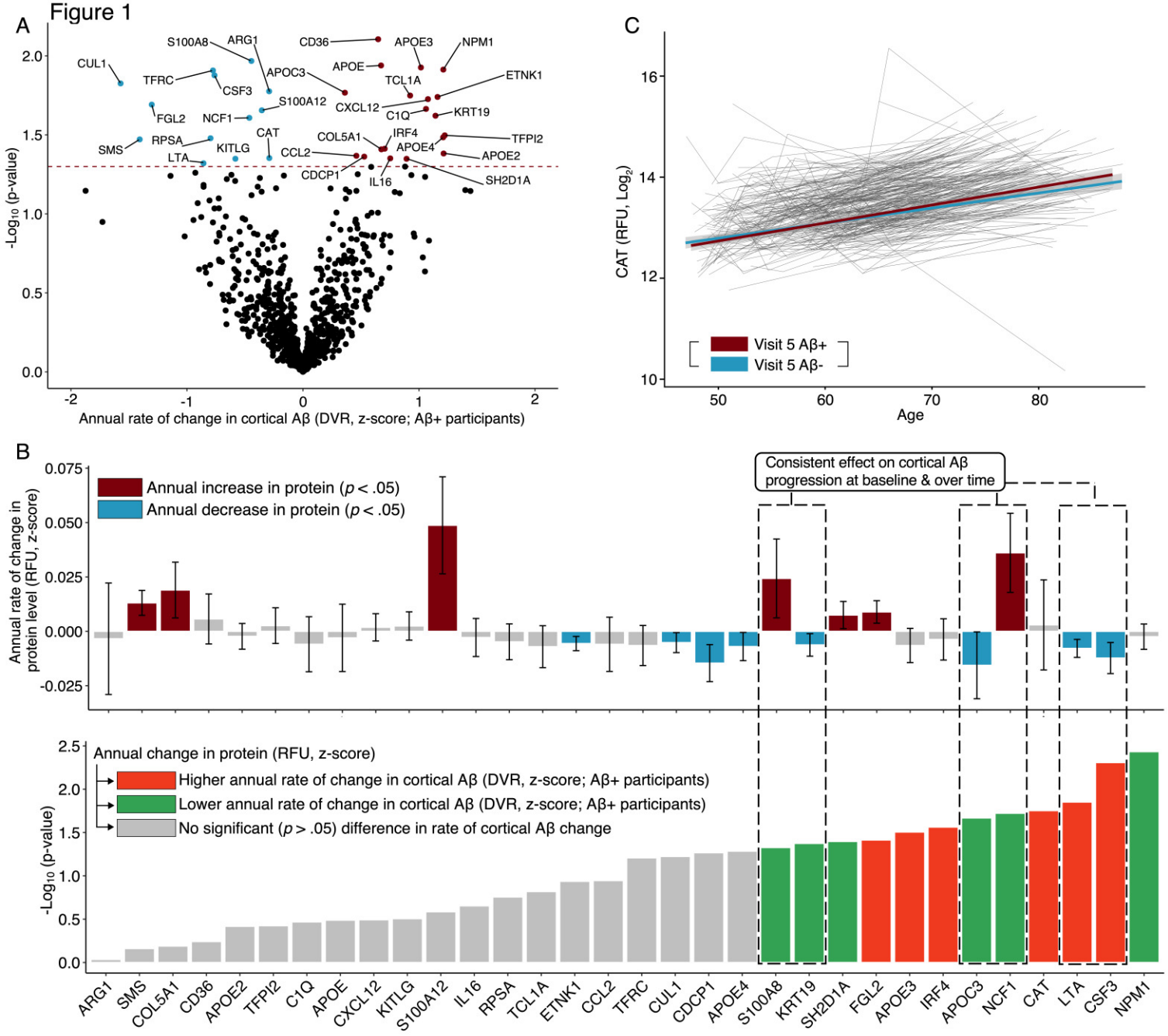

Figure 2

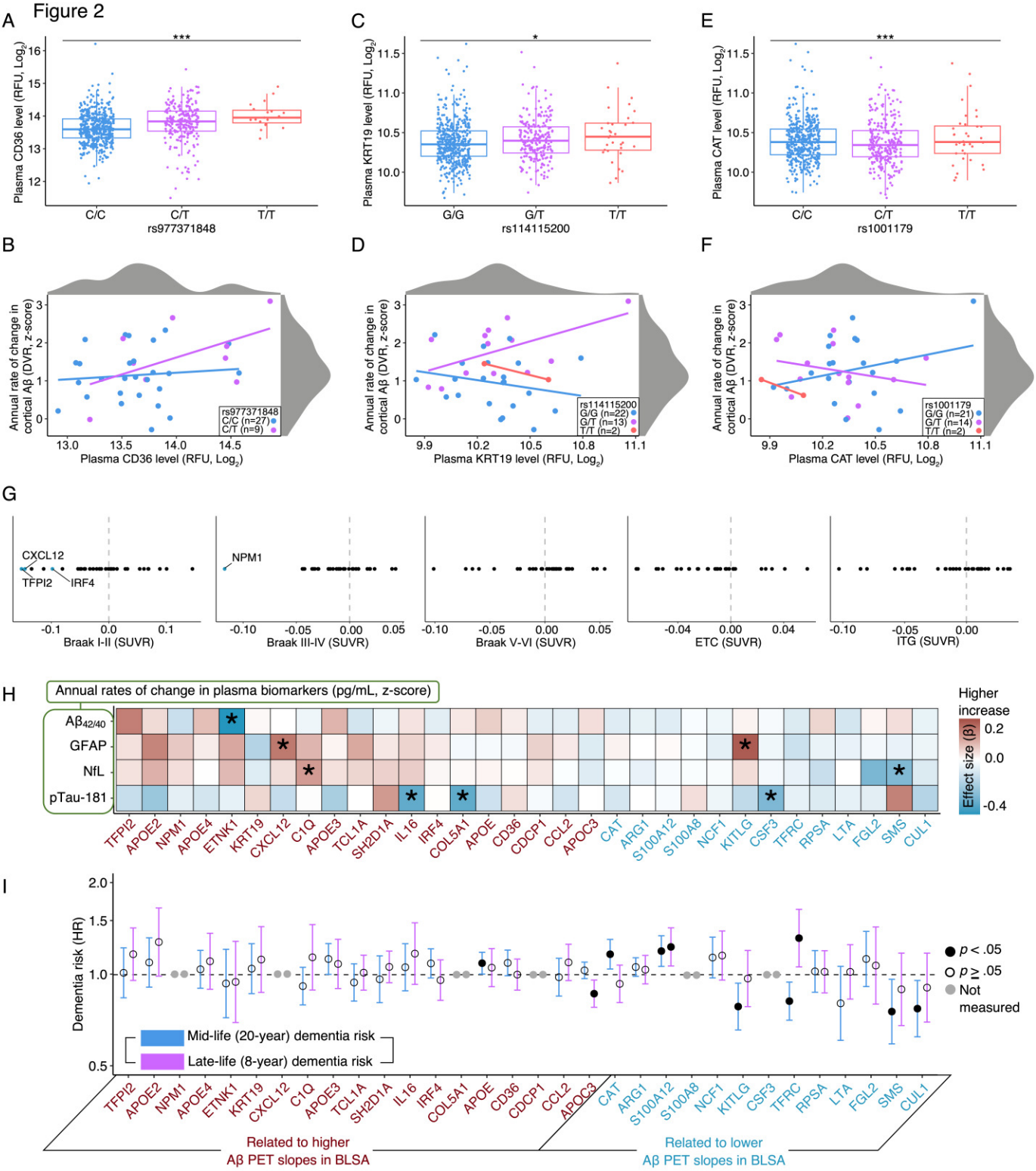
A
C
E
Plasma CD36 level (RFU, Log2)
Plasma KRT19 level (RFU, Log2)
Plasma CAT level (RFU, Log2)
C/C
C/T
T/T
G/G
G/T
rs977371848
rs114115200
rs1001179
B
D
F
Annual rate of change in cortical Aβ (DVR, z-score)
rs977371848 C/C (n=27) C/T (n=9)
rs114115200 G/G (n=22) G/T (n=13) T/T (n=2)
rs1001179 G/G (n=21) G/T (n=14) T/T (n=2)
G
CXCL12
TFPI2
IRF4
NPM1
Braak I-II (SUVR)
Braak III-IV (SUVR)
Braak V-VI (SUVR)
ETC (SUVR)
ITG (SUVR)
H
Annual rates of change in plasma biomarkers (pg/mL, z-score)
Aβ42/40
GFAP
NfL
pTau-181
Higher increase
Effect size (β)
TFPI2 APOE2 NPM1 APOE4 ETNK1 KRT19 CXCL12 C1Q APOE3 TCL1A SH2D1A IL16 IRF4 COL5A1 APOE CD36 CDCP1 CCL2 APOC3 CAT ARG1 S100A12 S100A8 NCF1 KITLG CSF3 TFRC RPSA LTA FGL2 SMS CUL1
I
Dementia risk (HR)
Mid-life (20-year) dementia risk
Late-life (8-year) dementia risk
p < .05
p ≥ .05
Not measured
Related to higher Aβ PET slopes in BLSA
Related to lower Aβ PET slopes in BLSA

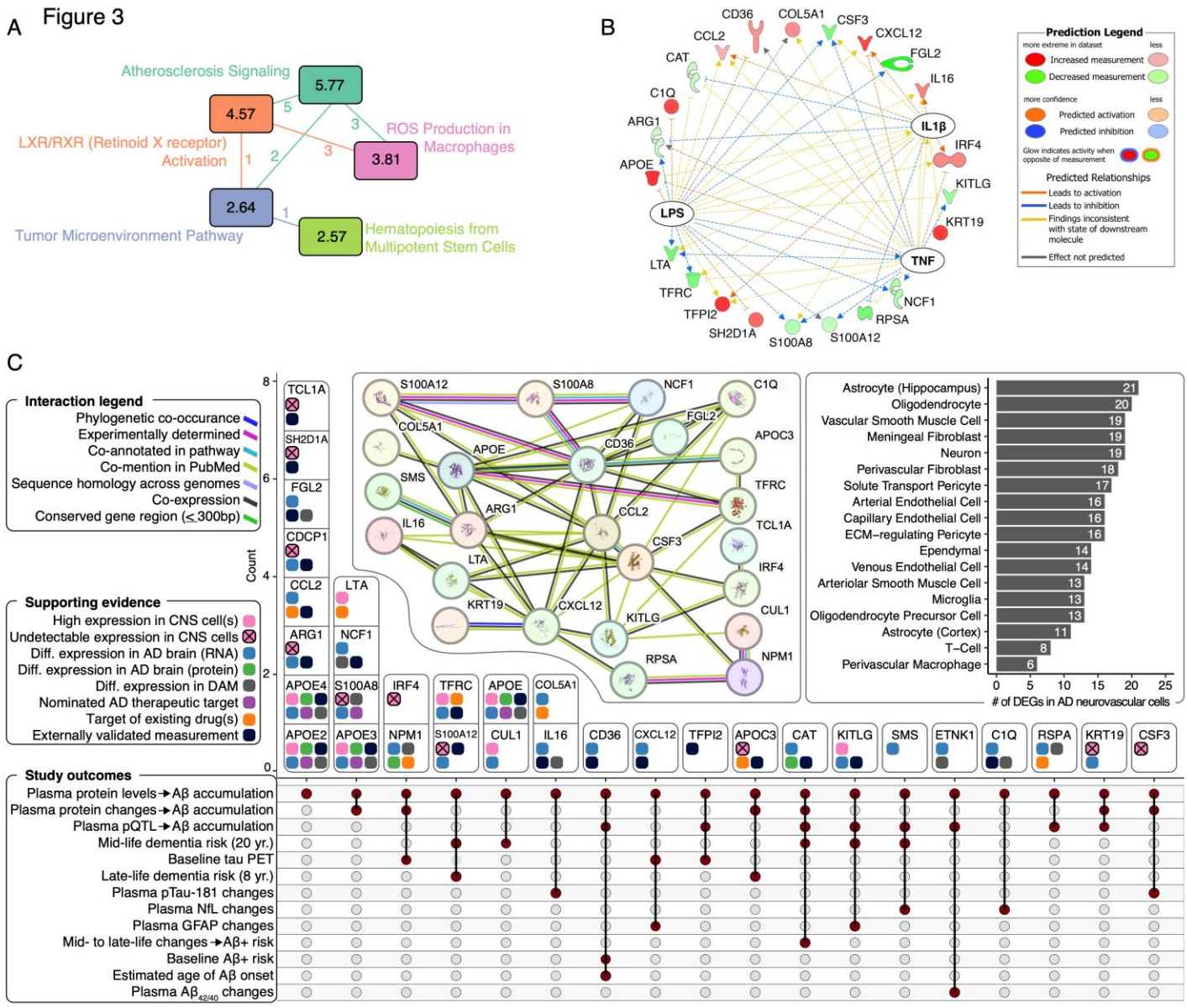

Keywords: PET, amyloid-beta, proteomics, immune

HAI 2024 IS MADE POSSIBLE THROUGH GRANTS AND SPONSORSHIP FROM THE FOLLOWING ORGANIZATIONS:

NIH National Institute on Aging

DIAMOND

Meilleur Technologies

LANTHEUS CERVEAU

PALLADIUM

Lilly

ALZHEIMER'S ASSOCIATION

GOLD

Genentech
A Member of the Roche Group

Eisai

SILVER AND SCHOLARSHIP

RAINWATER Charitable Foundation

Bristol Myers Squibb

SILVER

Invicro

Life Molecular Imaging

Johnson & Johnson Innovative Medicine

BRONZE

abbvie

C2N DIAGNOSTICS

CLARIO.

Quanterix
The Science of Precision Health